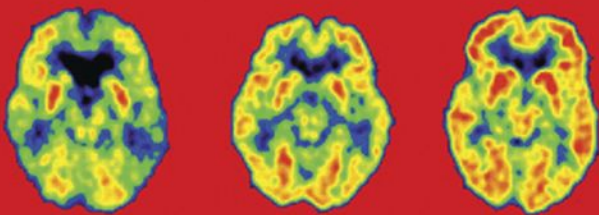
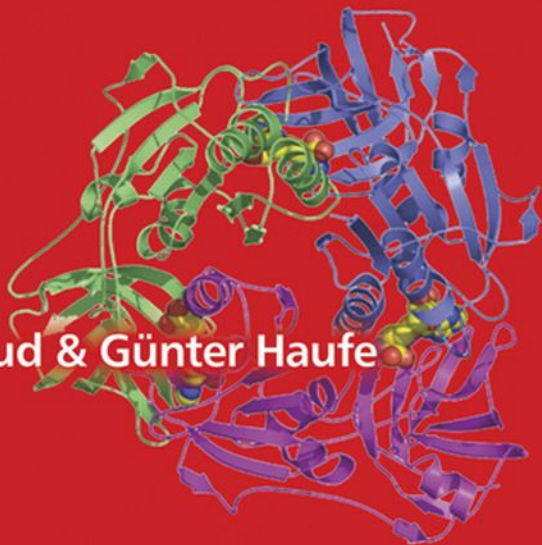




Fluorine and Health



*Molecular Imaging, Biomedical
Materials and Pharmaceuticals*



EDITED BY

Alain Tressaud & Günter Haufe

Fluorine and Health

**Molecular Imaging,
Biomedical Materials and
Pharmaceuticals**

Front cover illustrations:

- ^{18}F FDG PET scans depicting glucose metabolism in a monozygotic twin pair and in a control subject. Note the clear reduction in ^{18}F FDG uptake especially in temporo-parietal areas in the co-twin having Alzheimer disease (left) and similar, but less pronounced, reduction in same brain areas in the cognitively healthy co-twin (middle), as compared to the uptake in a control subject (right) [*Image by courtesy of K. Någren and J.O. Rinne, Turku, PET Centre, Finland and cf. chapter 2 in this book*].

-X-ray derived structure of the fluorinase showing the full structure as a hexamer (dimer of trimers) [*cf. chapter 18 by Hai Deng, D. O'Hagan et al. in this book*].

Fluorine and Health

Molecular Imaging, Biomedical Materials and Pharmaceuticals

Edited by

Alain Tressaud

ICMCB-CNRS

University of Bordeaux I

33608 Pessac Cedex,

France

Günter Haufe

Organisch-Chemisches Institut,

Westfälische Wilhelms-Universität Münster

Münster,

Germany



ELSEVIER

Amsterdam • Boston • Heidelberg • London • New York • Oxford • Paris
San Diego • San Francisco • Singapore • Sydney • Tokyo

Elsevier
Radarweg 29, PO Box 211, 1000 AE Amsterdam, The Netherlands
Linacre House, Jordan Hill, Oxford OX2 8DP, UK

First edition 2008

Copyright © 2008 Elsevier B.V. All rights reserved

No part of this publication may be reproduced, stored in a retrieval system or transmitted in any form or by any means electronic, mechanical, photocopying, recording or otherwise without the prior written permission of the publisher

Permissions may be sought directly from Elsevier's Science & Technology Rights Department in Oxford, UK: phone (+44) (0) 1865 843830; fax (+44) (0) 1865 853333; email: permissions@elsevier.com. Alternatively you can submit your request online by visiting the Elsevier web site at <http://elsevier.com/locate/permissions>, and selecting *Obtaining permission to use Elsevier material*

Notice

No responsibility is assumed by the publisher for any injury and/or damage to persons or property as a matter of products liability, negligence or otherwise, or from any use or operation of any methods, products, instructions or ideas contained in the material herein. Because of rapid advances in the medical sciences, in particular, independent verification of diagnoses and drug dosages should be made

Library of Congress Cataloging-in-Publication Data

A catalog record for this book is available from the Library of Congress

British Library Cataloguing in Publication Data

A catalogue record for this book is available from the British Library

ISBN: 978-0-444-53086-8

For information on all Elsevier publications visit our website at books.elsevier.com

Printed and bound in Hungary

08 09 10 11 12 10 9 8 7 6 5 4 3 2 1

Working together to grow
libraries in developing countries

www.elsevier.com | www.bookaid.org | www.sabre.org

ELSEVIER BOOK AID Sabre Foundation
International

CONTENTS

Contributors	ix
---------------------	----

Preface	xi
----------------	----

Part I: Molecular Imaging

1. Fluorine-18 Chemistry for Molecular Imaging with Positron Emission Tomography	3
<i>Frédéric Dollé, Dirk Roeda, Bertrand Kuhnast, and Marie-Claire Lasne</i>	
2. Application of ^{18}F -PET Imaging for the Study of Alzheimer's Disease	67
<i>Kjell Någren and Juha O. Rinne</i>	
3. ^{18}F -Labeled PET-Tracers for Cardiological Imaging	85
<i>Klaus Kopka, Stefan Wagner, Michael Schäfers, Andreas Faust, Otmar Schober, and Günter Haufe</i>	
4. [^{18}F]-Labeled PET and PET/CT Compounds in Oncology	141
<i>Ken Herrmann and Bernd Joachim Krause</i>	
5. Non-Invasive Physiology and Pharmacology Using ^{19}F Magnetic Resonance	197
<i>Jian-Xin Yu, Weina Cui, Dawen Zhao, and Ralph P. Mason</i>	

Part II: Biomedical Materials

6. Fluoride-Based Bioceramics	279
<i>Christian Rey, Christèle Combes, Christophe Drouet, and Hocine Sfihi</i>	
7. Fluoride in Dentistry and Dental Restoratives	333
<i>John W. Nicholson and Beata Czarnecka</i>	
8. Fluorinated Biomaterials for Cardiovascular Surgery	379
<i>Charles Baquey, Marie-Christine Durrieu, and Robert G. Guidoin</i>	

9. Fluorinated Molecules in Eye Surgery: Experimental and Clinical Benefit of a Heavy Silicone Oil Oxane Hd® (Mixture of Silicone Oil and RMN3 Fluorine Olefin) in the Treatment of Retinal Detachment 407
I. Rico-Lattes, J. C. Quintyn, V. Pagot-Mathis, X. Benouaich, and A. Mathis
10. Biocompatibility of Highly Fluorinated Liquids Used in Ophthalmic Surgery 421
Dirk-Henning Menz and Joachim H. Dresch
11. Perfluorochemical-Based Oxygen Therapeutics, Contrast Agents, and Beyond 447
Marie Pierre Krafft and Jean G. Riess
12. Exposure of Humans to Fluorine and Its Assessment 487
Maja Ponikvar

Part III: Pharmaceuticals

13. Biological Impacts of Fluorination: Pharmaceuticals Based on Natural Products 553
Jean-Pierre Bégué and Danièle Bonnet-Delpon
14. Synthesis and Pharmacological Properties of Fluorinated Prostanoids 623
Yasushi Matsumura
15. Synthesis and Biochemical Evaluation of Fluorinated Monoamine Oxidase Inhibitors 661
Kenneth L. Kirk, Shinichi Yoshida, and Günter Haufe
16. Fluoroolefin Dipeptide Isosteres: Structure, Syntheses, and Applications 699
John T. Welch
17. Molecular Interactions of Fluorinated Amino Acids in a Native Polypeptide Environment 737
Mario Salwiczek, Christian Jäckel, and Beate Koksck

18. Biological Fluorination in *Streptomyces cattleya*: The Fluorinase 761
Hai Deng, Fang-Lu Huang, James H. Naismith,
David O'Hagan, Jonathan B. Spencer, and Xiaofeng Zhu

Subject Index 779

Colour Plate Section at the end of this book

This page intentionally left blank

Contributors

Charles Baquey	379
Jean-Pierre Bégué	553
X. Benouaich	407
Danièle Bonnet-Delpon	553
Christèle Combes	279
Weina Cui	197
Beata Czarnecka	333
Hai Deng	761
Frédéric Dollé	3
Joachim H. Dresp	421
Christophe Drouet	279
Marie-Christine Durrieu	379
Andreas Faust	85
Robert G. Guidoin	379
Günter Haufe	xi,85,661
Ken Herrmann	141
Fang-Lu Huang	761
Christian Jäckel	737
Kenneth L. Kirk	661
Beate Kokschr	737
Klaus Kopka	85
Marie Pierre Krafft	447
Bernd Joachim Krause	141
Bertrand Kuhnast	3
Marie-Claire Lasne	3
Ralph P. Mason	197
A. Mathis	407
Yasushi Matsumura	623
Dirk-Henning Menz	421
Kjell Någren	67
James H. Naismith	761
John W. Nicholson	333
David O'Hagan	761
V. Pagot-Mathis	407
Maja Ponikvar	487

J. C. Quintyn	407
Christian Rey	279
I. Rico-Lattes	407
Jean G. Riess	447
Juha O. Rinne	67
Dirk Roeda	3
Mario Salwiczek	737
Michael Schäfers	85
Otmar Schober	85
Hocine Sfihi	279
Jonathan B. Spencer	761
Alain Tressaud	xi
Stefan Wagner	85
John T. Welch	699
Shinichi Yoshida	661
Jian-Xin Yu	197
Dawen Zhao	197
Xiaofeng Zhu	761

Preface

Recently it was stated that fluorine chemistry is experiencing a renaissance due to the multifaceted reactivity of fluorinating reagents and the outstanding, and sometimes unexpected, properties of compounds containing fluorine. The benefits of these compounds for our society are evident in many fields. Particularly the last two decades have witnessed a spectacular growth of interest in selectively fluorinated molecular compounds. Both low molecular weight molecules and polymers, as well as highly sophisticated materials, are crucial in manifold aspects of medicinal monitoring and health care. This book is designed to acknowledge the extraordinary impact of fluorinated compounds to the general topic of *Fluorine and Health*. The involved subjects are organized in three thematic parts devoted to *Molecular Imaging*, *Biomedical Materials*, and *Pharmaceuticals*.

The first chapters are focused on the key position in biochemical and medicinal analytics of both partially fluorinated low molecular weight compounds labeled with natural ^{19}F -isotope for Magnetic Resonance Imaging (MRI) and tracer molecules labeled with radioactive ^{18}F -isotope for Positron Emission Tomography (PET). The selective synthesis of molecules exhibiting specific properties or physiological effect constitutes the backbone of every medicinal application of fluorinated compounds. Consequently, the methodology for introducing fluorine itself or fluorinated groups into organic skeletons is largely developed in most chapters. Sensitive PET for high resolution molecular *in vivo* imaging requires the preparation of positron-emitting radiotracers. For this purpose, ^{18}F -labeled probes are becoming increasingly prerequisite molecules, due to their adequate physical, physiological, and nuclear characteristics, particularly the relatively long half-life of the ^{18}F -isotope of ~ 110 min as compared to other light positron-emitting isotopes such as ^{11}C (20 min), ^{13}N (10 min), or ^{15}O (2 min). Thus, the development of selective and fast synthetic methods for fluoroorganic compounds is an important issue.

The PET technique is particularly useful for *in vivo* imaging in oncology, neurology and in cardiology. PET and PET/CT (computed tomography) using ^{18}F -labeled compounds such as 2-deoxy-2- ^{18}F fluoro-D-glucose (^{18}F FDG) are becoming essential as *in vivo* imaging methods in oncological diagnostics, tumor prognosis and therapy monitoring. Moreover, innovative and more specific new ^{18}F -tracers for molecular imaging of tumor biology are highlighted in the

framework of their clinical value. Brain imaging using PET is one of the important new tools in monitoring of different neuronal diseases such as Alzheimer's disease, the devastating brain disorder of elderly humans. A number of recently developed [^{18}F]-radiopharmaceuticals have a unique potential for the study of several brain systems of clinical importance. Moreover, the molecular imaging of cardiovascular diseases with [^{18}F]-PET is of great clinical interest, offering the opportunity to investigate noninvasively the cardiovascular physiology and pathophysiology *in vivo* and to contribute to the diagnosis and treatment of diseases having the highest mortality in the industrialized countries. Similarly, the ^{19}F nucleus provides a powerful tool for spectroscopic studies and particularly for MRI, due to its high NMR sensitivity and the fact that there is essentially no background signal in the body. Furthermore, fluorine NMR allows multiple compounds to be examined simultaneously because of the very large chemical shift range of about 300 ppm.

The manifold facets of fluorinated biomaterials are illustrated by examples ranging from inorganic ceramics to perfluorinated organic molecules. Fluorine is an essential trace element in bone mineral, dentine and tooth enamel and is considered as one of the most efficient elements for the prophylaxis and treatment of dental caries. Fluoride-based treatments have been shown indeed to ensure populations developing and maintaining sound dental health. In particular, fluoride ion has an effect on the demineralization/remineralization equilibrium that exists at the tooth surface, shifting it back in favor of remineralization. Fluoride-containing bioactive glasses and ceramics have been found to have an important role in bone repairing materials. Resin-modified glass-ionomers and compomers are dental restoratives which allow fluoride releasing, thus bringing a greater availability and efficiency of the element. Highly diluted fluoridation of drinking water, fluoridated table salt, dentifrices, topical gels, varnishes and mouth-rinses are other types of possible ways to improve dental health, provided small amounts of fluoride are administered.

Another field of application of fluorinated biomaterials is connected to lesions or evolving disease pathology of blood vessels. In particular, arteries may become unable to insure an adequate transport of the blood to organs and tissues. Polytetrafluoroethylene (PTFE) and expanded e-PTFE are the preferred materials for vascular prostheses. The interactions of blood cells and blood plasma macromolecules with both natural and artificial vessel walls are discussed in terms of the mechanical properties of the vascular conduit, the morphology, and the physical and chemical characteristics of the blood contacting surface.

Conversely, the role of perfluorocarbons for oxygen transport and *in vivo* delivery is investigated. In addition to possible use as temporary blood substitute, these fluorocarbon molecules can be applied as respiratory gas carriers, for instance as lung surfactant replacement compositions for neonates and possibly for the treatment of acute respiratory distress syndrome for adults. Another

important issue concerns the applications of highly fluorinated liquids in ophthalmology. Retinal detachment, a disease that can result in blindness, is treated by performing a retinal scar around the tear and maintaining the retina in contact. For this purpose, dense fluorinated liquids are used in pure form or as mixtures with silicone oils. The state of the art of the application of these highly fluorinated liquids in ophthalmology and their biocompatibility and toxicity is discussed. Prospects concerning future applications of these molecules are also considered. Finally, the various origins of human exposure to fluoride species are detailed, together with invaluable recommendations for adequate intake of fluoride, methods for assessing exposure, and discussion of the benefits and drawbacks (fluorosis) of fluoride intake. These investigations should bring a better understanding of the effect of fluoride species on living organisms.

The main focus of the third part is the synthesis of medicinally relevant fluorinated molecules and their interaction with native proteins. New molecules fluorinated in strategic position are crucial for the development of pharmaceuticals with desired action and optimal pharmacological profile. Among the hundreds of marketed active drug components, there are more than 150 fluorinated compounds. It starts by illustrating how the presence of fluorine atoms modifies the properties of a bioactive compound at various biochemical steps, and possibly facilitates its emergence as a pharmaceutical agent. Recent advances in the development of fluorinated analogues of natural products led to new pharmaceuticals such as fluorinated nucleosides, alkaloids, macrolides, steroids, and amino acids.

More specifically, it is detailed how fluorine substitution of specific positions in prostaglandins and thromboxanes, locally produces hormones with a broad variety of biological functions, affecting not only the molecular conformation but also the drug–receptor complex through a contribution of fluorine to the nature and strength of the interaction. Amine oxidases have critically important functions in organisms for efficient deactivation of very potent biogenic amines and hence come into the focus for therapeutic intervention. These points include the development of selective inhibitors, tools for studies of reaction mechanisms, radiotracers for PET imaging, and of medicinal agents. Synthesis and biochemical evaluation of two types of medicinally relevant enzymes, the flavin-dependent monoamine oxidases (MAO) A and B, and the copper-containing amine oxidases (CAO) are highlighted.

The potential utility of peptides as therapeutics with clinical applications is limited by its metabolic instability or poor transmembrane mobility. Consequently, the preparation of metabolically stable peptide analogs that can either mimic or block the function of natural peptides or enzymes is an important area of medicinal chemistry research. Synthesis of fluoroolefin amide isosteres, its incorporation in peptidomimetics, and the influence of that isosteric substitution on the inhibition of several enzymes such as peptidyl prolyl isomerases, dipeptidyl peptidase IV, and thermolysin is described. Moreover, protein folding and activity

depend on a multitude of molecular interactions. Nevertheless, even interactions of single fluorinated amino acids can highly affect polypeptide folding. Though, the metabolic and structural stability of peptides and proteins containing fluorine substitutes have been studied extensively recently, the *de novo* design of relevant target molecules requires a detailed knowledge of molecular interactions introduced by the fluorine atom. Systematic investigation of different fluorinated amino acids incorporated in a model peptide system based on the α -helical coiled coil motive within a hydrophobic and hydrophilic protein environment led to new insights of protein structure.

Finally, recent developments on research into the first C–F bond forming enzyme are summarized. The fluorinase enzyme isolated from *Streptomyces catleya* catalyzes the formation of 5'-fluoro-5'-deoxyadenosine from S-adenosyl-L-methionine and fluoride. The substrate specificity and subsequent transformation of the fluorinated nucleoside to fluoroacetic acid and to fluoro threonine are discussed.

While conceiving the present book, we had outstanding support by a number of colleagues. We would like to express our deep gratitude to the Associate Advisors: B. Ameduri, P. Atkins, J. Knowles, T. Nakajima, M. Pontié, R. Syvret, S. Tavener, and J. Winfield for their encouraging advice and very helpful suggestions. In particular, we are deeply indebted to all the authors who compiled a truly excellent collection of important current facts connected to *Fluorine and Health*. We believe that the particular chapters constituting this book highlight the outstanding role of fluorine in different areas of medicinal monitoring and health care.

Alain Tressaud and Günter Haufe
Pessac and Münster, October 2007

SECTION 1

Molecular Imaging

This page intentionally left blank

CHAPTER 1

Fluorine-18 Chemistry for Molecular Imaging with Positron Emission Tomography

Frédéric Dollé,^{1,*} Dirk Roeda,¹ Bertrand Kuhnast,¹
and Marie-Claire Lasne²

¹*Institut d'Imagerie Biomédicale, CEA, Service Hospitalier Frédéric Joliot,
4 Place du Général Leclerc, F-91401 Orsay cedex, France*

²*CNRS, Département Chimie, 3 Rue Michel Ange, 75794 Paris cedex, France*

Contents

1. Introduction	4
2. The radionuclide fluorine-18 and some general considerations concerning short-lived positron emitters	5
2.1. The position of fluorine-18 among short-lived positron emitters for PET	5
2.2. Design of radiotracers and radiopharmaceuticals labelled with a short-lived positron emitter: The case of fluorine-18	7
2.3. Challenges in radiochemistry with short-lived positron emitters, including fluorine-18	8
2.4. Fluorine-18 production	10
2.5. Methods of radiofluorination	11
2.6. Early fluorine-18-labelled precursors	12
3. Electrophilic radiofluorination	14
3.1. Preparation of electrophilic fluorination reagents	15
3.1.1. Molecular [¹⁸ F]fluorine	15
3.1.2. Trifluoromethyl [¹⁸ F]hypofluorite	15
3.1.3. Acetyl [¹⁸ F]hypofluorite	15
3.1.4. Perchloryl [¹⁸ F]fluoride	16
3.1.5. Xenon d[¹⁸ F]fluoride	16
3.1.6. 1-[¹⁸ F]Fluoro-2-pyridone	17
3.1.7. N-[¹⁸ F]Fluoropyridinium triflate	17
3.1.8. N-[¹⁸ F]Fluoro-N-alkylsulphonamides	17
3.1.9. Bromo [¹⁸ F]fluoride	18
3.2. Fluorination of double-bond structures	18
3.2.1. Fluorination of alkenes	18
3.2.2. Fluorination of enol structures	21
3.3. Fluorination of carbanions	22
3.4. Fluorination of aromatic rings (other than via carbanions)	23
3.4.1. Fluorodehydrogenation	24
3.4.2. Fluorodemetalation	25

*Corresponding author. Tel.: +33-(0)1-69-86-77-04; Fax: +33-(0)1-69-86-77-49;
Email: frederic.dolle@cea.fr

4. Nucleophilic radiofluorination	28
4.1. Preparation of reactive [^{18}F]fluoride anion	28
4.2. Nucleophilic aliphatic substitution	29
4.2.1. Basic principles	29
4.2.2. Preparation of simple [^{18}F]fluoroalkyl-type molecular building blocks and some applications	30
4.2.3. One-step synthesis of a radiopharmaceutical involving an aliphatic nucleophilic fluorination	32
4.2.4. Multi-step synthesis of a radiopharmaceutical involving an aliphatic nucleophilic fluorination	32
4.3. Nucleophilic aromatic substitution	35
4.3.1. <i>Homoaromatic</i> series	35
4.3.2. <i>Heteroaromatic</i> series	41
5. Enzymatic carbon-[^{18}F]fluorine bond formation	43
6. The particular case of macromolecule labelling with fluorine-18	45
6.1. Reagents for the fluorine-18 labelling of peptides and proteins	45
6.2. Reagents for the fluorine-18 labelling of oligonucleotides	48
7. Conclusion and perspectives	49
References	50
Note from the Editors	65

Abstract

Molecular *in vivo* imaging with the high-resolution and sensitive positron emission tomography (PET) technique requires the preparation of positron-emitting radiolabelled probes or radiotracers. For this purpose, fluorine-18 is becoming increasingly the radionuclide of choice due to its adequate physical and nuclear characteristics. The successful use in clinical oncology of 2-[^{18}F]fluoro-2-deoxy-D-glucose ([^{18}F]FDG), currently the most widely used PET radiopharmaceutical, is manifestly also the motor behind the growing availability and interest for this positron emitter in radiopharmaceutical chemistry. The use of fluorine-18, however, presents some drawbacks, in particular the limited options in labelling strategies. Besides a few exceptions, radiofluorinations can be classified into two categories: nucleophilic and electrophilic reactions. The nucleophilic reactions usually involve no-carrier-added (high-specific-radioactivity) [^{18}F]fluoride as its $\text{K}[^{18}\text{F}]\text{F-K}_{222}$ complex and include $\text{S}_{\text{N}}2$ -type substitutions in the aliphatic series and $\text{S}_{\text{N}}\text{Ar}$ -type substitutions in the *homoaromatic* and *heteroaromatic* (particularly the pyridine family) series. The electrophilic reactions mainly use molecular [^{18}F]fluorine of moderately low specific radioactivity, or reagents prepared from it such as acetyl [^{18}F]hypofluorite, and include additions across double bonds, reactions with carbanions and especially fluorodehydrogenation and fluorodemetalation, where tin clearly appears to be the metal of choice. This chapter presents the bases and some recent advances in the field of fluorine-18 radiochemistry and highlights the potential of this radioisotope in the design and preparation of fluorine-18-labelled probes for PET imaging, often drug based but also macromolecules of biological interest such as peptides, proteins and oligonucleotides.

1. INTRODUCTION

Positron emission tomography (PET) is a high-resolution, sensitive, functional-imaging technique in nuclear medicine that permits repeated, non-invasive

assessment and quantification of specific biological and pharmacological processes at the molecular level in humans and animals. It is the most advanced technology currently available for studying *in vivo* molecular interactions in terms of distribution, pharmacokinetics and pharmacodynamics [1]. Molecular PET imaging requires the preparation of a positron-emitting radiolabelled probe or radiotracer [2,3]. For this purpose, fluorine-18 is becoming increasingly the radionuclide of choice not only due to its adequate physical and nuclear characteristics but also due to the successful use in clinical oncology of 2-[^{18}F]fluoro-2-deoxy-D-glucose ([^{18}F]FDG), currently the most widely used PET radiopharmaceutical and manifestly a motor behind the growing availability and interest for this positron emitter in radiopharmaceutical chemistry.

This chapter addresses this complex interdisciplinary and rapidly growing field from a radiochemist point of view, focusing on the synthesis of fluorine-18-labelled radiopharmaceuticals. We have tried to give the reader an extensive overview, without being exhaustive, covering the beginnings as well as the latest developments, from the production of the radioisotope and primary labelling precursors to sophisticated radiosynthetic procedures. Radiochemical yields appearing in this chapter are generally corrected for decay unless stated otherwise. Only a limited number of examples could be integrated in this text. For a more complete overview of fluorine-18-labelled structures we would like to draw the reader's attention to the regularly updated website of R. Iwata, at the Cyclotron and Radioisotope Center of Tohoku University: <http://kakuyaku.cyric.tohoku.ac.jp/indexe.html>.

2. THE RADIONUCLIDE FLUORINE-18 AND SOME GENERAL CONSIDERATIONS CONCERNING SHORT-LIVED POSITRON EMITTERS

2.1. The position of fluorine-18 among short-lived positron emitters for PET

Carbon-11, nitrogen-13, oxygen-15 and especially fluorine-18 are the short-lived positron-emitting radionuclides that have had the greatest impact on PET. This is understandable in view of the fact that the first three are isotopes of basic elements of life. They can substitute their stable counterparts without changing the properties of the target organic molecule. While fluorine is not a significant element in living systems, its longer half-life and its physico-chemical properties make it of considerable value. Table 1 lists some of the physical properties of these radionuclides, including two other radiohalogens, bromine-76 and iodine-124, for comparison.

Fluorine-18 is an artificial radionuclide, discovered in 1937. It decays with a half-life of 109.8 min for 97% by positron emission and for 3% by electron capture to the stable isotope oxygen-18. The maximum β^+ -particle energy is 0.635 MeV [4].

Table 1. Short-lived positron-emitting radionuclides for PET imaging

Radionuclide	Half-life	Decay (%)	Maximal particle energy (MeV)	Theoretical maximum specific activity (Ci/ μ mole)
^{11}C	20.4 min	β^+ (99)	0.960	9215
^{13}N	10.0 min	β^+ (100)	1.19	18,430
^{15}O	2.07 min	β^+ (100)	1.723	90,960
^{18}F	109.8 min	β^+ (97)	0.635	1712
^{76}Br	16.1 h	β^+ (57)	3.98	193
^{124}I	4.18 days	β^+ (24)	2.13	31

Specific activity (SA) defined as radioactivity per unit mass.

Compared with other positron-emitting radiohalogens used in PET such as bromine-76 (half-life: 16.1 h) or iodine-124 (half-life: 4.18 days), fluorine-18 displays simpler decay and emission properties with a high positron abundance [4]. As a result of its shorter half-life and its lower positron energy, fluorine-18-labelled radiopharmaceuticals give a lower radiation dose to patients. Compared with the other short-lived PET radionuclides carbon-11, nitrogen-13 and oxygen-15 with equally simple decay schemes, fluorine-18 has once more a relatively low positron energy and the shortest positron linear range in tissue (max 2.3 mm), resulting in the highest resolution in PET imaging. On the contrary, the radiation dose received by a patient exposed to the shorter-lived carbon-11, nitrogen-13 or oxygen-15 is considerably lower.

Its half-life is long enough to give access to relatively extended imaging protocols compared with what is possible with carbon-11. It facilitates kinetic studies and high-quality metabolite and plasma analysis because of higher count rates and better statistics over a longer time. On the contrary, the half-life is too long for repeated injection and imaging with the same or a different radiotracer, which is conceivable with carbon-11, nitrogen-13 and oxygen-15.

From a chemical point of view, the half-life of fluorine-18 allows multi-step synthetic approaches that can be extended over hours. Fluorine-18 has therefore, in spite of its somewhat limited chemical repertoire, been effectively used for the labelling of numerous both relatively simple and complex bioactive chemical structures [3,5–9], including high-molecular-weight macromolecules such as peptides, proteins [10–13] and oligonucleotides [14–18]. General considerations on radiochemistry involving short-lived positron emitters will be discussed in Section 2.3.

Finally, fluorine-18 can be reliably and routinely produced at the multi-Curie level [19] on widely implemented biomedical cyclotrons of relatively low-energy proton beam (e.g. 18 MeV). This fact, combined with its favourable half-life,

permits the transport and the use of fluorine-18-labelled radiopharmaceuticals (such as the archetype [^{18}F]FDG) at 'satellite' PET units that do not have the disposal of an on-site cyclotron facility [20,21]. Aspects on fluorine-18 production will be discussed in Section 2.4.

2.2. Design of radiotracers and radiopharmaceuticals labelled with a short-lived positron emitter: The case of fluorine-18

The design of radiotracers or radiopharmaceuticals labelled with short-lived positron emitters requires beside the inescapable selection of a chemical structure of interest to be labelled the choice of the radionuclide to be used.

The selection of a chemical structure is generally based on already existing and available information. Within the framework of receptor studies for example, the pharmacological characterisation of the target molecule is crucial. Qualitative data, such as selectivity, specificity, antagonist or agonist character, and quantitative data, such as affinity (K_D , K_i , IC_{50}) and localisation and number of binding sites (B_{max}), permit to classify potential candidates. Also other biological information, such as efficiency (ED_{50}), toxicology (LD_{50}) and pharmacokinetics as well as physico-chemical information, such as the partition coefficient, can influence the final selection. When known or foreseeable, the metabolic parameters of the target molecule can come into play. Other considerations, such as availability of the radionuclide, dosimetry of the radiotracer and its possible metabolites as well as radiotoxicity of the radioisotope, may have their say.

The choice of the radionuclide and the position of the labelling are generally determined by the chemical structure of the target molecule to label and the ease of introduction of the radionuclide from a chemical point of view. The physical half-life of the radionuclide should however match the timescale of the studied process. For example, in repeated blood flow measurements, oxygen-15 in the form of [^{15}O]water is ideal, while carbon-11 and especially fluorine-18 are preferable in the study of slower processes.

Native (or isotopic) labelling with fluorine-18 is limited to chemical structures already containing a fluorine atom. It implies the replacement of a native fluorine-19 atom with a fluorine-18 atom, which leaves the labelled compound with properties identical to the unlabelled one. The small isotope effect is negligible [22]. However, there are only a very limited number of molecules in living nature that contain fluorine. In fact, those fluorine-18-labelled radiotracers and radiopharmaceuticals that are based on natural molecules are always an analogue of the parent compound by hydroxy for fluorine or hydrogen for fluorine replacement, which is called foreign labelling [7,23]. Some controversy exists as to whether fluorine can be considered as isosteric to hydrogen. Fluorine has a small van der Waals radius of 1.33 Å, closer to that of oxygen (1.40 Å) than to that of hydrogen (1.20 Å) [24,25]. The C–F bond length, 1.38 Å, is comparable with that

of C–O, 1.43 Å (C–H, 1.10 Å) [24,26,27]. Finally, fluorine is also the most electronegative atom according to Pauling's scale, with the electronegativity of fluorine (4.0) close to that of oxygen (3.5) (only 2.2 for hydrogen). The carbon–fluorine bond is therefore highly polarised, generating a strong dipole moment in the molecule, favouring hydrogen-bond formation [28]. In any case, foreign labelling with a fluorine-18 atom changes the molecule's physical properties and consequently its biological and pharmacological properties [26]. The labelling strategy should be directed towards those positions that will cause as little effect as possible on the characteristics of the parent molecule. An ever expanding field in fluorine-18 chemistry concerns drug and drug-like compounds generated by the pharmaceutical industry [3,7,29]. These can be subject to native labelling if they contain a fluorine at a suitable position or to foreign labelling if they do not.

2.3. Challenges in radiochemistry with short-lived positron emitters, including fluorine-18

Most of the challenges associated with the handling of short-lived positron emitters are direct consequences of their physical properties, half-life and decay mode, from which also ensues very high maximum specific radioactivity and the associated practical minute amounts of material engaged in the radiosyntheses.

As an evident consequence of their short half-lives, these radioisotopes have to be produced immediately before use, normally on site by a dedicated biomedical cyclotron. Only fluorine-18 with its 110-min half-life permits off-site use.

The development of methods and techniques for the synthesis of short-lived positron-emitting compounds is of primordial importance, with time as the most critical parameter [30]. As a rule of thumb the preparation of a radiopharmaceutical, including radiosynthesis, purification and formulation for intravenous injection, should be achieved within three half-lives of the radioisotope. Minimising the radiosynthesis time will increase both the overall radiochemical yield and the final specific radioactivity, which is the radioactivity per unit of mass of product. The latter is of great importance in pharmacological studies of high-affinity receptors present in very low concentrations in tissues. Therefore, the radionuclide should be introduced as late as possible in the synthetic pathway and the number of radiochemical steps involved in the preparation, even if known as rapid reactions, must be kept to a minimum. As an additional limitation, the yield must be maximised with the shortest possible synthesis time for each radiochemical step. Since the radiochemical yield is a function of the chemical yield and the radioactive decay, the maximum radiochemical yield can be attained before the reaction has proceeded to completion. This effect is particularly important for carbon-11 and plays a less-significant role in the chemistry of the longer-lived fluorine-18. Synthetic methods are often modified relative to those applied in conventional organic synthesis. For example, drastic reaction conditions

may be used in labelling procedures, despite the fact that the chemical yield is lower, if the increase in reaction rate is large enough. Time optimisation also determines the type of procedures used for the synthesis, workup and final purification. Examples are the use of one-pot procedures in order to reduce preparation time by simplifying the technical handling, microwave technology in order to accelerate reaction rates and reduce heating times and Sep-Pak® cartridges in order to shorten the purification and formulation steps. The choice of reaction solvent is also important with respect to both the kinetic parameters of the reaction and the purification process.

In order to meet the rapid radioactive decay of a radiopharmaceutical labelled with carbon-11 or fluorine-18, the quantity of starting radioactivity engaged in their preparation should be very high, typically, at the Curie level or more (>37 GBq). As positron emission gives rise to secondary, highly penetrating 511-keV gamma radiation, the radiosyntheses are performed in closed and ventilated lead-shielded hot cells with a typical wall thickness of 50–75 mm in order to minimise the radiation dose to the chemist. Consequently, a radiopharmaceutical preparation imposes an exhaustive and advanced automation. The gamma rays facilitate hereby the process monitoring by easy and sensitive radioactivity detection. The susceptibility of the chemical reaction to automation should be taken into account at the early design stage of the radiochemical pathway. Certain manipulations of classical chemistry, such as liquid–liquid extraction or precipitation, are undesirable.

The specific radioactivity of a radiopharmaceutical labelled with a short-lived positron emitter like carbon-11 or fluorine-18 produced in a no-carrier-added way is in practice much lower than the theoretical one (Table 1). Values from 1 to 10 Ci/ μ mol are now often reached. These levels, taken together with the Curie amount of radioactivity currently used in a radiosynthesis, make that the quantity of starting radionuclide in terms of mass will be extremely low (less than 1 μ mol). This offers an opportunity to reduce the time of reactions, transfers and purifications. In view of the low mass of radioactive agent, the stoichiometrical ratio between the non-radioactive starting material (often called precursor for labelling) and the radioactive one is usually chosen in the range between 10,000 and 10. As a consequence, the starting radiolabelled reagent is consumed fast because of pseudo first-order reaction kinetics, independent of its concentration. Typically, concentrations in the sub-millimolar or even down to the low micromolar range are involved, implying that these radiosyntheses are compatible with high dilution. This radiochemistry also demands high-purity reagents in order to minimise the competitive reaction of impurities that can compromise this trace chemistry. The amount of non-radioactive reagent, although in large excess, remains relatively small in absolute terms, which is beneficial for the technical handling and offers possibilities of miniaturisation, facilitating automation and speeding up handling. This is exemplified by the convenient application of high performance liquid chromatography (HPLC) at the semi-preparative scale as

the purification process, often with direct injection of the crude reaction mixture. Beside its intrinsic efficiency, this separation method is perfectly well adapted to the low quantities in mass and is fast, thus compatible with short half-lives. The choice of the HPLC solvents in the purification is important with respect to the final formulation step.

Finally, radiopharmaceuticals are often prepared on a daily basis within the framework of clinical studies which often last several months or years. They demand a viable and reproducible production chain, leading to a sterile- and pyrogen-free radiopharmaceutical of high radiochemical purity. Therefore, microprocessor-controlled automated synthesis devices [31] are developed in order to ensure routine pharmaceutical production. They are becoming mandatory in order to meet the demands related to Good Laboratory Practice (GLP) and Good Manufacturing Practice (GMP).

2.4. Fluorine-18 production

Fluorine-18 can be produced with relative ease in both nuclear reactors and accelerators [32–34]. Nuclear reactor production involves fast neutron bombardment of a solid lithium carbonate target, preferably enriched in lithium-6, to generate the requisite energetic tritons to drive the $^{16}\text{O}(\text{t},\text{n})^{18}\text{F}$ nuclear reaction. The drawbacks of this method, compared with accelerator production, are the inherent contamination with radioactive tritium, the lower yield and the geographical distance between the sites of production and the sites of use. As accelerators became more and more available, the method fell into disuse. Today, the method of choice involves cyclotron acceleration of charged particles that induce a nuclear reaction in a suitable target. While a variety of cyclotrons of different size and energy have been employed for the production of medical radioisotopes since the 1930s, most fluorine-18 production sites have installed commercially available, compact cyclotrons over the last 20 years. These are either machines that exclusively produce a proton beam, for example with a kinetic energy of about 11 MeV, or dual-particle cyclotrons (protons and deuterons, e.g. at 18 and 9 MeV, respectively). The most commonly used nuclear transformations to produce fluorine-18 are the $^{18}\text{O}(\text{p},\text{n})^{18}\text{F}$ and $^{20}\text{Ne}(\text{d},\alpha)^{18}\text{F}$ reactions, with the first one providing significantly higher yields and specific radioactivities than the second one [35,36]. Other nuclear reaction pathways, such as $^{16}\text{O}(^3\text{He},\text{p})^{18}\text{F}$, $^{16}\text{O}(^4\text{He},\text{pn})^{18}\text{F}$ and $^{20}\text{Ne}(^3\text{He},\text{n})^{18}\text{Ne} \rightarrow ^{18}\text{F}$ [7], were also used in the past but are not of current interest anymore.

For the $^{18}\text{O}(\text{p},\text{n})^{18}\text{F}$ nuclear reaction, the oxygen-18 target material normally consists of highly enriched (>95%) liquid $[^{18}\text{O}]\text{water}$, but $[^{18}\text{O}]\text{dioxygen gas}$ has been used as well [19,37]. Appropriate cyclotron targetry allows a batch production of several Curies of $[^{18}\text{F}]\text{fluorine}$ in a single irradiation of a few hours. While the theoretical specific radioactivity of carrier-free fluorine-18 is 1.7×10^6

Ci/mmol (6.3×10^4 TBq/mmol), the practically achieved no-carrier-added specific radioactivity is in the region of 10^5 Ci/mmol (3.7×10^3 TBq/mmol). Fluorine-18 is generally recovered from the target as [^{18}F]fluoride anion in an aqueous solution and is then engaged in nucleophilic radiofluorinations (see Section 4.1).

The $^{20}\text{Ne}(\text{d},\alpha)^{18}\text{F}$ nuclear reaction is normally employed to generate fluorine-18 as molecular [^{18}F]fluorine gas ([^{18}F]F₂). It is a carrier-added method, since a small amount of 'cold' fluorine-19 gas (0.1%, 30–100 μmol) must be present in the target to allow recovery of the radioisotope. However, the $^{18}\text{O}(\text{p},\text{n})^{18}\text{F}$ nuclear reaction is recently gaining popularity in the production of molecular [^{18}F]F₂ gas by a procedure called the 'double-shoot' method [37]. An initial irradiation of enriched molecular [^{18}O]oxygen gas forms the radioisotope which sticks to the inside target chamber surface. This is followed by a second irradiation in the presence of a small amount of carrier fluorine in an inert gas (usually neon or argon) inducing a fluorine-18 for fluorine-19 exchange. Both processes produce fluorine-18 at a relatively low specific radioactivity (1–10 Ci/mmol or 37–370 GBq/mmol, depending on the total mass of added non-radioactive fluorine) and in much lower yields when compared to the [^{18}O]water/[^{18}F]fluoride target technology. Diluted gaseous [^{18}F]F₂ produced in either way is then engaged in electrophilic [^{18}F]radiofluorinations.

Noteworthy is a recent multi-step method for the production of molecular [^{18}F]F₂ of considerable higher specific radioactivity (100–925 Ci/mmol or 3.7–34 TBq/mmol) starting from aqueous [^{18}F]fluoride produced with the $^{18}\text{O}(\text{p},\text{n})^{18}\text{F}$ reaction [38]. The dried and activated [^{18}F]fluoride is reacted with methyl iodide to yield methyl [^{18}F]fluoride (CH₃[^{18}F]F) which is isolated by gas chromatography. The latter is then subjected to an electrical discharge (20–30 kV, 280 μA , 10 s) in the presence of small amounts of carrier fluorine (150 nmol) resulting in about 30% conversion of the original [^{18}F]fluoride into molecular [^{18}F]F₂.

2.5. Methods of radiofluorination

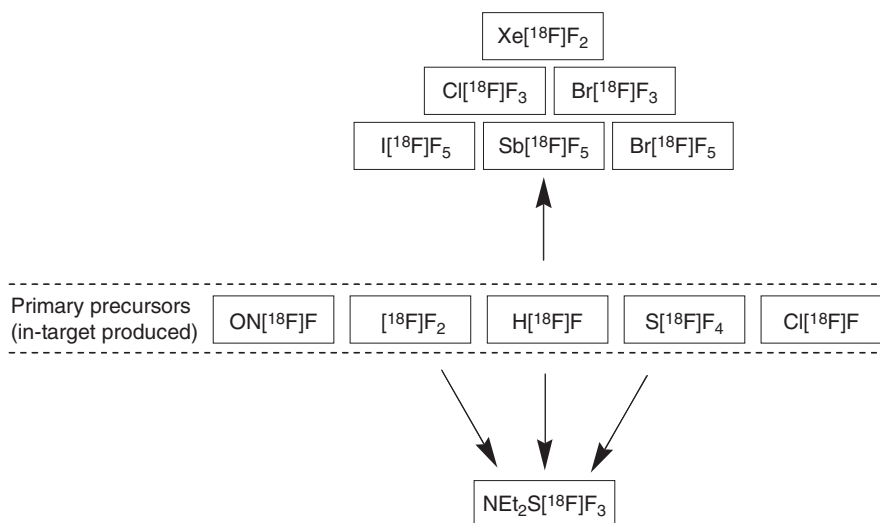
The chemical reactions used for the labelling of organic molecules with fluorine-18 fall broadly into two categories: nucleophilic and electrophilic reactions. This division is based on the availability of fluorine-18 in a nucleophilic form, the [^{18}F]fluoride anion, and an electrophilic form, molecular [^{18}F]fluorine, although there are some reactions which do not fit these simple categories [7,8,39–42]. Historically, a number of important fluorine-18-labelled radiopharmaceuticals were initially prepared using electrophilic fluorination, for example [^{18}F]FDG, and subsequently higher yielding nucleophilic routes were developed giving higher specific radioactivity.

2.6. Early fluorine-18-labelled precursors

In the early days of fluorine-18-chemistry the low reactivity of [^{18}F]fluoride ion in aqueous solution constituted a major obstacle to the advance of nucleophilic radiofluorination with high specific radioactivity, a problem that would later be solved with the introduction of the cryptand Kryptofix-222[®], giving the highly reactive $\text{K}[^{18}\text{F}]\text{F-K}_{222}$ complex (see Section 4.1) [3]. For this reason active research for anhydrous reactive fluorine-18 labelling species continued. Scheme 1 reviews a number of these early reagents.

From the beginning, molecular [^{18}F]fluorine ($[\text{F}_2]^{18}\text{F}$) has been the major source of anhydrous electrophilic fluorine produced in a neon target (see Section 2.4). It has the disadvantage of a low specific radioactivity because of mandatory addition of carrier fluorine gas, usually before the irradiation, in order to be able to extract the radioactivity from the cyclotron target. The replacement of this carrier fluorine in the neon target by other gases can lead to other, sometimes no-carrier-added, anhydrous fluorinating agents.

Hydrogen [^{18}F]fluoride ($\text{H}[^{18}\text{F}]\text{F}$) can be made in this way by irradiation of a neon–hydrogen mixture or by irradiation of a pure neon or a pure oxygen target followed by dislodging the activity from the target walls with hydrogen at elevated temperature. Much work was put into $\text{H}[^{18}\text{F}]\text{F}$ production [43–52] but surprisingly little was seen in terms of applications, perhaps because its preparation remains a tedious task. Anhydrous $\text{H}[^{18}\text{F}]\text{F}$ as such has weak nucleophilic properties. It has nevertheless been used in aromatic labelling in the triazene decomposition reaction (Wallach reaction, see Section 4.3.1.4) with relatively low yield. In aromatic [^{18}F]fluorine-for-iodine substitution, addition of potassium- or cesium



Scheme 1. Early fluorine-18-labelled anhydrous reagents.

carbonate to provide a cation proved mandatory [53,54]. This resembles much the modern nucleophilic [^{18}F]fluoride agents prepared from an aqueous [^{18}F]fluoride source by drying with Kryptofix-222[®] or *n*-tetrabutylammonium hydroxide (see Section 4.1), but with anhydrous $\text{H}[^{18}\text{F}]\text{F}$ there is in principle no residual hydration of the fluoride ‘anion’, which can be an advantage or a disadvantage [55,56]. However, its use in this way has not been explored further. Also hydrogen [^{18}F]fluoride was reported in the preparation by isotopic exchange of low-specific-activity bromine *tri*[^{18}F]fluoride ($\text{Br}[^{18}\text{F}]\text{F}_3$), bromine *penta*[^{18}F]fluoride ($\text{Br}[^{18}\text{F}]\text{F}_5$), iodine *penta*[^{18}F]fluoride ($\text{I}[^{18}\text{F}]\text{F}_5$), antimony *penta*[^{18}F]fluoride ($\text{Sb}[^{18}\text{F}]\text{F}_5$) and chlorine *tri*[^{18}F]fluoride ($\text{Cl}[^{18}\text{F}]\text{F}_3$) [45], now all sunk into oblivion. A more useful offspring of $\text{H}[^{18}\text{F}]\text{F}$ has been diethylaminosulphur *tri*[^{18}F]fluoride ($[\text{C}_2\text{H}_5]_2\text{N}[\text{S}[^{18}\text{F}]\text{F}_3]$), again by fluorine-18 for fluorine exchange [57]. This F-for-OH fluorinating agent was used in model preparations of methyl [^{18}F]fluoride, ethyl [^{18}F]fluoride and 2-[^{18}F]fluoroethanol from the corresponding alcohols and in the preparation of 3-[^{18}F]fluoro-3-deoxy-D-glucose from the appropriately protected precursor [58]. Another application of anhydrous $\text{H}[^{18}\text{F}]\text{F}$, this time generated by an exchange reaction between [^{18}F]fluoride ion, dried from an aqueous solution, and carrier hydrogen fluoride (HF), was the production of xenon *di*[^{18}F]fluoride ($\text{Xe}[^{18}\text{F}]\text{F}_2$), again by an exchange reaction. Alternatively, $\text{H}[^{18}\text{F}]\text{F}$ could be replaced by silicon *tetra*[^{18}F]fluoride ($\text{Si}[^{18}\text{F}]\text{F}_4$) or arsenic *penta*[^{18}F]fluoride ($\text{As}[^{18}\text{F}]\text{F}_5$) in this procedure. The latter two reagents were equally produced by exchange with [^{18}F]fluoride [59]. $\text{Xe}[^{18}\text{F}]\text{F}_2$ has been used in the synthesis of 6-[^{18}F]fluoro-L-DOPA [60] and 2-[^{18}F]fluoro-2-deoxy-D-glucose [61,62] but never got into routine use, probably because it is not easy to make. Most recently no-carrier-added $\text{H}[^{18}\text{F}]\text{F}$ was revived in the synthesis of perchloryl [^{18}F]fluoride ($\text{Cl}_3\text{O}[^{18}\text{F}]\text{F}$, see Section 3.1.4), providing an interesting electrophilic fluorinating agent of high specific radioactivity [63].

Sulphur *tetra*[^{18}F]fluoride ($\text{S}[^{18}\text{F}]\text{F}_4$) was obtained by irradiation of a neon– SF_4 mixture, giving rise to a low-specific-activity product by fluorine-18 for fluorine exchange. It was used as an alternative to $\text{H}[^{18}\text{F}]\text{F}$ in the preparation of [^{18}F]DAST [57]. $\text{S}[^{18}\text{F}]\text{F}_4$ has not found other applications so far.

When irradiating a neon–chlorine mixture chlorine, *mono*[^{18}F]fluoride ($\text{Cl}[^{18}\text{F}]\text{F}$) of high specific activity can be obtained [45]. In electrophilic reactions this reagent would rather introduce the less-electronegative non-radioactive chlorine atom. However, addition to a double bond should be feasible as has been shown for bromine [^{18}F]fluoride ($\text{Br}[^{18}\text{F}]\text{F}$) prepared more recently from activated [^{18}F]fluoride [64–66].

Irradiation of a mixture of neon and nitric oxide gives no-carrier-added nitrosyl [^{18}F]fluoride ($\text{ON}[^{18}\text{F}]\text{F}$) [45,67]. Hydrolysis yields [^{18}F]fluoride that was proposed for bone scanning. $\text{ON}[^{18}\text{F}]\text{F}$ was designed with steroid labelling in mind in which addition to a double bond should lead to an α -[^{18}F]fluoroketone entity, but this idea was not further pursued.

One may conclude that the above-mentioned anhydrous [^{18}F]fluorine compounds, except perhaps $\text{H}[^{18}\text{F}]\text{F}$, have been abandoned, partly because of their limited potential and difficulty of preparation and also because of the success of the main three agents of today, [^{18}F]fluoride (see Section 4), [^{18}F]fluorine gas (see Section 3.1.1) and acetyl [^{18}F]hypofluorite (see Section 3.1.3). The advent of the first one, ([^{18}F]fluoride), made less urgent the need for high-specific-activity electrophilic fluorine and the latter two, ([^{18}F]fluorine gas and acetyl [^{18}F]hypofluorite), are able to perform practically all low-specific-activity electrophilic syntheses (see Section 3), putting a brake on the development of alternatives.

3. ELECTROPHILIC RADIOFLUORINATION

Electrophilic fluorination is the process by which fluorine is delivered to an electron-donating reactant, such as an alkene, aromatic ring or carbanion, by a formal 'positive-fluorine' reagent to form a carbon–fluorine covalent bond. These reactions are fast and have proven extremely valuable for some important fluorine-18-labelled radiopharmaceuticals. Over the years several reviews on electrophilic fluorination were written. The reader is encouraged to seek out these works for greater detail on the subject [7,68–70].

The simplest reagent is molecular [^{18}F]fluorine ($[^{18}\text{F}]\text{F}_2$). It provides a facile means of introducing fluorine-18 into electron-donating compounds. The procedures are simple and basically involve bubbling the gas into the substrate solution. However, F_2 has a severe reputation as a poor reagent giving rise to low yields and low regioselectivity because of the destructive nature of this highly reactive molecule. The oxidising strength of fluorine often leads to exothermic radical chain reactions with the formation of side products and tars. It was found that its reactivity could be moderated and controlled by dilution with an inert gas (0.1–0.5% in neon or nitrogen) [71,72] and by performing the reaction in a strong acid medium [73,74]. The production of [^{18}F]F₂ (see Section 2.4) in fact involves fluorine–neon gas mixtures (0.1–2% F₂ in neon) that are well suited for subsequent fluorination reactions.

Other electrophilic reagents, less reactive and therefore less destructive, have been reported, such as trifluoromethyl [^{18}F]hypofluorite ($\text{CF}_3\text{O}[^{18}\text{F}]\text{F}$), acetyl [^{18}F]hypofluorite ($\text{CH}_3\text{CO}_2[^{18}\text{F}]\text{F}$), perchloryl [^{18}F]fluoride ($[^{18}\text{F}]\text{FCIO}_3$), xenon *d*[^{18}F]fluoride ($\text{Xe}[^{18}\text{F}]\text{F}_2$), 1-[^{18}F]fluoro-2-pyridone, *N*-[^{18}F]fluoropyridinium triflate and *N*-[^{18}F]fluoro-*N*-alkylsulphonamides [3,8]. Being practically always prepared from [^{18}F]F₂, which is produced in a carrier-added way, electrophilic radiofluorinations are necessarily carrier added and result in final products with low to at best moderate specific radioactivities (usually $\ll 10$ Ci/mmol or $\ll 370$ GBq/mmol). This has limited the utility of electrophilic radiofluorinations to the synthesis of tracers that do not need high specific radioactivity and that are not too toxic. Another drawback of these fluorination reactions is that the maximum achievable

radiochemical yield is often limited to 50%, for [^{18}F] F_2 usually passes only one of the two fluorine atoms on to the product.

3.1. Preparation of electrophilic fluorination reagents

In this section the production of a number of radioactive electrophilic fluorination agents that have not already been dealt with in Section 2.6 will be discussed.

3.1.1. Molecular [^{18}F]fluorine

Molecular [^{18}F]fluorine ([^{18}F] F_2) is produced in the cyclotron target usually during the irradiation for radioisotope production (see Section 2.4).

3.1.2. Trifluoromethyl [^{18}F]hypofluorite

Historically, trifluoromethyl [^{18}F]hypofluorite ($\text{CF}_3\text{O}[^{18}\text{F}]\text{F}$) was the first in a line of 'milder' gaseous electrophilic fluorinating reagents [75]. The synthesis starts with the production of fluorine-18 in an F_2 -passivated nickel target chamber containing neon gas and solid cesium fluoride. The gaseous target contents are then replaced by a mixture of neon, fluorine and carbonyl fluoride and the whole is heated in the target chamber at 100 °C for 35 min (Scheme 2). Exchange of the fluorine-18 activity, initially stuck to the CsF and the target chamber walls, with the gas phase gives predominantly [^{18}F] F_2 which reacts with COF_2 and CsF to give $\text{CF}_3\text{O}[^{18}\text{F}]\text{F}$ in 30% radiochemical yield but also some $\text{C}[^{18}\text{F}]\text{F}_3\text{OF}$.

3.1.3. Acetyl [^{18}F]hypofluorite

The original methodology to produce acetyl [^{18}F]hypofluorite ($\text{CH}_3\text{CO}_2[^{18}\text{F}]\text{F}$) involves the passage of [^{18}F] F_2 into glacial acetic acid to which a small amount of aqueous ammonium hydroxide [76] or ammonium acetate [77] has been added. Acetyl [^{18}F]hypofluorite can also be obtained in vapour form, circumventing the restriction to acetic acid as a reaction solvent in the above procedure [78]. This method involves passing [^{18}F] F_2 through a column containing a complex of potassium acetate with acetic acid at room temperature (Scheme 3). Although the reaction in both methods is complete, $\text{CH}_3\text{CO}_2[^{18}\text{F}]\text{F}$ is obtained in only about 50% radiochemical yield for half of the radioactivity ends up as [^{18}F]fluoride.



Scheme 2. (i) CsF, COF_2 , 100 °C, 35 min.

3.1.4. Perchloryl [^{18}F]fluoride

The standard method for the production of gaseous perchloryl [^{18}F]fluoride ([^{18}F] FCIO_3) involves passage of [^{18}F] F_2 through a column containing KClO_3 at 90°C (Scheme 4). The reaction gives [^{18}F] FCIO_3 in about 23% radiochemical yield [79].

Electrophilic fluorinating agents of high specific radioactivity are not routinely available. An attempt in this direction was recently made by producing perchloryl [^{18}F]fluoride from no-carrier-added $\text{H}[^{18}\text{F}]\text{F}$ and HClO_4 in about 6% radiochemical yield (Scheme 5). Its potential was demonstrated by the preparation of [^{18}F] fluorobenzene and diethyl 2-[^{18}F]fluoromalonate [63]. In this case the usual 50% radioactivity loss does not occur.

3.1.5. Xenon di[^{18}F]fluoride

Xenon di[^{18}F]fluoride ($\text{Xe}[^{18}\text{F}]\text{F}_2$) can be prepared through several approaches. The most common involves the thermal reaction between [^{18}F] F_2 and xenon gas in a sealed nickel vessel maintained at 390°C (Scheme 6, 70% radiochemical yield) [80].

Isotopic exchange between $\text{H}[^{18}\text{F}]\text{F}$ (or $\text{Si}[^{18}\text{F}]\text{F}_4$ or $\text{As}[^{18}\text{F}]\text{F}_5$, see Section 2.6) and XeF_2 was also reported (30% radiochemical yield) [59]. A more recent and simpler approach involves [^{18}F]fluoride anion exchange with XeF_2 that is catalysed by the Cs^+ -Kryptofix-222[®] complex (Scheme 7) [81]. The complex acts by ionising the XeF_2 when the reaction is performed in methylene chloride or chloroform. This efficient reaction produces nearly 60% of $\text{Xe}[^{18}\text{F}]\text{F}_2$ in 50 min at room temperature. Although the method potentially allows for higher specific radioactivities, the authors



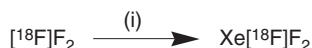
Scheme 3. (i) AcOH/AcOK , RT.



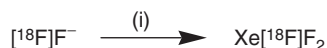
Scheme 4. (i) KClO_3 , 90°C , 10 min.



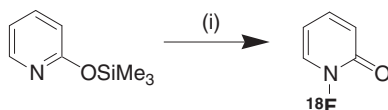
Scheme 5. (i) HClO_4 , RT, 30 min.



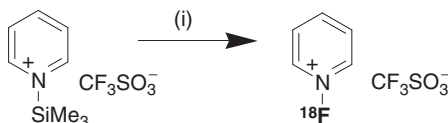
Scheme 6. (i) Xe gas, 390°C , 40 min.



Scheme 7. (i) Cs_2CO_3 -Kryptofix-222[®], CH_2Cl_2 , 20 °C, 50 min.



Scheme 8. (i) $[^{18}\text{F}]\text{F}_2$, CFCl_3 , -78 °C, 10 min.



Scheme 9. (i) $[^{18}\text{F}]\text{F}_2$, MeCN, -40 °C, 3 min.

did not optimise for this and reported a relatively low specific radioactivity using 50 mg (300 μmol) of XeF_2 in the exchange reaction.

3.1.6. 1-[¹⁸F]Fluoro-2-pyridone

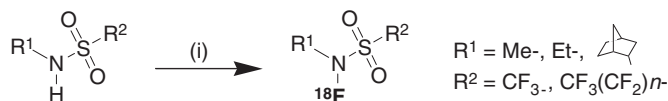
1-[¹⁸F]Fluoro-2-pyridone was prepared in about 20% radiochemical yield (50% being the maximum feasible yield) by bubbling $[^{18}\text{F}]\text{F}_2$ through a solution of 2-trimethylsilyloxypyridine in CFCl_3 (freon-11) at low temperature (Scheme 8) [82].

3.1.7. N-[¹⁸F]Fluoropyridinium triflate

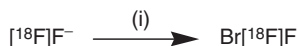
N-[¹⁸F]Fluoropyridinium triflate was readily prepared in about 45% radiochemical yield by direct reaction between $[^{18}\text{F}]\text{F}_2$ and N-trimethylsilylpyridinium triflate in acetonitrile at -40 °C (Scheme 9) [83].

3.1.8. N-[¹⁸F]Fluoro-N-alkylsulphonamides

N-[¹⁸F]Fluoro-N-alkylsulphonamides are readily prepared in nearly quantitative yield (50% maximum) by bubbling $[^{18}\text{F}]\text{F}_2$ through a solution of the appropriate sulphonamide in CFCl_3 (freon-11) at -78 °C (Scheme 10). The reaction is almost immediate and the solvent is easily removed through evaporation at room temperature. Examples include N-[¹⁸F]fluoro-N-methyltrifluoromethanesulphonamide, N-[¹⁸F]fluoro-N-methylperfluorobutanesulphonamide, N-[¹⁸F]fluoro-N-ethylperfluorooctanesulphonamide and N-[¹⁸F]fluoro-N-endo-norbornyl-*para*toluenesulphonamide [84].



Scheme 10. (i) $[^{18}\text{F}]\text{F}_2$, CFCl_3 , -78°C , 1 min.



Scheme 11. (i) 1,3-dibromo-5,5-dimethylhydantoin, H_2SO_4 , CH_2Cl_2 , $10\text{--}40^\circ\text{C}$, 15 min.

3.1.9. Bromo $[^{18}\text{F}]\text{fluoride}$

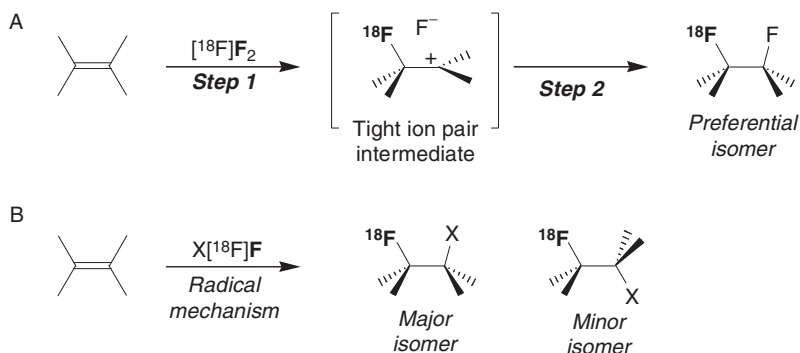
Bromo $[^{18}\text{F}]\text{fluoride}$ is different from the other electrophilic radiolabelling agents discussed so far in the sense that the electrophilic part of the molecule is not fluorine but bromine. This is reflected by its synthesis from nucleophilic $[^{18}\text{F}]\text{fluoride}$ and it can be obtained in high specific radioactivity. Bromo $[^{18}\text{F}]\text{fluoride}$ was developed for fluorine-18 labelling of steroids (see Section 3.2) [64–66]. It was prepared (Scheme 11) *in situ* by reaction of dried $[^{18}\text{F}]\text{fluoride}$ with 1,3-dibromo-5,5-dimethylhydantoin and sulphuric acid in dichloromethane containing also the substrate.

3.2. Fluorination of double-bond structures

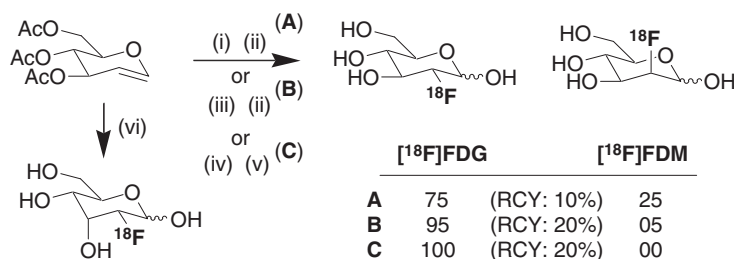
3.2.1. Fluorination of alkenes

The fluorination of a carbon–carbon double bond was widely utilised in the early times of fluorine-18 chemistry in the synthesis of $[^{18}\text{F}]\text{FDG}$ and was therefore an important type of reaction for over 10 years in the 1980s. The reaction of molecular $[^{18}\text{F}]\text{fluorine}$ with alkenes does probably not share the same two-step mechanism as accepted for chlorine, bromine and iodine (bimolecular electrophilic addition AdE2 [85]). It may involve an initial nucleophilic attack of the double bond on the fluorine molecule, resulting in the formation of a highly unstable tightly ion-paired α -fluorocation (Scheme 12A), which then collapses before any rotation around the carbon–carbon bond can take place [25]. As a consequence, an exclusive *syn*-addition is often observed, in contrast to the reaction with chlorine, bromine or iodine, involving a bridged halonium ion and leading to *anti*-addition. Reagents containing an $\text{O}-[^{18}\text{F}]\text{F}$ bond, such as acetyl $[^{18}\text{F}]\text{hypofluorite}$ ($\text{CH}_3\text{CO}_2[^{18}\text{F}]\text{F}$), also lead predominantly to a *syn*-addition (Scheme 12B), but are thought to proceed through a radical mechanism [25].

The early method for the preparation of 2- $[^{18}\text{F}]\text{fluoro-2-deoxy-D-glucose}$ ($[^{18}\text{F}]\text{FDG}$) was based on the reaction of molecular $[^{18}\text{F}]\text{fluorine}$ with 3,4,6-*tri-O*-acetyl



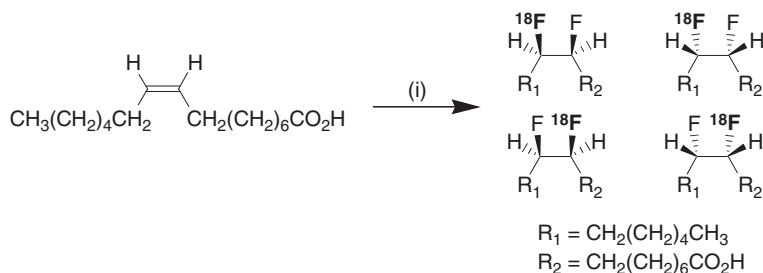
Scheme 12. Mechanisms of electrophilic fluorination of a carbon–carbon double bond.



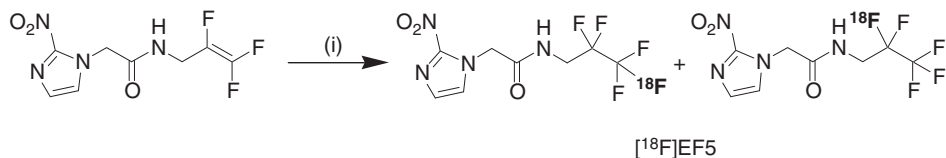
Scheme 13. (i) $[^{18}\text{F}]\text{F}_2$, 0.1–2% in neon, CFCl_3 , 0 °C, 3–5 min; (ii) aq. HCl, 100 °C, 15 min; (iii) $\text{CH}_3\text{CO}_2[^{18}\text{F}]\text{F}$, CFCl_3 , 0 °C, 3–5 min; (iv) $\text{Xe}[^{18}\text{F}]\text{F}_2$, BF_3 , Et_2O , RT, 15 min; (v) aq. HCl, 130 °C, 30 min; (vi) $[^{18}\text{F}]\text{F}_2$, HF, –60 °C, few min.

glucal in CFCl_3 (freon-11) (Scheme 13). The disadvantage of this method, due to the highly reactive nature of $[^{18}\text{F}]\text{F}_2$, was the concomitant production of the protected fluoromannose leading to the undesired 2- $[^{18}\text{F}]\text{fluoro-2-deoxy-D-mannose}$ ($[^{18}\text{F}]\text{FDM}$, $[^{18}\text{F}]\text{FDG}/[^{18}\text{F}]\text{FDM}$ ratio: 75/25), although FDM acts *in vivo* very similar to FDG [86]. The use of acetyl $[^{18}\text{F}]\text{hypofluorite}$ ($\text{CH}_3\text{CO}_2[^{18}\text{F}]\text{F}$) resulted in a more regioselective synthesis (95/5) of the desired glucosyl configuration [87] while xenon $d[^{18}\text{F}]\text{fluoride}$ was reported to give exclusively $[^{18}\text{F}]\text{FDG}$ [61]. These reactions can be seen as a 1,2-addition of two fluorine atoms (or a fluorine atom and an acetoxy group) across the double bond, followed by the subsequent loss of the fluorine or acetoxy group at the 1-position upon hydrolysis. Addition of $[^{18}\text{F}]\text{F}_2$ to 3,4,6-*tri-O*-acetyl glucal in liquid HF was recently shown to lead to 2-deoxy-2- $[^{18}\text{F}]\text{fluoro-D-allose}$ in 33% radiochemical yield, hydrolysis of the intermediate dioxolenium ion resulting in epimerisation at the 3-position [88].

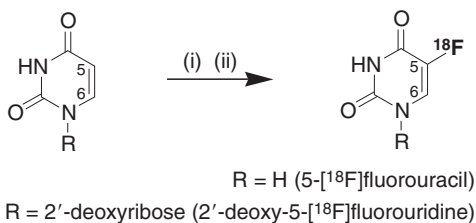
$[^{18}\text{F}]\text{F}_2$ adds across the double bond of *cis*-9,10-palmitoleic acid in a *syn* fashion (Scheme 14) to yield a mixture of racemic *erythro*-9,10- $d[^{18}\text{F}]\text{fluoropalmitic acid}$ in 12–16% radiochemical yield. It was designed for the study of fatty-acid metabolism [89].



Scheme 14. (i) $[\text{}^{18}\text{F}]\text{F}_2$, CFCl_3 , -70°C , 15–20 min.



Scheme 15. (i) $[\text{}^{18}\text{F}]\text{F}_2$, TFA, RT, 3–5 min.



Scheme 16. (i) $[\text{}^{18}\text{F}]\text{F}_2$, TFA, AcOH or AcOH/Ac₂O, -10°C to RT, 3–5 min; (ii) Δ with or without a base (TEA or NaOEt).

An example of fluorination of a *polyfluoroalkene* with $[\text{}^{18}\text{F}]\text{F}_2$ is the synthesis of [^{18}F]EF5 (Scheme 15), a radiotracer used to assess tissue hypoxia. The radiochemical yield was over 10% [90].

Addition of $[\text{}^{18}\text{F}]\text{F}_2$ (or $\text{CH}_3\text{CO}_2[\text{}^{18}\text{F}]\text{F}$) at the double bond of substituted 2,4-dioxypyrimidines (Scheme 16) allows the preparation of the fluorine-18-labelled nucleic acid base 5- $[\text{}^{18}\text{F}]$ fluorouracil [91–94] and the nucleoside 2'-deoxy-5- $[\text{}^{18}\text{F}]$ fluorouridine [95–97]. The reaction, usually carried out in acetic acid, demonstrates an excellent regioselectivity, with only the 5- $[\text{}^{18}\text{F}]$ fluoro derivatives obtained because the C-5 position is the unique activated position for reaction with an electrophile in these systems. The mechanism of this reaction has been studied and the intermediate 5,6-fluoro-acetoxy adduct (or the 5,6-fluoro-hydroxy adduct if the solvent is water) has been isolated and characterised [92].

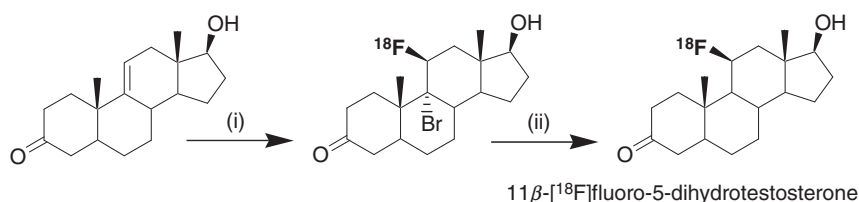
Consistent radiochemical yields of 20–30% were obtained for the preparation of 5- ^{18}F fluorouracil with either reagent and in a variety of solvents (trifluoroacetic acid, acetic acid, water). Similar fluorine-18-labelled products like 5'-deoxy-5- ^{18}F fluorouridine [95,98], 5- ^{18}F fluorouridine [95,99] and others [99] have been obtained in the same way.

Bromo ^{18}F fluoride (Section 3.9.1) addition across a double bond was used in the synthesis of fluorine-18-labelled steroids of high specific radioactivity. After addition, the bromine is removed by reduction or by dehydrobromination. 11 β - ^{18}F Fluoro-5 α -dihydrotestosterone was obtained in about 3% radiochemical yield (Scheme 17) [64] and 6 α - ^{18}F fluoroprogesterone in only 0.3% [65]. The yields were quite low but sufficient to allow for animal studies. These reactions had been tested out successfully with simpler model alkenes [66].

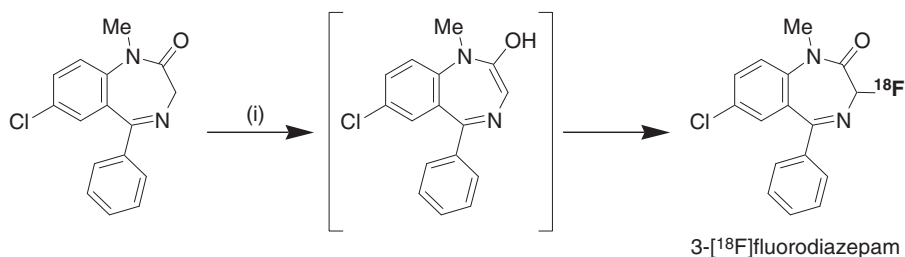
3.2.2. Fluorination of enol structures

An interesting variant of reactions with double bonds is the action of $^{18}\text{F}\text{F}_2$ or other electrophilic ^{18}F reagents on enol structures.

For example, the fluorination with $^{18}\text{F}\text{F}_2$ of diazepam, a 1,4-benzodiazepine (Scheme 18), gives the 3-fluoro derivative in up to 60% radiochemical yield [100]. The mechanism proposed is the electrophilic reaction of $^{18}\text{F}\text{F}_2$ with the enol form of the amide (stabilised by conjugation) yielding, after fluorine attachment and reformation of the carbonyl group, the α -fluoroketo derivative.



Scheme 17. (i) $\text{Br}^{18}\text{F}\text{F}$ *in situ* ($^{18}\text{F}\text{F}^-$, 1,3-dibromo-5,5-dimethylhydantoin, H_2SO_4 , CH_2Cl_2 , 40 °C, 15 min); (ii) Bu_3SnH , AIBN, C_6H_6 , 85 °C, 20 min.



Scheme 18. (i) $^{18}\text{F}\text{F}_2$ or $\text{CH}_3\text{CO}_2^{18}\text{F}\text{F}$, CHCl_3 or CFCl_3 or MeCN , 20 min.

The enol ether 1-methoxycyclohexene reacts with N -[^{18}F]fluoropyridinium triflate to give 6-[^{18}F]fluoro-1-methoxycyclohexene in 67% radiochemical yield (Scheme 19) [83]. Notice that the reaction leads to an allylic and not vinylic fluoride.

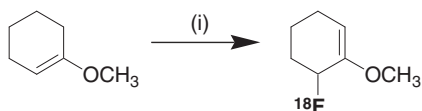
On the contrary, trimethylsilyl enol ethers yield α -fluoroketones when reacting with $\text{Xe}[^{18}\text{F}]\text{F}_2$ [81] or $[^{18}\text{F}]\text{F}_2$ [101] (Scheme 20). In this way several aryl- α -tri[^{18}F]fluoromethylketones were easily prepared in 22–28% radiochemical yields.

3.3. Fluorination of carbanions

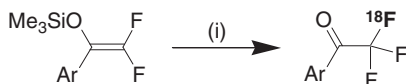
Carbanions in the form of organomagnesium, -sodium, or -lithium salts have been fluorinated with various reagents, including perchloryl [^{18}F]fluoride, 1-[^{18}F]fluoro-2-pyridone, N -[^{18}F]fluoropyridinium triflate and N -[^{18}F]fluoro- N -alkylsulphonamides.

Several phenyllithium compounds were fluorinated with perchloryl [^{18}F]fluoride ($[^{18}\text{F}]\text{FCIO}_3$, Scheme 21) to produce the corresponding [^{18}F]fluorobenzenes (2-[^{18}F]fluoroaniline, 2-[^{18}F]fluoroanisole and 3-[^{18}F]fluoroveratrole) in 21–34% radiochemical yields [79].

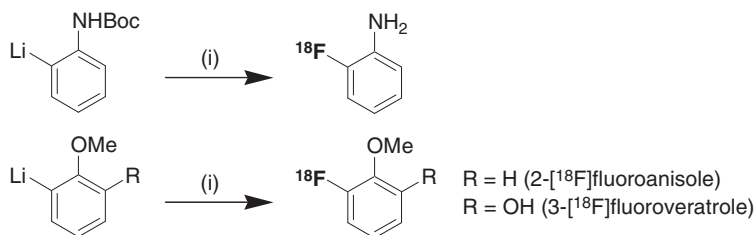
1-[^{18}F]Fluoro-2-pyridone was reacted with methyllithium yielding [^{18}F]fluoromethane quantitatively (Scheme 22) [82]. It should also react with aryl- and other alkyl lithium compounds to give the corresponding [^{18}F]fluoroarenes or -alkanes but no reports exist.



Scheme 19. (i) [^{18}F]FPy $^+$ ·CF $_3$ SO $_3^-$, CH $_2$ Cl $_2$, reflux, 40 min.



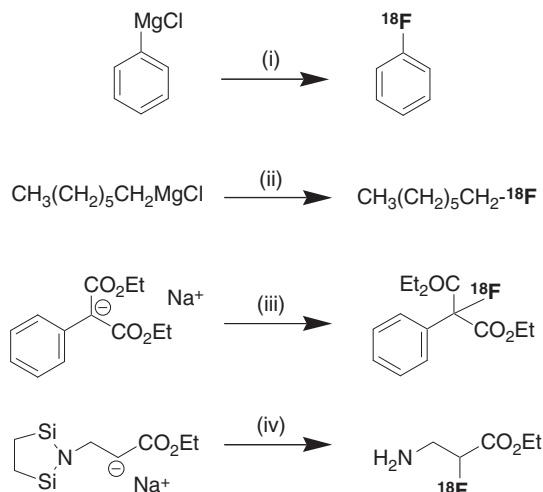
Scheme 20. (i) [^{18}F]F $_2$, MeCN, -45°C , 10 min.



Scheme 21. (i) [^{18}F]FCIO $_3$, KClO $_3$, Et $_2$ O or THF, -78°C , 5–10 min, then acidic hydrolysis.



Scheme 22. (i) 1-[¹⁸F]Fluoro-2-pyridone, Et₂O, −78 °C, 1 min.



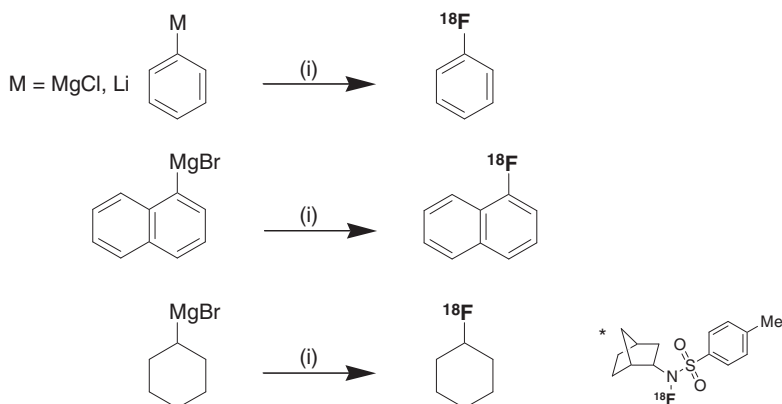
Scheme 23. (i) [¹⁸F]FPy⁺·CF₃SO₃[−], THF, 5 °C, 10 min; (ii) [¹⁸F]FPy⁺·CF₃SO₃[−], Et₂O, 5 °C, 10 min; (iii) [¹⁸F]FPy⁺·CF₃SO₃[−], THF, 0 °C, 10 min; (iv) [¹⁸F]FPy⁺·CF₃SO₃[−], THF, RT, 60 min.

N-[¹⁸F]Fluoropyridinium triflate reacts with alkyl- and arylmagnesium salts (Grignard reagents) as well as enolates (Scheme 23) to yield the corresponding radiofluorinated products, often in high radiochemical yields. Examples are the syntheses of [¹⁸F]fluorobenzene (62%), 1-[¹⁸F]fluorohexane (78%), diethyl 2-[¹⁸F]fluoro-2-phenylmalonate (58%) and ethyl 3-amino-2-[¹⁸F]fluoropropionate (23%) [83].

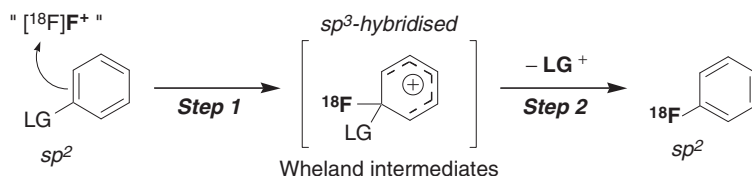
N-[¹⁸F]Fluoro-*N*-alkylsulphonamides react with a variety of carbanions and organometallic compounds [84]. For example, *N*-[¹⁸F]fluoro-*N*-endo-norbornyl-*para*toluenesulphonamide has been successfully used for the preparation of [¹⁸F]fluorobenzene (40 and 61% radiochemical yields from phenylmagnesium chloride and phenyllithium, respectively), 1-[¹⁸F]fluoronaphthalene (53%, from 1-naphthylmagnesium chloride) and [¹⁸F]fluorocyclohexane (29%, from cyclohexylmagnesium chloride) (Scheme 24).

3.4. Fluorination of aromatic rings (other than via carbanions)

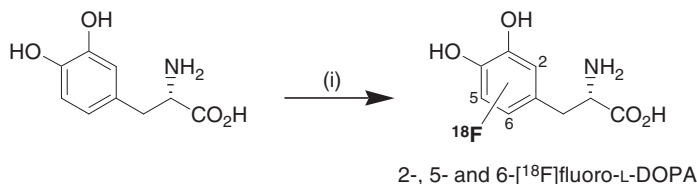
Fluorination of aromatic rings (other than those via carbanions described above) consists principally of fluorodehydrogenation and fluorodemetalation reactions, both of which are thought to proceed via an arenium ion mechanism (Scheme 25) [85].



Scheme 24. (i) *N*-[^{18}F]Fluoro-*N*-endo-norbornyl-*para*toluenesulphonamide ($*$), Et_2O , -78°C , 5 min.



Scheme 25. The arenium ion mechanism of electrophilic fluorination of aromatic rings via fluorodehydrogenation or fluorodemetalation reactions.



Scheme 26. (i) [^{18}F]F $_2$ or $\text{CH}_3\text{CO}_2[^{18}\text{F}]\text{F}$ or $\text{Xe}[^{18}\text{F}]\text{F}_2$, different solvents, -78 to 0°C , 5–15 min.

3.4.1. Fluorodehydrogenation

Direct fluorination of aromatic rings is possible using molecular [^{18}F]fluorine, acetyl [^{18}F]hypofluorite and xenon *di*[^{18}F]fluoride as electrophilic reagents. These fluorodehydrogenation reactions have been widely used even though they are often not very regioselective. Direct radiofluorination of L-DOPA (3,4-dihydroxy-L-phenylalanine) [102,103] with [^{18}F]F $_2$ yields the three possible regioisomers 2-[^{18}F]-, 5-[^{18}F]- and 6-[^{18}F]fluoro-L-DOPA in 12, 1.7 and 21% yield, respectively (Scheme 26). Isolation of the desired 6-fluoro isomer required careful HPLC and gave 6-[^{18}F]fluoro-L-DOPA in less than 5% radiochemical yield. From a design

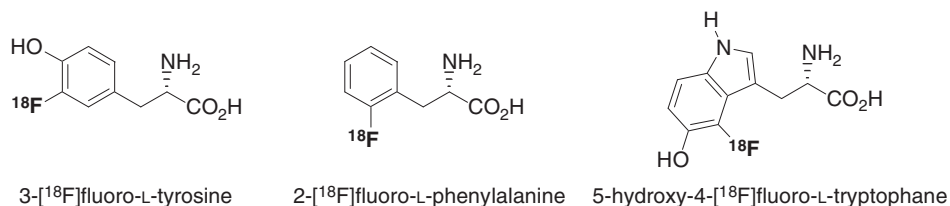
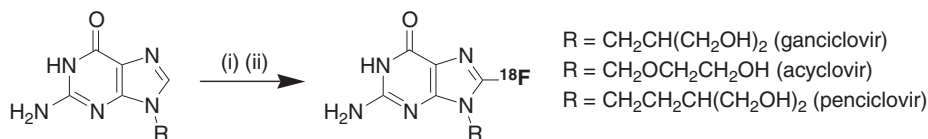


Fig. 1. Chemical structures of fluorinated analogues of amino acids naturally occurring in proteins and labelled with fluorine-18.



Scheme 27. (i) [^{18}F]F₂, Et₄NOH, EtOH, RT, 20 min; (ii) neutralisation with aq. AcOH (1 N).

point of view, note that in this radiopharmaceutical, fluorine-18 replaces an aromatic hydrogen and not one of the parent hydroxy groups (see also discussion in Section 2.2).

Reactivity and selectivity of [^{18}F]F₂ in the electrophilic fluorination of L-DOPA can be modulated by using different acidic solvents such as neat HF, neat TFA or 50% TFA in acetic acid. In this way, using 50% TFA in acetic acid, it was possible to produce useful quantities of the regioisomer 5-[^{18}F]fluoro-L-DOPA [104].

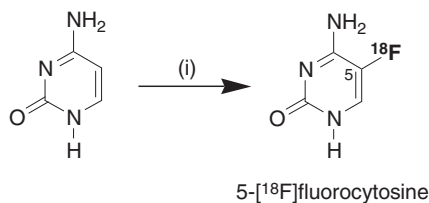
The naturally occurring aromatic amino acids phenylalanine, tryptophane and tyrosine (Fig. 1) have been labelled with fluorine-18 through similar electrophilic substitution methods [7]. Aromatic residues contained in peptides have been labelled with CH₃CO₂[^{18}F]F [105,106], an example of direct labelling of macromolecules. However, direct labelling of macromolecules is usually not the method of choice nowadays (see Section 6).

Another example of a direct electrophilic fluorination of aromatic rings is the synthesis of the purine derivatives 8-[^{18}F]fluoroganciclovir, 8-[^{18}F]fluoropenciclovir and 8-[^{18}F]fluoroacyclovir (Scheme 27). The radiochemical yields obtained for these compounds are low, about 1%, but no protecting group is required, allowing a one-step radiosynthesis [107].

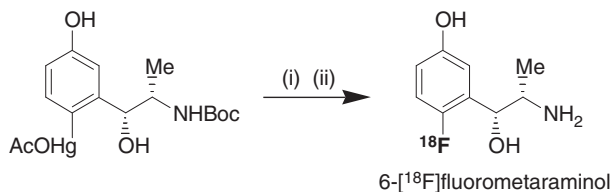
Also the preparation of the tumour imaging agents 5-[^{18}F]fluorocytosine [108] (Scheme 28) and cytosine derivative [^{18}F]capecitabine [109] can be considered as a direct *heteroaromatic* electrophilic dehydrogenation.

3.4.2. Fluorodemetalation

The consistent poor regioselectivity in direct aromatic electrophilic fluorination has privileged the use of fluorodemetalation reactions. Tin clearly appears to



Scheme 28. (i) [¹⁸F]F₂, HF, −5 °C, few min.

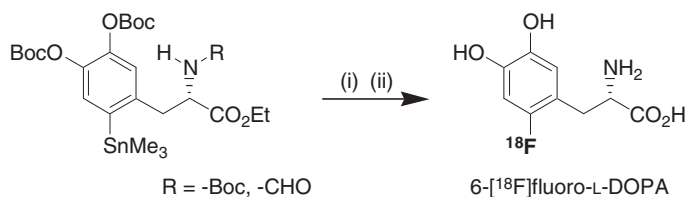


Scheme 29. (i) CH₃CO₂[¹⁸F]F, CH₂Cl₂, 0 °C, 5–15 min; (ii) HCl, MeCN, RT, 10 min.

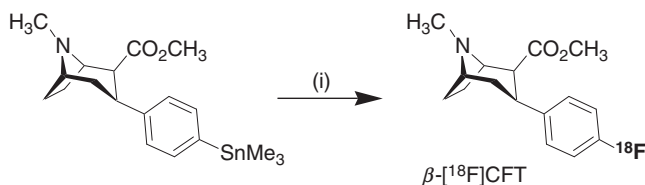
be the best metal [110], but several examples of the use of arylsilicon, -mercury, -selenium and -germanium compounds can be found in the literature [7]. In these methods the regioselectivity is accomplished by metal functionalisation of the aromatic ring with subsequent fluorination occurring only at the metal position, and this even when using the highly reactive molecular [¹⁸F]fluorine reagent.

The use of mercury has the merit of easy preparation of the aryl mercury compounds directly from the aromatic compound and an inorganic mercury salt, sometimes in complete regioselective manner. Preparation of the other metallated species generally involves more synthetic steps. An example of a radiofluorode-mercuration reaction (Scheme 29) is the synthesis of 6-[¹⁸F]fluorometaraminol [111]. This compound was later also prepared either by fluorodestannylation [112] or by using a nucleophilic approach (see Section 4) with [¹⁸F]fluoride [113].

The early preparations of 6-[¹⁸F]fluoro-L-DOPA involved reaction of a 6-substituted mercuric derivative with acetyl [¹⁸F]hypofluorite and yielded the expected compound in 11% radiochemical yield [114–116]. Nowadays fluorodestannylation is the reaction of choice for the preparation of this radiopharmaceutical. The most common precursor is a fully protected L-DOPA compound, bearing at the 6-position a trimethylstannyl group (Scheme 30). After fluorodestannylation, the phenol and amino acid protecting groups are removed with acid. The radiochemical yields were reported to be superior to 25%, using chlorotrifluoromethane (freon-11) or chloroform as the solvent. The yield obtained using [¹⁸F]F₂ [117–119] is better than the one obtained using CH₃CO₂[¹⁸F]F [120]. Fully automated computer-controlled modules for 6-[¹⁸F]fluoro-L-DOPA production using this two-step process are now commercially available (TRACERlabFX_{FDOPA}TM, GE Medical System).



Scheme 30. (i) [^{18}F]F₂, CFCl₃ or CHCl₃, -20 °C, 5–10 min; (ii) aq. HCl (4 N), 130 °C, 10 min.



Scheme 31. (i) [^{18}F]F₂, CFCl₃/AcOH (7/1 [v:v]), 0 °C or below, 5–15 min.

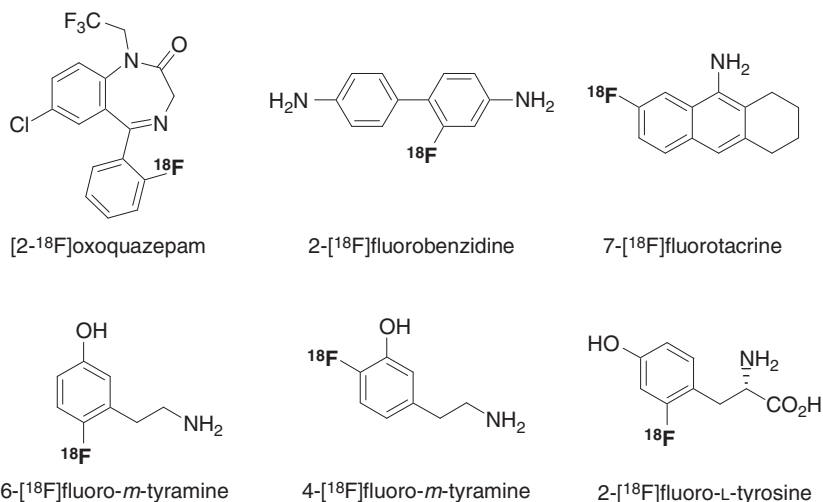


Fig. 2. Examples of fluorine-18-labelled compounds prepared by fluorodestannylation.

Another example is the radiosynthesis of β -[^{18}F]CFT ([^{18}F]WIN-35,428) [121,122] (Scheme 31). This radiopharmaceutical was prepared in 0.9–2.0% radiochemical yield using acetyl [^{18}F]hypofluorite as the fluorination reagent.

Figure 2 lists some other labelled compounds obtained by fluorodestannylation: 4- and 6-[^{18}F]fluoro-*m*-tyramine [123], 2-[^{18}F]fluoro-L-tyrosine [124], 2-[^{18}F]oxoquazepam, an agonist of benzodiazepine receptors [125], 7-[^{18}F]fluorotacrine, a potential agent for mapping acetylcholinesterase [126] and 2-[^{18}F]fluorobenzidine, a potential radioligand to image amyloid deposits in the brain [127].

4. NUCLEOPHILIC RADIOFLUORINATION

In the present decade, there has been an explosion in the fluorine-18 literature, both in the sheer number of new radiotracers published and in the number of those reaching at least preliminary evaluation in humans. Most of these fluorine-18-labelled radiotracers and radiopharmaceuticals have been synthesised using no-carrier-added [^{18}F]fluoride anion. The impetus for the latter includes the increasing availability of large quantities of [^{18}F]fluoride from low- to medium-energy cyclotrons utilising the $^{18}\text{O}(\text{p},\text{n})^{18}\text{F}$ nuclear reaction on [^{18}O] water (see Section 2.4), the generally higher specific radioactivities achievable with [^{18}F]fluoride ($\gg 2 \text{ Ci}/\mu\text{mol}$, $\gg 75 \text{ GBq}/\mu\text{mol}$) and the mastering of the techniques to render aqueous [^{18}F]fluoride chemically reactive. Nucleophilic radiofluorination can be divided into two principal categories: the aliphatic nucleophilic substitutions and the aromatic nucleophilic substitutions [3,7,8].

Aliphatic and aromatic nucleophilic substitutions with [^{18}F]fluoride are usually performed either on an immediate precursor of the target molecule (direct labelling using a one-step process) or on an indirect precursor followed by one or more chemical steps leading to the target radiotracer. The first approach, if highly desirable, is in fact rarely practicable. The reaction conditions are often not compatible with the structure or with the various chemical functions borne by the radiopharmaceutical. It is therefore common that the radiosynthesis comprises at least two chemical steps: first the introduction of fluorine-18 followed by what is often a (multi)deprotection step. It is not unusual either that fluorine-18 is first incorporated into a much simpler and chemically more robust molecule which is then coupled to a more sensitive entity under milder conditions, possibly still followed by a final deprotection step. Suchlike multi-step procedures are possible thanks to the favourable half-life of fluorine-18. However, the more complicated the process, the more chance of side reactions and complicated final purifications (see also Section 2.3), which may seriously hamper the automation of the process.

Both aliphatic and aromatic nucleophilic substitution procedures involve first pre-activation of cyclotron-produced, no-carrier-added, aqueous [^{18}F]fluoride.

4.1. Preparation of reactive [^{18}F]fluoride anion

[^{18}F]fluoride anion is in most cases produced by irradiation of oxygen-18-enriched water (see Section 2.4) and therefore provided in aqueous solution. Its highly solvated form is a poor nucleophile [28] but a strong base [128]. A number of procedures have been described for the isolation of [^{18}F]fluoride from the target water that render it more reactive and suitable for nucleophilic reactions.

Typically, the target content is passed through an anion exchange resin that permits both recovery of the expensive oxygen-18-enriched water and removal of some of the cationic contaminants that can impact on the reactivity of the [^{18}F]fluoride. The latter is then usually eluted with a dilute aqueous alkali metal carbonate solution. The carbonate has occasionally been substituted by the less-basic oxalate when sensitive substrates were used in the fluorination process [129,130]. Normally, potassium carbonate is preferred, even though the potassium counter-ion shows limited solubility in most of the solvents that are used. The larger alkali metals cesium and rubidium offer somewhat better fluoride solubility [131] and have been used successfully in radiofluorinations [132–134]. A number of alternative methodologies have been investigated to provide not only better solubility but above all higher reactivity, since a major reason for a limited fluoride reactivity is the latter's propensity to form tight ion pairs with metal cations. A number of *tetraalkyl ammoniums* ($^+\text{NR}_4$, R = ethyl, propyl, butyl) have therefore been used as counter-ions [135]. The corresponding [^{18}F]fluoride salts, besides providing reactive [^{18}F]fluoride, enlarge the choice of solvent for the radiofluorination reaction since they are soluble in a variety of organic solvents from non-polar to dipolar aprotic. However, they are more difficult to make anhydrous [136] and they are less stable at high temperatures [137].

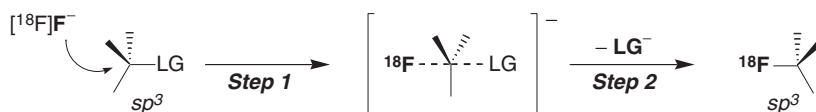
Since non-bound or non-coordinated nucleophiles are even more reactive, crown-ethers [138] and cryptands (polyaminoethers) [139,140] have been used to chelate the alkali metal cations, notably the potassium ion of $\text{K}[^{18}\text{F}]\text{F}$. This allows the [^{18}F]fluoride anion to be less tightly paired with the cation and therefore to be more reactive, which has been coined the 'naked' ion effect. In practice, the crown-ether (e.g. 18-crown-6) or better the polyaminoether Kryptofix-222[®] (4,7,13,16,21,24-hexaoxa-1,10-diazabicyclo[8.8.8]hexacosane) is added to the aqueous $\text{K}[^{18}\text{F}]\text{F}/\text{K}_2\text{CO}_3$ solution which is then concentrated to dryness [139,140]. The complex ($\text{K}[^{18}\text{F}]\text{F}-\text{K}_{222}$) can be further dried, if needed, by one or more cycles of addition of dry acetonitrile and azeotropic evaporation.

Other more anecdotic ways of activating [^{18}F]fluoride are its coordination with protonated 1,8-*bis*-(dimethylamino)naphthalene, its coordination with antimony oxide or its purification via an intermediate [^{18}F]fluorotrimethylsilane formation.

4.2. Nucleophilic aliphatic substitution

4.2.1. Basic principles

Aliphatic nucleophilic substitutions (at sp^3 centre) with [^{18}F]fluoride are principally $\text{S}_{\text{N}}2$ -type reactions (bimolecular nucleophilic substitution, Scheme 32). The nucleophile [^{18}F]fluoride attacks the substrate at the backside relative to the leaving group, resulting in substitution with inversion of configuration at the carbon centre [85]. The best leaving groups are the weakest bases, which is consistent with the principle that stable species make better leaving groups. Iodide is usually the best



Scheme 32. The S_N2 mechanism of nucleophilic aliphatic fluorination.

leaving group of the halides and fluoride the poorest. The sulphonic ester groups, such as the triflate (CFSO_3^-), tosylate ($p\text{-MeC}_6\text{H}_4\text{SO}_3^-$), mesylate (CH_3SO_3^-), brosylate ($p\text{-BrC}_6\text{H}_4\text{SO}_3^-$) and nosylate ($m\text{-NO}_2\text{C}_6\text{H}_4\text{SO}_3^-$), are better leaving groups than halides, leading to the following ranking order: $\text{RSO}_3^- > \text{I}^- > \text{Br}^- > \text{Cl}^- > \text{F}^-$. Of course, fluorine, in spite of its excellent leaving-group ability, is seldom used in fluorine-18 chemistry because of obvious isotopic dilution, leading to low specific radioactivity.

Aliphatic nucleophilic substitutions are usually performed under basic or neutral conditions, with a large assortment of solvents possible. Indeed, the effects of the solvent on S_N2 -type reactions depend on the charge dispersal in the transition state compared to the one in the reactants. However, in radiofluorinations with $[^{18}\text{F}]$ fluoride the solubility of the reactants appears to play a larger role in solvent choice than the solvent effects on reaction rates. The most common solvents are the polar aprotic ones, such as acetonitrile, in which the $[^{18}\text{F}]$ fluoride salt ($\text{K}[^{18}\text{F}]\text{F}$, $\text{Cs}[^{18}\text{F}]\text{F}$ or $\text{Bu}_4\text{N}[^{18}\text{F}]\text{F}$) or the $\text{K}[^{18}\text{F}]\text{F}\text{-K}_{222}$ complex and the organic precursors for labelling show good solubility. The reaction is often performed at reflux temperature of the solvent for a few minutes.

4.2.2. Preparation of simple $[^{18}\text{F}]$ fluoroalkyl-type molecular building blocks and some applications

Nucleophilic radiofluorination of small aliphatic molecules presenting two leaving groups (two halogens or two sulphonates), leaving one of them untouched in the labelling process, leads to an $[^{18}\text{F}]$ fluoroalkylating reagent ($[^{18}\text{F}]\text{F}-(\text{CH}_2)_n\text{-X}$ with $n = 1\text{--}3$ and $\text{X} = \text{halogen or sulphonate}$, Fig. 3). In particular, the radiosynthesis of bromo-, tosyloxy- and mesyloxy-1- $[^{18}\text{F}]$ fluoroalkanes from the reaction of the corresponding unbranched bifunctional alkanes with no-carrier-added $[^{18}\text{F}]$ fluoride as its activated $\text{K}[^{18}\text{F}]\text{F}\text{-K}_{222}$ complex [139,140] has received much attention [141]. In this way $[^{18}\text{F}]$ fluoriodomethane, a valuable tool for the introduction of a $[^{18}\text{F}]$ fluoromethyl group into radiopharmaceuticals, was prepared [142]. Its reactivity towards amine, acid, thiol or phenolate functions has been studied extensively.

$[^{18}\text{F}]$ Fluorocholine, an imaging agent used in oncology for detecting androgen-dependent and androgen-independent prostate cancers and its metastases, was prepared from bromo $[^{18}\text{F}]$ fluoromethane (Scheme 33) [143].

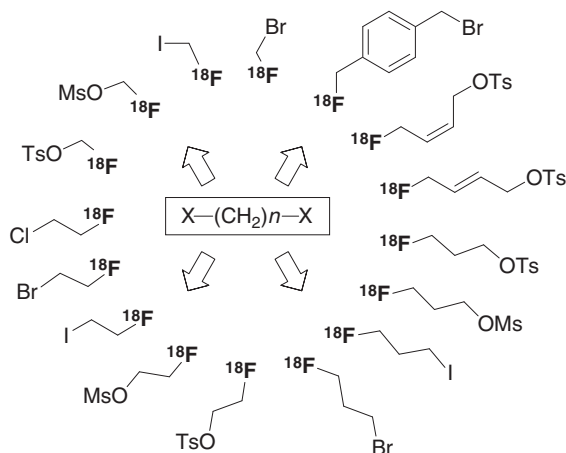
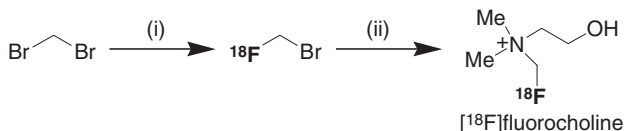


Fig. 3. Chemical structures of various halogeno- and sulphonyloxy-[¹⁸F]reagents.



Scheme 33. (i) $\text{K}[\text{F}(\text{F})\text{F}]\text{-K}_{222}$, MeCN, 110 °C, 3 min, then gas chromatography purification; (ii) $\text{Me}_2\text{NCH}_2\text{CH}_2\text{OH}$, acetone, 100 °C, 10 min, then concentration to dryness and cation exchange Sep-Pak® cartridge purification.

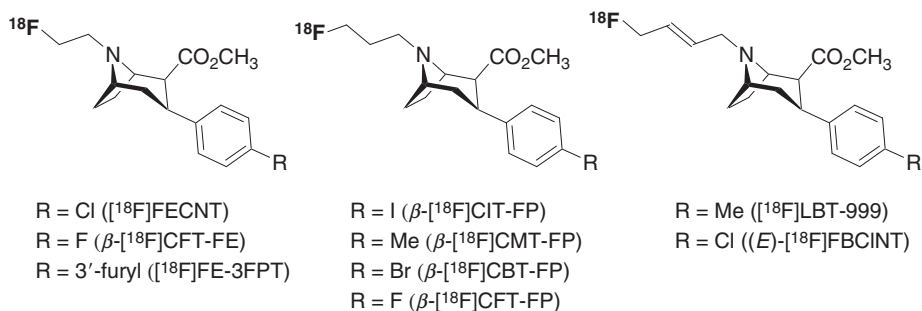


Fig. 4. Chemical structures of some *N*-[¹⁸F]fluoroalkyl- and *N*-[¹⁸F]fluoroalkenyltropane derivatives.

It was synthesised in 20–40% overall radiochemical yield (non-decay corrected) in less than 40 min. The radiochemical yield of the alkylation reaction of dimethylethanolamine with [^{18}F]fluorobromomethane was greater than 90%.

A prominent application of these halogeno- and sulphonyloxy [^{18}F]reagents is the robust and reliable pathway frequently proposed for the labelling of a series of fluoroalkyl- and fluoroalkenyltropane derivatives (Fig. 4), for example the

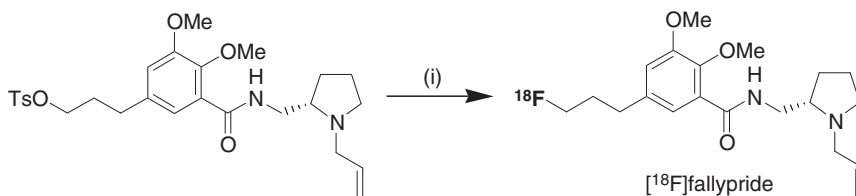
dopamine transporter ligands [^{18}F]FECNT, β -[^{18}F]CIT-FP, (*E*)-[^{18}F]FBCINT and more recently [^{18}F]LBT-999 [144].

4.2.3. One-step synthesis of a radiopharmaceutical involving an aliphatic nucleophilic fluorination

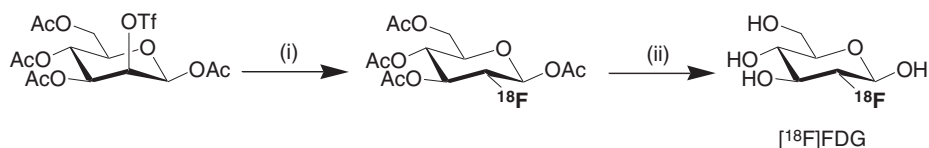
An example of a direct (one-step) preparation involving aliphatic nucleophilic substitution with [^{18}F]fluoride is the synthesis of [^{18}F]fallypride (Scheme 34), a high-affinity dopaminergic D_2 receptor ligand, from the corresponding tosylate in about 20% radiochemical yield [145].

4.2.4. Multi-step synthesis of a radiopharmaceutical involving an aliphatic nucleophilic fluorination

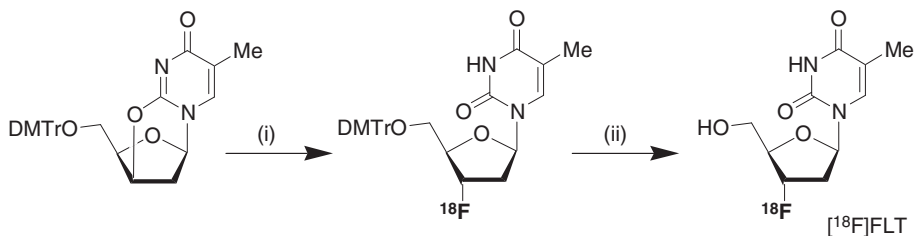
Many syntheses of fluorine-18-labelled radiopharmaceuticals prepared by aliphatic nucleophilic fluorination comprise at least two radiochemical steps: first the introduction of fluorine-18, followed by what is often a (multi)deprotection step. This is the case for the most frequently used PET radiopharmaceutical, 2-[^{18}F]fluoro-2-deoxy-D-glucose ([^{18}F]FDG). A few words about this revolutionary radiopharmaceutical are appropriate here. [^{18}F]FDG is a glucose analogue and is therefore taken up by glucose-using cells. It is then phosphorylated at the 6-position by hexokinase, whose mitochondrial form is upregulated in rapidly growing malignant tumours. Because the 2-hydroxy group of glucose (now replaced by a fluorine atom) is required for the next step in glucose metabolism in all cells, no further reactions occur. Furthermore, most tissues (with the notable exception of liver and kidneys) cannot reverse the 6-phosphorylation. This means that [^{18}F]FDG is trapped as [^{18}F]FDG-6-phosphate in any cell which takes it up, since phosphorylated sugars, due to their ionic charge, cannot diffuse passively out of the cell either. This results in intense labelling of tissues with high glucose uptake, such as the brain, the heart, the liver and most tumours. As a result [^{18}F]FDG-PET can be used in metabolic studies in various organs but above all for diagnosis, staging and treatment monitoring of cancers, particularly Hodgkin's disease, non-Hodgkin's lymphoma and lung cancer. Today, oncology scans using [^{18}F]FDG make up over 90% of all PET scans in current practice.



Scheme 34. (i) $\text{K}[^{18}\text{F}]\text{F-K}_{222}$, MeCN , $85-90^\circ\text{C}$, 30 min.



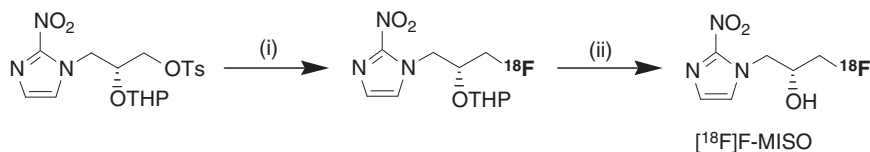
Scheme 35. (i) $K[^{18}\text{F}]\text{F-K}_{222}$, MeCN, 85 °C, 5 min; (ii) aq. HCl (1 M), 130 °C, 5 min (RCY: >>(50%).



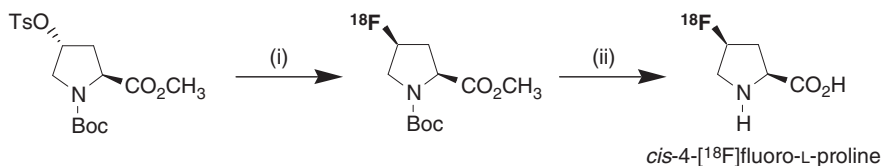
Scheme 36. (i) $K[^{18}\text{F}]\text{F-K}_{222}$, DMSO, 160 °C, 10 min; (ii) aq. HCl (1 N), 50 °C, 10 min (RCY: 14%).

$[^{18}\text{F}]\text{FDG}$ is currently produced by $[^{18}\text{F}]\text{fluoro-to-triflate}$ substitution, performed in acetonitrile at reflux temperature followed by acidic- or (preferred today) basic removal of the acetyl protective groups (Scheme 35). The increasing demand for $[^{18}\text{F}]\text{FDG}$ has led to significant effort directed towards the development of optimal, highly efficient, routine-production methods including the design and construction of automated systems [146]. The original synthetic process was developed in 1986 (Hamacher, Coenen and Stöcklin at the Jülich PET centre) [139,140] and modifications have been implemented to improve the final yield, for example solid-phase-supported basic hydrolysis of the radiolabelled O-protected intermediate [147–149]. State-of-the-art automation is provided by commercially available synthesis units, such as the TRACERlab MX_{FDG}TM and the TRACERlab FX_{FDG}TM (originally developed by Coincidence Technologies and Nuclear Interface, respectively, now both GE Medical Systems), giving $[^{18}\text{F}]\text{FDG}$ in over 50% radiochemical yield in less than 30 min. Recent progress in microfluidics has also been applied to the synthesis of $[^{18}\text{F}]\text{FDG}$, opening new perspectives in automation [150,151].

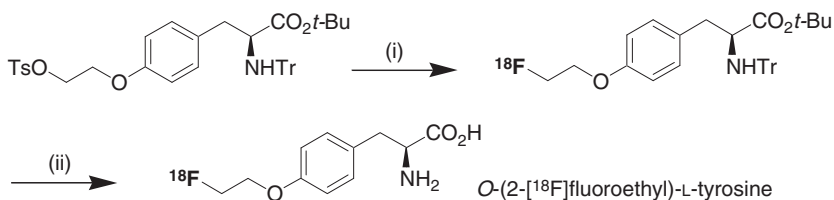
The successful use of $[^{18}\text{F}]\text{FDG}$ in oncology PET imaging has prompted the design of several other radiopharmaceuticals, such as $[^{18}\text{F}]\text{FLT}$ ($[^{18}\text{F}]\text{fluorothymidine}$, used as cellular proliferation marker, Scheme 36) [152–154], F-MISO ($[^{18}\text{F}]\text{fluoromisonidazole}$, used to assess tissue hypoxia, Scheme 37) [155], *cis*-4- $[^{18}\text{F}]\text{fluoro-L-proline}$ (used as abnormal collagen synthesis marker, Scheme 38) [156] and O-(2- $[^{18}\text{F}]\text{fluoroethyl}$)-L-tyrosine (used as amino acid transport and/or protein synthesis marker, Scheme 39) [157]. All these fluorine-18-labelled molecules have been prepared by aliphatic nucleophilic fluorination followed by a deprotection reaction.



Scheme 37. (i) K[¹⁸F]F-K₂₂₂, MeCN, 100 °C, 10 min; (ii) aq. HCl (1 N), 100 °C, 3 min (RCY: 21%).



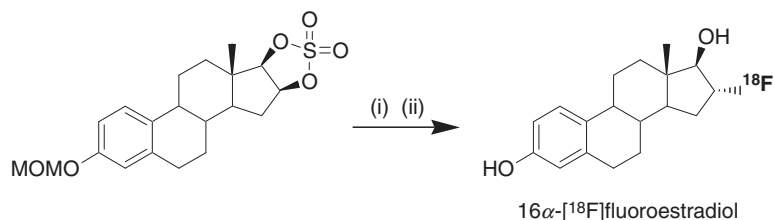
Scheme 38. (i) K[¹⁸F]F-K₂₂₂, MeCN, 85 °C, 10 min; (ii) CF₃SO₃H, 125–130 °C, 10 min (RCY: 36%).



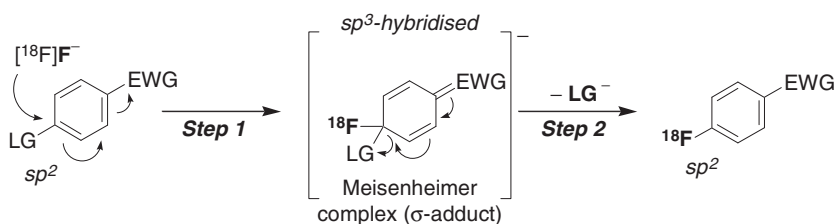
Scheme 39. (i) Bu₄N⁺[¹⁸F]F[−], MeCN, 85 °C, 5 min; (ii) TFA, CH₂Cl₂, 70 °C, 7 min (RCY: 60%).

The [¹⁸F]FLT and [¹⁸F]F-MISO preparations, the protocols of which resemble much that of [¹⁸F]FDG, have recently been automated by adapting a standard [¹⁸F]FDG module [158,159].

As illustrated above in the synthesis of [¹⁸F]FLT (Scheme 36), the leaving group used to facilitate the incorporation of [¹⁸F]fluoride can, in some instances, act simultaneously as a protective group for another function present in the substrate. In this case, it is the 2,3'-anhydro structure that serves as both the leaving group and the protecting group for the 3-*N*-position of the pyrimidine ring [152–154,160]. Another example of dual-mode leaving and protecting group can be found in the utilisation of 3-*O*-methoxymethyl-16 β ,17 β -*O*-epiestriol cyclic sulphone (Scheme 40) as precursor for the synthesis of 16 α -[¹⁸F]fluoroestradiol ([¹⁸F]FES, the only clinically relevant PET radiotracer for imaging estrogen-positive breast tumours) [161]. In this example, the cyclic sulphone acts both as a protective group for the 17 β -hydroxyl function and as an activating group for the [¹⁸F]fluoride



Scheme 40. (i) $\text{K}[^{18}\text{F}]\text{F}-\text{K}_{222}$, MeCN, 110 °C, 15 min; (ii) conc. H_2SO_4 in EtOH, 110 °C, 5 min (RCY: 30–45%).



Scheme 41. The $\text{S}_{\text{N}}\text{Ar}$ mechanism of nucleophilic aromatic fluorination.

incorporation from the α -face of the D-ring and at the C-16 position exclusively (the axial methyl group at the C-19 position prevents approach of the $[^{18}\text{F}]\text{fluoride}$ anion from the β -face and is possibly also responsible for the absence of displacement reaction at C-17 through hydrogen bonding with the adjacent oxygen). Various other examples of this type of reaction can be found in the literature [162–166].

4.3. Nucleophilic aromatic substitution

4.3.1. Homoaromatic series

Aromatic nucleophilic substitutions with $[^{18}\text{F}]\text{fluoride}$ in the *homoaromatic* series (typical $\text{S}_{\text{N}}\text{Ar}$ reactions) are by far the most commonly used for aromatic radiofluorination (Scheme 41). These reactions require the presence on the aromatic ring of both a good leaving group (LG) and a strong electron-withdrawing group (EWG) in the *ortho* or, better, *para* position [85]. Reactions in which a diazonium- or a triazene group is replaced by fluoride (known as the Balz-Schiemann and Wallach reactions) [85] are not largely used in fluorine-18 chemistry for reasons that will be discussed later. Worth mentioning is also the recently described reactions involving diaryliodonium salts as precursors (see Sections 4.3.1.1 and 4.3.1.2) in which an iodoarene is the leaving group. Like in the Balz-Schiemann and Wallach reactions, there is no need for an EWG in these nucleophilic radiofluorinations.

Leaving groups include the halogens and particularly the nitro group (with the following accepted order of decreasing leaving-group ability: $\text{F} > \text{NO}_2 > \text{Cl} > \text{Br}$

and I) [85]. However, this depends greatly on the nature of the nucleophile and with [^{18}F]fluoride, the trimethylammonium group [167,168] is often a better alternative, when available. Indeed, aryltrimethylammonium salts, which are relatively stable and easy to handle, tend to be more reactive than compounds with a neutral leaving group and usually require milder conditions and give higher radiochemical yields in [^{18}F]fluoride substitution. They are also particularly convenient because of their superior separation from the reaction product, the neutral aryl [^{18}F]fluoride, using HPLC or a solid-phase extraction (SPE)-cartridge, due to the large differences in physico-chemical properties. The possible side-reaction consisting of fluorodemethylation on the trimethylammonium group, leading to volatile [^{18}F]fluoromethane, is a limiting factor in the use of this leaving group. Again (see Section 4.2.1), fluorine, in spite of its excellent leaving-group ability, is seldom used in fluorine-18 chemistry because of obvious isotopic dilution, leading to low specific radioactivity.

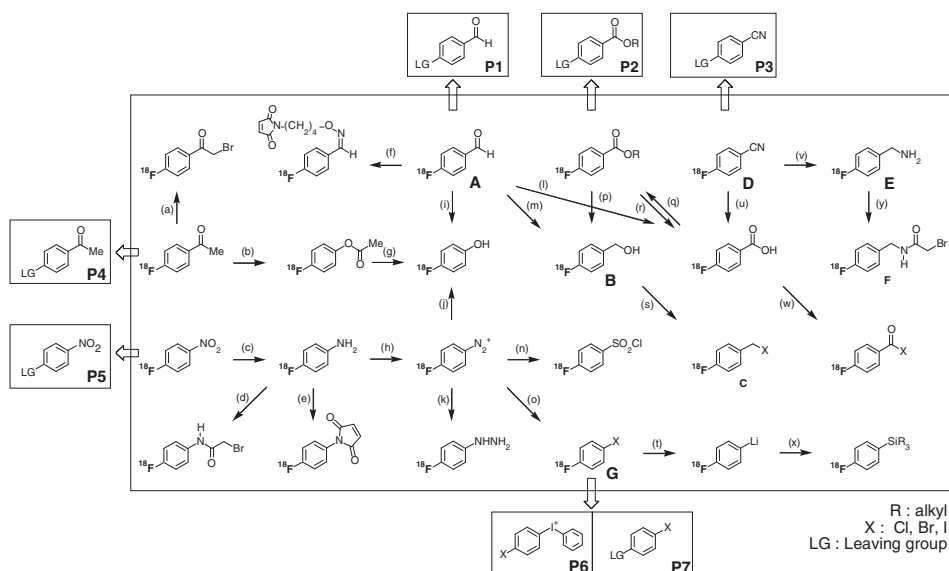
EWGs include the nitro-, trifluoromethyl- and cyano groups as well as the aldehyde, ketone, ester and carboxylic acid functions. An approximate ranking of the most common substituents in order of decreasing activation ability is $\text{NO}_2 > \text{CF}_3 > \text{CN} > \text{CHO} > \text{COR} > \text{COOR} > \text{CO}_2\text{H} > \text{Br, I, F, Me} > \text{NMe}_2 > \text{OH, NH}_2$ [7,167]. Attempts have been made to correlate the radiochemical yield in nucleophilic radiofluorination reactions with the carbon-13 nuclear magnetic resonance (^{13}C -NMR) chemical shift at the reaction centre in fluoro-, nitro- and trimethylammonium substituted aryl aldehydes, ketones and nitriles. While good to excellent agreement was found for the displacement of the fluoro and nitro groups, the trimethylammonium group did not show the same correlation pattern [7,168,169].

Aromatic nucleophilic radiofluorinations are usually performed in aprotic polar solvents, such as dimethyl sulfoxide (DMSO), sulfolane or dimethylacetamide, and often under basic conditions (because of the presence of Kryptofix-222®/potassium carbonate). Completion of the [^{18}F]fluoride incorporation often requires moderate to high temperatures (100–170 °C) for 10–30 min. Microwave technology can be a successful application here, resulting in improved yields and shorter reaction times [29,170–173].

4.3.1.1. Single- or multi-step preparation of [^{18}F]fluoroaryl-type molecular building blocks and some applications

A large number of no-carrier-added fluorine-18-labelled aromatic key-intermediates have been synthesised, opening the way to the preparation of more complicated radiopharmaceuticals via multi-step approaches. Scheme 42 non-exhaustively lists a number of *para*-substituted [^{18}F]fluorobenzene compounds indicating some of their possible chemical interconnections. It also shows some of the precursors for labelling (**P1–P7**) that have been used for their preparation.

For example, *p*-[^{18}F]fluorobenzaldehyde (**A**) is easily obtained in moderate to high yields from the corresponding nitro- [174–176] or trimethylammonium triflate precursor (**P1**) [167,168] using $\text{K}[^{18}\text{F}]\text{F-K}_{222}$ in DMSO at 120 °C for 10 min.



Scheme 42. Chemical structures of *para*-substituted [^{18}F]fluorobenzene reagents and their preparation: (a) Amberlyst A-26, Br_3 , THF, 60°C , 10 min; (b) H_2O_2 , H_2SO_4 , AcOH, 2–5 min; (c) NaBH_4 , Pd/C (10%), MeOH, RT or Pd/C, H_3PO_4 , THF, 65°C , 5 min; (d) BrCOCH_2Br , DMF, 80 – 90°C , 3–5 min; (e) maleic anhydride, AcOH, 65°C , 5 min, then Ac_2O , NaOAc, C_6H_6 , 100°C , 10 min; (f) *N*-[4-(amino-oxy)butyl]maleimide, MeOH, RT, 15 min; (g) aq. NaOH (1 M), 3–5 min; (h) NaNO_2 , aq. HCl (1 M), 0°C , 2 min; (i) *m*- $\text{ClC}_6\text{H}_4\text{CO}_3\text{H}$, TFA, CH_2Cl_2 , 120 – 130°C , 15 min; (j) Cu_2O , $\text{Cu}(\text{NO}_3)_2 \cdot 3\text{H}_2\text{O}$, 70°C , 10 min; (k) NaBH_3CN , 75°C , 1–2 min, then hydrolysis; (l) KMnO_4 or Jones' reagent ($\text{CrO}_3/\text{H}_2\text{SO}_4/\text{H}_2\text{O}$), MeCN, 80°C , 10 min; (m) NaBH_3CN , HCl (0.1 M in CH_3OH), RT or NaBH_4 fixed on Al_2O_3 , THF, RT or LiAlH_4 (1 M in THF), RT, 1 min, then aq. HCl (0.1 N); (n) SO_2 , CuCl, CuCl_2 , KCl, dioxane, 3–10 min; (o) CuX/HX ($\text{X} = \text{Cl}$ or Br), 75°C , 15 min; (p) BH_3 or LiAlH_4 , THF, reflux, 2 min, then hydrolysis; (q) ROX ($\text{X} = \text{H}$ or e.g. *N*-succinimidyl), MeCN, 90°C , 2–5 min; (r) aq. NaOH (1 N) then neutralisation, or HCl (1 N), 90°C , 5–10 min; (s) SOCl_2 or SOBr_2 , toluene, 120 – 130°C , 5 min or PBr_3 , PI_3 , P_2I_4 , Ph_3PBr_2 or Ph_3PI_2 , CH_2Cl_2 , RT (or 40°C), 2–15 min; (t) *n*-BuLi or Li, THF, -78°C , 1–2 min; (u) aq. NaOH (5 N), 120°C , 10 min then neutralisation; (v) LiAlH_4 , THF, reflux, 2 min, then hydrolysis; (w) SOX_2 , toluene or Et_2O , RT, 2–5 min; (x) R_3SiCl , THF, -78°C to RT, 5–10 min; (y) BrCOCH_2Br , CH_2Cl_2 , RT, 2 min.

Yields of up to 70–74% can be reached. *p*-[^{18}F]Fluorobenzaldehyde (**A**) can then be reduced to *p*-[^{18}F]fluorobenzylalcohol (**B**) using LiAlH_4 [177], NaBH_4 [175,178–180], NaBH_3CN [181] or SiH_2I_2 [182,183] and then converted to the corresponding *p*-[^{18}F]fluorobenzyl halides (**C**, $\text{X} = \text{chlorine, bromine or iodine}$) using HI [184,185], HBr [181], P_2I_4 , Ph_3PBr_2 [179,180], SOBr_2 [177,178,186] or SOCl_2 [187]. Radiochemical yields up to 90% can be obtained in 10 min for *p*-[^{18}F]fluorobenzyl iodide and 50–60% for *p*-[^{18}F]fluorobenzyl bromide in 30 min. An important application of these appropriately substituted [^{18}F]

fluorobenzyl halides is the asymmetric synthesis of aromatic amino acids and especially 6- ^{18}F fluoro-L-DOPA (*ortho*- ^{18}F fluoro in this case, see Section 4.3.1.3).

p- ^{18}F Fluorobenzonitrile (**D**) is an important key-intermediate that can be obtained in high yields (80–85% and up to 95%) by a nucleophilic substitution reaction on the corresponding trimethylammonium precursor (**P3**) [132]. It can be reduced to *p*- ^{18}F fluorobenzylamine (**E**) which has been transformed into *N*-4- ^{18}F fluorobenzyl- α -bromoacetamide (**F**) for the labelling of oligonucleotides [14,188,189] (see also Section 6).

The synthetic potential of palladium-mediated cross-coupling reactions (Heck, Suzuki, Stille, Sonogashira, Buchwald-Hartwig) led to the search for a practical synthesis of *p*- ^{18}F fluoroiodo- and *p*- ^{18}F fluorobromobenzene. *p*- ^{18}F Fluoroiodobenzene (**G**, X = iodine) can be obtained in poor yield from ^{18}F fluoride and a trimethylammonium precursor (**P7**). *p*- ^{18}F Fluorobromobenzene can be prepared in a more reproducible way from 5-bromo-2-nitrobenzaldehyde (radiochemical yields > 70%). The synthesis involves a two-step procedure: radiofluorination (F for NO₂ substitution), then a catalysed decarbonylation [190,191]. Also very efficient is the one-step reaction of ^{18}F fluoride with a suitable diaryliodonium salt (**P6**) giving >70% radiochemical yield [192–194].

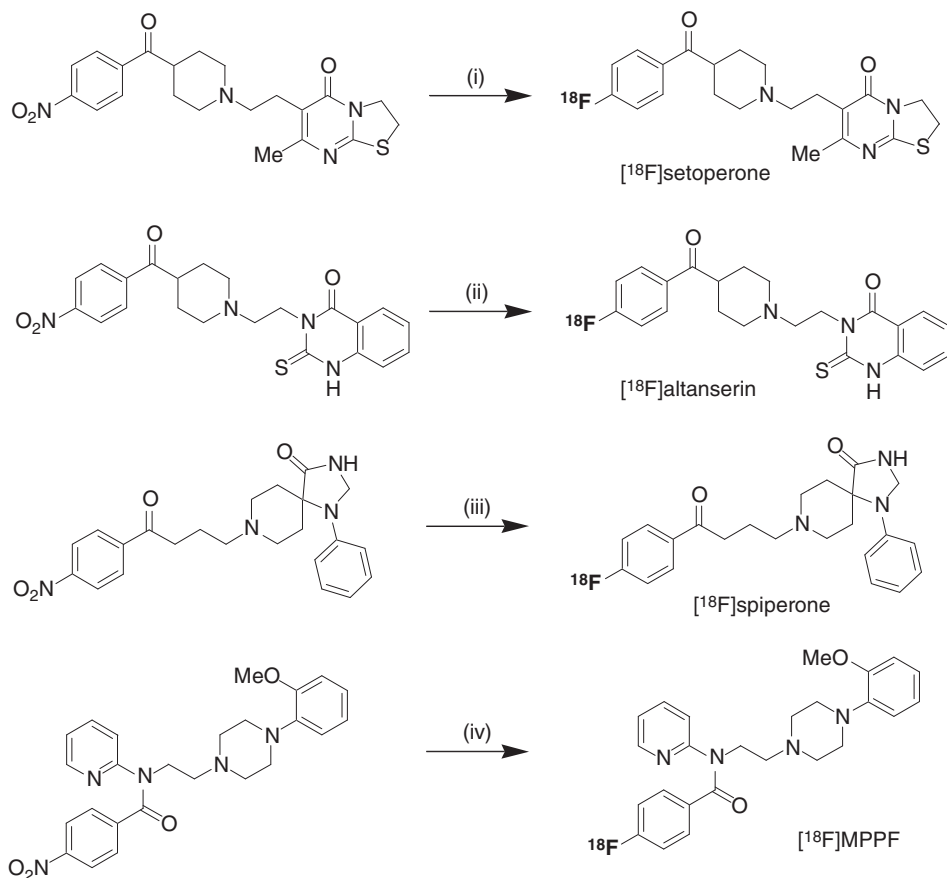
4.3.1.2. Other one-step syntheses involving aromatic nucleophilic radiofluorination

Examples of the relatively rare single-step nucleophilic aromatic radiofluorination of a more complex molecule are the syntheses of the two serotonergic 5HT_{2A} receptor ligands ^{18}F altanserin [195–197] and ^{18}F setoperone [198], the dopaminergic D₂ receptor ligand ^{18}F spiperone [130,199,200] and ^{18}F MPPF, a fluorinated analogue of the serotonergic 5HT_{1A} receptor ligand WAY-100635 [201]. They all illustrate the necessary activation of the aromatic nitro group, in this case by a carbonyl group *para* to the leaving group (Scheme 43).

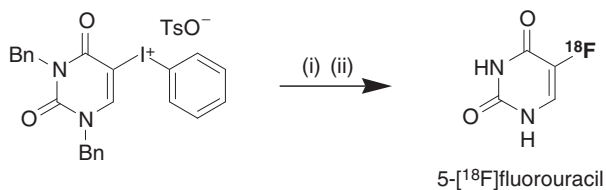
The exceptional case where no activating group is required is the use of diaryliodonium salts as precursors for labelling, permitting the fluorine-18-labelling of relatively electron-rich structures [192–194]. A recent example of successful application is the preparation of 5- ^{18}F fluorouracil in 40% radiochemical yield (Scheme 44) [202]. However, this methodology appears to be relatively difficult to use with complex structures [203–205].

4.3.1.3. Multi-step syntheses of a radiopharmaceutical involving an aromatic nucleophilic radiofluorination

An example of a multi-step radiosynthetic pathway is the no-carrier-added synthesis of 6- ^{18}F fluoro-L-DOPA (Scheme 45). The first step involves the preparation of 4,5-dimethoxy-2- ^{18}F fluorobenzaldehyde from the corresponding nitro-substituted benzaldehyde. The following steps involve its condensation with an asymmetric chiral inductor [206] followed by L-selectride reduction of the

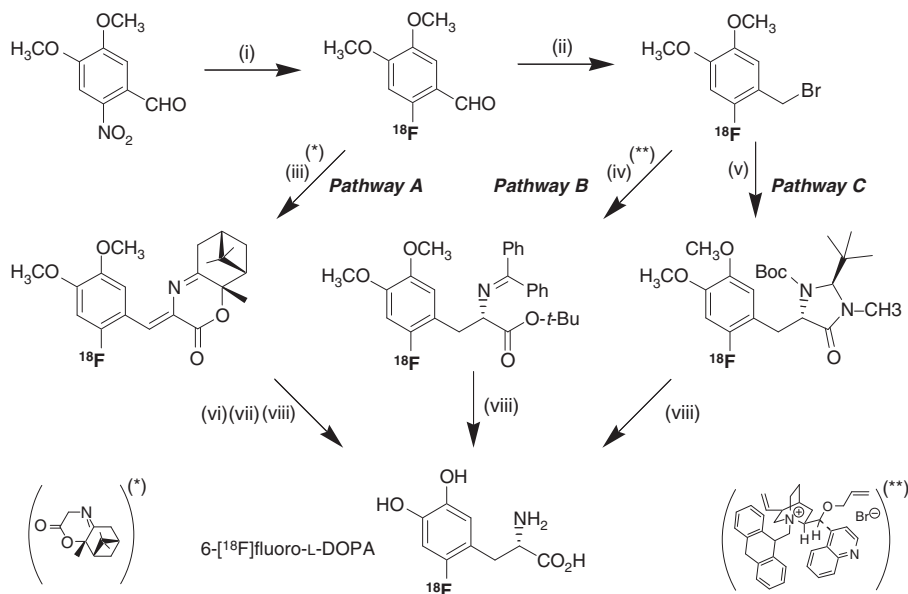


Scheme 43. (i) $\text{K}[^{18}\text{F}]\text{F-K}_{222}$, DMSO, $180\text{ }^{\circ}\text{C}$, 30 min (RCY: 55%); (ii) $\text{K}[^{18}\text{F}]\text{F-K}_{222}$, DMSO or DMF, microwave activation (300 W), 3–5 min (RCY: 32%); (iii) $\text{K}[^{18}\text{F}]\text{F-K}_{222}$, DMSO, $160\text{ }^{\circ}\text{C}$, 20–30 min (RCY: 15–20%); (iv) $\text{K}[^{18}\text{F}]\text{F-K}_{222}$, MeCN, microwave activation (500 W), 3 min (RCY: 25%).



Scheme 44. (i) $\text{K}[^{18}\text{F}]\text{F-K}_{222}$, MeCN, $90\text{ }^{\circ}\text{C}$, 40 min; (ii) BBr_3 , MeCN, $90\text{ }^{\circ}\text{C}$, 10 min.

olefinic double bond, hydrolysis and final deprotection of the hydroxy groups, leading to $6-[^{18}\text{F}]\text{fluoro-L-DOPA}$ in 3% radiochemical yield and an enantiomeric excess (ee) higher than 90% [Scheme 45, Pathway A: (i) (iii) (vi) (vii) (viii), total synthesis time: 125 min].

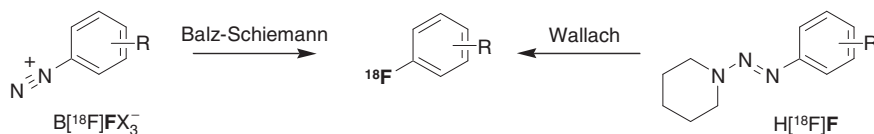


Scheme 45. (i) K[¹⁸F]F-K₂₂₂, DMSO, 140 °C, 20 min; (ii) NaBH₃CN or NaBH₄ (eventually fixed on alumina) then SOBr₂, THF, RT, 5 min; (iii) (6S,8S,8aS)-3,5,6,7,8,8a-hexahydro-7,7,8a-trimethyl-6,8-methano-2H-1,4-benzoxazin-2-one (*), NaH, THF, 20 min; (iv) *N*-(diphenylmethylene)glycine *tert*-butyl ester, (8 α ,9*R*)-*O*-allyl-1-(anthracen-9-ylmethyl)cinchonidinium bromide (**), toluene, CsOH or 50% KOH, 0 °C, 10 min; (v) (*S*)-1-(*tert*-butoxycarbonyl)-2-*tert*-butyl-3-methyl-4-imidazolidinone (Boc-BMI) lithium enolate, THF, −78 °C, 5 min; (vi) L-selectride, *tert*-BuOH, THF, −78 °C, 10 min; (vii) NH₂OH.HCl, EtOH, H₂O; (viii) aq. HI (47%), 200–220 °C, 15–20 min.

Alternative routes for the multi-step preparation of 6-[¹⁸F]fluoro-L-DOPA (given here as an example and also applicable to other amino acids) include the use of enantioselective benzylations using either a chiral auxiliary [Scheme 45, Pathway B: (i) (ii) (iv) (viii)] [207–209] or a chiral phase transfer catalyst [Scheme 45, Pathway C: (i) (ii) (v) (viii)] [210–212]. The latter approach, avoiding the use of dry reagents, is well suited to automation and enables the production of more than 200 mCi (7.4 GBq) of 6-[¹⁸F]fluoro-L-DOPA from 1.5 Ci (55.5 GBq) of starting [¹⁸F]fluoride [213].

4.3.1.4. The Balz-Schiemann and Wallach reactions

The Balz-Schiemann reaction (the thermal decomposition of an aryl diazonium salt, Scheme 46) was for many years the only practical method for the introduction of a fluorine atom into an aromatic ring not bearing electron-withdrawing substituents. This reaction, first reported in the late 1800s, was studied in fluorine-18 chemistry as early as 1967 [214]. It involves the generation of an aryl cation by thermal decomposition, which then reacts with solvent, nucleophiles or other species present to produce a substituted aromatic compound. Use of fluorine-18-labelled



Scheme 46. The Balz-Schiemann and the Wallach reactions.

tetrafluoroborate anion as the counter-ion for the diazonium salt led to the formation of the desired aryl ^{18}F fluoride. A drawback of this reaction is that only one fluorine atom is transferred from the tetrafluoroborate, giving maximum radiochemical yields of 25% (in practice 2–15% [215]). As the $\text{B}[^{18}\text{F}]\text{F}_4^-$ is formed by exchange with non-radioactive BF_4^- the specific radioactivities are low. Nevertheless, this labelling method has been successfully applied to the preparation of 4- ^{18}F fluorophenylalanine, 3- ^{18}F fluorotyrosine [215,216] and 5- ^{18}F fluoro-L-DOPA [217].

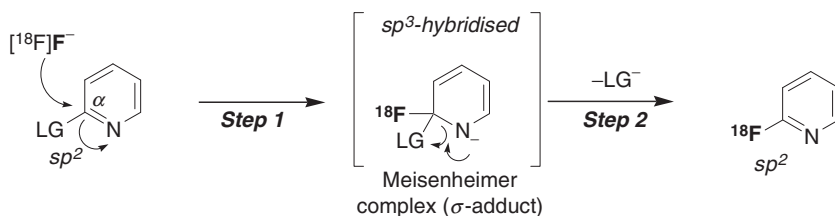
In order to increase the specific radioactivity, radiofluorinations have been carried out using aryl diazonium ^{18}F fluorotrichloroborates (prepared from *tetra*-butylammonium ^{18}F fluoride and the corresponding aryldiazoniumtetrachloroborates), giving on pyrolysis the expected aryl ^{18}F fluorides [218]. However, the development of this strategy has been limited by the difficulties encountered to prepare the tetrachloroborate in a pure and dry form and by the formation of chloroarenes as side products, which proved difficult to separate from the ^{18}F fluoroarene. Aryldiazonium compounds with no-halogen-containing anions have also been tried [219]. The best results were obtained with the 2,4,6-*tri-isopropyl*-phenylsulfonate anion, giving the expected aryl ^{18}F fluoride (4- ^{18}F fluorotoluene in this case) in 32% radiochemical yield.

The Wallach reaction, the thermal decomposition of an aryl triazene (Scheme 46), has also been attempted as an alternative to the Balz-Schiemann reaction [54,220,221]. Although a wide variety of experimental conditions have been tried, the radiochemical yields remain low.

4.3.2. Heteroaromatic series

4.3.2.1. The pyridine series

In the last decade the scope of nucleophilic radiofluorination has been open to *heteroaromatic* substitutions, particularly in the pyridine series [29,222–224], mainly promoted by the appearance of some important nicotinic receptor drug families, containing a fluoropyridine moiety. In stable-fluorine-19 chemistry one finds only a small number of examples of *heteroaromatic* nucleophilic fluorination leading to fluoropyridines and the like (fluoroquinolines, -isoquinolines, -naphthyridines and -pyridoquinolines). This is because these derivatives are usually prepared in good yields from the corresponding amino-substituted *heteroaromatic* compounds by treatment with sodium nitrite and HF or fluoboric acid. These methods, however, are unsuitable for high-specific-radioactivity fluorine-18 labelling.



Scheme 47. The addition–elimination mechanism of nucleophilic aromatic fluorination in the pyridine series.

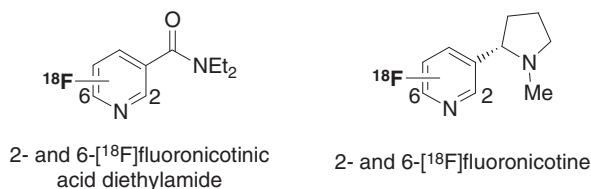


Fig. 5. Chemical structures of 2- and 6-[^{18}F]fluoronicotinic acid diethylamide as well as 2- and 6-[^{18}F]fluoronicotine.

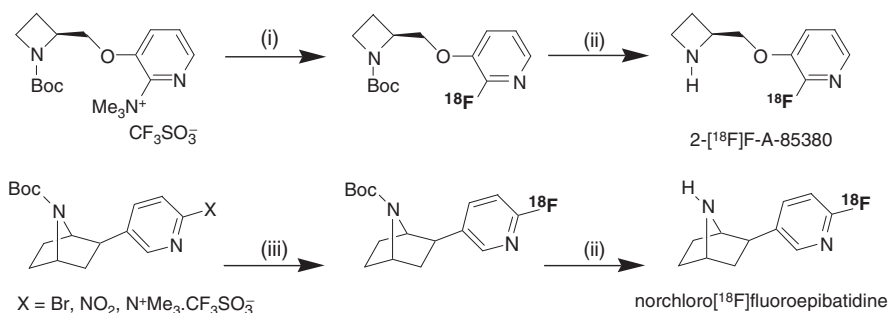
Heteroaromatic nucleophilic substitutions with [^{18}F]fluoride in the pyridine series (Scheme 47), like the aliphatic nucleophilic radiofluorinations (see Section 4.2), require only a good leaving group (a halogen or better a nitro- or a trimethylammonium group). There is no need for an electron-withdrawing substituent for activation of the aromatic ring as in *homoaromatic* nucleophilic radiofluorination, except if one considers fluorination *meta* to the ring nitrogen [85,225].

The earliest examples of such fluorine-18 labelling are 2- and 6-[^{18}F]fluoronicotinic acid diethylamide and 2- and 6-[^{18}F]fluoronicotine (Fig. 5). All were obtained in up to 40–50% radiochemical yield from the corresponding 2- and 6-chloro- (or bromo-) pyridine derivatives and [^{18}F]fluoride as its cesium salt, in melted acetamide or DMSO at about 200 °C for 30 min [226–229].

Today, these nucleophilic *heteroaromatic* radiofluorinations are generally performed in DMSO using the $\text{K}[^{18}\text{F}]\text{F}-\text{K}_{222}$ complex and conventional heating at a moderately high temperature (120–150 °C) or short 100-W microwave irradiation (1–2 min) and often lead to high radiochemical yields. Selected examples are the syntheses of the two selective central nicotinic cholinergic $\alpha_4\beta_2$ receptor ligands *norchloro*[^{18}F]fluoroepibatidine [230–233], obtained in overall 20–30% radiochemical yield, and 2-[^{18}F]F-A-85380 [234–236], obtained in overall 50–70% radiochemical yield (Scheme 48).

4.3.2.2. Other heterocyclic series

Heteroaromatic nucleophilic substitution with [^{18}F]fluoride was used once in the imidazo[4,5-d]pyrimidine series with the synthesis of 2- and 6-[^{18}F]fluoropurine (2- and 6-[^{18}F]fluoro-imidazo[4,5-b]pyrimidine) in 14 and 6% radiochemical yield,



Scheme 48. (i) K[¹⁸F]F-K₂₂₂, DMSO, 150 °C or microwave activation (100 W), 1–2 min; (ii) TFA, CH₂Cl₂, RT, 2–5 min; (iii) K[¹⁸F]F-K₂₂₂, DMSO, 150–180 °C, 10 min or K[¹⁸F]F-K₂₂₂, DMSO, microwave activation (100 W), 1–2.5 min.

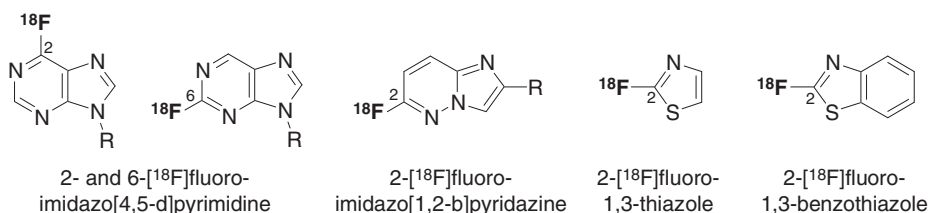


Fig. 6. Fluorine-18-labelled *heterocyclic* compounds other than [¹⁸F]fluoropyridines, obtained by nucleophilic radiofluorination.

respectively [237,238]. Recently fluorine-18-labelling of imidazo[1,2-b]pyridazine (43%), 1,3-thiazole (29%) and 1,3-benzothiazole (51%) derivatives was reported (Fig. 6) [239,240].

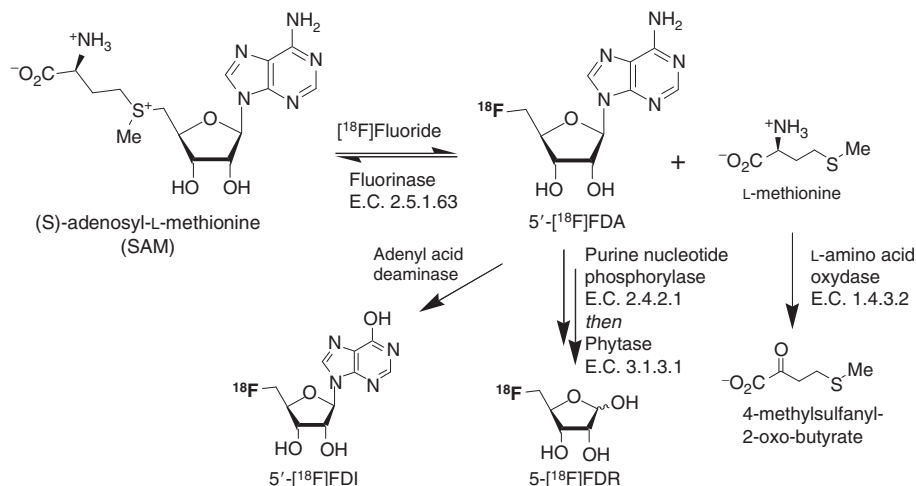
5. ENZYMATIC CARBON-[¹⁸F]FLUORINE BOND FORMATION

The use of enzymes in PET chemistry for the introduction of the radioactive label is an attractive strategy because enzymatic reactions are specific, often fast and without side products. Until recently this approach was restricted to carbon-11 chemistry and relatively few examples exist largely because of the lack of available suitable enzymes.

In fluorine-18 chemistry some enzymatic transformations of compounds already labelled with fluorine-18 have been reported: the synthesis of 6-[¹⁸F]fluoro-L-DOPA from 4-[¹⁸F]catechol by β -tyrosinase [241], the separation of racemic mixtures of [¹⁸F]fluoroaromatic amino acids by L-amino acylase [242] and the preparation of the coenzyme uridine diphospho-2-deoxy-2-[¹⁸F]fluoro- α -D-glucose from [¹⁸F]FDG-1-phosphate by UDP-glucose pyrophosphorylase [243]. In living nature compounds exhibiting a carbon–fluorine bond are very rare.

So far only a few dozen organofluorine compounds have been isolated from living organisms, for example fluoroacetic acid, 4-fluorothreonine and ω -fluoro-oleic acid [244–246]. The reason that nature has not invested in fluorine chemistry could be a combination of low availability of water-dissolved fluoride in the environment due to its tendency to form insoluble fluoride salts, and the low reactivity of water-solvated fluoride ion. However, in 2002, O'Hagan and collaborators [247] published the discovery of a biochemical fluorination reaction in a bacterial protein extract from *Streptomyces cattleya* converting S-adenosyl-L-methionine (SAM) to 5'-fluoro-5'-deoxyadenosine (5'-FDA). The same protein extract contained also the necessary enzymatic activity to convert 5'-FDA into fluoroacetic acid. In 2004, the same authors published the crystal structure of the enzyme and demonstrated a nucleophilic mechanism of fluorination [248,249].

Initial application of the wild-type enzyme, named fluorinase, to the radiosynthesis of 5'-[^{18}F]FDA gave only very low yields [250] but later great improvement was achieved with overexpressed recombinant fluorinase [251]. The enzyme catalyses a nucleophilic attack of [^{18}F]fluoride ion on SAM liberating one molecule of L-methionine as leaving group (Scheme 49). The enzymatic reaction being an equilibrium, yields could be improved considerably by a coupled enzyme strategy, either by taking away the L-methionine with L-amino acid oxidase (5'-[^{18}F]FDA yields up to 95%) or by concomitantly converting the 5'-[^{18}F]FDA to 5'-[^{18}F]fluoro-5'-deoxyinosine (5'-[^{18}F]FDI) by adenylic acid deaminase or to 5'-[^{18}F]fluoro-5-deoxy-D-ribose (5'-[^{18}F]FDR) by purine nucleotide phosphorylase and phytase in good radiochemical yields. Reaction times range between 1 and 4 h.



Scheme 49. Enzyme-assisted [^{18}F]fluorine-carbon bond formation using the recently discovered fluorinase.

6. THE PARTICULAR CASE OF MACROMOLECULE LABELLING WITH FLUORINE-18

Labelled high-molecular-weight bioactive chemical structures, such as single-stranded oligonucleotides, peptides and proteins, are increasingly proposed as radiopharmaceuticals and their applications are rapidly gaining importance in nuclear medicine [10,11,17]. The direct labelling of these macromolecules with fluorine-18 is, leaving aside some exceptions, not feasible. Labelling is therefore usually performed by conjugation of a prosthetic group, carrying the radioisotope, with a reactive function of the macromolecule (Fig. 7). This foreign-labelling strategy has the advantage of offering a flexibility in the choice of chemical routes, including those requiring drastic chemical conditions for the preparation of the labelled prosthetic group entity, while the conjugation of the latter with a macromolecule can then be done using the mild conditions needed to preserve the latter's integrity [11,12].

6.1. Reagents for the fluorine-18 labelling of peptides and proteins

Several fluorine-18-labelled reagents for coupling to peptides and proteins have been described (Fig. 8). Most of them were designed for coupling with the amino function of an amino acid residue (*N*-terminal α -NH₂ or internal lysine ϵ -NH₂) or

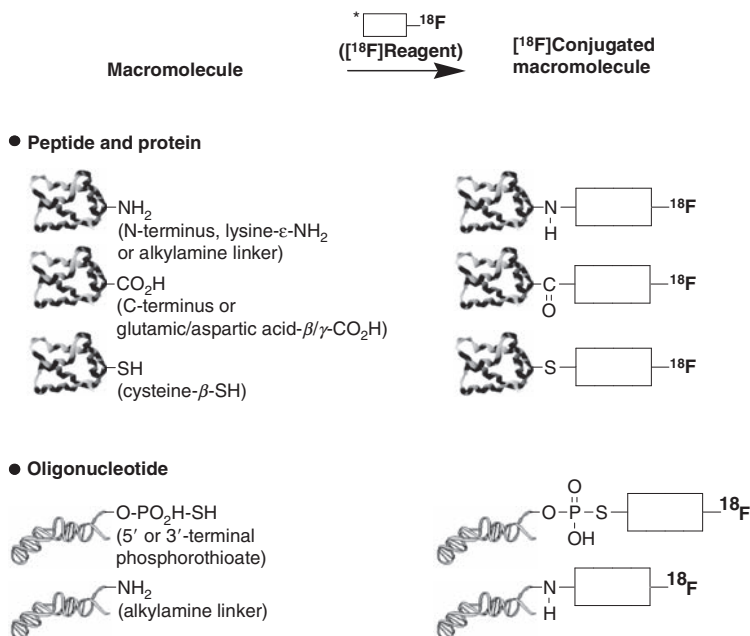


Fig. 7. Fluorine-18 labelling of macromolecules via conjugation strategies.

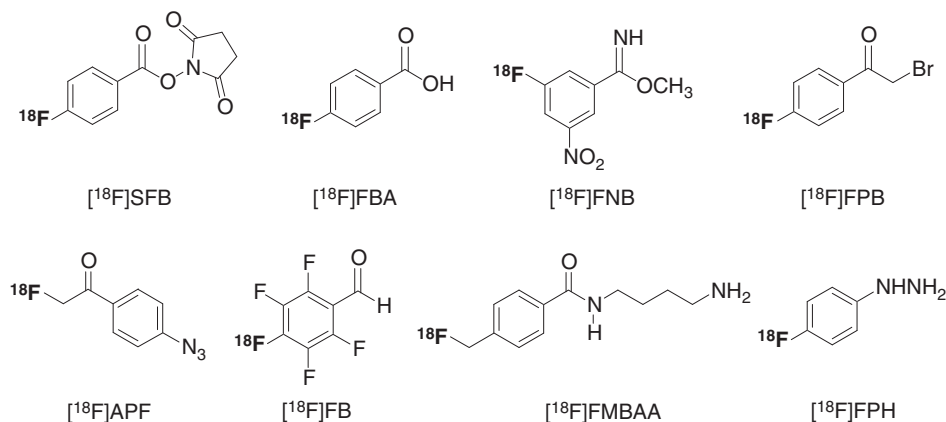


Fig. 8. Fluorine-18-labelled reagents for coupling with peptides and proteins via amino or carboxylic acid functions.

an alkylamine linker. The activated ester *N*-succinimidyl 4- $[^{18}\text{F}]$ fluorobenzoate ($[^{18}\text{F}]\text{SFB}$) [11,12,252–254] is the most popular prosthetic group, acting through an acylation reaction, besides other carboxylic acids or esters such as 4- $[^{18}\text{F}]$ fluorobenzoic acid ($[^{18}\text{F}]\text{FBA}$) [255], 2- $[^{18}\text{F}]$ fluoroacetic acid [256] or methyl 2- $[^{18}\text{F}]$ fluoropropionate [257] (the latter two not shown in Fig. 7). Activated esters such as *N*-succinimidyl 4- $[^{18}\text{F}]$ fluoromethylbenzoate [258,259] and *N*-succinimidyl 8-(4'- $[^{18}\text{F}]$ fluorobenzylamino)suberate [260] have also been reported (structures not shown). Imidation reactions, using 3- $[^{18}\text{F}]$ fluoro-5-nitrobenzimidate ($[^{18}\text{F}]\text{FNB}$) [10], have been described. Finally, alkylation reactions using 4- $[^{18}\text{F}]$ fluorophenacyl bromide ($[^{18}\text{F}]\text{FPB}$) [10] have been reported as well as photochemical conjugation using 4-azidophenacyl $[^{18}\text{F}]$ fluoride ($[^{18}\text{F}]\text{APF}$) [252,261] and reductive amination using *penta*[4- $[^{18}\text{F}]$ fluorobenzaldehyde ($[^{18}\text{F}]\text{FB}$) [262]. A much smaller number of fluorine-18-labelled reagents for the coupling to the carboxylic acid function (C-terminal $\alpha\text{-CO}_2\text{H}$ or internal glutamic/aspartic acid $\beta/\gamma\text{-CO}_2\text{H}$) have also been designed. To our knowledge, only two amines, 1-(4- $[^{18}\text{F}]$ fluoromethylbenzoyl)aminobutane-4-amine ($[^{18}\text{F}]\text{FMBA}$) [263] and 4- $[^{18}\text{F}]$ fluorophenylhydrazine ($[^{18}\text{F}]\text{FPH}$) [11], have been described for these amidation reactions.

Mainly because of the poor regioselectivity observed for the coupling of the above-mentioned reagents with macromolecules, which often leads to partial loss of the latter's biological properties, considerable attention has been paid to the design and development of thiol-selective key-derivatives. Indeed, the free thiol (or sulfhydryl) function is present only in cysteine residues (internal $\beta\text{-SH}$) and is not very common in most peptides and proteins. Thiol-reactive agents have therefore been used to modify peptides and proteins at specific sites [11,264,265], providing a means of high regioselectivity in contrast to the

carboxylate- and amine-reactive reagents described above. In the late 1980s, Shiue and collaborators described, in an abstract, the preparation of 1-(4-[^{18}F]fluorophenyl)pyrrole-2,5-dione ([^{18}F]FPPD) and *N*-[3-(2,5-dioxo-2,5-dihydropyrrol-1-yl)phenyl]-4-[^{18}F]fluorobenzamide ([^{18}F]DDPFB) and their coupling to proteins [266]. Based on this work some other *N*-substituted maleimides have now been reported and their coupling to peptides and proteins has been optimised (Fig. 9).

N-[4-[(4-[^{18}F]fluorobenzylidene)amino-oxy]butyl]maleimide ([^{18}F]FBABM) was synthesised in two steps, involving the preparation of 4-[^{18}F]fluorobenzaldehyde (see Section 4.3.1.1), in an overall radiochemical yield of 35% in 60 min [267], whereas *N*-[2-(4-[^{18}F]fluorobenzamido)ethyl]maleimide ([^{18}F]FBEM) was synthesised in three steps via 4-[^{18}F]fluorobenzoic acid (see Section 4.3.1.1) in an overall radiochemical yield of 12% in 150 min [268]. Finally, based on the successful use of nucleophilic *heteroaromatic ortho*-radiofluorination in the pyridine series (see Section 4.3.2.1), 1-[3-(2-[^{18}F]fluoropyridin-3-yloxy)propyl]pyrrole-2,5-dione was prepared in 17–20% non-decay-corrected radiochemical yield in a three-step pathway taking less than 110 min [13,269]. These three reagents have been successfully coupled to peptides and proteins (>80% radiochemical yield in 10 min).

Noteworthy is the labelling of so-called peptide nucleic acids (PNAs). These constitute a class of synthetic macromolecules where the deoxyribose phosphate backbone of DNA is replaced by the pseudo-peptide *N*-(2-aminoethyl)glycyl backbone, while retaining the nucleobases of DNA [270,271]. PNAs have been labelled at a terminal cysteine-site using *N*-(4-[^{18}F]fluorobenzyl)-2-bromoacetamide [272–274], a reagent belonging to another class of thiol-selective reagents,

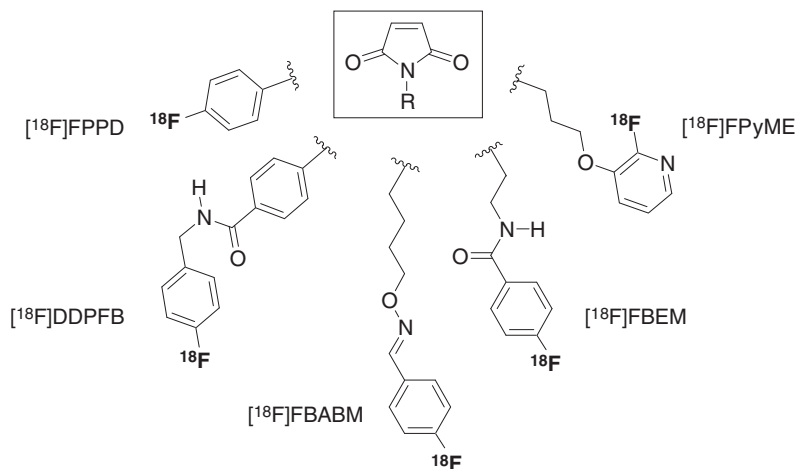


Fig. 9. Fluorine-18-labelled *N*-substituted maleimides for coupling to peptides and proteins via sulfhydryl functions.

the haloacetamide series, originally designed for the labelling of oligonucleotides (see Section 6.2).

A fast and straightforward approach to the large-scale production of fluorine-18-labelled peptides is based on the chemoselective oxime formation between an unprotected amino-oxy-functionalised peptide and 4- ^{18}F fluorobenzaldehyde (see Section 4.3.1.1). This reaction can be performed in aqueous media [275,276].

6.2. Reagents for the fluorine-18 labelling of oligonucleotides

According to the available literature, five fluorine-18-labelling reagents have been prepared and used for prosthetic conjugation with a single-stranded oligonucleotide [14,188,189,277–281].

N-(4- ^{18}F fluorobenzyl)-2-bromoacetamide (^{18}F FBnBrA, Fig. 10) was designed as a reagent of versatile application, the benzyl function carrying the fluorine-18 atom and the 2-bromoacetamide moiety ensuring regioselective conjugation with an oligonucleotide bearing a phosphorothioate monoester group at its 3'- or 5'-end [14,188,189,280,281]. This reagent could be obtained in 16–25% overall radiochemical yield in 90 min total synthesis time and has been applied to the fluorine-18 labelling of natural phosphodiester DNA oligodeoxyribonucleotides. The strategy has also been applied to all the common chemical modifications of oligonucleotides, such as full-length phosphorothioate diester internucleosidic-bond deoxyribonucleotides, hybrid methylphosphonate/phosphodiester internucleosidic-bond deoxyribonucleotides and 2'-*O*-methyl-modified oligoribonucleotides [14,15,188,189,280,282,283]. It has finally been applied to the labelling [272–274,281,284] of L-RNA and L-DNA (called Spiegelmers [285,286]) and PNAs (originally designed as ligands for the recognition of double-stranded DNA [270,271]). 4-(^{18}F Fluoromethyl)phenyl isothiocyanate (^{18}F FMPI) is a reagent that was conjugated with a single-stranded 18-mer oligonucleotide provided with a hexylamine linker at the 5'-end [277]. *N*-succinimidyl-4- ^{18}F fluorobenzoate (^{18}F SFB, see Section 6.1), known in the conjugation of proteins and peptides using an amino function (α or $\epsilon\text{-NH}_2\text{-Lys}$) [10–12], as well as the photosensitive 3-azido-5-nitrobenzyl ^{18}F fluoride (^{18}F ANBF) have been conjugated with single-stranded 18-mer oligonucleotides provided with a hexylamine linker at the 5'-end [278,279]. Finally, a new haloacetamide reagent

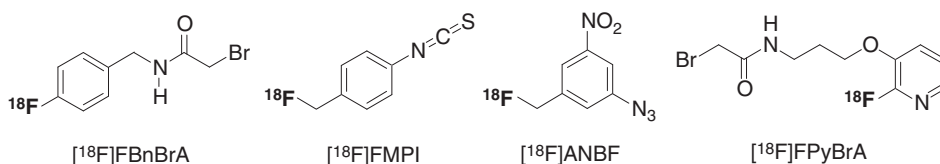


Fig. 10. Fluorine-18-labelled reagents for coupling to single-stranded oligonucleotides.

N-[3-(2-[^{18}F]fluoropyridin-3-yloxy)-propyl]-2-bromoacetamide ([^{18}F]FPyBrA) was recently prepared by nucleophilic *heteroaromatic* radiofluorination using a three-step radiochemical pathway and obtained in 20% overall non-decay-corrected yield in less than 85 min. In this reagent, the pyridinyl moiety carries the radioactive fluorine and the 2-bromoacetamide function ensures the alkylation of phosphorothioate monoester groups at the 3'- or 5'-end of a single-stranded oligonucleotide [18].

7. CONCLUSION AND PERSPECTIVES

The positron-emitting radiohalogen fluorine-18 is now probably the most widely used PET radionuclide as a result of its relative facile production in large quantities, its convenient half-life and its nearly optimal decay properties. Fluorine-18 has been successfully used for the labelling of thousands of molecules, many being drug based but also macromolecules of biological interest such as peptides, proteins and oligonucleotides.

As has been exemplified in this chapter, fluorinations with fluorine-18 can be classified into two categories: (1) the nucleophilic reactions, which usually involve no-carrier-added [^{18}F]fluoride of high-specific radioactivity as its $\text{K}[^{18}\text{F}]\text{F}-\text{K}_{222}$ complex and include substitutions in the aliphatic and the *homoaromatic* series and (2) the electrophilic reactions, which mainly use moderately low-specific radioactivity molecular [^{18}F]fluorine, or other reagents prepared from it, such as acetyl [^{18}F]hypofluorite, and include addition across double bonds, reactions with carbanions and especially fluorodehydrogenation and fluorodemetalation reactions.

The chemistry of fluorine-18 has now reached a certain maturity which is shown first of all in nucleophilic reactions with [^{18}F]fluoride. These now account for the vast majority of radiosyntheses and new developments will certainly continue to emerge. The recent use of iodonium salts as precursors for labelling and progress in *heteroaromatic* nucleophilic radiofluorination are two examples. Electrophilic radiofluorination methodology has been stagnant for a long time but is showing signs of new impetus with several recent attempts to increase the specific radioactivity of electrophilic radiofluorinating agents. This approach deserves more intensive research in the future as it might considerably enrich the arsenal of fluorine-18 chemistry. Technical progress in automation will remain essential in the further unfolding of fluorine-18 in nuclear medicine with microfluidics technology possibly playing an innovative role in this.

The availability of fluorine-18 is expected still to increase considerably in the near future seeing the growing demand for [^{18}F]FDG, which will be the most important PET radiopharmaceutical for times to come. Other fluorine-18-labelled analogues of natural compounds in the clinic are emerging such as [^{18}F]fluorothymidine and [^{18}F]fluorocholine for oncology and also 6-[^{18}F]fluoro-L-DOPA for brain studies. Moreover, the growing importance of fluorine-containing

compounds in industrial pharmaceutical drug design is opening up a wide field of possibilities of direct fluorine-18 labelling of drug-like compounds, either to aid the process of development and approval of such a drug or to provide new PET radiopharmaceuticals. Another research axe with a bright future is the prosthetic fluorine-18 labelling of peptides and other macromolecules.

The synthesis of complex structures labelled with fluorine-18 remains a challenge but undoubtedly, fluorine-18 is already, and will continue to be, a royal gateway to success in molecular imaging with PET.

REFERENCES

- [1] P.E. Valk, D.L. Bailey, D.W. Townsend, M.N. Maisey, *Positron Emission Tomography—Basic Science and Clinical Practice*, Springer, London - Berlin - Heidelberg - New York - Hong Kong - Milan - Paris - Tokyo, (2003).
- [2] G. Stöcklin, V.W. Pike, *Radiopharmaceuticals for Positron Emission Tomography*, Kluwer Academic Publishers, Dordrecht - Boston - London, (1993).
- [3] M.J. Welch, C.S. Redvanly, *Handbook of Radiopharmaceuticals—Radiochemistry and Applications*, Wiley, Chichester, (2003).
- [4] E. Browne, J.M. Dairiki, R.E. Doebl, *Table of Isotopes*, Wiley-Interscience Publishers, New York - Chichester - Brisbane - Toronto, (1978).
- [5] M.J. Welch, *Radiopharmaceuticals and other Compounds Labeled with Short-Lived Radionuclides*, Pergamon Press, Oxford - New York - Toronto - Sydney - Paris - Frankfurt, (1977).
- [6] M.R. Kilbourn, M.J. Welch, Fluorine-18 labeled receptor based radiopharmaceuticals, *Appl. Radiat. Isot.* 37 (1986) 677–683.
- [7] M.R. Kilbourn, *Fluorine-18 Labeling of Radiopharmaceuticals*, Nuclear Science Series, Washington, (1990).
- [8] M.C. Lasne, C. Perrio, J. Rouden, L. Barré, D. Roeda, F. Dollé, C. Crouzel, Chemistry of beta⁺-emitting compounds based on fluorine-18, in: W. Krause (Ed.), *Topics in Current Chemistry*, Vol. 222, Springer-Verlag, Berlin - Heidelberg, 2002, pp. 201–258.
- [9] N.S. Mason, C.A. Mathis, Radiohalogens for PET imaging, in: P.E. Valk, D.L. Bailey, D.W. Townsend, M.N. Maisey (Eds.), *Positron Emission Tomography—Basic Science and Clinical Practice*, Springer, London - Berlin - Heidelberg - New York - Hong Kong - Milan - Paris - Tokyo, 2003, pp. 217–236.
- [10] M.R. Kilbourn, C.S. Dence, M.J. Welch, C.J. Mathias, Fluorine-18 labeling of proteins, *J. Nucl. Med.* 28 (1987) 462–470.
- [11] D.S. Wilbur, Radiohalogenation of proteins: An overview of radionuclides, labeling methods, and reagents for conjugate labeling, *Bioconj. Chem.* 3 (1992) 433–470.
- [12] S.M. Okarvi, Recent progress in fluorine-18 labelled peptide radiopharmaceuticals, *Eur. J. Nucl. Med.* 28 (2001) 929–938.
- [13] B. de Bruin, B. Kuhnast, F. Hinnen, L. Yaouancq, M. Amessou, L. Johannes, A. Samson, R. Boisgard, B. Tavitian, F. Dollé, 1-[3-(2-[¹⁸F]Fluoropyridin-3-yloxy)propyl]pyrrole-2,5-dione: Design, synthesis and radiosynthesis of a new [¹⁸F]fluoropyridine-based maleimide reagent for the labeling of peptides and proteins, *Bioconj. Chem.* 16 (2005) 406–420.
- [14] F. Dollé, F. Hinnen, F. Vaufrey, B. Tavitian, C. Crouzel, A general method for labeling oligodeoxynucleotides with ¹⁸F for *in vivo* PET imaging, *J. Label. Compds Radiopharm.* 39 (1997) 319–330.

- [15] B. Tavitian, S. Terrazzino, B. Kuhnast, S. Marzabal, O. Stettler, F. Dollé, J.R. Deverre, A. Jobert, F. Hinnen, B. Bendriem, C. Crouzel, L. DiGiamberardino, *In vivo* imaging of oligonucleotides with positron emission tomography, *Nat. Med.* 4 (1998) 467–471.
- [16] B. Tavitian, *In vivo* imaging with oligonucleotides for diagnosis and drug development, *Gut* 52 (2003) 40–47.
- [17] B. Tavitian, Oligonucleotides as radiopharmaceuticals, in: Ernst Schering Research Foundation (Ed.), *Molecular Imaging*, Vol. 49, Springer-Verlag, Berlin - Heidelberg - New York, 2004, pp. 1–34.
- [18] B. Kuhnast, B. Lagnel - de Bruin, F. Hinnen, B. Tavitian, F. Dollé, Design and synthesis of a new [^{18}F]fluoropyridine-based haloacetamide reagent for the labeling of oligonucleotides: 2-Bromo-N-[3-(2-[^{18}F]fluoro-pyridin-3-yloxy)-propyl]-acetamide, *Bioconj. Chem.* 15 (2004) 617–627.
- [19] S.M. Qaim, G. Stöcklin, Production of some medically important short-lived neutron-deficient radioisotopes of halogens, *Radiochim. Acta* 34 (1983) 25–40.
- [20] G.L. Stöcklin, Is there a future for clinical fluorine-18 radiopharmaceuticals (excluding FDG)? *Eur. J. Nucl. Med.* 25 (1998) 1612–1616.
- [21] L. Varagnolo, M.P.M. Stokkel, U. Mazzi, E.K.J. Pauwels, ^{18}F -Labeled radiopharmaceuticals for PET in oncology, excluding FDG, *Nucl. Med. Biol.* 27 (2000) 103–112.
- [22] O. Matsson, J. Persson, B.S. Axelsson, B. Långström, Fluorine kinetic isotope effects, *J. Am. Chem. Soc.* 115 (1993) 5288–5289.
- [23] J.S. Fowler, A.P. Wolf, Positron-emitter-labeled compounds: Priorities and problems, in: M. Phelps, J. Mazziotta, H. Schelbert (Eds.), *Positron Emission Tomography and Autoradiography: Principles and Applications for the Brain and Heart*, Raven Press, New York, 1986, pp. 391–450.
- [24] A. Bondi, Van der Waals volumes and radii, *J. Phys. Chem.* 68 (1964) 441–451.
- [25] T. Hiyama, *Organofluorine Compounds—Chemistry and Applications*, Springer, Berlin - Heidelberg - New York - Barcelona - Hong Kong - London - Milan - Paris - Singapore - Tokyo, (2000).
- [26] B.E. Smart, Fluorine substituent effects (on bioactivity), *J. Fluor. Chem.* 109 (2001) 3–11.
- [27] R.C. Weast, M.J. Astle, *CRC Handbook of Chemistry and Physics*, 65th edition, CRC Press Inc., Boca Raton, (1984).
- [28] J.H. Clark, J.M. Miller, Hydrogen bonding in organic synthesis. 3. Hydrogen bond assisted reactions of cyclic organic hydrogen bond electron acceptors with halogenoalkanes in presence of potassium fluoride, *J. Am. Chem. Soc.* 99 (1977) 498–504.
- [29] F. Dollé, Fluorine-18-labelled fluoropyridines: Advances in radiopharmaceutical design, *Curr. Pharm. Des.* 11 (2005) 3221–3235.
- [30] B. Långström, T. Kihlberg, M. Bergström, G. Antoni, M. Björkman, B.H. Forngren, T. Forngren, P. Hartvig, K. Markides, U. Yngve, M. Ogren, Compounds labelled with short-lived beta-plus-emitting radionuclides and some applications in life sciences. The importance of time as a parameter, *Acta Chem. Scand.* 53 (1999) 651–669.
- [31] D.L. Alexoff, Automation for the synthesis and application of PET radiopharmaceuticals, in: M.J. Welch, C.S. Redvanly, (Eds.), *Handbook of Radiopharmaceuticals—Radiochemistry and Applications*, Wiley, Chichester, 2003, pp. 283–305.
- [32] D.J. Schlyer, Production of radionuclides in accelerators, in: M.J. Welch, C.S. Redvanly (Eds.), *Handbook of Radiopharmaceuticals—Radiochemistry and Applications*, Wiley, Chichester, 2003, pp. 1–70.
- [33] T.J. Ruth, Accelerators available for isotope production, in: M.J. Welch, C.S. Redvanly (Eds.), *Handbook of Radiopharmaceuticals—Radiochemistry and Applications*, Wiley, Chichester, 2003, pp. 71–86.
- [34] L.F. Mausner, S. Mirzadeh, Reactor production of radionuclides, in: M.J. Welch, C.S. Redvanly (Eds.), *Handbook of Radiopharmaceuticals—Radiochemistry and Applications*, Wiley, Chichester, 2003, pp. 86–118.

- [35] T.J. Ruth, A.P. Wolf, Absolute cross section for the production of ^{18}F via the $^{18}\text{O}(\text{p},\text{n})^{18}\text{F}$ reaction, *Radiochim. Acta* 26 (1979) 21–25.
- [36] M. Guillaume, A. Luxen, B. Nebeling, M. Argentini, J. Clark, V.W. Pike, Recommendations for F-18 production, *Appl. Radiat. Isot.* 42 (1991) 749–762.
- [37] R.J. Nickles, M.E. Daube, T.J. Ruth, An O_2 target for the production of $[\text{F-18}]\text{F}_2$, *Appl. Radiat. Isot.* 35 (1984) 117–122.
- [38] J. Bergman, O. Solin, Fluorine-18-labeled fluorine gas for synthesis of tracer molecules, *Nucl. Med. Biol.* 24 (1997) 677–683.
- [39] P.H. Elsinga, Radiopharmaceutical chemistry for positron emission tomography, *Methods* 27 (2002) 208–217.
- [40] H.J. Wester, ^{18}F : Labeling chemistry and labeled compounds, in: A. Vertes (Ed.), *Handbook of Nuclear Chemistry*, Vol. 4, Kluwer Academic Publishers, Dordrecht, 2003, pp. 167–209.
- [41] R.A. Ferrieri, Production and application of synthetic precursors labeled with carbon-11 and fluorine-18, in: M.J. Welch, C.S. Redvanly (Eds.), *Handbook of Radiopharmaceuticals—Radiochemistry and Applications*, Wiley, Chichester, 2003, pp. 229–282.
- [42] S.E. Snyder, M.R. Kilbourn, Chemistry of fluorine-18 radiopharmaceuticals, in: M. J. Welch, C.S. Redvanly (Eds.), *Handbook of Radiopharmaceuticals—Radiochemistry and Applications*, Wiley, Chichester, 2003, pp. 195–228.
- [43] T. Nozaki, Y. Tanaka, A. Shimamura, T. Karasawa, The preparation of anhydrous H^{18}F , *Int. J. Appl. Radiat. Isot.* 19 (1968) 27–32.
- [44] G. Blessing, H.H. Coenen, K. Franken, S.M. Qaim, Production of $[\text{F-18}]\text{F}_2$, HF (F-18) and F-18 (aq) using the $\text{Ne-20}(\text{d},\alpha)\text{F-18}$ process, *Appl. Radiat. Isot.* 37 (1986) 1135–1139.
- [45] R.M. Lambrecht, R. Neirinckx, A.P. Wolf, Cyclotron isotopes and radiopharmaceuticals—XXIII. Novel anhydrous ^{18}F -fluorinating intermediates, *Int. J. Appl. Radiat. Isot.* 29 (1978) 175–183.
- [46] C. Crouzel, D. Comar, Production of carrier-free ^{18}F -hydrofluoric acid, *Int. J. Appl. Radiat. Isot.* 29 (1978) 407–408.
- [47] J.C. Clark, F. Oberdorfer, Thermal characteristics of the release of fluorine-18 from an iconel-600 gas target, *J. Label. Compds Radiopharm.* 19 (1982) 1337.
- [48] F. Helus, W. Maierborst, U. Sahm, L.I. Wiebe, F-18 Cyclotron production methods, *Radiochem. Radioanal. Lett.* 38 (1979) 395–410.
- [49] R.A. Ferrieri, R.R. MacGregor, S. Rosenthal, D.J. Schlyer, J.S. Fowler, A.P. Wolf, A $\text{CF}_4\text{-H}_2\text{-Ne}$ gas target for reproducible high yields of anhydrous H^{18}F , *J. Label. Compds Radiopharm.* 19 (1982) 1620–1622.
- [50] J.C. Clark, R.W. Goulding, M. Roman, A.J. Palmer, Preparation of fluorine-18-labeled compounds using a recirculatory neon target, *Radiochem. Radioanal. Lett.* 14 (1973) 101–108.
- [51] J.R. Dahl, R. Lee, R.E. Bigler, B. Schmall, J.E. Aber, A new target system for the preparation of no-carrier-added F-18 fluorinated compounds, *Int. J. Appl. Radiat. Isot.* 34 (1983) 693–700.
- [52] R.E. Ehrenkauf, R.R. MacGregor, A.P. Wolf, J.S. Fowler, T.J. Ruth, D.J. Schlyer, B.W. Wieland, Production of H^{18}F by deuteron irradiation of a neon-hydrogen gas-target, *Radiochim. Acta* 33 (1983) 49–56.
- [53] M.S. Berridge, C. Crouzel, D. Comar, No-carrier-added ^{18}F -fluoride in organic solvents: Production and labeling results, *J. Label. Compds Radiopharm.* 19 (1982) 1639–1640.
- [54] M.S. Berridge, C. Crouzel, D. Comar, Aromatic fluorination with n.c.a. fluoride: A comparative study, *J. Label. Compds Radiopharm.* 22 (1985) 687–694.
- [55] E. Briard, V.W. Pike, Substitution-reduction: An alternative process for the $[\text{F-18}]\text{N}$ - (2-fluoroethylation) of anilines, *J. Label. Compds Radiopharm.* 47 (2004) 217–232.
- [56] A.D. Windhorst, R.P. Klok, C.L. Koolen, G.W.M. Visser, J.D.M. Herscheid, Labeling of $[\text{F-18}]\text{flumazenil}$ via instant fluorination, a new nucleophilic fluorination method, *J. Label. Compds Radiopharm.* 44 (2001) S930–S932.

- [57] M.G. Straatmann, M.J. Welch, ^{18}F -labeled diethylaminosulfur trifluoride. DAST: An F-for-OH fluorinating agent, *J. Nucl. Med.* 18 (1977) 151–158.
- [58] M.G. Straatmann, M.J. Welch, ^{18}F -DAST as a reagent in the synthesis of an ^{18}F -sugar, *J. Label. Compds Radiopharm.* 13 (1977) 210.
- [59] G. Schrobilgen, G. Firnau, R. Chirakal, E.S. Garnett, Synthesis of xenon difluoride- ^{18}F , a novel agent for the preparation of fluorine-18 radiopharmaceuticals, *J. Chem. Soc. Chem. Comm.* 4 (1981) 198–199.
- [60] G. Firnau, R. Chirakal, S. Sood, Radiofluorination with xenon difluoride: L-6- $^{[18]\text{F}}$ fluoro-DOPA, *J. Label. Compds Radiopharm.* 18 (1981) 7–8.
- [61] S. Sood, G. Firnau, E.S. Garnett, Radiofluorination with XeF_2 : A new high yield synthesis of ^{18}F -2-fluoro-2-deoxy-D-glucose, *Int. J. Appl. Radiat. Isot.* 34 (1983) 743–746.
- [62] C.Y. Shiue, K.C. To, A.P. Wolf, A rapid synthesis of 2-deoxy-2-fluoro-D-glucose from xenon difluoride suitable for labelling with ^{18}F , *J. Label. Compds Radiopharm.* 20 (1983) 157–162.
- [63] A. Jordanova, J. Steinbach, B. Johannsen, Radiofluorination of electron rich aromatic compounds with no carrier added $^{[18]\text{F}}$ perchlorylfluoride, *J. Label. Compds Radiopharm.* 44 (2001) S901.
- [64] Y.S. Choe, P.J. Lidström, D.Y. Chi, T.A. Bonasera, M.J. Welch, J.A. Katzenellenbogen, Synthesis of 11-beta- $^{[18]\text{F}}$ fluoro-5-alpha-dihydrotestosterone and 11-beta- $^{[18]\text{F}}$ fluoro-19-nor-5-alpha-dihydrotestosterone—Preparation via halofluorination-reduction, receptor-binding, and tissue distribution, *J. Med. Chem.* 38 (1995) 816–825.
- [65] Y.S. Choe, T.A. Bonasera, D.Y. Chi, M.J. Welch, J.A. Katzenellenbogen, 6-alpha- $^{[18]\text{F}}$ fluoroprogesterone—Synthesis via halofluorination-oxidation, receptor-binding and tissue distribution, *Nucl. Med. Biol.* 22 (1995) 635–642.
- [66] D.Y. Chi, P.J. Lidström, Y.S. Choe, T.A. Bonasera, M.J. Welch, J.A. Katzenellenbogen, Bromo $^{[18]\text{F}}$ fluorination of cyclohexenes—A method for the preparation of $^{[18]\text{F}}$ fluorocyclohexanes, *J. Fluor. Chem.* 71 (1995) 143–147.
- [67] M. Welch, J.F. Lifton, P.P. Gaspar, Production of ^{18}F for bone scanning from the $^{20}\text{Ne}(\text{d},\alpha)^{18}\text{F}$ reaction via fluorine-18 labeled nitrosyl fluoride. A selective fluorinating agent, *J. Nucl. Med.* 12 (1971) 405.
- [68] S. Rozen, Elemental fluorine as a legitimate reagent for selective fluorination of organic compounds, *Acc. Chem. Res.* 21 (1988) 307–312.
- [69] J.A. Wilkinson, Recent advances in the selective formation of the C-F bond, *Chem. Rev.* 92 (1992) 505–519.
- [70] M.S. Berridge, T.J. Tewson, Chemistry of ^{18}F -radiopharmaceuticals, *Appl. Radiat. Isot.* 37 (1986) 685–694.
- [71] V. Casella, T. Ido, A.P. Wolf, J.S. Fowler, R.R. MacGregor, T.J. Ruth, Anhydrous F-18 labeled elemental fluorine for radiopharmaceutical preparation, *J. Nucl. Med.* 21 (1980) 750–757.
- [72] G.T. Bida, R.L. Ehrenkaufer, A.P. Wolf, J.S. Fowler, R.R. MacGregor, T.J. Ruth, The effect of target-gas purity on the chemical form of F-18 during ^{18}F - F_2 production using the neon/fluorine target, *J. Nucl. Med.* 21 (1980) 758–762.
- [73] R.D. Chambers, C.J. Skinner, J. Hutchinson, J. Thomson, Elemental fluorine.1. Synthesis of fluoroaromatic compounds, *J. Chem. Soc. Perkin Trans. 1* (1996) 605–609.
- [74] J.S. Moilliet, The use of elemental fluorine for selective direct fluorinations, *J. Fluor. Chem.* 109 (2001) 13–17.
- [75] R.D. Neirircks, R.M. Lambrecht, A.P. Wolf, Cyclotron isotopes and radiopharmaceuticals-XXV: An anhydrous ^{18}F -fluorinating intermediate—trifluoromethyl hypofluorite, *Int. J. Appl. Radiat. Isot.* 29 (1978) 323–327.
- [76] C.Y. Shiue, P.A. Salvadori, A.P. Wolf, A new synthesis of 2-deoxy-2- $^{[18]\text{F}}$ fluoro-D-glucose from ^{18}F -labeled acetyl hypofluorite, *J. Nucl. Med.* 23 (1982) 899–903.
- [77] M. Haaparanta, J. Bergman, O. Solin, D. Roeda, A remotely controlled system for the routine synthesis of ^{18}F -2-fluoro-2-deoxy-D-glucose, *Nuklearmedizin* (suppl. 21) (1984) 823–825.

- [78] R.E. Ehrenkaufer, J.F. Potocki, D.M. Jewett, Simple synthesis of F-18-labeled 2-fluoro-2-deoxy-D-glucose, *J. Nucl. Med.* 25 (1984) 333–337.
- [79] R.E. Ehrenkaufer, R.R. MacGregor, Synthesis of [^{18}F]-perchloryl fluoride and its reactions with functionalized aryllithiums, *Int. J. Appl. Radiat. Isot.* 34 (1983) 613–615.
- [80] R. Chirakal, G. Firnau, J.G. Schrobilgen, J. McKay, E.S. Garnett, The synthesis of [^{18}F]xenon difluoride from [^{18}F]fluorine gas, *Int. J. Appl. Radiat. Isot.* 35 (1984) 401–404.
- [81] M. Constantinou, F.I. Aigbirhio, R.G. Smith, C.A. Ramsden, V.W. Pike, Xenon difluoride exchanges fluoride under mild conditions: A simple preparation of [^{18}F]xenon difluoride for PET and mechanistic studies, *J. Am. Chem. Soc.* 123 (2001) 1780–1781.
- [82] F. Oberdorfer, E. Hofmann, W. Maier-Borst, Preparation of a new fluorine-18-labelled precursor: 1-[^{18}F]fluoro-2-pyridone, *Appl. Radiat. Isot.* 39 (1988) 685–688.
- [83] F. Oberdorfer, E. Hofmann, W. Maier-Borst, Preparation of 18F-labeled N-fluoropyridinium triflate, *J. Label. Compds Radiopharm.* 25 (1988) 999–1005.
- [84] N. Satyamurthy, G.T. Bida, M.E. Phelps, J.R. Barrio, Fluorine-18 labeled N-[^{18}F] fluoro-N-alkylsulfonamides: Novel reagents for mild and regioselective radiofluorination, *Appl. Radiat. Isot.* 41 (1990) 733–738.
- [85] M.B. Smith, J. March, *March's Advanced Organic Chemistry—Reactions, Mechanisms, and Structure*, 5th edition, Wiley-Interscience Pub, New York - Chichester - Brisbane - Toronto, (2001).
- [86] T. Ido, C.N. Wan, V. Casella, J.S. Fowler, A.P. Wolf, M. Reivich, D.E. Kuhl, Labeled 2-deoxy-D-glucose analogs—F-18-labeled 2-deoxy-2-fluoro- D-glucose, 2-deoxy-2-fluoro- D-mannose and C-14-2-deoxy-2-fluoro- D-glucose, *J. Label. Compds Radiopharm.* 14 (1978) 175–183.
- [87] G.T. Bida, N. Satyamurthy, J. Barrio, The synthesis of 2-[^{18}F]fluoro-2-deoxy-D-glucose using glycals: A reexamination, *J. Nucl. Med.* 25 (1984) 1327–1334.
- [88] R. Ashique, R.V. Chirakal, D.W. Hughes, G.J. Schrobilgen, Two-step regio- and stereoselective syntheses of [F-19]- and [F-18]-2-deoxy-2-(R)-fluoro-beta-D-allose, *Carbohydr. Res.* 341 (2006) 457–466.
- [89] B. Schmall, R.D. Finn, S.I. Rapoport, J.G. Noronha, J.J. DeGeorge, D.O. Kiesewetter, N.R. Simpson, S.M. Larson, Synthesis of a fluorinated fatty acid, dl-erythro-9,10-[^{18}F]difluoropalmitic acid, and biodistribution in rats, *Nucl. Med. Biol.* 17 (1990) 805–809.
- [90] W.R. Dolbier, A.R. Li, C.J. Koch, C.Y. Shiue, A.V. Kachur, [^{18}F]EF5, a marker for PET detection of hypoxia: Synthesis of precursor and a new fluorination procedure, *Appl. Radiat. Isot.* 54 (2001) 73–80.
- [91] J.S. Fowler, R.D. Finn, R.M. Lambrecht, A.P. Wolf, The synthesis of ^{18}F -5-fluorouracil, *J. Nucl. Med.* 14 (1973) 63–64.
- [92] E.N. Vine, D.J. Yang, W.H. Vine, A.P. Wolf, An improved synthesis of ^{18}F -5-fluorouracil, *Int. J. Appl. Radiat. Isot.* 30 (1979) 401–405.
- [93] M. Diksic, S. Farrokhzard, Y.L. Yamamoto, W.A. Ferridel, A simple synthesis of ^{18}F -labelled 5-fluorouracil using acetylhypofluorite, *Nucl. Med. Biol.* 11 (1984) 141–142.
- [94] F. Oberdorfer, E. Hofmann, W. Maier-Borst, Preparation of ^{18}F -labelled 5-fluorouracil of very high purity, *J. Label. Compds Radiopharm.* 27 (1989) 137–145.
- [95] C.Y. Shiue, A.P. Wolf, M. Friedkin, Synthesis of 5'-deoxy-5-[^{18}F]fluorouridine and related compounds as probe for measuring tissue proliferation *in vivo*, *J. Label. Compds Radiopharm.* 21 (1984) 865–873.
- [96] K. Ishiwata, M. Monna, R. Iwata, T. Ido, Automated synthesis of 5-[^{18}F]fluoro-2'-deoxyuridine, *J. Label. Compds Radiopharm.* 21 (1984) 1231–1233.
- [97] K. Ishiwata, M. Monna, R. Iwata, T. Ido, Automated synthesis of 5-[^{18}F]fluoro-2'-deoxyuridine, *Appl. Radiat. Isot.* 38 (1987) 467–473.
- [98] C.Y. Shiue, A.P. Wolf, M. Friedkin, Synthesis of 5'-deoxy-5-[^{18}F]fluorouridine as a probe for measuring tissue proliferation *in vivo*, *J. Label. Compds Radiopharm.* 19 (1982) 1395.

- [99] G.W.M. Visser, P. Noordhuis, O. Zwaagstra, J.D.M. Herscheid, A. Hoekstra, A simplified synthesis of ^{18}F -labelled cytosine- and uracil-nucleosides, *Appl. Radiat. Isot.* 37 (1986) 1074–1076.
- [100] A. Luxen, J.R. Barrio, N. Satyamurthy, G.T. Bida, M.E. Phelps, Electrophilic and nucleophilic approaches to the synthesis of 3-fluorodiazepam, *J. Fluor. Chem.* 36 (1987) 83–92.
- [101] G.K.S. Prakash, M.M. Alauddin, J. Hu, P.S. Conti, G. Olah, Expedient synthesis of ^{18}F -labeled alpha-trifluoromethyl ketones, *J. Label. Compds Radiopharm.* 46 (2003) 1087–1092.
- [102] G. Firnau, R. Chirakal, E.S. Garnett, Aromatic radiofluorination with $[\text{F-18}]$ fluorine-gas—6- $[\text{F-18}]$ fluoro-L-DOPA, *J. Nucl. Med.* 25 (1984) 1228–1233.
- [103] H.H. Coenen, K. Franken, P. Kling, G. Stöcklin, Direct electrophilic radiofluorination of phenylalanine, tyrosine and DOPA, *Appl. Radiat. Isot.* 39 (1988) 1243–1250.
- [104] R. Chirakal, N. Vasdev, G.J. Schrobilgen, C. Nahmias, Radiochemical and NMR spectroscopic investigation of the solvent effect on the electrophilic elemental fluorination of L-DOPA: Synthesis of $[\text{F-18}]$ 5-fluoro-L-DOPA, *J. Fluor. Chem.* 99 (1999) 87–94.
- [105] W. Vaalburg, H.H. Coenen, C. Crouzel, P.H. Elsinga, B. Långström, C. Lemaire, G.J. Meyer, Amino acids for the measurement of protein synthesis *in vivo* by PET, *Nucl. Med. Biol.* 19 (1992) 227–237.
- [106] M. Ogawa, K. Hatano, S. Oishi, Y. Kawasumi, N. Fujii, M. Kawaguchi, R. Doi, M. Imamura, M. Yamamoto, K. Ajito, T. Mukai, H. Saji, K. Ito, Direct electrophilic radiofluorination of a cyclic RGD peptide for *in vivo* $\alpha(v)\beta(3)$ integrin related tumor imaging, *Nucl. Med. Biol.* 30 (2003) 1–9.
- [107] M. Namavari, J.R. Barrio, T. Toyokuni, S.S. Gambhir, S.R. Cherry, H.R. Herschman, M.E. Phelps, N. Satyamurthy, Synthesis of 8- $[\text{F-18}]$ fluoroguanine derivatives: *In vivo* probes for imaging gene expression with positron emission tomography, *Nucl. Med. Biol.* 27 (2000) 157–162.
- [108] F. Oberdorfer, U. Haberkorn, K. Weber, G. Firnau, The use of ^{18}F F_2 in anhydrous hydrogenfluoride. Preparation of 5- ^{18}F fluorocytosine and its conversion to 5- ^{18}F fluorouracil, *J. Label. Compds Radiopharm.* 37 (1995) 135–136.
- [109] B.S. Moon, A.Y. Shim, K.C. Lee, H.J. Lee, B.S. Lee, G.I. An, S.D. Yang, D.Y. Chi, C. W. Choi, S.M. Lim, K.S. Chun, Synthesis of F-18 labeled capecitabine using $[\text{F-18}]$ F_2 gas as a tumor imaging agent, *Bull. Kor. Chem. Soc.* 26 (2005) 1865–1868.
- [110] H.H. Coenen, S.M. Moerlein, Regiospecific aromatic fluorodemetalation of group IVb metalloarenes using elemental fluorine or acetyl hypofluorite, *J. Fluor. Chem.* 36 (1987) 63–75.
- [111] S.G. Mislankar, D.L. Gildersleeve, D.M. Wieland, C.C. Massin, G.K. Mulholland, S.A. Toorongan, 6- ^{18}F Fluorometaraminol: A radiotracer for *in vivo* mapping of adrenergic nerves of the heart, *J. Med. Chem.* 31 (1988) 362–366.
- [112] O. Eskola, T. Grönroos, J. Bergman, M. Haaparanta, P. Marjamäki, P. Lehtikoinen, S. Forsback, O. Langer, F. Hinnen, F. Dollé, C. Halldin, O. Solin, A novel electrophilic synthesis and evaluation of medium specific radioactivity (1R,2S)-4- ^{18}F fluorometaraminol, a tracer for the assessment of cardiac sympathetic nerve integrity with PET, *Nucl. Med. Biol.* 31 (2004) 103–110.
- [113] O. Langer, F. Dollé, H. Valette, C. Halldin, F. Vaufrey, C. Fuseau, C. Coulon, M. Ottaviani, K. Någren, M. Bottlaender, B. Mazière, C. Crouzel, Synthesis of high-specific-radioactivity 4- and 6- ^{18}F fluorometaraminol—PET tracers for the adrenergic nervous system of the heart, *Bioorg. Med. Chem.* 9 (2001) 677–694.
- [114] M.J. Adam, J.M. Berry, L.D. Hall, B.D. Pate, T. Ruth, The cleavage of aryl-metal bonds by elemental fluorine—Synthesis of aryl-fluorides, *Can. J. Chem.* 61 (1983) 658–660.
- [115] M.J. Adam, S. Jivan, Synthesis and purification of L-6- $[\text{F-18}]$ fluoro-DOPA, *Appl. Radiat. Isot.* 39 (1988) 1203–1206.

- [116] A. Luxen, M. Perlmutter, G.T. Bida, G. Van Moffaert, J.S. Cook, N. Satyamurthy, M.E. Phelps, J.R. Barrio, Remote, semiautomated production of 6-[F-18]fluoro-L-DOPA for human studies with PET, *Appl. Radiat. Isot.* 41 (1990) 275–281.
- [117] F. Dollé, S. Demphel, F. Hinnen, D. Fournier, F. Vaufrey, C. Crouzel, 6-[F-18]Fluoro-L-DOPA by radiofluorodestannylation: A short and simple synthesis of a new labelling precursor, *J. Label. Compds Radiopharm.* 41 (1998) 105–114.
- [118] E.F.J. de Vries, G. Luurtsema, M. Brüssermann, P.H. Elsinga, W. Vaalburg, Fully automated synthesis module for the high yield one-pot preparation of 6-[F-18]fluoro-L-DOPA, *Appl. Radiat. Isot.* 51 (1999) 389–394.
- [119] F. Füchtner, P. Angelberger, H. Kvaternik, F. Hammerschmidt, B. Peric-Simovc, J. Steinbach, Aspects of 6-[¹⁸F]fluoro-L-DOPA preparation: Precursor synthesis, preparative HPLC purification and determination of radiochemical purity, *Nucl. Med. Biol.* 29 (2002) 477–481.
- [120] M. Namavari, A. Bishop, N. Satyamurthy, G. Bida, J.R. Barrio, Regioselective radiofluorodestannylation with [F-18]F₂ and [F-18]CH₃COOF—A high-yield synthesis of 6-[F-18]fluoro-L-DOPA, *Appl. Radiat. Isot.* 43 (1992) 989–996.
- [121] M. Haaparanta, J. Bergmann, A. Laakso, J. Hietala, [¹⁸F]CFT ([¹⁸F]WIN 35,428), a radioligand to study the dopamine transporter with PET: Biodistribution in rats, *Synapse* 23 (1996) 321–327.
- [122] O. Rinne, H. Ruottinen, J. Bergman, M. Haaparanta, P. Sonninen, O. Solin, Usefulness of a dopamine transporter PET ligand [F-18]beta-CFT in assessing disability in Parkinson's disease, *J. Neurol. Neurosurg. Psych.* 67 (1999) 737–741.
- [123] M. Namavari, N. Satyamurthy, J.R. Barrio, Synthesis of 6-[F-18]fluorodopamine, 6-[F-18]fluoro-m-tyramine and 4-[F-18]fluoro-m-tyramine, *J. Label. Compds Radiopharm.* 36 (1995) 825–833.
- [124] E. Hess, S. Sichler, A. Kluge, H.H. Coenen, Synthesis of 2-[¹⁸F]fluoro-L-tyrosine via regiospecific fluoro-de-stannylation, *Appl. Radiat. Isot.* 57 (2002) 185–191.
- [125] T. Delffer, P. Johnström, S. Stone-Elander, A. Holland, C. Halldin, M. Haaparanta, O. Solin, J. Bergman, M. Steinman, G. Sedvall, The labeling of 2-oxoquazepam with electrophilic F-18, *J. Label. Compds Radiopharm.* 29 (1991) 1223–1239.
- [126] M.R. Akula, C.P.D. Longford, G.W. Kabalka, Synthesis of 9-amino-7-[¹⁸F]fluoro-1,2,3,4-tetrahydroacridine: A potential PET agent for evaluating acetylcholinesterase, *J. Label. Compds Radiopharm.* 42 (1999) S539–S540.
- [127] M.R. Akula, C.D.P. Longford, G.W. Kabalka, Synthesis of 2-[¹⁸F]fluorobenzidine: A precursor to bisdiazodyes: Potential radioligands to image amyloid deposits in the brain of alzheimer patients, *J. Label. Compds Radiopharm.* 42 (1999) S541–S542.
- [128] J.H. Clark, Fluoride-ion as a base in organic-synthesis, *Chem. Rev.* 80 (1980) 429–452.
- [129] A. Katsifis, K. Hamacher, J. Schnitter, G. Stöcklin, Optimization studies concerning the direct nucleophilic fluorination of butyrophenone neuroleptics, *Appl. Radiat. Isot.* 44 (1993) 1015–1020.
- [130] K. Hamacher, W. Hamkens, Remote-controlled one-step production of F-18 labeled butyrophenone neuroleptics exemplified by the synthesis of nca [F-18]N-methylspiperone, *Appl. Radiat. Isot.* 46 (1995) 911–916.
- [131] M. Attina, F. Cacace, A. Wolf, Labeled aryl fluorides from the nucleophilic displacement of activated nitro-groups by F-18-F⁻, *J. Label. Compds Radiopharm.* 20 (1983) 501–514.
- [132] C. Shiue, J.S. Fowler, A.P. Wolf, M. Watanabe, C.D. Arnett, Synthesis and specific activity determination of NCA ¹⁸F-labeled butyrophenone neuroleptics: Benperidol, haloperidol, spiroperidol and pipamperone, *J. Nucl. Med.* 26 (1985) 181–186.
- [133] C.Y. Shiue, L.Q. Bai, R. Teng, A.P. Wolf, Application of the nucleophilic substitution reactions to the synthesis of NCA ¹⁸F-labeled radioligands, *J. Label. Compds Radiopharm.* 23 (1986) 1038–1039.

- [134] C.Y. Shiue, J.S. Fowler, A.P. Wolf, D.W. McPherson, C.D. Arnett, L. Zecca, No-carrier-added fluorine-18 labeled N-methylspiperidol: Synthesis and biodistribution in mice, *J. Nucl. Med.* 27 (1986) 226–234.
- [135] J.W. Brodack, C.S. Dence, M.R. Kilbourn, M.J. Welch, Robotic production of 2-deoxy-2-[F-18]fluoro-D-glucose—A routine method of synthesis using tetrabutylammonium [F-18] fluoride, *Appl. Radiat. Isot.* 39 (1988) 699–703.
- [136] D.P. Cox, J. Terpinski, W. Lawrynowicz, Anhydrous tetrabutylammonium fluoride—A mild but highly efficient source of nucleophilic fluoride-ion, *J. Org. Chem.* 49 (1984) 3216–3219.
- [137] R.K. Sharma, J.L. Fry, Instability of anhydrous tetra-normal-alkylammonium fluorides, *J. Org. Chem.* 48 (1983) 2112–2114.
- [138] T. Irie, K. Fukushima, T. Ido, T. Nozaki, Y. Kasida, F-18-labeled fluorination by crown ether metal fluoride. 1. On labeling F-18–21-fluoroprogesterone, *Int. J. Appl. Radiat. Isot.* 33 (1982) 1449–1452.
- [139] F.K. Hamacher, H.H. Coenen, G. Stöcklin, Efficient stereospecific synthesis of no-carrier-added 2-[¹⁸F]-fluoro-2-deoxy-D-glucose using aminopolyether supported nucleophilic substitution, *J. Nucl. Med.* 27 (1986) 235–238.
- [140] H.H. Coenen, B. Klatte, A. Knöchel, M. Schüller, G. Stöcklin, Preparation of n.c.a. [^{17–18}F]fluoroheptadecanoic acid in high yields via aminopolyether supported, nucleophilic fluorination, *J. Label. Compds Radiopharm.* 23 (1986) 455–467.
- [141] D. Block, H.H. Coenen, G. Stöcklin, The N.C.A. nucleophilic ¹⁸F-fluorination of 1, N-disubstituted alkanes as fluoroalkylation agents, *J. Label. Compds Radiopharm.* 24 (1987) 1029–1042.
- [142] L. Zheng, M.S. Berridge, Synthesis of [F-18]fluoromethyl iodide, a synthetic precursor for fluoromethylation of radiopharmaceuticals, *Appl. Radiat. Isot.* 52 (2000) 55–61.
- [143] T.R. DeGrado, R.E. Coleman, S. Wang, S.W. Baldwin, M.D. Orr, C.N. Robertson, T.J. Polascik, D.T. Price, Synthesis and evaluation of ¹⁸F-labeled choline as an oncologic tracer for positron emission tomography: Initial findings in prostate cancer, *Cancer Res.* 61 (2001) 110–117.
- [144] F. Dollé, F. Hinnen, P. Emond, S. Mavel, Z. Mincheva, W. Saba, M.A. Schöllhorn-Peyronneau, H. Valette, L. Garreau, S. Chalon, C. Halldin, J. Helfenbein, J. Legaillard, J.C. Madelmont, J.B. Deloye, M. Bottlaender, D. Guilloteau, Radiosynthesis of [¹⁸F]LBT-999, a selective radioligand for the visualisation of the dopamine transporter with PET, *J. Label. Compds Radiopharm.* 49 (2006) 687–698.
- [145] J. Mukherjee, Z.Y. Yang, M.K. Das, T. Brown, Fluorinated benzamide neuroleptics-III. Development of (S)-N-[(1-allyl-2-pyrrolidinyl)methyl]-5-(3-[¹⁸F]fluoropropyl)-2,3-dimethoxybenzamide as an improved dopamine D-2 receptor tracer, *Nucl. Med. Biol.* 22 (1995) 283–296.
- [146] J.S. Fowler, T. Ido, Design and synthesis of 2-deoxy-2-[¹⁸F]fluoro-D-glucose (¹⁸FDG), in: M.J. Welch, C.S. Redvanly (Eds.), *Handbook of Radiopharmaceuticals—Radiochemistry and Applications*, Wiley, Chichester, 2003, pp. 307–322.
- [147] C. Mosdzianowski, C. Lemaire, B. Lauricella, J. Aerts, J.L. Morelle, F. Gobert, M. Herman, A. Luxen, Routine and multi-Curie level productions of [¹⁸F]FDG using an alkaline hydrolysis on solid support, *J. Label. Compds Radiopharm.* 42 (1999) S515–S516.
- [148] C. Mosdzianowski, C. Lemaire, F. Simoens, J. Aerts, J.L. Morelle, A. Luxen, Epimerization study on [¹⁸F]FDG produced by an alkaline hydrolysis on solid support under stringent conditions, *Appl. Radiat. Isot.* 56 (2002) 871–875.
- [149] C. Lemaire, P. Damhaut, B. Lauricella, C. Mosdzianowski, J.L. Morelle, M. Monclus, J. Van Naemen, E. Mulleneers, J. Aerts, A. Plenevaux, C. Brihaye, A. Luxen, Fast [¹⁸F]FDG synthesis by alkaline hydrolysis on a low polarity solid phase support, *J. Label. Compds Radiopharm.* 45 (2002) 435–447.
- [150] C.C. Lee, G. Sui, A. Elizarov, C.J. Shu, Y.S. Shin, A.N. Dooley, J. Huang, A. Daridon, P. Wyatt, D. Stout, H.C. Kolb, O.N. Witte, N. Satyamurthy, J.R. Heath, M.E. Phelps,

- S.R. Quake, H.R. Tseng, Multistep synthesis of a radiolabeled imaging probe using integrated microfluidics, *Science* 310 (2005) 1793–1796.
- [151] J.M. Gillies, C. Prenant, G.N. Chimon, G.J. Smethurst, W. Perrie, I. Hamblett, B. Dekker, J. Zweit, Microfluidic reactor for the radiosynthesis of PET radiotracers, *Appl. Radiat. Isot.* 64 (2006) 325–332.
- [152] H.J. Machulla, A. Blocher, M. Kuntzsch, M. Piert, R. Wei, J.R. Grierson, Simplified labeling approach for synthesizing 3'-deoxy-3'-[F-18]fluorothymidine ([F-18]FLT), *J. Radioanal. Nucl. Chem.* 243 (2000) 843–846.
- [153] C. Wodarski, J. Eisenbarth, K. Weber, M. Henze, U. Haberkorn, M. Eisenhut, Synthesis of 3'-deoxy-3'-[F-18]fluoro-thymidine with 2,3'-anhydro-5'-O-(4,4'-dimethoxytrityl)thymidine, *J. Label. Compds Radiopharm.* 43 (2000) 1211–1218.
- [154] B. Teng, S.Z. Wang, Z. Fu, Y.H. Dang, Z.H. Wu, L.Q. Liu, Semiautomatic synthesis of 3'-deoxy-3'-[F-18]fluorothymidine using three precursors, *Appl. Radiat. Isot.* 64 (2006) 187–193.
- [155] E.L. Kämäräinen, T. Kyllönen, O. Nihtilä, H. Björk, O. Solin, Preparation of fluorine-18-labeled fluoromisonidazole using two different synthesis methods, *J. Label. Compds Radiopharm.* 47 (2004) 37–45.
- [156] K. Hamacher, Synthesis of n.c.a. cis- and trans-4-[¹⁸F]fluoro-L-proline, radiotracers for PET-investigation of disordered matrix protein synthesis, *J. Label. Compds Radiopharm.* 42 (1999) 1135–1144.
- [157] F.K. Hamacher, H.H. Coenen, Efficient routine production of the ¹⁸F-labelled amino acid O-(2-[¹⁸F]fluoroethyl)-L-tyrosine, *Appl. Radiat. Isot.* 57 (2002) 853–856.
- [158] S.J. Oh, C. Mosdzianowski, D.Y. Chi, J.Y. Kim, S.H. Kang, J.S. Ryu, J.S. Yeo, D.H. Moon, Fully automated synthesis system of 3'-deoxy-3'-[¹⁸F]fluorothymidine, *Nucl. Med. Biol.* 31 (2004) 803–809.
- [159] S.J. Oh, D.Y. Chi, C. Mosdzianowski, J.Y. Kim, H.S. Gil, S.H. Kang, J.S. Ryu, D.H. Moon, Fully automated synthesis of [¹⁸F]fluoromisonidazole using a conventional [¹⁸F]FDG module, *Nucl. Med. Biol.* 32 (2005) 899–905.
- [160] A. Blocher, M. Kuntzsch, R. Wei, H.J. Machulla, Synthesis and labeling of 5'-O-(4,4'-dimethoxytrityl)-2,3 ϕ -anhydrothymidine for [F-18]FLT preparation, *J. Radioanal. Nucl. Chem.* 251 (2002) 55–58.
- [161] J.L. Lim, L. Zheng, M.S. Berridge, T.J. Tewson, The use of 3-methoxymethyl-16 β ,17 β -epiestriol-O-cyclic sulfone as the precursor in the synthesis of F-18 16 α -fluoroestradiol, *Nucl. Med. Biol.* 23 (1996) 911–915.
- [162] M.E. Van Dort, Y.W. Jung, P.S. Sherman, M.R. Kilbourn, D.M. Wieland, Fluorine for hydroxy substitution in biogenic amines: Asymmetric synthesis and biological evaluation of fluorine-18-labeled beta-fluorophenylalkylamines as model systems, *J. Med. Chem.* 38 (1995) 810–815.
- [163] J. McConathy, L. Martarello, E.J. Malveaux, V.M. Camp, N.E. Simpson, C.P. Simpson, G.D. Bowers, J.J. Olson, M.M. Goodman, Radiolabeled amino acid-sfor tumor imaging with PET: Radiosynthesis and biological evaluation of 2-amino-3-[F-18]fluoro-2-methylpropanoic acid and 3-[F-18]fluoro-2-methyl-2-(methylamino)propanoic acid, *J. Med. Chem.* 45 (2002) 2240–2249.
- [164] Y. Seimille, J. Rousseau, F. Benard, C. Morin, H. Ali, G. Avvakumov, G.L. Hammond, J.E. van Lier, F-18-labeled difluoroestradiols: Preparation and preclinical evaluation as estrogen receptor-binding radiopharmaceuticals, *Steroids* 67 (2002) 765–775.
- [165] Y. Seimille, F. Benard, J. Rousseau, E. Pepin, A. Aliaga, G. Tessier, J.E. van Lier, Impact on estrogen receptor binding and target tissue uptake of [F-18]fluorine substitution at the 16-alpha-position of fulvestrant, *Nucl. Med. Biol.* 31 (2004) 691–698.
- [166] F. Yamamoto, S. Sasaki, M. Maeda, Positron labeled antioxidants: Synthesis and tissue biodistribution of 6-deoxy-6-[¹⁸F]fluoro-L-ascorbic acid, *Appl. Radiat. Isot.* 43 (1992) 633–639.

- [167] G. Angelini, M. Speranza, A.P. Wolf, C.Y. Shiue, Nucleophilic aromatic-substitution of activated cationic groups by F-18-labeled fluoride—A useful route to no-carrier-added (nca) F-18-labeled aryl fluorides, *J. Fluor. Chem.* 27 (1985) 177–191.
- [168] M.S. Haka, M.R. Kilbourn, L. Watkins, S.A. Toorongan, Aryltrimethylammonium trifluoromethanesulfonates as precursors to aryl [F-18] fluorides—Improved synthesis of [F-18]GBR-13119, *J. Label. Compds Radiopharm.* 27 (1989) 823–833.
- [169] R. Rengan, P.K. Chakraborty, M.R. Kilbourn, Can we predict reactivity for aromatic nucleophilic substitution with [¹⁸F]fluoride ion? *J. Label. Compds Radiopharm.* 33 (1993) 563–572.
- [170] S. Stone-Elander, N. Elander, Microwave applications in radiolabelling with short-lived positron-emitting radionuclides, *J. Label. Compds Radiopharm.* 45 (2002) 715–746.
- [171] S. Stone-Elander, N. Elander, Microwave cavities: Some parameters affecting their use in radiolabeling reactions, *Appl. Radiat. Isot.* 42 (1991) 885–887.
- [172] N. Elander, J.R. Jones, S.Y. Lu, S. Stone-Elander, Microwave-enhanced radiochemistry, *Chem. Soc. Rev.* 29 (2000) 239–249.
- [173] D.R. Hwang, S.M. Moerlein, L. Lang, M.J. Welch, Application of microwave technology to the synthesis of short-lived radiopharmaceuticals, *J. Chem. Soc. Chem. Comm.* 23 (1987) 1799–1801.
- [174] C. Lemaire, M. Guillaume, L. Christiaens, A.J. Palmer, R. Cantineau, A new route for the synthesis of [F-18]fluoroaromatic substituted amino-acids—No carrier added L-p-[F-18]fluorophenylalanine, *Appl. Radiat. Isot.* 38 (1987) 1033–1038.
- [175] C. Lemaire, P. Damhaut, A. Plevenaux, R. Cantineau, L. Christiaens, M. Guillaume, Synthesis of F-18 substituted aromatic-aldehydes and benzyl bromides, new intermediates for nca [F-18] fluorination, *Appl. Radiat. Isot.* 43 (1992) 485–494.
- [176] Y.S. Ding, C.Y. Shiue, J.S. Fowler, A.P. Wolf, A. Plevenaux, No carrier added (nca) aryl [F-18]fluorides via the nucleophilic aromatic-substitution of electron-rich aromatic rings, *J. Fluor. Chem.* 48 (1990) 189–205.
- [177] A. Najafi, A. Peterson, M. Buchsbaum, S. O'Dell, F. Weihmuller, Preparation and preliminary biological evaluation of [F-18]NCQ-115—A new selective reversible dopamine D2 receptor ligand, *Nucl. Med. Biol.* 20 (1993) 549–555.
- [178] P. Damhaut, R. Cantineau, C. Lemaire, A. Plevenaux, L. Christiaens, M. Guillaume, 2-[F-18]fluorotropapride and 4-[F-18]fluorotropapride, 2 specific D2-receptor ligands for positron emission tomography—NCA syntheses and animal studies, *Appl. Radiat. Isot.* 43 (1992) 1265–1274.
- [179] R. Iwata, C. Pascali, A. Bogni, G. Horvath, Z. Kovacs, K. Yanai, T. Ido, A new convenient method for the preparation of 4-[F-18]fluorobenzyl halides, *Appl. Radiat. Isot.* 52 (2000) 87–92.
- [180] R. Iwata, G. Horvath, C. Pascali, A. Bogni, K. Yanai, Z. Kovacs, T. Ido, Synthesis of 3-[1H-imidazol-4-yl]propyl 4-[F-18]fluorobenzyl ether ([F-18]fluoroproxyfan): A potential radioligand for imaging histamine H-3 receptors, *J. Label. Compds Radiopharm.* 43 (2000) 872–893.
- [181] K. Hatano, T. Ido, R. Iwata, The synthesis of o- and p-[¹⁸F]fluorobenzyl bromides and their application to the preparation of labeled neuroleptics, *J. Label. Compds Radiopharm.* 29 (1991) 373–380.
- [182] C. Lemaire, P. Damhaut, A. Plevenaux, D. Comar, Enantioselective synthesis of 6-[fluorine-18]fluoro-L-DOPA from no-carrier-added fluorine-18-fluoride, *J. Nucl. Med.* 35 (1994) 1996–2002.
- [183] C.S. Dence, C.S. John, W.D. Bowen, M.J. Welch, Synthesis and evaluation of [F-18] labeled benzamides: High affinity sigma receptor ligands for PET imaging, *Nucl. Med. Biol.* 24 (1997) 333–340.
- [184] C. Halldin, T. Höglberg, L. Farde, Fluorine-18-labeled NCQ 115, a selective dopamine D-2 receptor ligand. Preparation and positron emission tomography, *Nucl. Med. Biol.* 21 (1994) 627–631.

- [185] R.H. Mach, S.T. Elder, T.E. Morton, P.A. Nowak, P.H. Evora, J.G. Scripko, R.R. Luedtke, C.D. Unsworth, T. Filtz, A.V. Rao, P.B. Molinoff, R.L.E. Ehrenkaufer, The use of [F-18] 4-fluorobenzyl iodide (FBI) in PET radiotracer synthesis—Model alkylation studies and its application in the design of dopamine-D(1) and dopamine-D(2) receptor-based imaging agents, *Nucl. Med. Biol.* 20 (1993) 777–794.
- [186] Y.S. Ding, J.S. Fowler, A.P. Wolf, Rapid, regiospecific syntheses of deuterium substituted 6-[F-18]fluorodopamine (alpha, alpha-D2 beta, beta-D2 and alpha, alpha, beta, beta-D4) for mechanistic studies with positron emission tomography, *J. Label. Compds Radiopharm.* 31 (1993) 645–654.
- [187] D.R. Hwang, C.S. Dence, Z.A. McKinnon, C.J. Mathias, M.J. Welch, Positron labeled muscarinic acetylcholine-receptor antagonist—2-[F-18]Fluorodexetimide and 4-[F-18]fluorodexetimide—Synthesis and biodistribution, *Nucl. Med. Biol.* 18 (1991) 247–252.
- [188] B. Kuhnast, F. Dollé, F. Vaufrey, F. Hinnen, C. Crouzel, B. Tavitian, Fluorine-18 labeling of oligonucleotides bearing chemically-modified ribose-phosphate backbones, *J. Label. Compds Radiopharm.* 43 (2000) 837–848.
- [189] B. Kuhnast, F. Dollé, S. Terrazzino, B. Rousseau, C. Loc'h, F. Vaufrey, F. Hinnen, I. Doignon, F. Pillon, C. David, C. Crouzel, B. Tavitian, A general method to label antisense oligonucleotides with radioactive halogens for pharmacological and imaging studies, *Bioconj. Chem.* 11 (2000) 627–636.
- [190] L. Allain-Barbier, M.-C. Lasne, C. Perrio-Huard, L. Barre, Synthesis of 4-[F-18]fluorophenylalkenes and -arenes via palladium-catalyzed coupling of 4-[F-18]fluoriodobenzene with vinyl and aryl tin reagents, *Acta Chem. Scand.* 52 (1998) 480–489.
- [191] T. Forngren, Y. Andersson, B. Lamm, B. Långström, Synthesis of [4-F-18]-1-bromo-4-fluorobenzene and its use in palladium-promoted cross-coupling reactions with organostannanes, *Acta Chem. Scand.* 52 (1998) 475–479.
- [192] V.W. Pike, F. Aigbirio, Reactions of cyclotron-produced [¹⁸F]fluoride with diaryliodonium salts—a novel single-step route to no-carrier-added [¹⁸F]fluoroarenes, *J. Chem. Soc. Chem. Comm.* 21 (1995) 2215–2216.
- [193] A. Shah, V.W. Pike, D.A. Widdowson, The synthesis of [F-18]fluoroarenes from the reaction of cyclotron-produced [F-18]fluoride ion with diaryliodonium salts, *J. Chem. Soc. Perkin Trans. I: Organic and Bio-Organic Chemistry* 13 (1998) 2043–2046.
- [194] J. Ermert, C. Hocke, T. Ludwig, R. Gail, H.H. Coenen, Comparison of pathways to the versatile synthon of no-carrier-added 1-bromo-4-[¹⁸F]fluorobenzene, *J. Label. Compds Radiopharm.* 47 (2004) 429–441.
- [195] C. Lemaire, R. Cantineau, M. Guillaume, A. Plenevaux, L. Christiaens, Fluorine-18-altanserine: A radioligand for the study of serotonin receptors with PET: Radiolabeling and *in vivo* biologic behavior in rats, *J. Nucl. Med.* 32 (1991) 2266–2272.
- [196] P.Z. Tan, R.M. Baldwin, R. Soufer, P.K. Garg, D.S. Charney, R.B. Innis, A complete remote-control system for reliable preparation of [F-18]altanserine, *Appl. Radiat. Isot.* 50 (1999) 923–927.
- [197] P.Z. Tan, R.M. Baldwin, T. Fu, D.S. Charney, R.B. Innis, Rapid synthesis of F-18 and H-2 dual-labeled altanserine, a metabolically resistant PET ligand for 5-HT_{2A} receptors, *J. Label. Compds Radiopharm.* 42 (1999) 457–467.
- [198] C. Crouzel, M. Venet, T. Irie, G. Sanz, C. Boullais, Labeling of a serotonergic ligand with fluorine-18: [¹⁸F]Setoperone, *J. Label. Compds Radiopharm.* 25 (1988) 403–414.
- [199] M. Gysemans, J. Mertens, Mechanistic approach of the nucleophilic ¹⁸F exchange on 4-NO₂-spiperone using TBA ¹⁸F or K₂.2.2/K¹⁸F, *J. Label. Compds Radiopharm.* 28 (1990) 73–81.
- [200] K. Hashizume, N. Hashimoto, Y. Miyake, Rapid and efficient synthesis of high-purity fluorine-18 labeled haloperidol and spiperone via the nitro precursor in combination with a new HPLC separation method, *Bull. Chem. Soc. Japan* 70 (1997) 681–687.

- [201] D. Le Bars, C. Lemaire, N. Ginovart, A. Plevenaux, J. Aerts, C. Brihaye, W. Hassoun, V. Leviel, P. Mekhsian, D. Weissmann, J.F. Pujol, A. Luxen, D. Comar, High-yield radiosynthesis and preliminary *in vivo* evaluation of p-[¹⁸F]MPPF, a fluoro analog of WAY-100635, Nucl. Med. Biol. 25 (1998) 343–350.
- [202] E.G. Robins, F. Brady, S.K. Luthra, Hypervalent iodine reagents as precursors for radiolabelling pyrimidines using n.c.a. [¹⁸F]fluoride, J. Label. Compds Radiopharm. 48 (2005) S145.
- [203] E.D. Hostetler, S.D. Jonson, M.J. Welch, J.A. Katzenellenbogen, Synthesis of 2-[F-18]fluoroestradiol, a potential diagnostic imaging agent for breast cancer: Strategies to achieve nucleophilic substitution of an electron-rich aromatic ring with [F-18]F, J. Org. Chem. 64 (1999) 178–185.
- [204] F. Wüst, J.M.H.M. Reul, T. Rein, A. Abel, G. Stöcklin, PET-corticosteroids as potential ligands for mapping brain glucocorticoid receptors (GR), J. Label. Compds Radiopharm. 44 (2001) S12–S14.
- [205] F. Wüst, K.E. Carlson, J.A. Katzenellenbogen, Synthesis of novel arylpyrazolo corticosteroids as potential ligands for imaging brain glucocorticoid receptors, Steroids 68 (2003) 177–191.
- [206] A. Horti, D.E. Redmond, R. Soufer, No-carrier-added (nca) synthesis of 6-[F-18] fluoro-L-DOPA using 3,5,7,8,8a-hexahydro-7,7,8a-trimethyl-[6S-(6- α , 8- α , 8- α -beta)]-6,8-methano-2H-1,4-benzoxazin-2-one, J. Label. Compds Radiopharm. 36 (1995) 409–423.
- [207] C. Lemaire, M. Guillaume, R. Cantineau, A. Plevenaux, L. Christiaens, An approach to the asymmetric synthesis of L-6-[¹⁸F]fluorodopa via NCA nucleophilic fluorination, Appl. Radiat. Isot. 42 (1991) 629–635.
- [208] C. Lemaire, A. Plevenaux, R. Cantineau, L. Christiaens, M. Guillaume, D. Comar, Nucleophilic enantioselective synthesis of 6-[¹⁸F]fluoro-L-DOPA via two chiral auxiliaries, Appl. Radiat. Isot. 44 (1993) 737–744.
- [209] P. Damhaut, C. Lemaire, A. Plevenaux, C. Brihaye, L. Christiaens, D. Comar, No-carrier-added asymmetric synthesis of alpha-methyl-alpha-amino acids labeled with fluorine-18, Tetrahedron 53 (1997) 5785–5796.
- [210] E.J. Corey, F. Xu, M.C. Noe, C. Mark, A rational approach to catalytic enantioselective enolate alkylation using a structurally rigidified and defined chiral quaternary ammonium salt under phase transfer conditions, J. Am. Chem. Soc. 119 (1997) 12414–12415.
- [211] E.J. Corey, M.C. Noe, F. Xu, Highly enantioselective synthesis of cyclic and functionalized alpha-amino acids by means of a chiral phase transfer catalyst, Tetrahedron Lett. 39 (1998) 5347–5350.
- [212] C. Lemaire, S. Gillet, S. Guillouet, A. Plevenaux, J. Aerts, A. Luxen, Highly enantioselective synthesis of no-carrier-added 6-[¹⁸F]fluoro-L-DOPA by chiral phase-transfer alkylation, Eur. J. Org. Chem. 13 (2004) 2899–2904.
- [213] S. Guillouet, C. Lemaire, G. Bonmarchand, L. Zimmer, D. Le Bars, Large scale production of 6-[¹⁸F]fluoro-L-DOPA in semi-automated system, J. Label. Compds Radiopharm. 44 (2001) S868–S870.
- [214] T. Nozaki, Y. Tanaka, Preparation of F-18-labelled aryl fluorides, Int. J. Appl. Radiat. Isot. 18 (1967) 111–119.
- [215] A.J. Palmer, J.C. Clark, R.W. Goulding, Preparation of F-18 labeled radiopharmaceuticals, Int. J. Appl. Radiat. Isot. 28 (1977) 53–65.
- [216] A.J. Palmer, J.C. Clark, R.W. Goulding, M. Roman, Preparation of fluorine-18-labeled DL-3-fluorotyrosine, Radiopharm. Label. Compds 1 (1973) 291–302.
- [217] M. Argentini, C. Wiese, R. Weinreich, Synthesis of 5-fluoro-D/L-DOPA and [F-18]5-fluoro-L-DOPA, J. Fluor. Chem. 68 (1994) 141–144.
- [218] A. Knöchel, O. Zwerneemann, Aromatic nca labeling with F-18(•) by modified Balz-Schiemann-decomposition, Appl. Radiat. Isot. 42 (1991) 1077–1080.

- [219] A. Knöchel, O. Zwerneemann, Development of a no-carrier-added method for F-18-labelling of aromatic compounds by fluorodediazotation, *J. Label. Compds Radiopharm.* 38 (1996) 325–336.
- [220] T.J. Tewson, M.J. Welch, Preparation of F-18 aryl fluorides—Piperidyl triazenes as a source of diazonium salts, *J. Chem. Soc. Chem. Comm.* 24 (1979) 1149–1150.
- [221] M.R. Kilbourn, M.J. Welch, C.S. Dence, T.J. Tewson, H. Saji, M. Maeda, Carrier-added and no-carrier-added synthesis of [F-18]spiroperidol and [F-18]haloperidol, *Int. J. Appl. Radiat. Isot.* 35 (1984) 591–598.
- [222] F. Dollé, [¹⁸F]Fluoropyridines: From conventional radiotracers to the labelling of macromolecules such as proteins and oligonucleotides, in: Ernst Schering Research Foundation (Ed.), *PETChemistry Vol. 62*, Springer-Verlag, Berlin - Heidelberg - New York, 2007, pp. 111–143.
- [223] L. Dolci, F. Dollé, S. Jubeau, F. Vaufrey, C. Crouzel, 2-[¹⁸F]Fluoropyridines by no-carrier-added nucleophilic aromatic substitution with K[¹⁸F]F-K₂₂₂—A comparative study, *J. Label. Compds Radiopharm.* 42 (1999) 975–985.
- [224] M. Karramkam, F. Hinnen, F. Vaufrey, F. Dollé, 2-, 3- and 4-[¹⁸F]Fluoropyridines by no-carrier-added nucleophilic aromatic substitution with K[¹⁸F]F-K₂₂₂—A comparative study, *J. Label. Compds Radiopharm.* 46 (2003) 979–992.
- [225] J.A. Joule, K. Mills, *Heterocyclic Chemistry*, 4th edition, Blackwell Science, Oxford - London - Edinburgh - Malden - Paris - Berlin - Tokyo, (2000).
- [226] E.J. Knust, M.J. Machulla, M. Molls, ¹⁸F-production in a water target with high yields for ¹⁸F-labelling of organic compounds: Synthesis of 6-[¹⁸F]nicotinic acid diethylamide, *J. Label. Compds Radiopharm.* 19 (1982) 1643–1644.
- [227] E.J. Knust, C. Mueller-Platz, M. Schueller, Synthesis, quality control and tissue distribution of 2-[¹⁸F]nicotinic acid diethylamide, a potential agent for regional cerebral function studies, *J. Radioanal. Chem.* 74 (1982) 283–291.
- [228] E.J. Knust, H.J. Machulla, C. Astfalk, *Radiopharmaceuticals V: ¹⁸F-Labeling with water target produced fluorine-18—Synthesis and quality control of 6-¹⁸F-nicotinic acid diethylamide*, *Radiochem. Radioanal. Lett.* 55 (1983) 249–255.
- [229] J. Ballinger, B.M. Bowen, G. Firnau, E.S. Garnett, F.W. Teare, Radiofluorination with reactor-produced cesium [¹⁸F]fluoride: No-carrier-added 2-[¹⁸F]fluoronicotine and 6-[¹⁸F]fluoronicotine, *Int. J. Appl. Radiat. Isot.* 35 (1984) 1125–1128.
- [230] Y.S. Ding, J. Gatley, J.S. Fowler, N.D. Volkow, D. Aggarwal, J. Logan, S.L. Dewey, F. Liang, F.I. Carroll, M.J. Kuhar, Mapping nicotinic acetylcholine receptors with PET, *Synapse* 24 (1996) 403–407.
- [231] F. Liang, H.A. Navarro, P. Abraham, P. Kotian, Y.S. Ding, J.S. Fowler, N.D. Volkow, M.J. Kuhar, F.I. Carroll, Synthesis and nicotinic acetylcholine receptor binding properties of exo-2-(2'-fluoro-5'-pyridinyl)-7-azabicyclo-[2.2.1]heptane: A new positron emission tomography ligand for nicotinic receptors, *J. Med. Chem.* 40 (1997) 2293–2295.
- [232] Y.S. Ding, F. Liang, J.S. Fowler, M.J. Kuhar, F.I. Carroll, Synthesis of [¹⁸F]norchloro-fluoroepibatidine and its N-methyl derivative: New PET ligands for mapping nicotinic acetylcholine receptors, *J. Label. Compds Radiopharm.* 39 (1997) 828–832.
- [233] L. Dolci, F. Dollé, H. Valette, F. Vaufrey, C. Fuseau, M. Bottlaender, C. Crouzel, Synthesis of a fluorine-18 labelled derivative of epibatidine for *in vivo* nicotinic acetylcholine receptor PET imaging, *Bioorg. Med. Chem.* 7 (1999) 467–479.
- [234] F. Dollé, H. Valette, M. Bottlaender, F. Hinnen, F. Vaufrey, I. Guenther, C. Crouzel, Synthesis of 2-[¹⁸F]fluoro-3-[2(S)-2-azetidylmethoxy]pyridine, a highly potent radioligand for *in vivo* imaging central nicotinic acetylcholine receptors, *J. Label. Compds Radiopharm.* 41 (1998) 451–463.
- [235] F. Dollé, L. Dolci, H. Valette, F. Hinnen, F. Vaufrey, I. Guenther, C. Fuseau, C. Coulon, M. Bottlaender, C. Crouzel, Synthesis and nicotinic acetylcholine receptor *in vivo* binding properties of 2-fluoro-3-[2(S)-2-azetidylmethoxy]pyridine: A new

- positron emission tomography ligand for nicotinic receptors, *J. Med. Chem.* 42 (1999) 2251–2259.
- [236] A. Horti, A.O. Koren, H.T. Ravert, J.L. Musachio, W.B. Mathews, E.D. London, R.F. Dannals, Synthesis of a radiotracer for studying nicotinic acetylcholine receptors: 2-[¹⁸F]Fluoro-3-(2(S)-azetidinylmethoxy)pyridine (2-[¹⁸F]F-A-85380), *J. Label. Compds Radiopharm.* 41 (1998) 309–318.
- [237] T. Irie, K. Fukushi, O. Inoue, T. Yamasaki, Y. Kasida, 18F-labelled 6-fluoro-purine derivatives as a new type brain scanning agent, *J. Label. Compds Radiopharm.* 19 (1982) 1641–1642.
- [238] T. Irie, K. Fukushi, O. Inoue, T. Yamasaki, T. Ido, T. Nozaki, Preparation of fluorine-18-labeled 6-fluoro-9-benzylpurine and 2-fluoro-9-benzylpurine as a potential brain scanning agent, *Int. J. Appl. Radiat. Isot.* 33 (1982) 633–636.
- [239] F. Zeng, J.A. Southerland, R.J. Voll, J.R. Votaw, L. Williams, B.J. Ciliax, M.M. Goodman, Synthesis and evaluation of ¹⁸F-labeled FIMPYD as a PET imaging agent for beta-amyloid plaques, *J. Label. Compds Radiopharm.* 48 (2005) S41.
- [240] F.G. Simeon, V.W. Pike, Radiosyntheses of 2-[¹⁸F]fluoro-1,3-thiazoles, *J. Label. Compds Radiopharm.* 48 (2005) S158.
- [241] S. Kaneko, K. Ishiwata, K. Hatano, H. Omura, K. Ito, M. Senda, Enzymatic synthesis of no-carrier-added 6-[F-18]fluoro-L-DOPA with beta-tyrosinase, *Appl. Radiat. Isot.* 50 (1999) 1025–1032.
- [242] M.N. Eakins, S. Somain, 18F-Labelled amino acids as pancreatic scanning agents, *J. Label. Compds Radiopharm.* 16 (1979) 148–149.
- [243] O. Prante, K. Hamacher, H.H. Coenen, Chemo-enzymatic n.c.a. synthesis of the coenzyme uridine diphospho-2-deoxy-2-[¹⁸F]fluoro-alpha-D-glucose, *J. Label. Compds Radiopharm.* 42 (1999) S111.
- [244] G.W. Gribble, Natural organohalogens: A new frontier for medicinal agents? *J. Chem. Educ.* 81 (2004) 1441–1449.
- [245] G.W. Gribble, The diversity of naturally produced organohalogens, *Chemosphere* 52 (2003) 289–297.
- [246] F.H. Vaillancourt, E. Yeh, D.A. Vosburg, S. Garneau-Tsodika, C. Walsh, Nature's inventory of halogenation catalysts: Oxidative strategies predominate, *Chem. Rev.* 106 (2006) 3364–3378.
- [247] D. O'Hagan, C. Schaffrath, S.L. Cobb, J.T.G. Hamilton, C.D. Murphy, Biosynthesis of an organofluorine molecule, *Nature* 416 (2002) 279.
- [248] C. Dong, F. Huang, H. Deng, C. Schaffrath, J. Spencer, D. O'Hagan, J.H. Naismith, Crystal structure and mechanism of a bacterial fluorinating enzyme, *Nature* 427 (2004) 561–565.
- [249] C.D. Cadicamo, J. Courtieu, H. Deng, A. Meddour, D. O'Hagan, Enzymatic fluorination in *Streptomyces cattleya* takes place with an inversion of configuration consistent with an S_N2 reaction mechanism, *ChemBioChem* 5 (2004) 685–690.
- [250] L. Martarello, C. Schaffrath, H. Deng, A.D. Gee, A. Lockhart, D. O'Hagan, The first enzymatic method for C-F-18 bond formation: The synthesis of 5'-[F-18]-fluoro-5'-deoxyadenosine for imaging with PET, *J. Label. Compds Radiopharm.* 46 (2003) 1181–1189.
- [251] H. Deng, S.L. Cobb, A.D. Gee, A. Lockhart, L. Martarello, R.P. McGlinchey, D. O'Hagan, M. Onega, Fluorinase mediated C-F-18 bond formation, an enzymatic tool for PET labelling, *Chem. Comm.* (2006) 652–654.
- [252] H.J. Wester, K. Hamacher, G. Stöcklin, A comparative study of N.C.A. fluorine-18 labeling of proteins via acylation and photoactivation, *Nucl. Med. Biol.* 23 (1996) 365–372.
- [253] G. Vaidyanathan, M.R. Zalutsky, Labeling of proteins with fluorine-18 using N-succinimidyl 4-[¹⁸F]fluorobenzoate, *Nucl. Med. Biol.* 19 (1992) 275–281.
- [254] G. Vaidyanathan, M.R. Zalutsky, Improved synthesis of N-succinimidyl 4-[¹⁸F]fluorobenzoate and its application to the labeling of monoclonal antibody fragment, *Bioconj. Chem.* 5 (1994) 352–356.

- [255] E.D. Hostetler, W.B. Edwards, C.J. Anderson, M.J. Welch, Synthesis of 4-[^{18}F] fluorobenzoyl octreotide and biodistribution in tumor-bearing Lewis rats, *J. Label. Compds Radiopharm.* 42 (1999) S720–S722.
- [256] C.M. Müller-Platz, G. Kloster, G. Legler, G. Stöcklin, ^{18}F -Fluoroacetate: An agent for introducing no-carrier-added fluorine-18 into urokinase without loss of biological activity, *J. Label. Compds Radiopharm.* 19 (1982) 1645–1646.
- [257] D. Block, H.H. Coenen, G. Stöcklin, N.C.A. ^{18}F -Fluoroacylation via fluorocarboxylic acid esters, *J. Label. Compds Radiopharm.* 15 (1988) 185–200.
- [258] L. Lang, W.C. Eckelman, One-step synthesis of ^{18}F -labelled [^{18}F]-N-succinimidyl 4-(fluoromethyl)benzoate for protein labelling, *Appl. Radiat. Isot.* 45 (1994) 1155–1163.
- [259] L. Lang, W.C. Eckelman, Labeling proteins at high specific radioactivity using N-succinimidyl 4-(^{18}F fluoromethyl)benzoate, *Appl. Radiat. Isot.* 48 (1997) 169–173.
- [260] P.K. Garg, S. Garg, D.D. Bigner, M.R. Zalutsky, Fluorine-18 labeling of monoclonal antibodies and fragments with preservation of immunoreactivity, *Bioconj. Chem.* 2 (1991) 44–49.
- [261] H.J. Wester, K. Hamacher, S. Gohlke, G. Stöcklin, A simple and fast ^{18}F -labeling of proteins by coupling with photogenerated [^{18}F]arylnitrene, *J. Nucl. Med.* 35 (1994) 73P.
- [262] L.W. Herman, A.J. Fischman, R.G. Tompkins, R.N. Hanson, C. Byon, H.W. Strauss, D.R. Elmaleh, The use of pentafluorophenyl derivatives for the ^{18}F labelling of proteins, *Nucl. Med. Biol.* 21 (1994) 1005–1010.
- [263] Y. Shai, L. Kirk, M.A. Channing, B.B. Dunn, M.A. Lesniak, R.C. Eastman, R.D. Finn, J. Roth, K.A. Jacobson, ^{18}F -labeled insulin: A prosthetic group methodology for incorporation of a positron emitter into peptides and proteins, *Biochem.* 28 (1989) 4801–4806.
- [264] M. Brinkley, A brief survey of methods for preparing protein conjugates with dyes, haptens, and cross-linking reagents, *Bioconj. Chem.* 3 (1992) 2–13.
- [265] G.T. Hermanson, *Bioconjugate Techniques*, Academic Press, San Diego (CA), (1996).
- [266] C.Y. Shiue, A.P. Wolf, J.F. Hainfeld, Synthesis of ^{18}F -labelled N-(p-[^{18}F]fluorophenyl) maleimide and its derivatives for labelling monoclonal antibody with ^{18}F , *J. Label. Compds Radiopharm.* 26 (1989) 287–289.
- [267] T. Toyokuni, J.C. Walsh, A. Dominguez, M.E. Phelps, J.R. Barrio, S.S. Gambhir, N. Satyamurthy, Synthesis of a new heterobifunctional linker, N-[4-(amino-oxy)butyl] maleimide, for facile access to a thiol-reactive ^{18}F -labeling agent, *Bioconj. Chem.* 14 (2003) 1253–1259.
- [268] W. Cai, X. Zhan, Y. Wu, X. Chen, A thiol-reactive ^{18}F -labeling agent, N-[2-(4- ^{18}F -fluorobenzamido)ethyl]maleimide, and synthesis of RGD peptide-based tracer for PET imaging of α -v- β -3-integrin expression, *J. Nucl. Med.* 47 (2006) 1172–1180.
- [269] F. Dollé, Preparation of [^{18}F]labeled maleimides, their use for marking macromolecules for medical imaging, *PCT Int. Appl.* (2004) 58 pp, WO 2004002984.
- [270] P.E. Nielsen, M. Egholm, R.H. Berg, O. Buchardt, Sequence-selective recognition of DNA by strand displacement with a thymine-substituted polyamide, *Science* 254 (1991) 1497–1500.
- [271] P.E. Nielsen, M. Egholm, *Peptide Nucleic Acids: Protocols and Applications*, Horizon Scientific Press, Norfolk, (1999).
- [272] B. Kuhnast, F. Dollé, B. Tavitian, Fluorine-18 labeling of peptide nucleic acids, *J. Label. Compds Radiopharm.* 45 (2001) 1–11.
- [273] R. Hamzavi, F. Dollé, B. Tavitian, O. Dahl, P. Nielsen, Modulation of the pharmacokinetic properties of PNA: Preparation of galactosyl, mannosyl, fucosyl, N-acetylgalactosaminyl and N-acetylglucosaminyl derivatives of aminoethylglycine peptide nucleic acid monomers and their incorporation into PNA oligomers, *Bioconj. Chem.* 14 (2003) 941–954.
- [274] B. Kuhnast, F. Hinnen, R. Hamzavi, R. Boisgard, B. Tavitian, P.E. Nielsen, F. Dollé, Fluorine-18 labelling of PNAs functionalized at their pseudo-peptidic backbone for imaging studies with PET, *J. Label. Compds Radiopharm.* 48 (2005) 51–61.

- [275] T. Poethko, M. Schottelius, G. Thumshirn, U. Hersel, M. Herz, G. Henriksen, H. Kessler, M. Schwaiger, H.J. Wester, Two-step methodology for high-yield routine radiohalogenation of peptides: ^{18}F -Labeled RGD and octreotide analogs, *J. Nucl. Med.* 45 (2004) 892–902.
- [276] T. Poethko, M. Schottelius, G. Thumshirn, U. Hersel, M. Herz, R. Haubner, G. Henriksen, H. Kessler, M. Schwaiger, H.J. Wester, Chemoselective pre-conjugate radiohalogenation of unprotected mono- and multimeric peptides via oxime formation, *Radiochim. Acta* 92 (2004) 317–327.
- [277] E. Hedberg, B. Långström, Synthesis of 4-([^{18}F]fluoromethyl)phenyl isothiocyanate and its use in labeling oligonucleotides, *Acta Chem. Scand.* 51 (1997) 1236–1240.
- [278] E. Hedberg, B. Långström, ^{18}F -Labeling of oligonucleotides using succinimido 4-[^{18}F]fluorobenzoate, *Acta Chem. Scand.* 52 (1998) 1034–1039.
- [279] C.W. Lange, H.F. VanBrocklin, S.E. Taylor, Photoconjugation of 3-azido-5-nitrobenzyl [^{18}F]fluoride to an oligonucleotide aptamer, *J. Label. Compds Radiopharm.* 45 (2002) 257–268.
- [280] B. Kuhnast, F. Hinnen, R. Boisgard, B. Tavitian, F. Dollé, Fluorine-18 labeling of oligonucleotides: Prosthetic labeling at the 5'-end using the N-(4-[^{18}F]fluorobenzyl)-2-bromoacetamide reagent, *J. Label. Compds Radiopharm.* 46 (2003) 1093–1103.
- [281] B. Kuhnast, S. Klussmann, F. Hinnen, R. Boisgard, B. Rousseau, J.P. Fürste, B. Tavitian, F. Dollé, Fluorine-18- and iodine-125 labelling of Spiegelmers, *J. Label. Compds Radiopharm.* 46 (2003) 1205–1219.
- [282] S. Marzabal, S. Terrazzino, B. Kuhnast, F. Dollé, J.R. Deverre, A. Jobert, C. Crouzel, L. DiGiamberardino, B. Tavitian, *In vivo* imaging and pharmacokinetics of oligonucleotides, *Nucleosides Nucleotides* 18 (1999) 1731–1733.
- [283] B. Tavitian, S. Marzabal, V. Boutet, B. Kuhnast, S. Terrazzino, M. Moynier, F. Dollé, J.R. Deverre, A.R. Thierry, Characterization of a synthetic anionic vector for oligonucleotide delivery using *in vivo* whole body dynamic imaging, *Pharm. Res.* 19 (2002) 367–376.
- [284] R. Boisgard, B. Kuhnast, S. Vonhoff, C. Younes, F. Hinnen, J.M. Verbavatz, B. Rousseau, J.P. Fürste, B. Wlotzka, F. Dollé, S. Klussmann, B. Tavitian, *In vivo* biodistribution and pharmacokinetics of ^{18}F -labelled Spiegelmers: A new class of oligonucleotidic radiopharmaceuticals, *Eur. J. Nucl. Med. Mol. Imaging* 32 (2005) 470–477.
- [285] A. Nolte, S. Klussmann, R. Bald, V. Erdmann, J.P. Fürste, Mirror-design of L-oligonucleotide ligands binding to L-arginine, *Nat. Biotech.* 14 (1996) 1116–1119.
- [286] B. Wlotzka, S. Leva, B. Eschgfäller, J. Burmeister, F. Kleinjung, C. Kaduk, P. Muhn, H. Hess-Stumpp, S. Klussmann, *In vivo* properties of an anti-GnRH Spiegelmer: An example of an oligonucleotide-based therapeutic substance class, *Proc. Nat. Acad. Sci. USA* 99 (2002) 8898–8902.

Note from the Editors

On the use of ^{18}F -labelled molecules, see also in this volume chapters by K. Kopka *et al.* on cardiological imaging, K. Någren and J. O Rinne on application to Alzheimer's disease and K. Herrmann and B. J. Krause on application to oncology.

This page intentionally left blank

CHAPTER 2

Application of ^{18}F -PET Imaging for the Study of Alzheimer's Disease

Kjell Någren* and Juha O. Rinne

*Turku PET Centre, Radiopharmaceutical Chemistry Laboratory,
FIN 20520 Turku, Finland*

Contents

1. Introduction	68
2. PET and SPECT imaging in AD	69
2.1. Special features of ^{18}F -radiopharmaceuticals	69
2.2. Glucose metabolism and blood flow	70
2.3. Serotonergic system	72
2.4. Dopaminergic system	73
2.5. Cholinergic system	74
2.6. Histamine and benzodiazepine receptors	76
2.7. Amyloid deposits	77
3. Conclusions	78
References	79
Note from the Editors	84

Abstract

Alzheimer's disease (AD) is a devastating brain disorder of elderly humans. In recent years, there has been a rapid development in the understanding of the underlying pathophysiological mechanisms of AD. The present treatment is mainly based on cholinesterase inhibitors and glutamate drugs. Nicotinic agonists, anti-amyloid therapies, and neuroprotective drugs are also under development. In order to develop an efficient treatment for this disease, a further understanding of the brain systems involved in the different stages of the disease is needed. Brain imaging using technologies such as positron emission tomography (PET) and single photon emission computed tomography (SPECT) are valuable tools in this search for new drug targets for the treatment of AD. These technologies have also proven to be useful to study the action of established or new drugs on these targets. Using PET, important information on the *in vivo* selectivity and the plasma concentration–target occupancy of these new drugs can be achieved.

2- ^{18}F Fluoro-2-deoxy-D-glucose (^{18}F FDG) is the most commonly used PET radiopharmaceutical, and it has also proven to be valuable in the early detection of AD and in the differentiation of AD from other causes of dementia. ^{18}F -Labeled radiopharmaceuticals have also successfully been used to study various components of the serotonergic brain

*Corresponding author. Tel.: +358-2-313-2865; Fax: +358-2-313-2882;
E-mail: kjell.nagren@utu.fi

system in patients with AD. For other neural systems, the first generation of PET and SPECT radiopharmaceuticals have been labeled with ^{11}C or ^{123}I . They have been useful to study brain systems such as the cholinergic and dopaminergic systems and to measure amyloid burden in patients with AD.

A number of recently developed ^{18}F -radiopharmaceuticals have great potential for the study of several brain systems of clinical importance in AD. These radiotracers will facilitate the exploration of patients with PET as they can be shipped to several satellite centers that rely on supply of radiopharmaceuticals from distributors.

The development of specific radiopharmaceuticals for various neurotransmitter systems could eventually help in the early detection, differential diagnosis, or evaluation of different treatments for AD.

1. INTRODUCTION

Alzheimer's disease (AD) is a neurodegenerative disorder that affects nearly 2% of the population in industrialized countries; the risk of AD dramatically increases in individuals beyond the age of 70 and it is predicted that the incidence of AD will increase threefold within the next 50 years [1]. Finding a treatment that could delay onset by 5 years could reduce the number of individuals with AD by nearly 50% after 50 years [2].

AD is characterized by a slowly progressive loss of memory and other cognitive functions and appearance of behavioral disturbances leading to loss of independence in daily life. The brain processes have most probably been ongoing for several years at a nonsymptomatic stage prior to symptomatic stage and the final stage of moderate to severe dementia. Alois Alzheimer first described a patient with the typical neuropathological hallmarks of AD, amyloid plaques and neurofibrillary tangles [3]. Currently, the amyloid cascade model is the prevailing hypothesis. However, the exact mechanism how amyloid pathology leads to neuronal degeneration, for instance to progressive neuronal loss and atrophy of the medial temporal lobe structures, is still unclear. According to the amyloid cascade hypothesis, the pathological amyloid process results in several biochemical deficits. Degeneration of various subcortical nuclei leads to deficits of cholinergic, dopaminergic, serotonergic, and noradrenergic neurotransmission. Other transmitter systems are also affected. The most convincing is the degeneration of the ascending cholinergic system, leading to cholinergic deficiency and cognitive deficits [4]. Changes in other neurotransmitter systems, such as the dopaminergic system, have also been found to contribute to aging-related cognitive decline [5]. Postmortem studies have found changes in peripheral benzodiazepine receptors [6], histamine content [7], and serotonergic systems [8]. AD thus affects a variety of neurotransmitter systems during the course of the disease. Molecular imaging is the only tool by which we can study these neurotransmitter systems in living humans. These studies can give unique possibilities for early diagnosis and improved differential diagnosis. Another area where molecular imaging can successfully be used is in the study of the relationship of neurotransmitter systems with specific AD symptoms (Table 1).

Table 1. Different fluorine-labeled PET tracers with their functional targets

Ligand	Brain function	Suggested AD-related functions/symptoms
[^{18}F]FDG	Metabolism	Neuronal function
[^{18}F]MPPF	Serotonin 5-HT _{1A} receptors	Mood
[^{18}F]FCWAY	Serotonin 5-HT _{1A} receptors	Anxiety
[^{18}F]Setoperone	Serotonin 5-HT _{2A} receptors	Sleep–wake cycle
[^{18}F]Altanserine	Serotonin 5-HT _{2A} receptors	Behavioral symptoms
[^{18}F]Fallypride	Dopamine D ₂ receptors	Motor functions
[^{18}F]CFT	Dopamine reuptake	Motivation, reward
[^{18}F]FP-CIT	Dopamine reuptake	Executive functions
[^{18}F]FECNT	Dopamine reuptake	and working memory
[^{18}F]A85380	Acetylcholine β_2 receptors	Cognition
[^{18}F]FP-TZTP	Muscarine M ₂ receptors	Attention
[^{18}F]FETp4A	Acetylcholinesterase	Behavioral symptoms
[^{18}F]FETpM2A	Acetylcholinesterase	
[^{18}F]FETpY3A	Acetylcholinesterase	
[^{18}F]FETpM4B	Butyrylcholinesterase	
[^{18}F]PK14105	Microglia	Neuroinflammation
[^{18}F]FEDAA1106	Microglia	
[^{18}F]FDDNP	Amyloid plaques, tangles	Amyloid and tangle
[^{18}F]FEPI	Amyloid plaques	pathology
[^{18}F]FPIIP	Amyloid plaques	

A number of earlier reviews have given summaries on the use of PET for the study of AD [e.g., 9–11]. In this chapter, we will also include recent work on ^{11}C - and ^{123}I -tracers, and present recently developed ^{18}F -tracers that would be useful for this imaging purpose.

2. PET AND SPECT IMAGING IN AD

2.1. Special features of ^{18}F -radiopharmaceuticals

The main feature of the short-lived positron-emitting isotope ^{18}F is the relative long half-life of 110 min. The ultrashort-lived isotopes ^{11}C , ^{13}N , and ^{15}O have half-lives of 2–20 min, and they must subsequently be produced in the vicinity of the PET scanner(s). Radiopharmaceuticals labeled with ^{18}F , on the contrary, can be shipped to distant “satellite” PET centers that are not equipped with a cyclotron. Several commercial companies are today producing 2-[^{18}F]fluoro-2-deoxy-D-glucose

(^{18}F FDG), which is distributed to customers within Europe, United States, or Asia. These companies are actively developing new ^{18}F -labeled radiopharmaceuticals, often in collaboration with academic research centers, with the hope to find new ^{18}F -labeled products that can be distributed to customers.

The second feature that distinguishes ^{18}F from the ultrashort-lived isotopes is that its stable counterpart ^{19}F is not commonly found in endogenous compounds. In most cases, the new ^{18}F -labeled radiopharmaceuticals are analogues of well-documented compounds. As the analogues are new chemical entities, a large documentation on toxicology and other aspects influencing their safe use in human has been a prerequisite before human PET studies could be initiated.

Fortunately, many of the new drugs that are presently developed contain fluorine atoms, and in these cases it is not necessary to develop analogues. The information on toxicology can in these cases often be found in the companies that produce the actual drugs. In recent years, regulatory bodies such as FDA in the United States and EMEA in Europe have adopted the microdosing concept [12] for exploratory studies with new PET radiopharmaceuticals. The basic principle of the microdosing concept is that while PET radiopharmaceuticals are administered only for a short period of time (often only once) and at doses more than 1000 times lower than the therapeutic dose, less safety documentation is required than for drugs developed for therapeutic use. The microdosing concept has reduced the amount of documentation on toxicology for exploratory studies and removed one of the obstacles for the evaluation of new PET radiopharmaceuticals in human.

2.2. Glucose metabolism and blood flow

The most commonly used radiopharmaceutical in PET is [^{18}F]FDG. PET imaging of glucose metabolism of patients with AD *in vivo* with [^{18}F]FDG has been carried out extensively [13]. These studies have revealed glucose metabolic reductions in the parietotemporal, frontal, and posterior cingulate cortices to be a hallmark of AD [13]. FDG is widely used, well-documented, and an important tracer in clinical and scientific studies on AD and related disorders, and its usefulness has been thoroughly reviewed, also very recently (for a review see Refs. [14] and [15]). [^{18}F]FDG has up to 90% sensitivity in the early detection of AD, although its specificity to differentiate AD from other causes of dementia is lower [14]. In the United States, Medicare covers [^{18}F]FDG-PET imaging for the indication of differentiation of possible AD from frontotemporal dementia. FDG-PET studies have shown that clinically normal individuals carrying the apolipoprotein E (apoE) $\epsilon 4$ allele (the presence of which increases the risk to develop AD) have reduced metabolism in same brain areas as patients with AD [16,17]. These metabolic changes are progressive and correlate with impairment of cognitive performance. However, it is still to be proven that these changes are due to very early AD.

Mild cognitive impairment (MCI), especially its amnesic type, is a prodrome of AD with 10–15% of individuals with MCI converting to AD annually [18]. Longitudinal [^{18}F]FDG-PET has been shown to predict normal elderly individuals developing MCI and also to predict conversion from MCI to AD [14,15]. In some studies, medial temporal hypometabolism was found to be most sensitive and specific in this respect [14], whereas in other studies regional hypometabolism of the posterior cingulate cortex was found to be the earliest and most sensitive marker predicting AD in MCI [19–22].

Another way to tap on early AD is to study individuals with increased genetic susceptibility for AD. Asymptomatic carriers of either amyloid precursor protein gene or presenilin gene mutations have been shown to have progressive parietotemporal hypometabolism resembling the pattern seen in clinical AD [14]. Recent twin studies indicate that in nonfamilial (sporadic) AD, 48% of the variation in liability to AD could be attributed to genetic variation [23]. Accordingly, an [^{18}F]FDG-PET study in monozygotic twin pairs where one twin has AD and the other is cognitively intact has demonstrated hippocampal and temporal hypometabolism already present in the asymptomatic cotwin (Fig. 1, [24]). Other genetic variation that has been shown to affect glucose metabolism is the apoE genotype. Individuals who are homozygous for apoE ϵ 4 allele show reduced metabolism compared to individuals without ϵ 4 allele [25,26]. These reductions are seen in brain areas typically affected in early AD. In a follow-up study, it was found that the ϵ 4 heterozygotes had significant glucose metabolism declines in the vicinity of temporal, posterior cingulate, and prefrontal cortex, basal forebrain, parahippocampal gyrus, and thalamus, and that these declines were significantly greater than those in the ϵ 4 noncarriers.

PET and SPECT are increasingly used in drug development. Characterization of longitudinal changes in glucose metabolism in AD and other dementias has

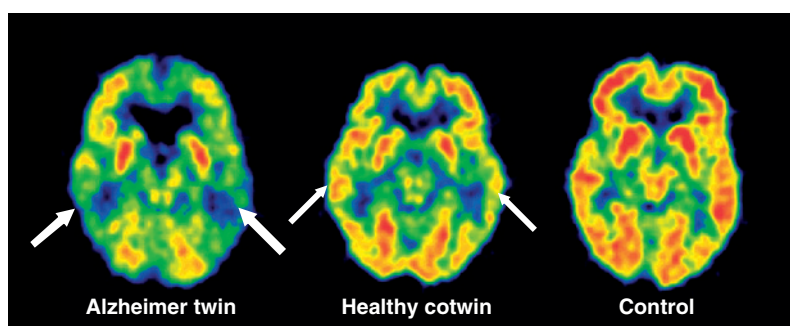


Fig. 1. An [^{18}F]FDG-PET scan depicting glucose metabolism in a monozygotic twin pair and in a control subject. Note the clear reduction in [^{18}F]FDG uptake especially in temporoparietal areas (thick arrows) in the cotwin having AD (on the left), and similar, but less pronounced reduction in same brain areas (thin arrows) in the cognitively healthy cotwin (in the middle) as compared with the uptake in a control subject (on the right). (See Colour Plate Section at the end of this book.)

been important regarding the possible use of [^{18}F]FDG as a tool for therapy monitoring [20,27,28]. Indeed, PET and SPECT measures of resting brain function appear to be sensitive to medication effects in clinical drug trials and relate to clinical measures in a manner that suggests their potential utility as surrogate markers [29,30]. In studies in AD patients given cholinesterase inhibitors, serial [^{18}F]FDG-PET measures parallel clinical measures in demonstrating stability or improvement in treated versus placebo groups or in predicting response in treated groups [31–33].

Another class of commonly used radiopharmaceuticals measure regional brain blood flow. In PET, [^{15}O]H₂O is used as a radiopharmaceutical and in SPECT, [$^{99\text{m}}\text{Tc}$]HMPAO, [$^{99\text{m}}\text{Tc}$]ECD, or [^{123}I]IMP are used. Studies of patients with AD with the use of these radiopharmaceuticals have been thoroughly reviewed elsewhere [e.g., 34–36] and it is out of the scope of this chapter to further discuss these studies.

2.3. Serotonergic system

Many behavioral and psychological symptoms of dementia (BPSD) and also cognitive functions have been linked with serotonergic system. Two different selective ^{18}F -labeled antagonists of the serotonin 2A (5-HT_{2A}) receptors have been used in the study of Alzheimer patients with PET. [^{18}F]Setoperone was used in a study of 9 nonmedicated patients with probable AD and 37 healthy controls [37]. Specific binding in the cerebral cortex, quantified using cerebellum as a reference, in patients with AD was reduced to 35–69% relative to healthy controls. [^{18}F]Altanserin was used in a study of 11 patients with depression, 9 with AD, including 3 with concurrent depression, and 10 age-matched healthy subjects [38]. No change in [^{18}F]altanserin binding was detected in depressed patients; however, the patients with AD had significantly lower [^{18}F]altanserin binding in several cortical areas of the brain.

An ^{18}F -labeled antagonist of the serotonin 1A (5-HT_{1A}) receptor, [^{18}F]MPPF, was recently used in a study of eight patients with AD, six patients with MCI, and five healthy controls [39]. 5-HT_{1A} receptor densities were reduced in the hippocampi and raphe nuclei, with larger reduction in patients with AD as compared to patients with MCI, 49% versus 24%. The tracer [^{18}F]MPPF gives a rather low target-to-background ratio which might explain the overlap of 5-HT_{1A} receptor densities in the three groups when examined with [^{18}F]MPPF. Two new ^{18}F -labeled tracers of the 5-HT_{1A} receptor with significantly increased target-to-background ratios, [^{18}F]FCWAY [40] and [^{18}F]DMPPF [41], have recently been developed. Of these two, [^{18}F]FCWAY suffers from defluorination *in vivo*, giving rise to [^{18}F]fluoride that is taken up in the bone, for instance in the skull [42]. Quantification of [^{18}F]FCWAY uptake in adjacent cortical areas is hampered by the radioactivity in skull. The second ^{18}F -labeled tracer, [^{18}F]DMPPF, has so far been studied only

in rat, but does not seem to suffer from defluorination, and is a promising candidate for the study of AD and MCI patients with PET. The molecular structures of ^{18}F -labeled tracers for the serotonergic system are shown in Fig. 2.

2.4. Dopaminergic system

A PET study using selective tracers for striatal dopamine D_1 ($[^{11}\text{C}]\text{NNC 756}$) and striatal dopamine D_2 ($[^{11}\text{C}]\text{raclopride}$) receptors showed that while striatal D_2 receptors were unaffected in patients with AD, striatal D_1 receptors were reduced by 14% in patients with AD compared with healthy age-matched controls [43]. At present, no ^{18}F -labeled dopamine D_1 tracers have been validated for human PET studies.

A subsequent PET study using a selective tracer for extrastriatal dopamine D_2 receptor, $[^{11}\text{C}]\text{FLB 457}$, showed that D_2 receptor binding potential was decreased by 12–34% in hippocampal and temporal cortical regions in patients with AD compared with healthy controls [44]. In addition, the D_2 receptor binding potential in the right hippocampus was found to correlate with memory functions, measured by the Wechsler Memory Scale (Revised version) and language function evaluated with the Boston Naming Test. Recently, an ^{18}F -labeled tracer for the extrastriatal dopamine D_2 receptor, $[^{18}\text{F}]\text{fallypride}$, has been developed [45,46]. So far, the use of this new tracer for the study of AD with PET has not been reported.

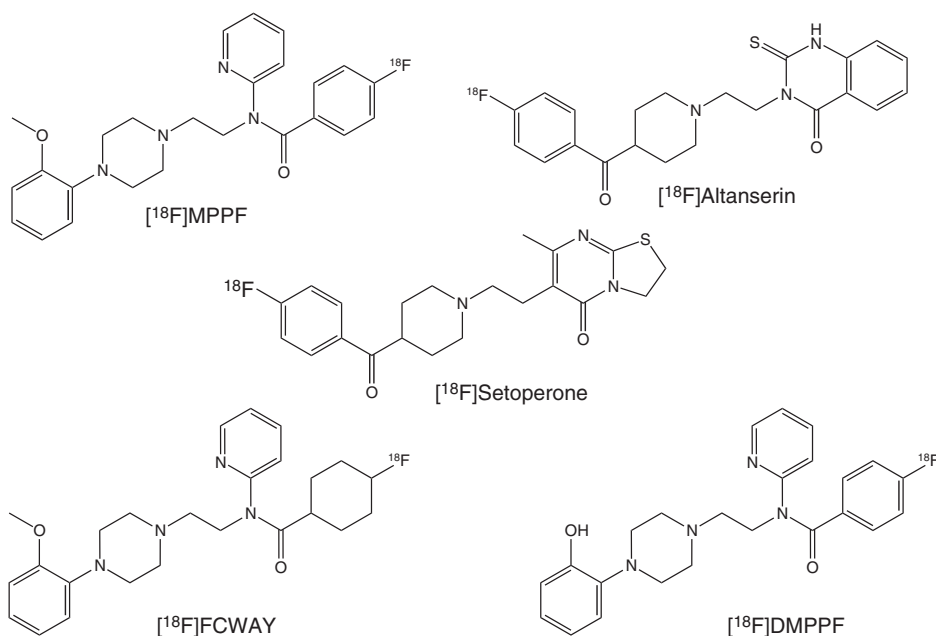


Fig. 2. ^{18}F -Labeled tracers for the serotonergic system.

A reduced binding of dopamine reuptake radioligands in the striatum of patients with AD when compared with healthy controls has been reported by using both [^{11}C]CFT and PET [47] and [^{123}I]FP-CIT and SPECT [48]. However, the reduction is rather small and in some studies no significant change in dopamine transporter imaging has been seen in patients with AD, whereas in dementia with Lewy bodies there is a marked reduction in SPECT tracer (FP-CIT) uptake [49]. This finding gives a possibility to use FP-CIT and other dopamine transporter markers in the differential diagnosis between AD and dementia with Lewy bodies, although before final conclusions more studies with pathological confirmation of the diagnosis are needed. Several ^{18}F -labeled tracers of dopamine reuptake have been developed and studied in human and among these, [^{18}F]CFT [50], [^{18}F]FP-CIT [51], and [^{18}F]FECNT [52] are the best characterized; however, so far they have not been used in studies of AD with PET. The molecular structures of ^{18}F -labeled tracers for the dopaminergic system are shown in Fig. 3.

2.5. Cholinergic system

Both nicotinic and muscarinic acetylcholinergic receptors have been found to be decreased in the brain of patients with AD. The changes in nicotinic acetylcholinergic

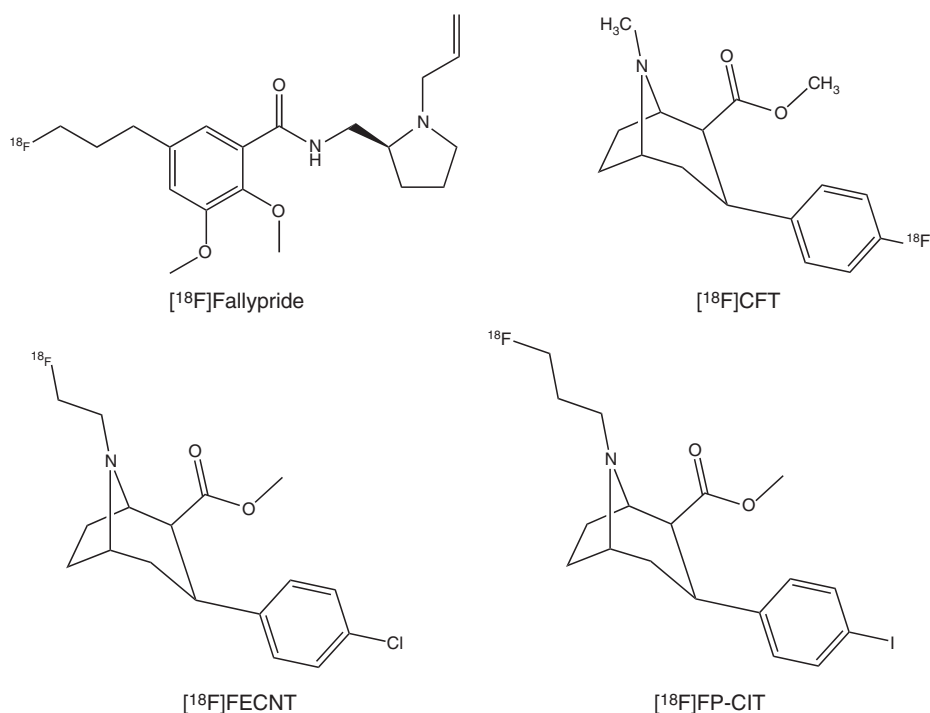


Fig. 3. ^{18}F -Labeled tracers for the dopaminergic system.

receptors (nAChRs) have been found using both *in vitro* [53,54] and [^{11}C]nicotine PET methods [55]. A recently developed tracer for the β_2 subtypes of the nAChRs, [^{18}F]A85380, has demonstrated decrease in AD *in vitro* [56] and this new tracer is a very promising tool for the study of AD patients using PET.

Decreases in muscarinic acetylcholinergic receptors (mAChRs) in patients with AD have also been demonstrated with SPECT using [^{123}I]IQNB [57] or [^{123}I]iododexetimide [58] and with PET using [^{11}C]NMPB [59]. [^{18}F]FP-TZTP is a recently developed tracer for the M2 subtype of the mAChRs. The binding of [^{18}F]FP-TZTP in the brain has been found to be higher in older healthy humans compared with younger ones, probably reflecting lower acetylcholine concentrations [60]. The binding of [^{18}F]FP-TZTP in the brain has also been found to be increased in subjects with an apoE $\epsilon 4$ allele [61]. [^{18}F]FP-TZTP is a promising new tool for the study of mAChRs in AD patients using PET.

Another strategy for the study of the brain cholinergic system using PET is to use labeled substrates for the enzymes acetylcholinesterase (AChE) and butyrylcholinesterase (BuChE). Postmortem brain studies have suggested that while AChE activity decreases during the course of AD, BuChE activity increases. Most of the currently used drugs for AD are inhibitors of AChE and/or BuChE, indirectly increasing the concentration of acetylcholine in the brain. Hydrolysis of the substrates by the enzymes yields labeled products that are trapped in the cell in analogy to [^{18}F]FDG, which is trapped as the corresponding phosphate. Study of these two enzymes, AChE and BuChE, *in vivo* in AD using PET is of special importance as many drugs for AD are targeting these two enzymes. By studying the action of established or new drugs on these enzymes using PET, important information on the *in vivo* selectivity (AChE vs BuChE) and the plasma concentration versus brain enzyme occupancy can be achieved.

The first generation of labeled AChE or BuChE substrates for PET has been labeled with ^{11}C . Brain AChE has been found to be reduced in patients with AD compared with healthy age-matched volunteers when studied with PET and [^{11}C]MP4A [62] or [^{11}C]MP4P [63]. By using [^{11}C]MP4A, it has also been suggested that a low cortical AChE activity in patients with MCI may be an indicator of impending dementia [64]. However, changes in AChE activity are relatively small and considerable overlap exists, and thus it seems unlikely that AChE ligands would be helpful in the early diagnosis of AD. In spite of this limitation, they might be very useful in drug development for AD, for instance in characterizing the properties of different drugs targeting cholinergic enzymes. In contrast, brain BuChE was not found to be changed in patients with AD compared with healthy age-matched volunteers when studied with PET and [^{11}C]MP4B [65]. However, since there may be changes in AChE and BuChE activities during the course of the disease, further studies are needed with patients at different stages of dementia.

As an example of the use of these tracers in drug development, [^{11}C]MP4A has been used to study the regional effects of donepezil and rivastigmine on cortical AChE activity in patients with AD [66]. Both drugs were found to reduce

AChE activity to a greater extent in the frontal cortex compared with the temporal cortex. Similar effects on brain AChE activity were found after 3 months of treatment with donepezil (10 mg/day) or after 3–5 months of treatment with rivastigmine (9 mg/day) [66].

Several ^{18}F -labeled substrates for AChE or BuChE have been developed and all of them are candidates for PET studies of the action of drugs on the brain AChE or BuChE. The most promising ^{18}F -labeled AChE radiotracers are [^{18}F]FETP4A ([^{18}F]N-fluoroethyl-4-piperidyl acetate) [67], [^{18}F]FETPM2A ([^{18}F]N-fluoroethyl-2-piperidinemethyl acetate), and [^{18}F]FETPy3A ([^{18}F]N-fluoroethyl-3-pyrrolidinyl acetate) [68]. ^{18}F -Labeled [^{18}F]FETPM4B ([^{18}F]N-fluoroethylpiperidine-4-ylmethyl butyrate) is the most promising radiotracer for BuChE[69]. As all of these compounds contain an [^{18}F]fluoroethyl group, they can be labeled from the same ^{18}F -labeled precursor. The molecular structures of ^{18}F -labeled tracers for the cholinergic system are shown in Fig. 4.

2.6. Histamine and benzodiazepine receptors

The selective ^{11}C -labeled antagonist of the histamine 1 (H_1) receptor [^{11}C]doxepin has been used in a study of 11 healthy subjects and 10 AD patients with PET. The binding potential of H_1 receptors showed a significant decrease especially in the frontal and temporal areas of the brain in patients with AD. In addition, the

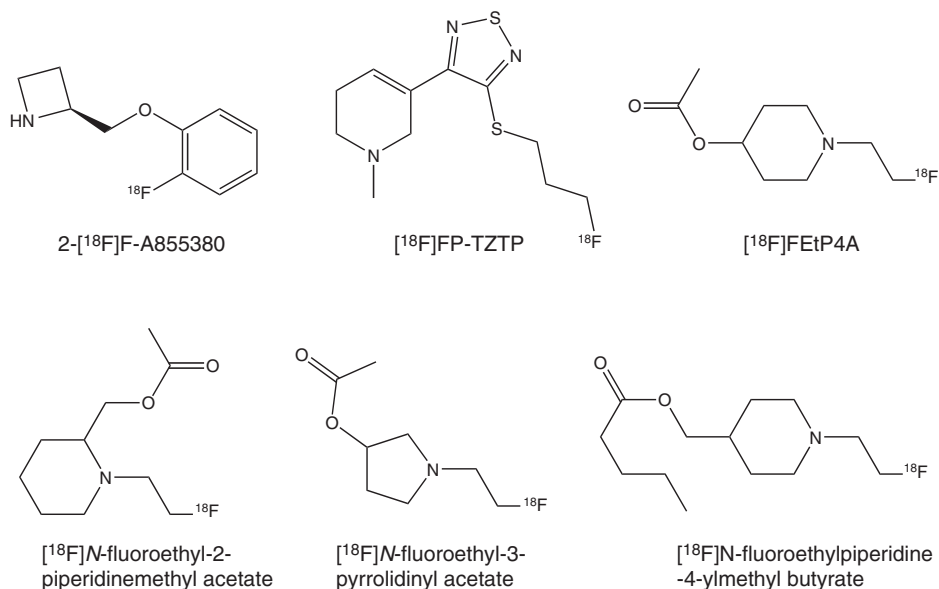


Fig. 4. ^{18}F -Labeled tracers for the cholinergic system.

receptor binding correlated closely to the severity of the AD assessed by the Mini-Mental State Examination score within several brain areas [70]. A disadvantage of doxepin has been its dependence on blood flow. Presently, no ^{18}F -labeled tracers have been developed for the H_1 receptor. Histamine receptors, especially H_3 receptors, are under vivid investigations as drug targets for AD and other central nervous system disorders [71]. Accordingly, new histaminergic PET tracers are likely to be developed in the near future.

A recent study found that cortical peripheral benzodiazepine receptors, as assessed with PET and $[^{11}\text{C}]\text{PK11195}$, were increased by 30–40% in patients with AD when compared with healthy controls. This suggests active inflammatory processes in AD since PK11195 binds to activated microglia [72]. Several ^{18}F -labeled tracers of the peripheral benzodiazepine receptor have been developed, and $[^{18}\text{F}]\text{PK14105}$ [73] and $[^{18}\text{F}]\text{FEDAA1106}$ [74] are the most well characterized. However, no reports have been published on the use of either of the two radiotracers in AD. The molecular structures of ^{18}F -labeled tracers for the peripheral benzodiazepine receptor are shown in Fig. 5.

2.7. Amyloid deposits

A new and exciting area in the field of PET studies of patients with MCI and AD is the use of positron-emitter-labeled tracers that bind to amyloid deposits in the brain. These ligands will help to evaluate the role of amyloid in the pathophysiology of AD and could also serve as surrogate markers in studies aiming to affect amyloid accumulation, although recent preliminary reports show little change in PIB uptake during the course of AD [75]. This indicates that if PIB uptake is to be used as a surrogate marker of anti-amyloid treatment, this kind of treatment need to start in the earliest detectable stage of the disease or should be directed toward reduction of the present amyloid plaque load. Also in this field most PET

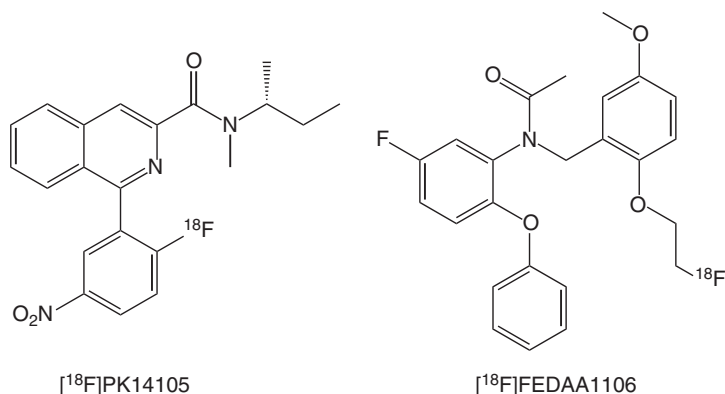


Fig. 5. ^{18}F -Labeled tracers for the peripheral benzodiazepine receptor.

imaging studies have been performed using ^{11}C -labeled tracers, mainly [^{11}C]6-OH-BTA-1 ([^{11}C]PIB). A proof-of-concept study showed a marked retention of [^{11}C]PIB in the association cortex of patients with mild AD compared with healthy controls [76]. Subsequent studies have demonstrated a widespread increase in PIB uptake in patients with AD [77] and also slight changes in a subpopulation of subjects with MCI [78]. Follow-up studies will show how well PIB uptake will predict who will eventually develop AD. Another [^{11}C]-labeled compound used for amyloid imaging is a stilbene derivative [^{11}C]SB-13 [79].

An ^{18}F -labeled tracer, [^{18}F]FDDNP, that labels both neurofibrillary tangles and β -amyloid plaques has also been used in a PET study of patients with AD and healthy controls, where the relative residence time for the tracer was significantly higher in patients with AD [80]. Recently, two ^{18}F -labeled tracers, [^{18}F]FEPIP and [^{18}F]FPPIP, have been shown to label amyloid plaques in human AD cortical tissues [81]. ^{18}F -Labeled tracers have the advantage of allowing longer scanning time than ^{11}C -labeled tracers, the usefulness of which in relation to amyloid imaging is still to be proven. The molecular structures of these ^{18}F -labeled tracers for the amyloid plaques are shown in Fig. 6. In addition, several other ^{18}F -labeled tracers for the amyloid plaques, such as ^{18}F derivatives of PIB, are under development; however, so far no human studies have been reported.

3. CONCLUSIONS

^{18}F -Labeled radiopharmaceuticals have a special advantage for clinical and academic PET studies due to the relatively long half-life of ^{18}F . The radiotracer can be used for several sequential PET studies of different patients, and it can also be shipped to remote PET centers that do not have a production of radiopharmaceuticals. [^{18}F]FDG is already an established tool in the diagnosis of patients with AD. A few ^{18}F -labeled tracers for serotonin receptors and amyloid plaques have

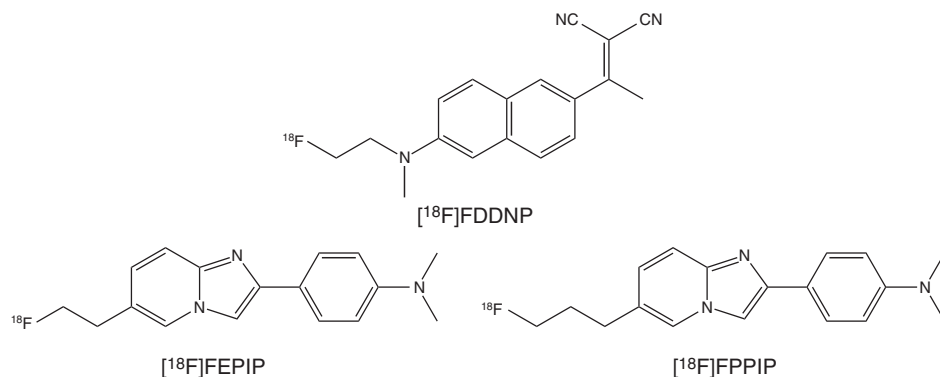


Fig. 6. ^{18}F -Labeled tracers for amyloid plaques.

also proven to be useful in the study of AD. There are several examples among other recently developed ^{18}F -labeled tracers that have potential for this imaging purpose. [^{18}F]Fallypride can be used to study both striatal and extrastriatal dopamine D_2 receptors. [^{18}F]A85380 is promising for the study of β_2 subtypes of the nAChRs. Several ^{18}F -labeled substrates for AChE or BuChE have been developed that are also promising for the study of new drugs for these enzymes. Tracers such as [^{18}F]FEDAA1106 can be used to study microglial activation. H_1 receptors have been shown to be dramatically reduced in AD by using a ^{11}C -labeled tracer, but we are still waiting for the development of the first useful ^{18}F -labeled tracer for H_1 or other types of histaminergic receptors. The development of specific ligands for various neurotransmitter systems could eventually help in the early detection, differential diagnosis, or evaluation of different treatments for AD.

REFERENCES

- [1] L.E. Hebert, P.A. Scherr, J.L. Bienias, D.A. Bennet, D.A. Evans, Alzheimer disease in the US population. Prevalence estimates using the 2000 census, *Arch. Neurol.* 60 (2003) 1119–1122.
- [2] R. Brookmeyer, S. Gray, C. Kawas, Projections of Alzheimer's disease in the United States and the public health impact of delaying disease onset, *Am. J. Public Health* 88 (1998) 1337–1342.
- [3] A. Alzheimer, über eine eigenartige Erkrankung der Hirnrinde, *Allgemeine Zeitschrift für Psychiatrie* 64 (1907) 146–148.
- [4] M.R. Farlow, Etiology and pathogenesis of Alzheimer's disease, *Am. J. Health Syst. Pharm.* 55 (Suppl. 2) (1998) S5–S10.
- [5] L. Bäckman, N. Ginovart, R.A. Dixon, T.-B. Robins Wahlin, Å. Wahlin, C. Halldin, L. Farde, Age-related cognitive deficits mediated by changes in the striatal dopamine system, *Am. J. Psychiatry* 157 (2000) 635–637.
- [6] D. Diorio, S.A. Welner, R.F. Butterworth, M.J. Meaney, B.E. Suranyi-Cadotte, Peripheral benzodiazepine binding sites in Alzheimer's disease frontal and temporal cortex, *Neurobiol. Aging* 12 (1991) 255–258.
- [7] P. Panula, J. Rinne, K. Kuokkanen, K.S. Eriksson, T. Sallmen, H. Kalimo, M. Relja, Neuronal histamine deficit in Alzheimer's disease, *Neuroscience* 82 (1998) 993–997.
- [8] C.C. Meltzer, G. Smith, S.T. DeKosky, B.G. Pollock, C.A. Mathis, R.Y. Moore, D.J. Kupfer, C.F. Reynolds Jr., Serotonin in Aging, late-time depression, and Alzheimer's disease: The emerging role of functional imaging, *Neuropsychopharmacology* 18 (1998) 407–430.
- [9] A. Nordberg, Clinical studies in Alzheimer patients with positron emission tomography, *Behav. Brain Res.* 57 (1993) 215–224.
- [10] A. Nordberg, Application of PET in dementia disorders, *Acta Neurol. Scand. Suppl.* 168 (1996) 71–76.
- [11] K. Herholz, PET studies in dementia, *Ann. Nucl. Med.* 17 (2003) 79–89.
- [12] M. Bergström, A. Grahnén, B. Långström, Positron emission tomography microdosing: A new concept with application in tracer and early clinical drug development, *Eur. J. Clin. Pharmacol.* 59 (2003) 357–366.
- [13] J. Neugroschl, K.L. Davis, Biological markers in Alzheimer disease, *Am. J. Geriatr. Psychiatry* 10 (2002) 660–677.
- [14] L. Mosconi, Brain glucose metabolism in the early and specific diagnosis of Alzheimer's disease FDG-PET studies in MCI and AD, *Eur. J. Nucl. Med. Mol. Imaging* 32 (2005) 486–510.

- [15] L. Mosconi, M. Brys, L. Glodzik-Sobanska, S. De Santi, H. Rusniek, M. de Leon, Early detection of Alzheimer's disease using neuroimaging, *Exp. Gerontol.* 42 (1–2) (2006) 129–138.
- [16] G.W. Small, J.C. Mazziotta, M.T. Collins, L.R. Baxter, M.E. Phelps, M.A. Mandelkern, A. Kaplan, A. La Rue, C.F. Adamson, L. Chang, B.H. Guze, E.H. Corder, A.M. Saunders, J.L. Haines, M.A. Pericak-Vance, A.D. Roses, Apolipoprotein E type 4 allele and cerebral glucose metabolism in relatives at risk for familial Alzheimer's disease, *J. Am. Med. Assoc.* 273 (1995) 942–947.
- [17] E.M. Reiman, K. Chen, G.E. Alexander, R.J. Caselli, D. Bandy, D. Osborne, A.M. Saunders, J. Hardy, Functional brain abnormalities in young adults at genetic risk for late-onset Alzheimer's dementia, *Proc. Natl. Acad. Sci. USA* 101 (2004) 284–289.
- [18] R.C. Petersen, G.E. Smith, S.C. Waring, R.J. Ivnik, E.G. Tangalos, E. Kokmen, Mild cognitive impairment: Clinical characterization and outcome, *Arch. Neurol.* 56 (1999) 303–308.
- [19] A. Drzezga, T. Grimmer, M. Riemenschneider, N. Lautenschlager, H. Siebner, P. Alexopoulos, S. Minoshima, M. Schwaiger, A. Kurz, Prediction of individual clinical outcome in MCI by means of genetic assessment and ^{18}F -FDG PET, *J. Nucl. Med.* 46 (2005) 1625–1632.
- [20] A. Drzezga, N. Lautenschlager, H. Siebner, M. Riemenschneider, F. Willoch, S. Minoshima, M. Schwaiger, A. Kurz, Cerebral metabolic changes accompanying conversion of mild cognitive impairment into Alzheimer's disease: A PET follow-up study, *Eur. J. Nucl. Med. Mol. Imaging* 30 (2003) 1104–1113.
- [21] S. Minoshima, N.L. Foster, D.E. Kuhl, Posterior cingulate cortex in Alzheimer's disease, *Lancet* 344 (1994) 895.
- [22] S. Minoshima, B. Giordani, S. Berent, K. Frey, N.L. Foster, D.E. Kuhl, Metabolic reduction in the posterior cingulate cortex in very early Alzheimer's disease, *Ann. Neurol.* 42 (1997) 85–94.
- [23] N.L. Pedersen, M. Gatz, S. Berg, B. Johansson, How heritable is Alzheimer's disease late in life? Findings from Swedish twins, *Ann. Neurol.* 55 (2004) 180–185.
- [24] T. Jarvenpää, I. Raiha, J. Kaprio, M. Koskenvuo, M. Laine, T. Kurki, T. Vahlberg, T. Viljanen, K. Ahonen, J.O. Rinne, Regional cerebral glucose metabolism in monozygotic twins discordant for Alzheimer's disease, *Dement. Geriatr. Cogn. Disord.* 16 (2003) 245–252.
- [25] E.M. Reiman, R.J. Caselli, L.S. Yun, K. Chen, D. Bandy, S. Minoshima, S.N. Thibodeau, D. Osborne, Preclinical evidence of Alzheimer's disease in persons homozygous for the epsilon 4 allele for apolipoprotein E, *N. Engl. J. Med.* 334 (1996) 752–758.
- [26] E.M. Reiman, R.J. Caselli, K. Chen, G.E. Alexander, D. Bandy, J. Frost, Declining brain activity in cognitively normal apolipoprotein E epsilon 4 heterozygotes: A foundation for using positron emission tomography to efficiently test treatments to prevent Alzheimer's disease, *Proc. Natl. Acad. Sci. USA* 98 (2001) 3334–3339.
- [27] J. Diehl-Schmid, T. Grimmer, A. Drzezga, S. Bornschein, R. Perneczky, H. Försti, M. Schwaiger, A. Kurz, Longitudinal changes of cerebral glucose metabolism in semantic dementia, *Dement. Geriatr. Cogn. Disord.* 22 (2006) 346–351.
- [28] J. Diehl-Schmid, T. Grimmer, A. Drzezga, S. Bornschein, M. Riemenschneider, H. Försti, M. Schwaiger, A. Kurz, Decline of cerebral glucose metabolism in frontotemporal dementia: A longitudinal ^{18}F -FDG-PET-study, *Neurobiol. Aging* 28 (2007) 42–50.
- [29] B. Matthews, E.R. Siemers, P.D. Mozley, Image-based measures of disease progression in clinical trials of disease-modifying drugs for Alzheimer disease, *Am. J. Geriatr. Psychiatry* 11 (2003) 146–159.
- [30] B.C. Dickerson, R.A. Sperling, Neuroimaging biomarkers for clinical trials of disease-modifying therapies in Alzheimer's disease, *NeuroRx* 2 (2005) 348–360.
- [31] M.S. Mega, J.L. Cummings, S.M. O'Connor, I.D. Dinov, E. Reback, J. Felix, D.L. Masterman, M.E. Phelps, G.W. Small, A.W. Toga, Cognitive and metabolic

- responses to metrifonate treatment in Alzheimer disease, *Neuropsychiatry Neuropsychol. Behav. Neurol.* 14 (2001) 63–68.
- [32] L. Tune, P.J. Tiseo, J. Ieni, C. Perdomo, R.D. Pratt, J.R. Votaw, R.D. Jewart, J.M. Hoffman, Donepezil HCl (E2020) maintains functional brain activity in patients with Alzheimer disease: Results of a 24-week double-blind, placebo-controlled study, *Am. J. Geriatr. Psychiatry* 11 (2003) 169–177.
- [33] E. Stefanova, A. Wall, O. Almkvist, A. Nilsson, A. Forsberg, B. Långström, A. Nordberg, Longitudinal PET evaluation of cerebral glucose metabolism in rivastigmine treated patients with mild Alzheimer's disease, *J. Neural Transm.* 113 (2006) 205–218.
- [34] M.D. Devous Sr., Functional brain imaging in the dementias: Role in early detection, differential diagnosis, and longitudinal studies, *Eur. J. Nucl. Med.* 29 (2002) 1685–1696.
- [35] N.J. Dougall, S. Bruggink, K.P. Ebmeier, Systematic review of the diagnostic accuracy of $^{99\text{m}}\text{Tc}$ -HMPAO SPECT in dementia, *Am. J. Geriatr. Psychiatry* 12 (2004) 554–570.
- [36] K. Ishii, S. Minoshima, A. Pupi, F.M. Nobili, PET is better than perfusion SPECT for early diagnosis of Alzheimer's disease. For–Against, *Eur. J. Nucl. Med. Mol. Imaging* 32 (2005) 1463–1472.
- [37] J. Blin, J.C. Baron, B. Dubois, C. Crouzel, M. Fiorelli, D. Attar-Lévy, B. Pillon, D. Fournier, M. Vidaihet, Y. Agid, Loss of brain 5-HT₂ receptors in Alzheimer's disease, *Brain* 116 (1993) 497–510.
- [38] C.C. Meltzer, J.C. Price, C.A. Mathis, P.J. Greer, M.N. Cantwell, P.R. Houck, B.H. Mulsant, D. Ben-Eliezer, B. Lopresti, S.T. DeKosky, C.F. Reynolds, PET imaging of serotonin type 2A receptors in late-life neuropsychiatric disorders, *Am. J. Psychiatry* 156 (1999) 1871–1878.
- [39] V. Kepe, J.R. Barrio, S.-H. Huang, L. Ercoli, P. Sissarth, K. Shoghi-Jarid, G.M. Cole, N. Satyamurthy, J.L. Cummings, G.W. Small, M.E. Phelps, Serotonin 1A receptors in the living brain of Alzheimer's disease patients, *Proc. Natl Acad. Sci. USA* 103 (2006) 702–707.
- [40] M.T. Toczek, R.E. Carson, L. Lang, Y. Ma, M.V. Spanaki, M.G. Der, S. Fazilat, L. Kopylev, P. Herscovitch, W.C. Eckelman, W.H. Theodore, PET imaging of 5HT_{1A} receptor binding in patients with temporal lobe epilepsy, *Neurology* 60 (2003) 749–756.
- [41] C. Defraiteur, C. Lemaire, A. Luxen, A. Plenevaux, Radiochemical synthesis and tissue distribution of p -[^{18}F]DMPF, a new 5-HT_{1A} ligand for PET, in rats, *Nucl. Med. Biol.* 33 (2006) 667–675.
- [42] D.N. Tipre, S.S. Zoghbi, J.-S. Liow, M.V. Green, J. Seidel, M. Ichise, R.B. Innis, V.W. Pike, PET imaging of brain 5-HT_{1A} receptors in rat in vivo with ^{18}F -FCWAY and improvement by successful inhibition of radioligand defluorination with miconazole, *J. Nucl. Med.* 47 (2006) 345–353.
- [43] N. Kempainen, H. Ruottinen, K. Någren, J.O. Rinne, PET shows that striatal dopamine D1 and D2 receptors are differently affected in AD, *Neurology* 55 (2000) 205–209.
- [44] N. Kempainen, M. Laine, M.P. Laakso, V. Kaasinen, K. Någren, T. Vahlberg, T. Kurki, J.O. Rinne, Hippocampal dopamine D2 receptors correlate with memory functions in Alzheimer's disease, *Eur. J. Neurosci.* 18 (2003) 149–154.
- [45] T. Siessmeier, Y. Zhou, H.-G. Buchholz, C. Landvogt, C.I. Vernaleken, M. Piel, R. Schirmacher, F. Rösch, M. Schreckenberger, D.F. Wong, P. Cumming, G. Gründer, P. Bartenstein, Parametric mapping of binding in human brain of D₂ receptor ligands of different affinities, *J. Nucl. Med.* 46 (2005) 964–972.
- [46] P. Riccardi, R. Li, M.S. Ansari, D. Zald, S. Park, B. Dawant, S. Anderson, M. Doop, N. Woodward, E. Schoenberg, D. Schmidt, R. Baldwin, R. Kessler, Amphetamine-induced displacement of [^{18}F] fallypride in striatum and extrastriatal regions in humans, *Neuropsychopharmacology* 31 (2006) 1016–1026.
- [47] J.O. Rinne, N. Sahlberg, H. Ruottinen, K. Någren, P. Lehtikoinen, Striatal uptake of the dopamine reuptake ligand [^{11}C]β-CFT is reduced in Alzheimer's disease assessed by positron emission tomography, *Neurology* 50 (1998) 152–156.

- [48] Z. Walker, D.C. Costa, R.W.H. Walker, K. Shaw, S. Gacinovic, T. Stevens, G. Livingston, P. Ince, I.G. McKeith, C.L.E. Katona, Differentiation of dementia with Lewy bodies from Alzheimer's disease using a dopaminergic presynaptic ligand, *J. Neurol. Neurosurg. Psychiatry* 73 (2002) 134–140.
- [49] J.T. O'Brien, S. Colloby, J. Fenwick, E.D. Williams, M. Firbank, D. Burn, D. Aarsland, I.G. McKeith, Dopamine transporter loss visualized with FP-CIT SPECT in the differential diagnosis of dementia with Lewy bodies, *Arch. Neurol.* 61 (2004) 919–925.
- [50] E. Nurmi, J. Bergman, O. Eskola, O. Solin, T. Vahlberg, P. Sonninen, J.O. Rinne, Progression of dopaminergic dysfunction in striatal subregions in Parkinson's disease using [^{18}F]CFT PET, *Synapse* 48 (2003) 109–115.
- [51] M. Carbon, Y. Ma, A. Barnes, V. Dhawan, T. Chaly, M.F. Ghilardi, D. Eidelberg, Caudate nucleus: Influence of dopaminergic input on sequence learning and brain activation in Parkinsonism, *Neuroimage* 21 (2004) 1497–1507.
- [52] M.R. Davis, J.R. Votaw, J.D. Bremner, M.G. Byas-Smith, T.L. Faber, R.J. Voll, J.M. Hoffman, S.T. Grafton, C.D. Kilts, M.M. Goodman, Initial human PET imaging studies with the dopamine transporter ligand ^{18}F -FECNT, *J. Nucl. Med.* 44 (2003) 855–861.
- [53] J.O. Rinne, T. Myllykylä, P. Lönnberg, P. Marjamäki, A postmortem study of brain nicotinic receptors in Parkinson's and Alzheimer's disease, *Brain Res.* 547 (1991) 167–170.
- [54] S. Oddo, F.M. LaFerla, The role of nicotinic acetylcholine receptors in Alzheimer's disease, *J. Physiol. (Paris)* 99 (2006) 172–179.
- [55] A. Nordberg, P. Hartvig, A. Lilja, M. Viitanen, K. Amberla, H. Lundqvist, Y. Andersson, J. Ulin, B. Winblad, B. Långström, Decreased uptake and binding of ^{11}C -nicotine in brain of Alzheimer patients as visualized by positron emission tomography, *J. Neural Transm. [P-D Sect]* 2 (1990) 215–224.
- [56] J. Schmaljohann, M. Minnerop, P. Karwath, D. Gündisch, P. Falkai, S. Gohlke, U. Wüllner, Imaging of central nAChReceptors with 2- ^{18}F]F-A85380: Optimized synthesis and in vitro evaluation in Alzheimer's disease, *Appl. Radiat. Isot.* 61 (2004) 1235–1240.
- [57] D.R. Weinberger, D. Jones, R.C. Reba, U. Mann, R. Coppola, R. Gibson, J. Gorey, A. Braun, T.N. Chase, A comparison of FDG PET and IQNB SPECT in normal subjects and in patients with dementia, *J. Neuropsychiatry Clin. Neurosci.* 4 (1992) 239–248.
- [58] K.L. Boundy, L.R. Barnden, A.G. Katsifis, C.C. Rowes, Reduced posterior cingulate binding of I-123 iodo-dexetimide to muscarinic receptors in mild Alzheimer's disease, *J. Clin. Neuroimaging* 12 (2005) 421–425.
- [59] J.-K. Zubieta, R.A. Koeppe, K.A. Frey, M.R. Kilbourn, T.J. Mangner, N.L. Foster, D.E. Kuhl, Assessment of muscarinic receptor concentrations in aging and Alzheimer disease with [^{11}C]NMPB and PET, *Synapse* 39 (2001) 275–287.
- [60] T.A. Podruchny, C. Connolly, A. Bokde, P. Herscovitch, W.C. Eckelman, D.A. Kiesewetter, T. Sunderland, R.E. Carson, R.M. Cohen, In vivo muscarinic 2 receptor imaging in cognitively normal young and older volunteers, *Synapse* 48 (2003) 39–44.
- [61] R.M. Cohen, T.A. Podruchny, A.L.W. Bokde, R.E. Carson, P. Herscovitch, D.A. Kiesewetter, W.C. Eckelman, T. Sunderland, Higher in vivo muscarinic-2 receptor distribution volumes in ageing subjects with an apolipoprotein E- ϵ 4 allele, *Synapse* 49 (2003) 150–156.
- [62] J.O. Rinne, V. Kaasinen, T. Järvenpää, K. Någren, A. Roivainen, M. Yu, V. Oikonen, T. Kurki, Brain acetylcholinesterase activity in mild cognitive impairment and early Alzheimer's disease, *J. Neurol. Neurosurg. Psychiatry* 74 (2003) 113–115.
- [63] D.E. Kuhl, R.A. Koeppe, S. Minoshima, S.E. Snyder, E.P. Ficaró, N.L. Foster, K.A. Frey, M.R. Kilbourn, In vivo mapping of cerebral acetylcholinesterase activity in aging and Alzheimer's disease, *Neurology* 52 (1999) 691–699.

- [64] K. Herholz, S. Weisenbach, E. Kalbe, N.J. Diederich, W.-D. Heiss, Cerebral acetylcholine esterase activity in mild cognitive impairment, *Neuroreport* 16 (2005) 1431–1434.
- [65] D.E. Kuhl, R.A. Koeppe, S.E. Snyder, S. Minoshima, K.A. Frey, M.R. Kilbourn, In vivo butyrylcholinesterase activity is not increased in Alzheimer's disease synapses, *Ann. Neurol.* 59 (2006) 13–20.
- [66] V. Kaasinen, K. Någren, T. Järvenpää, A. Roivainen, M. Yu, V. Oikonen, T. Kurki, J.O. Rinne, Regional effects of donepezil and rivastigmine on cortical acetylcholinesterase activity in Alzheimer's disease, *J. Clin. Psychopharmacol.* 22 (2002) 615–620.
- [67] M.-R. Zhang, A. Tsuchiyama, T. Haradahira, K. Furutsuka, Y. Toshida, T. Kida, J. Noguchi, T. Irie, K. Suzuki, Synthesis and preliminary evaluation of [^{18}F]FETp4A, a promising PET tracer for mapping acetylcholinesterase in vivo, *Nucl. Med. Biol.* 29 (2002) 463–468.
- [68] X. Shao, E.R. Butch, M.R. Kilbourn, S.E. Snyder, *N*-[^{18}F]fluoroethylpiperidinyl, *N*-[^{18}F]fluoroethylpiperidinemethyl and *N*-[^{18}F]fluoroethylpyrrolidinyl esters as radiotracers for acetylcholinesterase, *Nucl. Med. Biol.* 30 (2003) 491–500.
- [69] T. Kikuchi, M.-R. Zhang, N. Ikota, K. Fukushi, T. Okamura, K. Suzuki, Y. Arano, T. Irie, *N*-[^{18}F]fluoroethylpiperidin-4ylmethyl butyrate: A novel radiotracer for quantifying brain butyrylcholinesterase activity by positron emission tomography, *Bioorg. Med. Chem. Lett.* 14 (2004) 1927–1930.
- [70] M. Higuchi, K. Yanai, N. Okamura, K. Meguro, H. Arai, M. Itoh, R. Iwata, T. Ido, T. Watanabe, H. Sasaki, Histamine H1 receptors in patients with Alzheimer's disease assessed by positron emission tomography, *Neuroscience* 99 (2000) 721–729.
- [71] S. Celanire, M. Wijtmans, P. Talaga, R. Leurs, I.J. de Esch, Keynote review: Histamine H3 receptor antagonists reach out for the clinic, *Drug Discov. Today* 10 (2005) 1613–1627.
- [72] P. Edison, H. Archer, N. Fox, D.J. Brooks, Relationship between the distribution of microglial activation, amyloid plaque load and cerebral glucose metabolism in Alzheimer's disease (AD): An 11C-PK11195 18F-FDG and 11C-PIB PET study, *J. Am. Geriatr. Society* 54 (2006) S6–S7.
- [73] G.W. Price, R.G. Ahier, S.P. Hume, R. Myers, L. Manjil, J.E. Cremer, S.K. Luthra, C. Pascali, V. Pike, R.S.J. Frackowiak, In vivo binding to peripheral benzodiazepine binding sites in lesioned rat brain: Comparison between [^3H]PK11195 and [^{18}F]PK14105 as markers for neuronal damage, *J. Neurochem.* 55 (1990) 175–185.
- [74] M.-R. Zhang, J. Maeda, M. Ogawa, J. Noguchi, T. Ito, Y. Yoshida, T. Okauchi, S. Obayashi, T. Suhara, K. Suzuki, Development of a new radioligand, *N*-(5-fluoro-2-phenoxyphenyl)-*N*-(2[^{18}F]fluoroethyl-5-methoxybenzyl)acetamide, for PET imaging of peripheral benzodiazepine receptor in primate brain, *J. Med. Chem.* 47 (2004) 2228–2235.
- [75] H. Engler, A. Forsberg, O. Almkvist, G. Blomquist, E. Larsson, I. Savitcheva, A. Wall, A. Ringheim, B. Langstrom, A. Nordberg, , Two-year follow-up of amyloid deposition in patients with Alzheimer's disease, *Brain* 129 (2006) 2856–2866.
- [76] W.E. Klunk, H. Engler, A. Nordberg, Y. Wang, G. Blomqvist, D.P. Holt, M. Bergström, I. Savitcheva, G. Huang, S. Estrada, B. Ausén, M.L. Debnath, J. Barletta, J.C. Price, J. Sandell, B.J. Lopresti, A. Wall, P. Koivisto, G. Antoni, C.A. Mathis, B. Långström, Imaging brain amyloid in Alzheimer's disease with Pittsburgh compound-B, *Ann. Neurol.* 55 (2004) 306–319.
- [77] N.M. Kemppainen, S. Aalto, I.A. Wilson, K. Någren, S. Helin, A. Brück, V. Oikonen, M. Kailajärvi, M. Scheinin, M. Viitanen, R. Parkkola, J.O. Rinne, Voxel-based analysis of amyloid ligand [^{11}C]PIB uptake in Alzheimer disease, *Neurology* 67 (2006) 1575–1580.
- [78] M.A. Mintun, G.N. LaRossa, Y.I. Sheline, C.S. Dence, S.Y. Lee, R.H. Mach, W.E. Klunk, C.A. Mathis, S.T. DeKosky, J.C. Morris, [^{11}C]PIB in a nondemented population: Potential antecedent marker of Alzheimer disease, *Neurology* 67 (2006) 446–452.

- [79] N.P. Verhoeff, A.A. Wilson, S. Takeshita, L. Trop, D. Hussey, K. Singh, H.F. Kung, M.P. Kung, S. Houle, In-vivo imaging of Alzheimer disease beta-amyloid with [^{11}C]SB-13 PET, *Am. J. Geriatr. Psychiatry* 12 (2004) 584–595.
- [80] K. Shoghi-Jarid, G.W. Small, E.D. Agdeppa, V. Kepe, L.M. Ercoli, P. Siddarth, S. Read, N. Satyamurthy, A. Petric, S.-C. Huang, J.R. Barrio, Localization of neurofibrillary tangles and beta-amyloid plaques in the brains of living patients with Alzheimer disease, *Am. J. Geriatr. Psychiatry* 10 (2002) 24–35.
- [81] F. Zeng, J.A. Southerland, R.J. Voll, R.J. Votaw, L. Williams, B.J. Ciliax, A.I. Levey, M.M. Goodman, Synthesis and evaluation of two ^{18}F -labeled imidazo[1,2- α]pyridine analogues as potential agents for imaging β -amyloid in Alzheimer's disease, *Bioorg. Med. Chem. Lett.* 16 (2006) 3015–3018.

Note from the Editors

On the use of ^{18}F -labeled molecules, see also in this volume chapters by F. Dollé *et al.* on PET molecular imaging, K. Kopka *et al.* on cardiological imaging, and K. Herrmann and B. J. Krause on application to oncology.

CHAPTER 3

^{18}F -Labeled PET-Tracers for Cardiological Imaging

Klaus Kopka,^{1,5,†,*} Stefan Wagner,^{1,5,†} Michael Schäfers,^{1,2,5}
Andreas Faust,^{1,3,5} Otmar Schober,^{1,5} and Günter Haufe^{4,5}

¹*Department of Nuclear Medicine, University Hospital Münster,
D-48149 Münster, Germany*

²*Interdisciplinary Center of Clinical Research (IZKF) Münster, D-48149 Münster, Germany*

³*Department of Clinical Radiology, University Hospital Münster,
D-48149 Münster, Germany*

⁴*Organisch-Chemisches Institut, Universität Münster, D-48149 Münster, Germany*

⁵*European Institute of Molecular Imaging (EIMI), D-48149 Münster, Germany*

Contents

1. Molecular imaging of the myocardium	86
1.1. Background	86
1.2. 2-Deoxy-2- ^{18}F fluoro-D-glucose (^{18}F FDG)	87
1.2.1. Mechanism of accumulation in myocytes	87
1.2.2. Radiosynthesis	88
1.3. Fatty acids	89
2. Molecular imaging of vessels	91
2.1. Atherosclerosis	91
2.2. Endothelin-system	94
2.3. Perfusion	96
3. Innervation	99
3.1. Sympathetic and parasympathetic innervation	99
3.2. β -Adrenoceptors	100
3.3. ^{18}F -labeled radioligands for PET imaging of β -adrenoceptors	106
3.3.1. ^{18}F Fluoroacetone as radiolabeling building block	106
3.3.2. ^{18}F Fluoroisopropyl derivatives as radiolabeling building blocks	109
3.3.3. ^{18}F Fluoroethyl derivatives as radiolabeling building blocks	111
3.4. α -Adrenoceptors	113
3.5. Muscarinic acetylcholine receptors	113
3.6. Norepinephrine transporter and vesicular monoamine transporter	118
4. Summary and perspectives	125
Annex: ^{18}F -labeled PET-tracers for cardiological imaging — update	126

*Corresponding author. Tel.: + 49-251-8347362; Fax: +49-251-8347363;
Email: kopka@uni-muenster.de

† These authors contributed equally to this work.

Acknowledgments	127
References	128
Note from the Editors	139

Abstract

Molecular imaging of cardiovascular diseases is of great clinical interest. A suitable tool for this challenge are radiopharmaceuticals labeled with the positron-emitter ^{18}F that offer the opportunity to noninvasively investigate the cardiovascular physiology and pathophysiology *in vivo* with the prominent nuclear medicine technology positron emission tomography (PET). First of all, the molecular imaging of the myocardium with [^{18}F]FDG and ^{18}F -labeled fatty acids is illustrated in this chapter. Furthermore, the possibilities to image cardiac vessels with ^{18}F -labeled tracers for atherosclerosis, for the endothelin-system, and for perfusion studies are highlighted. Subsequently, the most important ^{18}F -labeled compounds for the evaluation of the sympathetic and parasympathetic innervation of the heart are described. Here, different receptors and transporters represent useful biological targets. Finally, the potential and perspectives of ^{18}F -labeled PET-tracers for cardiovascular imaging are summarized.

1. MOLECULAR IMAGING OF THE MYOCARDIUM

1.1. Background

Molecular imaging of the myocardium being the functionally most relevant tissue compartment of the mammalian heart has been proven valuable for clinical diagnostics, especially for the evaluation of cardiac physiology and pathophysiology. 2-Deoxy-2- ^{18}F fluoro-D-glucose ([^{18}F]FDG) and ^{18}F -labeled fatty acids are suitable tracers for the imaging of the metabolism of the myocardium and used for the investigation of metabolic abnormalities that underlie cardiac dysfunction [1].

Myocardial metabolism (Fig. 1) can be extensively and quantitatively investigated with positron emission tomography (PET). To maintain heart rate and cardiac contraction even in cardiac stress situations, the healthy human heart has to constantly extract arterial oxygen with high efficiency. However, myocardial oxygen extraction reaches its maximum already in the resting state. Thus, the only backdoor to further enhance myocardial oxygen supply in stress situations is the dilation of the coronary arteries to increase the myocardial blood volume. Because of changes in substrate utilization as a result of oxygen availability, it is useful to combine metabolic imaging and the assessment of myocardial blood flow (MBF, e.g., using injection of the perfusion tracers [^{15}O]H₂O or [^{13}N]NH₃) in one PET session [2] (Fig. 1).

During fasting, fatty acids are prevalently taken up by the myocytes and subsequently degraded by β -oxidation to acetyl-CoA. The resulting acetyl-CoA is further utilized during citrate synthesis within the tricarboxylic acid (TCA) cycle. Citrate inhibits glycolysis via a negative feedback mechanism. Fatty acids inhibit glucose metabolism with respect to glucose oxidation, glycolysis, and glucose uptake, thereby rerouting glucose toward glycogen synthesis. In the postprandial

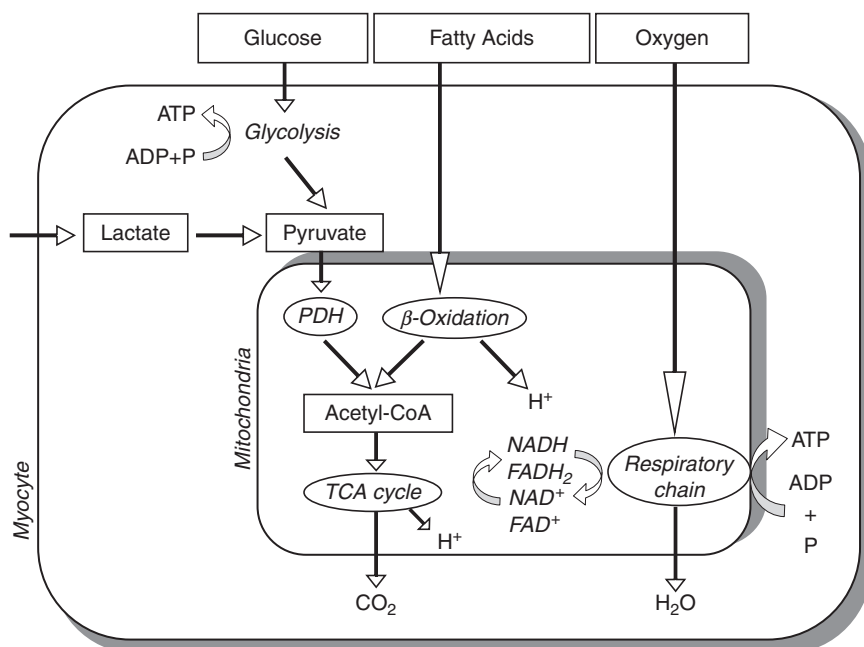


Fig. 1. Energy metabolism in the normal myocardium (ATP: adenosine-5'-triphosphate, ADP: adenosine-5'-diphosphate, P: phosphate, PDH: pyruvate dehydrogenase complex, acetyl-CoA: acetyl-coenzyme A, NADH and NAD^+ : nicotinamide adenine dinucleotide (reduced and oxidized), FADH_2 and FAD: flavin adenine dinucleotide (reduced and oxidized)).

state, when high glucose levels trigger the insulin production, glucose becomes the main energy source and circulating fatty acid levels are low. Glucose is transported into the cardiomyocyte by specific glucose transporters (activated by insulin) and is phosphorylated by hexokinases (see also Section 1.2.1.). Glucose-6-phosphate enters either the glycolytic pathway (catabolism to pyruvate) or the glycogen synthesis. Pyruvate accumulates in the mitochondria via a monocarboxylate carrier. Within the mitochondria, predominant amounts of pyruvate, either produced by glycolysis or by exogenous lactate, are oxidized to acetyl-CoA by pyruvate dehydrogenase (PDH). Oxidation of the acetyl groups in the TCA cycle results in the generation of CO_2 and H_2O . Pyruvate can also replenish the TCA cycle intermediates because of its transformation into oxaloacetate by pyruvate carboxylase or malic enzyme [2].

1.2. 2-Deoxy-2- ^{18}F fluoro-D-glucose (^{18}F FDG)

1.2.1. Mechanism of accumulation in myocytes

Since its first *in vivo* evaluation [3], the metabolic radiotracer ^{18}F FDG has become the most important radiopharmaceutical in clinical PET and is predominantly used for tumor imaging, particularly for the estimation of glucose uptake

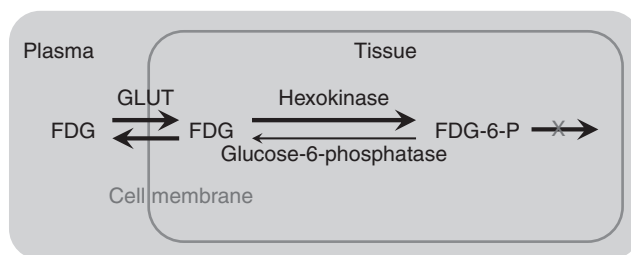


Fig. 2. Intracellular uptake of [^{18}F]FDG (metabolic trapping).

and utilization in malignant lesions (see Chapter 4). [^{18}F]FDG is also useful for the evaluation of myocardial viability and neuropathologies. Initially, the intracellular uptake of [^{18}F]FDG is similar to that of natural D-glucose. The accumulation of [^{18}F]FDG is a combination of active and stereospecific transport via glucose transport proteins, which are subdivided in transporters GLUT-1 to GLUT-7 as well as GLUT-10 to GLUT-12, and subsequent intracellular phosphorylation via the hexokinase isozymes (hexokinases I–IV) [4]. The GLUT-1 transporter and hexokinase II are the most common subtypes being involved in the glucose metabolism of tumor cells [5]. The uptake of glucose in myocytes is predominantly mediated by the GLUT-1 transporter and to a minor extent by GLUT-4 [6].

In contrast to the phosphorylated D-glucose, FDG-6-phosphate (FDG-6-P) is not a substrate of glycolysis because the next step of the glucose catabolism catalyzed by phosphoglucose-isomerase requires oxygen at the C-2-position. Therefore, FDG-6-P appears to be a terminal metabolite [7] which intracellularly “amplifies” over time. This process is termed *metabolic trapping*. However, ^{19}F -NMR spectroscopic investigations with macroscopic (mM) amounts of nonradioactive FDG *in vivo* show that FDG-6-P converts into 2-deoxy-2-fluoro-D-mannose-6-phosphate in specific organs, such as brain and heart [7]. In addition, glucose-6-phosphatase is able to dephosphorylate FDG-6-P, resulting in decreased metabolic trapping of FDG in other tissues. As a consequence, in organs with less intracellular glucose-6-phosphatase concentrations (e.g., in brain and heart) high FDG uptake rates are observable. On the other hand, high enterohepatic glucose-6-phosphatase concentrations result in low FDG uptake [6]. Figure 2 summarizes the mechanism of intracellular [^{18}F]FDG accumulation and retention.

1.2.2. Radiosynthesis

The radiosynthesis of [^{18}F]FDG is based on the nucleophilic substitution of a modified mannose precursor with [^{18}F]fluoride used as the nucleophilic reagent (Fig. 3).

The two-step procedure starts with the separation of the cyclotron-generated n.c.a. (no carrier added) [^{18}F]fluoride, mediated by an anion exchanger, and

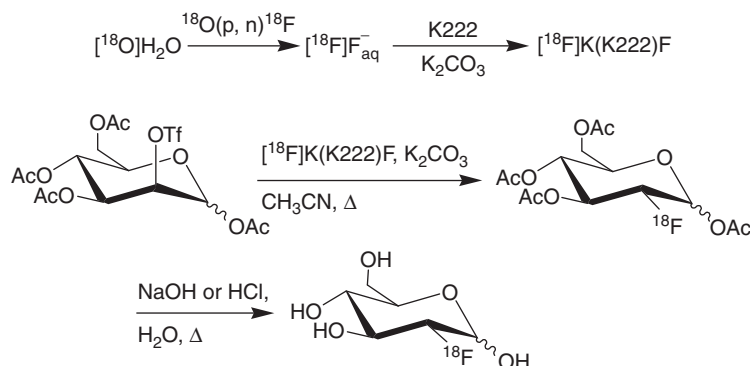


Fig. 3. Radiosynthesis of [^{18}F]FDG (K222: KryptofixTM 2.2.2).

addition of a KryptofixTM 2.2.2 solution which increases the nucleophilicity of the [^{18}F]fluoride anion. The precursor 1,3,4,6-tetra-O-acetyl-2-O-trifluoromethanesulfonyl- β -D-mannopyranose is subsequently converted into [^{18}F]FDG by nucleophilic substitution ($\text{S}_{\text{N}}2$ -type) and hydrolytic deprotection of the acetyl moieties. In this connection, a basic [8] and acidic variant [9] of the hydrolysis step is described. After purification via several cartridges, [^{18}F]FDG is diluted in a physiological buffer ready for injection [10]. The production of [^{18}F]FDG is established in many PET centers worldwide; networks that realize the distribution of [^{18}F]FDG are common practice in many countries.

1.3. Fatty acids

Fatty acids represent the predominant energy source of the myocardium. Actually, the healthy heart derives 60–80% of its energy need from the fatty acid oxidation (FAO) [11]. Significant dysregulation of FAO has been found to be associated with several cardiovascular diseases, including ischemic heart disease [12], heart failure [13], inherited disorders of FAO enzymes [14], and diabetes [15]. A diagnostic tool for FAO assessment in patients with cardiovascular diseases is important to monitor disease progression and drug therapy [16–18].

Several ^{18}F -labeled fatty acid derivatives have been successfully prepared and evaluated as potential FAO assessing tracers [19–24]. Methyl-branched-chain ω - ^{18}F -fluorofatty acids, such as 3-methyl-(**3-MFHA**) and 5-methyl-17- ^{18}F -fluoroheptadecanoic acid (**5-MFHA**), have been reported [23]. In a comparative study, it was found that ω - ^{18}F -fluoropalmitic acid (**FPA**) exhibits the highest myocardial uptake, followed by **5-MFHA** and **3-MFHA**. **FPA** possesses the fastest myocardial washout rate, and **3-MFHA** the slowest. In lipid analysis studies, **5-MFHA**

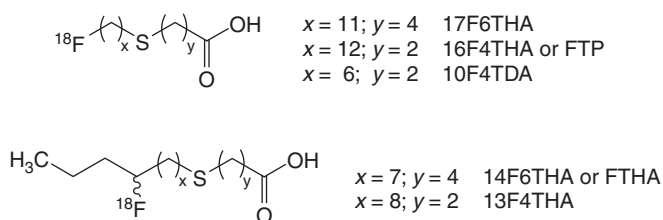


Fig. 4. Structures of ^{18}F -fluorothiafatty acids.

(similar to **FPA**) is mainly metabolized to triglycerides in the myocardium. However, all three tracers suffered from defluorination *in vivo*.

In alternative approaches several ^{18}F -fluorothiafatty acids were prepared and evaluated *in vivo* [19,20]. Figure 4 gives an overview of the relevant ^{18}F -fluorothiafatty acids.

14- ^{18}F Fluoro-6-thiaheptadecanoic acid (**14F6THA**) was shown to be metabolically retained in the myocardium, resulting in excellent imaging properties in normal human subjects and patients with coronary artery disease [25,26]. However, the tracer failed to detect the decrease in β -oxidation under hypoxic conditions [26], suggesting that β -oxidation is not solely responsible for intracellular retention of the radiolabeled compound. Nevertheless, **14F6THA** was evaluated in patients with congestive heart failure [27]. In conclusion, myocardial free fatty acid and glucose consumption can be complementarily and quantitatively assessed using **14F6THA** and ^{18}F FDG PET. Myocardial fatty acid uptake rates in the failing heart were higher than in the normal heart, whereby myocardial glucose uptake rates were found to be lower. This shift in myocardial substrate utilization may be an indication of impaired energy efficiency in the failing heart, providing a target for therapy directed to the improvement of myocardial energy efficiency.

Because of suboptimal specificity of **14F6THA**, several modified ^{18}F -labeled 4- and 6-thiafatty acid analogs have been prepared and evaluated [20]. Using an isolated perfused heart model, the ω -labeled 16- ^{18}F fluoro-4-thiahexadecanoic acid (**FTP**) was shown to track the inhibition of oxidation rate of palmitate under hypoxic conditions, whereby that of a 6-thia fatty acid (**17F6THA**) was insensitive to hypoxia. However, studies *in vivo* showed that **FTP** undergoes defluorination. Further validation of **FTP** as a metabolically trapped FAO probe in the isolated perfused rat heart model gave some insights into the changes of exogenous fatty acid availability under hypoxic conditions. The kinetic data for **FTP** demonstrated metabolic trapping of ^{18}F -radioactivity that was insensitive to changes in the mixture of fatty acids in the perfusion medium, but indeed sensitive to the inhibition of mitochondrial FAO by hypoxia [11]. To date, *in vivo* investigations of **FTP** in humans are not published to confirm the ability of an adequate FAO detection.

The iodinated precursor of **FTP** can be prepared in a one-step synthesis from 1,12-diiodododecane and 3-mercapto-propionic acid methyl ester. The

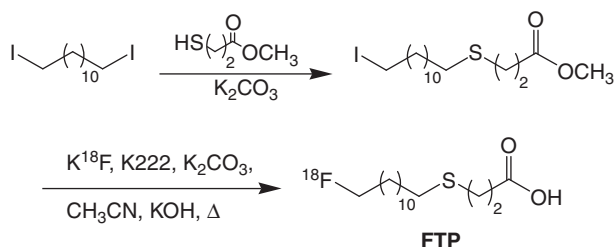


Fig. 5. Radiosynthesis of **FTP** [20].

nucleophilic substitution with [¹⁸F]fluoride and subsequent ester hydrolysis yielded **FTP** (Fig. 5) [20].

2. MOLECULAR IMAGING OF VESSELS

2.1. Atherosclerosis

Atherosclerosis is a progressive vascular fibroproliferative-inflammatory disease. It is triggered, maintained, and driven by risk factors such as hypercholesterolemia, hyperlipidemia, and hypertonus [28]. The characteristic clinical manifestation of atherosclerosis is the atherosclerotic lesion, developing in the vessel wall (atherosclerotic plaque).

The progression of the atherosclerotic lesion occurs silently in the course of a series of highly specific cellular and molecular responses to vessel wall injury, resulting in the development of different grades of disease progression [29]. The potentially most dangerous lesions are unstable and prone to rupture (so-called vulnerable plaques), leading to thrombus formation with subsequent occlusion of the vessel and its clinical sequelae, myocardial infarction, and stroke. Surprisingly, unstable plaques do not always narrow the lumen of the artery (stenoses) and, thus, can be missed by imaging methods which assess the lumen of the vessels. In fact, patients who had died from acute myocardial infarction due to plaque rupture can show culprit lesions exhibiting stenosis of less than 50% of the vessel diameter, or even no stenosis [30]. Unstable atherosclerotic lesions often grow outward or abluminally rather than inward so that substantial burden of atherosclerosis (“hidden lesions”) can exist without producing stenosis [31].

At autopsy, a ruptured plaque features a thin fibrous cap overlying cell-rich regions with a lipid-rich “necrotic” core (<3 mm²) containing cell debris. The indicators for plaque instability include an inflammatory infiltrate with lipid-rich macrophages (foam-cells) and a decreased collagen and smooth muscle cell (SMC) content in the fibrous caps as well as at the shoulders of the atheroma, respectively. Therefore, one of the challenges of modern medicine is the design of

techniques that enable the differentiation between stable and unstable atherosclerotic plaques in order to predict and prevent myocardial infarction or stroke [32].

One approach of imaging vulnerable atherosclerotic plaques is based on the assessment of the degree of inflammation within the unstable lesions. Therefore, the measurement of macrophage-based metabolic activity by [^{18}F]FDG PET is of potential use (see Section 1.2.). For different rabbit models [33,34] and patients several studies with PET or combined imaging modalities such as PET/CT (PET/computed tomography) or PET/HRMRI (PET/high-resolution magnetic resonance imaging) [35–38] suggested that atherosclerotic plaque inflammation could be imaged by [^{18}F]FDG.

In a second approach, the enzyme class matrix metalloproteinases (MMPs) can potentially be used as a molecular target *in vivo* and imaged by radiolabeled MMP inhibitors (MMPIs). MMPs are involved in many physiological processes but also take part in the pathophysiological mechanisms responsible for a wide range of diseases. Pathological expression and activation of MMPs are associated with cancer, atherosclerosis, stroke, arthritis, periodontal disease, multiple sclerosis, liver fibrosis, and others. MMPs are zinc- and calcium-dependent endopeptidases that are involved in the physiological and pathophysiological remodeling of connective tissue. The MMPs are secreted as inactive pro-enzymes or zymogens that are activated via the “cysteine switch.” Once activated, they degrade extracellular matrix proteins [39]. The progression of atherosclerosis is especially connected with locally upregulated MMP levels [37]. Strong local MMP overexpression and matrix-degrading activity *in situ* have been observed in the vulnerable human atheroma which coincides with areas of highest mechanical stress [40]. Radioiodinated derivatives of the broad-spectrum MMPI **CGS 27023A** [$K_i(\text{MMP-1}) = 33 \text{ nM}$, $K_i(\text{MMP-2}) = 20 \text{ nM}$, $K_i(\text{MMP-3}) = 43 \text{ nM}$, $K_i(\text{MMP-9}) = 8 \text{ nM}$] indeed showed the potential to specifically image MMP-rich vascular lesions that develop in ApoE $^{-/-}$ mice after carotid artery ligation and cholesterol-rich diet [41,42].

Two different lead structures were chosen for ^{18}F -labeled MMPIs. The PET-compatible ^{18}F -labeled analog [^{18}F]CGS 27023A (Fig. 6) was introduced in the year 2001 without giving detailed information about the synthesis. Its

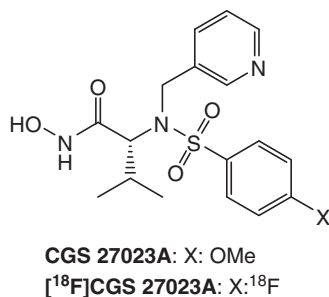


Fig. 6. MMPI **CGS 27023A** and the ^{18}F -labeled analog [^{18}F]CGS 27023A [43,44].

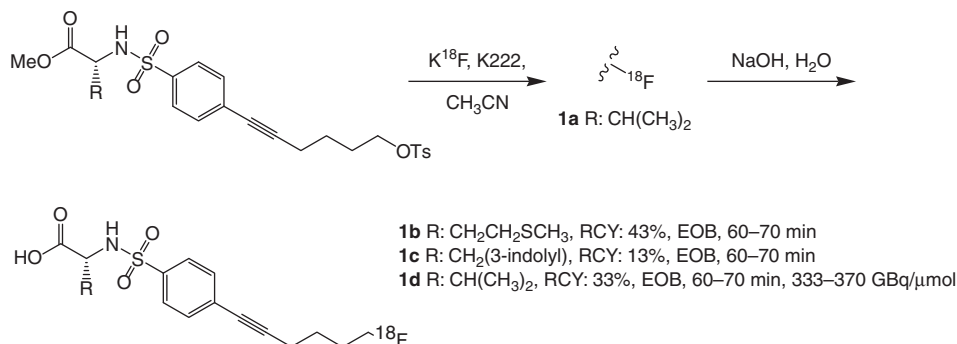


Fig. 7. Radiosyntheses of MMPis **1a-d** [45,46] (RCY: radiochemical yield, EOB: end of bombardment).

in vivo evaluation was prevented by low radiochemical yields, long reaction times, and complicated purification procedures [43,44].

One year later, Furumoto *et al.* presented the design and synthesis of ^{18}F -labeled MMPis **1a-d** with a linearly elongated and *p*-substituted alkyne aryl sulfonamide group (Fig. 7). The radiosynthesis of **1a-d** was achieved by nucleophilic substitution using ^{18}F [K(Kryptofix 2.2.2)F] and the corresponding tosylate precursors, and, if applicable, subsequent hydrolysis of the methylesters. The nonradioactive counterpart of **1d** inhibits MMP-2 with an IC_{50} -value of 1.9 μM [45,46] (Fig. 7).

Inadequate chemical stability of compound **1b** and low radiochemical yields of derivative **1c** prevented further evaluation of these potential imaging probes *in vitro* and *in vivo*. However, the stable MMPi **1d** was achievable with moderate radiochemical yields and its prodrug **1a** was examined in Ehrlich tumor-bearing mice. Ehrlich tumor cells expressed MMP-2 which was demonstrated by zymography. Biodistribution studies showed that the uptake of **1d** in the tumor was higher than in other organs except in the liver, small intestine, and bone. The administration of prodrug **1a** that is converted into the parent drug **1d** *in vivo* decreased the unintentional liver uptake compared to direct administration of **1d**, maybe due to a reduced first-pass effect that metabolized the tracer, giving the glucuronate conjugate. The improved *in vivo* behavior of **1a** was accompanied by a time-dependent increase in bone uptake, suggesting accumulation of ^{18}F fluoride that was generated by tracer defluorination [46]. Nevertheless, the forthcoming evaluation of atherosclerotic animal models with the ^{18}F -labeled MMPis **1a** and **1d** seems to be promising.

In summary, plaque imaging with ^{18}F -labeled MMPis remains a clinical challenge and is still in its infancy. The transfer of ^{18}F -labeled MMPis developed for oncological questions in the field of cardiovascular pathophysiology is one possible starting point.

2.2. Endothelin-system

Endothelin (ET) was first described by Hickey *et al.* [47] and subsequently isolated by Yanagisawa *et al.* [48] as a 21-amino acid peptide with vasoactive potential. Consecutive investigations pointed out the role of the ETs in several diseases, including atherosclerosis, congestive heart failure, and pulmonary hypertension [49–52]. In addition, the function of ET as a progression factor in many human tumor cell lines [53], its influence on renal function [54], and its relevance in the development of inflammation [55–56] have recently been discussed. To date, three isoforms of endothelin are characterized (ET-1, ET-2, and ET-3), transmitting their effects via two different G-protein-coupled receptors (GPCRs) (ET_A, ET_B). ET_A receptors are primarily located on vascular SMCs and are responsible for vasoconstriction and cell proliferation. On the other hand, ET_B receptors are located on SMCs and vascular endothelial cells, cause vasodilation via release of nitric oxide and prostacyclin, and are responsible for the clearance of ET-1 from plasma. The binding potency of the ETs for the ET_A receptor is ~100-fold higher for ET-1 and ET-2 than for ET-3, whereas the affinity for the ET_B receptor is equal for all three isoforms [57–60]. The system of the three ET peptides and the two ET receptors is referred to as the ET axis [53].

While normal concentrations of ET-1 and ET-3 in human plasma are relatively low (pg/ml, ET-2 concentrations are below detectable limits), plasma levels of ET-1 are elevated in many cardiovascular diseases. Therefore, ET receptor antagonists are utilized in the treatment of these diseases, and a number of

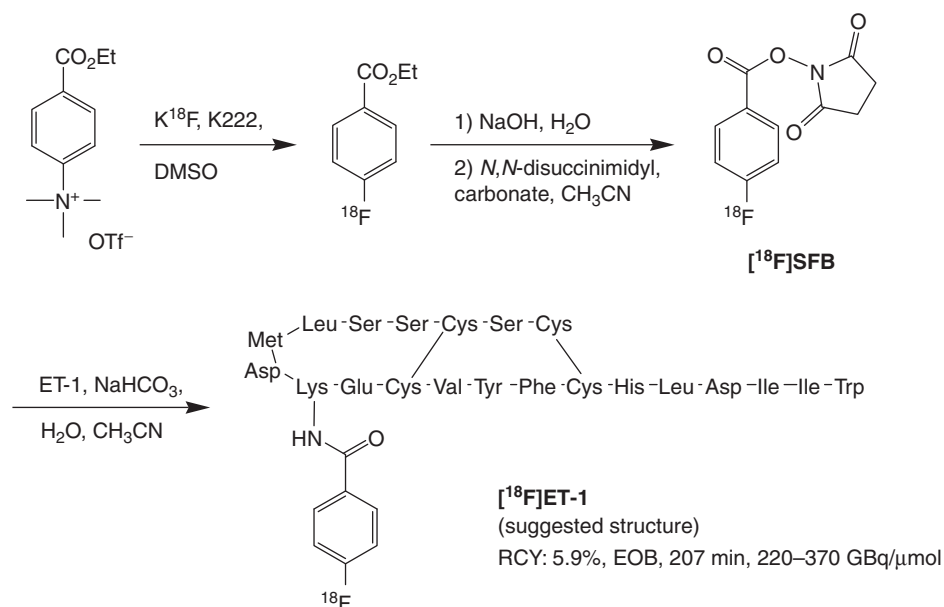


Fig. 8. Radiosynthesis of [¹⁸F]ET-1 [66].

different peptidyl and nonpeptidyl ligands, both selective and unselective, have been developed to improve efficacy [61–65].

Johnström *et al.* investigated the possibility to image ET receptors *in vivo* with ^{18}F -labeled ET-1 [66,67]. To make [^{18}F]ET-1 accessible for *in vivo* investigations, a four-step radiosynthesis was performed (Fig. 8).

Therefore, ethyl 4-trimethylammoniumbenzoate trifluoromethanesulfonate was labeled by nucleophilic aromatic substitution using [^{18}F]fluoride, and the resulting 4-[^{18}F]fluorobenzoic acid ethylester was hydrolyzed to produce 4-[^{18}F]fluorobenzoic acid which was functionalized with *N,N*-disuccinimidyl carbonate to yield the Bolton-Hunter-type reagent *N*-succinimidyl 4-[^{18}F]fluorobenzoate ([^{18}F]SFB). The active ester [^{18}F]SFB was utilized to conjugate ET-1, resulting in [^{18}F]ET-1. The structure of [^{18}F]ET-1 is not well-defined, but there is strong evidence that the side chain of the lysine residue was labeled and not the *N*-terminal cysteine [66] (Fig. 8).

Dynamic PET data of [^{18}F]ET-1 in male Sprague-Dawley rats demonstrated that the radioligand rapidly accumulates in the lung, kidney, and liver, which consists with receptor binding. However, the visualized receptor density in the heart was unexpectedly low compared with that predicted from investigations *in vitro*. The tracer binding in lungs could not be displaced by the ET_B -selective antagonist BQ788 in agreement with a proposed internalization of ET-1 (and [^{18}F]ET-1) by ET_B receptors. In contrast, predosing with BQ788 significantly reduced the amount of [^{18}F]ET-1 in the ET_B receptor-rich lung and kidneys, and the ET_A receptor-rich heart could be visualized by small-animal PET studies. In summary, the data suggest that [^{18}F]ET-1 clearance by ET_B receptors in the lung and kidneys prevents the tracer binding to receptors of the heart in the chosen animal model [67].

The same group labeled the ET_B -selective peptidyl agonist BQ3020 with [^{18}F]SFB starting from 4-trimethylammoniumbenzonitrile trifluoromethanesulfonate and [^{18}F]fluoride in a four-step synthesis similar to the labeling protocol of [^{18}F]ET-1 [68]. Investigations with the potential ET_B -selective radioligand [^{18}F]BQ3020 *in vivo* have not been published so far.

An ^{18}F -labeled nonpeptidyl ligand for ET receptors is represented by [^{18}F]SB209670 that was introduced by Johnström *et al.* in 2004 [69]. It was developed from the lead structure of the ET antagonist SB209670 with hydrogen displaced by ^{18}F . The compound was synthesized in a three-step procedure. In the first step 1,3-dibromopropane was reacted with [^{18}F]K(Kryptofix 2.2.2)F to yield 3-[^{18}F]fluoropropylbromide. *O*-Alkylation of SB421672 with this labeling building block and subsequent hydrolysis provided the target compound [^{18}F]SB209670 (Fig. 9).

The authors postulated that the affinity of [^{18}F]SB209670 to the ET receptors compared to the affinity of the lead structure SB209670 is not affected because the structure–activity relationships (SAR) of this series of compounds indicated that the propyloxy moiety has little effect on the binding potency of the ligands. This assumption was confirmed by the *in vitro* evaluation of [^{18}F]SB209670

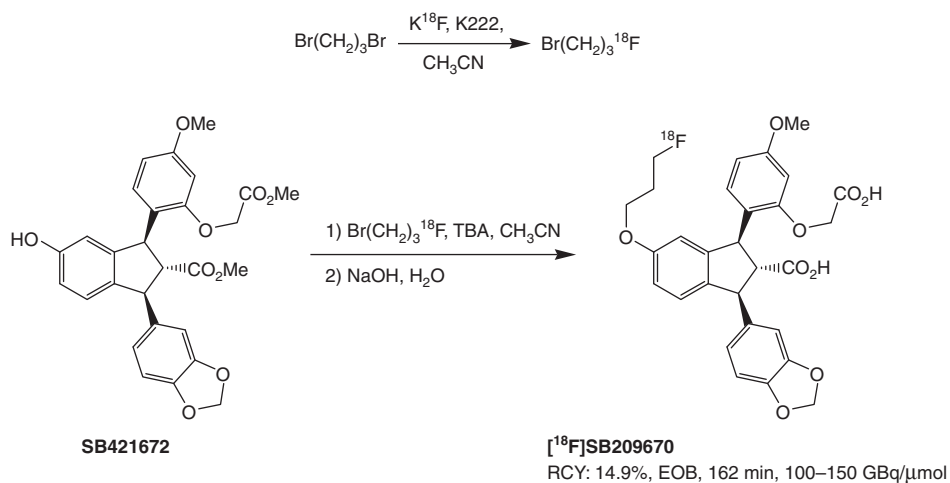


Fig. 9. Radiosynthesis of [¹⁸F]SB209670 [69].

[69,70]. Furthermore, the *in vitro* investigations suggested that [¹⁸F]SB209670 primarily binds to the ET_A receptor in the heart and kidneys. Despite a high degree of liver metabolism, binding of [¹⁸F]SB209670 to ET_A receptors in the heart of Sprague-Dawley rats *in vivo* was successfully imaged with small-animal PET [69].

In summary, several promising approaches to visualize ET receptors of the heart with ¹⁸F-labeled compounds have been developed. Nevertheless, the direct disadvantages of the tracers (e.g., [¹⁸F]ET-1 clearance by ET_B receptors, high degree of [¹⁸F]SB209670 metabolism) prevented further investigations *in vivo* and clinical studies in humans so far. Therefore, the existing ¹⁸F-labeled ET receptor ligands have to be improved or new generations of potential tracers have to be designed.

2.3. Perfusion

PET offers the possibility to quantitatively measure the myocardial blood flow (MBF). MBF tracers can be divided into two groups. The first group is freely diffusible and represented by [¹⁵O]H₂O. These tracers do not show any specific absorption and their distribution is completely determined by diffusion. Consequently, the measurement of the MBF is based on the first-pass extraction and clearance data. Because of the low heart-to-blood radioactivity ratio, the freely diffusible tracers provide myocardial images with low signal-to-background ratios. The second class is composed of highly extractable heart tracers. The tracer [¹³N]NH₃ belongs to this family. These radiolabeled compounds are characterized by a selective extraction and retention in the myocardium. The

accumulation of the extractable tracers is mediated by physiological processes and, thus, the measurement of MBF is susceptible to metabolic alterations. Actually, these effects are often insignificant in MBF measurements [71].

Studenov and Berridge introduced a series of potential ^{18}F -labeled extractable MBF tracers in the year 2001 that were accessible via reliable 1–2-step radiosynthesis sequences. Five ^{18}F -labeled amines and four quaternary ammonium salts were obtained by nucleophilic substitution either at aliphatic precursors or at aromatic compounds [71]. Figure 10 summarizes the synthesis of mentioned compounds.

Biodistribution studies in mice revealed that the ^{18}F -labeled secondary and tertiary amines did not possess the required properties of a high heart-to-blood ratio as well as high standard myocardial uptake. On the other hand, the *ex vivo* investigations identified the 4- ^{18}F fluoro-tri-*N*-methylanilinium cation (^{18}F FTMA) as the most potentially extractable MBF tracer. A comparative study using ^{18}F FTMA, efficient MBF tracers (e.g., $^{99\text{m}}\text{Tc}$ MIBI, $^{99\text{m}}\text{Tc}$ tetrofosmin, ^{13}N NH₃), and an unsuitable tracer (^{62}Cu [*N*-(2-pyridylmethyl)-*N'*-(salicylaldimino)-1,3-propanediamine]Cu(II) acetate) showed that heart-to-blood ratio and standard myocardial uptake of ^{18}F FTMA lie below the values of the efficient compounds, but above the data

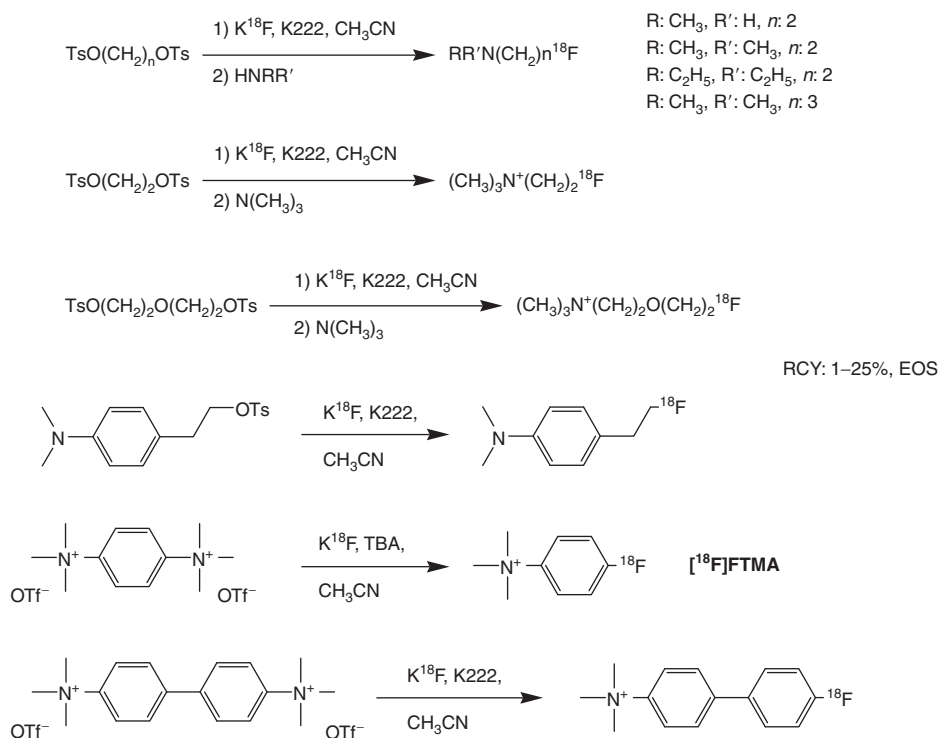


Fig. 10. Radiosyntheses of ^{18}F -labeled amines and quaternary ammonium salts as potential MBF tracers [71] (EOS: end of synthesis).

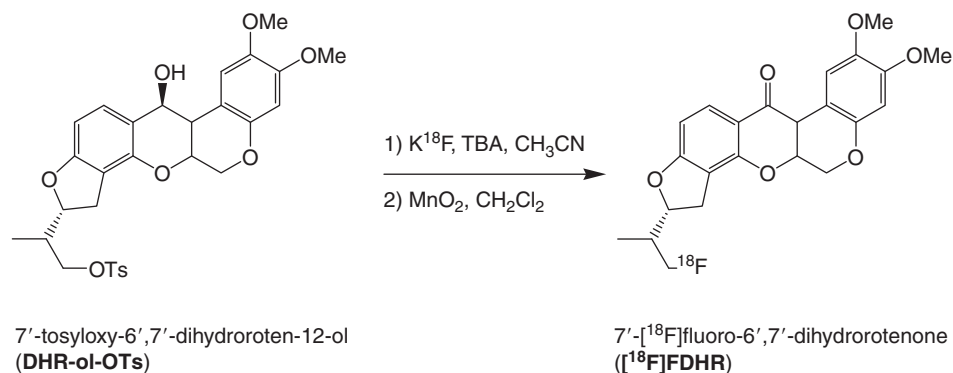


Fig. 11. Radiosynthesis of [^{18}F]FDHR [72].

of the unsuccessful tracer. In general, the relative low myocardial accumulation of the synthesized compounds was attributed to a fast renal clearance as well as to a medium-to-low affinity for any myocardial uptake mechanism [71]. Therefore, the family of simply ^{18}F -labeled amines or quaternary ammonium salts seems to represent an unsuitable compound class for the measurement of MBF (Fig. 10).

Furthermore, Marshall *et al.* developed the extractable MBF tracer 7'-[^{18}F] fluoro-6',7'-dihydrotrotenone ([^{18}F]FDHR) [72]. [^{18}F]FDHR is a derivative of the neutral and lipophilic lead compound rotenone that binds to the complex I of the mitochondrial electron transport chain [73–76]. It was prepared from 7'-tosyloxy-6',7'-dihydrotroten-12-ol (DHR-ol-OTs) in two steps. After nucleophilic substitution of DHR-ol-OTs with [^{18}F]fluoride, the intermediate was oxidized with manganese dioxide to yield the target compound [^{18}F]FDHR (Fig. 11).

In a comparative study, [^{18}F]FDHR, the well-known extractable MBF SPECT (single photon emission computed tomography) tracer [^{201}Ti]TlCl, and the vascular reference tracer [^{131}I]albumin were evaluated in 22 isolated erythrocyte- and albumin-perfused rabbit hearts. A superior retention of [^{18}F]FDHR was observed and the net uptake of this ^{18}F -labeled compound was better correlated with the blood flow than that of [^{201}Ti]TlCl, indicating that [^{18}F]FDHR is a better flow tracer than [^{201}Ti]TlCl in isolated rabbit hearts [72].

In summary, the encouraging results obtained by [^{18}F]FDHR should give rise to further *in vitro* and *in vivo* investigations. If similar results can be achieved in patients, [^{18}F]FDHR could be used with PET for a more accurate assessment of MBF. In this case, an on-site cyclotron that is obligatory for the production of the short-lived nuclides ^{15}O and ^{13}N (half-lives: 2 and 10 min, respectively) used for the synthesis of the common MBF–PET tracers [^{15}O]H $_2$ O and [^{13}N]NH $_3$, respectively, would not be needed.

3. INNERVATION

3.1. Sympathetic and parasympathetic innervation

In addition to perfusion and metabolism in the heart the myocardial innervation is a key player in the physiology and the pathophysiology of the heart [77]. The processes of myocardial neurotransmission happen in three principal parts of the nerve terminals, the synaptic cleft, and the pre- and postsynaptic sites. Myocardial nerves are important for heart functions such as heart rhythm, conduction, and repolarization. The innervation of the heart is provided by the sympathetic and the parasympathetic nervous system. They belong to the autonomic nervous system with (–)-norepinephrine (NE, configuration: 1*R*) and acetylcholine (ACh) as the related endogenous neurotransmitters [78,79] which define the stimulatory and inhibitory physiological effects of each system. The noradrenergic system stimulates the cardiac functions such as contractility and acceleration of heart rate mainly via the β_1 -adrenoceptors, whereas the cholinergic system induces a decreased force of heart contraction and inhibition of conduction via the action of ACh on M_2 muscarinic cholinergic receptors [79]. The dysfunction of the cardiac nervous system plays a fundamental role in the pathophysiology of cardiac diseases (e.g., heart failure, myocardial infarction, and diabetic autonomic neuropathy). Furthermore, cardiovascular innervation constitutes an important target for cardiovascular drugs such as β -adrenoceptor blockers. The human heart has been widely studied with PET and SPECT, but

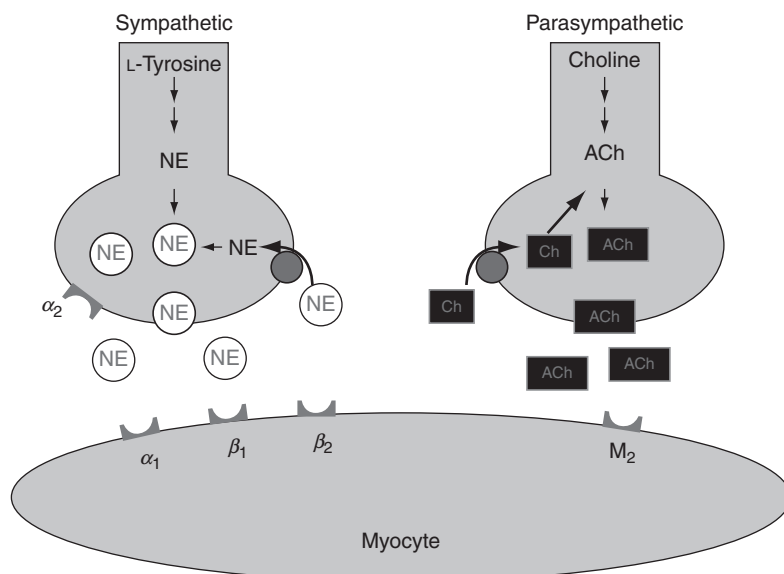


Fig. 12. Sympathetic and parasympathetic innervation of a myocardial myocyte.

until now the assessment of MBF and substrate metabolism using these scintigraphic techniques predominates [79] (Fig. 12).

Recently, several reviews have reported on a variety of ^{11}C - and ^{18}F -labeled radiotracers aiming at mapping cardiac innervation [79–82]. These radioligands are, or could be, useful for visualizing the different aspects of cardiac neurotransmission (Fig. 12). Besides the quantification of postsynaptic receptor densities, radiotracers can also be used for the *in vivo* imaging of presynaptic elements of neurotransmission such as uptake and storage of neurotransmitters as well as binding of neurotransmitters to specific sites within the nerve terminals. Some of the promising ^{18}F -labeled radiotracers are highlighted in the next paragraphs.

3.2. β -Adrenoceptors

The postsynaptic β -adrenoceptors (β -ARs) belong to the rhodopsin/ β_2 adrenergic receptor-like receptors that belong to one of three major subfamilies of the GPCRs [83]. The β -AR family is subdivided into at least three discrete subtypes, the β_1 -, β_2 -AR [84], and the atypical β_3 -AR [85,86]. Additionally, a putative subtype has been identified in cardiac tissue, classified as the β_4 -AR [87]. The β_1 - and β_2 -AR are G_S -protein coupled, thereby elevating the intracellular level of cyclic adenosine monophosphate (cAMP) and causing positive inotropic and chronotropic effects [88]. The β_2 -AR can also couple to the G_i -protein.

Because of the extensive presence of β_1 -ARs in the non-failing myocardium, the heart can be defined as a β_1 -AR organ. The β_1/β_2 -AR ratio within the ventricles of the healthy human heart is $\sim 80/20$ and the average β -AR density (B_{\max}) in atria and ventricles is normally 70–100 fmol/mg protein [89]. In the heart, β_1 -AR agonists are responsible for the increase in cardiac contractility and heart rate, whereas bronchodilation and vasodepression can be mediated by β_2 -selective agonists.

In heart diseases like hypertension, heart failure, ischemia, and hypertrophic cardiomyopathy (HCM) as well as dilated cardiomyopathies (DCM), total myocardial β -AR density is reduced [90–94]. A selective reduction of β_1 -ARs without change of β_2 -AR density is often observed in the failing human heart [89]. Therefore, there is a clinical need for the noninvasive assessment of β -AR density *in vivo*. PET is capable of assessing receptor concentrations *in vivo*, provided that a radioligand radiolabeled with a positron emitter specifically and selectively binds to the target receptor, and metabolism of the radiotracer does not occur in target tissue.

In the following section, all literature known predominantly 3-aryloxy-2-propanolamine-type β -AR radioligands are considered concerning their accessibility for ^{18}F -radiolabeling. In addition, the radioligands are discussed from the radiopharmacological point of view. The feasibility to specifically image pulmonary, cardiac as well as cerebral β -ARs *in vivo* is also considered.

Table 1. Characteristics of potential ¹⁸F-labeled β-adrenoceptor PET radioligands

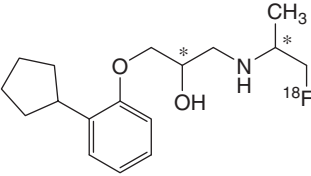
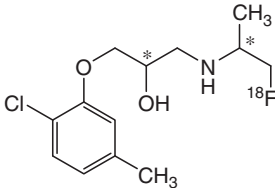
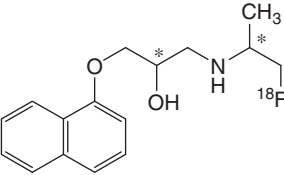
Structure	<i>K</i> _D (β ₁) ¹	<i>K</i> _D (β ₂) ¹	Log <i>D</i> / log <i>P</i> ²	Configuration, [reference]
	—	—	3.35/3.63	(<i>S,S</i>)(<i>S,R</i>) ³ , [95]
[¹⁸ F]Fluoroisopropyl-penbutolol 1				
	—	—	2.18/2.43	(<i>S,S</i>)(<i>S,R</i>) ³ , [95]
[¹⁸ F]Fluoroisopropyl-bupranolol 2				
	—	0.5 nM	2.63/2.90	(<i>S,S</i>)(<i>S,R</i>) ³ , [96]
[¹⁸ F]Fluoropropranolol 3				

Table 1. Continued

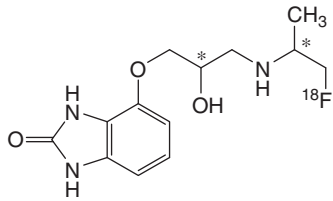
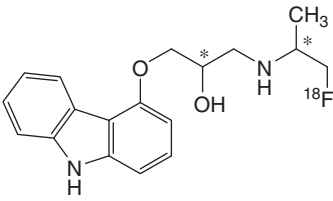
Structure	K_D (β_1) ¹	K_D (β_2) ¹	Log <i>D</i> / log <i>P</i> ²	Configuration, [reference]
 [¹⁸ F]Fluoro CGP 12388 4	–	–	0.30/0.56	(<i>S,S</i>)(<i>S,R</i>) ³ , [97]
 [¹⁸ F]Fluorocarazolol 5	0.41 nM	0.10 nM	2.88/3.18	(<i>S,S</i>)(<i>S,R</i>) ³ , [98]

Table 1. Continued

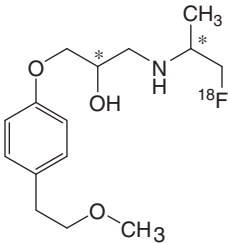
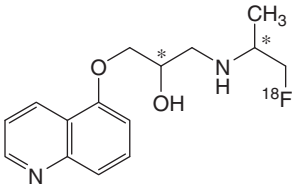
Structure	K_D (β_1) ¹	K_D (β_2) ¹	Log <i>D</i> / log <i>P</i> ²	Configuration, [reference]
 <p>[¹⁸F]Fluorometoprolol 6</p>	350 nM	17 μM	1.31/1.60	All isomers, [103]
 <p>1-(2-[¹⁸F]Fluoro-1-methyl-ethylamino)-3-(quinolin-5-yloxy)- propan-2-ol 7</p>	—	—	1.77/2.02	(<i>S,S</i>)(<i>S,R</i>) ³ , [104]

Table 1. Continued

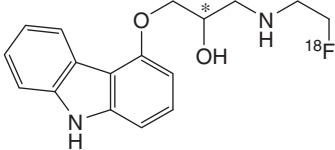
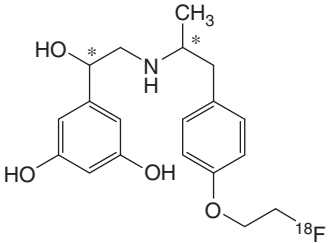
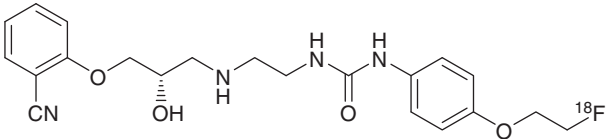
Structure	$K_D (\beta_1)^1$	$K_D (\beta_2)^1$	$\text{Log}D/\text{log}P^2$	Configuration, [reference]
 <p>$[^{18}\text{F}]$Fluoroethyl-carazolol 8</p>	0.50 nM	0.40 nM	2.52/2.83	(S), [105]
 <p>$[^{18}\text{F}]$Fluoroethyl-fenoterol 9</p>	—	$\text{IC}_{50} = 60 \text{ nM}$	0.33/1.77	(R,R)(S,S) ³ , [106]

Table 1. Continued

Structure	K_D (β_1) ¹	K_D (β_2) ¹	Log <i>D</i> / log <i>P</i> ²	Configuration, [reference]
	0.049 nM	2000 nM	0.17/1.44	(<i>S</i>), [107]
(S)- <i>N</i> -[2-[3-(2-cyano-phenoxy)-2-hydroxy-propylamino]-ethyl]- <i>N'</i> -[4-(2-[¹⁸ F]fluoroethoxy)-phenyl]-urea 10				

¹ K_D values found for the nonradioactive counterparts of the β -AR PET radioligands in the here quoted configurations.

² Log*P* values of the neutral form and log*D* values calculated by ACD/Log*D* Suite (Log*D* = Log*P* at physiological pH 7.4 with consideration of charged species).

³ Mixture of stereoisomers of compounds with two chiral centers (e.g., (*S,S*)(*S,R*) = mixture of (*S,S*)- and (*S,R*)-isomers); first configuration in the parentheses refers to the left stereocenter in the structural formula, second configuration in the parentheses refers to the right one (e.g., (*S,R*) = isomer with a (*S*)-configuration at the left and a (*R*)-configuration at the right stereocenter of the shown structural formula).

3.3. ^{18}F -labeled radioligands for PET imaging of β -adrenoceptors

Table 1 shows the characteristics of potential ^{18}F -labeled β -adrenoceptor PET radioligands.

3.3.1. [^{18}F]Fluoroacetone as radiolabeling building block

[^{18}F]Fluoroacetone represents a radiochemically attractive alternative in addition to the short-lived radiolabeling building block 2- ^{11}C acetone. In [^{18}F]fluoroacetone a hydrogen is exchanged by a fluorine atom without changing its sterical demand. Therefore, [^{18}F]fluoroacetone offers the possibility to radiosynthesize β -AR radioligands with extended *in vivo* half-life. [^{18}F]Fluoroacetone can easily be obtained by reaction of acetone tosylate with [^{18}F]K(Kryptofix 2.2.2)F. Acetone tosylate itself is prepared from 1-bromo-2,2-dimethoxypropane and silver tosylate following acidic hydrolysis of the ketal function [96]. Similar to 2- ^{11}C acetone, the [^{18}F]fluoro analog is introduced into the amine function of the β -AR radioligand under reductive alkylation conditions using sodium cyanoborohydride. The presence of fluorine in the isopropyl moiety of the amino function of the β -AR radioligand results in a second chiral center at the secondary isopropyl carbon, and consequently in mixtures of diastereomers. (Table 2).

Using this radiolabeling method, (S,S)(S,R)-[^{18}F]fluoroisopropyl-penbutolol **1** and (S,S)(S,R)-[^{18}F]fluoroisopropyl-bupranolol **2** were synthesized as putative cerebral β -AR radioligands [98]. Despite high *in vitro* binding potencies of both compounds for β -ARs (subnanomolar and nanomolar affinity) as well as significant accumulation in brain tissues of male Wistar rats *in vivo*, uptake of (S,S)(S,R)-[^{18}F]fluoroisopropyl-penbutolol **1** or (S,S)(S,R)-[^{18}F]fluoroisopropyl-bupranolol **2** is dominated by nonspecific binding, both in the brain and in the β -AR-rich peripheral organs heart, lung, and spleen. Therefore, (S,S)(S,R)-[^{18}F]fluoroisopropyl-penbutolol **1** and (S,S)(S,R)-[^{18}F]fluoroisopropyl-bupranolol **2** are unsuitable for β -AR imaging *in vivo*.

(S,S)(S,R)- and (R,R)(R,S)-[^{18}F]fluoropropranolol **3** have also been prepared by reductive alkylation using [^{18}F]fluoroacetone [96]. Both diastereomers were examined as β_2 -AR selective radioligands in male Sprague-Dawley rats *in vivo*. Obviously, the biodistribution data of the (S,S)(S,R)-diastereomer show that binding in the lung between 5 and 30 min post injection (p.i.) could be blocked in the presence of nonradioactive propranolol, but not that of the (R,R)(R,S)-diastereomer of compound **3**. Later time-points were less clear concerning uptake and less affected by propranolol blocking. Altogether, the β -AR affinity of the (S,S)(S,R)-ligand ($K_D = 0.5$ nM) is fivefold higher than that of the (R,R)(R,S)-compound ($K_D = 2.5$ nM).

(S,S)(S,R)-[^{18}F]Fluoro-CGP 12388 **4** was prepared as the less hydrophilic counterpart of the promising non-subtype-selective β -AR radioligand (S)-[^{11}C]CGP 12388 [97]. PET studies of both, the ^{18}F - and ^{11}C -derivative, in male Wistar rats resulted in pulmonary total-to-nonspecific binding ratios of 2.0 for

Table 2. Synthesis of [¹⁸F]fluoroisopropyl-substituted radioligands with [¹⁸F]fluoroacetone

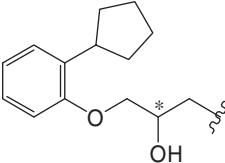
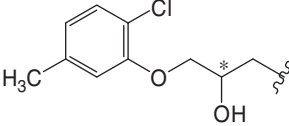
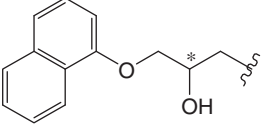
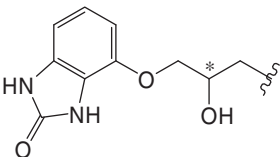
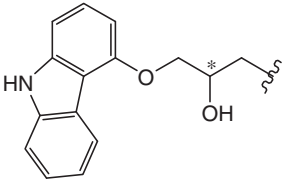
$\text{R-NH}_2 + \text{O}=\text{C}(\text{CH}_3)\text{CH}_2^{18}\text{F} \xrightarrow[\text{solvent, acid, } \Delta]{\text{NaCNBH}_3} \text{R-NH}-\text{CH}(\text{CH}_3)\text{CH}_2^{18}\text{F}$				
Radioligand ¹ , [reference]	R	Radiochemical yield (%)	Synthesis time (min)	Specific activity (GBq/μmol)
(<i>S,S</i>)(<i>S,R</i>)-[¹⁸ F]Fluoroisopropyl-penbutolol 1 [95, 98]		5–21, EOB	20	26–100
(<i>S,S</i>)(<i>S,R</i>)-[¹⁸ F]Fluoroisopropyl-bupranolol 2 [95, 98]		10, EOB	20	11–18
(<i>S,S</i>)(<i>S,R</i>)- and (<i>R,R</i>)(<i>R,S</i>)-[¹⁸ F]Fluoro-propranolol 3 [96]		20–25, EOS	90	37–111
(<i>S,S</i>)(<i>S,R</i>)-[¹⁸ F]Fluoro CGP 12388 4 [97]		12, EOS	105	>74

Table 2. Continued

Radioligand ¹ , [reference]	R	Radiochemical yield (%)	Synthesis time (min)	Specific activity (GBq/μmol)
(<i>S,S</i>)- and (<i>S,R</i>)- [¹⁸ F]Fluorocarazolol 5 [99]		3, EOS	180	19–74

¹ Please notice Footnote 3 of Table 1 regarding the stereochemistry.
EOB, end of bombardment; EOS, end of synthesis.

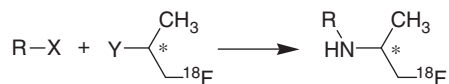
(S)-[¹⁸F]fluoro-CGP 12388 **4** and 5.6 for (S)-[¹¹C]CGP 12388, which corresponds with a certain loss (4–5-fold) in affinity of (S,S)(S,R)-[¹⁸F]fluoro-CGP 12388 **4** for β -ARs resulting from fluorine substitution in the isopropyl group. In addition, (S,S)(S,R)-[¹⁸F]fluoro-CGP 12388 **4** shows a faster (2–3-fold) washout compared with (S)-[¹¹C]CGP 12388.

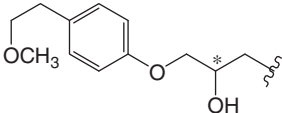
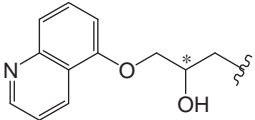
The same group radiosynthesized both the (S,S)- and (S,R)-diastereomers of [¹⁸F]fluorocarazolol **5** [99]. Both diastereomers proved to show a similar biodistribution behavior in male Wistar rats with high receptor-mediated lung and heart accumulation which can be blocked with propranolol. However, in a PET study using male Wistar rats the lungs can clearly be visualized, but not the heart. At 90 min p.i. the specific-to-nonspecific binding ratio was 3.6. In a blocking study with propranolol the lungs were not visible. The visualization of the lung without detecting the heart was reproduced in a PET study in lambs suggesting [¹⁸F]fluorocarazolol **5** as pulmonary β -AR radioligand. In healthy volunteers, (S,R)-[¹⁸F]fluorocarazolol **5** was evaluated as promising cerebral β -AR radioligand (total-to-nonspecific binding ratio 2.0 at 60 min) [100] as well as pulmonary (tissue-to-plasma concentration ratio 11.6) and myocardial radioligand (tissue-to-plasma concentration ratio 18.0) [101] with β -AR binding characteristics. However, [¹⁸F]fluorocarazolol **5** indicated a positive Ames test in extensive toxicological screening experiments with the consequence that the use of this radioligand as radiotracer in clinical PET studies was discontinued [102].

3.3.2. [¹⁸F]Fluoroisopropyl derivatives as radiolabeling building blocks

Another route to introduce the 1-[¹⁸F]fluoroisopropyl residue into the propanolamine radioligands is represented by the model radiotracers listed in Table 3. [¹⁸F]Fluorometoprolol **6** exemplifies the less affine ¹⁸F-labeled counterpart of the β_1 -AR-selective radioligand [¹¹C]metoprolol [103]. 1-[¹⁸F]Fluoroisopropyl tosylate is the building block of choice used to prepare (+/–)-[¹⁸F]fluorometoprolol **6**. 1-[¹⁸F]Fluoroisopropyl tosylate itself is accessible via the reaction of 1,2-propanediol di(p-toluenesulfonate) with [¹⁸F]K(Kryptofix 2.2.2)F. (+/–)-[¹⁸F]Fluorometoprolol **6** was proven to possess a similar β_1 -AR selectivity like [¹¹C]metoprolol, but its affinity appeared to be too low to potentially visualize β -ARs in the heart with PET.

1-(Isopropylamino)-3-(quinolin-5-yloxy)propan-2-ol (β_1/β_2 selectivity = 1.2×10^4) is one of the available β_1 -AR candidate ligands with high β_1 -AR selectivity which was chosen as lead compound to develop a subtype-selective β_1 -AR radioligand. Starting from quinolin-5-yloxy-methyl-oxirane or 1-iodo-3-(quinolin-5-yloxy)-2-(tetrahydropyran-2'-yloxy)propan and the ¹⁸F-labeled building block 2-[¹⁸F]fluoro-1-methyl-ethylamine, the model radiotracer (S,S)(S,R)-1-(2-[¹⁸F]fluoro-1-methyl-ethyl-amino)-3-(quinolin-5-yloxy)propan-2-ol **7** was obtained, but radiochemical yields were too low for further evaluation as β_1 -AR-selective radioligand [104].

Table 3. Synthesis of [¹⁸F]fluoroisopropyl-substituted radioligands with a 1-[¹⁸F]fluoroisopropyl building block

Radioligand ¹ , [reference]	R	XY	Radiochemical yield (%)	Synthesis time (min)	Specific activity (GBq/μmol)
(S,S)(S,R) (R,S)(R,R)- [¹⁸ F]Fluorometoprolol 6 [103]		NH ₂ OTos	2, EOB	90	≥80
(S,S)- and (S,R)-1-(2-[¹⁸ F]Fluoro-1-methyl-ethyl-amino)-3-(quinolin-5-yloxy)-propan-2-ol 7 [104] ²		I NH ₂	Low yields	—	—

¹ Please notice Footnotes 3 and 4 of Table 1 regarding the stereochemistry.² Deprotection via hydrolysis after labeling.

EOB, end of bombardment.

3.3.3. [^{18}F]Fluoroethyl derivatives as radiolabeling building blocks

A common feasibility to introduce a ^{18}F -labeled building block into a precursor compound is the application of 2- ^{18}F fluoroethyl derivatives (e.g., 2- ^{18}F fluoroethyl tosylate). In this section, three model radiotracers are mentioned that represent putative radioligands with β -AR binding properties.

The non-subtype-selective β -AR radioligand (S)- ^{18}F fluoroethylcarazocol **8** is prepared by reaction of 2- ^{18}F fluoroethyl amine with the corresponding epoxide (S)-4-(2,3-epoxypropoxy)carbazole (Fig. 13).

2- ^{18}F Fluoroethyl amine arises from ^{18}F fluorination of *N*-[2-(toluene-4-sulfonyloxy)-ethyl]-phthalimide, followed by hydrazinolysis. (S)- ^{18}F Fluoroethylcarazocol **8** is the successor of the model radioligand ^{18}F fluorocarazocol **5** that showed a positive Ames test during toxicological screening studies [102]. (S)- ^{18}F Fluoroethylcarazocol **8** was examined as β -AR radioligand for cerebral β -AR imaging in male Wistar rats and found to be a high-affinity ligand that specifically binds to cerebral β -ARs *in vivo*. Biodistribution studies showed radioactivity in all brain regions except medulla and pons that could be significantly blocked by nonradioactive fluoroethylcarazocol. Propranolol was able to block (S)- ^{18}F fluoroethylcarazocol **8** uptake in the brain regions, frontal cortex, and striatum, while pindolol additionally reduced radioactivity levels in the cerebellum. Nonradioactive fluoroethylcarazocol, propranolol, and pindolol also blocked (S)- ^{18}F fluoroethylcarazocol **8** accumulation in the peripheral β -AR-rich organs lung, heart, and spleen. In a PET study using rats, the brain was visualized by (S)- ^{18}F fluoroethylcarazocol **8** [105]; thus this radioligand might be useful for the evaluation of cerebral β -ARs with PET.

(*R,R*)(S,S)- ^{18}F Fluoroethylfenoterol **9** was preliminary evaluated as β_2 -AR-selective radioligand for the quantification of the β_2 -AR status in the lung [106]. (*R,R*)(S,S)- ^{18}F Fluoroethylfenoterol **9** arises from the phenolic ^{18}F fluoroethylation reaction of the desfluoroethyl β_2 -AR agonist fenoterol with 2- ^{18}F fluoroethyl tosylate (Fig. 14) which itself can be achieved as radiolabeling building block by ^{18}F fluorination of ethylene glycol di-*p*-tosylate.

2- ^{18}F Fluoroethylation of fenoterol does not change the *in vitro* affinity toward β_2 -ARs as evaluated with isolated guinea pig trachea. In a PET study (*R,R*)(S,S)-

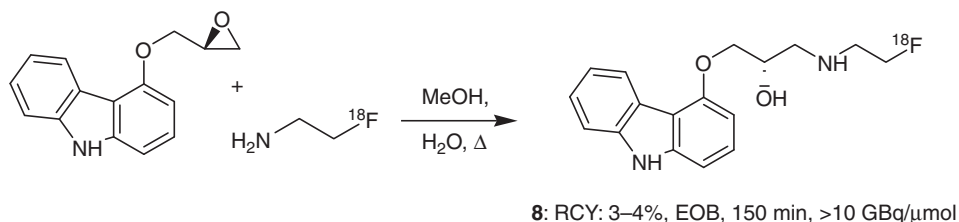
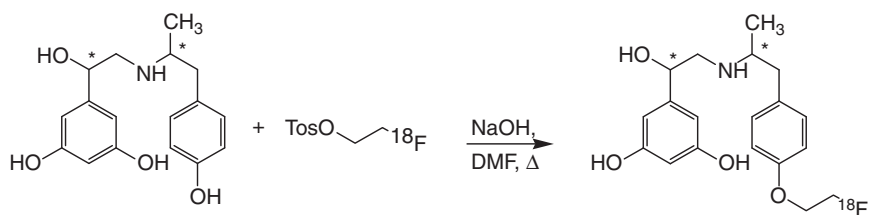
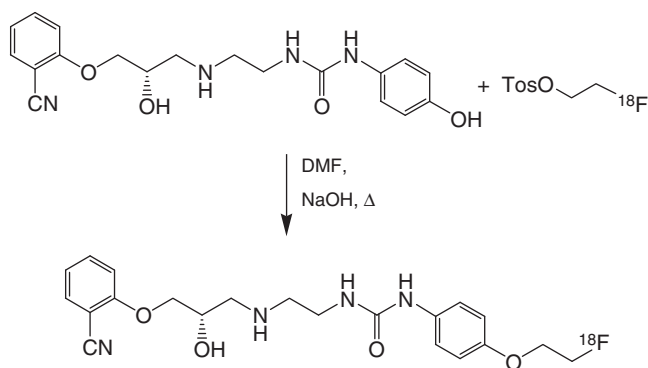


Fig. 13. Radiosynthesis of (S)- ^{18}F fluoroethylcarazocol **8** [105].



9: RCY: 20%, EOB, 65 min, 50–60 GBq/μmol

Fig. 14. Radiosynthesis of (*R,R*)(*S,S*)-[^{18}F]fluoroethylfenoterol **9** [106].



10: RCY: 16%, EOB, 174 min, 40 GBq/μmol

Fig. 15. Radiosynthesis of (*S*)-*N*-[2-[3-(2-cyano-phenoxy)-2-hydroxy-propylamino]-ethyl]-*N'*-[4-(2-[^{18}F]fluoroethoxy)-phenyl]-urea **10** [107].

[^{18}F]fluoroethylfenoterol **9** showed specific pulmonary β_2 -AR binding in guinea pigs that was displaceable by nonradioactive fenoterol by 50%.

Recently, the 2-[^{18}F]fluoroethylation of a phenolic desalkyl precursor based on the β_1 -AR-selective antagonist ICI 89,406 was realized via a two-step synthesis starting with the [^{18}F]fluorination of ethylene glycol di-*p*-tosylate. The radiosynthesis yielded (*S*)-*N*-[2-[3-(2-cyano-phenoxy)-2-hydroxy-propylamino]-ethyl]-*N'*-[4-(2-[^{18}F]fluoroethoxy)-phenyl]-urea **10**, representing a potent ^{18}F -labeled high affinity β_1 -AR-selective radioligand with a β_1 -AR-selectivity of >40,000 (Fig. 15) [107].

The β -AR binding potency of **10** *in vitro* was achieved using the corresponding nonradioactive fluorinated compound and ventricular membrane preparations from dilute brown agouti (DBA) mouse hearts. First preclinical evaluation studies *in vivo* using compound **10** that aim at the visualization of cardiac β_1 -AR receptors in small animals are planned.

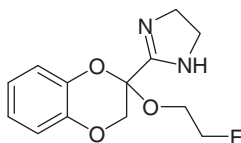


Fig. 16. 2-Fluoroethoxy-idazoxan (RX841018), suggested as nonradioactive counterpart of a potential ^{18}F -labeled α_2 -AR radioligand.

3.4. α -Adrenoceptors

The α -Adrenoceptors (α -ARs) are also G-protein coupled [83] and were differentiated in the 1970s into postsynaptic α_1 -ARs as well as pre- and postsynaptic α_2 -ARs (Fig. 12) [108, 109]. The density of cardiac α_1 -ARs is only 10–15% of that of β_1 -ARs [88, 110]. Cardiac α_1 -ARs which presumably couple via the $G_{q/11}$ -protein [88] are considered to function as backup for the β_1 -ARs. The decrease of β -AR density during heart disease occurs with a simultaneous upregulation of α_1 -ARs that may preserve heart function as compensatory mechanism [111, 112]. Thus, when the number of β -ARs is decreased, increasing amounts of α_1 -ARs may be observed. In the normal situation, the presynaptic α_2 -ARs regulate the norepinephrine release and both the α_1 -AR- and the α_2 -AR-subtype contribute to coronary vasoconstriction and vascular tone [109]. α_1 -ARs are linked to arrhythmogenesis and the development of ventricular hypotrophy [81]. Actually, it is known that each α -AR type can be subdivided further into three subtypes: the α_1 -ARs include the α_{1A} -, α_{1B} -, and α_{1D} -ARs; the present classification of α_2 -ARs consists of the $\alpha_{2A/D}$ -, α_{2B} -, and α_{2C} -ARs [109–113] (Fig. 12).

To date, ^{18}F -labeled α -AR radioligands are not described in the literature. However, a novel fluorinated α_2 -AR antagonist 2-fluoroethoxy-idazoxan based on 2-ethoxy-idazoxan (RX811059) has been evaluated as potential brain imaging agent [114] (Fig. 16). *Ex vivo* binding assays showed the potential of 2-fluoroethoxy-idazoxan to cross the blood–brain-barrier. 2-Fluoroethoxy-idazoxan (RX841018) displayed selectivity over β -ARs as well as the imidazoline₂ binding site and was able to displace tritiated 2-methoxy-idazoxan ($[^3\text{H}]$ RX821002) from whole brain membranes prepared from rat, mouse, and guinea pig with nanomolar α_2 -AR affinity (rat: $K_i = 3.5$ nM; mouse: $K_i = 8.7$ nM; guinea pig: $K_i = 4.5$ nM). This ligand appears to provide a new direction toward developing α_2 -AR ligands for PET [114, 115].

3.5. Muscarinic acetylcholine receptors

At present five different muscarinic receptor subtypes are known that mediate the parasympathetic activity of the autonomic nervous system: M_1 -, M_2 -, M_3 -, M_4 -, and M_5 -receptors [88, 116]. The odd-numbered muscarinic receptors are

$G_{q/11}$ -protein coupled; the even-numbered muscarinic receptors are $G_{i/o}$ -protein coupled [88]. In the human heart, the M_2 -receptor subtype is predominant with reported densities of 243 fmol/mg protein [80–116]. Stimulated muscarinic M_2 -receptors result in negative inotropic and chronotropic effects. Recently, it was demonstrated that the muscarinic M_3 -receptor subtype also exists in the human heart, but its function has still to be elucidated [117]. In contrast to the β -ARs, the density of muscarinic receptors in the failing human heart often does not differ from that in the normal heart [88]. However, in the aging human heart the muscarinic receptor density (the G_i -coupled M_2 -receptor density) decreases. Only a single PET study using (*R*)-[^{11}C]MQNB [(*R*)-methylquinuclidinyl benzilate] — a hydrophilic non-subtype-selective antagonist suitable for imaging peripheral muscarinic receptors — has found a slight, but significant increase in cardiac muscarinic receptors in patients with chronic heart failure [118].

Two ^{18}F -labeled diastereomers, analogs of (*R*)-[^{11}C]MQNB, (*R,R*)- and (*R,S*)-quinuclidinyl-4-[^{18}F]fluoromethyl-benzilate ([^{18}F]FMeQNB), developed for the imaging of muscarinic receptors in the brain, were prepared via a multistep radiosynthesis, resulting in radioligands with high binding potency for muscarinic ACh receptors [119] (Fig. 17). Interestingly, the (*R,R*)-diastereomer [$K_i(M_1) = 0.11\text{ nM}$; $K_i(M_2) = 0.84\text{ nM}$] displays an eightfold selectivity for the M_1 - over the M_2 -receptor while the (*R,S*)-diastereomer [$K_i(M_1) = 0.89\text{ nM}$; $K_i(M_2) = 0.13\text{ nM}$]

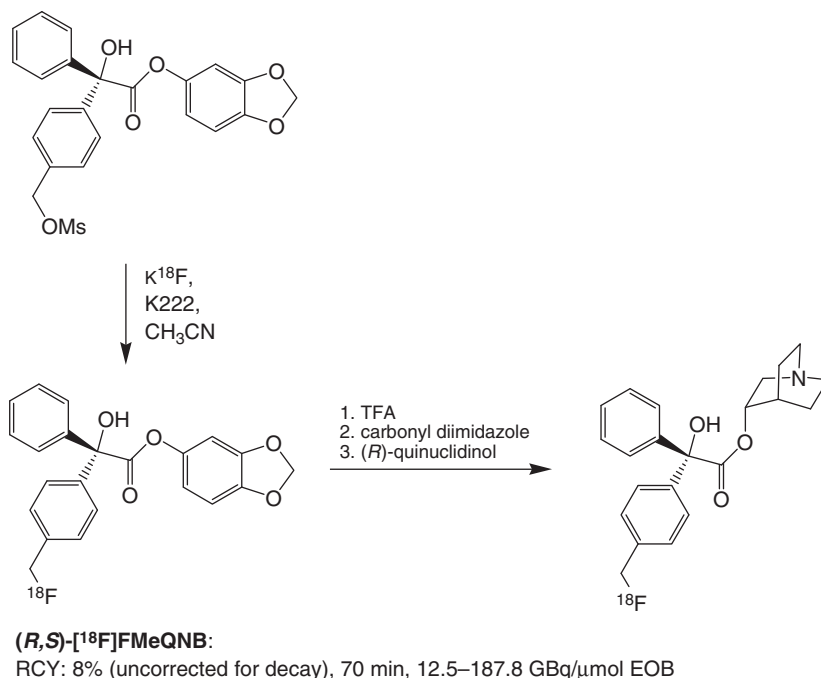


Fig. 17. Two-step radiosynthesis of (*R,S*)-[^{18}F]FMeQNB [119].

possesses a sevenfold selectivity for the M_2 -receptor over the M_1 -receptor [120]. **(R,S)-[^{18}F]FMeQNB** preferably binds to the M_2 -receptor subtype of the heart as shown in rats, but radioligand binding was also detected in some brain regions with the highest portions of the M_2 -subtype (pons, medulla, and cerebellum). In contrast, the uptake of **(R,R)-[^{18}F]FMeQNB** was higher in those brain regions with increased concentrations of the M_1 -subtype (cortex, hippocampus, and caudate). The uptake of **(R,R)-[^{18}F]FMeQNB** in the heart was 4–9 times lower compared with the **(R,S)**-diastereomer. Corresponding experiments in rhesus monkeys showed uptake of **(R,S)-[^{18}F]FMeQNB** in the heart 30–40 min after bolus injection (59 MBq) with good contrast between myocardium and blood pool (activity in myocardium $\sim 26 \text{ kBq/cm}^3$) evidencing that the **(R,S)**-diastereomer has potential for imaging cardiac muscarinic receptors (Fig. 17).

Recently, another fluorinated muscarinic receptor radioligand **[^{18}F]FP-TZTP** selective for the M_2 -subtype [$K_i(M_1) = 7.4 \text{ nM}$; $K_i(M_2) = 2.2 \text{ nM}$; $K_i(M_3) = 79.7 \text{ nM}$] [121] was introduced for the *in vivo* imaging of downregulated M_2 -receptor density in Alzheimer's disease. The M_2 -selectivity of this agonist 3-(3-(3-[^{18}F]-fluoropropyl)thio)-1,2,5-thiadiazol-4-yl)-1,2,5,6-tetrahydro-1-methylpyridine (**[^{18}F]FP-TZTP**) *in vivo* was shown in 2.5-month-old muscarinic receptor-deficient mice whereupon the M_2 knockout mouse was the only one that showed significantly reduced **[^{18}F]FP-TZTP** uptake in all brain tissues [122]. Studies in rhesus monkeys *in vivo* [123, 124] proved the M_2 -receptor selective binding potency of **[^{18}F]FP-TZTP** in the brain. In addition, it was discovered by equilibrium binding and dissociation kinetic studies *in vitro* using rat brain tissue that the M_2 -receptor selectivity of **[^{18}F]FP-TZTP** is based neither on selective internalization of this agonist nor on equilibrium constant differences, but rather on a significantly slower off-rate from the M_2 -receptor [125]. **[^{18}F]FP-TZTP** becomes immediately metabolized in blood; the parent compound decreased to 4–6% in mouse serum at 30 min p.i. while the radioactivity in the brain tissue represented $>87\%$ unmetabolized **[^{18}F]FP-TZTP** [122]. The original two-step synthesis of **[^{18}F]FP-TZTP** using the precursor 3-(3-thiol-1,2,5-thiadiazol-4-yl)-1,2,5,6-tetrahydro-1-methylpyridine oxalate (**SH-TZTP**) and 1-[^{18}F]fluoropropyl toluenesulfonate as intermediate building block was described by Kiesewetter *et al.* [121] and was recently re-developed as one-step synthesis by direct ^{18}F -fluorination of the precursor 3-methanesulfonyloxypropyl-TZTP (Fig. 18) [122].

Moreover, the moderate-affinity ($K_i = 1.7 \text{ nM}$) non-subtype-selective muscarinic ACh receptor antagonist *N*-(2-[^{18}F]fluoroethyl)-4-piperidyl benzilate (**4-[^{18}F]FEPB**) was established for the examination of its sensitivity to changes in ACh levels in the brain, that is, for measuring changes in endogenous ACh levels induced by acetylcholinesterase inhibitors as shown in the brain of male CD rats (rats maintained from birth on a chemically defined diet) [126]. The preparation of **4-[^{18}F]FEPB** can be realized by a two-step synthesis, starting with the ^{18}F -fluorination of the bis-triflate of ethylene glycol (Fig. 19). The formed 2-[^{18}F]fluoroethyltriflate was further

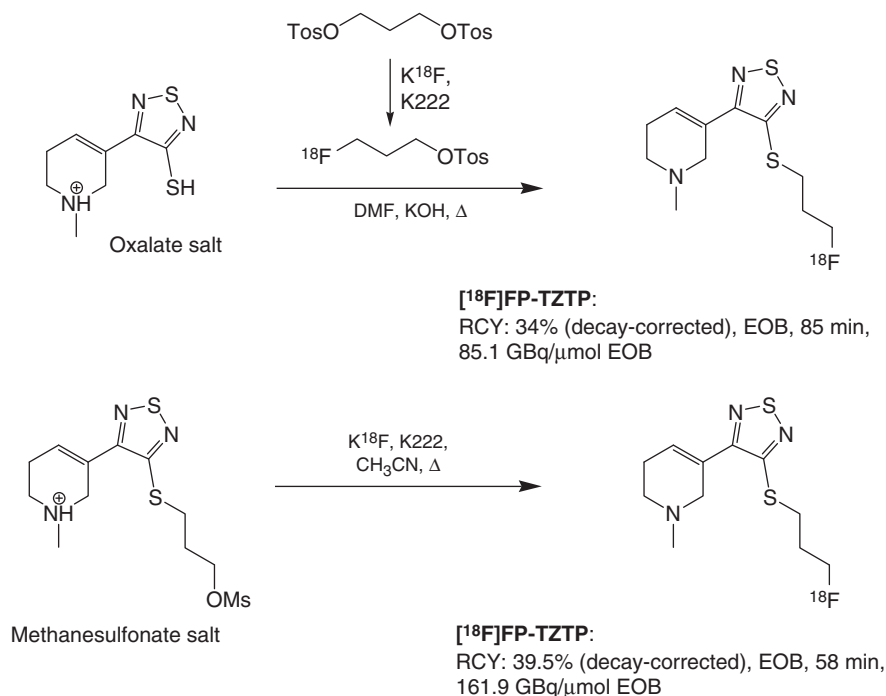


Fig. 18. Radiosyntheses of [¹⁸F]FP-TZTP [121,122].

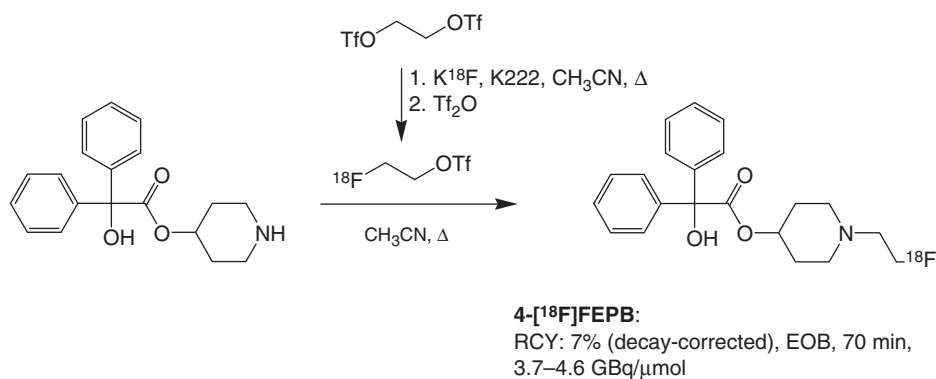


Fig. 19. Two-step radiosynthesis of 4-[¹⁸F]FEPB [127].

reacted with the norpiperidyl precursor hydroxydiphenylacetic acid piperidin-4-yl ester to yield 4-[¹⁸F]FEPB within 4 min by heating [127].

Some years ago, a ¹⁸F-labeled analog of dextetimide, 4-[¹⁸F]fluorodextetimide (4-[¹⁸F]FDEX), was suggested as potential non-subtype-selective muscarinic receptor radioligand for the imaging of muscarinic acetylcholine receptor

(mAChR) density in the brain [128, 129]. The amount of radioactivity peaked at 60 min p.i. in the striatum and cortex of male CD1 mice and cleared slowly. Pre-administration (2 mg/kg) of dextetimide and unlabeled 4-FDEX reduced radioactivity uptake by more than 90% in striatal and cortical regions, indicating specific mAChR binding of **4- ^{18}F FDEX** [129]. The radiosynthesis of **4- ^{18}F FDEX** follows two possible routes. One is the reductive alkylation of (*S*)-nordexetimide with 4- ^{18}F fluorobenzaldehyde using acetic acid and sodium cyanoborohydride in methanol at 80 °C which appeared to be not successful; the second is arranged for the alkylation of (*S*)-nordexetimide with 4- ^{18}F fluorobenzylchloride. The second alkylation approach was realized in a synthesis time of 2.5 h with an overall yield of 10–12% at the end of synthesis (EOS) and a specific activity of >22 GBq/ μmol (Fig. 20) [128].

Alternative QNB analogs were evaluated resulting in the preparation of 1-azabicyclo[2.2.2]oct-3-yl α -(1-fluoropent-5-yl)- α -hydroxy- α -phenylacetate (FQNPe), which demonstrated high binding potency for mAChR [$K_i(\text{M}_1) = 0.33 \text{ nM}$; $K_i(\text{M}_2) = 0.1 \text{ nM}$; $K_i(\text{M}_3) = 0.34$] *in vitro* [130]. Pretreatment of female Fisher rats with FQNPe prior to intravenous (i.v.) administration of Z-(*R,R*)- ^{131}I IQNB, a high-affinity muscarinic ligand, significantly blocked the uptake of radioactivity in the brain and in the heart, which was measured 3 h p.i. [131]. Subsequently, the ^{18}F -labeled (*R,R*)-diastereomer of FQNPe was radiosynthesized via a two-step synthesis yielding (*R,R*)- ^{18}F FQNPe in 12–21% radiochemical yield (decay-corrected) after 3 h (Fig. 21) [130]. Specific activity values of (*R,R*)- ^{18}F FQNPe (<62 MBq/ μmol) were very low owing to a present unidentified non-radioactive compound in the product solution. Anyway, 12 nmol of (*R,R*)- ^{18}F FQNPe were calculated to not block muscarinic receptors *in vivo* and, thus, injected into female Fisher rats. (*R,R*)- ^{18}F FQNPe accumulates in brain regions with high M_1 -subtype (cortex, striatum, thalamus) as well as with high M_2 -subtype concentrations (pons, medulla, superior colliculli), indicating nonselective

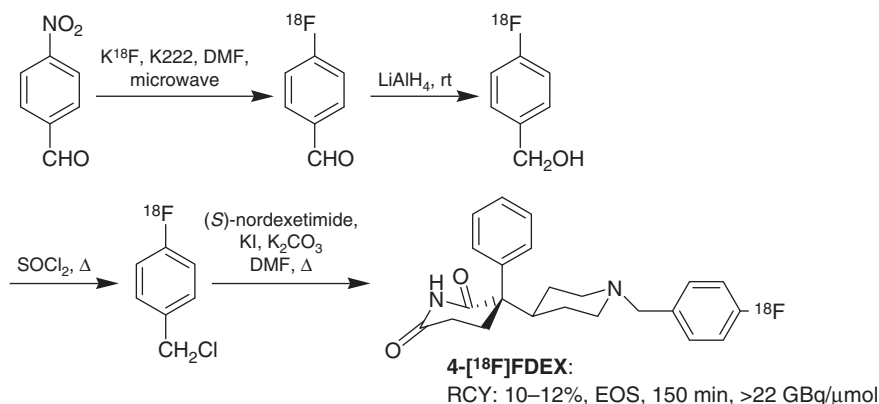
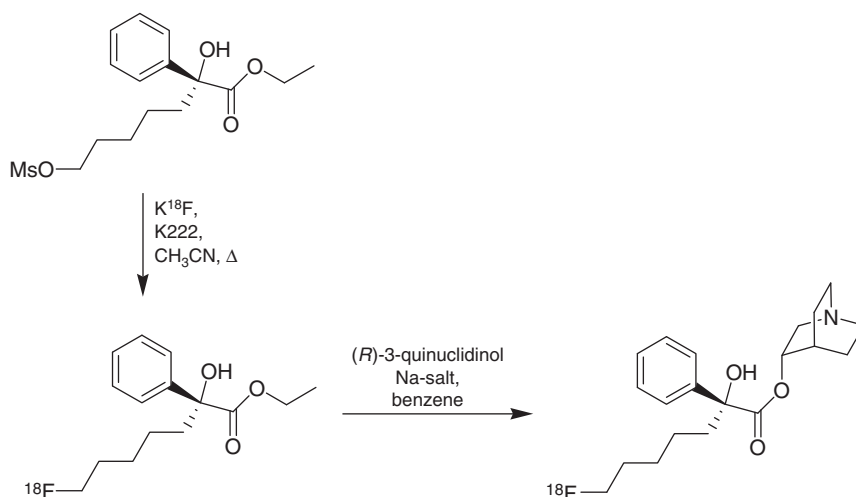


Fig. 20. Four-step radiosynthesis of **4- ^{18}F FDEX** [128].



(*R,R*)-[¹⁸F]FQNPe:

RCY: 12–21% (decay-corrected to start of synthesis), 180 min, <62 MBq/μmol

Fig. 21. Two-step radiosynthesis of (*R,R*)-[¹⁸F]FQNPe [130].

muscarinic receptor binding of (*R,R*)-[¹⁸F]FQNPe. A modest uptake of radioactivity was also observed in the heart, assuming cardiac M₂-subtype binding potency of (*R,R*)-[¹⁸F]FQNPe [130]. Preblocking with 3 mg/kg (*R*)-QNB decreased the (*R,R*)-[¹⁸F]FQNPe uptake by ~90% (Fig. 21).

3.6. Norepinephrine transporter and vesicular monoamine transporter

The norepinephrine transporter (NET) and the vesicular monoamine transporter (VMAT) are presynaptic components of the sympathetic neurons. NET is a Na⁺/Cl[−]-dependent transport protein and responsible for the neurotransmitter uptake from the synaptic cleft into the cytoplasm of the neurons. This transport process, called “uptake-1,” reduces the amount and, thus, the effect of **NE** released into the synaptic cleft. **NE** is stored in the cytoplasm of the neurons in specialized vesicles by the H⁺-dependent transport protein VMAT. Two isoforms VMAT1 and VMAT2, are known. VMAT is localized in the vesicle membranes, and the vesicular storage protects **NE** from metabolism by monoamine oxidase (MAO), which is localized on the surface membrane of the mitochondria. Vice versa, nerve depolarisation causes **NE** release from the vesicles into the synaptic cleft by Ca⁺-mediated exocytose (Fig. 12) [79,132–136].

Several ^{18}F -labeled compounds have been evaluated and established for the *in vivo* investigation of the cardiac “uptake-1” mechanism in physiological and pathological processes. These tracers can be subdivided into two groups. The first group includes the ^{18}F -labeled catecholamines (e.g., derivatives of dopamine and NE). The second group is composed of ^{18}F -labeled catecholamine analogs [e.g., derivatives of metaraminol (**MR**)] and analogs of the antihypertensive drug **guanethidine** (e.g., derivatives of *meta*-iodobenzylguanidine). The catecholamine analogs possess similar characteristics compared to the endogenous neurotransmitters regarding uptake, storage, and release mechanism but display decreased receptor binding potency as well as increased metabolic stability. Therefore, these compounds are called false neurotransmitters [137].

A prominent radiotracer represented in the first group is 6- ^{18}F fluorodopamine (**6- ^{18}F FDA**). This compound was developed from the knowledge that dopamine binds not only to the dopamine transporter (DAT) but also to NET with high binding affinity [138].

Among the different radiosyntheses for **6- ^{18}F FDA** a nucleophilic n.c.a. approach is highlighted in Fig. 22 [139].

The nucleophilic aromatic substitution of 6-nitropiperonal with [^{18}F]K(Kryptofix 2.2.2)F yielded 6- ^{18}F fluoropiperonal that was condensed with nitromethane. Reduction and subsequent hydrolysis of the intermediate nitroalkene provided the target compound **6- ^{18}F FDA**. In comparison to more direct approaches which utilize electrophilic aromatic substitution with positive polarized [^{18}F]fluorine [140–142], this type of preparation is characterized by high specific radioactivity, which is requested for human PET studies with vasopressor compounds, like **6-FDA** [139,143].

PET imaging of cardiac sympathetic innervation with **6- ^{18}F FDA** was evaluated in healthy volunteers regarding its safety, efficacy, validity, and significance. As a conclusion, the uptake of **6- ^{18}F FDA** reflects the distribution of cardiac sympathetic innervation, and the tracer represents a suitable ^{18}F -labeled compound for

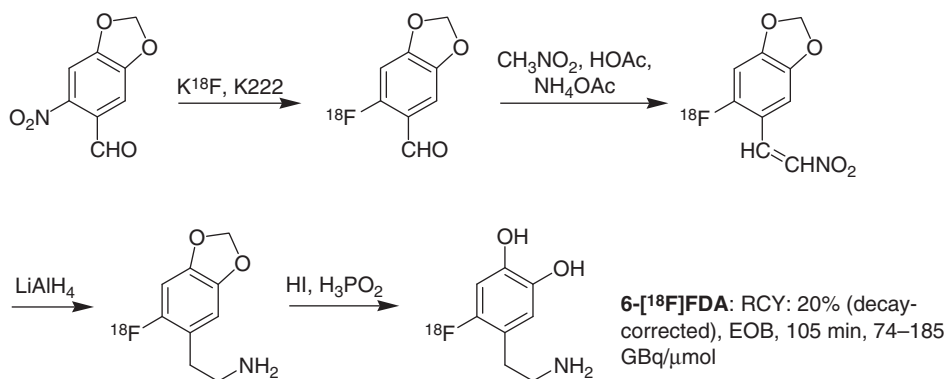


Fig. 22. Four-step radiosynthesis of **6- ^{18}F FDA** [139].

noninvasively assessing sympathetic innervation and function of the human heart [140,144]. Furthermore, **6-[¹⁸F]FDA** PET was useful to detect effects of stressors and drugs on specific aspects of cardiac sympathoneural function in healthy volunteers because alterations in post-ganglionic sympathoneural traffic, neuronal catecholamine uptake, and vesicular turnover of monoamines produced distinct changes in myocardial **6-[¹⁸F]FDA** uptake after tracer injection [145].

This proof of principle was subsequently transferred to pathological processes. The results of **6-[¹⁸F]FDA** PET and neurochemical analyses in patients with dysautonomias supported a new clinical pathophysiological classification of dysautonomias [146]. Another example using **6-[¹⁸F]FDA** PET showed evidence of sympathetic reinnervation of the area at risk 2 weeks and 3 months after acute myocardial infarction [147]. **6-[¹⁸F]FDA** was also used to investigate cardiac sympathetic denervation in patients with Parkinson's disease (PD) [148]. The results of **6-[¹⁸F]FDA** PET were consistent with decreased cardiac uptake of catecholamines in patients with HCM [149]. Furthermore, **6-[¹⁸F]FDA** PET confirmed that cardiac "uptake-1" activity decreases with normal human aging [150]. Additionally, the same group found that at high plasma concentrations endogenous NE competed with sympathetic imaging agents such as **6-[¹⁸F]FDA** for "uptake-1" in patients with pheochromocytoma [151]. Recently, **6-[¹⁸F]FDA** PET studies showed that bilateral upper thoracic sympathectomy partly decreases cardiac sympathetic innervation density [152].

A second ¹⁸F-labeled catecholamine is represented by **6-[¹⁸F]fluoronorepinephrine (6-[¹⁸F]FNE)**. It was developed from the knowledge that the nonradioactive counterpart **6-FNE** possesses a similar *in vivo* behavior regarding storage in the adrenergic nerve terminals and release during sympathetic nerve stimulation, respectively, compared to norepinephrine [153]. Several new asymmetric syntheses of nonradioactive **6-FNE** and **2-FNE** have recently been reviewed [154, 155]. The preparation of **6-[¹⁸F]FNE** corresponds to the synthesis of **6-[¹⁸F]FDA**. Nucleophilic aromatic substitution of 3,4-O-isopropylidene-6-nitrobenzaldehyde by [¹⁸F]K(Kryptofix 2.2.2)F provided 3,4-O-isopropylidene-6-[¹⁸F]fluorobenzaldehyde that was converted into the corresponding cyanohydrins trimethylsilyl ether. Subsequent reduction with lithium aluminium hydride and hydrolysis with formic acid yielded racemic **6-[¹⁸F]FNE**. Resolution of the racemic mixture was achieved via a chiral high performance liquid chromatography (HPLC) column to obtain the pure enantiomers, **(R)-(-)-6-[¹⁸F]FNE** and **(S)-(+)-6-[¹⁸F]FNE** (Fig. 23) [156].

An alternative approach for the synthesis of the **(R)-(-)-6-[¹⁸F]FNE** enantiomer was described by Lui *et al.* Here **6-[¹⁸F]FDA** was converted into **(R)-(-)-6-[¹⁸F]FNE** enzymatically by dopamine β-hydroxylase with an optical purity of at least 90%. Compared to the aforementioned synthesis approach, the enzymatic method offers the advantage of avoiding the enantiomeric resolution [157].

Actually, a comparative PET study using **(R)-(-)-6-[¹⁸F]FNE**, **(S)-(+)-6-[¹⁸F]FNE**, and **6-[¹⁸F]FDA** was performed in baboons. These investigations showed

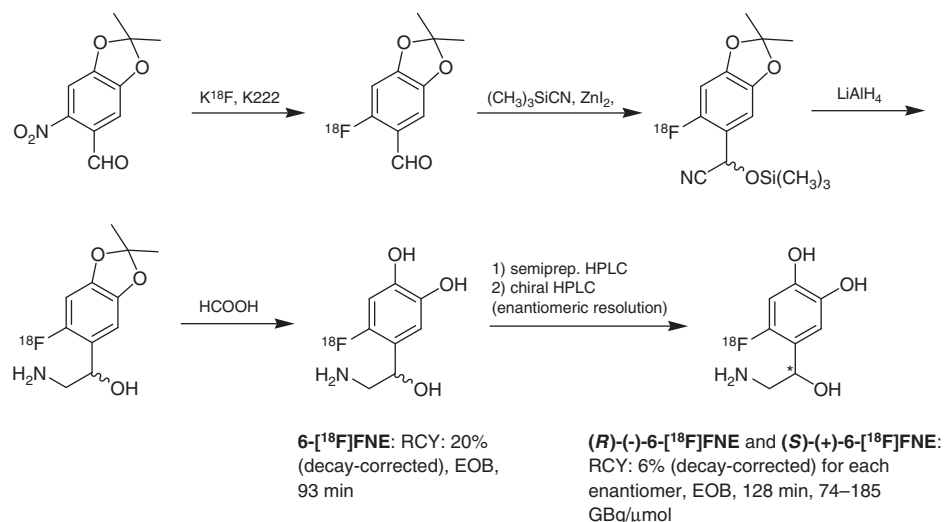


Fig. 23. Radiosynthesis and resolution of 6- ^{18}F FNE [156].

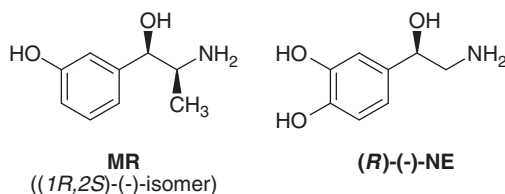


Fig. 24. Chemical structures of MR and (*R*)-(-)-NE.

that (*R*)-(-)-6- ^{18}F FNE and (*S*)-(+)-6- ^{18}F FNE behave like (-)- and (+)-NE concerning the metabolism and clearance characteristics in the heart, and it was found that (*R*)-(-)-6- ^{18}F FNE is a promising tracer for the endogenous biologically more active (-)-NE enantiomer [158]. In further PET studies, (*R*)-(-)-6- ^{18}F FNE was used to evaluate the influence of cocaine on NE “uptake-1” in baboons [159]. It was demonstrated that (*R*)-(-)-6- ^{18}F FNE is a metabolism product of 6- ^{18}F FDA and shares the NET with 6- ^{18}F FDA, but the clearance of the NE analog is slower than that of 6- ^{18}F FDA [160]. To date, human PET studies with 6- ^{18}F FNE are not yet published.

Compared to NE, the metabolism of the false neurotransmitter metaraminol (MR), mediated by catechol-O-methyl transferase (COMT) and MAO, is reduced because of the absence of the catechol function and the presence of an α -methyl group, respectively (Fig. 24) [161].

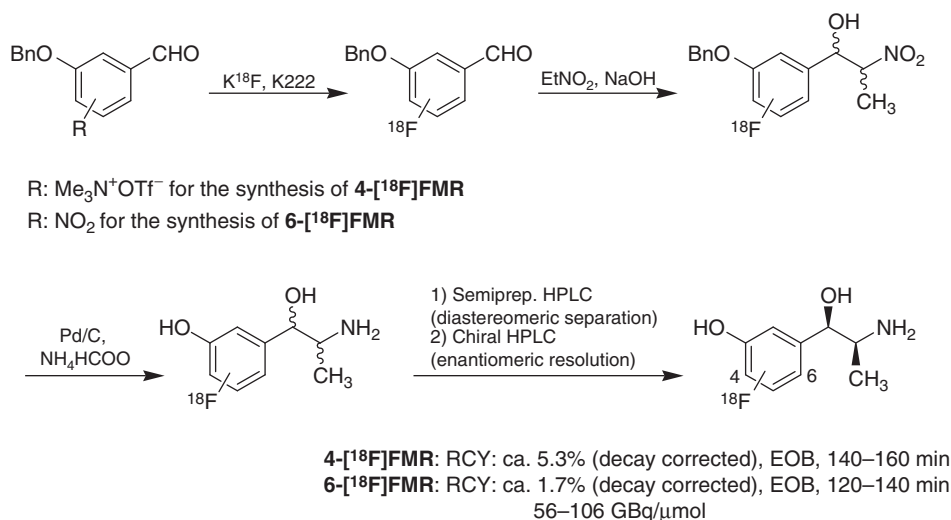


Fig. 25. Radiosynthesis of **4-[¹⁸F]FMR** and **6-[¹⁸F]FMR** [173].

Nevertheless, **MR** possesses similar characteristics regarding the uptake, storage, and release pathways compared to **NE** [162–167]. The superior behavior *in vivo* resulted in the synthesis and evaluation of ¹⁸F-labeled analogs of **MR** for mapping the adrenergic nervous system of the heart *in vivo*. Therefore, the two regioisomers 4- and 6-[¹⁸F]fluorometaraminol (**4-[¹⁸F]FMR** and **6-[¹⁸F]FMR**) were prepared by different electrophilic [168–170] and nucleophilic methods [171–173]. A general approach that yielded **4-[¹⁸F]FMR** or **6-[¹⁸F]FMR** was published by Langer *et al.* in the year 2001 (Fig. 25) [173].

The radiosynthesis starts with the nucleophilic ¹⁸F-fluorination of 2-benzyloxy-4-formyl-*N,N,N*-trimethylanilinium trifluoromethanesulfonate or 5-benzyloxy-2-nitrobenzaldehyde. Subsequent condensation with nitroethane yielded the corresponding 2-nitro-1-propanol derivatives. Reduction of the nitro moiety and deprotection provided the four stereoisomers of ¹⁸F-labeled 2-amino-1-(4-fluoro-3-hydroxyphenyl)-1-propanol and 2-amino-1-(2-fluoro-5-hydroxyphenyl)-1-propanol, respectively. **4-[¹⁸F]FMR** was isolated from the 2-amino-1-(4-fluoro-3-hydroxyphenyl)-1-propanol stereoisomer mixture via semipreparative HPLC and additional chiral HPLC for enantiomeric resolution. In a similar manner enantiomeric pure **6-[¹⁸F]FMR** was obtained. From a synthetic point of view, **4-[¹⁸F]FMR** appeared to be the more promising candidate for PET investigations due to higher radiochemical yields. The main advantage of the nucleophilic approach over the electrophilic methods is the obtained high specific radioactivity (56–106 GBq/μmol) that is desired for safe use in humans with tracer doses far beyond the pharmacological level [173].

In the year 1988, the selective accumulation of **6-[¹⁸F]FMR** in adrenergic nerves of rats was proven by Mislankar *et al.* Systemic blockade of the neuronal

“uptake-1” carrier with desmethylinipramine (a NE “uptake-1” inhibitor) or systemic destruction of the adrenergic nerves with 6-hydroxydopamine reduced the accumulation of **6- ^{18}F FMR** in the heart regions by $\geq 85\%$ [168]. Metabolism studies in rats, dogs, baboons, and guinea pigs with **6- ^{18}F FMR** did not show any significant accumulation of tracer metabolites in the heart, suggesting **6- ^{18}F FMR** as a suitable radioligand for quantitative cardiac imaging [174]. Continuative **6- ^{18}F FMR** PET investigations in closed-chest dogs, bearing phenol-induced left ventricular (LV) neuronal defects, demonstrated the feasibility to delineate the regions of neuronal impairment. Furthermore, tracer accumulation correlated closely with endogenous NE concentrations: **NE** is a commonly used marker of sympathetic nerve density [169].

Similar results were obtained in a group of dogs with neuronal impairments induced by ischemia. Postmortem regional myocardial ^{18}F -radioactivities of **6- ^{18}F FMR** were reduced by 34% compared to the control animals [175]. The regioisomers **4- ^{18}F FMR** and **6- ^{18}F FMR** were compared in a tissue distribution study in rats. The results suggested a similar affinity of both isomers toward the pre-synaptic adrenergic nerve terminals of the heart [173]. Furthermore, **4- ^{18}F FMR** did not show any metabolic degradation in the left ventricle of the rat heart and the uptake was high, rapid, and specific [170]. Blockage of NET or VMAT in rats reduced the myocardial uptake of **4- ^{18}F FMR** by 76–80%. These results were confirmed by **4- ^{18}F FMR** PET in dogs. High cardiac uptake with barely detectable washout was observed during the time course of the experiment. On the other hand, blockage of the NET prior to injection of **4- ^{18}F FMR** reduced the effective half-life of the radioligand by 90% in the heart compared with the control [172]. A comparative study of **4- ^{18}F FMR** and *meta*- ^{123}I iodobenzylguanidine (**^{123}I MIBG**) (Fig. 26), a commercially available and commonly used SPECT-radiopharmaceutical for cardiac neuronal imaging, in spontaneously hypertensive rats suggested that **4- ^{18}F FMR** reflected alterations in “uptake-1” better than **^{123}I MIBG** [176].

The potential of **4- ^{18}F FMR** for the imaging of sympathetic innervation is further confirmed by the development of analytical methods such as planar chromatographic analysis for the detection of its metabolites. This analytical method is well suited for microdialysis samples which have small volumes and low concentrations of compounds [177].

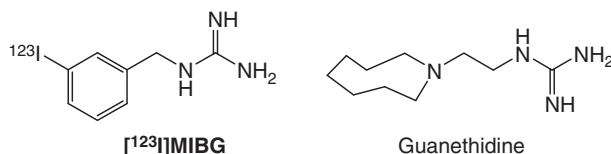
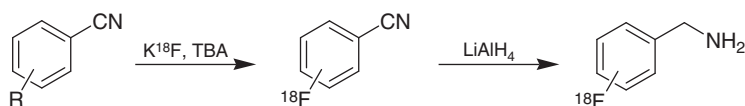
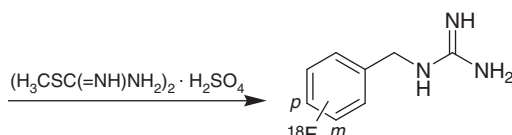


Fig. 26. Chemical structure of ^{123}I MIBG, a single photon emission computed tomography (SPECT)-radiopharmaceutical for cardiac neuronal imaging, and its lead structure guanethidine.



R: NO₂ for the synthesis of [¹⁸F]MFBG

R: Me₃N⁺OTf⁻ for the synthesis of [¹⁸F]PFBG



[¹⁸F]MFBG: RCY: 10–15% (decay corrected), EOB, 60 min

[¹⁸F]PFBG: RCY: 50–55% (decay corrected), EOB, 50 min

Fig. 27. Radiosynthesis of [¹⁸F]MFBG and [¹⁸F]PFBG [178].

¹⁸F-Labeled examples of guanethidine analogs (Fig. 26) are represented by *meta*-[¹⁸F]fluorobenzylguanidine ([¹⁸F]MFBG), *para*-[¹⁸F]fluorobenzylguanidine ([¹⁸F]PFBG), and 4-[¹⁸F]fluoro-3-iodobenzylguanidine ([¹⁸F]FIBG). [¹⁸F]MFBG and [¹⁸F]PFBG were prepared by Garg *et al.* as shown in Fig. 27 [178].

The nucleophilic ¹⁸F-fluorination of 3-nitrobenzonitrile or 4-cyano-*N,N,N*-trimethylanilinium trifluoromethanesulfonate yielded the corresponding [¹⁸F]fluorobenzonitriles. Reduction of the nitrile moiety and subsequent substitution with 2-methyl-2-thiopseudourea completed the three-step radiosyntheses of [¹⁸F]MFBG and [¹⁸F]PFBG, respectively.

In a comparative binding study using the human neuroblastoma cell line SK-N-SH, *in vitro*-specific uptake of [¹³¹I]MIBG, [¹⁸F]MFBG, and [¹⁸F]PFBG was observed but the magnitude of binding was lower than that of [¹³¹I]MIBG. Similar results for heart uptake were obtained in biodistribution studies of mice [178]. Furthermore, the specific accumulation of [¹⁸F]PFBG was demonstrated in the isolated perfused rat heart to clarify uptake and retention mechanism [179]. In subsequent investigations, [¹⁸F]PFBG PET was used to image canine pheochromocytomas and to characterize the area at risk in a canine coronary artery occlusion model [180, 181].

Vaidyanathan *et al.* hypothesized that the unfavorable properties of [¹⁸F]MFBG and [¹⁸F]PFBG, compared to [¹³¹I]MIBG, are caused by the lower lipophilicity of the ¹⁸F-labeled radiotracer, thus suggesting the more lipophilic [¹⁸F]FIBG as PET tracer for the imaging of sympathetic innervation of the heart. The synthesis of this compound was performed similar to that of [¹⁸F]MFBG and [¹⁸F]PFBG (Fig. 28) [182].

4-[¹⁸F]Fluoro-3-iodobenzonitrile was synthesized via nucleophilic aromatic ¹⁸F-fluorination of 4-cyano-3-iodo-*N,N,N*-trimethylanilinium trifluoromethanesulfonate. Subsequent reduction with sodium borohydride, condensation with bis

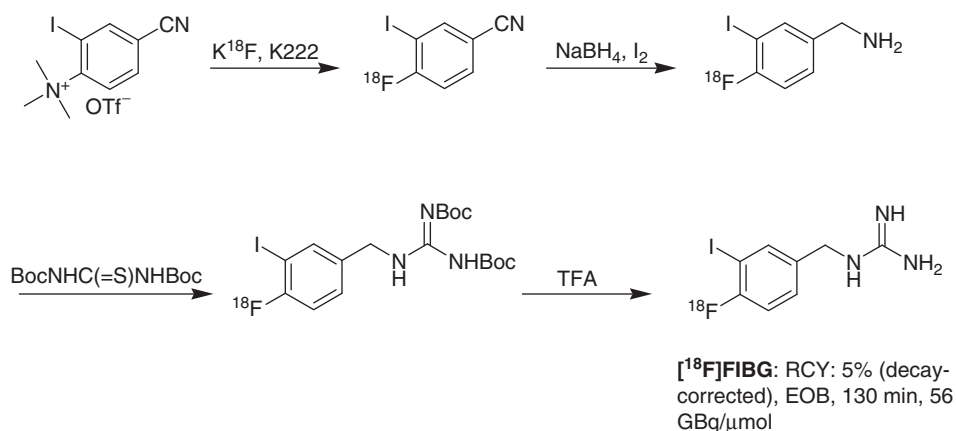


Fig. 28. Radiosynthesis of [^{18}F]FIBG [182].

(*t*-butyloxycarbonyl)thiourea, and deprotection with trifluoroacetic acid yielded [^{18}F]FIBG. [^{18}F]FIBG and [$^{125/131}\text{I}$]MIBG were investigated in SK-N-SH human neuroblastoma cells and in biodistribution studies *in vitro*. As postulated, superior tracer properties of [^{18}F]FIBG compared to [^{18}F]MFBG and [^{18}F]PFBG were described. Additionally, a comparable behavior of [^{18}F]FIBG and [$^{125/131}\text{I}$]MIBG *in vitro/ex vivo* was found regarding specific uptake, concentration-dependent inhibition in the neuroblastoma cells, and specific accumulation in hearts of mice [182,183]. These results demonstrate that FIBG is a true MIBG analog and further evaluation of [^{18}F]FIBG needs to be favored.

In summary, several ^{18}F -labeled radioligands for the imaging of the sympathetic innervation of the heart are available. Several 6-[^{18}F]FDA PET studies in humans have already been performed. It is indeed worthwhile to also continue with the evaluation of the preclinical cardiac innervation tracers, such as 4-[^{18}F]FMR and [^{18}F]FIBG, because of their partly superior *in vivo* potential.

4. SUMMARY AND PERSPECTIVES

In summary, molecular and functional imaging of myocytes, vessels, and nerves in the human heart is already established using different ^{18}F -containing compounds and highly promising for future diagnostic use in patients. However, apart from [^{18}F]FDG none of the other radiotracers discussed here has been really implemented in clinical routine so far. To improve this, science should aim at the automation and simplification of the radiosynthesis and quality control procedures, as well as at the distribution of established tracers. Along with the ever ongoing discovery of new molecular targets, molecular imaging with ^{18}F -labeled compounds should prove useful in clinical decision making in the cardiovascular field.

ANNEX: ¹⁸F-LABELED PET-TRACERS FOR CARDIOLOGICAL IMAGING — UPDATE

Fluorinated fatty acids (FFA): Several clinical FFA metabolism studies have been performed using ¹⁸F-labeled **14F6THA** (**[¹⁸F]FTHA**). Especially, metabolic abnormalities in patients with genetically identical cause for HCM but with variable LV hypertrophy were examined. It was shown that FFA metabolism is increased in mentioned HCM patients and inversely related to LV hypertrophy [184]. At the same time, the biodistribution and partitioning of **14F6THA** in pigs across different lipid pools in plasma and in metabolically important organs in response to insulin were investigated. **14F6THA** was announced as promising tracer in PET imaging of metabolically important organs. The tissue-to-plasma ratio of intact **14F6THA** was highest in the heart [185]. The effect of hyperinsulinemia on myocardial distribution of **14F6THA** was also determined in male Wistar rats. Mitochondrial [¹⁸F]-activity in the heart was increased under hyperinsulinemia conditions; that is, **14F6THA** is sensitive to insulin-induced modifications of FFA oxidative metabolism in the rat heart [186].

A recent study aiming at validating the fatty acid analog **FTP** in the isolated perfused rat heart showed that **FTP** as a metabolically trapped FAO probe is capable of indicating rates of myocardial oxidation of exogenous long-chain fatty acids [187].

Lately, the ¹⁸F-fluorinated fatty acid analog trans-9(*RS*)-[¹⁸F]fluoro-3,4(*RS*, *RS*)-methyleneheptadecanoic acid (**FCPHA**), containing a cyclopropyl group in the β,γ-position, was introduced as a new probe for assessing myocardial FFA metabolism. The cyclopropyl moiety obviously causes an enhanced myocardial uptake of this new tracer in rats, that is, 10-fold higher heart-to-blood ratios 60 min p.i. compared to known ¹⁸F-labeled fatty acids. Additionally, **FCPHA** produces remarkable myocardial PET images in rhesus monkeys, which underlines the potential of this new class of labeled fatty acids in studying heart disease by PET [188].

Atherosclerosis: The imaging of atherosclerosis with [¹⁸F]**FDG** PET was advanced and recent studies in rabbits showed that the tracer accumulated in macrophage-rich atherosclerotic plaques. It was assumed that the vascular macrophage activity can be quantified by [¹⁸F]**FDG** PET [189]. Further studies in rabbits demonstrated that this imaging modality is useful for the clinical evaluation of therapeutic effects of drugs as well as for the development of new drugs that can reduce and inhibit inflammation of vulnerable plaques [190].

Additionally, human studies of atherosclerosis, mainly located in the carotid arteries and thoracic aorta, with [¹⁸F]**FDG** PET were performed. These investigations strengthen the status of [¹⁸F]**FDG** PET as noninvasive plaque-imaging technique [191–196].

In a second approach, ^{18}F -labeled broad-spectrum MMPis have been suggested for the identification and assessment of the vulnerability of atherosclerotic plaques. Corresponding (radio)syntheses of potential PET tracers have been presented. ^{18}F -labeled **CGS 27023A** (see Fig. 6) and **CGS 25966** derivatives (picolyl subunit is replaced by a benzyl subunit, see Fig. 6) were synthesized. These compounds possess a 2- ^{18}F fluoroethoxy-group that replaces the methoxy-group of the lead structures and showed high *in vitro* binding potencies for MMP-2, -8, -9, and -13, respectively [197,198]. Currently, the substances are evaluated in suitable animal models characterized by elevated levels of activated MMPs.

Endothelin-system: Meanwhile, the ^{18}F -labeled ET_B -selective agonist [^{18}F]**BQ3020** has been validated *in vivo* by microPET. As expected, the *in vivo* study indicated high radioactivity accumulation of [^{18}F]**BQ3020** in ET_B receptor-rich tissues such as lungs and kidneys. Interestingly, high levels of radioactivity were found to colocalise to macrophages in atherosclerotic coronary arteries. The biodistribution behavior corresponds to that of [^{18}F]**ET-1**. [^{18}F]**BQ3020** has been suggested as a feasible radioligand for elucidating the proposed role of the ET_B subtype as ET-1 clearing receptor [199].

Perfusion: Recently, a new ^{18}F -labeled cationic myocardial flow tracer has been introduced, that is, the lipophilic *p*-fluorobenzyl triphenyl phosphonium cation ([^{18}F]**FBnTP**). Preliminary pharmacokinetic studies in dogs *in vivo* showed a maximal myocardial uptake within minutes, which was retained throughout the scanning time of >60 min. Sixty minutes after i.v. application, the radioactivity uptake expressed as LV wall-to-blood, -lung, and -liver ratios was 16.6, 12.2, and 1.2, respectively, pointing at the potential of this new PET tracer for cardiac imaging [200]. The same group demonstrated that [^{18}F]**FBnTP** can be used for rapid noninvasive detection and assessment of myocardial perfusion defect severity [201] and as a new sensor for detection of physiological and pathological processes associated with mitochondrial dysfunction [202].

Innervation. NET: **6- ^{18}F FDA** was used in patients with PD with orthostatic hypotension. It was ascertained that PD with orthostatic hypotension features inter alia sympathoneural failure and cardiac sympathetic denervation, independent of levodopa treatment [203]. Based on a profoundly decreased LV myocardial **6- ^{18}F FDA**-derived radioactivity 4 years before the onset of symptoms of PD, the same group hypothesize that cardiac noradrenergic denervation may occur early in the pathogenesis of PD [204,205].

ACKNOWLEDGMENTS

This work was supported by the Deutsche Forschungsgemeinschaft (DFG), Sonderforschungsbereich SFB 656 *Molecular cardiovascular imaging — from mouse to man (MoBil)*, University of Münster, Germany.

REFERENCES

- [1] M.J. Welch, C.S. Redvanly, *Handbook of Radiopharmaceuticals*, John Wiley & Sons Ltd, Chichester, West Sussex, UK, 2003.
- [2] D. Neglia, G. Sambuceti, P. Iozzo, A. L'Abbate, H.W. Strauss, Myocardial metabolic and receptor imaging in idiopathic dilated cardiomyopathy, *Eur. J. Nucl. Med.* 29 (2002) 1403–1413.
- [3] B.M. Gallagher, J.S. Fowler, N.I. Guttererson, R.R. McGregor, C.N. Wan, A.P. Wolf, Metabolic trapping as a principle of radiopharmaceutical design: Some factors responsible for the biodistribution of [^{18}F]-2-deoxy-2-fluoro-D-glucose, *J. Nucl. Med.* 19 (1978) 1154–1161.
- [4] T.A. Smith, Mammalian hexokinases and their abnormal expression in cancer, *Br. J. Biomed. Sci.* 57 (2000) 170–178.
- [5] M. Mamede, T. Higashi, M. Kitaichi, K. Ishizu, T. Ishimori, Y. Nakamoto, K. Yanagihara, M. Li, F. Tanaka, H. Wada, T. Manabe, T. Saga, [^{18}F]FDG uptake and PCNA, Glut-1, and Hexokinase II expressions in cancers and inflammatory lesions of the lung, *Neoplasia* 7 (2005) 369–379.
- [6] R. Southworth, J.L. Darling, R.A. Medina, A.A. Flynn, R.B. Pedley, P.B. Garlick, Dissociation of glucose tracer uptake and glucose transporter distribution in the regionally ischemic isolated rat heart: Application of a new autoradiographic technique, *Eur. J. Nucl. Med. Mol. Imaging* 29 (2002) 1334–1341.
- [7] C.S. Brock, S.R. Meikle, P. Price, Does fluorine-18 fluorodeoxyglucose metabolic imaging of tumors benefit oncology? *Eur. J. Nucl. Med.* 24 (1997) 691–705.
- [8] F. Füchtner, J. Steinbach, P. Mäding, B. Johannsen, Basic hydrolysis of 2-[^{18}F]-fluoro-1,3,4,6-tetra-O-acetyl-D-glucose in the preparation of 2-[^{18}F]-fluoro-2-deoxy-D-glucose, *Appl. Radiat. Isot.* 47 (1996) 61–66.
- [9] K. Hamacher, H.H. Coenen, G. Stöcklin, Efficient stereospecific synthesis of no-carrier-added 2-[^{18}F]-fluoro-2-deoxy-D-glucose using aminopolyether supported nucleophilic substitution, *J. Nucl. Med.* 27 (1986) 235–238.
- [10] H. Schicha, O. Schober, *Nuklearmedizin. Basiswissen und klinische Anwendung*, 5th Edition, Schattauer, Stuttgart, New York, 2003, pp. 20–54.
- [11] T.R. de Grado, M.T. Kitapci, S. Wang, J. Ying, Validation of ^{18}F -fluoro-4-thia-palmitate as a PET probe for myocardial fatty acid oxidation: Effects of hypoxia and composition of exogenous fatty acids, *J. Nucl. Med.* 47 (2006) 173–181.
- [12] M. Schwaiger, H.R. Schelbert, R. Keen, Retention and clearance of C-11 palmitic acid in ischemic and reperfused canine myocardium, *J. Am. Coll. Cardiol.* 6 (1985) 311–320.
- [13] W.C. Stanley, F.A. Recchia, G.D. Lopaschuk, Myocardial substrate metabolism in the normal and failing heart, *Physiol. Rev.* 85 (2005) 1093–1129.
- [14] S.R. Bergmann, P. Herrero, R. Sciacca, Characterization of altered myocardial fatty acid metabolism in patients with inherited cardiomyopathy, *J. Inherit. Metab. Dis.* 24 (2001) 657–674.
- [15] W.C. Stanley, G.D. Lopaschuk, J.G. McCormack, Regulation of energy substrate metabolism in the diabetic heart, *Cardiovasc. Res.* 34 (1997) 25–33.
- [16] C.D. Folmes, A.S. Clanachan, G.D. Lopaschuk, Fatty acid oxidation inhibitors in the management of chronic complications of atherosclerosis, *Curr. Atheroscler. Rep.* 7 (2005) 63–70.
- [17] P. Di Napoli, A.A. Taccardi, A. Barsotti, Long term cardioprotective action of trimetazidine and potential effect on the inflammatory process in patients with ischemic dilated cardiomyopathy, *Heart* 91 (2005) 161–165.
- [18] R.B. Wambolt, G.D. Lopaschuk, R.W. Brownsey, Dichloroacetate improves postischemic function of hypertrophied rat hearts, *J. Am. Coll. Cardiol.* 36 (2000) 1378–1385.

- [19] T.R. de Grado, H.H. Coenen, G. Stöcklin, (*R,S*)-14- ^{18}F -fluoro-6-thiaheptadecanoic acid (FTHA): Evaluation in mouse of a new probe of myocardial utilization of long chain fatty acids, *J. Nucl. Med.* 32 (1991) 1888–1896.
- [20] T.R. de Grado, S. Wang, J.E. Holden, R.J. Nickles, M. Taylor, C.K. Stone, Synthesis and preliminary evaluation of ^{18}F -labelled 4-thia palmitate a pet tracer of myocardial fatty acid oxidation, *Nucl. Med. Biol.* 27 (2000) 221–231.
- [21] M.M. Goodman, F.F. Knapp Jr, Radiochemical synthesis of ^{18}F -3-methyl-branched omega fluorofatty acids, *J. Label. Compd. Radiopharm.* 26 (1989) 233–235.
- [22] E.J. Knust, C. Kupfernagel, G. Stöcklin, Long chain ^{18}F -fatty acids for the study of regional metabolism in heart and liver; odd-even effects of metabolism in mice, *J. Nucl. Med.* 20 (1979) 1170–1175.
- [23] T. Takahashi, S. Nishimura, T. Ido, K. Ishiwata, R. Iwata, Biological evaluation of 5-methyl-branched-chain omega- ^{18}F -fluorofatty acid: A potential myocardial imaging tracer for positron emission tomography, *Nucl. Med. Biol.* 23 (1996) 303–308.
- [24] R.D. Timothy, C.M. Detlef, Non- β -oxidizable ω - ^{18}F -fluoro long chain fatty acid analogues show cytochrome P-450 mediated defluorination; implication for the design of PET-tracers of myocardial fatty acid utilization, *Nucl. Med. Biol.* 19 (1992) 389–397.
- [25] A. Ebert, H. Herzog, G.L. Stöcklin, M.M. Henrich, T.R. de Grado, H.H. Coenen, L.E. Feinendegen, Kinetics of (*R,S*)-14- ^{18}F -fluoro-6-thiaheptadecanoic acid in normal human hearts at rest, during exercise and after dipyridamole injection, *J. Nucl. Med.* 35 (1994) 51–56.
- [26] M.T. Maki, M. Haaparanta, P. Nuutila, V. Oikonen, M. Luotolahti, O. Eskola, J.M. Knuuti, Free fatty acid uptake in the myocardium and skeletal muscle using fluorine-18-fluoro-6-thia heptadecanoic acid, *J. Nucl. Med.* 39 (1998) 1320–1327.
- [27] M. Taylor, T.R. Wallhaus, T.R. de Grado, D.C. Russell, P. Stanko, R.J. Nickles, C.K. Stone, An evaluation of myocardial fatty acid and glucose uptake using PET with ^{18}F -fluoro-6 thiaheptadecanoic acid and ^{18}F -FDG in patients with congestive heart failure, *J. Nucl. Med.* 42 (2001) 55–62.
- [28] P. Libby, Inflammation in atherosclerosis, *Nature* 420 (2002) 868–874.
- [29] H.C. Stary, A.B. Chandler, R.E. Dinsmore, V. Fuster, S. Glagov, W. Insull Jr, M.E. Rosenfeld, C.J. Schwartz, W.D. Wagner, R.W. Wissler, A definition of advanced types of atherosclerotic lesions and a histological classification of atherosclerosis. A report from the Committee on Vascular Lesions of the Council on Arteriosclerosis, American Heart Association, *Circulation* 92 (1995) 1355–1374.
- [30] R. Virmani, A.P. Burke, F.D. Kolodgie, A. Farb, Pathology of the thin-cap fibroatheroma: A type of vulnerable plaque, *J. Interv. Cardiol.* 16 (2003) 267–272.
- [31] P. Libby, P. Theroux, Pathophysiology of coronary artery disease, *Circulation* 111 (2005) 3481–3488.
- [32] Z.S. Galis, Vulnerable plaque: The devil is in the details, *Circulation* 110 (2004) 244–246.
- [33] R.J. Lederman, R.R. Raylman, S.J. Fisher, P.V. Kison, H. San, E.G. Nabel, R.L. Wahl, Detection of atherosclerosis using a novel positron-sensitive probe and 18-fluorodeoxy-glucose (FDG), *Nucl. Med. Commun.* 22 (2001) 747–753.
- [34] M. Ogawa, S. Ishino, T. Mukai, D. Asano, N. Teramoto, H. Watabe, N. Kudomi, M. Shiomi, Y. Magata, H. Iida, H. Saji, ^{18}F -FDG accumulation in atherosclerotic plaques: Immunohistochemical and PET imaging study, *J. Nucl. Med.* 45 (2004) 1245–1250.
- [35] M. Yun, S. Jang, A. Cucchiara, A.B. Newberg, A. Alavi, ^{18}F -FDG uptake in the large arteries: A correlation study with the atherogenic risk factors, *Semin. Nucl. Med.* 32 (2002) 70–76.
- [36] J.H. Rudd, E.A. Warburton, T.D. Fryer, H.A. Jones, J.C. Clark, N. Antoun, P. Johnström, A.P. Davenport, P.J. Kirkpatrick, B.N. Arch, J.D. Pickard, P.L. Weissberg, Imaging atherosclerotic plaque inflammation with ^{18}F -fluorodeoxy-glucose positron emission tomography, *Circulation* 105 (2002) 2708–2711.

- [37] M. Tatsumi, C. Cohade, Y. Nakamoto, R.L. Wahl, Fluorodeoxyglucose uptake in the aortic wall at PET/CT: Possible finding for active atherosclerosis, *Radiology* 229 (2003) 831–837.
- [38] J.R. Davies, J.H. Rudd, T.D. Fryer, M.J. Graves, J.C. Clark, P.J. Kirkpatrick, J.H. Gillard, E.A. Warburton, P.L. Weissberg, Identification of culprit lesions after transient ischemic attack by combined ^{18}F -fluorodeoxyglucose positron-emission tomography and high-resolution magnetic resonance imaging, *Stroke* 36 (2005) 2642–2647.
- [39] N. Borkakoti, Structural studies of matrix metalloproteinases, *J. Mol. Med.* 78 (2000) 261–268.
- [40] A.C. Newby, Dual role of matrix metalloproteinases (matrixins) in intimal thickening and atherosclerotic plaque rupture, *Physiol. Rev.* 85 (2005) 1–31.
- [41] K. Kopka, H.J. Breyholz, S. Wagner, M.P. Law, B. Riemann, S. Schröer, M. Trub, B. Guilbert, B. Levkau, O. Schober, M. Schäfers, Synthesis and preliminary biological evaluation of new radioiodinated MMP inhibitors for imaging MMP activity *in vivo*, *Nucl. Med. Biol.* 31 (2004) 257–267.
- [42] M. Schäfers, B. Riemann, K. Kopka, H.J. Breyholz, S. Wagner, K.P. Schäfers, M.P. Law, O. Schober, B. Levkau, Scintigraphic imaging of matrix metalloproteinase activity in the arterial wall *in vivo*, *Circulation* 109 (2004) 2554–2559.
- [43] Q.H. Zheng, G.D. Hutchins, B.H. Mock, W.L. Winkle, MMP Inhibitor Radiotracer [^{11}C] Methyl-CGS27023A: A new PET breast cancer imaging agent, *J. Label. Compd. Radiopharm.* 44 (2001) S104–S106.
- [44] X. Fei, Q.H. Zheng, G.D. Hutchins, X. Liu, K.L. Stone, K.A. Carlson, B.H. Mock, W.L. Winkle, B.E. Glick-Wilson, K.D. Miller, R.S. Fife, G.W. Sledge, H.B. Sun, R.E. Carr, Synthesis of MMP inhibitor radiotracers [^{11}C]methyl-CGS 27023A and its analogs, new potential PET breast cancer imaging agents, *J. Label. Compd. Radiopharm.* 45 (2002) 449–470.
- [45] S. Furumoto, R. Iwata, T. Ido, Design and synthesis of fluorine-18 labeled matrix metalloproteinase inhibitors for cancer imaging, *J. Label. Compd. Radiopharm.* 45 (2002) 975–986.
- [46] S. Furumoto, K. Takashima, K. Kubota, T. Ido, R. Iwata, H. Fukuda, Tumor detection using ^{18}F -labeled matrix metalloproteinase-2 inhibitor, *Nucl. Med. Biol.* 30 (2003) 119–125.
- [47] K.A. Hickey, G. Rubanyi, R.J. Paul, R.F. Highsmith, Characterization of a coronary vasoconstrictor produced by cultured endothelial cells, *Am. J. Physiol.* 248 (1985) C550–C556.
- [48] M. Yanagisawa, H. Kurihara, S. Kimura, Y. Tomobe, M. Kobayashi, Y. Mitsui, Y. Yazaki, K. Goto, A novel potent vasoconstrictor peptide produced by vascular endothelial cells, *Nature* 332 (1988) 411–415.
- [49] Y. Saito, K. Nakao, M. Mukoyama, H. Imura, Increased plasma endothelin level in patients with essential hypertension, *N. Engl. J. Med.* 322 (1990) 205.
- [50] J. Teerlink, B.M. Loeffler, P. Hess, J.P. Maire, M. Clozel, J.P. Clozel, Role of endothelin in the maintenance of blood pressure in conscious rats with chronic heart failure. Acute effects of the endothelin receptor antagonist Ro 47–0203 (bosentan), *Circulation* 90 (1994) 2510–2518.
- [51] A. Giaid, M. Yanagisawa, D. Langleben, R. Michel, R. Levy, H. Shennib, S. Kimura, T. Masaki, W. Duguid, F.R.C. Path, D.J. Stewart, Expression of endothelin-1 in the lungs of patients with pulmonary hypertension, *N. Engl. J. Med.* 328 (1993) 1732–1739.
- [52] T. Masaki, M. Yanagisawa, K. Goto, Physiology and pharmacology of endothelins, *Med. Res. Rev.* 12 (1992) 391–421.
- [53] J. Nelson, A. Bagnato, B. Battistini, P. Nisen, The endothelin axis: Emerging role in cancer, *Nat. Rev. Cancer* 3 (2003) 110–116.
- [54] N. Dhaun, J. Goddard, D. Webb, The endothelin system and its antagonism in chronic kidney disease, *J. Am. Soc. Nephrol.* 17 (2006) 943–955.

- [55] Q.J. Pittman, Endothelin—an emerging role in proinflammatory pathways in brain, *Am. J. Physiol. Regul. Integr. Comp. Physiol.* 290 (2006) R162–R163.
- [56] T. Plusczyk, B. Witzel, M.D. Menger, M. Schilling, ET_A and ET_B receptor function in pancreatitis-associated microcirculatory failure, inflammation, and parenchymal injury, *Am. J. Physiol. Gastrointest. Liver Physiol.* 285 (2003) G145–G153.
- [57] T. Sakurai, M. Yanagisawa, T. Masaki, Molecular characterization of endothelin receptors, *Trends Pharmacol. Sci.* 13 (1992) 103–108.
- [58] B. Battistini, P. Chailier, P. D'Orleans-Juste, N. Briere, P. Sirios, Growth regulatory properties of endothelins, *Peptides* 14 (1993) 385–399.
- [59] E.R. Levin, Endothelins, *N. Engl. J. Med.* 333 (1995) 356–363.
- [60] R.G. Goldie, Endothelins in health and disease: An overview, *Clin. Exp. Pharmacol. Physiol.* 26 (1999) 145–148.
- [61] A.P. Davenport, B. Battistini, Classification of endothelin receptors and antagonists in clinical development, *Clin. Sci.* 103 (2002) 1S–3S.
- [62] M.L. Webb, T.D. Meek, Inhibitors of endothelin, *Med. Res. Rev.* 17 (1997) 17–67.
- [63] S.A. Boyd, R.A. Mantei, A.S. Tasker, G. Liu, B.K. Sorensen, K.J. Henry Jr, T.W. von Geldern, M. Winn, J.R. Wu-Wong, W.J. Chiou, D.B. Dixon, C.W. Hutchins, K.C. Marsh, B. Nguyen, T.J. Opgenorth, Discovery of a series of pyrrolidine-based endothelin receptor antagonists with enhanced ET_A receptor selectivity, *Bioorg. Med. Chem.* 7 (1999) 991–1002.
- [64] J. Sakaki, T. Murata, Y. Yuamoto, I. Nakamura, T. Frueh, T. Pitterna, G. Iwasaki, K. Oda, T. Yamamura, K. Hayakawa, Discovery of IRL 3461: A novel and potent endothelin antagonist with balanced ET_A/ET_B affinity, *Bioorg. Med. Chem. Lett.* 8 (1998) 2241–2246.
- [65] W. Amberg, S. Hergenröder, H. Hillen, R. Jansen, G. Kettschau, A. Kling, D. Klinge, M. Raschak, H. Riechers, L. Unger, Discovery and synthesis of (S)-3-[2-(3,4-dimethoxyphenyl)ethoxy]-2-(4,6-dimethylpyrimidin-2-yloxy)-3,3-diphenylpropionic acid (LU 302872), a novel orally active mixed ET_A/ET_B receptor antagonist, *J. Med. Chem.* 42 (1999) 3026–3032.
- [66] P. Johnström, N.G. Harris, T.D. Fryer, O. Barret, J.C. Clark, J.D. Pickard, A.P. Davenport, ¹⁸F-Endothelin-1, a positron emission tomography (PET) radioligand for the endothelin receptor system: Radiosynthesis and in vivo imaging using microPET, *Clin. Sci.* 103 (2002) 4S–8S.
- [67] P. Johnström, T.D. Fryer, H.K. Richards, N.G. Harris, O. Barret, J.C. Clark, J.D. Pickard, A.P. Davenport, Positron emission tomography using ¹⁸F-labelled endothelin-1 reveals prevention of binding to cardiac receptors owing to tissue-specific clearance by ET_B receptors *in vivo*, *Br. J. Pharmacol.* 144 (2005) 115–122.
- [68] P. Johnström, F.I. Aigbirhio, J.C. Clark, S.P.M.J. Downey, J.D. Pickard, A.P. Davenport, Syntheses of the first endothelin-A- and -B-selective radioligands for positron emission tomography, *J. Cardiovasc. Pharmacol.* 36 (2000) S58–S60.
- [69] P. Johnström, T.D. Fryer, H.K. Richards, O. Barret, J.C. Clark, E.H. Ohlstein, J.D. Pickard, A.P. Davenport, *In vivo* imaging of cardiovascular endothelin receptors using the novel radiolabelled antagonist [¹⁸F]-SB209670 and positron emission tomography (microPET), *J. Cardiovasc. Pharmacol.* 44 (2004) S34–S38.
- [70] J.D. Elliott, M.A. Lago, R.D. Cousins, A. Gao, J.D. Leber, K.F. Erhard, P. Nambi, N.A. Elshourbagy, C. Kumar, J.A. Lee, J.B. Bean, C.W. DeBrosse, D.S. Eggleston, D.P. Brooks, G. Feuerstein, R.R. Ruffolo, J. Weinstock, J.G. Gleason, C.E. Peishoff, E.H. Ohlstein, 1,3-Diarylindan-2-carboxylic acids potent and selective non-peptide endothelin receptor antagonists, *J. Med. Chem.* 37 (1994) 1553–1557.
- [71] A.R. Studenov, M.S. Berridge, Synthesis and properties of ¹⁸F-labeled potential myocardial blood flow tracers, *Nucl. Med. Biol.* 28 (2001) 683–693.
- [72] R.C. Marshall, P. Powers-Risius, B.W. Reutter, J.P. O'Neil, M. La Belle, R.H. Huesman, H.F. VanBrocklin, Kinetic analysis of ¹⁸F-fluorodihydrorotenone as a deposited myocardial flow tracer: Comparison to ²⁰¹Tl, *J. Nucl. Med.* 45 (2004) 1950–1959.

- [73] H. Ueno, H. Miyoshi, K. Ebisui, H. Iwamura, Comparison of the inhibitory action of natural rotenone and its stereoisomers with various NADH-ubiquinone reductases, *Eur. J. Biochem.* 225 (1994) 411–417.
- [74] H. Ueno, H. Miyoshi, M. Inoue, Y. Niidome, H. Iwamura, Structural factors of rotenone required for inhibition of various NADH-ubiquinone oxidoreductases, *Biochim. Biophys. Acta* 1276 (1996) 195–202.
- [75] J.T. Greenamyre, D.S. Higgins, R.V. Ellers, Quantitative autoradiography of dihydrotrotenone binding to complex I of the electron transport chain, *J. Neurochem.* 59 (1992) 746–749.
- [76] R.R. Ramsay, M.J. Krueger, S.K. Youngster, M.R. Gluck, J.E. Casida, T.P. Singer, Interaction of 1-methyl-4-phenylpyridinium ion (MPP⁺) and its analogs with the rotenone/piericidin binding site of NADH dehydrogenase, *J. Neurochem.* 56 (1991) 1184–1190.
- [77] B. Riemann, M. Schäfers, M.P. Law, T. Wichter, O. Schober, Radioligands for imaging myocardial α - and β -adrenoceptors, *Nuklearmedizin* 42 (2003) 4–9.
- [78] I. Carrio, Cardiac neurotransmission imaging, *J. Nucl. Med.* 42 (2001) 1062–1076.
- [79] O. Langer, C. Halldin, PET and SPET tracers for mapping the cardiac nervous system, *Eur. J. Nucl. Med. Mol. Imaging* 29 (2002) 416–434.
- [80] P.H. Elsinga, A. van Waarde, W. Vaalburg, Receptor imaging in the thorax with PET, *Eur. J. Pharmacol.* 499 (2004) 1–13.
- [81] V.W. Pike, M.P. Law, S. Osman, R.J. Davenport, O. Rimoldi, D. Giardina, P.G. Camici, Selection design and evaluation of new radioligands for PET studies of cardiac adrenoceptors, *Pharm. Acta Helv.* 74 (2000) 191–200.
- [82] K. Kopka, M.P. Law, H.J. Breyholz, A. Faust, C. Höltke, B. Riemann, O. Schober, M. Schäfers, S. Wagner, Non-invasive molecular imaging of β -adrenoceptors *in vivo*: Perspectives for PET-radioligands, *Curr. Med. Chem.* 12 (2005) 2057–2074.
- [83] U. Gether, Uncovering molecular mechanisms involved in activation of G protein-coupled receptors, *Endocr. Rev.* 21 (2000) 90–113.
- [84] A.M. Lands, A. Arnold, J.P. McAuliff, F.P. Luduena, T.G. Brown, Differentiation of receptor systems activated by sympathomimetic amines, *Nature* 214 (1967) 597–598.
- [85] J.R. Arch, A.T. Ainsworth, M.A. Cawthorne, V. Piercy, M.V. Sennitt, V.E. Thody, C. Wilson, S. Wilson, Atypical β -adrenoceptor on brown adipocytes as target for anti-obesity drugs, *Nature* 309 (1984) 163–165.
- [86] R.A. Bond, D.E. Clarke, Agonist and antagonist characterization of a putative adrenoceptor with distinct pharmacological properties from the α - and β -subtypes, *Br. J. Pharmacol.* 95 (1988) 723–734.
- [87] D. Sarsero, P. Molenaar, A.J. Kaumann, N.S. Freestone, Putative β_4 -adrenoceptors in rat ventricle mediate increases in contractile force and cell Ca²⁺: Comparison with atrial receptors and relationship to (–)-[3H]-CGP 12177 binding, *Br. J. Pharmacol.* 128 (1999) 1445–1460.
- [88] O.E. Brodde, K. Leineweber, Autonomic receptor systems in the failing and aging human heart: Similarities and differences, *Eur. J. Pharmacol.* 500 (2004) 167–176.
- [89] O.E. Brodde, β_1 - and β_2 -adrenoceptors in the human heart: Properties, function, and alterations in chronic heart failure, *Pharmacol. Rev.* 43 (1991) 203–242.
- [90] M. Castellano, M. Böhm, The cardiac β -adrenoceptor-mediated signaling pathway and its alterations in hypertensive heart disease, *Hypertension* 29 (1997) 715–722.
- [91] M. Khamssi, O.E. Brodde, The role of cardiac β_1 - and β_2 -adrenoceptor stimulation in heart failure, *J. Cardiovasc. Pharmacol.* 16(Suppl 5) (1990) S133–S137.
- [92] O.E. Brodde, H.R. Zerkowski, N. Doetsch, S. Motomura, M. Khamssi, M.C. Michel, Myocardial β -adrenoceptor changes in heart failure: Concomitant reduction in β_1 - and β_2 -adrenoceptor function related to the degree of heart failure in patients with mitral valve disease, *J. Am. Coll. Cardiol.* 14 (1989) 323–331.
- [93] R.L. Anthonio, O.E. Brodde, D.J. van Veldhuisen, E. Scholtens, H.J. Crijns, W.H. van Gilst, β -adrenoceptor density in chronic infarcted myocardium: A subtype specific decrease of β_1 -adrenoceptor density, *Int. J. Cardiol.* 72 (2000) 137–141.

- [94] S. Yamada, T. Ohkura, S. Uchida, K. Inabe, Y. Iwatani, R. Kimura, T. Hoshino, T. Kaburagi, A sustained increase in β -adrenoceptors during long-term therapy with metoprolol and bisoprolol in patients with heart failure from idiopathic dilated cardiomyopathy, *Life Sci.* 58 (1996) 1737–1744.
- [95] P.H. Elsinga, P. Doze, A. Maas, A. van Waarde, T. Wegman, W. Vaalburg, Synthesis and evaluation of radiolabelled antagonists for β -adrenoceptor imaging in the brain with PET, *J. Label. Compd. Radiopharm.* 44 (2001) S262–S264.
- [96] T.J. Tewson, S. Stekhova, B. Kinsey, L. Chen, L. Wiens, R. Barber, Synthesis and biodistribution of *R*- and *S*-isomers of [^{18}F]-fluoropropranolol, a lipophilic ligand for the β -adrenergic receptor, *Nucl. Med. Biol.* 26 (1999) 891–896.
- [97] P.H. Elsinga, A. van Waarde, K.A. Jaeggi, G. Schreiber, M. Helderdoorn, W. Vaalburg, Synthesis and evaluation of (*S*)-4-(3-(2'-[^{11}C]isopropylamino)-2-hydroxypropoxy)-2*H*-benzimidazol-2-one ((*S*)-[^{11}C]CGP 12388) and (*S*)-4-(3-((1'-[^{18}F]-fluoroisopropyl)amino)-2-hydroxypropoxy)-2*H*-benzimidazol-2-one ((*S*)-[^{18}F]fluoro-CGP 12388) for visualization of β -adrenoceptors with positron emission tomography, *J. Med. Chem.* 40 (1997) 3829–3835.
- [98] P. Doze, P.H. Elsinga, B. Maas, A. van Waarde, T. Wegman, W. Vaalburg, Synthesis and evaluation of radiolabeled antagonists for imaging of β -adrenoceptors in the brain with PET, *Neurochem. Int.* 40 (2002) 145–155.
- [99] P.H. Elsinga, M.G. Vos, A. van Waarde, A.H. Braker, T.J. de Groot, R.L. Anthonio, A.A. Weemaes, O.E. Brodde, G.M. Visser, W. Vaalburg, (*S,S*)- and (*S,R*)-1'-[^{18}F]fluorocarazolol ligands for the visualization of pulmonary β -adrenergic receptors with PET, *Nucl. Med. Biol.* 23 (1996) 159–167.
- [100] A. van Waarde, T.J. Visser, P.H. Elsinga, B. de Jong, T.W. van der Mark, J. Kraan, K. Ensing, J. Pruijm, A.T. Willemsen, O.E. Brodde, G.M. Visser, A.M. Paans, W. Vaalburg, Imaging β -adrenoceptors in the human brain with (*S*)-1'-[^{18}F]fluorocarazolol, *J. Nucl. Med.* 38 (1997) 934–939.
- [101] T.J. Visser, A. van Waarde, T.W. van der Mark, J. Kraan, P.H. Elsinga, J. Pruijm, K. Ensing, T. Jansen, A.T. Willemsen, E.J. Franssen, G.M. Visser, A.M. Paans, W. Vaalburg, Characterization of pulmonary and myocardial β -adrenoceptors with (*S*)-1'-[fluorine-18]fluorocarazolol, *J. Nucl. Med.* 38 (1997) 169–174.
- [102] P. Doze, P.H. Elsinga, E.F. de Vries, A. van Waarde, W. Vaalburg, Mutagenic activity of a fluorinated analog of the β -adrenoceptor ligand carazolol in the Ames test, *Nucl. Med. Biol.* 27 (2000) 315–319.
- [103] T.J. de Groot, A. van Waarde, P.H. Elsinga, G.M. Visser, O.E. Brodde, W. Vaalburg, Synthesis and evaluation of 1'-[^{18}F]fluorometoprolol as a potential tracer for the visualization of β -adrenoceptors with PET, *Nucl. Med. Biol.* 20 (1993) 637–642.
- [104] J.J. Posakony, T.J. Tewson, [^{18}F]-Labeled β_1 -selective ligands for imaging the adrenergic receptors of the heart, *J. Label. Compd. Radiopharm.* 44 (2001) S416–S417.
- [105] P. Doze, A. van Waarde, T.J. Tewson, W. Vaalburg, P.H. Elsinga, Synthesis and evaluation of (*S*)-[^{18}F]-fluoroethylcarazolol for *in vivo* β -adrenoceptor imaging in the brain, *Neurochem. Int.* 41 (2002) 17–27.
- [106] E. Schirmacher, R. Schirmacher, O. Thews, W. Dillenburg, A. Helisch, I. Wessler, R. Buhl, S. Hohnemann, H.G. Buchholz, P. Bartenstein, H.J. Machulla, F. Rösch, Synthesis and preliminary evaluation of (*R,R*)(*S,S*) 5-(2-(2-[4-(2-[^{18}F]fluoroethoxy)phenyl]-1-methylethylamino)-1-hydroxyethyl)-benzene-1,3-diol ([^{18}F]FEFE) for the *in vivo* visualisation and quantification of the β_2 -adrenergic receptor status in lung, *Bioorg. Med. Chem. Lett.* 13 (2003) 2687–2692.
- [107] S. Wagner, M.P. Law, B. Riemann, V.W. Pike, H.J. Breyholz, C. Hölte, A. Faust, C. Renner, O. Schober, M. Schäfers, K. Kopka, Synthesis of an ^{18}F -labelled high affinity β_1 -adrenoceptor PET radioligand based on ICI 89,406, *J. Label. Compd. Radiopharm.* 49 (2006) 177–195.
- [108] K. Starke, α -Adrenoceptor subclassification, *Rev. Physiol. Biochem. Pharmacol.* 88 (1981) 199–236.

- [109] B. Civantos Calzada, A. Aleixandre de Artinano, α -Adrenoceptor subtypes, *Pharmacol. Res.* 44 (2001) 195–208.
- [110] M.R. Bristow, Changes in myocardial and vascular receptors in heart failure, *J. Am. Coll. Cardiol.* 22(4 Suppl A) (1993) 61A–71A.
- [111] M.R. Bristow, W. Minobe, R. Rasmussen, R.E. Hershberger, B.B. Hoffman, (α_1 -Adrenergic receptors in the nonfailing and failing human heart, *J. Pharmacol. Exp. Ther.* 247 (1988) 1039–1045.
- [112] G. Heusch, α -Adrenergic mechanisms in myocardial ischemia, *Circulation* 81 (1990) 1–13.
- [113] J.P. Hieble, Adrenoceptor subclassification: An approach to improved cardiovascular therapeutics, *Pharm. Acta. Helv.* 74 (2000) 163–171.
- [114] E.S. Robinson, R.J. Tyacke, L. Finch, G. Willmott, S. Husbands, D.J. Nutt, A.L. Hudson, Pharmacological characterisation of novel α_2 -adrenoceptor antagonists as potential brain imaging agents, *Neuropharmacology* 46 (2004) 847–855.
- [115] S.P. Hume, A.A. Lammertsma, J. Opacka-Juffry, R.G. Ahier, R. Myers, J.E. Cremer, A.L. Hudson, D.J. Nutt, V.W. Pike, Quantification of *in vivo* binding of [3 H]RX 821002 in rat brain: Evaluation as a radioligand for central α_2 -adrenoceptors, *Int. J. Rad. Appl. Instrum. B* 19 (1992) 841–849.
- [116] S. Dhein, C.J. van Koppen, O.E. Brodde, Muscarinic receptors in the mammalian heart, *Pharmacol. Res.* 44 (2001) 161–182.
- [117] I. Hellgren, A. Mustafa, M. Riazi, I. Suliman, C. Sylven, A. Adem, Muscarinic M_3 receptor subtype gene expression in the human heart, *Cell Mol. Life Sci.* 57 (2000) 175–180.
- [118] D. Le Guludec, A. Cohen-Solal, J. Delforge, N. Delahaye, A. Syrota, P. Merlet, Increased myocardial muscarinic receptor density in idiopathic dilated cardiomyopathy: an *in vivo* PET study, *Circulation* 96 (1997) 3416–3422.
- [119] D.O. Kiesewetter, R.E. Carson, E.M. Jagoda, C.J. Endres, M.G. Der, P. Herscovitch, W.C. Eckelman, *In vivo* muscarinic binding selectivity of (R,S)- and (R,R)-[18 F]-fluoromethyl QNB, *Bioorg. Med. Chem.* 5 (1997) 1555–1567.
- [120] D.O. Kiesewetter, J.V. Silverton, W.C. Eckelman, Syntheses and biological properties of chiral fluoroalkyl quinuclidinyl benzilates, *J. Med. Chem.* 38 (1995) 1711–1719.
- [121] D.O. Kiesewetter, J. Lee, L. Lang, S.G. Park, C.H. Paik, W.C. Eckelman, Preparation of 18 F-labeled muscarinic agonist with M_2 selectivity, *J. Med. Chem.* 38 (1995) 5–8.
- [122] E.M. Jagoda, D.O. Kiesewetter, K. Shimoji, L. Ravasi, M. Yamada, J. Gomez, J. Wess, W.C. Eckelman, Regional brain uptake of the muscarinic ligand, [18 F]FP-TZTP, is greatly decreased in M_2 receptor knockout mice but not in M_1 , M_3 and M_4 receptor knockout mice, *Neuropharmacology* 44 (2003) 653–661.
- [123] B.E. Benson, R.E. Carson, D.O. Kiesewetter, P. Herscovitch, W.C. Eckelman, R.M. Post, T.A. Ketter, A potential cholinergic mechanism of procaine's limbic activation, *Neuropsychopharmacology* 29 (2004) 1239–1250.
- [124] R.E. Carson, D.O. Kiesewetter, E. Jagoda, M.G. Der, P. Herscovitch, W.C. Eckelman, Muscarinic cholinergic receptor measurements with [18 F]FP-TZTP: Control and competition studies, *J. Cereb. Blood Flow Metab.* 18 (1998) 1130–1142.
- [125] L. Ravasi, D.O. Kiesewetter, K. Shimoji, G. Lucignani, W.C. Eckelman, Why does the agonist [18 F]FP-TZTP bind preferentially to the M_2 muscarinic receptor? *Eur. J. Nucl. Med. Mol. Imaging* 33 (2006) 292–300.
- [126] M.B. Skaddan, M.R. Kilbourn, S.E. Snyder, P.S. Sherman, Acetylcholinesterase inhibition increases *in vivo* N-(2-[18 F]fluoroethyl)-4-piperidyl benzilate binding to muscarinic acetylcholine receptors, *J. Cereb. Blood Flow Metab.* 21 (2001) 144–148.
- [127] M.B. Skaddan, M.R. Kilbourn, S.E. Snyder, P.S. Sherman, T.J. Desmond, K.A. Frey, Synthesis, 18 F-labeling, and biological evaluation of piperidyl and pyrrolidyl benzilates as *in vivo* ligands for muscarinic acetylcholine receptors, *J. Med. Chem.* 43 (2000) 4552–4562.

- [128] D.R. Hwang, C.S. Dence, Z.A. McKinnon, C.J. Mathias, M. Welch, Positron labeled muscarinic acetylcholine receptor antagonist: 2- and 4- ^{18}F fluorodexetimide. Syntheses and biodistribution, *Int. J. Rad. Appl. Instrum. B* 18 (1991) 247–252.
- [129] A.A. Wilson, U.A. Scheffel, R.F. Dannals, M. Stathis, H.T. Ravert, H.N. Wagner Jr, *In vivo* biodistribution of two ^{18}F -labelled muscarinic cholinergic receptor ligands: 2- ^{18}F - and 4- ^{18}F -fluorodexetimide, *Life Sci.* 48 (1991) 1385–1394.
- [130] H. Luo, A.L. Beets, M.J. McAllister, M. Greenbaum, D.W. McPherson, F.F. Knapp Jr, Resolution, *in vitro* and *in vivo* evaluation of fluorine-18-labeled isomers of 1-azabicyclo[2.2.2]oct-3-yl α -(1-fluoropent-5-yl)- α -hydroxy- α -phenylacetate (FQNPe) as new PET candidates for the imaging of muscarinic-cholinergic receptor, *J. Label. Compd. Radiopharm.* 41 (1998) 681–704.
- [131] H. Luo, A. Hasan, V. Sood, R.C. McRee, B. Zeeberg, R.C. Reba, D.W. McPherson, F.F. Knapp Jr, Evaluation of 1-azabicyclo[2.2.2]oct-3-yl α -fluoroalkyl- α -hydroxy- α -phenylacetates as potential ligands for the study of muscarinic receptor density by positron emission tomography, *Nucl. Med. Biol.* 23 (1996) 267–276.
- [132] S.G. Amara, Neurotransmitter transporters: Recent progress, *Annu. Rev. Neurosci.* 16 (1993) 73–79.
- [133] M.J. Brownstein, B.J. Hoffman, Neurotransmitter transporters, *Recent Prog. Hormone Res.* 49 (1994) 27–42.
- [134] B. Borowsky, B.J. Hoffmann, Neurotransmitter transporters: Molecular biology function and regulation, *Int. Rev. Neurobiol.* 38 (1995) 139–198.
- [135] S.M. Parsons, Transport mechanism in acetylcholine and monoamine storage, *FASEB J.* 14 (2000) 2423–2434.
- [136] E. Weihe, L.E. Eiden, Chemical neuroanatomy of the vesicular amine transporters, *FASEB J.* 14 (2000) 2435–2449.
- [137] I.J. Kopin, False adrenergic transmitters, *Annu. Rev. Pharmacol.* 8 (1968) 377–394.
- [138] E.L. Barker, R.D. Blakely, in: F.E. Bloom, D.J. Kupfer (Eds.), *Psychopharmacology: The fourth generation of progress*, Raven Press, New York, 1995, pp. 321–333.
- [139] Y.S. Ding, J.S. Fowler, S.J. Gatley, S.L. Dewey, A.P. Wolf, D.J. Schlyer, Synthesis of high specific activity 6- ^{18}F fluorodopamine for positron emission tomography studies of sympathetic nervous tissue, *J. Med. Chem.* 34 (1991) 861–863.
- [140] D.S. Goldstein, G. Eisenhofer, B.B. Dunn, I. Armando, J. Lenders, E. Grossman, C. Holmes, K.L. Kirk, S. Bacharach, R. Adams, P. Herscovitch, I.J. Kopin, Positron emission tomographic imaging of cardiac sympathetic innervation using 6- ^{18}F fluorodopamine: Initial findings in humans, *J. Am. Coll. Cardiol.* 22 (1993) 1961–1971.
- [141] T. Chaly, J.R. Dahl, R. Maccacchieri, D. Bandyopadhyay, A. Belakhlef, V. Dhawan, S. Takikawa, W. Robeson, D. Margouleff, D. Eidelberg, Synthesis of 6- ^{18}F fluorodopamine with a synthetic unit made up of primarily sterile disposable components and operated by master slave manipulator, *Appl. Radiat. Isot.* 44 (1993) 869–873.
- [142] R. Chirakal, G. Coates, G. Firna, G.J. Schrobilgen, C. Nahmias, Direct radiofluorination of dopamine: ^{18}F -labeled 6-fluorodopamine for imaging cardiac sympathetic innervation in humans using positron emission tomography, *Nucl. Med. Biol.* 23 (1996) 41–45.
- [143] D.S. Goldstein, P.C. Chang, G. Eisenhofer, R. Mileti, R. Finn, J. Bacher, K.L. Kirk, S. Bacharach, I.J. Kopin, Positron emission tomographic imaging of cardiac sympathetic innervation and function, *Circulation* 81 (1990) 1606–1621.
- [144] G. Coates, R. Chirakal, E.L. Fallen, G. Firna, E.S. Garnett, M.V. Kamath, A. Scheffel, C. Nahmias, Regional distribution and kinetics of ^{18}F 6-fluorodopamine as a measure of cardiac sympathetic activity in humans, *Heart* 75 (1996) 29–34.
- [145] D.S. Goldstein, C. Holmes, J.E. Stuhlmuller, J.W. Lenders, I.J. Kopin, 6- ^{18}F fluorodopamine positron emission tomographic scanning in the assessment of cardiac sympathetic neuronal function—studies in normal humans, *Clin. Auton. Res.* 7 (1997) 17–29.
- [146] D.S. Goldstein, C. Holmes, R.O. Cannon 3rd, G. Eisenhofer, I.J. Kopin, Sympathetic cardioneuropathy in dysautonomias, *N. Engl. J. Med.* 336 (1997) 696–702.

- [147] E.L. Fallen, G. Coates, C. Nahmias, R. Chirakal, R. Beanlands, L. Wahl, G. Woodcock, M. Thomson, M. Kamath, Recovery rates of regional sympathetic reinnervation and myocardial blood flow after acute myocardial infarction, *Am. Heart J.* 137 (1999) 863–869.
- [148] D.S. Goldstein, C. Holmes, S.T. Li, S. Bruce, L.V. Metman, R.O. Cannon 3rd, Cardiac sympathetic denervation in Parkinson disease, *Ann. Intern. Med.* 133 (2000) 338–347.
- [149] S.T. Li, C.J. Tack, L. Fananapazir, D.S. Goldstein, Myocardial perfusion and sympathetic innervation in patients with hypertrophic cardiomyopathy, *J. Am. Coll. Cardiol.* 35 (2000) 1867–1873.
- [150] S.T. Li, C. Holmes, I.J. Kopin, D.S. Goldstein, Aging-related changes in cardiac sympathetic function in humans, assessed by 6-¹⁸F-fluorodopamine PET scanning, *J. Nucl. Med.* 44 (2003) 1599–1603.
- [151] B.A. Eldadah, K. Pacak, G. Eisenhofer, C. Holmes, I.J. Kopin, D.S. Goldstein, Cardiac uptake-1 inhibition by high circulating norepinephrine levels in patients with pheochromocytoma, *Hypertension* 43 (2004) 1227–1232.
- [152] J.P. Moak, B. Eldadah, C. Holmes, S. Pechnik, D.S. Goldstein, Partial cardiac sympathetic denervation after bilateral thoracic sympathectomy in humans, *Heart Rhythm* 2 (2005) 602–609.
- [153] C.C. Chiueh, Z. Zukowska-Grojec, K.L. Kirk, I.J. Kopin, 6-Fluorocatecholamines as false adrenergic neurotransmitters, *J. Pharmacol. Exp. Ther.* 225 (1983) 529–533.
- [154] K.L. Kirk, B. Jayachandran, B. Herbert, S.F. Lu, W.L. Padgett, J.W. Daly, G. Haufe, K.W. Laue, Chemical and biological approaches to non-racemic fluorinated catecholamines and amino acids, *ACS Symposium Series* 746 (2000) 194–209.
- [155] S.F. Lu, G. Haufe, K.W. Laue, W.L. Padgett, O. Oshunlet, J.W. Daly, K.L. Kirk, Syntheses of (R)- and (S)-2- and 6-fluoronorepinephrine and (R)- and (S)-2- and 6-fluoro-epinephrine: Effect of stereochemistry on fluorine-induced adrenergic selectivities, *J. Med. Chem.* 43 (2000) 1611–1619.
- [156] Y.S. Ding, J.S. Fowler, S.J. Gatley, S.L. Dewey, A.P. Wolf, Synthesis of high specific activity (+)- and (–)-6-[¹⁸F]fluoronorepinephrine via the nucleophilic aromatic substitution reaction, *J. Med. Chem.* 34 (1991) 767–771.
- [157] E. Lui, R. Chirakal, G. Firmau, Enzymatic synthesis of (–)-6-[¹⁸F]fluoronorepinephrine from 6-[¹⁸F]fluorodopamine by dopamine β -hydroxylase, *J. Label. Compd. Radiopharm.* 41 (1998) 503–521.
- [158] Y.S. Ding, J.S. Fowler, S.L. Dewey, J. Logan, D.J. Schlyer, S.J. Gatley, N.D. Volkow, P.T. King, A.P. Wolf, Comparison of high specific activity (–) and (+)-6-[¹⁸F]fluoronorepinephrine and 6-[¹⁸F]fluorodopamine in baboons: Heart uptake, metabolism and the effect of desipramine, *J. Nucl. Med.* 34 (1993) 619–629.
- [159] J.S. Fowler, Y.S. Ding, N.D. Volkow, T. Martin, R.R. MacGregor, S. Dewey, P. King, N. Pappas, D. Alexoff, C. Shea, S.J. Gatley, D.J. Schlyer, A.P. Wolf, PET studies of cocaine inhibition of myocardial norepinephrine uptake, *Synapse* 16 (1994) 312–317.
- [160] Y.S. Ding, J.S. Fowler, S.J. Gatley, J. Logan, N.D. Volkow, C. Shea, Mechanistic positron emission tomography studies of 6-[¹⁸F]fluorodopamine in living baboon heart: Selective imaging and control of radiotracer metabolism using the deuterium isotope effect, *J. Neurochem.* 65 (1995) 682–690.
- [161] R.W. Fuller, H.D. Snoddy, K.W. Perry, J.R. Bernstein, P.J. Murphy, Formation of α -methylnorepinephrine as a metabolite of metaraminol in guinea pigs, *Biochem. Pharmacol.* 30 (1981) 2831–2836.
- [162] N.E. Andén, On the mechanism of noradrenaline depletion by α -methyl metatyrosine and metaraminol, *Acta Pharmacol. Toxicol.* 21 (1964) 260–271.
- [163] P.A. Shore, D. Busfield, H.S. Alpers, Binding and release of metaraminol: Mechanism of norepinephrine depletion by α -methyl-m-tyrosine and related reagents, *J. Pharmacol. Exp. Ther.* 146 (1964) 194–199.
- [164] J.R. Crout, H.S. Alpers, E.L. Tatum, P.A. Shore, Release of metaraminol (aramine) from the heart by sympathetic nerve stimulation, *Science* 145 (1964) 828–829.

- [165] A. Carlsson, B. Waldeck, Release of ³H-metaraminol by different mechanisms, *Acta Physiol. Scand.* 67 (1966) 471–480.
- [166] A. Carlsson, B. Waldeck, Different mechanisms of drug-induced release of noradrenaline and its congeners α -methyl-noradrenaline and metaraminol, *Eur. J. Pharmacol.* 4 (1968) 165–168.
- [167] R.G. Johnson, S.E. Carty, S. Hayflick, A. Scarpa, Mechanisms of accumulation of tyramine, metaraminol, and isoproterenol in isolated chromaffin granules and ghosts, *Biochem. Pharmacol.* 31 (1982) 815–823.
- [168] S.G. Mislankar, D.L. Gildersleeve, D.M. Wieland, C.C. Massin, G.K. Mulholland, S.A. Toorongan, 6-[¹⁸F]fluorometaraminol: A radiotracer for in vivo mapping of adrenergic nerves of the heart, *J. Med. Chem.* 31 (1988) 362–366.
- [169] D.M. Wieland, K.C. Rosenspire, G.D. Hutchins, M. Van Dort, J.M. Rothley, S.G. Mislankar, H.T. Lee, C.C. Massin, D.L. Gildersleeve, P.S. Sherman, M. Schwaiger, Neuronal mapping of the heart with 6-[¹⁸F]fluorometaraminol, *J. Med. Chem.* 33 (1990) 956–964.
- [170] O. Eskola, T. Gronroos, J. Bergman, M. Haaparanta, P. Marjamäki, P. Lehtiköinen, S. Forsback, O. Langer, F. Hinnen, F. Dollé, C. Halldin, O. Solin, A novel electrophilic synthesis and evaluation of medium specific radioactivity (1*R*,2*S*)-4-[¹⁸F]fluorometaraminol, a tracer for the assessment of cardiac sympathetic nerve integrity with PET, *Nucl. Med. Biol.* 31 (2004) 103–110.
- [171] J. Ermert, K. Hamacher, H.H. Coenen, Convenient synthesis route to n.c.a ¹⁸F-labelled sympathomimetics based on norepinephrine, *J. Label. Compd. Radiopharm.* 40 (1997) 53–56.
- [172] O. Langer, H. Valette, F. Dollé, C. Halldin, C. Loc'h, C. Fuseau, C. Coulon, M. Ottaviani, M. Bottlaender, B. Mazière, C. Crouzel, High specific radioactivity (1*R*,2*S*)-4-[¹⁸F]fluorometaraminol: A PET radiotracer for mapping sympathetic nerves of the heart, *Nucl. Med. Biol.* 27 (2000) 233–238.
- [173] O. Langer, F. Dollé, H. Valette, C. Halldin, F. Vaufrey, C. Fuseau, C. Coulon, M. Ottaviani, K. Någren, M. Bottlaender, B. Mazière, C. Crouzel, Synthesis of high-specific-radioactivity 4- and 6-[¹⁸F]fluorometaraminol-PET tracers for the adrenergic nervous system of the heart, *Bioorg. Med. Chem.* 9 (2001) 677–694.
- [174] K.C. Rosenspire, D.L. Gildersleeve, C.C. Massin, S.G. Mislankar, D.M. Wieland, Metabolic fate of the heart agent [¹⁸F]6-fluorometaraminol, *Int. J. Rad. Appl. Instrum. B* 16 (1989) 735–739.
- [175] M. Schwaiger, H. Guibourg, K. Rosenspire, T. McClanahan, K. Gallagher, G. Hutchins, D.M. Wieland, Effect of regional myocardial ischemia on sympathetic nervous system as assessed by fluorine-18-metaraminol, *J. Nucl. Med.* 31 (1990) 1352–1357.
- [176] M. Pissarek, J. Ermert, G. Oesterreich, D. Bier, H.H. Coenen, Relative uptake, metabolism, and β -receptor binding of (1*R*,2*S*)-4-¹⁸F-fluorometaraminol and [¹²³I]-MIBG in normotensive and spontaneously hypertensive rats, *J. Nucl. Med.* 43 (2002) 366–373.
- [177] M. Haaparanta, T. Gronroos, O. Eskola, J. Bergman, O. Solin, Planar chromatographic analysis and quantification of short-lived radioactive metabolites from microdialysis fractions, *J. Chromatogr. A* 1108 (2006) 136–139.
- [178] P.K. Garg, S. Garg, M.R. Zalutsky, Synthesis and preliminary evaluation of para- and meta-[¹⁸F]fluorobenzylguanidine, *Nucl. Med. Biol.* 21 (1994) 87–103.
- [179] C.R. Berry, P.K. Garg, M.R. Zalutsky, R.E. Coleman, T.R. DeGrado, Uptake and retention kinetics of para-fluorine-18-fluorobenzylguanidine in isolated rat heart, *J. Nucl. Med.* 37 (1996) 2011–2016.
- [180] C.R. Berry, T.R. DeGrado, F. Nutter, P.K. Garg, E.B. Breitschwerdt, K. Spaulding, K.D. Concannon, M.R. Zalutsky, R.E. Coleman, Imaging of pheochromocytoma in 2 dogs using p-[¹⁸F]fluorobenzylguanidine, *Vet. Radiol. Ultrasound* 43 (2002) 183–186.

- [181] C.R. Berry, P.K. Garg, T.R. DeGrado, P. Hellyer, W. Weber, S. Garg, B. Hansen, M.R. Zalutsky, R.E. Coleman, Para-[^{18}F]fluorobenzylguanidine kinetics in a canine coronary artery occlusion model, *J. Nucl. Cardiol.* 3 (1996) 119–129.
- [182] G. Vaidyanathan, D.J. Affleck, M.R. Zalutsky, (4-[^{18}F]fluoro-3-iodobenzyl)guanidine, a potential MIBG analogue for positron emission tomography, *J. Med. Chem.* 37 (1994) 3655–3662.
- [183] G. Vaidyanathan, D.J. Affleck, M.R. Zalutsky, Validation of 4-[^{18}F]fluoro-3-iodobenzylguanidine as a positron-emitting analog of MIBG, *J. Nucl. Med.* 36 (1995) 644–650.
- [184] H. Tuunanen, J. Kuusisto, J. Toikka, P. Jaaskelainen, P. Marjamäki, K. Peuhkurinen, T. Viljanen, P. Sipola, K.Q. Stolen, J. Hannukainen, P. Nuutila, M. Laakso, J. Knuuti, Myocardial perfusion, oxidative metabolism, and free fatty acid uptake in patients with hypertrophic cardiomyopathy attributable to the Asp175Asn mutation in the α -tropomyosin gene: A positron emission tomography study, *J. Nucl. Cardiol.* 14 (2007) 354–365.
- [185] L. Guiducci, T. Gronroos, M.J. Jarvisalo, J. Kiss, A. Viljanen, A.G. Naum, T. Viljanen, T. Savunen, J. Knuuti, E. Ferrannini, P.A. Salvadori, P. Nuutila, P. Iozzo, Biodistribution of the fatty acid analogue ^{18}F -FTHA: Plasma and tissue partitioning between lipid pools during fasting and hyperinsulinemia, *J. Nucl. Med.* 48 (2007) 455–462.
- [186] X. Ci, F. Frisch, F. Lavoie, P. Germain, R. Lecomte, J.E. van Lier, F. Benard, A.C. Carpentier, The effect of insulin on the intracellular distribution of 14(R,S)-[^{18}F] Fluoro-6-thia-heptadecanoic acid in rats, *Mol. Imaging Biol.* 8 (2006) 237–244.
- [187] T.R. DeGrado, M.T. Kitapci, S. Wang, J. Ying, G.D. Lopaschuk, Validation of ^{18}F -fluoro-4-thia-palmitate as a PET probe for myocardial fatty acid oxidation: Effects of hypoxia and composition of exogenous fatty acids, *J. Nucl. Med.* 47 (2006) 173–181.
- [188] T.M. Shoup, D.R. Elmaleh, A.A. Bonab, A.J. Fischman, Evaluation of trans-9- ^{18}F -fluoro-3,4-methyleneheptadecanoic acid as a PET tracer for myocardial fatty acid imaging, *J. Nucl. Med.* 46 (2005) 297–304.
- [189] A. Tawakol, R.Q. Migrino, U. Hoffmann, S. Abbata, S. Houser, H. Gewirtz, J.E. Muller, T.J. Brady, A.J. Fischman, Noninvasive in vivo measurement of vascular inflammation with F-18 fluorodeoxyglucose positron emission tomography, *J. Nucl. Cardiol.* 12 (2005) 294–301.
- [190] M. Ogawa, Y. Magata, T. Kato, K. Hatano, S. Ishino, T. Mukai, M. Shiomi, K. Ito, H. Saji, Application of ^{18}F -FDG PET for monitoring the therapeutic effect of anti-inflammatory drugs on stabilization of vulnerable atherosclerotic plaques, *J. Nucl. Med.* 47 (2006) 1845–1850.
- [191] J.H.F. Rudd, K.S. Myers, S. Bansilal, J. Machac, A. Rafique, M. Farkouh, V. Fuster, Z.A. Fayad, ^{18}F Fluorodeoxyglucose positron emission tomography imaging of atherosclerotic plaque inflammation is highly reproducible: Implications for atherosclerosis therapy trials, *J. Am. Coll. Cardiol.* 50 (2007) 892–896.
- [192] Y.W. Wu, H.L. Kao, M.F. Chen, B.C. Lee, W.Y. Tseng, J.S. Jeng, K.Y. Tzen, R.F. Yen, P.J. Huang, W.S. Yang, Characterization of plaques using ^{18}F -FDG PET/CT in patients with carotid atherosclerosis and correlation with matrix metalloproteinase-1, *J. Nucl. Med.* 48 (2007) 227–233.
- [193] K. Okane, M. Ibaraki, H. Toyoshima, S. Sugawara, K. Takahashi, S. Miura, E. Shimosegawa, J. Satomi, K. Kitamura, T. Satoh, ^{18}F -FDG accumulation in atherosclerosis: Use of CT and MR co-registration of thoracic and carotid arteries, *Eur. J. Nucl. Med. Mol. Imaging* 33 (2006) 589–594.
- [194] N. Tahara, H. Kai, M. Ishibashi, H. Nakaura, H. Kaida, K. Baba, N. Hayabuchi, T. Imaizumi, Simvastatin attenuates plaque inflammation: Evaluation by fluorodeoxyglucose positron emission tomography, *J. Am. Coll. Cardiol.* 48 (2006) 1825–1831.
- [195] A. Tawakol, R.Q. Migrino, G.G. Bashian, S. Bedri, D. Vermeylen, R.C. Cury, D. Yates, G.M. LaMuraglia, K. Furie, S. Houser, H. Gewirtz, J.E. Muller, T.J. Brady, A.J. Fischman, In vivo ^{18}F -fluorodeoxyglucose positron emission tomography

- imaging provides a noninvasive measure of carotid plaque inflammation in patients, *J. Am. Coll. Cardiol* 48 (2006) 1818–1824.
- [196] G.G. Bural, D.A. Torigian, W. Chamroonrat, K. Alkhalwaleh, M. Houseni, G. El-Haddad, A. Alavi, Quantitative assessment of the atherosclerotic burden of the aorta by combined FDG-PET and CT image analysis: A new concept, *Nucl. Med. Biol* 33 (2006) 1037–1043.
- [197] H.J. Breyholz, S. Wagner, B. Levkau, O. Schober, M. Schäfers, K. Kopka, A ^{18}F -radiolabeled analogue of CGS 27023A as a potential agent for assessment of matrix-metalloproteinase activity *in vivo*, *Q. J. Nucl. Med. Mol. Imaging* 51 (2007) 24–32.
- [198] S. Wagner, H.J. Breyholz, M.P. Law, A. Faust, C. Hölthke, S. Schröer, G. Haufe, B. Levkau, O. Schober, M. Schäfers, K. Kopka, Novel fluorinated derivatives of the broad-spectrum MMP inhibitors *N*-hydroxy-2(*R*)-[[[(4-methoxyphenyl)sulfonyl](benzyl)- and (3-picolyl)-amino]-3-methyl-butanamide as potential tools for the molecular imaging of activated MMPs with PET, *J. Med. Chem.* 50 (2007) 5752–5764.
- [199] P. Johnström, J.H. Rudd, H.K. Richards, T.D. Fryer, J.C. Clark, P.L. Weissberg, J.D. Pickard, A.P. Davenport, Imaging endothelin ET_B receptors using [^{18}F]-BQ3020: *In vitro* characterization and positron emission tomography (microPET), *Exp. Biol. Med.* (Maywood) 231 (2006) 736–740.
- [200] I. Madar, H.T. Ravert, Y. Du, J. Hilton, L. Volokh, R.F. Dannals, J.J. Frost, J.M. Hare, Characterization of uptake of the new PET imaging compound ^{18}F -fluorobenzyl triphenyl phosphonium in dog myocardium, *J. Nucl. Med.* 47 (2006) 1359–1366.
- [201] I. Madar, H. Ravert, A. Dipaula, Y. Du, R.F. Dannals, L. Becker, Assessment of severity of coronary artery stenosis in a canine model using the PET agent ^{18}F -fluorobenzyl triphenyl phosphonium: Comparison with $^{99\text{m}}\text{Tc}$ -tetrofosmin, *J. Nucl. Med.* 48 (2007) 1021–1030.
- [202] I. Madar, H. Ravert, B. Nelkin, M. Abro, M. Pomper, R. Dannals, J.J. Frost, Characterization of membrane potential-dependent uptake of the novel PET tracer ^{18}F -fluorobenzyl triphenylphosphonium cation, *Eur. J. Nucl. Med. Mol. Imaging*, 2007 Sep 5, [Epub ahead of print].
- [203] D.S. Goldstein, B.A. Eldadah, C. Holmes, S. Pechnik, J. Moak, A. Saleem, Y. Sharabi, Neurocirculatory abnormalities in Parkinson disease with orthostatic hypotension: Independence from levodopa treatment, *Hypertension* 46 (2005) 1333–1339.
- [204] D.S. Goldstein, Y. Sharabi, B.I. Karp, O. Benthó, A. Saleem, K. Pacak, G. Eisenhofer, Cardiac sympathetic denervation preceding motor signs in Parkinson disease, *Clin. Auton. Res.* 17 (2007) 118–121.
- [205] D.S. Goldstein, Cardiac denervation in patients with Parkinson disease, *Cleve. Clin. J. Med.* 74(Suppl. 1) (2007) S91–S94.

Note from the Editors

On the use of ^{18}F -labeled molecules, see also in this volume chapters by F. Dollé *et al.* on PET molecular imaging, K. Någren and J.O. Rinn on application to Alzheimer's disease, K. Herrmann and B. J. Krause on application to oncology.

This page intentionally left blank

CHAPTER 4

[¹⁸F]-Labeled PET and PET/CT Compounds in Oncology

Ken Herrmann and Bernd Joachim Krause*

*Nuklearmedizinische Klinik und Poliklinik, Klinikum rechts der Isar,
Technische Universität München, Ismaninger Str. 22, D-81675 München, Germany*

Contents

1. Introduction	142
2. [¹⁸ F]-FDG-PET and -PET/CT in oncology	144
2.1. Main indications of [¹⁸ F]-FDG-PET and -PET/CT	144
2.1.1. Colorectal cancer	144
2.1.2. Lung cancer	153
2.1.3. Lymphoma	155
2.1.4. Breast cancer	157
2.1.5. Esophageal cancer	159
2.2. Therapy monitoring with [¹⁸ F]-FDG-PET and [¹⁸ F]-FDG-PET/CT	162
2.2.1. Gastrointestinal tract (GI)	163
2.2.2. Lung cancer	166
2.2.3. Lymphoma	167
2.2.4. Gastrointestinal stromal tumors (GIST)	167
2.2.5. Head and neck	168
2.2.6. Breast cancer	168
2.2.7. Ovarian cancer	168
2.3. Methodical considerations and limitations	169
3. Innovative [¹⁸ F] fluorine-based radiotracers	170
3.1. Molecular imaging of proliferation with 3'-deoxy-3'-[¹⁸ F]-fluorothymidine	170
3.2. PET/CT studies of tumor hypoxia	173
3.3. [¹⁸ F]-Galacto-RGD-PET: Imaging of $\alpha_v\beta_3$ integrin expression	175
3.4. [¹⁸ F]-Fluorocholine-PET: Imaging of prostate cancer	176
3.4.1. Biochemical rationale	176
3.4.2. Compounds, biodistribution, and imaging	177
3.4.3. Clinical studies	178
3.5. [¹⁸ F]-Fluoride-PET: Imaging of bone metastases	178
3.6. [¹⁸ F]FET-PET: Imaging with amino acids	179
3.7. [¹⁸ F]Fluorodopa-PET: Imaging with amino precursors	181
Acknowledgments	182
References	182
Note from the Editors	196

*Corresponding author.;

E-mail: bernd-joachim.krause@tum.de

Abstract

[^{18}F]-labeled compounds are widely used in PET and PET/CT imaging in oncology. Among these [^{18}F]-FDG is the most commonly used tracer in clinical routine. This chapter will discuss the use and the main indications of (1) [^{18}F]-FDG-PET and PET/CT in oncology with special emphasis on therapy monitoring (among other tumors the focus is on colorectal cancer, lung cancer, lymphoma, breast cancer, esophageal cancer and head and neck cancer) and (2) further [^{18}F]-based radiotracers such as [^{18}F]-FLT, [^{18}F]-RGD, [^{18}F]-FAZA, [^{18}F]-fluoride, [^{18}F]-FMISO, [^{18}F]-FCH, [^{18}F]-FET and [^{18}F]-DOPA.

(1) A review of the current literature will be given with respect to primary diagnosis, diagnosis of recurrent disease (local, lymph node, and distant metastases) and prognostic factors derived from PET imaging as well as therapy monitoring studies using [^{18}F]-FDG. (2) Additionally innovative and more specific tracers for molecular imaging of tumor biology will be highlighted and discussed in the framework of their clinical value: [^{18}F]-FLT for imaging of tumor proliferation, [^{18}F]-RGD for imaging of tumor angiogenesis, [^{18}F]-FCH for imaging cell membrane metabolism, [^{18}F]-fluoride for bone metabolism imaging, [^{18}F]-FMISO/[^{18}F]-FAZA for imaging of hypoxia, [^{18}F]-FET as radiolabeled amino acid and [^{18}F]-DOPA as radiolabeled amino precursor.

1. INTRODUCTION

In clinical routine, imaging modalities play a steadily increasing role, especially in staging and restaging of oncological patients. In contrast to conventional imaging modalities, comprising endoluminal ultrasound, computed tomography (CT) and magnetic resonance imaging (MRI), which are limited to morphological information, positron emission tomography (PET) is based on imaging biochemical processes *in vivo* representing molecular processes underlying metabolic activity. PET is a very sensitive modality to image biologically active substances and even concentrations as low as picomolar can be visualized. The basis for PET imaging is the positron emission of neutron-deficient isotopes in which a proton in the nucleus decays to a neutron, a positron and a neutrino. Depending on their energy, the emitted positrons travel inside the body in a range of few millimeters. While traveling in tissue, a positron loses energy in collisions with atomic electrons. It eventually annihilates with an atomic electron, resulting in the emission of two 511 keV photons leaving the atom in opposite directions. These positron-emitting isotopes (e.g. elements such as carbon [^{11}C], nitrogen [^{13}N], oxygen [^{15}O] and fluorine [^{18}F]) may be used for synthesis of tracers, which are similar to naturally occurring substances in the body and can be used for the imaging of biochemical and physiological processes *in vivo* (for fluorine-labeled compounds, see Table 1).

Among the [^{18}F]-labeled compounds 2'-[^{18}F]-fluoro-2'-deoxy-D-glucose ([^{18}F]-FDG) is the most widely used tracer in oncology. [^{18}F]-FDG is relatively easy to synthesize with a high radiochemical yield [1]. It follows a metabolic pathway similar to glucose *in vivo*, except that it is not further metabolized but is trapped within cells. Increased consumption of glucose is a characteristic of most tumor

Table 1. [¹⁸F]-Fluorine based radiotracers

Tracer compound	Physical process or function	Typical application
Fluoro-deoxy-glucose ([¹⁸ F]-FDG)	Glucose metabolism	Oncology, neurology, and cardiology
Fluoride ion ([¹⁸ F]fluoride)	Bone metabolism	Oncology
Fluoro-misonidazole ([¹⁸ F]-MISO)	Hypoxia	Oncology—response to radiotherapy
Fluoro-azomycin arabinoside ([¹⁸ F]-FAZA)	Hypoxia	Oncology—response to radiotherapy
Galacto-RGD ([¹⁸ F]-RGD)	Angiogenesis	Oncology
Fluoro-choline ([¹⁸ F]-FCH)	Cell membrane metabolism	Oncology
Fluoro-thymidine ([¹⁸ F]-FLT)	Proliferation	Oncology
Fluoro-ethyl-tyrosine ([¹⁸ F]-FET)	Radiolabeled amino acid	Oncology
Fluoro-dihydroxyphenyl-alanine ([¹⁸ F]-DOPA)	Amino precursor	Oncology and neurology

cells and is partially related to over-expression of the GLUT-1 glucose transporters and increased hexokinase activity. This principle enables to visualize regional tumor glucose metabolism with a high sensitivity and specificity.

Despite the high sensitivity of [¹⁸F]-FDG-PET false-positive findings—due to physiological processes such as brown fat, colonic and gynecologic activity, infectious and inflammatory processes and rebound thymic hyperplasia—pose a major challenge.

[¹⁸F]-FDG-PET allows the quantification of biochemical and physiological processes in tumors. The most accurate method to analyze the acquired data is to quantitatively assess the [¹⁸F]-FDG metabolism, for example, by using kinetic modeling together with nonlinear regression techniques. One simplified quantitative technique is the linearized Patlak analysis, which still requires dynamic scanning but fewer frames and is therefore less time-consuming. Other methodologies include visual and semiquantitative evaluations of the accumulated [¹⁸F]-FDG. The principle of semiquantitative analyses is the estimation of the radiotracer concentration from attenuation-corrected images of a region of interest. The most commonly used technique is the standardized uptake value (SUV):

a semiquantitative index of tumor uptake normalized to the injected dose and a measure of the total volume of distribution, such as the patient's body weight. This method turned out to be highly reproducible [2]. Nevertheless, due to only low GLUT-1 expression and hexokinase activities some tumors—such as prostate cancer and mucinous carcinomas—show in part only low [^{18}F]-FDG uptake and may not be detected by [^{18}F]-FDG-PET.

In 1998, the first PET/CT scanner, combining functional information with morphological information, was introduced by Townsend and co-workers [3]. Combined PET/CT devices offer an efficient tool for whole-body staging and restaging functional assessment within one imaging modality. PET/CT scanners allow a merging of complementary information from CT and PET, leading to a more accurate anatomic localization. Furthermore, a more precise assessment of tumor volume is possible in comparison to PET.

This chapter will focus on the (1) main indications of [^{18}F]-FDG-PET and -PET/CT and (2) the innovative [^{18}F]-labeled compounds in oncology.

2. [^{18}F]-FDG-PET AND -PET/CT IN ONCOLOGY

2.1. Main indications of [^{18}F]-FDG-PET and -PET/CT

In recent years, numerous studies have evaluated the use of [^{18}F]-FDG-PET for staging and restaging of tumor patients. Based on this data, the Centers for Medicare and Medicaid Services (CMS) have approved Medicare reimbursement for [^{18}F]-FDG-PET imaging in 10 oncological conditions so far (Table 2).

2.1.1. Colorectal cancer

Colorectal cancer is one of the most common neoplasms in Western countries. In frequency, colorectal cancer ranked second for men and women in Germany in 2002 [4]. After a slight increase in frequency over the last years, the incidence is expected to remain stable over the next years. Epidemiological and experimental studies suggest that an unbalanced fatty nutrition with low dietary fibers may promote tumor growth. Two inherited syndromes, familial adenomatous polyposis (FAP) and hereditary nonpolyposis colorectal cancer (HNPCC), going along with colorectal cancer have been identified so far. In Germany, the mortality rate for colorectal cancer in 2000 was 29.8/100,000 for men and 19.3/100,000 for women [4].

In most cases colorectal cancer is located in the rectum (40%), followed by the sigmoid and caecum. Of the diagnosed tumors, around 70% are resectable. However, around 40% of the patients undergoing surgery will relapse in the first 2 years after initial resection. Up to 30% develop hepatic metastases and around 15% lung metastases. Reported 5-year survival rates range between 40% and 60%. Early stages (Dukes A) are well curable, resulting in 5-year survival rates of around

Table 2. CMS (the Centers for Medicare and Medicaid Services) coverage for FDG-PET in oncology

Clinical condition	Coverage
Solitary pulmonary nodule	Characterization (January 1998)
Lung cancer (NSCLC)	Initial staging (January 1998) Diagnosis, staging, and restaging (July 2001)
Esophageal cancer	Diagnosis, staging, and restaging (July 2001)
Colonrectal cancer	Tumor localization if CEA suggests recurrence (July 1999) Diagnosis, staging, and restaging (July 2001)
Melanoma	Diagnosis, staging, and restaging (July 2001)
Lymphoma	Diagnosis, staging, and restaging (July 2001)
Head and neck cancer	Diagnosis, staging, and restaging (July 2001)
Breast cancer	Adjunct for diagnosis, staging, restaging, and monitoring response (October 2002)
Thyroid cancer (follicular cell)	Evaluating recurrent or residual follicular cell tumors (treated previously by thyroidectomy and radioiodine ablation) when serum thyroglobulin >10 ng/ml and ¹³¹ I whole-body scan is negative (October 2003)
Cervical cancer	Detecting pretreatment metastases in newly diagnosed cervical cancer after negative conventional imaging (January 2005)

90%. However, only 39% of colorectal cancers are diagnosed at this early stage. For advanced stages (Dukes D), the reported 5-year survival rate is only around 10% [5]. The goal of treatment is cure in early stages (Dukes A and B), prolongation of survival in stage C, and palliation in stage D. Resection of isolated metastatic disease to the liver has been associated with improved survival [6,7].

Initial detection of primary colorectal cancer is a domain of endoscopy. Additional imaging for therapy planning is discussed controversially, especially due to the lack of a single comprehensive imaging method [8]. Conventional imaging modalities, comprising endoluminal ultrasound, CT and MRI are limited to give

morphological information. Differentiation between malign and benign lesions is not always reliable. Assessment of lymph node size and morphology remains the only criteria. Regarding MRI and CT, lymph nodes >1 cm are considered to be suspicious, but of course also smaller lymph nodes can contain malignancies. Therefore, we have a high demand for imaging methods providing functional information.

Imaging modalities play an even more important role in the setting of suspected recurrence of colorectal cancer. Around 30% of the patients with recurrence within 2 years of initial diagnosis appear to have limited recurrent disease, but only 25% of them are actually curable by surgery [9]. At surgery, up to 75% of the patients reveal to have non-resectable disease due to distant metastases or widespread disease [10,11]. In order to decrease the number of futile surgeries, it is essential to improve the accuracy of preoperative detection of recurrent disease.

Since the first reported [^{18}F]-FDG-PET study in patients with colorectal cancer by Strauss *et al.* in 1989 [12], a considerable number of [^{18}F]-FDG-PET studies of different groups regarding staging [13], detection of recurrence [9,14–22] and changes on therapy management [23–25] have been published (for reviews see [9,16]).

2.1.1.1. [^{18}F]-FDG-PET

Staging. In 1994, Falk *et al.* [26] reported a comparison of [^{18}F]-FDG-PET and CT for preoperative staging of colorectal carcinoma in 16 patients. [^{18}F]-FDG-PET proved to be more accurate than CT (accuracy 83% for [^{18}F]-FDG-PET vs. 56% for CT). Abdel-Nabi *et al.* [13] preoperatively investigated 48 consecutive patients with biopsy-proven or clinically high-suspected colorectal cancer. [^{18}F]-FDG-PET depicted all primaries resulting in a sensitivity of 100%; the related specificity was 43%. [^{18}F]-FDG-PET also proved to be very sensitive for detection of liver metastases (sensitivity: 83%), whereas it was positive in only 29% of the lymph node metastases. Overall, Abdel-Nabi *et al.* concluded that [^{18}F]-FDG-PET was superior to CT in staging of primary colorectal carcinoma. In a study of 24 patients, Mukai *et al.* [19] confirmed earlier published results by reporting a sensitivity of 96% for staging of primary colorectal cancer. Only 22% of the histologically confirmed lymph node metastases were depicted by [^{18}F]-FDG-PET. In a more recent publication, Kantorova *et al.* [17] compared [^{18}F]-FDG-PET with CT in the preoperative staging of colorectal cancer. In 38 consecutive patients with histologically proven colorectal cancer [^{18}F]-FDG-PET was more sensitive than CT and ultrasound (95%, 49% and 14%, respectively) in staging primary disease. Despite a low sensitivity of 29% [^{18}F]-FDG-PET had an accuracy of 75% in depicting lymph node metastases. Compared with ultrasound (accuracy: 81%), [^{18}F]-FDG-PET and CT appeared to be more accurate (both 91%). Additional information provided by [^{18}F]-FDG-PET led to a change of treatment modality for 8% of patients and influenced the range of surgery for 13%.

Regarding the prognostic relevance of the initial SUV_{max} , Calvo *et al.* [15] showed that initial SUV_{max} in the staging $[^{18}\text{F}]$ -FDG-PET was predictive for long-term patient outcome in a cohort of 25 consecutive patients. Definition of a cut-off of $\text{SUV}_{\text{max}} \leq 6$ correlated with a significantly better 3-year survival (92% vs. 60%).

The T-staging is the domain of morphological imaging methods (CT and MRI). Sensitivity for N-staging remains low for both, morphological and functional imaging modalities. $[^{18}\text{F}]$ -FDG-PET can provide important additional information regarding the M-staging.

Recurrent Disease. In 1989, a first study of $[^{18}\text{F}]$ -FDG-PET in patients with recurrent colorectal cancer was published comparing $[^{18}\text{F}]$ -FDG-PET with CT. The aim of the study was to differentiate between scar tissue and recurrent disease in the follow-up of patients with colorectal cancer. In a group of 29 patients, Strauss *et al.* detected recurrent disease in 21 patients all showing an increased $[^{18}\text{F}]$ -FDG uptake in the $[^{18}\text{F}]$ -FDG-PET cross sections [27]. In a meta-analysis by Huebner *et al.* 11 studies met the inclusion criteria defined and the reported data were analyzed [9]. The overall sensitivities and specificities of $[^{18}\text{F}]$ -FDG-PET for the local/pelvic region on patient basis, for hepatic metastases on patient and lesion-by-lesion basis, and for the whole body on patient basis were determined separately. Imaging results for detection of local/pelvic recurrence were available for a total of 366 patients. Analysis of the pooled data resulted in a sensitivity of 94% (range: 90–97%) and a specificity of 98% (range: 89–100%). Analysis of the imaging results of $[^{18}\text{F}]$ -FDG-PET in the liver in a total of 393 patients included in five studies showed a sensitivity ranging between 94% and 100% and a specificity reaching from 67% to 100%. Hepatic involvement reported in lesion data was published in two studies with a total of 182 patients. Sensitivity (90% vs. 91%) and specificity (96% vs. 100%) were similar in both publications. Five studies reported sensitivity and specificity data for $[^{18}\text{F}]$ -FDG-PET depicting colorectal recurrences in the whole body. In a total of 281 patients, the sensitivity ranged from 95% to 100% whereas the specificity showed a wider spread (69–83%). This led to an overall sensitivity of 97% and an overall specificity of 76%.

Whiteford *et al.* [22] compared the clinical efficacy of $[^{18}\text{F}]$ -FDG-PET with CT plus other conventional imaging methods in patients with recurrent or metastatic colorectal cancer. In the detection of clinically relevant tumors or metastases $[^{18}\text{F}]$ -FDG-PET showed a significantly higher sensitivity (87% vs. 66%) and specificity (68% vs. 59%) than CT plus other conventional imaging modalities. Reported sensitivities for $[^{18}\text{F}]$ -FDG-PET were higher than for conventional imaging including CT regarding detection of hepatic metastases (89% vs. 71%), extrahepatic metastases (94% vs. 67%) and local recurrence (90% vs. 71%). The determined specificities showed no significant difference for both imaging methods.

In another study by Staib *et al.* the influence of $[^{18}\text{F}]$ -FDG-PET on surgical decisions was studied in 100 patients. $[^{18}\text{F}]$ -FDG-PET showed an overall sensitivity of 98% and specificity of 90% for detecting malignant lesions compared with CT, 91% and 72%, respectively, and to carcinoembryonic antigen (CEA) level

measurements, 76% and 90%, respectively [20]. [^{18}F]-FDG-PET was more sensitive in detection of hepatic metastases than ultrasound (98% vs. 87%), whereas ultrasound revealed a higher specificity than [^{18}F]-FDG-PET (96% vs. 90%), resulting in similar accuracies ([^{18}F]-FDG-PET: 95%, ultrasound: 93%). According to this study, additional [^{18}F]-FDG-PET information influenced surgical decisions in 61% of cases [separated into very high relevance (14%) and high relevance (47%)] by disclosing correct diagnosis of hepatic and distant metastases.

Arulampalam *et al.* [14] investigated the impact of [^{18}F]-FDG-PET on the clinical management in a group of 42 patients with suspected recurrence. Because of the additional information provided by [^{18}F]-FDG-PET, 27% of the patients were upstaged and in a total of 16 patients (38%) the clinical management was altered. Follow-up and histological confirmation of diagnosis proved in 14 cases a change of treatment to the benefit of the patient, whereas two patients ultimately did not benefit from the alteration of clinical management. Determination of sensitivity for detection of recurrence showed that [^{18}F]-FDG-PET is more sensitive than CT (93% vs. 73%). Related specificity of [^{18}F]-FDG-PET was 58% compared with the specificity of 75% for CT. In staging local recurrence, [^{18}F]-FDG-PET (sensitivity: 100%, specificity: 86%) proved to be more accurate than CT (sensitivity: 75%, specificity: 100%). Additionally, [^{18}F]-FDG-PET proved to be superior to CT for the detection of liver metastases (sensitivity: 100% vs. 45% and specificity both 100%).

In a study of 79 patients with known or suspected recurrence, Lonneux *et al.* [18] analyzed the impact of [^{18}F]-FDG-PET on selecting candidates for curative resection more accurately than with conventional imaging modalities. [^{18}F]-FDG-PET predicted resectability significantly more accurate (82% vs. 65%, $p = 0.02$) than conventional imaging modalities consisting of CT abdomen, CT pelvis, and chest x-ray and led to a reduction of unnecessary surgeries of 53%. [^{18}F]-FDG-PET was also more accurate (overall sensitivity: 97%, specificity: 72%) than conventional imaging modalities (overall sensitivity: 61%, specificity: 36%) in detecting recurrence at all sites except the liver.

2.1.1.2. [^{18}F]-FDG-PET/CT

The combination of whole-body anatomical (CT) and functional (PET) imaging offers an efficient tool for whole-body staging, restaging and therapy control and functional assessment in one device. PET/CT enables the assessment of the exact tumor volume. Recently, studies evaluating the impact of [^{18}F]-FDG-PET/CT on diagnosing and treating colorectal cancer have been published (Fig. 1) [28–31].

In 45 patients with known colorectal cancer, Cohade *et al.* [28] compared retrospectively the accuracies for staging and restaging of [^{18}F]-FDG-PET/CT versus [^{18}F]-FDG-PET alone. All [^{18}F]-FDG-PET and [^{18}F]-FDG-PET/CT studies were separately evaluated in randomized order. [^{68}Ge] attenuation-corrected images were assessed to reassure that only the added value of CT information was

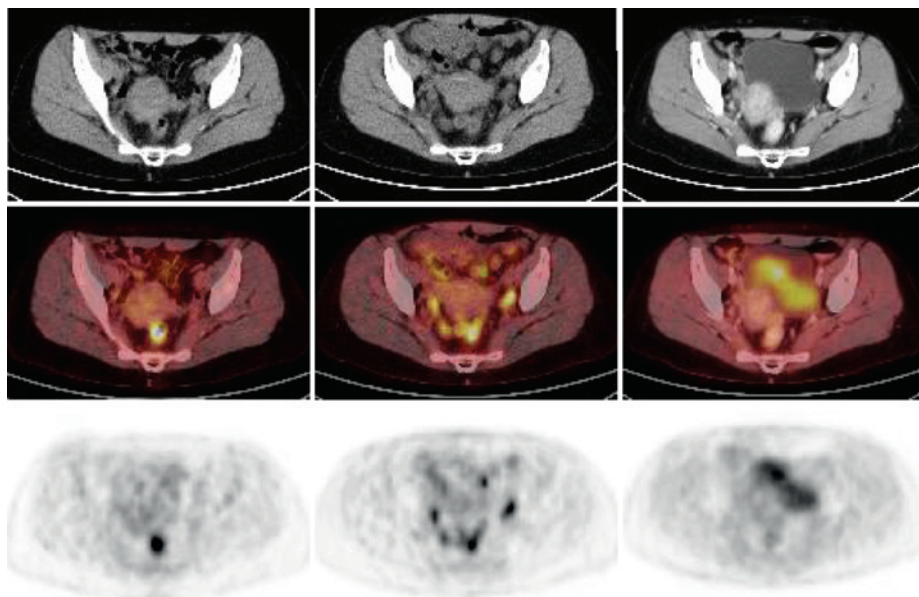


Fig. 1. Example of FDG-PET/CT studies in a patient with rectal cancer and metabolic response. FDG uptake decreases 14 days after initiation and after completion of radiochemotherapy. First row shows the CT-scan, second row displays the fusion of FDG-PET and CT-scans and the third row represents the corresponding FDG-PET scan. (See Colour Plate Section at the end of this book.)

evaluated. Patient scans were evaluated on a lesion-by-lesion and on a patient-by-patient basis. Lesion location was scored on a 3-point scale (0 = uncertain, 1 = probable and 2 = certain) and certainty of lesion characterization on a 5-point scale (0 = definitely benign, 1 = probably benign, 2 = equivocal, 3 = probably malignant and 4 = definitely malignant). [^{18}F]-FDG-PET/CT reduced the number of lesions rated as uncertain location by 55% and the number of lesions characterized as equivocal or probable by 50%. On a patient-by-patient basis, the overall accuracy was raised by 11% ([^{18}F]-FDG-PET/CT: 89%, [^{18}F]-FDG-PET alone: 78%) resulting in a reduction of incorrectly staged patients by 50%. Additional information provided by [^{18}F]-FDG-PET/CT in comparison to [^{18}F]-FDG-PET alone seems to be of greater importance for the evaluation of extrahepatic disease than for liver evaluation. In extrahepatic regions, a better localization of [^{18}F]-FDG uptake appeared to be crucial for staging. In this study, follow-up data for at least 6 months were available only in 56% of the analyzed patients.

Kamel *et al.* [29] evaluated the contribution of dedicated CT interpretation to the accuracy of [^{18}F]-FDG-PET/CT in patients with suspected primary or metastatic colorectal carcinoma. In 100 [^{18}F]-FDG-PET/CT scans in 90 consecutive patients, this group analyzed the impact of the additional CT information to the overall accuracy of [^{18}F]-FDG-PET/CT. The CT component of the

[^{18}F]-FDG-PET/CT scans was retrospectively reviewed by two experienced CT radiologists and findings classified as primary lesion, local recurrence or distant metastases. Comparison of sensitivity, specificity and accuracy of combined [^{18}F]-FDG-PET/CT with dedicated CT interpretation (99%, 100%, and 98%, respectively) to the [^{18}F]-FDG-PET/CT reports (91%, 63%, and 83%, respectively) showed a statistically significant higher accuracy ($p < 0.05$). The increased overall accuracy of 15% was mainly due to an increase of specificity by a significant reduction of false-positive scans related to post-liver resection or radiofrequency ablation, inflammatory pulmonary or hilar uptake, and non-neoplastic increased activity. These results demonstrate the high impact of combined [^{18}F]-FDG-PET/CT devices in clinical routine by combining functional information with anatomic and pathological information.

Kim *et al.* [30] compared the accuracies of [^{18}F]-FDG-PET, in-line [^{18}F]-FDG-PET/CT and software fusion for restaging of recurrent colorectal cancer. A total of 51 patients underwent a [^{18}F]-FDG-PET/CT examination and 34 patients of this cohort received an additional CT scan within 4 weeks of [^{18}F]-FDG-PET/CT. For evaluation of the accuracy of the software fusion-defined landmarks including normal anatomic structures such as the lower poles of both kidneys and the lower pole of the spleen were identified on CT and [^{18}F]-FDG-PET scan and the distances measured. [^{18}F]-FDG-PET, [^{18}F]-FDG-PET/CT and software fusion of [^{18}F]-FDG-PET and CT were interpreted separately by independent observers. Findings were validated by histological evaluation or clinical follow-up of at least 6 months. Staging accuracy on a patient basis was significantly higher for [^{18}F]-FDG-PET/CT (88%) than for [^{18}F]-FDG-PET alone (71%; $p = 0.01$) due to an additional identification of metastases in five regions and correct exclusion of metastases in seven regions. Additionally detected metastases included peritoneal lesions, small pulmonary metastases and a sclerotic bone metastasis. Better anatomic localization of increased FDG uptake led to a reduction of false-positive findings. Analysis of software fusion of independently acquired [^{18}F]-FDG-PET and CT scans revealed a comparable accuracy to in-line [^{18}F]-FDG-PET/CT (95% vs. 97%, respectively), but software fusion was successful in only 76% of the patients. In accordance with the results published by Kamel *et al.* [29], Kim *et al.* [30] concluded that the CT scans should be evaluated for signs of metastatic disease and not only for anatomic localization of abnormalities identified in the [^{18}F]-FDG-PET study, leading to significant higher accuracies than [^{18}F]-FDG-PET alone.

In a cohort of 29 patients with suspected recurrent colorectal carcinoma referred for restaging Strunk *et al.* [31] retrospectively compared [^{18}F]-FDG-PET alone, CT alone, [^{18}F]-FDG-PET and CT virtually fused with simultaneously coregistered [^{18}F]-FDG-PET/CT scans. Detection of lesions was most sensitive with coregistered [^{18}F]-FDG-PET/CT scans. Discrepancies were mainly found in the lung and lymph nodes, where [^{18}F]-FDG-PET alone detected often lymph nodes and soft tissue masses where CT alone was often negative. Coregistered [^{18}F]-FDG-PET/CT scans provided additional information in 7 of

29 patients, leading to a greater accuracy in diagnosis and anatomic localization of metastases in colorectal cancer patients.

2.1.1.3. Disease Management

Additional information provided by $[^{18}\text{F}]$ -FDG-PET is important for the clinical therapy management of patients with recurrent colorectal carcinoma. Visualization of CT negative lesions by $[^{18}\text{F}]$ -FDG-PET allows an earlier treatment change. Detection of distant metastases and better preoperative assessment of tumor spread can avoid unnecessary surgery, leading to a reduction of morbidity and mortality associated with aggressive and futile therapeutic approaches.

Seven of the eleven studies reviewed by Huebner *et al.* [9] evaluated the change of therapy management as a consequence of $[^{18}\text{F}]$ -FDG-PET imaging. In a total of 349 patients, the pooled change of management rate was 29% (range: 20–44%). In the study by Whiteford *et al.* [22], clinical management based on the results of $[^{18}\text{F}]$ -FDG-PET was changed in 30 patients (30%). Histological analysis and clinical follow-up proved that in 26 cases (26%) $[^{18}\text{F}]$ -FDG-PET had a beneficial effect by upstaging disease from resectable to unresectable ($n = 14$), disproving a positive CT finding ($n = 8$) or detecting a previously unrecognized resectable ($n = 4$) tumor. In four cases, false-positive $[^{18}\text{F}]$ -FDG-PET scans had a negative clinical effect leading to non-therapeutic interventions. Arulampalam *et al.* [14] reported a change of clinical management in a beneficial manner due to additional information provided by $[^{18}\text{F}]$ -FDG-PET in 14 of 42 patients (33%). In nine patients with negative CT scan $[^{18}\text{F}]$ -FDG-PET detected local recurrence and in five patients $[^{18}\text{F}]$ -FDG-PET allowed a more accurate staging of liver metastases, avoiding futile surgery in three cases. In two other cases (5%) $[^{18}\text{F}]$ -FDG-PET led to invasive investigations that had no benefit for the patient.

In a study by Lonneux *et al.* [18], $[^{18}\text{F}]$ -FDG-PET correctly modified the disease stage in 33 of 79 patients (41%). In 18 patients, recurrence was detected by $[^{18}\text{F}]$ -FDG-PET. $[^{18}\text{F}]$ -FDG-PET ruled out recurrence in seven patients and upstaged the disease in eight cases, avoiding surgery in seven patients. Kalff *et al.* [23] aimed to confirm the beneficial influence of $[^{18}\text{F}]$ -FDG-PET in treatment planning in a prospective study. In a total of 102 patients, an alteration of clinical management was found in 59% (60 patients) of the cases. Three patients were lost to follow-up. In 52 of the 57 evaluable patients, follow-up revealed a beneficial effect of management changes induced by $[^{18}\text{F}]$ -FDG-PET. In five patients, consisting of one case with a false-positive $[^{18}\text{F}]$ -FDG-PET and four studies underestimating disease spread, changes of therapy management had no therapeutic benefit for the patients. Because of incremental $[^{18}\text{F}]$ -FDG-PET findings, planned surgery was abandoned in 26 of 43 patients (60%). In 5 cases futile radiotherapy could be prevented, whereas surgery was initiated in 8 patients and radiotherapy in 10 cases.

In another study with 120 patients, $[^{18}\text{F}]$ -FDG-PET led to a major management change in 58 (48%) of the referred patients [25]. Clinical management changes

due to additional information provided by [^{18}F]-FDG-PET had a beneficial effect in 54 (45%) cases. Three patients with negative [^{18}F]-FDG-PET scan relapsed within 9 months of follow-up and another one referred for preoperative planning showed no [^{18}F]-FDG uptake in histologically proven lesion. Ruers *et al.* [24] prospectively investigated the value of [^{18}F]-FDG-PET for treatment planning in candidates for resection of colorectal liver metastases. In 10 of 51 patients (20%), additional information provided by [^{18}F]-FDG-PET resulted in a change of clinical management. In six cases, [^{18}F]-FDG-PET detected unresectable metastases (pulmonary $n = 5$, hepatic $n = 1$). In two patients, extrahepatic disease and in another two hepatic disease could be ruled out by [^{18}F]-FDG-PET. Regarding the additional information provided by [^{18}F]-FDG-PET in a retrospective analysis, [^{18}F]-FDG-PET revealed a potential change of management in 15 patients (29%). [^{18}F]-FDG-PET and conventional imaging consisting of spiral CT of lung, abdomen and pelvis showed discordant results for extrahepatic disease in 11 patients (22%) and for hepatic disease in 8 patients ($n = 16\%$). According to follow-up and histological confirmation of discrepant results in [^{18}F]-FDG-PET and conventional imaging, [^{18}F]-FDG-PET resulted in true upstaging ($n = 11$, 22%), true downstaging ($n = 5$, 10%), false upstaging ($n = 1$, 2%) and false downstaging ($n = 2$, 4%). Pooling the data of all reviewed studies with a total of 927 patients shows that additional information provided by [^{18}F]-FDG-PET led to a change of clinical management in around 35% of the cases.

2.1.1.4. Cost-effectiveness

New techniques must be assessed with respect to efficiency and cost-effectiveness in comparison to already existing ones. So far only a few cost-effective analyses of management of recurrent colorectal cancer based on decision analysis models have been published. Cost calculations of two studies were based on US Medicare reimbursement rates [32–34], whereas one other economic analysis was performed from the French national health insurance's perspective [35].

Gambhir *et al.* compared CEA + CT with CEA + CT + [^{18}F]-FDG-PET for detecting and restaging patients with suspected hepatic metastases [32]. In comparison to the CEA + CT strategy, the calculations for the CEA + CT + [^{18}F]-FDG-PET resulted in savings of \$220 per patient and were accompanied by a calculated gain in life expectancy of 2 days. The study by Park *et al.* also focused on patients with a positive CEA and suspected hepatic recurrence who were potentially curable through surgical hepatic resection [33]. Compared with the CEA + CT strategy, the CEA + CT + [^{18}F]-FDG-PET strategy was higher in mean cost by \$429 per patient but was associated with a calculated increase of life expectancy of 9.5 days. The incremental cost-effectiveness ratio (ICER) of \$16,437 per life-year gained, calculated by $\text{ICER} = (\text{COST}_a - \text{COST}_b) / (\text{Life Expectancy}_a - \text{Life Expectancy}_b)$, was significantly lower than the maximum ICER (\$50,000 per life-year gained) accepted by many health care economists as indicating a cost-effective strategy. Recently, Lejeune *et al.* [35] published a

study assessing the cost-effectiveness of $[^{18}\text{F}]$ -FDG-PET in the management of liver metastases of colorectal cancer based on a decision analysis model and survival data provided by the Burgundy Digestive Cancer Registry (France). In contrast to the other two studies, patient selection was based on an abdominal ultrasound with suspicious findings. The CT + $[^{18}\text{F}]$ -FDG-PET strategy presented an expected incremental cost saving of \$3213 per patient mainly caused by a decreasing number of futile surgeries (88% less than CT alone). CT + $[^{18}\text{F}]$ -FDG-PET did not generate an additional survival effectiveness compared with CT alone. In conclusion, the use of $[^{18}\text{F}]$ -FDG-PET for diagnosis and staging of recurrent colorectal cancer might prove to be cost-effective and its introduction into clinical routine economically justifiable.

2.1.2. Lung cancer

In approximately 3 million patients every year lung cancer is newly diagnosed. Because of its high-mortality lung cancer is the most common cause of cancer-related death in the Western world. As a consequence of the good results of $[^{18}\text{F}]$ -FDG-PET in staging and restaging lung cancer, the CMS approved the coverage of $[^{18}\text{F}]$ -FDG-PET scanning for characterization of solitary pulmonary nodules (SPN) (1998), initial staging (1998) and diagnosis, and staging and restaging (2001) of non-small cell lung cancers (NSCLC).

2.1.2.1. $[^{18}\text{F}]$ -FDG-PET

Initial staging: T-staging. Prospective studies have shown that $[^{18}\text{F}]$ -FDG-PET provides a high accuracy in characterization of SPN. So far, chest x-ray and CT are the most frequently performed imaging modalities on patients with suspected lung cancer. Both modalities provide only a limited accuracy in distinguishing between benign and malignant lesions. In a review by Reske and Kotzerke the sensitivity and specificity of $[^{18}\text{F}]$ -FDG-PET in 2512 patients for differentiation of benign and malign pulmonary nodules were 96% and 80%, respectively [36]. This correlates with the accuracies published in a review by Vansteenkiste and Stroobants in which prospective studies with at least 50 patients were reviewed: accuracy ranged from 89% to 96% [37]. Corresponding sensitivities ranged from 89% to 100% and specificities from 52% to 100%, respectively. Causes of false-negative lesions were small size (<1 cm) or low-metabolic activity, for example in carcinoid tumors and bronchioloalveolar cell carcinoma.

Nevertheless, determination of tumor size remains the domain of CT because of its excellent anatomical resolution and cost-effectiveness.

Initial staging: N-staging. Assessment of locoregional lymph node involvement and determination of the N-stage are the most important indications for $[^{18}\text{F}]$ -FDG-PET in patients with lung cancer. In comparison to CT, $[^{18}\text{F}]$ -FDG-PET proved to be significantly more accurate in nearly all of the adequately

powered studies. For nodal staging, Reske *et al.* determined a sensitivity of 88% and a specificity of 92% [36] for [^{18}F]-FDG-PET. In their review Vansteenkiste and Stroobants obtained an overall sensitivity of 89% (range: 67–93), specificity of 92% (range: 82–97) and accuracy of 90% (range: 84–94), respectively [37]. In a study by Birim *et al.* the receiver operating characteristic (ROC) curve with equal sensitivity and specificity for [^{18}F]-FDG-PET was $Q^* = 0.90$ (point of maximum joint sensitivity and specificity) and for CT it was 0.70 [39]. This resulted in a highly significant difference ($p < 0.0001$).

Because of the high accuracy of [^{18}F]-FDG-PET in locoregional lymph node staging, Vansteenkiste *et al.* stated that mediastinoscopy could be omitted in patients with normal mediastinal [^{18}F]-FDG-PET readings [39]. This suggestion is now widely accepted and was implemented in the Lung Cancer Guidelines of the American College of Chest Physicians [40].

Initial staging: M-staging. Routine staging workup is based on conventional imaging such as CT and MRI. In the review by Reske *et al.*, [^{18}F]-FDG-PET detected unsuspected extrathoracic metastases in 12% of the cases. The calculated sensitivity and specificity for detection of distant metastases were 94% and 97%, respectively. [^{18}F]-FDG-PET also revealed to be a useful tool in the assessment of adrenal masses and suspected liver metastases.

One of the major impacts of [^{18}F]-FDG-PET in staging patients with lung cancer is the improvement of treatment planning. Depending on the existence of distant metastases and determination of N-stage, patients undergo local or systemic treatment. In a publication by van Tinteren *et al.* it was shown that the addition of a [^{18}F]-FDG-PET to conventional workup led to a relative reduction of futile thoracotomies of 51% [41]. This resulted in a prevention of unnecessary surgery in 1 of 5 patients.

Recurrence. Differentiation between post-therapeutic changes and recurrent lung cancer by conventional imaging remains difficult. [^{18}F]-FDG-PET is very sensitive in detecting viable tumor tissue and proved to be superior to CT in detection of recurrence. The pooled data of 423 patients reviewed by Hellwig *et al.* revealed a sensitivity of 96% (range: 93–100) and specificity of 84% (range: 62–100), respectively [42]. False-positive findings can be evoked by radiation pneumonitis or macrophage glycolysis in tumor necrosis. Therefore, it is recommended to leave an interval of 4–6 months between end of radiation therapy and [^{18}F]-FDG-PET imaging.

2.1.2.2. [^{18}F]-FDG-PET/CT

Initial staging. The first study comparing the diagnostic accuracy of integrated [^{18}F]-FDG-PET/CT with CT alone, [^{18}F]-FDG-PET alone and conventional visual correlation of [^{18}F]-FDG-PET and CT in patients with NSCLC was published by Lardinois *et al.* [43]. Integrated [^{18}F]-FDG-PET/CT provided additional information beyond that provided by visually correlated [^{18}F]-FDG-PET and CT in 41% of the included patients. [^{18}F]-FDG-PET/CT also revealed to be significantly

more accurate in tumor staging than CT alone ($p = 0.001$), $[^{18}\text{F}]$ -FDG-PET alone ($p < 0.001$) and visual correlation of $[^{18}\text{F}]$ -FDG-PET and CT ($p = 0.013$). In nodal staging $[^{18}\text{F}]$ -FDG-PET/CT was also significantly more accurate than $[^{18}\text{F}]$ -FDG-PET alone ($p = 0.013$). In another study by Shin *et al.* 106 patients underwent surgical resection (tumor resection and lymph node dissection) after stand-alone CT followed by integrated $[^{18}\text{F}]$ -FDG-PET/CT [44]. $[^{18}\text{F}]$ -FDG-PET/CT correctly staged the primary tumor in 86% of the patients versus 79% with CT alone. For the depiction of SPN, $[^{18}\text{F}]$ -FDG-PET/CT revealed to be significantly more accurate than CT (85% vs. 70%, $p < 0.001$); corresponding sensitivities: 84% vs. 69%, $p < 0.001$, and specificities: 84% vs. 69%, $p < 0.001$. De Wever *et al.* determined the TNM status for CT, $[^{18}\text{F}]$ -FDG-PET, visually correlated $[^{18}\text{F}]$ -FDG-PET/CT and integrated $[^{18}\text{F}]$ -FDG-PET/CT and compared it with the post-surgical TNM status [45]. In this study integrated $[^{18}\text{F}]$ -FDG-PET/CT was the most accurate imaging technique by predicting correctly the T status, N status, M status and TNM status in, respectively, 86%, 80%, 98%, 70% versus 68%, 66%, 88%, 46% with CT, 46%, 70%, 96%, 30% with $[^{18}\text{F}]$ -FDG-PET and 72%, 68%, 96%, 54% with visually correlated $[^{18}\text{F}]$ -FDG-PET/CT.

These results lead to the conclusion that integrated $[^{18}\text{F}]$ -FDG-PET/CT improves the staging of lung cancer through a better anatomic localization and characterization of lesions and is superior to CT alone and $[^{18}\text{F}]$ -FDG-PET alone.

Recurrence. Additional information provided by the use of a combined $[^{18}\text{F}]$ -FDG-PET/CT scanner led to an improvement of accuracy in detection of recurrent disease in a study of 52 patients with suspected recurrence of NSCLC. According to Keidar *et al.* sensitivity was unchanged (96% vs. 96%) but $[^{18}\text{F}]$ -FDG-PET/CT revealed to be more specific than $[^{18}\text{F}]$ -FDG-PET alone (82% vs. 53%) [46]. In this study $[^{18}\text{F}]$ -FDG-PET/CT changed the $[^{18}\text{F}]$ -FDG-PET lesion classification in 22 patients (52%) by determining the precise localization of sites of increased $[^{18}\text{F}]$ -FDG uptake. $[^{18}\text{F}]$ -FDG-PET/CT changed the management of 12 patients (29%) by eliminating previously planned diagnostic procedures (5 patients), by initiating a previously unplanned treatment option (4 patients) or by inducing a change in the planned therapeutic approach (3 patients).

2.1.3. Lymphoma

Malignant lymphomas consist of two entities—Hodgkin's disease (HD) and non-Hodgkin's lymphomas (NHL). As a result of a high number of studies investigating the role of $[^{18}\text{F}]$ -FDG-PET in malignant lymphomas, $[^{18}\text{F}]$ -FDG-PET is now clinically accepted and introduced into the clinical routine for staging, restaging and treatment evaluation of lymphomas. As a consequence, the CMS approved the coverage of $[^{18}\text{F}]$ -FDG-PET scanning for diagnosis, staging and restaging of Hodgkin's and non-Hodgkin's lymphomas in 2001.

2.1.3.1. [^{18}F]-PET

Initial staging. The use of [^{18}F]-FDG-PET for the initial staging of newly diagnosed HD summarizing the results up to the year 2000 was published in a meta-analysis by Reske and Kotzerke [47]. This review of 11 studies with a total of 514 patients showed a 10% increase of sensitivity compared with conventional imaging such as CT, related specificities ranged from 85% to 90%. This review suggests a sensitivity of more than 90% for staging of HD with [^{18}F]-FDG-PET. In a more recent study by Naumann *et al.*, which investigates the impact of [^{18}F]-FDG-PET on the therapy decision of 88 patients with early-stage HD, the sensitivity and specificity were 93.1% and 100%, respectively [48]. Additional information provided by [^{18}F]-FDG-PET led to a different clinical stage in 20% of the patients and would have resulted in a change of therapy management in 18%.

Even though the studies published often represent a combination of HD and NHL patients, it is appropriate to state that [^{18}F]-FDG-PET quite reliably exceeds conventional imaging also for patients with NHL.

Schöder *et al.* recently showed that [^{18}F]-FDG uptake is lower in indolent than in aggressive NHL [49]. A SUV >10 resulted in a higher likelihood for aggressive disease and excluded indolent lymphomas with a sensitivity of 81%. But nevertheless differentiation between aggressive and indolent lymphomas depending on the SUV leaves around 45% of the patients in a gray area.

Restaging: Therapy control. The data pool for restaging of HD and NHL is much larger than for initial staging. Especially in the detection of tumor viability after chemotherapy with a high negative predictive value [^{18}F]-FDG-PET has proven to be extremely valuable. For restaging studies with mixed patient populations of HD/NHL [^{18}F]-FDG-PET revealed high sensitivities (range: 71–88%) and specificities (range: 83–86%) and was compared with CT (sensitivity: 88%, specificity: 31%) significantly more accurate [47,50].

In a meta-analysis Isasi *et al.* reviewed 47 studies evaluating the role of [^{18}F]-FDG-PET for staging and restaging of lymphoma patients [51]. Twenty studies published between 1995 and 2004 met the inclusion criteria and were eligible for the meta-analysis. Among the studies with patient-based data the pooled sensitivity was 90.9% and the related pooled false-sensitive rate was 10.3%. This resulted in a maximum joint sensitivity and specificity of 87.8%. Separate meta-analysis for HD yielded a pooled sensitivity of 92.6% and a false-positive rate of 13.6%. In contrast, among patients with NHL the pooled sensitivity and false-positive rates were 89.4% and 11.4%, respectively. For HD the maximum joint sensitivity and specificity appeared to be slightly higher (89.4% vs. 85.0%) than for NHL.

2.1.3.2. [^{18}F]-PET/CT

In a study of 99 consecutive patients with HD, Hutchings *et al.* compared [^{18}F]-FDG-PET with or without CT regarding primary staging [52]. The use of [^{18}F]-FDG-PET alone would have upstaged 19% of patients and downstaged

5% of patients, leading to a different treatment in 9%. The corresponding figures for ^{18}F -FDG-PET/CT were 17%, 5% and 7%. ^{18}F -FDG-PET alone and ^{18}F -FDG-PET/CT also revealed to be more sensitive in nodal regions (sensitivity 92% each) than CT (83%). The number of false-positive nodal sites revealed to be lowest for ^{18}F -FDG-PET/CT (0.5%). Corresponding figures for ^{18}F -FDG-PET alone and CT are 1.6% and 0.7%, respectively.

In another study, la Fougere *et al.* compared the value of ^{18}F -FDG-PET/CT versus ^{18}F -FDG-PET and CT for staging and restaging as separate investigations in patients with HD and NHL [53]. Region-based evaluation revealed the following sensitivities for ^{18}F -FDG-PET/CT, ^{18}F -FDG-PET and CT: 98% versus 98% versus 85%. The related specificities were 99%, 99% and 91%, respectively. It was therefore concluded that ^{18}F -FDG-PET was superior to CT alone, but introduction of in-line ^{18}F -FDG-PET/CT led to no significant difference in staging and restaging accuracy.

2.1.4. Breast cancer

Breast cancer is the leading cause of cancer in women and the second leading cause of cancer death in women in the United States [54]. ^{18}F -FDG-PET scanning has gained widespread acceptance for the diagnosis, staging, restaging and therapy management of breast cancer. As a consequence, the CMS approved coverage for ^{18}F -FDG-PET scanning for the following indications in breast cancer: as an adjunct to standard imaging modalities for staging patients with distant metastases or restaging patients with locoregional recurrence of metastases; and as an adjunct to standard imaging modalities for monitoring tumor response to treatment for women with locally advanced and metastatic breast cancer when a change in therapy is anticipated.

However, currently CMS have not yet decided to cover ^{18}F -FDG-PET for primary staging of breast cancer and the staging of axillary lymph nodes, since research studies for these indications showed inconsistent results. Nevertheless, the role of ^{18}F -FDG-PET in clinical diagnosis and management of breast cancer patients is increasing and evolving and the range of the CMS coverage will likely be expanded in the near future.

2.1.4.1. ^{18}F -FDG-PET

Initial staging: Primary staging. The majority of ^{18}F -FDG-PET studies have been performed on patients with invasive breast cancer, because previously performed studies showed that ^{18}F -FDG-PET only poorly images noninvasive breast cancer [55]. In a review by Wu *et al.* an overall sensitivity, specificity and accuracy of ^{18}F -FDG-PET in the detection of primary invasive breast cancer of 90%, 92% and 93%, respectively, were reported [56]. Even though there was a significant variation between the studies, all larger series (≥ 20 patients) showed high sensitivities, ranging from 80% to 93%. The related specificities were relatively high, but inflammatory changes and fibroadenoma led to

false-positive-findings. Two histological types of invasive breast cancer can be differentiated—infiltrating ductal, infiltrating lobular and a combination of both—which show differences in [^{18}F]-FDG uptake. Studies have shown that infiltrating ductal carcinomas are detected at a significantly higher sensitivity than carcinomas of the infiltrating lobular type [55,57]. Furthermore, several studies have shown that lesions larger than 1 cm are much better detected, with sensitivities and specificities in the range of 96% to 100%, and more recent series proved that small tumor sizes (ranging from 0.4 to 1.5 cm) show only low FDG accumulation because of partial volume effects or are non-detectable by [^{18}F]-FDG-PET [58–60].

Initial staging: N-staging. The evaluation of [^{18}F]-FDG-PET imaging for staging of breast cancer refers to the staging of axillary lymph nodes and the staging of mediastinal and internal mammary lymph nodes and distant metastases. Studies investigating the role of [^{18}F]-FDG-PET for staging of axillary lymph nodes—a very important indicator of prognosis and determination of therapy strategies—showed mixed results. In contrast, many studies have proved that [^{18}F]-FDG-PET is superior to CT in the detection of internal mammary and/or mediastinal lymph nodal metastases.

[^{18}F]-FDG-PET has been extensively studied for noninvasive staging of the axilla. These results have been promising but have not shown consistent results. Although [^{18}F]-FDG-PET has an overall sensitivity of 88%, specificity of 92% and accuracy of 89% when surveying across the multitude of prior reports, several of the studies achieved higher sensitivity at the expense of lower specificity or vice versa [56].

A review by Wu *et al.* revealed consistently better results for [^{18}F]-FDG-PET (sensitivity: 85%, specificity: 90% and accuracy: 88%) versus CT (54%, 85% and 73%, respectively) in detecting internal mammary and/or mediastinal lymph nodal metastases [56].

Initial staging: M-staging. [^{18}F]-FDG-PET has also proved effectiveness in detecting distant lesions and providing staging information even at the time of initial diagnosis. Several investigators have shown that [^{18}F]-FDG-PET is relatively sensitive (84–93%) and has a good negative predictive value (>90%) in the evaluation of distant metastases [61–63]. Whole-body [^{18}F]-FDG-PET is able to detect metastases involving the liver, lymph nodes, bone, lung, and bone marrow. Specificity and positive predictive values are not quite as high, in the range of 55–86% and 82%, respectively, largely due to false-positive findings caused by muscle uptake, inflammation, blood-pool activity and bowel uptake [61].

Recurrence. Local recurrence appears in 80% of all cases within the 5 years following surgery. In 50% of the patients, local recurrence is the only site of tumor remanifestation. Pecking *et al.* evaluated [^{18}F]-FDG-PET for detection of recurrence in a series of 132 patients [64]. According to this study, [^{18}F]-FDG-PET detected lesions in 106 patients with an overall sensitivity of 94%, resulting in a

positive predictive value of 96%. In a study by Suarez *et al.* in patients with complete remission but with elevated tumor markers [¹⁸F]-FDG-PET revealed a recurrence in 24 of 45 included patients, which was superior to the combination of several anatomic imaging modalities (CT, MRI, ultrasound and x-rays) that only detected recurrence in 21 patients [65].

2.1.4.2. [¹⁸F]-FDG-PET/CT

So far only two studies have been addressing the role of [¹⁸F]-FDG-PET/CT in the evaluation of breast cancer. Fueger *et al.* compared [¹⁸F]-FDG-PET and integrated [¹⁸F]-FDG-PET/CT for staging and restaging of 58 female patients with breast cancer [66]. According to this study, [¹⁸F]-FDG-PET/CT provided a higher sensitivity (94% vs. 85%) and specificity (84% vs. 72%) than [¹⁸F]-FDG-PET alone. Overall, [¹⁸F]-FDG-PET/CT reduced the number of incorrectly staged patients by 65%. Nevertheless, the staging accuracy of [¹⁸F]-FDG-PET/CT was not significantly better than that of [¹⁸F]-FDG-PET alone ($p = 0.059$). In another study of 85 patients with breast cancer, Tatsumi *et al.* demonstrated that [¹⁸F]-FDG-PET/CT (86%) had a significantly better accuracy in staging than CT alone did (77%; $p > 0.05$). [¹⁸F]-FDG-PET/CT also added additional incremental diagnostic confidence to [¹⁸F]-FDG-PET in 60% of the 50 patients with increased [¹⁸F]-FDG uptake.

2.1.5. Esophageal cancer

Esophageal cancer ranks among the 10 most common malignancies in the world and is a frequent cause of cancer-related death. However, carcinomas of the esophagus are a heterogeneous group of tumors in terms of etiology, histopathology and epidemiology. Depending on the tumor stage, the available therapeutic approaches for esophageal cancer are endoscopic mucosal resection, primary esophagectomy, neoadjuvant or palliative chemotherapy/radiotherapy followed by surgery and palliative resection. Most of the therapeutic modalities are associated with substantial morbidity and mortality. Accurate pre-therapeutic staging is crucial in order to select the appropriate kind of therapy.

2.1.5.1. [¹⁸F]-FDG-PET

Initial staging: T-staging. Several studies report a high sensitivity of [¹⁸F]-FDG-PET for staging squamous cell carcinoma (SCC) and adenocarcinomas of the esophagus. Detection rates for the primary tumor range from 69% to 100% [67–73]. In most studies, [¹⁸F]-FDG-PET is more sensitive than CT. Rasanen *et al.* investigated 42 patients who had undergone [¹⁸F]-FDG-PET and CT before esophagectomy [74]. They found that the primary tumor was correctly detected in 35 (83%) of 42 patients by [¹⁸F]-FDG-PET and in 28 (67%) patients by CT. Furthermore, Heeren *et al.* reported that the primary tumor was visualized in 95% (70 of 74 patients) with [¹⁸F]-FDG-PET and in 84% (62 of 74 patients) with CT [67]. False-negative [¹⁸F]-FDG-PET findings in SCC are often due to a small

tumor size. This is a consequence of the limited spatial resolution of [^{18}F]-FDG-PET which is approximately 5–8 mm. A small percentage of adenocarcinomas shows a limited or absent [^{18}F]-FDG accumulation regardless of tumor size. This seems to be related to the histological type: limited or absent [^{18}F]-FDG uptake has been found in diffusely growing and/or mucus producing subtypes.

Initial staging: N-staging. Locoregional lymph node metastases seem to represent one of the most important prognostic factors in patients with esophageal cancer. Not only the number and location of regional metastatic lymph nodes but also the lymph node size is predictive for the patient's outcome. Nevertheless, the noninvasive staging is still not accurate enough for a reliable N-staging. Depending on the criteria used for detection of regional lymph node involvement, the values for sensitivity and specificity vary substantially between different studies.

In a meta-analysis, Westreenen *et al.* analyzed 12 studies concerning the diagnostic accuracy of [^{18}F]-FDG-PET in staging the locoregional lymph node status [75]. The pooled sensitivity and specificity of [^{18}F]-FDG-PET in detecting locoregional lymph node involvement were 51% and 84%, respectively.

Flamen *et al.* prospectively studied 74 patients with esophageal cancer with regard to lymph node staging [71]. Endoscopic ultrasound (EUS) was more sensitive (81% vs. 33%) but less specific (67% vs. 89%) than [^{18}F]-FDG-PET for the detection of regional lymph node metastases. Compared with the combined use of CT and EUS, [^{18}F]-FDG-PET had a higher specificity (98% vs. 90%) and a similar sensitivity (43% vs. 46%) for the assessment of regional and distant lymph node involvement. Choi *et al.* compared the diagnostic accuracy of [^{18}F]-FDG-PET and CT/EUS in 61 consecutive patients [76]. Forty-eight patients (13 excluded because of nonsurgical treatment) underwent transthoracic esophagectomy with lymph node dissection. Three hundred eighty-eight lymph nodes were dissected, of which 100 in 32 patients were malignant on histological examination. On a patient basis, N-staging was correct in 83% of the patients on [^{18}F]-FDG-PET, whereas it was correct in 60% on CT and in 58% by using EUS ($p < 0.05$). However, in the neighborhood of the primary tumor, the authors report a low sensitivity of [^{18}F]-FDG-PET for detecting metastatic lymph nodes due to the limited spatial resolution of the [^{18}F]-FDG-PET-scanners and scatter effects arising from FDG accumulation in the primary tumor. In contrast to other tumor types, regional lymph node metastases in esophageal cancer are frequently located very close to the primary tumor making it difficult to differentiate lymph node metastases from the primary tumor on [^{18}F]-FDG-PET.

Lerut *et al.* prospectively included 42 patients in a staging study of esophageal carcinoma [77]. All patients underwent [^{18}F]-FDG-PET, CT and EUS. For the diagnosis of regional lymph node metastases [^{18}F]-FDG-PET was not considered to be useful because of a lack of sensitivity, which was 22% compared with 83% for CT and EUS.

Initial staging: M-staging. Computed tomography of the chest and the abdomen currently presents the standard noninvasive test for evaluating distant metastases with a sensitivity of 37–66%. In a meta-analysis by van Westreenen *et al.* 12 studies investigating patients with newly diagnosed cancer of the esophagus were included [75]. Pooled sensitivity and specificity for detection of distant metastases were 67% and 97%, respectively. Flamen *et al.* evaluated 74 patients with potentially resectable esophageal cancer in a prospective study and compared the diagnostic accuracy for $[^{18}\text{F}]$ -FDG-PET, CT and EUS [71]. For detecting distant metastases, the sensitivities for $[^{18}\text{F}]$ -FDG-PET, CT and EUS were 74%, 41% and 42%, the corresponding specificities were 90%, 83% and 94%. The diagnostic accuracy of $[^{18}\text{F}]$ -FDG-PET was 82% while it was only 64% for a combination of CT and EUS mainly by virtue of a superior sensitivity of $[^{18}\text{F}]$ -FDG-PET. These findings changed patient management in 22% of the studied patients by upstaging 11 patients (15%) and downstaging 5 patients (7%). In two patients $[^{18}\text{F}]$ -FDG-PET falsely understaged disease because of false-negative $[^{18}\text{F}]$ -FDG-PET findings with regard to supra-diaphragmatic lymph nodes.

Heeren *et al.* compared $[^{18}\text{F}]$ -FDG-PET with a combination of CT/EUS in the pre-therapeutic staging for distant lymph node metastases and distant organ metastases in 74 patients [67]. $[^{18}\text{F}]$ -FDG-PET was able to identify distant nodal disease in 17/24 (71%) of the patients while this ratio was only 7/24 patients (29%) for CT/EUS. The sensitivity for detection of distant metastases was also significantly higher for $[^{18}\text{F}]$ -FDG-PET (70%) than for the combined use of CT and EUS (30%). $[^{18}\text{F}]$ -FDG-PET correctly upstaged 15 patients (20%) who were missed on CT/EUS and correctly downstaged 4 patients (5%). However, in this study $[^{18}\text{F}]$ -FDG-PET also misclassified 8 of the 74 patients (11%) by falsely upstaging in 5 patients (7%) and false downstaging in 3 patients (4%).

In all studies published so far, the diagnostic accuracy of $[^{18}\text{F}]$ -FDG-PET in detection of distant metastases of esophageal cancer has been found to be higher than that of morphological imaging techniques like CT or EUS. This seems to apply to both, the detection of distant lymph node metastases and organ metastases. $[^{18}\text{F}]$ -FDG-PET exceeds by an outstanding sensitivity for bone metastases and appears to have a higher specificity than CT for detection of lung metastases and liver metastases. CT, on the other hand, appears to have a higher sensitivity for lung metastases.

In summary, the value of $[^{18}\text{F}]$ -FDG-PET for staging esophageal carcinoma mainly resides in better characterization of distant metastases (lymph nodes and organs). However, $[^{18}\text{F}]$ -FDG-PET should be regarded a supplemental procedure (e.g. in addition to CT), as it does not enable accurate determination of the local tumor extent and locoregional lymph node involvement. Furthermore, $[^{18}\text{F}]$ -FDG-PET plays an important role for the early response evaluation of tumors to neoadjuvant chemo- and radiochemotherapy (see section about therapy monitoring).

Recurrence. Kato *et al.* studied 55 patients with thoracic SCC who had undergone radical esophagectomy [78]. Twenty-seven of the 55 patients had recurrent

disease in a total of 37 organs. The accuracy of [^{18}F]-FDG-PET and CT in detecting recurrences during follow-up was always calculated by using the first images, which suggested the presence of recurrent disease. [^{18}F]-FDG-PET showed 100% sensitivity, 75% specificity and 84% accuracy for detecting locoregional recurrence. The corresponding values for CT were 84%, 86% and 85%, respectively. The specificity of [^{18}F]-FDG-PET was lower because of unspecific [^{18}F]-FDG uptake in gastric tissue and in thoracic lymph nodes of the lung hilum or the pretracheal region. Distant recurrence was observed in 15 patients in 18 organs. Most of the recurrences were located in liver, lung and bone. The sensitivity, specificity and accuracy for [^{18}F]-FDG-PET was 87%, 95% and 93% versus 87%, 98% and 95% for CT. The diagnostic accuracy of [^{18}F]-FDG-PET for distant recurrence was similar to that of CT. The sensitivity of [^{18}F]-FDG-PET in detecting bone metastases was higher than that of CT. The sensitivity for lung metastases was higher on CT because of the excellent spatial resolution and high tumor-to-tissue contrast in lung. Similar sensitivities for [^{18}F]-FDG-PET and CT were observed for both liver and distant lymph node metastases.

Flamen *et al.* used [^{18}F]-FDG-PET in 41 symptomatic patients for diagnosis and staging of recurrent disease after radical esophagectomy [79]. All patients underwent a whole-body [^{18}F]-FDG-PET and a conventional diagnostic workup including a combination of CT and EUS. Recurrent disease was present in 33 patients (40 locations). Nine lesions were located at the anastomotic site, 12 at regional and 19 at distant sites. For the diagnosis of a recurrence at the anastomotic site, no significant difference between [^{18}F]-FDG-PET and CT/EUS was found. The sensitivity, specificity and accuracy of [^{18}F]-FDG-PET was 100%, 57% and 74% versus 100%, 93% and 96% for conventional diagnostic workup. A reason for the high incidence of false-positive [^{18}F]-FDG-PET findings at the perianastomotic region might have been progressive benign anastomotic strictures in these patients, requiring repetitive endoscopic dilatation. Probably the dilatation-induced trauma resulted in an inflammatory reaction. For the diagnosis of regional and distant recurrence [^{18}F]-FDG-PET showed 94% sensitivity, 82% specificity and 87% accuracy versus 81%, 84% and 81% for CT/EUS. On a patient basis, [^{18}F]-FDG-PET provided additional information in 27% (11/41) of the patients. In summary, [^{18}F]-FDG-PET is associated with a similar clinical benefit in restaging esophageal carcinoma as in primary staging. However, the perianastomotic site often remains equivocal as an unspecific increase of metabolic activity may be present owing to inflammatory or reparative processes.

2.2. Therapy monitoring with [^{18}F]-FDG-PET and [^{18}F]-FDG-PET/CT

One of the most promising future indications of [^{18}F]-FDG-PET imaging in the clinical routine will be the evaluation of therapy response, tumor control and prediction of prognosis. Weber *et al.* [2] showed that [^{18}F]-FDG-PET provides

several highly reproducible quantitative parameters of tumor glucose metabolism and concluded that changes of glucose consumption that are outside the 95% normal range may be used to define a metabolic response to therapy [2]. From the perspective of a clinician it is very important to differentiate nonresponders to chemotherapy or radiochemotherapy early in the course of treatment to possibly change the therapeutic management. The following section gives an overview of the role of [¹⁸F]-FDG-PET and [¹⁸F]-FDG-PET/CT in the assessment of therapy response and prognosis with special emphasis on the early therapy response evaluation (Table 3).

2.2.1. Gastrointestinal tract (GI)

In general, response rates to neoadjuvant chemotherapy and/or radiotherapy in esophageal cancer are below 50% for all carcinoma types as measured by histopathologic examination of the surgical specimen (after termination of therapy, e.g. in a neoadjuvant setting). A common criterion for histopathologic response to therapy is the absence of tumor cells or the presence of only scattered tumor cells (<10% viable tumor cells) in the resected specimen [80–82]. In a neoadjuvant (preoperative) setting, the overall survival of patients is correlated with histopathologic response [81]. However, because of the tumor heterogeneity after neoadjuvant therapy small biopsies of the tumor tissue are not representative for the whole tumor mass. A complete tumor resection and a histopathologic examination of the whole tumor including resection borders are necessary to define the histopathologic tumor response.

In contrast to pre- or post-therapeutic biopsies used for histopathologic analysis, the whole tumor mass can be analyzed noninvasively by imaging techniques such as contrast-enhanced CT or EUS. However, morphological changes are not always representative of tumor response to therapy as large tumor masses may remain despite response, therapy-induced fibrosis or edema may mimic residual tumor and shrinking tumors may still contain vital tumor cells. The overall accuracy for response assessment is relatively low when determining post-therapeutic T-stage or comparing pre- and post-therapeutic T-stage by using morphological imaging. As a consequence, following chemotherapy or chemoradiotherapy, tumor response may not be reliably assessed by CT or EUS.

Despite these limitations, changes in tumor size have been used to assess tumor response in patients with esophageal cancer. According to criteria of the World Health Organization (WHO), the size of the tumor has to be measured in 2 perpendicular diameters. Tumor response is defined as a therapy-induced reduction of the product of these 2 diameters by at least 50%. In 2000, Therasse *et al.* published the so-called RECIST criteria introducing a model by which a combined assessment of all existing lesions, characterized by target lesions (to be measured) and non-target lesions, is used to extrapolate an overall response to treatment [83,84]. Previous studies have shown that mean changes in tumor

Table 3. Early assessment of response by FDG-PET and clinical outcome

Tumor	Author	Year	N	Criteria	Assessment of response after (in months)	Responder	Non- Responder (in months)	p-value
<i>Lymphoma</i>								
M. Hodgkin	Hutchings	2005	77	Visual	8 wks.	96%**	0%**	<0.0001
NHL	Mikhaeel	2005	121	Visual	8 wks.	89%***	16%***	<0.0001
<i>Esophagus</i>								
AGE	Weber	2001	40	−35%	2 wks.	>48	20	0.04
AEG	Ott	2006	65	−35%	2 wks.	n.e	18	0.01
AGE	Lordick	2007	111	−35%	2 wks.	n.e	26	0.01
SCC	Wieder	2004	27	−30%	2 wks.	38	18	0.011
Gastric	Ott	2003	44	−35%	2 wks.	n.e	19	0.001
Breast	Schelling	2000	24	−45%	4 wks.			<0.05
Ovarial	Avril	2005	33	−20%	2 wks.	38	23	0.008
Head/Neck	Brun	2002	47	Median	3 wks.	>120	40	0.004
Lung	Weber	2003	57	−20%	2 wks.	9	5	0.005
GIST	Stroobants	2003	21	Visual	8 days	92%*	12%*	0.0011

* 1-year progression free survival.

** 2-year progression free survival.

*** 5-year progression free survival.

NHL, non-Hodgkin's lymphoma; AEG, adenocarcinoma of the esophagogastric junction; SCC, squamous cell carcinoma; GIST, gastrointestinal stromal tumor.

size of 50% and more are seen in esophageal cancer at the end of chemotherapy. However, these changes show no strong correlation with histopathologic response. It is well known that the esophageal wall often shows pathological thickening and irregularities regardless of the degree of therapy response.

Therefore, anatomical imaging modalities usually do not allow to distinguish residual tumor from therapy-related changes like inflammatory reaction, edema, and scar tissue.

The reproducibility of the [¹⁸F]-FDG-PET signal arising from [¹⁸F]-FDG accumulation in tumors has been shown to be stable across repeated examinations [2]. The inter-study variability of repeated [¹⁸F]-FDG measurements within 3 weeks is <20% [2]. In other words, during therapy, any change in tumor [¹⁸F]-FDG uptake greater than $\pm 20\%$ between baseline [¹⁸F]-FDG-PET and follow-up [¹⁸F]-FDG-PET can possibly be considered a true change.

The metabolic effects of a neoadjuvant chemotherapy/radiochemotherapy can be assessed during and after treatment. Evaluation late in the course of treatment and after completion of treatment may predict survival and may be associated with the amount of residual viable tumor cells and histopathologic tumor response. However, the therapeutic relevance of this prognostic information is limited, as it is obtained too late for alteration of therapeutic strategy. Therefore, it is considered important to differentiate between response and nonresponse early in the course of neoadjuvant therapy.

2.2.1.1. Upper GI

In 2001, Weber *et al.* [82] showed in a study cohort of 40 patients with locally advanced adenocarcinoma of the esophagogastric junction that prediction of histopathologic response is possible by metabolic imaging with [¹⁸F]-FDG as early as 2 weeks after induction of chemotherapy. Application of the criterion metabolic response—defined as a reduction of baseline SUV of more than 35%—allowed prediction of clinical response with a sensitivity of 93% and specificity of 95%, respectively (Fig. 2).

Wieder *et al.* [80] evaluated the time course of therapy-induced changes in tumor glucose metabolism during chemoradiotherapy of esophageal SCC in a cohort of 38 patients. Early metabolic response, defined as a reduction of baseline SUV of more than 30%, predicted histopathologic response 2 weeks after induction of chemotherapy with a sensitivity of 93% and a specificity of 88%, respectively. Changes in tumor metabolic activity early in the time course of preoperative chemoradiotherapy were also significantly correlated with patient survival ($p < 0.011$).

In a study investigating the prediction of response to preoperative chemotherapy in gastric carcinoma, Ott *et al.* [85] included 44 patients with locally advanced gastric cancer. Using the same criterion for differentiating metabolic responders and nonresponders as defined by Weber *et al.* [82], early response assessment by [¹⁸F]-FDG-PET turned out to predict histopathologic response with a sensitivity of 77% and specificity of 86%, respectively. Lordick *et al.* [222] prospectively

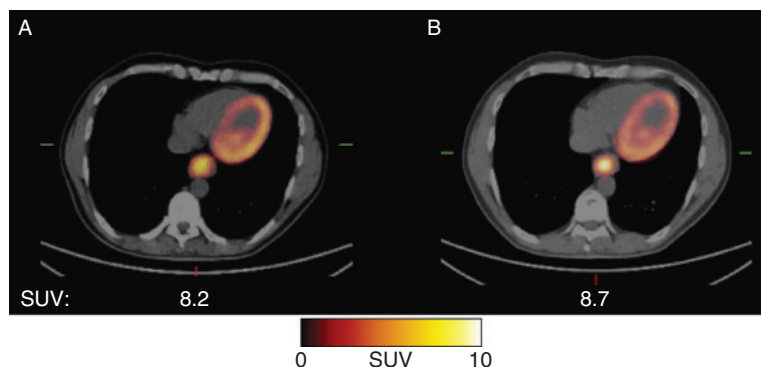


Fig. 2. Example of FDG-PET/CT studies (fused images) in a patient with adenocarcinomas of the esophagus and metabolic non-response. High focal initial FDG uptake in the tumor (A) which is almost unchanged 14 days (B) after initiation of chemotherapy. (See Colour Plate Section at the end of this book.)

confirmed the value of early metabolic response in patients with AEG I/II tumors and showed for the first time the feasibility of a PET guided treatment algorithm.

2.2.1.2. Lower GI

Calvo *et al.* [86] investigated the prognostic value of initial SUV_{max} in 25 patients with locally advanced rectal cancer. An initial $SUV_{max} < 6$ was correlated with a significant better 3-year overall survival than for the group with a $SUV_{max} \geq 6$ (93% vs. 60%, $p = 0.04$).

In a study by Guillem *et al.* [87] 15 patients with locally advanced rectal cancer underwent a [^{18}F]-FDG-PET scan before and 4–5 weeks after the completion of neoadjuvant radiochemotherapy. A reduction of SUV_{mean} of more than 62.5% was defined as metabolic response and correlated significantly with better recurrence-free survival ($p = 0.02$). In a recently published study by Cascini *et al.* [88] early assessment of response to radiochemotherapy by [^{18}F]-FDG-PET was investigated in 33 patients with locally advanced rectal cancer. Patients underwent [^{18}F]-FDG-PET scans before the start of therapy, 12 days after starting treatment and half of the included patients a third [^{18}F]-FDG-PET scan before surgery (Fig. 1). Retrospective ROC analysis revealed that a cut-off of 52% SUV mean decrease separated histological responders from nonresponders with a high sensitivity, specificity and accuracy. In the future, this cut-off will have to be verified in a prospective study.

2.2.2. Lung cancer

[^{18}F]-FDG-PET revealed to be of great importance for the prediction of prognosis for patients with lung cancer, as published by Downey *et al.* [89]. In a retrospective analysis an initial $SUV_{max} < 9$ was correlated with significant better 2-year survival (96% vs. 68%; $p < 0.01$). In a prospective study with a total of 57 patients Weber *et al.* [90] showed that in NSCLC the reduction of metabolic activity after one cycle

of chemotherapy determined by $[^{18}\text{F}]$ -FDG-PET is closely correlated with the final outcome of therapy. Metabolic response, defined as a reduction of tumor $[^{18}\text{F}]$ -FDG uptake by more than 20% as assessed by SUVs, was significantly correlated with histopathologic response ($p < 0.001$) and better overall survival ($p = 0.005$). Sensitivity and specificity for the prediction of histopathologic response by $[^{18}\text{F}]$ -FDG-PET were 95% and 74%, respectively. Weber *et al.* concluded that $[^{18}\text{F}]$ -FDG-PET is a suitable tool for early response evaluation and may decrease the morbidity and costs of therapy in nonresponding patients.

2.2.3. Lymphoma

Zinzani *et al.* showed in a study of 75 patients with malignant lymphomas that $[^{18}\text{F}]$ -FDG-PET positivity after induction of treatment is highly predictive for the presence of residual disease, with significant differences in terms of recurrence free survival (9% vs. 91%). Conventional imaging methods such as CT and MRI cannot differentiate reliably between scar tissue and vital tumor tissue. Therefore, $[^{18}\text{F}]$ -FDG-PET was recently introduced into clinical routine for therapy control and evaluation of early treatment response [91].

Mikhaeel *et al.* [92] evaluated the role of $[^{18}\text{F}]$ -FDG-PET for prediction of progression free survival and overall survival after two to three cycles of chemotherapy in 121 patients with high-grade NHL. Graduation of $[^{18}\text{F}]$ -FDG-PET scans into positive, minimal residual uptake (MRU), and negative was correlated with progression free survival and overall survival. The $[^{18}\text{F}]$ -FDG-PET-negative group revealed to have a significant better 5-year progression free survival (89%) than the MRU—and the $[^{18}\text{F}]$ -FDG-PET-positive group (59% and 16%, respectively; $p < 0.0001$). Kaplan–Meier analyses showed strong associations between $[^{18}\text{F}]$ -FDG-PET results and progression free survival ($p < 0.0001$) and overall survival ($p < 0.01$). Mikhaeel *et al.* concluded that an early interim $[^{18}\text{F}]$ -FDG-PET is an accurate and independent predictor of both, progression free and overall survival [92]. In a study of 77 patients with HD by Hutchings *et al.* [93], $[^{18}\text{F}]$ -FDG-PET proved to predict treatment failure and progression free survival. For prediction of progression free survival, early $[^{18}\text{F}]$ -FDG-PET was as accurate after two cycles as later during treatment and superior to CT at all times. A positive early $[^{18}\text{F}]$ -FDG-PET scan revealed to be highly predictive of progression in patients with advanced stage or extranodal disease. In a publication by Romer *et al.* [94] it was shown that standard chemotherapy of patients with NHL causes rapid decrease of tumor $[^{18}\text{F}]$ -FDG uptake as early as 7 days after treatment initiation and therefore remains a promising tool for early prediction of response to chemotherapy as early as day 7 after initiation of therapy.

2.2.4. Gastrointestinal stromal tumors (GIST)

Stroobants *et al.* [95] evaluated the role of $[^{18}\text{F}]$ -FDG-PET for early response evaluation to treatment with Glivec in a group of 21 patients with soft tissue

sarcoma. [^{18}F]-FDG-PET response, defined according to the European Organization for Research on Treatment of Cancer (EORTC) [^{18}F]-FDG-PET recommendations, as early as at day 8 after initiation of Glivec treatment was associated with a significant longer progression-free survival (1-year progression-free survival: 92% vs. 12%, $p = 0.001$). Response evaluation by [^{18}F]-FDG-PET preceded CT response by a median of 7 weeks (range: 4–48).

2.2.5. Head and neck

Brun *et al.* [96] assessed the value of [^{18}F]-FDG-PET in prediction of therapy outcome in 47 patients with locally advanced head and neck squamous cell carcinoma (HNSCC). As early as 5–10 days after initiation of radiotherapy, determination of the metabolic rate was correlated with 5-year survival. Patients with a metabolic rate lower than the median turned out to have a significantly higher 5-year survival (72% vs. 35%, $p = 0.004$), whereas determination of SUV showed no correlation at this time point.

2.2.6. Breast cancer

Schelling *et al.* [97] assessed the role of [^{18}F]-FDG-PET in predicting histopathologic response in 24 patients with locally advanced breast cancer. Metabolic response, defined as a decrease of more than 45% of baseline SUV, revealed a high accuracy (88%) in predicting histopathologic response already after one cycle of chemotherapy—related sensitivity and specificity were 100% and 85%, respectively. In another study by Dose Schwarz *et al.* [98] investigating 11 patients with metastatic breast cancer, patients with a negative [^{18}F]-FDG-PET scan after the first cycle of chemotherapy showed a longer overall survival than nonresponders (19.2 vs. 8.8 months). Comparison of responding and nonresponding lesions revealed a statistically significant difference in SUV uptake at both time points, after the first and the second cycle ($p = 0.02$ and $p = 0.003$, respectively). The authors therefore concluded that [^{18}F]-FDG-PET imaging as a surrogate endpoint for monitoring therapy response offers improved patient care by individualizing treatment and avoiding ineffective chemotherapy.

2.2.7. Ovarian cancer

Avril *et al.* [99] evaluated sequential [^{18}F]-FDG-PET to predict patient outcome after the first and the third cycle of neoadjuvant chemotherapy in 33 patients with advanced-stage ovarian cancer. A significant correlation was observed between [^{18}F]-FDG-PET metabolic response after the first ($p = 0.008$) and the third ($p = 0.005$) cycle of chemotherapy and overall survival. After the first cycle, a threshold of 20% SUV decrease for differentiation of metabolic responders and nonresponders revealed the following median overall survival: 38.3 months for metabolic responders compared to 23.1 months for metabolic nonresponders.

Therefore, $[^{18}\text{F}]$ -FDG-PET also appears to be a promising tool for early prediction of response to neoadjuvant chemotherapy in patients with ovarian cancer.

2.3. Methodical considerations and limitations

Spatial resolution of PET scanners is lower as compared with morphological imaging techniques such as CT and MR. One of the consequences of the low-spatial resolution is a partial loss of the signal in structures that are smaller than twice the resolution of the PET scanner, leading to measured activity concentrations that are lower than the real-activity concentration. This effect, described as partial volume effect, represents one of the main limitations of qualitative and quantitative analysis of PET studies of small anatomical structures. As a result, PET has a great difficulty in detecting lesions <1 cm such as small lymph nodes and lesions in liver and lung. As a consequence, specific molecular markers for PET are used resulting in high lesion-to-background contrasts.

A wide spectrum of methods and algorithms for evaluation and interpretation of $[^{18}\text{F}]$ -FDG metabolism signals from $[^{18}\text{F}]$ -FDG-PET reaching from visual analysis to kinetic modeling is available. For quantitation of $[^{18}\text{F}]$ -FDG metabolism individual rate constants and uptake kinetics have to be determined, requiring arterial blood sampling or arterialized venous blood sampling simultaneously with dynamic image acquisition or lookup tables. Because of its complexity, kinetic modeling mainly remains limited to scientific investigations. Semiquantitatively analysis of static $[^{18}\text{F}]$ -FDG-PET images using the SUVs proved to be suitable for clinical routine. Calculation of SUVs is defined as the ratio of measured activity in the lesion in [mCi/ml] and the injected dose in [mCi/g of body weight]. Normalization of SUV to body surface area [100], lean body weight [101] and blood glucose level [102] has been reported. Graham *et al.* [103] compared in a study population of 40 patients with colon cancer and liver metastases complex kinetic modeling methods with simplified quantitative analysis methods of $[^{18}\text{F}]$ -FDG uptake. Best predictor for outcome and best discriminator between normal tissue and tumor was the Patlak graphical analysis, but SUV normalized to body surface area also revealed comparable results. Regarding therapy monitoring, Stahl *et al.* [104] investigated the influence of different imaging protocols and SUV normalizations on the prediction of tumor response in a cohort of 43 patients with gastric carcinomas. The SUV decrease was not essentially influenced by any of the methodological variations investigated, demonstrating the robustness of $[^{18}\text{F}]$ -FDG SUV for therapeutic monitoring.

Metabolic response plays a decisive role for therapy monitoring and evaluation of tumor response to therapy. So far only a reduction of SUV has been taken into account, whereas a change of tumor volume is not included in semiquantitative analysis. The $[^{18}\text{F}]$ -FDG-PET/CT technique, combining metabolic and anatomic information, allowing a precise location of $[^{18}\text{F}]$ -FDG uptake might

potentially lead to a more detailed evaluation of therapy response. Comparison of in-line [^{18}F]-FDG-PET/CT with software fusion of [^{18}F]-FDG-PET and CT, with the so-called mental fusion of [^{18}F]-FDG-PET and CT, with [^{18}F]-FDG-PET only proved superiority of the new in-line devices in staging and restaging of colorectal carcinoma [30,31].

Image acquisition in PET scanners takes several minutes per acquisition field of view during which the patient breathes freely. As a consequence, PET images represent an average of different organ positions during the breathing cycles. In contrast, state-of-the-art CT scans are performed in a few seconds and can be acquired in any desirable state of respiratory arrest [105]. Motion artifacts can result in a suboptimal coregistration of PET and CT images, leading to breathing-related nonrigid mismatches and possible misinterpretation of lesions especially in lung and liver. Respiratory gating, a possible approach to solve this problem, was introduced by Nehmeh *et al.* [106], proving a reduction of respiratory motion artifact in PET imaging. Another approach reported by Shekhar *et al.* [107] was the development of an automated three-dimensional elastic registration algorithm of whole-body PET and CT correcting nonrigid misalignments as well as improving mechanical registration.

Another limitation of [^{18}F]-FDG-PET are false-positive findings. [^{18}F]-FDG is an excellent tumor-localizing tracer but is not tumor specific. Benign processes associated with increased glucose uptake include physiological processes such as brown fat, colonic and gynecologic activity, infectious and inflammatory processes, hyperplastic bone marrow and rebounding thymic hyperplasia in children and young adults [108].

3. INNOVATIVE [^{18}F] FLUORINE-BASED RADIOTRACERS

Introduction of new tracers such as [^{18}F]-fluorothymidine ([^{18}F]-FLT) for proliferation imaging, [^{18}F]-fluoromisonidazole ([^{18}F]-FMISO) and [^{18}F]-fluoroazomycin arabinoside ([^{18}F]-FAZA) for hypoxia imaging, [^{18}F]-galacto-RGD for angiogenesis imaging, [^{18}F]-FCH for imaging phospholipid metabolism and [^{18}F]-fluoride for bone metabolism imaging makes PET a promising noninvasive tool to accurately characterize individual tumor biology and offering the potential to optimize and individualize therapy for cancer patients. The next section presents the most commonly used fluorine-based radiotracers beside [^{18}F]-FDG.

3.1. Molecular imaging of proliferation with 3'-deoxy-3'-[^{18}F]-fluorothymidine

Treatment strategies of malignant tumors rely on histology and tumor stage. PET using the glucose analog [^{18}F]-FDG is now an established imaging modality for staging and restaging of malignant tumors [109,110]. [^{18}F]-FDG-PET is also a

valuable clinical tool for predicting tumor response to therapy and patient survival [111]. However, $[^{18}\text{F}]$ -FDG is not tumor specific and can also accumulate in inflammatory lesions such as tuberculosis (granulomas) abscesses, and sarcoidosis, leading to a reduced diagnostic accuracy [112,113]. Therefore, to increase specificity for malignant lesions, other tracers that complement the information provided by $[^{18}\text{F}]$ -FDG are required. Measurement of tumor growth and DNA synthesis might be appropriate for assessment of proliferative activity in malignant tumors. So far, several DNA precursors have been investigated, including $[^{11}\text{C}]$ -thymidine that represents the native pyrimidine base used for DNA synthesis *in vivo* [114]. Because of the short half-life of $[^{11}\text{C}]$ and rapid degradation of $[^{11}\text{C}]$ -thymidine, this tracer was considered less suitable for clinical use.

Recently, the thymidine analog 3'-deoxy-3'- $[^{18}\text{F}]$ -FLT was suggested for noninvasive assessment of proliferation and more specific tumor imaging [115]. The effort to synthesize $[^{18}\text{F}]$ -FLT is similar to that of the standard radiotracer $[^{18}\text{F}]$ -FDG [116]. $[^{18}\text{F}]$ -FLT that is derived from the cytostatic drug azidovudine (AZT) has been reported to be stable *in vitro* and to accumulate in proliferating tissues and malignant tumors [114]. Thymidine kinase 1 (TK1) was revealed as key enzyme responsible for the intracellular trapping of $[^{18}\text{F}]$ -FLT [117,118]. Recently, $[^{18}\text{F}]$ -FLT uptake in various malignant tumors has been described including breast cancer [119], colorectal cancer [120], lung cancer (Fig. 3) [121], lymphomas [122], gastric cancer (Herrman, 2007) JNM. In a pilot study comprising 34 patients with malignant lymphomas, linear regression analysis indicated a significant correlation of tumoral $[^{18}\text{F}]$ -FLT uptake and proliferation fraction in biopsied tissues as indicated by Ki-67 immunohistochemistry ($r = 0.84$, $p < 0.0001$) [123]. All patients with indolent or aggressive lymphomas

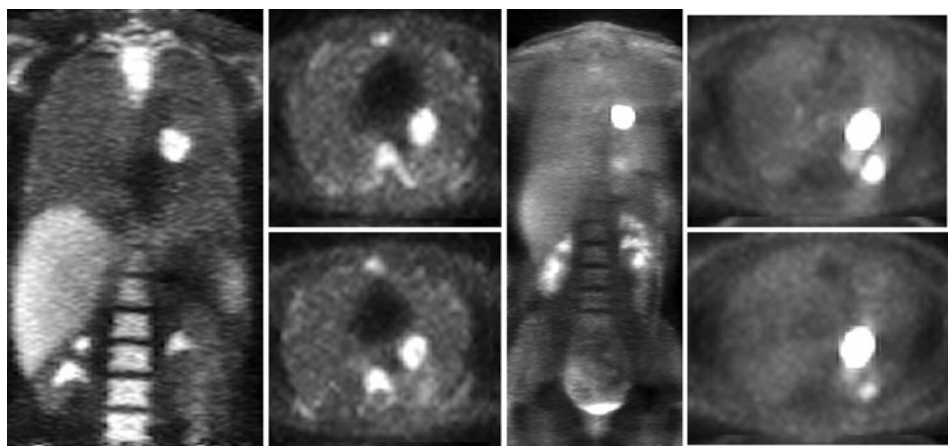


Fig. 3. Patient with lung cancer: Staging with $[^{18}\text{F}]$ -FLT-PET versus $[^{18}\text{F}]$ -FDG-PET.

exhibited focal [^{18}F]-FLT uptake in lesions also described by routine staging procedures, indicating a sensitivity of 100%. [^{18}F]-FLT uptake in lymphomas was significantly lower compared with respective [^{18}F]-FDG uptake (mean SUV-values 4.6 and 5.1, respectively). A reduced uptake of [^{18}F]-FLT compared with [^{18}F]-FDG has also been observed in a series of non-small cell lung cancer (mean SUV-values 3.7 and 6.0, respectively) [124] whereas sensitivity of [^{18}F]-FLT-PET was 90% for malignant primaries. Detection rates for mediastinal lymph node metastases (53%) and distant metastases (67%) were significantly lower compared with [^{18}F]-FDG-PET (77% and 100% respectively) and [^{18}F]-FLT was interpreted less suitable for tumor staging. In contrast, [^{18}F]-FLT-PET was accurate for imaging malignant lymphomas.

[^{18}F]-FLT is not or only marginally incorporated into DNA (<2%) and therefore not a direct measure of proliferation [122]. *In vitro* studies indicated that [^{18}F]-FLT uptake is closely related to thymidine kinase 1 (TK1) activity and respective protein levels [117,118]. [^{18}F]-FLT is therefore considered to reflect TK1 activity and hence, S-phase fraction rather than DNA synthesis. Although being a poor substrate for type 1 equilibrative nucleoside transporters (ENT), cellular uptake of [^{18}F]-FLT is further facilitated by redistribution of nucleoside transporters to the cellular membrane after inhibition of endogenous synthesis of thymidylate (TMP) (*de novo* synthesis of TMP) [125]. However, the detailed uptake mechanism of [^{18}F]-FLT is yet unknown and the influence of membrane transporters and various nucleoside metabolizing enzymes remains to be determined.

[^{18}F]-FLT-PET produces images of high contrast of both malignant tumors and proliferating tissues. Because of high physiological tracer uptake in proliferating bone marrow, the sensitivity of [^{18}F]-FLT for detecting tumor manifestations in bone marrow may be reduced. [^{18}F]-FLT undergoes glucuronization, leading to enhanced liver uptake. Decreased sensitivity rates were described for liver metastases from various solid tumors [120,124]. Because of negligible background uptake of [^{18}F]-FLT in the brain, specific imaging of proliferation may be appropriate for detection of tumors or metastases in the central nervous system.

Recently, [^{18}F]-FLT was suggested for therapeutic monitoring using various experimental settings. In an animal model of fibrosarcoma it was reported that [^{18}F]-FLT uptake decreased early after antiproliferative treatment with 5-fluorouracil or cisplatin [126,127]. In a mouse lymphoma xenotransplant model, significant decrease of [^{18}F]-FLT uptake was observed already 48 h after chemotherapy with cyclophosphamide [126]. An early reduction of tumoral [^{18}F]-FLT uptake was further demonstrated 48 h after treatment with tyrosine kinase inhibitors in a lung cancer xenograft model [128]. However, data are preliminary and clinical trials are needed to further validate [^{18}F]-FLT as marker for therapy response. Moreover, the lower uptake of [^{18}F]-FLT compared with [^{18}F]-FDG may result in a reduced sensitivity to detect residual disease after treatment. As previously reported for the standard radiotracer [^{18}F]-FDG, false-positive findings may also occur at [^{18}F]-FLT-PET because an increased proliferation rate is

not specific for malignant tumors. However, false-positive results have not yet been described in the literature.

In conclusion, specific imaging of proliferative activity with $[^{18}\text{F}]$ -FLT is feasible. The use of $[^{18}\text{F}]$ -FLT as PET tracer showed advantages for detection of lymphomas in the central nervous system and the mediastinum. $[^{18}\text{F}]$ -FLT-PET was suitable to differentiate indolent and aggressive tumors and to indicate progression to a more aggressive histology. However, a significantly reduced tracer uptake compared with the standard radiotracer $[^{18}\text{F}]$ -FDG has been observed in a variety of solid neoplasms, indicating that $[^{18}\text{F}]$ -FDG is superior to $[^{18}\text{F}]$ -FLT regarding detection of tumor manifestation sites. $[^{18}\text{F}]$ -FLT-PET has a potential especially for early assessment of therapy response which has to be validated in further experimental and clinical studies.

3.2. PET/CT studies of tumor hypoxia

Malignant tumors often exhibit increased levels of hypoxia. Hypoxia is associated with poor response to therapy and poor clinical outcome. With hypoxia, an increase in the malignant potential of the tumor cell has been observed. Oxygen is an important factor for the sustained action of radiation-induced cytotoxic products in tissues. Well-oxygenated cells are more sensitive to the cytotoxic effects of ionizing radiation compared with poorly oxygenated cells. Hypoxic tumors are not sensitive to conventional doses of radiation therapy. In fact, the doses of radiation therapy have to be increased in order to achieve the same cytotoxic effects compared to tissues with normal oxygenation. Furthermore, hypoxia promotes resistance to antitumor chemotherapeutic agents. A systemic or local increase of the oxygen supply to tumors (hyperbaric oxygen, hyper fractionation, pretreatment transfusion and radiation sensitizers) has generally failed to demonstrate significant treatment benefits if performed in conjunction with radiation therapy.

Since tumor hypoxia constitutes a major difference between tumor and normal tissues, therapeutic approaches based on that phenomenon have been introduced. Examples are bioreductive drugs or hypoxia-selective cytotoxins, which are inactive prodrugs that are favorably activated by reductive enzymes only in the hypoxic environment of tumors. Upon activation they release toxic metabolites that can cause cell damage and death by various mechanisms. In lung cancer and head and neck cancer promising results have been achieved with hypoxia-activated drugs such as tirapazamine in addition to chemotherapy. Because tumor size or grade, extent of necrosis and blood hemoglobin status show only weak correlation with tumor hypoxia, these clinical and pathological parameters are not suitable to select patients for hypoxia-directed therapies. Furthermore, these parameters are too unreliable to accurately predict tumor prognosis.

Methods to assess tumor hypoxia can be classified as *in vivo* (invasive—polarographic measurements/non-invasive—imaging) and *ex vivo* (invasive—biopsy)

approaches. Several methods have been introduced to evaluate tumor oxygenation and to predict patient outcome in cervix [129], lung [130], head and neck cancers [131–133] as well as gliomas [134]. A major finding in all these studies is the considerable heterogeneity exhibited by these malignancies as well as marked interpatient variability. PET imaging has emerged as a promising noninvasive tool to accurately characterize tumor oxygenation. PET and PET/CT allow the *in vivo* mapping of regional tumor hypoxia with adequate anatomical resolution as well as monitoring of therapy through follow-up mapping of hypoxia.

Derivatives of misonidazole—an azomycin-based hypoxic cell sensitizer that was introduced in radiation oncology decades ago—have been successfully labeled with positron emitters. [^{18}F]-fluoromisonidazole is a radiopharmaceutical directly derived from misonidazole and is the most extensively studied PET agent for hypoxia of these derivatives. Alternative nitroimidazole radiopharmaceuticals for PET imaging have been developed by changing the properties of the tracers, especially with respect to blood clearance [135,136]. [^{18}F]-fluoroerythronitroimidazole ([^{18}F]-FETNIM) has been introduced as a more hydrophilic derivative of misonidazole with potentially more rapid plasma clearance. [^{18}F]-fluoroazomycin arabinoside is currently being evaluated in *in vitro* and clinical studies [137]. Besides nitroimidazole compounds, the direct reduction of metal complexes such as Tc- $^{99\text{m}}$ -labeled dioximes (HL91) and Cu-60,62,64-labeled methylthiosemicarbazone (Cu-ATSM) [138] have been evaluated for tumor hypoxia imaging.

Molecular imaging with hypoxia-specific PET tracers has great potential as a tool to identify patients who may benefit from changes in their therapeutic regimen. Numerous PET studies evaluating hypoxia in different tumor types have been conducted over recent years including cervical cancer [139], head and neck cancer [140–148, Souvatoglou 2007], lung cancer [139,145,149–151], soft tissue carcinoma [141,152], colorectal cancer [153], breast cancer [141], brain tumors [141,154,155], renal cancer [156] and prostate cancer [141,147].

Several groups have demonstrated the potential to monitor the effect of a therapy in cancer using PET-based imaging of hypoxia [148,150,152]. Other authors have shown that hypoxia imaging predicts response (responders vs. nonresponders) in patients undergoing radiation therapy, chemotherapy or both [139, 145,157]. Furthermore, studies provide evidence that pre-therapy hypoxia is predictive of disease free survival and overall survival [139,157]. More recently it has been demonstrated that PET/CT allows quantification of regional hypoxia within a tumor independent of its anatomical localization. Additionally, PET/CT at the same time offers an efficient tool for whole-body staging and functional assessment within one imaging modality. A particular advantage of PET/CT lies in its ability to assess exact tumor volume; and volumetry is important for the analysis of hypoxic fractional volume when planning radiation treatment.

PET and PET/CT therefore enable to assess regional tumor hypoxia and associated tumor heterogeneity. Less spatial heterogeneity in hypoxia might represent a more localized process. The former is more likely to be accessible by a

more general or systemic approach such as hypoxic cell cytotoxines (e.g. tirapazamine). The latter more focal hypoxia probably would be treated with a local/regional approach such as intensity-modulated radiation therapy (IMRT).

3.3. $[^{18}\text{F}]$ -Galacto-RGD-PET: Imaging of $\alpha_v\beta_3$ integrin expression

A variety of disorders is characterized by an imbalance of the angiogenic process or induction of neovascularization. Thus, noninvasive monitoring of molecular processes during angiogenesis would supply helpful information for clinicians as well as for basic scientists. One target structure involved is the integrin $\alpha_v\beta_3$, which mediates migration of activated endothelial cells [158]. Integrins are heterodimeric transmembrane glycoproteins consisting of an α - and a β -subunit. It was found that several extracellular matrix (ECM) proteins like vitronectin, fibrinogen and fibronectin interact via the amino acid sequence arginine-glycine-aspartic acid (RGD, amino acid single letter code) with the integrins. Based on these findings, linear as well as cyclic peptides including the RGD sequence have been introduced as tracers (for review see [159]). Kessler and co-workers developed the pentapeptide cyclo(-Arg-Gly-Asp-DPhe-Val-) [160], which showed high affinity and selectivity for $\alpha_v\beta_3$. This peptide is the most prominent lead structure for the development of radiotracers for the noninvasive determination of $\alpha_v\beta_3$ expression [161]. In the last few years various radiolabeled peptides have been developed for the noninvasive determination of $\alpha_v\beta_3$ expression using nuclear medicine tracer techniques. Most of the radiolabeled peptides show high affinity and selectivity for the integrin $\alpha_v\beta_3$ *in vitro* and receptor-specific accumulation in the tumor *in vivo*. Most studies have been carried out with the glycosylated RGD peptides $[^*\text{I}]\text{gluco-RGD}$ and $[^{18}\text{F}]\text{-galacto-RGD}$. With $[^{18}\text{F}]\text{-galacto-RGD}$ it was demonstrated in a murine melanoma model that noninvasive quantification of the $\alpha_v\beta_3$ expression as well as repetitive monitoring of the inhibition of the receptor with $\alpha_v\beta_3$ antagonists is possible. Moreover, additional studies showed that $[^{18}\text{F}]\text{-galacto-RGD}$ and PET are sensitive enough to image $\alpha_v\beta_3$ expression on activated endothelial cells during tumor-induced angiogenesis [162]. Initial patient studies have demonstrated that $[^{18}\text{F}]\text{-galacto-RGD}$ has a favorable biodistribution in humans with a slowly reversible, specific tracer uptake [163]. The dosimetry revealed very similar results as the commonly applied PET tracer $[^{18}\text{F}]\text{-FDG}$ [164]. Finally it was also confirmed in patients that the tracer accumulation in the tumor correlates with $\alpha_v\beta_3$ expression (Fig. 4) [165].

However, $\alpha_v\beta_3$ can be expressed on tumor cells as well as on endothelial cells, making it difficult to attribute the resulting signal exclusively to molecular processes during tumor-induced angiogenesis. Thus, in cancer the most obvious use of this class of tracer could be for planning and controlling $\alpha_v\beta_3$ -directed therapies. The value of noninvasive techniques for appropriate selection of patients who may benefit from such therapies is demonstrated by initial clinical

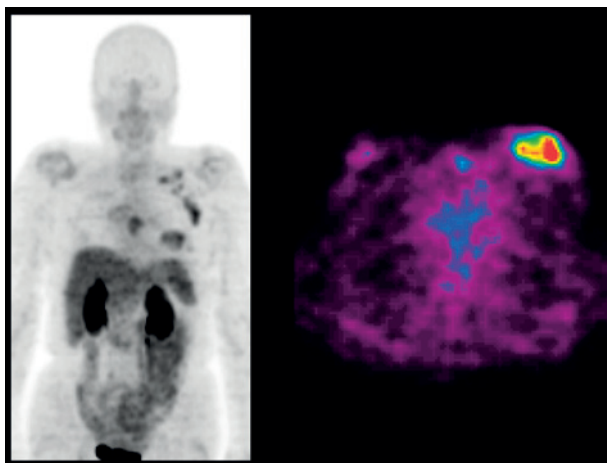


Fig. 4. Patient with breast cancer: Staging with [^{18}F]-RGD-PET. (See Colour Plate Section at the end of this book.)

studies using [^{18}F]-galacto-RGD and PET [163,165]. These studies also revealed high inter- and intraindividual variance in tracer accumulation in lesions, indicating great diversity in receptor expression. Whether this new technique may have an additional impact as a novel prognostic indicator in cancer will need to be demonstrated in further studies. However, some evidence of prognostic value has been provided by Gasparini *et al.* [166], who found $\alpha_v\beta_3$ expression in tumor vasculature to be a significant prognostic factor.

Integrin $\alpha_v\beta_3$ expression is found on endothelial cells not only during tumor-induced angiogenesis but also for example during wound healing, in rheumatoid arthritis, in psoriatic plaques and during restenosis [167]. Preclinical studies showing that radiolabeled RGD peptides specifically accumulate in chronic inflamed tissue and preliminary data from patients with villonodular synovitis indicate that this new technique may become a new biomarker for disease activity in inflammatory processes [168]. Moreover, for diseases where no tumor mass is involved, the corresponding signal should predominantly correlate with $\alpha_v\beta_3$ expression on endothelial cells and may thus allow monitoring of molecular processes during neovascularization.

3.4. [^{18}F]-Fluorocholine-PET: Imaging of prostate cancer

3.4.1. Biochemical rationale

In the human body choline is needed for the synthesis of phospholipids in cell membranes, methyl metabolism, transmembrane signaling and lipid cholesterol transport and metabolism [169]. It is transported into mammalian cells by a high-affinity sodium-dependent transport system. Intracellular choline is metabolized to phosphorylcholine, the reaction being catalyzed by the enzyme choline

kinase. This is followed by the synthesis of phosphatidyl choline, which constitutes a main component of cell membranes. It may also undergo acetylation to form acetylcholine or oxidation to form betaine. Once phosphorylated the polar phosphorylcholine molecule is trapped within the cell. Various studies have revealed an upregulation of high-affinity choline transport system as well as increase choline kinase activity in cancer cells [170–172].

Based on these observations, choline was radiolabeled and introduced for imaging of malignancies [173–176]. Its main application is in the assessment of prostate cancer. Although $[^{18}\text{F}]$ -FDG has gained an established role in the diagnosis and in staging and restaging of various malignancies, its value in the assessment of patients with prostate cancer is limited. $[^{18}\text{F}]$ -FDG is excreted by the kidneys, an undesirable property when pelvic malignancies are to be examined. Additionally a large fraction of prostate cancer exhibits a relatively slow metabolic rate leading to lower $[^{18}\text{F}]$ -FDG uptake compared with other cancers [177].

3.4.2. Compounds, biodistribution, and imaging

Initially choline, $(\text{CH}_3)_3\text{N}^+\text{CH}_2\text{CH}_2\text{OH}$ = trimethyl-2-hydroxyethylamminium, was introduced for tumor imaging labeled with $[^{11}\text{C}]$ by Hara *et al.* [175,176]. However, the short half-life of $[^{11}\text{C}]$ (20 min) limits its use in institutions with a cyclotron on site. This led to the development of $[^{18}\text{F}]$ (half-life 110 min) labeled choline taking also advantage of the better physical properties for imaging of ^{18}F compared with $[^{11}\text{C}]$ [178]. Two compounds of $[^{18}\text{F}]$ -labeled choline analoga are currently in use: 2- $[^{18}\text{F}]$ -fluoroethyl-dimethyl-2-hydroxyethyl-ammonium ($[^{18}\text{F}]$ -FEC) and $[^{18}\text{F}]$ -fluoromethyl-dimethyl-2-hydroxyethylammonium choline ($[^{18}\text{F}]$ -FCH) [178,179].

The normal biodistribution is similar for both compounds: they both show rapid clearance from the blood pool and accumulate in the salivary glands, the liver, the spleen, and the renal cortex. The primary mode of excretion is via the urinary tract, appearing in the urinary bladder 3–5 min after injection. This necessitates early imaging, which should commence at about 1 min after intravenous injection. The typical injected dose is about 250 MBq and the effective dose equivalent calculated for $[^{18}\text{F}]$ -FCH is 3.5×10^{-2} mSv/MBq, the critical organ being the kidney receiving 0.17 mSv/MBq [180]. However, there are some distinct differences characterizing the two analoga. First, $[^{18}\text{F}]$ -FEC concentration in the prostate reaches its highest activity at 55 min p.i., whereas $[^{18}\text{F}]$ -FCH uptake shows a peak at approximately 3 min p.i. followed by a plateau [178,179]. Therefore, an additional late image after bladder emptying is recommended when $[^{18}\text{F}]$ -FEC is used. Second, *in vitro* studies (cultured PC-3 human prostate cells) revealed that cellular uptake and phosphorylation by cholin kinase are very similar for $[^{18}\text{F}]$ -FCH and natural choline but are lower for $[^{18}\text{F}]$ -FEC [181].

3.4.3. Clinical studies

The role of [^{18}F]-choline in the primary diagnosis and staging of prostate cancer is still under debate. First studies indicate that there is increased uptake of [^{18}F]-FEC and [^{18}F]-FCH in the prostate tumor and in lymph node and bone metastases [178,179,182–184]. In a direct comparison with [^{18}F]-FDG, [^{18}F]-FCH proved to be better for detecting androgen-dependent and androgen-independent prostate cancer and its metastases [185]. However, like [^{18}F]-FDG, [^{18}F]-choline is not a cancer-specific agent. Nonspecific uptake of [^{18}F]-choline in granulocytes and macrophages has been described [186]. In the prostate it accumulates, apart from the tumor, in benign prostate hyperplasia (BPH) and in prostatitis and it remains unclear if these can be discriminated by means of intensity of the uptake. In a study correlating the histopathologic prostate specimen with the transversal slice of the PET/CT images obtained after [^{18}F]-FCH injection in nine patients who underwent prostatectomy because of prostate cancer Schmid *et al.* [183] reported that it was not possible to discriminate benign hyperplasia from cancerous prostate lesions by means of SUV. In contrast to those results, Kwee *et al.* reported in a study in which in five patients the histopathologic prostate specimen was compared with the [^{18}F]-fluorocholine-PET scan on a sextant-to-sextant basis, that they could discriminate benign hyperplasia from cancerous prostate lesions based on the wash out the benign lesions showed in late imaging [182].

First studies indicate that [^{18}F]-fluorocholine is a promising imaging tracer for localizing biochemical recurrence after prostate cancer. Heinisch *et al.* localized the PSA relapse in 8/17 patients with a PSA < 5 ng/ml [184]. Schmid *et al.* localized the biochemical recurrence in 9/9 patients with a mean PSA of 14.1 ng/ml \pm 15.3 ng/ml (range: 0.7–46.3 ng/ml) [183]. In the first study in a large patient cohort (n = 100) Cimitan *et al.* detected one or more areas of high [^{18}F]-FCH uptake in 54/100 patients (PSA range: 0.22–511.79 ng/ml). Most of the patients with a negative [^{18}F]-FCH-PET/CT scan (87%) had a Gleason score of the primary tumor ≤ 7 [187].

Despite these initial promising results, further studies are needed to determine the exact indications for using [^{18}F]-fluorocholine in the diagnostic algorithm of patients with prostate cancer and to assess the influence of different factors including hormonal therapy, PSA level and PSA doubling time on the uptake of the tracer in the cancer lesions.

3.5. [^{18}F]-Fluoride-PET: Imaging of bone metastases

[^{18}F]-fluoride has a long history as a tracer for bone imaging. In 1962, this tracer was first introduced by Blau *et al.* [188]. [^{18}F]-fluoride-PET imaging combines the superior pharmacokinetic properties of ^{18}F -fluoride (compared with those of [$^{99\text{m}}\text{Tc}$]-polyphosphonates) and the improved spatial resolution and lesion

contrast of PET technology (compared with those of planar and even SPECT gamma camera imaging). $[^{18}\text{F}]$ -fluoride has higher bone uptake and faster blood clearance, resulting in a better target-to-background ratio [189–192].

Schirrmeyer *et al.* prospectively evaluated the clinical value of planar bone scans, SPECT and $[^{18}\text{F}]$ -labeled sodium fluoride in 53 patients with newly diagnosed lung cancer [193]. Twelve of the 53 patients turned out to have bone metastases. $[^{18}\text{F}]$ -fluoride-PET detected all patients with bone metastases, whereas bone scan and SPECT produced false-negative results (6 vs. 1). An area under the curve analysis (ROC) proved $[^{18}\text{F}]$ -fluoride-PET to be the most accurate whole-body imaging modality for screening of bone metastases in this study.

$[^{18}\text{F}]$ -fluoride-PET is a very sensitive method for detection of bone lesions; however, increased $[^{18}\text{F}]$ -fluoride uptake is not specific for tumoral bone involvement and may also lead to a higher detection rate of benign bone lesions. Even the lesion-to-background ratios cannot differentiate benign from malignant $[^{18}\text{F}]$ -fluoride uptake [192]. In clinical practice $[^{18}\text{F}]$ -fluoride findings have to be correlated with morphological imaging modalities such as CT and MRI.

The introduction of integrated PET/CT devices suggested an improved diagnostic accuracy in tumor detection using $[^{18}\text{F}]$ -fluoride as the tumor-imaging agent. In 2004, Even-Sapir *et al.* compared $[^{18}\text{F}]$ -fluoride-PET and $[^{18}\text{F}]$ -fluoride-PET/CT for the assessment of bone lesions in a study population of 44 patients with oncological disease and malignant osseous disease [194]. In a patient-based analysis, $[^{18}\text{F}]$ -fluoride-PET/CT revealed to be significantly more sensitive than $[^{18}\text{F}]$ -fluoride-PET (100% vs. 88%; $p < 0.05$). The corresponding specificity was also higher (88% vs. 56%) but not statistically significant. The authors therefore concluded that $[^{18}\text{F}]$ -fluoride-PET/CT accurately differentiates malignant from benign bone lesions.

In another study by the same group, $[^{18}\text{F}]$ -fluoride-PET/CT was compared with $[^{18}\text{F}]$ -fluoride-PET, bone scintigraphy and SPECT in 44 patients with high-risk prostate cancer [195]. For detection of skeletal metastatic spread $[^{18}\text{F}]$ -fluoride-PET/CT revealed to be significantly more sensitive and specific than bone scintigraphy ($p < 0.05$) and SPECT ($p < 0.05$), and significantly more specific than $[^{18}\text{F}]$ -fluoride-PET ($p < 0.001$).

According to Langsteger *et al.* $[^{18}\text{F}]$ -fluoride seems to better visualize bone metastases in $[^{18}\text{F}]$ -FDG negative tumors, such as renal cell and thyroid carcinoma and in $[^{18}\text{F}]$ -FDG avid tumors under therapy [196].

3.6. $[^{18}\text{F}]$ FET-PET: Imaging with amino acids

Malignant neoplasms of the nervous system occur with an incidence of 5–6/100,000 inhabitants/year [197]. Besides meningiomas cerebral gliomas are the most frequent primary brain tumors. Primary treatment comprises surgical resection, irradiation and chemotherapy. However, survival and quality of life are still limited. For the diagnosis and differential diagnosis of brain tumors,

MRI is the diagnostic modality of choice. Tumor localization as well as alterations of the blood brain barrier can be characterized for most tumors. However, the differentiation of tumor tissue and cerebral edema is difficult.

Radiolabeled amino acids have been introduced as SPECT and PET tracers that allow a precise delineation of brain tumor in cerebral gliomas and differentiation of tumor tissue and edema. Radiolabeled amino acids are taken up by specific amino acid transporters in glioma cells [198–201]. Recently O-(2-[^{18}F] fluorethyl)-L-tyrosin ([^{18}F]FET) has been introduced as PET brain tumor imaging tracer [202,203].

The assessment of the extent of a brain tumor and the localization of the area with the highest proliferation is important for the characterization of the tumor, prognosis and therapy management. In a recent study by Pauleit *et al.* with [^{18}F]FET-PET it was shown that in patients with cerebral gliomas and a characterization of tumor extent based on MRI only in 53% of the cases the MR signal corresponded to tumor tissue as verified by biopsy [204]. Combined MRI and [^{18}F]FET-PET could increase the percentage of correctly identified tumor manifestation to 94% of the cases documenting the important diagnostic value of [^{18}F]FET-PET. Therefore, imaging with radiolabeled amino acids improves the guidance of biopsies and minimizes biopsies in brain tissue not affected by tumor. Moreover imaging of cerebral gliomas with radiolabeled amino acids holds promise to enable a more precise surgical management and improved radiation treatment planning [205].

Studies have demonstrated a correlation of amino acid uptake with the grading in cerebral gliomas. However, a considerable overlap has been observed in most studies so that an exact assessment of the differentiation of gliomas remains difficult. Recent studies provide evidence that based on kinetic analyses [^{18}F]FET-PET data might allow to differentiate between low- and high-grade gliomas as well as recurrence of gliomas [206,207].

The differentiation of recurrent glioma from post-therapeutic changes by MRI is difficult, because recurrent disease as well as necrotic tissue after radiotherapy or chemotherapy is accompanied by contrast agent enhancement [208–210]. [^{18}F]FET-PET as other radiolabeled amino acid tracers has a high sensitivity and specificity for the detection of recurrent disease and differentiation of post-therapeutic changes from tumor manifestation. In a study in 53 patients with suspected recurrence of cerebral glioma, [^{18}F]FET-PET correctly revealed recurrence in 42 patients and excluded recurrence in 11 patients [211]. Comparing [^{18}F]FET-PET and MRI, Rachinger *et al.* showed a sensitivity of 100% and a specificity of 93% for [^{18}F]FET-PET and a sensitivity of 93% and a specificity of 50% for MRI [212].

In recent therapy assessment studies promising results with [^{18}F]FET-PET have been obtained. Sequential [^{18}F]FET-PET studies during locoregional chemotherapy and radioimmunotherapy show a high correlation between the [^{18}F]FET uptake and the response of the tumor to treatment [213,214].

3.7. $[^{18}\text{F}]$ Fluorodopa-PET: Imaging with amino precursors

Fluorinated dihydroxyphenylalanine $[^{18}\text{F}]$ DOPA is a precursor for the neurotransmitter dopamine and is commonly used in the imaging of Parkinson's disease. In oncological imaging $[^{18}\text{F}]$ DOPA has been assessed for imaging of brain tumors, advanced neuroendocrine tumors and medullary thyroid cancer [215].

Becherer *et al.* evaluated $[^{18}\text{F}]$ DOPA for brain tumor imaging in 20 patients with primary brain lesions, cerebral metastases or nonneoplastic cerebral lesions and compared it with $[^{11}\text{C}]$ methionine ($[^{11}\text{C}]$ -MET). $[^{18}\text{F}]$ DOPA and $[^{11}\text{C}]$ MET matched in all patients and showed all lesions as hot spots with higher uptake than in the contralateral brain [216]. Becherer *et al.* therefore concluded that $[^{18}\text{F}]$ DOPA is equivalent to MET imaging in amino acid transport in malignant cerebral lesions and combines the good physical properties of $[^{18}\text{F}]$ with the pharmacological properties of methionine. In a study by Chen *et al.* $[^{18}\text{F}]$ DOPA-PET revealed a high-diagnostic accuracy for detection of brain tumors (sensitivity: 98%, specificity: 86%) but showed no significant difference in tumor uptake between low- and high-grade tumors. In comparison to $[^{18}\text{F}]$ FDG-PET, $[^{18}\text{F}]$ DOPA-PET proved to be more accurate for evaluation of recurrent tumors and imaging of low-grade tumors [217].

Another interesting entity for $[^{18}\text{F}]$ DOPA-PET is the imaging of neuroendocrine tumors (NETs). NETs are capable of taking up amino acids, converting them by means of decarboxylation into biogenic amines, which are finally stored in cell vesicles; the physiological distribution of DOPA is mostly seen in the gallbladder, bile and intestine (duodenum, pancreas). Becherer *et al.* compared $[^{18}\text{F}]$ DOPA-PET with $[^{111}\text{In}]$ somatostatin receptor scintigraphy (SRS) in 23 patients with histologically verified NETs in advanced stages. $[^{18}\text{F}]$ DOPA was most accurate in detecting skeletal lesions but was limited in the lung. However, it was more accurate than SRS in all organs [218]. Montravers *et al.* investigated if $[^{18}\text{F}]$ DOPA-PET is accurate for the diagnosis and follow-up of any type of well-differentiated digestive endocrine tumor [219]. In 30 patients referred for documented well-differentiated digestive endocrine tumor, $[^{18}\text{F}]$ DOPA-PET revealed a significantly better sensitivity and accuracy for carcinoid tumors than for noncarcinoid tumors (93% and 89% vs. 25% and 36%; $p < 0.01$). In contrast, SRS showed no significant difference in accuracy according to the carcinoid or noncarcinoid type. Therefore, Montravers *et al.* concluded that $[^{18}\text{F}]$ DOPA-PET appears to be useful in carcinoid tumors, but for noncarcinoid tumors SRS appeared to be the better diagnostic tool.

In 11 patients with medullary thyroid carcinoma Hoegerle *et al.* compared $[^{18}\text{F}]$ -DOPA-PET with $[^{18}\text{F}]$ FDG-PET, SRS and conventional imaging [220]. A total of 27 tumors were studied and the corresponding sensitivities were 63% for $[^{18}\text{F}]$ DOPA-PET, 44% for $[^{18}\text{F}]$ -FDG-PET, 52% for SRS and 81% for conventional imaging. With respect to lymph node staging, the best results were obtained with $[^{18}\text{F}]$ DOPA-PET.

ACKNOWLEDGMENTS

We appreciate the excellent contributions made by our colleagues PD Dr. Andreas Buck, Dr. Ambros Beer, Dr. Michael Souvatzoglou, and Mrs. Christine Praus.

REFERENCES

- [1] K. Hamacher, H.H. Coenen, G. Stocklin, Efficient stereospecific synthesis of no-carrier-added 2- ^{18}F -fluoro-2-deoxy-D-glucose using aminopolyether supported nucleophilic substitution, *J. Nucl. Med.* 27(2) (1986) 235–238.
- [2] W.A. Weber, S.I. Ziegler, R. Thodtmann, A.R. Hanauske, M. Schwaiger, Reproducibility of metabolic measurements in malignant tumors using FDG PET, *J. Nucl. Med.* 40(11) (1999) 1771–1777.
- [3] T. Beyer, D.W. Townsend, T. Brun, P.E. Kinahan, M. Charron, R. Roddy, J. Jerin, J. Young, L. Byars, R. Nutt, A combined PET/CT scanner for clinical oncology, *J. Nucl. Med.* 41(8) (2000) 1369–1379.
- [4] Krebs in Deutschland, Häufigkeiten und Trends, Robert Koch Institut; (2006).
- [5] I.J. Adam, M.O. Mohamdee, I.G. Martin, N. Scott, P.J. Finan, D. Johnston, M. F. Dixon, P. Quirke, Role of circumferential margin involvement in the local recurrence of rectal cancer, *Lancet* 344(8924) (1994) 707–711.
- [6] W. Willmanns, D. Huhn, K. Wilms, *Internistische Onkologie*, Georg Thieme, Stuttgart, 1994.
- [7] B. Djulbegovic, D.M. Sullivan, *Decision Making in Oncology: Evidence-Based Management*, Churchill Livingstone, New York, 1997.
- [8] D.J. Ott, N.T. Wolfman, E.S. Scharling, R.J. Zagoria, Overview of imaging in colorectal cancer, *Dig. Dis.* 16(3) (1998) 175–182.
- [9] R.H. Huebner, K.C. Park, J.E. Shepherd, J. Schwimmer, J. Czernin, M.E. Phelps, S. S. Gambhir, A meta-analysis of the literature for whole-body FDG PET detection of recurrent colorectal cancer, *J. Nucl. Med.* 41(7) (2000) 1177–1189.
- [10] N.C. Saenz, B. Cady, W.V. McDermott Jr., G.D. Steele Jr., Experience with colorectal carcinoma metastatic to the liver, *Surg. Clin. North Am.* 69(2) (1989) 361–370.
- [11] G. Steele Jr., R. Bleday, R.J. Mayer, A. Lindblad, N. Petrelli, D. Weaver, A prospective evaluation of hepatic resection for colorectal carcinoma metastases to the liver: Gastrointestinal Tumor Study Group Protocol (6584), *J. Clin. Oncol.* 9(7) (1991) 1105–1112.
- [12] L.G. Strauss, J.H. Clorius, B. Kimmig, A. Dimitrakopoulou, M. Marin-Grez, R. Engenhart, P. Schraube, Imaging positron emitting radionuclides generated during radiation therapy, *Eur. J. Radiol.* 9(4) (1989) 200–202.
- [13] H. Abdel-Nabi, R.J. Doerr, D.M. Lamonica, V.R. Cronin, P.J. Galantowicz, G. M. Carbone, M.B. Spaulding, Staging of primary colorectal carcinomas with fluorine-18 fluorodeoxyglucose whole-body PET: Correlation with histopathologic and CT findings, *Radiology* 206(3) (1998) 755–760.
- [14] T. Arulampalam, D. Costa, D. Visvikis, P. Boulos, I. Taylor, P. Ell, The impact of FDG-PET on the management algorithm for recurrent colorectal cancer, *Eur. J. Nucl. Med.* 28(12) (2001) 1758–1765.
- [15] F.A. Calvo, M. Domper, R. Matute, R. Martinez-Lazaro, J.A. Arranz, M. Desco, E. Alvarez, J.L. Carreras, ^{18}F -FDG positron emission tomography staging and restaging in rectal cancer treated with preoperative chemoradiation, *Int. J. Radiat. Oncol. Biol. Phys.* 58(2) (2004) 528–535.
- [16] M. Dietlein, W. Weber, M. Schwaiger, H. Schicha, ^{18}F -Fluorodeoxyglucose positron emission tomography in restaging of colorectal cancer, *Nuklearmedizin* 42(4) (2003) 145–156.

- [17] I. Kantorova, L. Lipska, O. Belohlavek, V. Visokai, M. Trubac, M. Schneiderova, Routine (18)F-FDG PET preoperative staging of colorectal cancer: Comparison with conventional staging and its impact on treatment decision making, *J. Nucl. Med.* 44(11) (2003) 1784–1788.
- [18] M. Lonneux, A.M. Reffad, R. Detry, A. Kartheuser, J.F. Gigot, S. Pauwels, FDG-PET improves the staging and selection of patients with recurrent colorectal cancer, *Eur. J. Nucl. Med. Mol. Imaging* 29(7) (2002) 915–921.
- [19] M. Mukai, S. Sadahiro, S. Yasuda, H. Ishida, N. Tokunaga, T. Tajima, H. Makuuchi, Preoperative evaluation by whole-body ¹⁸F-fluorodeoxyglucose positron emission tomography in patients with primary colorectal cancer, *Oncol. Rep.* 7(1) (2000) 85–87.
- [20] L. Staib, H. Schirrmeister, S.N. Reske, H.G. Beger, Is (18)F-fluorodeoxyglucose positron emission tomography in recurrent colorectal cancer a contribution to surgical decision making, *Am. J. Surg.* 180(1) (2000) 1–5.
- [21] L.G. Strauss, J.H. Clorius, P. Schlag, B. Lehner, B. Kimmig, R. Engenhart, M. Marin-Grez, F. Helus, F. Oberdorfer, P. Schmidlin, Recurrence of colorectal tumors: PET evaluation, *Radiology* 170(2) (1989) 329–332.
- [22] M.H. Whiteford, H.M. Whiteford, L.F. Yee, O.A. Ogunbiyi, F. Dehdashti, B.A. Siegel, E.H. Birnbaum, J.W. Fleshman, I.J. Kodner, T.E. Read, Usefulness of FDG-PET scan in the assessment of suspected metastatic or recurrent adenocarcinoma of the colon and rectum, *Dis. Colon. Rectum.* 43(6) (2000) 759–767.
- [23] V. Kalff, R.J. Hicks, R.E. Ware, A. Hogg, D. Binns, A.F. McKenzie, The clinical impact of (18)F-FDG PET in patients with suspected or confirmed recurrence of colorectal cancer: A prospective study, *J. Nucl. Med.* 43(4) (2002) 492–499.
- [24] T.J. Ruers, B.S. Langenhoff, N. Neeleman, G.J. Jager, S. Strijk, T. Wobbes, F. H. Corstens, W.J. Oyen, Value of positron emission tomography with [F-18] fluorodeoxyglucose in patients with colorectal liver metastases: A prospective study, *J. Clin. Oncol.* 20(2) (2002) 388–395.
- [25] M. Simo, F. Lomena, J. Setoain, G. Perez, P. Castellucci, J.M. Costansa, J. Setoain-Quinquer, F. Domenech-Torne, I. Carrio, FDG-PET improves the management of patients with suspected recurrence of colorectal cancer, *Nucl. Med. Commun.* 23(10) (2002) 975–982.
- [26] P.M. Falk, N.C. Gupta, A.G. Thorson, M.P. Frick, B.M. Boman, M.A. Christensen, G. J. Blatchford, Positron emission tomography for preoperative staging of colorectal carcinoma, *Dis. Colon. Rectum.* 37(2) (1994) 153–156.
- [27] L.G. Strauss, J.H. Clorius, P. Schlag, B. Lehner, B. Kimmig, R. Engenhart, M. Marin-Grez, F. Helus, F. Oberdorfer, P. Schmidlin, Recurrence of colorectal tumors: PET evaluation, *Radiology* 170(2) (1989) 329–332.
- [28] C. Cohade, M. Osman, J. Leal, R.L. Wahl, Direct comparison of (18)F-FDG PET and PET/CT in patients with colorectal carcinoma, *J. Nucl. Med.* 44(11) (2003) 1797–1803.
- [29] I.R. Kamel, C. Cohade, E. Neyman, E.K. Fishman, R.L. Wahl, Incremental value of CT in PET/CT of patients with colorectal carcinoma, *Abdom. Imaging* 29(6) (2004) 663–668.
- [30] J.H. Kim, J. Czernin, M.S. Len-Auerbach, B.S. Halpern, B.J. Fueger, J.R. Hecht, O. Ratib, M.E. Phelps, W.A. Weber, Comparison between ¹⁸F-FDG PET, in-line PET/CT, and software fusion for restaging of recurrent colorectal cancer, *J. Nucl. Med.* 46(4) (2005) 587–595.
- [31] H. Strunk, J. Bucerius, U. Jaeger, A. Joe, S. Flacke, M. Reinhardt, N. Hortling, H. Palmedo, Combined FDG PET/CT imaging for restaging of colorectal cancer patients: Impact of image fusion on staging accuracy, *Rofo* 177(9) (2005) 1235–1241.
- [32] S.S. Gambhir, P. Valk, J.E. Shepherd, C.K. Hoh, M. Allen, M.E. Phelps, Cost-effective analysis modeling of the role of FDG PET in the management of patients

- with recurrent colorectal cancer, *J. Nucl. Med.* 38(38) (1997) 90–91Ref Type: Abstract.
- [33] K.C. Park, J. Schwimmer, J.E. Shepherd, M.E. Phelps, J.R. Czernin, C. Schiepers, S.S. Gambhir, Decision analysis for the cost-effective management of recurrent colorectal cancer, *Ann. Surg.* 233(3) (2001) 310–319.
 - [34] P.E. Valk, T.R. Pounds, R.D. Tesar, D.M. Hopkins, M.K. Haseman, Cost-effectiveness of PET imaging in clinical oncology, *Nucl. Med. Biol.* 23(6) (1996) 737–743.
 - [35] C. Lejeune, M.J. Bismuth, T. Conroy, C. Zanni, P. Bey, L. Bedenne, J. Faivre, P. Arveux, F. Guillemin, Use of a decision analysis model to assess the cost-effectiveness of ^{18}F -FDG PET in the management of metachronous liver metastases of colorectal cancer, *J. Nucl. Med.* 46(12) (2005) 2020–2028.
 - [36] S.N. Reske, J. Kotzerke, FDG-PET for clinical use. Results of the 3rd German Interdisciplinary Consensus Conference, “Onko-PET III”, 21 July and 19 September 2000, *Eur. J. Nucl. Med.* 28(11) (2001) 1707–1723.
 - [37] J.F. Vansteenkiste, S.G. Stroobants, Positron emission tomography in the management of non-small cell lung cancer, *Hematol. Oncol. Clin. North. Am.* 18(1) (2004) 269–288.
 - [38] O. Birim, A.P. Kappetein, T. Stijnen, A.J. Bogers, Meta-analysis of positron emission tomographic and computed tomographic imaging in detecting mediastinal lymph node metastases in nonsmall cell lung cancer, *Ann. Thorac. Surg.* 79(1) (2005) 375–382.
 - [39] J.F. Vansteenkiste, S.G. Stroobants, P.R. De Leyn, P.J. Dupont, J.A. Verschakelen, K.L. Nackaerts, L.A. Mortelmans, Mediastinal lymph node staging with FDG-PET scan in patients with potentially operable non-small cell lung cancer: A prospective analysis of 50 cases. Leuven Lung Cancer Group, *Chest* 112(6) (1997) 1480–1486.
 - [40] G.A. Silvestri, L.T. Tanoue, M.L. Margolis, J. Barker, F. Dettterbeck, The noninvasive staging of non-small cell lung cancer: The guidelines, *Chest* 123(1 Suppl.) (2003) 147S–756S.
 - [41] T.H. van, O.S. Hoekstra, E.F. Smit, J.H. van den Bergh, A.J. Schreurs, R.A. Stallaert, P.C. van Velthoven, E.F. Comans, F.W. Diepenhorst, P. Verboom, J.C. van Mourik, P.E. Postmus, M. Boers, G.J. Teule, Effectiveness of positron emission tomography in the preoperative assessment of patients with suspected non-small-cell lung cancer: The PLUS multicentre randomised trial, *Lancet* 359(9315) (2002) 1388–1393.
 - [42] D. Hellwig, A. Groschel, T.P. Graeter, A.P. Hellwig, U. Nestle, H.J. Schafers, G. W. Sybrecht, C.M. Kirsch, Diagnostic performance and prognostic impact of FDG-PET in suspected recurrence of surgically treated non-small cell lung cancer, *Eur. J. Nucl. Med. Mol. Imaging* 33(1) (2006) 13–21.
 - [43] D. Lardinois, W. Weder, T.F. Hany, E.M. Kamel, S. Korom, B. Seifert, G.K. von Schulthess, H.C. Steinert, Staging of non-small-cell lung cancer with integrated positron-emission tomography and computed tomography, *N. Engl. J. Med.* 348(25) (2003) 2500–2507.
 - [44] S.S. Shim, K.S. Lee, B.T. Kim, M.J. Chung, E.J. Lee, J. Han, J.Y. Choi, O.J. Kwon, Y. M. Shim, S. Kim, Non-small cell lung cancer: prospective comparison of integrated FDG PET/CT and CT alone for preoperative staging, *Radiology* 236(3) (2005) 1011–1019.
 - [45] W. De Wever, S. Leyssens, L. Mortelmans, S. Stroobants, G. Machal, J. Bogaert, J. A. Verschakelen, Additional value of PET-CT in the staging of lung cancer: Comparison with CT alone, PET alone and visual correlation of PET and CT, *Eur Radiol* 17(1) (2007) 23–32.
 - [46] Z. Keidar, N. Haim, L. Guralnik, M. Wollner, R. Bar-Shalom, A. Ben-Nun, O. Israel, PET/CT using ^{18}F -FDG in suspected lung cancer recurrence: Diagnostic value and impact on patient management, *J. Nucl. Med.* 45(10) (2004) 1640–1646.
 - [47] S.N. Reske, J. Kotzerke, D.G.P.E.T. for clinical use, Results of the 3rd German Interdisciplinary Consensus Conference, “Onko-PET III”, 21 July and 19 September 2000, *Eur. J. Nucl. Med.* 28(11) (2001) 1707–1723F.

- [48] R. Naumann, B. Beuthien-Baumann, A. Reiss, J. Schulze, A. Hanel, J. Bredow, G. Kuhnel, J. Kropp, M. Hanel, M. Laniado, J. Kotzerke, G. Ehninger, Substantial impact of FDG PET imaging on the therapy decision in patients with early-stage Hodgkin's lymphoma, *Br. J. Cancer* 90(3) (2004) 620–625.
- [49] H. Schoder, A. Noy, M. Gonen, L. Weng, D. Green, Y.E. Erdi, S.M. Larson, H. W. Yeung, , Intensity of 18fluorodeoxyglucose uptake in positron emission tomography distinguishes between indolent and aggressive non-Hodgkin's lymphoma, *J. Clin. Oncol.* 23(21) (2005) 4643–4651.
- [50] P.L. Zinzani, F. Chierichetti, M. Zompatori, M. Tani, V. Stefoni, G. Garraffa, P. Albertini, L. Alinari, G. Ferlin, M. Baccarani, S. Tura, Advantages of positron emission tomography (PET) with respect to computed tomography in the follow-up of lymphoma patients with abdominal presentation, *Leuk. Lymphoma.* 43(6) (2002) 1239–1243.
- [51] C.R. Isasi, P. Lu, M.D. Blafox, A metaanalysis of ¹⁸F-2-deoxy-2-fluoro-D-glucose positron emission tomography in the staging and restaging of patients with lymphoma, *Cancer* 104(5) (2005) 1066–1074.
- [52] M. Hutchings, A. Loft, M. Hansen, L.M. Pedersen, A.K. Berthelsen, S. Keiding, F. D'Amore, A.M. Boesen, L. Roemer, L. Specht, Position emission tomography with or without computed tomography in the primary staging of Hodgkin's lymphoma, *Haematologica* 91(4) (2006) 482–489.
- [53] C. La Fougere, W. Hundt, N. Brockel, T. Pfluger, A. Haug, B. Scher, M. Hacker, K. Hahn, M. Reiser, R. Tiling, Value of PET/CT versus PET and CT performed as separate investigations in patients with Hodgkin's disease and non-Hodgkin's lymphoma, *Eur. J. Nucl. Med. Mol. Imaging* 33(12) (2006) 1417–1425.
- [54] American Cancer Society; American Cancer Society: Breast Cancer Facts and Figures, Atlanta, GA, (2002).
- [55] N. Avril, C.A. Rose, M. Schelling, J. Dose, W. Kuhn, S. Bense, W. Weber, S. Ziegler, H. Graeff, M. Schwaiger, Breast imaging with positron emission tomography and fluorine-18 fluorodeoxyglucose: Use and limitations, *J. Clin. Oncol.* 18(20) (2000) 3495–3502.
- [56] D. Wu, S.S. Gambhir, Positron emission tomography in diagnosis and management of invasive breast cancer: Current status and future perspectives, *Clin. Breast Cancer* 4(Suppl. 1) (2003) S55–S63.
- [57] F. Crippa, R. Agresti, E. Seregini, M. Greco, C. Pascali, A. Bogni, C. Chiesa, S. De, V. V. Delledonne, B. Salvadori, M. Leutner, E. Bombardieri, Prospective evaluation of fluorine-18-FDG PET in presurgical staging of the axilla in breast cancer, *J. Nucl. Med.* 39(1) (1998) 4–8.
- [58] K. Yutani, E. Shiba, H. Kusuoka, M. Tatsumi, T. Uehara, T. Taguchi, S.I. Takai, T. Nishimura, Comparison of FDG-PET with MIBI-SPECT in the detection of breast cancer and axillary lymph node metastasis, *J. Comput. Assist. Tomogr.* 24(2) (2000) 274–280.
- [59] R.L. Wahl, K. Zasadny, M. Helvie, G.D. Hutchins, B. Weber, R. Cody, Metabolic monitoring of breast cancer chemohormonotherapy using positron emission tomography: Initial evaluation, *J. Clin. Oncol.* 11(11) (1993) 2101–2111.
- [60] L.P. Adler, J.P. Crowe, N.K. al-Kaisi, J.L. Sunshine, , Evaluation of breast masses and axillary lymph nodes with [¹⁸F] 2-deoxy-2-fluoro-D-glucose PET, *Radiology* 187 (3) (1993) 743–750.
- [61] W.Y. Lin, S.C. Tsai, K.Y. Cheng, R.F. Yen, C.H. Kao, Fluorine-18 FDG-PET in detecting local recurrence and distant metastases in breast cancer—Taiwanese experiences, *Cancer Invest.* 20(5–6) (2002) 725–729.
- [62] C.H. Kao, J.F. Hsieh, S.C. Tsai, Y.J. Ho, R.F. Yen, Comparison and discrepancy of ¹⁸F-2-deoxyglucose positron emission tomography and Tc-99m MDP bone scan to detect bone metastases, *Anticancer Res.* 20(3B) (2000) 2189–2192.

- [63] M. Lonneux, I. Borbath, M. Berliere, C. Kirkove, S. Pauwels, The place of whole-body PET FDG for the diagnosis of distant recurrence of breast cancer, *Clin. Positron. Imaging* 3(2) (2000) 45–49.
- [64] A.P. Pecking, C. Mechelany-Corone, F. Bertrand-Kermorgant, J.L. Alberini, J.L. Floiras, A. Goupil, M.F. Pichon, Detection of occult disease in breast cancer using fluorodeoxyglucose camera-based positron emission tomography, *Clin. Breast Cancer* 2(3) (2001) 229–234.
- [65] M. Suarez, M.J. Perez-Castejon, A. Jimenez, M. Domper, G. Ruiz, R. Montz, J. L. Carreras, Early diagnosis of recurrent breast cancer with FDG-PET in patients with progressive elevation of serum tumor markers, *Q. J. Nucl. Med.* 46(2) (2002) 113–121.
- [66] B.J. Fueger, W.A. Weber, A. Quon, T.L. Crawford, M.S. Ien-Auerbach, B.S. Halpern, O. Ratib, M.E. Phelps, J. Czernin, Performance of 2-deoxy-2-[F-18]fluoro-D-glucose positron emission tomography and integrated PET/CT in restaged breast cancer patients, *Mol. Imaging Biol.* 7(5) (2005) 369–376.
- [67] P.A. Heeren, P.L. Jager, F. Bongaerts, D.H. van, W. Sluiter, J.T. Plukker, Detection of distant metastases in esophageal cancer with (18)F-FDG PET, *J. Nucl. Med.* 45(6) (2004) 980–987.
- [68] Y.C. Yoon, K.S. Lee, Y.M. Shim, B.T. Kim, K. Kim, T.S. Kim, Metastasis to regional lymph nodes in patients with esophageal squamous cell carcinoma: CT versus FDG PET for presurgical detection prospective study, *Radiology* 227(3) (2003) 764–770.
- [69] K. Kim, S.J. Park, B.T. Kim, K.S. Lee, Y.M. Shim, Evaluation of lymph node metastases in squamous cell carcinoma of the esophagus with positron emission tomography, *Ann. Thorac. Surg.* 71(1) (2001) 290–294.
- [70] C.C. Meltzer, J.D. Luketich, D. Friedman, M. Charron, D. Strollo, M. Meehan, G. K. Urso, M.A. Dachille, D.W. Townsend, Whole-body FDG positron emission tomographic imaging for staging esophageal cancer comparison with computed tomography, *Clin. Nucl. Med.* 25(11) (2000) 882–887.
- [71] P. Flamen, A. Lerut, C.E. Van, W.W. De, M. Peeters, S. Stroobants, P. Dupont, G. Bormans, M. Hiele, L.P. De, R.D. Van, W. Coosemans, N. Ectors, K. Haustermans, L. Mortelmans, Utility of positron emission tomography for the staging of patients with potentially operable esophageal carcinoma, *J. Clin. Oncol.* 18(18) (2000) 3202–3210.
- [72] D. McAteer, F. Wallis, G. Couper, M. Norton, A. Welch, D. Bruce, K. Park, M. Nicolson, F.J. Gilbert, P. Sharp, Evaluation of ¹⁸F-FDG positron emission tomography in gastric and oesophageal carcinoma, *Br. J. Radiol.* 72(858) (1999) 525–529.
- [73] H. Kato, H. Kuwano, M. Nakajima, T. Miyazaki, M. Yoshikawa, N. Masuda, M. Fukuchi, R. Manda, K. Tsukada, N. Oriuchi, K. Endo, Usefulness of positron emission tomography for assessing the response of neoadjuvant chemoradiotherapy in patients with esophageal cancer, *Am. J. Surg.* 184(3) (2002) 279–283.
- [74] J.V. Rasanen, E.I. Sihvo, M.J. Knuuti, H.R. Minn, M.E. Luostarinen, P. Laippala, T. Viljanen, J.A. Salo, Prospective analysis of accuracy of positron emission tomography, computed tomography, and endoscopic ultrasonography in staging of adenocarcinoma of the esophagus and the esophagogastric junction, *Ann. Surg. Oncol.* 10 (8) (2003) 954–960.
- [75] H.L. van Westreenen, M. Westerterp, P.M. Bossuyt, J. Pruijm, G.W. Sloof, J.J. van Lanschot, H. Groen, J.T. Plukker, Systematic review of the staging performance of ¹⁸F-fluorodeoxyglucose positron emission tomography in esophageal cancer, *J. Clin. Oncol.* 22(18) (2004) 3805–3812.
- [76] J.Y. Choi, K.H. Lee, Y.M. Shim, K.S. Lee, J.J. Kim, S.E. Kim, B.T. Kim, Improved detection of individual nodal involvement in squamous cell carcinoma of the esophagus by FDG PET, *J. Nucl. Med.* 41(5) (2000) 808–815.
- [77] T. Lerut, P. Flamen, N. Ectors, C.E. Van, M. Peeters, M. Hiele, W.W. De, W. Coosemans, G. Decker, L.P. De, G. Deneffe, R.D. Van, L. Mortelmans,

- Histopathologic validation of lymph node staging with FDG-PET scan in cancer of the esophagus and gastroesophageal junction: A prospective study based on primary surgery with extensive lymphadenectomy, *Ann. Surg.* 232(6) (2000) 743–752.
- [78] H. Kato, T. Miyazaki, M. Nakajima, M. Fukuchi, R. Manda, H. Kuwano, Value of positron emission tomography in the diagnosis of recurrent oesophageal carcinoma, *Br. J. Surg.* 91(8) (2004) 1004–1009.
- [79] P. Flamen, A. Lerut, C.E. Van, J.P. Cambier, A. Maes, W.W. De, M. Peeters, L.P. De, R.D. Van, L. Mortelmans, The utility of positron emission tomography for the diagnosis and staging of recurrent esophageal cancer, *J. Thorac. Cardiovasc. Surg.* 120(6) (2000) 1085–1092.
- [80] H.A. Wiedner, B.L. Brucher, F. Zimmermann, K. Becker, F. Lordick, A. Beer, M. Schwaiger, U. Fink, J.R. Siewert, H.J. Stein, W.A. Weber, Time course of tumor metabolic activity during chemoradiotherapy of esophageal squamous cell carcinoma and response to treatment, *J. Clin. Oncol.* 22(5) (2004) 900–908.
- [81] A.M. Mandard, F. Dalibard, J.C. Mandard, J. Marnay, M. Henry-Amar, J.F. Petiot, A. Roussel, J.H. Jacob, P. Segol, G. Samama, Pathologic assessment of tumor regression after preoperative chemoradiotherapy of esophageal carcinoma, clinicopathologic correlations, *Cancer* 73(11) (1994) 2680–2686.
- [82] W.A. Weber, K. Ott, K. Becker, H.J. Dittler, H. Helmberger, N.E. Avril, G. Meisetschlager, R. Busch, J.R. Siewert, M. Schwaiger, U. Fink, Prediction of response to preoperative chemotherapy in adenocarcinomas of the esophagogastric junction by metabolic imaging, *J. Clin. Oncol.* 19(12) (2001) 3058–3065.
- [83] P. Therasse, S.G. Arbuck, E.A. Eisenhauer, J. Wanders, R.S. Kaplan, L. Rubinstein, J. Verweij, G.M. Van, A.T. van Oosterom, M.C. Christian, S.G. Gwyther, New guidelines to evaluate the response to treatment in solid tumors, European Organization for Research and Treatment of Cancer, National Cancer Institute of the United States, National Cancer Institute of Canada, *J. Natl. Cancer Inst.* 92(3) (2000) 205–216.
- [84] P. Therasse, E.A. Eisenhauer, J. Verweij, RECIST revisited: A review of validation studies on tumor assessment, *Eur. J. Cancer* 42(8) (2006) 1031–1039.
- [85] K. Ott, U. Fink, K. Becker, A. Stahl, H.J. Dittler, R. Busch, H. Stein, F. Lordick, T. Link, M. Schwaiger, J.R. Siewert, W.A. Weber, Prediction of response to preoperative chemotherapy in gastric carcinoma by metabolic imaging: Results of a prospective trial, *J. Clin. Oncol.* 21(24) (2003) 4604–4610.
- [86] F.A. Calvo, M. Domper, R. Matute, R. Martinez-Lazaro, J.A. Arranz, M. Desco, E. Alvarez, J.L. Carreras, ¹⁸F-FDG positron emission tomography staging and restaging in rectal cancer treated with preoperative chemoradiation, *Int. J. Radiat. Oncol. Biol. Phys.* 58(2) (2004) 528–535.
- [87] J.G. Guillem, H.G. Moore, T. Akhurst, D.S. Klimstra, L. Ruo, M. Mazumdar, B. D. Minsky, L. Saltz, W.D. Wong, S. Larson, Sequential preoperative fluorodeoxyglucose-positron emission tomography assessment of response to preoperative chemoradiation: A means for determining longterm outcomes of rectal cancer, *J. Am. Coll. Surg.* 199(1) (2004) 1–7.
- [88] G.L. Cascini, A. Avallone, P. Delrio, C. Guida, F. Tatangelo, P. Marone, L. Aloj, M.F. De, P. Comella, V. Parisi, S. Lastoria, ¹⁸F-FDG PET is an early predictor of pathologic tumor response to preoperative radiochemotherapy in locally advanced rectal cancer, *J. Nucl. Med.* 47(8) (2006) 1241–1248.
- [89] R.J. Downey, T. Akhurst, M. Gonen, A. Vincent, M.S. Bains, S. Larson, V. Rusch, Preoperative F-18 fluorodeoxyglucose-positron emission tomography maximal standardized uptake value predicts survival after lung cancer resection, *J. Clin. Oncol.* 22(16) (2004) 3255–3260.
- [90] W.A. Weber, V. Petersen, B. Schmidt, L. Tyndale-Hines, T. Link, C. Peschel, M. Schwaiger, Positron emission tomography in non-small-cell lung cancer: Prediction of response to chemotherapy by quantitative assessment of glucose use, *J. Clin. Oncol.* 21(14) (2003) 2651–2657.

- [91] P.L. Zinzani, S. Fanti, G. Battista, M. Tani, P. Castellucci, V. Stefoni, L. Alinari, M. Farsad, G. Musuraca, A. Gabriele, E. Marchi, C. Nanni, R. Canini, N. Monetti, M. Baccarani, Predictive role of positron emission tomography (PET) in the outcome of lymphoma patients, *Br. J. Cancer* 91(5) (2004) 850–854.
- [92] N.G. Mikhaeel, M. Hutchings, P.A. Fields, M.J. O'Doherty, A.R. Timothy, FDG-PET after two to three cycles of chemotherapy predicts progression-free and overall survival in high-grade non-Hodgkin lymphoma, *Ann. Oncol.* 16(9) (2005) 1514–1523.
- [93] M. Hutchings, A. Loft, M. Hansen, L.M. Pedersen, T. Buhl, J. Jurlander, S. Buus, S. Keiding, F. D'Amore, A.M. Boesen, A.K. Berthelsen, L. Specht, FDG-PET after two cycles of chemotherapy predicts treatment failure and progression-free survival in Hodgkin lymphoma, *Blood* 107(1) (2006) 52–59.
- [94] W. Romer, A.R. Hanauske, S. Ziegler, R. Thodtman, W. Weber, C. Fuchs, W. Enne, M. Herz, C. Nerl, M. Garbrecht, M. Schwaiger, Positron emission tomography in non-Hodgkin's lymphoma: Assessment of chemotherapy with fluorodeoxyglucose, *Blood* 91(12) (1998) 4464–4471.
- [95] S.G. Stroobants, I. D'Hoore, C. Dooms, P.R. De Leyn, P.J. Dupont, W.W. De, G. T. De, J.A. Verschakelen, L.A. Mortelmans, J.F. Vansteenkiste, Additional value of whole-body fluorodeoxyglucose positron emission tomography in the detection of distant metastases of non-small-cell lung cancer, *Clin. Lung Cancer* 4(4) (2003) 242–247.
- [96] E. Brun, E. Kjellen, J. Tennvall, T. Ohlsson, A. Sandell, R. Perfekt, J. Wennerberg, S. E. Strand, FDG PET studies during treatment: Prediction of therapy outcome in head and neck squamous cell carcinoma, *Head Neck* 24(2) (2002) 127–135.
- [97] M. Schelling, N. Avril, J. Nahrig, W. Kuhn, W. Romer, D. Sattler, M. Werner, J. Dose, F. Janicke, H. Graeff, M. Schwaiger, Positron emission tomography using [(18)F] fluorodeoxyglucose for monitoring primary chemotherapy in breast cancer, *J. Clin. Oncol.* 18(8) (2000) 1689–1695.
- [98] J. Dose Schwarz, M. Bader, L. Jenicke, G. Hemminger, F. Janicke, N. Avril, Early prediction of response to chemotherapy in metastatic breast cancer using sequential ¹⁸F-FDG PET, *J. Nucl. Med.* 46(7) (2005) 1144–1150.
- [99] N. Avril, S. Sassen, B. Schmalfeldt, J. Naehrig, S. Rutke, W.A. Weber, M. Werner, H. Graeff, M. Schwaiger, W. Kuhn, Prediction of response to neoadjuvant chemotherapy by sequential F-18-fluorodeoxyglucose positron emission tomography in patients with advanced-stage ovarian cancer, *J. Clin. Oncol.* 23(30) (2005) 7445–7453.
- [100] C.K. Kim, N.C. Gupta, B. Chandramouli, A. Alavi, Standardized uptake values of FDG: Body surface area correction is preferable to body weight correction, *J. Nucl. Med.* 35(1) (1994) 164–167.
- [101] K.R. Zasadny, R.L. Wahl, Standardized uptake values of normal tissues at PET with 2-[fluorine-18]-fluoro-2-deoxy-D-glucose: Variations with body weight and a method for correction, *Radiology* 189(3) (1993) 847–850.
- [102] R. Calvo, J.M. Marti-Climent, J.A. Richter, I. Penuelas, A. Crespo-Jara, L.M. Villar, M. J. Garcia-Velloso, Three-dimensional clinical PET in lung cancer: Validation and practical strategies, *J. Nucl. Med.* 41(3) (2000) 439–448.
- [103] M.M. Graham, L.M. Peterson, R.M. Hayward, Comparison of simplified quantitative analyses of FDG uptake, *Nucl. Med. Biol.* 27(7) (2000) 647–655.
- [104] A. Stahl, K. Ott, M. Schwaiger, W.A. Weber, Comparison of different SUV-based methods for monitoring cytotoxic therapy with FDG PET, *Eur. J. Nucl. Med. Mol. Imaging* 31(11) (2004) 1471–1478.
- [105] G.W. Goerres, C. Burger, M.R. Schwitter, T.N. Heidelberg, B. Seifert, G.K. von Schulthess, PET/CT of the abdomen: Optimizing the patient breathing pattern, *Eur. Radiol.* 13(4) (2003) 734–739.
- [106] S.A. Nehmeh, Y.E. Erdi, T. Pan, A. Pevsner, K.E. Rosenzweig, E. Yorke, G. S. Mageras, H. Schoder, P. Vernon, O. Squire, H. Mostafavi, S.M. Larson,

- J. L. Humm, Four-dimensional (4D) PET/CT imaging of the thorax, *Med. Phys.* 31(12) (2004) 3179–3186.
- [107] R. Shekhar, V. Walimbe, S. Raja, V. Zagrodsky, M. Kanvinde, G. Wu, B. Bybel, Automated 3-dimensional elastic registration of whole-body PET and CT from separate or combined scanners, *J. Nucl. Med.* 46(9) (2005) 1488–1496.
- [108] M.E. Juweid, B.D. Cheson, Positron-emission tomography and assessment of cancer therapy, *N. Engl. J. Med.* 354(5) (2006) 496–507.
- [109] G.K. von Schulthess, H.C. Steinert, T.F. Hany, Integrated PET/CT: Current applications and future directions, *Radiology* 238(2) (2006) 405–422.
- [110] J. Barentsz, S. Takahashi, W. Oyen, R. Mus, M.P. De, R. Reznick, M. Oudkerk, W. Mali, Commonly used imaging techniques for diagnosis and staging, *J. Clin. Oncol.* 24(20) (2006) 3234–3244.
- [111] M.E. Juweid, B.D. Cheson, Positron-emission tomography and assessment of cancer therapy, *N. Engl. J. Med.* 354(5) (2006) 496–507.
- [112] P.D. Shreve, Y. Anzai, R.L. Wahl, Pitfalls in oncologic diagnosis with FDG PET imaging: Physiologic and benign variants, *Radiographics* 19(1) (1999) 61–77.
- [113] R. Kubota, K. Kubota, S. Yamada, M. Tada, T. Ido, N. Tamahashi, Microautoradiographic study for the differentiation of intratumoral macrophages, granulation tissues and cancer cells by the dynamics of fluorine-18-fluorodeoxyglucose uptake, *J. Nucl. Med.* 35(1) (1994) 104–112.
- [114] P. Wells, R.N. Gunn, M. Alison, C. Steel, M. Golding, A.S. Ranicar, F. Brady, S. Osman, T. Jones, P. Price, Assessment of proliferation *in vivo* using 2-[(11)C]thymidine positron emission tomography in advanced intra-abdominal malignancies, *Cancer Res.* 62(20) (2002) 5698–5702.
- [115] A.F. Shields, J.R. Grierson, B.M. Dohmen, H.J. Machulla, J.C. Stayanoff, J.M. Lawhorn-Crews, J.E. Obradovich, O. Muzik, T.J. Mangner, Imaging proliferation *in vivo* with [F-18]FLT and positron emission tomography, *Nat. Med.* 4(11) (1998) 1334–1336.
- [116] H.J. Machulla, A. Blocher, M. Kuntzsch, Simplified. labeling. approach. for. synthesizing. 3'-deoxy-3'-[¹⁸F]fluorothymidine. ([¹⁸F]FLT), *J. Radioanal. Nucl. Chem.*, 2000 (abstract).
- [117] J.S. Rasey, J.R. Grierson, L.W. Wiens, P.D. Kolb, J.L. Schwartz, Validation of FLT uptake as a measure of thymidine kinase-1 activity in A549 carcinoma cells, *J. Nucl. Med.* 43(9) (2002) 1210–1217.
- [118] H. Barthel, M. Perumal, J. Latigo, Q. He, F. Brady, S.K. Luthra, P.M. Price, E. O. Aboagye, The uptake of 3'-deoxy-3'-[¹⁸F]fluorothymidine into L5178 Y tumors *in vivo* is dependent on thymidine kinase 1 protein levels, *Eur. J. Nucl. Med. Mol. Imaging* 32(3) (2005) 257–263.
- [119] L.M. Kenny, D.M. Vigushin, A. Al-Nahhas, S. Osman, S.K. Luthra, S. Shousha, R. C. Coombes, E.O. Aboagye, Quantification of cellular proliferation in tumor and normal tissues of patients with breast cancer by [¹⁸F]fluorothymidine-positron emission tomography imaging: Evaluation of analytical methods, *Cancer Res.* 65(21) (2005) 10104–10112.
- [120] D.L. Francis, D. Visvikis, D.C. Costa, T.H. Arulampalam, C. Townsend, S.K. Luthra, I. Taylor, P.J. Ell, Potential impact of [¹⁸F]3'-deoxy-3'-fluorothymidine versus [¹⁸F] fluoro-2-deoxy-D-glucose in positron emission tomography for colorectal cancer, *Eur. J. Nucl. Med. Mol. Imaging* 30(7) (2003) 988–994.
- [121] A.K. Buck, H. Schirrmeister, M. Hetzel, H.M. Von Der, G. Halter, G. Glatting, T. Mattfeldt, F. Liewald, S.N. Reske, B. Neumaier, 3-deoxy-3-[(18)F]fluorothymidine-positron emission tomography for noninvasive assessment of proliferation in pulmonary nodules, *Cancer Res.* 62(12) (2002) 3331–3334.
- [122] M. Wagner, U. Seitz, A. Buck, B. Neumaier, S. Schultheiss, M. Bangerter, M. Bommer, F. Leithauser, E. Wawra, G. Munzert, S.N. Reske, 3'-[¹⁸F]fluoro-3'-deoxythymidine ([¹⁸F]-FLT) as positron emission tomography tracer for imaging

- proliferation in a murine B-cell lymphoma model and in the human disease, *Cancer Res.* 63(10) (2003) 2681–2687.
- [123] A.K. Buck, M. Bommer, S. Stilgenhauer, M. Juweid, G. Glatting, H. Schirrmeister, T. Mattfeldt, D. Tepsic, D. Bunjes, F.M. Mottaghy, B.J. Krause, B. Neumaier, H. Döhner, P. Möller, S.N. Reske, Molecular imaging of proliferation in malignant lymphoma, *Cancer Res* 66(22) (2006) 11055–11061.
 - [124] A.K. Buck, M. Hetzel, H. Schirrmeister, G. Halter, P. Moller, C. Kratochwil, A. Wahl, G. Glatting, F.M. Mottaghy, T. Mattfeldt, B. Neumaier, S.N. Reske, Clinical relevance of imaging proliferative activity in lung nodules, *Eur. J. Nucl. Med. Mol. Imaging* 32(5) (2005) 525–533.
 - [125] M. Perumal, R.G. Pillai, H. Barthel, J. Leyton, J.R. Latigo, M. Forster, F. Mitchell, A. L. Jackman, E.O. Aboagye, Redistribution of nucleoside transporters to the cell membrane provides a novel approach for imaging thymidylate synthase inhibition by positron emission tomography, *Cancer Res.* 66(17) (2006) 8558–8564.
 - [126] A.K. Buck, A.T.J. Vogg, G. Glatting, [^{18}F]FLT for monitoring response to antiproliferative therapy in a mouse lymphoma xenotransplant model, *J. Nucl. Med.*, 2004 (abstract).
 - [127] J. Leyton, J.R. Latigo, M. Perumal, H. Dhaliwal, Q. He, E.O. Aboagye, Early detection of tumor response to chemotherapy by 3'-deoxy-3'-[^{18}F]fluorothymidine positron emission tomography: The effect of cisplatin on a fibrosarcoma tumor model in vivo, *Cancer Res.* 65(10) (2005) 4202–4210.
 - [128] C. Waldherr, I.K. Mellinghoff, C. Tran, B.S. Halpern, N. Rozengurt, A. Safaei, W. A. Weber, D. Stout, N. Satyamurthy, J. Barrio, M.E. Phelps, D.H. Silverman, C. L. Sawyers, J. Czernin, Monitoring antiproliferative responses to kinase inhibitor therapy in mice with 3'-deoxy-3'- ^{18}F -fluorothymidine PET, *J. Nucl. Med.* 46(1) (2005) 114–120.
 - [129] M. Hockel, K. Schlenger, C. Knoop, P. Vaupel, Oxygenation of carcinomas of the uterine cervix: Evaluation by computerized O_2 tension measurements, *Cancer Res.* 51(22) (1991) 6098–6102.
 - [130] W.J. Koh, K.S. Bergman, J.S. Rasey, L.M. Peterson, M.L. Evans, M.M. Graham, J. R. Grierson, K.L. Lindsley, T.K. Lewellen, K.A. Krohn, Evaluation of oxygenation status during fractionated radiotherapy in human nonsmall cell lung cancers using [^{18}F]fluoromisonidazole positron emission tomography, *Int. J. Radiat. Oncol. Biol. Phys.* 33(2) (1995) 391–398.
 - [131] M. Nordmark, M. Overgaard, J. Overgaard, Pretreatment oxygenation predicts radiation response in advanced squamous cell carcinoma of the head and neck, *Radiother. Oncol.* 41(1) (1996) 31–39.
 - [132] E. Lartigau, A. Lusinchi, P. Weeger, P. Wibault, B. Lubinski, F. Eschwege, M. Guichard, Variations in tumour oxygen tension (pO_2) during accelerated radiotherapy of head and neck carcinoma, *Eur. J. Cancer* 34(6) (1998) 856–861.
 - [133] D.M. Brizel, G.S. Sibley, L.R. Prosnitz, R.L. Scher, M.W. Dewhirst, Tumor hypoxia adversely affects the prognosis of carcinoma of the head and neck, *Int. J. Radiat. Oncol. Biol. Phys.* 38(2) (1997) 285–289.
 - [134] P.E. Valk, C.A. Mathis, M.D. Prados, J.C. Gilbert, T.F. Budinger, Hypoxia in human gliomas: Demonstration by PET with fluorine-18-fluoromisonidazole, *J. Nucl. Med.* 33 (12) (1992) 2133–2137.
 - [135] T. Gronroos, O. Eskola, K. Lehtio, H. Minn, P. Marjamäki, J. Bergman, M. Haaparanta, S. Forsback, O. Solin, Pharmacokinetics of [^{18}F]FETNIM: A potential marker for PET, *J. Nucl. Med.* 42(9) (2001) 1397–1404.
 - [136] D.J. Yang, S. Wallace, A. Cherif, C. Li, M.B. Gretzer, E.E. Kim, D.A. Podoloff, Development of F-18-labeled fluoroerythronitroimidazole as a PET agent for imaging tumor hypoxia, *Radiology* 194(3) (1995) 795–800.
 - [137] M. Piert, H.J. Machulla, M. Picchio, G. Reischl, S. Ziegler, P. Kumar, H.J. Wester, R. Beck, A.J. McEwan, L.I. Wiebe, M. Schwaiger, Hypoxia-specific tumor imaging with ^{18}F -fluoroazomycin arabinoside, *J. Nucl. Med.* 46(1) (2005) 106–113.

- [138] B.G. Siim, W.T. Laux, M.D. Rutland, B.N. Palmer, W.R. Wilson, Scintigraphic imaging of the hypoxia marker (99m)technetium-labeled 2,2'-(1,4-diaminobutane)bis (2-methyl-3-butanone) dioxime (99mTc-labeled HL-91; prognox): Noninvasive detection of tumor response to the antivascular agent 5,6-dimethylxanthenone-4-acetic acid, *Cancer Res.* 60(16) (2000) 4582–4588.
- [139] F. Dehdashti, M.A. Mintun, J.S. Lewis, J. Bradley, R. Govindan, R. Laforest, M. J. Welch, B.A. Siegel, *In vivo* assessment of tumor hypoxia in lung cancer with ^{60}Cu -ATSM, *Eur. J. Nucl. Med. Mol. Imaging* 30(6) (2003) 844–850.
- [140] D. Rischin, R.J. Hicks, R. Fisher, D. Binns, J. Corry, S. Porceddu, *et al.*, Prognostic significance of ^{18}F -misonidazole positron emission tomography-detected tumor hypoxia in patients with advanced head and neck cancer randomly assigned to chemoradiation with or without tirapazamine: A substudy of Trans-Tasman Radiation Oncology Group Study 98,02, *J. Clin. Oncol.* 24(13) (2006) 2098–2104.
- [141] J.G. Rajendran, D.A. Mankoff, F. O'Sullivan, L.M. Peterson, D.L. Schwartz, E.U. Conrad, A.M. Spence, M. Muzi, D.G. Farwell, K.A. Krohn, Hypoxia and glucose metabolism in malignant tumors: Evaluation by ^{18}F fluoromisonidazole and ^{18}F fluorodeoxyglucose positron emission tomography imaging, *Clin. Cancer Res.* 10 (7) (2004) 2245–2252.
- [142] K. Lehtio, O. Eskola, T. Viljanen, V. Oikonen, T. Gronroos, L. Sillanmaki, R. Grenman, H. Minn, Imaging perfusion and hypoxia with PET to predict radiotherapy response in head-and-neck cancer, *Int. J. Radiat. Oncol. Biol. Phys.* 59(4) (2004) 971–982.
- [143] K. Lehtio, V. Oikonen, T. Gronroos, O. Eskola, K. Kalliokoski, J. Bergman, O. Solin, R. Grenman, P. Nuutila, H. Minn, Imaging of blood flow and hypoxia in head and neck cancer: Initial evaluation with $[(15)\text{O}]\text{H}_2\text{O}$ and $[(18)\text{F}]\text{fluoroerythronitroimidazole}$ PET, *J. Nucl. Med.* 42(11) (2001) 1643–1652.
- [144] B. Gagel, P. Reinartz, E. Dimartino, M. Zimny, M. Pinkawa, P. Maneschi, S. Stanzel, K. Hamacher, H.H. Coenen, M. Westhofen, U. Bull, M.J. Eble, pO_2 Polarography versus positron emission tomography ($[(18)\text{F}]\text{fluoromisonidazole}$, $[(18)\text{F}]\text{-2-fluoro-2'-deoxyglucose}$), an appraisal of radiotherapeutically relevant hypoxia, *Strahlenther. Onkol.* 180(10) (2004) 616–622.
- [145] S.M. Eschmann, F. Paulsen, M. Reimold, H. Dittmann, S. Welz, G. Reischl, H. J. Machulla, R. Bares, Prognostic impact of hypoxia imaging with ^{18}F -misonidazole PET in non-small cell lung cancer and head and neck cancer before radiotherapy, *J. Nucl. Med.* 46(2) (2005) 253–260.
- [146] S.H. Yeh, R.S. Liu, L.C. Wu, D.J. Yang, S.H. Yen, C.W. Chang, T.W. Yu, K.L. Chou, K.Y. Chen, Fluorine-18 fluoromisonidazole tumor to muscle retention ratio for the detection of hypoxia in nasopharyngeal carcinoma, *Eur. J. Nucl. Med.* 23(10) (1996) 1378–1383.
- [147] J.S. Rasey, W.J. Koh, M.L. Evans, L.M. Peterson, T.K. Lewellen, M.M. Graham, K. A. Krohn, Quantifying regional hypoxia in human tumors with positron emission tomography of ^{18}F fluoromisonidazole: A pretherapy study of 37 patients, *Int. J. Radiat. Oncol. Biol. Phys.* 36(2) (1996) 417–428.
- [148] R.J. Hicks, D. Rischin, R. Fisher, D. Binns, A.M. Scott, L.J. Peters, Utility of FMISO PET in advanced head and neck cancer treated with chemoradiation incorporating a hypoxia-targeting chemotherapy agent, *Eur. J. Nucl. Med. Mol. Imaging* 32(12) (2005) 1384–1391.
- [149] J.S. Rasey, W.J. Koh, M.L. Evans, L.M. Peterson, T.K. Lewellen, M.M. Graham, K. A. Krohn, Quantifying regional hypoxia in human tumors with positron emission tomography of ^{18}F fluoromisonidazole: A pretherapy study of 37 patients, *Int. J. Radiat. Oncol. Biol. Phys.* 36(2) (1996) 417–428.
- [150] W.J. Koh, K.S. Bergman, J.S. Rasey, L.M. Peterson, M.L. Evans, M.M. Graham, J. R. Grierson, K.L. Lindsley, T.K. Lewellen, K.A. Krohn, Evaluation of oxygenation status during fractionated radiotherapy in human nonsmall cell lung cancers using

- [F-18]fluoromisonidazole positron emission tomography, *Int. J. Radiat. Oncol. Biol. Phys.* 33(2) (1995) 391–398.
- [151] B. Gagel, P. Reinartz, C. Demirel, H.J. Kaiser, M. Zimny, M. Piroth, M. Pinkawa, S. Stanzel, B. Asadpour, K. Hamacher, H.H. Coenen, U. Buell, M.J. Eble, [¹⁸F] fluoromisonidazole and [¹⁸F] fluorodeoxyglucose positron emission tomography in response evaluation after chemo-/radiotherapy of non-small-cell lung cancer: A feasibility study, *BMC Cancer* 6 (2006) 51.
- [152] J.G. Rajendran, D.C. Wilson, E.U. Conrad, L.M. Peterson, J.D. Bruckner, J.S. Rasey, L.K. Chin, P.D. Hofstrand, J.R. Grierson, J.F. Eary, K.A. Krohn, [(18F)FMISO and [(18F)FDG PET imaging in soft tissue sarcomas: Correlation of hypoxia, metabolism and VEGF expression, *Eur. J. Nucl. Med. Mol. Imaging* 30(5) (2003) 695–704.
- [153] S. Loi, S.Y. Ngan, R.J. Hicks, B. Mukesh, P. Mitchell, M. Michael, J. Zalcborg, T. Leong, D. Lim-Joon, J. Mackay, D. Rischin, Oxaliplatin combined with infusional 5-fluorouracil and concomitant radiotherapy in inoperable and metastatic rectal cancer: A phase I trial, *Br. J. Cancer* 92(4) (2005) 655–661.
- [154] M. Bruehlmeier, U. Roelcke, P.A. Schubiger, S.M. Ametamey, Assessment of hypoxia and perfusion in human brain tumors using PET with ¹⁸F-fluoromisonidazole and ¹⁵O-H₂O, *J. Nucl. Med.* 45(11) (2004) 1851–1859.
- [155] L.M. Cher, C. Murone, N. Lawrentschuk, S. Ramdave, A. Papenfuss, A. Hannah, G. J. O’Keefe, J.I. Sachinidis, S.U. Berlangieri, G. Fabinyi, A.M. Scott, Correlation of hypoxic cell fraction and angiogenesis with glucose metabolic rate in gliomas using ¹⁸F-fluoromisonidazole, ¹⁸F-FDG PET, and immunohistochemical studies, *J. Nucl. Med.* 47(3) (2006) 410–418.
- [156] N. Lawrentschuk, A.M. Poon, S.S. Foo, L.G. Putra, C. Murone, I.D. Davis, D. M. Bolton, A.M. Scott, Assessing regional hypoxia in human renal tumors using ¹⁸F-fluoromisonidazole positron emission tomography, *BJU Int.* 96(4) (2005) 540–546.
- [157] F. Dehdashti, P.W. Grigsby, M.A. Mintun, J.S. Lewis, B.A. Siegel, M.J. Welch, Assessing tumor hypoxia in cervical cancer by positron emission tomography with ⁶⁰Cu-ATSM: Relationship to therapeutic response—A preliminary report, *Int. J. Radiat. Oncol. Biol. Phys.* 55(5) (2003) 1233–1238.
- [158] E. Ruoslahti, M.D. Pierschbacher, New perspectives in cell adhesion: RGD and integrins, *Science* 238(4826) (1987) 491–497.
- [159] R. Haubner, D. Finsinger, H. Kessler, Stereoisomeric peptide libraries and peptidomimetics for designing selective inhibitors of the alpha-v-beta-3 integrin for a new cancer therapy, *Angew. Chem. Int. Ed. Engl.* (1997) 1374–1389.
- [160] M. Aumailley, M. Gurrath, G. Muller, J. Calvete, R. Timpl, H. Kessler, Arg-Gly-Asp constrained within cyclic pentapeptides, strong and selective inhibitors of cell adhesion to vitronectin and laminin fragment P1, *FEBS. Lett.* 291(1) (1991) 50–54.
- [161] R. Haubner, H.J. Wester, Radiolabeled tracers for imaging of tumor angiogenesis and evaluation of anti-angiogenic therapies, *Curr. Pharm. Des.* 10(13) (2004) 1439–1455.
- [162] R. Haubner, W.A. Weber, A.J. Beer, E. Vabulien, D. Reim, M. Sarbia, K.F. Becker, M. Goebel, R. Hein, H.J. Wester, H. Kessler, M. Schwaiger, Noninvasive visualization of the activated alphavbeta3 integrin in cancer patients by positron emission tomography and [¹⁸F]galacto-RGD, *PLoS Med.* 2(3) (2005) e70.
- [163] A.J. Beer, R. Haubner, M. Goebel, S. Luderschmidt, M.E. Spilker, H.J. Wester, W. A. Weber, M. Schwaiger, Biodistribution and pharmacokinetics of the alphav-beta3-selective tracer ¹⁸F-galacto-RGD in cancer patients, *J. Nucl. Med.* 46(8) (2005) 1333–1341.
- [164] A.J. Beer, R. Haubner, I. Wolf, M. Goebel, S. Luderschmidt, M. Niemeyer, A. L. Grosu, M.J. Martinez, H.J. Wester, W.A. Weber, M. Schwaiger, PET-based human dosimetry of ¹⁸F-galacto-RGD, a new radiotracer for imaging alpha v beta3 expression, *J. Nucl. Med.* 47(5) (2006) 763–769.

- [165] A.J. Beer, R. Haubner, M. Sarbia, M. Goebel, S. Luderschmidt, A.L. Grosu, O. Schnell, M. Niemeyer, H. Kessler, H.J. Wester, W.A. Weber, M. Schwaiger, Positron emission tomography using [¹⁸F]galacto-RGD identifies the level of integrin alpha(v)beta3 expression in man, *Clin. Cancer Res.* 12(13) (2006) 3942–3949.
- [166] G. Gasparini, P.C. Brooks, E. Biganzoli, P.B. Vermeulen, E. Bonoldi, L.Y. Dirix, G. Ranieri, R. Miceli, D.A. Cheresch, Vascular integrin alpha(v)beta3: A new prognostic indicator in breast cancer, *Clin. Cancer Res.* 4(11) (1998) 2625–2634.
- [167] C.M. Storgard, D.G. Stupack, A. Jonczyk, S.L. Goodman, R.I. Fox, D.A. Cheresch, Decreased angiogenesis and arthritic disease in rabbits treated with an alphavbeta3 antagonist, *J. Clin. Invest.* 103(1) (1999) 47–54.
- [168] B.J. Pichler, M. Kneilling, R. Haubner, H. Braumuller, M. Schwaiger, M. Rocken, W. A. Weber, Imaging of delayed-type hypersensitivity reaction by PET and ¹⁸F-galacto-RGD, *J. Nucl. Med.* 46(1) (2005) 184–189.
- [169] S.H. Zeisel, J.K. Blusztajn, Choline and human nutrition, *Annu. Rev. Nutr.* 14 (1994) 269–296.
- [170] R. Katz-Brull, H. Degani, Kinetics of choline transport and phosphorylation in human breast cancer cells; NMR application of the zero trans method, *Anticancer Res.* 16 (3B) (1996) 1375–1380.
- [171] E. Ackerstaff, B.R. Pflug, J.B. Nelson, Z.M. Bhujwala, Detection of increased choline compounds with proton nuclear magnetic resonance spectroscopy subsequent to malignant transformation of human prostatic epithelial cells, *Cancer Res.* 61(9) (2001) 3599–3603.
- [172] S. Ratnam, C. Kent, Early increase in choline kinase activity upon induction of the H-ras oncogene in mouse fibroblast cell lines, *Arch. Biochem. Biophys.* 323(2) (1995) 313–322.
- [173] O. Kabori, Y. Kirihaara, N. Kosaka, T. Hara, Positron emission tomography of esophageal carcinoma using (11)C-choline and (18)F-fluorodeoxyglucose: A novel method of preoperative lymph node staging, *Cancer* 86(9) (1999) 1638–1648.
- [174] T. Hara, K. Inagaki, N. Kosaka, T. Morita, Sensitive detection of mediastinal lymph node metastasis of lung cancer with 11C-choline PET, *J. Nucl. Med.* 41(9) (2000) 1507–1513.
- [175] T. Hara, N. Kosaka, N. Shinoura, T. Kondo, PET imaging of brain tumor with [methyl-11C]choline, *J. Nucl. Med.* 38(6) (1997) 842–847.
- [176] T. Hara, N. Kosaka, H. Kishi, PET imaging of prostate cancer using carbon-11-choline, *J. Nucl. Med.* 39(6) (1998) 990–995.
- [177] S. Jana, M.D. Blafox, Nuclear medicine studies of the prostate, testes, and bladder, *Semin. Nucl. Med.* 36(1) (2006) 51–72.
- [178] T. Hara, N. Kosaka, H. Kishi, Development of (18)F-fluoroethylcholine for cancer imaging with PET: Synthesis, biochemistry, and prostate cancer imaging, *J. Nucl. Med.* 43(2) (2002) 187–199.
- [179] T.R. DeGrado, R.E. Coleman, S. Wang, S.W. Baldwin, M.D. Orr, C.N. Robertson, T. J. Polascik, D.T. Price, Synthesis and evaluation of ¹⁸F-labeled choline as an oncologic tracer for positron emission tomography: Initial findings in prostate cancer, *Cancer Res.* 61(1) (2001) 110–117.
- [180] T.R. DeGrado, R.E. Reiman, D.T. Price, S. Wang, R.E. Coleman, Pharmacokinetics and radiation dosimetry of ¹⁸F-fluorocholine, *J. Nucl. Med.* 43(1) (2002) 92–96.
- [181] T.R. DeGrado, S.W. Baldwin, S. Wang, M.D. Orr, R.P. Liao, H.S. Friedman, R. Reiman, D.T. Price, R.E. Coleman, Synthesis and evaluation of (18)F-labeled choline analogs as oncologic PET tracers, *J. Nucl. Med.* 42(12) (2001) 1805–1814.
- [182] S.A. Kwee, H. Wei, I. Sesterhenn, D. Yun, M.N. Coel, Localization of primary prostate cancer with dual-phase ¹⁸F-fluorocholine PET, *J. Nucl. Med.* 47(2) (2006) 262–269.

- [183] D.T. Schmid, H. John, R. Zweifel, T. Cservenyak, G. Westera, G.W. Goerres, G. K. von Schulthess, T.F. Hany, Fluorocholine PET/CT in patients with prostate cancer: Initial experience, *Radiology* 235(2) (2005) 623–628.
- [184] M. Heinisch, A. Dirisamer, W. Loidl, F. Stoiber, B. Gruy, S. Haim, W. Langsteger, Positron emission tomography/computed tomography with F-18-fluorocholine for restaging of prostate cancer patients: meaningful at PSA < 5 ng/ml, *Mol. Imaging Biol.* 8(1) (2006) 43–48.
- [185] D.T. Price, R.E. Coleman, R.P. Liao, C.N. Robertson, T.J. Polascik, T.R. DeGrado, Comparison of [18F]fluorocholine and [18F]fluorodeoxyglucose for positron emission tomography of androgen dependent and androgen independent prostate cancer, *J. Urol.* 168(1) (2002) 273–280.
- [186] M.T. Wyss, B. Weber, M. Honer, N. Spath, S.M. Ametamey, G. Westera, B. Bode, A.H. Kaim, A. Buck, ¹⁸F-choline in experimental soft tissue infection assessed with autoradiography and high-resolution PET, *Eur. J. Nucl. Med. Mol. Imaging* 31(3) (2004) 312–316.
- [187] M. Cimitan, R. Bortolus, S. Morassut, V. Canzonieri, A. Garbeglio, T. Baresic, E. Borsatti, A. Drigo, M.G. Trovo, [(18)F]fluorocholine PET/CT imaging for the detection of recurrent prostate cancer at PSA relapse: Experience in 100 consecutive patients, *Eur. J. Nucl. Med. Mol. Imaging*, 2006.
- [188] M. Blau, W. Nagler, M.A. Bender, Fluorine-18: A new isotope for bone scanning, *J. Nucl. Med.* 3 (1962) 332–334.
- [189] C. Schiepers, J. Nuyts, G. Bormans, J. Dequeker, R. Bouillon, L. Mortelmans, A. Verbruggen, R.M. De, Fluoride kinetics of the axial skeleton measured *in vivo* with fluorine-18-fluoride PET, *J. Nucl. Med.* 38(12) (1997) 1970–1976.
- [190] G.M. Blake, S.J. Park-Holohan, G.J. Cook, I. Fogelman, Quantitative studies of bone with the use of ¹⁸F-fluoride and ^{99m}Tc-methylene diphosphonate, *Semin. Nucl. Med.* 31(1) (2001) 28–49.
- [191] R.A. Hawkins, Y. Choi, S.C. Huang, C.K. Hoh, M. Dahlbom, C. Schiepers, N. Satyamurthy, J.R. Barrio, M.E. Phelps, Evaluation of the skeletal kinetics of fluorine-18-fluoride ion with PET, *J. Nucl. Med.* 33(5) (1992) 633–642.
- [192] G.J. Cook, I. Fogelman, The role of positron emission tomography in the management of bone metastases, *Cancer* 88(12 Suppl.) (2000) 2927–2933.
- [193] H. Schirrmeister, G. Glatting, J. Hetzel, K. Nussle, C. Arslanemir, A.K. Buck, K. Dziuk, A. Gabelmann, S.N. Reske, M. Hetzel, Prospective evaluation of the clinical value of planar bone scans, SPECT, and (18)F-labeled NaF PET in newly diagnosed lung cancer, *J. Nucl. Med.* 42(12) (2001) 1800–1804.
- [194] E. Even-Sapir, U. Metser, G. Flusser, L. Zuriel, Y. Kollender, H. Lerman, G. Lievshitz, I. Ron, E. Mishani, Assessment of malignant skeletal disease: Initial experience with ¹⁸F-fluoride PET/CT and comparison between ¹⁸F-fluoride PET and ¹⁸F-fluoride PET/CT, *J. Nucl. Med.* 45(2) (2004) 272–278.
- [195] E. Even-Sapir, U. Metser, E. Mishani, G. Lievshitz, H. Lerman, I. Leibovitch, The detection of bone metastases in patients with high-risk prostate cancer: ^{99m}Tc-MDP planar bone scintigraphy, single- and multi-field-of-view SPECT, ¹⁸F-fluoride PET, and ¹⁸F-fluoride PET/CT, *J. Nucl. Med.* 47(2) (2006) 287–297.
- [196] W. Langsteger, L. Jorg, C. Tausch, M. Heinisch, B. Wieser, E. Rechberger, P. J. Panholzer, W. Segal, M. Aufschneider, The value of F-18 fluorodeoxyglucose in positron emission tomography diagnosis of breast carcinoma, *Wien. Med. Wochenschr.* 152(11–12) (2002) 255–258.
- [197] H. Ohgaki, P. Kleihues, Population-based studies on incidence, survival rates, and genetic alterations in astrocytic and oligodendroglial gliomas, *J. Neuropathol. Exp. Neurol.* 64(6) (2005) 479–489.
- [198] B. Riemann, F. Stogbauer, K. Kopka, H. Halfter, M. Lasic, A. Schirmacher, T. Kuwert, M. Weckesser, E.B. Ringelstein, O. Schober, Kinetics of 3-[(123)I]iodo-L-alpha-methyltyrosine transport in rat C6 glioma cells, *Eur. J. Nucl. Med.* 26(10) (1999) 1274–1278.

- [199] K.J. Langen, H. Muhlensiepen, M. Holschbach, H. Hautzel, P. Jansen, H.H. Coenen, Transport mechanisms of 3-[^{123}I]iodo- α -methyl-L-tyrosine in a human glioma cell line: Comparison with [3H]methyl-L-methionine, *J. Nucl. Med.* 41(7) (2000) 1250–1255.
- [200] K.J. Langen, M. Jarosch, H. Muhlensiepen, K. Hamacher, S. Broer, P. Jansen, K. Zilles, H.H. Coenen, Comparison of fluorotyrosines and methionine uptake in F98 rat gliomas, *Nucl. Med. Biol.* 30(5) (2003) 501–508.
- [201] P. Heiss, S. Mayer, M. Herz, H.J. Wester, M. Schwaiger, R. Senekowitsch-Schmidtke, Investigation of transport mechanism and uptake kinetics of O-(2-[^{18}F]fluoroethyl)-L-tyrosine *in vitro* and *in vivo*, *J. Nucl. Med.* 40(8) (1999) 1367–1373.
- [202] K. Hamacher, T. Hirschfelder, H.H. Coenen, Electrochemical cell for separation of [^{18}F]fluoride from irradiated ^{18}O -water and subsequent no carrier added nucleophilic fluorination, *Appl. Radiat. Isot.* 56(3) (2002) 519–523.
- [203] H.J. Wester, M. Herz, W. Weber, P. Heiss, R. Senekowitsch-Schmidtke, M. Schwaiger, G. Stocklin, Synthesis and radiopharmacology of O-(2-[^{18}F]fluoroethyl)-L-tyrosine for tumor imaging, *J. Nucl. Med.* 40(1) (1999) 205–212.
- [204] D. Pauleit, F. Floeth, K. Hamacher, M.J. Riemenschneider, G. Reifenberger, H.W. Muller, K. Zilles, H.H. Coenen, K.J. Langen, O-(2-[^{18}F]fluoroethyl)-L-tyrosine PET combined with MRI improves the diagnostic assessment of cerebral gliomas, *Brain* 128(Pt 3) (2005) 678–687.
- [205] A.L. Grosu, W.A. Weber, M. Franz, S. Stark, M. Piert, R. Thamm, H. Gumprecht, M. Schwaiger, M. Molls, C. Nieder, Reirradiation of recurrent high-grade gliomas using amino acid PET (SPECT)/CT/MRI image fusion to determine gross tumor volume for stereotactic fractionated radiotherapy, *Int. J. Radiat. Oncol. Biol. Phys.* 63(2) (2005) 511–519.
- [206] M. Weckesser, K.J. Langen, C.H. Rickert, S. Kloska, R. Straeter, K. Hamacher, G. Kurlmann, H. Wassmann, H.H. Coenen, O. Schober, O-(2-[^{18}F]fluoroethyl)-L-tyrosine PET in the clinical evaluation of primary brain tumours, *Eur. J. Nucl. Med. Mol. Imaging* 32(4) (2005) 422–429.
- [207] G. Popperl, F.W. Kreth, J. Herms, W. Koch, J.H. Mehrkens, F.J. Gildehaus, H. A. Kretschmar, J.C. Tonn, K. Tatsch, Analysis of ^{18}F -FET PET for grading of recurrent gliomas: Is evaluation of uptake kinetics superior to standard methods? *J. Nucl. Med.* 47(3) (2006) 393–403.
- [208] S.J. Nelson, Imaging of brain tumors after therapy, *Neuroimaging Clin. N. Am.* 9(4) (1999) 801–819.
- [209] N.E. Leeds, E.F. Jackson, Current imaging techniques for the evaluation of brain neoplasms, *Curr. Opin. Oncol.* 6(3) (1994) 254–261.
- [210] T.N. Byrne, Imaging of gliomas, *Semin. Oncol.* 21(2) (1994) 162–171.
- [211] G. Popperl, C. Gotz, W. Rachinger, F.J. Gildehaus, J.C. Tonn, K. Tatsch, Value of O-(2-[^{18}F]fluoroethyl)-L-tyrosine PET for the diagnosis of recurrent glioma, *Eur. J. Nucl. Med. Mol. Imaging* 31(11) (2004) 1464–1470.
- [212] W. Rachinger, C. Goetz, G. Popperl, F.J. Gildehaus, F.W. Kreth, M. Holtmannspotter, J. Herms, W. Koch, K. Tatsch, J.C. Tonn, Positron emission tomography with O-(2-[^{18}F]fluoroethyl)-L-tyrosine versus magnetic resonance imaging in the diagnosis of recurrent gliomas, *Neurosurgery* 57(3) (2005) 505–511.
- [213] G. Popperl, C. Gotz, W. Rachinger, O. Schnell, F.J. Gildehaus, J.C. Tonn, K. Tatsch, Serial O-(2-[(^{18}F]fluoroethyl)-L-tyrosine PET for monitoring the effects of intracavitary radioimmunotherapy in patients with malignant glioma, *Eur. J. Nucl. Med. Mol. Imaging* 33(7) (2006) 792–800.
- [214] G. Popperl, R. Goldbrunner, F.J. Gildehaus, F.W. Kreth, P. Tanner, M. Holtmannspotter, J.C. Tonn, K. Tatsch, O-(2-[^{18}F]fluoroethyl)-L-tyrosine PET for monitoring the effects of convection-enhanced delivery of paclitaxel in patients with recurrent glioblastoma, *Eur. J. Nucl. Med. Mol. Imaging* 32(9) (2005) 1018–1025.

- [215] W. Langsteger, M. Heinisch, I. Fogelman, The role of fluorodeoxyglucose, ^{18}F -dihydroxyphenylalanine, ^{18}F -choline, and ^{18}F -fluoride in bone imaging with emphasis on prostate and breast, *Semin. Nucl. Med.* 36(1) (2006) 73–92.
- [216] A. Becherer, G. Karanikas, M. Szabo, G. Zettinig, S. Asenbaum, C. Marosi, C. Henk, P. Wunderbaldinger, T. Czech, W. Wadsak, K. Kletter, Brain tumor imaging with PET: A comparison between [^{18}F]fluorodopa and [^{11}C]methionine, *Eur. J. Nucl. Med. Mol. Imaging* 30(11) (2003) 1561–1567.
- [217] W. Chen, D.H. Silverman, S. Delaloye, J. Czernin, N. Kamdar, W. Pope, N. Satyamurthy, C. Schiepers, T. Cloughesy, ^{18}F -FDOPA PET imaging of brain tumors: Comparison study with ^{18}F -FDG PET and evaluation of diagnostic accuracy, *J. Nucl. Med.* 47(6) (2006) 904–911.
- [218] A. Becherer, M. Szabo, G. Karanikas, P. Wunderbaldinger, P. Angelberger, M. Raderer, A. Kurtaran, R. Dudczak, K. Kletter, Imaging of advanced neuroendocrine tumors with (18)F-FDOPA PET, *J. Nucl. Med.* 45(7) (2004) 1161–1167.
- [219] F. Montravers, D. Grahek, K. Kerrou, P. Ruszniewski, V. De Beco, N. Aide, F. Gutman, J.D. Grangé, J.P. Lotz, J.N. Talbot, Can fluorodihydroxyphenylalanine PET replace somatostatin receptor scintigraphy in patients with digestive endocrine tumors, *J. Nucl. Med.* 47(9) (2006) 1455–1462.
- [220] S. Hoegerle, C. Althoefer, N. Ghanem, I. Brink, E. Moser, E. Nitzsche, ^{18}F -DOPA positron emission tomography for tumor detection in patients with medullary thyroid carcinoma and elevated calcitonin levels, *Eur. J. Nucl. Med.* 28(1) (2001) 64–71.
- [221] K. Herrmann, K. Ott, A.K. Buck, F. Lordick, D. Wilhelm, M. Souvatzoglou, K. Becker, T. Sehuster, H.J. Wester, J.R. Siewert, M. Schwaiger, B.J. Krause, Imaging Gastric Cancer with PET and the Radiotracers ^{18}F -FLT and ^{18}F -FDG: A Comparative Analysis, *J. Nucl. Med.* 48(12) (2007) 1945–1950.
- [222] F. Lordick, K. Ott, B.J. Krause, W.A. Weber, K. Becker, H.J. Stein, S. Lorenzen, T. Schuster, H. Wiedner, K. Herrmann, R. Bredenkamp, H. Höfler, U. Fink, C. Peschel, M. Schwaiger, J.R. Siewert, PET to assess early metabolic response and to guide treatment of adenocarcinoma of the oesphagogastric junction: The MUNICON phase II trial, *Lancet Oncol.* 8(9) (2007) 797–805.
- [223] M. Souvatzoglou, A.L. Grosu, B. Roper, B.J. Krause, R. Beck, G. Reischl, M. Picchio, H.J. Machulla, H.J. Wester, M. Pietsch, Tumor hypoxia imaging with [^{18}F] FAZA PET in head and neck cancer patients: A pilot study, *Eur. J. Nucl. Med. Mol. Imaging* 34(10) (2007) 1566–1575.

Note from the Editors

On the use of ^{18}F -labeled molecules, see also in this volume chapters by F. Dollé *et al.* on PET molecular imaging, K. Kopka *et al.* on cardiological imaging, K. Nägren and J. O Rinne on application to Alzheimer's disease.

CHAPTER 5

Non-Invasive Physiology and Pharmacology Using ^{19}F Magnetic Resonance

Jian-Xin Yu, Weina Cui, Dawen Zhao, and Ralph P. Mason*

*Laboratory of Prognostic Radiology, Department of Radiology, The University of Texas
Southwestern Medical Center at Dallas, TX 75390, USA*

Contents

1. Introduction	198
1.1. Context and perspective	199
1.2. ^{19}F as an <i>in vivo</i> NMR probe	201
2. ^{19}F NMR for pharmacology	215
2.1. Cancer chemotherapeutics	216
2.1.1. Fluoropyrimidines	216
2.1.2. Other anticancer drugs	217
2.2. Other drugs	218
3. Active reporter molecules	220
3.1. Physical interactions	220
3.1.1. <i>In vivo</i> oximetry	220
3.1.2. pH	231
3.1.3. Metal ions	235
3.1.4. Caveats	242
3.2. Chemical interactions	243
3.2.1. Metabolism of FDG	243
3.2.2. Hypoxia	244
3.2.3. Enzyme reporters	245
4. Passive reporter molecules	252
5. Potential innovations and improvements	253
6. Conclusions	253
References	254

Abstract

^{19}F provides a powerful tool for nuclear magnetic resonance (NMR) investigations. It has been widely exploited for both spectroscopic studies and increasingly for magnetic resonance imaging (MRI). The ^{19}F atom has high NMR sensitivity while there is essentially no background signal in the body. Many diverse reporter molecules have been designed, which exploit the unique sensitivity of the fluorine atom to its microenvironment and these

*Corresponding author. Tel.: +1-(214)-648-8926; Fax: +1-(214)-648-2991;
E-mail: Ralph.Mason@UTSouthwestern.edu

cover such diverse aspects as pO_2 , pH, metal ion concentrations (e.g., calcium, magnesium), gene reporter molecules, hypoxia reporters, vascular flow, and volume. There are also numerous drugs in clinical use (e.g., the cancer chemotherapeutics 5-fluorouracil and gemcitabine, anesthetics, and psychoactive drugs such as fluoxetine) and agrochemicals, which include a fluorine atom. This review examines the properties of the fluorine atom that make it an ideal tool for NMR, consider the many properties that are available for interrogation and examine applications. NMR is a particularly flexible technology, since it can provide information through multiple parameters including chemical shift, relaxation processes (R_1 and R_2), scalar coupling, and chemical exchange. Moreover, fluorine NMR has a very large chemical shift range (~ 300 ppm) allowing multiple agents to be examined simultaneously.

1. INTRODUCTION

MRI has become the technology of choice for radiology and detection of many diseases. Today, clinical MRI uses almost exclusively the proton nucleus of the hydrogen atom, which occurs naturally in tissue water. Thus, there is a particularly strong signal, which is sensitive to tissue status and provides exquisite indications of soft tissue anatomy. Increasingly, the development of specific contrast agents and selective pulse sequences allows more detailed analysis of tissue properties such as diffusion, flow, and changes in vascular oxygenation [1,2]. Much information may also be obtained from metabolites; however, these typically occur at millimolar concentrations (or less) requiring prodigious water suppression [3]. Heteronuclei can provide metabolic tracers and physiological reporters while avoiding the intense water and lipid signals. The ^{19}F atom has sensitivity of the order of 80% of that of proton, but there is essentially no endogenous signal from tissues. Most of the fluorine in the body is in the form of solid state fluoride ions, which give very broad lines, essentially undetectable using standard NMR equipment. There are also a few fluorine containing molecules that occur in nature, but these are almost exclusively in plants, are highly toxic, and thought to be part of inherent defense mechanisms [4]. Thus, any molecular fluorine introduced into the body in the form of reporter molecules or drugs is readily detected with high sensitivity.

The importance of fluorine in the Life Sciences continues to be recognized in journals such as the *Journal of Fluorine Chemistry*, reviews in regular journals devoted to technology, and the current series *Advances in Fluorine Science*. Many reviews beginning in the 1980s were devoted to fluorine NMR with seminal work from Thomas, Selinsky and Burt, Prior, and London [5–8]. More recently, Mason reviewed the use of perfluorocarbons (PFCs) for measuring tissue oxygenation [9,10] and fluorinated derivatives of vitamin B6 as probes of pH *in vivo* [11]. McSheehy *et al.* [12] discussed applications of fluorine NMR to oncology, Menon [13] examined fluorinated anesthetics, and Passe *et al.* [14] reviewed neuropsychiatric applications. Several reviews have concerned the pharmacokinetics of

fluoropyrimidine drugs based on fluorine NMR including notable contributions from Bachert, Martino, and Wolf [15–17] and, indeed, Wolf *et al.* contributed the succeeding article in this volume. Use of fluorine NMR to investigate physiology and pharmacology from an organic chemical perspective was the focus of a review by us [18]. Given the continuing appearance of novel applications in the field and developing interest in fluorine NMR, this current article will provide both a historical perspective and review state of the art. Readers are also directed to many relevant reviews that consider pharmacology, organic chemistry, or synthetic methods relating to fluorine [19–30]. Examples include recent reviews from Jescke [26]: on the unique role of fluorine in the design of active ingredients for modern crop protection, Dolbie: a review of fluorine chemistry at the millennium [21], Shimizu and Hiyama [24]: examining modern synthetic methods for fluorine substituted target molecules, Isanbor and O'Hagan [28]: reviewing fluorinated anticancer agents, Jäckel and Kokschi [23]: on fluorine in peptide design approaching engineering, and Plenio: on the coordination chemistry of fluorine in fluorocarbons [25].

1.1. Context and perspective

In many disciplines, investigators have a deep understanding of their own speciality, but lack perspective of competing technologies. Historically, NMR investigators were physicists, who could develop sophisticated pulse sequences to manipulate nuclear spins, or radiofrequency engineers specialized in wave propagation and coil design. Alternatively, NMR investigators were chemists who could design new reporter molecules and assess metabolic processes. Today, the field is far more diverse. Beyond the integration of multiple disciplines into NMR, increasingly, there is recognition that often no single technology will optimally solve a problem, but multidisciplinary teams need to understand the strengths and weakness of diverse technologies and exploit multiple modalities. This review will promote the virtues and unique capabilities of ^{19}F NMR, but it is important to recognize competing technologies. In the United States, increased emphasis on multimodality imaging and cross-disciplinary research is now driven by the formation of the National Institute for Biomedical Imaging and Bioengineering (NIBIB) [31] and Cancer Imaging Program (CIP) of the NCI [32]. Moreover, new learned societies are dedicated to imaging in general, for example, Society of Molecular Imaging (SMI) [33], as opposed to being devoted to a specific modality (e.g., International Society of Magnetic Resonance in Medicine (ISMRM) [34] or Society of Nuclear Medicine [35]) and many journals have published issues reviewing diverse imaging methods [36–39].

Proton MRI has the great advantage of using spin physics to interrogate tissue water revealing anatomy and pathophysiology based on cellular and tissue properties. Nonetheless, it is often enhanced by the introduction of paramagnetic contrast agents at micromolar concentrations. Fluorine MRI typically requires

millimolar concentrations of reporter molecules. In this respect, radionuclide and optical imaging techniques can offer far superior sensitivity, potentially with pico to nanomolar requirements. Fluorescence imaging is becoming more attractive with the commercial availability of many labeling kits [40] and new instrumentation, which allows spectral deconvolution [41]. However, fluorescence imaging can suffer from signal quenching and is generally a two-dimensional technique. Recently, 3D fluorescence is becoming feasible in small animals [42,43]. Nanoparticles (quantum dots) offer particularly high sensitivity although current generations would be inappropriate for human application, since they use highly toxic elements, such as cadmium and mercury [44]. Fluorescent proteins can also be generated *in situ*; cellular transfection can generate green fluorescent protein (GFP) or longer wavelength proteins [45]. Alternatively, cells may be transfected with a bioluminescent imaging (BLI) reporter such as luciferase, which emits light upon interaction with luciferin substrate [38,46]. Again, this is becoming feasible in three dimensions in small animals [47]. Generally, optical imaging technologies can use relatively cheap instrumentation.

Radionuclide imaging has similar sensitivity to optical imaging and is routinely used for studies of biodistribution, planar γ -scintigraphy, positron emission tomography (PET), and single photon emission computed tomography (SPECT) [48,49]. A major drawback with radionuclides is the limited shelf life of substrates, which may either decay (short half-life) or be subject to long-term radiolysis. Radioactivity also poses specific safety issues during production, reagent preparation, and ultimate disposal. Nonetheless, several PET and SPECT agents are in routine clinical use (e.g., fluorodeoxyglucose [FDG], Prostascint, ^{99m}Tc [50–52]). Other materials are effective for tracing the pharmacokinetics of labeled substrates. A major problem is ensuring that the label remains part of the molecule, since radioactivity provides no molecular characterization and unless specific analytical techniques such as high performance liquid chromatography (HPLC) are applied, only experience can indicate whether metabolic transformation has occurred.

Ultrasound and X-ray imaging are routine in the clinic and examine endogenous molecules based on signal reflection and/or absorption. These are starting to find application in small animal research [53]. Currently, they provide primarily anatomical information, although addition of contrast agents promises new applications [54].

Relatively, ^{19}F NMR has multiple strengths and virtues as described in the following sections. Briefly, fluorine containing molecules tend to be metabolically stable and have indefinite shelf life. The fluorine nucleus offers sufficient sensitivity for imaging, but also provides a very large chemical shift range immediately revealing metabolic transformations and allowing multiple molecules to be observed and identified simultaneously with potential applications to metabolomics. Fluorine MRI is readily combined with anatomical proton MRI providing high spatial resolution anatomy.

1.2. ¹⁹F as an *in vivo* NMR probe

¹⁹F is 100% naturally abundant and the only stable isotope of fluorine. The nucleus has a nuclear spin $I = \frac{1}{2}$ and a gyromagnetic ratio of 40.05 MHz/T, providing a sensitivity approximately 83% that of protons. The high gyromagnetic ratio generally allows the use of existing proton NMR instrumentation with the minimum of component adjustments. NMR has multiple strengths and virtues. Modern NMR instrumentation can be user friendly allowing a well-trained technician to undertake studies. However, NMR is intrinsically a complex tool providing potentially a multitude of information based on diverse parameters including signal intensity (SI), chemical shift (δ), and changes of chemical shift ($\Delta\delta$). In addition, signals are characterized by the transverse dephasing rate ($R_2^* = 1/T_2^*$), spin–spin or transverse relaxation rate ($R_2 = 1/T_2$) and spin–lattice or longitudinal relaxation rate ($R_1 = 1/T_1$). Indeed, each of these parameters have been exploited for specific ¹⁹F NMR reporter molecules (Table 1). With care, the NMR signal can be quantitative, so that the integral (area under the peak) of a signal is directly proportional to the amount of material being interrogated. However, NMR may be considered relatively insensitive compared with some other modalities. Typically, millimolar concentrations are required to achieve a good signal in a reasonable amount of time. The precise detection sensitivity is governed by numerous parameters including the volume of interrogation, the required spatial resolution, and relaxation properties of the molecule, and its tendency to accumulate or disperse from a region of interest. Perhaps, most important is the temporal resolution since signals may be averaged over many hours. Increasingly, there are attempts to target fluorinated agents to accumulate at a site of interest, for example, using specific antibodies [55,56] and low-molecular weight ligands [57].

The simplest concept of NMR is that of chemical shift. In this context, ¹⁹F is exceptionally sensitive to molecular and microenvironmental changes. Fluorine NMR has a chemical shift range of approximately 300 ppm, as opposed to approximately 10 ppm for proton. Multiple different fluorinated agents may readily be detected simultaneously with minimal danger of signal overlap. To allow comparison between data from different molecules and different investigators, chemical shifts must be referred to a standard. The International Union of Pure and Applied Chemistry (IUPAC) ¹⁹F NMR chemical shift standard is fluorotrichloromethane (CFCl₃) [58]. Using this agent, the range of chemical shifts of most organic fluorinated compounds is 0–250 ppm. However, this volatile solvent is not convenient for most biomedical applications and thus, secondary standards are usually preferred. We favor sodium trifluoroacetate (CF₃CO₂Na or NaTFA). This has the advantage of being readily available, quite nontoxic, and may be used as either an external, or indeed, internal chemical shift standard in biological investigations. It should be noted that fluorine chemical shifts can be strongly solvent dependent and vary with dilution [59]. Fluorine may ultimately be described on a ϕ scale, extrapolated to infinite dilution, under which

Table 1. Fluorinated reporter molecules

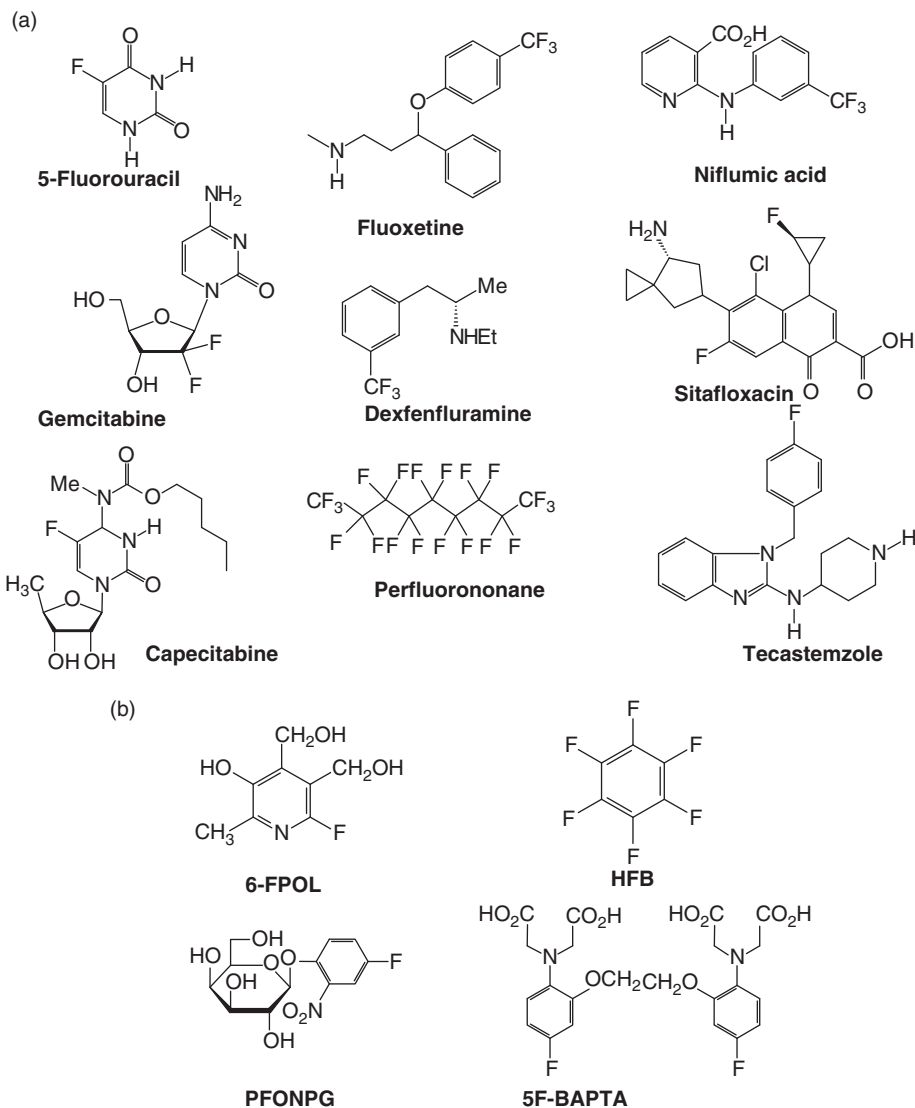
Parameter	Indicator (example)	NMR parameter	References (representative)
Physical interactions			
pO_2	Perfluorocarbons	R_1 (R_2)	[9,10,222,351,407]
	For example, hexafluorobenzene	$\Delta\delta$	[408]
pH	FPOL, DFMO, ZK150471	$\Delta\delta$, J	[11,280,301,303,409]
[Na ⁺]	F-cryp-1	δ , ratio	[410]
[Ca ²⁺]	5F-BAPTA	δ , ratio	[8,295,311]
[Mg ²⁺]	5F-APTRA	δ , ratio	[321]
Membrane/chloride potential	TFA	ratio	[287,411]
Chemical interactions			
Gene activity	PFONPG, 5FC	$\Delta\delta$	[147,294,374,378]
Nitric oxide	NN ^{•a}	$\Delta\delta$	[412]
Hypoxia	F-misonidazoles	Integral	[351,413]
Glycolysis	FDG	Integral	[331]
Drug metabolism	5FU, gemcitabine	Integral	[17,63]
Protein catabolism	DLBA	Integral	[414]
Disease specific receptors	Nanoparticles	Integral	[56,57]
Passive reporters			
Temperature	PFCs	Ratio	[5,207,415]
Blood flow	Freon FC-23	Integral	[401]
Cell volume	TFM	integral	[287]
Diffusion	FDG	ADC	[416]
Vascular volume	Fluorocarbon emulsion	Integral	[398,417]
Lung function	PFC; SF ₆	Integral	[384,386,387]
GI function	PFC	Integral	[69,392]
Myocardial infarction	MP-312	Integral	[418]

^a 2-(2,6-Difluorophenyl)-4,4,5,5-tetramethyl-4,5-dihydro-1H-imidazol-3-oxide-1-oxyl.

conditions $\text{CF}_3\text{CO}_2\text{H}$ is quoted as -76.530 ppm. For precise measurements, it may be critical for both the chemical shift standard and molecule of investigation to be under precisely the same conditions (necessitating an internal standard). External standards, for example, in glass capillaries, may be subject to small susceptibility effects causing errors in estimation of absolute chemical shift. However, they provide more reliable quantitation standards for SI. Chemical shift is the mainstay of detecting and classifying molecules and detecting and identifying metabolic products of agents. While there have been many theoretical exercises on fluorine chemical shift it can often be quite unpredictable and occurs across an exceptionally large range. In 1971, Emsley and Phillips [60] published a 520-page review of the theory relating to ^{19}F NMR chemical shifts followed by a 673 page compilation of coupling constants [61].

Scalar coupling constants of fluorine are typically much larger than proton. For geminal fluorine atoms, $^2J_{\text{FF}}$ may be in the range of 200–800 Hz, while $^3J_{\text{FF}}$ is often less than 1 Hz, yet $^4J_{\text{FF}}$ may reach 20 Hz: such nonmonotonicity can be confusing and large long range couplings $^{6\text{or}7}J_{\text{FF}}$ are also encountered [18,59,61,62]. Proton fluorine coupling constants are $^2J_{\text{FH}} \sim 45\text{--}90$ Hz and $^3J_{\text{FH}}$: 0–53 Hz. While fluorine carbon coupling is typically large ($^1J_{\text{CF}} > 200$ Hz), it is generally not observed unless the carbon is enriched with ^{13}C . However, as a corollary, fluorine coupling is observed clearly and extensively in ^{13}C NMR spectra. To avoid complexity of fluorine–fluorine coupling, it may be important to include fluorine as a symmetrical moiety, for example, a trifluoromethyl group, as opposed to asymmetric geminal fluorine atoms or a single fluorine atom. Likewise, a CF_3 moiety will generally avoid fluorine–hydrogen couplings. Since ^{19}F NMR is often detected by retuning a proton channel, proton decoupling may not be available.

Representative drugs, which include fluorine atoms and for which *in vivo* NMR has been reported are shown in Fig. 1 [17,63–73]. Furthermore, many drugs in early preclinical testing include fluorine atoms: the prevalence of fluorine atoms may reach 20% of all candidate agents [19]. Introduction of fluorine requires care. While the carbon fluorine bond is particularly strong, any release of fluoride or metabolites such as mono- or difluoroacetate can lead to exceedingly toxic products. For reporter molecules or pharmacological drugs, it is clearly important to minimize inadvertent toxicity. In this respect, the trifluoromethyl (CF_3) group is particularly suitable, since it resists degradation and for NMR avoids fluorine–fluorine couplings. In pharmaceuticals and agrochemicals, fluorine occurs in many forms ranging from a single fluorine atom to as many as six or nine identical fluorines (Table 2). In terms of NMR detection, the more equivalent fluorines, the stronger the signal. However, fluorine will modulate the properties of a molecule, since the fluorine atom is exceedingly electronegative and the CF bond strongly polarized. While the van der Waals radius of a fluorine atom is quite similar to a proton, the electronegativity alters electronic configuration modulating $\text{p}K_{\text{a}}$. For the series of acetic acids $\text{p}K_{\text{a}}(\text{CH}_3\text{CO}_2\text{H}) = 4.76$, $\text{p}K_{\text{a}}(\text{CH}_2\text{FCO}_2\text{H}) = 2.59$, $\text{p}K_{\text{a}}(\text{CHF}_2\text{CO}_2\text{H}) = 1.24$, and $\text{p}K_{\text{a}}(\text{CF}_3\text{CO}_2\text{H}) = 0.23$ [19]. Similar changes have been reported for a

**Fig. 1.** Continued

series of fluoromethyl alanines (Table 3) [74]. The trifluoromethyl group is often considered to be equivalent to the introduction of an isopropyl group. Fluorine not only perturbs the electronic structure of a molecule, but also alters the hydrophobicity [75]. Indeed, in many cases, particularly for agrochemicals, fluorine is specifically added to reduce the water solubility of molecules, so they are retained more effectively on the waxy cuticle of plants [26]. Fluorine modifies lipophilicity and ability to cross membranes, such as the blood–brain barrier, which is pertinent to the extensive applications in anesthetics and psychiatric drugs [76].

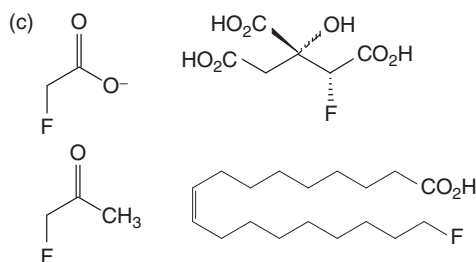


Fig. 1. (a) Representative fluorinated molecules. Pharmaceuticals for which clinical or preclinical *in vivo* NMR studies have been reported: 5-fluorouracil (5FU) [16,17,63], gemcitabine [65], and capecitabine [73] are anticancer drugs; fluoxetine [162] and dexfenfluramine [72] have neurological activity, sitafloxacin [66] is an antimicrobial, niflumic acid [67] is a nonsteroidal anti-inflammatory, tecastemizole [68] is an experimental antihistamine and perfluorononane has been proposed for GI imaging [69]. (b) Published ^{19}F NMR reporter molecules: 6-FPOL (6-fluoropyridoxol) is a pH reporter [11], hexafluorobenzene (HFB) is used for oximetry [10], PFONPG is a gene reporter for β -gal [294], and 5FBAPTA measures $[\text{Ca}^{2+}]$ [295]. (c) Natural products incorporating fluorine atoms: fluoroacetate, fluorocitrate, fluoroacetone, and fluorooleic acid [4].

Fluorine chemistry has made major progress over the last 10–15 years and now many reagents are available for derivatization [24]. However, many require quite severe conditions using such materials as hydrogen fluoride [77], various metal halides such as SeF_4 [78], WF_6 [79], XeF_2 [80], and SbF_5 [81], or fluorine itself [82]. In some cases, a fluorine moiety may be introduced with S-ethyl trifluoroacetate (SETFA) [83] or trifluoroacetic anhydride [84]. It is often preferable to use a starting material that already includes a fluorine or multiple fluorine atoms, which may be introduced using relatively mild conditions, as explored extensively in the generation of fluorinated peptides [23].

While only a single isotope of fluorine is available for NMR, fluorine is finding increasing use as ^{18}F for PET (see other articles in this volume). While ^{18}F has a limited half-life ($t_{1/2} = 110$ min), it has found major application in the detection of tumors including Medicare reimbursed studies with FDG within the last 5 years. There is active interest in the pursuit of other ^{18}F agents to detect parameters such as hypoxia or mitosis [85–90]. The greatest strength of PET is that it may use nano to femtomolar concentrations, as opposed to the milli to micromolar concentrations required for NMR. However, ^{18}F simply provides a count of molecular concentration, that is, detecting radioactive decay with no indication of multiple substrates or metabolites. Thus, it may require rigorous HPLC or other analyses to strictly determine the fate of a drug. Meanwhile, ^{19}F can allow the detection of multiple agents, and metabolites simultaneously based on chemical shift. ^{19}F is indefinitely stable and the lack of radioactivity provides not only a long shelf life, but minimizes any issues of disposal of hazardous waste. Moreover, any fluorine MRI detection is readily correlated with the exquisite anatomy provided by routine proton MRI.

Table 2. Fluorine-containing pharmaceuticals and agrochemicals [22,26,28]

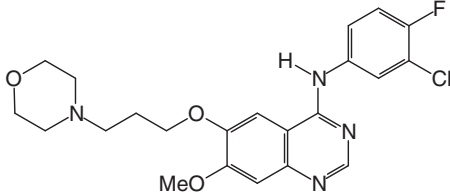
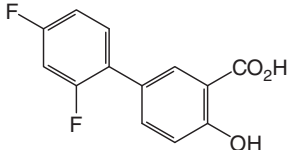
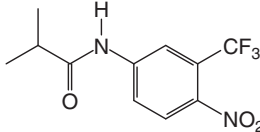
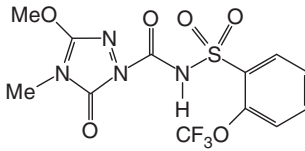
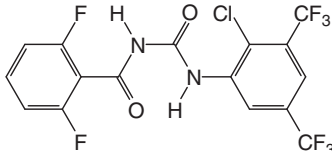
Number of equivalent F-atoms	Molecular structure	Name	Use	Relevant references
1		Gefitinib ZD1839 Iressa®	Anticancer drug	[419,420]
1 + 1		Diflunisal Dolobid®	Anti-inflammatory drug	[182]
3		Flutamide Eulexin®	Anti-androgen drug	[181,421]
3		Flucarbazone	Herbicide	[422]
3 + 3 + 2		Bistrifluron	Insecticide	[423]

Table 2. Continued

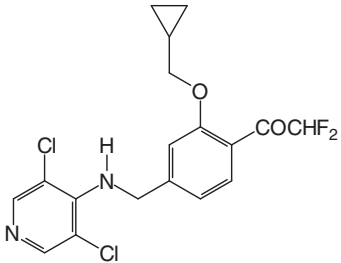
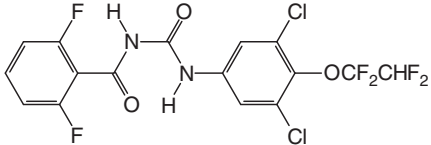
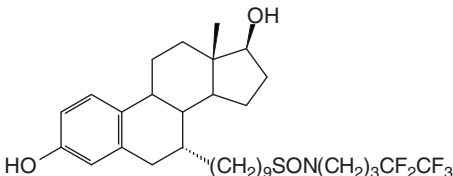
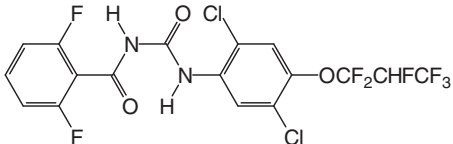
Number of equivalent F-atoms	Molecular structure	Name	Use	Relevant references
2		Roflumilast	Anti-inflammatory(asthma) phosphodiesterase (PDE) 4 inhibitor	[424]
2 + 2 + 2		Hexaflumuron	Insecticide	[425]
3 + 2		Fulvestrant Faslodex [®]	Anti-androgens drug	[426]
3 + 2 + 2 + 1		Lufenuron	Insecticide	[427]

Table 2. Continued

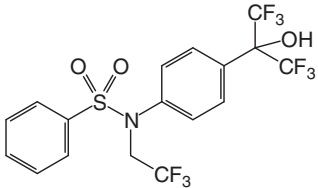
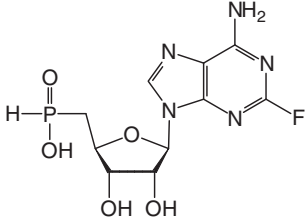
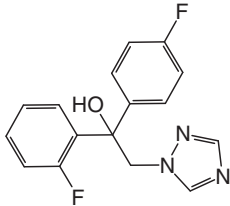
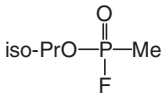
Number of equivalent F-atoms	Molecular structure	Name	Use	Relevant references
6 + 3		T 0901317	Anticancer drug	[183]
1		Fludarabine	Topoisomerase inhibitor	[428]
1 + 1		Flutriafol	Fungicide	[429]
1		Sarin	Toxicant	[430]

Table 3. ¹⁹F NMR pH indicators

Reporter	Structure	pK _a	δ _{F(acid)} [*] (ppm)	δ _{F(base)} [*] (ppm)	Δδ (ppm)	Reported applications
3-Fluoro-2-methyl alanine		8.5	−143.2	−145.3	2.05	Intracellular pH, perfused liver, lymphocytes [74]
3,3-Difluoro-2-methyl alanine		7.3	−53.95	−55.95	2.00	Figure 8 [74]
3,3,3-Trifluoro- 2-methyl alanine		5.9	−0.25	−2.35	2.10	[74]
DFMO		6.4	4.60	4.30	0.30	[286]
6-FPOL		8.2	−9.84	−19.56	9.72	Transmembrane pH gradient, blood, heart, tumor [11,290]

Table 3. Continued

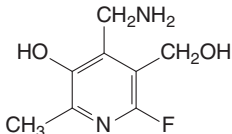
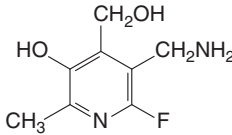
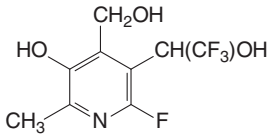
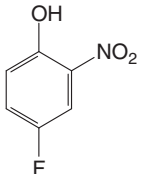
Reporter	Structure	pK _a	$\delta_{\text{F(acid)}}^*$ (ppm)	$\delta_{\text{F(base)}}^*$ (ppm)	$\Delta\delta$ (ppm)	Reported applications
6-FPAM		7.05	−9.19	−19.19	10.07	Transmembrane pH gradient, blood, heart, tumor [11,291]
6-FPOL-5-NH ₂		8.0	−7.57	−19.55	11.98	[291]
6-FPOL-5- α -CF ₃		7.6	−4.45	−14.09	9.64	[291]
PFONP		6.9	−44.44	−55.76	11.32	Transmembrane pH gradient, blood [294,374]

Table 3. Continued

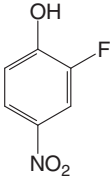
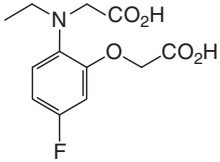
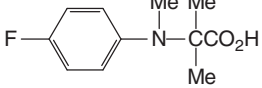
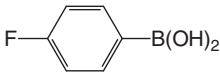
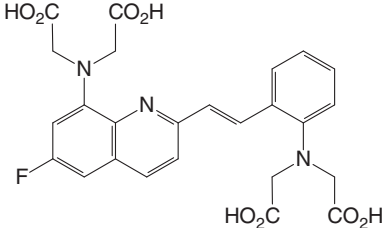
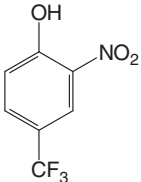
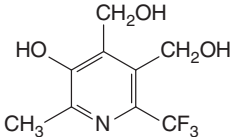
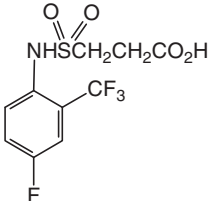
Reporter	Structure	pK _a	δ _{F(acid)} [*] (ppm)	δ _{F(base)} [*] (ppm)	Δδ (ppm)	Reported applications
OFPNP		6.0	−58.77	−61.01	2.24	Extracellular pH [294]
5FNEAP-1		6.85	35.60 [*]	24.70 ^{**}	10.90	Extracellular pH [298]
<i>N,N</i> -(methyl-2-carboxyisopropyl)-4-fluoroaniline		6.8	−36.00	−49.50	13.50	<i>In vivo</i> pH measurement agents [297]
4-Fluoro benzene boronate (FBA)		8.7	−34.50	−43.50	8.80	<i>In vivo</i> pH measurement agents [431]
Fquene		6.7	11.82 ^{***}	8.73 ^{***}	3.09	Intracellular pH, liver of rats [296]

Table 3. Continued

Reporter	Structure	pK _a	$\delta_{\text{F}(\text{acid})}^*$ (ppm)	$\delta_{\text{F}(\text{base})}^*$ (ppm)	$\Delta\delta$ (ppm)	Reported applications
PCF ₃ ONP		5.6	13.49	14.52	1.03	Extracellular pH [299]
CF ₃ POL		6.8	15.15	16.76	1.7	Extracellular pH [18]
ZK 150471		7.16	−52.74****	−62.87****	−10.13	<i>In vivo</i> pH probe, tumor and tissue [301,303, 304]

* Unless otherwise noted, dilute CF₃CO₂[−] was used as chemical shift reference

** tetrafluoroterphthalic acid was used as standard, though variously in the experimental section NaF and hexafluorobenzene were used as standards

*** chemicals shifts quoted with respect to 5FBAPTA

**** intramolecular chemical shift difference.

NMR is a particularly facile approach to analysis requiring minimal sample preparation: mixtures, turbid media, and organisms including biopsy specimens or living plants and animals or even patients may be examined directly. Feasibility is governed by sample volume and the need for appropriate magnetic resonance systems and radio frequency (RF) coils [91,92]. For small specimens (<1 ml), magnetic fields exceed 22 T (950 MHz proton) and routine analysis is available at and above 7 T. These high field systems usually use vertical narrow bore magnets which can accommodate small samples of solutions (analytical and *in vitro* investigations) and sometimes mice. Small animal studies are most commonly performed in horizontal bore systems at 4.7 T, but increasingly systems are available at 7 and 9.4 T. Humans are now routinely studied at 3 T with research systems up to 12 T. Figure 1 shows representative drugs, which have been studied by ^{19}F NMR in clinical trials.

Proton NMR is potentially more versatile, since protons are essentially ubiquitous. However, this also provides a major drawback—crowded signals across limited chemical shift dispersion. Moreover, the water component of tissues can approach 70% water leading to signals approaching 80 M, as compared with mM metabolites. Elegant water suppression methods have evolved over the years, but often obliterate extended spectral windows around water or are limited to specific molecular structures exhibiting multiquantum detectability [93–95]. Lipid signals may also interfere with detection. Samples may be subjected to D_2O exchange, but this is perturbing. Deuterium enrichment is feasible providing up to 6,400-fold amplification [96], but the gyromagnetic ratio (γ) is much lower reducing ultimate sensitivity. Carbon is also ubiquitous in biological systems, but only 1.1% is NMR active as ^{13}C . This does provide the opportunity for selective isotopic enrichment and has proven fruitful for many studies [97], though ^{13}C can be expensive. Again, the gyromagnetic ratio is relatively low, precluding effective clinical studies at low fields.

The virtues of ^{19}F have led to the design and use of many reporter molecules in preclinical investigations (Table 1 and Fig. 1b). Since, there are few naturally occurring compounds containing fluorine, fluorinated molecules do not have to compete with background signal. Fluorine does occur extensively in bones and teeth, but the solid matrix causes very short T_2 values providing exceedingly broad signals, which can either be removed by deconvolution or electronic timing. Indeed, special rapid electronics are required for detecting solid state ^{19}F [98]. The spin lattice relaxation time T_1 can be quite long, but efficient use of rapid pulsing at the Ernst angle can accelerate spectral acquisition [99]. For aqueous solutions, relaxation agents, such as Gadolinium diethylenetriamine penta-acetic acid (Gd-DTPA), can be added to accelerate relaxation [100–102], and indeed, this has been used to identify cellular compartmentation based on the ability of the contrast agent to relax extracellular material, but not intracellular [103]. Data acquisition efficiency can also be enhanced by interleaving or acquiring simultaneously ^1H and ^{19}F NMR providing both anatomical and

pharmacological/physiological data simultaneously [91,92,104,105]. T_1 relaxation is extensively exploited with PFCs to measure pO_2 , as described in detail in Section 3.1.1.

A few natural organofluorine compounds exist, most notably in plants (Fig. 1c). These are generally noted for their toxicity; most importantly, fluoroacetate enters the tricarboxylic acid (TCA) cycle and as fluorocitrate inhibits *cis*-aconitase [4,106,107]. Of course, toxicity provides an opportunity to generate specific poisons and fluoroacetate is widely used as a rodenticide providing opportunities for NMR [108]. ^{19}F NMR has been used for extensive studies of body fluids such as milk and urine with respect to xenobiotica [109–115].

Fluorine is increasingly used in industrial products ranging from fluoropolymers (e.g., Teflon) and liquid crystal components to anesthetics (e.g., isoflurane) to refrigerants and fire suppressants (halocarbons), numerous agrochemicals and several medicines [21,22,26,28]. While application of fluoro molecules will lead to increasingly crowded spectra, the large chemical shift range ensures that multiple molecules may be detected simultaneously. For example, in a study to investigate influence of tumor pH, on the anticancer drug 5FU in rat breast tumors, four molecules were detectable simultaneously (Fig. 2), the drug 5FU at -93.6 ppm, the extracellular pH reporter CF_3POL at $+16.69$ ppm, a chemical shift standard NaTFA (0 ppm) and two signals for the gaseous veterinary anesthetic isoflurane (-5.1 , -10.99 ppm). As noted above, we favor NaTFA as an internal standard for biological investigation, as compared with the IUPAC

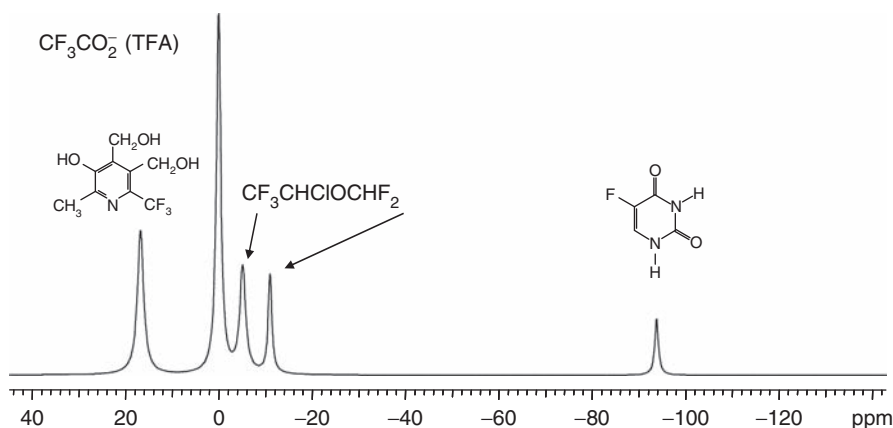


Fig. 2. Simultaneous detection of multiple fluorinated molecules *in vivo*. To explore the hypothesis that uptake of the anticancer drug 5FU by tumors is pH dependant, we infused 5FU (0.4 ml (50 mg/ml) IV), the extracellular pH reporter CF_3POL (400 mg/kg IP), and the chemical shift standard NaTFA (200 mg/kg IP) into an anesthetized rat (1% isoflurane) with a subcutaneous 13762NF breast tumor ($1.4 \times 1.5 \times 1.1$ cm). Thirty minutes after administration, all four molecules were detectable simultaneously in 17 min. At this stage, no metabolites of 5FU were detected.

standard (CFCl₃). In principle, the NaTFA was unnecessary here, since the isoflurane signals could have served as a secondary standard. However, it is important to note that the signals from anesthetics tend to have very short T_2^* [116–118], and thus, while they are visible in this pulse-acquire spectrum, they will tend to be “lost” in spin echo investigations, such as chemical shift imaging (CSI). While ¹⁹F NMR investigations can generally be performed using existing ¹H equipment, some care is required, since probe and RF components may include fluorinated material which can give rise to spurious signals [119].

In the following sections, this review will separately consider industrial pharmacological and agrochemical agents (Section 2) followed by active (Section 3) and passive (Section 4) reporter molecules. Active reporter molecules may further be differentiated as those based on physical interaction with a substrate (Section 3.1) or those that undergo a chemical reaction (Section 3.2).

2. ¹⁹F NMR FOR PHARMACOLOGY

Fluorine is often added to modulate biological activity of pharmaceuticals. Numerous reports describe changes in pK_a [74,75] (see also Table 3), lipophilicity [19,26,75], retention, resistance to degradation [22], enhanced binding [19,120] induced by selective incorporation of F atom or atoms. In other cases, F atoms have been used to probe molecular interactions or binding sites in order to enhance drug design, even if fluorine is ultimately not included in the drugs. It has been recognized that ¹⁹F chemical shift is not only highly dependant on molecular structure and ionization, but also on the microenvironment. In early works, Dwek [121] and Gerig [122] reported the use of F moieties to probe interactions of oxy- and deoxyhemoglobin with cofactors such as diphosphoglycerate (DPG) under differential protonation [123]. Trifluoroacetylated chitotriose and *N*-trifluoroacetylglucosamine were used to probe active sites in lysozyme [124]. Many fluoro sugars have been used to study enzyme specificity, substrates, or inhibitors of enzymes such as glycogen phosphorylase and glucosidases [125–127].

Essentially, no background ¹⁹F signal occurs and the sensitivity is sufficient to examine biological mixtures, for example, body fluids such as urine, blood, or milk for fluorinated metabolites [109–115,128,129]. This is being used both by academic laboratories and pharmaceutical companies to examine the fate of xenobiotica. In some cases, metabolites (degradation products or excretory bioconjugates) are derived from fluorine containing drugs; in other cases, ¹⁹F labels may be added for the ADME (absorption, distribution, metabolism, and excretion toxicity) process to learn about pathways, even though the labels are not included in the ultimate pharmaceuticals. In several cases, glucuronides have been identified as key detoxification products [130–132].

2.1. Cancer chemotherapeutics

2.1.1. Fluoropyrimidines

With the significant developments in fluorination technology, inclusion of F atoms into pharmaceuticals and agrochemicals is becoming more feasible and popular [26,28]. Fluorine can yield subtle, but significant changes in drug activity [19,22,28]. The F atom is generally considered to have a structural size between H and OH, while CF_3 is similar to an isopropyl group [75]. The strong electronegativity can modulate electronic distributions influencing pK_a , particularly in proximity to delocalized aromatic structures [19,75]. F may be involved in hydrogen bonding altering binding and entry into enzyme pockets [23]. Many new industrial pharmaceuticals and agrochemicals incorporate a fluorine group providing a tool for NMR investigations. Figure 1 show drugs, which have been examined by ^{19}F NMR in clinical or advanced preclinical studies, while Table 2 shows diverse molecules including pharmaceuticals and agrochemicals, which could be strong candidates for ^{19}F NMR investigations, but for which reports are lacking in the public domain. Most studies to date have examined pharmacokinetics and metabolism of fluoropyrimidines, particularly 5-fluorouracil (5FU). 5FU was first developed in the 1950s and remains a primary drug in treatment of many cancers, but it has a narrow range of efficacy/toxicity [28,63,133]. Presumably, both response and toxicity are related to pharmacokinetics and there is interest in assessing dynamics of uptake, biodistribution, and metabolism. Patients with enhanced tumor retention of 5FU ("trappers") may be expected to exhibit better response [134]. Such trapping is apparently a requisite, though not in itself sufficient for efficacy [17].

Given the importance and prevalence of 5FU, over 200 studies have reported ^{19}F NMR investigations in clinical trials and evaluation in animal models. Several detailed reviews consider metabolism, pharmacokinetics, and detectability of 5FU and its metabolites and the reader is referred to these [15–17,63]. 5FU requires anabolic conversion to nucleosides (e.g., FdUrd, FdUmp) and nucleotides for cytostatic activity, requiring the activity of various kinases and phosphorylases [17]. However, competing catabolic reactions convert 5FU to 5,6-dihydrofluorouracil (DHFU) and α -fluoro β -alanine (FBAL) in liver, in addition to several other molecules offering little toxicity [15,17,135]. FBAL is excreted by the kidneys. Localized NMR spectroscopy and low resolution CSI have examined pharmacokinetics [103,136–138]. NMR of excised tissue and body fluids has also provided insight into metabolism and can provide much higher sensitivity (e.g., μM). While studies *in vivo* are most attractive, studies of cultured cells can also provide important information.

The pharmacokinetics of 5FU are reported to be pH sensitive and thus, measurements of tumor pH may have prognostic value for drug efficacy. In tumors with lower pH, the retention of 5FU is considerably enhanced [139–141]. This has prompted

investigations of the ability to alter pharmacokinetics by modulation of tumor pH to increase activity, for example, by breathing carbogen [142,143]. 5FU, its metabolites, and fluorinated pH reporter molecules can all be detected simultaneously by ¹⁹F NMR (Fig. 2). Intriguingly, fluoronucleotides derived *in vivo* from 5FU exhibit sensitivity to changes in pH and could be used to measure intracellular pH (pHi), although the presence of a mixture of products may complicate interpretation [141,144,145].

Given the inherent dose-limiting toxicity of 5FU, various prodrugs and mixture formulations have been developed (e.g., capecitabine (Xeloda), Tegafur-uracil (Uftoral®), emitefur (3 (3-(6-benzoyloxy-3-cyano-2-pyridyloxycarbonyl)benzoyl)-1-ethoxymethyl-5-fluorouracil)) and ¹⁹F NMR has played a role in analysis and development [16,63]. A new and potentially exciting application is assessment of prodrug therapy in conjunction with gene therapy; specifically, the use of cytosine deaminase (CD), to convert the relatively innocuous 5-fluorocytosine (5FC) to 5FU [146–150]. Several investigations have now reported ¹⁹F NMR of the conversion of 5FC to 5FU based on the ¹⁹F NMR chemical shift, $\Delta\delta = 2$ ppm [18,147,150,151].

Gemcitabine (Gemzar®) is a newer anticancer drug with a more favorable toxicity profile than 5FU. It comprises both sugar and pyrimidine moieties. In cells, it is phosphorylated and incorporated into DNA and to a lesser extent RNA, where it can inhibit DNA polymerases. It can also inhibit thymidine synthase. Given the significant clinical results and successful combination with radiotherapy, there is interest in optimizing activity based on ¹⁹F NMR. Unlike 5FU, fluorine is now on the deoxyribosyl ring and the two geminal fluorines give rise to an AB quartet at -42 ppm ($\delta_{\text{TFA}} = 0$ ppm). This has been detected in human tumor xenografts by ¹⁹F NMR following IP injection and kinetics have been investigated with respect to vasoactive drugs [65,152]. Metabolite signals have been observed in liver and bladder using CSI [153]. At low pH, the signals appear as an AB quartet, but they appear to collapse and broaden to a single signal at pH 8 (Fig. 3).

2.1.2. Other anticancer drugs

McSheehy *et al.* [154] presented a preliminary report of a novel thymidine synthase inhibitor, ZD9331, where both parent and metabolite peaks were detected at 4.7 T. Brix *et al.* [155] evaluated a trifluoromethylated derivative of 3-aminobenzamide, an inhibitor of poly(ADP-ribo) polymerase1 (PARP-1), as a potential radio sensitizer in Dunning prostate rat tumors and using CSI, detected separate signals from liver, muscle, and tumor revealing maximum tissue signals after 2 days. Spees *et al.* [156] followed pharmacokinetics of fluorine-labeled methotrexate in sensitive and resistant tumor xenografts in mice and found an inverse correlation between surviving fraction and area under the curve.

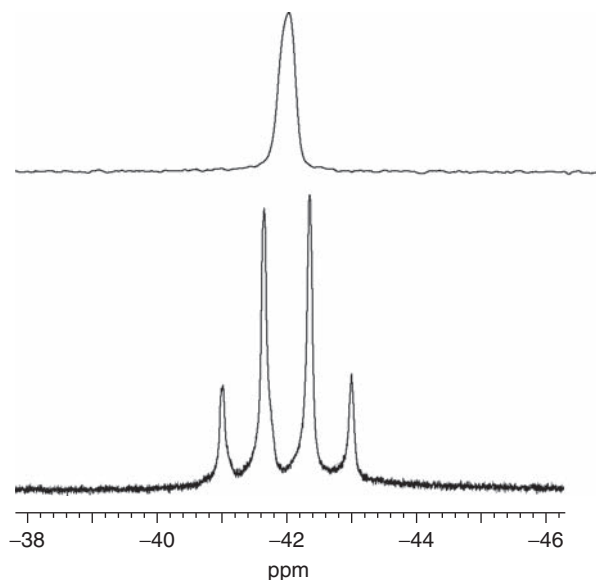


Fig. 3. ^{19}F NMR of gemcitabine. Lower spectrum shows a solution of gemcitabine hydrochloride at pH 3.2. For comparison, the upper spectrum was obtained in the presence of sodium hydroxide at pH 8.4. Each spectrum required about 1 min at 376 MHz (9.4 T) (data acquired in collaboration with Dr. Peter Peschke, DKFZ, Heidelberg, Germany).

2.2. Other drugs

Recognizing the exquisite sensitivity of ^{19}F NMR to microenvironment, inclusion of fluorine atoms in libraries of ligands has been used to probe molecular interactions based on changes in line width and chemical shift [157–160].

Following cancer chemotherapeutics, most *in vivo* ^{19}F NMR has examined psychiatric agents [14,161]. These can be particularly favorable when they incorporate a CF_3 moiety. Several reports investigated fluoxetine (Prozac) with studies ranging from biopsy tissue extracts to preclinical animal models and human volunteers [70,71,162]. The primary goal has been correlation of concentration with efficacy, for example, Henry *et al.* [70] explored the relative brain concentrations of *R* and *S* enantiomers versus a racemic mixture of fluoxetine in separate groups of patients. Other studies have examined fluvoxamine (a selective serotonin reuptake inhibitor—SSRI) to counter a possessive compulsive disorder [71,163]. Dexfenfluramine has been observed at brain concentrations $<10\ \mu\text{M}$ [72]. ^{19}F NMR of trifluoperazine revealed multiple metabolites in rat brain extracts, but these were too weak and unresolved *in vivo* at 4.7 T [164]. Such studies have provided a single unlocalized spectrum corresponding to whole brain volume and lines are generally quite broad (2–3 ppm). Sassa *et al.* [165] used ^{19}F chemical shift imaging to detect haloperidol decanoate in schizophrenic patients.

Other studies have examined fluoroquinolone antibiotics (fleroxacin) [166], antimicrobials (sitafloracin) [66], nonsteroidal anti-inflammatory (niflumic acid [67]), and anti-histamines (tecastemizole [68]). However, the tecastemizole was only detected from 3 of 23 patients and the retention was found to be much shorter than the psychotropic drugs such as fluoxetine. Attempts to detect dexamethasone in the eye at 1.5 T failed [167]. PFCs have been used as a tamponade in eye surgery and residual PFC has been detected in patients at 1.5 T [168,169]. Indeed, this allowed pO_2 measurements based on spin lattice relaxation, as discussed in detail in Section 3.1.1.1. The PFC emulsion synthetic blood substitute Fluosol was proposed as a method of modulating tumor oxygenation [170] and it could be detected from surrounding tissues as long as 1 year after administration and tumor resection [171]. Perfluorononane has been used to explore GI tract in man and mice at 1.5 T [69]. This may provide insight into GI function or serve as a model for all drug delivery.

Many gaseous anesthetics are fluorinated, for example, halothane, enflurane, isoflurane, sevoflurane, and desflurane. NMR studies of fluorinated anesthetics form some of the earliest *in vivo* applications of ¹⁹F NMR [172–174]. Issues regarding the use of anesthetics are site of anesthetic action, duration of residence in the brain, and toxicity of metabolic byproducts. The results have been a source of debate and controversy. Wyrwicz and coworkers [175] addressed the issue of residence times of anesthetics in the brain and observed signals for prolonged durations after cessation of anesthesia. Global spectroscopy is straightforward, but anesthetics have a short transverse relaxation time (T_2^*) and signals may be lost in localized spectroscopy or imaging approaches. Very few clinical studies have reported ¹⁹F NMR of anesthetics in the brain, though Menon *et al.* [13] demonstrated the feasibility of such studies and found halothane signal up to 90 min after the withdrawal of anesthetic. Lockwood *et al.* [176] studied isoflurane kinetics and showed biphasic elimination with decay halftimes of 9.5 and 130 min. Selinsky *et al.* [177,178] have studied the metabolism of volatile anesthetics showing generation of potentially toxic metabolites such as methoxydifluoroacetate, dichloroacetate, and fluoride ion from methoxyflurane.

The ability to detect drugs *in vivo* depends on multiple considerations. Obviously, the concentration at which drugs are administered is important together with the tendency to localize or clear from tissues. One would also expect multiple fluorine atoms to provide enhanced signal-to-noise over a single fluorine atom. Of course, they must be spectrally equivalent. Table 2 shows multiple diverse commercial molecules from the pharmaceutical and agrochemical fields, each of which has one or more fluorine atoms. Although no particular *in vivo* fluorine NMR has been reported, they are clearly prime candidates. Indeed, ¹⁹F NMR has been exploited to assess pesticides as contaminants in food [179]: in oils and wine levels >1 mg/l, while in food extracts detection levels may approach parts per billion [180]. In particular, we note that some agents have multiple equivalent fluorine atoms. Flutamide [181] has a trifluoromethyl

group and while there appear to be no references to *in vivo* NMR, ^{19}F NMR has been used to investigate drug formulation [181,182]. Bistrifluoron has two trifluoromethyl groups, but they are spectrally nonequivalent. By contrast, T009317 [183] has a hydroxyditrifluoromethylisopropyl group and would be expected to give high NMR sensitivity.

To obtain detectable signals (spectra, or images), sufficient fluorinated probe must be administered, though the concentration of probe in studies of living organisms should be as low as possible to avoid physiological perturbations or toxic side effects. For pharmaceuticals, fluorine labels are added for development, but their ultimate presence depends on optimal drug activity. By contrast, for reporter molecules, the fluorine atom is the key to efficacy and design is optimized for NMR detectability.

3. ACTIVE REPORTER MOLECULES

Many reporter molecules have been designed specifically to exploit fluorine chemical shift, coupling, or relaxation to reveal physiological parameters. Active agents typically fall into three categories: (i) molecules which enjoy a physical interaction, for example, PFCs, which exhibit exceptional gas solubility and reveal oxygen tension based on modification of relaxation parameters (Section 3.1.1); (ii) ligands designed to trap/bind specific entities, such as ions, specifically, but reversibly, for example, H^+ (pH) (Section 3.1.2), metal ions (Ca^{2+} , Mg^{2+}) (Section 3.1.3); and (iii) molecules which undergo irreversible chemical interaction modifying their structure, as revealed by a change in chemical shift (Section 3.2). These are represented by gene reporter molecules (Section 3.2.3), where substrates are cleaved by specific enzyme activity, and hypoxia agents (Section 3.2.2), which are modified by reductases and trapped. There are also passive agents, which occupy and hence reveal a space, compartment, or volume, for example, tumor blood volume (Section 4).

3.1. Physical interactions

3.1.1. *In vivo oximetry*

Oxygen is vital to the well being of normal mammalian tissues and deficits are associated with myocardial infarct, stroke, diabetic neuropathy, and cancer. In each case, lack of oxygen is associated with poor prognosis and a clinical goal is often to enhance tissue oxygenation. There is increasing evidence that hypoxia influences such critical characteristics as angiogenesis, tumor invasion, and metastasis [184–187]. Moreover, it has long been appreciated that hypoxic tumor cells are more resistant to radiotherapy [188]. Given that hypoxic tumors are more resistant to certain therapies, it becomes important to assess tumor oxygenation as part of therapeutic planning [189]. Patients could be stratified

according to baseline hypoxia to receive adjuvant interventions designed to modulate pO_2 , or more intense therapy as facilitated by intensity modulated radiation therapy (IMRT). Tumors, which do not respond to interventions, may be ideal candidates for hypoxia selective cytotoxins (e.g., tirapazamine [190]).

Thus, there is a vital need to be able to measure tissue pO_2 and many diverse technologies have been presented, as reviewed previously [10,191,192]. Some, such as near infrared spectroscopy and blood oxygen level dependent (BOLD) contrast MRI provide an indication of vascular oxygenation [2,193,194]. PET has been used to examine oxygen extraction fraction and hence metabolic activity based on uptake of $^{15}O_2$, but the half-life of oxygen-15 is exceedingly short ($t_{1/2} \sim 2$ min) [195,196]. Other modalities provide an indication of hypoxia [197,198]. In many cases, there is a desire to measure pO_2 directly and this may be achieved using polarographic electrodes [199,200], fiber optic probes [201], free radical probes with electron spin resonance (ESR) [191,202], or PFC probes with NMR [9,10], as described below.

3.1.1.1. PFC pO_2 reporters

NMR oximetry is based on the paramagnetic influence of dissolved oxygen on the ^{19}F NMR spin lattice relaxation rate of a PFC, as reviewed previously [10]. The solubility of gas, notably oxygen, in PFCs occurs as an ideal gas liquid mixture and thus, R_1 varies linearly with pO_2 , as predicted by Henry's Law [5,10,203]. R_1 is sensitive to temperature, and magnetic field, but importantly, R_1 of PFCs is essentially unresponsive to pH, CO_2 , charged paramagnetic ions, mixing with blood, or emulsification [204–206] and for the PFC emulsion of perfluorotributylamine (PFTB) (Oxypherol), we have shown that calibration curves obtained in solution are valid *in vivo* [207]. At any given magnetic field (B_0) and temperature (T)

$$R_1 = A + B pO_2, \quad (1)$$

where A is the anoxic relaxation rate and B represents the sensitivity of the reporter molecule to the paramagnetic contribution of oxygen and the ratio $\eta = B/A$ has been proposed as a sensitivity index [208]. Several PFCs have been used successfully for NMR oximetry and characteristics are summarized in Table 4. A particular PFC molecule may have multiple ^{19}F NMR resonances, and each resonance has a characteristic R_1 response to pO_2 and temperature [9,62]. Many PFCs (e.g., PFTB, perflubron (often referred to as perfluorooctylbromide [PFOB]) and TheroxTM (F44-E)) have several ^{19}F NMR resonances, which can be exploited to provide additional information in spectroscopic studies, but complicate effective imaging [209–211]. PFCs with a single resonance provide optimal signal-to-noise ratio (SNR) and simplify imaging: two agents hexafluorobenzene (HFB) [10,36,200,212–217], and perfluoro-15-crown-5-ether (15C5) [218–221] have found extensive use. While most pO_2 investigations have exploited the R_1 sensitivity, R_2 is also sensitive as reported by Girard *et al.* [222].

Table 4. ^{19}F NMR characteristics and applications of PFCs for tissue oximetry

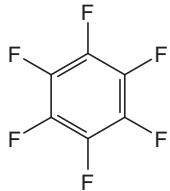
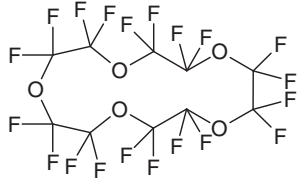
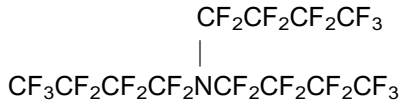
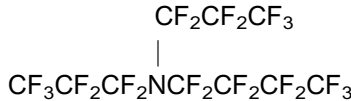
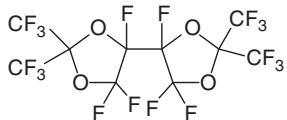
Name	Structure	Sensitivity to $p\text{O}_2^a$	Number of ^{19}F resonances	Applications
HFB		$A = 0.0835;$ $B = 0.001876$	1	Rat breast tumor, prostate tumor, human lymphoma xenograft [10,214, 215,217,267,270] (Fig. 7)
Perfluoro-15-crown-5-ether		$A = 0.345;$ $B = 0.0034$	1	Tumor cells, mouse tumor, spleen, liver, rat breast tumor, rat brain [218,247,254]
FC-43 (OxypheroI TM)		$A = 1.09;$ $B = 0.00623$	4	Liver, spleen, lung, eye, tumors, heart [5,243,244,256]
PFTP (Fluosol TM)		$A = 0.301;$ $B = 0.00312$	3	Rat spleen, lung, tumors, cells [232,252,406]

Table 4. Continued

Name	Structure	Sensitivity to pO_2^a	Number of ¹⁹ F resonances	Applications
F-44E (Therox™)	<chem>CF3(CF2)3CH=CH(CF2)3CF3</chem>	$A = 0.2525;$ $B = 0.16527$	4	Rat spleen, liver, aorta, mouse Tumors [235,253]
PFOB (Imagent™, Oxygent™)	<chem>Br(CF2)7CF3</chem>	$A = 0.2677;$ $B = 0.12259$	7	Rat heart, rat prostate tumor, rabbit liver, pig lungs, phantom [241,250,432,433]
PTBD		$A = 0.50104;$ $B = 0.1672$	2	Phantom [434]

^a $R_1 (s^{-1}) = A + B pO_2 (Torr)$.

HFB, hexafluorobenzene.

R_1 is sensitive to temperature and even a relatively small error in temperature estimate can introduce a sizable discrepancy into the apparent pO_2 based on some PFCs. The relative error introduced into a pO_2 determination by a 1 °C error in temperature estimate ranges from 8 Torr/°C for PFTB [207] to 3 Torr/°C for PFOB (perflubron) [223] or 15-Crown-5-ether [218] when pO_2 is actually 5 Torr. HFB exhibits remarkable lack of temperature dependence and the comparative error would be 0.1 Torr/°C [224]. Recognizing differential sensitivity of pairs of resonances within a single molecule to pO_2 and temperature, Mason *et al.* [207,225] patented a method to simultaneously determine both parameters by solving simultaneous equations. However, generally it is preferable for a pO_2 sensor to exhibit minimal response to temperature, since this is not always known precisely *in vivo* and temperature gradients may occur across tumors.

PFCs are extremely hydrophobic and do not dissolve in blood directly, but may be formulated as biocompatible emulsions for intravenous (IV) infusion. PFC emulsions have been developed commercially both as potential synthetic blood substitutes [226–229] and as ultrasound contrast agents [230,231]. Following IV infusion, a typical blood substitute emulsion circulates in the vasculature with a half-life of 12 h providing substantial clearance within 2 days [227]. Some investigators have examined tissue vascular pO_2 , while PFC remained in the blood [206,232–235]. Flow can generate artifacts and correction algorithms have been proposed [236,237]. Primary clearance is by macrophage activity leading to extensive accumulation in the liver, spleen, and bone marrow [238,239]. This is ideal for investigating pO_2 in the liver or spleen, but a major shortcoming for other tissues, since animals may exhibit extensive hepatomegaly or splenomegaly though there is no apparent toxicity [227,238,240]. Long-term retention in tissues allows pO_2 measurements to be made *in vivo* and extensive studies have been reported in liver, spleen, abscess, perfused heart, and tumors [5,9,62,218,241–254].

3.1.1.2. Myocardial oxygenation

Due to motion, the heart is a particularly complex organ for measuring pO_2 , yet understanding myocardial physiology with respect to infarcts has important implications for the clinical practice. Sponsored by the American Heart Association, we sought to develop a noninvasive approach for monitoring dynamic changes in myocardial oxygenation [243]. In Figs. 4 and 5, we present a case study demonstrating the ability to evaluate dynamic changes in myocardial oxygenation. Following IV or IP administration of PFC, some becomes sequestered in heart tissue. This is detectable using a surface coil placed over the heart of an open-chest rabbit, but for proof of principle investigations, we examined excised crystalloid perfused Langendorff rat hearts [243]. To achieve effective ^{19}F NMR signal, Sprague–Dawley rats were loaded with PFTB (Oxypherol: 1 ml/100g/day) for 9 days via tail vein injections. Hearts containing the sequestered PFC

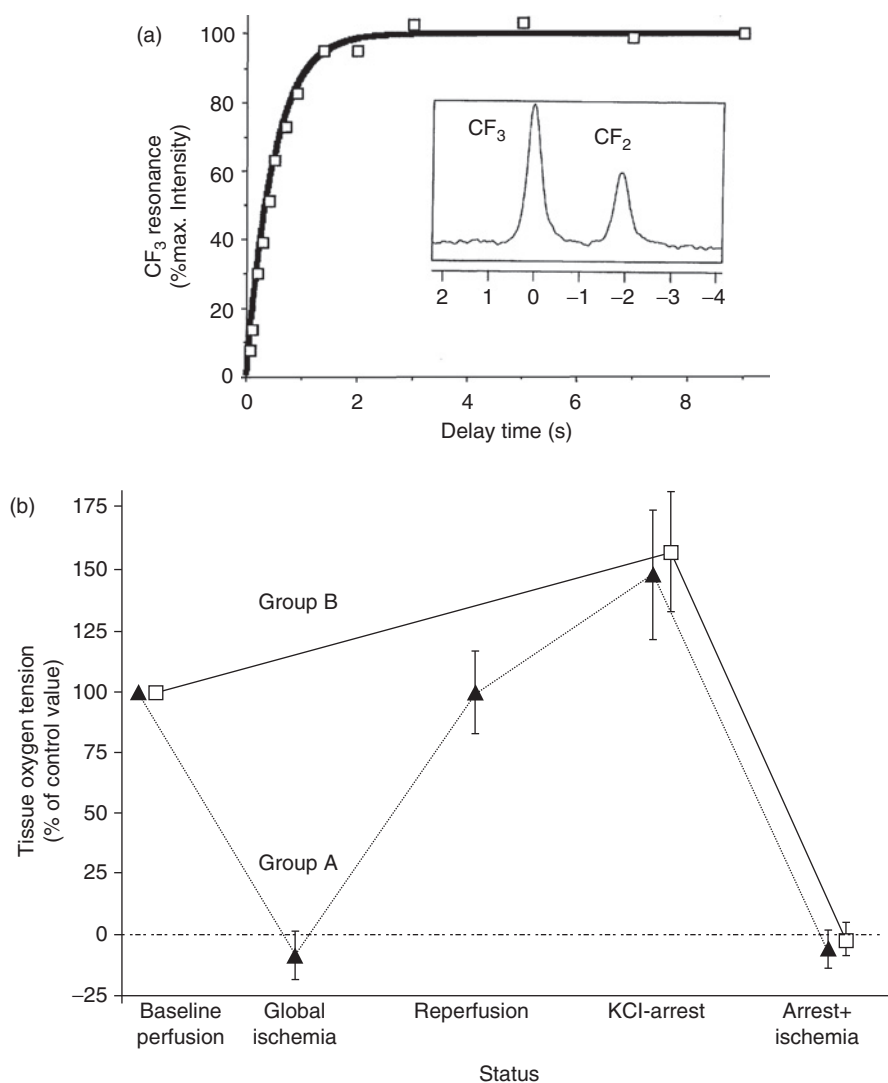


Fig. 4. Monitoring myocardial oxygenation using ^{19}F NMR of sequestered perfluorotributylamine. (a) Spin lattice relaxation (R_1) recovery curve obtained in 2 min for the CF_3 resonance from an isolated Langendorff perfused rat heart that had sequestered oxyphenol. $R_1 = 2.11 \pm 0.08 \text{ s}^{-1}$ indicates $510 \pm 30 \text{ Torr}$ at 37°C . Inset shows partial ^{19}F NMR spectrum with resolved downfield CF_3 and CF_2 resonances. (b) Steady-state R_1 -measured $p\text{O}_2$ values of perfused rat hearts as percentage of normalized initial tissue $p\text{O}_2$ with respect to interventions. Hearts in Group A (\blacktriangle) showed $p\text{O}_2$ equivalent to 0 Torr during total global ischemia (TGI), but returned to 100% upon reperfusion. KCl arrest resulted in increased tissue $p\text{O}_2$ from the excess available oxygen. Elevated $p\text{O}_2$ was observed in hearts in both Group B (\square) (experiencing immediate arrest) and those in Group A (experiencing prior TGI). The previous ischemia experienced by Group A did not “condition” the hearts in terms of the

were excised and retrograde perfused by the Langendorff method at a pressure of 70 cm H₂O with modified Krebs–Henseleit buffer. A fluid-filled latex balloon was inserted into the left ventricle and connected to a pressure transducer to monitor developed pressure. Total global ischemia (TGI) was induced by halting flow to the aorta *in situ*. Cardiac arrest was induced by increasing the KCl in the perfusate to 20 mM.

In the absence of spatial selection, a ¹⁹F NMR signal of PFTB could be obtained representing the whole heart in one pulse at 7 T using a volume coil [243]. Using a full T_1 relaxation sequence (e.g., Fig. 4), precise pO_2 values could be obtained. Global R_1 measurements provided an accuracy of 20–40 mmHg (Torr) and showed significant differences in cardiac tissue before and during ischemia ($p < 0.001$) and before and during KCl-induced cardiac arrest ($p < 0.001$, Fig. 4b). However, it was apparent that pO_2 changes occurred far more rapidly than could be assessed using a full T_1 curve. More rapid T_1 estimates are feasible using fewer recovery time delays on the relaxation curve, and indeed, a two-point comparison based on partial saturation allowed dynamic changes in pO_2 to be assessed with 1-s time resolution [243]. While any individual pO_2 estimate is less precise, the dynamics are apparent (Fig. 5). The decline in myocardial tissue pO_2 in KCl-arrested hearts undergoing ischemia was four to eight times slower than that of the normally beating hearts. Following the onset of ischemia, there was close correlation ($R = 0.93$) between the decline of pO_2 and developed pressure (Fig. 5e).

Global measurements related to TGI have some value, but clinical infarction is more likely to generate regional ischemia requiring spatial resolution for useful models. We have undertaken ¹⁹F MRI of arrested hearts with respect to regional ischemia induced by ligation of the lower anterior descending (LAD) artery and found spatial heterogeneity of hypoxia [246]. However, acquisition times for the images were excessive (hours), so that monitoring pO_2 dynamics in the heart is restricted to preclinical studies. Use of a PFC with a single resonance could improve SNR and reduce imaging times. Targeting cardiac tissue directly could also improve SNR and this has been a goal of Wickline *et al.* [56].

3.1.1.3. Tumor oxygenation

The most extensive use of ¹⁹F NMR oximetry has been to investigate tumor oxygenation with both acute studies of interventions and chronic studies of growth. Many investigations, including our own initial studies, used PFC emulsions to probe tumor oxygenation. Uptake and deposition of PFC emulsions in tumors is highly variable and heterogeneous with most signal occurring in well-perfused

R_1 -measured pO_2 . Global ischemia showed complete hypoxia for both groups with or without KCl arrest. Error bars represent one standard deviation of measurements from multiple hearts (data adapted from Ph.D. thesis of Himu Shukla, UT Southwestern 1994) [405].

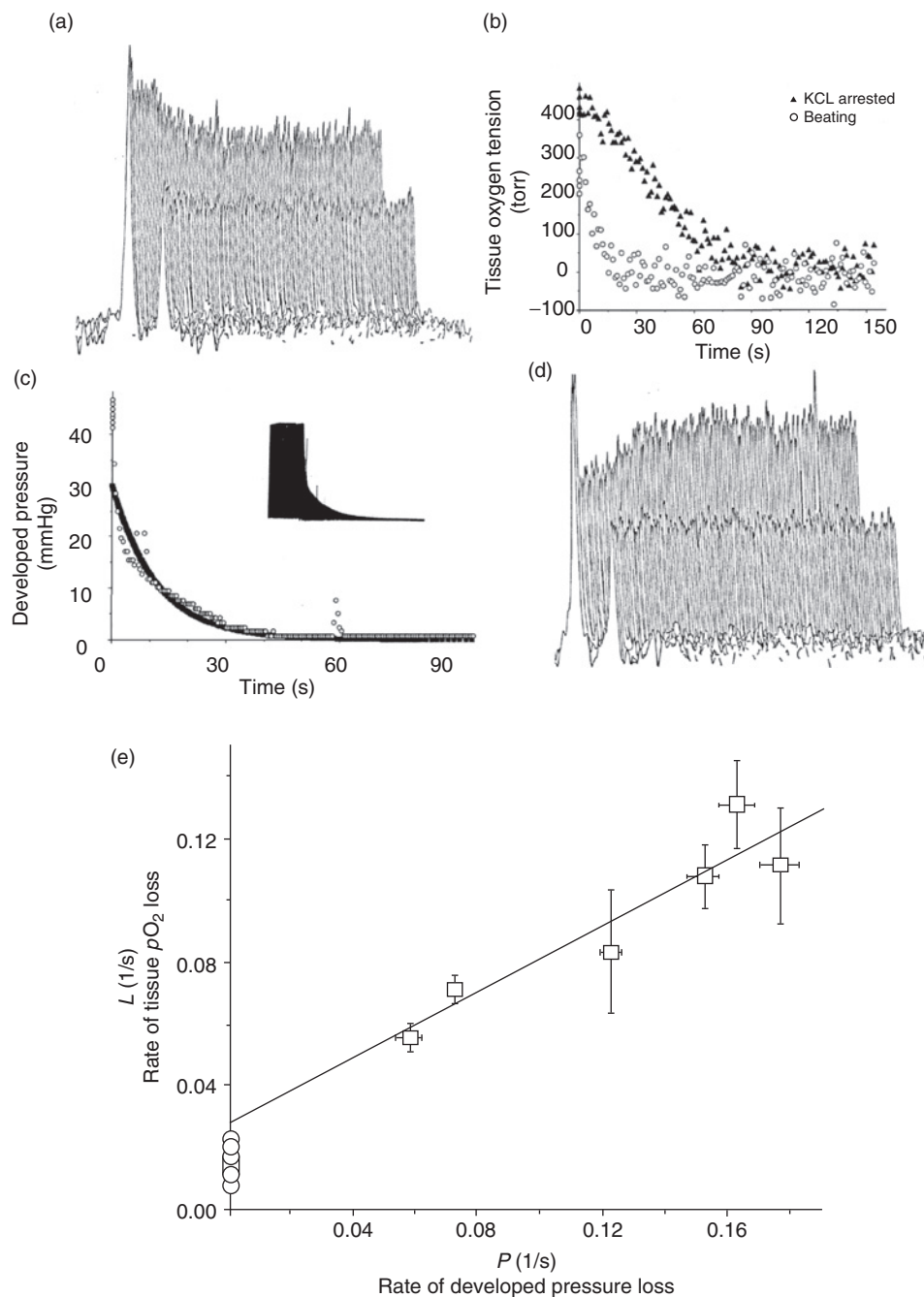


Fig. 5. Correlation of myocardial oxygenation and developed pressure in excised Langendorff perfused rat hearts. (a) When NMR signals are acquired more rapidly than the time required for full relaxation, there is signal loss due to partial saturation. Comparing the

regions [242,254]. Indeed, pO_2 values measured soon after intravenous infusion, but following vascular clearance (typically 2 days), are generally high, approaching arterial pO_2 [242]. Thus, physiological measurements with respect to intervention are biased towards the well-perfused, well-oxygenated regions, which are often less important than hypoxic regions. Interestingly, following sequestration, PFC does not seem to redistribute within tissue, but remains associated with specific locations. Figure 6 shows residual PFC in the center of a tumor 18 days after systemic administration of Oxypherol. This was found to be essentially hypoxic tissue. When fresh PFC emulsion was administered and allowed to clear for two days, the original signal was still clearly delineated in shape, form, and intensity. However, a new signal was detected around the tumor periphery indicating the newly well-perfused regions. Such long-term tissue marking has been proposed as a form of noninvasive histology [255]. Long tissue retention has the advantage of facilitating chronic studies during tumor development and progressive tumor hypoxiation has been observed over many days [242,245].

To avoid the bias towards well-perfused regions and need to await vascular clearance, we developed an approach using direct intratumoral (IT) injection of neat PFC, which allows any region of interest in a tumor to be interrogated immediately [10]. Use of a fine needle ensures minimal tissue damage. Direct injection of neat PFC has been used by others to investigate retinal oxygenation [256–258] and cerebral oxygenation in the interstitial and ventricular spaces [221] and for the first time here, we show results in rat thigh muscle (Fig. 7).

We have identified HFB as an ideal reporter molecule [224]. Symmetry provides a single narrow ^{19}F NMR signal and the spin lattice relaxation rate is highly

intensity of a partially saturated signal to fully relaxed signal indicates R_1 and hence, pO_2 . In (a), the larger CF_3 signal shows a decrease of about 15% compared with baseline under fully perfused, well-oxygenated conditions. Induction of TGI caused rapid loss of signal commensurate with increasing T_1 and reduced pO_2 . Individual spectra were acquired in 1.1 s. The transition was complete within about 40 s. T_1 of the CF_3 resonance increased from 540–1240 ms causing the signal to decline from 86% to 68% accompanying TGI. The CF_2 resonance only changed from about 390 to 570 ms and this had minimal effect on signal intensity (SI) under these partial saturation conditions. (b) Dynamic data (the partial saturation spectra quantified using decay of the CF_3 resonance) from hearts made globally ischemic showed that an arrested heart (\blacktriangle) consumed residual oxygen in the heart more slowly than a beating heart (\square). Note that the arrested heart started from a higher state of tissue oxygenation due to reduced oxygen demand. The monoexponential rate constants representing the loss of tissue pO_2 are: beating $L = 0.11 \text{ s}^{-1}$, arrested $L = 0.02 \text{ s}^{-1}$. (c) The pressure tracing of a perfused rat heart based on an intraventricular balloon catheter was digitized to quantitate the rate of ventricular pressure failure during ischemia. For this heart, a monoexponential curve fit to the pressure amplitude yielded a decay rate constant $P = 0.085 \text{ s}^{-1}$. (d) Reperfusion following 5 min TGI led to rapid reoxygenation of the rat hearts, revealed by increase in the CF_3 signal corresponding to shortening of T_1 . (e) A strong linear relationship was found between the rate of heart tissue hypoxiation and ventricular pressure failure for rat hearts upon acute TGI ($r > 0.9$).

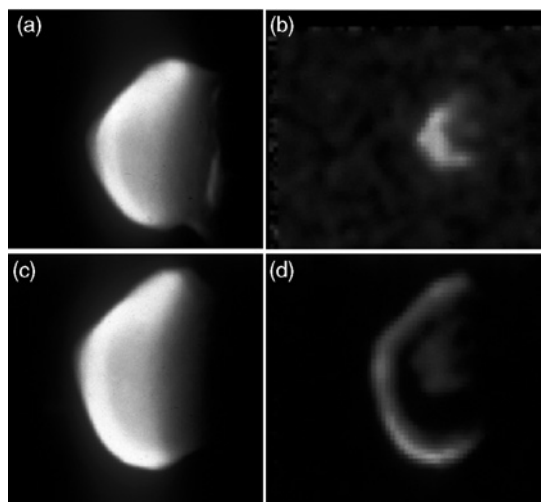


Fig. 6. *In vivo* MR histology. Following administration of Oxypherol (perfluorocarbon, PFC) blood substitute emulsion of perfluorotributylamine (PFTB)) to a Copenhagen rat bearing an AT1 tumor, ^{19}F NMR signal was initially detected around the tumor periphery [242]. Comparison of thin slices from 3D ^1H (a) and ^{19}F (b) MRI data sets obtained 18 days later showed that new tumor tissue grew around the labeled tissue and the ^{19}F label was exclusively in the central region and ^{19}F NMR oxygen tension measurements showed mean $p\text{O}_2 = 2.5$ Torr for a group of six such tumors. When fresh Oxypherol was administered (4×2.5 ml IV) and allowed to clear for 48 h, the new PFC was found around the tumor periphery, but the original signal was retained in the center (c) and (d). These data reveal the differential perfusion of tumor regions and tendency of IV administered reporters to target well-perfused regions (unpublished data obtained in collaboration with Drs. Anca Constantinescu and Peter Peschke).

sensitive to changes in $p\text{O}_2$, yet minimally responsive to temperature [224,259,260]. HFB also has a long spin–spin relaxation time (T_2), which is particularly important for imaging investigations. HFB is well characterized in terms of lack of toxicity [261,262], exhibiting no mutagenicity [263], teratogenicity or fetotoxicity [264], and the manufacturer's material data safety sheet indicates $\text{LD}_{50} > 25$ g/kg (oral-rat) and LC_{50} 95 g/m 3 /2 h (inhalation-mouse). HFB had been proposed as a veterinary anesthetic and has been used in many species including ponies, sheep, cats, dogs, rats, and mice, but was abandoned due to its flammability [265]. Flammability is not a problem for NMR oximetry, where small quantities of liquid (typically, 50 μl) are injected directly into the tumor.

Initial studies used 10–20 μl HFB injected directly into the center or periphery of a tumor and $p\text{O}_2$ measurements indicated tumor heterogeneity [224,266]. Although data were acquired using nonlocalized spectroscopy, the highly localized signal ensured that regional $p\text{O}_2$ was measured. Subsequently, we developed an imaging approach: *FREDOM* (Fluorocarbon Relaxometry using Echo planar imaging for Dynamic Oxygen Mapping) [10], which typically provides

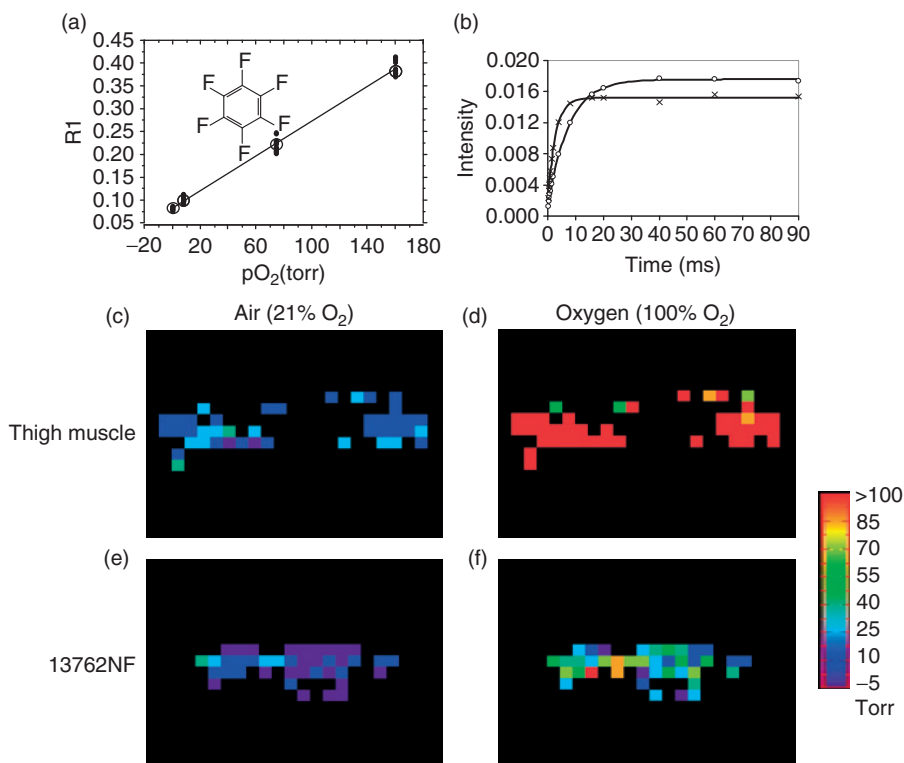


Fig. 7. FREDOM-tissue oxygen dynamics. (a) A linear relationship is found between the spin lattice relaxation rate R_1 of hexafluorobenzene (HFB) and pO_2 (reprinted from *Methods in Enzymology*, 386, Zhao D, Jiang L, Mason RP, Measuring Changes in Tumor Oxygenation., 378–418, Copyright (2004), with permission from Elsevier) [10]. (b) ^{19}F NMR relaxation curves from a single voxel in rat leg muscle after direct administration of 50 μ l HFB. Curves are shown during air breathing (circles; $T_1 = 7.37$ s, $pO_2 = 28$ Torr) and following switch to oxygen for about 20 min (crosses; $T_1 = 2.65$ s, $pO_2 = 156$ Torr), respectively. (c) pO_2 map of rat thigh muscle during air breathing. Data obtained in 6.5 min, showing heterogeneity of baseline oxygenation. Mean $pO_2 = 20 \pm 1$ Torr. (d) Following 20 min oxygen breathing, all the voxels in (c) showed increased pO_2 reaching a new mean $pO_2 = 158 \pm 6$ Torr. (e) pO_2 map of 13762NF rat breast tumor, while rat breathed air (mean $pO_2 = 13 \pm 2$ Torr). Oxygenation is clearly lower than for muscle, above. (f) During oxygen breathing, tumor pO_2 increased, though showing considerable heterogeneity of response with mean $pO_2 = 52 \pm 4$ Torr. (See Colour Plate Section at the end of this book.)

50–150 individual pO_2 measurements across a tumor simultaneously in about 6.5 min with a precision of 1–3 Torr in relatively hypoxic regions based on 50 μ l injected dose (Fig. 7). In both muscle and tumor tissues, pO_2 heterogeneity is apparent when rats breathe air (pO_2 ranged from 0 to 100 Torr). Upon challenge with oxygen breathing, essentially all muscle regions showed a significant increase in oxygenation. Many tumors show little response to hyperoxic gas, but the 13762NF mammary tumor generally shows extensive response [217],

as seen in Fig. 7. We have used *FREDOM* to examine the effects of vascular targeting agents [36,267], vasoactive agents [215] and hyperoxic gases [10,200, 212–217,268–270]. We have shown that measurements are consistent with sequential determinations made using electrodes [271,272] and fiber optic probes (FOXYTM and OxyLite[®]) [201,216]. Repeat measurements are highly reproducible and generally quite stable in tumors under baseline conditions. Results are also consistent with hypoxia estimates using the histological marker pimonidazole [212]. Most significantly, estimates of *pO*₂ and modulation of tumor hypoxia are found to be consistent with modified tumor response to irradiation [213,273]. Such prognostic capability could be important in the clinic, since it is known that relatively hypoxic tumors tend to be more aggressive and respond less well to radiation therapy [274–276]. Hitherto, we have lacked a ¹⁹F MRI capability in our human systems in Dallas. However, Philips is promoting dual ¹⁹F MRI capabilities on the new 3 T human systems [91,277] and we expect to be able to pursue translation of the *FREDOM* approach in the near future.

3.1.2. pH

pH is an important indicator of tissue health and acidosis may reflect ischemia and hypoxia. Historically, tumors were believed to be acidic (Warburg hypothesis) and the detection of neutral or basic environments by NMR led to initial controversy [278]. It was ultimately realized that ³¹P NMR of endogenous inorganic phosphate (Pi) reflects primarily the cytosolic pH, which is often in the range 7.0–7.4, whereas tumor interstitial (pHe) may indeed be acidic, as previously observed using polarographic electrodes. This reversed pH gradient has important implications for partitioning of weak acid or base drugs, and thus, considerable effort has been applied to developing robust reporter molecules. ¹⁹F NMR pH indicators (Table 3) represent three strategies: (i) development of molecules specifically designed for ¹⁹F NMR, (ii) fluorinated analogues of existing fluorescent indicators, and (iii) exploitation of the ¹⁹F NMR chemical shift sensitivity inherent in cytotoxic drugs. Many molecules exhibit chemical shift response to changes in pH, for example, the ¹⁹F NMR resonance of 6-fluoropyridoxol (6-FPOL) [11,279]. On the NMR timescale, protonated and deprotonated moieties are generally in fast exchange, so that a single signal is observed representing the amplitude weighted mean of acid and base forms. pH is measured using the Henderson–Hasselbalch equation:

$$\text{pH} = \text{p}K_{\text{a}} + \log_{10} \left[\frac{\delta_{\text{obs}} - \delta_{\text{acid}}}{\delta_{\text{base}} - \delta_{\text{obs}}} \right] \quad (2)$$

where δ_{acid} is the limiting chemical shift in acid, δ_{base} is the limiting chemical shift in base, and δ_{obs} is the chemical shift observed at a given pH. Due to the nonlinear form of the equation, greatest sensitivity is found close to the $\text{p}K_{\text{a}}$.

Reporter molecules may readily access the interstitial compartment, but intracellular measurements are more difficult. Deutsch *et al.* [74,280] championed the use of ^{19}F NMR to measure intracellular pH primarily based on the series of agents 3-monofluoro-, 3,3-difluoro-, and 3,3,3-trifluoro-2-amino-2-methyl propionic acid (Table 3). pH sensitivity is predicated on protonation of the amino group and it is immediately apparent that additional fluorine atoms influence the pK_a . These molecules have been successfully applied to pH measurements in cells [74,281–283] and isolated organs [74,284]. A significant problem is loading indicators into cells, but esters are relatively permeable, stable in water, and undergo nonspecific enzymatic hydrolysis intracellularly, liberating the pH-sensitive molecules [280]. This approach can lead to complex spectra including overlapping multiline ester and liberated free acid resonances from both intra- and extracellular compartments (Fig. 8) [285]. Widespread use of these molecules has been hindered by the problem of loading the indicators into cells and the relatively small chemical shift range approximately 2 ppm. Difluoromethyl ornithine (DFMO) represents another ^{19}F NMR sensitive amino acid, which is also a

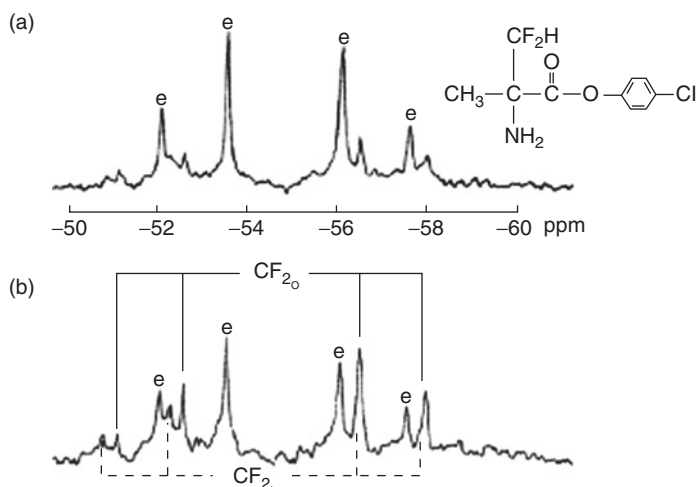


Fig. 8. pH measurement in cells. ^{19}F NMR of difluoromethylalanine *para*-chlorophenyl ester (1 mM) added to suspension of RINm5F cells (4% cytochrome c). Spectra were taken at 4-min intervals (1,600 scans, 30° pulse, repetition rate = 5/s) with broadband proton decoupling. The resonances marked “e” arise from the ester form of the amino acid. The resonances in the lower spectrum marked “o” arise from extracellular free amino acid, whereas those marked “i” arise from intracellular free amino acid. Spectrum (a) 1–5 min; (b) 5–9 min after addition of ester to the cell suspension. The ester quartet (e) lines decreased in intensity, while the quartets of lines from the product of ester hydrolysis, intracellular difluoromethylalanine (CF_2i) and extracellular difluoromethylalanine (CF_2e), increased with time [partial figure reproduced from J. Taylor and C.J. Deutsch, ^{19}F nuclear magnetic resonance: measurements of $[\text{O}_2]$ and pH in biological systems. *Biophys. J.* 1988; 53: 227–233 [406] with permission of the Biophysical Society].

therapeutic drug. Unfortunately, its chemical shift response is even smaller and the chemical response is not monotonic, going through a reversal above the pK_a [286]. A large chemical shift range is important to ensure precise measurements of pH. When multiple cellular compartments are present there is less problem with signal overlap. Perhaps more importantly, any chemical shift perturbations due to other factors, such as susceptibility become also important [287–289]. Furthermore, the pK_a should be matched to the pH range of interest since the largest chemical shift response occurs close to the pK_a [74].

Aromatic reporter molecules tend to have a much larger chemical shift pH response. Analogs of vitamin B6, for example, 6-FPOL are highly sensitive to pH [11,279,290–292]. We showed that 6-FPOL itself readily enters cells and provides well-resolved resonances reporting both intra- and extracellular pH (pHi and pHe), simultaneously, in whole blood (Fig. 9) [279] and the perfused rat heart [290]. Ease of entry into blood cells may be related to facilitated transport, since vitamin B6 is naturally stored, transported, and redistributed by erythrocytes [293]. Intriguingly, most tumors cells show a single resonance only, suggesting that 6-FPOL does not enter. The somewhat basic $\text{pK}_a = 8.2$ is appropriate for investigations of cellular alkalosis, but it is not ideal for studies in the normal physiological range (6.5–7.5) [290].

Ring substitution allowed us to alter the pK_a and 6-fluoropyridoxamine (6-FPAM) offered superior characteristics with $\text{pK}_a = 7.05$ [291]. As for 6-FPOL, we have observed intra- and extracellular signals in whole blood and perfused rat hearts [11,291] and in addition, specific tumor cells (Morris hepatoma

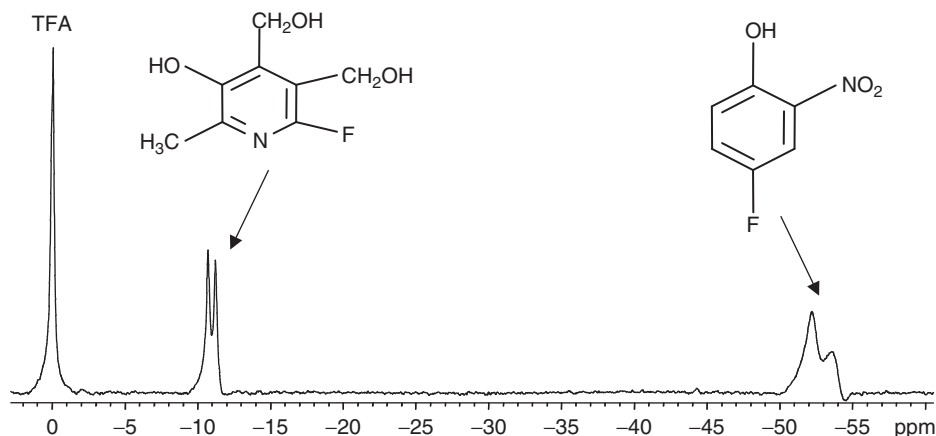


Fig. 9. Transmembrane pH gradient in red blood cells. ^{19}F NMR of 6-fluoropyridoxol (4.2 mg), PFONP (4.8 mg), and NaTFA in whole fresh rabbit blood (600 μl). Both pH indicators show split peaks arising from intra- and extracellular signals. Extracellular pH was measured using polarographic electrode $\text{pHe} = 7.66$ and compared with $\text{pHe}_{(\text{PFONP})} = 7.55$ and $\text{pHe}_{(\text{FPOL})} = 7.55$. ^{19}F NMR showed intracellular pH $\text{pHi}_{(\text{PFONP})} = 7.16$; $\text{pHi}_{(\text{FPOL})} = 7.29$.

MH-Tk) showed uptake [18]. While modification of the 4-hydroxymethyl group to aminomethyl altered the pK_a favorably, the 5-isomer was minimally changed (Table 3) [291].

Noting the large chemical shift response of pyridines, we also explored fluorophenols as pH indicators. Like 6-FPOL, *p*-fluorophenols show a large chemical shift response $\Delta\delta$ 6.4–11.3 ppm, whereas *o*-fluorophenols have a smaller chemical shift range (\sim 0.3–2.2 ppm) (Table 3) [294]. For comparison both 6-FPOL and PFONP (*p*-fluoro-*o*-nitrophenol) are shown to reveal pH gradients in whole blood giving comparable results and consistent with electrode measurements (Fig. 9). Fluorophenols must be used cautiously, since PFONP appears cytolytic for certain tumor cells and may act as an ionophore, by analogy with dinitrophenol.

Other aromatic pH reporters have been presented including analogs of fluorescent pH indicators. FQuene, a ^{19}F NMR sensitive analog of the fluorescent pH indicator quene-1, was used to measure intracellular pH in a perfused heart [295] and liver [296]. *o*-Methoxy-*N*-(2-carboxyisopropyl)-4-fluoroaniline has a chemical shift range approximately 17 ppm, but the pK_a (5.8) is less suitable for *in vivo* investigations. Modification to *N,N*-(methyl-2-carboxyisopropyl)-4-fluoroaniline [297] retained a substantial chemical shift range ($\Delta\delta$ 12 ppm) and produced a physiologically suitable pK_a (6.8), however, no biological studies have been reported. Metafluoro isomers showed considerably smaller chemical shift response to changes in pH. *N*-ethylaminophenol (NEAP) has been described with various analogs to detect pH or metal ions [298].

To enhance SNR, or reduce the required dose, a pH sensitive CF_3 moiety could be introduced in place of the F-atom. Trifluoromethylphenols show titration response, though by comparison with the fluorophenols (Table 3), the chemical shift response is typically smaller $\Delta\delta = 1.25$ ppm (*p*- CF_3ArOH , pK_a 8.5) to 0.4 ppm (*o*- $\text{CF}_3\text{-Ar}$, pK_a 7.92), as expected since electronic sensing must be transmitted through an additional C–C bond [299]. Importantly, the ^{19}F NMR signal occurs downfield from NaTFA, so that unlike 6-FPOL there is no interference from isoflurane signals [18]. While FPOL and FPAM provide both intra- and extracellular signals with varying ratios depending on cell type, 6-trifluoromethylpyridoxol (CF_3POL) is found to occur exclusively in the extracellular compartment, and thus reports pHe, or interstitial pH [18,300]. Frenzel *et al.* [301] have described a fluoroaniline sulfonamide (ZK150471) and its use has been demonstrated in mice and rats to investigate tumor pH [302,303]. This molecule is restricted to the extracellular compartment only [301,304], but combination with ^{31}P NMR of Pi to determine pH_i has been used to reveal the transmembrane pH gradient in mouse tumors [141]. A distinct problem with ZK150471 is that the pK_a differs in saline and plasma [304]. Most indicators require an additional chemical shift reference standard, for example, sodium trifluoroacetate, but NEAP [298], 6-FPOL-5- α - CF_3 [291], and ZK150471 [301] all have nontitrating intramolecular chemical shift references. pH measurements using 2-amino-3,3-difluoro-2-methyl propanoic acid is based on changes in the

splitting of the AB quartet and this again avoids need for a chemical shift reference, but the splitting increases the complexity of the spectrum and reduces SNR (Fig. 8).

3.1.3. Metal ions

Since metal ions play key roles in cellular physiological processes many specific reporter molecules have been developed, mostly as fluorescent indicators incorporating extended aromatic and conjugated structures, where the wavelength of fluorescence depends upon specific binding of a metal ion. Several ¹⁹F NMR reporters have been created by addition of fluorine atoms (Table 5).

Tsien [305] made an important breakthrough by establishing an approach for loading fluorescent metal ion chelators into cells using acetoxymethyl esters. He demonstrated 1,2-bis(*o*-aminophenoxy)ethane-*N,N,N',N'*-tetraacetic acid (BAPTA) for detecting intracellular calcium ions and subsequently Metcalfe *et al.* [295] added *para*-fluoro atoms to the aromatic ring yielding a ¹⁹F NMR responsive agent (5,5-difluoro-1,2-bis(*o*-aminophenoxy)ethane-*N,N,N',N'*-tetraacetic acid (5FBAPTA)) (Table 5). Upon binding calcium, there is a change in chemical shift (Fig. 10).

Ideally, such a reporter molecule would have high specificity for the metal ion of interest. In fact, the F-BAPTA agents are found to bind several divalent metal ions, including Ca²⁺, Zn²⁺, Pb²⁺, Fe²⁺, and Mn²⁺ (Fig. 10) [306,307], but importantly, each metal ion chelate has an individual chemical shift, so that they can be detected simultaneously [308]. 5FBAPTA includes two fluorine atoms symmetrically placed to provide a single signal. Upon binding, there is slow exchange of Ca²⁺, on and off the indicator, on the NMR timescale, so that separate signals are seen for the free and metal ion bound moieties, with chemical shifts of several ppm. Measurements are based on the signal ratio, avoiding the need for a chemical shift reference, in contrast to pH reporters, which are usually in the fast exchange regimen. Calcium concentration may be calculated from the formula [308]

$$[\text{Ca}^{2+}] = K_D \frac{[\text{Ca} - \text{FBAPTA}]}{[\text{FBAPTA}]} \quad (3)$$

However, the dissociation constant (K_D) does depend on pH, ionic strength, and the concentration of free Mg²⁺, which need to be estimated independently. 5FBAPTA has been used extensively [308] in studies of cells [306,309,310], and the perfused beating heart, revealing calcium transients during the myocardial cycle (Fig. 11) [311–313]. Kirschenlohr *et al.* [313] reported that developed pressure in the perfused heart was reduced after addition of 5FBAPTA, but this could be reversed by including 50 μM ZnCl₂ in the perfusion medium.

Table 5. ^{19}F NMR metal ions indicators^a

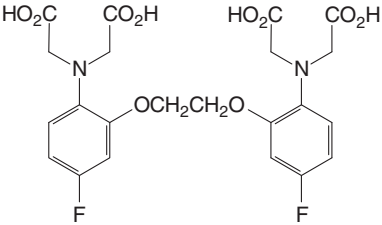
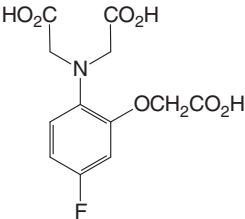
Detected Ion	Agent	Structure	$\delta_{\text{F(Ligand)}}$ (ppm)	$\Delta\delta$ (ppm)	References
[Ca ²⁺] [Zn ²⁺] [Pb ²⁺] [Cd ²⁺] [Hg ²⁺] [Co ²⁺] [Ni ²⁺] [Fe ²⁺]	5FBAPTA		2.08 ^b	5.8 3.7 4.6 4.8 5.3 28.1 32.4 31.1	[307]
[Mg ²⁺]	5FAPTRA		0.80 ^b	8.00	[322]

Table 5. Continued

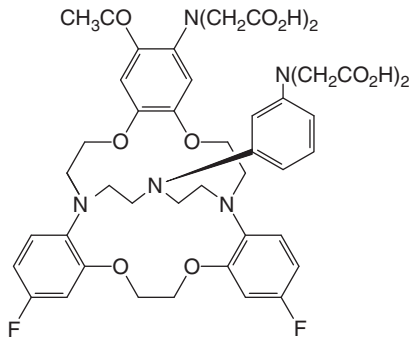
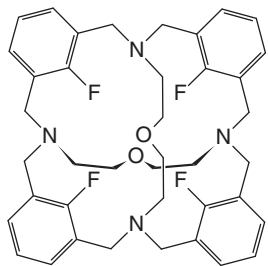
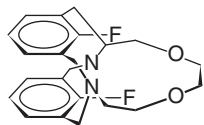
Detected Ion	Agent	Structure	$\delta_{\text{F(Ligand)}}$ (ppm)	$\Delta\delta$ (ppm)	References
[Na ⁺]	F-cryp-1		5.50	1.9	[410]
[Li ⁺] [Na ⁺] [K ⁺] [Rb ⁺]	F ₄ -Cage		−116.70	4.20 −13.5 −6.8 −4.2	[325]
[Li ⁺]	F ₂ -[2.1.1]-Cryptand		−100.70	28.53	[324]

Table 5. Continued

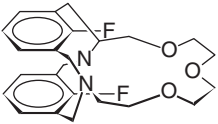
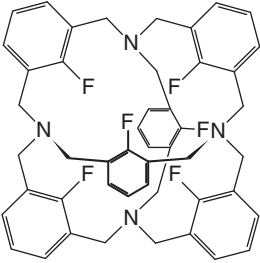
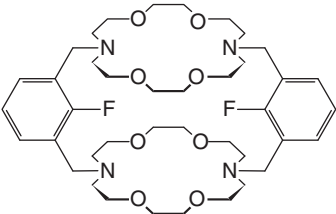
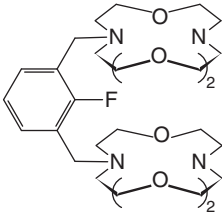
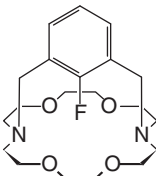
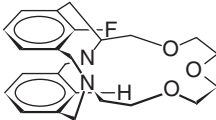
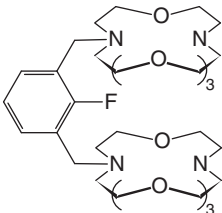
Detected Ion	Agent	Structure	$\delta_{\text{F(Ligand)}} \text{ (ppm)}$	$\Delta\delta \text{ (ppm)}$	References
[Na ⁺]	F ₂ -[3.1.1]-Cryptand		−105.80	−16.00	[324]
[K ⁺]	F ₆ -Carcerand		−110.50	−15.76	[325]
[Rb ⁺]	(FN ₂ O ₄) ₂		−124.46	5.40	[25,314]

Table 5. Continued

Detected Ion	Agent	Structure	$\delta_{\text{F(Ligand)}} \text{ (ppm)}$	$\Delta\delta \text{ (ppm)}$	References
[Cs ⁺]	F(NO ₄) ₂		−123.70	5.50	[25,314]
[Ca ²⁺]	F-[2.2.1]-Cryptand		−114.38	−11.90	[25,314]
[Sr ²⁺]	HF-[3.1.1]-Cryptand		−110.38	−5.87	[324]
[Ba ²⁺]	F(NO ₅) ₂		−123.78	7.90	[25,314]

^a Unless otherwise noted, CFCl₃ was used as a chemical shift standard, solvent: CH₃CN.

^b 6-Fluorotryptophan was used as a chemical shift standard.

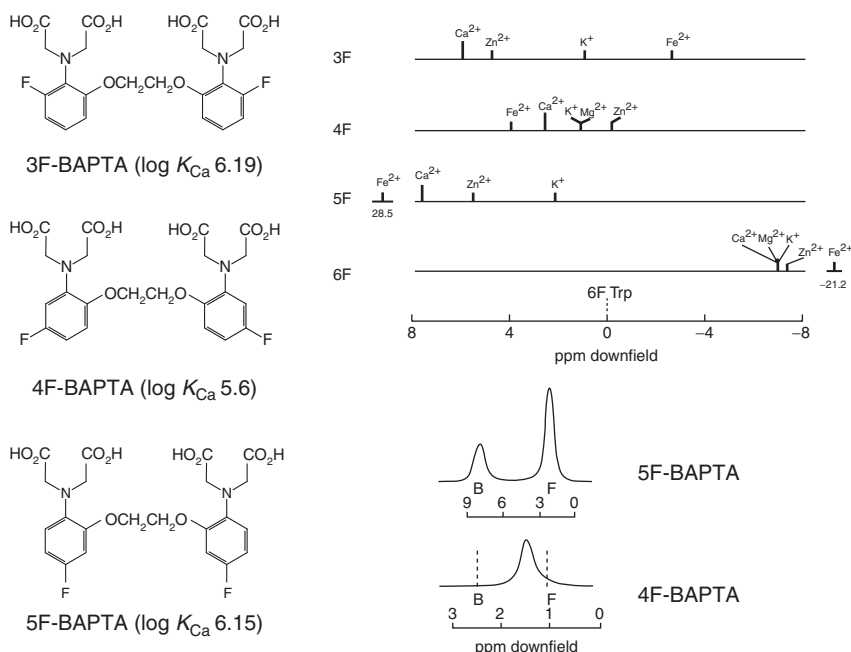


Fig. 10. Detection of $[\text{Ca}^{2+}]$ using ^{19}F NMR of F-BAPTA. Left: molecular structures of three F-BAPTA isomers with Ca^{2+} binding constants. Top right: chemical shifts of F-BAPTA isomers upon binding divalent metal ions with respect to F-tryptophan. Bottom right: ^{19}F NMR spectra of F-BAPTA in presence of Ca^{2+} . 5F-BAPTA is in slow exchange showing response for free and bound forms, whereas 4F-BAPTA is in fast exchange showing weighted average (modified from Smith *et al.*, *Proc. Natl. Acad. Sci. (USA) Biological Sciences* 80, 7178–7182 (1983)—with permission [306]).

In an effort to find an optimal reporter, isomers and derivatives were developed (Fig. 10). 4FBAPTA has a somewhat lower binding constant $K_D = 0.7 \mu\text{M}$, but exhibits fast exchange [308], so that the signals from the bound and unbound forms are averaged, and it is the absolute chemical shift, which is related to the ratio of the two components (Fig. 10).

Plenio and Diodone have also reported fluorocrown ethers (Table 5), which exhibit chemical shift response upon binding Ca^{2+} [314]. Of course, calcium could potentially be analyzed directly by ^{43}Ca NMR, however, its natural abundance is $<0.2\%$, its sensitivity is $<1\%$ that of ^1H , and being quadrupolar, it is liable to extensive line broadening [59]. Thus, the application of ^{19}F NMR with appropriately designed reporter molecules gives insight into cytosolic $[\text{Ca}^{2+}]$.

Magnesium ions are also involved in biological processes and occur in cells at millimolar concentrations [315]. Magnesium can be estimated based on the chemical shift difference of the resonances of adenosine triphosphate (ATP) using ^{31}P NMR [316–318], though ^{31}P NMR has intrinsically low signal-to-noise, exacerbated under many pathophysiological conditions, such as ischemia.

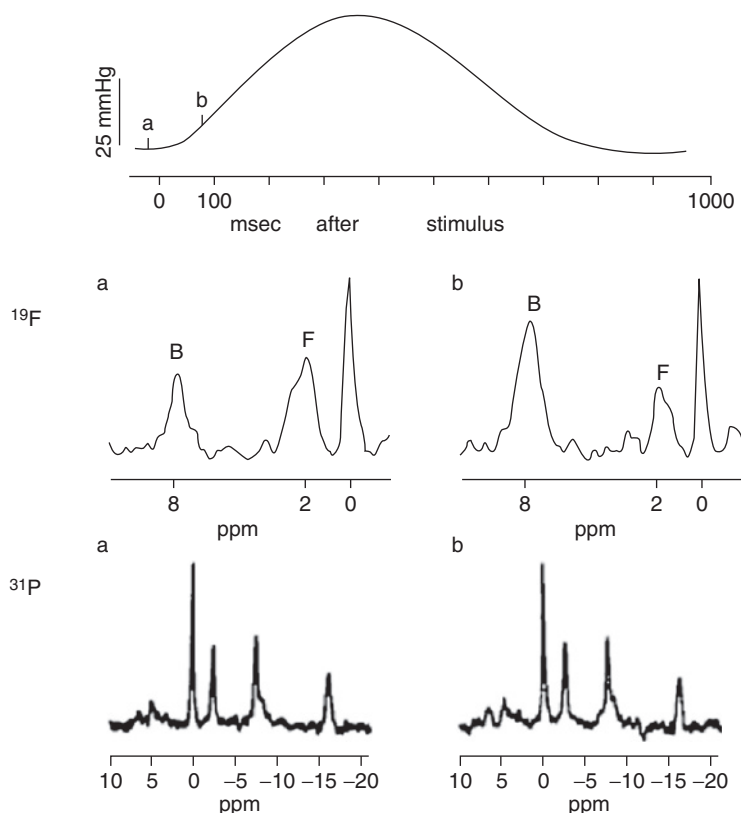


Fig. 11. Changes in gated NMR spectra during the cardiac cycle. Top panel: isovolumic left ventricular pressure in a ferret heart paced at 0.99 Hz in 8 mM $[\text{Ca}^{2+}]$. NMR spectra were acquired at the two times indicated on the pressure record: (a) 10 ms prior to stimulation; (b) 75 ms after stimulation. Middle panel shows gated ^{19}F NMR spectra (each from 800 acquisitions) recorded at (a) and (b), as indicated. The bound (B) and free (F) peaks of 5F-BAPTA exhibit distinct chemical shifts at approximately 8 and 2 ppm, respectively, downfield from a standard of 1 mM 6-Ftryptophan at 0 ppm. It appears that the free $[\text{Ca}^{2+}]$ varied during the cardiac cycle. Bottom panel shows gated ^{31}P spectra (400 scans) acquired at times a and b in the same heart. The major peaks correspond to phosphocreatine (0 ppm), ATP (the three peaks upfield from phosphocreatine), and inorganic phosphate (the small peak at 4–5 ppm) (Reproduced from Marban *et al. Circ. Res.* 1988; 63: 673–678 [311] with permission of Lippincott, Williams & Wilkins).

There are many fluorescent indicators for detection of $[\text{Mg}^{2+}]$ [319] and fluorinated NMR reporters have been proposed. The simplest is fluorocitrate [313], which shows a change in chemical shift upon binding Mg^{2+} . However, it is critical that the reporter molecule be used as the + isomer only, which has relatively little toxicity [320]. Levy *et al.* [8,321] developed the *o*-aminophenol-*N,N,O*-triacetic acid (APTRA) structure both for fluorescent application and by incorporation of fluorine atoms for ^{19}F NMR, which have been used in the perfused rat heart [322].

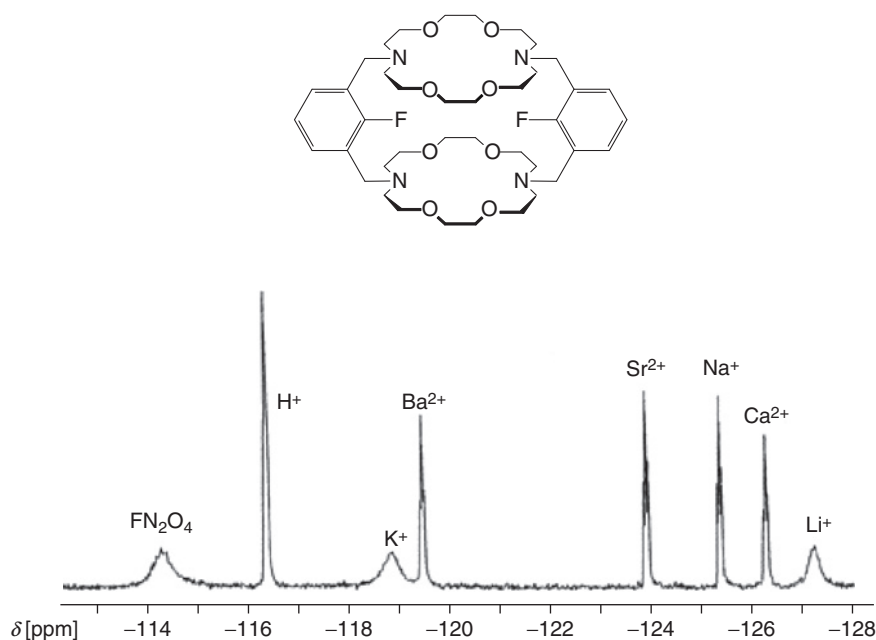


Fig. 12. ^{19}F NMR spectrum of FN_2O_4 ligand with mixture of mono- and divalent cations: Li^+ , Na^+ , K^+ , Rb^+ , Mg^{2+} , Ca^{2+} , Sr^{2+} , and Ba^{2+} . Due to slow exchange all species are detected simultaneously (reprinted with permission from Plenio and Diodone, JACS 118, 356–367 [314], Copyright 1996 American Chemical Society).

While indicators are normally designed for a specific ion they often also interact with other ions, for example, FBAPTA provides a unique chemical shift with many divalent metal ions (Fig. 10) [306,307] and has been used to estimate $[\text{Zn}^{2+}]$, $[\text{Pb}^{2+}]$ [323], and $[\text{Cd}^{2+}]$ [307]. Plenio and Diodone [314,324] have developed series of fluorocyclophanes and fluoro crown ethers to explore specific cation binding (e.g., K^+ , Li^+ , Na^+ , Ba^{2+} , Sr^{2+} , Ca^{2+}) though in many cases, multiple ions may be bound (Table 5 and Fig. 12). Takemura [325] reported macrocycles designed to bind K^+ , NH_4^+ , and Ag^+ . In addition to the metal binding ligands shown in Table 5, many others have been reported, but these were selected since they exhibit particularly large chemical shift responses.

While most reporter molecules have been designed to interact with cations, Plenio and Diodone [326] reported fluorine containing cryptands, which interact with perchlorate. London and Gabel [327] reported fluorobenzene boronic acid, which interacted with specific sugars.

3.1.4. Caveats

A number of criteria are pertinent to the development and exploitation of reporter molecules. The fluorine NMR spectrum must respond to interaction with the ion of interest, for example, through the formation of a second signal, as in the slow

exchange regime, or chemical shift in a fast exchange regime. For many ions, agents should be water soluble, although a degree of lipophilicity may help in transport. The reporter molecule must reach the cellular compartment of interest. Some molecules penetrate cells directly, while for others, this is facilitated using acetoxymethyl esters. A critical issue for intracellular interrogation is loading the reporter molecule into cells. The tetra-carboxylates do not penetrate cells, however, derivatization as acetoxymethyl esters, which has been very widely used in association with analogous fluorescent indicators provides a more lipophilic entity, which can equilibrate across cell membranes [305]. These esters are specifically designed so that intracellular esterases cleave the acetoxymethyl ester, releasing the charged reporter molecule, which is then essentially trapped in the intracellular compartment. The release of acetic acid and formaldehyde are considered to be relatively innocuous. In other cases, specific cellular exclusion is important, so that any signal can unambiguously be attributed to the extracellular or interstitial compartment in a tissue. Such measurements would be analogous to electrode measurements.

It is critical that the reporter molecule not perturb the system under investigation. For ions, there is inevitably some binding and complexation. Provided there is sufficient reservoir of the ions, there can be rapid re-equilibration, and the concentration may give a realistic indication of the free concentration. In unregulated systems, this may be less reliable. The binding constant must be compatible with the typical concentration encountered *in vivo*. Ideally, the reporter ligand is highly selective for the ion of interest and of course the molecule should exhibit minimal toxicity. Signals should be narrow to enhance both the signal-to-noise and spectral resolution.

3.2. Chemical interactions

In the previous section, we considered reporter molecules, which interact reversibly in a physical sense, for example, solvation of gas, protonation, or binding of metal ion by a ligand. Other reporter molecules reveal activity based on irreversible bond cleavage to release a distinct product. This may be more akin to the metabolism of drugs, but these reporters can be tailored to interrogate specific biological processes.

3.2.1. Metabolism of FDG

Steric and electrostatic considerations allow a fluorine atom to replace a hydroxyl group in many sugars, while retaining enzyme substrate activity. Many tumors are characterized by a high glycolytic rate and FDG is a fluorinated glucose analogue used in PET to measure metabolic activity [328]. It is particularly useful for staging tumors and monitoring metastases. FDG is recognized by glucose transporters and enters cells where it is effectively phosphorylated, trapping it

intracellularly, but phosphorylated FDG (FDG-6-P) is not a substrate for phosphofructose isomerase. FDG accumulates in metabolically active cells, such as tumors, brain, and myocardium. FDG PET is currently the method of choice for detecting many cancer metastases and differentiating recurrent disease from scar tissue. While PET can assess retention with great sensitivity, it provides no metabolic information, whereas ^{19}F NMR can be used to differentiate individual metabolites from anabolic and catabolic processes. Of course, NMR studies typically require mM concentrations as opposed to nM/ μM for PET and thus, metabolic fates may differ, but 2-FDG has been used in metabolic studies using ^{19}F NMR [329–332]. The 3-fluoro-3-deoxy-D-glucose isomer (3-FDG) has also been used in the eye, particularly with respect to exploring onset of cataracts [333,334]. It is a poor substrate for hexokinase and the binding affinity of phosphohexose isomerase is low relative to glucose, but it has been used to probe aldose reductase activity in brain [335].

NMR not only provides spectral resolution for a given nucleus allowing multiple fluorine-labeled substrates to be observed simultaneously together with metabolic products, but other nuclei may also be detected. In particular, ^{13}C and ^2H NMR have been used extensively to probe metabolism, both confirming well-known pathways (e.g., glycolysis) and revealing novel detoxification products of xenobiotica [96,97,336,337]. ^{13}C NMR may be considered preferable for such studies since isotopic enrichment is less perturbing than introduction of a fluorine label. As for ^{19}F NMR, ^{13}C NMR normally has minimal background signal, since the natural abundance of ^{13}C is only 1.1% allowing almost 100-fold enrichment. Isotopomer analysis can reveal substrate preferences and mechanisms of enzyme activity and kinetic isotope effects are minimal for ^{13}C , though may be sizable for ^2H -examined substrates [338].

3.2.2. Hypoxia

While FDG has a role in detecting tumors, a new thrust is characterizing tumors so as to individualize therapy and optimize outcome. To this end, hypoxia is recognized as a critical characteristic. In Section 3.1.1, we described ^{19}F NMR methods for measuring $p\text{O}_2$. As an alternative approach, fluoronitroimidazoles have been used to detect hypoxia. Nitroimidazoles are bioreductive agents that are reduced by intracellular reductases to generate reactive intermediates. In the presence of oxygen, the intermediates are rapidly reoxidised and may clear from cells, but under hypoxic conditions they become covalently bound to cellular constituents, indicating the presence of cellular hypoxia. Nitroimidazoles have been used extensively in the past as hypoxic cell radiosensitizers [339] and more recently have gained a role as markers of tumor hypoxia [85,340–344]. EF5 and pimonidazole are widely used to assess hypoxia in histological analysis of biopsy specimens [198,345–347], but noninvasive approaches would be preferable for therapeutic prognosis. Retention of ^{18}F misonidazole in hypoxic tumors has been

observed using PET. Given the importance of hypoxia other PET and SPECT sensitive agents have been proposed and tested (e.g., Cu-ATSM [348,349] and iodinated azomycin galactoside (IAZG) [350]), but nonradioactive approaches would be preferable.

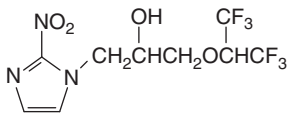
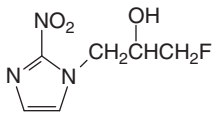
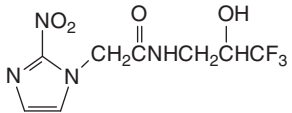
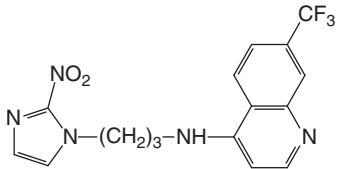
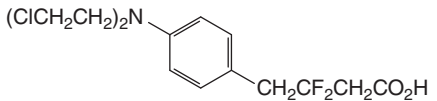
Fluorine-19 labels have been introduced into the nitroimidazole structure providing NMR-sensitive agents [351,352]. Studies have reported the fluorinated nitroimidazoles CCI-103F [353], Ro 07-0741 [354], and SR4554 [351,355,356], which contain 6, 1, and 3 fluorine atoms per molecule, respectively (Table 6). Subsequent to administration, a washout period sufficient for elimination of unbound marker is required, since there is apparently no difference detectable *in vivo* in the chemical shifts of the parent molecule and the metabolites [351]. Li *et al.* [357] investigated the predictive potential of CCI-103F retention as an indicator of tumor radiosensitivity and found a weak correlation indicating that factors other than hypoxia are involved and glutathione concentration may be pertinent [351].

Aboagye *et al.* [358] found increased retention of SR4554 in hypoxic tumors, but no linear correlation with pO_2 . Lack of correlation with pO_2 measurements [355,358] and pimonidazole uptake [351] suggest that additional factors influence hypoxia marker retention and indeed blood flow/perfusion has been implicated [351]. Robinson and Griffiths found differential uptake of SR4554 in diverse tumors known to exhibit different levels of hypoxia. Surprisingly, there was no retention detected in C6 gliomas, which are widely reported to have extensive hypoxia (Fig. 13). Trapping is predicated on nitroreductase activity, which may be lacking in some tumors. Unlike radiochemical approaches, which detect all labeled molecules, NMR offers potential benefits, but added complexity. Diverse adducts, and metabolites may exhibit multiple chemical shifts, each at very low concentration. There is also concern that polymeric adducts may have exceedingly short T_2 , so that they become essentially invisible for many NMR sequences [359]. The biggest problem with ¹⁹F hypoxia agents is that they merely provide a qualitative impression of hypoxia rather than a definitive pO_2 . Seddon *et al.* [356] reported a correlation between retention of SR4554 and pO_2 , but a Phase I clinical ¹⁹F NMR study [356] required infusion at doses of 400–1600 mg/m², which could have adverse side effects.

3.2.3. Enzyme reporters

A ¹⁹F atom can be substituted for a hydroxyl group in sugars with little overall structural perturbation. As such, fluorosugars were widely used to explore mechanisms of enzyme activity [124,126,360]. We adopted a different strategy by including ¹⁹F into the aglycon moiety of a substrate to detect β -galactosidase activity (Figs. 1 and 14 and Table 7) [294]. This provides insight into activity of the lacZ gene, which has historically been the most popular reporter gene in molecular biology.

Table 6. ^{19}F NMR hypoxia indicators

Name	Structure	Number of F atoms	Application
CCI 103F		6	Tumors, cells [353,413]
RO 070741		1	Tumors, cells [354]
SR4554		3	Tumors, cells [355,356,351]
NLTQ-1		3	Tumors, cells [435]
3,3-Difluorochlorambucil		2 ABq	Tumors, cells [354]

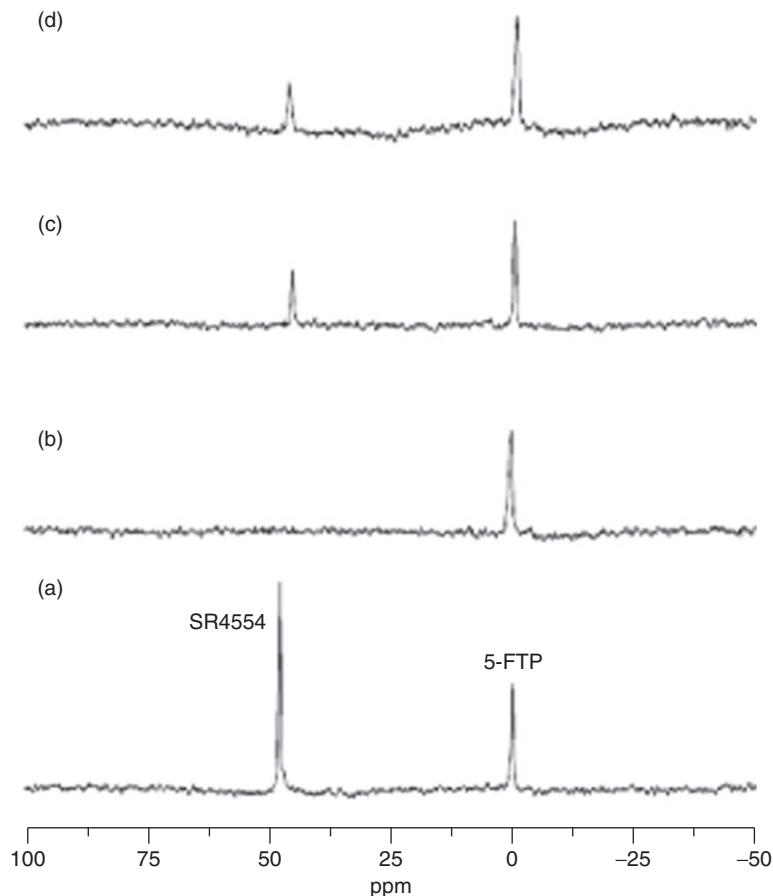


Fig. 13. ^{19}F NMR of hypoxia reporter SR4554 in tumors. ^{19}F NMR spectra obtained from (a) a vial containing 6 mg/ml SR4554 resonating at ca. 45 ppm relative to a 5-fluorotryptophan (5-FTP) external standard; (b) a wild-type C6 glioma; (c) a RIF-1 fibrosarcoma; and (d) an HT29 colon adenocarcinoma all acquired 45 min after administration of 180 mg/kg SR4554 IP. The degree of retention of the reduced adducts of SR4554, measured by ^{19}F MRS, affords a noninvasive assessment of tumor hypoxia. No ^{19}F resonance was detected in C6 gliomas, although they are expected to exhibit considerable hypoxia. The RIF-1 fibrosarcoma grown in C3H mice and HT29 colon adenocarcinoma grown in nude mice showed clear ^{19}F resonances from SR4554 (reproduced with permission from Robinson and Griffiths, *Phil. Trans. R. Soc. London B Biol. Sci.* 359, 987–996, Fig. 6 (2004) [351]).

Gene therapy holds great promise for the treatment of diverse diseases. However, widespread implementation is hindered by difficulties in assessing the success of transfection in terms of spatial extent, gene expression, and longevity of expression. The development of noninvasive reporter techniques based on appropriate molecules and imaging modalities may help to assay gene expression and this is often achieved by including a reporter gene in tandem with the

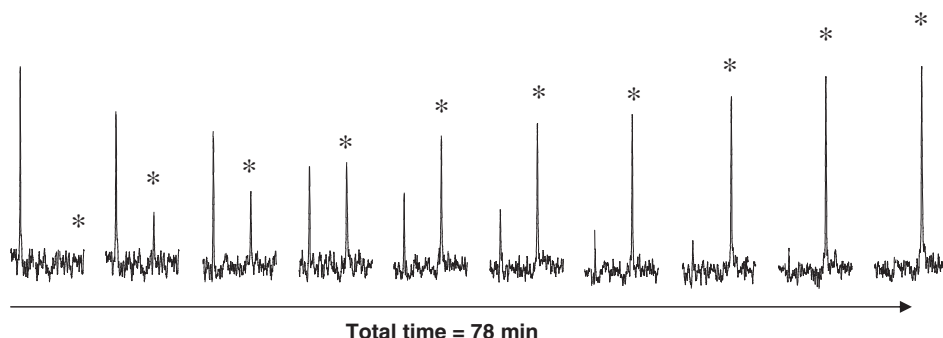


Fig. 14. Detection of β -galactosidase activity in cells using ^{19}F NMR. Sequential ^{19}F NMR spectra of LNCaP C4–2 prostate cancer cells transiently transfected with *lacZ* (1.0×10^7) in phosphate buffered saline (PBS) (0.1 M, pH = 7.4, 700 ml) at 37 °C following addition of GFPOL (1.84 mg, 5.27 mmol). ^{19}F NMR spectra were acquired in 102 s each, and enhanced with an exponential line broadening 40 Hz. In each spectrum, GFPOL occurs on the left with liberated FPOL aglycon appearing at right (*).

therapeutic gene [38,361]. Currently, reporter genes associated with optical imaging are most popular, e.g., BLI of luciferase [38,362] and fluorescent imaging of GFP and longer wavelength variants [45], since they are cheap modalities, and highly sensitive results are rapidly available. These techniques are very useful in superficial tissues and have extensive applications in mice, but application to larger bodies is limited by depth of light penetration. For deeper tissues and larger animals, nuclear medicine approaches based on thymidine kinase or the sodium iodine symporter (hNIS) have been used [49,363]. For cancer, thymidine kinase has the advantage that the gene serves not only as a reporter, but gene products can themselves have therapeutic value [146]. CD activates the minimally toxic 5-fluorocytosine (5FC) to the highly toxic 5-fluorouracil (5FU) [146,147]. The conversion of 5FC to 5FU causes a ^{19}F NMR chemical shift approximately 1.5 ppm, hence, revealing gene activity, which has been demonstrated in a number of systems *in vivo* [147,150].

We have focused on substrates for *lacZ*, recognizing its popularity as a reporter gene. Given the popularity of *lacZ* [364–366] diverse reporter agents are commercially available, but mostly for optical and histological applications (e.g., X-gal, o-nitrophenylgalactopyranoside (ONPG), S-GalTM, and S-Galacton-StarTM) [367–369]. Recently, ^1H MRI [370], fluorescent [371], and radionuclide [372] substrates have been presented for *in vivo* work, prompting us to consider ^{19}F NMR active analogs. It appeared that introduction of a fluorine atom into the popular colorimetric biochemical indicator *ortho*-nitrophenyl β -galactopyranoside (ONPG) could produce a strong candidate molecule. Fluoronitrophenol galactosides were used by Yoon *et al.* [373], to explore β -gal activity, but they placed the fluorine atom on the sugar moiety, which would be expected to provide much

Table 7. ¹⁹F NMR lacZ gene reporters^a

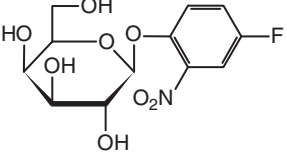
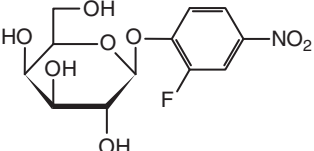
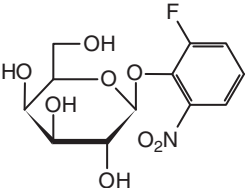
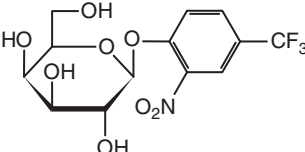
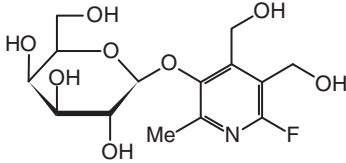
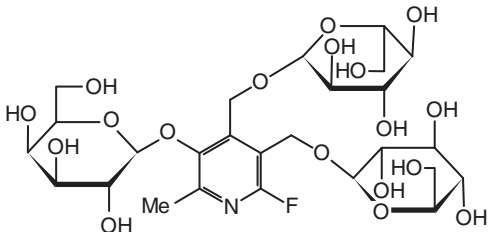
Reporter	Structure	$\delta_{\text{F(Substrate)}}$ (ppm)	$\delta_{\text{F(aglycone)}}$ (ppm)	$\Delta\delta$ (ppm)	References
PFONPG		−42.87	−52.71	−9.84	[294,374]
OFPNPG		−54.93	−61.04	−6.11	[294,375]
OFONPG		−50.67	−58.67	−8.00	[294]
PCF ₃ ONPG		13.40	14.54	1.14	[299]

Table 7. Continued

Reporter	Structure	$\delta_{\text{F}}(\text{Substrate})$ (ppm)	$\delta_{\text{F}}(\text{aglycone})$ (ppm)	$\Delta\delta$ (ppm)	References
GFPOL		−3.22	−11.21	−8.00	[377]
GDUFPOL		−2.85	−12.16	−9.31	[378]

^a NaTFA was used as a chemical shift standard in PBS (0.1 M, pH = 7.4) buffer at 37 °C.

less chemical shift response to cleavage and they do not appear to have used ¹⁹F NMR in these investigations.

Our prototype molecule 4-fluoro-2-nitrophenyl β -D-galactopyranoside (PFONPG, Table 7) proved effective as a substrate for β -galactosidase [374]. It provides a single ¹⁹F NMR signal with a narrow line width and good stability in solution. It is stable in normal wild-type cells and whole blood, but exposure to the enzyme or cells transfected to express β -galactosidase causes rapid cleavage in line with anticipated levels of transfection [374]. Upon cleavage of the glycosidic bond, a chemical shift difference $\Delta\delta > 3.6$ ppm is observed, though the chemical shift of the product may have a range of about 9 ppm, since the released aglycone is pH sensitive and the pK_a is in the physiological range. Significantly, there is no overlap between the chemical shift of the substrate and the product and the chemical shift difference is sufficient to permit chemical shift selective imaging to reveal distribution of each entity separately [375].

To seek optimal ¹⁹F NMR reporters, we synthesized diverse agents and the broad range of substrate structures is consistent with enzyme promiscuity (lack of substrate specificity) (Table 7). The released aglycone PFONP is somewhat toxic and can cause lysis of fragile cells. We have synthesized series of analogues with the fluorine atom placed at various locations on the phenolic ring and incorporating alternate substituents, such as Cl and Br [294]. Each adduct and aglycone provides a unique chemical shift allowing ready comparison of susceptibility to enzyme activity. The chemical shift accompanying cleavage depends strongly on the orientation of the F-atom with largest response for *para*-F and less for *ortho*-F. The rate of cleavage was closely related to the pK_a of the aglycone [294] commensurate with enzyme studies reported previously [376].

One approach to reducing toxicity is introduction of a trifluoromethyl (CF₃) reporter group, as opposed to the single F-atom to enhance signal-to-noise. The chemical shift response is much smaller (Table 7), due to transmission of the electron density redistribution through an additional carbon-carbon bond [299]. Spectroscopic detection is still feasible *in vivo* and deconvolution allows CSI, but it is unlikely to be feasible *in vivo* [299]. Toxicity may also be altered by using alternate aglycons, such as the pH reporter 6-FPOL [11]. 3-O-(β -D-galactopyranosyl)-6-fluoropyridoxol (GFPOL) is found to be a much less good substrate and reactivity is much slower [377]. It is also less water soluble. However, we have found that water solubility may be enhanced by polyglycosylation of the hydroxymethyl arms [378]. The polyglycosylated substrate was also highly reactive for β -gal, but when galactose was used for all sugar residues multiple products were rapidly generated causing complex spectra. Differential glycosylation using glucose or mannose as the secondary sugars overcame this problem [378].

Given the different chemical shifts of individual substrates and products, we believe there will be opportunities to use multiple reporters simultaneously. Indeed, we have investigated using 4-fluoro-2-nitrophenyl β -D-galactopyranoside (PFONPG) and 2-fluorine-4-nitrophenyl β -D-galactopyranoside (OFPNPG) as

substrates simultaneously to differentiate wild type and lacZ expressing tumors in mice [379].

4. PASSIVE REPORTER MOLECULES

Many active ^{19}F NMR reporter molecules have been designed, developed, and exploited, but other methods use a passive approach. In essence, fluorinated molecules occupy a space and a signal magnitude provides an indication of anatomical properties such as lung volume, bowel function, vascular volume, or flow.

PFCs exhibit remarkable gas solubility, and based on the high carrying capacity for oxygen and carbon dioxide, have been developed in emulsion form as synthetic blood substitutes [231]. PFCs may also be relevant as pure liquids. In a classic experiment, Clark and Gollan [380] submersed a living mouse in PFC liquid and far from drowning, it inhaled the PFC facilitating effective oxygen transport to the lungs. Thus, PFCs have potential application as surfactants to aid breathing in extremely premature infants, as explored in clinical trials [381]. PFC may be administered as liquid or aerosols. Thomas *et al.* [382,383] applied ^{19}F MRI to show the extent of lung filling. Further, by applying relaxation measurements (as described in Section 3.1), they could estimate regional $p\text{O}_2$ in the lungs of mice, rats, dogs, and pigs [208,383]. Various PFCs and PFC emulsions have been introduced into the lung as aerosols, sometimes with animals under forced ventilation, following thorocotomy [383]. The ^{19}F signal provides an opportunity to image lungs. By contrast ^1H MRI is handicapped by lack of water signal. In a novel approach, Huang *et al.* [384] applied ^1H MRI to the water in a PFC emulsion and found considerably enhanced structural information. Liquid and aerosol ventilation can be stressful, whereas inhalation of inert gas may be more practical, as shown by proof of principle using CF_4 or C_2F_6 [385]. More recent studies used SF_6 with potential application for detection of lung cancer, emphysema, or allograft rejection [386,387]. Gas detection does require special MR instrumentation, due to the exceedingly short T_1 and T_2 relaxation.

Increasing awareness of colon cancer demands improved screening. Traditional barium meals provide contrast in CT, and virtual colonoscopy is competing with traditional fiber optic probes [388]. MR procedures have lagged behind CT, but several potential contrast agents have been presented, ranging from paramagnetic zeolite formulations [389] and ferric ammonium citrate [390] to PFC emulsions [391,392] and recently images were shown in mice based on perfluorononane [69].

Angiogenesis is associated with tumor development and many clinical trials have found correlations between vascular density and prognosis. Traditional analysis required biopsy and histology, with CD31 antibodies to provide blood vessel counts [393], and dyes such as India ink or Hoechst 33342 to reveal

perfusion [394]. ^{19}F NMR provides a robust indication of vascular volume *in vivo* based on intravenous PFC emulsions, which are retained in the vasculature for a period of hours [395,396]. Noninvasive measurements revealed acute modulation of tumor blood volume and have provided validation of noninvasive near infrared (NIR) methods [397,398]. This approach has also been applied to other organs and tissues, for example, demonstrating reactive hyperemia in muscles [399]. Studies have validated signal using traditional radioisotope-labeled approaches and dyes [400].

Fluorinated gases (e.g., trifluoromethane (FC-23) and chlorofluoromethane (FC-22)) have been used to examine cerebral blood flow based on inflow and outflow kinetics, sometimes with pulsed delivery to facilitate compartmental analysis [401,402]. The observation that HFB clears from tumors over a period of hours suggests this could provide insight into tissue perfusion [224,266].

5. POTENTIAL INNOVATIONS AND IMPROVEMENTS

Implementation and application of ^{19}F MRI in the clinic awaits further developments. As described above, many reporter molecules have been presented and are undergoing further refinement and evaluation. Sensitivity can be enhanced incrementally by exploiting molecular symmetry as emphasized in Table 2: bis-fluorine atoms can enhance SNR twofold, a CF_3 group threefold, a bis- CF_3 sixfold and tris- CF_3 ninefold. Perhaps the most satisfying increase in SNR is gained by better targetability and localization following systemic delivery. Widespread utility of agents will depend on ready commercial availability. Other sensitivity gains can arise from enhanced radiofrequency coils and parallel imaging (e.g., SiMultaneous Aequisition of Spatial Harmonics (SMASH) or Sensitivity encoding (SENSE) technologies [403,404]) and higher magnetic field. While ^{19}F MRI on human NMR systems is feasible, it still remains to be established as part of a routine commercial inventory. Clearly, use and need will stimulate widespread provision and availability which could occur quite rapidly.

6. CONCLUSIONS

Since there is essentially no ^{19}F NMR background signal in tissues, fluorinated drugs, and reporter molecules may be detected without interference. Huge diversity of application has been demonstrated in the biochemical and small animal areas, with some limited clinical application. To date, clinical application is hindered by the lack of availability of clinical ^{19}F NMR, but manufacturers are increasingly recognizing the value of including such capability. Given that ^{19}F NMR offers the potential to investigate many diverse parameters (Table 1), it will become increasingly available and useful in the future.

ACKNOWLEDGMENTS

Supported in part by the Cancer Imaging Program, NCI Pre-ICMIC P20 CA086354, SAIRP U24 CA126608 and IDEA awards from the DOD Breast Cancer Initiative DAMD 17-99-1-9381, and 17-03-1-0343 and Prostate Cancer Initiative W81XWH-06-1-0149. NMR experiments were conducted at the Mary Nell and Ralph B. Rogers NMR Center, an NIH BTRP facility #P41-RR02584. We are grateful to Drs. Mark Jeffrey, Himu Shukla, and Peter Peschke, for collegial support and allowing us to include unpublished collaborative studies here. Melody Simmons provided expert assistance in preparing this manuscript. Over the past 15 years, our development of expertise in ^{19}F NMR has been supported by the NIH, Department of Defense Breast and Prostate Cancer Initiatives, the American Cancer Society, the American Heart Association, and The Whitaker Foundation.

REFERENCES

- [1] Z. Zhang, S.A. Nair, T.J. McMurry, Gadolinium meets medicinal chemistry: MRI contrast agent development, *Curr. Med. Chem.* 12 (2005) 751–778.
- [2] C. Baudelet, B. Gallez, Current issues in the utility of blood oxygen level dependent MRI for the assessment of modulations in tumor oxygenation, *Curr. Med. Imag. Rev.* 1 (2005) 229–243.
- [3] D. Liebfritz, J.D. de Certaines, W.M.M.J. Bovee, F. Podo Water Suppression, Pergamon, Oxford, 1992, pp. 149–168.
- [4] D. O'Hagan, D.B. Harper, Fluorine-containing natural products, *J. Fluorine Chem.* 100 (1999) 127–133.
- [5] S.R. Thomas, C.L. Partain, R.R. Price, J.A. Patton, M.V. Kulkarni, A.E.J. James (Eds.), *The Biomedical Applications of Fluorine-19 NMR*, Vol. 2, W.B. Saunders Co., London, 1988, pp. 1536–1552.
- [6] B.S. Selinsky, C.T. Burt, L.J. Berliner, J. Reuben (Eds.), *In Vivo ^{19}F NMR*, Vol. 11, Plenum, New York, 1992, pp. 241–276.
- [7] M.J.W. Prior, R.J. Maxwell, J.R. Griffiths, M. Rudin (Eds.), *Fluorine- ^{19}F NMR Spectroscopy and Imaging *In-Vivo**, Springer-Verlag, Berlin, 1992, pp. 103–130.
- [8] R.E. London, R.J. Gillies (Eds.), *In Vivo NMR Studies Utilizing Fluorinated NMR Probes Academic*, San Diego, 1994, pp. 263–277.
- [9] R.P. Mason, Non-invasive physiology: ^{19}F NMR of perfluorocarbon, *Artif. Cells Blood Substit. Immobil. Biotechnol.* 22 (1994) 1141–1153.
- [10] D. Zhao, L. Jiang, R.P. Mason, Measuring changes in tumor oxygenation, *Meth. Enzymol.* 386 (2004) 378–418.
- [11] R.P. Mason, Transmembrane pH gradients *in vivo*: Measurements using fluorinated vitamin B6 derivatives, *Curr. Med. Chem.* 6 (1999) 481–499.
- [12] P.M.J. McSheehy, L.P. Lemaire, J.R. Griffiths, D.M. Grant, in: R.K. Harris (Eds.), *Fluorine-19 MRS: Applications in Oncology*, Wiley, Chichester, 1996, pp. 2048–2051.
- [13] D.K. Menon, Fluorine-19 MRS: General Overview and Anesthesia R.K. Harris (Eds.), Wiley, Chichester, 1995, pp. 2052–2063.
- [14] T.J. Passe, H.C. Charles, P. Rajagopalan, K.R. Krishnan, Nuclear magnetic resonance spectroscopy: A review of neuropsychiatric applications, nuclear magnetic resonance spectroscopy: A review of neuropsychiatric applications, *Prog. Neuropsychopharmacol. Biol. Psychiatry* 19 (1995) 541–563.

- [15] P. Bachert, Pharmacokinetics using fluorine NMR *in vivo*, Prog. Nucl. Magn. Reson. Spectrosc. 33 (1998) 1–56.
- [16] R. Martino, M. Malet-Martino, V. Gilard, Fluorine nuclear magnetic resonance, a privileged tool for metabolic studies of fluoropyrimidine drugs, Curr. Drug Metab. 1 (2000) 271–303.
- [17] W. Wolf, C.A. Presant, V. Waluch, ^{19}F -MRS studies of fluorinated drugs in humans, Adv. Drug Deliv. Rev. 41 (2000) 55–74.
- [18] J.X. Yu, V. Kodibagkar, W. Cui, R.P. Mason, ^{19}F : A versatile reporter for non-invasive physiology and pharmacology using magnetic resonance, Curr. Med. Chem. 12 (2005) 818–848.
- [19] H.J. Bohm, D. Banner, S. Bendels, M. Kansy, B. Kuhn, K. Muller, U. Obst-Sander, M. Stahl, Fluorine in medicinal chemistry, Chembiochem 5 (2004) 637–643.
- [20] I. Ojima, Use of fluorine in the medicinal chemistry and chemical biology of bioactive compounds—A case study on fluorinated taxane anticancer agents, Chembiochem 5 (2004) 628–635.
- [21] W.R. Dolbier, Fluorine chemistry at the millennium, J. Fluorine Chem. 126 (2005) 157–163.
- [22] B.K. Park, N.R. Kitteringham, P.M. O'Neill, Metabolism of fluorine-containing drugs, Annu. Rev. Pharmacol. Toxicol. 41 (2001) 443–470.
- [23] C. Jackel, B. Koksche, Fluorine in peptide design and protein engineering, Eur. J. Org. Chem. 21 (2005) 4483–4503.
- [24] M. Shimizu, T. Hiyama, Modern synthetic methods for fluorine-substituted target molecules, Angew. Chem. Int. Ed. 44 (2005) 214–231.
- [25] H. Plenio, The coordination chemistry of fluorine in fluorocarbons, Chembiochem 5 (2004) 650–655.
- [26] P. Jeschke, The unique role of fluorine in the design of active ingredients for modern crop protection, Chembiochem 5 (2004) 570–589.
- [27] F.M.D. Ismail, Important fluorinated drugs in experimental and clinical use, J. Fluorine Chem. 118 (2002) 27–33.
- [28] C. Isanbor, D. O'Hagan, Fluorine in medicinal chemistry: A review of anti-cancer agents, J. Fluorine Chem. 127 (2006) 303–319.
- [29] C.E. Oyiliagu, M. Novalen, L.P. Kotra, Fluorine containing molecules for peptidomimicry: A chemical act to modulate enzymatic activity, Mini-Rev. Organic Chem. 3 (2006) 99–115.
- [30] M. Zanda, Trifluoromethyl group: An effective xenobiotic function for peptide backbone modification, New J. Chem. 28 (2004) 1401–1411.
- [31] <http://www.nibib.nih.gov/in> Vol. 2006.
- [32] <http://imaging.cancer.gov/in> Vol. 2007.
- [33] <http://www.molecularimaging.org>.
- [34] <http://www.ismrm.org/>.
- [35] <http://interactive.snm.org/in> Vol. 2007.
- [36] R.P. Mason, S. Ran, P.E. Thorpe, Quantitative assessment of tumor oxygen dynamics: Molecular Imaging for Prognostic Radiology, J. Cell. Biochem. 87(Suppl.) (2002) 45–53.
- [37] J.A. Karam, R.P. Mason, K.S. Koeneman, P.P. Antich, E.A. Benaim, J.T. Hsieh, Molecular imaging in prostate cancer, J. Cell. Biochem. 90 (2003) 473–483.
- [38] C.H. Contag, B.D. Ross, It's not just about anatomy: *In vivo* bioluminescence imaging as an eyepiece into biology, J. Magn. Reson. Imaging 16 (2002) 378–387.
- [39] R. Kumar, S. Jana, Positron emission tomography: An advanced nuclear medicine imaging technique from research to clinical practice, Methods Enzymol. 385 (2004) 3–19.
- [40] <http://probes.invitrogen.com/handbook/in> Vol. 2007.
- [41] <http://www.cri-inc.com/products/maestro.aspin> Vol. 2007.
- [42] M. Oldham, H. Sakhalkar, T. Oliver, Y.M. Wang, J. Kirpatrick, Y.T. Cao, C. Badea, G.A. Johnson, M. Dewhirst, Three-dimensional imaging of xenograft tumors using optical computed and emission tomography, Med. Phys. 33 (2006) 3193–3202.

- [43] G. Zacharakis, H. Kambara, H. Shih, J. Ripoll, J. Grimm, Y. Saeki, R. Weissleder, V. Ntziachristos, Volumetric tomography of fluorescent proteins through small animals *in vivo*, *Proc. Natl. Acad. Sci. USA* 102 (2005) 18252–18257.
- [44] A.M. Derfus, W.C.W. Chan, S.N. Bhatia, Probing the cytotoxicity of semiconductor quantum dots, *Nano Lett.* 4 (2004) 11–18.
- [45] R. Hoffman, Green fluorescent protein imaging of tumour growth, metastasis, and angiogenesis in mouse models, *Lancet Oncol.* 3 (2002) 546–556.
- [46] C.H. Contag, S.D. Spilman, P.R. Contag, M. Oshiro, B. Eames, P. Dennerly, D.K. Stevenson, D.A. Benaron, Visualizing gene expression in living mammals using a bioluminescent reporter, *Photochem. Photobiol.* 66 (1997) 523–531.
- [47] E. Richer, N. Slavine, M.A. Lewis, E. Tsyganov, G.C. Gellert, Z. Gunnur Dikmen, V. Bhagwandin, J.W. Shay, R.P. Mason, P.P. Antich, Society of Molecular Imaging (St. Louis) 2004.
- [48] F. Blankenberg, W.C. Eckelman, H.W. Strauss, M.J. Welch, A. Alavi, C. Anderson, S. Bacharach, R.G. Blasberg, M.M. Graham, W. Weber, Role of radionuclide imaging in trials of antiangiogenic therapy. [Review], *Acad. Radiol.* 7 (2000) 851–867.
- [49] U. Haberkorn, W. Mier, M. Eisenhut, Scintigraphic imaging of gene expression and gene transfer, *Curr. Med. Chem.* 12 (2005) 779–794.
- [50] D. Vranjesevic, J.E. Filmont, J. Meta, D.H. Silverman, M.E. Phelps, J. Rao, P.E. Valk, J. Czernin, Whole-body (18)F-FDG PET and conventional imaging for predicting outcome in previously treated breast cancer patients, *J. Nucl. Med.* 43 (2002) 325–329.
- [51] Y. Seo, B.L. Franc, R.A. Hawkins, K.H. Wong, B.H. Hasegawa, Progress in SPECT/CT imaging of prostate cancer, *Technol. Cancer Res. Treat.* 5 (2006) 329–336.
- [52] C. Love, A.S. Din, M.B. Tomas, T.P. Kalapparambath, C. Palestro, Radionuclide bone imaging: An illustrative review, *Radiographics* 23 (2003) 341–358.
- [53] E. Cherin, R. Williams, A. Needles, G.W. Liu, C. White, A.S. Brown, Y.Q. Zhou, F.S. Foster, Ultrahigh frame rate retrospective ultrasound microimaging and blood flow visualization in mice *in vivo*, *Ultrasound Med. Biol.* 32 (2006) 683–691.
- [54] M. Tepel, P. Aspelin, N. Lameire, Contrast-induced nephropathy: A clinical and evidence-based approach, *Circulation* 113 (2006) 1799–1806.
- [55] H. Mishima, T. Kobayashi, M. Shimizu, Y. Tamaki, M. Baba, In vivo F-19 chemical shift imaging with FTPA and antibody-coupled FMIQ, *J. Magn. Reson. Imaging* 1 (1991) 705–709.
- [56] A.M. Morawski, P.M. Winter, X. Yu, R. Fuhrhop, M.J. Scott, F. Hockett, J.-D. Robertson, P.J. Gaffney, G.M. Lanza, S.A. Wickline, Quantitative “magnetic resonance immunohistochemistry” with ligand-targeted (19)F nanoparticles, *Magn. Reson. Med.* 52 (2004) 1255–1262.
- [57] M. Higuchi, N. Iwata, Y. Matsuba, K. Sato, K. Sasamoto, T.C. Saido, F-19 and H-1 MRI detection of amyloid beta plaques *in vivo*, *Nat. Neurosci.* 8 (2005) 527–533.
- [58] R.K. Harris, E.D. Becker, S.M. Cabral de Menezes, R. Goodfellow, P. Granger, NMR nomenclature. Nuclear spin properties and conventions for chemical shifts (IUPAC Recommendations 2001), *Pure Appl. Chem.* 73 (2001) 1795–1818.
- [59] F.A. Bovey, *Nuclear Magnetic Resonance Spectroscopy*, Academic Press, San Diego, 1988, p. 653.
- [60] J.W. Emsley, L. Phillips, Fluorine chemical shifts, *Prog. Nucl. Magn. Reson. Spectrosc.* 7 (1971) 1–520.
- [61] J.W. Emsley, L. Phillips, V. Wray, Fluorine coupling constants, *Prog. Nucl. Magn. Reson. Spectrosc.* 10 (1976) 83–756.
- [62] H.P. Shukla, R.P. Mason, D.E. Woessner, P.P. Antich, A comparison of three commercial perfluorocarbon emulsions as high field NMR probes of oxygen tension and temperature, *J. Magn. Reson. Series B.* 106 (1995) 131–141.
- [63] H.W.M. van Laarhoven, C.J.A. Punt, Y.J.L. Kamm, A. Heerschap, Monitoring fluoropyrimidine metabolism in solid tumors with *in vivo* 19F magnetic resonance spectroscopy, *Crit. Rev. Oncol./Hematol.* 56 (2005) 321–343.

- [64] M.C. Malet-Martino, J.P. Armand, A. Lopez, J. Bernadou, J.P. Beteille, M. Bon, R. Martino, Evidence for the importance of 5'-deoxy-5-fluorouridine catabolism in humans from ¹⁹F nuclear magnetic resonance spectrometry, *Cancer Res.* 46 (1986) 2105–2112.
- [65] A.W. Blackstock, H. Lightfoot, L.D. Case, J.E. Tepper, S.K. Mukherji, B.S. Mitchell, S. G. Swarts, S.M. Hess, Tumor uptake and elimination of 2',2'-difluoro-2'-deoxycytidine (gemcitabine) after deoxycytidine kinase gene transfer: Correlation with *in vivo* tumor response, *Clin. Cancer Res.* 7 (2001) 3263–3268.
- [66] G.S. Payne, D.J. Collins, P. Loynds, G. Mould, P.S. Murphy, A.S.K. Dzik-Jurasz, P. Kessar, N. Haque, M. Yamaguchi, S. Atarashi, M.O. Leach, Quantitative assessment of the hepatic pharmacokinetics of the antimicrobial sitafloxacin in humans using *in vivo* F-19 magnetic resonance spectroscopy, *Br. J. Clin. Pharmacol.* 59 (2005) 244–248.
- [67] D. Bilecen, A.C. Schulte, A. Kaspar, E. Kustermann, J. Seelig, D. von Elverfeldt, K. Scheffler, Detection of the non-steroidal anti-inflammatory drug niflumic acid in humans: A combined F-19-MRS *in vivo* and *in vitro* study, *NMR Biomed.* 16 (2003) 144–151.
- [68] E. Schneider, N.R. Bolo, B. Frederick, S. Wilkinson, F. Hirashima, L. Nassar, I. K. Lyoo, P. Koch, S. Jones, J. Hwang, Y. Sung, R.A. Villafuerte, G. Maier, R. Hsu, R. Hashoian, P.F. Renshaw, Magnetic resonance spectroscopy for measuring the biodistribution and *in situ in vivo* pharmacokinetics of fluorinated compounds: Validation using an investigation of liver and heart disposition of tecastemizole, *J. Clin. Pharm. Ther.* 31 (2006) 261–273.
- [69] R. Schwarz, A. Kaspar, J. Seelig, B. Kunnecke, Gastrointestinal transit times in mice and humans measured with ²⁷Al and ¹⁹F nuclear magnetic resonance, *Magn. Reson. Med.* 48 (2002) 255–261.
- [70] M.E. Henry, M.E. Schmidt, J. Hennen, R.A. Villafuerte, M.L. Butman, P. Tran, L.T. Kerner, B. Cohen, P.F. Renshaw, A comparison of brain and serum pharmacokinetics of R-fluoxetine and racemic fluoxetine: A 19-F MRS study, *Neuropsychopharmacology* 30 (2005) 1576–1583.
- [71] W.L. Strauss, A.S. Unis, C. Cowan, G. Dawson, S.R. Dager, Fluorine magnetic resonance spectroscopy measurement of brain fluvoxamine and fluoxetine in pediatric patients treated for pervasive developmental disorders, *Am. J. Psychiatry* 159 (2002) 755–760.
- [72] J.D. Christensen, D.A. Yurgelun-Todd, S.M. Babb, S.A. Gruber, B.M. Cohen, P.F. Renshaw, Measurement of human brain dexfenfluramine concentration by ¹⁹F magnetic resonance spectroscopy, *Brain Res.* 834 (1999) 1–5.
- [73] Y.L. Chung, H. Troy, I.R. Judson, R. Leek, M.O. Leach, M. Stubbs, A.L. Harris, J.R. Griffiths, Noninvasive measurements of capecitabine metabolism in bladder tumors overexpressing thymidine phosphorylase by fluorine-19 magnetic resonance spectroscopy, *Clin. Cancer Res.* 10 (2004) 3863–3870.
- [74] C.J. Deutsch, J.S. Taylor, R.K. Gupta (Eds.), ¹⁹F NMR Measurements of Intracellular pH CRC Press, Boca Raton, 1987, pp. 55–73.
- [75] B.E. Smart, Fluorine substituent effects (on bioactivity), *J. Fluorine Chem.* 109 (2001) 3–11.
- [76] G. Gerebtzoff, X. Li-Blatter, H. Fischer, A. Frentzel, A. Seelig, Halogenation of drugs enhances membrane binding and permeation, *Chembiochem* 5 (2004) 676–684.
- [77] B.A. Shainyan, Y.S. Danilevich, A.A. Grigor'eva, Y.A. Chuvashov, Electrochemical fluorination of benzamide and acetanilide in anhydrous HF and in acetonitrile, *Russian J. Org. Chem. (Trans. Zh. Organ. Khim.)* 40 (2004) 513–517.
- [78] G.A. Olah, M. Nojima, I. Kerekes, Synthetic methods and reactions. I. Selenium tetrafluoride and its pyridine complex. Convenient fluorinating agents for fluorination of ketones, aldehydes, amides, alcohols, carboxylic acids, and anhydrides, *J. Am. Chem. Soc.* 96 (1974) 925–927.

- [79] A. Haas, T. Maciej, Fluorination by tungsten hexafluoride, *J. Fluorine Chem.* 20 (1982) 581–587.
- [80] T.B. Patrick, L. Zhang, Q. Li, Rearrangement and double fluorination in the deiodinative fluorination of neopentyl iodide with xenon difluoride, *J. Fluorine Chem.* 102 (2000) 11–15.
- [81] G.G. Belen'kii, V.A. Petrov, P.R. Resnick, Electrophilic, catalytic alkylation of polyfluoroolefins by some fluoroalkanes, *J. Fluorine Chem.* 108 (2001) 15–20.
- [82] K. Adachi, Y. Ohira, G. Tomizawa, S. Ishihara, S. Oishi, Electrophilic fluorination with N,N'-difluoro-2,2'-bipyridinium salt and elemental fluorine, *J. Fluorine Chem.* 120 (2003) 173–183.
- [83] V. Mehta, P.V. Kulkarni, R.P. Mason, A. Constantinescu, P.P. Antich, Novel molecular probes for ^{19}F magnetic resonance imaging: Synthesis & characterization of fluorinated polymers, *Bioorg. Med. Chem. Lett.* 2 (1992) 527–532.
- [84] J. Joubert, S. Roussel, C. Christophe, T. Billard, B.R. Langlois, T. Vidal, Trifluoroacetamides from amino alcohols as nucleophilic trifluoromethylating reagents, *Angew. Chem. Int. Ed.* 42 (2003) 3133–3136.
- [85] J.S. Rasey, J.J. Casciari, P.D. Hofstrand, M. Muzi, M.M. Graham, L.K. Chin, Determining hypoxic fraction in a rat glioma by uptake of radiolabeled fluoromisonidazole, *Radiat. Res.* 153 (2000) 84–92.
- [86] W.R. Dolbier Jr., A.R. Li, C.J. Koch, C.Y. Shiue, A.V. Kachur, [18F]-EF5, a marker for PET detection of hypoxia: Synthesis of precursor and a new fluorination procedure, *Appl. Radiat. Isot.* 54 (2001) 73–80.
- [87] C.S. Yap, J. Czernin, M.C. Fishbein, R.B. Cameron, C. Schiepers, M.E. Phelps, W.A. Weber, Evaluation of thoracic tumors with ^{18}F -fluorothymidine and ^{18}F -fluoro-deoxyglucose-positron emission tomography, *Chest* 129 (2006) 393–401.
- [88] P. Zanzonico, J. Campa, D. Polcarpe-Holman, G. Forster, R. Finn, S. Larson, J. Humm, C. Ling, Animal-specific positioning molds for registration of repeat imaging studies: Comparative microPET imaging of F18-labeled fluoro-deoxyglucose and fluoro-misonidazole in rodent tumors, *Nucl. Med. Biol.* 33 (2006) 65–70.
- [89] N.J. Spratt, U. Ackerman, H.J. Tochon-Danguy, G.A. Donnan, D.W. Howells, Characterization of fluoromisonidazole binding in stroke, *Stroke* 37 (2006) 1862–1867.
- [90] J. Bussink, E.G.C. Troost, P. Laverman, M. Philippens, J. Lok, O.C. Boerman, J. Kaanders, A.J. van der Kogel, Characterization of human squamous cell head and neck carcinoma xenografts using 18F-FLT and 18F-MISO autoradiography and immunohistochemistry, *Radiother. Oncol.* 78 (2006) S33.
- [91] J. Keupp, P.C. Mazurkewitz, I. Gräßlin, T. Schaeffter, *Proc. Intl. Soc. Mag. Reson. Med.* 2006, p. 102.
- [92] G. Schnur, R. Kimmich, R. Lietzenmayer, Hydrogen/Fluorine retuning tomography. Applications to ^1H image-guided volume-selective ^{19}F spectroscopy and relaxometry of perfluorocarbon emulsions in tissue, *Magn. Reson. Med.* 13 (1990) 478–489.
- [93] J. Sanders, B. Hunter, *Modern NMR Spectroscopy*, Oxford University Press, New York 1987, p. 308.
- [94] R.P. Mason, G. Cha, G.H. Gorrie, E.E. Babcock, P.P. Antich, Glutathione in whole blood: A novel determination using double quantum coherence transfer proton NMR spectroscopy, *FEBS Lett.* 318 (1993) 30–34.
- [95] R.E. Hurd, D.M. Freeman, Metabolite specific proton magnetic-resonance imaging, *Proc. Natl. Acad. Sci. USA* 86 (1989) 4402–4406.
- [96] R.P. Mason, J.K.M. Sanders, *In vivo* enzymology: A deuterium NMR study of formaldehyde dismutase in *Pseudomonas putida* F61a and *Staphylococcus aureus*, *Biochemistry* 28 (1989) 2160–2168.
- [97] R.P. Mason, J.K.M. Sanders, A. Crawford, B.K. Hunter, Formaldehyde metabolism by *E. coli*: Detection using *in vivo* ^{13}C NMR spectroscopy of S-(hydroxymethyl) glutathione as a transient intracellular intermediate, *Biochemistry* 25 (1986) 4504–4507.
- [98] R.F. Code, J.E. Harrison, K.G. McNeill, M. Szykowski, *In vivo* ^{19}F spin relaxation in index finger bones, *Mag. Reson. Med.* 13 (1990) 358–369.

- [99] D.W.J. Klomp, H.W.M. van Laarhoven, A.P.M. Kentgens, A. Heerschap, Optimization of localized F-19 magnetic resonance spectroscopy for the detection of fluorinated drugs in the human liver, *Magn. Reson. Med.* 50 (2003) 303–308.
- [100] A.V. Ratner, S. Quay, H.H. Muller, B.B. Simpson, R. Hurd, S.W. Young, ^{19}F relaxation rate enhancement and frequency shift with Gd-DTPA, *Invest. Radiol.* 24 (1989) 224–227.
- [101] V.D. Mehta, R.P. Mason, P.V. Kulkarni, P. Lea, A. Constantinescu, P.P. Antich, E.H. Emram (Eds.), ^{19}F MR Characterization of Fluorinated Proteins and Relaxation Rate Enhancement with Gd-DTPA for Faster Imaging, Plenum, New York, 1995, pp. 305–313.
- [102] H. Lee, R.R. Price, G.E. Holburn, C.L. Partain, M.D. Adams, W.P. Cacheris, *In-Vivo* F-19 MR-Imaging—Relaxation Enhancement with Gd-DTPA, *J. Magn. Reson. Imaging* 4 (1994) 609–613.
- [103] G. Brix, M.E. Bellemann, L. Gerlach, U. Haberkorn, Intra- and extracellular fluorouracil uptake: Assessment with contrast-enhanced metabolic F-19 MR imaging, *Radiology* 209 (1998) 259–267.
- [104] B.S.Y. Li, G.S. Payne, D.J. Collins, M.O. Leach, H-1 decoupling for *in vivo* F-19 MRS studies using the time-share modulation method on a clinical 1.5 T NMR system, *Magn. Reson. Med.* 44 (2000) 5–9.
- [105] R.D. Kendrick, C.S. Yannoni, High-Power H-1-F-19 Excitation in a Multiple-Resonance Single-Coil Circuit, *J. Magn. Reson.* 75 (1987) 506–508.
- [106] H.B. Lantum, R.B. Baggs, D.M. Krenitsky, M.W. Anders, Nephrotoxicity of chloro-fluoroacetic acid in rats, *Toxicol. Sci.* 70 (2002) 261–268.
- [107] B. Hassel, U. Sonnewald, G. Unsgard, F. Fonnum, NMR-spectroscopy of cultured astrocytes—Effects of glutamine and the gliotoxin fluorocitrate, *J. Neurochem.* 62 (1994) 2187–2194.
- [108] R.L. Frost, R.W. Parker, J.V. Hanna, Detection of the pesticide compound-1080 (sodium monofluoroacetate) using F-19 nuclear magnetic-resonance spectroscopy, *Analyst* 114 (1989) 1245–1248.
- [109] O. Corcoran, J.C. Lindon, R. Hall, I.M. Ismail, J.K. Nicholson, The potential of F-19 NMR spectroscopy for rapid screening of cell cultures for models of mammalian drug metabolism, *Analyst* 126 (2001) 2103–2106.
- [110] M. Spraul, M. Hofmann, I.D. Wilson, E. Lenz, J.K. Nicholson, J.C. Lindon, Coupling of Hplc with F-19-NMR and H-1-NMR spectroscopy to investigate the human urinary-excretion of flurbiprofen metabolites, *J. Pharm. Biomed. Anal.* 11 (1993) 1009–1015.
- [111] M.E. Bollard, E. Holmes, C.A. Blackledge, J.C. Lindon, I.D. Wilson, J.K. Nicholson, H-1 and F-19-nmr spectroscopic studies on the metabolism and urinary excretion of mono- and disubstituted phenols in the rat, *Xenobiotica* 26 (1996) 255–273.
- [112] A. Preiss, J. Kruppa, J. Buschmann, C. Mugge, The determination of trifluoroacetic acid in rat milk samples by F-19-NMR spectroscopy and capillary gas chromatography, *J. Pharm. Biomed. Anal.* 16 (1998) 1381–1385.
- [113] M. Tugnait, E.M. Lenz, M. Hofmann, M. Spraul, I.D. Wilson, J.C. Lindon, J.K. Nicholson, The metabolism of 2-trifluormethylaniline and its acetanilide in the rat by ^{19}F NMR monitored enzyme hydrolysis and $^1\text{H}/^{19}\text{F}$ HPLC-NMR spectroscopy, *J. Pharm. Biomed. Anal.* 30 (2003) 1561–1574.
- [114] C.J. Duckett, J.C. Lindon, H. Walker, F. Abou-Shakra, I.D. Wilson, J.K. Nicholson, Metabolism of 3-chloro-4-fluoroaniline in rat using [C-14]-radiolabelling, F-19-NMR spectroscopy, HPLC-MS/MS, HPLC-ICPMS and HPLC-NMR, *Xenobiotica* 36 (2006) 59–77.
- [115] C.A. Blackledge, J.K. Nicholson, J.A. Evans, C. Rodgers, I.D. Wilson, Application of H-1- and F-19-NMR spectroscopy in the investigation of the urinary and biliary excretion of 3,5-, 2,4-ditrifluoromethylbenzoic and pentafluorobenzoic acids in rat, *Xenobiotica* 32 (2002) 605–613.

- [116] B.W. Dubois, A.S. Evers, 19F-NMR spin-spin relaxation (T2) method for characterizing volatile anesthetic binding to proteins. Analysis of isoflurane binding to serum albumin, *Biochemistry*. 31 (1992) 7069–7076.
- [117] W.M. Chew, M.E. Moseley, P.A. Mills, D. Sessler, R. Gonzalez-Mendez, T.L. James, L. Litt, Spin-echo fluorine magnetic resonance imaging at 2 T: *In vivo* spatial distribution of halothane in the rabbit head, *Magn. Reson. Imaging* 5 (1987) 51–56.
- [118] D.K. Menon, G.G. Lockwood, C.J. Peden, I.J. Cox, J. Sargentoni, J.D. Bell, G.A. Coutts, J.G. Whitwam, *In-vivo* F-19 magnetic-resonance spectroscopy of cerebral halothane in postoperative-patients—preliminary-results, *Magn. Reson. Med.* 30 (1993) 680–684.
- [119] E.E. Babcock, J.T. Vaughan, B. Lesan, R.L. Nunnally, Multinuclear NMR investigations of probe construction materials at 4.7-T, *Magn. Reson. Med.* 13 (1990) 498–503.
- [120] T.A. Morinelli, A.K. Okwu, D.E. Mais, P.V. Halushka, V. John, C.K. Chen, J. Fried, Difluorothromboxane-A2 and stereoisomers—stable derivatives of thromboxane-A2 with differential-effects on platelets and blood-vessels, *Proc. Natl.Acad. Sci. USA* 86 (1989) 5600–5604.
- [121] R.A. Dwek, R.A. Dwek (Ed.), *The Use of Fluorine-19 as a Detecting Shift Probe*, Clarendon, Oxford, 1975, pp. 158–173.
- [122] J.T. Gerig, Fluorine magnetic resonance of fluorinated ligands, *Meth. Enzymol.* 177 (1989) 3–23.
- [123] W.H. Huestis, M.A. Raftery, Study of cooperative interactions in hemoglobin using fluorine nuclear magnetic resonance, *Biochemistry* 11 (1972) 1648–1654.
- [124] F. Millett, M.A. Raftery, Fluorine-19 nuclear magnetic resonance study of the binding of trifluoroacetylglucosamine oligomers to lysozyme, *Biochemistry* 11 (1972) 1639–1643.
- [125] S.G. Withers, K. Rupitz, I.P. Street, 2-Deoxy-2-fluoro-D-glycosyl fluorides—a new class of specific mechanism-based glycosidase inhibitors, *J. Biol. Chem.* 263 (1988) 7929–7932.
- [126] S.G. Withers, I.P. Street, M.D. Percival, Fluorinated carbohydrates as probes of enzyme specificity and mechanism, *ACS Symposium Series* 374 (1988) 59–77.
- [127] W.G. Stirtan, S.G. Withers, Phosphonate and alpha-fluorophosphonate analogue probes of the ionization state of pyridoxal 5'-phosphate (PLP) in glycogen phosphorylase, *Biochemistry* 35 (1996) 15057–15064.
- [128] P. Szczecinski, D. Bartusik, F-19 NMR measurements—A potential tool for the determination of amino acids in body fluids, *Pol. J. Chem.* 77 (2003) 321–328.
- [129] L.A. Sylvia, J.T. Gerig, Fluorine NMR-studies of the metabolism of flumecinol (3-trifluoromethyl-alpha-ethylbenzhydrol), *Drug Metab. Dispos.* 21 (1993) 105–113.
- [130] U. Sidelmann, S.H. Hansen, C. Gavaghan, A.W. Nicholls, H.A.J. Carless, J.C. Landon, I.D. Wilson, J.K. Nicholson, Development of a simple liquid chromatographic method for the separation of mixtures of positional isomers and anomers of synthetic 2-, 3- and 4-fluorobenzoic acid glucuronides formed via acyl migration reactions, *J. Chromatogr. B: Biomed. Sci. Appl.* 685 (1996) 113–122.
- [131] G.B. Scarfe, M. Tugnait, I.D. Wilson, J.K. Nicholson, Studies on the metabolism of 4-fluoroaniline and 4-fluoroacetanilide in rat: Formation of 4-acetamidophenol (paracetamol) and its metabolites via defluorination and N-acetylation, *Xenobiotica* 29 (1999) 205–216.
- [132] M.K. Ellis, J.L. Naylor, T. Green, M.A. Collins, Identification and quantification of fluorine-containing metabolites of 1-chloro-2,2,2-trifluoroethane (Hcfc133a) in the rat by F-19-Nmr spectroscopy, *Drug Metab. Dispos.* 23 (1995) 102–106.
- [133] C. Heidelberger, Fluorinated pyrimidines, a new class of tumour-inhibitory compounds, *Nat. Chem. Biol.* 179 (1957) 663–666.
- [134] C.A. Presant, W. Wolf, V. Waluch, C. Wiseman, P. Kennedy, D. Blayney, R.R. Brechner, Association of intratumoral pharmacokinetics of fluorouracil with clinical response, *Lancet* 343 (1994) 1184–1187.

- [135] G.F.J. Peters, Fluorouracil: Biochemistry and pharmacology, *J. Clin. Oncol.* 6 (1988) 1653–1664.
- [136] G. Brix, M.E. Bellemann, U. Haberkorn, L. Gerlach, W.J. Lorenz, Assessment of the biodistribution of 5-fluorouracil as monitored by ¹⁸F PET and ¹⁹F MRI: A comparative animal study, *Nucl. Med. Biol.* 23 (1996) 897–906.
- [137] G. Brix, M.E. Bellemann, L. Gerlach, U. Haberkorn, Direct detection of intratumoral 5-fluorouracil trapping using metabolic F-19 MR imaging, *Magn. Reson. Imaging* 17 (1999) 151–155.
- [138] G. Brix, M.E. Bellemann, U. Haberkorn, L. Gerlach, P. Bachert, W.J. Lorenz, Mapping the biodistribution and catabolism of 5-fluorouracil in tumor-bearing rats by chemical-shift selective F-19 MR-imaging, *Magn. Reson. Med.* 34 (1995) 302–307.
- [139] J.L. Guerquin-Kern, F. Leteurtre, A. Croisy, J.M. Lhoste, pH dependence of 5-fluorouracil uptake observed by *in vivo* ³¹P and ¹⁹F NMR spectroscopy, *Cancer Res.* 51 (1991) 5770–5773.
- [140] A.S.E. Ojugo, P.M.J. McSheehy, M. Stubbs, G. Alder, C.L. Bashford, R.J. Maxwell, M.O. Leach, I.R. Judson, J.R. Griffiths, Influence of pH on the uptake of 5-fluorouracil into isolated tumour cells, *Br J. Cancer* 77 (1998) 873–879.
- [141] P.M.J. McSheehy, S.P. Robinson, A.S.E. Ojugo, E.O. Aboagye, M.B. Cannell, M.O. Leach, I.R. Judson, J.R. Griffiths, Carbogen breathing increases 5-Fluorouracil uptake and cytotoxicity in hypoxic Rif-1 tumors: A magnetic resonance study *in vivo*, *Cancer Res.* 58 (1998) 1185–1194.
- [142] J.R. Griffiths, D.J.O. McIntyre, F.A. Howe, P.M.J. McSheehy, A.S.E. Ojugo, L.M. Rodrigues, P. Wadsworth, N.M. Price, F. Lofts, G. Nicholson, K. Smid, P. Noordhuis, G.J. Peters, M. Stubbs, Issues of normal tissue toxicity in patient and animal studies—Effect of carbogen breathing in rats after 5-fluorouracil treatment, *Acta Oncol.* 40 (2001) 609–614.
- [143] H. van Laarhoven, G. Gambarota, J. Lok, M. Lammens, Y. Kamm, T. Wagener, C. Punt, A. van der Kogel, A. Heerschap, Carbogen breathing differentially enhances blood plasma volume and 5-fluorouracil uptake in two murine colon tumor models with distinct vascular structures. *Proc. Intl. Soc. Mag. Reson. Med. (Seattle)* 2006, p. 1766.
- [144] P.E. Sijens, N.J. Baldwin, T.C. Ng, Multinuclear MR investigation of the metabolic response of murine RIF-1 tumor to 5-fluorouracil chemotherapy, *Magn. Reson. Med.* 19 (1991) 337–385.
- [145] N.W. Lutz, W.E. Hull, Assignment and pH dependence of the ¹⁹F-NMR resonances from the fluorouracil anabolites involved in fluoropyrimidine chemotherapy, *NMR Biomed.* 12 (1999) 237–248.
- [146] S.O. Freytag, M. Khil, H. Stricker, J. Peabody, M. Menon, M. DePeralta-Venturina, D. Nafziger, J. Pegg, D. Paielli, S. Brown, K. Barton, M. Lu, E. Aguilar-Cordova, J.H. Kim, Phase I study of replication-competent adenovirus-mediated double suicide gene therapy for the treatment of locally recurrent prostate cancer, *Cancer Res.* 62 (2002) 4968–4976.
- [147] L.D. Stegman, A. Rehemtulla, B. Beattie, E. Kievit, T.S. Lawrence, R.G. Blasberg, J.G. Tjuvajev, B.D. Ross, Noninvasive quantitation of cytosine deaminase transgene expression in human tumor xenografts with *in vivo* magnetic resonance spectroscopy, *Proc. Natl. Acad. Sci. USA* 96 (1999) 9821–9826.
- [148] L.D. Stegman, A. Rehemtulla, D.A. Hamstra, D.J. Rice, S.J. Jonas, K.L. Stout, T.L. Chenevert, B.D. Ross, Diffusion MRI detects early events in the response of a glioma model to the yeast cytosine deaminase gene therapy strategy, *Gene Ther.* 7 (2000) 1005–1010.
- [149] M. Aghi, C.M. Kramm, T.C. Chou, X.O. Breakefield, E.A. Chiocca, Synergistic anticancer effects of ganciclovir/thymidine kinase and 5-fluorocytosine/cytosine deaminase gene therapies, *J. Natl. Cancer Inst.* 90 (1998) 370–380.
- [150] H. Corban-Wilhelm, W.E. Hull, G. Becker, U. Bauder-Wust, D. Greulich, J. Debus, Cytosine deaminase and thymidine kinase gene therapy in a dunning rat prostate

- tumour model: Absence of bystander effects and characterisation of 5-fluorocytosine metabolism with ^{19}F -NMR spectroscopy, *Gene Ther.* 9 (2002) 1564–1575.
- [151] T. Dresselaers, J. Theys, L. Dubois, W. Landuyt, P. Van Hecke, P. Lambin, Evaluation of salmonella-based suicide gene transfer in a rodent tumor model using *in vivo* ^{19}F MR spectroscopy. *Proc. Intl. Soc. Mag. Reson. Med.* (2006) p. 3175.
 - [152] G.O. Cron, N. Beghein, R. Ansiaux, B. Gallez, Botulinum toxin increases tumor uptake of gemcitabine chemotherapy as measured with fluorine spectroscopy. *Proc. Intl. Soc. Mag. Reson. Med.* (Seattle) 2006, p. 1764.
 - [153] M.E. Bellemann, U. Haberkorn, L. Gerlach, J. Blatter, G. Brix, Fluorine-19 NMR imaging of the biodistribution and metabolization of the antienoplastic agent gemcitabine in tumor-bearing rats. *Proceedings of the 7th Scientific Meeting ISMRM* (Philadelphia, PA), (1999) p. 1352.
 - [154] P.M.J. McSheehy, A.S.E. Ojugo, M.O. Leach, I.R. Judson, J.R. Griffiths, ^{19}F -MRS studies of the novel Thymidylate Synthase (TS) Inhibitor, ZD9331. *Proceedings of the 7th Annual Meeting ISMRM* (Philadelphia) (1999), p. 1347.
 - [155] G. Brix, A. Schlicker, W. Mier, P. Peschke, M.E. Bellemann, Biodistribution and pharmacokinetics of the F-19-labeled radiosensitizer 3-aminobenzamide: Assessment by F-19 MR imaging, *Magn. Reson. Imaging* 23 (2005) 967–976.
 - [156] W.M. Spees, T.P.F. Gade, G.L. Yang, W.P. Tong, W.G. Bornmann, R. Gorlick, J.A. Koutcher, An F-19 magnetic resonance-based *in vivo* assay of solid tumor methotrexate resistance: Proof of principle, *Clin. Cancer Res.* 11 (2005) 1454–1461.
 - [157] T. Tengel, T. Fex, H. Emtenas, F. Almqvist, I. Sethson, J. Kihlberg, Use of F-19 NMR spectroscopy to screen chemical libraries for ligands that bind to proteins, *Org. Biomol. Chem.* 2 (2004) 725–731.
 - [158] T. Tarrago, S. Frutos, R.A. Rodriguez-Mias, E. Giralt, Identification by F-19 NMR of traditional chinese medicinal plants possessing prolyl oligopeptidase inhibitory activity, *Chembiochem* 7 (2006) 827–833.
 - [159] S. Frutos, T. Tarrago, E. Giralt, A fast and robust F-19 NMR-based method for finding new HIV-1 protease inhibitors, *Bioorg. Med. Chem. Lett.* 16 (2006) 2677–2681.
 - [160] L.P. Yu, P.J. Hajduk, J. Mack, E.T. Olejniczak, Structural studies of Bcl-xL/ligand complexes using F-19 NMR, *J. Biomol. NMR* 34 (2006) 221–227.
 - [161] M. Bartels, K. Albert, Detection of psychoactive drugs using ^{19}F MR spectroscopy, *J. Neural Transm. Gen Sect.* 99 (1995) 1–6.
 - [162] N.R. Bolo, Y. Hode, J.P. Macher, Long-term sequestration of fluorinated compounds in tissues after fluvoxamine or fluoxetine treatment: A fluorine magnetic resonance spectroscopy study *in vivo*, *MAGMA* 16 (2004) 268–276.
 - [163] W.L. Strauss, M.E. Layton, S.R. Dager, Brain elimination half-life of fluvoxamine measured by ^{19}F magnetic resonance spectroscopy, *Am. J. Psychiatry* 155 (1998) 380–384.
 - [164] D.M. Lindquist, M. Dachtler, R.M. Hawk, C.N. Karson, K. Albert, R.A. Komoroski, Contribution of trifluoperazine metabolites to the *in vivo* F-19 NMR spectrum of rat brain, *Magn. Reson. Med.* 43 (2000) 756–759.
 - [165] T. Sassa, T. Suhara, H. Ikehira, T. Obata, F. Girard, S. Tanada, Y. Okubo, ^{19}F -magnetic resonance spectroscopy and chemical shift imaging for schizophrenic patients using haloperidol decanoate, *Psychiatry Clin. Neurosci.* 56 (2002) 637–642.
 - [166] P. Jynge, T. Skjetne, I. Gribbestad, C.H. Kleinbloesem, H.F.W. Hoogkamer, O. Antonsen, J. Krane, O.E. Bakoy, K.M. Furuheim, O.G. Nilsen, *In vivo* tissue pharmacokinetics by fluorine magnetic-resonance spectroscopy—a study of liver and muscle disposition of fleroxacin in humans, *Clin. Pharmacol. Ther.* 48 (1990) 481–489.
 - [167] O. Saether, A. Midelfart, O. Risa, O. Haraldseth, J. Krane, Proton decoupled F-19 NMR spectroscopy of drugs used in eye treatment, *Spectrosc. Lett.* 39 (2006) 135–144.
 - [168] B. Gewiese, W. Noske, A. Schilling, D. Stiller, K. Wolf, M. Foerster, Human eye: Visualization of perfluorodecalin with F-19 MR imaging, *Radiology* 185 (1992) 131–133.

- [169] C. Wilson, B. Berkowitz, B. McCuen, C. Charles, Measurement of preretinal pO_2 in the vitrectomized human eye using ^{19}F NMR, *Arch. Ophthalmol.* 110 (1992) 1098–1100.
- [170] R.P. Mason, E.E. Babcock, R.L. Nunnally, Proceedings of the XIII International Congress of Magnetic Resonance in Biological Systems (Madison, WI) 1988.
- [171] R. Nunnally, P. Antich, P. Nguyen, E. Babcock, G. McDonald, R. Mason, Fluosol adjuvant therapy in human cancer: Examinations *in vivo* of perfluorocarbons by F-19 NM, in: Proceedings of the SMRM 7th Meeting San Francisco, 1988, p. 342.
- [172] A.M. Wyrwicz, C.B. Conboy, Multiecho ^{19}F NMR imaging of halothane in rabbit brain, Proceedings of the 7th SMRM San Francisco 1988, p. 597.
- [173] T. Takeda, K. Makita, S. Ishikawa, K. Kaneda, K. Yokoyama, K. Amaha, Uptake and elimination of sevoflurane in rabbit tissues - an *in vivo* magnetic resonance spectroscopy study, *Can. J. Anaesth.* 47 (2000) 579–584.
- [174] Y. Xu, P. Tang, W.G. Zhang, L. Firestone, P.M. Winter, F-19 nuclear-magnetic-resonance imaging and spectroscopy of sevoflurane uptake, distribution, and elimination in rat-brain, *Anesthesiology* 83 (1995) 766–774.
- [175] P.N. Venkatasubramanian, Y.J. Shen, A.M. Wyrwicz, *In vivo* ^{19}F one-dimensional chemical shift imaging study of isoflurane uptake in rabbit brain, *NMR Biomed.* 6 (1993) 377–382.
- [176] G.G. Lockwood, D.P. Dob, D.J. Bryant, J.A. Wilson, J. Sargentoni, S.M. Sapsed-Byrne, D.N.F. Harris, D.K. Menon, Magnetic resonance spectroscopy of isoflurane kinetics in humans. 1. Elimination from the head, *Br. J. Anaesth.* 79 (1997) 581–585.
- [177] B.S. Selinsky, M.E. Perlman, R.E. London, *In vivo* nuclear magnetic resonance studies of hepatic methoxyflurane metabolism. I. Verification and quantitation of methoxydifluoroacetate, *Mol. Pharmacol.* 33 (1988) 559–566.
- [178] B.S. Selinsky, M.E. Perlman, R.E. London, *In vivo* nuclear magnetic-resonance studies of hepatic methoxyflurane metabolism. 2. A reevaluation of hepatic metabolic pathways, *Mol. Pharmacol.* 33 (1988) 567–573.
- [179] E.P. Mazzola, A.P. Borsetti, S.W. Page, D.W. Bristol, Determination of pesticide-residues in foods by F-19 fourier-transform nuclear magnetic-resonance spectroscopy, *J. Agric. Food Chem.* 32 (1984) 1102–1103.
- [180] R.D. Mortimer, B.A. Dawson, Using F-19 Nmr for trace analysis of fluorinated pesticides in food-products, *J. Agric. Food. Chem.* 39 (1991) 1781–1785.
- [181] Z. Zuo, G. Kwon, B. Stevenson, J. Diakur, L.I. Wiebe, Flutamide—Hydroxypropyl-beta-cyclodextrin complex: Formulation, physical characterization, and absorption studies using the Caco-2 *in vitro* model, *J. Pharm. Pharm. Sci.* 3 (2000) 220–227.
- [182] M. Masson, J.F. Sigurjonsdottir, S. Jonsdottir, T. Loftsson, Examination of F-19-NMR as a tool for investigation of drug-cyclodextrin complexes, *Drug Dev. Ind. Pharm.* 29 (2003) 107–112.
- [183] J. Fukuchi, J.M. Kokontis, R.A. Hiipakka, C.P. Chuu, S. Liao, Antiproliferative effect of liver X receptor agonists on LNCaP human prostate cancer cells, *Cancer Res.* 64 (2004) 7686–7689.
- [184] E.K. Rofstad, T. Danielsen, Hypoxia-induced metastasis of human melanoma cells: Involvement of vascular endothelial growth factor-mediated angiogenesis, *Br. J. Cancer* 80 (1999) 1697–1707.
- [185] M. Höckel, P. Vaupel, Tumor hypoxia: Definitions and current clinical, biologic, and molecular aspects, *J. Natl. Cancer Inst.* 93 (2001) 266–276.
- [186] J. Folkman, Angiogenesis and apoptosis, *Semin. Cancer Biol.* 13 (2003) 159–167.
- [187] H.J. Knowles, A.L. Harris, Hypoxia and oxidative stress in breast cancer. Hypoxia and tumorigenesis. [Review], *Breast Cancer Res.* 3 (2001) 318–322.
- [188] L. Gray, A. Conger, M. Ebert, S. Hornsey, O. Scott, The concentration of oxygen dissolved in tissues at time of irradiation as a factor in radiotherapy, *Br. J. Radiol.* 26 (1953) 638–648.

- [189] J.L. Tatum, G.J. Kelloff, R.J. Gillies, J.M. Arbeit, J.M. Brown, K.S. Chao, J.D. Chapman, W.C. Eckelman, A.W. Fyles, A.J. Giaccia, R.P. Hill, C.J. Koch, M.C. Krishna, K.A. Krohn, J.S. Lewis, R.P. Mason, G. Melillo, A.R. Padhani, G. Powis, J.G. Rajendran, R. Reba, S.P. Robinson, G.L. Semenza, H.M. Swartz, P. Vaupel, D. Yang, B. Croft, J. Hoffman, G. Liu, H. Stone, D. Sullivan, Hypoxia: Importance in tumor biology, noninvasive measurement by imaging, and value of its measurement in the management of cancer therapy, *Int. J. Radiat. Biol.* 82 (2006) 699–757.
- [190] J.M. Brown, Exploiting the hypoxic cancer cell: Mechanisms and therapeutic strategies, *Mol. Med. Today* 6 (2000) 157–162.
- [191] H.M. Swartz, J.F. Dunn, J.F. Dunn, H.M. Swartz (Eds.), *Measurements of Oxygen in Tissues: Overview and Perspectives on Methods*, Vol. 530, Kluwer Academic, New York, 2003, pp. 1–12.
- [192] H.B. Stone, J.M. Brown, T. Phillips, R.M. Sutherland, Oxygen in human tumors: Correlations between methods of measurement and response to therapy, *Radiat. Res.* 136 (1993) 422–434.
- [193] H. Liu, Y. Gu, J.G. Kim, R.P. Mason, Near infrared spectroscopy and imaging of tumor vascular oxygenation, *Methods Enzymol.* 386 (2004) 349–378.
- [194] R.P. Mason, Non-Invasive assessment of kidney oxygenation: A role for BOLD MRI, *Kidney Int.* 70 (2006) 10–11.
- [195] S.H. Yee, K. Lee, P.A. Jerabek, P.T. Fox, Quantitative measurement of oxygen metabolic rate in the rat brain using microPET imaging of briefly inhaled ^{15}O -labelled oxygen gas, *Nucl. Med. Commun.* 27 (2006) 573–581.
- [196] J.P. Coles, T.D. Fryer, P.G. Bradley, J. Nortje, P. Smielewski, K. Rice, J.C. Clark, J.D. Pickard, D.K. Menon, Intersubject variability and reproducibility of ^{15}O PET studies, *J. Cereb. Blood Flow Metab.* 26 (2006) 48–57.
- [197] C.J. Koch, Measurement of absolute oxygen levels in cells and tissues using oxygen sensors and 2-nitroimidazole EF5, *Methods Enzymol.* 352 (2002) 3–31.
- [198] J.A. Raleigh, S.C. Chou, G.E. Arteel, M. Horsman, Comparison among pimonidazole binding oxygen electrode measurements, and radiation response in C3H mouse tumors, *Radiat. Res.* 151 (1999) 580–589.
- [199] C. Song, I. Lee, T. Hasegawa, J. Rhee, S. Levitt, Increase in pO_2 and radiosensitivity of tumors by Fluosol and carbogen, *Cancer Res.* 47 (1987) 442–446.
- [200] J.G. Kim, D. Zhao, A. Constantinescu, R.P. Mason, H. Liu, Interplay of tumor vascular oxygenation and tumor pO_2 observed using NIRS, oxygen needle electrode, and ^{19}F MR pO_2 mapping, *J. Biomed. Opt.* 8 (2003) 53–62.
- [201] Y. Gu, V. Bourke, J.G. Kim, A. Constantinescu, R.P. Mason, H. Liu, Dynamic response of breast tumor oxygenation to hyperoxic respiratory challenge monitored with three oxygen-sensitive parameters, *Appl. Opt.* 42 (2003) 1–8.
- [202] B. Gallez, C. Baudelet, B.F. Jordan, Assessment of tumor oxygenation by electron paramagnetic resonance: Principles and applications, *NMR Biomed.* 17 (2004) 240–262.
- [203] P. Parhami, B.N. Fung, Fluorine-19 relaxation study of perfluorochemicals as oxygen carriers, *J. Phys. Chem.* 87 (1983) 1928–1931.
- [204] S.R. Thomas, R.G. Pratt, R.W. Millard, R.C. Samarasinghe, Y. Shiferaw, L.C. Clark Jr., R.E. Hoffmann, Evaluation of the influence of the aqueous phase bioconstituent environment on the F-19 T1 of perfluorocarbon blood substitute emulsions, *J. Magn. Reson. Imag.* 4 (1994) 631–635.
- [205] C.S. Lai, S. Stair, H. Mizioro, J.S. Hyde, Effect of oxygen and the spin label TEMPO-Laurate on ^{19}F and proton relaxation rates of the perfluorochemical blood substitute FC-43 emulsion, *J. Magn. Reson.* 57 (1984) 447–452.
- [206] D. Eidelberg, G. Johnson, D. Barnes, P.S. Tofts, D. Delpy, D. Plummer, W.I. McDonald, ^{19}F NMR imaging of blood oxygenation in the brain, *Magn. Reson. Med.* 6 (1988) 344–352.

- [207] R.P. Mason, H.P. Shukla, P.P. Antich, *In vivo* oxygen tension and temperature: Simultaneous determination using ¹⁹F spectroscopy of perfluorocarbon, *Magn. Reson. Med.* 29 (1993) 296–302.
- [208] S.R. Thomas, R.G. Pratt, R.W. Millard, R.C. Samarasinghe, Y. Shiferaw, A.J. McGoron, K.K. Tan, *In vivo* pO₂ imaging in the porcine model with perfluorocarbon F-19 NMR at low field, *Magn. Reson. Imaging* 14 (1996) 103–114.
- [209] R.P. Mason, N. Bansal, E.E. Babcock, R.L. Nunnally, P.P. Antich, A novel editing technique for ¹⁹F MRI: Molecule-specific imaging, *Magn. Reson. Imaging* 8 (1990) 729–736.
- [210] E.E. Babcock, R.P. Mason, P.P. Antich, Effect of homonuclear J modulation on ¹⁹F spin-echo images, *Magn. Reson. Med.* 17 (1991) 178–188.
- [211] C.H. Sotak, P.S. Hees, H.N. Huang, M.H. Hung, C.G. Krespan, S. Raynolds, A new perfluorocarbon for use in fluorine-19 MRI and MRS, *Magn. Reson. Med.* 29 (1993) 188–195.
- [212] D. Zhao, S. Ran, A. Constantinescu, E.W. Hahn, R.P. Mason, Tumor oxygen dynamics: Correlation of *in vivo* MRI with histological findings, *Neoplasia* 5 (2003) 308–318.
- [213] D. Zhao, A. Constantinescu, C.H. Chang, E.W. Hahn, R.P. Mason, Correlation of tumor oxygen dynamics with radiation response of the dunning prostate R3327-HI tumor, *Radiat. Res.* 159 (2003) 621–631.
- [214] D. Zhao, C. Constantinescu, E.W. Hahn, R.P. Mason, Differential oxygen dynamics in two diverse Dunning prostate R3327 rat tumor sublines (MAT-Lu and HI) with respect to growth and respiratory challenge, *Int. J. Radiat. Oncol. Biol. Phys.* 53 (2002) 744–756.
- [215] D. Zhao, A. Constantinescu, L. Jiang, E.W. Hahn, R.P. Mason, Prognostic radiology: Quantitative assessment of tumor oxygen dynamics by MRI, *Am. J. Clin. Oncol.* 24 (2001) 462–466.
- [216] D. Zhao, A. Constantinescu, E.W. Hahn, R.P. Mason, Tumor oxygen dynamics with respect to growth and respiratory challenge: Investigation of the Dunning prostate R3327-HI tumor, *Radiat. Res.* 156 (2001) 510–520.
- [217] Y. Song, A. Constantinescu, R.P. Mason, Dynamic breast tumor oximetry: The development of prognostic radiology, *Technol. Cancer Res. Treat.* 1 (2002) 471–478.
- [218] B.J. Dardzinski, C.H. Sotak, Rapid tissue oxygen tension mapping using ¹⁹F inversion-recovery echo-planar imaging of Perfluoro-15-crown-5-ether, *Magn. Reson. Med.* 32 (1994) 88–97.
- [219] Z. Wang, M.Y. Su, O. Nalcioglu, Applications of dynamic contrast enhanced MRI in oncology: Measurement of tumor oxygen tension, *Technol. Cancer Res. Treat.* 1 (2002) 29–38.
- [220] B.J.P. van der Sanden, A. Heerschap, L. Hoofd, A.W. Simonetti, K. Nicolay, A. van der Toorn, W.N.M. Colier, A.J. van der Kogel, Effect of carbogen breathing on the physiological profile of human glioma xenografts, *Magn. Reson. Med.* 42 (1999) 490–499.
- [221] T.Q. Duong, C. Iadecola, S.G. Kim, Effect of hyperoxia, hypercapnia, and hypoxia on cerebral interstitial oxygen tension and cerebral blood flow, *Magn. Reson. Med.* 45 (2001) 61–70.
- [222] F. Girard, P. Poulet, I.J. Namer, J. Steibel, J. Chambron, Localized T-2 measurements using an osiris-CPMG method—application to measurements of blood oxygenation and transverse relaxation free of diffusion effect, *NMR Biomed.* 7 (1994) 343–348.
- [223] R.P. Mason, H.P. Shukla, P.P. Antich, Oxygent: A novel probe of tissue oxygen tension, *Biomater. Artif. Cells Immobilization. Biotechnol.* 20 (1992) 929–935.
- [224] R.P. Mason, W. Rodbumrung, P.P. Antich, Hexafluorobenzene: A sensitive ¹⁹F NMR indicator of tumor oxygenation, *NMR Biomed.* 9 (1996) 125–134.
- [225] R.P. Mason, P.P. Antich, Application of ¹⁹F MR to Non Invasively Assess pO₂ and Temperature *In Vivo* with Rapid Time Resolution (Ed. US patent No.5, 397, 562), 1995.
- [226] J.G. Riess, Overview of progress in the fluorocarbon approach to *in vivo* oxygen delivery, *Biomater. Artif. Cells Immobilization Biotech.* 20 (1992) 183–202.

- [227] R.J. Kaufman, J. Goldstein (Ed.), *Medical Oxygen Transport Using Perfluorochemicals* Butterworth-Heinemann, N.Y., 1991, pp. 127–158.
- [228] T.F. Zuck, J.G. Riess, Current status of injectable oxygen carriers. [Review], *Crit. Rev. Clin. Lab. Sci.* 31 (1994) 295–324.
- [229] M.P. Krafft, Fluorocarbons and fluorinated amphiphiles in drug delivery and biomedical research, *Adv. Drug Deliv. Rev.* 47 (2001) 209–228.
- [230] E.G. Schutt, D.H. Klein, R.M. Mattrey, J.G. Riess, Injectable microbubbles as contrast agents for diagnostic ultrasound imaging: The key role of perfluorochemicals, *Angew. Chem. Int. Ed.* 42 (2003) 3218–3235.
- [231] J.G. Riess, Oxygen carriers (“blood substitutes”)—raison d’être, chemistry, and some physiology, *Chem. Rev.* 101 (2001) 2797–2920.
- [232] J.E. Fishman, P.M. Joseph, T.F. Floyd, B. Mukherji, H.S. Sloviter, Oxygen-sensitive ^{19}F NMR imaging of the vascular system *in vivo*, *Magn. Reson. Imag.* 5 (1987) 279–285.
- [233] J.E. Fishman, P.M. Joseph, M.J. Carvlin, M. Saadi-Elmandjra, B. Mukherji, H.S. Sloviter, *In vivo* measurements of vascular oxygen tension in tumors using MRI of a fluorinated blood substitute, *Invest. Radiol.* 24 (1989) 65–71.
- [234] D. Eidelberg, G. Johnson, P.S. Tofts, J. Dobbin, H.A. Crockard, D. Plummer, ^{19}F imaging of cerebral blood oxygenation in experimental middle cerebral artery occlusion: Preliminary results, *J. Cereb. Blood Flow Metab.* 8 (1988) 276–281.
- [235] U. Noth, S.P. Morrissey, R. Deichmann, H. Adolf, C. Schwarzbauer, J. Lutz, A. Haase, *In vivo* measurement of partial oxygen pressure in large vessels and in the reticuloendothelial system using fast ^{19}F -MRI, *Magn. Reson. Med.* 34 (1995) 738–745.
- [236] K.M. Hoard, *Measurement of Flow Rates Using Surface Coil Nuclear Magnetic Resonance* Vol. MSc. University of Arlington, Arlington, 1989.
- [237] T. Higuchi, S. Naruse, Y. Horikawa, K. Hirakawa, C. Tanaka, *In vivo* measurement of the partial pressure of oxygen in brain tissue using ^{19}F NMR, in: *Proceedings of the 7th SMRM*, 1988, p. 435.
- [238] R.P. Mason, P.P. Antich, E.E. Babcock, J.L. Gerberich, R.L. Nunnally, Perfluorocarbon imaging *in vivo*: A ^{19}F MRI study in tumor-bearing mice, *Magn. Reson. Imag.* 7 (1989) 475–485.
- [239] R.F. Mattrey, D.C. Long, Potential role of PFOB in diagnostic imaging, *Invest. Radiol.* 23 (1988) s298–301.
- [240] W.I. Rosenblum, M.G. Hadfield, A.J. Martinez, P. Schatzki, Alterations of liver and spleen following intravenous infusion of fluorocarbon emulsions, *Arch. Pathol. Lab. Med.* 100 (1976) 213–217.
- [241] R.P. Mason, P.P. Antich, Tumor oxygen tension: Measurement using OxygentTM as a ^{19}F NMR probe at 4.7 T, *Artif. Cells Blood Substit. Immobil. Biotechnol.* 22 (1994) 1361–1367.
- [242] R.P. Mason, P.P. Antich, E.E. Babcock, A. Constantinescu, P. Peschke, E.W. Hahn, Non-invasive determination of tumor oxygen tension and local variation with growth, *Int. J. Radiat. Oncol. Biol. Phys.* 29 (1994) 95–103.
- [243] R.P. Mason, F.M.H. Jeffrey, C.R. Malloy, E.E. Babcock, P.P. Antich, A noninvasive assessment of myocardial oxygen tension: ^{19}F NMR spectroscopy of sequestered perfluorocarbon emulsion, *Magn. Reson. Med.* 27 (1992) 310–317.
- [244] R.P. Mason, R.L. Nunnally, P.P. Antich, Tissue oxygenation: A novel determination using ^{19}F surface coil spectroscopy of sequestered perfluorocarbon emulsion, *Magn. Reson. Med.* 18 (1991) 71–79.
- [245] N.J. Baldwin, T.C. Ng, Oxygenation and metabolic status of KHT tumors as measured simultaneously by ^{19}F magnetic resonance imaging and ^{31}P magnetic resonance spectroscopy, *Magn. Reson. Imaging* 14 (1996) 541–551.
- [246] H.P. Shukla, R.P. Mason, N. Bansal, P.P. Antich, Regional myocardial oxygen tension: ^{19}F MRI of sequestered perfluorocarbon, *Magn. Reson. Med.* 35 (1996) 827–833.
- [247] B.P.J. van der Sanden, A. Heerschap, A.W. Simonetti, P.F.J.W. Rijken, H.P.W. Peters, G. Stüben, A.J. van der Kogel, Characterization and validation of non-invasive oxygen

- tension measurements in human glioma xenografts by ¹⁹F-MR relaxometry, *Int. J. Radiat. Oncol. Biol. Phys.* 44 (1999) 649–658.
- [248] H.T. Tran, Q. Guo, D.J. Schumacher, R.B. Buxton, R.F. Mattrey, ¹⁹F chemical shift imaging technique to measure intracellular pO₂ *in vivo* using perflubron, *Acad. Radiol.* 2 (1995) 756–761.
- [249] K.G. Helmer, S. Han, C.H. Sotak, On the correlation between the water diffusion coefficient and oxygen tension in RIF-1 tumors, *NMR Biomed.* 11 (1998) 120–130.
- [250] B.R. Barker, R.P. Mason, N. Bansal, R.M. Peshock, Oxygen tension mapping by ¹⁹F echo planar NMR imaging of sequestered perfluorocarbon, *J. Magn. Reson. Imaging* 4 (1994) 595–602.
- [251] X. Fan, J.N. River, M. Zamora, H.A. Al-Hallaq, G.S. Karczmar, Effect of carbogen on tumor oxygenation: Combined fluorine-19 and proton MRI measurements, *Int. J. Radiat. Oncol. Biol. Phys.* 54 (2002) 1202–1209.
- [252] S.K. Holland, R.P. Kennan, M.M. Schaub, M.J. D'Angelo, J.C. Gore, Imaging oxygen tension in liver and spleen by ¹⁹F NMR, *Magn. Reson. Med.* 29 (1993) 446–458.
- [253] P.S. Hees, C.H. Sotak, Assessment of changes in murine tumor oxygenation in response to nicotinamide using ¹⁹F NMR relaxometry of a perfluorocarbon emulsion, *Magn. Reson. Med.* 29 (1993) 303–310 and erratum 329 716 (1993).
- [254] D.J.O. McIntyre, C.L. McCoy, J.R. Griffiths, Tumour oxygenation measurements by ¹⁹F MRI of perfluorocarbons, *Curr. Sci.* 76 (1999) 753–762.
- [255] P.P. Antich, R.P. Mason, A. Constantinescu, P. Peschke, E.W. Hahn, MRI staining: A novel approach to tumor architecture using perfluorocarbons, *Proc. Soc. Nucl. Med.* 35(5) (1994) 216P.
- [256] B.A. Berkowitz, C.A. Wilson, D.L. Hatchell, Oxygen kinetics in the vitreous substitute perfluorotributylamine: A ¹⁹F NMR study *in vivo*, *Invest. Ophthalmol. Vis. Sci.* 32 (1991) 2382–2387.
- [257] C.A. Wilson, B.A. Berkowitz, D.L. Hatchell, Oxygen kinetics in preretinal perfluorotributylamine, *Exp. Eye Res.* 55 (1992) 119–126.
- [258] W. Zhang, Y. Ito, E. Berlin, R. Roberts, B.A. Berkowitz, Role of hypoxia during normal retinal vessel development and in experimental retinopathy of prematurity, *Invest. Ophthalmol. Vis. Sci.* 44 (2003) 3119–3123.
- [259] J.J. Delpuech, M.A. Hamza, G. Serraticce, M.J. Stébé, Fluorocarbons as oxygen carriers. I. An NMR study of oxygen solutions in hexafluorobenzene, *J. Chem. Phys.* 70 (1979) 2680–2687.
- [260] M.A. Hamza, G. Serraticce, M.J. Stebe, J.J. Delpuech, Solute-solvent interactions in perfluorocarbon solutions of oxygen. An NMR study, *J. Am. Chem. Soc.* 103 (1981) 3733–3738.
- [261] I.M.C.M. Rietjens, A. Steensma, C. den Besten, G. van Tintelen, J. Haas, B. van Ommen, P.J. van Bladeren, Comparative biotransformation of hexachlorobenzene and hexafluorobenzene in relation to the induction of porphyria, *Eur. J. Pharmacol.* 293 (1995) 292–299.
- [262] Y.S. Gorsman, T.A. Kapitonenko, Pharmacology and toxicology of hexafluorobenzene, *Izv. Estestvennonauchu. Inst. Pevinsk.* 15 (1973) 155–163.
- [263] K.M. Mortelmans, V.F. Simmon, “*In vitro*” microbiological mutagenicity assays of eight fluorocarbon taggant samples, *Gov. Rep. Announce. Index. (US).* 81 (1981) 2555–2587.
- [264] K.D. Courtney, J.E. Andrews, Teratogenic evaluation and fetal deposition of hexabromobenzene (HBB) and hexafluorobenzene (HFB) in CD-1 mice, *J. Environ. Sci. Health B* 19 (1984) 83–94.
- [265] L.W. Hall, S.R.K. Jackson, G.M. Massey, A. Arias, R. Llauro, M.A. Nalda, J.N. Lunn (Eds.), *Hexafluorobenzene in veterinary anaesthesia*, Excerpta Medica, Oxford, 1975, pp. 201–204.
- [266] S. Hunjan, R.P. Mason, A. Constantinescu, P. Peschke, E.W. Hahn, P.P. Antich, Regional tumor oximetry: ¹⁹F NMR spectroscopy of hexafluorobenzene, *Int. J. Radiat. Oncol. Biol. Phys.* 40 (1998) 161–171.

- [267] D. Zhao, L. Jiang, E.W. Hahn, R.P. Mason, Tumor physiological response to combretastatin A4 phosphate assessed by MRI, *Int. J. Radiat. Oncol. Biol. Phys.* 62 (2005) 872–880.
- [268] D. Le, R.P. Mason, S. Hunjan, A. Constantinescu, B.R. Barker, P.P. Antich, Regional tumor oxygen dynamics: ^{19}F PBSR EPI of hexafluorobenzene, *Magn. Reson. Imaging*, 15 (1997) 971–981.
- [269] S. Hunjan, D. Zhao, A. Constantinescu, E.W. Hahn, P.P. Antich, R.P. Mason, Tumor oximetry: Demonstration of an enhanced dynamic mapping procedure using fluorine-19 echo planar magnetic resonance imaging in the Dunning prostate R3327-AT1 rat tumor, *Int. J. Radiat. Oncol. Biol. Phys.* 49 (2001) 1097–1108.
- [270] M. Xia, V. Kodibagkar, H. Liu, R.P. Mason, Tumour oxygen dynamics measured simultaneously by near infrared spectroscopy and ^{19}F magnetic resonance imaging in rats, *Phys. Med. Biol.* 51 (2006) 45–60.
- [271] R.P. Mason, S. Hunjan, A. Constantinescu, Y. Song, D. Zhao, E.W. Hahn, P.P. Antich, P. Peschke, J.F. Dunn, H.M. Swartz (Eds.), Tumor oximetry: Comparison of ^{19}F MR EPI and electrodes, Vol. 530, Kluwer, New York, 2003, pp. 19–28.
- [272] R.P. Mason, A. Constantinescu, S. Hunjan, D. Le, E.W. Hahn, P.P. Antich, C. Blum, P. Peschke, Regional tumor oxygenation and measurement of dynamic changes, *Radiat. Res.* 152 (1999) 239–249.
- [273] V. Bourke, J. Gilio, D. Zhao, A. Constantinescu, V. Kodibagkar, L. Jiang, E.W. Hahn, R.P. Mason, Correlation of radiation response with tumor oxygenation in the Dunning prostate R3327-AT1 Tumor, *Int. J. Radiat. Oncol. Biol. Phys.* 67(2007) 1179–1186.
- [274] E.K. Rofstad, K. Sundfor, H. Lyng, C.G. Trope, Hypoxia-induced treatment failure in advanced squamous cell carcinoma of the uterine cervix is primarily due to hypoxia-induced radiation resistance rather than hypoxia-induced metastasis, *Br. J. Cancer* 83 (2000) 354–359.
- [275] A.W. Fyles, M. Milosevic, R. Wong, M.C. Kavanagh, M. Pintile, A. Sun, W. Chapman, W. Levin, L. Manchul, T.J. Keane, R.P. Hill, Oxygenation predicts radiation response and survival in patients with cervix cancer, *Radiother. Oncol.* 48 (1998) 149–156.
- [276] M. Höckel, K. Schlenger, B. Aral, M. Mitze, U. Schäffer, P. Vaupel, Hypoxia and radiation response in human tumors, *Semin. Radiat. Oncol.* 6 (1996) 3–9.
- [277] J. Keupp, T. Schaeffter, *Proc. Intl. Soc. Mag. Reson. Med. (Seattle) 2006*, p. 916.
- [278] J.R. Griffiths, Are cancer cells acidic? *Br. J. Cancer* 64 (1991) 425–427.
- [279] V.D. Mehta, P.V. Kulkarni, R.P. Mason, A. Constantinescu, S. Aravind, N. Goomer, P.P. Antich, 6-Fluoropyridoxol: A novel probe of cellular pH using ^{19}F NMR spectroscopy, *FEBS Lett.* 349 (1994) 234–238.
- [280] C.J. Deutsch, J.S. Taylor, Intracellular pH measured by ^{19}F NMR, *Ann. N. Y. Acad. Sci.* 508 (1987) 33–47.
- [281] C. Deutsch, J.S. Taylor, D.F. Wilson, Regulation of intracellular pH of human peripheral blood lymphocytes as measured by ^{19}F NMR, *Proc. Natl. Acad. Sci. USA* 79 (1982) 7944–7948.
- [282] C. Deutsch, J.S. Taylor, M. Price, pH homeostasis in human lymphocytes: Modulation by ions and mitogen, *J. Cell Biol.* 98 (1984) 885–894.
- [283] T. Kashiwagura, C.J. Deutsch, J. Taylor, M. Erecinska, D.F. Wilson, Dependence of gluconeogenesis, urea synthesis, and energy metabolism of hepatocytes on intracellular pH, *J. Biol. Chem.* 259 (1984) 237–243.
- [284] W.J. Thoma, K. Ugurbil, pH and compartmentation of isolated perfused rat liver studied by ^{19}F and ^{31}P NMR, *NMR Biomed.* 1 (1988) 95–100.
- [285] J.S. Taylor, C.J. Deutsch, Fluorinated α -methylamino acids as ^{19}F NMR indicators of intracellular pH, *Biophys. J.* 43 (1983) 261–267.
- [286] A. Joseph, C. Davenport, L. Kwock, C.T. Burt, R.E. London, Fluorine-19 NMR studies of tumor-bearing rats treated with difluoromethylornithine, *Magn. Reson. Med.* 4 (1987) 137–143.

- [287] R.E. London, S.A. Gabel, Determination of membrane potential and cell volume by ¹⁹F NMR using trifluoroacetate and trifluoroacetamide probes, *Biochemistry* 28 (1989) 2378–2382.
- [288] A.S.L. Xu, J.R. Potts, P.W. Kuchel, The phenomenon of separate intracellular and extracellular resonances of difluorophosphate in P-31 and F-19 Nmr-spectra of erythrocytes, *Magn. Reson. Med.* 18 (1991) 193–198.
- [289] A.S.L. Xu, A.R. Waldeck, P.W. Kuchel, Transmembrane F-19 Nmr chemical-shift difference of fluorinated solutes in liposomes, erythrocytes and erythrocyte-ghosts, *NMR Biomed.* 6 (1993) 136–143.
- [290] S. Hunjan, R.P. Mason, V.D. Mehta, P.V. Kulkarni, S. Aravind, V. Arora, P.P. Antich, Simultaneous intra- and extra-cellular pH measurement using ¹⁹F NMR of 6-Fluoropyridoxol, *Magn. Reson. Med.* 39 (1998) 551–556.
- [291] S. He, R.P. Mason, S. Hunjan, V.D. Mehta, V. Arora, R. Katipally, P.V. Kulkarni, P.P. Antich, Development of novel ¹⁹F NMR pH indicators: Synthesis and evaluation of a series of fluorinated vitamin B₆ analogs, *Bioorg. Med. Chem.* 6 (1998) 1631–1639.
- [292] W. Korytnyk, R.P. Singh, Proton magnetic resonance spectra of compounds in the vitamin B₆ group, *J. Am. Chem. Soc.* 85 (1963) 2813–2817.
- [293] K. Yamada, M. Tsuji, Transport of vitamin B₆ in human erythrocytes, *J. Vitaminol.* 16 (1970) 237–242.
- [294] J.X. Yu, P. Otten, Z. Ma, W. Cui, L. Liu, R.P. Mason, A novel NMR platform for detecting gene transfection: Synthesis and evaluation of fluorinated phenyl β-D-Galactosides with potential application for assessing LacZ gene expression, *Bioconjug. Chem.* 15 (2004) 1334–1341.
- [295] J.C. Metcalfe, T.R. Hesketh, G.A. Smith, Free cytosolic Ca²⁺ measurements with fluorine labelled indicators using ¹⁹F NMR, *Cell Calcium* 6 (1985) 183–195.
- [296] J.S. Beech, R.A. Iles, ¹⁹F NMR indicators of hepatic intra cellular pH *in vivo*, *Biochem. Soc. Trans.* 15 (1987) 871–872.
- [297] C.J. Deusch, J.S. Taylor, New class of ¹⁹F pH indicators: Fluoroanilines, *Biophys. J.* 55 (1989) 799–804.
- [298] C.K. Rhee, L.A. Levy, R.E. London, Fluorinated o-aminophenol derivatives for measurement of intracellular pH, *Bioconjug. Chem.* 6 (1995) 77–81.
- [299] J.X. Yu, L. Liu, V.D. Kodibagkar, W. Cui, R.P. Mason, Synthesis and evaluation of novel enhanced gene reporter molecules: Detection of β-Galactosidase activity using ¹⁹F NMR of trifluoromethylated Aryl β-D-galactopyranosides, *Bioorg. Med. Chem.* 14 (2006) 326–333.
- [300] W. Cui, P. Otten, J. Yu, V. Kodibagkar, R.P. Mason, 6-trifluoromethyl pyridoxol, a novel reporter molecule for tumor extracellular pH. *Proc. ISMRM (Toronto, Canada)2003*, p. 675.
- [301] T. Frenzel, S. Koszler, H. Bauer, U. Niedballa, H.J. Weinmann, Noninvasive *in vivo* pH measurement using a fluorinated pH probe and fluorine-19 magnetic resonance spectroscopy, *Invest. Radiol.* 29 (1994) S220–222.
- [302] T. Miyazawa, Y. Aoki, K. Akagi, M. Takahashi, B. Fritz-Zieroth, T. Frenzel, H.J. Weinmann, Application of ZK150 471, a fluorinated pH probe for ¹⁹F MRS, to *in vivo* pH measurement after hyperthermic treatment of tumors in mice, *Acad. Radiol.* 3 (1996) S363–S364.
- [303] A.S. Ojugo, P.M. McSheehy, D.J. McIntyre, C. McCoy, M. Stubbs, M.O. Leach, I.R. Judson, J.R. Griffiths, Measurement of the extracellular pH of solid tumours in mice by magnetic resonance spectroscopy: A comparison of exogenous (19)F and (31)P probes, *NMR Biomed.* 12 (1999) 495–504.
- [304] Y. Aoki, K. Akagi, Y. Tanaka, J. Kawai, M. Takahashi, Measurement of intratumor pH by pH indicator used in ¹⁹F MR spectroscopy, *Invest. Radiol.* 31 (1996) 680–689.
- [305] R.Y. Tsien, A non-disruptive technique for loading calcium buffers and indicators into cells, *Nature* 290 (1981) 527–528.
- [306] G.A. Smith, R.T. Hesketh, J.C. Metcalfe, J. Feeney, P.G. Morris, Intracellular calcium measurements by F-19 Nmr of fluorine-labeled chelators, *Proc. Natl. Acad. Sci. USA* 80 (1983) 7178–7182.

- [307] J. Benders, U. Flogel, T. Schafer, D. Leibfritz, S. Hechtenberg, D. Beyersmann, Study of the interactions of cadmium and zinc ions with cellular calcium homeostasis using F-19-NMR spectroscopy, *Biochem. J.* 322 (1997) 793–799.
- [308] R.K. Gupta, R.J. Gillies, R.K. Gupta (Ed.), *¹⁹F NMR Measurement of Intracellular Free Calcium Ions In Intact Cells and Tissues*, Vol. 2, CRC, Boca Raton, 1987, pp. 45–53.
- [309] F.A. Schanne, J.R. Moskal, R.K. Gupta, Effect of lead on intracellular free calcium ion concentration in a presynaptic neuronal model: ¹⁹F-NMR study of NG108–15 cells, *Brain Res.* 503 (1989) 308–311.
- [310] F.A. Schanne, T.L. Dowd, R.K. Gupta, J.F. Rosen, Lead increases free Ca^{2+} concentration in cultured osteoblastic bone cells: Simultaneous detection of intracellular free Pb^{2+} by ¹⁹F NMR, *Proc. Natl. Acad. Sci. USA* 86 (1989) 5133–5135.
- [311] E. Marban, M. Kitakaze, V.P. Chacko, M.M. Pike, Ca^{2+} transients in perfused hearts revealed by gated F-19 NMR-spectroscopy, *Circ. Res.* 63 (1988) 673–678.
- [312] H. Kusuoka, P.H. Backx, M.C. Camilion de Hurtado, M. Azan-Backx, E. Marban, H.E. Cingolani, Relative roles of intracellular Ca^{2+} and pH in shaping myocardial contractile response to acute respiratory alkalosis, *Am. J. Physiol.* 265 (1993) H1696–1703.
- [313] H.L. Kirschenlohr, J.C. Metcalfe, P.G. Morris, G.C. Rodrigo, G.A. Smith, Ca^{2+} Transient, Mg^{2+} , and pH Measurements in the cardiac cycle by F-19 NMR, *Proc. Natl. Acad. Sci. USA* 85 (1988) 9017–9021.
- [314] H. Plenio, R. Diodone, Covalently bonded fluorine as a σ -donor for groups I and II metal ions in partially fluorinated macrocycles, *JACS* 118 (1996) 356–367.
- [315] J.L. Noronha, G.M. Matuschak, Magnesium in critical illness: Metabolism, assessment, and treatment, *Intensive Care Med.* 28 (2002) 667–679.
- [316] R.K. Gupta, P. Gupta, R.K. Gupta (Ed.), *³¹P NMR Measurement of Intracellular Free Magnesium in Cells and Organisms*, Vol. 2, CRC, Boca Raton, 1987, pp. 34–43.
- [317] E. Weller, P. Bachert, H.M. Meinck, B. Friedmann, P. Bartsch, H. Mairbaurl, Lack of effect of oral Mg-supplementation on Mg in serum, blood cells, and calf muscle, *Med. Sci. Sports Exerc.* 30 (1998) 1584–1591.
- [318] C.V. Odvina, R.P. Mason, C.Y.C. Pak, Prevention of thiazide-induced hypokalemia without magnesium depletion by potassium-magnesium citrate, *Am. J. Ther.* 13 (2006) 101–108.
- [319] E. Murphy, Measurement of intracellular ionized magnesium, *Miner. Electrolyte Metab.* 19 (1993) 250–258.
- [320] B. Tecle, J.E. Casida, Enzymatic defluorination and metabolism of fluoroacetate, fluoroacetamide, fluoroethanol, and (-)-erythro-fluorocitrate in rats and mice examined by ¹⁹F and ¹³C NMR, *Chem. Res. Toxicol.* 2 (1989) 429–435.
- [321] L.A. Levy, E. Murphy, B. Raju, R.E. London, Measurement of cytosolic free magnesium concentration by ¹⁹F NMR, *Biochemistry* 27 (1988) 4041–4048.
- [322] E. Murphy, C. Steenbergen, L.A. Levy, B. Raju, R.E. London, Cytosolic free magnesium levels in ischemic rat-heart, *J. Biol. Chem.* 264 (1989) 5622–5627.
- [323] G.J. Long, J.F. Rosen, F.A.X. Schanne, Lead activation of protein-kinase-C from rat-brain - determination of free calcium, lead, and zinc by F-19-Nmr, *J. Biol. Chem.* 269 (1994) 834–837.
- [324] H. Plenio, J. Hermann, R. Diodone, The coordination chemistry of fluorocarbons: Difluoro-m-cyclophane-based fluorocryptands and their group I and II metal ion complexes, *Inorg. Chem.* 36 (1997) 5722–5729.
- [325] H. Takemura, H. Kariyazono, M. Yasutake, N. Kon, K. Tani, K. Sako, T. Shinmyozu, T. Inazu, Syntheses of macrocyclic compounds possessing fluorine atoms in their cavities: Structures and complexation with cations, *Eur. J. Org. Chem.* 1 (2000) 141–148.
- [326] H. Plenio, R. Diodone, A fluorine-containing cryptand for the complexation of anions and the utility of F-19 Nmr-spectroscopy for the determination of host guest association, *Z. Naturforsch. Section. B- J. Chem. Sci.* 50 (1995) 1075–1078.

- [327] R.E. London, S.A. Gabel, F-19 NMR-studies of fluorobenzenboronic acids.1. Interaction kinetics with biologically significant, JACS 116 (1994) 2562–2569.
- [328] J.S. Fowler, N.D. Volkow, G.J. Wang, Y.S. Ding, 2-deoxy-2-[18F]fluoro-D-glucose and alternative radiotracers for positron emission tomography imaging using the human brain as a model, Semin. Nucl. Med. 34 (2004) 112–121.
- [329] T. Nakada, I.L. Kwee, C.B. Conboy, Noninvasive *in vivo* demonstration of 2-fluoro-2-deoxy-D-glucose metabolism beyond the hexokinase reaction in rat-brain by F-19 nuclear-magnetic-resonance spectroscopy. J. Neurochem. 46 (1986) 198.
- [330] T. Nakada, I.L. Kwee, P.J. Card, N.A. Matwiyoff, B.V. Griffey, R.H. Griffey, F-19 NMR imaging of glucose-metabolism, Magn. Reson. Med. 6 (1988) 307–313.
- [331] T. Nakada, I.L. Kwee, B.V. Griffey, R.H. Griffey, F-19 Mr imaging of glucose-metabolism in the rabbit, Radiology 168 (1988) 823–825.
- [332] B.A. Berkowitz, J.J.H. Ackerman, Proton decoupled fluorine nuclear-magnetic-resonance spectroscopy *in situ*, Biophys. J. 51 (1987) 681–685.
- [333] M.J. Lizak, K. Mori, P.F. Kador, Determination of aldose reductase activity in the eye by localized magnetic resonance spectroscopy, J. Ocul. Pharmacol. Ther. 17 (2001) 475–483.
- [334] E.F. Secchi, M.J. Lizak, S. Sato, P.F. Kador, 3-Fluoro-3-deoxy-D-galactose: A new probe for studies on sugar cataract, Curr. Eye Res. 18 (1999) 277–282.
- [335] I.L. Kwee, H. Igarashi, T. Nakada, Aldose reductase and sorbitol dehydrogenase activities in diabetic brain: *In vivo* kinetic studies using F-19 3-FDG NMR in rats, Neuroreport 7 (1996) 726–728.
- [336] R.G. Shulman, D.L. Rothman, C-13 NMR of intermediary metabolism: Implications for systemic physiology, Annu. Rev. Physiol. 63 (2001) 15–48.
- [337] F.M.H. Jeffrey, A. Rajagopal, C.R. Malloy, A.D. Sherry, C-13-Nmr - a simple yet comprehensive method for analysis of intermediary metabolism, Trends Biochem. Sci. 16 (1991) 5–10.
- [338] R.P. Mason, J.K.M. Sanders, A. Cornish, *In vivo* enzymology—C-13 Nmr measurement of a kinetic isotope effect for methanol oxidation in *methylosinus-trichosporium* Ob3b, FEBS Lett. 216 (1987) 4–6.
- [339] I.J. Stratford, G.E. Adams, G.G. Steel, G.E. Adams, A. Horwich (Eds.), Radiation Sensitizers and Bioreductive Drugs, Elsevier, Amsterdam, 1989, pp. 145–162.
- [340] S.S. Foo, D.F. Abbott, N. Lawrentschuk, A.M. Scott, Functional imaging of intratumoral hypoxia, Mol. Imaging. Biol. 6 (2004) 291–305.
- [341] A. Franko, C. Koch, D. Boisvert, Distribution of misonidazole adducts in gliosarcoma tumors and spheroids: Implications for oxygen distribution, Cancer Res. 52 (1992) 3831–3837.
- [342] J.R. Ballinger, Imaging hypoxia in tumors, Semin. Nucl. Med. 31 (2001) 321–329.
- [343] R.J. Hodgkiss, Use of 2-nitroimidazoles as bioreductive markers for tumour hypoxia, Anticancer Drug Des. 13 (1998) 687–702.
- [344] J.G. Rajendran, K.A. Krohn, Imaging hypoxia and angiogenesis in tumors, Radiol. Clin. North Am. 43 (2005) 169–187.
- [345] S.M. Evans, S. Hahn, D.R. Pook, W.T. Jenkins, A.A. Chalian, P. Zhang, C. Stevens, R. Weber, G. Weinstein, I. Benjamin, N. Mirza, M. Morgan, S. Rubin, W.G. McKenna, E.M. Lord, C.J. Koch, Detection of hypoxia in human squamous cell carcinoma by EF5 binding, Cancer Res. 60 (2000) 2018–2024.
- [346] C.J. Koch, S.M. Hahn, K.J. Rockwell, J.M. Covey, W.G. McKenna, S.M. Evans, Pharmacokinetics of EF5 [2-(2-nitro-1-H-imidazol-1-yl)-N-(2,2,3,3,3-pentafluoropropyl) acetamide] in human patients: Implications for hypoxia measurements *in vivo* by 2-nitroimidazoles, Cancer Chemother. Pharmacol. 48 (2001) 177–187.
- [347] A.S.E. Ljungkvist, J. Bussink, P.F.J.W. Rijken, J.A. Raleigh, J. Denekamp, A.J. Van Der Kogel, Changes in tumor hypoxia measured with a double hypoxic marker technique, Int. J. Radiat. Oncol. Biol. Phys. 48 (2000) 1529–1538.
- [348] J.S. Lewis, D.W. McCarthy, T.J. McCarthy, Y. Fujibayashi, M.J. Welch, Evaluation of Cu-64-ATSM *in vitro* and *in vivo* in a hypoxic tumor model, J. Nucl. Med. 40 (1999) 177–183.

- [349] F. Dehdashti, P.W. Grigsby, M.A. Mintun, J.S. Lewis, B.A. Siegel, M.J. Welch, Assessing tumor hypoxia in cervical cancer by positron emission tomography with ^{60}Cu -ATSM: Relationship to therapeutic response—a preliminary report, *Int. J. Radiat. Oncol. Biol. Phys.* 55 (2003) 1233–1238.
- [350] J.D. Chapman, E.L. Engelhardt, C.C. Stobbe, R.F. Schneider, G.E. Hanks, Measuring hypoxia and predicting tumor radioresistance with nuclear medicine assays, *Radiother. Oncol.* 46 (1998) 229–237.
- [351] S.P. Robinson, J.R. Griffiths, Current issues in the utility of ^{19}F nuclear magnetic resonance methodologies for the assessment of tumour hypoxia, *Philos. Trans. R. Soc. Lond. B Biol. Sci.* 359 (2004) 987–996.
- [352] D. Procissi, F. Claus, J. Koziorowski, P. Burgman, C. Matei, S. Thakur, C. Ling, J.A. Koutcher, *In vivo* ^{19}F MRS and ^{19}F 2D-CSI investigation of a fluorine labeled 2-Nitroimidazole (TF-MISO). A potential functional reporter of hypoxia in solid tumors. *Proc. Intl. Soc. Mag. Reson. Med.* 2006, p. 1260.
- [353] J.M. Cline, G.L. Rosner, J.A. Raleigh, D.E. Thrall, Quantification of CCI-103F labeling heterogeneity in canine solid tumors, *Int. J. Radiat. Oncol. Biol. Phys.* 37 (1997) 655–662.
- [354] P. Workman, R.J. Maxwell, J.R. Griffiths, Noninvasive MRS in New Anticancer Drug Development, *NMR Biomed.* 5 (1992) 270–272.
- [355] B.M. Seddon, R.J. Maxwell, D.J. Honess, R. Grimshaw, F. Raynaud, G.M. Tozer, P. Workman, Validation of the fluorinated 2-nitroimidazole SR-4554 as a noninvasive hypoxia marker detected by magnetic resonance spectroscopy, *Clin. Cancer Res.* 8 (2002) 2323–2335.
- [356] B.M. Seddon, G.S. Payne, L. Simmons, R. Ruddle, R. Grimshaw, S. Tan, A. Turner, F. Raynaud, G. Halbert, M.O. Leach, I. Judson, P. Workman, A phase I study of SR-4554 via intravenous administration for noninvasive investigation of tumor hypoxia by magnetic resonance spectroscopy in patients with malignancy, *Clin. Cancer Res.* 9 (2003) 5101–5112.
- [357] S.J. Li, G.Y. Jin, J.E. Moulder, Prediction of tumor radiosensitivity by hexafluoromisonidazole retention monitored by $[\text{H}-1]/[\text{F}-19]$ magnetic-resonance spectroscopy, *Cancer Commun.* 3 (1991) 133–139.
- [358] E.O. Aboagye, R.J. Maxwell, M.R. Horsman, A.D. Lewis, P. Workman, M. Tracy, J.R. Griffiths, The relationship between tumour oxygenation determined by oxygen electrode measurements and magnetic resonance spectroscopy of the fluorinated 2-nitroimidazole SR-4554, *Br. J. Cancer* 77 (1998) 65–70.
- [359] H.W. Salmon, D.W. Siemann, Utility of ^{19}F MRS detection of the hypoxic cell marker EF5 to assess cellular hypoxia in solid tumors, *Radiother. Oncol.* 73 (2004) 359–366.
- [360] J.K. Fairweather, M. Faijes, H. Driguez, A. Planas, Specificity studies of bacillus 1,3–1,4-beta-glucanases and application to glycosynthase-catalyzed transglycosylation, *Chembiochem* 3 (2002) 866–873.
- [361] T. Ichikawa, D. Hogemann, Y. Saeki, E. Tyminski, K. Terada, R. Weissleder, E.A. Chiocca, J.P. Basilion, MRI of transgene expression: Correlation to therapeutic gene expression, *Neoplasia* (New York) 6 (2002) 523–530.
- [362] Z. Paroo, R.A. Bollinger, D.A. Braasch, E. Richer, D.R. Corey, P.P. Antich, R.P. Mason, Validating bioluminescence imaging as a high-throughput, quantitative modality for assessing tumor burden, *Mol. Imaging* 3 (2004) 117–124.
- [363] J.G. Tjuvajev, M. Doubrovina, T. Akhurst, S. Cai, J. Balatoni, M.M. Alauddin, R. Finn, W. Bornmann, H. Thaler, P.S. Conti, R.G. Blasberg, Comparison of radiolabeled nucleoside probes (FIAU, FHBG, and FHPG) for PET imaging of HSV1-tk gene expression, *J. Nucl. Med.* 43 (2002) 1072–1083.
- [364] A. Kruger, V. Schirmacher, R. Khokha, The bacterial lacZ gene: An important tool for metastasis research and evaluation of new cancer therapies, *Cancer Metastasis Rev.* 17 (1999) 285–294.

- [365] I.G. Serebriiskii, E.A. Golemis, Uses of lacZ to study gene function: Evaluation of beta-galactosidase assays employed in the yeast two-hybrid system, *Anal. Biochem.* 285 (2000) 1–15.
- [366] J.R. Beckwith, D. Zipser, The Lactose Operon Cold Spring Harbor Laboratory, Cold Spring Harbor, 1970, p. 435.
- [367] J. Kawaguchi, V. Wilson, P.J. Mee, Visualization of whole-mount skeletal expression patterns of LacZ reporters using a tissue clearing protocol, *Biotechniques* 32 (2002) 68–73.
- [368] K. Heuermann, J. Cosgrove, S-Gal: An autoclavable dye for color selection of cloned DNA inserts, *Biotechniques* 30 (2001) 1142–1147.
- [369] I. Bronstein, B. Edwards, J.C. Voyta, 1,2-Dioxetanes—novel chemi-luminescent enzyme substrates—applications to immunoassays, *J. Chemilum. Biolum.* 4 (1989) 99–111.
- [370] A.Y. Louie, M.M. Huber, E.T. Ahrens, U. Rothbacher, R. Moats, R.E. Jacobs, S.E. Fraser, T.J. Meade, *In vivo* visualization of gene expression using magnetic resonance imaging, *Nat. Biotechnol.* 18 (2000) 321–325.
- [371] C.H. Tung, Q. Zeng, K. Shah, D.E. Kim, D. Schellingerhout, R. Weissleder, *In vivo* imaging of beta-galactosidase activity using far red fluorescent switch, *Cancer Res.* 64 (2004) 1579–1583.
- [372] K.H. Lee, S.S. Byun, J.H. Choi, J.Y. Paik, Y.S. Choe, B.T. Kim, Targeting of lacZ reporter gene expression with radioiodine-labelled phenylethyl-beta-d-thiogalactopyranoside, *Eur. J. Nucl. Med. Mol. Imaging* 31 (2004) 433–438.
- [373] S. Yoon, H.G. Kim, K.H. Chun, J.E.N. Shin, 4-deoxy-analogs of p-nitrophenyl β -D-galactopyranosides for specificity study with β -galactosidase from escherichia coli, *Bull. Korean Chem. Soc.* 17 (1996) 599–604.
- [374] W. Cui, P. Otten, Y. Li, K. Koeneman, J. Yu, R.P. Mason, A novel NMR approach to assessing gene transfection: 4-fluoro-2-nitrophenyl- β -D-galactopyranoside as a prototype reporter molecule for β -galactosidase, *Magn. Reson. Med.* 51 (2004) 616–620.
- [375] V.D. Kodibagkar, J. Yu, L. Liu, H.P. Hetherington, R.P. Mason, Imaging b-galactosidase activity using ¹⁹F chemical shift imaging of LacZ gene-reporter molecule 2-fluoro-4-nitrophenol- β -D-galactopyranoside, *Magn. Reson. Imaging* 24 (2006) 959–962.
- [376] J.P. Richard, J.G. Westerfeld, S. Lin, Structure-reactivity relationships for beta-galactosidase (Escherichia coli, lac Z). 1. Bronsted parameters for cleavage of alkyl beta-D-galactopyranosides, *Biochemistry* 34 (1995) 11703–11712.
- [377] J.X. Yu, Z. Ma, Y. Li, K.S. Koeneman, L. Liu, R.P. Mason, Synthesis and evaluation of a novel gene reporter molecule: Detection of β -galactosidase activity using ¹⁹F NMR of a fluorinated vitamin B6 conjugate, *Med. Chem.* 1 (2005) 255–262.
- [378] J.X. Yu, R.P. Mason, Synthesis and characterization of novel lacZ gene reporter molecules: Detection of b-galactosidase activity using ¹⁹F NMR of polyglycosylated fluorinated vitamin B6, *J. Med. Chem.* 49 (2006) 1991–1999.
- [379] L. Liu, V.D. Kodibagkar, J.-X. Yu, R.P. Mason, ¹⁹F-NMR detection of lacZ gene expression via the enzymic hydrolysis of 2-fluoro-4-nitrophenyl β -D-galactopyranoside *in vivo* in PC3 prostate tumor xenografts in the mouse, *Faseb J.* 21(2007) 2014–2019.
- [380] L.C. Clark Jr., F. Gollan, Survival of mammals breathing organic liquids equilibrated with oxygen at atmospheric pressure, *Science* 152 (1966) 1755–1756.
- [381] J.S. Greenspan, W.W. Fox, S.D. Rubenstein, M.R. Wolfson, S.S. Spinner, T.H. Shaffer, Partial liquid ventilation in critically ill infants receiving extracorporeal life support. Philadelphia Liquid Ventilation Consortium, *Pediatrics* 99 (1997) E2.
- [382] S.R. Thomas, L.C. Clark Jr., J. Ackerman, R.G. Pratt, R.E. Hoffmann, L.J. Busse, R.A. Kinsey, R.C. Samarutunga, MRI imaging of the lung using liquid perfluorocarbons, *J. Comput. Asst. Tomogr.* 10 (1986) 1–9.

- [383] S.R. Thomas, L. Gradon, S.E. Pratsinis, R.G. Pratt, G.P. Fotou, A.J. McGoron, A.L. Podgorski, R.W. Millard, Perfluorocarbon compound aerosols for delivery to the lung as potential ^{19}F magnetic resonance reporters of regional pulmonary pO_2 , *Invest. Radiol.* 32 (1997) 29–38.
- [384] M.Q. Huang, Q. Ye, D.S. Williams, C. Ho, MRI of lungs using partial liquid ventilation with water-in-perfluorocarbon emulsions, *Magn. Reson. Med.* 48 (2002) 487–492.
- [385] E. Heidelberg, P.C. Lauterbur, 1982, pp. 70–71.
- [386] D.O. Kuethe, V.C. Behr, S. Begay, Volume of rat lungs measured throughout the respiratory cycle using F-19 NMR of the inert gas SF_6 , *Magn. Reson. Med.* 48 (2002) 547–549.
- [387] J. Ruiz-Cabello, J.M. Perez-Sanchez, R.P. de Alejo, I. Rodriguez, N. Gonzalez-Mangado, G. Peces-Barbas, M. Cortijo, Diffusion-weighted F-19-MRI of lung periphery: Influence of pressure and air- SF_6 composition on apparent diffusion coefficients, *Resp. Physiol. Neurobiol.* 148 (2005) 43–56.
- [388] W.F. Remy, R.W. Geenen, S.M. Hussain, F. Cademartiri, J.W. Poley, P.D. Siersema, G.P. Krestin, CT and MR colonography: Scanning techniques, postprocessing, and emphasis on polyp detection, *Radiograph.* 24 (2004) e18.
- [389] D.L. Rubin, K.L. Falk, M.J. Sperling, M. Ross, S. Saini, B. Rothman, F. Shellock, E. Zerhouni, D. Stark, E.K. Outwater, U. Schmiedl, L.C. Kirby, J. Chezmar, T. Coates, M. Chang, J.M. Silverman, N. Rofsky, K. Burnett, J. Engel, S.W. Young, A multicenter clinical trial of Gadolite Oral Suspension as a contrast agent for MRI. [Clinical Trial. Clinical Trial, Phase II. Clinical Trial, Phase III, J. Magn. Reson. Imaging 7 (1997) 865–872.
- [390] S. Hirohashi, H. Uchida, K. Yoshikawa, N. Fujita, K. Ohtomo, Y. Yuasa, Y. Kawamura, O. Matsui, Large scale clinical evaluation of bowel contrast agent containing ferric ammonium citrate in MRI, *Magn. Reson. Imaging* 12 (1994) 837–846.
- [391] G.S.I. Bisset, K.H. Emery, M.P. Meza, N.K. Rollins, S. Don, J.S. Shorr, Perflubron as a gastrointestinal MR imaging contrast agent in the pediatric population, *Pediatr. Radiol.* 26 (1996) 409–415.
- [392] R.F. Mattrey, M.A. Trambert, J.J. Brown, S.W. Young, J.N. Bruneton, G.E. Wesbey, Z.N. Balsara, Perflubron as an oral contrast agent for MR imaging: Results of a phase III clinical trial, *Radiology* 191 (1994) 841–848.
- [393] B. Uzzan, P. Nicolas, M. Cucherat, G.Y. Perret, Microvessel density as a prognostic factor in women with breast cancer: A systematic review of the literature and meta-analysis, *Cancer Res.* 64 (2004) 2941–2955.
- [394] S.P. Robinson, P.F. Rijken, F.A. Howe, P.M. McSheehy, B.P. van der Sanden, A. Heerschap, M. Stubbs, A.J. Van Der Kogel, J.R. Griffiths, Tumor vascular architecture and function evaluated by non-invasive susceptibility MRI methods and immunohistochemistry, *J. Magn. Reson. Imaging.* 17 (2003) 445–454.
- [395] T.L. Ceckler, S.L. Gibson, R. Hilf, R.G. Bryant, In situ assessment of tumor vascularity using fluorine NMR imaging, *Magn. Reson. Med.* 13 (1990) 416–433.
- [396] K.L. Meyer, P.M. Joseph, B. Mukherji, V.A. Livolsi, R. Lin, Measurement of vascular volume in experimental rat-tumors by F-19 magnetic-resonance-imaging, *Invest. Radiol.* 28 (1993) 710–719.
- [397] T. Sogabe, T. Imaizumi, T. Mori, M. Tominaga, K. Koga, Y. Yabuuchi, Effects of vasodilators on the signal intensity of perfluorocarbon monitored by *in vivo* F-19-NMR spectroscopy, *Magn. Reson. Imaging* 15 (1997) 341–345.
- [398] Y. Gu, R.P. Mason, H. Liu, Estimated fraction of tumor vascular blood contents sampled by near infrared spectroscopy and ^{19}F magnetic resonance spectroscopy, *Opt. Express.* 13 (2005) 1724–1733.
- [399] B. Authier, Reactive hyperemia monitored on rat muscle using perfluorocarbons and F-19 NMR, *Magn. Reson. Med.* 8 (1988) 80–83.

- [400] N.J. Baldwin, Y. Wang, T.C. Ng, *In situ* ¹⁹F MRS measurement of RIF-1 tumor blood volume: Corroboration by radioisotope-labeled [¹²⁵I]-albumin and correlation to tumor size, *Magn. Reson. Imaging* 14 (1996) 275–280.
- [401] J.R. Ewing, C.A. Branch, S.C. Fagan, J.A. Helpert, R.T. Simkins, S.M. Butt, K.M. A. Welch, Fluorocarbon-23 measure of cat cerebral blood flow by NMR, *Stroke* 21 (1990) 100–106.
- [402] S.M. Eleff, M.D. Schnall, L. Ligetti, M. Osbakken, V.H. Subramanian, B. Chance, J.S. Leigh, concurrent measurements of cerebral blood-flow, sodium, lactate, and high-energy phosphate-metabolism using F-19, Na-23, H-1, and P-31 nuclear magnetic-resonance spectroscopy, *Magn. Reson. Med.* 7 (1988) 412–424.
- [403] J.S. van den Brink, Y. Watanabe, C.K. Kuhl, T. Chung, R. Muthupillai, M. Van Cauteren, K. Yamada, S. Dymarkowski, J. Bogaert, J.H. Maki, C. Matos, J.W. Casselman, R.M. Hooijveen, Implications of SENSE MR in routine clinical practice, *Eur. J. Radiol.* 46 (2003) 3–27.
- [404] K.P. Pruessmann, M. Weiger, M.B. Scheidegger, P. Boesiger, SENSE: Sensitivity encoding for fast MRI, *Magn. Reson. Med.* 42 (1999) 952–962.
- [405] H.P. Shukla, Application of Perfluorocarbon Emulsions as Fluorine-19 Nuclear Magnetic Resonance Molecular Probes of Cardiac Tissue Oxygen Tension, University of Texas Southwestern Graduate School of Biomedical Sciences, 1994Ph.D..
- [406] J. Taylor, C.J. Deutsch, ¹⁹F nuclear magnetic resonance: Measurements of [O₂] and pH in biological systems, *Biophys. J.* 53 (1988) 227–233.
- [407] Q. Guo, R.F. Mattrey, C. Guclu, R.B. Buxton, O. Nalcioğlu, Monitoring of pO₂ by spin-spin relaxation rate 1/T₂ of ¹⁹F in a rabbit abscess model, *Artif Cells Blood Substit. Immobil. Biotechnol.* 22 (1994) 1449–1454.
- [408] J.J. Delpuech, M.A. Hamza, G. Serratrice, Determination of oxygen by a nuclear magnetic-resonance method, *J. Magn. Reson.* 36 (1979) 173–179.
- [409] N. Raghunand, R.J. Gillies, pH and chemotherapy, Novartis Foundation Symposium 240 (2001) 199–211.
- [410] G.A. Smith, P.G. Morris, T.R. Hesketh, J.C. Metcalfe, Design of an indicator of intracellular free Na⁺ concentration using ¹⁹F-NMR, *Biochim. Biophys. Acta* 889 (1986) 72–83.
- [411] R. Ramasamy, P. Zhao, W.L. Gitomer, A.D. Sherry, C.R. Malloy, Determination of chloride potential in perfused rat hearts by NMR spectroscopy, *Am. J. Physiol.* 263 (1993) H1958–1962.
- [412] A.A. Bobko, S.V. Sergeeva, E.G. Bagryanskaya, A.L. Markel, V.V. Khramtsov, V.A. Reznikov, N.G. Kolosova, ¹⁹F NMR measurements of NO production in hypertensive ISIAH and OXYS rats, *Biochem. Biophys. Res. Commun.* 330 (2005) 367–370.
- [413] J. Raleigh, A. Franko, D. Kelly, L. Trimble, P. Allen, Development of an *in vivo* ¹⁹F MR method for measuring oxygen deficiency in tumors, *Magn. Reson. Med.* 22 (1991) 451–466.
- [414] A. Daugherty, N.N. Becker, L.A. Scherrer, B.E. Sobel, J.J.H. Ackerman, J.W. Baynes, S.R. Thorpe, Non-invasive detection of protein-metabolism *In vivo* by NMR-spectroscopy—Application of a novel F-19-containing residualizing label, *Biochem. J.* 264 (1989) 829–835.
- [415] B.A. Berkowitz, J.T. Handa, C.A. Wilson, Perfluorocarbon temperature measurement using ¹⁹F NMR, *NMR Biomed* 5 (1992) 65–68.
- [416] T.Q. Duong, J.J.H. Ackerman, H.S. Ying, J.J. Neil, Evaluation of extra- and intracellular apparent diffusion in normal and globally ischemic rat brain via F-19 NMR, *Magn. Reson. Med.* 40 (1998) 1–13.
- [417] C. Thomas, C. Counsell, P. Wood, G.E. Adams, Use of F-19 nuclear-magnetic-resonance spectroscopy and hydralazine for measuring dynamic changes in blood perfusion volume in tumors in mice, *J. Natl. Cancer Inst.* 84 (1992) 174–180.

- [418] R.L. Nunnally, E.E. Babcock, S.D. Horner, R.M. Peshock, Fluorine-19 NMR spectroscopy and imaging investigations of myocardial perfusion and cardiac function, *Magn. Reson. Imaging* 3 (1985) 399–405.
- [419] R. Tibes, J. Trent, R. Kurzrock, Tyrosine kinase inhibitors and the dawn of molecular cancer therapeutics, *Ann. Rev. Pharmacol. Toxicol.* 45 (2005) 357.
- [420] M.H. Cohen, G.A. Williams, R. Sridhara, G. Chen, R. Pazdur, FDA drug approval summary: Gefitinib (ZD1839) (Iressa(R)) Tablets, *Oncologist* 8 (2003) 303–306.
- [421] R. Neri, Pharmacology and pharmacokinetics of flutamide, *Urology* 34 (1989) 19–21.
- [422] R. Eliason, J.J. Schoenau, A.M. Szmigielski, W.M. Lavery, Phytotoxicity and persistence of flucarbazone-sodium in soil, *Weed Sci.* 52 (2004) 857–862.
- [423] J.K. Moon, J.H. Kim, S. Rhee, G. Kim, H. Yun, B.J. Chung, S. Lee, Y. Lim, Structural investigation of bistrifluron using X-ray crystallography, NMR spectroscopy, and molecular modeling, *Bull. Korean Chem. Soc.* 23 (2002) 1545–1547.
- [424] P. Christie, Roflumilast: A selective phosphodiesterase 4 inhibitor, *Drugs Today* 41 (2005) 667–675.
- [425] K.A. Haagsma, M.K. Rust, Effect of hexaflumuron on mortality of the Western subterranean termite (Isoptera: Rhinotermitidae) during and following exposure and movement of hexaflumuron in termite groups, *Pest. Manag. Sci.* 61 (2005) 517–531.
- [426] A. Howell, Fulvestrant ('Faslodex'): Current and future role in breast cancer management, *Crit. Rev. Oncol. Hematol.* 57 (2006) 265–273.
- [427] K.A. Santora, M. Zakson-Aiken, C. Rasa, W. Shoop, Development of a mouse model to determine the systemic activity of potential flea-control compounds, *Vet. Parasitol.* 104 (2002) 257–264.
- [428] E. Van Den Neste, S. Cardoen, F. Offner, F. Bontemps, Old and new insights into the mechanisms of action of two nucleoside analogs active in lymphoid malignancies: Fludarabine and cladribine (Review), *Int. J. Oncol.* 27 (2005) 1113–1124.
- [429] C. Blasco, G. Font, J. Manes, Y. Pico, Solid-phase microextraction liquid chromatography/tandem mass spectrometry to determine postharvest fungicides in fruits, *Anal. Chem.* 75 (2003) 3606–3615.
- [430] A.W. Abu-Qare, M.B. Abou-Donia, Sarin: Health effects, metabolism, and methods of analysis, *Food Chem. Toxicol.* 40 (2002) 1327–1333.
- [431] R.E. London, S.A. Gabel, F-19 NMR-studies of fluorobenzeneboronic acids.1. Interaction kinetics with biologically significant ligands, *J. Am. Chem. Soc.* 116 (1994) 2562–2569.
- [432] R.F. Mattrey, D.J. Schumacher, H.T. Tran, Q. Guo, R.B. Buxton, The use of Imagent in diagnostic imaging research and ¹⁹F magnetic resonance for pO₂ measurements, *Biomater. Artif. Cells Immobilization Biotechnol.* 20 (1992) 917–920.
- [433] S. Laukemper-Ostendorf, A. Scholz, K. Burger, C.P. Heussel, M. Schmittner, N. Weiler, K. Markstaller, B. Eberle, H.U. Kauczor, M. Quintel, M. Thelen, W. G. Schreiber, ¹⁹F-MRI of perflubron for measurement of oxygen partial pressure in porcine lungs during partial liquid ventilation, *Magn. Reson. Med.* 47 (2002) 82–89.
- [434] C.H. Sotak, P.S. Hees, H.H. Huang, M.H. Hung, C.G. Krespan, S. Reynolds, A new perfluorocarbon for use in fluorine-19 magnetic resonance spectroscopy, *Magn. Reson. Med.* 29 (1993) 188–195.
- [435] M.V. Papadopoulou, R. Pouremad, M.K. Rao, M. Ji, W.D. Bloomer, *In vitro* evaluation of 4-[3-(2-nitro-1-imidazolyl)-7-trifluoromethylquinoline hydrochloride (NLTQ-1), a new bioreductive agent as a hypoxia marker by F-19-magnetic resonance spectroscopy (F-19-MRS), *In Vivo* 15 (2001) 365–371.

SECTION 2

Biomedical Materials

This page intentionally left blank

CHAPTER 6

Fluoride-Based Bioceramics

Christian Rey,^{1,*} Christèle Combes,¹ Christophe Drouet,¹ and
Hocine Sfihi^{2,3}

¹*Centre Inter-universitaire de Recherche et d'Ingénierie des Matériaux (CIRIMAT)
Ecole Nationale Supérieure des Ingénieurs en Arts Chimiques et Technologiques 118,
route de Narbonne, 31077 Toulouse Cedex 04, France*

²*Laboratoire de Physique Quantique UMR CNRS 7142, ESPCI,
10 rue Vauquelin 75005 Paris, France*

³*Département de Physique, UFR SMBH, Université Paris 13,
74 rue Marcel Cachin 93012 Bobigny Cedex, France*

Contents

1. Introduction	281
2. Overview of bioceramics and related biomaterials incorporating fluoride ions	281
3. Fluorapatite and fluoridated apatites: Structure and characterisation	284
3.1. Crystal structure of stoichiometric fluorapatite	284
3.2. Substituted fluoridated apatites	286
3.3. Physico-chemical characterisation of fluoridated apatites	288
3.3.1. X-ray diffraction	288
3.3.2. FTIR spectroscopy	289
3.3.3. Solid-state NMR	290
3.3.4. Difficulties related to the characterisation of fluoridated apatites	296
4. Physico-chemical properties of fluoridated apatites	296
4.1. Dissolution properties of fluoridated apatites	296
4.2. Fluoridation reactions	297
4.3. Thermal stability	298
4.4. Thermodynamic characteristics	299
4.5. Surface characteristics	299
4.5.1. Surface energy	299
4.5.2. Surface charge	300
4.5.3. Adsorption properties	300
4.6. Fluoridation effects	300
4.7. Mechanical properties of fluoridated apatite ceramics	301
5. Fluor-containing glasses and cements	302
5.1. Fluor-containing glasses	302
5.2. Fluoridated cements	305

*Corresponding author: Christian Rey, CIRIMAT; ENSIACET, 118 route de Narbonne,
31077 Toulouse Cedex 04, France. Tel.: +33 (0)5-62-88-56-35; Fax: 33 (0)5-62-88-57-73;
E-mail: Christian.Rey@ensiacet.fr

6. Preparation and synthesis routes of fluoride-containing apatites	306
6.1. High-temperature methods	306
6.1.1. Solid–gas reaction	306
6.1.2. Pyrolysis method	307
6.1.3. Crystal growth method	307
6.2. Low-temperature methods	308
6.2.1. Hydrolysis method	308
6.2.2. Precipitation method	308
6.2.3. Exchange and/or dissolution–reprecipitation reactions	309
6.2.4. Sol-gel method	310
6.2.5. Crystal growth method	310
7. Processing techniques for fluoride-containing bioceramics	311
7.1. Processing of massive bioceramics containing fluoride	311
7.2. Fluoride-containing bioceramic coatings	312
7.2.1. High-energy processing	312
7.2.2. Solution-mediated processing	314
8. Fluoride ions in biological apatites	316
9. Biological properties of fluoride-containing bioceramics	319
9.1. Biological properties of fluoride ions in solution	319
9.1.1. Effect of fluoride ion on mineralising cells	319
9.1.2. Effect of the fluoride ion on osteoclasts	319
9.1.3. Effect of fluoride ions on bacteria	320
9.1.4. Other alterations in biological fluids related to fluoride ions	321
9.2. Effect of fluoride-containing substrates on bone cells	321
9.2.1. Osteoblast cells	321
9.2.2. Osteoclast cells	321
10. Conclusion	322
References	322
Note from the Editors	331

Abstract

Fluoride ions enter in the composition of several bioceramics, coatings, and composite materials for orthopaedic applications. Because of their physico-chemical effects, they favour processing and shaping of the biomaterials; in addition, they generally confer a specific biological activity to bioceramics and improve bone-cell behaviour and the bone–implant interface. Fluoride ions have mainly been used as additives in hydroxyapatite (HA), one of the most widely used bioceramics, and they participate in the composition of different bioglasses. The effect of fluoride on the physico-chemical properties of HA is well known and documented, fluoride ions can partly or totally substitute the hydroxide ions of HA. In addition to its effect on the unit-cell dimensions, the fluoridation of HA allows the formation of hydrogen bonds with residual OH ions which stabilise fluorhydroxyapatites. Fluoride incorporation in apatites has been shown to considerably decrease their aqueous solubility even at very low substitution levels. Fluoride-containing apatites also exhibit a higher thermal stability than HA. The synthesis of fluoridated apatites for biomedical applications has been accomplished in various ways from simple ion exchange in solution to more elaborate techniques involving sol-gel routes or thermal processes. Because of their stability fluorapatite ceramics can be processed by thermal techniques at temperatures up to 1600°C, well above the decomposition temperature of HA. In bioglasses, fluoride ions are used to favour the formation of fluorapatite crystals and/or to

modulate the biological behaviour. The biomedical effects of fluoride ions have been extensively studied, especially their cariostatic activity and its effect on bone formation and turnover. Generally materials based on fluoridated apatite favour osteoblast adhesion and proliferation. Because of their physicochemical properties, on contact with body fluids, these apatites induce the formation of a bone-like apatite layer on their surface, this event being possibly related to their biological activity. The very low solubility of fluoridated apatites added to the specific action of fluoride ions on osteoblasts determines their very low resorption rate and the *in vivo* stability of their interface with bone tissues. This behaviour may explain the reported improvement of bone-implant bonding.

1. INTRODUCTION

Fluorine is an essential element involved in several enzymatic reactions in various organs, it is present as a trace element in bone mineral, dentine and tooth enamel and is considered as one of the most efficient elements for the prophylaxis and treatment of dental caries. In addition to their direct effect on cell biology, fluoride ions can also modify the physico-chemical properties of materials (solubility, structure and microstructure, surface properties), resulting in indirect biological effects. The biological and physico-chemical roles of fluoride ions are the main reasons for their incorporation in biomaterials, with a pre-eminence for the biological role and often both in conjunction. This chapter focuses on fluoridated bioceramics and related materials, including cements. The specific role of fluorinated polymers and molecules will not be reviewed here.

Most uses of fluoride ions in biomaterials involve apatite compounds either as initial compounds or as a terminal location for fluoride ions. A description of fluoridated apatites will first be given, including structural and characterisation aspects, thermodynamics, solubility and reactivity.

Several biomaterials such as bioglasses and cements contain fluoride; they will be described, followed by a review of the preparation and processing techniques for fluoridated biomaterials.

The role of fluoride ions will be discussed with regard to their incorporation in mineralised tissues, and the biological behaviour of fluoridated biomaterials will also be reviewed.

2. OVERVIEW OF BIOCERAMICS AND RELATED BIOMATERIALS INCORPORATING FLUORIDE IONS

There are multiple applications of fluoridated bioceramics, essentially as bone and tooth substitutes (Table 1), involving bulk ceramics, glasses, composite materials and coatings for medical devices and surface treatments. In some cases, fluoride ions can leach out of the material inducing a direct biological effect in a soluble form. However, considering the affinity of fluoride ions for apatite

Table 1. Applications of fluoridated bioceramics and related biomaterials

Type of material	Application	Main fluorine-related effects
Ceramics	Bone substitutes	Improvement of surface and interface properties and processing techniques
Biological glasses	Bone replacement	
	Tissue engineering	
Ca-P ionic cements	Bone substitute	Improvement of cement setting. Biological effect of released F ions
	Dental applications	
Glass ionomer cements (GIC) and related materials	Dental filling	Biological effect of released F ions
Coatings	Coating of metallic prostheses	Improvement of processing techniques and surface properties
Mineral-organic composites	Bone replacement and bone substitution	Improvement of mechanical and surface properties

minerals, the ultimate location of fluoride ions is generally bone, dentine and enamel mineral where they induce structural and micro-structural changes.

Several effects of fluoride ions have been claimed (Table 1) concerning the stability of the biomaterials, the implant–tissue interface, or the tissue itself. The incorporation of fluoride ions in apatitic materials is generally aimed at increasing their stability and decreasing their solubility.

The increased thermal stability of fluoride-containing apatites compared to hydroxyapatite (HA) enables high-temperature thermal processing (for ceramics, coatings) to be used, which would deteriorate HA. In addition the thermal decomposition scheme is different (Fig. 1). In the case of HA, the decomposition depends on the water partial pressure: usually, at processing temperatures (1250°C for sintering and higher in the case of plasma spraying), in air, apatites decompose partly into CaO and tricalcium phosphate (TCP). Although these reactions are totally reversible for stoichiometric apatites, in several processing techniques, such as plasma spraying, the high cooling rate and the heterogeneity of the phase distribution do not allow a complete reconstitution of the apatite lattice, and thermally very stable CaO may subsist in the material. The rehydration of such residual CaO (either during the storage period or after implantation)

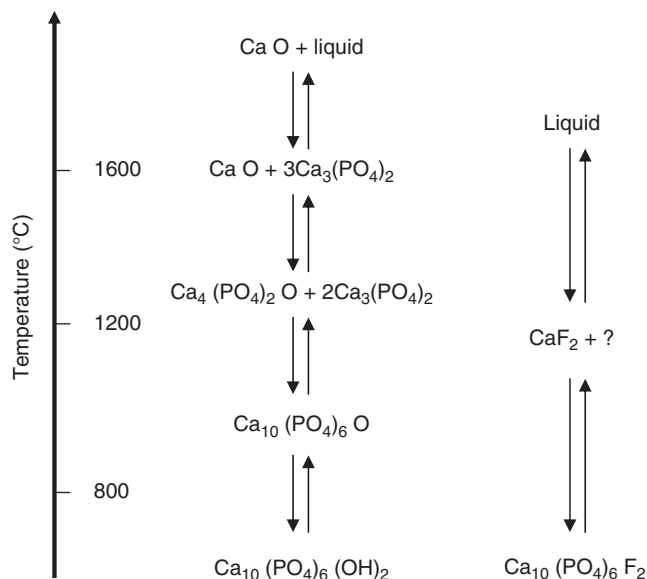


Fig. 1. Thermal stability of hydroxyapatite (HA) and fluorapatite. HA decomposes through a series of reactions into very stable CaO (melting point: 2650°C) and a liquid phase. In the case of fluorapatite, the release of CaF_2 has been reported at very high temperature, before melting; however, the associated phases have not been identified.

may then lead to a swelling and cracking of the ceramics or the coatings. Fluorapatite (FA) on the contrary melts without decomposing; although hydrolysis may occur in the presence of water vapour, the formation of CaO is minimised and the stability of the materials considerably improves (Fig. 1).

Stoichiometric FA is less soluble than stoichiometric HA at physiological pH. In addition, as fluoridated apatites obtained in aqueous media are generally closer to stoichiometry than hydroxylated apatites obtained in the same conditions, the difference in solubility is even larger. The formation of FA is thus favoured in aqueous media containing calcium and phosphate ions, and fluoride ions have been shown to accelerate the hydrolysis of most calcium phosphate salts into fluoridated apatite. In materials science this ability has been utilised, for example, to accelerate the setting reaction of calcium phosphate-based cements. The main use of this property is, however, related to biological apatites. It is now well established that fluoridated enamel and dentine have an improved resistance to caries formation, and that fluoride can even promote remineralisation of early lesions (white spots). Fluoride ions have been shown to increase the bone mineral density (BMD) and they have been used in the treatment of osteoporosis, although the expected decrease in fracture occurrences was not observed in the case of long bones to the extent it was in the case of vertebra.

The ability of fluoride ions to alter the solubility of biological apatites can be useful regarding biomaterials. Fluoride-releasing materials are used for improving the resistance of enamel and dentine to caries and for enhancing remineralisation. In bone substitute materials, fluoride ions are susceptible to locally modifying bone mineral and to inhibiting remodelling, resulting in a stable bone tissue interface. Local applications of fluoride may additionally result in accelerated bone reconstruction, considering the reported effect of these ions on osteoblast proliferation and expression. In these last cases, however, fluoride ions need to be released into the surrounding biological fluids during the reconstruction period.

3. FLUORAPATITE AND FLUORIDATED APATITES: STRUCTURE AND CHARACTERISATION

3.1. Crystal structure of stoichiometric fluorapatite

Fluorapatite (FA) corresponds to the chemical formula $\text{Ca}_{10}(\text{PO}_4)_6\text{F}_2$ and crystallises in the hexagonal space group $\text{P6}_3/\text{m}$, with $Z = 1$ and unit-cell parameters $a = b = 9.367 \text{ \AA}$ and $c = 6.884 \text{ \AA}$ [1] (Fig. 2). From a structural viewpoint, fluorapatite is often considered as a crystalline model for other apatites and is seen as a reference apatitic array [2]. It is one of the very first apatite structures to have been solved. It has been thoroughly studied since the 1930s [3] and is well documented in the literature. In particular, Sudarsanan *et al.* [1] reported the single crystal refinement of X-ray diffraction (XRD) data, and the detailed description of atomic positions and local symmetry is fully available [4,5].

The elementary unit cell can be quite easily described starting from the four mineral ion sites of the crystal: F^- , Ca(I)^{2+} , Ca(II)^{2+} and PO_4^{3-} , where the symbols I and II represent the two different crystallographic sites of the cations, with the application of all the symmetry operations relevant to the space group $\text{P6}_3/\text{m}$. Among the principal symmetry elements, one can cite mirror planes perpendicular to the c -axis (at $z = 1/4$ and $3/4$), which contain most of the ions of the structure (F^- , $\text{Ca}^{2+}(\text{II})$, PO_4^{3-}), three-fold axes parallel to the c -axis (at $x = 1/3$, $y = 2/3$ and $x = 2/3$, $y = 1/3$) along which are located the $\text{Ca}^{2+}(\text{I})$ ions, screw axes 6_3 at the corners of the unit cell and parallel to the c -axis and screw axes 2_1 parallel to the c -axis and located at the midpoints of the cell edges and at the centre of the unit cell itself [3].

The entire unit cell involves seven non-equivalent atoms: F, Ca(I), Ca(II), P, O(I), O(II) and O(III), distributed as $\text{Ca(I)}_4\text{Ca(II)}_6$ [$\text{PO(I)O(II)O(III)}_2$] $_6$ F_2 , and Table 2 reports the corresponding atomic positions in the unit cell.

As stated above, in the stoichiometric FA structure, calcium ions are distributed into two crystallographic sites. Ca(I) sites, often referred to as 'columnar' sites, are spaced by one half of the c -axis parameter, along the three-fold axes. Each Ca(I) $^{2+}$ ion is nine-fold coordinated to oxygen ions, three oxygen atoms being slightly

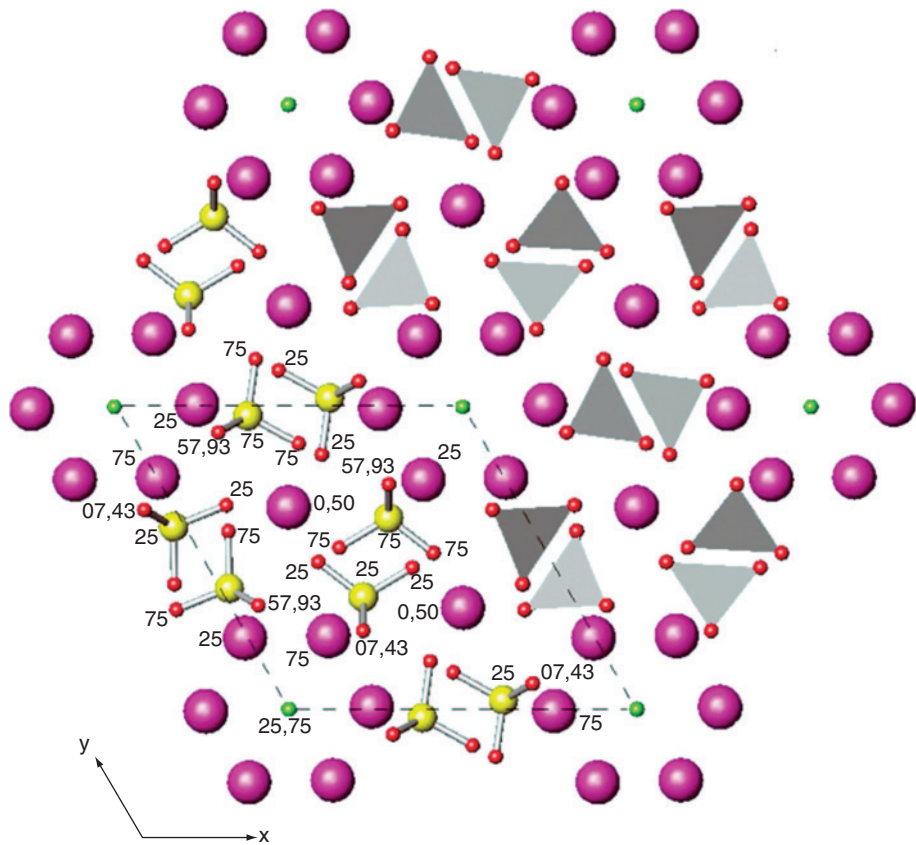


Fig. 2. Structure of fluorapatite. Projection on the (001) cristallographic plane, perpendicular to the *c* axis of the hexagonal structure. (Reproduced by permission of IUCr from Ref. [2]). Purple: Calcium; green: Fluorine; red: Oxygen; yellow: Phosphorus. (See Colour Plate Section at the end of this book.)

Table 2. Atomic positions in stoichiometric fluorapatite

Atom	Site symmetry	Crystallographic position		
		<i>x</i>	<i>y</i>	<i>z</i>
F	C _{3h}	0	0	0.2500
Ca (I)	C ₃	0.3333	0.6667	0.0001
Ca (II)	C _s	−0.0071	0.2423	0.2500
P	C _s	0.3690	0.3985	0.2500
O (I)	C _s	0.4849	0.3273	0.2500
O (II)	C _s	0.4667	0.5875	0.2500
O (III)	E	0.2575	0.3421	0.0705

farther away than the other six. These calcium and oxygen atoms are linked together via PO_4 tetrahedra. This array of phosphate groups leads to channels that coincide with the six-fold screw axes. Ca(II) sites are located at the internal border of these channels, forming two equilateral Ca(II)_3 triangles rotated by 60° from each other around the c -axis, and the F^- ions occupy the centre of these triangles. Thus, the F^- ions are three-fold coordinated by coplanar Ca(II)^{2+} ions.

3.2. Substituted fluoridated apatites

Interestingly, the substitution of small fluoride ions by larger ions like OH^- or Cl^- leads to a displacement of the position of the anionic monovalent sites away from the centre of the Ca(II)_3 triangles. A typical example is that of stoichiometric chlorapatite, $\text{Ca}_{10}(\text{PO}_4)_6\text{Cl}_2$, where Cl^- ions are distributed in the channels at positions slightly above and below $z = 1/2$, in an ordered way leading to a lowering of symmetry from hexagonal to monoclinic ($\text{P2}_1/\text{b}$ space group) with a b parameter doubled from that of FA [6].

It is possible to substitute F^- ions of FA while keeping the overall apatitic structure, possibly accompanied by variations in the atomic positions and unit-cell symmetry. This is the case with HA, $\text{Ca}_{10}(\text{PO}_4)_6(\text{OH})_2$, often considered as a model for biological apatites. In stoichiometric HA, the oxygen atoms of the hydroxyl ions are slightly displaced from the centre of the Ca(II)_3 triangles, giving rise to local distortions [7]. For a perfectly stoichiometric HA sample, the ordering of the OH^- ions, similar to that of Cl^- ions in chlorapatite, leads to the space group $\text{P2}_1/\text{b}$ (with a pseudo-hexagonal structure also involving a doubling of the b parameter) [4,7].

The physico-chemical characteristics of solid solutions are, however, dependent on the type (and amount) of substituting ions, as will be discussed later. Fluorhydroxyapatites (F-OH substitutions) are the most common solid solutions in biological apatites and biomaterials. They exhibit a hexagonal structure and the ion distribution is generally considered to obey statistical laws. Other substitution types are also encountered, both in natural specimens and in synthetic samples. These can involve the substitution of Ca^{2+} ions or phosphate groups. For example, rare earth-doped FA with rare earth elements replacing some of the calcium ions have been used for their fluorescence properties [8]. Because of the existence of two cationic crystallographic sites, Ca(I) and Ca(II) , several types of cationic substitutions can be considered depending on which sites are preferentially targeted by the foreign ion. It is generally accepted that large cations show a preference for the Ca(II) sites located within the channels of the apatite structure [4,9], whereas the substitution of small monovalent cations, such as Na^+ , seems to take place in Ca(I) sites.

The substitution of phosphate groups by other trivalent ions or ions with a different charge has also been observed. Among the most important in terms of

biological relevance and biomedical applications are B-type carbonate-apatites, where CO_3^{2-} ions occupy phosphate positions [10,11]. In this case, however, two major modifications of the original apatite array are involved: (1) the necessity to compensate the charge imbalance involves the creation of ionic vacancies, and (2) the lack of one oxygen atom in carbonate ion compared to phosphate ion results in one oxygen vacancy. Some spectroscopic and XRD data using the Rietveld refinement method [4,12] have established that carbonate oxygen is located (Fig. 3) on sites O(I), O(II) and on one of the two equivalent positions O(III) or O(III'). One oxygen site O(III or III') is vacant and it has been suggested that it could be occupied by OH^- or F^- ions [13,14] explaining, thus, the 'excess' of fluoride and OH^- ions sometimes found in synthetic and natural apatites. In this case, the ion couples $(\text{CO}_3, \text{F})^{3-}$ and $(\text{CO}_3, \text{OH})^{3-}$ would substitute the PO_4^{3-} groups and there is no need for a charge compensation

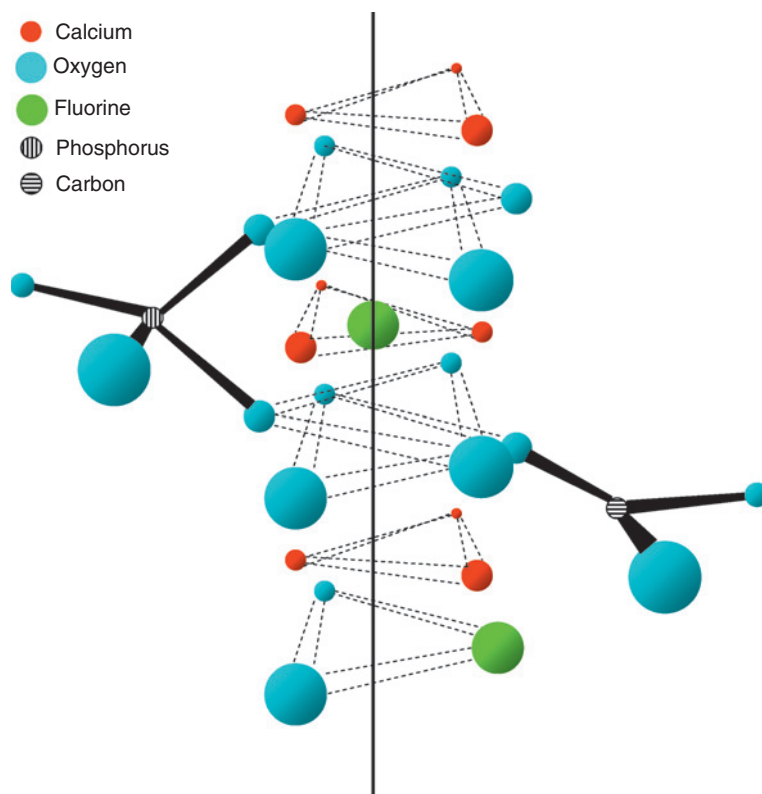


Fig. 3. Split view of atoms along the c axis of the hexagonal structure showing the two possible fluoride ion locations. In stoichiometric fluorapatite, fluoride ions locate in the equilateral triangle formed by Ca(II) ions. In type B carbonate apatite, the replacement of PO_4^{3-} ions by CO_3^{2-} ions creates an oxygen atom vacancy which may be occupied by a second kind of fluoride ion (adapted from Ref. [4]). (See Colour Plate Section at the end of this book.)

mechanism. In most cases, however, and especially in biological apatites, such couples do not form or are rare, and the charge compensation mechanism which occurs involves the creation of one cationic vacancy, on a Ca(II) site, and one monovalent anionic vacancy (OH^- or F^-) [12].

Substituting the original ions of calcium phosphate fluorapatite often leads to changes in the unit-cell parameters. Frequently, the variations of the unit-cell dimensions are proportional to the substitution ratio and follow 'Vegard's law' (i.e. the unit-cell parameter varies linearly with the substitution ratio). This is the case, for example, with chlor-fluorapatite.

3.3. Physico-chemical characterisation of fluoridated apatites

Several techniques have been used to characterise fluoridated apatites, especially XRD, fourier transform infrared (FTIR) spectroscopy and solid-state nuclear magnetic resonance (NMR).

3.3.1. X-ray diffraction

The XRD pattern of FA is reported in Fig. 4. It is characteristic of the apatite structure. This pattern is very analogous to that of HA. Fluoride substitution for OH is related to a decrease in the *a* unit-cell dimension and a very slight increase in the *c* unit-cell parameter.

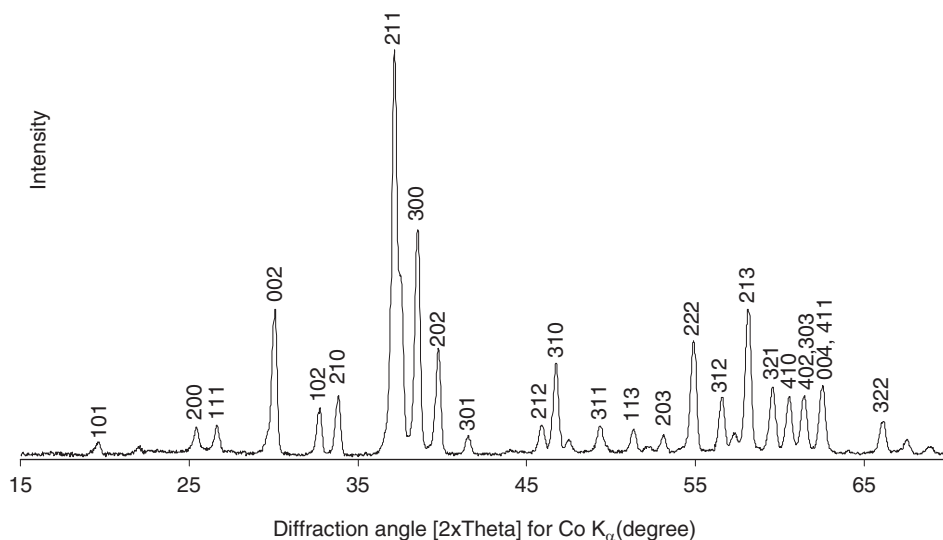


Fig. 4. X-ray diffraction (XRD) pattern of nearly stoichiometric fluorapatite.

3.3.2. FTIR spectroscopy

Many vibrational spectroscopic investigations (FTIR and Raman) concerning FA have been reported, in particular, in the early works of Baddiel and Berry [15], Bhatnagar [16], Levitt *et al.* [17] and Klee [18]. Some studies also relate, among others, to the far-infrared region [19] and to the influence of high-pressure conditions [20]. In particular, these techniques have been used for comparative analysis of FA with other apatites, such as HA or chlorapatite.

The vibration bands relative to phosphate groups in the apatite structure differ from the normal modes of the PO_4^{3-} isolated ion, due to distortions of the PO_4 tetrahedra in the apatite lattice and vibrational coupling [4]. Therefore, site-group and factor-group analyses were applied [15,16,18,21] to elucidate the vibrational spectra observed (Fig. 5) and band assignments of infrared (IR) and Raman bands have been given (Table 3).

Interesting observations have been made on mixed fluorhydroxyapatites. Several additional OH bands were observed in the stretching domain and in the librational domain depending on the substitution ratio [4,21,22]. In stoichiometric HA, the OH bands appear at 3570 and 633 cm^{-1} , respectively. In fluorapatite containing few OH^- ions, these have F^- ions as neighbours, and the OH band positions are shifted to 3540 and 747 cm^{-1} because of strong hydrogen bonding with the electronegative F^- . When the OH^- content is increased several other bands may appear (3547 ; 720 cm^{-1} and 670 cm^{-1}), depending on the different possible environments of OH^- ions with uncertain assignments, as discussed in the following paragraph.

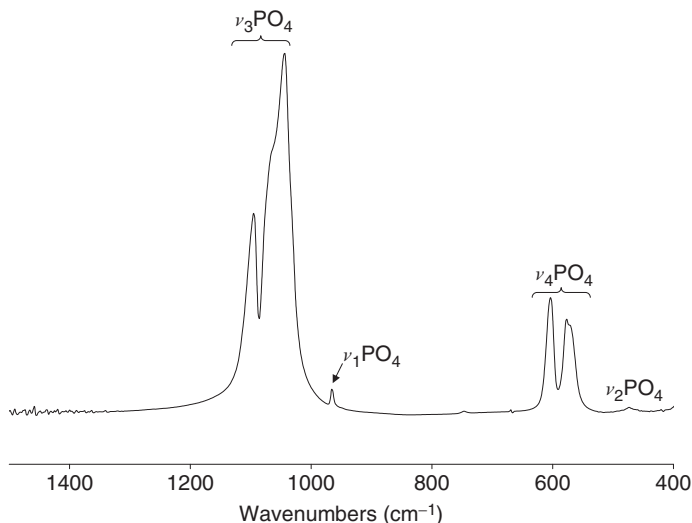


Fig. 5. FTIR spectrum (ν_1 , ν_2 , ν_3 and ν_4 PO_4 domains) of nearly stoichiometric fluorapatite.

Table 3. Infrared (IR) and Raman band positions and assignments for stoichiometric fluorapatite

Vibrational domain	Assignment C _{6h} factor group symmetry	Raman (cm ⁻¹)	IR (cm ⁻¹)
ν_1	A _g , E _{2g} , E _{1u}	965	965
ν_2	E _{1g}	432	
	E _{2g}		
	A _g	449	
	E _{1u}		460
	A _u		470
ν_3	A _u , E _{2g}	1034	1032
	E _{1g} , E _{1u}	1042	1040
	A _g	1053	
	E _{2g}	1061	
	A _g	1081	
	E _{1u}		1090
	A _u		560
ν_4	E _{1u}		575
	E _{2g}	581	
	A _g , E _{1g}	592	
	E _{1u}		601
	A _g	608	
	E _{2g}	617	

3.3.3. Solid-state NMR

In the last two decades, high-resolution solid-state nuclear magnetic resonance (NMR) has become the method of choice for investigating the chemical environments and local structures of calcium phosphate biomaterials and related materials such as bone mineral and dental enamel. Although the main constituents (Ca, O, H, F, C, P) of these biomaterials have a nuclear spin, only ¹H, ¹⁹F, ¹³C and ³¹P solid-state NMR have been measured. The ⁴³Ca and ¹⁷O, both of which should give interesting results, particularly on the local structure of apatite, have a very low natural abundance (0.045% for ⁴³Ca and 0.037% for ¹⁷O) and lead to very poor NMR detection; therefore, they have not been studied. The NMR detection of these two nuclear spins requires the samples to be isotopically labelled. This labelling is excluded because of the very high cost of these isotopes, in particular ⁴³Ca.

Concerning synthetic fluoridated calcium phosphate biomaterials (i.e. fluorapatites, fluorhydroxyapatites, carbonated fluorhydroxyapatites and other calcium

phosphates grown with F^- ions), few solid-state NMR studies have been reported [23–50] by comparison with other calcium phosphates. These studies mainly focus on the local environments of hydrogen, fluorine and phosphorus atoms located in the bulk as well as at the sample surface, and on the effect of some substitution on these local environments. In addition, the existence of a quasi one-dimensional distribution of fluorine and hydrogen spins in apatites presents, from a solid-state NMR theoretical standpoint, an interesting model for developing multi-quantum (MQ) coherences [27,32,36,46] and for studying spin echo formation and line shape of spins coupled with dipole–dipole interactions in a linear chain [47,48].

3.3.3.1. ^{19}F NMR

Except in fluorapatite doped with Sb^{3+} [49], weakly hydroxylated carbonate-fluorapatite [39] and apatite/OCP/apatite lamellar mixed crystals grown in the presence of F^- [35], the ^{19}F NMR spectrum of fluorapatite and fluorhydroxyapatite, obtained either by single-pulse (SPE) [24,31,32] or multi-pulse [30] excitations, both combined with magic angle spinning (MAS), consists of a single line whose position and width significantly depend on the fluorine content [24,29,34]. For pure stoichiometric fluorapatite, the position of the ^{19}F MAS NMR line was located at 62–64 ppm from C_6F_6 [24,30,31,34,37,45]. In fluorhydroxyapatite with low fluorine content (13%), this line is located at ~ 59 ppm and gradually shifts downfield as the relative fluorine content increases [34]. This shift is accompanied by a decrease in the linewidth from ca. 3 ppm to ca. 1.1 ppm when the relative fluorine content goes from ca. 13% to ca. 90%. For comparison, the ^{19}F SPE-MAS NMR linewidth measured for pure fluorapatite is 0.5 ppm [32]. This linewidth value could, however, differ from one sample to another, depending on the preparation conditions and therefore on the crystallinity of the pure fluorapatite. The presence of OH groups in fluorhydroxyapatite is the main cause of the change in both the ^{19}F isotropic chemical shift and the linewidth versus the fluorine content. The latter is mainly due to a chemical shift distribution. The presence of OH groups induces a modification in the fluorine environments, involving displacements of both OH groups and fluorine from their normal position (with respect to the positions of fluorine and OH groups in fluorapatite and HA, respectively). These displacements lead to a distortion of the fluorine electronic environment and, therefore, to a modification of the isotropic chemical shift. The decrease in the ^{19}F linewidth with increasing fluorine content (or decreasing OH groups content) is related to a reduction in the ^{19}F isotropic chemical shift distribution. This distribution of the chemical shift arises from the different arrangements of the fluorine atoms along the apatitic channel (e.g. F-F-F, OH-F-F, OH-F-OH). In addition, some of these arrangements, such as the last two, offer different possibilities depending on the hydrogen-bonding scheme of OH^- with adjacent F^- . Therefore the decrease in the chemical shift distribution is directly related to the decrease in the number of both arrangements and configurations with increasing fluorine content. These fluorine arrangements lead to the formation of fluorine cluster chains of different sizes as shown by ^{19}F MQ NMR measurements [36]. Similar

results were obtained by the same authors by using ^1H MQ NMR measurements. In addition, the use of ^{31}P - ^{19}F rotational echo double resonance (REDOR) NMR experiments made it possible to determine in pure fluorapatite and in fluorhydroxyapatite, the P-F connectivities and the nearest inter-nuclear distance of the two nuclei, by observing ^{31}P and ^{19}F , respectively [50]. In the case of pure fluorapatite, this distance was found to be consistent with that determined by XRD (3.6 Å). When some of the PO_4^{3-} ions were replaced by CO_3^{2-} ions (weakly hydroxylated type B carbonate-fluorapatite), the ^{19}F SPE-MAS NMR spectrum (Fig. 6-c) contained one additional peak (78 ppm) besides that (64 ppm) of the unperturbed fluoride ions in the apatitic channel [39].

The 2-D heterocorrelation chemical shift (HetCor) NMR measurements [39] have clearly shown that the additional peak would correspond to fluoride ions closer to CO_3^{2-} ions located at the sites of the phosphate groups (two CO_3^{2-} occupancy sites were revealed by $^1\text{H} \rightarrow ^{13}\text{C}$ CP-MAS NMR: located at PO_4^{3-} and in the vicinity of water molecules probably near the apatite surface, respectively), rather than to PO_4^{3-} ions (Figs. 6 and 7). Indeed, the intensity of the additional peak at 78 ppm was considerably enhanced by ^{13}C of carbonate ions, and less so by the ^{31}P of phosphate groups. Therefore, this additional peak was assigned to fluoride ions located at the oxygen vacancies arising from the replacement of some PO_4^{3-} ions by CO_3^{2-} (as shown in Fig. 3). In addition, the 2-D $^{13}\text{C}\{^{19}\text{F}\}$ HetCor revealed that the peak assigned to unperturbed fluoride ions (64 ppm) is structured, indicating therefore

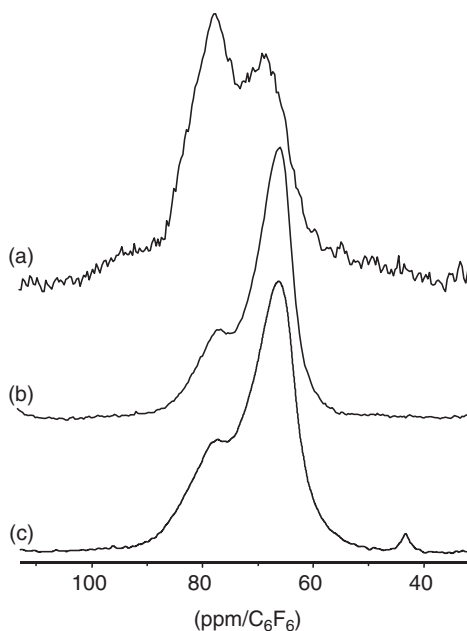


Fig. 6. ^{19}F 1-D MAS-NMR spectra of type B carbonated fluoroapatite weakly hydroxylated (a) ^{19}F projection of $^{13}\text{C}\{^{19}\text{F}\}$ HetCor MAS-NMR spectra, (b) ^{19}F projection of 2-D $^{31}\text{P}\{^{19}\text{F}\}$ HetCor MAS NM, (c) ^{19}F SPE-MAS NMR spectrum.

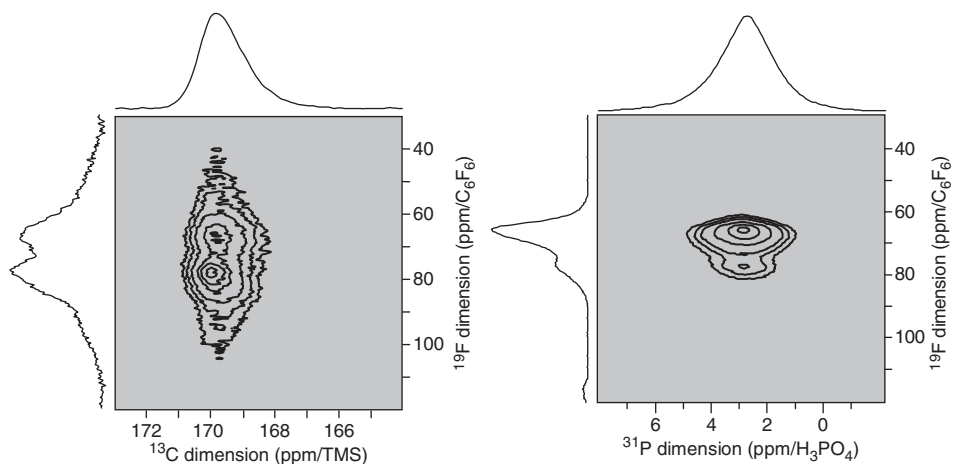


Fig. 7. Contours plots and projections of 2-D $^{13}\text{C}\{^{19}\text{F}\}$ (left) and $^{31}\text{P}\{^{19}\text{F}\}$ (right) HetCor MAS NMR of type B carbonate fluorapatite weakly hydroxylated [39].

the existence of different fluorine sites in the apatitic channel and the presence of ammonium fluoride impurity in the sample (peak at ca. 90 ppm, see Fig. 6a).

Another interesting aspect of ^{19}F SPE-MAS NMR measurements concerned the monitoring of the fluoridation of HA surfaces [24,27,29,31,50]. This aspect is particularly important for better understanding the effective proven role of fluoride in the prevention of dental caries. When the HA sample was exposed for several days after its preparation to a low concentration of fluoride ions, the ^{19}F SPE-MAS NMR spectrum contained a single peak located at 1.4 ppm upfield from that of fluorapatite [24,27]. This peak, position and spinning sideband intensity both resembled the spectrum of the fluorhydroxyapatite solid-solution sample (with a fluorine substitution ratio in the range 40–80%), was identified as an initially formed fluoride species. This result enabled the authors, on the basis of the surface area and the percentage of fluoride present in the sample, to determine the number of fluoride ions per surface hydroxyl. After 6 months, the ^{19}F SPE-MAS NMR spectrum of the same powder sample changed to one characteristic of fluorapatite and did not change further over additional months. For these authors, this solid transformation was due to the fluoride ions diffusing over the surface of the crystallites. When the HA sample was exposed to a high concentration of fluoride ions, the ^{19}F SPE-MAS NMR measurements indicated the presence of a mixture of calcium fluoride and fluorapatite, characterised by a broad and narrow line, respectively, located at about the same position.

3.3.3.2. ^1H NMR

The use of ^1H NMR to investigate the structure of fluoridated apatite appears to be of crucial importance, particularly for determining the active surface sites, suggested to be calcium hydroxyl (Ca-OH) and phosphorus (POH) groups [51],

as well the location of water molecules (particularly important for understanding their role in bone mineral structure and architecture), and the configuration of hydroxide and fluoride ions along the apatitic channel. The ^1H SPE-MAS NMR spectrum of pure fluorapatite [25] mentioned earlier contained a very intense line at ca. 6 ppm and a tiny peak at ca. 1.5 ppm from tetramethylsilan (TMS). They were attributed to adsorbed water and to hydroxyl groups singly hydrogen-bonded to fluorine ($\text{O-H}\cdots\text{F}$) in the apatitic channel, respectively. The presence of the tiny peak has therefore revealed that the OH groups cannot be entirely replaced by fluoride ions in precipitated samples. However, the amount of the non-substituted OH remains very low (trace amount). More recently, the ^1H SPE-MAS NMR spectra obtained from various pure fluorapatites prepared in different experimental conditions (pH and temperature) were more structured, particularly in the region 5–9 ppm [41,42,43]. Indeed, in addition to the peak of adsorbed water (5.9 ppm), two unresolved peaks at 6.9 and 7.8 ppm were observed and two resolved peaks at 3.8 and 0.9 ppm. The two peaks at 6.9 and 7.8 ppm were assigned to surface protonated phosphates. However, this assignment, particularly the peak at 6.9 ppm is, as far as we know, questionable: it is well known that NH_4F groups and NH_4^+ ions, used in the preparation of the samples as $(\text{NH}_4)_2\text{HPO}_4$ and NH_4F , give ^1H NMR peaks at ~ 7 ppm. Therefore the presence of one or both species in fluorapatite lattice, as clearly shown in weakly hydroxylated carbonate-fluorapatite [39], cannot be excluded. The peak at 0.9 ppm, which increased in intensity with decreasing pH, was assigned by the authors to surface Ca–OH sites, contrary to a previous assignment to apatitic OH (peak at 1.5 ppm) proposed by Yesinowski [25]. The peak at 3.8 ppm, which also increased in intensity with decreasing pH, was not assigned. When some of the fluorapatite samples were dried at 200°C , the peak at 5.9 ppm split into three weakly resolved peaks (5.9, 5.3 and 4.7 ppm) attributed to different surface protons, and that at 0.9 ppm split into two peaks (0.9 and 1.3 ppm).

The difference in the ^1H MAS NMR results obtained by the different authors mentioned indicated that the structure of fluorapatite is not uniform and seems to depend greatly on the preparation conditions (pH, temperature treatment, etc.) of the samples.

The ^1H SPE-MAS NMR spectra of fluorhydroxyapatites, having different fluorine content, are similar to those of the pure fluorapatite [25], except in the 1.2–2.5 ppm region, related to hydroxyl groups in the apatitic channel. Indeed, the single peak observed at 1.5 ppm in pure fluorapatite splits into four peaks (0.3, 1.2, 1.5 and 2.5 ppm), reflecting the perturbation of the OH electronic environments by the presence of fluoride ions, similarly to the ^{19}F SPE-MAS NMR results discussed above. More precisely, the splitting into four peaks means the existence of four different environments or configurations of OH^- ions in the apatitic channel characterised by different electronic environments. In other words, the result means that the OH groups were perturbed differently, probably among their positions inside the apatitic channel.

The existence of different peaks in the 0–2 ppm region was also observed in carbonate-fluorapatite [39]. The peak at 0.3 ppm, which decreases in intensity with increasing fluorine content and which is at practically the same position (0.2 ppm) as that of apatitic OH in pure HA, was assigned to unperturbed OH groups. The peak at 1.2 ppm, which was better resolved in samples with a low fluorine content (high hydroxide content), was assigned to the $\text{OH}\cdots\text{F}\cdots\text{HO}$ configuration and the one at 1.5 ppm, whose relative intensity increased with the increasing fluorine content, to the ' $\text{O-H}\cdots\text{F}$ ' and/or ' $\text{OH}\cdots\text{F HO}$ ' configurations. The distribution of OH groups in the apatitic channel was also investigated by ^1H MQ NMR [36], and the results obtained show the existence of an OH cluster chain, as for the fluoride ions discussed above in the ^{19}F NMR section.

3.3.3.3. ^{31}P NMR

Unlike the ^1H and more particularly the ^{19}F NMR, only very few NMR results were reported for the ^{31}P NMR of fluoridated apatites, including fluorapatites, fluorhydroxyapatites and carbonate-fluorapatites [34,39,41–43,49]. This fact is probably related to the smaller quantity of chemical and structural information that could be obtained by ^{31}P NMR, compared to the observation of ^{19}F and ^1H . In the case of pure fluorapatite, as well as for isostructural HA, one should expect a single ^{31}P SPE–NMR line whose characteristics (particularly width) would depend mainly on the crystallisation state of the investigated sample. However, the different ^{31}P NMR results reported in the literature differ between authors, particularly in the chemical structure point of view. This appears as a consequence of the non-uniformity of the fluorapatite structure, which seems to depend significantly on the preparation conditions, as mentioned above. As expected, the first ^{31}P SPE–MAS NMR spectra, obtained from pure fluorapatite [23,49], exhibited a single narrow line (0.4 ppm width at half maximum) located at the same position as that of HA (2.8 ppm from 80% H_3PO_4). This line, similar to that observed in weakly hydroxylated carbonate-fluorapatite [39], although slightly asymmetric in the latter case, was due to bulk phosphate groups. In addition to this line, the ^{31}P SPE–MAS NMR spectra obtained by Braun *et al.* [34] in non-heat-treated and heat-treated pure fluorapatite showed a supplementary resolved peak at 5.1 ppm and a less resolved one at 0 ppm. These two peaks, whose intensities considerably decreased in the heat-treated sample, were assigned to TCP impurities ($\alpha\text{-Ca}_3(\text{PO}_4)_2$ and $\beta\text{-Ca}_3(\text{PO}_4)_2$). In more recent work reporting on various fluorapatites obtained in different preparation conditions (pH, temperature) [41–43], the ^{31}P SPE–MAS NMR line originating from bulk phosphate groups (2.9 ppm) was accompanied by an upfield shoulder (0.8–1 ppm) of relatively very weak intensity. The use of $^1\text{H} \rightarrow ^{31}\text{P}$ CP–MAS, making it possible to distinguish phosphorus strongly coupled with the protons from weakly coupled phosphorus, revealed the presence of one or two additional peaks (5.4 and—4.5 ppm) depending on the preparation conditions (particularly

the pH) of the sample. On the basis of the cross-polarisation times, these peaks (-4.5 , 0.8 and 5.4 ppm) were assigned to surface protonated (0.8 and 4.5 ppm) and un-protonated (5.4 ppm) phosphate groups.

3.3.4. Difficulties related to the characterisation of fluoridated apatites

One of the main problems, rarely addressed, raised by solid solutions involving apatite compounds, concerns the homogeneity of distribution of the ions between the different parts of the apatite crystals. Several cases of heterogeneous distribution of mineral ions have been reported in tooth enamel crystals, for example, where fluoride ions have been found to preferentially concentrate at the surface of the crystals [52]. It can be considered that for samples heated at high temperatures, there is either a decomposition into different phases or a homogeneous distribution of the different ions of the solid solution in the crystal due to thermal agitation mixing. The homogeneous distribution may be preserved at low temperatures depending on the cooling rate and the ions involved.

When considering samples obtained at low temperature, however, ion diffusion cannot reasonably be involved, and several cases of inhomogeneous ion distribution have been reported. This heterogeneous distribution affecting the surface ions particularly enables the crystal surface to equilibrate with the surrounding fluids, whereas the core of the crystal keeps its original composition. This effect could explain some divergences in peak assignments and positions using spectroscopic methods and discrepancies appearing in the physico-chemical properties of solid solutions, especially those obtained at low temperatures compared to those obtained at high temperatures.

4. PHYSICO-CHEMICAL PROPERTIES OF FLUORIDATED APATITES

Fluoride ions considerably change the physico-chemical properties of apatites and particularly their dissolution properties.

4.1. Dissolution properties of fluoridated apatites

Fluorapatite is a highly insoluble calcium phosphate phase. The solubility product of stoichiometric fluorapatite at 37°C is $3.19 \pm 0.14 \times 10^{-61} \text{ mol l}^{-1}$ (for $\text{Ca}_5(\text{PO}_4)_3\text{F}$ as reported by Moreno *et al.* [53]) and appears significantly lower than that of HA in the same conditions ($7.36 \pm 0.93 \times 10^{-60} \text{ mol l}^{-1}$ for $\text{Ca}_5(\text{PO}_4)_3\text{OH}$). A suggested explanation for this very low solubility product is that cohesive forces are stronger in fluorapatite than in other apatites due to smaller unit-cell dimensions. The complete solid solution $\text{Ca}_{10}(\text{PO}_4)_6(\text{OH})_{2-x}\text{F}_x$ can be obtained. Initial solubility determinations have shown a solubility minimum for x close to 1 [54], related to the formation of hydrogen bonding between F^- and OH^- ions. These results were subsequently

discussed and it was concluded [55] that, at low pH levels, the solubility of solid solutions was reduced for increasing values of x . Verbeeck *et al.* [56] have indeed shown that at pH 4 and 5 substituting a few per cent of OH^- by F^- was sufficient to reduce solubility by a factor of 2. However, in this case it is probable that fluoride ions are mainly located at the surface of the crystals, thus inducing large composition and solubility changes with a low-bulk concentration. At higher pH values though, greater substitution levels were needed to obtain the same effect.

Solid solutions between carbonated HA and fluorapatite occur naturally in the body, in bone and teeth. In particular, the presence of fluoride ions offers the low solubility and good acid resistance needed for protecting teeth [57]. Note, however, that at very high pH levels, the HA end-member becomes less soluble than fluorapatite [58]. That is why it is often difficult to prepare stoichiometric fluorapatite by precipitation methods involving generally alkaline pH levels.

Also, substituting fluoride ions for OH^- in HA generally leads to a phase with greater crystallinity [59].

4.2. Fluoridation reactions

When HA is in contact with a fluoride-containing solution at low concentration, this F^-/OH^- substitution mostly occurs at the crystal surface [60] and can be accompanied by the formation of CaF_2 as a secondary phase in acidic media (Fig. 8). The fluoride ions fixed on the HA crystal surface after exposure to a fluoride-containing solution were found to be coordinated by three calcium ions, as with the regular fluorapatite structure [61]. The fluoride uptake was shown to

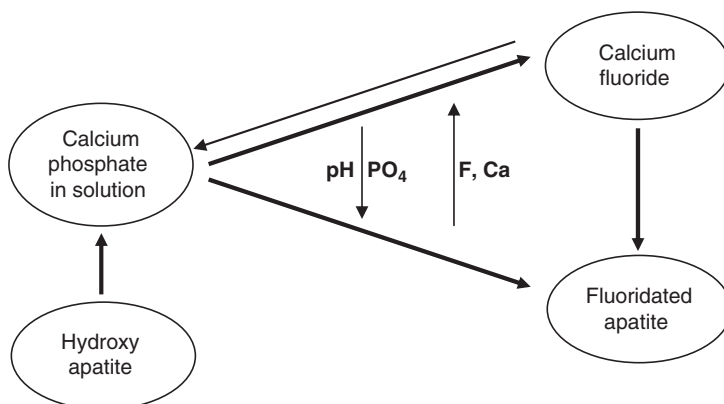


Fig. 8. Evolution of synthetic and biological apatites in the presence of fluoride ions. The increase of pH and/or phosphate concentration in solution favours the formation of fluoridated apatite, whereas the increase of fluoride and/or calcium concentration favours CaF_2 formation. At physiologic pH and mineral ions concentrations (in all body fluids), the formation of fluoridated apatite is favoured.

be dependent on the fluoride solution pH [62]. At low pH (typically around 4), the partial decomposition of HA was observed, accompanied by the precipitation of CaF_2 . In contrast, at higher pH values, HA progressively converted to FA. However, these reactions generally gave rise to very heterogeneous apatite solid solutions. It has been suggested that loosely bound (sometimes qualified as 'adsorbed') fluoride ions play a determining role in the fluoridation of apatite, especially in the case of dental enamel [63].

4.3. Thermal stability

Other physico-chemical characteristics of fluorhydroxyapatites also vary with the amount of fluoride. In particular, Chen *et al.* [64] showed, based on thermogravimetry and XRD data, that the thermal stability of $\text{Ca}_{10}(\text{PO}_4)_6(\text{OH})_{2-x}\text{F}_x$ phases increased remarkably for x values greater than 0.8, as compared to pure HA. These authors also reported an increase in the sintering onset temperature for fluoridated HA-based ceramics, as well as a retardation of the densification of such ceramics compared to fluoride-free compacts. Other authors [65] indicated, in the case of the HA–FA solid solutions, a minimum of densification for the compound $\text{Ca}_{10}(\text{PO}_4)_6(\text{OH})_{2-x}\text{F}_x$ with $x = 1$, corresponding to the substitution of 50% of the hydroxide ions in HA by fluoride. The sintering ability of such compounds was related to the diffusion of hydroxide and fluoride ions. The existence of hydrogen bonding between these ions [22] induced a stabilising effect becoming maximum for $x = 1$, assuming a homogeneous distribution of fluoride and hydroxyl ions in the channels. This variation with x is also paralleled by the evolution of the solubility product as shown by Moreno *et al.* [53].

The thermal decomposition of non-stoichiometric FA and HA seems very close and depends on the Ca/P ratio, although the presence of fluoride in precipitating solutions generally tends to decrease the vacancy content [66]. Ca/P ratios lower than 1.67 lead to the formation of fluor- (or fluorhydroxy-) apatites and TCPs, whereas Ca/P ratios higher than 1.67, observed, for example, in the case of carbonate-fluorapatites, lead to the presence of calcium oxide and fluorapatite, possibly associated with CaF_2 according to the amount of fluoride in the structure. The high-temperature thermal decomposition of stoichiometric FA and HA on the contrary shows great dissimilarities. Depending on the water partial pressure, HA can decompose at temperatures as low as 800°C [67], giving rise to oxyapatite which then decomposes into TCP and calcium oxide and/or tetracalcium phosphate. Fluorapatite on the contrary appears much more stable and melts at 1644°C [68]. A surface hydrolysis of FA crystals was observed on heating in the presence of water vapour above 900°C [115], leading to the formation of hydroxylated apatite associated with a loss of fluoride.

4.4. Thermodynamic characteristics

The standard enthalpies and free energies of FA and HA have been extensively studied (see review by Tacker and Stormer [69]). Despite some discrepancies among the values reported, probably due for the most part to the presence of impurities in the samples investigated, substantive differences can be pointed out between the thermodynamic data corresponding to the two phases. Of particular importance is the difference in standard (Gibbs) free energy $\Delta G^\circ_{298.15}$ between the two phases. It can be estimated from averaging the values listed by Tacker and Stormer [69] (and thus disregarding possible discrepancies) to about -6459.2 kJ/mol for FA and -6315.8 kJ/mol for HA, considering the chemical formula $\text{Ca}_5(\text{PO}_4)_3\text{X}$ with $\text{X} = \text{OH}$ or F . This point establishes the greater thermodynamic stability of fluorapatite.

Interestingly, the standard entropies (and in turn heat capacities) of both phases were found to be rather similar [69,70]. Considering the difference in standard entropy between $\text{F}_2(\text{gas})$ and the mixture $\text{O}_2(\text{gas}) + \text{H}_2(\text{gas})$ taken in their standard states (which can be extracted from general thermodynamic tables), the difference between the entropy terms of the Gibbs function relative to HA and FA, around room temperature, is about 6.5 times lower than the difference between enthalpy terms (close to 125 kJ/mol as estimated from Tacker and Stormer [69]). This indicates that FA higher stability is mostly due to the lower enthalpy of formation of FA (more exothermic than for HA), and that it is not greatly affected by entropic factors. Jemal *et al.* [71] have studied some of the thermodynamic properties of FA and HA with varying cationic substitutions, and these authors linked the lower enthalpy of formation of FA compared to HA to the decrease in lattice volume in FA.

In addition to end-member phases, such as fluorapatite and HA, several studies have reported thermodynamic data related to solid solutions of apatite with various cations involving substitutions like Ca-Mg, Ca-Cd, Ca-Pb and Ca-Sr [72–74]. The related enthalpies of mixing were obtained, and their variation versus composition was generally indicative of a non-statistical occupancy of the cationic sites of the apatitic structure. In some instances, the limits of cationic substitution for calcium were estimated (e.g. in the range 0.073–0.101 for Ca-Mg fluorapatites according to Ben Abdelkader *et al.* [74]).

4.5. Surface characteristics

4.5.1. Surface energy

The surface energy of fluorapatite as compared to HA was recently determined by Wu and Nancollas using different techniques [75]. The data indicate that, whatever the technique used, FA exhibits a higher surface tension than HA (e.g. 18.5 mJ m^{-2} for FA compared to 10 mJ m^{-2} for HA, using contact angle

determinations). This observation may be related to the adsorption properties, although physical parameters seem to explain only part of the adsorption behaviour.

4.5.2. Surface charge

The surface charge of FA and HA is determined by several ions from the solution (hydroxide, fluoride, phosphate, calcium, but also foreign species such as magnesium and carbonate) [76]. The apatite surface at low pH levels is more positive than at a high pH probably because of the greater hydrolysis of surface PO_4^{3-} groups, giving surface HPO_4^{2-} groups. The point of zero charge for FA (6.8) is lower than that for HA (8.5) [77], indicating possibly a change in the hydrolysis properties of surface phosphate groups (more difficult protonation).

4.5.3. Adsorption properties

The adsorption of tooth enamel-related proteins has been investigated on apatite samples with varying F/OH ratios [78]. The results obtained in this study showed that the amount of adsorbed proteins increased with the degree of fluoridation. These effects could be related to a less polar surface for fluorapatite compared to HA [75], although stronger chemical interactions cannot be discarded in protein adsorption. Biological studies have also revealed that fluoridation induced a stronger retention of proteins involved in developing enamel, especially ameloblastin, impairing the development of mineralisation [79]. The use of atomic force microscopy (AFM) in chemical force mode has shown that the binding strength of carboxyl- or hydroxyl-groups was stronger on apatite surfaces when fluoride was present [80]. These enhanced adsorption properties of fluorapatite compared to HA have led to the commercialisation of fluoridated apatites for chromatographic separation.

4.6. Fluoridation effects

Eanes and Hailer [81] studied the effect of fluoride addition on the size and morphology of apatite crystals in close-to-physiological conditions. These authors in particular reported that fluoride uptake was accompanied by some anisotropic growth of the apatite crystals: the width and/or thickness of the crystals increased with F uptake while no noticeable change in length was observed. In addition, LeGeros *et al.* [66] pointed out the decrease in calcium deficiency linked to a progressive fluoride incorporation.

Finally, other effects of fluoride addition to HA have been investigated. In particular, the electrical conductivity of HA was found to be modified with fluoride substitution, as an increase in conductivity was observed [82] for OH–F apatites where up to 50% of OH^- ions were replaced by F^- . Beyond this proportion, however, a sharp drop in conductivity was pointed out. It seems, however, difficult to

explain these data. Another point of interest is that the HA surface is more negatively charged when F^- ions are attached to the crystal surface, in agreement with the variations of the points of zero charge, whereas it becomes more positively charged when CaF_2 forms [79]. This behaviour might be crucial in protein adsorption and cell attachment, which depend closely on the surface charge of the substrate.

The effect of fluoride ions on nanocrystalline (poorly crystallised) apatites analogous to bone mineral has only recently been investigated [83]. This effect was studied using a solution containing both fluoride (at low concentration) and phosphate ions, as the presence of F^- alone (especially at high concentrations) could lead to the precipitation of CaF_2 . Precipitated biomimetic nanocrystalline apatite crystals are characterised by the presence on their surface of a hydrated layer containing bivalent mineral ions corresponding to labile non-apatitic environments identifiable using spectroscopic methods [84]. This layer determines the evolution and chemical properties of apatite nanocrystals. After treatment of nanocrystalline carbonate-apatites with the phosphate–fluoride solution, a noticeable increase in the $Ca/(P+C)$ ratio was observed, testifying to a decrease in the amount of cationic vacancies. FTIR observation of the ν_3 vibration mode of carbonate ions showed that after treatment in the phosphate–fluoride solution, the relative intensity of the bands attributable to apatitic carbonate environments increased, whereas that of the band located close to 1500 cm^{-1} and assigned to non-apatitic carbonate species decreased. In the ν_2CO_3 vibration domain, a new thin carbonate band was noticed at 866 cm^{-1} in addition to type A (880 cm^{-1}) and type B (871 cm^{-1}) present in the original sample. The additional band has already been observed in synthetic well-crystallised apatites and assigned to a (CO_3^{2-}, F^-) association replacing PO_4^{3-} groups [85]. The amount of labile PO_4^{3-} groups in the solid, as determined by self-deconvolution of FTIR spectra, was found to decrease slightly after contact with the phosphate–fluoride solution. These findings were explained by the evolution of the solid towards a more stoichiometric and stable apatitic structure upon fluoride incorporation, related in part to an alteration of the hydrated surface layer. These points also illustrate the difference in surface reactivity between stoichiometric apatites and non-stoichiometric poorly crystallised apatites analogous to bone mineral.

4.7. Mechanical properties of fluoridated apatite ceramics

The fatigue behaviour of pure hydroxy- and fluorhydroxyapatite-sintered bioceramics has been studied in ambient air, distilled water and simulated human saliva [86]. The authors observed that, as a general trend, HA ceramics exhibited a lower resistance to fatigue than fluoridated ones. Another work [87] showed that the hardness remained essentially unchanged until 80% of OH^- were replaced with F^- , whereas it noticeably increased with greater fluoride contents. The elastic

modulus was found to increase linearly with the amount of fluoride. Fracture toughness was found to be dependent on F incorporation. In the case of 95%-dense sintered pellets, the fracture toughness increased up to a fluoride substitution of about 60%, however, for greater F contents, it decreased rapidly indicating the existence of optimised fluoride content for mechanical resistance.

5. FLUOR-CONTAINING GLASSES AND CEMENTS

5.1. Fluor-containing glasses

Since the discovery of Bioglass® by Hench *et al.* in the early 1970s [88], several bioactive glasses and glass-ceramics have been found to bond to living bone and thus occupy important roles in bone-repairing materials. The bioactivity of bio-glasses is related to the diffusion of active ions such as calcium ions outside the glass; an apatitic layer can form heterogeneously on the glass surface involving ions both from the glass and the biological fluids [89]. First produced as ordinary glassware and then transformed into crystalline ceramics by thermal treatment, glass-ceramics combined the advantages of an ability to form complex shapes economically and precisely (initial glass stage) and fine-grained microstructure with little or no porosity (final crystallisation stage). Crystallisation is not always complete and the residual glass phase fills the grain boundary volume helping to create the pore-free microstructure. Several glass and glass-ceramic biomaterials have been extensively studied. However, from 1994 (when Vrouwenvelder *et al.* [90] pointed out the need to further investigate the physico-chemical properties and *in vivo* behaviour of fluoride-doped bioactive 45S5 Bioglass®) until now, the presence of fluorine and its role in these materials has not been well documented in the literature.

In Japan, a two-phase silica and fluor-containing phosphate material known as apatite-wollastonite glass-ceramic (AW-GC) has been studied and developed by Yamamuro and Kokubo's groups [91,92]. It consists of crystalline apatite ($\text{Ca}_{10}(\text{PO}_4)_6(\text{OH},\text{F})_2$) and β -wollastonite ($\text{CaO} \cdot \text{SiO}_2$) and a residual glassy matrix. Bioactive AW-GC are used clinically, especially in vertebral reconstruction and iliac crest repair [88,93]. AW-GC has a very regular structure with a small grain size and is resistant to interphase boundary attack. Despite their good mechanical strength, glass-ceramics cannot be implanted in load-bearing sites. The clinical use of bioactive glasses and glass-ceramic coatings on metallic implants has been limited because of interfacial degradation between metal and glass [88,92].

In Germany, a silica-phosphate glass-ceramic has been developed and used clinically. It consists of fluorhydroxyapatite ($\text{Ca}_{10}(\text{PO}_4)_6(\text{OH},\text{F})_2$) and phlogopite ($(\text{Na},\text{K})\text{Mg}_3(\text{AlSi}_3\text{O}_{10})\text{F}_2$), a type of mica [88,94–96].

Other examples of fluor-containing glasses and glass-ceramics have been studied in different systems [97,98]. For example, the preparation of glasses

and glass-ceramics with composition ranging in the ternary system tetrasilicic mica and fluorapatite-diopside (50/50% wt) has been reported to lead to materials exhibiting features such as attractive aesthetics, structural integrity and dense structure [98]. However, the mineralisation capability of the different glass-ceramics needs to be investigated to consider such compositions for biomedical applications.

Biocompatibility and castability of modified fluorcanasite ($\text{Ca}_5\text{Na}_4\text{K}_2\text{Si}_{12}\text{O}_{30}\text{F}_4$) glass-ceramics have been investigated and Bandyopadhyay-Ghosh *et al.* showed that incorporation of an excess of CaO or P_2O_5 in stoichiometric fluorcanasite glass composition along with controlled heat treatment improved osteoblast-like cell activity *in vitro* [99].

Generally, the composition ranges in which glasses and glass-ceramics bond with bone and other tissues is limited. Examples of composition and bending strength of commercialised fluor-containing glass-ceramics are reported in Table 4.

AW-GC has also been used as powder to prepare a bioactive cement for bone filling. The paste made from AW-GC powder and an acrylic resin (bisphenol- α -glycidyl methacrylate) hardens in a few minutes exhibiting a much lower curing temperature than a polymethylmethacrylate (PMMA) cement [100]. Yamamuro *et al.* showed that the mechanical and biological properties of such bioactive cements bonding directly with bone in 4–8 weeks *in vivo* are significantly higher than those of PMMA cements. The amount of AW-GC powder in the cement was found to be an important parameter for bone-bonding strength [101].

Glasses and glass-ceramics can also be used as coatings to impart enhanced biological properties to bioinert ceramics and metal implants. Bosetti *et al.* applied a fluorapatite-based glass-ceramic coating to a full-density alumina ceramic claiming to combine the mechanical properties of the bioinert alumina substrate with the bioactivity of the glass-ceramic coating involving the system fluorapatite-mullite glassy film ($\text{SiO}_2\text{-Al}_2\text{O}_3\text{-P}_2\text{O}_5\text{-K}_2\text{O-CaO-F}$) [102]. This coating consisted of hollow needle-shaped fluorapatite crystals embedded in glass and the authors showed that the coating favoured binding with plasma fibronectin, a protein that enhances osteoblast-like cell adhesion and spreading on its surface.

Ignatius *et al.* showed that a coating with Bioverit® I (see Table 4) improved osseointegration of alumina ceramics (higher interfacial shear strength and high quantity of newly formed bone in direct contact with the implant surface) especially in load-bearing conditions [103]. Verne *et al.* reported a vacuum plasma-sprayed composite coating consisting of Bioverit® I and titanium particles as a toughening phase, deposited on titanium alloy Ti6Al4V [104]. An example of a middle ear implant made of apatite-phlogopite glass-ceramics and titanium is given in Fig. 9.

Finally, Ti6Al4V can be coated with $\text{SiO}_2\text{-Al}_2\text{O}_3\text{-P}_2\text{O}_5\text{-CaO-CaF}_2$ using a sputtering process [105].

Table 4. Composition and mechanical properties of fluor-containing-glass-ceramics used clinically [88]

Glass-ceramics	Composition (wt %)								Phase Composition	Bending strength (MPa)
	Na ₂ O	K ₂ O	MgO	CaO	Al ₂ O ₃	SiO ₂	P ₂ O ₅	CaF ₂		
Cerabone® AW	0	0	4.6	44.7	0	34.0	16.2	0.5	Apatite and β -wollastonite	215
Ilmaplant®	4.6	0.2	2.8	31.9	0	44.3	11.2	5.0	Apatite and β -wollastonite	160
Bioverit®	3–8	3–8	2–21	10–34	8–15	19–54	2–10	3–23	Apatite and Phlogopite	100–160



Fig. 9. Photograph of two different shapes of middle ear implants made of Bioverit® II and titanium used for tympanoplasty (with permission of 3di) [<http://www.3di.de>].

5.2. Fluoridated cements

Another important use of fluoridated glass is in glass ionomer cements (GIC), covered in another chapter of this book. The main characteristic of the fluoridated glasses used in the GIC is to release active fluorine species, mainly fluoride ions and AlF_x . One may distinguish two types of fluoride releases: dissolution of a fluoridated precursor, which is an irreversible process in which the fluoride release is determined by the solubility properties of the precursor and diffusion in the matrix, or a reversible ion exchange process involving the glass or matrix constituents [106]. In the latter case, the GIC can function as a fluoride ion reservoir and can be reloaded with fluoride through topical applications or fluoridated mouth rinse [107–108].

An interesting use of fluoride ions was made to control the setting and hardening properties of self-hardening hydraulic calcium phosphate cements (CPC). These cements were first proposed by Chow [109]. They generally consist of a mixture of an acidic calcium phosphate salt with an alkaline calcium phosphate salt. On mixing in aqueous media the reaction leads to the formation of acicular apatite crystals which resulted in hardening. Several modifications of the original formula have been proposed [110,111] and some of them include fluoride ions as a soluble salt (NaF , generally) [112–113]. Fluoride ions favour the formation of apatite crystals and accelerate the hydrolysis reaction of the calcium salts originally present in the cement paste. The hardening reaction is accelerated and the mechanical properties are improved. In these cements the final product is a fluoridated apatite and, unlike in GIC, there is no spontaneous release of fluoride in the surrounding media after the hardening has been completed.

6. PREPARATION AND SYNTHESIS ROUTES OF FLUORIDE-CONTAINING APATITES

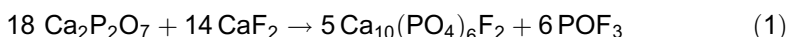
Synthetic fluor-containing apatites are prepared and investigated for biomedical applications and serve also as models to understand the formation of biological fluorapatites and some of their properties. The synthesis of fluoridated apatites has been accomplished in various ways from simple ion exchange in solution to more elaborate techniques involving sol-gel routes or thermal processes. Two main classes of synthesis routes are presented in this chapter: high-temperature routes and low-temperature solution routes.

6.1. High-temperature methods

Several high-temperature methods leading to fluoridated apatites can be found in the literature; they involve solid–gas reaction, pyrolysis or crystal growth processes.

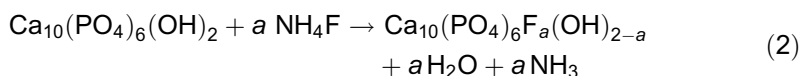
6.1.1. Solid–gas reaction

Fluorapatite can be prepared by heating a mixture of calcium pyrophosphate ($\text{Ca}_2\text{P}_2\text{O}_7$) and CaF_2 at 750°C [114,115]. POF_3 gas is formed according to the following chemical reaction equation:



Heating an intimate stoichiometric mixture of TCP ($\text{Ca}_3(\text{PO}_4)_2$) and CaF_2 for several hours at 900°C also leads to fluorapatite, which is better crystallised if the reaction is carried out at a higher temperature (1370°C) for 30 min and in a current of dry nitrogen with CaF_2 upstream to reduce volatilisation of fluorine [4,116].

Solid solutions of fluorhydroxyapatite ($\text{Ca}_{10}(\text{PO}_4)_6(\text{OH})_{2-x}(\text{F})_x$) can be prepared at high temperatures by gaseous fluoridation of HA powder; this leads to water and ammonia release, as follows [115]:

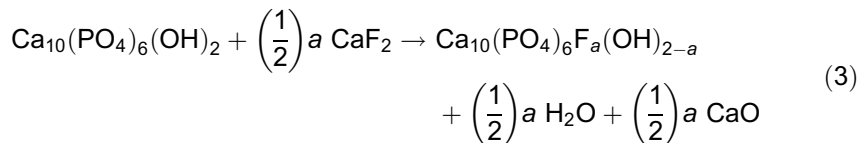


Other fluoridation agents can be involved. After 2 h at 900°C , fully fluoridated apatite ($a = 2$) is formed [115]. Applying this process to HA-dense ceramics leads to similar results.

This reaction involves ion diffusion in apatites and the reaction rate depends on the temperature, the size of the crystals and the porosity of the ceramics. At 900°C , the reaction is relatively fast and crystals of a few hundred microns can be totally exchanged in a few hours. The advantage of these processes is that they can be easily performed from existing HA powders or ceramics and

they do not generally disturb the ceramic microstructure (crystal size, porosity) provided that the exchange temperature is lower than 1000°C.

An alternative method for the fluoridation of HA involves solid-state reactions, for example, with CaF_2 above 900°C [116].



This method, however, leads to CaO formation which is not suitable for ceramic and coatings' stability in aqueous media.

The direct solid-state reaction of FA and HA can also be used to synthesise fluorhydroxyapatites. This reaction is, however, rather slow and gaseous fluoridation is preferred.

6.1.2. Pyrolysis method

More recently, Loher *et al.* reported the preparation of fluorapatite nanoparticles by the flame spray pyrolysis process [117]. The liquid precursor is obtained by dissolving calcium oxide in 2-ethylhexanoic acid and tributyl phosphate and has a molar ratio of $\text{Ca/P} = 1.67$. This liquid mixture, including trifluoroacetic acid as a fluoride source, is fed through a capillary into a methane/oxygen flame. Oxygen at 5 ml/min allows the liquid leaving the capillary to disperse. The set-up providing a stable pressure drop and stable combustion (sheath gas) leads to nanoparticles of fluorapatite. The as-synthesised fluorhydroxyapatite particles are spherical and highly agglomerated [0–30 nm in diameter with a specific surface area (SSA) of around 90 m²/g]. Then a thermal treatment at 700°C for 30 min followed by a quenching in air at ambient temperature leads to an open structure with interconnecting pores (SSA around 55 m²/g). This study showed that the flame pyrolysis process already established as an industrial-scale process for oxide nanoparticles preparation offers an interesting tool for calcium phosphate-based bioceramics engineering.

6.1.3. Crystal growth method

Single crystals (hexagonal prisms) of fluorapatite can be grown from melt composition at, or near, stoichiometry and in an argon atmosphere using the Czochralski method [118]. The hydrothermal method also allows fluorapatite single crystals to be obtained from an apatitic calcium phosphate phase and CaF_2 heated at 700°C for 72 h and under a pressure equal to $7.5 \times 10^7 \text{ N m}^{-2}$ [119].

6.2. Low-temperature methods

Several low-temperature methods involving different types of reactions (precipitation, hydrolysis, ion exchange, sol-gel processes) leading to fluoridated apatites can be found in the literature.

Figure 8 gathers the various schemes that can be involved in these solution-mediated synthesis routes depending on solution parameters (pH, fluorine, calcium and phosphate concentrations).

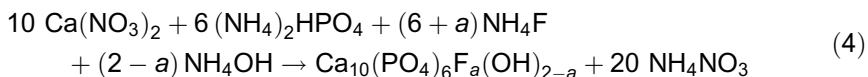
6.2.1. Hydrolysis method

When present in solution, fluoride ions readily become incorporated in the forming apatite prepared by either the hydrolysis or the precipitation method [120].

The hydrolysis of CaF_2 in solutions containing phosphates and carbonate ions results in the formation of fluor-, fluor-hydroxy- or fluor-carbonate-apatites. Fluor and fluor-hydroxy-apatites can also be formed by the hydrolysis of dicalcium phosphate (anhydrous or dihydrate), DCPA or DCPD, respectively, in solutions containing fluoride ions [121] or from the hydrolysis of any other calcium phosphate salt.

6.2.2. Precipitation method

Fluorhydroxyapatite can be synthesised by the traditional double-decomposition method generally used for apatite precipitation. An ammonium phosphate and fluoride solution (solution B) is added, dropwise, into a hot (generally at boiling temperature) calcium solution (solution A) at a basic pH level as previously published [122,123]. Fluorapatites close to stoichiometry are obtained ($a = 2$, see the following reaction equation); however, a very small residual amount of OH^- always seems to be present. Filtration and several washing operations are necessary to remove the counter-ions. The reaction is almost total due to the very low solubility of fluorhydroxyapatites.



Control of the pH and temperature of the precipitating solution is important to provide optimised conditions for stoichiometric, homogeneous, fluorhydroxyapatite formation. Similar conditions and set-up can be used for the synthesis of fluoride-substituted apatite crystals with varying size, crystallinity and morphology depending on the preparation temperature [124]; a purge of the synthesis system with nitrogen gas ensures the preparation of carbonate-free fluorhydroxyapatite at ambient temperature [125].

The synthesis of B-type carbonate-fluoroapatites was reported by Montel *et al.* with fluoride ions present in two kinds of sites in the apatitic structure [126]. Moreover, the correlation between the respective amounts of fluoride and

carbonate ions in such carbonate-fluorapatite solid solutions suggested a substitution of phosphate ions in apatite partially by the $(\text{CO}_3, \text{F})^{3-}$ association and partially by CO_3^{2-} .

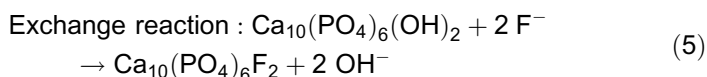
Okazaki *et al.* showed that for the same fluoride level supplied, the precipitation of fluorapatite using an organic phosphate source (phosphate ester monomer) instead of an inorganic phosphate source led to higher fluoride contents [127].

The synthesis of well-crystallised heterogeneous fluoridated apatites using a multi-step fluoride supply at 80°C and a physiological pH level was also reported [128]. This system allows the apatite crystal growth to be studied step by step with the increasing fluoride content. The authors proposed a multilayer fluoridated apatite crystal model including a HA core covered by several layers of fluoridated apatite whose boundaries were difficult to distinguish by high resolution transmission electron microscopy (HR-TEM).

Finally, control of fluorapatite particle size (from 15 nm to $200\text{ }\mu\text{m}$) and morphology can be achieved by varying precipitation conditions using aqueous precipitation from a micro-emulsion or by biomimetic synthesis in a gelatin matrix [129].

6.2.3. Exchange and/or dissolution–reprecipitation reactions

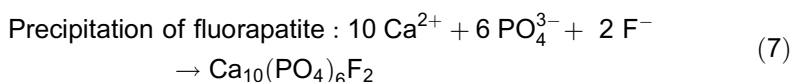
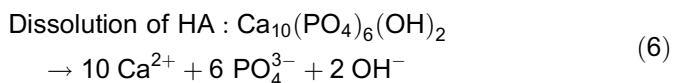
Low-temperature exchange reactions have been described for fluorhydroxyapatite solid solutions [115, 130, 131]. They generally occur in aqueous media and in most instances involve a dissolution–reprecipitation mechanism. Such reactions may be used to partly or totally modify the surface composition of ceramics or coatings. In order to observe such reactions, the resulting apatites should be less soluble than the starting compounds in the solution conditions [132]. This is the case, for example, with fluoride uptake by HA.



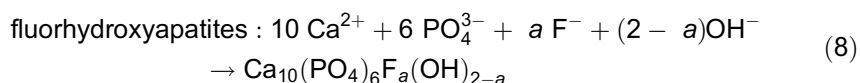
The reaction rate is strongly dependent on the size and stoichiometry of the crystals. For stoichiometric HA, this reaction is very slow especially at physiological temperature. Furthermore, because of the existence of a solid solution and epitaxial growth, surface equilibration may often occur, limiting the extent of the pseudo-exchange phenomenon. Such reactions may, however, be useful and they have been proposed for the transformation of coatings and ceramics surfaces [133]. They essentially lead to more stable, less resorbable coatings with increased surface area, nucleation ability and adsorption properties (see in the Fluoride-containing coatings sub-section).

The reactions between HA and fluoride ions in solution appeared complex and not fully understood. The most important factor controlling the course of the reaction is the fluoride ions concentration, but pH, surface area of the solid, its Ca/P

ratio, temperature and the presence of phosphate in the solution are other parameters affecting the reaction rate and products (Fig. 8). Having extensively studied fluoridation of HA at low temperature, Amrah Bouali showed that at a low fluoride concentration in solution, fluoridation may occur by superficial ion exchange ($F^- \leftrightarrow OH^-$) or by precipitation of fluorapatite or fluorhydroxyapatite [115]. However, the solution's ionic strength can limit the fluoride ion uptake. At high fluoride concentrations in solution, precipitation of calcium fluoride occurs, which is strongly dependent on solution composition and pH. The presence of phosphate ions in solution limits the dissolution of HA, prevents the formation of CaF_2 and favours precipitation of fluorapatite at the extreme surface according to the following equations:



or



6.2.4. Sol-gel method

Fluorhydroxyapatite solid solutions can be prepared by the sol-gel method [134,135]. Cheng *et al.* reported the control of fluoride content in fluorhydroxyapatite solid solutions by the amounts of triethanolamine ($N(CH_2CH_2OH)_3$) and trifluoroacetic acid (CF_3COOH) in the mixed ethanol solutions of $Ca(NO_3)_2$ and $PO(CH_2CH_2OH)_x(OH)_{3-x}$ with a Ca/P ratio of 1.67 [134]. After evaporation of the mixed ethanol solution at $150^\circ C$ on a hot plate, the powder obtained, comprising a homogeneous mixture of calcium nitrate crystallites and amorphous calcium phosphates, is then heated at 500 or $900^\circ C$ for 1 h to be transformed into the pure apatitic phase.

6.2.5. Crystal growth method

Fluoridated apatite crystals can grow using the dual membrane system involving on the one hand a calcium acetate solution and on the other hand a phosphate solution at physiological temperature with a pH of 6.5. Iijima *et al.* showed that the combination of fluoride ions, added to the phosphate solution, and amelogenin (a major protein in the enamel extracellular matrix), present in the reaction space between the two membranes, controlled the transformation of octacalcium phosphate (OCP) into fine rod-like fluoridated apatite crystals with habit, size

and orientation similar to those of tooth enamel crystals [136]. This study highlights the potential of this system to investigate the matrix-mediated enamel biomineralisation and also to prepare engineered enamel-like materials.

7. PROCESSING TECHNIQUES FOR FLUORIDE-CONTAINING BIO CERAMICS

7.1. Processing of massive bioceramics containing fluoride

Most processing methods developed for the preparation of traditional ceramics can generally also be applied to the elaboration of fluoride-containing ceramics. This includes in particular reactive sintering processes starting from intimate mixtures of a calcium salt, a phosphate salt and a fluoride-containing compound (e.g. CaF_2), followed by sintering at high temperature, typically around 1300°C . Examples of such solid-state reactions, with varying compositions and initial relative amounts, are given in the literature [137,138]. In some instances [139], lower sintering temperatures, of the order of 1000°C , can otherwise be applied in order to obtain less crystallised fluorapatite-based compounds. Fluorhydroxyapatite ceramics can, however, also be directly obtained by sintering, generally above 1000°C , F–OH apatite solid solutions obtained by co-precipitation [65].

In view of biomedical applications, both dense ceramics and porous tridimensional scaffolds can be prepared. In the latter case, the creation of interconnected pores is ensured by the incorporation of a pore-forming agent into the initial mixture of solid phases [140]. After pressing, organic porogenic agents are generally removed by calcination whereas inorganic agents are often washed out by soaking in water, for more or less extended periods of time (generally several hours), possibly followed by a complementary thermal treatment. Another popular processing method for porous ceramics consists in using polymer foams impregnated with a slurry followed by drying, removal of the polymer shape by heating, then sintering at high temperature [141]. Direct foaming methods have also been investigated [142].

Biphasic materials associating FA with other phases can also be prepared. For example, combining it with ZrO_2 micro-particles has been studied [140,143] in order to enhance the mechanical properties of FA-based bioceramics. Associations with other phases like Al_2O_3 [137] or crystalline calcium silicate [144] have also been reported. Generally, such composite ceramics are processed using solid-state reactions, after mixing the constituents and fusing under pressure at relatively high temperatures (above 1200°C). Although the initial mixtures are usually pressed during sintering, often uniaxially, some reports denote processing techniques without applying mechanical pressure during the heat treatment. An example of this is given by Kim *et al.* [145], who prepared dense biphasic materials involving fluoride-substituted HA and yttria-doped zirconia and/or

alumina, using a three-step process: mixing of FA, HA, and ZrO_2 and/or Al_2O_3 , then submitting the mixture to cold isostatic pressing at 300 MPa and finally sintering at $1,440^\circ\text{C}$ for 3 h without pressure. In this case, the yttria-doped zirconia or alumina was considered as reinforcing agents that were found to be well dispersed in the F–OH apatitic matrix. Interestingly, superior mechanical properties (e.g. hardness and elastic modulus) were obtained for F–OH ceramic composites as compared to HA composites. The suppression of decomposition during the sintering step, which the authors attributed to the formation of a stable F–OH apatite solid solution, led to ceramic composites with fewer pores (higher density), thus explaining the improved mechanical behaviour observed. Similar results were obtained when CaF_2 was added to the mixture of HA and alumina before sintering.

In addition to solid-state reactions, other processing techniques of such ceramics have also been sporadically investigated, and have generally been the subject of new patents in the biomedical field.

An example of alternative processing methods is given by the use of a hydrothermal treatment at moderate temperatures ($100\text{--}500^\circ\text{C}$), positioning the sample either above the water or in total immersion (possibly in the presence of sodium fluoride) of the powder mixture, which was proposed [146] in view of the preparation of both stoichiometric and nonstoichiometric apatite bioceramics, eventually followed by thermal treatment.

Other non-conventional processing methods include the use of microwave irradiation [147] for the preparation of biphasic TCP/apatite bioceramics enriched with ions such as Mg^{2+} and F^- , known for their effects on these two phases stability.

7.2. Fluoride-containing bioceramic coatings

7.2.1. High-energy processing

The main subject of concern with the well-known metallic prostheses is the quality of the interface between the surrounding bone and the implant surface. During the last two decades, various coating methods leading to HA-coated prostheses combining the good mechanical properties of metals with the excellent biocompatibility and bioactivity of calcium phosphate have been studied. HA-coating is known to improve bone formation when in contact with bone tissue (osteoconduction) and to facilitate the anchorage between the bone tissue and the prosthesis (biointegration) especially during the first few months [148]. Currently, HA plasma spraying is the most common and successful process for enhancing the bioactivity of metallic implants (orthopaedic and dental implants) and for improving early bone-implant bonding [149].

However, several drawbacks still limit the quality of the interface and the implant biointegration: the poor adhesion of the coating on the titanium surface and its scaling either during implantation or in the long run, and the decomposition of

the HA during the plasma spray process (formation of an amorphous phase), which consequently has a negative effect as it initiates the degradation of the coating [149,150]. Fluorapatite-based coatings have been studied with a view to partly solve these problems due to the higher stability of fluor-containing well-crystallised apatites, which can lead to coatings with greater resistance to dissolution and biodegradation [151–155]. However, the main challenge is to improve the quality and the biological function of the coatings through the modification of their chemical composition at the lowest cost.

Other coating processes involving fluoridated apatite have been investigated to improve the long-term adhesion and promote osteointegration of cementless titanium-based metal implants: pulsed laser deposition, electron beam deposition and ion beam sputter deposition techniques, and sol-gel methods, for example. They lead to fluor-containing calcium phosphates (apatites in most cases) with different compositions and crystallinity states.

Ferro *et al.* reported the deposition of a thin, dense film of poorly crystalline fluoridated calcium phosphate on titanium using pulsed neodymium-doped yttrium aluminium garnet (Nd:YAG) laser deposition [156]. The coating was obtained using a high-intensity laser beam and a sintered HA-10% FA mixture as the target; it led to an amorphous deposit and a greatly improved hardness compared to initial ceramic targets, probably due to melting and phase decomposition of the initial phases in the laser plasma.

Apatite coatings fluoridated at different levels obtained by the electron beam deposition method have been studied [157]. Fluorhydroxyapatite solid solutions were used as initial evaporants. A subsequent heat treatment at 500°C of the initial amorphous deposit resulted in the crystallisation of the coating into the apatite structure. The as-prepared coatings showed good adhesion strength and a lower dissolution rate than a pure HA coating but no statistically significant difference was found between the different coatings regarding *in vitro* osteoblast-like cell response. Studying the dissolution/reprecipitation of the initial amorphous coating obtained from FA targets and using an ion beam sputter deposition technique, Zeng *et al.* also reported a lower dissolution rate for a FA-based coating [158]. In addition, they showed that the presence of bovine serum albumin in the environmental milieu had an effect on the extent of coating dissolution (increase dissolution) and on its final surface morphology.

Despite its clinical success, the plasma spray technique used for HA and/or FA coatings on metallic implants and the other high-energy (ion, laser, temperature) techniques cited above present intrinsic drawbacks: (1) the high energy involved in these techniques restricts the process to the deposition of stable phases like HA–FA solid solutions presenting a low SSA (around 1 m²/g) and thus low reactivity without any possibility of associating biologically active (macro)molecules (growth factors, e.g.) with the coating, (2) the limitations of this technique to covering complex surfaces and/or inside porous materials, (3) the partial and superficial decomposition of HA and/or FA powders or targets into several possible

phases under a high-energy physical source which could modify the chemical, mechanical and biological behaviour of the biomaterial. Moreover, the actual plasma spray systems do not allow the deposition of very thin homogeneous coatings because of the coarse minimum particle size allowed. In addition, they have a low efficiency with about 10–20% of the apatite material injected used for coating the metal; the yield is even lower for the coating of small implant devices such as dental implants. Finally, it appears difficult to control the coating's chemical composition, homogeneity and microstructure using such high-energy deposition techniques.

7.2.2. *Solution-mediated processing*

Within the framework of a previous European Community program (Brite Euram-CRAFT II), our research group studied plasma-sprayed coatings of HA and fluorhydroxyapatites with and without aqueous fluoridation post-treatment. For example, as described in the 'low-temperature solution methods' sub-section, aqueous fluoridation of plasma-sprayed HA coatings can be obtained by treating the raw coating with a fluoride-containing solution (KF: 0.05 M at 100°C). The addition of phosphate (F/P = 1/3) in the solution and the neutral pH prevent the formation of calcium fluoride and favour the formation of fluoridated apatites with a fluoridation rate close to 80%. [133]. The treatment is completed after 10 h and results in the formation of fluoridated apatite crystals on the surface of the coating, essentially at the expense of the amorphous fraction of the plasma-sprayed coating. A layer of more stable and less soluble needle-like fluorhydroxyapatite crystals is formed on the coating surface (see Fig. 10).

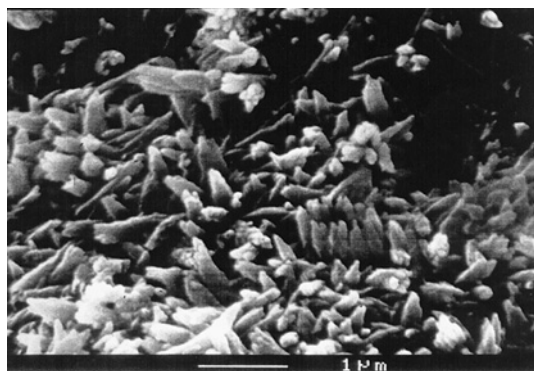


Fig. 10. Scanning electron microscope (SEM) micrograph of the surface of vacuum plasma sprayed hydroxyapatite (HA) coating after treatment in the fluoridating solution (KF: 0.05 M; KH_2PO_4 : 0.15 M; pH: 7, temperature: 100°C). A layer of thin needle-like fluorhydroxyapatite crystals (0.5–3 μm long, 0.1–0.3 μm width) can be observed. (With kind permission of Springer Science and Business Media).

An *in vitro* dissolution test showed that fluorhydroxyapatite coatings decomposed less than HA coatings and gave superior adhesive strength to the titanium substrate [133]. Implantation results were also very good and superior to HA coatings; however, the development of such coatings was rendered difficult due to preparation difficulties of the starting powders on an industrial scale.

Finally, the modified surfaces have been tested in cell culture with human osteoblasts. Although cell adhesion was found to be roughly equivalent on treated and raw surfaces, cell proliferation greatly improved after 10 days on the fluoridated surface [159]. In addition, the fluoridation treatment considerably reduced the degradation of the coating.

With a view to better control the composition, crystallinity and microstructure of fluorhydroxyapatite films, the sol-gel method can provide a means to tailor, for example, a homogeneous fluoride content at lower temperature and lower cost. Recently, a few research groups, using several kinds of precursors (triethyl phosphite ($\text{P}(\text{C}_2\text{H}_5\text{O})_3$), P_2O_5 , ammonium fluoride (NH_4F), hexafluorophosphoric acid (HPF_6) and calcium nitrate ($\text{Ca}(\text{NO}_3)_2 \cdot 4\text{H}_2\text{O}$)), reported studies on fluorhydroxyapatite deposition by the sol-gel route; the literature remains limited, however, on the deposition of a fluor-containing apatite film [134,135,160]. Generally, the coating process by the sol-gel route involves several steps: (1) the preparation of the sols (calcium sol on the one hand and phosphate and fluoride sol on the other hand), (2) the mixture of the sols, (3) the gelation of the mixture under stirring over several days, (4) the coating process using the ready-to-dip gel mixture either with dip- or spin-coating techniques, (5) the drying of the film, and (6) a final heat treatment at a moderate temperature (500°C – 600°C) to achieve the film crystallisation. This procedure can be repeated several times to increase the thickness of the film or to achieve a multi-layer deposit involving layers with different compositions (different fluoride content, e.g.) and structures which would determine the biological behaviour of the implant [134,160]. The sols are prepared in aqueous, hydroalcoholic or pure ethanol solutions. Dense, pure, homogeneous and strongly adherent apatite film can be obtained. However, as generally observed for apatite coating using the sol-gel route, one of the main problems is the aging time for the precursor sol (several days), which can influence the phase composition, homogeneity and textural properties of the deposit. *In vitro* testing showed that HA–FA coatings obtained by the sol-gel route led to more stable coatings compared to HA coating obtained by the same method, and to improved activity of cell functions compared to uncoated titanium [160,135]. Fluorhydroxyapatite coating by the sol-gel method on a zirconia substrate has also been reported, resulting in similar conclusions to the case of titanium substrate [160].

Even if the fluoride content in the HA–FA solution deposited can be tailored by the amount of fluoridated sol precursor, the potential benefit and/or dose effect of the fluoride content on the resulting coating bioactivity is not well documented [134].

Another solution proposed for the low-temperature deposit process for fluorhydroxyapatite onto porous zirconia bone scaffold was reported by Kim *et al.* [161]. It is based on the immersion of the scaffold in a slurry of dispersed HA–FA powders in polyvinylbutyl for several hours, followed by drying and subsequent heat treatments at 800°C and 1200°C for binder (polyvinylbutyl) burnout. The process can be repeated for a multilayer film deposit.

The coating of glass and glass-ceramics is developed in the fluoride-containing glasses part of this section. The techniques used are similar to those described for ceramic coatings.

8. FLUORIDE IONS IN BIOLOGICAL APATITES

Fluoride has been described as a bone-seeking element. It predominates and accumulates in mineralised tissues and is considered to be located essentially in the apatite mineral component of the tissues. This location has been confirmed by chemical analysis after removal of the organic matrix and by spectroscopic techniques such as solid-state NMR [162], as well as indirectly by FTIR spectroscopy [163] due to its effect on carbonate location. It is generally considered that fluoride ions substitute for the OH^- ions in the HA. However, recent data show that the OH^- content of bone mineral is very low, less than 0.2 ion per unit cell (work to be published); thus the incorporation of fluoride, which can be as high as 0.6 ion per unit cell, cannot be considered as a simple substitution of OH^- . Studies involving synthetic samples suggest a decrease in HPO_4^{2-} and in the carbonate content of apatites incorporating fluoride ions [66,83]. Fluoride thus induces a shift in bone apatite composition towards stoichiometry, which adds to the observed decrease in solubility.

The fluoride content of biological apatites can vary over a wide range depending essentially on diet (Table 5) and individual sensibilities [164].

In the same individual, however, the distribution of fluoride also appears quite erratic. Thus it has been found that the amount of fluoride was higher in trabecular than in cortical bone. This phenomenon has been observed for many other

Table 5. Fluoride concentration in mineralised tissues [164]

Tissue	Fluoride content (ppm of dry weight)
Bone	654–6180 (639–2108)
Dentine	140–157
Enamel	293– 2640 (54.3–752)

Values in parentheses represent literature values.

bone-seeking elements than fluoride and has been found, for example, with lead and strontium [165–167]. Several explanations have been proposed. One of the most prevalent is that a high turnover rate favours the uptake of trace elements from body fluids [168]. The trace elements drained in body fluids would be located first in zones where active precipitation takes place. However, after a complete turnover of the skeleton the fluoride concentration should be identical in the whole skeleton, which, according to observations, is never the case. This explanation neglects the specific reactivity of fluoride with apatite mineral. *In vitro* experiments [169] indicate that even at very low concentrations, fluoride is taken up by existing apatite crystals probably through a fast dissolution-precipitation process due to its effect on solubility. These experiments clearly show that fluoride could be fixed even in the absence of remodelling, like in enamel and dentine, through its reaction with existing bone crystals. Assuming that this fast physico-chemical process is predominant, fluoride ions driven by the bloodstream would first react in bone tissues with large bone-blood contact, that is, trabecular bone. An additional phenomenon involved in the faster uptake of fluoride in trabecular than cortical bone could be the ion recycling rate during remodelling. This phenomenon is not well known; however, several observations indicate that ions are partially recycled during remodelling. These mechanisms would be superimposed on the effect of the remodelling rate but it would not be exactly equivalent as each ion would have its own recycling rate. These recycling rates are complex and related to the local precipitation condition (local ionic concentrations and volumes, diffusion rates), they can, however, be roughly linked to the solubility products of the substituted apatitic phases. Thus fluoride and lead, which give more insoluble apatites than regular bone apatite, show a high recycling rate, whereas Sr-containing apatites, whose solubility seems higher than that of regular bone mineral, would involve a low recycling rate. This phenomenon explains, for instance, the difficult elimination of fluoride from bone and the easy elimination of strontium. These recycling rates could also be different in trabecular and cortical bone and they are, in addition, modified by the uptake of the element. Thus assuming that the recycling of ions is globally higher for cortical bone (smaller volumes, lower ion diffusion) the uptake of new ions would be reduced and the removal of trapped ions would be slower. Another important factor relates to the specific structure and properties of bone apatite nanocrystals as reported in a previous section, which suggests that freshly precipitated crystals would be more sensitive to fluoride uptake than old mature crystals.

Owing to the very long turnover rate of fluoride ions in the skeleton [170], it is generally admitted that fluoride concentration increases with age although this is difficult to ascertain considering the great variability of fluoride content between individuals and within tissues.

As there is no remodelling for enamel and dentine mineral, the incorporation process of fluoride appears in these cases rather different. Two processes have been considered: the fluoride uptake during tooth formation and the uptake resulting from saliva and/or topical applications. The fluoridation process of

apatite during tooth formation is essentially similar to that occurring in bone tissue. Frequently, fluoride supplements are given to children during second dentition formation to increase the fluoride content of enamel and to develop a resistance to caries. The cariostatic role of fluoride is believed to be essentially related to its effect on apatite solubility possibly superimposed on bactericidal properties. However, the process of enamel demineralisation and remineralisation related to circadian variations in pH involves an additional complexity. Saliva has been shown to be supersaturated with regard to stoichiometric HA at physiological pH; thus if enamel mineral were stoichiometric HA and if there were no pH variations, it would not dissolve. However, although enamel crystals composition approaches that of stoichiometric HA, they still correspond to a carbonate and hydrogen phosphate-containing calcium deficient-HA with a higher solubility than stoichiometric HA. In addition, the pH in the mouth can vary considerably because of contact with acidic beverages or food and the circadian activity of the bacterial flora. Thus the partial dissolution of enamel crystals cannot be avoided, although it can be slowed down by adsorption of saliva proteins [171]. This phenomenon is counterbalanced by enamel's ability to remineralise from saliva when the natural pH of the mouth is restored. This phenomenon may lead to a modification of the initial enamel crystals characteristics known as post-eruptive maturation [172]. Thus the enamel surface is submitted to cycles of dissolution and reprecipitation and the enamel surface composition depends to a considerable extent on the conditions of these events. Without the constant refuelling of fluoride ions through saliva, the enamel crystals would probably lose any acquired caries resistance related to initial fluoride intake during enamel formation. The presence of fluoride in saliva on the contrary can significantly change the characteristics of the reprecipitated crystals, leading to more stoichiometric stable apatites [173]. The fluoride ion content of saliva seems determined in part by food and beverage intake. However, additional sources may come from a fluoride reservoir possibly formed by the reaction of fluoridated solutions with saliva and/or enamel apatite. At acidic pH especially and at moderate fluoride concentrations, the formation of CaF_2 may be favoured forming a fluoride reservoir (Fig. 8). When normal saliva pH is re-established, fluoridated apatite becomes the most stable phase and CaF_2 progressively dissolves, leading to a release of fluoride. These reactions have been verified *in vitro* [131]. Analogous reactions could occur using fluoride-releasing materials such as glass ionomers and cements. In this case, the local fluoride concentration can be rather high after implantation, and associated with the local acidic pH similar phenomena would occur.

Despite many advantages fluoridation may also have some drawbacks. One of the most important is increased formation of dental calculi. As fluoridation considerably reduces the solubility of apatites, the supersaturation of saliva with respect to apatite is appreciably increased and may favour the spontaneous precipitation of fluoridated apatites and the formation of dental calculi. This phenomenon would occur especially in the case of fluoridated toothpaste, and most of them

have inhibitors of calculi formation and growth included in their composition. This risk seems very limited, however, for fluoride-releasing materials considering the slow release rate and the low amount of fluoride ions reaching saliva.

From a macroscopic point of view, fluoride ions have been consistently shown to increase the BMD. It seems that fluoride treatments decrease the rate of vertebral fractures but fail to reduce that of long bones [174].

9. BIOLOGICAL PROPERTIES OF FLUORIDE-CONTAINING BIOCERAMICS

The biological properties of fluoridated bioceramics depend on numerous factors besides the amount of fluoride (porosity, surface roughness, surface properties, degradation process) and it is often difficult to discern the specific role of fluoride. It seems useful to begin by summarising the biological properties of fluoride ions in solution.

9.1. Biological properties of fluoride ions in solution

Several excellent reviews on the biological role of fluoride have been published recently [79,175–176]. The main effect of fluoride is related to osteoblast cell proliferation.

9.1.1. Effect of fluoride ion on mineralising cells

Two processes have been proposed to explain the mitogenic effect of fluoride on bone cells involving either fluoride ions directly or the AlF_x complex (Fig. 11). Fluoride ions have been shown to directly inhibit an enzyme (tyrosine phosphorylase phosphatase) resulting in an enhancement of the tyrosine phosphorylation part of the mitogen-activated protein kinase system (MAPK) [177]. The other activation pathway involves a complex of aluminium and fluoride which activates the G-protein and stimulates tyrosine phosphorylation resulting in an enhanced mitogenic effect [176].

The effect of fluoride on odontoblast seems to follow similar pathways; however, fluoride does not seem to show any effect on the proliferation of ameloblast cells. In addition to direct biological effects, fluoride ions may also exhibit indirect effects related to the decrease in Calcium concentration they can involve, and the change in the surface properties of biological apatites.

9.1.2. Effect of the fluoride ion on osteoclasts

Osteoclast cells generally require an apatitic substrate (dentine, enamel, bone slices or synthetic apatite coatings) to attach to and act on and the effect of fluoride ions in solution cannot be readily distinguished from the effect of fluoride on

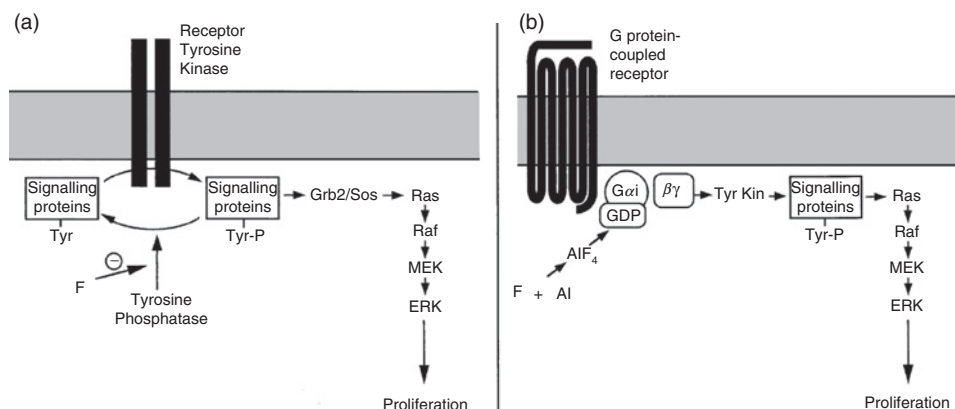


Fig. 11. Modes of action of fluoride on osteoblastic cells. (a) Tyrosine phosphatase hypothesis: in osteoblastic cells, fluoride ion directly inhibits tyrosine phosphatase. Inhibition of this enzyme enhances the tyrosine phosphorylation of signalling molecules induced by receptor tyrosine kinase, which leads to activation of the extracellular signal-regulated kinase (ERK) through the Ras pathway and enhanced cell proliferation. (b) G-protein hypothesis: in osteoblast-like cells, fluoride ions form a complex with aluminum, probably fluoroaluminate, which interacts with guanosine 5'-diphosphate (GDP) to form guanosine 5'-triphosphate (GTP)-like molecule. Activation of the G_i protein stimulates the tyrosine phosphorylation of signalling molecules by a yet unknown tyrosine kinase (Tyr Kin) and activation of the ERK kinase through the Ras pathway leads to enhanced cell proliferation. (Reproduced by permission of Elsevier from Ref. [175]).

the substrates they live on. In general, the investigators did not consider possible changes in the solution composition over time related to the substrate fluoridation. Such alteration may possibly explain discrepancies in the data. It is generally accepted [178,179] that fluoride decreases the resorptive capability of osteoclast cells; however, it is not yet clear if these properties are related to the direct effect of fluoride ions or to the alteration of the substrate surface and dissolution properties. The inhibitory effect of fluoride on osteoclast activity has been shown to be dose-dependent; however, it seems significant only for fluoride concentrations above 1 µg/L, the average concentration of blood.

9.1.3. Effect of fluoride ions on bacteria

Several experiments have shown the bactericidal effect of fluoride ions at high concentrations [180,181]. This effect generally occurs at concentrations well above those generally observed in saliva; however, the use of fluoridated toothpaste or dental topical applications of fluoride may temporarily elevate the fluoride concentration in the oral cavity to bactericidal levels. It has been demonstrated that fluoride affects the metabolism of oral bacteria and reduces its acid tolerance. It is most effective at acidic pH values and, for example, fluoride levels as low as 0.1 mM can cause the complete arrest of glycolysis by *Streptococcus mutans*. It has been suggested that modifying the biological fluids related to the presence

of fluoride could determine a selection of buccal bacterial strains. Despite a proven antibacterial effect, it is generally accepted that fluoride ions have only a marginal effect on dental plaque cariogenicity.

9.1.4. Other alterations in biological fluids related to fluoride ions

Significant alterations in biological fluids in the presence of fluoride ions are mainly related to the disturbance of the solubility equilibrium of calcium phosphate apatites in relation to fluoridation. Calcium depletion of biological fluids induced by fluoride ions has been suggested to be a cause of dental fluorosis resulting in a decrease in protease activity and the inefficient removal of dental proteins preventing the growth of enamel crystals [182], although this issue seems controversial [79]. Calcium ions are heavily involved in bone-cell behaviour and the depletion of the local calcium levels related to fluoridation could contribute to some biological effects [183].

9.2. Effect of fluoride-containing substrates on bone cells

9.2.1. Osteoblast cells

The data concerning the effect of fluoride-containing apatites on cell adhesion, proliferation and expression seem rather disparate, probably because of the variation of other surface characteristics and the use of different cell strains. No real negative effect of fluoride-containing substrates has been reported so far and the osteoblast cells seem to behave similarly [184,185] or better [183,186,187] on fluoridated apatites than on HA surfaces. Some reports mention weaker attachment and proliferation, compensated for by improved collagen matrix production [188]. The shape of cells appeared different on fluoridated apatites than on HA. Other authors have found an improvement in cell attachment [183] which has been attributed to the change in surface charge of FA compared to HA.

The positive effect of different surface treatments for titanium with fluoride ions has essentially been related to changes in surface roughness [189,190]. Concerning bioglass [90] incorporating fluoride ions seems to show a slight beneficial effect, especially regarding cell expression, although this effect could be related to some release of fluoride ions in the solution.

9.2.2. Osteoclast cells

Only a very few experiments have been published concerning the behaviour of osteoclast cells on fluoridated biomaterial surfaces, although this point seems crucial concerning the mode of action of osteoclast cells. Most studies report on the effect of fluoride ions in the solution, which may also change the surface on which these cells are cultivated. Ramaswamy *et al.* [191] have shown that osteoclasts attach to FA ceramic surfaces but that the resorption pits were barely observed. It is accepted that due to the very slow solubility of fluorapatite

the degradation rate by osteoclast cells should be very low. This fact has been confirmed by *in vivo* studies on plasma-sprayed coatings, stressing the greater stability of fluoridated apatites [192,193]. The poor stability of FA coatings sometimes reported can possibly be attributed to specific coating characteristics due to the presence of an amorphous phase [194].

10. CONCLUSION

The only wide-range application and commercialisation area of fluoride-containing biomaterials concern ionomer glasses for dental applications. The improved biological effect of these compounds is related to a slow release of active fluoride ions in biological fluids and the direct effect of fluoride ions on mineralised biological tissues.

Many biomaterials containing fluoride ions aimed at orthopaedic applications have not yet reached industrial development despite the existence of many positive studies showing an improvement in several properties concerning the materials themselves (mechanical properties, stability) and/or their biological behaviour (especially bone reconstruction and biodegradation). These difficulties are mainly related to difficulties in the preparation of FA and to the reluctance of practitioners to involve fluoride ions, considering their relative lack of success in treating osteoporotic patients. In addition, the data reporting the biological behaviour of fluoridated compounds, especially those related to osteoblast cells, show significant discrepancies, probably related to other surface characteristics, alterations of the materials or experimental conditions, which need to be investigated further. Among the most promising properties which do not seem to raise any doubts are the slower degradation rate of fluoridated apatites and the better stability of the bone-implant interface, which should favour their development as coatings and ceramics for permanent implant devices.

REFERENCES

- [1] K. Sudarsanan, P.E. Mackie, R.A. Young, Comparison of synthetic and mineral fluorapatite, $\text{Ca}_5(\text{PO}_4)_3\text{F}$, in crystallographic detail, *Mat. Res. Bull.* 7 (1972) 1331–1338.
- [2] T.J. White, D. Zhili, Structural derivation and crystal chemistry of apatites, *Acta Crystallogr. B* B59 (2003) 1–16.
- [3] S. Naray-Szabo, The structure of apatite $(\text{CaF})\text{Ca}_4(\text{PO}_4)_3$, *Z. Kristallogr. Kristallgeometrie Kristallphys. Kristallchem.* 75 (1930) 387–398.
- [4] J.C. Elliott, Structure and chemistry of the apatites and other calcium orthophosphates, in: *Studies in Inorganic Chemistry*, Vol. 18. Elsevier, Amsterdam, 1994.
- [5] N. Leroy, E. Bres, Structure and substitutions in fluorapatite, *Eur. Cell. Mater.* 2 (2001) 36–48.
- [6] P.E. Mackie, J.C. Elliott, R.A. Young, Monoclinic structure of synthetic $\text{Ca}_5(\text{PO}_4)_3\text{Cl}$, chlorapatite, *Acta Crystallogr. B* 28 (1972) 1840–1848.

- [7] J.M. Hughes, M. Cameron, K.D. Crowley, Structural variations in natural F, OH, and Cl apatites, *Am. Mineral.* 74 (1989) 870–876.
- [8] P.R. Suitch, J.L. Lacout, A. Hewat, R.A. Young, The structural location and role of Mn^{2+} ions partially substituted for Ca^{2+} in fluorapatite, *Acta Crystallogr. B* 41 (1985) 173–179.
- [9] E.R. Kreidler, F.A. Hummel, The crystal chemistry of apatite: Structure fields of fluor- and chlorapatite, *Am. Mineral.* 55 (1970) 170–184.
- [10] R. LeGeros, O.R. Trautz, E. Klein, J.P. LeGeros, Two types of carbonate substitution in the apatite structure, *Experientia* 25 (1969) 5–7.
- [11] M. Vignoles, G. Bonel, D.W. Holcomb, R.A. Young, Influence of preparation conditions on the composition of type B carbonated hydroxyapatite and on the localization of the carbonate ions, *Calcif. Tissue Int.* 43 (1988) 33–40.
- [12] R.M. Wilson, J.C. Elliott, S.E.P. Dowker, R.I. Smith, Rietveld structure refinement of precipitated carbonate apatite using neutron diffraction data, *Biomaterials* 25 (2004) 2205–2213.
- [13] D. McConnell, *Apatite, Its Crystal Chemistry, Mineralogy, Utilization, and Geologic and Biologic Occurrences*, Springer-Verlag, New York, 1973.
- [14] M. Vignoles, G. Bonel, Sur la localisation des ions fluorures dans les carbonate apatites de type B, *C.R. Acad. Sci. (Paris)* 287 (1978) 321–324.
- [15] C.B. Baddiel, E.E. Berry, Spectra-structure correlations in hydroxyapatite and fluorapatite, *Spectrochim. Acta* 22 (1966) 1407–1416.
- [16] V.M. Bhatnagar, Infrared spectra of hydroxyapatite and fluorapatite, *Bull. Soc. Chim. Fr.* (special issue) (1968) 1771–1773.
- [17] S.R. Levitt, K.C. Blakeslee, R.A. Condrate, Infrared spectra and laser-Raman spectra of several apatites, *Mémoires de la Société Royale des Sciences de Liège, Collection in 8* 20 (1970) 121–141.
- [18] W.E. Klee, Vibrational spectra of the phosphate ions in fluorapatite, *Z. Kristallogr. Kristallgeometrie Kristallphys. Kristallchem.* 131 (1970) 95–102.
- [19] P.M. Nikolic, W.B. Roys, V. Blagojevic, Far infrared properties of fluoroapatite, *Fizika (Zagreb)* 10(suppl. 2) (1978) 367–370.
- [20] Q. Williams, E. Knittle, Infrared and Raman spectra of fluorapatite at high pressures: Compression-induced changes in phosphate site and Davydov splittings, *J. Phys. Chem. Sol.* 57 (1996) 417–422.
- [21] G. Penel, G. Leroy, C. Rey, B. Sombret, J.P. Huvenne, E. Bres, Infrared and Raman microspectrometry study of fluor- fluor-hydrox- and hydroxy-apatite powders, *J. Mater. Sci. Mater. Med.* 8 (1997) 271–276.
- [22] F. Freund, R.M. Knobel, Distribution of fluorine in hydroxyapatite studied by infrared spectroscopy, *J. Chem. Soc. Dalton* 11 (1977) 1136–1140.
- [23] W.P. Rothwell, J.S. Waugh, J.P. Yesinowski, High resolution variable temperature ^{31}P NMR of solid calcium phosphates, *J. Am. Chem. Soc.* 102 (1980) 2637–2643.
- [24] J.P. Yesinowski, M.J. Mobley, ^{19}F MAS-NMR of fluoridated hydroxyapatite surfaces, *J. Am. Chem. Soc.* 105 (1983) 6191–6193.
- [25] J.P. Yesinowski, H. Eckert, Hydrogen environments in calcium phosphates: 1H MAS NMR at high spinning speeds, *J. Am. Chem. Soc.* 109 (1987) 6274–6282.
- [27] J.P. Yesinowski, Nuclear magnetic resonance spectroscopy of calcium phosphates, in: Z. Amjad (Ed.), *Calcium Phosphates in Biological and Industrial Systems*, Kluwer Academic Publishers, Norwell, MA, 1998, pp. 103–143.
- [29] D.J. White, W.D. Bowman, F.V. Faller, M.J. Mobley, R.A. Wolfgang, J.P. Yesinowski, ^{19}F MAS-NMR and solution chemical characterization of the reactions of fluoride with hydroxyapatite and powder enamel, *Acta Odontol. Scand.* 46 (1988) 375–389.
- [30] K.A. Smith, D.P. Burum, Application of Fluorine-19 CRAMPS to the analysis of calcium fluoride/fluorapatite mixtures, *J. Magn. Reson.* 84 (1989) 85–94.
- [31] A.T. Kreinbrink, C.D. Sazavsky, J.W. Pyrz, D.G.A. Nelson, R.S. Honkonen, Fast magic angle spinning ^{19}F NMR of inorganic fluorides and fluoridated apatitic surfaces, *J. Magn. Reson.* 88 (1990) 267–276.

- [32] L.B. Moran, J.P. Yesinowski, Chemical-shift selective multiple quantum NMR as probe of the correlation length of chemical shielding tensors, *Chem. Phys. Lett.* 222 (1994) 363–370.
- [33] P. Regnier, A.C. Lasaga, R.A. Berner, O.H. Han, K.W. Zilm, Mechanism of CO_3^{2-} substitution in carbonate-fluorapatite: Evidence from FTIR spectroscopy, ^{13}C NMR, and quantum mechanical calculations, *Am. Mineral.* 79 (1994) 809–818.
- [34] M. Braun, C. Jana, ^{19}F NMR spectroscopy of fluoridated apatites, *Chem. Phys. Lett.* 245 (1995) 19–22.
- [35] M. Iijima, D.G.A. Nelson, Y. Pan, A.T. Kreinbrink, M. Adachi, T. Goto, Y. Moriwaki, Fluoride analysis of apatite crystals with a central planar OCP inclusion: Concerning the role of F^- ions on apatite/OCP/apatite structure formation, *Calcif. Tissue Int.* 59 (1996) 377–384.
- [36] G. Cho, J.P. Yesinowski, ^1H and ^{19}F multiple quantum dynamics in Quasi-one-dimensional spin clusters in apatites, *J. Phys. Chem.* 100 (1996) 15716–15725.
- [37] J.M. Miller, Fluorine-19 magic-angle spinning NMR, *Prog. Nucl. Magn. Reson. Spectrosc.* 28 (1996) 255–281.
- [38] J.C.C. Chan, C-REDOR: Rotational double resonance under very fast magic angle spinning, *Chem. Phys. Lett.* 335 (2001) 289–297.
- [39] H. Sfihi, C. Rey, 1-D and 2-D Double heteronuclear magnetic resonance study of the local structure of type B carbonate fluorapatite, in: J. Fraissard, B. Lapina (Eds.), *Magnetic Resonance in Colloid and Interface Science*, Nato ASI Series II, Vol. 76, Kluwer Academic Publishers, Dordrecht, 2002, pp. 409–422.
- [40] C.J.L. Silwood, I. Abrahams, D.C. Apperly, N.P. Lockyer, E. Lynch, M. Motevalli, R.M. Nix, M. Grootveld, Surface analysis of novel hydroxyapatite bioceramics containing titanium (IV) and fluoride, *J. Mat. Chem.* 15 (2005) 1626–1636.
- [41] M. Jarlbring, Surface Reaction in Aqueous Suspensions of Fluorapatite and iron Oxides, Doctoral Thesis, Luleå University of Technology, Luleå, Sweden, 2006.
- [42] M. Jarlbring, D.E. Sandström, O.N. Antzutkin, W. Forsling, Characterization of active phosphorus surface sites at synthetic carbonate-free fluorapatite using single pulse ^1H , ^{31}P , and ^{31}P CP-MAS NMR, *Langmuir* 22 (2006) 4787–4792.
- [43] D.E. Sandström, O.N. Antzutkin, W. Forsling, A spectroscopic study of calcium surface sites and adsorbed iron species at aqueous fluorapatite by means of ^1H and ^{31}P MAS NMR, *Langmuir* 22 (2006) 11060–11064.
- [44] D.E. Sandström, Solid State Nuclear Magnetic Resonance of Synthetic Mineral Surfaces, Thesis, Luleå University of Technology, Luleå, Sweden, 2006.
- [45] H. Chen, K. Sun, Z. Tang, R.V. Law, J.F. Mansfield, A. Czajka-Jakubowska, B.H. Clarkson, Synthesis of fluorapatite nanorods and nanowires by direct precipitation from solution, *Crystal Growth and Design* 6 (2006) 1504–1508.
- [46] G. Cho, J.P. Yesinowski, ^1H and ^{19}F multiple quantum dynamics in Quasi-one-dimensional spin clusters in apatites, *J. Phys. Chem.* 100 (1996) 15716–15725.
- [47] N. Gelman, R.F. Code, A simple model of ^{19}F spin-echo formation in polycrystalline fluorapatite, *J. Magn. Res. A* 107 (1994) 185–193.
- [48] M. Engelsberg, I.J. Lowe, J.L. Carolan, Nuclear magnetic resonance line shape of linear chain of spins, *Phys. Rev. B* 7 (1973) 924–929.
- [49] L.B. Moran, J.K. Berkowitz, J.P. Yesinowski, ^{19}F and ^{31}P magic angle spinning nuclear magnetic resonance of antimony (III) doped fluorapatite phosphors: Dopant sites and spin diffusion, *Phys. Rev. B* 45 (1992) 5347–5360.
- [50] Y. Pan, ^{31}P - ^{19}F rotational-echo double resonance nuclear magnetic resonance experiment on fluoridated hydroxyapatite, *Solid State Nucl. Magn. Reson.* 5 (1995) 263–268.
- [51] L. Wu, W. Forsling, P.W. Schindler, Surface complexation of calcium mineral in aqueous solution, surface protonation at fluorapatite surface, *J. Colloid Interface Sci.* 147 (1991) 178–185.
- [52] K. Takeuchi, H. Nakagaki, Y. Toyama, N. Kimata, C. Robinson, J.A. Weatherell, L. St-ossier, W. Kunzel, Fluoride concentration and distribution in premolars of children from low and optimal fluoride areas, *Caries Res.* 30 (1996) 76–82.

- [53] E.C. Moreno, M. Kresak, R.T. Zahradnik, Fluoridated hydroxyapatite solubility and caries formation, *Nature* 247 (1974) 64–65.
- [54] E.C. Moreno, M. Kresak, R.T. Zahradnik, Physicochemical aspects of fluoride-apatite systems relevant to the study of dental caries, *Caries Res.* 11(suppl. 1) (1977) 142–171.
- [55] F.C.M. Driessens, in *Mineral Aspects of Dentistry*, Karger, Basel, 1982, pp. 113–128.
- [56] R.M.H. Verbeeck, R.A. Khan, H.P. Thun, F.C.M. Driessens, Solubility of thermal synthesized fluorhydroxyapatites, *Bull. Soc. Chim. Belge* 88 (1979) 751–759.
- [57] J.M. Ten Cate, J.D. Featherstone, Mechanistic aspects of the interactions between fluoride and dental enamel, *Crit. Rev. Oral Biol. Med.* 2 (1991) 283–296.
- [58] L.C. Chow, M. Markovic, Physicochemical properties of fluorapatite, in: Z. Amjad (Ed.), *Calcium Phosphates in Biological and Industrial Systems*, Kluwer, Norwell, 1998, pp. 67–83.
- [59] L.C. Chow, Solubility of calcium phosphates, in: L.C. Chow, E.D. Eanes (Eds.), *Octacalcium Phosphate, Monographs in Oral Science Vol. 18*, 2001, pp. 94–111.
- [60] S. Chander, D.W. Fürstenau, On the dissolution and interfacial properties of hydroxyapatite, *Colloids Surf.* 4 (1982) 101–120.
- [61] J.P. Yesinowski, R.A. Wolfgang, M.J. Mobley, New NMR methods for the study of hydroxyapatite surfaces, in: D.N. Misra (Ed.), *Adsorption on and Surface Chemistry in Hydroxyapatite*, Plenum Press, New York, 1984.
- [62] A.C. Ramsey, E.J. Duff, L. Paterson, J.L. Stuart, The uptake of F⁻ by hydroxyapatite at varying pH, *Caries Res.* 7 (1973) 231–244.
- [63] J. Arends, J. Christoffersen, Nature and role of loosely bound fluoride in dental caries, *J. Dent. Res.* 69 (1990) 601–605.
- [64] Y. Chen, X. Miao, Thermal and chemical stability of fluorhydroxyapatite ceramics with different fluorine contents, *Biomaterials* 26 (2004) 1205–1210.
- [65] N. Senamaud, D. Bernache-Assollant, E. Champion, M. Heughebaert, C. Rey, Calcination and sintering of hydroxyfluorapatite powders, *Solid State Ionics* 101–103 (1997) 1357–1362.
- [66] R.Z. LeGeros, D. Mijares, F. Yao, J.P. LeGeros, T. Bromage, V. La, Q. Xi, S. Tannous, R. Kijkowska, Consequences of fluoride incorporation on properties of apatites, *Key Eng. Mater.* 309–311 (2006) 697–700.
- [67] P.V. Riboud, Composition et stabilité des phases à structure d'apatite dans le système CaO-P₂O₅-oxyde de fer-H₂O à haute température, *Ann. Chim. (Paris)* 8 (1973) 381–390.
- [68] R. Mazelsky, R.H. Hopkins, W.E. Kramer, Czochralski growth of calcium fluorophosphate, *J. Cryst. Growth* 3,4 (1968) 260–264.
- [69] R.C. Tacker, J.C. Stormer Jr., A thermodynamic model for apatite solid solutions, applicable to high-temperature geologic problems, *Am. Miner.* 74 (1989) 877–888.
- [70] E.P. Egan, Z.T. Wakefield, K.L. Elmore, Thermodynamic properties of fluorapatite, 15 to 1600 °K, *J. Am. Chem. Soc.* 73 (1951) 5581–5582.
- [71] M. Jemal, A. Ben Cherifa, I. Khattech, I. Ntahomvukiye, Standard enthalpies of formation and mixing of hydroxy- and fluorapatites, *Thermochim. Acta* 259 (1995) 13–21.
- [72] I. Ntahomvukiye, I. Khattech, M. Jemal, Synthesis, characterization and thermochemistry of calcium-lead fluorapatites Ca_(10-x)Pb_x(PO₄)₆F₂, 0 ≤ x ≤ 10, *Ann. Chim. (Paris)* 22 (1997) 435–446.
- [73] I. Khattech, M. Jemal, Thermochemistry of phosphate products. Part II: Standard enthalpies of formation and mixing of calcium and strontium fluorapatites, *Thermochim. Acta* 298 (1997) 23–30.
- [74] S. Ben Abdelkader, I. Khattech, C. Rey, M. Jemal, Synthesis, characterization and thermochemistry of calcium-magnesium hydroxyapatite and fluorapatite, *Thermochim. Acta* 376 (2001) 25–36.
- [75] W. Wu, G.H. Nancollas, Determination of interfacial tension from crystallization and dissolution data: A comparison with other methods, *Adv. Colloid Interface Sci.* 79 (1999) 229–279.

- [76] M.S. Tung, D. Skrtic, Interfacial properties of hydroxyapatite in fluorapatite and octacalcium phosphate, in: L.C. Chowm, E.D. Eanes (Eds.), *Octacalcium Phosphate*, Karger, Basel, 2001, pp. 112–129.
- [77] L.C. Bell, A.S. Posner, J.P. Quirk, The point of zero charge of hydroxyapatite and fluorapatite in aqueous solutions, *J. Col. Inter. Sci.* 42 (1973) 250–261.
- [78] T. Tanabe, T. Aoba, E.C. Moreno, M. Fukae, Effect of fluoride in the apatitic lattice on adsorption of enamel proteins onto calcium apatites, *J. Dent. Res.* 67 (1988) 536–542.
- [79] C. Robinson, S. Connell, J. Kirkham, S.J. Brookes, R.C. Shore, A.M. Smith, The effect of fluoride on the developing tooth, *Caries Res.* 38 (2004) 268–276.
- [80] C. Robinson, K. Yamamoto, S.D. Connell, J. Kirkham, H. Nakagaki, A.D. Smith, The effect of fluoride on the nanostructure and surface pK of enamel crystals: An atomic force microscopy study of human and rat enamel, *Eur. J. Oral Sci.* 114 (2006) 99–104.
- [81] E.D. Eanes, A.W. Hailer, The effect of fluoride on the size and morphology of apatite crystals grown from physiological solutions, *Calcif. Tissue Int.* 63 (1998) 250–257.
- [82] G.C. Maiti, F. Freund, Influence of fluorine substitution on proton conductivity of hydroxyapatite, *J. Chem. Soc. Dalton Trans.* 4 (1981) 949–955.
- [83] A. Hina, Etude de la Réactivité en Milieu Aqueux d'apatites Phosphocalciques d'intérêt Biologique, Ph.D. Thesis, INPT, France, 1996.
- [84] C. Rey, C. Combes, C. Drouet, H. Sfihi, A. Barroug, Physico-chemical properties of nanocrystalline apatites: Implications for biominerals and biomaterials, *Mat. Sci. Eng. C* 27 (2007) 198–205.
- [85] M. Vignoles-Montrejaud, Contribution à l'étude des Apatites Carbonatées de Type B, Thesis INPT, France, 1984.
- [86] S.M. Barinov, I.V. Fadeeva, L.V. Fateeva, S.V. Tumanov, Delayed fatigue of hydroxy- and fluorhydroxyapatite ceramics in simulated body fluid, *Key Eng. Mater.* 290 (2005) 366–369.
- [87] K.A. Gross, L.M. Rodriguez-Lorenzo, Sintered hydroxyfluorapatites. Part II: Mechanical properties of solid solutions determined by microindentation, *Biomaterials* 25 (2004) 1385–1394.
- [88] L.L. Hench, Bioactive glasses and glass-ceramics, *Mater. Sci. Forum* 293 (1999) 37–64.
- [89] H. Matsuoka, H. Akiyama, Y. Okada, C. Shigeno, J. Konishi, T. Kokubo, T. Nakamura, In vitro analysis of the stimulation of bone formation by highly bioactive apatite- and wollastonite-containing glass-ceramic: Released calcium ions promote osteogenic differentiation in osteoblastic ROS17/2.8 cells, *J. Biomed. Mater. Res.* 47 (1999) 176–188.
- [90] W.C. Vroouwenvelder, C.G. Groot, K. de Groot, Better histology and biochemistry for osteoblasts cultured on titanium-doped bioactive glass: Bioglass 45S5 compared with iron-, titanium-, fluorine- and boron-containing bioactive glasses, *Biomaterials* 15 (1994) 97–106.
- [91] T. Kitsugi, T. Yamamuro, T. Nakamura, T. Kokubo, Bone bonding behavior of MgO-CaO-SiO₂-P₂O₅-CaF₂ glass (mother glass of AW-glass-ceramics), *J. Biomed. Mater. Res.* 23 (1989) 631–648.
- [92] T. Kokubo, Novel biomedical materials based on glasses, *Mater. Sci. Forum* 293 (1999) 65–82.
- [93] T. Yamamuro, K. Shimizu, Clinical application of AW glass-ceramic prosthesis in spinal surgery, *Nippon Seikeigeka Gakkai Zasshi* 68 (1994) 505–515.
- [94] W. Holand, W. Vogel, K. Nauman, J. Gummel, Interface reactions between machinable bioactive glass-ceramics and bone, *J. Biomed. Mater. Res.* 19 (1985) 303–312.
- [95] T. Bartels, W. Hein, C. Taube, G. Berger, H.J. Mest, The significance of Ilmaplant as a bone substitute with reference to prostaglandin biosynthesis in bones. An animal experiment-clinical study, *Beitr. Orthop. Traumatol.* 36 (1989) 207–213.
- [96] J.F. Shackelford, Bioceramics-current status and future trends, *Mater. Sci. Forum* 293 (1999) 99–106.
- [97] R. Hill, D. Wood, Apatite-mullite glass-ceramics, *J. Mater. Sci. Mater. Med.* 6 (1995) 311–318.

- [98] D.U. Tulyaganov, S. Agathopoulos, H.R. Fernandes, J.M. Ventura, J.M.F. Ferreira, Preparation and crystallization of glasses in the system tetrasilicic mica-fluorapatite-diopside, *J. Eur. Ceram. Soc.* 24 (2004) 3521–3528.
- [99] S. Bandyopadhyay-Ghosh, I.M. Reaney, K. Hurrell-Gillingham, I.M. Brook, P.V. Hatton, Evaluation of modified fluorcanasite glass-ceramics for bone tissue augmentation, *Key Eng. Mater.* 284–286 (2005) 557–560.
- [100] T. Yamamuro, T. Nakamura, H. Iida, K. Kawanabe, Y. Matsuda, K. Ido, J. Tamura, Y. Seneba, Development of bioactive bone cement and its clinical applications, *Biomaterials* 19 (1998) 1479–1482.
- [101] H. Fujita, T. Nakamura, J. Tamura, M. Kobayashi, Y. Katsura, T. Kokubo, T. Kikutani, Bioactive bone cement: Effect of the amount of glass-ceramic powder on bone-bonding strength, *J. Biomed. Mater. Res.* 40 (1998) 145–152.
- [102] M. Bosetti, E. Vernè, C. Vitale-Brovarone, C. Moisescu, M. Sabbatini, M. Cannas, Fluoroapatite glass-ceramic coating on alumina: Surface behavior with biological fluids, *J. Biomed. Mater. Res.* 66 (2003) 615–621.
- [103] A. Ignatius, M. Peraus, S. Schorlemmer, P. Augat, W. Burger, S. Leyen, L. Claes, Osseointegration of alumina with a bioactive coating under load-bearing and unloaded conditions, *Biomaterials* 26 (2005) 2325–2332.
- [104] E. Vernè, M. Ferraris, C. Jana, L. Paracchini, Bioverit® base glass/Ti particulate biocomposite: « *in situ* » vacuum plasma spray deposition, *J. Eur. Ceram. Soc.* 20 (2000) 473–479.
- [105] J.K. Bibby, N.L. Bubb, D.J. Wood, P.M. Mummery, Fluorapatite-mullite glass sputter coated Ti6Al4V for biomedical applications, *J. Mater. Sci. Mater. Med.* 16 (2005) 379–385.
- [106] J.F. McCabe, Resin-modified glass ionomers, *Biomaterials* 19 (1998) 521–527.
- [107] L. Forsten, Fluoride release and uptake by glass ionomer and related materials and its clinical effect, *Biomaterials* 19 (1998) 503–508.
- [108] A.M.J.C. de Witte, E.A.P. De Maeyer, R.M.H. Verbeeck, L.C. Martens, Fluoride release profiles of mature restorative glass ionomer cements after fluoride application, *Biomaterials* 21 (2000) 475–482.
- [109] Y. Fukase, E.D. Eanes, S. Takagi, L.C. Chow, W.E. Brown, Setting reaction and compressive strengths of calcium phosphate cements, *J. Dent. Res.* 69 (1990) 1852–1856.
- [110] C. Rey, A. Tofghi, S. Mounic, C. Combes, D. Lee, Biomimetism and calcium phosphate cements, in: D. Mainard (Ed.), *Actualités en Biomatériaux*, Vol VI, Romillat, Paris, 2002, pp. 27–37.
- [111] M. Bohner, U. Gbureck, J.E. Barralet, Technological issues for the development of more efficient calcium phosphate bone cements: A critical assessment, *Biomaterials* 26 (2005) 6423–6429.
- [112] A.A. Mirtchi, J. Lemaître, E. Münting, Calcium phosphate cements: Effect of fluorides on the setting and hardening of beta-tricalcium phosphate-dicalcium phosphate-calcite cements, *Biomaterials* 12 (1991) 505–510.
- [113] Y. Fukase, E.D. Eanes, S. Takagi, L.C. Chow, W.E. Brown, Setting reactions and compressive strengths of calcium phosphate cements, *J. Dent. Res.* 69 (1990) 1852–1856.
- [114] G. Montel, Synthesis and decomposition reactions of fluorapatite involving liberation of fluorides of phosphorus, *Colloq. Sek. Anorg. Chem. Intern. Union Reineu. Angew. Chem. Munster* (1955) 178–183.
- [115] S. Amrah-Bouali, Etude de la Fluoruration Gazeuse et Aqueuse de l'hydroxyapatite, PhD Thesis, INPT, Toulouse, France, 1993.
- [116] R. Wallaëys, G. Chaudron, Preparation of certain mixed apatites, *Compte Rendus de l'Académie des Sciences* 231 (1950) 355–357.
- [117] S. Loher, W.J. Stark, M. Maciejewski, A. Baiker, S.E. Pratsinis, D. Reichardt, F. Maspero, F. Krumeich, D. Günther, Fluoro-apatite and calcium phosphate nanoparticles by flame synthesis, *Chem. Mater.* 17 (2005) 36–42.

- [118] R. Mazelsky, R.H. Hopkins, W.E. Kramer, Czochralski-growth of calcium fluorophosphate, *J. Cryst. Growth* 3–4 (1968) 260–264.
- [119] D. Lapraz, A. Baumer, Thermoluminescence properties of synthetic and natural fluorapatite single $\text{Ca}_5(\text{PO}_4)_3\text{F}$, *Phys. Stat. Sol.* 80 (1983) 353–366.
- [120] G. Daculsi, J.M. Bouler, R.Z. Legeros, Adaptive crystal formation in normal and pathological calcifications in synthetic calcium phosphate and related biomaterials, *Int. Rev. Cytol.* 172 (1997) 129–191.
- [121] R.Z. Legeros, Biological and synthetic apatites. in: P.W. Brown, B. Constantz (Eds.), *Hydroxyapatite and Related Materials*, CRC Press, Boca Raton, 1994, pp. 3–28.
- [122] J.C. Trombe, Contribution à l'étude de la décomposition et de la réactivité de certaines apatites hydroxylées, carbonatées ou fluorées alcalino-terreuses, Thesis, Paul Sabatier University, Toulouse, 1972.
- [123] G. Penel, G. Leroy, C. Rey, B. Sombret, J.P. Huvenne, E. Brès, Infrared and Raman microspectroscopy study of fluor-hydroxy- and hydroxy-apatite powders, *J. Mater. Sci. Mater. Med.* 8 (1997) 271–276.
- [124] L.J. Jha, S.M. Best, J.C. Knowles, I. Rehman, J.D. Santos, W. Bonfield, Preparation and characterization of fluoride-substituted apatites, *J. Mater. Sci. Mater. Med.* 8 (1997) 185–191.
- [125] L.M. Rodriguez-Lorenzo, J.N. Hart, K.A. Gross, Influence of fluorine in the synthesis of apatites. Synthesis of solid solutions of hydroxy-fluorapatite, *Biomaterials* 24 (2003) 3777–3785.
- [126] G. Montel, G. Bonel, J.C. Heughebaert, J.C. Trombe, C. Rey, New concepts in the composition, crystallization and growth of the mineral component of calcified tissues, *J. Cryst. Growth* 53 (1981) 74–99.
- [127] M. Okazaki, Fluoridated hydroxyapatites synthesized with organic phosphate ester, *Biomaterials* 12 (1991) 46–49.
- [128] M. Okazaki, Y. Miake, H. Tohda, T. Yanagisawa, J. Takahashi, Fluoridated apatite synthesized using a multi-step fluoride supply system, *Biomaterials* 20 (1999) 1303–1307.
- [129] S.F. Willigeroth, K. Beneke, M. Hannig, R. Zimehl, Preparation strategies for phosphate-based mineral biomaterials, *Prog. Colloid Polym. Sci.* 121 (2002) 1–6.
- [130] J. Lin, S. Raghavan, D.W. Fuerstenau, The adsorption of fluoride ions by hydroxyapatite from aqueous solution, *Colloids Surf.* 3 (1981) 357–370.
- [131] J. Szilagyi, Contribution à l'étude de la réactivité de l'émail dentaire et d'apatites synthétiques en présence d'ions fluorure: Mécanismes réactionnels, Thesis, National Polytechnique Institute of Toulouse, Toulouse, 1981.
- [132] M.R. Christoffersen, J. Christoffersen, J. Arends, Kinetics of dissolution of calcium hydroxyapatite. VII. The effect of fluoride, *J. Cryst. Growth* 67 (1984) 107–114.
- [133] X. Ranz, Développement et caractérisation de dépôts d'apatite obtenus par projection plasma sur prothèses orthopédiques, PhD Thesis, INPT, Toulouse, France, 1996.
- [134] K. Cheng, W. Weng, H. Qu, P. Du, G. Shen, G. Han, J. Yang, J.M.F. Ferreira, Sol-gel preparation and in vitro test of fluoroapatite/hydroxyapatite films, *J. Biomed. Mater. Res.* 69 (2004) 33–37.
- [135] W. Weng, S. Zhang, K. Cheng, H. Qu, P. Du, G. Shen, J. Yuan, G. Han, Sol-gel preparation of bioactive apatite films, *Surf. Coat. Technol.* 167 (2003) 292–296.
- [136] M. Iijima, J. Moradian-Oldak, Control of apatite crystal growth in a fluoride containing amelogenic-rich matrix, *Biomaterials* 26 (2005) 1595–1603.
- [137] V. Burghilea, A. Melinescu, C. Tardei, A. Lanculescu, Fluorapatite bioceramics, *Materiale de Constructii (Bucharest)* 30 (2000) 9–11.
- [138] E.J. Lee, H.W. Kim, H.E. Kim, Biocompatibility of fluor-hydroxyapatite bioceramics, *J. Am. Ceram. Soc.* 88 (2005) 1309–1311.
- [139] R. Fabian, L. Kotsis, P. Halmos, E. Veszprem, H. Veszprem, Synthesis of fluorapatite by using solid phase reactions, *Epitoanyag* 52 (2000) 2–7.
- [140] Y. Huang, Porous calcium phosphate bioceramic material and its manufacture, Chinese Patent, CN1488602A, 2004.

- [141] H.X. Peng, Z. Fan, J.R.G. Evans, J.J.C. Busfield, Microstructure of ceramic foams, *J. Eur. Ceram. Soc.* 20 (2000) 807–813.
- [142] X. Miao, Y. Hu, J. Liu, A.P. Wong, Porous calcium phosphate ceramics prepared by coating polyurethane foams with calcium phosphate cements, *Mater. Lett.* 58 (2004) 397–402.
- [143] J. Ruan, B. Huang, FHA bioceramic composite materials enhanced by ZrO_2 , *J. Central South Univ. Technol.* 1 (1994) 19–22.
- [144] C.K. Seo, H.K. Kim, Manufacture of bioceramics comprising wollastonite and apatite, Korean Patent, KR9711448, 1997.
- [145] H.W. Kim, Y.J. Noh, Y.H. Koh, H.E. Kim, Enhanced performance of fluorine substituted hydroxyapatite composites for hard tissue engineering, *J. Mat. Sci. Mat. Med.* 14 (2003) 899–904.
- [146] J. Carpena, B. Donazzon, J.L. Lacout, M. Frèche, Process for production of apatite ceramics, especially for biological use, French Patent, FR2772746, WO9933766, 1999.
- [147] I. Manjubala, T.S. Kumar, Preparation of biphasic calcium phosphate doped with magnesium fluoride for osteoporotic applications, *J. Mater. Sci. Lett.* 20 (2001) 1225–1227.
- [148] O. Mouzin, K. Soballe, J.E. Bechtold, Loading improves anchorage of hydroxyapatite implants more than titanium implants, *J. Biomed. Mater. Res.* 58 (2001) 61–68.
- [149] L. Sun, C.C. Berndt, K.A. Gross, A. Kucuk, Material fundamentals and clinical performance of plasma-sprayed hydroxyapatite coatings: A review, *J. Biomed. Mater. Res.* 58 (2001) 570–592.
- [150] P. Cheang, K.A. Khor, Addressing processing problems associated with plasma spraying of hydroxyapatite coatings, *Biomaterials* 17 (1996) 537–544.
- [151] W.J. Dhert, C.P. Klein, J.G. Wolke, E.A. van der Velde, K. de Groot, P.M. Rozing, A mechanical investigation of fluorapatite, magnesium whitlockite, and hydroxylapatite plasma-sprayed coatings in goats, *J. Biomed. Mater. Res.* 25 (1991) 1183–1200.
- [152] W.J. Dhert, C.P. Klein, J.A. Jansen, E.A. van der Velde, R.C. Vriesde, P.M. Rozing, K. de Groot, A histological and histomorphometrical investigation of fluorapatite, magnesium whitlockite, and hydroxylapatite plasma-sprayed coatings in goats, *J. Biomed. Mater. Res.* 27 (1993) 127–138.
- [153] C.P.A.T. Klein, J.G.C. Wolke, J.M.A. de Blieck-Hogervorst, K. de Groot, Calcium phosphate plasma-sprayed coatings and their stability: An *in vivo* study, *J. Biomed. Mater. Res.* 28 (1994) 909–917.
- [154] L. Gineste, M. Gineste, X. Ranz, A. Elleftherion, A. Guilhem, N. Rouquet, P. Frayssinet, Degradation of hydroxyapatite, fluorapatite, and fluorhydroxyapatite coatings of dental implants in dogs, *J. Biomed. Mater. Res.* 48 (1999) 224–234.
- [155] K. Cheng, W. Weng, G. Han, P. Du, G. Shen, J. Yang, J.M.F. Ferreira, The effect of triethanolamine on the formation of sol-gel derived fluoroapatite/hydroxyapatite solid solution, *Mater. Chem. Phys.* 78 (2003) 767–771.
- [156] D. Ferro, S.M. Barinov, J.V. Rau, R. Teghil, A. Latini, Calcium phosphate and fluorinated calcium phosphate coatings on titanium deposited by Nd:YAG laser at a high fluence, *Biomaterials* 26 (2005) 805–812.
- [157] E.J. Lee, S.H. Lee, H.W. Kim, Y.M. Kong, H.E. Kim, Fluoridated apatite coatings on titanium obtained by electron-beam deposition, *Biomaterials* 26 (2005) 3843–3851.
- [158] H. Zheng, K.K. Chittur, W.R. Lacefield, Dissolution/precipitation of calcium phosphate thin films produced by ion beam sputter deposition technique, *Biomaterials* 20 (1999) 443–451.
- [159] S. Cazalbou, D. Eichert, X. Ranz, C. Drouet, C. Combes, M.F. Harmand, C. Rey, Ion exchanges in apatites for biomedical applications, *J. Mater. Sci. Mater. Med.* 16 (2005) 405–409.
- [160] H.W. Kim, H.E. Kim, J.C. Knowles, Fluor-hydroxyapatite sol-gel coating on titanium substrate for hard tissue implants, *Biomaterials* 25 (2004) 3351–3358.
- [161] H.W. Kim, S.Y. Lee, C.J. Bae, Y.J. Noh, H.E. Kim, H.M. Kim, J.S. Ko, Porous ZrO_2 scaffold coated with hydroxyapatite with fluorapatite intermediate layer, *Biomaterials* 24 (2003) 3277–3284.

- [162] R.F. Code, N. Gelman, R.L. Armstrong, R.S. Hallsworth, C. Lemaire, P.T. Cheng, Field dependence of ^{19}F NMR in rat bone powders, *Phys. Med. Biol.* 35 (1990) 1271–1286.
- [163] M. Gryn timer, C. Rey, The effect of fluoride treatment on bone mineral crystals in the rat, *Bone* 13 (1992) 423–429.
- [164] G.V. Iyengar, L. Tandon, Minor and trace elements in human bones and teeth, in: International Atomic Energy Agency, NAHRES-39 report, Vienna, 1999.
- [165] E.J. O'Flaherty, Modeling bone mineral metabolism, with special reference to calcium and lead, *Neurotoxicology* 13 (1992) 789–797.
- [166] M.B. Rabinowitz, Toxicokinetics of bone lead, *Environ. Health Perspect.* 91 (1991) 33–37.
- [167] S.G. Dahl, P. Allain, P.J. Marie, Y. Mauras, G. Boivin, P. Ammann, Y. Tsouderos, P.D. Delmas, C. Christiansen, Incorporation and distribution of strontium in bone, *Bone* 28 (2001) 446–453.
- [168] S.G. Kshirsager, E. Lloyd, J. Vaughan, Discrimination between strontium and calcium in bone and the transfer from blood to bone in the rabbit, *Br. J. Radiol.* 39 (1966) 131–140.
- [169] A. Barry, H. Zhuang, A.A. Baig, W.I. Higuchi, Effect of fluoride pretreatment on the solubility of synthetic carbonated apatite, *Calcif. Tissue Int.* 72 (2003) 236–242.
- [170] C.H. Turner, G. Boivin, P.J. Meunier, A mathematical model for fluoride uptake by the skeleton, *Calcif. Tissue Int.* 52 (1993) 130–138.
- [171] A. van Nieuw Amerongen, J.G.M. Bolscher, E.C.I. Veerman, Saliva proteins: Protective and diagnostic value in cariology, *Caries Res.* 38 (2004) 247–253.
- [172] J. Hicks, F. Garcia-Godoy, C. Flaitz, Biological factors in dental caries enamel structure and the caries process in the dynamic process of demineralization and remineralization, *J. Clin. Pediatr. Dent.* part 1: 28 (2003) 47–52; part 2: 28 2004 119–124; part 3: 28 2004 303–314.
- [173] G.S. Ingram, E.A. Agalany, S.M. Higham, Caries and fluoride processes, *J. Dent.* 33 (2005) 187–191.
- [174] M. Kleerekoper, D.B. Mendlovic, Sodium fluoride therapy of postmenopausal osteoporosis, *Endocr. Rev.* 14 (1993) 312–323.
- [175] J. Caverzacio, G. Palmer, J.P. Bonjour, Fluoride: Mode of action, *Bone* 22 (1998) 585–589.
- [176] L. Li, The biochemistry and physiology of metallic fluoride: Action, mechanism, and implications, *Crit. Rev. Oral Biol. Med.* 14 (2003) 100–114.
- [177] K.H. Lau, T.K. Freeman, D.J. Baylink, A proposed mechanism of the mitogenic action of fluoride on bone cells. Inhibition of the activity of an osteoblastic acid phosphatase, *Metabolism* 38 (1989) 858–868.
- [178] A. Okuda, J. Kanehisa, J.N. Heersche, The effect of sodium fluoride on the resorptive activity of isolated osteoclasts, *J. Bone Miner. Res.* 5(suppl.1) (1990) S115–120.
- [179] M.L. Taylor, A. Boyde, S.J. Jones, The effect of fluoride on the patterns of adherence of osteoclasts cultured on and resorbing dentine: A 3-D assessment of vinculin-labelled cells using confocal optical microscopy, *Anat. Embryol. (Berl.)* 180 (1989) 427–435.
- [180] G.H. Bowden, Effect of fluoride on the microbial ecology of dental plaque, *J. Dent. Res.* 69 (spec no) (1990) 653–659.
- [181] R.E. Marquis, Antimicrobial action of fluoride for oral bacteria, *Can. J. Microbiol.* 41 (1995) 955–964.
- [182] T. Aoba, O. Fejerskov, Dental fluorosis: Chemistry and biology, *Crit. Rev. Oral Biol. Med.* 13 (2002) 155–170.
- [183] K. Cheng, W. Weng, H. Wang, S. Zhang, In vitro behavior of osteoblast-like cells on fluoridated hydroxyapatite coatings, *Biomaterials* 26 (2005) 6288–6295.
- [184] H.W. Kim, J.C. Knowles, L.H. Li, H.E. Kim, Mechanical performance and osteoblast-like cell responses of fluorine-substituted hydroxyapatite and zirconia dense composite, *J. Biomed. Mater. Res.* 72 (2005) 258–268.

- [185] A.J.S. Peaker, K.A. Hing, I.R. Gibson, L. DiSilvio, S.M. Best, L.L. Hench, W. Bonfield, Activity of human osteoblast-like cells on bioglass, hydroxyapatite and fluoride-substituted hydroxyapatite, *Bioceramics* 11 (1998) 285–288.
- [186] M. Wei, D. Vellinga, D. Lavesley, J. Evans, Z. Upton, Cell attachment and proliferation on hydroxyapatite and ion substituted hydroxyapatites, *Key Eng. Mater.* 240–242 (2003) 671–674.
- [187] H. Qu, M. Wei, The effect of fluoride content in fluoridated hydroxyapatite on osteoblast behavior, *Acta Biomaterials* 2 (2006) 113–119.
- [188] M. Inoue, R.Z. LeGeros, M. Inoue, H. Tsujigiwa, H. Nagatsuka, T. Yamamoto, N. Nagai, *In vitro* response of osteoblast-like and odontoblast-like cells to unsubstituted and substituted apatites, *J. Biomed. Mater. Res.* 70A (2004) 585–593.
- [189] A.S. Santiago, E.A. Santos, M.S. Sader, M.F. Santiago, G.A. Soares, Response of osteoblastic cells to titanium submitted to three different surface treatments, *Pesqui. Odont. Bras.* 19 (2005) 203–208.
- [190] Z.M. Isa, G.B. Schneider, R. Zaharias, D. Seabold, C.M. Stanford, Effects of fluoride-modified titanium surfaces on osteoblast proliferation and gene expression, *Int. J. Oral Maxillofac. Implants* 21 (2006) 203–211.
- [191] Y. Ramaswamy, D.R. Haynes, G. Berger, R. Gildenhaar, H. Lucas, C. Holding, H. Zreiqat, Bioceramic composition modulate resorption of human osteoclast, *J. Mater. Sci. Mater. Med.* 6 (2005) 1199–1205.
- [192] L. Gineste, M. Gineste, X. Ranz, A. Ellefterion, A. Guilhem, N. Rouquet, P. Frayssinet, Degradation of hydroxylapatite, fluorapatite and fluorhydroxyapatite coatings of dental implants in dogs, *J. Biomed. Mater. Res.* 48 (1999) 224–234.
- [193] S. Overgaard, K. Soballe, M. Lind, C. Büniger, Resorption of hydroxyapatite and fluorapatite coatings in man. An experimental study in trabecular bone, *J. Bone Joint Surg. (British Volume)* 79 (1997) 654–659.
- [194] S. Overgaard, M. Lind, K. Josephsen, A. Maunsbach, C. Büniger, K. Soballe, Resorption of hydroxyapatite and fluorapatite coatings on weight-bearing implants: A quantitative and morphological study in dogs, *J. Biomed. Mater. Res.* 39 (1996) 141–152.

Note from the Editors

In this volume, another chapter deals with inorganic and/or composite biomaterials by J. W. Nicholson and B. Czarnecka.

This page intentionally left blank

CHAPTER 7

Fluoride in Dentistry and Dental Restoratives

John W. Nicholson,^{1,*} and Beata Czarnecka²

¹*Department of Chemical and Pharmaceutical Sciences, School of Science, University of Greenwich, Medway Campus, Chatham, Kent ME4 4TB, UK*

²*Department of Biomaterials and Experimental Dentistry, University of Medical Sciences, Ul Bokowska 70, 60–812 Poznań, Poland*

Contents

1. Introduction	334
2. Fluoride in dentistry	335
2.1. The importance of fluoride in dental health	335
2.1.1. Fluoride in dentistry	335
2.1.2. Demineralisation/remineralisation behaviour of the tooth surface	338
2.1.3. Possible antimicrobial effect of fluoride	339
2.2. Interaction of fluoride with hydroxyapatite	340
2.2.1. Basic chemistry	340
2.2.2. Fluoride and oral health: practical aspects	343
2.3. Adverse effects of fluoride	344
2.3.1. Fluorosis	344
2.3.2. Potential systemic effects	345
3. Methods of delivering fluoride	347
3.1. Drinking water	347
3.2. Salt and milk	350
3.3. Dentifrices	351
3.4. Fluoride mouthrinses	353
3.5. Topical fluoride applications	354
3.5.1. Gels	354
3.5.2. Varnishes	355
3.6. Fluoride-releasing restorative materials	355
3.6.1. Glass-ionomers	356
3.6.2. Resin-modified glass-ionomers	361
3.6.3. Compomers	362
3.6.4. Fluoride-containing composite resins	364
4. Conclusions	365
References	366
Note from the Editors	378

*Corresponding author. Tel.: +44-208-331-9965; Fax: +44-208-331-9805;
E-mail: J.W.Nicholson@gre.ac.uk

Abstract

Fluoride has been shown to be a key element in ensuring that populations develop and maintain sound dental health. At the atomic level, it has an effect on the demineralisation/reminerisation equilibrium that exists at the tooth surface, shifting it back in favour of remineralisation. Fluoride does this by a variety of mechanisms, including reducing the solvating power of saliva towards the tooth mineral, reducing the solubility of the apatite phase, and improving the crystallisation kinetics of the mineralisation process. It may also have an effect on the bacterial populations living in the oral biofilms, through inhibition of their enzyme activity.

Fluoride is supplied to large number of populations throughout the world in drinking water and, at the levels used, it is safe and effective, and has been accepted as such by numerous public health agencies worldwide. Fluoride can be delivered partly as a public health measure, mainly through the domestic water supply but also through its introduction to table salt or milk, and partly on an individual basis. The latter includes the use of fluoridated dentifrices, mouthrinses, topical gels and varnishes, and the use of fluoride-releasing restorative materials to repair teeth damaged by caries. These tailored individual treatment measures are particularly important in reducing caries in high-risk groups within any population.

The use of fluoridated products, as well as fluoridation of domestic water supplies, has been one of the most successful approaches ever adopted to improve any aspect of public health. Continued use of such products, albeit under careful control and supervision by the dental profession, will remain important if the advances in oral health of the past 50 years are to be maintained in the future.

1. INTRODUCTION

The element fluorine in the form of the fluoride ion is well known to be associated with sound dental health [1]. This association has been known since at least the 1930s when in a classic epidemiological study, Dean *et al.* [2] showed an inverse relationship between mottled enamel and the occurrence of dental caries. Mottling had previously been shown to be caused by the presence of fluoride [3], so Dean *et al.* concluded that this element was responsible for reducing the incidence of dental caries [2]. They demonstrated that 1 part per million (ppm) of fluoride in drinking water was optimal, as it gave the greatest reduction in dental caries without also causing mottling of the teeth. As a result of this study, the condition of tooth mottling was renamed 'dental fluorosis', and the study paved the way for extensive fluoridation of domestic water supplies throughout the developed world. Though controversial, this step has undoubtedly led to a reduction in caries in populations so treated. An example of the data supporting this can be seen in Table 1 [4].

Toothpaste containing fluoride became available in this period, and has also contributed to the reduction in the incidence of caries over the period covered. However, it is apparent that the reduction was greater in the cohort from the Republic of Ireland, who also had the benefit of fluoride in their drinking water. Similar findings have been reported in numerous similar studies worldwide [4],

Table 1. Mean DMFT (damaged, missing, filled teeth) in two regions of Ireland, showing the effect of water fluoridation [4]

Northern Ireland (northern region) (nonfluoridated)			Republic of Ireland (eastern region) (fluoridated)		
1963	1983	1996/1997	1961–1963	1984	1993
5.5	4.4	3.3	4.7	2.6	1.4

demonstrating beyond reasonable doubt that that there is an improvement in the dental health of populations with fluoridated drinking water.

Fluoridation of drinking water is only one of the ways that fluoride has been delivered to the community and improved dental health. Others include (i) fluoridated table salt and fluoridated milk, (ii) fluoridated dentifrices, (iii) topical fluoride gels, varnishes, and mouthrinses, and (iv) fluoride-releasing dental restorative materials. All of these are reviewed in the current chapter, along with the most recent findings on their clinical effectiveness. First, the role of fluoride in dentistry is considered in detail. An understanding of the underlying chemistry involved is critical to an appreciation of the clinical function of fluoride. We have now reached the point where the effect of fluoride on the mineral phase of the tooth, hydroxyapatite, is reasonably well understood, and can be used as starting point for considering the contribution of fluoride to dental health.

2. FLUORIDE IN DENTISTRY

2.1. The importance of fluoride in dental health

2.1.1. Fluoride in dentistry

Following the discovery of the link between fluoride and reduced incidence of dental caries community fluoridation programmes were instituted in America. The first of these were Grand-Rapids, Michigan, and Newburg, New York, and the effects were monitored by comparing both of these against control cities without fluoridated water, namely Muskegon and Kingston. By the early 1950s, it was apparent that dental caries had been reduced by around 50% in those areas that had a fluoridated water supply [4–6]. Since then, most cities across the world have moved to provide fluoridated water as standard to their populations.

Exposure to fluoride has to be closely regulated, and current estimates of optimum level of exposure to fluoride are between 0.05 and 0.07 mg/kg of body weight [7]. Some researchers have suggested that even lower levels, for

example, 0.03–0.04 mg/kg, are appropriate [8], though these are lower than those typically aimed for in public health programmes. Fluoride is especially important for children to prevent caries. However, it is important to regulate intake, as excessive exposure to fluoride can result in fluorosis. There are several sources of fluoride available to typical children in the developed world, including dentifrices, milk and other foodstuffs, as well as drinking water [4]. All these sources need to be taken into consideration when setting the level of fluoride to be added to public drinking water supplies.

Current levels of fluoride in water were based on findings of Galagan and Vermilion [9] from the late 1950s, though they have since been modified downwards slightly. Thus, the World Health Organisation recommends levels of fluoride between 0.5 and 1.0 ppm [10]. Levels of water consumption do not vary particularly widely with climate, but are only about 20% higher in regions with higher average air temperatures [10]. Also, they vary throughout the year, again reflecting the local air temperature, with water consumption being greater in warmer conditions [10]. Consequently, there is no need to adjust the overall level of fluoride to take account of local climate and local variations in patterns of water consumption.

Dental caries is one of the most common diseases in humans, and is mediated by bacteria, mainly *Streptococcus mutans*. It has been estimated to affect between 60 and 90% of school children in the developed world and the majority of adults [11], and is consequently a major public health concern. In addition to the developed world, it is the most widespread oral disease in many Asian and Latin American countries, though it currently appears to be less of a problem in Africa. However, changes in living conditions and increases in sugar consumption within a changing diet suggest that, in Africa too, the incidence of caries will increase, and that it will become a major public health issue here, too.

The presence of *S. mutans* and other cariogenic bacteria contributes towards the formation of a biofilm known as dental plaque, and their metabolism of fermentable carbohydrates in the diet leads to the formation of acids [12]. Dental caries has been described as 'a complex imbalance in physiologic equilibrium between tooth mineral and biofilm' [13]. Biofilms imply the involvement of micro-biological species [14], but the key concept included within this definition is that the bacteria involved are native to the body, not a group of specific invasive bacteria causing infection [14].

The resident microbes within the mouth readily form biofilms on teeth. A biofilm consists of a population of bacteria coexisting in an orderly structure at the interface of a solid and a liquid [14] and, within a biofilm, bacteria living in colonies encapsulated in a matrix of extracellular polymer. Oral biofilms are known to vary extensively in structure throughout the colony, with regions of densely packed microorganisms surrounded by open water channels. Each type of bacteria exists in reasonably defined environments which are influenced by surrounding cells, distance from the outer surface and local structure, all of which influence availability of nutrients and ambient pH.

As far as caries is concerned, lesions develop where biofilms accumulate and are allowed to mature for prolonged periods of time. This includes occlusal surfaces, interproximal areas and along the margin of the gingiva. Once a frank cavity forms, it becomes an altered environment that becomes populated with biofilm organisms capable of adapting to the reducing local pH. In such cavities, the metabolism of the biofilm and the diffusion of substances through it become different from those of the biofilms over either sound or inactive caries [15].

The bacteria within a biofilm produce organic acids, the proportions of which vary depending on whether caries is active, that is, progressing through the tooth, or arrested; and also with depth into the cavity, whether present in enamel or dentine [16]. Active caries has been shown to have a pH of 4.9 ± 0.2 , with the acid mainly being lactic acid ($88.2 \pm 8.3\%$) together with some ethanoic (acetic) acid ($9.6 \pm 5.9\%$), whereas arrested caries consists mainly of ethanoic acid ($64.0 \pm 14.4\%$) with some propionic acid ($18.2 \pm 9.2\%$) [17]. There is destruction of both mineral and organic phase of the tooth as a result of the action of these acids, though most damage is done to the mineral phase [12]. Its loss results in a greater amount of organic phases in the tooth, and this in turn becomes discoloured as a result of the action of these organic acids. The result is the yellowy-brown lesion characteristic of advanced dental caries.

When fluoride therapy was first used it was widely assumed that its effect was systemic. In particular, it was assumed to become incorporated into the tooth during development, forming the less acid-soluble fluorapatite rather than hydroxyapatite [18,19]. There was evidence to support this view. For example, studies showed that incidence of caries was lower in areas with fluoridated water and that fluoride concentration was higher in the surface of teeth of subjects in high fluoride areas [20,21]. However, over the last three decades or so, there has been a shift in our understanding, and it is now known that the principal effects of fluoride take place after eruption of the tooth [22].

The modern view is that fluoride interferes with the progression of caries through a number of mechanisms, all of which apply after the tooth has erupted. These include the following:

- (i) inhibition of demineralisation;
- (ii) promotion of mineralisation;
- (iii) development of a mineral phase of enhanced acid resistance; and
- (iv) damage to oral bacteria through inhibition of their enzymes [12].

Exposure to fluoride, by whatever means, leads to moderately elevated levels of fluoride in the saliva and the plaque. This is sufficient to help caries prevention by inhibiting demineralisation and assisting remineralisation. These processes are discussed in detail in the following sections of this chapter.

For many years, the process of caries was thought to be irreversible and to result in permanent loss of tooth material. This process eventually leads to the development of a cavity, and a considerable part of the dental professions' time

is taken up with diagnosing and repairing such cavities. However, in recent years, it has become apparent that caries is not irreversible. Rather, as the process of tooth maintenance represents a balance of demineralisation and remineralisation, so caries can be considered to be a shift in this balance, a shift, moreover, that can be reversed under the appropriate conditions.

Remineralisation occurs when partly dissolved crystals are induced to grow by precipitation of the mineral-forming ions Ca^{2+} and PO_4^{3-} . This is a natural process that occurs as a result of the concentration of these ions in saliva [23] and it serves to oppose the demineralising effects of caries. The processes involved are complex [24] and involve dynamic activity at the interface between the tooth, the saliva, the pellicle and the plaque. Fluoride plays a role in enhancing these processes, and though this is not the only contribution that fluoride makes to protect the tooth from caries, it is nonetheless an important one.

2.1.2. Demineralisation/remineralisation behaviour of the tooth surface

The first sign of caries in the enamel is the so-called 'white spot lesion', a feature which arises due to sub-surface demineralisation [23]. Although at this stage the structure appears reasonably intact, it may have lost up to 50% of its original mineral content [25]. One of the difficulties in clinical dentistry is the fact that these early lesions may be difficult to detect, particularly when they are hidden in fissures and pits. By the time they are apparent, they may have progressed significantly and extended well into the dentine [26]. Fluoride, in promoting remineralisation, may contribute to a clinical problem with certain lesions. By encouraging only the surface layer to undergo remineralisation, it may cause the underlying lesions to be concealed [27]. In such cases, remineralisation of the sub-structure is inhibited because the mineralised surface that forms is relatively impermeable to calcium and phosphate ions, which consequently cannot penetrate the surface layer [28].

It is now known that teeth undergo a continuous process of demineralisation and remineralisation (see Table 2), which is driven by changes in the plaque composition [29]. In the presence of fermentable carbohydrates plaque microorganisms generate characteristic organic acids, that is, lactic and acetic [17], and these diffuse through the pellicle to the tooth surface and cause demineralisation [30]. Ions are then liberated from the mineral phase into this low pH liquid [31], and they diffuse outwards and re-precipitate at the surface layer of the demineralised lesion [32,33]. If this process is sufficiently rapid, there is a net loss of tooth mineral and irreversible cavity formation.

On the other hand, remineralisation may occur at such a rate that the surface layer is retained (Table 2). This requires continuous renewal of ions, either from among those newly solubilised or from those present anyway in the saliva. This process has been discussed in terms of thermodynamics, in particular of the solubilities of the various possible calcium phosphate salts [34]. The present authors are wary of this approach, as what is involved is essentially a kinetic

Table 2. Factors influencing the position of the demineralisation–remineralisation equilibrium and clinical outcomes

Factors	Poor oral hygiene Active biofilm High levels of fermentable carbohydrate in diet	Good oral hygiene Biofilm absent/inactive Low levels of fermentable carbohydrate in diet Fluoride in saliva
Biofilm activity	Active Acid production pH circa 4.5	In active Little or no acid pH 5.5 or higher
Favoured process	Demineralisation	Remineralisation
Clinical outcome	Carious lesion	Healthy tooth surface

process, and it may in fact take place at conditions far removed from equilibrium. Consideration of thermodynamic properties, such as solubilities and phase diagrams, needs to be balanced with an appreciation of kinetic factors to achieve a full picture of the chemistry of the tooth surface (Table 2).

Useful insights can undoubtedly be obtained by consideration of the likely chemical species present, and their behaviour at varying pH. Saliva is known to be metastable and supersaturated with respect to hydroxyapatite [35], which is further evidence that the purely thermodynamic approach is suspect. It does mean though that there is a significant driving force for remineralisation, as the supersaturated saliva approaches equilibrium with the consequent precipitation of hydroxyapatite. The development or arrest of a carious lesion is therefore dependent on the frequency and duration of the remineralisation and demineralisation processes, and also on their respective rates. These in turn depend on factors such as sucrose consumption, salivary flow, oral hygiene [36] and, of course, fluoride exposure [37]. It is the latter that is of greatest interest in the present chapter, and its role will be considered in detail in the next section.

2.1.3. Possible antimicrobial effect of fluoride

There is some evidence that one potential effect of the release of fluoride is for it to act as an antimicrobial agent. It is known that millimolar concentrations of fluoride ion in water will affect a variety of activities in several types of cell [38]. It does this by denaturing the enzymes. In bacteria, the most important enzyme which can be affected is enolase, and this is responsible for the conversion of 2-P-glycerate to 2-enol pyruvate in the glycolic pathway. Enolase is a magnesium-containing

enzyme and, without Mg^{2+} ions, is deactivated. Fluoride, probably as monofluorophosphate ion, reacts preferentially with Mg^{2+} , removing it from the catalytic site in the enzyme and thereby inhibiting its activity [39,40]. Fluoride has other adverse effects on the biochemistry of bacteria, including inhibition of phosphatases [41], which also contain magnesium. There is also evidence that fluoride generally has an adverse effect on bacterial growth [42,43].

Unfortunately, however, there is evidence that achieving sufficient fluoride levels *in vivo* to impair enzyme activity and inhibit bacterial growth is difficult [44]. It may therefore be that such potential action of fluoride, for example on cariogenic bacteria such as *S. mutans*, has little or no part to play in practical caries prevention.

In addition, it seems that *S. mutans* can adapt to the presence of fluoride in such a way that its cariogenic potential is reduced. In *in vitro* tests in rats, fluoride-resistant strains of *S. mutans* were found to produce cariogenic acids more slowly than normal strains [45]. However, this effect has not been demonstrated in human subjects.

2.2. Interaction of fluoride with hydroxyapatite

2.2.1. Basic chemistry

The mineral phase of the tooth is predominantly hydroxyapatite, with the enamel containing a greater proportion than the dentine. This phase is very far from inert, but undergoes chemical exchange of ions with the surrounding saliva [46] driven by factors such as local fluctuations in pH of the plaque [47,48], and the presence of fermentable carbohydrates [49,50]. The major cariostatic effect of fluoride is that it influences these processes, even at very low concentrations, that is, 0.2–1 ppm, and in particular it facilitates precipitation of calcium phosphate [51]. This is consistent with *in vitro* observations that fluoride is capable of inducing hydroxyapatite to form from solutions of calcium and phosphate ions [52]. The inorganic composition of saliva is such that it is readily able to precipitate calcium phosphate in this way [53], and thus leads to remineralisation at the tooth surface. The presence of fluoride at slightly elevated concentrations enhances this ability as pH is lowered from the level of active to the level of arrested caries (pH 5.5 and above) [53].

In addition, the presence of low concentrations of fluoride in saliva also has the effect of preventing dissolution of hydroxyapatite from enamel at low pH, an effect that has been shown to apply at values of pH as low as 4.2 [54,55]. Thus, it is the fluoride in solution that has the effect of reducing solubility, rather than the fluoride in the mineral phase [51]. This effect requires extremely small amounts of fluoride, typically in the sub-ppm range [51,56], and has the effect of shifting the balance between demineralisation and remineralisation so that loss of the hard tissue is inhibited.

Nevertheless, fluoride does lead to a reduction in the solubility of hydroxyapatite in aqueous solution, even in the absence of trace levels of fluoride in solution, and hence can be seen to have an effect in the solid state as well [57]. Apatites are complex and diverse materials which have the general formula $\text{Ca}_{10}(\text{PO}_4)_6\text{X}_2$ ($\text{X} = \text{F}, \text{Cl}, \text{OH}$) and they represent a crystallographic system, in which there can be considerable replacement of species. Thus, with little or no change in the dimensions of the crystal lattice, there can be exchanges of OH^- for F^- , Ca^{2+} for Sr^{2+} , and PO_4^{3-} for CO_3^{2-} ; and all of these are known to occur in biological systems. Natural hydroxyapatite, for example, is often partially carbonate substituted [58].

The incorporation of fluoride in place of hydroxyl groups is chemically straightforward [59,60] and, as we have seen, results in a substance of greater resistance to acid attack. This is partly due to the greater electronegativity of fluorine, which means that the electrostatic attraction between Ca^{2+} and F^- is greater than that between Ca^{2+} and OH^- . As a result, the fluoridated apatite lattice is more stable than hydroxyapatite [61–63]. It is also more crystalline [64].

Fluoride also brings about a change in composition in natural hydroxyapatite, since it not only undergoes a simple exchange with hydroxyl ions but also promotes the formation of a phase containing less carbonate than the initial hydroxyapatite [65]. Fluoride is taken up more readily by demineralised enamel than by sound enamel [66], which means its availability causes a 'self-healing' effect in the mineral phase of the hard tissue.

In a recent paper, the effect of fluoride for hydroxyl ion exchange as it affects the individual atomic layers of hydroxyapatite in a crystal has been modelled, using a computational approach [67]. Computational methods of this type are able to calculate both the energy changes in exchanging hydroxyl ions for fluoride, and also to determine the expected distribution of the fluoride in the resulting crystal. These calculations provide interesting results about the overall process.

For example, substitution of hydroxyl ions by fluoride ions has been shown to be energetically favourable when that substitution takes place in the uppermost surface layer. It is highly exothermic, with an enthalpy change of 193 kJ/mol. Incorporation of fluoride into lower layers, though, is less favoured. In the second layer, it yields 164 kJ/mol and in the third layer only 68 kJ/mol. Beyond that, there is almost no energy change associated with this exchange, values of about 4 kJ/mol being calculated [67], which means that there is little or no driving force for fluoride to penetrate deep into the bulk of the hydroxyapatite crystal. These results show that it is relatively easy to replace the surface layer hydroxyl groups with fluoride ions, but go on to predict that fluoride will not penetrate much below about three atomic layers of the bulk crystal. As a result, whether fluoride is taken up by replacement of OH^- ions, or whether the mechanism of deposition involves re-precipitation of dissolved hydroxyapatite, the fluoridated form of apatite is found in the surface layers only [67].

The effect of water on the surface has also been modelled [67], and the calculations have shown that surface layers of water are able to take up OH^- ions

from hydroxyapatite more readily than they can take up F^- ions from the substituted apatite structure. Hence, F^- tends to remain in its place in the crystal lattice. The ease of dissolution can be determined from the calculated diffusion coefficients, which have been found to be respectively for OH^- and F^- $5.74 \times 10^{-9} \text{ cm}^2/\text{s}$ and 0. By comparison, the calculated diffusion coefficient for molecules of water in the region close to the surface was 1.50×10^{-7} . This is similar to that for the hydroxyl ions, and demonstrates the significance of dissolution in water as part of the mechanism of movement of these ions. Sub-surface OH^- ions, by contrast, have been shown to have a very low diffusion coefficient, that is 1.23×10^{-12} , which suggests that these ions are almost completely immobile compared with surface layer ones [67].

In the presence of fluoride, calcium ions have been found to be more firmly anchored than in pure hydroxyapatite [67]. This enhances the overall resistance to dissolution. Thus, the presence of a thin stable film of fluorapatite on the surface of hydroxyapatite crystals has two effects, namely (i) resistance to diffusion and dissolution of the anion and (ii) firmer binding of calcium ions into the surface. Both of these make the resulting apatite structure more resistant to dissolution, regardless of the pH of the external medium, and they thereby increase the resistance of the mineral phase to the onset of caries.

Hydroxyapatite (with some carbonate inclusions) is the most stable of the possible calcium phosphate salts that can be formed under physiological conditions. However, it is not the most rapid one to form. Instead, octacalcium phosphate (OCP) will precipitate more readily than hydroxyapatite. This led Brown in 1987 to propose that, as the kinetically favoured compound, OCP precipitates first, and then undergoes irreversible hydrolysis to a transition product 'OCP hydrolyzate' [68]. This hypothesis is consistent with the observation that enamel comprises hydroxyapatite crystals that have the long, plate-like morphology that is generally considered characteristic of OCP crystals [69]. Overall, it seems that enamel crystals, with their elongated form, result from early precipitation of OCP, which forms a template on which hydroxyapatite units grow epitaxially [70,71]. This leads to enamel mineralisation with the observed thin, ribbon-like structure of crystals.

The role of fluoride in this mineralisation process seems to be in promoting the conversion of OCP to hydroxyapatite, and producing plate-like crystals of the more thermodynamically stable mineral. Fluoride is effective at promoting the formation of an apatite lattice through a solid-state transformation of OCP at levels between 0.05 and 0.4 ppm [72].

Under neutral conditions, fluoride is also able to induce nucleation and growth of apatite crystals without the involvement of OCP [72]. This requires fluoride concentrations of 0.5 ppm or higher, which are rarely achieved *in vivo* except in cases where fluorosis may result. It is significant that in severe cases of fluorotic enamel, ultra-structural studies [73] have shown the occurrence of a proliferation of apatite nuclei, suggesting that the presence of fluoride may act to encourage precipitation of crystals of fluorapatite.

The various findings about fluoride and its interaction with the hydroxyapatite at the molecular level show that the relationship is complicated and multifaceted. The broad conclusion from the enormous volume of work that has led to our current understanding of the role of fluoride is that it is overwhelmingly beneficial. It promotes numerous desirable properties in tooth mineral, reducing solubility through action in both the saliva and in the mineral phase, it shifts the demineralisation/remineralisation equilibrium in favour of remineralisation, and through its actions in the solid state, ensures that the kinetically favoured OCP is transformed into the more thermodynamically stable hydroxyapatite. Research continues, and there is no doubt that there is still more to learn about the complexities of the interaction of fluoride with hydroxyapatite under physiological conditions.

2.2.2. Fluoride and oral health: practical aspects

There has been a large volume of work on the chemistry of the effect of fluoride on caries. Typically, studies have employed an artificial caries medium, and exposed extracted teeth to acidified buffer solutions or gels. Buffers are typically adjusted to pH 4–6 using lactic acid or acetic acid. Such studies have demonstrated that fluoride reduces the rate of formation of carious lesions *in vitro* [74–76], and also that the appearance of the resulting lesion is modified [76]. Chemical analysis of white spot lesions have shown them to contain more fluoride than the surrounding sound enamel [77,78], which suggests that fluoride has a greater affinity for demineralised regions. As a result of this, precipitation of hydroxyapatite is accelerated, particularly around the edges of the lesion. Overall, this shows that the relationship between local pH and the presence of fluoride is complicated. One factor is that a decrease in pH reduces the OH^- concentration, leading to relatively enhanced F^- concentration. This results in an increase in the rate of fluoride uptake as a consequence of mass action effects.

Fluoride is also employed clinically to reduce hypersensitivity in patients. It may be employed at low levels, that is, less than 1%, in solutions, and as such it is effective in reducing reported pain levels in patients experiencing hypersensitivity [79]. Fluoride-containing varnishes have also been shown to reduce such pain [80], though not to a greater extent than non-fluoridated varnishes. On the contrary, fluoridated toothpastes seem to have a positive effect on reducing hypersensitivity [81,82]. Fluoride is not the only possible agent to promote such pain reduction; compounds such as strontium chloride [83] and potassium nitrate [84] are also known to be effective. This suggests that a variety of mechanisms of pain reduction are possible. In the case of fluoride, it appears linked to the ease of precipitation, for example of CaF_2 through interaction with saliva, leading to sealing of structural imperfections in the tooth surface. This reduces the ease with which hot or cold liquids can diffuse into the tooth and eventually through to the pulp, causing the sensation of pain.

Although not the most important effect of fluoride, the effect on hypersensitivity is further evidence of generally beneficial role of this element. More important is its effect of caries. The rest of the chapter is concerned with the ways in which fluoride can be delivered to the teeth of individuals in various populations and how its positive effects are harnessed to promote improved oral health.

2.3. Adverse effects of fluoride

2.3.1. Fluorosis

Fluorosis is regarded as the most serious adverse effect of exposure to relatively low doses of fluoride [85]. In extreme cases, fluorosis manifests itself as brown mottling of the enamel, and also results in overall yellowing of the teeth, and a greater degree of brittleness. It occurs as the result of excessive consumption of fluoride, though at levels significantly higher than the 0.7–1.2 ppm used in fluoridated water. As ever, the dose critically determines whether there will be any adverse effects, and this depends *inter alia* on the amount taken in, the proportion absorbed by the body and the weight of the patient. In response to these considerations, the medical profession tends to advise mothers not to make up infant feeds from fluoridated water, though there is as much concern with the fact that ingested fluoride promotes removal of calcium from the body as CaF_2 in the faeces as with any adverse effects of retained fluoride. Another group who are advised against consuming fluoridated water are patients on kidney dialysis [85].

Fluorosis affects the enamel of the tooth, causing it to become hypomineralised. This is detected as visual changes in the opacity, and it is only in extreme cases that this leads to an adverse appearance as mottling of the tooth surface [86]. The severity of the discolouration depends on the dose of fluoride, its duration and timing of consumption.

Teeth are most susceptible to the adverse effects of excess fluoride at the transition and early maturation stages of enamel development [87]. The timing of these stages varies with the type of tooth [88]. For the most prominent teeth, the upper central incisors, the most sensitive period appears to be 13–24 months, with some indication that the timing varies slightly for boys and girls [87,88].

The risk of fluorosis is only of concern for children below about 8 years of age, because enamel can no longer be affected once pre-eruptive maturation has occurred [89]. As far as cosmetic effects are concerned, the critical age is somewhat younger because at this age the central incisors are undergoing development, and hence are at a stage that makes them susceptible to fluorosis. For children at the age likely to be affected, the main sources of fluoride are drinking water, processed food and beverages, toothpaste and other dental products (i.e., tablets or drops).

In its mildest form, fluorosis appears on the enamel surface as chalky, lace-like marks, and these may not be apparent to the casual observer [90]. As severity

increases, over half of the enamel surface may appear white and opaque. In its most severe form, fluorosis causes the enamel to become pitted and brittle. Despite this embrittlement, fluorosis rarely causes the teeth to suffer from severe mechanical problems, so the condition is considered to be an aesthetic rather than a functional problem [91,92]. Both moderate and severe fluorosis may be accompanied by the development of a brown discolouration.

In general, moderate and severe fluorosis is rare. However, mild fluorosis has been detected at significant levels, for example, in 26% of subjects in one recent study [93]. However, the mildness of the fluorosis detected is associated with only very slight changes in the appearance of the teeth, which suggests that, even at these levels, it is not a major public health problem. Nonetheless, it is appropriate to ensure that parents or guardians of children continue to receive sound advice on safe levels of fluoride for those in their care to be exposed to and, since the cariostatic effect of fluoride is known to occur well after enamel formation during tooth development, treatment to reduce caries should concentrate on those measures that carry the lowest possible risks of fluorosis [91].

In most cases, fluoridated toothpastes are acceptable substances for use, but even for these products, there is some risk of fluorosis. For example, children who began using them before the age of 2 were shown to be at higher risk of developing fluorosis than children who do not use it at all [94,95]. However, the relative importance of the various factors that govern exposure to fluoride from this source (age of starting to use fluoridated toothpastes, amount used and frequency) is not known.

One contributor to this risk of fluorosis in children is the lack of control in the swallowing reflex, particularly in children younger than 3 years of age [96]. Children are also known to like the taste of toothpaste, and hence to swallow it deliberately. A small toothbrush of the size appropriate for use by a child holds in the region of 0.75–1.0 g of toothpaste, which means that an individual blob of toothpaste provides between 0.75 and 1.0 mg of fluoride. It has been estimated that children below the age of six swallow a mean of 0.3 of toothpaste per brushing and this may be sufficient to lead to ingestion of enough fluoride to cause the mottling associated with fluorosis [97].

2.3.2. Potential systemic effects

Fluoridation of drinking water causes every member of the population to be exposed to fluoride treatment, though its principal benefits are for children. This is the basis for one of the widely used arguments against fluoridation of water supplies. The concern which underlies this argument has led to certain public organisations across the world ceasing to fluoridate the water. An example of this was the Gold Coast Council in Queensland, Australia, which stopped fluoridation in 1979 [98].

Another much discussed concern is the potential effect on bone, with conditions such as skeletal fluorosis, osteosarcomas, osteoporosis and greater incidence of fractures being considered.

Animal studies have demonstrated that, with sufficiently high doses of fluoride, bone strength decreases. In rats, this required at least 50 ppm/day [99,100] or 0.23 mg/kg/day [101], with at least three months treatment needed before loss of strength was significant [101,102]. In rabbits, high dose rates of fluoride were similarly required, for example, 16 mg/day, in order to produce an effect [103]. By contrast, exposure to low amounts of fluoride increased bone strength in rats without increasing femoral bone density [100]. For comparison, consuming a typical amount of water (1 L/day) at a concentration of 1 ppm provides a dose of 0.02 mg/kg/day for a 60-kg person, that is, some 150th of the dose given to cause adverse effects in rats [98].

Hip fracture has been reported to increase in two studies, respectively after 4 years [104] and 7 years [105] of exposure to fluoridated water. However, other studies have shown either no effect after 6 years [106] or 10 years [107], or a reduction in incidence [108,109]. The problem with such studies is that there may be bias due to lack of ability to control such variables as age, race, poverty, activity levels or overall health status.

Clinical trials have been reported, and these are not subject to the same levels of uncertainty. They have concentrated on bone mineral density, because this parameter is an acceptable measure of bone mass, is sensitive to the occurrence of osteoporosis and correlates well with the likelihood of bone fracture in patients affected by osteoporosis. Bone mineral density is known to increase in childhood and adolescence, to reach a maximum around the age of 40, then to decline [110,111]. In women in the years immediately following the menopause, it may sharply reduce, and if it reaches a level $2\frac{1}{2}$ standard deviations below the young adult mean value, the condition is defined by the WHO as osteoporosis [110,111].

When fluoride dose has been tested in a controlled clinical trial, no adverse effects on bone mineral density have been detected. As expected from this finding, there have been no reports of increased susceptibility to bone fracture in these studies either.

Daily doses studied have ranged from 9 to 22.6 mg of fluoride over time periods of 1–4 years [98]. These trials were particularly concerned with the use of slow-release NaF [112,113] or sodium monofluorophosphate preparations [114,115], and they generally led to reductions in the incidence of bone fracture, as shown in Table 3. In addition, they typically caused increased bone density at the neck of the femur, the femoral condyle and the lower spine [98] (Table 3).

These results confirm the findings of animal studies that lower doses have greater beneficial effects. Overall, they are consistent with the general conclusion from a large number of studies in different regions and with highly varied populations that fluoridated water has no adverse effect on bone. On the contrary, there is clear evidence that it is beneficial [98].

Table 3. Clinical trial results of fluoride exposure

Treatment (dose/day)	Fluoride equivalent (dose/day)	Time until reduction in incidence of fractures (years)	Reference
50 mg NaF	22.6 mg	2	[116]
50 mg NaF	22.6 mg	2.5	[117]
75 mg NaF	33.9 mg	No effect	[118]
114 mg NaMFP	15 mg	3	[119]
200 mg NaMFP	20 mg	4	[115]

3. METHODS OF DELIVERING FLUORIDE

3.1. Drinking water

Water fluoridation is regarded by the World Health Organisation as one of the key means of delivering improved oral health to populations throughout the world [120]. Recent reports have emphasised the great improvements in oral health, but note that problems remain. This is especially true in underprivileged groups within populations of both the developed and the developing countries of the world.

Fluoridation of the drinking water supply involves treating with appropriate fluorides to produce levels in low fluoride areas that mimic those occurring in naturally high fluoride areas [121]. When fluoridated water is consumed regularly, a low concentration of fluoride develops in the mouth that assumes a more or less steady state. This fluoride becomes distributed between the dental plaque, the saliva and the enamel surfaces [122]. It becomes attached to the latter with increasing degrees of binding strength, starting as loosely bound, but eventually becoming fully incorporated into the hydroxyapatite structure of the mineral phase.

As far as the addition of fluoride to drinking water is concerned, the key requirement is that the compound chosen should yield free fluoride ions readily on dissolution in water [123]. Sodium fluoride can be used as it is reasonably soluble and dissolves readily [124]. However, even by the 1950s it was proving relatively expensive, and so the use of alternative compounds was investigated [125]. This identified fluorosilicic acid and its disodium salt as possible alternatives (Table 4), and their use as the source of fluoride in drinking waters continues to this day.

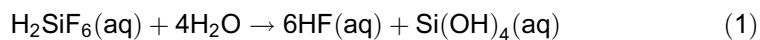
The choice of fluoride compound is dictated by technical aspects of the treatment process. Sodium fluoride is easily handled, and tends to be used by smaller utility companies. The fluorosilicates are more difficult to handle, and are employed by larger utilities, where the reduced costs of large volumes

Table 4. Sources of fluoride ion and their use in drinking water in the United States [125]

Compound	Number of utilities employing	Population receiving (millions of people)
NaF	2491	11.7
H ₂ SiF ₆	5876	80.0
Na ₂ SiF ₆	1635	36.1

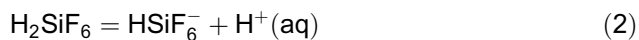
compensates for the increased cost of handling what are difficult substances. Fluorosilicates pose similar hazard problems to hydrofluoric acid, which they yield on dissolution, and also potentially on contact with the skin or mucous membranes of operatives, and hence the storage and handling of significant volumes of concentrated stocks requires a particular degree of care [125].

The complex fluorosilicate compounds were chosen for use because it was widely assumed that they yielded free fluoride rapidly and quantitatively [126], as follows:



For this reason, many subsequent laboratory studies of effectiveness and/or toxicity have employed simpler fluorides, typically NaF. They have generally ignored the fluorosilicates that are widely used in practice in drinking water supplies. Recent findings suggest that this may be a mistake, and that the behaviour of these fluorosilicates in aqueous solution is not as straightforward as was once thought. Consequently, modelling health impacts, adverse or otherwise, of drinking water by study of aqueous solutions of NaF may not be scientifically relevant [123].

Hexafluorosilicic acid is similar to sulphuric acid in that it is a strong acid as far as the first proton is concerned, but very much weaker with respect to the second proton. Its dissociations are:



The first dissociation is complete, as is characteristic of a strong acid. The second dissociation occurs to an extremely limited extent, with an estimated dissociation constant K_{a2} of between $10^{-0.65}$ and $10^{-1.83}$ [123]. The hexafluorosilicate anion is formed from either the hexafluorosilicic acid or from the sodium

salt in drinking water supplies. It dissociates on dilution, and releases the fluoride ion. At the same time, it also produces a range of water-soluble aquo-, hydroxo- and oxosilicates which, to add to the complexity of the chemistry, are capable of undergoing polymerisation. This has led to suggestions that a large number of chemical species may be present in water treated with hexafluorosilicate compounds. These are shown in Table 5.

So far, there have been no studies to confirm or refute the suggestion that water supplies contain polymeric species, and there have been only very few studies on the relevant equilibria which are involved in liberating free fluoride ions from the hexafluorosilicate additives [123]. What data there are, though, suggest that equilibrium will have been reached by the time the water reaches the consumer, even though it may not have been achieved when the water left the waterworks.

Natural waters used to supply drinking water contain a number of elements in their cationic form capable of forming complexes with fluoride ions. The F^- ion is particularly noted for binding strongly to trivalent metal ions such as Fe^{3+} and Al^{3+} . Concern has been expressed about aluminium in particular that complexation may be responsible for lowering the concentration of free fluoride significantly, so that it is below the level required to confer any beneficial effects [127]. Fluoride would be expected to be present substantially complexed with metal ions, with precise details depending on the respective concentrations of metal ion, fluoride ion and hydrogen ion [123], but it seems unlikely that these would be sufficient to suppress the level of available fluoride irreversibly to a level below that is needed for any beneficial effect.

Fluoridation of drinking water has been shown to be highly effective in reducing the incidence of childhood dental caries [128,129]. Earlier results were better,

Table 5. Possible fluorosilicates and resulting species in aqueous solution [123]

Co-ordination number of Si	Fluorosilicates	Aquo/hydroxo/ oxosilicates	Aquo/hydroxo/oxo/ fluorosilicates
6	SiF_6^{2-} $HSiF_6^-$	$Si(OH)(H_2O)_2$ $Si(OH)_5^-$	$SiF_5(H_2O)^-$ $SiF_5(OH)^{2-}$ $SiF_4(OH)_2^{2-}$ $SiF(OH)_2(H_2O)_3^+$
5	SiF_5^- $HSiF_5$	$Si(OH)_4$	$SiF(OH)^-$
4	SiF_4	$SiO(OH)_3$ $SiO_2(OH)_2^{2-}$	$SiF_3(OH)$ $SiF_2(OH)_2$ $SiF(OH)_3$
3	None	$SiO(OH)_2$ $SiO_2(OH)^-$	$Si(OH)_2F^+$

with differences between fluoridated and non-fluoridated areas in the range 50–60%. By contrast more recent reports show lower differences, in the range 18–40% [130,131]. This change is attributed to the fact that there are now many other sources of fluoride available to children, notably toothpaste, and there is no significant variation in the use of these products between fluoridated and non-fluoridated regions. There is also the possibility that food and drinks prepared with fluoridated water can be transported to non-fluoridated areas, so that children in these areas may be subject to infrequent exposure to fluoride in the food and drinks they consume. This so-called diffusion effect causes the differences between populations exposed to fluoridated and non-fluoridated water supplies to be smaller than in the past [132].

A major benefit of water fluoridation to children is that it reduces disparities between socio-economic groups [133,134]. Children in lower socio-economic groups tend to suffer more severely from dental caries, and though the reasons for this are not clear, the result has been confirmed in many parts of the world. Children in these groups therefore benefit enormously from fluoridation of the water supply and in areas where the water supply is fluoridated, the differences in dental caries experience between the social classes are much less than in non-fluoridated areas [135].

The effect of fluoridation on adult dental health is harder to quantify. There are several reasons for this. Adults vary in the extent to which they may have been exposed to fluoride while growing up, and they may experience tooth loss for reasons other than dental caries, for example, trauma or periodontal disease. However, despite these difficulties, what evidence there is points to fluoride being beneficial for adult healthcare [136,137], and for older adults in particular, conditions such as root caries has been demonstrated quite clearly to be less prevalent in regions where the drinking water is fluoridated [138,139]. The overall conclusion from all of these studies is that the whole population benefits from fluoridation in terms of improvements to their overall dental health.

3.2. Salt and milk

In certain countries, rather than fluoridating drinking water, table salt is fluoridated instead [140]. Countries favouring this approach include France and Germany, Jamaica and parts of Switzerland [140]. Jamaica is a particularly useful example to consider because almost all salt for human consumption has been fluoridated since 1987 [141]. Concentrations used vary around the world, but range from 90 to 350 mg/kg, with either 200 or 250 g/kg being considered optimal [142]. Results suggest that this measure is as effective as water fluoridation in reducing the incidence of caries, especially in children [143].

Production of fluoridated salt is generally carried out at large salt factories in tropical or subtropical locations, using solar energy [140]. Fluoride is added as

NaF, KF or CaF_2 using wet- or dry-mix methods. In wet-mix methods, the previously extracted pure salt is sprayed with a concentrated solution, usually of potassium fluoride at a controlled rate onto a continuous flow of salt [140]. To ensure correct dosage, both the volume delivered by the spraying nozzle and the amount of salt passing under the nozzle are carefully monitored and controlled.

Concern has been expressed that because the consumption of salt is associated with the risk of hypertension, promotion of the health benefits of fluoridated salt will confuse the public. However, populations in countries such as France or Germany are not encouraged to increase their salt intake in order to improve their oral health. Rather they accept fluoridation of salt as a passive means of improving their dental health and do not appear to be consuming more salt in order to enhance any effect [142].

Milk fluoridation is an alternative method that is used to provide fluoride to a population. It has the advantage that, as milk is mainly consumed by children, this approach targets the most caries-susceptible individuals within the community [143]. Against that, it has long been known that children from lower socio-economic groups, who are most at risk from caries, drink the least quantity of fresh milk [144]. There is also the disadvantage that the rate of absorption of fluoride from milk is lower than from water [145], which given that fluoride acts topically, suggests that milk is a much less efficient vehicle for delivering fluoride than water [143]. Nonetheless, fluoridation of milk is an acceptable means of providing fluoride, and has been shown to bring about reductions in caries incidence [146,147]. Fluoride delivered in milk has been shown to have various desirable effects, including increasing F-concentrations in enamel [148,149], increasing pH adjacent to tooth surface and reductions in proportions of *S. mutans* in biofilms [150]. This latter effect shows that fluoridated milk produces biofilms of reduced cariogenic potential.

Despite these positive features, milk fluoridation is used in only a limited number of places, and both water- and salt-fluoridation are more widely employed.

3.3. Dentifrices

Dentifrices, more commonly called toothpastes, are a widely used source of fluoride for the majority of the population in the developed world. First introduced in the 1970s, fluoride-containing toothpastes accounted for over 90% of the market in the industrialised nations by the 1990s [151]. Because not all countries fluoridate their drinking water, fluoridated toothpastes are, for many people in the world, the most important source of this element for oral health.

Fluoride is added to toothpaste, typically at levels equivalent to 1000 ppm in fluoride, usually as an inorganic compound, typically sodium fluoride, sodium

monofluorophosphate or stannous fluoride. However, organic aminofluorides can also be used and are effective [152]. For many years, it was assumed that all of these fluoride compounds were more or less equivalent in their effectiveness, but there are reports that suggest differences between them. For example, a meta-analysis has demonstrated that toothpastes containing NaF are more effective in protecting against caries than toothpastes containing monofluorophosphate by an amount that is small but statistically significant [153]. Also, an experimental (*in vitro*) study has suggested that stannous fluoride is more effective in protecting against demineralisation of enamel than sodium fluoride [154]. This study used resistance to enamel dissolution in citric acid as the criterion of effectiveness, and showed clearly that there was less dissolution following treatment with SnF_2 .

However, as has been discussed earlier in this chapter, demineralisation is not the only process that occurs at the surface of the tooth. Remineralisation is also occurring, and the effect of the various forms of fluoride on this process has also been studied. For example, one study used three experimental toothpastes, two of them containing respectively sodium monofluorophosphate and sodium fluoride, and one containing a mixture of sodium fluoride and water-soluble copolymer [155]. In addition, fluoride-free toothpaste was used as a placebo. In the case of each of three fluoride-containing toothpastes, treatment for two weeks led to statistically significant increases in percent mineral content in both the enamel and the dentine specimens, whereas in the placebo there was no effect. There were no differences between the fluoridated toothpastes [155], showing that as far as the remineralisation part of the process is concerned, the form of the fluoride component has no effect. In view of the findings on the effect of stannous fluoride on dissolution, it would be desirable to extend this study of remineralisation to include a toothpaste containing SnF_2 .

When fluoridated toothpastes are used, one of the effects is that fluoride levels increase, and such an effect is detectable after a single use [156]. This fluoride is taken up both by the dental plaque [157,158] and by the demineralised enamel [159] as a result of increases in fluoride levels in saliva between 100 and 1000 times the initial level. Although this initial elevation in concentration lasts for only 1–2 h [160], regular use of fluoridated toothpaste can raise the general level of fluoride in the saliva. This shift in baseline fluoride level can be maintained over considerable periods of time [157,158].

Studies have shown that fluoridated toothpastes are effective at reducing the incidence of caries in children [161,162], with reductions typically being in the range 15–30%. This is much lower than the effect that has been reported for fluoridation of the drinking water supply, although it must be remembered that studies of drinking water fluoridation have tended to be over much longer time periods. It is likely that regular brushing with fluoridated toothpastes over a lifetime will confer similar benefits as consuming fluoridated drinking water. Results have shown, though, that combining use of fluoridated toothpastes with

consumption of fluoridated drinking water offers greater protection than either one on its own [153,163].

Most people brush their teeth at least once per day [164], though it is generally considered that twice a day is readily accommodated within a daily routine. Hence, this frequency has become the one recommended to provide the basic level of oral care [165]. It is doubtful whether increasing the frequency of brushing above twice per day has any effect on lowering the incidence of caries [165]. The extent of rinsing after tooth-brushing affects the fluoride level in the mouth, and hence the resulting caries experience [166], and it has been suggested that children below the age of 6 tend to retain greater amounts of fluoride, because of their tendency not to rinse, or to rinse in a perfunctory way [167].

One approach to overcome the possibility of consuming excess fluoride is to provide low strength toothpastes made especially for children [168]. However, clinical trials have shown that a toothpaste containing only 250 ppm fluoride is not clinically effective at preventing caries [169]. This suggests that an intermediate fluoride concentration, say 500–550 ppm, might be sufficiently efficacious for children, and not have the potential to cause the extent of fluorosis that toothpastes containing 1000 ppm have [170]. There has been a study which has shown that the incidence of diffuse enamel opacities, an indicator of mild enamel fluorosis, in upper anterior incisors was reduced by using a toothpaste formulated to contain 550 ppm fluoride [171]. From this it can be inferred that lower levels of fluoride will, as suggested, prove clinically effective in reducing caries with at least a reduced incidence of the adverse side effect of fluorosis.

3.4. Fluoride mouthrinses

Mouthrinses containing fluoride consist of a concentrated solution that is prepared for use at daily or weekly intervals. As is the case for toothpastes, fluoride from mouthrinses is retained by the dental plaque and increases the concentration in saliva [172]. Mouthrinses have the advantage that their viscosity is low [173], which is aided by the use of ethanol as at least part of the carrier liquid. This enables mouthrinses to penetrate into interproximal regions, and hence carry the fluoride to parts of the tooth that are difficult to access by other means, for example, with toothpastes.

Sodium fluoride is the most commonly used active compound in mouthrinses, and typically proprietary brands of mouthrinses sold over the counter contain 0.05% NaF, equivalent to 230 ppm fluoride. These preparations are not suitable for children below 6 years of age, because of the high levels of fluoride. In addition, more concentrated solutions are available and used under the supervision of dental professionals [174].

Studies have shown that the use of fluoride mouthrinses reduces the incidence of caries in children [175,176]. An average caries reduction of 31% has been

determined for studies carried out in the 1970s and 1980s [177]. However, the extent of success appears to have declined, and more recent studies in America [178,179] suggest that these substances have only limited effectiveness. This is possibly due to the fact that the children concerned were anyway exposed to fluoridated water, which itself is responsible for significant reductions in caries rates.

3.5. Topical fluoride applications

3.5.1. Gels

The use of high-concentration gels and varnishes has been practised clinically for many years by dentists and dental hygienists [180]. When originally formulated, they were designed to be used in application procedures based on the concept that fluoride becomes incorporated into the crystalline phase of the enamel and leads to the development of a more acid-resistant form of apatite. They were not expected to make any difference to the levels of fluoride in saliva, or to influence the demineralisation/dissolution phase of the behaviour of tooth mineral.

More recently, it has been shown that topical fluoride preparations do not lead to fluoridation of the hydroxyapatite crystal [181]. Rather they form a calcium fluoride-like substance that is deposited onto the tooth surface and dissolves when the local pH is lowered [182]. The resulting dissolution adjacent to the tooth surface provides a source of soluble fluoride that can be incorporated into the mineral structure, and thus augment remineralisation.

A very early study suggested that fluoride uptake was enhanced in a low pH environment [180]. Because of this, fluoride gels are often formulated to be quite acidic, typically of pH around 3. Typical products include an acidic phosphate fluoride gel that is 1.23% fluoride (equivalent to 12,300 ppm), an acidic sodium fluoride gel (0.5% fluoride, 5000 ppm) and a stannous fluoride gel (0.15% fluoride, 1000 ppm) [183]. All of these formulations are acidic, and are generally designed for use by dental professionals. There are also products for home use, which are also on the acid side of neutral, and which also contain high levels of fluoride [184].

Clinical trials have shown that relatively infrequent application of these gels, for example, at six-monthly intervals with treatments of 4 min duration, are effective at reducing caries [183,185]. In clinical practice, there is evidence that much shorter times are used, though there have been no studies of the effectiveness of such briefer treatment regimes. Similarly, there are no data available on the optimum schedule for treatments, and what studies there are have reported mixed results for the most effective treatment regimes for preventing and controlling caries. The current evidence suggests that six-monthly treatment with fluoridated gels is an acceptable frequency, and that this enhances resistance to caries [186,187]. Also, because the applications are infrequent, there seems little risk of enamel fluorosis occurring as a result of using professionally applied fluoride gels.

3.5.2. *Varnishes*

Fluoride-containing varnishes are designed to be painted onto the teeth and retained for a few hours at least, during which they release fluoride close to the tooth surface [188]. Like fluoride gels, they are intended for use by dental professionals, but have the advantage that they are considered to be easy to apply. They have an acceptable taste and contain lower amounts of fluoride than gels. They contain either sodium fluoride or difluorosilane as the active ingredient.

Fluoride varnishes have been used since the 1970s, and found to be effective in preventing caries. Their use has been predominantly in Europe, and also Canada, because there have been legal difficulties in the United States over the therapeutic claims of such varnishes to be anticariogenic. As they are intended to remain in place beyond the period of time for which the treatment is under the direct supervision of a clinician, this implies that this product is a drug. As such, proper clinical trials are required before the product can be marketed in the United States [189].

Fluoride varnishes have, though, been shown to be effective in preventing caries in children [190,191]. Applied at six month intervals, these varnishes were found to be as effective as fluoride gel [191]. Some reports conclude that more frequent applications are desirable, for example, four times a year and there is also some evidence that three applications within a week, at yearly intervals might be beneficial [192,193]. However, overall the evidence is inconclusive.

Fluoride varnishes have been shown to prevent decalcification beneath orthodontic bands [194] and also to reduce the rate of progression of enamel lesions [195]. They have thus been shown to be effective against one of the early stages of dental caries. They also have the advantage that there is no published evidence that fluorosis is a problem when fluoride varnishes are applied by dental professionals. In addition, proper application methods as practised by the profession reduce the possibility of accidentally swallowing varnish and also limit the amount of fluoride that can be ingested. Chair-time is less, as varnishes are easier to apply than gels [196]. Thus, fluoride varnishes have some overall modest advantages over fluoridated gels as a means of applying fluoride to the tooth surface.

The overall mode of action of fluoride varnishes is the same as gels, namely that they deposit soluble fluoride as calcium fluoride. When local pH adjacent to this deposit falls, fluoride is solubilised and then proceeds to become incorporated into the tooth mineral as fluorapatite [196].

3.6. Fluoride-releasing restorative materials

A variety of materials are employed in the repair of teeth damaged by caries. The main ones are: amalgams, composite resins and glass-ionomers (conventional and resin-modified). Table 6 shows the proportion of these materials used in the United Kingdom, based on a comprehensive survey of 9000 restorations placed.

Table 6. Proportions of restorative materials used in the United Kingdom [197]

Material	Proportion used (%)
Amalgam	54
Composite resin	30
Glass-ionomer	16

This survey showed that restorations are fairly evenly divided between initial repairs (49%) and replacements (51%) [197]. The principal reason for failure of restorations is secondary caries [198,199], a finding which appears to be world-wide, including in the United Kingdom [200]. Other reasons may include material failure, including discolouration, fracture of the tooth, or the need for endodontic intervention. Of the available materials, amalgams have the greatest median and mean survival times [201], though the survival of the other types of material is highly variable [202,203], reflecting the importance of clinical skill in their deployment and of the state of oral hygiene in the patient [204].

Secondary caries is caries detected at the margins of an existing restoration [205], and has certain distinctive features [205–207]. It generally develops along the cervical and interproximal margins, and presents as discolouration, a white spot indicating active recurrent caries [201]. The adjacent enamel surface may develop a slight but distinct hue, varying from brown to grey, that arises from the undermining spread of caries below the surface. The most important factor in the development of secondary caries is the presence of microfissures around the restoration. Other risk factors are the same as those for primary caries [201,205–207], and include consumption of fermentable carbohydrates, and inadequate oral hygiene. Application of fluoride reduces the risk of the condition developing, and one clinically straightforward approach is to employ fluoride-releasing restorative material. These are considered in the following sections of the chapter.

3.6.1. *Glass-ionomers*

Glass-ionomers have been used in various areas of restorative dentistry since the mid 1970s. They were invented and originally described by Wilson and Kent [208], and consist of a basic glass powder and a water-soluble acidic polymer. The most widely used polymer is poly(acrylic acid), but acrylic/maleic acid copolymer is also widely used [209]. The glass powder is a complex calcium (or strontium) aluminofluorosilicate [210] that is typically at least partially phase separated.

Setting of the cements occurs by neutralisation, and involves initial formation of calcium or strontium polyacrylate and later formation of aluminium polyacrylate. There is also evidence for a later, slow reaction involving the ion-depleted

inorganic species from the acid-attacked glass [211]. This appears to be responsible for the various changes that occur on maturation, including improvements in compressive strength and translucency, and reduction in water sensitivity [211].

Glass-ionomers may be divided into three categories, namely conventional, metal-reinforced and resin modified [209,212,213]. All involve the acid-base setting chemistry of the original glass-ionomer, but in the case of resin-modified glass-ionomers there is also a polymerisation reaction involving an additional monomer, typically 2-hydroxyethyl methacrylate, HEMA. These materials are discussed in more detail in Section 3.6.2. Metal-reinforced glass-ionomers set only by the acid-base process, and are strengthened by the inclusion of finely divided metal powders, typically the silver-tin alloy of dental amalgams [214].

Recently fast-setting, high-viscosity conventional glass-ionomers have been developed [215]. These were made available during the early 1990s for use with the atraumatic restorative treatment (ART) technique in developing countries. They are considered later in this article, and the clinical success of the ART approach has relied on the improved properties of these newer glass-ionomer materials.

Glass-ionomers form a natural adhesive bond to tooth structure (enamel or dentine) [216]. This seals the cavity, preventing leakage at the margins, protecting the pulp and eliminating secondary caries [217]. The adhesive bond arises due to an ion-exchange process at the interface [209,218], and in strontium-based glass-ionomers, this has been shown to result in strontium migrating from the cement to well inside the tooth surface, and calcium migrating from the tooth to well inside the cement [219]. The result is a very durable bond to the tooth [217].

When determined relatively soon after placement, reported shear bond strengths of glass-ionomers are of the order of 3–7 MPa [213,220]. However, because the material fails cohesively, this is actually a measure of the tensile strength. As the cement matures, the tensile strength increases, and failure rates in clinical service are very low [221].

Despite the good adhesion, conventional glass-ionomers show some micro-leakage at the margins of restorations. One *in vitro* study showed that conventional glass-ionomers were less reliable in sealing enamel margins than composite resin [222], and that there was significant dye penetration at the gingival margins.

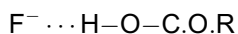
Conventional glass-ionomers are tooth coloured, and have a degree of translucency. This gives them reasonable aesthetics, though they are less aesthetic than composite resins, mainly because they remain relatively opaque compared with the tooth itself [218].

The glasses from which these cements are made are fluoride-containing, and some of the fluoride is transferred to the matrix during setting. From there it can be released, essentially without altering the physical properties of the cement [223]. Release has been shown to occur by two mechanisms, an early 'wash-out' process, and a longer-term diffusion process [224]. The long-term release can continue for at least 5 years [225].

Ion release by glass-ionomers, including fluoride release, has generally been thought to originate in the matrix. However, the glass itself has also been shown to be capable of releasing ions into neutral water [226]. Using the glass G338, which has been widely studied and whose composition is given in Table 7, it was shown that glass can release a total of 5.6 mg/g of fluoride into water in 21 days. Calculation showed that this represents $\sim 3.3\%$ of the fluoride content of the glass [226].

Not surprisingly, the use of acidified water increased the level of fluoride release from the glass, and this effectively models what happens in a setting cement. The acid-base reaction between the glass and the water-soluble polymeric acid liberates fluoride from the glass, causing it to move to the matrix, from where it is gradually leached as the cement releases fluoride [227,228].

Ions released into the matrix as the cement sets may interact with the organic part of the matrix. Metal ions, such as Ca^{2+} and Al^{3+} , may be chelated by carboxylate groups, either on the polymer or on the tartaric acid additive. These have been considered in reasonable detail in the literature [230]. What has received far less attention is the possibility that fluoride ions might interact with carboxylic acid groups, either to modify the setting reaction or to become relatively securely anchored within the set cement. This possibility was raised in a review published in 1998 [230], but has not been followed up subsequently. It is based on the well-established observation that fluoride ion will form extremely strong hydrogen bonds with carboxylic acids in aqueous solution. They are of the type:



Calculation shows that these are strong and that the strongest hydrogen bond of all is that formed between fluoride ion (from CaF) and formic acid in aqueous solution [231]. In view of the strength of such hydrogen bonds and their ease of

Table 7. Composition of G338 glass as used in glass-ionomer cement [229]

Component	Weight % in pre-firing composition
SiO_2	24.9
Al_2O_3	14.2
CaF_2	12.8
Na_3AlF_6	19.2
AlF_3	4.6
AlPO_4	24.3

formation it is highly unlikely that they are absent from glass-ionomer cements. However, what their effect is or how they influence cement properties, has still not been investigated.

As mentioned, fluoride release from set cements follows a distinctive pattern. First, there is a rapid burst of ion release that is non-linear with respect to time. This has sometimes been referred to as 'early wash-out', but actually is not confined to particularly early periods in a cement's life, as it has been shown to be discernible after 28 days [224].

Later, there is a period of sustained release, typically showing release proportional to $t^{1/2}$, indicating that the process of fluoride release is diffusion controlled [228]. Alternatively, in some studies, release has been shown to be proportional to t , which means that for those cements, release is dissolution controlled [232]. This sustained release phase is the one that prevails over long periods of time. For example, Forsten [225] carried out a study in which cement specimens were exposed to running tap water for 5 years, with short periods in static water to allow samples to be collected for analysis, after which they were returned to the running tap water. The data he obtained have been analysed by Billington *et al.* [233], who showed that the pattern of fluoride release right up to the end of the experiment (i.e., 5 years) continued to show a linear relationship with $t^{1/2}$. Fluoride release is thus diffusion controlled for a considerable period of time.

In artificial saliva, release of fluoride has been shown to be reduced [234,235], a finding that may be the case for all ions released by glass-ionomer cements. There are two possible explanations for this: (i) that the higher ionic strength of the external medium reduces the rate at which ions can be dissolved into it, and (ii) that the artificial saliva contained calcium ions [236], which may precipitate CaF_2 on the surface, and thus impede ion transfer from that surface [237].

Glass-ionomer cements have been shown to be dynamic materials and, following the suggestion of Walls [238], to be capable of taking up fluoride from surrounding media. There have been several reports that fluoride release is enhanced following prior exposure to fluoride solution [239–243]. This effect has been demonstrated both *in vitro* and *in vivo*, and has been claimed to be evidence of fluoride uptake and re-release.

However, this does not necessarily follow. Exposure to fluoride ion has been shown to alter the structure of the cement [244] and to roughen the surface [245,246]. It may be the case, therefore, that exposure to fluoride alters the surface layers in such a way that more of the fluoride initially present in the cement becomes available for release.

Against that, studies have been carried out using fluoride-free glass-ionomer cement [247], and immersing it in potassium fluoride solution. Following this treatment, the cement was found to release fluoride, thus demonstrating that this cement, at least, was indeed capable of taking up and re-releasing fluoride ion.

Overall, these various studies lead to the conclusion that exposing a conventional fluoride-containing glass-ionomer cement to an external source of fluoride

results in improvements in fluoride release levels, and that at least some of this increase is likely to be the result of fluoride uptake and re-release.

The way in which fluoride is taken up by glass-ionomers has been studied using surface analysis techniques. Dynamic secondary ion mass spectroscopy (SIMS) shows that most of the fluoride becomes concentrated in the surface [248]. Its concentration with depth varies as an error function relationship [248]. X-ray photoelectron spectroscopy (XPS) has suggested that fluoride taken up becomes associated with calcium [249]. However, the form of this association is unclear, because calcium fluoride as such is very insoluble, and when added to a fluoride-free glass-ionomer cement, caused no fluoride to be released [234]. It therefore seems unlikely that the calcium-fluoride association results in formation of CaF_2 , and further research is necessary to determine the precise nature of the calcium-fluoride association, and thus to resolve this paradox.

Fluoride release is most frequently determined using an ion-selective electrode. Because such electrodes are incapable of detecting complexed fluoride, a decomplexing agent is generally added to the mixture prior to analysis. This frees up fluoride from most complexes as the F^- ion, and the total quantity of fluoride released can then be determined by the ion-selective electrode. The usual complexing agent is TISAB (total ionic solubility acid buffer) [250].

Fluoride is assumed to complex with aluminium in the form of aluminofluoride ions (AlF_2^+ and AlF_2^{2+}), and such complexes are dissociated in TISAB to liberate all of the fluoride as free F^- ions. This is consistent with the observation that ion release under acidic conditions tends to show proportionately greater aluminium release yet lower amounts of free fluoride [251].

This approach may not account for all the fluoride released by glass-ionomers [252]. A recent study has used two methods of decomplexation of fluoride, using the same solutions for both methods, by dividing a given storage volume into two and treating each aliquot differently. One aliquot was diluted with an equal volume of TISAB, as is usual in the determination of fluoride by ion-selective electrode. The other solution was treated with a small volume of 4 M hydrochloric acid, allowed to stand for 3 h, then neutralised with an equal amount of 4 M sodium hydroxide. A volume of TISAB equal to the initial volume of the aliquot was added. This technique is known to liberate fluoride from monofluorophosphate as well as from aluminofluoride complexes [253].

Results showed that the overall fluoride release, including of fluoride that could have been present as monofluorophosphate, was much higher than that detected by TISAB decomplexation alone. In other words, almost all of the published reports of fluoride release appear to have underestimated the total amount of fluoride released by glass-ionomer cements. Billington *et al.* also noted that a plot of 'additional fluoride' against $t^{1/2}$ was linear, suggesting that this fluoride, presumably as monofluorophosphate, is released in a diffusion-controlled process. They also carried out preliminary studies to determine other ions, using ICP, and showed that there was sufficient phosphorus released to give the

required P:F ratio for monofluorophosphate. Phosphorus has been recorded as being released in several other studies [251,254], which is also consistent with the occurrence of monofluorophosphate among the ions released by glass-ionomers.

One significance of these results is that it may imply a greater availability of fluoride to the tooth surface than had been thought. Fluoride release as F^- ion is likely to lead to precipitation as CaF_2 following interaction with calcium ions in saliva [255]. However, the calcium salt of the monofluorophosphate ion is more soluble than CaF_2 by a factor of ~ 500 , so that it would not be expected to experience the same degree of suppression of release *in vivo*. This in turn suggests that fluoride as monofluorophosphate may be the form in which clinically useful amounts of this element are delivered in the mouth [252].

Whatever its precise form, fluoride release is assumed to make glass-ionomers cariostatic when used clinically [256]. This is supported by *in vitro* studies using an artificial caries gel, when teeth restored with glass-ionomer and stored in this gel showed less decalcification than unrestored teeth stored similarly [257,258]. However, clinical results are less clear. For example, studies of the reasons given by dentists for replacement of restorations have shown that glass-ionomers are likely to be associated with secondary caries [259,260], and this suggests that they may not be as cariostatic as has been anticipated. It is the present authors' view that care needs to be taken with interpretation of these findings, since they rest heavily on the ability of busy clinicians to identify the materials that are being replaced, and they are contradicted by numerous reports from clinicians who recommend glass-ionomers for high caries risk patients [209,212,223].

Lastly, it should be noted that, in service, glass-ionomers are exposed to a variety of fluoride-containing products, for example, dentifrices, mouthwashes and topical fluoride solutions [261,262]. Given the evidence that glass-ionomers are able to take up fluoride, this suggests that under clinical conditions they are continually undergoing fluoride replenishment. This would make glass-ionomers permanent suppliers of fluoride, a feature that further emphasises the advantages of these materials for patients with high susceptibility to dental caries.

3.6.2. Resin-modified glass-ionomers

As already mentioned, resin-modified glass-ionomers are a subset of the glass-ionomer family in which the acid-base setting reaction is augmented with an addition polymerisation [213]. In order to achieve this, the monomer 2-hydroxyethyl methacrylate (HEMA) is usually employed, together with the appropriate free-radical initiator system [213,263]. These are typically light sensitive, and are designed to be activated by blue light at 470 nm wavelength from a conventional dental curing lamp [263]. The earliest forms of these materials were designed as liners and bases [264], but they were soon followed by restorative grade materials. These have now been in use for a few years, and seem to give acceptable clinical results.

Resin-modified glass-ionomers, like their conventional counterparts, are capable of releasing fluoride [224,264,265], and in greater amounts under acid conditions than neutral ones [265]. Release rates and release profiles have been shown to be comparable with those from conventional glass-ionomer cements [264,265]. Other ions have also been shown to be released by these materials and, as for fluoride, these ions show a greater release under low pH conditions [265]. However, the level of phosphorus released has been shown to be much lower from resin-modified glass-ionomers than from conventional ones [263]. This suggests that there is little or no possibility of association of fluoride as monofluorophosphate, but rather that almost all of the fluoride is released either as the free fluoride ion or as alumino-fluoride complex ions.

3.6.3. *Compomers*

Compomers are properly called polyacid-modified composite resins and are a group of aesthetic materials chemically similar to the well-established composite resins [266]. They were introduced to the dental profession in the early 1990s [267], and were intended to combine the benefits of traditional composite resins and glass-ionomer cements, and their trivial name reflects this, being derived from the names of these two 'parent' materials, the 'comp' coming from composite, and 'omer' from ionomer [268]. These materials are now considered a distinct class of dental restorative, with well established uses in clinical restoration, particularly in children's dentistry [269].

Compomers are set by an addition polymerisation reaction that is usually light-initiated using blue light at 470 nm, the initiator being camphorquinone with amine accelerator [269]. There is, though, at least one brand, designed for use as luting cement that is a two-paste system [270], where cure is brought about as a result of mixing the two pastes, each of which contains a component of the free radical initiator system.

Compomers contain no water, but rather are mainly formulated from the same components as conventional composite resins. Typically this means macromonomers, such as bis-glycidyl ether dimethacrylate (bisGMA) or its derivatives and/or urethane dimethacrylate, blended with viscosity-reducing diluents, such as triethylene glycol dimethacrylate (TEGDMA). These polymer systems are filled with non-reactive inorganic powders, for example, quartz or a silicate glass [271].

In addition, compomers contain extra monomers from conventional composites, and these contain acidic functional groups. The most widely used monomer of this type is so-called TCB, which is a di-ester of 2-hydroxyethyl methacrylate with butane tetracarboxylic acid [271]. This acid-functional monomer is a very minor component and compomers also contain some reactive glass powder of the type used in glass-ionomer cements [266].

Despite the presence of these additional components, compomers are set by a polymerisation reaction. It is only once they are set that they draw in a small amount

of water to promote a secondary neutralisation reaction [271]. They lack the ability to bond to tooth tissues [272,273], so they require the use of bonding agents [273]. Their fluoride release levels are significantly lower than those of glass-ionomer cements [274,275] and this compromises the degree of protection given by these materials in *in vitro* experiments using an artificial caries medium [276].

Fluoride in compomers is present in the reactive glass filler, and becomes available for release following reaction of this glass with the acid functional groups, triggered by moisture uptake. Commercial compomers also contain fluoride compounds such as strontium fluoride or ytterbium fluoride, and these are capable of releasing free fluoride ion under clinical conditions, thus augmenting the low level of release from the poly-salt species that forms in the presence of moisture.

Fluoride release is enhanced in acidic conditions [277,278], and in lactate buffer has been shown to be diffusion based [277]. A plot of cumulative fluoride release against square root of time was found to remain linear for up to 169 h, and to follow the equation:

$$M = a + b\sqrt{t}$$

throughout this time. Materials exposed to lactate buffer were examined by SEM and shown to develop voids and other surface irregularities, which were assumed to assist fluoride release [277].

Other equations have been used to describe fluoride release profiles from compomers. For example, Xu and Burgess [278] suggested two possible equations (a) for high-fluoride releasing compomers:

$$[F]_c = [F]_{(i)}(1 - \exp(-bt)) + \beta t$$

(b) for more regular compomers, and also fluoride-releasing composite resins:

$$[F]_c = [F]_{(i)} + \alpha t$$

($t^{1/2} + t$)

Fluoride release in compomers can be regenerated by using a topical fluoride agent and high-release compomers greater recharge capacity than low-release ones [278].

The proportion of free and complexed fluoride has been determined in one study of ion release from compomers [279], by measuring the amount of fluoride with and without TISAB. Results obtained are shown in Table 8.

These results demonstrate that the amount of free fluoride is much less in acidic conditions than in neutral ones, even though the total fluoride release is greater. In this study, the authors assumed that, as for glass-ionomers, the complexation was caused by the elevated levels of aluminium that were also released under acidic conditions. As an example, for Compoglass F, aluminium

Table 8. Free and total fluoride concentrations in solutions in which compomers had been stored for one week (from [279])

Material/conditions	Free fluoride	Total fluoride	% free fluoride
Compoglass F			
Neutral	2.8	4.5	62.2
Acidic	0.5	15.5	3.2
Dyract AP			
Neutral	19.1	21.3	89.7
Acidic	0.3	21.3	1.4
F2000			
Neutral	2.2	6.2	35.5
Acidic	0.2	15.5	1.3

concentration rose from 4.68 ppm in water to 104 ppm in lactic acid solution. As already noted for glass-ionomers, aluminium is reported to form complexes of the type AlF_2^+ and AlF^{2+} [280], and these have been widely assumed to occur in glass-ionomer cements [229]. Since similar glasses are used in compomers, it was possible that these types of complex also occur in these materials.

However, following the suggestion that some of the fluoride released from glass-ionomers is complexed as monofluorophosphate [252], it seems likely that the techniques used have underestimated the total fluoride released from compomers, too, and that in addition to free fluoride and alumino-fluoride complexes, some monofluorophosphate ions are also present among the ions eluted from compomers. Certainly an increase in the level of phosphorus release from compomers was noted under acidic conditions. This is an aspect that needs further study and, as with glass-ionomers, further research is necessary before every aspect of fluoride release from compomers is fully understood.

3.6.4. Fluoride-containing composite resins

Unlike glass-ionomers or compomers, composite resins are not inherently fluoride-releasing and they do not generally contain any fluoride compounds. However, they can be formulated with such compounds [281], for example NaF, YbF_3 or ion-leachable glass [201]. Organic fluorides can be used, too, such as methacryloyl fluoride-methyl methacrylate (MF-MMA) or tetrabutyl ammonium tetrafluoroborate. These latter substances impart the property of slow release of fluoride to the surrounding tissue without the creation of voids within the material.

Fluoride release from composite resins differs from that in glass-ionomers (conventional or resin-modified) in two important respects. First, it tends to be a gradual, sustained process throughout the life time of the restoration

[281,282], and lacks the initial burst immediately after placement that characterises glass-ionomers. Possibly as result of this, fluoride-releasing composite resins tend not to form inhibition zones in the cavosurface tooth structure.

Second, these materials are unable to undergo fluoride recharge [283]. Their predominantly hydrophobic composition means that there is no basis for interaction with, or uptake of, the strongly hydrophilic F^- ion *in situ*. Hence, exposure to fluoridated drinking water or fluoridated toothpastes has no effect, and these materials are unable to function as 'fluoride reservoirs' [284].

Despite these differences from glass-ionomers of both types, there is evidence that fluoride-releasing composite resins are effective [201]. For example, they have been shown to reduce the incidence of wall lesions at the tooth-restorative interface [285,286]. They have also been shown to reduce the depth of lesions at sites adjacent to the restoration, and to reduce mineral loss [287]. Enamel adjacent to such restorations has been demonstrated to have taken up fluoride, showing that they are efficient vehicles for delivering fluoride to the tooth tissue [288]. Despite these successes, fluoride-releasing composite resins are generally less effective at supplying fluoride or protecting adjacent tooth surfaces than glass-ionomer cements [201,284].

4. CONCLUSIONS

Fluoride has been shown to be a key element in ensuring that populations develop and maintain sound dental health. At the atomic level, it has an effect on the demineralisation/remineralisation equilibrium that exists at the tooth surface, shifting it back in favour of remineralisation. Fluoride does this by a variety of mechanisms, including reducing the solvating power of saliva towards the tooth mineral, reducing the solubility of the apatite phase, and improving the crystallisation kinetics of the mineralisation process. It may also have an effect on the bacterial populations living in the oral biofilms, through inhibition of their enzyme activity.

Fluoride is supplied to large numbers of populations throughout the world in drinking water and, at the levels used, it is safe and effective, and has been accepted as such by numerous public health agencies worldwide. Fluoride can be delivered partly as a public health measure, mainly through the domestic water supply, but also through its introduction to table salt or milk, and partly on an individual basis. The latter includes the use of fluoridated dentifrices, mouthrinses, topical gels and varnishes, and the use of fluoride-releasing restorative materials to repair of teeth damaged by caries. These tailored individual treatment measures are particularly important in reducing caries in high risk groups within any population.

The use of fluoridated products, as well as fluoridation of domestic water supplies, has been one of the most successful approaches ever adopted to

improve any aspect of public health. Continued use of such products, albeit under careful control and supervision by the dental profession, will remain important if the advances in oral health of the past 50 years are to be maintained in the future.

REFERENCES

- [1] J.J. Murray, A.J. Rugg-Gunn, G.N. Jenkins, *Fluoride in Caries Prevention*, 3rd edition, Wright, Oxford, 1991.
- [2] H.T. Dean, F.A. Arnold Jr., E. Elvove, Additional studies of the relation of fluoride domestic waters to dental caries experience in 4,425 white children aged 12–14 years of 13 cities in 4 states, *Public Health Rep.* 65 (1942) 1403–1408.
- [3] H.V. Churchill, Occurrence of fluorides in some drinking waters of the United States, *J. Ind. Eng. Chem.* 23 (1931) 996–998.
- [4] J.J. Clarkson, J. McLoughlin, Role of fluoride in oral health promotion, *Int. Dent. J.* 50 (2000) 119–128.
- [5] F.A. Arnold Jr., H.T. Dean, J. Knutson, Effect of fluoridated public water supplies on dental caries incidence. Results of the seventh year of study at Grand Rapids, Muskegon, Mich., *Public Health Rep.* 68 (1953) 141–148.
- [6] D.B. Ast, D.J. Smith, B. Wachs, K.T. Cantwell, The Newburgh-Kingston caries-fluoride study. XIV. Combined clinical and roentgenographic dental findings after ten years of fluoride experience, *J. Am. Dent. Assoc.* 52 (1956) 314–325.
- [7] B.A. Burt, The changing patterns of systemic fluoride intake, *J. Dent. Res.* 71 (1992) 1228–1237.
- [8] O. Fejerskov, K.W. Stephen, A. Richards, R. Speirs, Combined effect of systemic and topical fluoride treatments on human deciduous teeth—Case studies. *Caries Res.* 21 (1987) 452–459.
- [9] D.J. Galagan, J.R. Vermilion, Determining optimum fluoride concentrations, *Public Health Rep.* 72 (1957) 491–493.
- [10] K.E. Heller, W. Sohn, B.A. Burt, S.A. Eklund, Water consumption in the United States in 1994–96 and implications for the water fluoridation policy, *J. Public Health Dent.* 59 (1999) 3–11.
- [11] P.E. Petersen, M.A. Lennon, Effective use of fluorides for the prevention of dental caries in the 21st century: The WHO approach, *Commun. Dent. Oral Epidemiol.* 32 (2004) 319–321.
- [12] J.D. Featherstone, Prevention and reversal of dental caries: Role of low level fluoride, *Commun. Dent. Oral Epidemiol.* 27 (1999) 31–40.
- [13] O. Fejerskov, B. Nyvad, Is dental caries an infectious disease? Diagnostic and treatment consequences for the practitioner, in: L. Schon (Ed.), *Nordic Dentistry 2003 Yearbook*, Quintessence Publishing, Copenhagen, 2003, pp. 141–151.
- [14] O. Fejerskov, Changing paradigms in concepts on dental caries: Consequences for oral health care, *Caries Res.* 38 (2004) 182–191.
- [15] O. Fejerskov, A.A. Scheie, F. Manti, The effect of sucrose on plaque pH in the primary and permanent dentition of caries-inactive and -active Kenyan children, *J. Dent. Res.* 71 (1992) 25–31.
- [16] S. Hojo, M. Komatsu, R. Okuda, N. Takahashi, T. Yamada, Acid profiles and pH of carious dentine in active and arrested caries, *J. Dent. Res.* 73 (1994) 1853–1857.
- [17] S. Hojo, N. Takahashi, T. Yamada, Acid profiles in caries dentin, *J. Dent. Res.* 70 (1991) 182–186.
- [18] F.J. McClure, R.C. Likins, Fluorine in human teeth studied in relation to fluorine in drinking water, *J. Dent. Res.* 30 (1951) 172–176.

- [19] F.S. McKay, The study of mottled enamel (dental fluorosis), J. Am. Dent. Assoc. 44 (1952) 133–137.
- [20] J.T. Chan, C.C. Qiu, G.M. Whitford, J.G. Weathered, R.K. Clardy, The distribution of fluoride of pre-natal origin in the rat: A pilot study, Arch. Oral Biol. 34 (1989) 885–888.
- [21] K. Takeuchi, H. Nakagaki, Y. Toyama, N. Kimala, F. Ito, C. Robinson, J.A. Weatherell, L. Stosser, W. Kunzel, Fluoride concentrations and distribution in premolars of children from low and optimal fluoride areas, Caries Res. 30 (1996) 76–82.
- [22] E. Hellwig, A.M. Lennon, Systemic versus topical fluoride, Caries Res. 38 (2004) 258–262.
- [23] W.M. Edgar, S.M. Highman, Role of saliva in caries models, Adv. Dent. Res. 9 (1995) 235–238.
- [24] C.A. Robinson, R.C. Shore, S.J. Brookes, S. Stafford, S.R. Wood, J. Kirkholm, The chemistry of enamel caries, Crit. Rev. Oral Biol. Med. 11 (2000) 481–495.
- [25] L.M. Silverstone, The structure of carious enamel, including the early lesion, Oral Sci. Rev. 3 (1973) 100–160.
- [26] K.L. Weerheijm, R.J.M. Gruythusen, W.E. van Amerongen, Prevalence of hidden caries, J. Dent. Child. 59 (1992) 408–412.
- [27] K.L. Weerheijm, E.A.M. Kidd, H.J. Groen, The effect of fluoridation on the occurrence of hidden caries in clinically sound occlusal surfaces, Caries Res. 31 (1997) 30–34.
- [28] M.J. Larsen, A. Richards, The influence of saliva on the formation of calcium fluoride-like material on human dental enamel, Caries Res. 35 (2001) 57–60.
- [29] X.J. Gao, Y. Fan, R.L. Kent Jr., J. Van Houte, H.C. Margolis, Association of caries activity with the composition of dental plaque fluid, J. Dent. Res. 80 (2001) 1834–1839.
- [30] J.W.E. van Dijk, J.M.P.M. Borggreven, F.C.M. Driessens, Diffusion in mammalian tooth enamel in relation to the caries process, Arch. Oral Biol. 28 (1983) 591–597.
- [31] Y.P. Zhang, R.L. Kent Jr., H.C. Margolis, Enamel demineralization under driving forces found in dental plaque fluid, Eur. J. Oral Sci. 108 (2000) 207–213.
- [32] W.E. Brown, Physicochemical mechanisms in dental caries, J. Dent. Res. 53 (1974) 204–255.
- [33] E.C. Morino, T. Aoba, Comparative solubility study of human dental enamel, dentin and hydroxyapatite, Calcif. Tissue Int. 49 (1991) 6–13.
- [34] T. Aoba, Solubility properties of human tooth mineral and pathogenesis of dental caries, Oral Dis. 10 (2004) 249–257.
- [35] F.C.M. Driessens, Mineral aspects of dentistry, in: H.M. Myers (Ed.), Monographs in Oral Science, Vol. 10. Karger, Basle, Switzerland, 1982.
- [36] G. Nikiforuk, Understanding Dental Caries, Etiology and Mechanisms. Basic and Clinical Aspects, Karger, Bale, Switzerland, 1985.
- [37] O. Fejerskov, J. Ekstrand, B.A. Burt, Fluoride in Dentistry, Munksgaard, Copenhagen, 1996.
- [38] H.C. Hodge, F.A. Smith, in: J.H. Simons (Ed.), Fluoride Chemistry, Academic Press, Orlando, FL, 1965, Chapter 4.
- [39] I.R. Hamilton, Biochemical effects of fluoride on oral bacteria, J. Dent. Res. 69 (1996) 660–667.
- [40] I.R. Hamilton, D.C. Ellwood, Effects of fluoride on carbohydrate metabolism by washed cells of *Streptococcus mutans* grown at various pH values in a chemostat, Infect. Immunol. 48 (1985) 664–670.
- [41] H. Luoma, Phosphorus translocation between enamel and *Streptococcus mutans* in the presence of sucrose and fluoride with observations on the acid phosphatase of *S. mutans*, Caries Res. 14 (1980) 248–257.
- [42] N.A. Yoon, C.W. Berry, The antimicrobial effect of fluorides (acidulated phosphate, sodium and stannous) on *Actinomyces viscosus*, J. Dent. Res. 58 (1979) 1824–1829.
- [43] Y.H. Li, G.H.W. Bowden, The effect of surface fluoride on the accumulation of biofilms of oral bacteria, J. Dent. Res. 73 (1994) 1615–1626.
- [44] L.S. Kaminsky, M.C. Mahoney, J. Leach, J. Melius, M.J. Miller, Fluoride: Benefits and risks of exposure, Crit. Rev. Oral Biol. Med. 1 (1990) 261–281.

- [45] C. Van Loveren, The antimicrobial action fluoride and its role in caries inhibition, *J. Dent. Res.* 69 (1990) 676–681.
- [46] H.C. Margolis, J.H. Duchworth, E.C. Moreno, Composition of pooled resting plaque fluid from caries-free and caries susceptible individuals, *J. Dent. Res.* 67 (1988) 1468–1475.
- [47] A. Kuseler, V. Baelum, O. Fejerskov, J. Heidmann, Accuracy and precision in vitro of Beetrode® microelectrodes used for intraoral pH measurements, *Caries Res.* 27 (1993) 183–190.
- [48] V. Baelum, O. Fejerskov, A. Kuseler, Approximal plaque pH following topical applications of standard buffers *in vivo*, *Caries Res.* 28 (1994) 116–122.
- [49] R.M. Stephan, Changes in hydrogen ion concentration on tooth surfaces and in carious lesions, *J. Am. Dent. Assoc.* 27 (1940) 718–723.
- [50] O. Fejerskov, A.A. Scheie, F. Manji, The effect of sucrose on plaque pH in the primary and permanent dentition of caries-inactive and -active Kenyan children, *J. Dent. Res.* 71 (1992) 25–31.
- [51] O. Fejerskov, A. Thylstrup, M.J. Larsen, Rational use of fluoride in caries prevention: A concept based on possible cariostatic mechanisms, *Acta Odontol. Scand.* 39 (1981) 241–249.
- [52] F. Brudevold, H.G. McCann, P. Gron, Caries resistance as related to the chemistry of enamel, in: G.E.W. Wolstenholm, M. O'Conner (Eds.), *Caries Resistant Teeth*, Ciba Foundation Symposium, Churchill, London, 1965.
- [53] T. Koulourides, F.F. Feagin, W. Pigman, Remineralisation of dental enamel by saliva *in vitro*, *Ann. N.Y. Acad. Sci.* 131 (1965) 751–757.
- [54] R.S. Manly, D.P. Harrington, Solution rate of tooth enamel in acetate buffer, *J. Dent. Res.* 38 (1959) 910–919.
- [55] M.J. Larsen, F.R. von der Fehr, J.M. Birkeland, Effect of fluoride on the saturation of an acetate buffer with respect to hydroxyapatite, *Arch. Oral Biol.* 21 (1976) 723–728.
- [56] F. Lagerlof, A. Oliveby, Caries-protective factors in saliva, *Adv. Dent. Res.* 8 (1994) 229–238.
- [57] F.A. Arnold Jr., The use of fluoride compounds for the prevention of dental caries, *Int. Dent. J.* 7 (1957) 54–72.
- [58] G. Penel, G. Leroy, C. Rey, E. Bres, Micro-Raman spectral study of the PO₄ and CO₃ vibrational modes in synthetic and biological apatites, *Calcif. Tissue Int.* 63 (1998) 475–481.
- [59] M.I. Kay, R.A. Young, A.S. Posner, Crystal structure of hydroxyl-apatite, *Nature* 204 (1964) 1050–1052.
- [60] J.C. Elliott, Recent progress in the chemistry, crystal chemistry and structure of the apatite, *Calcif. Tissue Res.* 3 (1969) 293–307.
- [61] H. Kutnerian, A.C. Kuyper, The influence of fluoride on the solubility of bone salt, *J. Biol. Chem.* 233 (1957) 760–763.
- [62] W.E. Brown, T.M. Gregory, L.C. Chow, Effects of fluoride on enamel solubility and cariostasis, *Caries Res.* 11 (1977) 118–141.
- [63] R.A. Young, Biological apatite vs hydroxyapatite at the atomic level, *Clin. Orthop.* 113 (1975) 249–262.
- [64] D.J. White, G.H. Nancollas, Physical and chemical considerations of the role of firmly and loosely bound fluoride in caries prevention, *J. Dent. Res.* 69 (1990) 587–594.
- [65] J.D.B. Featherstone, Prevention and reversal of dental caries: Role of low level fluoride, *Commun. Dent. Oral Epidemiol.* 27 (1999) 31–40.
- [66] A. Thylstrup, O. Fejerskov, C. Bruun, J. Kann, Enamel changes and dental caries in 7-year-old children given fluoride tablets from shortly after birth, *Caries Res.* 13 (1979) 265–276.
- [67] N.H. de Leeuw, Resisting the onset of hydroxyapatite dissolution through incorporation of fluoride, *J. Phys. Chem. B* 108 (2004) 1809–1811.
- [68] W.E. Brown, N. Eidelman, B.B. Tomzaic, Octa-calcium phosphate as a precursor in biomineral formation, *Adv. Dent. Res.* 1 (1987) 306–313.

- [69] T. Aoba, H. Komatsu, Y. Shimazu, H. Yagishita, Y. Taya, Enamel mineralisation and an initial crystalline phase, *Connect. Tissue Res.* 38 (1998) 129–137.
- [70] M. Iijima, H. Tohda, Y. Moriwaki, Growth and structure of lamellar mixed crystals of octacalcium phosphate and apatite in model system of enamel formation, *J. Cryst. Growth* 116 (1992) 319–326.
- [71] Y. Miaka, S. Shimoda, M. Fukase, T. Aoba, Epitaxial overgrowth of apatite crystals on the thin-ribbon precursor at early stages of porcine enamel mineralisation, *Calcif. Tissue Int.* 53 (1993) 257–261.
- [72] M.J. Mura-Galelli, H. Narusawa, T. Simada, M. Iijima, T. Aoba, Effect of fluoride on precipitation and hydrolysis of octacalcium phosphate in an experimental model simulating enamel mineralization during amelogenesis, *Cells Mater.* 2 (1992) 221–230.
- [73] T. Yanagisawa, S. Takuma, H. Tohda, O. Fejerskov, R.W. Fearnhead, High resolution electron microscopy of enamel crystals in cases of human dental fluorosis, *J. Electron Microsc.* 38 (1989) 441–448.
- [74] R.S. Manly, D.P. Harrington, Solution rate of tooth enamel in an acetate buffer, *J. Dent. Res.* 38 (1959) 910–919.
- [75] R.L. Spiers, M. Spinelli, F. Brudevold, Solution rate of hydroxyapatite in acetate buffer containing low concentrations of foreign ions, *J. Dent. Res.* 42 (1963) 811–820.
- [76] M.J. Larsen, O. Fejerskov, Surface etching and subsurface demineralization of dental enamel induced by a strong acid, *Scand. J. Dent. Res.* 85 (1977) 320–326.
- [77] J.M. ten Cate, Review on fluoride, with special emphasis on calcium fluoride mechanisms in caries prevention, *Eur. J. Oral Sci.* 105 (1997) 461–465.
- [78] N.Y. Sakkab, W.A. Cilley, J.P. Haberman, Fluoride in deciduous teeth from an anti-carries clinical study, *J. Dent. Res.* 63 (1984) 1201–1205.
- [79] W.J. Thrash, D.L. Jones, W.J. Dodds, Effect of a fluoride solution on dentinal hypersensitivity, *Am. J. Dent.* 5 (1992) 299–302.
- [80] A.V. Ritter, W.L. de Dias, P. Miguez, D.J. Caplan, E.J. Swift Jr., Treating cervical dentin hypersensitivity with fluoride varnish, *J. Am. Dent. Assoc.* 137 (2006) 1013–1020.
- [81] M. Addy, P. Mostafa, R.G. Newcombe, Dentine hypersensitivity: A comparison of five toothpastes used during a 6-week period, *Br. Dent. J.* 163 (1987) 45–50.
- [82] D. MacCarthy, Dentine hypersensitivity: A review of the literature, *J. Irish Dent. Assoc.* 50 (2004) 36–41.
- [83] S. Minkoff, S. Axelrod, Efficacy of strontium chloride in dental hypersensitivity, *J. Periodontol.* 58 (1987) 470–474.
- [84] G. Silverman, The sensitivity reducing effect of brushing with a potassium nitrate-sodium monofluorophosphate dentifrice, *Compend. Contin. Educ. Dent.* 6 (1985) 131–133.
- [85] M.S. McDonagh, P.F. Whiting, P.M. Wilson, A.J. Sutton, I. Chestnutt, J. Cooper, K. Misso, M. Bradley, E. Treasure, J. Kleijnen, Systematic review of water fluoridation, *Br. Med. J.* 321 (2000) 855–859.
- [86] A. Thylstrup, O. Fejerskov, Clinical appearance of dental fluorosis in permanent teeth in relation to histologic changes, *Commun. Dent. Oral Epidemiol.* 6 (1978) 315–328.
- [87] A. Bardsen, K. Bjorvath, Risk periods in the development of dental fluorosis, *Clin. Oral Invest.* 2 (1998) 155–160.
- [88] R.W. Evans, J.W. Stamm, An epidemiologic estimate of the critical period during which human maxillary central incisors are most susceptible to fluorosis, *J. Public Health Dent.* 51 (1991) 251–259.
- [89] R.D. Jackson, S.A. Kelly, B. Katz, E. Brizendine, G.K. Stookey, Dental fluorosis in children residing in communities with different water fluoride levels: 33 month follow-up, *Pediatr. Dent.* 21 (1999) 248–254.
- [90] A. Thylstrup, O. Fejerskov, Clinical appearance of dental fluorosis in permanent teeth in relation to histologic changes, *Commun. Dent. Oral Epidemiol.* 6 (1978) 315–328.
- [91] O. Fejerskov, M.J. Larsen, A. Richards, V. Baelum, Dental tissue effects of fluorine, *Adv. Dent. Res.* 8 (1994) 15–31.

- [92] W.H. Bowen, Fluorosis: Is it really a problem? *J. Am. Dent. Assoc.* 133 (2002) 1405–1407.
- [93] S.O. Griffen, E.D. Beltran, S.A. Lockwood, L.K. Barker, Esthetically objectionable fluorosis attributable to water fluoridation, *Commun. Dent. Oral Epidemiol.* 30 (2002) 199–209.
- [94] D.G. Pendrys, R.V. Katz, D.R. Morse, Risk factors for enamel fluorosis in fluoridated population, *Am. J. Epidemiol.* 140 (1994) 461–471.
- [95] J.A. Lalumandier, R.G. Rozier, The prevalence and risk factors of fluorosis among patients in a pediatric dental practice, *Pediatr. Dent.* 17 (1995) 19–25.
- [96] P.L. Simard, H. Naccache, D. Lachapelle, J.M. Brodeur, Ingestion of fluoride from dentifrices by children aged 12 to 24 months, *Clin. Pediatr.* 30 (1991) 614–617.
- [97] J.M. Levy, A review of fluoride intake from fluoride dentifrice, *J. Dent. Child.* 61 (1993) 115–124.
- [98] L.L. Demos, H. Kazda, F.M. Cicuttini, M.I. Sinclair, C.K. Fairley, Water fluoridation, osteoporosis, fractures—Recent developments, *Aust. Dent. J.* 46 (2001) 80–87.
- [99] T.A. Einhorn, G.K. Wakley, S. Linkhart, E.B. Rush, S. Maloney, E. Faierman, D. J. Baylink, Incorporation of sodium fluoride into cortical bone does not impair the mechanical properties of the appendicular skeleton in rats, *Calcif. Tissue Int.* 51 (1992) 127–131.
- [100] C.H. Turner, M.P. Akhter, R.P. Heaney, The effects of fluoridated water on bone strength, *J. Orthop. Res.* 10 (1992) 581–587.
- [101] Y. Jiang, J. Zhao, R. Van Audekercke, J. Dequeker, P. Geusens, Effects of low-dose long-term sodium fluoride preventive treatment on rat bone mass and biomechanical properties, *Calcif. Tissue Int.* 58 (1996) 30–39.
- [102] C.H. Turner, K. Hasegawa, W. Zhang, M. Wilson, Y. Li, A.J. Dunipace, Fluoride reduces bone strength in older rats, *J. Dent. Res.* 74 (1995) 1475–1481.
- [103] C.H. Turner, L.P. Garetto, A.J. Dunipace, W. Zhang, M.E. Wilson, M.D. Grynpas, D. Chachra, R. McClintock, M. Peacock, G.K. Stookey, Fluoride treatment increased serum IGF-1, bone turnover, but not bone strength, in rabbits, *Calcif. Tissue Int.* 61 (1997) 77–83.
- [104] S.J. Jacobsen, J. Golberg, C. Cooper, S.A. Lockwood, The association between water fluoridation and hip fracture among white women and men aged 65 years and older, *Ann. Epidemiol.* 2 (1992) 617–626.
- [105] C. Danielson, J.L. Lyon, M. Egger, G.K. Goodenough, Hip fractures and fluoridation in Utah's elderly population, *J. Am. Med. Assoc.* 268 (1992) 746–748.
- [106] M.E. Suarez-Almazor, G. Flowerdew, L.D. Saunders, C.L. Soskolne, A.S. Russell, The fluoridation of drinking water and hip fracture hospitalization rates in two Canadian communities, *Am. J. Public Health* 83 (1993) 689–693.
- [107] S.J. Jacobsen, W.M. O'Fallon, L.J. Melton, Hip fracture incidence before and after the fluoridation of the public water supply, Rochester, Minnesota, *Am. J. Public Health* 83 (1993) 743–745.
- [108] L. Fabiani, V. Leoni, M. Vitali, M. Parafati, S. Rodolico, C. Cremisini, Fluoride in water as a protective factor for bone fractures: Preliminary data of an epidemiological study in Italy, in: E.G. Reichard, G.A. Zapponi (Eds.), *Assessing and Managing Health Risks from Drinking Water Contamination: Approaches and Applications*, International Association for Hydrological Sciences Publication No. 233, 1995.
- [109] M.R. Karagas, J.A. Baron, J.A. Barrett, S.J. Jacobsen, Patterns of fracture among United States elderly: Geographic and fluoride effects, *Ann. Epidemiol.* 6 (1996) 209–216.
- [110] B. Lentle, Osteoporosis and bone densitometry, *Can. Med. Assoc. J.* 159 (1998) 1261–1264.
- [111] E.C. Mirsky, T.A. Einhorn, Bone densitometry in orthopaedic practice, *J. Bone Joint Surg.* 80A (1998) 1687–1698.

- [112] C.Y.C. Pak, K. Sakheee, B. Adams-Huet, V. Piziak, R.D. Peterson, J.R. Poindexter, Treatment of postmenopausal osteoporosis with slow-release sodium fluoride: Final report of a randomized controlled trial, *Ann. Intern. Med.* 123 (1995) 401–408.
- [113] C.Y.C. Pak, K. Sakhaee, N.H. Bell, A. Licata, C. Johnston, B. Dubin, S. Bonnick, V. Piziak, H. Graham, J. Ballard, R. Berger, W. Fears, N. Breslau, C. Rubin, B. Adams-Huet, Comparison of non- randomized trials with slow-release sodium fluoride with a randomized placebo-controlled trial in postmenopausal osteoporosis, *J. Bone Miner. Res.* 11 (1996) 160–168.
- [114] J.L. Sebert, P. Richard, I. Mennecier, J.P. Bisset, G. Loeb, Monofluorophosphate increases lumbar bone density in osteopenic patients: A double-masked randomized study, *Osteoporos. Int.* 5 (1995) 108–114.
- [115] J.Y. Reginster, L. Meurmans, B. Zegels, C. Gosset, The effect of sodium monofluorophosphate plus calcium on vertebral fracture rate in postmenopausal women with moderate osteoporosis. A randomized, controlled trial, *Ann. Intern. Med.* 129 (1998) 1–8.
- [116] P.J. Meunier, J.-L. Sebert, J.Y. Reginster, D. Briancon, T. Appelboom, P. Netter, G. Loeb, A. Rouillon, S. Barry, J.C. Evereux, B. Avouac, X. Marchandise, Fluoride salts are no better at preventing new vertebral fractures than calcium-vitamin D in postmenopausal osteoporosis, The FAVO study, *Osteoporos. Int.* 8 (1998) 4–12.
- [117] C.Y.C. Pak, K. Sakhaee, V. Piziak, R. Peterson, N.A. Breslau, P. Boyd, J.R. Poindexter, J. Herzog, A. Heard-Sakhaee, S. Haynes, B. Adams-Huet, J.S. Reisch, Slow-release sodium fluoride in the management of postmenopausal osteoporosis. A randomized controlled trial, *Ann. Intern. Med.* 120 (1994) 625–632.
- [118] M. Kleerekoper, D.B. Mendlovic, Sodium fluoride therapy of postmenopausal osteoporosis, *Endocr. Rev.* 14 (1993) 312–323.
- [119] J.D. Ringe, A. Dorst, C. Kipshoeven, L.C. Rovati, I. Setnikar, Avoidance of vertebral fractures in men with idiopathic osteoporosis by a three year therapy with calcium and low-dose intermittent monofluorophosphate, *Osteoporos. Int.* 8 (1998) 47–52.
- [120] World Health Organisation, Fluorides and Oral Health. WHO Technical Report Series 846, WHO, Geneva, 1994.
- [121] D.J. Galagan, J.R. Vermillion, Determining optimum fluoride concentrations. *Public Health Rep* 72 (1957) 491–493.
- [122] L. Singer, B.A. Jarvey, P. Venkateswarlu, W.D. Armstrong, Fluoride in plaque. *J. Dent. Res.* 49 (1970) 455.
- [123] E.T. Urbansky, Fate of fluorosilicate drinking water additives, *Chem. Rev.* 102 (2002) 2837–2854.
- [124] D.R. Lide, (Editor-in-Chief), *Handbook of Chemistry, Physics*, CRC, Boca Raton, Florida, 2001/2002.
- [125] I. Zipkin, F.J. McClure, Complex fluorides, caries reduction and fluoride retention in bones and teeth of white rats, *Public Health Rep.* 66 (1951) 1523–1532.
- [126] F.J. McClure, Availability of fluoride in sodium fluoride vs sodium fluorosilicate, *Public Health Rep.* 65 (1950) 1175–1186.
- [127] P. Pitter, Forms of occurrence of fluorine in drinking water, *Water Res.* 19 (1985) 281–284.
- [128] F.A. Arnold Jr., R.C. Likins, A.L. Russell, D.B. Scott, Fifteenth year of the Grand Rapids Fluoridation Study, *J. Am. Dent. Assoc.* 65 (1962) 780–785.
- [129] D.B. Ast, B. Fitzgerald, Effectiveness of water fluoridation, *J. Am. Dent. Assoc.* 65 (1962) 581–587.
- [130] J.A. Brunelle, J.P. Carlos, Recent trends in dental caries in U.S. children and the effect of water fluoridation, *J. Dent. Res.* 69 (1990) 723–727.
- [131] E. Newbrun, Effectiveness of water fluoridation, *J. Public Health Dent.* 49 (1989) 279–289.
- [132] L.W. Ripa, A half-century of community water fluoridation in the United States: Review and commentary, *J. Public Health Dent.* 53 (1993) 17–44.

- [133] C.M. Jones, G.O. Taylor, J.G. Whittle, D. Evans, D.P. Trotter, Water fluoridation, tooth decay in 5 year olds, and social deprivation measured by the Jarman score: Analysis of data from British dental surveys. *Br. Med. J.* 315 (1997) 514–517.
- [134] G.D. Slade, A.J. Spencer, M.J. Davies, J.F. Stewart, Influence of exposure to fluoridated water on socioeconomic inequalities in children's caries experience, *Commun. Dent. Oral Epidemiol.* 24 (1996) 89–100.
- [135] R.C. Graves, H.M. Bohannon, J.A. Disney, J.W. Stamm, J.D. Bader, J.R. Abernathy, Recent dental caries and treatment patterns in US children, *J. Public Health Dent.* 46 (1986) 23–29.
- [136] D. Grembowski, L. Fiset, A. Spadafora, How fluoridation affects adult dental caries: Systemic and topical effects are explored, *J. Am. Dent. Assoc.* 123 (1992) 49–54.
- [137] S.A. Eklund, B.A. Burt, A.I. Ismail, J.J. Calderone, High fluoride drinking water, fluorosis, and dental caries in adults, *J. Am. Dent. Assoc.* 114 (1987) 324–328.
- [138] B. Brustman, Impact of exposure to fluoride-adequate water on root surface caries in elderly, *Gerodontology* 2 (1986) 203–207.
- [139] J.S. Stamm, D.W. Banting, P.B. Imrey, Adult root caries survey of two similar communities with contrasting natural water fluoride levels, *J. Am. Dent. Assoc.* 120 (1990) 143–149.
- [140] T.M. Marthaler, P.E. Petersen, Salt fluoridation—An alternative in automatic prevention of dental caries, *Int. Dent. J.* 55 (2005) 351–358.
- [141] S.R. Estupinan-Day, R. Baez, H. Horowitz, R. Warpela, B. Sutherland, M. Thamer, Salt fluoridation and dental caries in Jamaica, *Commun. Dent. Oral Epidemiol.* 29 (2001) 247–252.
- [142] S. Jones, B.A. Burt, P.E. Petersen, M.A. Larsen, The effective use of fluorides in public health, *Bull. World Health Org.* 83 (2005) 670–676.
- [143] B.A. Burt, T.M. Marthaler, Fluoride tablets, salt fluoridation and milk fluoridation, in: O. Fejerskov, J. Ekstrand, B.A. Burts (Eds.), *Fluoride in Dentistry*, 2nd edition, Munksgaard, Copenhagen, 1996.
- [144] J.W. Stamm, Milk fluoridation as a public health measure, *J. Can. Dent. Assoc.* 38 (1972) 446–448.
- [145] Y. Ericsson, State of fluorine in milk and its absorption and retention when administered in milk. Investigations with radioactive fluorine, *Acta Odontol. Scand.* 16 (1958) 51–72.
- [146] K.W. Stephen, I.T. Boyle, D. Campbell, S. McNee, P. Boyle, Five-year double-blind fluoridated milk study in Scotland, *Commun. Dent. Oral Epidemiol.* 12 (1984) 223–229.
- [147] G.N. Pakhomov, K. Ivanova, I.J. Moller, M. Vrabcheva, Dental caries-reducing effects of a milk fluoridation project in Bulgaria, *J. Public Health Dent.* 55 (1995) 234–237.
- [148] Z. Toth, Z. Gintner, J. Banoczy, P.C. Phillips, The effect of fluoridated milk on human dental enamel in an *in vitro* demineralization model, *Caries Res.* 31 (1997) 212–215.
- [149] J. Pratten, R. Bedi, M. Wilson, An *in vitro* study of the effect of fluoridated milk on oral bacterial biofilms, *Appl. Environ. Microbiol.* 66 (2000) 1720–1723.
- [150] H.T. Meyer-Lueckel, T. Satzinger, A.M. Keielbassa, Caries prevalence among 6- to 16-year-old students in Jamaica 12 years after the introduction of salt fluoridation, *Caries Res.* 36 (2002) 170–173.
- [151] S.M. Levy, Review of fluoride exposures and ingestion, *Commun. Dent. Oral Epidemiol.* 22 (1994) 173–180.
- [152] A. Richards, D.W. Banting, Fluoride toothpastes: Current status and future prospects, in: O. Fejerskov, J. Ekstrand, B.A. Burt (Eds.), *Fluoride in Dentistry*, 2nd edition, Munksgaard, Copenhagen, 1996.
- [153] M.F. Johnson, Comparative efficacy of NaF and SMFP dentifrices in caries prevention: A meta-analytic overview *Caries, Res.* 27 (1993) 328–336.

- [154] A. Young, P.S. Thrane, E. Saxegaard, G. Jonski, G. Rolla, Effect of stannous fluoride toothpaste on erosion-like lesions: An *in vivo* study, *Eur. J. Oral Sci.* 114 (2006) 180–183.
- [155] R.J. Sullivan, R. Fletcher, R. Bachiman, B. Penugonda, R.Z. LeGeros, Intra-oral comparison and evaluation of the ability of fluoride dentifrices to promote remineralisation of caries-like lesions in dentin and enamel, *J. Clin. Dent.* 6 (1995) 135–138.
- [156] R.M. Duckworth, S.N. Morgan, R.J. Gilbert, Oral fluoride measurements for estimation of the anti-caries efficacy of fluoride treatments, *J. Dent. Res.* 71 (1992) 836–840.
- [157] R.M. Duckworth, S.N. Morgan, C.K. Burchell, Fluoride in plaque following use of dentifrices containing sodium monofluorophosphate, *J. Dent. Res.* 68 (1989) 130–133.
- [158] R.M. Duckworth, S.N. Morgan, Oral fluoride retention after use of fluoride dentifrices, *Caries Res.* 25 (1991) 123–129.
- [159] H. Rentsema, J. Schuthof, J. Arends, An *in vivo* investigation of the fluoride uptake in partially demineralised human enamel from several different dentifrices, *J. Dent. Res.* 64 (1985) 19–23.
- [160] C. Bruun, H. Givskov, A. Thylstrup, Whole saliva fluoride after toothbrushing with NaF and MFP dentifrices with different F concentrations, *Caries Res.* 18 (1984) 282–288.
- [161] J.W. Stamm, The value of dentifrices and mouthrinses in caries prevention, *Int. Dent. J.* 43 (1993) 517–527.
- [162] J.R. Mellberg, Fluoride dentifrices: Current status and prospects, *Int. Dent. J.* 41 (1991) 9–16.
- [163] R.M. Davies, R.P. Ellwood, G.M. Davies, The rational use of fluoride toothpaste, *Int. J. Dent. Hyg.* 1 (2003) 3–8.
- [164] O.P. Lind, J.R. von der Fehr, M. Joost Larsen, I.J. Moller, Anti-caries effect of a 2% Na₂PO₃F-dentifrice in a Danish fluoride area, *Commun. Dent. Oral Epidemiol.* 4 (1976) 7–14.
- [165] D.M. O' Mullane, J. Clarkson, T. Holland, S. O'Hickey, H. Whelton, Effectiveness of water fluoridation in the prevention of dental caries in Irish children, *Commun. Dent. Health* 5 (1988) 331–344.
- [166] R.K. Chesters, E. Huntington, C.K. Buchell, K.W. Stephen, Effect of oral care habits on caries in adolescents, *Caries Res.* 26 (1992) 299–304.
- [167] I.G. Chesnutt, F. Schafer, A.P.M. Jacobson, K.W. Stephen, The influence of toothbrushing frequency and post-brushing rinsing on caries experience in a caries clinical trial, *Commun. Dent. Oral Epidemiol.* 26 (1998) 406–411.
- [168] E.D. Beltran, S.M. Szpunar, Fluoride in toothpastes for children: Suggestion for change, *Pediatr. Dent.* 10 (1988) 185–188.
- [169] G. Koch, L-G. Petersen, E. Kling, L. Kling, Effect of 250 and 1000 ppm fluoride dentifrice on caries: A three-year clinical study, *Swed. Dent. J.* 2 (1982) 233–238.
- [170] G.B. Winter, R.D. Holt, B.F. Williams, Clinical trial of a low-fluoride toothpaste for young children, *Int. Dent. J.* 39 (1989) 227–235.
- [171] R.D. Holt, C.E. Morris, G.B. Winter, M.C. Downer, Enamel opacities and dental caries in children who use a low fluoride toothpaste between 2 and 5 years of age, *Int. Dent. J.* 44 (1991) 331–341.
- [172] D.T. Zero, R.F. Raubertas, J. Fu, A.M. Pedersen, A.L. Hayes, J.D.B. Featherstone, Fluoride concentrations in plaque, whole saliva, and ductal saliva after application of home-use topical fluorides, *J. Dent. Res.* 71 (1992) 1768–1775.
- [173] J.F. Perdok, H.C. van der Mei, H.J. Busscher, Physicochemical properties of commercially available mouthrinses, *J. Dent.* 18 (1990) 147–150.
- [174] B.A. Burt, S.A. Eklund, *Dentistry, Dental Practice, and the Community*, 5th edition, WB Saunders, Philadelphia, 1999.
- [175] A.J. Rugg-Gunn, P.J. Holloway, T.G.H. Davies, Caries prevention by daily fluoride mouthrinsing: Report of a three-year clinical trial, *Br. Dent. J.* 135 (1973) 353–360.

- [176] D.H. Leverett, O.B. Sveen, Ø.E. Jensen, Weekly rinsing with a fluoride mouthrinse in an unfluoridated community: Results after seven years, *J. Public Health Dent.* 45 (1985) 95–100.
- [177] L.W. Ripa, A critique of topical fluoride methods (dentifrices, mouthrinses, operator-, and self-applied gels) in an era of decreased caries and increased fluorosis prevalence, *J. Public Health Dent.* 51 (1991) 23–41.
- [178] J.A. Disney, R.C. Graves, J.W. Stamm, H.M. Bohannon, J.R. Abernathy, Comparative effects of a 4-year fluoride mouthrinse program on high and low caries forming grade 1 children, *Commun. Dent. Oral Epidemiol* 17 (1989) 139–143.
- [179] S.P. Klein, H.M. Bohannon, R.M. Bell, J.A. Disney, C.B. Foch, R.C. Graves, The cost and effectiveness of school-based preventive dental care, *Am. J. Public Health* 75 (1985) 382–391.
- [180] F. Brudevold, A. Savory, D.E. Gardner, M. Spinelli, R. Speirs, A study of acidulated fluoride solutions. I. *In vitro* effects on enamel, *Arch. Oral Biol.* 8 (1963) 167–177.
- [181] M. Hout, S. Koenigsberg, Z. Shey, The effect of prior toothcleaning on the efficacy of topical fluoride treatment: Two-year results, *Clin. Prev. Dent.* 5 (1983) 8–10.
- [182] T.G. Dijkman, J. Arends, The role of 'CaF₂-like' material in topical fluoridation of enamel *in situ*, *Acta Odontol. Scand.* 46 (1988) 391–397.
- [183] P.P. Hagen, R.G. Rozier, J.W. Bawden, The caries-preventive effect of full- and half-strength topical acidulated phosphate fluoride, *Pediatr. Dent.* 7 (1985) 185–191.
- [184] American Dental Association, ADA Guide to Dental Therapeutics, 1st edition, American Dental Association, Chicago, 1998.
- [185] L.W. Ripa, An evaluation of the use of professional (operator-applied) topical fluorides, *J. Dent. Res.* 69 (1990) 786–796.
- [186] H.S. Horowitz, J. Doyle, The effect on dental caries of topically applied acidulated phosphate-fluoride: Results after three years, *J. Am. Dent. Assoc.* 82 (1971) 359–365.
- [187] D.W. Johnston, D.W. Lewis, Three-year randomized trial of professionally applied topical fluoride gel comparing annual and biannual application with/without prior prophylaxis, *Caries Res.* 29 (1995) 331–336.
- [188] H.S. Horowitz, A.I. Ismail, Topical fluorides in caries prevention, in: O. Fejerskov, J. Ekstrand, B.A. Burt (Eds.), *Fluorides in Dentistry*, 2nd edition, Munksgaard, Copenhagen, 1996.
- [189] L.M. Wakeen, Legal implications of using drugs and devices in the dental office, *J. Public Health Dent.* 52 (1992) 403–408.
- [190] S. Twetman, L.G. Petersson, G.N. Pakhomov, Caries incidence in relation to salivary mutans streptococci and fluoride varnish applications in preschool children from low- and optimal-fluoride areas, *Caries Res.* 30 (1996) 347–353.
- [191] L. Seppä, T. Leppänen, H. Hausen, Fluoride varnish versus acidulated phosphate fluoride gel: A 3-year clinical trial, *Caries Res.* 29 (1995) 327–330.
- [192] L.G. Petersson, L. Arthursson, C. Östberg, P. Jönsson, A. Gleerup, Caries-inhibiting effects of different modes of Duraphat varnish reapplication: A 3-year radiographic study, *Caries Res.* 25 (1991) 70–73.
- [193] L. Sköld, B. Sundquist, B. Eriksson, C. Edeland, Four-year study of caries inhibition of intensive Duraphat application in 11–15-year-old children, *Commun. Dent. Oral Epidemiol.* 22 (1994) 8–12.
- [194] M.L. Adriaens, L.R. Dermaut, R.M.H. Verbeeck, The use of 'Fluor Protector,' a fluoride varnish, as a caries prevention method under orthodontic molar bands, *Eur. J. Orthod.* 12 (1990) 316–319.
- [195] M. Peyron, L. Matsson, D. Birkhed, Progression of approximal caries in primary molars and the effect of Duraphat treatment, *Scand. J. Dent. Res.* 100 (1992) 314–318.
- [196] B. Ogard, L. Seppä, G. Rolla, Professional topical fluoride applications—Clinical efficacy and mechanism of action, *Adv. Dent. Res.* 8 (1994) 190–201.

- [197] F.J.T. Burke, S.W. Cheung, I.A. Mjor, N.H.F. Wilson, Restoration longevity and analysis of reasons for the placement and replacement of restorations provided by vocational dental practitioners and their trainees in the United Kingdom, *Quintessence Int.* 30 (1999) 234–242.
- [198] I.A. Mjor, The reasons for replacement and the age of failed restorations in general dental practice, *Acta Odontol. Scand.* 55 (1997) 58–63.
- [199] L-K. Wendt, G. Koch, D. Birkhed, Replacement of restorations in the primary and young permanent dentition, *Swed. Dent.* 22 (1998) 149–155.
- [200] N.H.F. Wilson, F.J.T. Burke, I.A. Mjor, Reasons for placement and replacement of restorations in direct restorative materials by a selected group of practitioners in the United Kingdom, *Quintessence Int.* 28 (1997) 245–248.
- [201] J. Hicks, F. Garcia-Godoy, K. Donly, C. Flaitz, Fluoride-releasing restorative materials and secondary caries, *J. Calif. Dent. Assoc.* 31 (2003) 229–245.
- [202] W.S. Hawthorne, R.J. Smales, Factors influencing long term restoration survival in three private dental practices in Australia, *Aust. Dent. J.* 42 (1997) 59–63.
- [203] C. Bentley, C.W. Drake, Longevity of restorations in a dental school school clinic, *J. Dent. Educ.* 50 (1986) 594–600.
- [204] R. Hickel, J. Manhart, Longevity of restorations in posterior teeth and reasons for failure, *J. Adhes. Dent.* 3 (2001) 45–64.
- [205] E.A.M. Kidd, Caries diagnosis with restored teeth, *Adv. Dent. Res.* 4 (1990) 10–13.
- [206] E.A.M. Kidd, S. Johnston-Bechal, D. Beighton, Diagnosis of secondary caries: A laboratory study, *Br. Dent. J.* 176 (1994) 135–139.
- [207] I.A. Mjor, The location of clinically diagnosed secondary caries, *Quintessence Int.* 29 (1998) 313–317.
- [208] A.D. Wilson, B.E. Kent, The glass ionomer cement, a new translucent dental filling material, *J. Appl. Chem. Biotechnol.* 21 (1971) 313.
- [209] A.D. Wilson, J.W. McLean, *Glass Ionomer Cement*, Quintessence Publishers, Chicago, 1988.
- [210] R.G. Hill, A.D. Wilson, Some structural aspects of glasses used in ionomer cements, *Glass Technol.* 29 (1988) 150–167.
- [211] S. Matsuya, T. Maeda, M. Ohta, IR and NMR analyses of hardening and maturation of glass-ionomer cement, *J. Dent. Res.* 75 (1996) 1920–1927.
- [212] G. Mount, Making the most of glass ionomer cements, *Dent. Update* 18 (1991) 276–279.
- [213] J. Burgess, M. Norling, J. Summit, Resin ionomer restorative materials: The new generation, *J. Esthet. Dent.* 6 (1994) 207–215.
- [214] E.A. Wasson, Reinforced glass-ionomer cements—A review of properties and clinical use, *Clin. Mater.* 12 (1993) 181–190.
- [215] R. Frankenberger, J. Sindel, N. Kramer, Viscous glass-ionomer cements: A new alternative to amalgam in the primary dentition? *Quintessence Int.* 28 (1997) 667–676.
- [216] M.J. Tyas, Milestones in adhesion: Glass-ionomer cements, *J. Adhes. Dent.* 5 (2003) 259–266.
- [217] A.D. Wilson, H.J. Prosser, D.R. Powis, Mechanism of adhesion of polyelectrolyte cements to hydroxyapatite, *J. Dent. Res.* 62 (1983) 590–592.
- [218] S.-Y. Cho, A.C. Cheng, A review of glass ionomer restorations in the primary dentition, *J. Can. Dent. Assoc.* 65 (1999) 491–495.
- [219] H. Ngo, G.J. Mount, M.C.R.B. Peters, A study of glass-ionomer cement and its interface with enamel and dentin using a low-temperature, high-resolution scanning electron microscopic technique, *Quintessence Int.* 28 (1997) 63–69.
- [220] R.L. Erickson, E.A. Glasspole, Bonding to tooth structure: A comparison of glass-ionomer composite resin systems, *J. Esthet. Dent.* 6 (1994) 227–244.
- [221] M.J. Tyas, Cariostatic effect of glass ionomer cement: A five-year clinical study, *Aust. Dent. J.* 36 (1991) 236–239.

- [222] E.D. Smith, F.E. Martin, Microleakage of glass ionomer/composite resin restorations: A laboratory study. I. The influence of glass ionomer cement, *Aust. Dent. J.* 37 (1992) 23–30.
- [223] G.J. Mount, Clinical placement of modern glass-ionomer cements, *Quintessence Int.* 24 (1993) 99–107.
- [224] R.M.H. Verbeeck, E.A.P. De Maeyer, L.A.M. Marks, R.G.J. De Moor, A.M.C.J. De Witte, L.M. Trimpeneers, Fluoride release process of (resin-modified) glass-ionomer cements versus (polyacid-modified) composite resins, *Biomaterials* 19 (1998) 509–519.
- [225] L. Forsten, Short- and long-term fluoride release from glass ionomers and other fluoride-containing filling materials *in vitro*, *Scand. J. Dent. Res.* 98 (1990) 179–185.
- [226] A.D. Wilson, D. Clinton, R.P. Miller, The formation and microstructure of dental silicate cements, *J. Mater. Sci.* 7 (1972) 220.
- [227] L. Forsten, Fluoride release from a glass ionomer cement, *Scand. J. Dent. Res.* 8 (1977) 503–504.
- [228] W.M. Tay, M. Braden, Fluoride diffusion from polyalkenoate (glass-ionomer) cements, *Biomaterials* 9 (1988) 454–456.
- [229] A.D. Wilson, J.W. Nicholson, *Acid-Base Cements*, The University Press, Cambridge, 1993.
- [230] J.W. Nicholson, Chemistry of glass-ionomer cements: A review, *Biomaterials* 19 (1998) 485–494.
- [231] O.P.A. Hoyte, J. Emsley, Caesium fluoride solutions in carboxylic acids, *J. Chem. Soc. Dalton Trans.* (1976) 2219–2226.
- [232] R.W. Billington, J.A. Williams, G.J. Pearson, Ion processes in glass ionomer cements, *J. Dent.* 34 (2006) 544–555.
- [233] R.W. Billington, P.C. Hadley, J.A. Williams, G.J. Pearson, Kinetics of fluoride release from zinc oxide-based cements, *Biomaterials* 22 (2000) 2507–2513.
- [234] J.A. Williams, R.W. Billington, G.J. Pearson, A long term study of fluoride release from metal containing conventional and resin modified glass ionomer cements, *J. Oral Rehabil.* 28 (2001) 41–47.
- [235] B.F. El Mallakh, N.K. Sarkar, Fluoride release from glass ionomer cements in deionized water and artificial saliva, *Dent. Mater.* 6 (1990) 118–122.
- [236] T. Fusayama, T. Katayori, S. Nomoto, Corrosion of gold and amalgam placed in contact with each other, *J. Dent. Res.* 42 (1963) 1183–1197.
- [237] B. Levallois, F. Yannick, L. Lapeyre, J.Y. Gal, In vitro fluoride from restorative materials in water versus artificial saliva medium (SAGF), *Dent. Mater.* 14 (1998) 441–447.
- [238] A.W.G. Walls, Glass polyalkenoate (glass-ionomer) cements: A review, *J. Dent.* 14 (1986) 231–246.
- [239] L. Forsten, Fluoride release and uptake by glass ionomers, *Scand. J. Dent. Res.* 91 (1991) 241–245.
- [240] L. Seppa, H. Forss, B. Ogaard, The effect of fluoride application on fluoride release and the antibacterial action of glass ionomers, *J. Dent. Res.* 72 (1993) 1310–1314.
- [241] S. Hatibovic-Kofman, G. Koch, Fluoride release from glass ionomer cement *in vivo* and *in vitro*, *Swed. Dent. J.* 5 (1991) 253–258.
- [242] A.J. Preston, E.A. Agalamany, S.M. Higham, L.H. Mair, The recharge of aesthetic dental restorative materials with fluoride *in vitro*—Two year results, *Dent. Mater.* 19 (2003) 32–37.
- [243] A.M. De Witte, E.A.P. De Maeyer, R.M.H. Verbeeck, L.C. Martens, Fluoride release profiles of mature glass ionomer cements after fluoride application, *Biomaterials* 21 (2000) 475–482.
- [244] J.P. Akselsen, J. Afseth, G. Rolla, In vitro damage to glass-ionomer cements by fluoride ion, *Caries Res.* 21 (1987) 188 (Abs No 81).
- [245] R.W. Billington, J.A. Williams, R. Strang, Effects of neutral sodium fluoride on glass-ionomers *in vitro*, *J. Dent. Res.* 66 (1987) 844 (Abs No 88).

- [246] A.M.J. De Witte, E.A.P. De Maeyer, R.M.H. Verbeeck, Surface roughening of glass ionomer cements by neutral NaF solutions, *Biomaterials* 24 (2003) 1995–2000.
- [247] J.A. Williams, R.W. Billington, G.J. Pearson, Comparison of ion release from a glass ionomer cement as a function of the method of incorporation of added ions, *Biomaterials* 20 (1999) 589–594.
- [248] P.C. Hadley, E. Milella, C. Cerardi, R.G. Hill, R.W. Billington, Distribution of fluoride in glass ionomer cement using SIMS, *Biomaterials* 22 (2001) 1563–1569.
- [249] F.H. Jones, B.M. Hutton, P.C. Hadley, A.J. Eccles, T.A. Steele, R.W. Billington, G. J. Pearson, Fluoride uptake by glass ionomer cements: A surface analysis approach, *Biomaterials* 24 (2003) 107–119.
- [250] A.D. Wilson, D.M. Groffman, A.T. Kuhn, The release of fluoride and other chemical species from a glass ionomer cement, *Biomaterials* 6 (1985) 431–433.
- [251] B. Czarnecka, H. Limanowska-Shaw, J.W. Nicholson, Buffering and ion-release by a glass-ionomer cement under near neutral; and acidic conditions, *Biomaterials* 23 (2002) 2783–2788.
- [252] R.W. Billington, J.A. Williams, A. Dorban, G.J. Pearson, Glass ionomer cement: Evidence pointing to fluorine release in the form of monofluorophosphate in addition to fluoride ion, *Biomaterials* 25 (2004) 3399–3402.
- [253] F.N. Hattab, Analytical methods for the determination of various forms of fluoride in toothpastes, *J. Dent.* 17 (1989) 77–83.
- [254] R.G. Hill, E. de Barra, F. Griffin, G. Henn, J. Devlin, P.V. Hatton, I. Brook, K. Johal, G. Craig, Ion release from glass polyalkenoate (ionomer) cements, *Key Eng. Mater.* 99/100 (1995) 315–322.
- [255] B. Levallois, Y. Fovet, L. Lapeyre, J.Y. Gal, In vitro fluoride release from restorative materials in water versus artificial saliva medium (SAGF), *Dent. Mater.* 14 (1998) 441–447.
- [256] G.J. Mount, Glass ionomer cements: Past, present and future, *Oper. Dent.* 19 (1994) 82–90.
- [257] E.J. Swift Jr., An update on glass ionomer cements, *Quintessence Int.* 19 (1988) 125–130.
- [258] M. Souto, K.J. Donly, Caries inhibition of glass ionomers, *Am. J. Dent.* 7 (1994) 122–124.
- [259] I.A. Mjor, Glass-ionomer cement restorations and secondary caries: A preliminary report, *Quintessence Int.* 27 (1996) 171–174.
- [260] N.H.F. Wilson, F.J.T. Burke, I.A. Mjor, Reasons for placement and replacement of restorations of direct restorative materials by a selected group of practitioners in the United Kingdom, *Quintessence Int.* 28 (1997) 245–248.
- [261] C.B. Marinelle, K.J. Donly, J.S. Wefel, J.R. Jakobsen, G.E. Denehy, An *in vitro* comparison of 3 fluoride regimens on enamel remineralization, *Caries Res.* 31 (1997) 418–422.
- [262] K.J. Donly, J.J. Nelson, Fluoride release of restorative materials exposed to a fluoridated dentifrice, *J. Dent. Child.* 64 (1997) 249–250.
- [263] B. Czarnecka, J.W. Nicholson, Ion release by resin-modified glass-ionomer cements into water and lactic acid solutions, *J. Dent.* 34 (2006) 539–543.
- [264] S.B. Mitra, In vitro fluoride release from a light-cured glass-ionomer liner/base, *J. Dent. Res.* 70 (1991) 75–78.
- [265] H. Forss, Release of fluoride and other elements from light cured glass ionomers in neutral and acidic conditions, *J. Dent. Res.* 72 (1993) 1257–1262.
- [266] J.W. McLean, J.W. Nicholson, A.D. Wilson, Proposed nomenclature for glass-ionomer dental cements and related materials, *Quintessence Int.* 25 (1994) 587–589.
- [267] J-M. Meyer, M.A. Cattani-Lorente, V. Dupuis, Compomers: Between glass-ionomer cements and composites, *Biomaterials* 19 (1998) 529–539.
- [268] N.D. Ruse, What is a compomer? *J. Can. Dent. Assoc.* 65 (1999) 500–504.
- [269] J.W. Nicholson, Polyacid modified composite resins (“compomers”) and their use in clinical dentistry, *Dent. Mater.* 23 (2006) 615–622.

- [270] J.W. Nicholson, M.A. McKenzie, The properties of polymerizable luting cements, *J. Oral Rehabil.* 26 (1999) 767–774.
- [271] G. Eliades, A. Kakaboura, G. Palaghias, Acid base reaction and fluoride release profiles in visible light-cured polyacid modified composite resin restorations, *Dent. Mater.* 14 (1998) 57–63.
- [272] R. Martin, S.J. Paul, H. Luthy, P. Scharer, Dentin bond strength of Dyract Cem, *Am. J. Dent.* 10 (1997) 27–31.
- [273] D. Moodley, S.R. Grobler, Compomers: Adhesion and setting reactions, *S. Afr. Dent. J.* 58 (2003) 24–28.
- [274] A.J. Shaw, T. Carrick, J.F. McCabe, Fluoride release from glass-ionomer and compomer restorative materials: 6 month data, *J. Dent.* 26 (1998) 355–356.
- [275] S.R. Grobler, R.J. Rossouw, K. Van Wyk, A comparison of fluoride release from various dental materials, *J. Dent.* 26 (1998) 256–265.
- [276] B.J. Millar, F. Abiden, J.W. Nicholson, In vitro caries inhibition by polyacid-modified composite resins (“compomers”), *J. Dent.* 26 (1998) 133–136.
- [277] D. Sales, D. Sae-Lee, S. Matsuya, I.D. Ana, Short-term fluoride and cations release from polyacid-modified composites in distilled water and an acidic lactate buffer, *Biomaterials* 21 (2003) 1687–1696.
- [278] X. Xu, J.O. Burgess, Compressive strength, fluoride release and recharge of fluoride-releasing materials, *Biomaterials* 24 (2003) 2451–2461.
- [279] J.W. Nicholson, B. Czarnecka, The release of ions by compomers under neutral and acidic conditions, *J. Oral Rehabil.* 31 (2004) 665–670.
- [280] J.W. Akitt, N.N. Greenwood, G.D. Lester, Nuclear magnetic resonance and Raman studies of aluminium complexes formed in aqueous solutions of aluminium salts containing phosphoric acids and fluoride ions, *J. Chem. Soc. A* (1971) 2450–2457.
- [281] P. Karantakis, M. Helvatjoglou-Antoniades, S. Theodoridou-Pahini, Y. Papadogiannis, Fluoride release from three glass ionomers, a compomer, and a composite resin in water, artificial saliva, and lactic acid, *Oper. Dent.* 25 (2000) 20–25.
- [282] F.C. Eichmiller, W.A. Marjenhoff, Fluoride-releasing dental restorative materials, *Oper. Dent.* 23 (1998) 213–218.
- [283] A.R. Veira, I.P.R. De Souza, A. Modesto, Fluoride uptake and release by composites and glass ionomers in a high caries challenge situation, *Am. J. Dent.* 12 (1999) 14–18.
- [284] P. Weidlich, L.M. Miranda, M. Maltz, S.M.W. Samuel, Fluoride release and uptake from glass ionomer cements and composite resins, *Braz. Dent. J.* 11 (2000) 89–96.
- [285] J. Arends, G.E.H.M. Dijkman, A.G. Dijkman, Review of fluoride release and secondary caries reduction by fluoridating composites, *Adv. Dent. Res.* 9 (1995) 367–376.
- [286] J. Arends, J. Ruben, A.G. Dijkman, The effect of fluoride release from a fluoride-containing composite resin on secondary caries: An *in vitro* study, *Quintessence Int.* 21 (1990) 671–674.
- [287] G.E.H.M. Dijkman, J. de Vries, A. Lodding, J. Arends, Long-term fluoride release of visible light-activated composites *in vitro*: A correlation with *in situ* demineralization data, *Caries Res.* 27 (1993) 117–123.
- [288] K. Kawai, D. Tantbirojn, A.S. Kamalawat, T. Hasegawa, D.H. Retief, In vitro enamel and cementum fluoride uptake from three fluoride-containing composites, *Caries Res.* 32 (1998) 463–469.

Note from the Editors

In this volume, another chapter deals with inorganic and/or composite biomaterials by C. Rey *et al.*, and the effects of exposure of humans to fluorine are presented by M. Ponikvar.

CHAPTER 8

Fluorinated Biomaterials for Cardiovascular Surgery

Charles Baquey,^{1,*} Marie-Christine Durrieu,¹ and Robert G. Guidoin²

¹INSERM, U577, Bordeaux, F-33076 France; Univ. Victor Ségalen Bordeaux 2, F-33076 France 146, rue Léo Saignat, 33076 Bordeaux Cédex, France

²Department of Surgery (Biomaterials), Faculté de Médecine, Pavillon Ferdinand-Vandry, Université Laval, Québec G1K7P4, Canada

Contents

1. Introduction	380
2. Blood–vessel wall relationships (interactions of flowing blood with the vessel/vascular prosthesis wall)	380
2.1. Role of the surface free energy or surface tension	381
2.2. Role of electrical parameters	381
2.3. Scenario for blood–material interactions	382
2.4. Role of dynamic factors	384
2.5. Role of the morphology	385
3. Requirements for a cardiovascular biomaterial	386
4. From polytetrafluoroethylene to microporous teflon-based vascular prostheses	388
4.1. State of the art related to vessel repair or replacement: Evolution and role of PTFE	389
4.2. How to improve the functional patency of ePTFE-based prostheses?	392
4.3. Chemical modifications of fluorinated polymers: A way to the improvement of their haemocompatibility	394
4.3.1. PTFE case	394
4.3.2. PVDF case	396
4.3.3. P(VDF-HFP) case	401
5. Conclusions	402
References	404
Note from the Editors	406

Abstract

The biomedical area did not miss the tremendous development of macromolecular materials and their applications, which has followed the rapid expansion of petrochemistry during the twentieth century. In fact, these materials are widely used to design a lot of

*Corresponding author.;
Email: charles@baquey.com

medical devices that are at physicians' disposal to care patients. Some of these devices, commonly used in medical care units, such as syringes or tubings, are disposable, whereas others, such as joint prostheses, vascular substitutes, artificial lens, suture thread, are implanted in the body for an unlimited time, hopefully. Considering the cardiovascular area only, the introduction of polymeric materials induced outstanding advances, as they allowed, for instance, the design of arterial substitutes from woven, knitted and non-woven synthetic fabrics, thus opening a new therapeutic option for the replacement of diseased arterial segments beside the grafting of an autologous venous segment, the availability of which is necessarily limited. The polyethylene terephthalate (PET) takes a prominent place among the materials which are used for this application, but it meets the strong competition of the expanded polytetrafluoroethylene (ePTFE). Known for its chemical inertia and great thermal stability, this polymer, which is not easily processed, has many assets (biostability, heat sterilisable) in comparison with its main competitor, the PET, even if like the latter, it does not satisfy all the requirements a material used for the making of arterial substitutes has to comply with. However, different approaches are proposed to improve the situation, such as surface processings specifically designed to increase the polytetrafluoroethylene (PTFE) haemocompatibility on the one hand, or the choice of other fluorinated polymers on the other.

1. INTRODUCTION

Because of inherited lesions or of an evolutive disease of their wall, arteries may become unable to ensure an adequate transport of the blood to organs and tissues, which may create a risk of myocardium infarctus or aneurysm rupture followed by a fatal haemorrhage for patients concerned by such (or suffering such) vascular diseases. After Gluck's pioneering works [1], which paved the way to the modern vascular surgery concepts, the replacement of a carotid segment by an autologous venous graft was no longer a dream, and these patients could be surged to repair or replace their diseased arteries. In this respect, vascular surgeons have at their disposal, various devices which do not satisfy all the requirements which are listed below, but which may compensate some of the functional deficiencies their patients encounter. Following Gluck's works, various materials including metals and glass have been used for the design and making of vascular substitutes, but the first clinical studies related to the use of flexible prostheses made from a non-biological material were reported only after 1952 by Woorhees *et al.* [2]. Taking into account what is known about the flowing blood-artery wall relationship, different criteria which have to be satisfied by a blood-contacting material, and more specifically by an arterial substitute, can be identified. This rationally designed strategy, mainly documented by studies carried out during the seventies and later on, was not given the priority as surgeons chose 20 years earlier, pragmatic solutions based on the use of polymeric materials among which polyethylene terephthalate (PET) and polytetrafluoroethylene (PTFE) a little later took leading positions.

2. BLOOD–VESSEL WALL RELATIONSHIPS (INTERACTIONS OF FLOWING BLOOD WITH THE VESSEL/VASCULAR PROSTHESIS WALL)

Interactions of blood, or more precisely of plasma macromolecules and blood cells with the vessel wall, should the latter be natural or artificial, depend upon several parameters: the mechanical properties of the vascular conduit, on the one hand, the morphology and the physical and chemical characteristics of the blood-contacting surface on the other.

2.1. Role of the surface free energy or surface tension

Surface tension, or surface free energy, is a parameter which corresponds to the residual binding capacity of a material surface, that is, the binding capacity of atoms or groups of atoms which constitute the border surface of the material of interest. This binding capacity may be uniform, as is the case for non-oxidised metals, but most of the time it is the resultant of several components that are respectively related to the various types of atoms or atom groups present on this surface including ionic sites, hydrophobic sites, polar sites or hydrogen atom donors or acceptors. Accordingly, most of the material surfaces appear as mosaic-like structures. The nature of the potential sites of interaction and the micro-topography determine the interaction phenomena of materials with biological media and especially with blood.

2.2. Role of electrical parameters

Blood cells and vessels walls are negatively charged, the corresponding isoelectric point lying at a pH between 4.8 and 5. Sawyer and Srinivasan [3] measured a voltage difference between endothelial layer and blood. Negatively charged surfaces give rise in the presence of an electrolyte solution to a double electric layer responsible for the recorded potential value Ψ_0 (Fig. 1a). As the distance from the wall increases, Ψ_0 decreases linearly down to a value equal to $\Psi_0/2.3$ according to the Stern theory. The corresponding distance (λ) to the wall is known as the Debye length. At distances greater than λ , the potential decreases exponentially to zero, the decaying potential being characterised by the so-called zeta (ζ) potential (Fig. 1b). The distance from the wall, corresponding to ζ , defines the shear plane and depends upon the flow conditions. For a given electrolyte solution (i.e. the nature and concentrations of ions in blood are known), ζ increases linearly with the flow rate [4].

Since the vessel wall is negatively charged, it repels the negatively charged platelets, and it helps in preventing thrombogenic phenomena. Experimentally, Sawyer *et al.* [5] demonstrated that on positively charged surfaces [>200 mV/normal

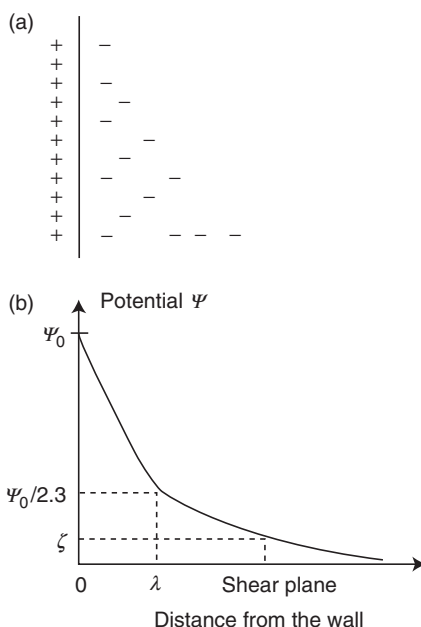


Fig. 1. Variation of the electric potential near a surface in the presence of an electrolyte solution. (a) Electrical double layer at the surface of a solid positively charged, in contact with an electrolyte solution. (b) The variation of the electrical potential when the measurement is made at an increasing distance from the surface, and when the liquid phase is mobile at a given flow rate. The zeta potential (ζ) can be calculated from the streaming potential, which can be measured according to the method described by Thubikar *et al.* [4].

hydrogen electrode (NHE)] thrombosis occurred systematically, while thrombosis never occurred on surfaces with a negative potential (<0 mV/NHE).

However, surface potential cannot be the unique criterion of non-thrombogenicity. The superficial distribution of the charged site plays an important role as far as plasma protein adsorption is concerned and, upon their adsorption, these biomolecules may trigger the coagulation cascade in spite of exposing a net negative charge to the bloodstream.

2.3. Scenario for blood–material interactions

According to the above developed considerations, surfaces can be described as a mosaic-like structure of which individual elements contribute locally and specifically to their residual binding capacity and their electrical potential. The individual characteristics of these elements and their microtopography determine, via a first series of interactions with water molecules and small solutes, which plasma

proteins adsorb and how they do it, when blood comes into contact with these surfaces, according to the following scenario.

At first, and according to their surface tension, materials show an affinity for water which corresponds to their wettability. Polar materials and materials bearing ionic sites, whether these properties are intrinsic or brought about by the contacting medium through adsorption phenomena of ions, are obviously the most wettable. Hydrophobic materials do not interact with water, but instead promote its intermolecular organisation, as in the case of oil or parafins. The contribution of water to the entropy of the system is thus decreased. This first step may occur simultaneously with (or may be immediately followed by) the interaction of free ions in solution on the one hand, which interact with ionic sites present on the material surface for previously mentioned reasons, and the interaction of small solutes in solution on the other. Obviously, ions and small solutes contribute to a local alteration of the water organisation in the interfacial region. The second step concerns proteins and other biological macromolecules, which will adsorb at the blood–material interface. These adsorption phenomena are controlled by the nature and distribution of available binding sites as determined by the type of material and the state of its surface after the previous step. Biological macromolecules are themselves characterised by a superficial distribution of binding sites when they are free in solution. If there is a good fit between this distribution and the one exposed by the material surface, macromolecules may adsorb without any conformational change; among available macromolecules, those for which this fit is the best have the greatest probability to adsorb. However, adsorption may occur together with a conformational change if such behaviour is thermodynamically favoured [6]. Furthermore, these adsorption phenomena may give macromolecules an opportunity to be activated, that is, zymogens will give active enzymes. In this way, the so-called coagulation contact phase starts.

The third and final step involves blood cells, and more particularly platelets and polymorphonuclear neutrophil leukocyte also known as granulocytes. According to the material surface state after the various events which have occurred previously, cells may or may not adhere to the material; for platelets, adhesion may be the initiating step for their activation and aggregation, since activation of platelets involves the release by their cytoplasmic granules of active promoters for thrombogenesis and platelet aggregation. Cell adhesion is not only due to physical and chemical phenomena as for protein adsorption, but also implies biochemical mechanisms involving cell membrane glycoproteins.

C5 to C9 complement[†] components may bind to platelets and amplify platelet release and aggregation already induced by thrombin. It may be noticed that platelet activation may also result from contact with air, which cannot occur under

[†] The so-called complement system consists in a set of 21 proteins aimed at contributing to the defence of the organism against foreign bodies or microorganisms or even abnormal cells.

implantation conditions, but which is possible during a session of extracorporeal circulation. Similarly, neutrophil adhesion arises from an increase of their adhesiveness due to the effect of the anaphylatoxin C5a on the expression of adhesines at the membrane of the neutrophils; C5a is generated by the complement activation processes, which may occur during the plasma protein–material interaction step.

2.4. Role of dynamic factors

Surface physics and chemistry play a major role as far as blood–material interactions are concerned. However, the observed processes depend as much on the local flow patterns of the blood near the material surface as on these surface characteristics.

It has been shown that plasma protein adsorption, which occurs as soon as blood comes into contact with a given surface, is clearly influenced by the local shear stress [7].

As discussed by Leonard [8], the concentrations of activated coagulation proteins in the interfacial layer (i.e. the layer sitting between the main stream in a vessel and the wall) are strongly influenced by flow factors, and the net concentrations are determined both by biochemical reactions producing activated coagulation factors and by convective–diffusive factors that serve to moderate the concentrations of inactivated and activated coagulation proteins. Furthermore, the presence of high concentrations of activated coagulation proteins may favour the activation of platelets and leukocytes. These two blood cell types are able to undergo activation via collisions, which are favoured by turbulent flow or particular conditions such as those created by vortices.

Platelet and fibrin deposition are strongly influenced by plasma and cellular factors, by properties of the vessel wall and by flow, as shown experimentally with the model of the everted deendothelialised rabbit aorta, used by Baumgartner [9].

Platelet attachment to subendothelium[‡] is determined predominantly by physical factors controlling the rate of platelet transport to the subendothelium at low shear rates (800 s^{-1}). In addition, platelet deposition was found to be highly dependent on the concentration of red cells, an effect attributed in part to the fact that red cells, by increasing the radial movement of platelets, enhance their diffusivity by several orders of magnitude compared to that theoretically predicted and experimentally measured in platelet-rich plasma.

Weiss *et al.* [10] have shown that platelet deposition is at a minimum at a shear rate of 50 s^{-1} , while fibrin deposition on subendothelium from non-anticoagulated blood is at a maximum at the same shear rate. At low shear rates (250 s^{-1}), fibrin

[‡] The inner surface of vessel is composed by a monolayer of adjacent endothelial cells. This layer is called endothelium and the underlying tissue is called subendothelium.

deposition is independent of platelet density and integrity. At a higher shear rate (650 s^{-1}), platelets must possess all their physiological properties to promote fibrin deposition. At much higher shear rates (2600 s^{-1}), fibrin deposition decreases despite increasing platelet deposition.

It will be later proposed that an ideal blood-contacting surface would be one on which endothelial cells could adhere and grow normally to create a complete endothelium endowed with the physiological functions of such tissue. But the correct expression of such physiological functions requires normal blood flow conditions. And the correlation of thrombosis with regions of disturbed flow suggests that shear stress may alter the production of endothelial cell-derived products and directly affect endothelial cell function.

Secretion of tissue plasminogen activator by cultured endothelial cells increases within an hour after exposure to arterial levels of shear stress [11], while secretion of the related inhibitor (plasminogen inhibitor-1) by the same cells is unaffected by shear forces over the physiological range.

Endothelial cells produce vasoactive substances, which modulate the permeability of vessel walls; accordingly, shear stresses may indirectly affect this wall parameter by influencing the secretory activity of endothelial cells.

Prostacyclin, a potent inhibitor of platelet aggregation, is derived from metabolism of arachidonic acid by endothelial cells, and shear stress increases its production rate [12]. It is postulated that this effect is due to perturbations of the permeability of the plasma membrane changing the cytosolic Ca^{2+} content and leading to an increase in phospholipase C activity (through the by-passing of the receptor requirement), which contributes to a higher production of arachidonic metabolites.

Shear stresses may also affect the construction and secretion by human endothelial cells of von Willebrand Factor polymeric forms that are involved together with fibronectin and fibrinogen during shear-induced platelet aggregation. In addition, shear stresses may play a role in the mechanism of platelet aggregation, probably through an increase in the readily available amounts of ADP, should the latter be due to an increased lysis of platelets, or to a greater release of their granules content.

2.5. Role of the morphology

Materials may be compact or porous. In the case of compact materials, smooth surfaces are preferred, as blood cells will encounter fewer opportunities to be injured by asperities or morphological singularities when blood flows in contact with such surfaces. The chance of cell trauma of mechanical origin depends obviously upon the size of these morphological irregularities and upon local flow conditions (shear stress, tubulences, vortices, etc.). Wurzingger and Schmid-Schonbein [13] have shown that the number of platelets adhering to PVC

surfaces could be multiplied by a factor of 3 with surfaces featuring peaks or valleys with averaged heights or depths around 9 μm compared to polished surfaces, knowing that the diameter of platelets sits around 1.5 μm .

Porous materials may have a closed porosity, which lowers their density and can be varied to optimise their mechanical properties, as this is carried out for some kinds of vascular grafts. For such materials, surface morphology must fulfil same requirements as those fulfilled by compact materials.

Materials with an open porosity are not generally directly exposed to flowing blood for long. A widespread example of such materials is found with knitted or woven PET-based vascular grafts. These grafts may be immersed into blood to allow the latter to invade the fabric mesh where it coagulates, the resulting matrix acting as a new lining offered to the flowing blood.

3. REQUIREMENTS FOR A CARDIOVASCULAR BIOMATERIAL

The above considerations show how it is important for the design of a vascular substitute to pay attention to its mechanical properties, to get similarity of dynamic behaviour between this substitute and the vessel it is to partly replace. The bloodstream that will flow through this artificial conduit must not suffer any alteration able to induce any local turbulences or high wall shear rate. This requirement may be satisfied insofar as the mechanical compliancy of the prosthesis (see Table 1 for definition) is equivalent to that of the natural artery it will replace. In fact, the arterial blood flow is pulsatile and characterised by a pressure wave which should propagate itself across any section of the arterial tree without encountering any sudden change of mechanical impedancy (potentially responsible for energy consuming reflected waves). The viscoelastic properties of their wall, featuring a composite structure, allow natural arteries to increase

Table 1. Comparison of the respective evolution of the compliances of a natural artery on the one hand and of an expanded polytetrafluoroethylene prosthesis on the other hand when the blood pressure increases

	Blood pressure (mmHg)			
	60	80	100	120
Femoral artery	6.5	4.7	4.1	3.8
Expanded polytetrafluoroethylene	0.9	0.85	0.78	0.8

Compliancy: Measures the ability of an artery to increase its section (and obviously the volume of blood, which can be contained in a given segment of this artery) upon an increase of TransMural Pressure (PTM) compliancy is expressed as $((\Delta V/V) \times 100)/\Delta P$ as % per mmHg.

their diameter according to a non-linear pattern, as the blood pressure increases; the greater this pressure, the smaller the relative increase of the diameter (see Table 1). It is expected that the laminar blood flow regimen will not turn to a turbulent one, when it crosses over an anastomosis between a natural artery and an arterial prosthesis (or between the latter and again the natural artery), if the prosthesis has a compliancy similar to that of the natural artery. The turbulent regimen is undesirable as it increases the probability of collision between blood cells and causes great variations of the wall shear rate, the consequences of which are detrimental in several respects: intimal lesions, platelet activation, peri-anastomotic hyperplasia and false aneurysms formation.

Whichever is the targeted application several fundamental requirements must be satisfied. Devices designed for the replacement of arteries, and then the materials used for the making of these devices, must be mechanically adapted to suffer for many years stresses resulting from the pulsatile blood pressure. They must feature as well, an adequate level of haemocompatibility, this criterion being easier to satisfy as vessels to be replaced have a larger diameter. Lastly, they must be biocompatible, which means that they are able to promote adhesion and healing of surrounding tissues without inducing any heavy inflammatory process or fibrosis or any other undesirable process. As a matter of fact, chemically inert materials, such as polyesters like PET on the one hand, or PTFE on the other, drew the interest of specialists, and were used as woven or knitted fabrics (for PET and PTFE initially), or as non-woven fabrics for PTFE (later on) to make tubular conduits; the porous wall of the latter was supposed to favour the above mentioned healing process. In fact, the wall porosity allows a transmural ingrowth of blood capillaries, the latter providing a potential source of cells for the endoluminal endothelialisation of the artificial substitute on the one hand, and oxygen and nutriment to the neointima on the other as does the *vaso vasorum* capillary network through the wall of native vessels. In addition, this parietal microvasculature helps to strengthen the host's defences against infectious processes, of which the risk is objectively increased by the implantation of a prosthesis, as bacteria easily adhere onto the surface of the latter. However, a compromise must be established between the above mentioned advantages brought by vessel substitutes with a porous wall and the blood loss suffered by the patient as soon as his blood is allowed to flow through such substitutes. In fact, the blood stops leaking rather rapidly as it clots when it comes into contact with the artificial surface of the vascular prosthesis. Nevertheless, and as a consequence of this blood loss, patients may need a blood transfusion, which may expose them to specific risks. That is the reason why vascular prostheses makers proposed in the early eighties, devices with an impervious wall. Such devices were prepared by soaking classical woven or knitted polyester prostheses into an albumin or collagen solution, and by a further cross-linking of the absorbed protein [14]. *In vivo*, the resulting proteinaceous reticulum is

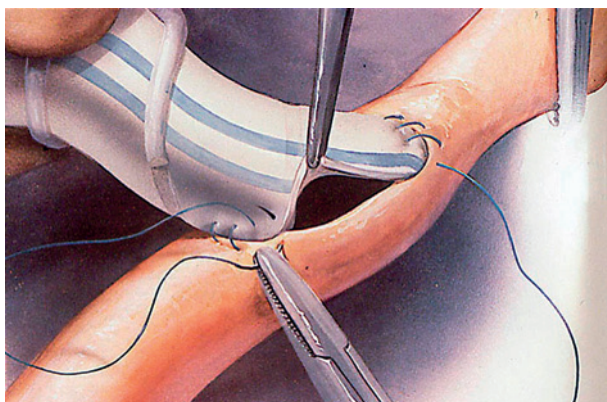


Fig. 2. A type of surgical vascular suture. (See Colour Plate Section at the end of this book.)

progressively resorbed, and a few days after implantation, the primary porosity of the prostheses is again available for an eventual ingrowth of blood capillaries.

Last but not least requirement, artificial arterial substitutes must be able to be connected to the host's vessels using sutures, the only reliable mean surgeons trust (Fig. 2). The connections performed must be stable and blood tight for as long as the prosthesis will remain patent. This last condition has supported the interest of surgeons for vascular prostheses made of woven or non-woven and knitted synthetic fabrics. The following sections give an outline of the different steps that line the evolution of materials for the cardiovascular system, and present some prospective solutions that have been proposed and supposed to improve the performances of these materials.

4. FROM POLYTETRAFLUOROETHYLENE TO MICROPOROUS TEFLON-BASED VASCULAR PROSTHESES

Among these materials, two polymers the PET and the PTFE, which was discovered in 1938 by Roy J. Plunkett (after Peska *et al.* [15]), hold a predominant place, and obviously our comments will mainly concern the second one. The perfluorination of ethylene leads to the starting vinyl monomer for the synthesis of the polyethylene perfluorinated homologue; according to the propylene content of the starting hydrocarbon, the resulting fluorinated polymer may include a more or less great proportion of perfluorinated statistic copolymers of ethylene and propylene; the so-called Teflon FEP corresponds to one of such blends. Because of the high energy of the C–F bond, PTFE is extremely stable; its high molecular weight ($>10^6$ g/mole) renders it insoluble in all usual organic solvents, and resistant to relatively high temperatures, as it can suffer permanently as high temperatures as 260°C. Because of the strong electronegativity of fluorine, PTFE is not

flammable, and demonstrates a high chemical inertia. Moreover, its surface free energy (18 ergs/cm^2) is the lowest in comparison to that of usual polymeric materials; in fact, PTFE is the hydrophobic reference material, its hydrophobicity being likely responsible for conformational changes (with already mentioned biological consequences) proteins suffer when they adsorb onto its surface. Its high melting temperature ($>320^\circ\text{C}$) and the high viscosity of the melted polymer prevent its transformation according to procedures used with classical thermoplastics. Accordingly, a specific transformation protocol, derived from the powder metallurgy technology, has been developed to produce flexible tubings fitting with surgeons' wishes.

According to this protocol, PTFE pellets are mixed with naphthalene, which plays a role of lubricant during the high temperature extrusion of this blend into tubes. The latter are modified by a process including several cycles of heating and mechanical stretching. This process, which is carried out at a temperature close to the PTFE melting point and favours the coalescence of PTFE crystallites, as well as induces the elimination of residual naphthalene, strongly alters the structure of the wall and create a macroporous, non-woven fabric with a high percentage of its volume composed of transmural void spaces. The structure that is formed is called expanded polytetrafluoroethylene (ePTFE), consists of layers of short, interlocking, circumferentially oriented, solid bands of the polymers (nodes), which are linked together by numerous, fine, filamentous bands (fibrils) that are longitudinally oriented, respect to the graft, and perpendicular to the nodes (Fig. 3A,B). Grafts have been investigated with internodal distances ranging from 5 to $90 \mu\text{m}$ in an effort to optimise haemocompatibility and endothelial cell attachment; however, the grafts in current clinical use, all have average internodal spacing of about $30 \mu\text{m}$. These grafts are easily handled by surgeons and can be sutured securely; however, they have two drawbacks: they are prone to kink under severe bending and to collapse under the compressive action of surrounding tissues. To prevent these bad phenomena, companies have proposed to stake the graft wall with a propylene rib, but the abrasive effect of the latter on the material wall during the prostheses use induced potentially more severe risks for the patients.

4.1. State of the art related to vessel repair or replacement: Evolution and role of PTFE

Like PET, which further became more and more popular under various trade names (Dacron in USA, Rhodergon in France, Dallon in Russia and European Eastern countries), PTFE was initially used as thread, which could be woven or knitted to obtain vascular prostheses. These resulting woven devices, in which two sets of threads, respectively called weft and warp, cross each other perpendicularly, are known to easily fray near anastomoses. For knitted devices, in

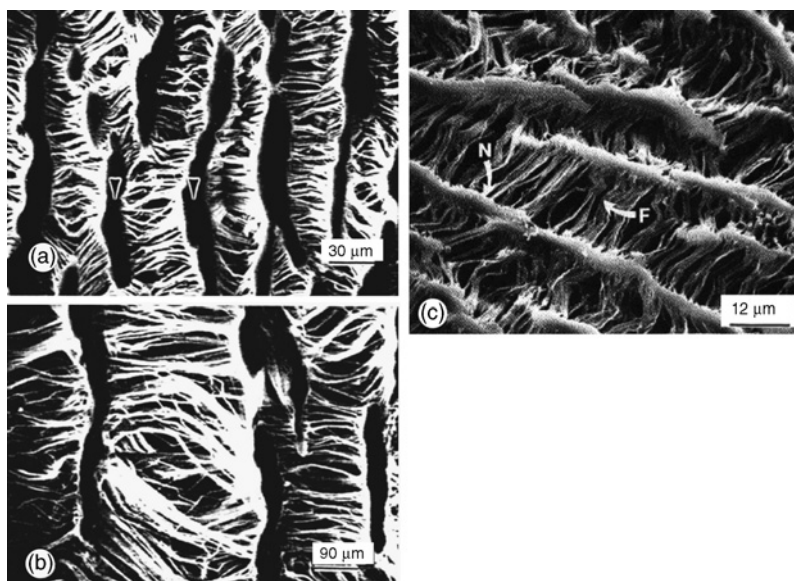


Fig. 3. Microstructure of expanded polytetrafluoroethylene as shown by scanning electron microscopy with different internodular species (a) 30 μm ; (b) 90 μm ; (c) 12 μm . (N: Nodules, F: Fibrilles)

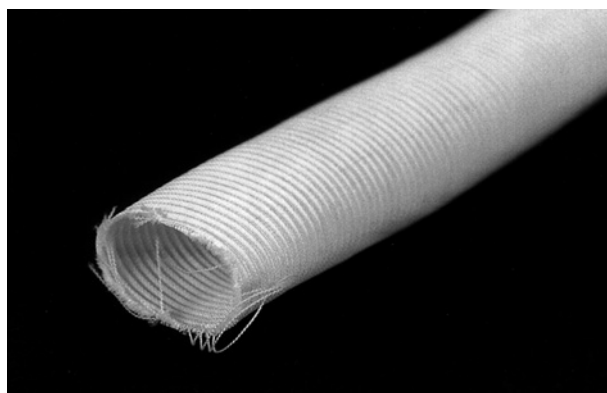


Fig. 4. Vascular prosthesis made of woven polytetrafluoroethylene. The photograph shows the great ability of the fabric to fray.

which these two sets of threads may not only interlace but also lock up with each other, fraying is less important, but still occurs due to the PTFE fibre characteristics.

The ends of the primary devices as proposed by Edwards [16] (after Harisson experiments [17]) frayed rather easily (Fig. 4), especially when they were bevel-edged. However, these devices showed rather good clinical performances in spite of an uncertain healing. Ruptures might occur near the anastomoses when

silk was used to realise the sutures, as silk is partly biodegradable, while Teflon fibres kept unaltered for several decades after implantation [18]. Nevertheless, woven PTFE arterial prostheses were no longer used, as surgeons preferred to use prostheses made from woven or knitted PET yarns. Later on, these polyester-based prostheses met the competition with prostheses made from microporous Teflon (Fig. 5) or ePTFE, better known under various trade names such as Gore-Tex, IMPRA, Vitaflon, etc.

Microporous Teflon was first used by Ben Eiseman in 1972 [19] for the making of membranes fitting oxygenators used for extracorporeal circulatory assistance. As several benefits seemed to be related to the use of this material (less damaged blood cells, no or little protein depletion, no or few clot deposition, neither embol release), he tried with his team to extend its applications. They carried out a series of experiments with piglets, such as the implantation of microporous Teflon conduits as substitutes for the portal vein, the inferior vena cava, the external iliac vein, and obtained a permeability rate equal to 80%, 2 months after implantation, taking into account the data from 27 experiments. In a pancreatectomised patient (pancreatectomy being a consequence of a cancer), 32 months after the implantation of such an artificial graft as a substitute for the portal vein, these graft was still permeable. Such success encouraged major companies, such as W.L. Gore and IMPRA, and vascular surgeons to develop the use of such grafts as arterial substitutes, and several teams carried out experimental studies which show them performant for various implantation sites.

The first series of femoro-popliteal shunts, including 15 patients suffering a severe lower limb arterite (level III, even IV) and for whom the saphenous vein could not be used, was reported by Campbell in 1976 [20]; the patency rate at 8 months was 87%. These ePTFE prostheses made surgeons very enthusiastic and at least one of them, Veith [21], argued in their favour through an impressive



Fig. 5. Vascular prosthesis made of microporous polytetrafluoroethylene, also known as expanded polytetrafluoroethylene.

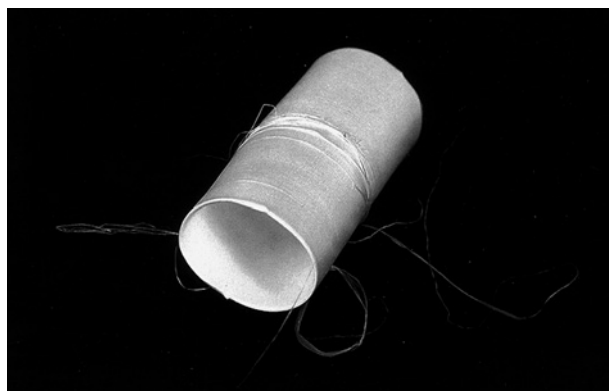


Fig. 6. Tubular conduit made of expanded polytetrafluoroethylene wrapped into a thin sheath, which is also made of polytetrafluoroethylene; the photograph shows the ability of the sheath to detach from the main wall surface.

clinical experience. Few cardiac surgeons attempted to use these prostheses for aortocoronary bypass, but they gave up very soon with this practice.

The analysis of microporous Teflon-based arterial prostheses, which were retrieved along autopsies or along revision surgeries, confirmed the excellent biostability of these devices insofar as they had been carefully implanted. Few ruptures or tears were observed but had been likely caused either by a bad handling or by fibrosis expansion, the latter being more frequent for non-sheathed devices (Formichi *et al.* [22,23]). Taking into account the lack of stability of the prosthesis wall, the two major makers made tremendous efforts to improve this situation. W.L. Gore chose to fit their prostheses with a very thin external sheath, made also of microporous PTFE but almost impervious (Fig. 6).

4.2. How to improve the functional patency of ePTFE-based prostheses?

These prostheses need to be improved in at least two respects: their haemocompatibility that must be increased if they are to be used for the replacement of small diameter artery ($\phi < 4.5$ mm) on the one hand, and their dynamic mechanical properties on the other. To resolve the first issue, two strategies that in fact do not apply specifically to ePTFE-based prostheses have been proposed. According to a first strategy, the triggering of the blood coagulation cascade, which generates thrombin as soon as blood comes into contact with the artificial material, cannot be avoided, and the latter must be endowed along appropriate chemical modifications, with the ability to catalyse the inhibition of thrombin by its naturally circulating inhibitor, that is, the so-called antithrombin. Among the proposed modifications, one can distinguish the covalent binding of either heparin [24],

a specific glycosaminoglycan of which the catalytic effect on the thrombin–antithrombin reaction is well known, or synthetic polymers that are functionalised along a further stage to endow them with heparin-like properties [25].

A second strategy aims at avoiding the triggering of the blood coagulation cascade by preventing in a non-specific way, the adsorption of the so-called contact phase proteins and their conformational changes upon adsorption on a surface as hydrophobic as PTFEs, these conformational changes being responsible for their activation. Pre-adsorption of human serum albumin has been shown empirically to be somewhat efficient in this respect. According to a more rational approach, irreversible adsorption of proteins in general, and more particularly of proteins belonging to the coagulation system, can be prevented by the presence at the surface of the PTFE of a hydrophilic layer of which the main constituent may be polyethyleneglycol molecules. The latter can be bound to the PTFE insofar as it has been previously adequately functionalised; a plasma treatment, as described in a further section, allows such a functionalisation [26].

However, the expected best way to prevent blood to clot upon its contact with prostheses wall is to coat the latter with endothelial cells, which are used to regulate the blood–vessel wall relationship. To carry out this coating, the material surface has to be endowed with pro-adhesive properties towards endothelial cells; such properties may be brought by peptidic ligands able to be specifically recognised by specialised membrane receptors (integrins) sitting at the surface of the cells. These ligands are characterised by the presence in their sequence of the RGD (arginin-glycin-aspartic acid) triade [27], the latter being also included in the sequence of extracellular matrix proteins (collagen, fibronectin, vitronectin, etc.). Thus, such tripeptides may be also brought onto a prosthetic surface by coating the latter with an aqueous solution of collagen or of any other extracellular matrix protein. To control their availability and their superficial distribution density, pro-adhesive synthetic peptides may be used, as reported in a subsequent section. Endothelial cells anticoagulant properties are partly due to their ability to express at their membrane, thrombomodulin (TM) a glycoprotein, which tightly binds thrombin. So TM works as a direct anticoagulant by inhibiting the thrombin cleavage of fibrinogen, the first step of the fibrin clot formation; more importantly, TM is the essential cofactor that promotes thrombin cleavage of protein C; the resultant activated protein C inactivates factors Va and VIIIa and thus shuts down coagulation and haemostasis. This explains the choice made by Vasilets *et al.* [28] who proposed to immobilise TM onto PTFE previously grafted with acrylic acid (AA) through a microwave CO₂ plasma initiated process.

Considering the second requirement, that is, good dynamic mechanical properties ePTFE-based arterial prostheses must satisfy to improve their functional patency, there are not so many ways to reach this goal. Unfortunately, and due to the intrinsic mechanical characteristics of PTFE, the mechanical behaviour of these prostheses cannot be easily modified. However, different ways have been explored; on the one hand, an optimisation of the design of the prostheses

has been attempted; on the other, the replacement of PTFE by other fluorinated polymers with a lower Young's modulus has been envisaged.

As far as the design of the prostheses is concerned, the replacement of strictly cylindrical conduits, by tapered ones that better conform to the anatomic reality, has been proposed and deeply documented by theoretical and experimental studies [29]. ePTFE-based tapered arterial prostheses have been commercialised, but did not appear to bring any clinical benefit. The design of prostheses with an oval section, instead of a circular one, offers a way to get a gain in compliancy as the section area of such prostheses increases via a simple change of its shape (oval \rightarrow circular) as blood pressure increases, without any change of its circumference. However, to our knowledge, no arterial prosthesis designed according to this concept has ever been commercialised.

The poor ability of ePTFE to reversibly stretch is not compatible with the making of arterial substitutes with a good compliancy; thus, specialists considered other polymeric materials combining the chemical inertia and the biostability of PTFE with a mechanical behaviour similar to that of elastomers, and their interest moved towards polyvinylidene difluoride (PVDF) and even more towards copolymers of vinylidenedifluoride and hexafluoropropylene (HFP), which may have pseudo-elastomeric properties. Until now, only PVDF has been processed into yarns [while yarns of P(VDF-HFP) copolymers are not commercially available] from which tubular conduits, prefiguring vascular prostheses, have been woven (see Section 4.3). Even if the mechanical behaviour of these woven PVDF-based conduits, when they are experimentally exposed to a pulsatile flow with characteristics analogous to that of blood flow, is better than that of ePTFE-based prostheses or PET-based ones, it is far from conforming specialists' expectations. Nevertheless, the faisability of the chemical modification of PVDF to improve its haemocompatibility, according to the previously described principles, has been investigated. A further step will concern the modification of P(VDF-HFP) copolymers (hopefully, the same procedure as the one used with PVDF will be applicable), as soon as corresponding yarns from which tubular conduits demonstrating the expected mechanical behaviour could be woven, will be available.

4.3. Chemical modifications of fluorinated polymers: A way to the improvement of their haemocompatibility

This section will successively deal with the treatment of PTFE, the treatment of PVDF and the treatment of P(VDF-HFP) copolymers.

4.3.1. PTFE case

Because of its high chemical inertia, the chemical modification of PTFE may appear as a challenge. However, although this polymer resists to acidic or alkaline attacks,

it is vulnerable to the action of ionising radiations and to gaseous plasmas. Unfortunately, when PTFE is exposed to γ -rays or to accelerated electrons beams, it degrades even if the adsorbed doses (a few kilograys) are relatively low; its molecular weight and its tensile strength decrease dramatically, as a lot of structural bonds are broken in the whole bulk of the material. Plasma treatment offers the opportunity to break bonds that belong only to the very first layers of macromolecules sitting at and under the surface of the material, without any noticeable bulky effect. Among others authors, Vasilets *et al.* [28] already quoted and Baquey *et al.* [26] demonstrated the interest of such an approach to introduce some functionality at the surface of ePTFE. After their paper, Baquey *et al.* exposed ePTFE samples to a Radio Frequency Glow Discharge fed with an argon/oxygen mixture (flow rate ratio 1:1) in a classical reactor. The latter was fitted with two internal aluminium electrodes, one being grounded and the other powered by a 13.56 MHz generator and acting as a sample holder. The pressure was set at 100 mTorr, and the treatments were driven at 100 W for 1 min. Then the samples were exposed to air atmosphere for 1 h before further grafting by AA via their immersion in an aqueous Acrylic Acid (AA) solution (25%, v/v) contained in glass flasks; following vigorous degassing, the flasks were sealed and kept for 5 h in a water bath at 65°C. The AA-grafted samples were taken out of the flasks, and appropriately washed to remove any adsorbed homopolymers.

Along a further step, the carboxylic groups available at the surface of the AA-grafted samples were exploited for the coupling of bNH₂PEG, which is intended to be used as an anchor arm between the surface and peptidic molecules of interest via amide bonds. In this respect, Baquey *et al.* [26] chose a tetrapeptide, containing the RGD sequence and being, for that reason, a potential ligand for integrins (adhesion molecules), which sits at the membrane of cells, and particularly, of endothelial cells. The different steps of the procedure were monitored by X-ray photoelectron spectroscopy (XPS) quantitative analysis. It appeared that after plasma treatment (according to the above described protocol here) the oxygen content of the material surface was significantly increased, this being possibly attributed to the formation of peroxides. The latter were supposed to give rise upon heating, to peroxy radicals able to induce the grafting of AA. In fact, the oxygen content of the material surface further increased after AA-grafting, and the presence of carboxylic groups was confirmed by a colorimetric assay based on the reactivity of these groups towards toluidine blue. So was confirmed the coupling of the AA-grafted surface with bNH₂PEG, as the presence of nitrogen could be detected as significant by XPS. The final coupling of the RGDC tetrapeptide (Arg-Gly-Asp-Cys) was confirmed, as well as the presence of sulfur due to its cysteine amino acid component, and could be detected by XPS also. As far as their biological properties are concerned, the treated ePTFE samples showed their ability to better induce the adhesion of endothelial cells than does the pristine material. The number of cells adhered to the material

after 2 h of culture in the absence of serum were four times larger for the treated ePTFE than for the pristine material; the mechanism of this adhesion was specific as the phenomena could be inhibited by the introduction of soluble RGDC peptides in the immersion medium of the samples containing the cells.

4.3.2. PVDF case

PVDF is mainly obtained by radical polymerisation of 1,1-difluoroethylene; 'head to tail' is the preferred mode of linking between the monomer units, but according to the polymerisation conditions, 'head to head' or 'tail to tail' links may appear. The inversion percentage, which depends upon the polymerisation temperature (3.5% at 20°C, around 6% at 140°C), can be quantified by ^{19}F or ^{13}C NMR spectroscopy [30] or FTIR spectroscopy [31], and affects the crystallinity of the polymer and its physical properties. The latter have been extensively summarised by Lovinger [30]. Upon recrystallisation from the melted state, PVDF features a spherulitic structure with a crystalline phase representing 50% of the whole material [32]. Four different crystalline phases (α , β , γ , δ) may be identified, but the α phase is the most common as it is the most stable from a thermodynamic point of view. Its helical structure is composed of two antiparallel chains. The other phases may be obtained, as shown by the conversion diagram (Fig. 7), by applying a mechanical or thermal stress or an electrical polarisation. The β phase owns ferroelectric, piezoelectric and pyroelectric properties.

The interest for this polymer came as already said, from its relatively high chemical inertia, although lower than that of PTFE, and its lower Young's modulus (1.45 GPa) in comparison to that of PET (10.56 GPa) and PTFE. In addition, the availability of multifilament yarns obtained by extrusion from bulky PVDF offers the possibility to weave or to knit, as it is the case for PET yarns, tubular conduits usable as vascular prostheses (Fig. 8). Moreover, threads made of PVDF have long been actually used in surgery for suturing purposes [33] and have demonstrated a clinical biocompatibility [34] equivalent to that of other non-biodegradable polymeric materials used for this application. In parallel, the possibility to endow this polymer with 'heparin-like' properties was demonstrated [35–37]. Briefly, the polymer available as 25- μm -thick films was grafted with polystyrene along a first step including its irradiation either with γ -rays delivered by a $^{137}\text{Cesium}$ source, or with swift heavy ions (SHI; mainly Argon) available from the GANIL (Grand Accélérateur National d'Ions Lourds) facility in Caen, France. Different grafting yields ($Y\%$) were obtained according to the type of radiation that was used, the adsorbed dose and the time of exposure to the vinylic monomer, that is, styrene; then the phenyl rings of the grafted polystyrene were chlorosulfonated and the chlorosulfonate groups reacted with the aspartic acid dimethylester; lastly, an alkaline treatment regenerated the carboxylic groups of the aspartic acid residues and generated sulfonate functions from the unreacted chlorosulfonate.

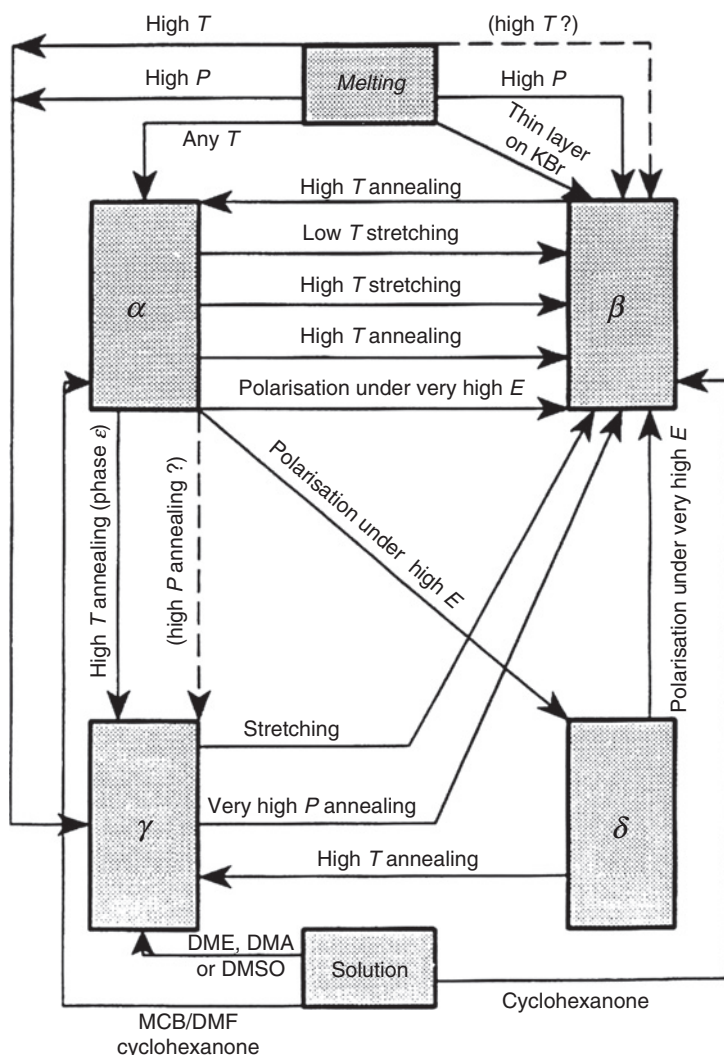


Fig. 7. Polyvinylidene difluoride conversion diagram.

Knowing the deleterious effects of ionising radiations on PTFE, much attention was paid on their effects on PVDF although the latter had been told to behave well under irradiation. As an example, PVDF multifilament yarns can be γ irradiated up to the absorption of 80 kGy without any effect on their Young's modulus [38]. However, the structure of the polymer was somewhat modified as its energy to break kept constant and even increased by about 50% while the adsorbed dose was less than 8 kGy but decreased for higher adsorbed doses, down to 1/3 of its maximum value (1/2 of its initial value) when the adsorbed dose reached 81 kGy. To avoid these bulky effects, the interest of

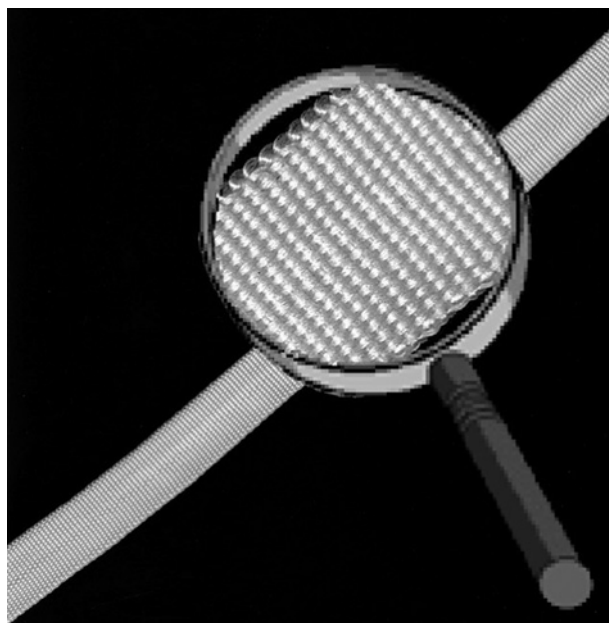


Fig. 8. Tubular conduit made of woven polyvinylidene difluoride.

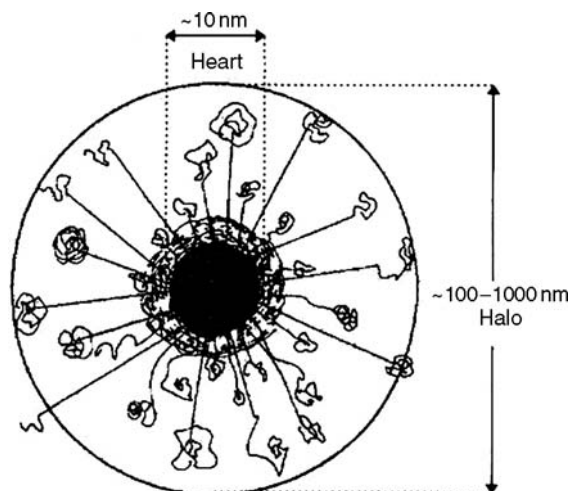


Fig. 9. Scheme of a swift heavy ion latent track.

the irradiation by SHI has been investigated. Instead of being homogeneously distributed in the whole bulk of the irradiated material when γ -rays are used, the energy (or the absorbed dose) brought by heavy ions is deposited very locally along so-called latent tracks (Fig. 9) related to their very short range inside the

material. According to the fluence (i.e. the average number of ions crossing a 1 cm^2 section) of the heavy ions beam that is operated, these latent tracks may be either completely separated or overlap with one another. Moreover, due to their high Linear Energy Transfer (LET), SHI are rapidly stopped; thus, their interactions with the irradiated polymer only concern the very superficial layers of the latter. As a matter of fact, the subsequent grafting of polystyrene can only occur onto the related surface microdomains, where the density of precursors of polymerisation initiators is relatively high. This appears clearly on microphotographs obtained by Scanning Electron Microscopy (SEM) of treated films which show the presence of circular islands (Fig. 10), the diameter of which depends upon the adsorbed dose. In addition, the elemental analysis of these films by Energy-Dispersive X-ray Analysis (EDXA) evidenced a decrease of the relative concentration of fluorine related to an increase of the grafting yield, and this decrease being maximum when the microprobe targets the centre of the above mentioned islands. Fourier Transform IR, transmission and internal reflection spectroscopies have been used to calculate the PS grafting yields at different depths; the observed gradient is higher in the case of γ -ray-induced grafting than in that of a SHI one. This might be explained by the fact that the PS growing chains diffusion is accelerated in the latent tracks formed after irradiation with SHI. The existence of a grafting can be linked to the monomer ability to diffuse towards the grafting centres. The subsequent steps of the treatment aimed at endowing the PVDF with heparin-like properties lead as well, to a non-homogenous distribution of the related functional groups; as a matter of fact the hydrophobicity of the material surface depends upon the coordinates of the point around which the wettability is measured. In fact, the surface has acquired a mosaic-like structure; in other words, it consists of two classes of microdomains more or less delimited, respectively characterised by the original hydrophobicity of PVDF for some of them, and by a relative hydrophilicity for the others. According to the concept developed by Okano *et al.* [39], such surfaces, insofar as they are properly designed in terms of size and specific characteristics of their constitutive microdomains, could express a low thrombogenicity as they could suppress platelet adhesion, and not induce any activation of the coagulation cascade. In spite of these very promising perspectives, there was a lot of work to carry out to apply this concept to the processing of PVDF multifilament yarns. So and considering practical reasons (i.e. the necessity to rapidly obtain tubular conduits which could be experimentally implanted *in vivo* as arterial substitutes), Marmey *et al.* [37] decided to initiate the chemical functionalisation of this material through its irradiation with γ -rays; even under such conditions, the resulting functions are homogeneously distributed at the surface of the material. To evaluate the effect of the treatment on the haemocompatibility of the PVDF yarns, the so-called thrombin time (TT) of human plasma was measured, whether a given amount of PVDF yarns, either treated or not was, immersed into a plasma aliquot or not. The immersion of pristine PVDF did not change the value

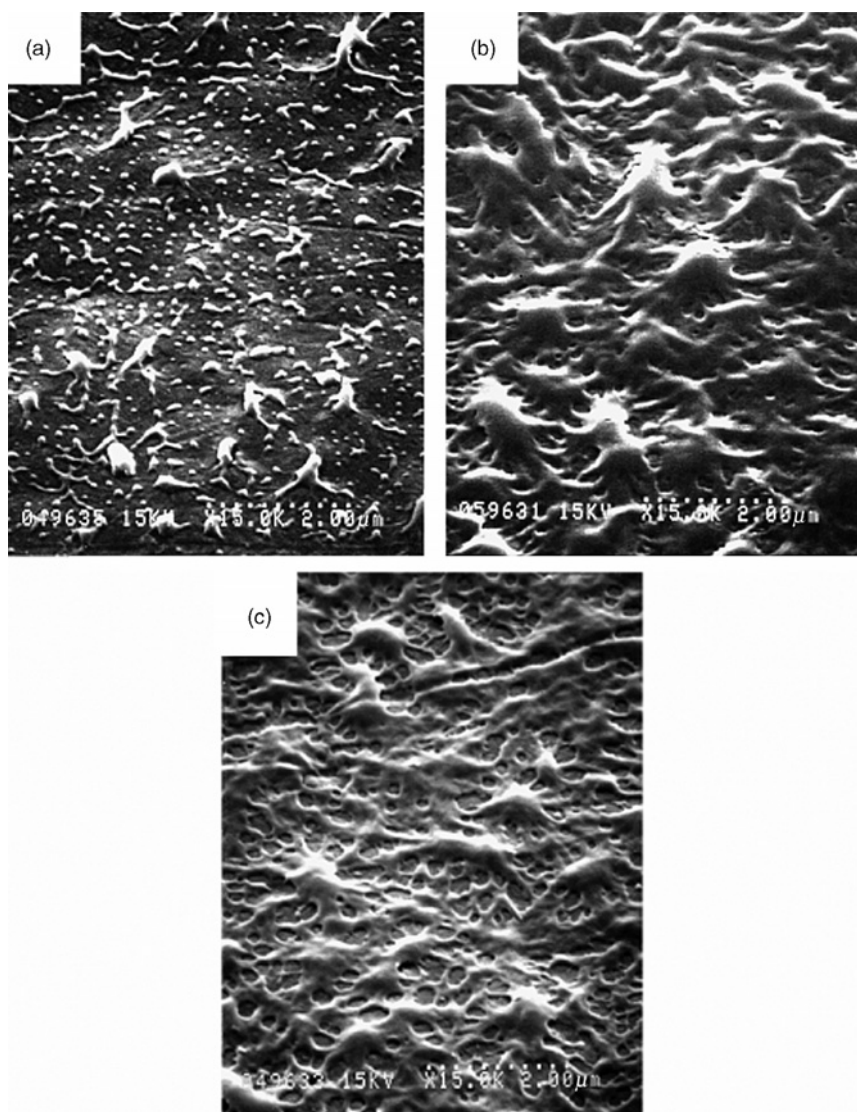


Fig. 10. Scanning electron microscopy microphotographies of the surface of different polystyrene-grafted polyvinylidene difluoride (PVDF) surfaces; the grafting was performed upon irradiation with Argon ions with various fluences or absorbed doses. (a) PVDF-gAr-PS ($Y = 2.5\%$), $D = 3.72$ kGy, $\Phi_t = 1.1 \times 10^9$ ions/cm²; (b) PVDF-gAr-PS ($Y = 19\%$), $D = 3.72$ kGy, $\Phi_t = 1.1 \times 10^9$ ions/cm² and (c) PVDF-gAr-PS ($Y = 12\%$), $D = 37.2$ kGy, $\Phi_t = 1.1 \times 10^{10}$ ions/cm².

of TT in comparison with the value (18 s) measured for plasma alone, while the immersion of treated PVDF dramatically increased the TT up to values greater than 120 s. Thus, a first requirement seemed to be fulfilled before knitting haemocompatible tubular conduits from chemically modified PVDF multifilament yarns; unfortunately the available yarns had a too big diameter, which rendered impossible the

making of enough supple tubular conduits able to be used as vascular substitutes. Except for this application, such yarns seem to not find any other commercial application, which explains the lack of interest from specialised companies to transform PVDF into multifilament yarns.

4.3.3. *P(VDF-HFP) case*

A particular copolymer for which the molar fractions of the two constitutive monomers were 93% and 7%, respectively was available as films prepared by MS Techniques (France) with a 1.78 g/cm^3 density.

The interest for this copolymer comes from its mechanical properties, which should render it better adapted for making compliant tubings, and from its relatively high radiation resistance. Unfortunately, the availability of multifilament yarns is a bigger concern than it is for PVDF. Nevertheless, the faisability of the modification of this copolymer to endow it with heparin-like properties has been investigated according to the same protocol. During the grafting stage, the styrene can diffuse more easily into this copolymer than it does through PVDF as the latter has a higher level of crystallinity [Fig. 11 clearly shows the presence of $1\text{-}\mu\text{m}$ -large spherulites at the surface of PVDF, whereas such features do not appear at the surface of the P(VDF-HFP)]. In fact, swelling measurements performed with styrene at 60°C on pristine and irradiated polymers, show that the diffusion coefficient is almost 15 times smaller for PVDF than for P(VDF-HFP), this result being attributed to the difference of crystallinity between the two materials [36]. At the same time, the plasticising effect of HFP increases the

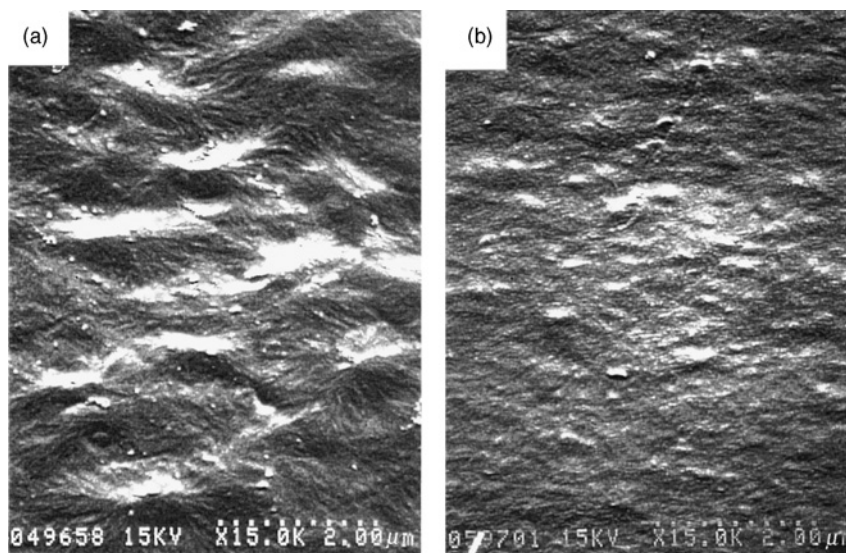


Fig. 11. Comparison of PVDF (a) and P(VDF-HFP) (b) surface respective morphologies as shown by scanning electron microscopy.

mobility of the radicals created upon irradiation and their ability to recombine, which explains a lower global grafting yield of styrene on P(VDF-HFP) in comparison to the grafting yield on PVDF following the same absorbed dose. The previously mentioned authors [36] have investigated in details the role of different parameters: radiation kind (γ or SHI) adsorbed dose or fluence for SHI, duration of exposure to the monomer, on the distribution of the grafted polystyrene. The latter may consist in separated islands, when SHI are used at low fluence and the exposure to the monomer is short (Fig. 10), or in a continuous and more or less thick film, which confers to the polymer surface a smooth appearance when γ -rays are used and the grafting yield is high (Fig. 12).

5. CONCLUSIONS

More than 30 years after it has been proposed for the manufacture of arterial substitutes, microporous PTFE stands more than ever among the biomaterials that are widely used by vascular surgeons. As it may be transformed into tubular conduits, they use the latter to replace arterial segments, or to build femoro-popliteal by-pass, or even to build arterio-venous shunts for patients needing recurrent haemodialysis. Its biostability has been established along many years of clinical use, and according to manufacturers, more than 2 millions of microporous Teflon-based vascular prostheses have been implanted all over the world since they have been launched in the market. In the meantime, the original products have suffered very few modifications. Its wall has been made thinner to make its implantation easier, and a gelatin coating may be applied to prevent any bleeding through suture stitches. However, the relative success of such devices is beyond any rational analysis; their compliancy is rather poor and their integration into the host tissues is uneven; moreover, their internal surface may be colonised *in vivo* but without any positive bioactivity as it may turn thrombogenic again upon biochemical or mechanical stimulation [40]. In fact, despite spectacular clinical results, microporous Teflon-based vascular prostheses do not objectively perform better than the autologous venous graft, which still stands as the gold standard. Clinical studies do not establish as well that these prostheses perform better than polyester-based ones when they are used to build a femoro-popliteal by-pass. If one considers more demanding applications such as the replacement of coronary arteries, the lack of performant prostheses is still pending, and the only chance to fill the gap is to consider other polymeric materials (including other fluorinated polymers) and new strategies aimed at designing vascular substitutes. Among these strategies, those which are based on tissue engineering concepts appears as very promising, and almost ready to be developed. The availability of more compliant fluorinated polymers or copolymers than ePTFE has been evoked in this chapter as well as the availability of methods allowing the functionalisation of their surface to endow the latter with

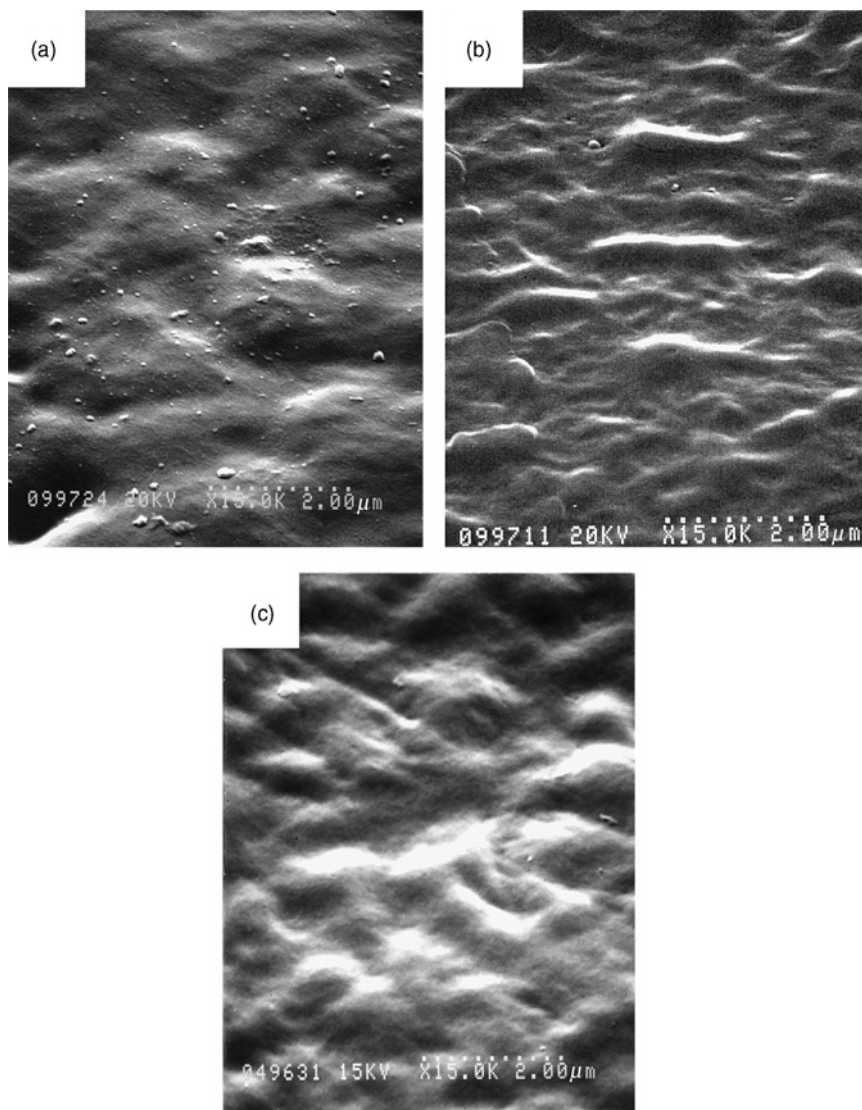


Fig. 12. Scanning electron microscopy microphotographies of different polystyrene grafted polyvinylidene difluoride (PVDF) surfaces; the grafting was performed upon gamma irradiation with various absorbed doses; the grafting yield (Y) was also modulated by the time of exposure of the irradiated surfaces to the styrene. (a) PVDF- $g\gamma$ -PS ($Y = 6\%$), $D = 10$ kGy; (b) PVDF- $g\gamma$ -PS ($Y = 20\%$), $D = 10$ kGy; (c) PVDF- $g\gamma$ -PS ($Y = 50\%$), $D = 30$ kGy.

pro-adhesive properties towards endothelial cells. It is just necessary to develop the appropriate processing techniques, enabling the manufacture of compliant small diameter tubular conduits from these materials, these conduits being able to be sutured by the surgeons to the natural vessels.

REFERENCES

- [1] T. Gluck, Die modern chirurgie des circulations apparates, Berl. Klin 120 (1898) 1–29.
- [2] A.B.Ja. Woorhees, A.III. Jaretzki, A.H. Blakemore, The use of tubes contracted from vinyon = N? cloth in bridging arterial defects, *Ann. Surg.* 135 (1952) 332–336.
- [3] P.N. Sawyer, S. Srinivasan, The role of electrochemical surface properties in thrombosis at vascular interfaces: cumulative experience of studies in animals and man, *Bull. N. Y. Acad. Med.* 48 (1972) 235–256.
- [4] M. Thubrikar, T. Reich, I. Cadoff, Study of surface charge of the intima and artificial materials in relation to thrombogenicity, *J. Biomech.* 13(8) (1980) 663–666.
- [5] P.N. Sawyer, B. Stanczewski, N. Ramasamy, G.W. Kammlott, J.G. Stempak, S. Srinivasan, Electrochemical and chemical methods for production of non-thrombogenic metal heart valves: Combined bio-physical, electron microscopic and scanning electron microscopic studies, *Trans. Am. Soc. Artif. Organs* 195, 1973.
- [6] A.S. Hoffmann, Principles governing biomolecule interactions at foreign interfaces, *J. Biomed. Mater. Res.* 8(3) (1974) 77–83.
- [7] R.G. Lee, S.W. Kim, Adsorption of protein onto hydrophobic polymer surfaces: adsorption isotherms and kinetics, *J. Biomed. Mater. Res.* 8 (1974) 251–259.
- [8] E.F. Leonard, in: W. Coleman, J. Hirsch, V.S. Marder, E.W. Salzman (Eds.), *Hemostasis and Thrombosis*, J.B. Lippincott, Philadelphia p. 755.
- [9] H.R. Baumgartner, The role of blood flow in platelet adhesion, fibrin deposition, and formation of mural thrombi, *Microvasc. Res.* 5(2) (1973) 167–179.
- [10] H.J. Weiss, V.T. Turitto, H.R. Baumgartner, Role of shear rate and platelets in promoting fibrin formation on rabbit subendothelium. Studies utilizing patients with quantitative and qualitative platelet defects, *J. Clin. Invest.* 78 (1986) 1072–1082.
- [11] S.L. Diamond, S.G. Eskin, L.V. McIntire, Fluid flow stimulates tissue plasminogen activator secretion by cultured human endothelial cells, *Science* 243(4897) (1989) 1483.
- [12] J.A. Frangos, L.V. McIntire, S.G. Eskin, C.L. Ives, Flow effects on prostacyclin production by cultured human endothelial cells, *Science* 227 (1985) 1477–1479.
- [13] L.J. Wurzinger, H. Schmid-Schönbein, The interaction of fluid-dynamic, physicochemical and cell biological reactions in thrombus formation, *Annals of the New York academy of sciences* 516 (1987) 316–332.
- [14] D. Domurado, R. Guidoin, M. Marois, L. Martin, C. Gosselin, J. Awad, Albuminated dacron prostheses as improved blood vessel substitutes, *J. Bioeng.* 2 (1978) 79.
- [15] D.N. Peska, L.A. Rea, L.L. Bondini, Common prostheses in the practice of vascular surgery, *J. Am. Osteopath. Assoc.* 80(8) (1981) 529–533.
- [16] W.S. Edwards, Progress in synthetic graft development; an improved crimped graft of Teflon, *Surgery* 45 (1959) 298–309.
- [17] J.H. Harrison, The use of Teflon as a blood vessel replacement in experimental animals, *Surg. Gynecol. Obstet.* 104 (1957) 81.
- [18] J. Couture, R. Guidoin, M. King, M. Marois, Textile Teflon arterial prostheses: How successful are they, *Can. J. Surg.* 27 (1984) 575.
- [19] B. Eiseman, D. Birnbaum, R. Leonard, F.J. Martinez, A new gas permeable membrane for blood oxygenators, *Surg. Gynecol. Obstet.* 135 (1972) 732.
- [20] C.D. Campbell, D.H. Brooks, M.W. Webster, H.T. Bahnson, The use of expanded microporous polytetrafluoroethylene for limb salvage. A preliminary report, *Surgery* 79 (1976) 485–491.
- [21] F.J. Veith, S.K. Gupta, E. Ascer, S. White-Flores, R.H. Samson, L.A. Scher, J.B. Town, V.M. Bernard, P. Bonier, W.R. Flinn, P. Astelford, J.S.T. Yao, J.J. Bergan, Six-year prospective multicenter randomized comparison of autologous saphenous vein and expanded polytetrafluoroethylene grafts in infrainguinal arterial reconstructions, *J. Vasc. Surg.* 3(1) (1986) 104–114.

- [22] M. Formichi, J.M. Jausseran, R. Guidoin, M. Marois, P. Bergeron, C. Gosselin, R. Courbier, Analyse de prothèses artérielles en téflon microporeux après exérèse chirurgicale = Analysis of expanded PTFE arterial prostheses after surgical explantation, *J. Mal. Vasc.* 11(3) (1986) 248–255.
- [23] M.J. Formichi, R.G. Guidoin, J.-M. Jausseran, J.A. Awad, K.W. Johnston, M.W. King, R. Courbier, M. Marois, C. Rouleau, M. Batt, J.-F. Girard, C. Gosselin, Expanded PTFE prostheses as arterial substitute in humans: late pathological findings in 73 excised grafts, *Ann. Vasc. Surg.* 2(1) (1988) 14–27.
- [24] C. Baquey, A. Beziade, D. Ducassou, P. Blanquet, Intérêt du greffage radiochimique de monomères vinyliques pour améliorer l'hémocompatibilité des matériaux artificiels. I. Tentative d'association covalente d'héparine au Dacron, *Itbml* 2(4) (1981) 378.
- [25] V. Migonney, C. Baquey, B. Basse-Cathalinat, B. Masson, S. Winnock, D. Ducassou, E. Serne, D. Labarre, C. Fougnot, M. Jozefowicz, Haemocompatibility of polyethylene-polystyrene modified tubings, *Life Support Syst.* 1(Suppl 1) (1983) 227–230.
- [26] C. Baquey, F. Palumbo, M.C. Porte-Durrieu, G. Legeay, A. Tressaud, R. d'Agostino, Plasma-treatment of expanded PTFE offers a way to a biofunctionalization of its surface, *NIM Nucl. Instrum. Methods Phys. Res. B* 151 (1999) 255–262.
- [27] E. Ruoslahti, M.D. Pierschbacher, New perspectives in cell adhesion: RGD and integrins, *Science* 238 (1987) 491–497.
- [28] V.N. Vasilets, G. Hermel, U. König, C. Werner, M. Muller, F. Simon, K. Grundke, Y. Ikada, H.J. Jacobasch, Microwave CO₂ plasma-initiated vapour phase graft polymerization of acrylic acid onto polytetrafluoroethylene for immobilization of human thrombomodulin, *Biomaterials* 18 (1997) 1139–1145.
- [29] R.A. Black, T.V. How, Attenuation of flow disturbances in tapered arterial grafts, *ASME J. Biomech. Eng.* 111 (1989) 303–310.
- [30] A.J. Lovinger, Poly(vinylidene fluoride), in: D.C. Bassett(Ed.), *Developments in Crystalline Polymers*, Applied Science, London, England, 1982, pp. 195–273.
- [31] M. Kobayashi, K. Tashiro, H. Tadokoro, Molecular vibrations of three crystal forms of poly(vinylidene fluoride), *Macromolecules* 8(2) (1975) 158–171.
- [32] M.G. Broadhurst, G.T. Davis, J.E. Mc Kinney, R.E. Collins, Piezoelectricity and pyroelectricity in PVDF—a model, *J. Appl. Phys.* 49(10) (1978) 4992–4997.
- [33] G. Laroche, Y. Marois, R. Guidoin, M.W. King, L. Martin, T. How, Y. Douville, Polyvinylidene fluoride (PVDF) as a biomaterial: From polymeric raw material to monofilament vascular suture, *J. Biomed. Mater. Res.* 29(12) (1995) 1525–1536.
- [34] S.R. Saba, K.M. Brinkhous, Thrombogenicity of some biomedical materials: platelet-interface reactions. Mason RG, Scarborough DE, *J. Biomed. Mater. Res.* 3(4) (1969) 615–644.
- [35] M.C. Porte-Durrieu, C. Aymes-Chodur, N. Betz, Ch. Baquey, Development of “heparin-like” polymers using swift heavy ion and gamma radiation. I. Preparation and characterization of the materials, *J. Biomed. Mater. Res.* 52(1) (2000) 119–127.
- [36] C. Aymes-Chodur, N. Betz, M.C. Porte-Durrieu, Ch. Baquey, A. Le Moël, A FTIR and SEM study of PS radiation grafted fluoropolymers: Influence of the nature of the ionizing radiation on the film structure, *Nucl. Instrum. Methods Phys. Res. B* 151 (1999) 377–385.
- [37] P. Marmey, M.C. Porte-Durrieu, C. Baquey, PVDF multifilament yarns grafted with polystyrene induced by gamma-irradiation: Influence of the grafting parameters on the mechanical properties, *Nucl. Instrum. Methods Phys. Res. B* 208 (2003) 429–435.
- [38] J. Scheirs, in: *Modern Fluoropolymers: High Performance Polymers for Diverse Applications*, Vol. I, Wiley, New York, 1997.
- [39] T. Okano, T. Aoyagi, K. Kataoka, K. Abe, Y. Sakurai, M. Shimada, I. Shinohara, Hydrophilic-hydrophobic microdomains surfaces having an ability to suppress platelet adhesion and their *in vitro* antithrombogenicity, *J. Biomed. Mater. Res.* 20 (1986) 919–927.

- [40] E. Chignier, J. Guidollet, Y. Heynen, M. Serres, G. Clendinnen, P. Louisot, R. Eloy, Macromolecular, histological, ultrastructural and immunocytochemical characteristics of the neointima developed within PTFE vascular grafts. Experimental study in dogs, J. Biomed. Mater. Res. 17(4) (1983) 623–636.

Note from the Editors

Partially adapted from “*Biomatériaux fluorés pour la chirurgie cardio-vasculaire*”, C. Baquey and R. Guidoin, Actualité Chimique, No. 301–302, November 2006. Actualité Chimique and Société Française de Chimie are acknowledged for authorization.

CHAPTER 9

Fluorinated Molecules in Eye Surgery: Experimental and Clinical Benefit of a Heavy Silicone Oil Oxane Hd[®] (Mixture of Silicone Oil and RMN3 Fluorine Olefin) in the Treatment of Retinal Detachment

I. Rico-Lattes,^{1,*} J. C. Quintyn,^{1,2} V. Pagot-Mathis,²
X. Benouaich,² and A. Mathis²

¹*Laboratoire des IMRCP, UMR CNRS 5623, Université Paul Sabatier,
31062 Toulouse Cedex 9, France*

²*Service d'Ophthalmologie, CHU Rangueil-TSA 50032, 31059 Toulouse Cedex 9, France*

Contents

1. Introduction	407
2. State of the art	408
3. Synthesis of RMN3	412
4. Biocompatibility of RMN3 and Oxane Hd [®]	413
5. Clinical study with Oxane Hd [®]	415
6. Conclusion	417
References	418
Note from the Editors	420

Abstract

Rhegmatogenous retinal detachment (RD) is a pathology that can result in blindness. Treatment consists in performing a retinal scar (retinopexy) around the tear and maintaining the retina in contact by gas or silicone oil tamponade being less dense than water. The development of 'heavier than water' fluids is the most recent system serving to prolong internal tamponades with benefit in complex RD. Therefore, Oxane Hd[®] (Bausch & Lomb Inc., Rochester, NY, USA) (a mixture of silicone oil and RMN3, a synthetic fluorine compound) showed good performances with high tolerance for several months.

1. INTRODUCTION

Rhegmatogenous retinal detachment (RD) is defined by fluid accumulation in the subretinal space through retinal tear, inducing separation of the neurosensory retina from the retinal pigmentary epithelium (Fig. 1).

*Corresponding author.;
Email: rico@chimie.ups-tlse.fr

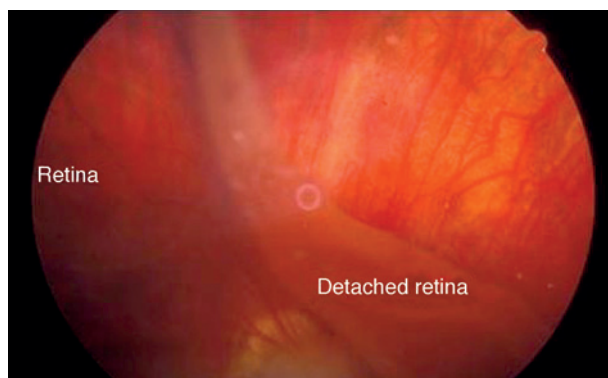


Fig. 1. Photograph of fundus with a retinal detachment. (See Colour Plate Section at the end of this book.)

The incidence of that pathology is as low as 1/10,000 per year but it may result in blindness. Treatment consists in performing a retinal scar (retinopexy) around the tear and maintaining the retina in contact by gas or silicone oil tamponade. Complex, inferior dehiscence RD often recur by lesion reopening and/or by vitrorretinal inflammation [vitro-retinal proliferation (VRP)] secondary to ineffective inferior internal tamponade. Indeed, silicone oil and protracted action gases, which are internal tamponades whose tolerance has been proven in vitreoretinal surgery, are less effective in the internal tamponade of inferior lesions their density being lower than that of water. Supplemental actions are required to improve inferior internal tamponade, such as the fitting of inferior episcleral indentation or inferior retinectomy, often combined with intensive positioning of patients in strict ventral decubitus, facing ground or even sometimes in declive posture so as to achieve better tamponade of the inferior part. In the 80s, the introduction of liquid perfluorocarbons (LPFC) as perioperative tools [1–4] led to contemplating the development of other ‘heavier than water’ fluids to serve as prolonged internal tamponades. Semifluorinated alkanes and hydrofluorocarbon oligomers appeared to induce inflammatory reactions [5–7]. Heavy silicone oils, solutions comprising a fluorinated compound and standard silicone oil, are expected to prove beneficial in that application. This is a report on animal study and a prospective one in man [8] conducted with the ‘heavy’ silicone oil marketed under the Oxane Hd® brand name since 2003. Oxane Hd® is a mixture of standard silicone oil and hydrogenated, fluorinated, mixed olefin RMN3 [9]. It is noteworthy that very recently another ‘heavy’ silicone oil has been marketed. It is a mixture of a fluorinated alkane and a silicone oil named Densiron 68® (Fluoron GmbH, Neu-Ulm, Germany) [10].

The purpose of this chapter is to summarise some experimental results concerning Oxane Hd®, especially clinical results obtained before the commercialisation of Oxane Hd®. Since 2003, the compound was used extensively in the world and many clinical studies were realised but are not discussed in this chapter.

2. STATE OF THE ART

The principle of ocular tamponade is represented in Fig. 2.

Internal tamponade potency is the capacity to obdurate a dehiscence. It is correlated to the surface pressure of the product used. Schematically, the higher the tension, the stronger the tendency of the fluid to form a single bubble and to remain in the vitreous cavity without running through retinal dehiscences into the subretinal space. As a result, no fluid is passing through retinal dehiscences, which makes retinal reapplication possible. The internal tamponade potency is unrelated to the viscosity of the product.

Retinal reapplication force is the capacity to move the subretinal fluid. It is proportional to the density difference between serum and the product used for internal tamponade. Combined with subretinal fluid (SRF) drainage, it makes retinal reapplication possible.

The use of expanding perfluorocarbon gases was initiated by Norton with sulphur hexafluoride (SF_6) [11]. Then in the 80s were introduced perfluoropropane (C_3F_8) by Lincoff and perfluoroethane (C_2F_6) [12]. Their density being much lower than that of serum, they have a very strong reapplication force. Their surface tension is very high, hence their high internal tamponade potency. Fluorine-containing gases possess expanding properties by incorporating blood nitrogen. They can be used alone or as non-expanding gaseous mixtures: SF_6 -air (20%), C_2F_6 -air (17%) and C_3F_8 -air (14%). Their spontaneous resorption and their lifespan vary according to gases.

In the 60s, Cibis [13,14] introduced silicone oil injection in non-vitrectomized eyes. Then, Haut combined silicone oil with pars plana vitrectomy [15]. The technique was later refined by Zivojnovic [16]. Silicone oil was then used as a means of permanent internal tamponade. It was only in 1983 that Gonvers used silicone oil as a means for temporary internal tamponade [17].

Unlike gases, silicone oil permits prolonged internal tamponade with a constant volume. The absence of spontaneous resorption requires a second surgical operation to remove it. Its effectiveness in the surgical treatment of RD and

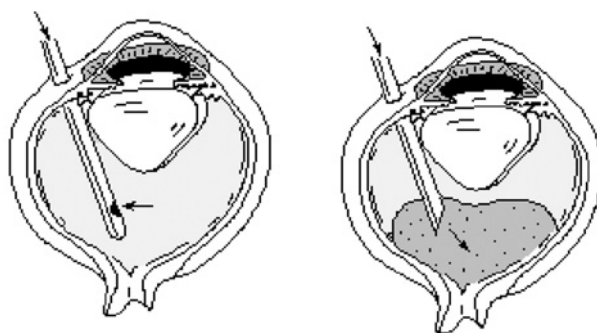


Fig. 2. Principle of ocular tamponade.

of tractional retinal detachment in diabetic patients has been demonstrated by several studies [18–21].

Silicone oil is a dimethylsiloxane polymer presenting as a transparent, hydrophobic viscous fluid. Standard silicone oil is marketed in various viscosities ranging from 1000 cSt to 5000 cSt. It possesses a strong internal tamponade potency because of its high surface tension. In contrast, its density being close to that of serum, its reapplication force is weak. It will preferentially ensure tamponade of superior dehiscences because its density is slightly lower than that of serum. Classic complications of silicone oil are keratopathy (11–49%), glaucoma (11–33%) and cataract (49–100%). Their occurrence being correlated to the duration of internal tamponade, their prevention requires early removal of the silicone oil after a few weeks [22–28]. Emulsification is defined as the fractioning of the silicone oil bubble into variable-size droplets. It is reversely proportional to fluid viscosity and surface tension. It is promoted by surface impurities (low molecular weight catalytic residues), by mechanical constraints (motion), contact with other fluids of different densities and by surface irregularities (vitreous bridles, edge of an ocular implant, premacular membrane,...). Emulsification consequences are the loss of internal tamponade potency, poor fundus visualisation, switching to anterior chamber, keratopathy and ocular hypertonia [29,30]. Retinopathy occurrence is highly controversial: indeed, the retinal toxicity of silicone oil has never really been proven; minor histological lesions limited to the external plexiform layer have been described after 6 weeks of internal tamponade; also, prolonged tamponade with silicone oil does not significantly modify electroretinogram results and it has been shown that 50% of eyes with a flat retina maintained their visual function after 10-year protracted internal tamponade [31–33].

The first 'heavier than water' internal tamponade was introduced in 1987 by Chang with LPFC [1]. The two perfluorocarbons most used are perfluorooctane and perfluorodecaline. Perfluorotributylamine, perfluoropolyether, perfluorooctylbromide and perfluorophenanthrene are less used. LPFC are transparent fluids and are not miscible in water and their main characteristic is their high density (1.76–2.03) [2]. Their properties are summarised in Table 1.

As a result, their reapplication force is high and applied from back to front (contrary to air or standard silicone oil). Their surface tension is high, close to that of silicone oil, hence their high internal tamponade potency. Their viscosity is low, facilitating manipulation during their injection or exchange with air, gases or silicone oil. Lastly, their refraction index being close to 1.30, interface with water, serum or silicone oil is clearly visible during exchanges. They have been considered as pre-operative instruments to manipulate and reapply the retina [1–4, 34,35], especially in such indications as giant tears, retinal detachments with vitreoretinal proliferation, retinal detachments by perforating trauma diabetic retinopathy complicated by tractional retinal detachment, crystalline lens or ocular implant posterior spraining and posterior dehiscence retinopathy. Their use as

Table 1. Physical characteristics of LPFC perfluorocyclohexan (PFE), perfluorotributylamine (PFBA), perfluoro-*n*-octan (PFO), perfluorodecaline (PFD) bromo perfluoro-*n*-octan (PFOB), perfluorophenanthren (PFPN)

	PFE	PFBA	PFO	PFD	PFOB	PFPN
Formula	C ₆ F ₁₂	C ₁₂ F ₂₇ N	C ₈ F ₁₈	C ₁₀ F ₁₈	C ₈ F ₁₇ Br	C ₁₄ F ₂₄
Molecular weight	400	671	449	462	499	624
Density (g/cm ³ , 25°C)	1.83	1.89	1.76	1.94	1.918	2.03
Refraction index (25°C)	1.29	1.29	1.27	1.31	1.30	1.33
Viscosity (cSt, 25°C)	0.94	2.06	0.80	2.70	2.90	8.03
Boiling point (°C)	51	177	99	141	143	215
Surface tension (mN/m, 25°C)		55.10	54.20	55.30	51.30	51.30

a temporary internal tamponade, however, is not recommended because of their early emulsification and their short-term corneal and retinal toxicity, as demonstrated by several experimental studies [35–44].

More recently, other 'heavier than water' products have been developed for temporary internal tamponade. These are fluorosilicones [46,47], semifluorinated alkanes [1,7], heavy fluorocarbon liquid (HFCL) oligomers [5,7] and solutions of fluorine-containing compound and silicone oil [8–10,47].

Semifluorinated alkanes or liquid hydrofluorocarbons are partially hydrogenated HFCL. Those most studied are perfluorohexyloctane (F₆H₈), perfluorohexylhexane (F₆H₆), perfluorobutylbutane (O44) and perfluorohexylethane (O62). Their density, below that of LPFC, is 1.35 g/cm³ for F₆H₈ and 1.42 g/cm³ for F₆H₆. Their properties make them excellent candidates as heavy internal tamponade products. They can be used pre-operatively for the same indications as LPFC, although their miscibility in silicone oil contraindicates direct exchanges between these two products [5,6]. F₆H₈, developed by Kirchlof's team, is used essentially during operations to remove silicone oil. Injected in the vitreous cavity, it acts as a solvent on the residual silicone oil droplets, on the posterior face of intraocular implants [7]. Used as an internal tamponade product in complex retinal detachment surgery, it would pose the problem of early dispersion and emulsification [6], sometimes associated with an inflammatory reaction [8]. To reduce these complication risks, Gabel's team developed HFCL oligomers with a density of 1.62 g/cm³ [7]. Their higher viscosity reduces the risk of dispersion. Despite good tolerance in animals

[7], they nonetheless appeared to induce major inflammatory reactions post-operatively [5] and presented emulsification problems.

In this content, we developed and studied a solution of a fluorine-containing compound, RMN3, and silicone oil. This so-called 'heavy silicone oil' has been on the market since May 2003 under the name of Oxane Hd®.

It is noteworthy that this formulation is different from fluorosilicones. Fluorosilicones are fluorine-containing silicone oils with a 1.35 g/cm³ density. Their poor tolerance in animals and men was demonstrated by experimental studies [45,46]: ocular hypertonia, keratopathy, early emulsification and severe inflammatory reactions. They cannot therefore be used as a heavy internal tamponade product.

The formulation of silicone oil and RMN3 is therefore a solution of a fluorine-containing compound, RMN3, and of a 5700-cSt silicone oil. It is the result of cooperation between the IMRCP laboratory of the Paul Sabatier University in Toulouse (Dr. Rico-Lattes), the Ophthalmology Department team of the Rangueil Teaching Hospital of Toulouse (Professor Mathis) and Chauvin Baush & Lomb® Laboratories and Opsia® companies (Toulouse). This 'heavy' silicone oil has been marketed since May 2003 by Chauvin Baush & Lomb® Laboratories. The characteristics of Oxane Hd® are summarised in Table 2.

The product is packaged as 10-ml, single-use glass syringes. The mixture is composed of silicone oil (Oxane 5700) and RMN3. The silicone oil is standard dimethylsiloxane polymer (Table 2). RMN3 is soluble in silicone oil up to 12% (in volume). After purification, the two compounds were mixed and sterilised. Final filtration to 0.2 µm under a laminar flow hood preceded packaging and autoclave sterilisation.

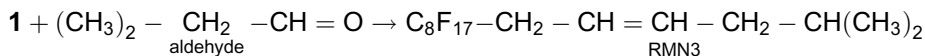
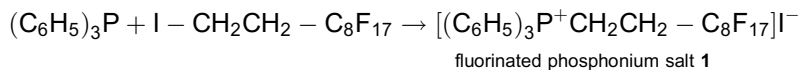
3. SYNTHESIS OF RMN3

RMN3 was designed in the team of I. Rico-Lattes and synthesised following a procedure previously described [10] and developed now in Bausch & Lomb Laboratory.

Table 2. Characteristics of Oxane Hd® compared to oligomers HFCL and standard silicone oil

Physical characteristics	Standard silicone oil	HFCL	HFCL oligomers	Heavy oil (Oxane 5700– RMN3 formulation)
Viscosity (cSt, 20°C)	1000–5000	2500	90–2000	3700
Surface tension (mN/m, 25°C)	> 40	22–50	35	> 40
Density (g/cm ³ , 25°C)	0.98	1.35–1.42	1.6	1.03
Refraction index (25°C)	1.40	1.3	1.3	1.391

RMN3 was prepared with a yield of 70% by a Wittig reaction:



The structure of RMN3 is represented in Fig. 3.

4. BIOCOMPATIBILITY OF RMN3 AND OXANE Hd[®]

Tolerance to RMN3 was demonstrated *in vitro* and *in vivo* by experimental studies conducted in cooperation with Opsia-Chauvin-Baush & Lomb laboratories, in Toulouse.

The first study involved the eyes of 11 rabbits and 5 minipigs. We compared ocular tolerance to RMN3 with that of vitrectomized eyes. Pars plana vitrectomy was performed and followed by fluorocarbon fluid injection so as to fill more than half the vitreous cavity. Nine rabbits' eyes and three minipigs' eyes were vitrectomized without RMN3 injection and served as controls. Clinical examination and fundus indirect ophthalmoscopy were performed weekly until the animals were sacrificed. Enucleation was performed after 7 days in 8 rabbits' eyes and after

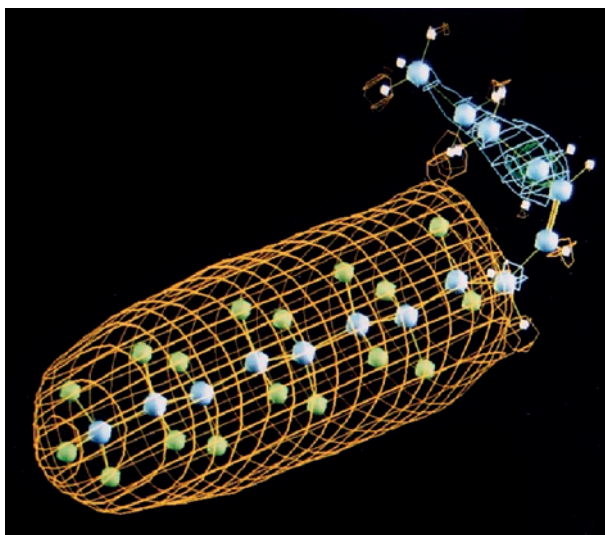


Fig. 3. Structure of RMN3. (See Colour Plate Section at the end of this book.)

1 month in 12 rabbits' and 8 minipigs' eyes. Tissue specimens were taken from the lower part of the globes.

The second study explored the intraocular tolerance to the mixture of RMN3–silicone oil Oxane Hd® (Fig. 4) in 27 albino rabbits [8]. Pars plana vitrectomy was performed in 22 eyes with mixture injection; 5 eyes received only silicone oil 1300 cSt, and the 27 adelpic eyes were used as controls. Clinical examinations were performed on D7, D30, D60 and D190, when the animals were sacrificed and tissue specimens were taken from the lower part of the ocular globes.

In the first animal study, the clinical tolerance to RMN3 appeared to be good in all eyes regardless of the duration of internal tamponade, with a clear vitreous cavity and a normally looking retina. Moderate whitish deposits occurred on the

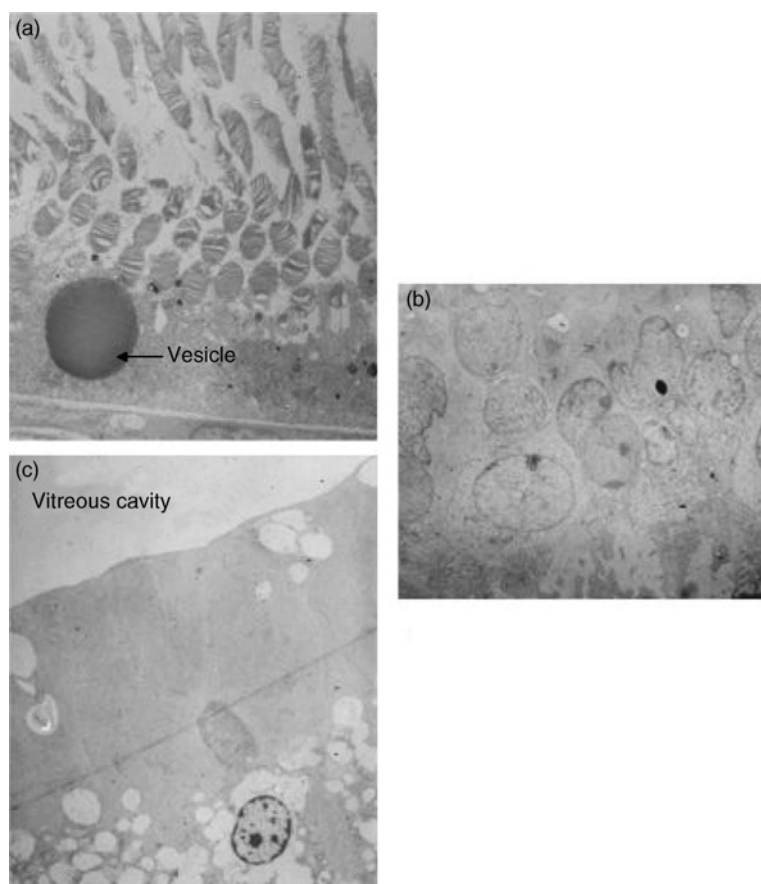


Fig. 4. Experimental study of RMN3–silicone oil mixture in rabbits (electron microscopy after 1-month internal tamponade with heavy silicone oil): (a) moderate intercellular oedema between photoreceptor external articles; note the presence of a mundane vesicle; (b) normal aspect of retina internal layers; and (c) normal aspect of internal limiting layer and vitreous cavity.

RMN3 bubble surface in one rabbit's eye after 7 days and in three rabbits' and one minipig's eyes after 1 month. Study of semi-thin sections under an optical microscope revealed moderate retinal lesions. In rabbits' eyes, a moderate cellular reaction was noted in the form of monocytes and macrophages containing optically empty vacuoles. The presence of vesicles in internal layers, as well as an intercellular oedema affecting all external layers, was frequently observed with RMN3 and also in control eyes. In the treated eyes, there was some degree of photoreceptor intracellular space disorganisation, nuclear densifications in the external nuclear layer and irregularities in the external limiter. The presence of vesicles was observed in the pigmentary epithelium and also in control eyes; in minipigs after 1 month of internal tamponade, intracellular oedema was the main observation noted; there was no 'drop-down' phenomenon in photoreceptors.

Moderate, pre-retinal cellular reaction in the form of a few macrophages was noted on one eye only. Electron microscopy revealed only moderate lesions after 7 days of internal tamponade in rabbits, and equally after 30 days in rabbits and minipigs. Intracellular oedema was the main lesion noted after 7 days, predominantly in external layers. Interphotoreceptor space disorganisation was variously observed in all eyes, although external segment structure appeared normal.

In the second animal experiment, involving albino rabbits, the clinical tolerance of Oxane Hd[®] appeared to be good with no inflammatory reaction and no retinal vascular lesion. No emulsification was noted. Optical microscopy of semi-thin layers elicited only a few retinal lesions: atrophy of the retinal external layers was observed in one eye treated with the mixture and one treated with standard silicone oil. We found a few rare cells in the vitreous cavity, which contained intra-cytoplasmic vacuoles. Electron microscopy confirmed the absence of damage to the pigmentary epithelium and to the retinal internal layers and atrophy of the retinal external layers in two cases treated with the mixture and in one case treated with standard silicone oil (Fig. 2).

5. CLINICAL STUDY WITH OXANE Hd[®]

The clinical study involved all the patients operated on for retinal detachment with insertion of heavy silicone oil in the Ophthalmology Department of the Rangueil Hospital in Toulouse, from December 1998 to December 2002. It involved 17 eyes from 17 patients, including 10 right and 7 left eyes. There were 5 women and 12 men, mean age 53.2 years. It was RD recurrence in 9 patients. Pre-operative vision was below 1/20 in 16 patients. All patients underwent posterior vitrectomy through the pars plana and as complete as possible peripheral vitrectomy with scleral depression using the slit lamp of the operative microscope without any wide field system. Silicone oil injection was administered actively in all cases, using an automatic injector. The technique for injecting heavy silicone

oil is the same as for injecting 5000 cSt standard silicone oil. Lesion retinopexia was ensured in all cases by laser endophotocoagulation, performed under HFCL in 2 cases and under silicone oil in 15. Inferior episcleral indentation was performed in three patients. In most cases, no post-operative posture was imposed on patients. Indeed, the product density ($d = 1.02$) ensured effective tamponade of the lower retina in standing posture throughout the day. Silicone oil was removed from all patients after 9.3 weeks on average (range 3 weeks–5 months). Heavy silicone oil was actively removed by aspiration because of its density and viscosity. This active extraction was performed under visual control via the three approaches to pars plana, using the vitrectomy extraction module at the highest suction power, with the help of a 19-gauge extraction canula (Fig. 5).

In the clinical study, perioperative complications were highlighted by two cases of early and unexplained emulsification, impairing fundus visualisation but not precluding reapplication. Post-operative complications were emulsification in seven case, including one very severe one. No corneal dystrophy and no ocular hypertonia were reported.

After a 40-month mean follow-up period (range 3–66 months after removal of the heavy oil), total retinal reapplication was achieved in 16 cases. Three patients suffered from RD recurrence under silicone oil by proliferative vitreoretinopathy (PVR) and one after silicone oil removal. Post-operative visual acuity, better than quantitative vision, making deambulation possible, was achieved in 10 patients with a mean acuity of 1/20 and at least 3/10 in 3 patients.

A multicentre, prospective study was conducted in cooperation with three vitreoretinal surgery centres (CHU de Rangueil, Hôtel Dieu, Paris, CHNO des XV-XX, Paris) in 30 patients operated on between 1998 and 2000, which confirmed the effectiveness and tolerance of the RMN3–5700 cSt silicone oil 12%/88% mixture, with a density of 1.03, in the treatment of retinal detachment, especially inferior and/or posterior dehiscences [8,9]. In particular, only one case

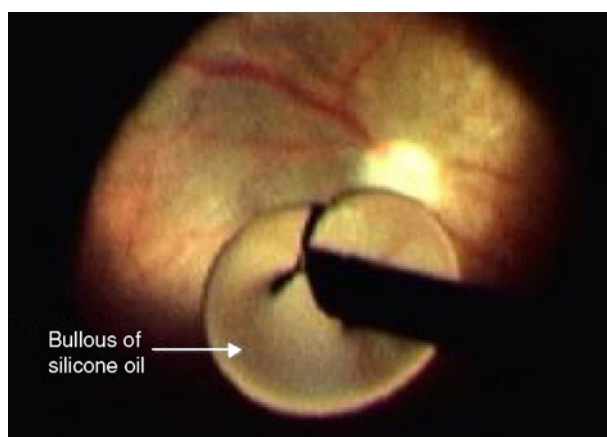


Fig. 5. Preoperative picture showing the 'heavy oil' extraction system. (See Colour Plate Section at the end of this book.)

of unusual post-operative inflammatory reaction was noted and there was no post-operative major emulsification. Three cases of slight emulsification out of 30 were recorded by this French study. Two cases of unexplained pre-operative major emulsification were noted, one of which spontaneously resorbed within 24 h. The second case was complicated by post-operative inflammatory reaction with iridocrySTALLINE synechiae and early cataract. No retinal vascular complication was noted. A study was conducted in parallel by Wolf [48] in 35 patients with the same mixture. Results were consistent with those of the French study. In particular, a single pseudophakic patient presented with post-operative inflammatory reaction with marked posterior synechiae; no emulsification higher than grade I was observed; one patient presented with an occlusion of the retinal central artery post-operatively.

In our series, full retinal reapplication was achieved in 16 of 17 patients (95%). There was only one case of major emulsification immediately after surgery. This was consistent with Wolf's results [47], who reported no case of emulsification with Oxane Hd[®]. Only once did we note silicone passage into the anterior chamber. Wolf reported the post-operative passage of heavy silicone oil (1.03 g/cm³) into the anterior chamber in two aphatic patients despite superior peripheral iridectomy. The incidence of post-operative glaucoma was lower in our series than that reported by Wolf [47] and other publications on standard silicone oil complications [16,17]. Heavy oil removal was uneventful in all patients in Wolf's series, who used 1.03 g/cm³ density silicone oil. Likewise, in all our patients operated on with the same density (1.03 g/cm³) heavy silicone oil (17 eyes), active extraction with the extraction module of the vitrectomy apparatus posed no problem.

6. CONCLUSION

On the basis of the results, it appears that heavy silicone oil Oxane Hd[®], the first formulation of this type on the market, as a temporary internal tamponade is equally tolerated as standard silicone oil in the surgical treatment of complex retinal detachment. It does not pose any emulsification or major fragmentation problem, as encountered with other 'heavier than water' products. Its effectiveness on inferior and posterior dehiscence tamponade appears to be very effective to currently available anatomical results. Oxane Hd[®], moreover, presents in this context a real benefit in the treatment of complex retinal detachment [48]. Retinopexy quality and the absence of residual subretinal fluid in internal tamponade of inferior lesions, extensive inferior retinectomies in particular, may reduce the risk of recurrence of complex retinal detachment by PVR. More extensive studies are now in course to see the limits of Oxane Hd[®] in comparison with new analogues such as Densiron 68[®], which has been marketed recently.

REFERENCES

- [1] S. Chang, Low viscosity liquid fluorochemicals in vitreous surgery, *Am. J. Ophthalmol.* 103 (1987) 38–43.
- [2] G. Brasseur, *Pathologie du vitré*, Masson, Paris, 2003, pp. 421–441.
- [3] S. Chang, V. Reppucci, N.J. Zimmerman, M.H. Heinemann, D.J. Coleman, Perfluorocarbon liquids in the management on traumatic retinal detachments, *Ophthalmology* 96 (1989) 785–792.
- [4] S. Chang, E. Ozmert, N.J. Zimmerman, Intraoperative perfluorocarbon liquids in the management of proliferative vitreoretinopathy, *Am. J. Ophthalmol.* 106 (1988) 668–674.
- [5] J. Roider, H. Hoerauf, K. Kobuch, V.P. Gabel, Clinical findings on the use of long-term heavy tamponades (semifluorinated alkanes and their oligomers) in complicated retinal detachment surgery, *Graefes Arch. Clin. Exp. Ophthalmol.* 240 (2002) 965–971.
- [6] B. Kirchhof, D. Wong, J.V. Meurs, R.D. Hilgers, M. Macek, N. Lois, Use of perfluorohexyloctane as a long-term internal tamponade agent in complicated retinal detachment surgery, *Am. J. Ophthalmol.* 133 (2002) 95–101.
- [7] K. Kobuch, D.H. Menz, H. Hoerauf, J.H. Dresch, V.P. Gabel, New substances for intraocular tamponades: Perfluorocarbon liquids, hydrofluorocarbon liquids and hydrofluorocarbon oligomers in vitreoretinal surgery, *Graefes Arch. Clin. Exp. Ophthalmol.* 239 (2001) 635–642.
- [8] (a) A. Mathis, V. Grosmaire, P. Garcia, J.Y. Driot, *et al.* Etude expérimentale de la tolérance intraoculaire d'un nouveau produit de tamponnement interne en chirurgie vitréorétinienne: Résultats préliminaires. 104^{ème} congrès de la Société Française d'Ophthalmologie, 17-21 mai, Masson (Paris), Paris p. 92.
 (b) A. Mathis, V. Pagot-Mathis, D. Chauvaud, C. Monin, J.F. Le Rouic, P. Larricart, *et al.* Tolérance d'un nouveau produit de tamponnement interne en chirurgie vitréorétinienne 107^{ème} congrès de la Société Française d'Ophthalmologie, 5-mai, Masson (Paris), Paris p. 119.
 (c) A. Mathis, V. Payrou, V. Pagot-Mathis, I. Ricco, M.T. Pieraggi, J. Pynson, B. Feurer, Etude expérimentale de la tolérance intraoculaire d'un nouveau liquide fluorocarboné en chirurgie vitréorétinienne 103^{ème} congrès de la Société Française d'Ophthalmologie, 11-15 mai, Masson (Paris), Paris p. 68.
- [9] I. Rico-Lattes, B. Ferrer, B. Guidetti, V. Payrau, BF n° 940480 (25/02/1994) and PCT n° 95012696 (25/08/1995), Baush and Lomb.
- [10] D. Wong, J.C. van Meurs, T. Stappler, C. Groenewald, I.A. Pearce, J.N. McGalliard, E. Manousakis, E.N. Herbert, A pilot study on the use of a perfluorohexyloctane/silicone oil solution as a heavier than water internal taponade agent, *Br. J. Ophthalmol.* 89 (2005) 662–665.
- [11] E.W.D. Norton, Edward Jackson Memorial lecture, Intraocula gas in the management of selected retinal detachments, *Trans. Am. Acad. Ophthalmol. Otolaryngol.* 77 (1973) 85–98.
- [12] H. Lincoff, J. Coleman, I. Kreissing, G. Richard, S. Chary, L.M. Wilcof, The perfluorocarbon gases in the treatment of retinal dataachment, *Ophthalmology* 90 (1983) 546–551.
- [13] P.A. Cibis, *Vitreoretinal Pathology and Surgery in Retinal Detachment*, The CV Mosby Company, St Louis, USA, 1965.
- [14] P.A. Cibis, B. Becker, E. Okun, S. Canaan, The use of liquid silicone in retinal detachment surgery, *Arch. Ophthalmol.* 68 (1962) 590–599.
- [15] J. Haut, L'intervention vitrectomie-silicone: à propos de 1000 cas, Masson, Paris, 1984.
- [16] R. Zivovnjovic, *Silicone Oil in Vitreoretinal Surgery*, Martinus Nijhoff/W. Junk, Dordrecht, 1987.
- [17] M. Gonvers, Temporary use of silicone oil in the treatment of special cases of retinal detachment, *Ophthalmologica* 187 (1983) 202–209.

- [18] D. McLeod, Silicone-oil injection during closed microsurgery for diabetic retinal detachment, *Graefes Arch. Clin. Exp. Ophthalmol.* 224 (1986) 55–59.
- [19] N.D. Brouman, M.S. Blumenkranz, M.S. Cox, M.T. Trese, Silicone oil for the treatment of severe proliferative diabetic retinopathy, *Ophthalmology* 96 (1989) 759–764.
- [20] J.S. Rinkoff, E. de Juan Jr, B.W. Mc Cuen, Silicone oil of retinal detachment with advanced proliferative vitreoretinopathy following failed vitrectomy for proliferative diabetic retinopathy, *Am. J. Ophthalmol.* 101 (1986) 181–186.
- [21] K. Heimann, B. Dalh, S. Dimopoulos, K.D. Lemmen, Pars plana vitrectomy and silicone oil injection in proliferative diabetic retinopathy, *Graefes Arch. Clin. Exp. Ophthalmol.* 227 (1989) 152–156.
- [22] H.C. Sell, B.W. Mc Cuen, M.B. Landers, R. Machemer, Long-term results of successful vitrectomy with silicone oil for advanced proliferative vitreoretinopathy, *Am. J. Ophthalmol.* 103 (1987) 24–28.
- [23] Silicon study group. Vitrectomy with silicone oil or sulfur hexafluoride gas in eyes with severe proliferative vitreoretinopathy: Results of a randomized clinical trial. Silicone study report 1, *Arch. Ophthalmol.* 110 (1992) 770–779.
- [24] Silicon study group. Vitrectomy with silicone oil or sulfur hexafluoride gas in eyes with severe proliferative vitreoretinopathy: Results of a randomized clinical trial. Silicone study report 2, *Arch. Ophthalmol.* 110 (1992) 780–793.
- [25] J.H. Yeo, B.M. Glaser, R.G. Michels, Silicone oil in the treatment of complicated retinal detachments, *Ophthalmology* 94 (1987) 1109–1113.
- [26] C. Chan, E. Okun, The question of ocular tolerance to intravitreal liquid silicone. A long-term analysis, *Ophthalmology* 93 (1986) 651–660.
- [27] E. De Juan, M. Hardy, D.L. Hatchell, M.C. Hatchell, The effect of intraocular silicone oil on anterior chamber oxygen pressure in cats, *Arch. Ophthalmol.* 104 (1986) 1063–1064.
- [28] J.L. Federman, H.D. Schubert, Complications associated with the use of silicone oil in 150 eyes after retina-vitreous surgery, *Ophthalmology* 95 (1988) 870–875.
- [29] A. Crisp, E. de Juan, J. Tiedeman, Effect of silicone oil viscosity on emulsification, *Arch. Ophthalmol.* 105 (1987) 546–550.
- [30] K. Nakamura, M.F. Refojo, D.V. Crabtree, Factors contributing to the emulsification of intraocular silicone and fluorosilicone oils, *Invest. Ophthalmol. Vis. Sci.* 31 (1990) 647–656.
- [31] (a) M. Soheilian, G.A. Peyman, T. Moritera, H. Wafapoor, Experimental retinal tolerance to very low viscosity silicone oil (100 cs) as a vitreous substitute compared to higher viscosity silicone oil (5000 cs), *Int. Ophthalmol.* 19 (1995) 57–61.
(b) M. Gonvers, *Intralocular Silicone Oil: An Experimental Study. Basic and Advanced Surgery. Internal Tamponade. III Complications of Silicone Oil* Livina Press, Padova, 1986, pp. 403–405.
- [32] M. Gonvers, J.P. Kornung, C. de Courten, The effect of liquid silicone on the rabbit retina, *Arch. Ophthalmol.* 104 (1986) 1057–1062.
- [33] S. Langefeld, B. Kirchlof, H. Meinert, T. Roy, A. Aretz, N.F. Schrage, A new way of removing silicone oil from the surface of silicone intraocular lenses, *Graefes Arch. Clin. Exp. Ophthalmol.* 237 (1999) 201–206.
- [34] A. Mathis, V. Pagot, J.L. David, The use of perfluorodecalin in diabetic vitrectomy, *Fortschr. Ophthalmol.* 88 (1991) 148–150.
- [35] M. Velikay, U. Stolba, A. Wedrich, Y. Li, P. Datlinger, S. Binder, The effect of chemical stability and purification of perfluorocarbon liquids in experimental extended-term vitreous substitution, *Graefes Arch. Clin. Exp. Ophthalmol.* 233 (1995) 26–30.
- [36] S. Chang, J.R. Sparrow, T. Iwamoto, A. Gershbein, R. Ross, R. Ortiz, Experimental studies of tolerance to intravitreal perfluoro-n-octane liquid, *Retina* 11 (1991) 367–374.
- [37] C. Eckardt, U. Nicolai, M. Winter, E. Knop, Experimental intraocular tolerance to liquid perfluorooctane and perfluoropolyether, *Retina* 11 (1991) 375–384.

- [38] M. Nabih, G.A. Peyman, L.C. Clark Jr, *et al.* Experimental evaluation of perfluorophenanthrene as a high specific gravity vitreous substitute: A preliminary report, *Ophthalmic Surg.* 20 (1989) 286–293.
- [39] U. Stolba, K. Krepler, R. Pflug, M. Velikay, A. Wedrich, S. Binder, Experimental vitreous and aqueous replacement with perfluorophenanthrene. Clinical, histologic, and electrophysiologic results, *Retina* 17 (1997) 146–153.
- [40] S. Chang, N.J. Zimmerman, T. Iwamoto, R. Ortiz, D. Faris, Experimental vitreous replacement with perfluorotributylamine, *Am. J. Ophthalmol.* 103 (1987) 29–37.
- [41] H. Terauchi, S. Okinami, Z. Kozaki, H. Tanihara, M. Nagata, Y. Sagawa, Experimental study on the effects of a replacement of the vitreous body with perfluorotributylamine on the rabbit eye, *Nippon Ganka Gakkai Zasshi* 93 (1989) 294–301.
- [42] K. Miyamoto, M.F. Refojo, F.I. Tolentino, G.A. Fournier, D.M. Albert, Perfluoroether liquid as a long-term vitreous substitute. An experimental study, *Retina* 4 (1984) 264–268.
- [43] M. Flores-Aguilar, D. Munguia, E. Loeb, J.A. Crapotta, C. Vuong, S. Shakiba, G. Bergeron-Lynn, C.A. Wiley, J. Weers, W.R. Freeman, Intraocular tolerance of perfluorooctylbromide (perflubron), *Retina* 15 (1995) 3–13.
- [44] K. Miyamoto, M.F. Refojo, F.I. Tolentino, G.A. Fournier, D.M. Albert, Fluorinated oils as experimental vitreous substitutes, *Arch. Ophthalmol.* 104 (1986) 1053–1056.
- [45] V.P. Gabel, A. Kampik, C.H. Gabel, D. Spiegel, Silicone oil with specific gravity for intraocular use, *Br. J. Ophthalmol.* 71 (1987) 262–267.
- [46] C.M. Gremillion, G.A. Peyman, K.R. Lui, K.S. Naguib, Fluorosilicone oil in the treatment of retinal detachment, *Br. J. Ophthalmol.* 74 (1990) 643–646.
- [47] S. Wolf, V. Schön, P. Meier, P. Wiedemann, Silicone oil–RMN3 mixture (“heavy silicone oil”) as internal tamponade for complicated retinal detachment, *Retina* 23 (2003) 335–342.
- [48] V. Pagot-Mathis, X. Benouaich, A. Mathis, I. Rico-Lattes, A. Dumoulin, Management of complicated retinal detachment using a heavy silicon oil as temporary tamponade, *J. Fr. Ophthalmol.* 29 (2006) 137–145.

Note from the Editors

For the use of perfluorocarbon molecules for ophthalmologic applications, see also in this volume the chapter by D. Menz and J.H. Dresch.

CHAPTER 10

Biocompatibility of Highly Fluorinated Liquids Used in Ophthalmic Surgery

Dirk-Henning Menz,^{1,*} and Joachim H. Dresch²

¹*Pharmpur GmbH, Messerschmittring 33, D-86343 Königsbrunn, Germany*

²*Bausch & Lomb Inc., Hans-Riedl-Str.7–9, D-85622 Feldkirchen, Germany*

Contents

1. Introduction	422
1.1. Anatomy of the human eye	422
1.2. Vitreoretinal diseases	422
1.3. Vitreoretinal surgery	424
1.4. The particularity of the use of highly fluorinated liquids as ocular endotamponades	425
2. Biocompatibility	425
2.1. Perfluorooctane and perfluorodecalin	427
2.2. New ocular endotamponades	428
2.3. Biocompatibility test scheme adjusted for FCLs for ophthalmic use	431
2.3.1. Toxicological tests	431
2.3.2. Modified test procedures for FCLs	433
2.4. Evaluation of undesirable local effects of ocular endotamponades	435
2.4.1. Effects of the high density	435
2.4.2. Oxygen content	436
2.4.3. Effects based on physicochemical behaviours	436
2.4.4. Effects based on the structure	437
2.4.5. Shape of the droplet/contact angle	439
2.4.6. Effect of impurities	440
3. New developments	441
References	443
Note from the Editors	445

Abstract

In different medical disciplines, highly fluorinated liquids are directly used, like in the case of ocular endotamponades in ophthalmology, of gas carriers in liquid ventilation, or of preservation and transport media in transplantation medicine. For these applications, the highly fluorinated liquids are used in a purified form or as mixtures. The extraordinary

*Corresponding author; Tel.: +49-8231-95770; Fax: +49-8231-957722;
E-mail: dirk-menz@pharmpur.de

behaviour of the fluorocarbon liquids (FCLs) requires specialised biocompatibility testing, adjusted to this class of components. The use of FCLs in ophthalmology can be regarded as an exotic application of FCLs as well, as this class of components is an exotic group of substances used in ophthalmology. The biocompatibility of FCLs and the special requirements related to the tests for this group of substances will be discussed with special emphasis on ophthalmic applications. An outlook into the possible future of highly fluorinated compounds as drug-delivering ocular endotamponades will be given.

1. INTRODUCTION

This chapter presents the state of the art of the use of highly fluorinated liquids in ophthalmology and perspectives of future applications in the eye. In different medical disciplines, the characteristics of these fluids are directly used, like in the case of ocular endotamponades in ophthalmology, of gas carriers in liquid ventilation, or of preservation and transport media in transplantation medicine [1–3]. For these applications, the highly fluorinated liquids are used in a purified form or as mixtures. The intended effect is created by the physicochemical characteristics themselves. The extraordinary behaviour of the fluorocarbon liquids (FCLs) requires specialised biocompatibility testing, adjusted to this class of components.

The use of FCLs in ophthalmology can be regarded as an exotic application of FCLs as well, as this class of components is an exotic group of substances used in ophthalmology.

The biocompatibility of FCLs and the special requirements related to the tests for this group of substances will be discussed with special emphasis on ophthalmic application.

Finally, an outlook into the possible future of highly fluorinated compounds as drug-delivering ocular endotamponades will be given.

1.1. Anatomy of the human eye

The human eye is a more or less spherical organ located in the orbit, a cavity in the skull of the anterior head. The main task of the eye is the dioptric function, focusing the ambient light on the retina to evoke electric potentials which can be transmitted via the optic nerve to the brain to create visual impressions (Fig. 1).

After refraction of the light in the cornea and the crystalline lens, the light has to pass through the vitreous before it reaches the neural component of the retina.

With an approximate volume of 4 ml, the vitreous is the largest structure within the eye. It has a refractive index of 1.33 and consists of 98–99% water with a scaffold of collagen fibres and macromolecules of hyaluronic acid winding through the scaffold. The healthy human vitreous does not contain blood vessels and has a consistency comparable to that of egg white.

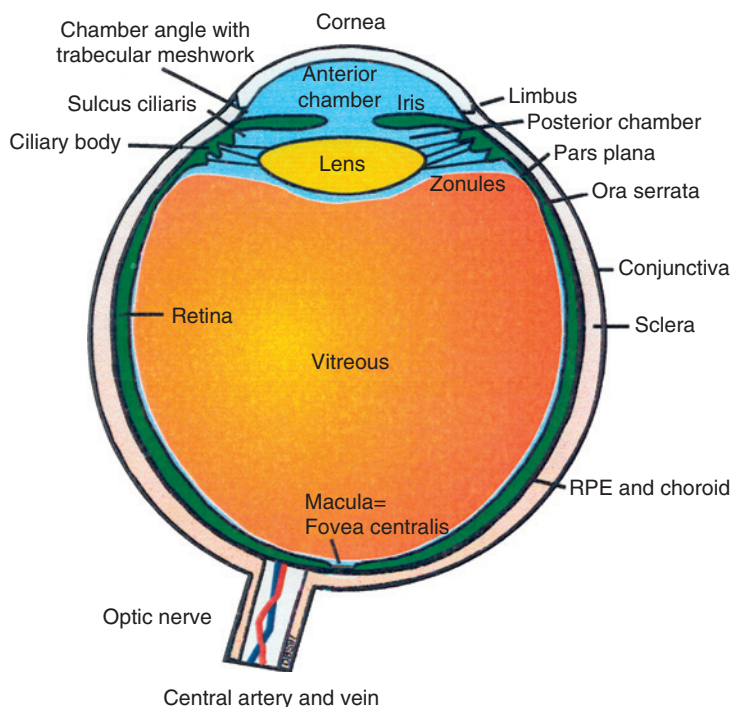


Fig. 1. Cross section of the human eye. (See Colour Plate Section at the end of this book.)

1.2. Vitreoretinal diseases

Various diseases of the natural vitreous itself, like opacification, haemorrhage, inflammation, as well as retinal detachment, may require its removal by so-called vitrectomy.

Primary (idiopathic, rhegmatogenous) retinal detachment is induced by a retinal tear, followed by penetration of vitreous fluid between the sensoric retina and the pigment epithelium.

Tractional retinal detachment is the result of the shrinkage of membranes. This is a frequent event in proliferative vitreoretinopathy (PVR), which is characterised by the growth of membranes on the outer as well as on the inner side of the detached retina. The shrinkage of these membranes results in further detachments of the retina and additional retinal holes.

Proliferative diabetic vitreoretinopathy (PDR) is characterised by the growth of blood vessels into the vitreous and neovascularisation of the retina. These neovascularisations lead to vitreous haemorrhage, creating additional fibrous epiretinal proliferations.

1.3. Vitreoretinal surgery

Standard procedure for a vitrectomy is the introduction of a vitrectomy cutter through the pars plana with subsequent alternating cuts and aspiration steps to remove the vitreous gel from the eye (Figs. 2 and 3).

Concomitantly, the removed volume has to be replaced to avoid ocular hypotension. This volume replacement is performed with a balanced salt solution. At the end of the vitrectomy, the vitreous gel has been removed—ideally completely—and the vitreous cavity is filled now with balanced salt solution.

The status of the retina has not changed; it is still detached, very frequently with idiopathic or iatrogenic liquid between the sensoric retina tissue and the underlying vascular layer (choroidea).

Perfluorocarbon liquids (PFCLs) are used in vitreoretinal (VR) surgery to stabilise the retina after vitrectomy. These surgical techniques use the hydrodynamic force created by the high specific gravity of the substances.

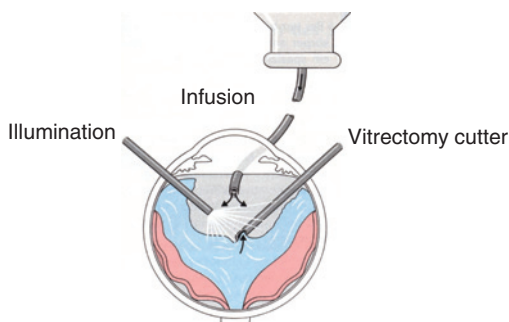


Fig. 2. Vitrectomy. (See Colour Plate Section at the end of this book.)

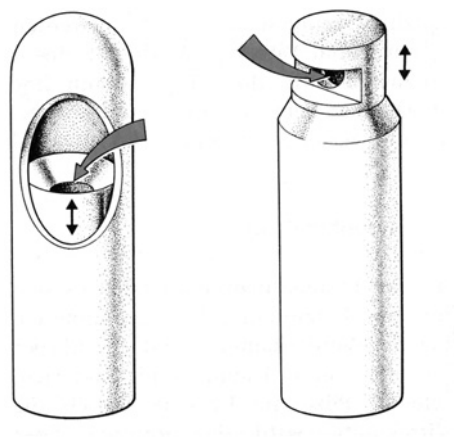


Fig. 3. Vitrectomy cutters.

1.4. The particularity of the use of highly fluorinated liquids as ocular endotamponades

At the end of the 70s of the last century, an impressive experiment was controversially discussed; a living mouse was completely submersed in a PFCL and could survive. This drastic demonstration of the efficacy of artificial respiration, and the tolerance to the substance used, is completely controversial. On the other hand, this test has become a milestone in the development of different medical applications of PFCLs. Not only the possibility of respiration from PFCL (liquid ventilation [3]) was proven, it could be demonstrated simultaneously that these PFCLs were tolerated by the skin and even by the eye and no toxic side effects were observed.

The demonstration of the potential of this stable and obviously excellently tolerated compound has inspired a great number of scientists to develop PFCLs as special tools for medical applications and to introduce therapies using the outstanding behaviours of PFCLs, like the well-known concepts of complete and partial liquid ventilation [4], oxygen support of the skin, wound treatment [5], artificial tears [6], and ocular endotamponade media [1], to name only a few. Until now, the mouse submersed in PFCLs is often used as an eye-catcher for the demonstration of the biocompatibility of PFCLs even in cases where the topic of the presentation is not reflected by this experiment.

However, a critical review shows that most of these developments are still in an experimental stage. Because of the complexity of the effects to be optimised, and the concomitant improvement of classical treatments, in the majority of cases the initial success could not be transferred to a routine procedure.

An exception is the ophthalmic use of PFCLs (see Table 1) like perfluorooctane (PFO) and perfluorodecalin (PFD). Since the introduction of PFCLs into VR surgery in the 80s [6–8], more than 2 million patients have been treated with PFCLs intra-operatively. In addition, animal studies with at least 3 months exposure have been published [9–11]. This experience based on the high number of well-documented patient cases and the consolidated findings on the effects of a long-term treatment opens the possibility of an exemplary discussion of opportunities and drawbacks of the use of highly fluorinated liquids.

The interoperative use of PFCLs has become a standard procedure in VR surgery during the last 15 years.

2. BIOCOMPATIBILITY

The term ‘biocompatibility’ needs some explanation and has to be defined for each application separately. The historical definition was based on unimpaired cell growth in the presence of the test article [12]. More recent definitions of the biocompatibility of implantable devices ask for the ability of the device to perform its intended function, without eliciting any undesirable local or systemic effects in the host.

Table 1. Perfluorocarbons used as ocular endotamponade and their behaviour

	Perfluoro- 1,3- dimethyl- cyclohexane	Perfluoro- n-octane	Perfluor- decaline (cis+trans Isomere)	Perfluoro- perhydro- phenan- threne
Molecular weight (g/mol)	400	438	462	624
Boiling point (°C)	102	104	142	215
Melting point (°C)	−70		trans >10 cis <−10	−20
Density (g/ml)	1.828	1.780	1.917	2.030
Refractive index (20°C)	1.2895	1.2700	1.3130	1.3348
Viscosity mPas (25°C)	1.92	1.4	5.53	28.40
Surface tension (mN/m)	16.6	14.0	17.6	19.0
Vapor pressure (mbar)	48	43	9	<1
CTSH (°C) lipophilicity	21	37	22	45
O ₂ -solubility volume(%)	—	48–52	40–44	—

An ocular endotamponade has to fulfil the related requirements of the particularities for this special application.

Additionally, it must fulfil the general requirements for biocompatibility/non-toxicity of medical devices. The compliance with the global requirements affirms that generally accepted limits of toxicological standard tests are met [13].

But it is too simple to justify the biocompatibility of an FCL with the result of toxicological tests only.

The biocompatibility of a device can only be given if the functionality of the tool for the main purpose—here the tamponade effect—and the functionality of the treated tissues or organs are unrestricted as well, keeping in mind the need of an assessment of the degree of restriction for each individual case.

The completely different polarity, electrical resistance and insolubility of the tamponade media compared to aqueous material can inhibit or change the functionality of the tissues or rearrange tissue parts, resulting in a loss of function, inflammatory reactions or immune reactions caused by the physical–mechanical contact only.

2.1. Perfluorooctane and perfluorodecalin

Based on the inventions of Clark [14] and Haidt [15], a rapid development of the ophthalmological use was initiated in the late 80s of the last century. The inertness of the PFCLs, the ease of injection, and the extremely high interfacial tension in combination with the high density of the material were the keys for revolutionising VR surgery [1,7,16].

From a classification point of view, ocular endotamponades are classical medical devices. Their application inside the human eye requires, besides ultra-purity, special controls during the manufacturing as well as for the release of finished products. They must be non-toxic and sterile and have to meet the general requirements of the European Medical Device Directive (MDD).

One of the main requirements is the verification of the biocompatibility and a risk management, which have to consider the results of a clinical study and post-marketing (vigilance) studies [17].

The chemical inertness of PFCLs is undeniable. Nevertheless, at least during long-term treatment, undesirable side effects have been observed [9].

One reason, at that time, was the insufficient purity of the compounds [18]. Because of the drastic reaction conditions during manufacturing of PFCLs, toxic by-products, like hydrogen containing fluorine compounds (HF) or fluoroolefins, can be generated and become an impurity of technical grade material. These by-products must be removed completely to avoid inflammatory effects in the eye.

This is an equivalent situation to that of the raw material for blood substitutes, and the impurity limits developed for this special application can be used directly. The content of extractable fluorine is a sensitive parameter to characterise the quality of PFCLs. The correlation between the concentration of extractable fluorine in a PFCL and its toxicity was reported by Gervits [19]. Using cell cultures, he was able to correlate the inhibition rate of cell growth to the content of extractable fluorine. Table 2 shows that only very low concentration could be tolerated.

Table 2. Cell growth inhibition caused by different concentration of extractable fluoride according to Gervits [19]

Cell growth of lymphoid human Raji cells	Content extractable Fluorid (10^{-4} M)
100–120	0.6
70–80	5.0
0	43.0

The compliance with these basic requirements can only be met using a well-balanced combination of chemical treatment and purification techniques [20]. Most of the side effects reported in the 1980s and beginning of 1990s were caused by toxic impurities in the PFCLs. But even highly purified substances cannot avoid all side effects, like epiretinal foam cells, the vacuolization of the inner retinal surface, the hypertrophy of Müller cells and slight disarrangements of the plexiform layer and outer nuclear layers, loss of photoreceptor cells and thinning of the retina [16,21,22]. Until recently, the high density of the PFCLs, necessary and responsible for a good tamponade effect, was regarded as the reason for these damages. But this approach was too simple to explain all effects observed in the past.

Table 1 shows the products used and tested as ocular endotamponades and their characteristics. In addition to the specific density, the interfacial tension against water is also an important parameter for the use. The drainage of subretinal fluids is achieved, but the interfacial tension prevents the passage of the PFCL into the subretinal space.

The preference for one of the products is more or less a matter of habit. Therefore, it is no surprise that over the years the best available and least expensive products, PFO and PFD, have dominated the ophthalmic market completely.

Based on general experience and the confirmation of the results by different groups all over the world and the availability of many approved and certified products, it should be easily possible to characterise the biocompatibility of these products.

Surprisingly, the fact remains that the question if these FCLs are biocompatible cannot be answered with a simple yes or no, even not in this obviously well-investigated field.

2.2. New ocular endotamponades

Developments to improve ocular endotamponades were focused initially on lower-density FCLs as alternatives to the PFCLs [23–25].

At the end of this development phase, partially fluorinated compounds of the RFRH type [27], with different ratios of alkane and perfluoroalkane chains linked together, were introduced into the market [26].

They could not replace the PFCL in interoperative use because their performance was not better than that of PFCLs, and they were more expensive. The hydrodynamic force and, consequently, the tamponade effect are limited by the reduced density. Possibly, they will find a niche in special applications in which the different shape of the droplet, in comparison to PFCLs, may support special manoeuvres or processes in which their higher potential to dissolve substances is needed (removal of silicone oil remnants). Especially the expectations for a better long-term tolerance have not been fulfilled.

The histological findings after 3 months treatment show lesser damages of the tissues as in case of PFCLs, but inflammatory effects, the formation of precipitates and a distinctive emulsification are non-tolerable side effects [28,29] (Table 3).

The advantage of the partially fluorinated compounds lies more in their potential to mix with silicone oil. Various groups started activities to diversify the portfolio of silicone oils used as long-term endotamponades to enable a reattachment of a detached retina. Dimethylsiloxanes of different viscosities are well established but their use is limited to the treatment of the upper quadrants of the retina. This is because a 100% filling of the vitreous cavity cannot be achieved, which means that because of their specific gravity, which is 0.97 g/ml, they float on top of the aqueous material present in the vitreous

Table 3. Behaviours of partial fluorinated liquids used and tested in ophthalmic use

	Perfluoro-ethyl-hexane O26	Perfluoro-hexyl-ethane O62	Perfluoro-butyl-butane O44	Perfluoro-hexyl-hexane F6H6® (Fluoron GmbH)	Perfluoro-hexyl-octane F6H8® (Fluoron GmbH)
Purity (%)	>98	>99	>99	>99	>99
Boiling point (°C)	115	114	103	187	223
Specific gravity (g/ml)	1.08	1.62	1.24	1.42	1.35
Refractive index	1.33	1.29	1.31	1.32	1.34
Viscosity (mPas)	0.67	0.75	0.77	1.85	2.50
Surface tension (mN/m)	16.7	14.7	17.4	20.0	21.0
Interfacial tension against water (mN/m)	n.b.	39	22	50	49

cavity. Therefore, the VR surgeons wanted a 'heavier than water' silicone oil to tamponade the lower quadrant of the retina and to replace the so-called PVR milieu [30].

All attempts to introduce fluorosilicone oils, in which the fluoro-alkyl group was covalently bound to the Si-O-Si backbone, were without success [31,32]. A new approach to create a 'heavier than water' silicone oil was the mixture of partially fluorinated compounds and ultra-purified silicone oil. The first product on the market was Oxane Hd® (Bausch&Lomb Inc., Rochester, NY, USA), a mixture of 1-perfluorooctyl-5-methylhex-2-en and silicone oil 5000 mPas. The specific density of this clear mixture is 1.02 g/ml. This creates the possibility to treat the lower quadrant of the retina. An intra-ocular bubble of Oxane Hd® has an ideal spherical shape as demonstrated in Fig. 4.

This is an example of a real rolling tamponade, which has the advantage that no area of the retina is permanently separated from aqueous contact.

In the meantime, corresponding mixtures of different perfluoralkyl-alkanes with silicone oil are available (Densiron 68®, Fluoron GmbH, Neu-Ulm, Germany).

The negative side effects of the partially fluorinated compounds are masked if these components are dissolved in silicone oil. Here they are completely enclosed by the silicone oil matrix and have no direct contact to the intraocular tissue [33,34] (Table 4).

All these mixtures are ideal mixtures at temperatures above 30°C. Lower temperatures increase the risk of aggregates. These aggregates can be observed by light scattering. Ultimately, a reversible separation may take place. The specific density, viscosity, and the separation temperature of all the mixtures mentioned above depend on the chemical structure and the amount of partially fluorinated substance dissolved ([28], own results).

Within certain limits, these 'heavier than water' silicone oils can be adjusted to the particular needs.



Fig. 4. A nearly ideal spherical bubble of Oxane Hd under water.

Table 4. 'Heavier than water' silicone oil tamponades

	Oxane Hd® (Bausch&Lomb Inc.)	Densiron 68® (Fluoron GmbH)
Specific gravity (g/ml)	1.02	1.06
Viscosity (mPas)	3500	1400
Components	Silicone oil 5000 mPas and RMN3	Silicone oil 5000 mPas and F6H8®

The new ocular endotamponades extend the portfolio of available intra-operative tools, but they do not overcome the side effects already described for the established products.

2.3. Biocompatibility test scheme adjusted for FCLs for ophthalmic use

The evaluation of the biocompatibility starts with the toxicological characterisation of the products. There are generally accepted standard tests and guidelines for each type of product available for this purpose [13,17].

2.3.1. Toxicological tests

Tamponade media are classic medical devices. The general requirement for an approval of such a product is the conformation of the non-toxicity as an important part of the biocompatibility. There are detailed guidelines available which determine the tests necessary, dependent on the intended use of the product.

For FCLs as a short-term ocular endotamponade, the following tests must be performed:

- Test of cytotoxicity ISO 10993–5
- Test of sensitisation ISO 10993–10, OECD, 406
- Test of irritation and intra-cutaneous reactivity ISO 10993–10, OECD 404, 405
- Test of acute systemic toxicity ISO 10993–11, OECD 423
- Test of genotoxicity ISO 10993–3 OECD 471, 473

In general, the first toxicological test in the development of a new material is the test for cytotoxicity.

There are standardised test procedures described in the pharmacopoeia (e.g., EP and USP) and in the standards referenced above. These are general test procedures developed and applicable for 'normal' products. Testing products

absolutely non-soluble in water creates difficulties and can lead to false positive or negative results. Especially for FCLs (perfluorinated as well as partially fluorinated), the test procedures have to be validated for these substances and the procedures have to be adjusted to the non-aqueous behaviours of these compounds.

The cytotoxicity test described in ISO 10993-5 is a good example. It is a rapid, standardised test, very sensitive and can characterise materials and significant quantities of harmful extractables and their effect on cellular growth. Because of the high sensitivity, mouse fibroblasts L929 are used as the test cells routinely.

The basic idea is to monitor the cell growth by determining the increase in concentration of compounds which are formed during cell proliferation. There is a correlation between cell growth and the toxic behaviour of compounds which are part of the surrounding media of the cells. Any toxic effect of a component in the surrounding media would lead to a cell growth inhibition. In this case, the test material, usually an extract, is placed in a cell culture plate containing a confluent monolayer of the test cells. After incubation (72 h, 37 °C), the treated cells or cell components are stained and quantitatively determined by a photometric system. In the same way, positive and negative controls must be performed. If the relative inhibition of the cell growth is >30%, then the product has to be characterised as cytotoxic.

In the so-called disk diffusion test, a carrier (paper disk) impregnated with a known amount of the test material is placed on the surface of an agar medium, which has previously been inoculated with a cell suspension. The agar acts as a cushion to protect the cells from mechanical damage while allowing the diffusion of leachable chemicals from test material into the monolayer culture of cells (incubation time 24 h, 37 °C). The idea is that toxic products diffuse from the carrier into the medium with the cell suspension, producing a concentration gradient. Cell growth in the vicinity of the carrier occurs only when the concentration diffusing from the carrier is no longer sufficient to inhibit cell growth. If the concentrations are sufficient to achieve inhibition, a circular region of no cell growth develops. If such a zone can be observed, the criteria of cytotoxicity are met.

All these standard tests have the water solubility of the toxic materials or impurities or extractables as a provision of the test strategy. In the case of PFCLs, this can result in an incorrect classification. Therefore, the test design has to be adjusted to the special behaviours of PFCLs.

Because of the water insolubility of the PFCLs and of the potential toxic by-products, the investigation of extracts or the use of diffusion gradients is not sufficient. If PFCL is added to the culture plates, where the cells grow on the plate surface and are covered by the growth media, the heavy PFCL sinks to the bottom of the culture plate, insulating the cells from the nutrient and occupying space needed for cell proliferation. Both situations create an inhibition of cell growth. This inhibition is not caused by a toxic but by a mechanical effect.

2.3.2. Modified test procedures for FCLs

The following test procedures reflect the experiences with the characterisation of perfluorinated and partially fluorinated compounds used as ocular endotamponades but should also be used for other, similar applications. A risk assessment shows that toxic effects from a completely water-insoluble substance can be caused by

- Toxic effects of extractables
- Toxic effects by direct contact

These different origins of cytotoxicity should be investigated in separate tests using the following test designs.

Test for toxic effects of extractables

- Simulation of biological conditions for an extraction of any toxic substances from a water-insoluble and nonpolar phase by shaking and incubating the test samples with culture media as the extraction agent for 72 h at 37°C
- Complete separation of the extract and test sample by centrifugation
- Dosage-dependent test of the clear (!) extracts and pure test samples according to ISO 10993
- Evaluation of the cell growth by the growth inhibition test according to ISO 10993–5 using mouse fibroblasts L929 and crystal violet as staining substance

Test for toxic effects induced by the direct contact

- Performing the cell inhibition test with pure test materials in different amounts

In order to separate effects of cell growth inhibition not induced by toxic potential, an extra microscopic evaluation of the test cells must be performed in each case.

The following tables illustrate typical results of toxic and non-toxic products (Tables 5–8).

Examples for non-cytotoxicity of ultra-purified PFC and HPFC

Table 5. Test results of the extracts

Sample	Average growth inhibition (%)					
	Concentration of dilution tested					
	100%	30%	10%	3%	1%	0.3%
O44	1	0	–2	0		
O62	7	9	4	2		
PFD	8	4	7	3		
DMEM Neg. control	0					
DMSO Pos. control			107	85	24	1

Table 6. Test results of direct exposition

Sample	Average growth inhibition (%)			
	Amount of sample tested			
	5 μ l	10 μ l	20 μ l	50 μ l
O44	7	5	7	12
O62	−1	2	2	9
PFD	6	4	7	32

Table 7. Test results of the extracts

Sample	Average growth inhibition (%)					
	Concentration of dilution tested					
	100%	30%	10%	3%	1%	0.3%
O26	11	−8	−3	−5		
UN36	32	−4	0	−6		
DMEM Neg. control	−1					
DMSO Pos. control			101	80	10	−5

Table 8. Test results of direct exposition

Sample	Average growth inhibition (%)			
	Amount of sample tested			
	5 μ l	10 μ l	20 μ l	50 μ l
O26	8	30	86	99
UN36	100	100	99	87

Equivalent results were obtained with other ultra purified compounds like PFO, RMN3 or F6H8®.

Examples of cytotoxicity: perfluorpropyloctane (UN36) and perfluorohexyl-ethane (O26)

The cytotoxicity is related to the direct contact; the extracts show no significant cytotoxic reaction.

Examples for the need of additional microscopic evaluation

Monitoring of the manufacturing process of perfluoralkyl-alkenes: the test results of the extractables are inconspicuous; the direct contact tests show no

Table 9. Test results of direct exposition

Sample	Average growth inhibition (%)			
	Amount of sample tested			
	5 μ l	10 μ l	20 μ l	50 μ l
Crude material	83	41	20	8
Treated material	46	23	24	6
Purified RMN3	56	n.d.	n.d.	n.d.

Table 10. Microscopic evaluation of the cells

Sample	Cell damage*microscopic evaluation			
	Amount of sample tested			
	5 μ l	10 μ l	20 μ l	50 μ l
Crude material	4	1–2	1	0
Treated material	1	0	0	0
Purified RMN3	0	n.d.	n.d.	n.d.

*Definition of cell damage according to USP27: 0 = no reactivity, 1 = weak reactivity, 2 = small reactivity, 3 = middle reactivity and 4 = strong reactivity.

significant differences between the samples. The microscopic evaluation shows that only the crude material reacts cytotoxic; the growth inhibition of the other two samples is caused by mechanical and not toxic effects (Tables 9 and 10).

2.4. Evaluation of undesirable local effects of ocular endotamponades

2.4.1. Effects of the high density

The retina of eyes filled with PFCLs is exposed to a media which has a density nearly twice as high as that of the natural vitreous. Mechanical damage by increased pressure on the retinal vessels was used as a simple explanation for the necrotic retina observed after longer (2 weeks) exposure.

Calculations performed by Winter [35] showed that the increase in hydrostatic pressure (3–6 Torr) is within the physiological limits and should be well tolerated by the eye (normal intra-ocular pressure 20 Torr).

This was verified by Kobuch and Hoerauf by histological studies [36,28]. Different fluorinated compounds with a linear backbone of 8 C-atoms and a different degree of fluorination were filled into the vitreous cavity of vitrectomised rabbit eyes.

Table 11. Compounds investigated for potential retinal damage caused by the specific gravity

	Perfluoro-decalin	Perfluoro-roctane	Perfluorohexyl-ethane	Perfluorobutyl-butane
Purity (%)	>99	>99	>99	>99
Density (g/ml)	1.92	1.78	1.62	1.24
Induced hydrostatic pressure (Torr)		1.34	1.04	0.60

All compounds used had equivalent purity (see Table 11). The test design was focused on the evaluation of histological differences after a tamponade time of 6 weeks. The density of the PFCLs used was 1.32 g/ml (perfluorobutylbutane), 1.62 g/ml (perfluorohexyl-ethane) and 1.78 g/ml (PFO). There was no dose–response relationship; that means there is no evidence that a higher density creates more severe histological damage. Therefore, the simple explanation of the insufficient long-term tolerance for PFCLs could not be verified.

2.4.2. Oxygen content

The potential of PFCLs to solve high volumes of gases, especially oxygen and carbon dioxide, was the key for most of the medical applications and was described recently [37].

In ophthalmological application, this characteristic of the PFCLs is not used yet. In general, the products used are air equilibrated with the consequence that the oxygen partial pressure in the eye is increased from 15 Torr to 160 Torr and the CO₂ partial pressure drops down from 50 Torr to 3 Torr initially. These differences are equilibrated intra-ocularly by diffusion processes, but the initial difference to the physiological level of gas concentration activates the constriction of the retinal vessels, resulting in an increase of the blood flow. In rabbit eyes, a damage of the retina could be attributed to this mechanism [38,39]. On the other hand, endotamponade media with controlled levels of dissolved gases could not only avoid such a scenario but should also be useable for a therapeutic manipulation of the retinal perfusion.

2.4.3. Effects based on physicochemical behaviours

Our own investigations concentrated on compounds with different densities (PFO and perfluorohexyl-ethane) and additionally on compounds with comparable densities but different viscosities. Perfluorohexyl-ethane was tested as a monomer and in two oligomeric configurations with the same molecular unit but

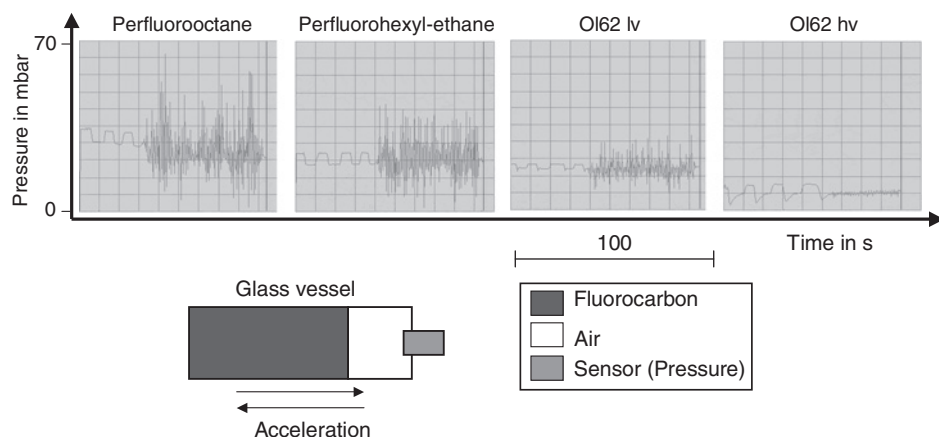


Fig. 5. Pressure spikes induced by shaking low dense fluorocarbons *in vitro*.

different viscosities, OL62lv (70 mPas) and OL62hv (1750 mPas, for more details see Section 3.).

These test samples were filled into glass vials. The closure included a pressure sensor. The vials were turned upside down three to four times and shaken by hand subsequently, simulating head and eye movements. Figure 5 shows the pressure spikes recorded. Liquids of low viscosity create pressure spikes which are significantly higher than those of higher viscosity (see also [51]). These high-pressure peaks may be responsible for the necrosis of the retina, seen after long-term exposure to PFCLs, all the more considering the fact that in some cases the tissue changes were located at the PFCL/aqueous interface [10,18].

The combination of low viscosity and high density creates a risk situation, which might be described as 'Tanker effect'. Assuming a tanker without separators and with a 50% filling of the tank accelerates, the inertia of the fluid mass creates pressure on the inner back side of the tank. If the driver pushes the break firmly, all liquid will move to the front and will create pressure on the inner front side of the tank.

These findings should have two consequences. First, the development of potential long-term ocular endotamponades should consider harmonising viscosity and density to avoid mechanically induced side effects. And secondly, the evaluation of the biocompatibility should include effects not directly related to classic toxic phenomena.

2.4.4. Effects based on the structure

Some of the compounds described above are not perfluorocarbons. Partially fluorinated compounds of the type RFRH like perfluorohexyl-octane (F6H8®, Geuder GmbH, Heidelberg, Germany) or perfluorohexyl-ethane became a matter of particular interest for ophthalmic endotamponades. They combine sufficient chemical stability with high interfacial tension against water but have a significantly lower density than perfluorinated compounds.

The different PFCLs used as intraoperative tools can be categorised as a group of compounds with more or less uniform behaviour. On the contrary, the partially fluorinated species have to be regarded as individuals each. This is due to the hybrid character of these compounds, which combine the behaviours of alkanes and perfluoroalkanes. Especially, the toxicological behaviour cannot be optimised by simple modifications of the degree of fluorination. If the two molecule parts are combined in the right balance, the cytotoxic behaviour of the alkyl chain can be overcompensated by the inert perfluorinated part of the compound. But each compound should be tested individually to ensure its suitability as a candidate for ophthalmic use.

Perfluoroalkyl-alkenes like 1-perfluorooctyl-5-methylhex-2-en (usually abbreviated as RMN3, [24]) can be regarded in the same way. In addition to the saturated analogues, it has to be ensured by the molecular structure that no inter- or intra-molecular rearrangements take place, generating acid by-products.

A further important issue is the balance between the perfluoroalkane and the alkane part in the RFRH molecules and the branching ratio in both these compartments. This is of special importance if penetration processes into tissues must be taken into consideration. Especially low molecular weight species or partial fluorinated liquids with their distinctly higher lipophilic potential as PFCLs can easily penetrate tissues.

This was demonstrated by GC/MS measurements using a headspace sampler. Equivalent tissue segments of freshly enucleated and vitrectomised eyes of pig were prepared and rinsed for 30 min with PFD after a simulated VR surgery using different types of partially fluorinated liquids as endotamponade media. PFO was used as a reference. At the end of treatment, they were rinsed with PFD to clean the surfaces.

Table 12 shows the differences in penetration of ocular tissues of the different tamponade media [28].

Table 12. Penetration of ocular tissues of pig eyes in the result of a simulated eye surgery [28]

	Concentration [ppm] in the tissue after a simulated surgery (30 min contact time)		
	Retina	Choroidea	Sclera
O26	0.70	0.20	0.20
O44v	0.12	0.10	–
O62	0.31	0.20	0.29
OL62LV	0.14	0.10	–
PFO	0.01	0.02	0.10 (without rinsing)

Tissue penetration of endotamponade media should be avoided because of non-calculable side effects. One way to reduce the penetration rate is the use of branched species. In a similar experiment as described above, small pieces of fatty tissue and muscle tissue from pig were immersed in the test liquids for 15 min and then rinsed with PFD to clean the surfaces. Table 13 shows the reduced ratio of penetration of branched perfluorobutyl-butane in comparison to the linear form (O44: perfluorobutyl-n-butane and O44v:1-perfluorobutyl-2-methylpropane, own unpublished results). The relative penetration ratio was determined on the basis of the concentration of the two types of perfluorobutyl-butane indicated by GC/MS measurements.

But it has to be taken into consideration that a complete suppression of tissue penetration may have not only surgical advantages.

If the intra-operative use of PFCL is followed by a silicone oil tamponade and residual PFCL is still present (up to 3 months) during the removal of silicone oil, then sticky behaviour of the silicone oil can be promoted [40].

2.4.5. Shape of the droplet/contact angle

The use of PFCLs as interoperative tools requires the phase separation to the aqueous environment in the vitrectomised eye. Simultaneously, this requirement is the reason for some undesirable side effects.

Winter *et al.* [41] could demonstrate that the intra-operative treatment of retinal detachments with PFCLs, followed by an exchange to intraocular gas, resulted in total coating of the retinal surface with the fatal effect of complete sealing, creating an interruption of essential transretinal exchange processes. Equivalent scenarios have to be taken into consideration in the situation of a completely filled eye or if the droplets of an endotamponade media show a non-spherical shape.

Table 13. Difference in tissue penetration of branched and unbranched species

	Muscle tissue	Muscle tissue	Fatty tissue
Cleaning procedure after immersion	Two times dipping in PFD, rinsing with water	Mechanical cleaning followed by rinsing	Mechanical cleaning followed by rinsing
Relative concentration of O44v	1	1	1
Relative concentration of O44	11	5	4

Because of the differences in the interfacial tension and the density of the tamponade media, differences in the drop shape (see Fig. 6) and in the contact angles between the media and the retina can be observed. This has an impact on the manoeuvre which has to be avoided (see slippage—complete drainage of the aqueous part before removing PFCL [42]) or supported (see macular translocation—rotation could be facilitated by smaller contact angles like in the case of partially fluorinated alkanes [28]). From a toxicological point of view, the complete coating of the retina over a long time leads to disarrangements, especially in the Müller cells because the exchange of water-soluble components is blocked by the insulating effect of non-water-soluble PFCL-layers. Silicone oil should have the same insulating behaviour, but in this case no direct contact between silicone oil and the retina occurs, at least not in the lower quadrant of the vitreous cavity. Because of the movement of the eye, this aqueous interface is moving too and can obviously compensate the insulating effect of the tamponade media itself (see rolling tamponade and [42]).

2.4.6. *Effect of impurities*

The effect of toxic impurities formed during the manufacturing of PFCL and the need of the use of ultra-purified products was already discussed. But small amounts of highly fluorinated and non-toxic by-products can also induce side effects because they can alter the interfacial tension. Table 14 shows the effect of small amounts of 1H-perfluorooctane in PFO [own, non-published results]. The differences in the surface tension and interfacial tension against water between pure and spiked PFO are not significant. Nevertheless, such a change in interfacial tension can alter the interaction with the tissues in contact. Because of the greater number of different types of ocular endotamponades now used in

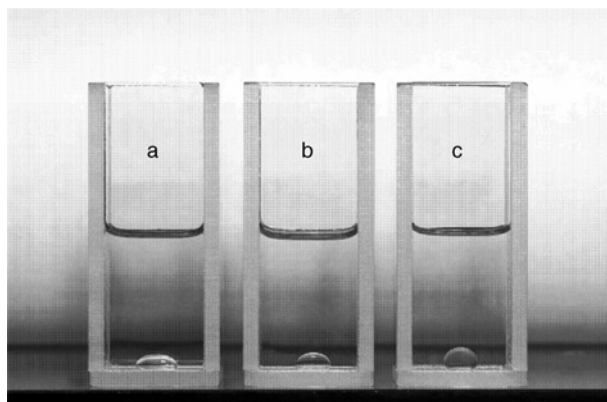


Fig. 6. Different drop shapes of endotamponade materials in water: (a) PFCL, (b) partial fluorinated liquid and (c) 'heavier than water' silicone oil.

Table 14. Alteration of surface behaviours of PFO spiked with 1H-Perfluorooctane

	Surface tension (mN/m)	Interfacial tension against water (mN/m)
Perfluorooctane	14.2	51.4
1-H-perfluorooctane	15.4	32.0
Perfluorooctane spiked with 0.55% 1-H-perfluorooctane	13.7	50.9

routine procedures, such a small alteration may gain more significance in the future because of the possibility to initiate unexpected side effects by a combined use with other endotamponades like the stickiness of silicone oil [54].

Summarising all the experiences of biocompatibility studies and the description of local side effects, the ocular endotamponades in use have to be characterised as non-toxic, but with a limited biocompatibility. Tissue alterations induced by local side effects can be accumulated in such a way that an immunological response may occur. Therefore, it is impossible to set strict boundaries between the elements of biocompatibility and the development must be focused on the reduction on local effects.

3. NEW DEVELOPMENTS

The introduction of the 'heavier than water' tamponades into the market was a milestone in the development of long-term ocular endotamponades (vitreous substitute).

The development of partially fluorinated substances of higher viscosity was based on the idea that the retinal damages induced by PFCLs are caused by the combination of low viscosity and high density.

Simultaneously, the tendency of emulsification can be reduced in the same way [43].

Oligomers of perfluorohexyl-ethene fulfilled these expectations in all preclinical studies, *in vitro* tests as well in animal tests. A radical polymerisation, followed by ultra-purification steps, created a crystal clear gel-like substance. The behaviours of the mixture of dimeric, trimeric and tetrameric star-shaped species with an inner core of hydrocarbon bonds and an outer layer of perfluoro-alkyl chains could be adjusted by the ratio of the dimeric, trimeric and tetrameric species, using a thin layer distillation. In dependence on this ratio, the viscosity could be adjusted in the range between 90 mPas and 1700 mPas, the specific density between 1.60 g/ml and 1.66 g/ml and the interfacial tension against water between

33 mN/m and 35 mN/m. The refractive index of 1.33, which is similar to that of water, did not create refractive changes in the eye.

All these parameters are very close to the requirements which a long-term ocular endotamponade has to fulfil. Also the *in vivo* tests in a rabbit eye model were extremely promising: no emulsification, no changes in the vascular structure of the retina and no increase of the intra-ocular pressures. All negative side effects, seen with the monomeric FCLs, seemed to be eliminated. In addition, some additional advantages could be claimed: reduced tissue penetration and the potential to dissolve drugs [44,45].

The first results after clinical use were disappointing: emulsification, inflammation and formation of precipitates [28]. All these non-tolerable side effects could not be reproduced in the rabbit eye, that is, the substance used fulfilled all requirements of biocompatibility testing according to the international standards. These discrepancies are not completely clarified yet. One explanation could be a sealing effect. Because of the fact that the highly viscous oligomer acts as a steady tamponade, instead of a rolling tamponade, the pump function of the Müller cells may have been compromised [46]. Another explanation for these findings is discussed by Hoerauf. He found that the formation of precipitates can be traced back to a degradation/derivatisation of albumin, in addition to mechanically induced changes [47,48,53]. It seems possible that an immune response to such a reaction could be the reason for incompatibility and that healthy, untreated eyes, which are required in the international standards as test models, have a higher tolerance against such challenges.

This experience is an indication that biocompatibility testing has to be adjusted for each device, and established animal models must be questioned if new classes of substances are to be tested. Standardised toxicological tests may be suitable for substances known at that time when these tests were developed. There is a need for the introduction of new types of cell culture tests as well as for better animal models and more suitable *in vivo* tests [49].

Ocular endotamponades based on FCL are and will be interoperative tools. They have to be removed after use. The risk–benefit analysis must be the base for defining the maximum treatment period. The main task of these devices is space filling/maintenance.

The ocular endotamponades of the future could be a combination of tamponading and drug delivery device. Vitrectomy removes the natural vitreous after it has become opaque, inflamed, or unable to keep the retina in place. In many cases, the necessity to remove it is the result of retinal disorders, which are still existent after vitrectomy [50]. In equivalence to the blood–brain barrier, there is also a blood–retina barrier, with the effect that it is difficult to treat retinal disorders systemically. Therefore, the delivery of appropriate drugs via the vitreous cavity would open new treatment options.

All existing ocular endotamponades have a neglectable dissolution potential for approved drug substances. This situation could be significantly improved by

using gel-like substances with polyaphron structure [51]. These foam-like substances consist of three components: water, fluorocarbon and a fluorine-containing surfactant [52]. The foam-like structure with a discontinuous phase (bubbles of fluorocarbons) covered by a continuous phase (mixture of surfactant and water) makes the gel viscoelastic, injectable, autoclavable and permeable for water and ions. A well-balanced selection of the components can vary the behaviours of the gel in wide ranges up to a reversal of the character of the continuous and discontinuous phase [51].

The combination of aqueous-like behaviour with a tamponading effect is one of the big challenges.

REFERENCES

- [1] S. Chang, E. Ozmert, N.J. Zimmerman, Intraoperative perfluorocarbon liquids in the management of proliferative retinopathy, *Am. J. Ophthalmol.* 106 (1988) 668–674.
- [2] Y. Kuroda, T. Kawamura, Y. Suzuki, A new simple method for cold storage of the pancreas using perfluorochemicals, *Transplantation* 46 (1988) 457.
- [3] T.H. Shaffer, D. Rubenstein, D. Moskowitz, M. Delivoria-Papadopoulos, Gaseous exchange and acid-base balance in premature lambs during liquid ventilation since birth, *Pediatr. Res.* 10 (1976) 227–231.
- [4] M. Quintel, K.F. Waschke, J. Meinhardt, Flüssigkeitsbeatmung mit Perfluorocarbon, *Anästhesiol Intensivmed Notfallmed Schmerzther* 31 (1996) 461–469.
- [5] D.C. Withe, Use of perfluorocarbons as wound treatment, US Patent No. 4,366169, (1981).
- [6] S.J. Haidt, L.C. Clark, J. Ginsberg, Liquid perfluorocarbon replacement of the eye, *Invest. Ophthalmol. Vis. Sci.* 22(Suppl.) (1982) 233.
- [7] S. Chang, H. Lincoff, N.J. Zimmermann, W. Fuchs, Giant retinal tears. Surgical techniques and results using perfluorocarbon liquids, *Arch. Ophthalmol.* 107 (1989) 761–766.
- [8] K. Miyamoto, M.F. Refojo, F. Tolentino, G.A. Fournier, D.M. Albert, Fluorinated oils as exp. Vitreous substitutes, *Arch. Ophthalmol.* 104 (1986) 1053–1056.
- [9] C. Eckardt, U. Nicolai, Klinische und histologische Befunde nach mehrwöchiger intraokularer Tamponade mit Perfluorodekalin, *Ophthalmologie* 90 (1993) 443–447.
- [10] M. Velikay, A. Wedrich, U. Stolba, P. Datlinger, Y. Li, S. Binder, Experimental long-term vitreous replacement with purified and non-purified perfluorodecalin, *Am. J. Ophthalmol.* 116 (1993) 565–570.
- [11] S. Binder, M. Velikay, A. Wedrich, U. Stolba, P. Datlinger, Die klinische Anwendung flüssiger Perfluorcarbone in der Netzhautchirurgie, *Spektrum Augenheilkund.* 6 (1992) 4–7.
- [12] D. Williams, Revisiting the definition of biocompatibility, *Med. Device Technol.* 14 (2003) 10–13.
- [13] ISO 10993 standards for evaluating biocompatibility, ISO 10993-5, *Biological evaluation of medical devices—Part 5: Tests for cytotoxicity: in vitro methods.*
- [14] L.C. Clark, Methods of treating disorders of the eye with liquid perfluorocarbons, US Patent No. 4,490351, (1984).
- [15] S.J. Haidt, Extraocular method of treating the eye with liquid perfluorocarbons, US Patent No. 4,452818, (1984).
- [16] G.A. Peyman, J.A. Schulman, B. Sullivan, Perfluorocarbon liquids in ophthalmology, *Surv. Ophthalmol.* 39 (1995) 375–395.
- [17] ISO 14971, *Medical device risk management.*

- [18] M. Velikay, U. Stolba, A. Wedrich, Y. Li, P. Datlinger, S. Binder, The effect of chemical stability and purification of perfluorocarbon liquids in experimental extended-term vitreous substitutes, *Graefes Arch. Clin. Exp. Ophthalmol.* 233 (1995) 26–30.
- [19] L.L. Gervits, Perfluorocarbon-based blood substitutes: Russian experience, *Fluorine in medicine in the 21st Century*, Paper 22, Manchester (UK), (1994).
- [20] H. Meinert, Method of purifying perfluorocarbons, and use of the perfluorocarbons thus purified, US Patent No. 5,563,306, (1996).
- [21] S. Chang, J.R. Sparrow, T. Iwamoto, A. Gershbein, R. Ross, R. Ortiz, Experimental studies of tolerance to intravitreal perfluoro-n-octane liquid, *Retina* 11 (1991) 367–374.
- [22] M. Nabih, G.A. Peyman, L.C. Clarc, Experimental evaluation of perfluorophenanthrene as high specific gravity vitreous substitute: A preliminary report, *Ophthalmic Surg.* 20 (1989) 286–293.
- [23] H. Meinert, Semifluorierte Alkane und ihre Verwendung, Patent Nr. DE 19536504 A1; PCT/EP96/03542, (1995).
- [24] I. Lattes, B. Feurer, B. Guidetti, V. Payrou, Fluorinated organic compounds, ophthalmological applications thereof and method for making same, US Patent No. 6,040,485, (2000).
- [25] D.H. Menz, Fluorierte Alkane und ihre Verwendung, Patent Nr. DE 197 19 280, (1997).
- [26] H. Meinert, T. Roy, Semifluorinated alkanes—a new class of compounds with outstanding properties for use in ophthalmology, *Eur. J. Ophthalmol.* 10 (2000) 189–197.
- [27] M. Napoli, Diblock and triblock semifluorinated n-alkanes: Preparations, structural aspects and applications, *J. Fluorine Chem.* 79 (1996) 59–69.
- [28] H. Hoerauf, Flüssige Hydrofluorkarbonate als Netzhauttamponade und intraoperative Hilfsmittel in der Glaskörperchirurgie—Experimentelle Befunde und klinische Anwendung, *Habilitationsschrift Lübeck* (2003).
- [29] J. Roider, H. Hoerauf, K. Kobuch, V.P. Gabel, Clinical findings on the use of long-term heavy tamponades (semifluorinated alkanes and their oligomers) in complicated retinal detachment surgery, *Graefes Arch. Clin. Exp. Ophthalmol.* 240 (2002) 965–971.
- [30] B. Kirchhof, N. Sorgente, Pathogenesis of proliferative vitreoretinopathy. Modulation of retinal pigment epithelial cell functions by vitreous and macrophages. *Dev. Ophthalmol.* 16 (1989) 1–53.
- [31] M. Doi, M.F. Refojo, Histopathology of rabbit eyes with silicone-fluorosilicone copolymer oil as six months internal retinal tamponade, *Exp. Eye Res.* 61 (1995) 469–478.
- [32] K. Nakamura, M.F. Refojo, D.V. Crabtree, F.L. Leang, Analysis and fractionation of silicone and fluorosilicone oils for intraocular use, *Invest. Ophthalmol. Vis. Sci.* 31 (1990) 2059–2069.
- [33] (a) S. Wolf, V. Schön, P. Meier, P. Wiedemann, Schweres Silikonöl als Endotamponade bei komplizierter Netzhautablösung, *Ophthalmologie* 104(Suppl. 1) (2000) 45.
(b) S. Wolf, V. Schön, P. Meier, P. Wiedemann, Silicone Oil-RMN3 mixture ("Heavy Silicone Oil") as internal tamponade for complicated retinal detachment, *Retina* 23 (Suppl. 3) (2003) 335.
- [34] D. Wong, J.C. Van Meurs, T. Stappler, C. Groenewald, I.A. Pearce, J.N. McGalliard, E. Manousakis, E.N. Herbert, A pilot study on the use of a perfluorohexyloctane/silicone oil solution as a heavier than water internal tamponade agent, *Br. J. Ophthalmol.* 89 (2005) 662–665.
- [35] M. Winter, S. Behrendt, D.H. Menz, G. Pfister, Retinale Druckbelastung durch Perfluorodekalin, *Ophthalmologie* 103(Suppl. 1) (1999) 421.
- [36] V.P. Gabel, K. Kobuch, H. Hoerauf, D.H. Menz, J. Dresch, H. Laqua, Specific gravity, the cause of retinal damage induced by perfluorocarbon liquids ? *Invest. Ophthalmol. Vis. Sci.* 41(Suppl.) (2000) 662.
- [37] M.F. Costa Gomes, J. Deschamps, D.-H. Menz, Solubility of dioxygen in seven fluorinated liquids, *J. Fluorine Chem.* 125 (2004) 1325–1329.
- [38] K. Kobuch, B. Fuchs, A. Tomi, J. Roider, V.P. Gabel, The influence of O₂ and Co₂ concentrations in perfluorocarbon liquids as vitreous substitute on the retinal perfusion, *IOVS abstract book* 40 (1999) 4052.

- [39] B. Fuchs, Der Einfluß von verschiedenen synthetischen Glaskörperersatzstoffen auf den intravitrealen Sauerstoffpartialdruck, Inaugural Dissertation, (2003) Regensburg.
- [40] D.H. Menz, Side effects of ocular endotamponades caused by surface behaviors of fluorocarbons, *Poster presentation 14th European Symposium on Fluorine Chemistry, Poznan, Pologne*, 11–16 juillet, (2004).
- [41] M. Winter, C. Winter, B. Wiechens, Quantification of intraocular retained perfluorodecaline after macroscopic removal, *Graefes Arch. Clin. Exp. Ophthalmol.* 237 (1999) 153–156.
- [42] D. Wong, R.L. Williams, M.J. German, Exchange of perfluorodecalin for gas or oil: A model for avoiding slippage, *Graefes Arch. Clin. Exp. Ophthalmol.* 236 (1998) 234–237.
- [43] U. Groß, D.H. Menz, K. Kobuch, H. Hoerauf, Verwendung eines hochfluorierten oligomeren Alkans in der Ophthalmologie, Patent Nr. DE 19926890. (2000) 8–41.
- [44] K. Kobuch, D.H. Menz, H. Hoerauf, J.H. Dresch, V.P. Gabel, New substances for intraocular tamponades: Perfluorocarbon liquids, hydrofluorocarbon liquids and hydro-fluorocarbon-oligomers in vitreoretinal surgery, *Graefes Arch. Clin. Exp. Ophthalmol.* 239 (2001) 635–642.
- [45] K. Kobuch, D.H. Menz, V.P. Gabel, in: G.K. Kriegelstein (Ed.), *Retinologie heute*, München, Ad. manum medici (publ.). 2000, pp. 98–104.
- [46] M. Winter, W. Eberhardt, C. Scholz, A. Reichenbach, Failure of potassium siphoning by Müller cells: A new hypothesis of perfluorocarbon liquid induced retinopathy, *Invest. Ophthalmol. Vis. Sci.* 41 (2000) 256–261.
- [47] M. Winter, C. Eckardt, B. Havsteen, Vitreous changes after contact with high-density substances: an *in vitro* experiment, *Ger. J. Ophthalmol.* 1(1992)268A.
- [48] N. Schrage, J. Becker, White precipitation after F₆H₈ endotamponade. ESEM and EDXA analysis, Presented at the *First Meeting on Heavy Tamponades*, Telfs, (2003).
- [49] F. Malchiodi-Albedi, A. Matteucci, G. Formisano, S. Paradisi, G. Carnovale-Scalzo, G. Scorgia, H. Hoerauf, Induction of apoptosis in rat retinal cell cultures by partially fluorinated alkanes, *Am. J. Ophthalmol.* 139 (2005) 737–739.
- [50] B. Kirchhof, Fluorkarbonate in der Netzhaut-Glaskörperchirurgie, *Ophthalmol. Chirurgie* 11 (1999) 153–158.
- [51] D.H. Menz, J.H. Dresch, Plastically deformable implant, PCT/EPOO/05208, Appl. No. 2,377,155, (2000).
- [52] M.P. Krafft, J.G. Riess, Stabile hochkonzentrierte Fluorkohlenwasserstoffgele, *Angew. Chem.* 106 (1994) 1146–1147.
- [53] H. Hoerauf, D.H. Menz, J. Dresch, H. John, R. Moll, H. Laqua, Modification of vitreous serum albumin by hydrofluorocarbons as a cause of severe inflammatory reaction, Lecture at the *First Meeting on heavy tamponades*, Telfs, (2003).
- [54] H. Hoerauf, K. Kobuch, J. Dresch, D.H. Menz, Combined use of partially fluorinated alkanes, perfluorocarbon liquids and silicone oil—an experimental study, *Graefes Arch. Clin. Exp. Ophthalmol.* 239 (2001) 373–381.

Note from the Editors

For the use of perfluorocarbon molecules for ophthalmologic applications, see also in this volume the chapter by I. Rico-Lattes *et al.*

This page intentionally left blank

CHAPTER 11

Perfluorochemical-Based Oxygen Therapeutics, Contrast Agents, and Beyond

Marie Pierre Krafft,^{1,*} and Jean G. Riess²

¹*Systèmes Organisés Fluorés à Finalité Thérapeutique, Institut Charles Sadron,
6 rue Boussingault, 67000 Strasbourg, France*

²*MRI Institute, University of California, 410 Dickinson Street, San Diego, CA 92103, USA*

Contents

1. Introduction	448
1.1. Brief reminder of basic properties of perfluorocarbons relevant to biomedical uses	448
1.2. Perfluorocarbons: biocompatibility and environmental issues	451
2. Oxygen Transport to Tissues	452
2.1. Challenges in the development of a PFC-based oxygen carrier	454
2.2. Product development status	455
2.3. Prospects	458
3. Improving Diagnosis	460
3.1. Development of micron-size injectable gas bubbles as contrast agents for improved us imaging	462
3.1.1. The challenges: stabilizing microbubbles	462
3.1.2. Osmotic stabilization of micron-size bubbles using a perfluorochemical	463
3.1.3. Products and status	465
3.1.4. Prospects	465
3.2. Targeted particles for molecular imaging using US and magnetic resonance	466
3.3. Further potential uses of perfluorocarbons in diagnosis	469
4. Perfluorocarbons as Drugs and Drug Delivery Systems	469
4.1. Lung ventilation	469
4.2. Lung-surfactant replacement	470
4.3. Miscellaneous therapeutic innovations	471
4.4. Drug and gene delivery	471
5. Surgical Aids	472
6. Research Tools for the Life Sciences	474
6.1. Abiotic tags for controlled recognition, selection, and pairing of biopolymers	474
6.2. "Abiotic" environments—"super-nonpolar" fluoruous compartments for segregation and confinement	476
6.3. Tools for nanogram-scale bioassays and protein crystallization	478

*Corresponding author. Tel.: +33-3-88-41-40-60; Fax: +33-3-88-41-40-99;
Email: krafft@ics.u-strasbg.fr

7. Conclusions and Perspectives	479
References	481
Note from the Editors	486

Abstract

Perfluorocarbons display outstanding chemical and biological inertness, and intense hydrophobic and lipophobic effects. The latter effects provide a powerful, yet labile, noncovalent binding interaction that can promote selective self-assembly. Perfluoro compounds do not mimic nature, yet they can offer abiotic building blocks for the *de novo* design of functional biopolymers. They offer new tags useful for molecular recognition, selective sorting, and templated binding (e.g., selective peptide and nucleic acid pairing). They also stabilize membranes and provide micro- and nanocompartimented fluoruous environments. Perfluorocarbons provide inert, apolar carrier fluids for lab-on-a-chip experiments and assays using microfluidic technologies. Low water solubility, combined with high vapor pressure, allows stabilization of injectable microbubbles that serve as contrast agents for diagnostic ultrasound (US) imaging. Several such agents are commercially available. High gas solubilities are the basis for an abiotic means for intravascular oxygen delivery. A fluorocarbon emulsion that is intended for preventing organ ischemia during surgery and as a blood substitute is in advanced clinical trials. Other biomedical applications of fluorocarbons include lung-surfactant replacement and ophthalmologic aids. Diverse colloids with fluorocarbon phases and/or shells are being investigated for molecular imaging using US or magnetic resonance, and for targeted drug delivery. Highly fluorinated polymers provide a range of inert materials (e.g., fluorosilicons, expanded polytetrafluoroethylene) for contact lenses, reconstructive surgery (e.g., vascular grafts) and other devices.

1. INTRODUCTION

This chapter intends to briefly overview, for each of the major areas of uses of perfluorochemicals (PFCs) in medicine, biology, and biochemistry, the medical needs and therapeutic objectives; the challenges facing product definition and development; the solutions and products that are or could be provided by PFC-based materials; as well as some present research trends and perspectives. The increasing number of pharmaceuticals and agrochemicals that contain individual fluorine atoms or trifluoromethyl groups is out of the scope of this chapter [1,2].

Detailed information, background reviews, or highlights from the authors about the specific properties of PFCs and fluorinated colloids in relation to biomedical applications can be found in Refs. [3–9]. These papers also provide insight into the surface properties of PFCs, their hydrophobic and lipophobic characters, self-aggregation properties, tendency to stabilize interfaces, and ability to promote nanocompartmentation in self-assembled systems.

1.1. Brief reminder of basic properties of perfluorocarbons relevant to biomedical uses

Perfluorocarbons exhibit a range of specific attributes and combinations of attributes that make them unique [4]. Several of them are of interest in life sciences

and medicine [5]. The most important common basis for the biomedical uses of PFCs is certainly their outstanding chemical and biological inertness. One reason for this inertness arises from the strength of the C–F and skeletal C–C bonds and from the repulsive dense electron coating that protects perfluoroalkyl chains (*F*-chains, C_nF_{2n+1} ; the italicized prefixal symbol *F*- conventionally stands for *perfluoro*)¹. Another reason derives from their pronounced hydro- and lipophobia, which promote segregation of PFC material and prevent *F*-chains from meddling with other material. PFCs are also characterized by a unique and extreme contrast between the strength of their *intramolecular* C–C and C–F bonds and the weakness of their *intermolecular* interactions. The low polarizability of the fluorine atom results indeed into low van der Waals forces. Consequently, liquid PFCs display very low intermolecular cohesiveness, a feature they share with gases. Low cohesiveness is reflected by the highest vapor pressures (relative to molecular weight), lowest surface tensions and lowest water solubilities of all liquids, and an exceptional propensity for liquid PFCs to dissolve gases. Concurrently, higher *F*-chain rigidity translates into higher melting points than for the corresponding hydrocarbon compounds, resulting in a narrower liquid phase domain. *F*-chains are also more bulky than alkyl chains, with cross-sections of 30 and 20 Å, respectively, and their conformational freedom is strongly reduced.

Because of the powerful noncovalent and reversible “super-hydrophobic” effects that *F*-chains engender, which are accompanied by substantial lipophobic effects as well, they tend to segregate and self-assemble into well-organized films, membranes, vesicles, and other stable and often nanocompartimented supramolecular constructs. These effects enrich the toolbox of the chemist dealing with fluorinated colloids and interfaces [10] or developing supramolecular constructs and practicing complex constitutional dynamic chemistry [11]. They also provide an abiotic implement to biochemists seeking alternatives to natural (Watson and Crick) hydrogen bonding for nucleic acid pairing or selective protein interactions [9]. In this respect, it is noteworthy that fluorine appears to display little capacity to act as a hydrogen bond acceptor. On the other hand, a strong “halogen” bonding force between halo-PFCs and diverse electron-donor atoms has led to extensive self-associated arrays of hybrid PFC and hydrocarbon derivatives, and could play a role in recognition processes [12].

Reversible temperature-dependent partitioning of PFC-tagged molecules between a PFC phase and an organic solvent is the basis for “fluorous” synthesis, catalysis, and separation technologies [13,14]. These technologies are now being extensively applied to biologically important molecules.

It should be emphasized that it is the *combination* of biological inertness and unmatched gas-dissolving capacity of PFCs that creates the potential for an injectable oxygen carrier. Likewise, it is the combination of their inertness and

¹ The IUPAC-authorized italicized prefixal symbol *F* conveys the sense of perfluoro (e.g., *F*-alkyl = perfluoroalkyl = C_nF_{2n+1}). By extension, the symbol *F*- will be used to designate entities (*F*-chains, *F*-compounds, *F*-amphiphiles, *F*-colloids) that comprise a highly fluorinated moiety or phase.

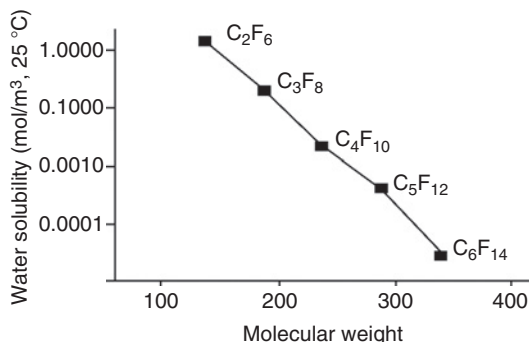


Fig. 1. Solubility of perfluorochemicals (PFCs) in water decreases rapidly with increasing molecular weight. The solubility of *F*-octyl bromide used in injectable oxygen carriers is 5×10^{-9} mol/l.

of their extremely low solubility in water (Fig. 1) that allows stabilization of the micron-size gas bubbles used in contrast US imaging.

Further specific properties of PFCs or PFC-enhanced properties that participate to their biomedical potential include the very high specific gravity of liquid PFCs; their high fluidity, compressibility, and low spreading coefficient; high contact angle with water, translating into low friction materials; their refractivity index and magnetic susceptibility close to that of water, the absence of protons, and the abundance of ^{19}F nuclei that provides a valuable, sensitive nuclear magnetic resonance probe.

PFCs for biomedical uses should be pure and well defined. PFCs can be synthesized industrially by substitution of hydrogen atoms by fluorine atoms in an organic compound using electrochemical fluorination, reaction with heavy metal fluorides, or direct action of molecular difluorine. If not properly controlled, these highly exothermal processes tend, however, to yield complex, often ill-defined mixtures. Alternately, PFCs can be obtained by assembling small building blocks that are already fluorinated. Telomerization of tetrafluoroethylene provides very pure materials, as separation of successive terms of a homologous series of *F*-compounds is straightforward. Among the PFCs most investigated for biomedical applications, one can list *F*-propane, *F*-butane, *F*-hexane, *F*-decalin, *F*-octyl bromide, *F*-1,8-dichlorooctane, as well as various fluorinated polymers such as expanded polytetrafluoroethylene (ePTFE). Semi-fluorinated diblock compounds [(*F*-alkyl)alkanes, $\text{C}_n\text{F}_{2n+1}\text{C}_m\text{H}_{2m+1}$], constitute further valuable components for the engineering of fluorinated colloidal systems. Their biological inertness and the *in vivo* behavior appears to be similar to that of PFCs, while their amphiphilic character enables them to self-assemble and participate to organized supramolecular and colloidal systems. A range of *F*-alkylated surfactants, with a large variety of polar head groups, has also been synthesized [15]. In terms of surface activity, *F*-surfactants are both more effective and more efficient than their hydrogenated counterparts. Small amounts of such materials

allow reducing surface tensions to values that cannot be attained otherwise. Numerous reagents have been developed for tagging molecules with *F*-alkyl chains, some of which are now commercially available [14].

1.2. Perfluorocarbons: biocompatibility and environmental issues

The exceptional biological inertness of PFCs is well established. It is illustrated by the fact that liter-size doses of *F*-octyl bromide, $C_8F_{17}Br$, can be ingested to serve as a contrast agent for bowel wall delineation by magnetic resonance imaging (MRI) (Fig. 2a) [16]. Likewise, clinical research on liquid ventilation, involving the instillation of the same material in the lungs in liter-size doses, uncovered no serious untoward effects (Fig. 2b) [17]. As yet, hundred of thousands of patients have received PFC-based US contrast agents, with only few minor side effects. Also noteworthy is that the standard PFCs are not metabolized. When administered parenterally, in the form of an emulsion or a dispersion of microbubbles, PFCs are excreted unchanged in the expired air.

Yet, a note of caution is here appropriate concerning possible environmental issues that may be associated with the use of *F*-compounds. Ideally, microorganisms should be discovered or developed that would digest PFCs into harmless metabolites. However, our understanding of the biochemistry of the C–F bond is still rudimentary and only concerns isolated C–F bonds. Alternatively, recovery or sequestration of used PFCs could be envisaged. Meanwhile, only low tonnage medical applications, as is the case for essentially all the products presently commercialized or under development, seem sustainable. The environment protection agencies appear, at this time, to consider that the risk associated with these products, in the required amounts, is insignificant.

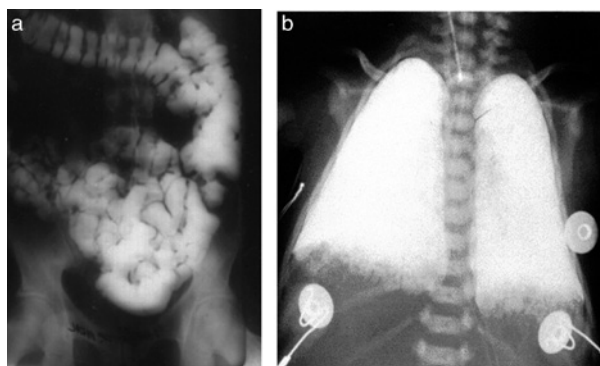


Fig. 2. (a) X-ray image of the bowels of an adult patient filled with *F*-octyl bromide (the bromine atom makes the compound radioopaque, hence clear on the radiograph). Courtesy Alliance Pharmaceutical Corporation (b) Lungs of an infant patient filled with the same material. From Ref. [17], with permission.

Fluorinated surfactants pose different problems: the bioaccumulation and toxicity of some of them, including *F*-alkyl acids such as *F*-decanoic acid, or of their metabolites, are well documented [18]. In other cases, including *F*-alkylated phospholipids, acute toxicity appears to be very low, but prolonged retention in the organism (which increases rapidly when the *F*-chain exceeds eight carbon atoms) may limit the length of the *F*-chain used or the dose administered or the frequency of their use [19]. Some components that may be acceptable for occasional use, for example, perioperatively, may not be tolerable for chronic daily use (e.g., delivery of antiasthma drugs through metered-dose inhalers), when the rate of accumulation exceeds the rate of excretion.

2. OXYGEN TRANSPORT TO TISSUES

Development of a "blood substitute" was initially aimed at providing an alternative to allogeneic (donor) blood banking and transfusion. The emergence of AIDS provided momentums to such research. Considerable advances in blood safety progressively led to defining new therapeutic indications for an oxygen carrier, different from those of red blood cells, for which oxygen delivery to tissues is needed. Several substantial problems continue, however, to plague banked blood. Concerns have shifted from safety to availability. Blood shortages are, in many countries, a matter of concern. Alternatives based on autologous blood harvesting and use have not succeeded in resolving this issue. Practice of predonation or acute normovolemic hemodilution (ANH) is actually regressing. Further open questions concern the effects of allogeneic blood on the immune system. Delivering oxygen to tissues and organs at risk of hypoxia thus remains as an important unsatisfied need [20].

The mechanisms that underlie *in vivo* oxygen transport and delivery by PFCs and by hemoglobin (Hb) are widely different (Fig. 3). In the case of Hb, a strong, localized chemical coordination bond is established between the dioxygen molecule and the iron atom of a heme. Successive binding of four O₂ molecules to the four hemes present in each Hb molecule is cooperative and saturation occurs when all four iron atoms are coordinated. Hence, the sigmoid shape of the O₂ uptake curve (Fig. 3, curve d). In the case of PFCs, there is a simple physical dissolution of O₂, characterized by loose, nondirectional van der Waals interactions among like materials. Indeed, liquid PFCs and gases both have very low cohesive energy densities, as expressed by close Hildebrandt coefficients. O₂ dissolution follows Henry's law, that is, is linearly dependent upon O₂ partial pressure (Fig. 3, line c). Because PFCs are not miscible with water, PFCs for *in vivo* O₂ delivery are administered in the form of emulsions. Figure 3 shows that in order to achieve full benefit of PFC emulsion administration, the patient should breathe pure or close-to-pure oxygen. O₂ release to tissues can then reach 90% of emulsion content [20].

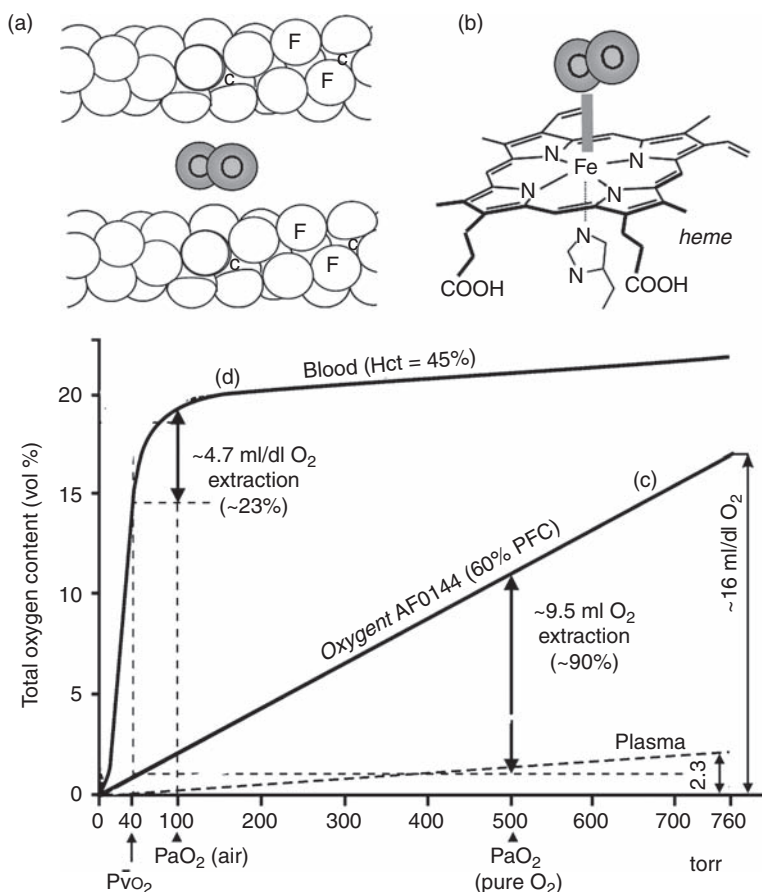


Fig. 3. Oxygen transport by perfluorocarbons versus hemoglobin (Hb): (a) In the case of PFCs, O₂ dissolution is characterized by loose, nondirectional van der Waals interactions. Oxygen solubility follows Henry's law, that is, is directly proportional to the gas's partial pressure (curve c). (b) In the case of Hb, a strong, localized chemical bond is established with the iron atom of a heme. Successive binding of four O₂ molecules to the four hemes of Hb is cooperative, and saturation occurs when all four iron atoms are bound. Hence, the sigmoid shape of the O₂ uptake curve, which levels off when the partial pressure of O₂ on earth is attained (curve d) [20].

The fact that no satisfactory oxygen carrier has reached commercialization after over half a century of intensive research, first on hemoglobin-based oxygen carriers and subsequently also on PFC-based products, attests that the challenges were more formidable than anticipated. This chapter will consider only the PFC approach. Since this approach has recently been reviewed extensively by the authors [8,20–22], it will be limited to a brief overview of the challenges, solutions, present state of clinical evaluation, and most recent developments.

2.1. Challenges in the development of a PFC-based oxygen carrier

The challenges encountered when developing a PFC-based oxygen carrier are very different from those of the hemoglobin-based products. They concern both the PFC itself and its formulation into a stable, biocompatible emulsion, allowing intravascular administration.

Defining the selection criteria for an adequate PFC candidate was a lengthy process. Eventually, it was recognized that the optimal PFC needed to be well defined and pure, manufacturable in large tonnages at a reasonable cost, amenable to producing stable submicron-size emulsions and be excreted from the body within a matter of days. While increased molecular weight promotes emulsion stability by decreasing water solubility, it also increases organ retention time exponentially. The latter could be mitigated by selecting a slightly lipophilic PFC. Excretion is indeed dependent on solubility of the PFC in the blood lipoproteins that carry the PFC to the lungs for exhalation. The desired lipophilic touch can be obtained by introducing one or two heavier halogens or a hydrocarbon fragment into the PFC molecule, as in *F*-octyl bromide (PFOB, perflubron), α,ω -dichloro-*F*-octane (PFDCO), or *F*-octylethane. Eventually *F*-octyl bromide appears to meet the above listed requirements best. It can be produced in large tonnage from *F*-octyl iodide, which is the precursor of many industrial *F*-compounds (Fig. 4).

PFC emulsions for injection need to be concentrated, yet fluid, small-sized, stable and sterile, and ready for use. Stability is required for convenient long-term storage and easy transportation. Needless to say that stability is a prerequisite for safety. Achieving PFC emulsion stability constitutes a significant challenge. Reconstitution of an injectable emulsion from a frozen stem emulsion, a situation found with some early emulsions, is too inconvenient and not acceptable. Particle growth in PFC emulsions over time is primarily driven by molecular diffusion (Ostwald ripening). Counteracting this process can be achieved in various ways, the most commonly used being to reduce the solubility of the dispersed PFC

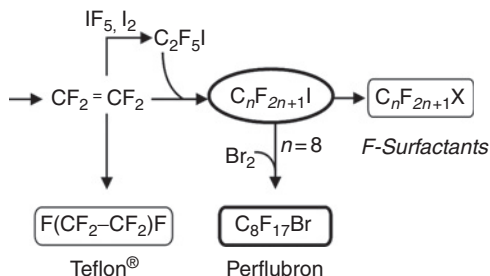


Fig. 4. Synthesis of *F*-octyl bromide by bromination of *F*-octyl iodide produced by telomerization of tetrafluoroethylene, the monomer of Teflon[®]. *F*-octyl iodide is the precursor of numerous fluorosurfactants.

phase in water by adding a secondary, less soluble, higher molecular weight PFC [20].

The emulsifier needs to provide a very low PFC/water interfacial tension, be biocompatible and preferably listed among those already well accepted in pharmaceuticals. The emulsions currently under development all use egg yolk phospholipids (EYP) for this purpose, an emulsifier that has been employed for over 30 years to manufacture the fat emulsions used for parenteral nutrition and, more recently, to produce liposomes and drug-carrying emulsions. PFC emulsions are terminally heat-sterilized, preferably in a rotary sterilizer that ensures homogeneous heat distribution. The emulsion needs also to be small-sized, below 200 nm, and narrowly distributed. Inadequate droplet size or coating can cause macrophage activation that translates into fever and other flu-like symptoms. Although it implements existing parenteral emulsion-production technology, manufacture of stable, small-sized, sterile PFC emulsions has required development of specific know-how [23].

The pharmacokinetics of PFCs can be roughly described by two key parameters, namely, PFC half-life in the circulation ($t_{1/2}$) and in the organs of the reticuloendothelial system (RES) ($T_{1/2}$). PFC emulsion droplets, when injected into the vasculature, are opsonized and progressively phagocytized by circulating monocytes and macrophages from the RES, and cleared from the bloodstream. These initial steps are responsible for the limited intravascular persistence, $t_{1/2}$, of the PFC. PFCs are then temporarily stored in the organs of the RES, primarily the liver, spleen, and bone marrow, with an average organ persistence $T_{1/2}$. They eventually diffuse across cell membranes back into the blood vessels, where they are taken up by lipid carriers and delivered to the lungs for excretion. The circulatory half-life of PFCs is dependent on emulsion droplet characteristics (size and coating), dose (Fig. 5), and species. For the *Oxygent*TM emulsion described below, $t_{1/2}$ is on the order of 12 h for a 2.7 g/kg body weight dose in humans. On the other hand, $T_{1/2}$ depends primarily on PFC characteristics (primarily lipophilicity) and dose, and increases exponentially with molecular weight. For *F*-octyl bromide, $T_{1/2}$ is about 4 days when used at the above dose.

Further issues concern the design of appropriate protocols for evaluation of efficacy of a “blood substitute” so different from blood, the definition of indications, and conditions of use that benefit PFC emulsions and provide maximum benefit for the patient. The latter issues depend largely on our understanding of the *in vivo* behavior of PFCs and PFC emulsions.

2.2. Product development status

The first commercially developed PFC emulsion, *Fluosol*, consisted of a mixture of *F*-decalin and *F*-tripropylamine emulsified with Pluronic F-68 [a poly(oxyethylene) poly(oxypropylene) block co-polymer] as the main surfactant. It gained

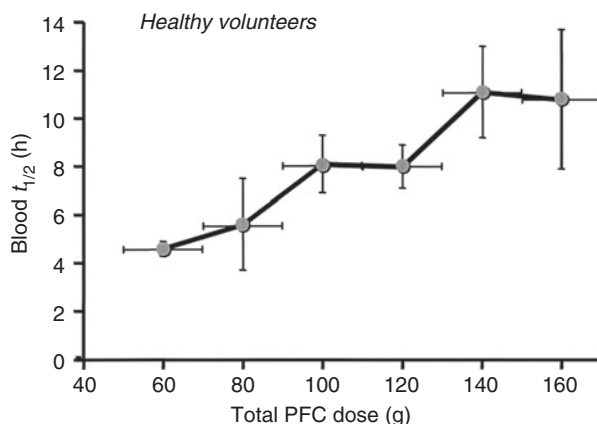


Fig. 5. Intravascular half-life $t_{1/2}$ of an emulsion of *F*-octyl bromide (*Oxygent* AF0144) in humans as a function of dose administered.

approval from the U.S. Food and Drug Administration as a means of providing oxygen to the heart muscle during transluminal coronary angioplasty. *Fluosol* failed to achieve commercial success because of the development of autoperfusion catheters and also because of the lack of user friendliness due to a lengthy and cumbersome reconstitution procedure [20]. *Fluosol* came indeed as a frozen emulsion concentrate that had to be thawed and mixed with two annex solutions prior to administration; it then had to be used within a few hours. Perftoran, a mixture of *F*-decalin and *F*-[*N*-(4-methylcyclohexyl)piperidine], emulsified with a Pluronic F-68-type poloxamer, was licensed in Russia [24,25]. Development of *Oxyfluor*, an α,ω -dichloro-*F*-octane/EYP/saffoil emulsion, was abandoned, possibly because of insufficient emulsion stability.

The most advanced injectable O_2 -carrier under development, *Oxygent*, consists of a 60% w/v concentrated submicronic emulsion of *F*-octyl bromide with a small percentage of *F*-decyl bromide added [8,20]. Selection of *F*-octyl bromide as the primary PFC has resulted from a compromise between adequate emulsion stability and acceptable excretion rate. The terminal bromine atom of *F*-octyl bromide is the lipophilic element needed in order to mitigate the organ retention of the PFC. The less water-soluble added *F*-decyl bromide stabilizes the emulsion by reducing the rate of molecular diffusion. Here again, the lipophilic bromine termination augments the excretion rate. Commonly used EYP provide an effective emulsifier. The emulsion is terminally heat-sterilized, can be stored for 2 years under standard refrigeration conditions, and is ready for use.

Safety and effective O_2 delivery has been established for *Oxygent* in numerous animal models. Figure 6 shows, for example, the effect of the emulsion in a canine model mimicking surgical blood loss. Mixed venous O_2 tension, Po_2 (the O_2 tension after tissues and organs have been irrigated; y-axis) reflects

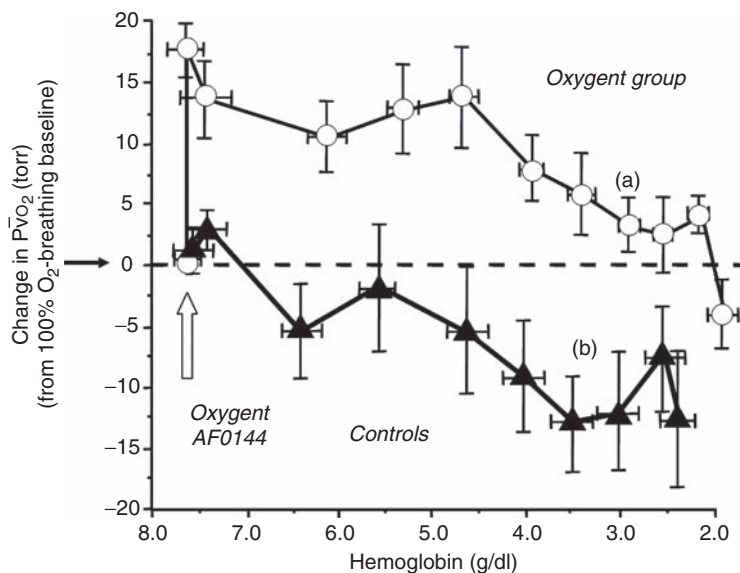


Fig. 6. Efficacy of the perfluorocarbon emulsion *Oxygent* AF0144 in a canine model mimicking surgical blood loss after acute normovolemic hemodilution (ANH). Both the test group and the control group animals were hemodiluted (Hb brought down from ca. 14 to ca. 8 g/dl), breathed oxygen, and lost blood, hence Hb (x-axis), in a controlled manner. Mixed venous O₂ tension (PvO₂, the O₂ tension after tissues and organs have been irrigated; y-axis) reflects the adequacy of tissue oxygenation. The difference in tissue oxygenation between treatment (a) and control groups (b) is significant. The perfluorochemical (PFC)-treated dogs (1.35 g of PFC per kilogram body weight in this experiment) still benefit from adequate tissue oxygenation at Hb levels one-fifth of normal. From Ref. [105], with permission.

the adequacy of tissue oxygenation. The difference in tissue oxygenation between the treated animals and the control animals is significant. In humans, a total of 20 different clinical trials have been performed to evaluate the safety and efficacy of the emulsion. These trials have enrolled close to 1500 subjects (of which over 800 have received *Oxygent*, the control patients receiving a saline solution). They consisted of Phase I, II, and III studies that have included healthy volunteers, cancer patients, general surgery patients, and cardiac surgery patients. In general, the safety profiles from these trials were considered acceptable for further clinical development of the product [26]. These clinical studies have also demonstrated the efficacy of *Oxygent* in terms of drug activity (i.e., ability to deliver oxygen and reverse physiological transfusion triggers). Use of the emulsion in a Phase III clinical trial conducted in general surgery patients undergoing ANH led to statistically significant avoidance and reduction of transfusion of banked blood (Fig. 7) [27]. *Oxygent* also enabled surgical patients to be physiologically stable and well oxygenated at substantially lower intraoperative Hb levels than the control patients. No significant side effects were reported

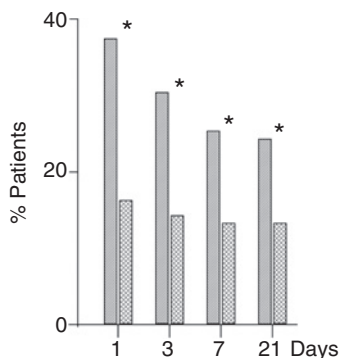


Fig. 7. Percentage of surgical patients avoiding donor blood transfusion in the protocol-defined target population (blood loss ≥ 20 ml per kilogram body weight) from postoperative day 1 through day 21 (or hospital discharge). First bar is the *Oxygent*-treated patients; second bar, control group (* $p < 0.05$ between groups). From Ref. [27], with permission.

as being attributable to the emulsion. The clinical data indicated that a dose of *Oxygent* of 2.7 g of PFC per kilogram body weight was equivalent to about 4 g/dl of Hb [28].

Subsequently, a second Phase III trial in cardiac surgery patients undergoing cardiopulmonary bypass (CPB), with, in addition to ANH, a second blood withdrawal procedure called intraoperative blood donation (IAD), was initiated, during which untoward neurological and bleeding events were observed. Although the overall rates of these adverse events were within clinical expectations and within the ranges reported in the literature, the rates of these events were higher in the patients who had received *Oxygent* as compared to the control group of patients, causing suspension of the trial [26]. Analysis of the clinical data indicated that the imbalance in the adverse events rates was caused by excessive hemodilution in the patients receiving *Oxygent*, meaning that the testing protocol, and not the drug, was responsible for the observed untoward effects. In parallel, extensive hemostasis and hemolysis studies investigated possible interactions between the emulsion and the circulating fluids present in the patients during CPB surgery. However, these studies found no link between the presence of *Oxygent* and the observed imbalance in adverse events. The presence of the emulsion induced no increase in viscosity or tendency for coagulation in the blood mixtures tested [22].

2.3. Prospects

Clinical development is now being initiated in Europe to decrease the incidence of postoperative organ failure. In China, development is directed toward reduction of exposure to allogeneic blood and blood sparing during surgery. A promising indication under investigation for *Oxygent* concerns the protection

of organs at risk of ischemia during surgery and, in particular, the prevention of post-op ileus (intestinal occlusion). During major surgery, the body often reacts by decreasing blood flow to intraabdominal tissues, thereby conserving O_2 supply to vital organs, such as the heart and brain. As a result, gastrointestinal organs receive less oxygen and postoperative bowel function may be impaired. Clinical evidence for intestinal mucosal protection by *Oxygent* was obtained during a Phase III study in which gastric tonometry was performed in a subset of patients at one clinical study site by looking at differences between CO_2 tensions in the arterial blood and those in the tonometer balloon (the “ CO_2 gap”). During CPB, control patients had elevated CO_2 gaps and calculated intestinal mucosal pH significantly higher than patients treated with the emulsion, in which these values were normal (Fig. 8) [29]. This benefit translated into significantly shorter postoperative time to first bowel movement and a strong trend to earlier consumption of solid food. The clinical endpoints utilized, for example, time to recovery of upper gastrointestinal function (consumption of solid food) and lower gastrointestinal function (bowel movement), have been accepted by Food and Drug Administration as approvable endpoints for other drugs. Therefore, a study has been initiated, the objective of which is to determine if *Oxygent* can reverse the gastric arterial P_{CO_2} gap, which has been shown to be predictive of postoperative morbidity and organ dysfunction.

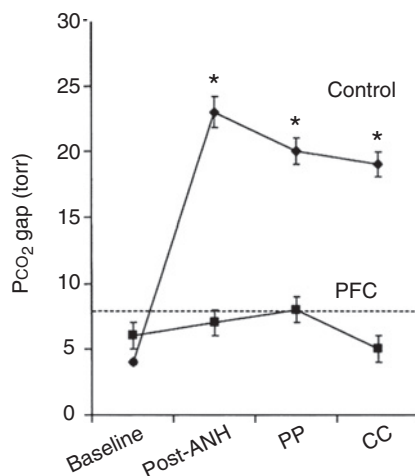


Fig. 8. Assessment of gut oxygenation status during surgery. Changes in CO_2 gap in surgical patients randomized to *Oxygent* (PFC) or placebo (controls) (ANH = acute normovolemic hemodilution; PP = post-protamine administration; CC = chest closure; * $p < 0.05$ between groups). The dashed line represents the upper limit of normal for CO_2 gap (8 torr). Postoperative recovery of gut function was determined by shorter time to first bowel movement (2 vs. 5 days; $p < 0.007$) and earlier consumption of solid food (1.8 vs. 4.1 days; $p = 0.056$). From Ref. [29], with permission.

Further applications of PFC-based oxygen carriers that are being investigated include use during CPB to reduce gaseous microemboli (the probable cause for the neurological and psychological deficits frequently observed in patients after cardiac surgery) [30]; resuscitation of hemorrhagic shock; treatment of decompression sickness; treatment of sickle cell disease; enhancement of tumor sensitivity to radiation and chemotherapy; and preservation and storage of tissues and organs [20]. Other PFC emulsion products are in early development phases, but little is published in the scientific literature about their characteristics and status [21].

Ongoing physicochemical research aims at further increasing PFC emulsion stability, controlling particle sizes, and prolonging intravascular persistence. Incorporation of fluorocarbon-hydrocarbon diblocks compounds (e.g., $C_6F_{13}C_{10}H_{21}$) in the formulation was found to increase emulsion stability considerably (Fig. 9a) and to reduce droplet size [8,20]. The diblock molecules were shown to incorporate, at least in part, into the EYP film that coats the emulsion droplets (Fig. 9d), hence to stabilize emulsions by a mechanism that is different from a simple reduction of the water solubility of the PFC phase. Evidence for such incorporation includes a dramatic decrease in PFC/water interfacial tension (typically from about 24 to 2 mN/m) between *F*-octyl bromide and aqueous phospholipids solutions upon addition of a diblock to the PFC phase (Fig. 9b) [31]. Use of a nonamphiphilic higher molecular weight stabilizer (e.g., $C_{10}F_{21}Br$) does not reduce interfacial tension (Fig. 9c). Surface tension is a critical parameter of the Lifshitz-Slyozov equation that characterizes the molecular diffusion mechanism. Such a diblock-stabilized emulsion, when used to resuscitate rabbits from severe hemorrhagic shock, increased skeletal muscle oxygen delivery without measurable deleterious effects [32].

Another approach to tissue oxygenation, which consists of administering an aqueous suspension of O_2 nanobubbles osmotically stabilized by a volatile PFC (e.g., *F*-pentane) and a fluorinated surfactant, appears promising. Experimental proof of efficacy for this system includes survival of erythrocyte-depleted rats and pigs, and of pigs with potentially lethal hemorrhagic shock and with severe right-to-left shunt [33].

3. IMPROVING DIAGNOSIS

Earlier detection, detection of smaller masses of pathologic tissue and more detailed, higher quality images are expected to lead to earlier, more accurate diagnosis and characterization of disease, reduction of time-consuming and costly downstream testing, and increased physician confidence. These elements may play a decisive role in the selection and initiation of treatment and monitoring of therapeutic progress, and hence, may improve patient outcome.

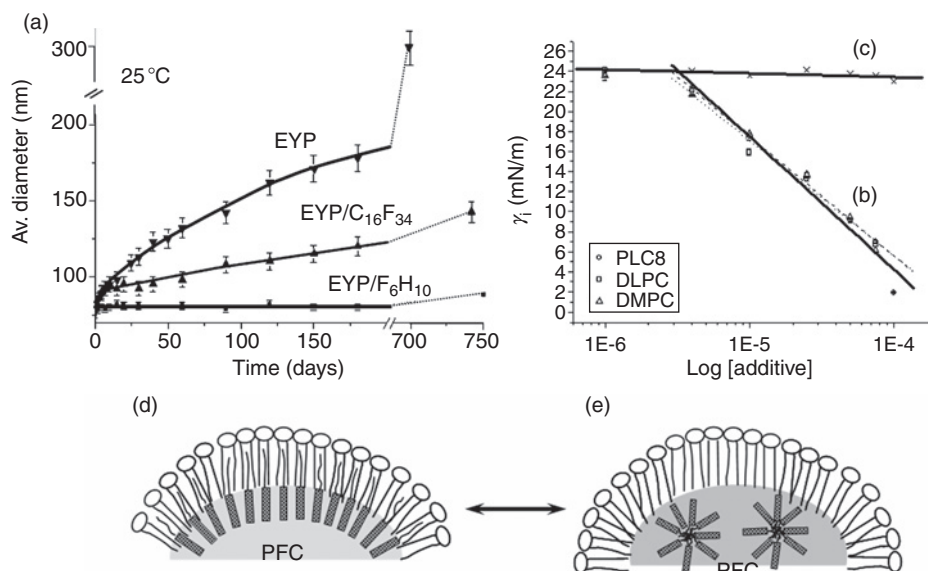


Fig. 9. Increased stability of perfluorocarbon/hydrocarbon diblock-containing emulsions. (a) Two-year aging at 25 °C of 60% w/v concentrated emulsions of perfluorooctyl bromide emulsified with 3% w/v of egg yolk phospholipids (EYP). The emulsions contained EYP only, or a combination of EYP and C₁₆F₃₄, or of EYP and F₆H₁₀ in equimolar proportions. (b) Variation of the interfacial tension (γ_i) between solutions of F₈H₁₆ in C₈F₁₇Br and solutions of phospholipids in water, as a function of the logarithm of the concentration of F₈H₁₆ in C₈F₁₇Br. The phospholipids investigated were DMPC, triangles, 1.66×10^{-11} mol/l; dilaurylphosphatidylcholine (DLPC), squares, 1.25×10^{-9} mol/l; and dioctanoylphosphatidylcholine (PLC8), circles, 3.73×10^{-5} mol/l. (c) Absence of variation of γ_i between solutions of C₁₀F₂₁Br in C₈F₁₇Br and a DMPC solution (1.66×10^{-11} mol/l). The amphiphilic diblock molecules can, *a priori*, be located in the surfactant membrane that coats the perfluorochemical (PFC) droplets (d) or could form micelles within the dispersed PFC phase (e). The above data establish that there is an effective contribution of (d).

Several imaging modalities do or could benefit from PFC-based contrast agents, primarily US imaging, but also MRI and X-ray radiography. The role of a contrast agent is to increase the signal difference between normal and pathologic tissue or structure. PFC gases have been key to the development of several commercial injectable microbubble products that serve as contrast agents for US imaging. Targeted microbubbles and emulsion droplets are being investigated for molecular characterization of disease using both US and MRI. Additionally, ¹⁹F (spin 1/2, natural abundance 100%) is the second most sensitive nuclei available for nuclear magnetic resonance investigations. PFCs can also be made opaque to X-rays by introduction of a heavy halogen (Fig. 2), as, for example, in *F*-octyl bromide. General information on US contrast agents, contrast echography, and targeted magnetic resonance can be found in Refs. [34–39].

3.1. Development of micron-size injectable gas bubbles as contrast agents for improved us imaging

Ultrasound (US) imaging (echography, echosonography) is the most widespread and most frequently used, least invasive, most portable, only bedside, and cheapest diagnostic imaging modality. It allows diagnosis of numerous pathological conditions. Yet, contrary to the other major imaging modalities, US has, until recently, not benefited from an effective contrast agent. As for any imaging technique, there are instances where contrast between normal and abnormal tissues is not strong enough to allow reliable, conclusive diagnosis. In the absence of a contrast agent, the information provided by US imaging on the cardiovascular system, blood flow, and organ perfusion can be insufficient.

The ideal contrast agent for US imaging is a highly compressible micron-size gas bubble that can be injected in the patient's circulation. Gas bubbles scatter US several orders of magnitude more effectively than blood, providing powerful echo and bright contrast.

3.1.1. The challenges: stabilizing microbubbles

The main challenge was to develop injectable micron-size gas bubbles that would last long enough in the patient's cardiovascular system to allow effective US examination. Simple micron-size air bubbles, when administered in the circulation, dissolve very rapidly in the blood under the combined action of surface tension (Laplace pressure, whose variation is reciprocal to bubble radius, and hence increases rapidly as bubble shrink), arterial pressure, oxygen metabolism, and US energy. Because they are so short-lived, these air bubbles have little utility. As several minutes are needed for an effective examination, bubbles need to survive multiple passages through the lung and heart. Substantial bubble stabilization was indispensable for effective widespread use.

Bubble-size control was also critical. The intensity of scattering by nonresonant gas bubbles is proportional to the sixth power of the radius of the bubble. Hence, the larger the bubble, the better the scattering intensity. However, the acceptable upper size limit for *in vivo* administration is determined by the need for bubbles to cross capillary beds. Bubbles larger than 6–8 μm should be avoided as they are trapped in the lung capillaries. The current accepted sizes are in 1–7 μm , preferably around 3 μm , with as narrow a size distribution as possible. Bubble shell material needs to be biodegradable. Soft shells are generally preferable, as they minimally impede US backscatter.

Other objectives were to maximize contrast between tissues and image quality, and hence efficacy, by cutting background signals. A further desirable goal is to provide dynamic information on blood flow. The ability to see blood flowing through organs as the microbubbles percolate through their vascular tree is important for the diagnostician in his assessment of pathology.

3.1.2. Osmotic stabilization of micron-size bubbles using a perfluorochemical

The properties of PFCs that are brought into play in US diagnosis applications consist, beside the biological inertness, in the unique combination of extreme hydrophobicity, which translates into very low water solubility, and high vapor pressure relative to molecular weight. In order to effectively hinder bubble dissolution in the blood, the gas inside the bubble needs to be substantially less soluble in water than in air. Perfluorochemical gases are obvious candidates for this role, as their water solubility is much lower than that of any other chemical of similar volatility. When used as the filling gas or part of the filling gas of a bubble, PFC vapor counterbalances the surface tension and blood pressure forces that push the gases inside the bubble toward dissolution. An osmotic equilibrium sets in when the rates of diffusion of the water-soluble gases in and out of the bubble are equal (Fig. 10). Bubble dissolution is then delayed very effectively, thus providing ample time for patient examination. Prominent examples of osmotic bubble-stabilizing agents include *F*-propane, *F*-butane, and *F*-pentane. The most effective ones are those that combine the lowest water solubility with the highest vapor pressure. These are represented by SF_6 , *F*-hexane, *n*- C_6F_{14} , and *F*-diglyme $\text{CF}_3(\text{OCF}_2\text{CF}_2)_2\text{OCF}_3$ [37,40,41]. The wall of the microbubbles typically consists of a 2–3-nm-thick phospholipid monolayer. Thicker walls and more rigid membranes have been made from heat-denatured albumin or a biodegradable polymer.

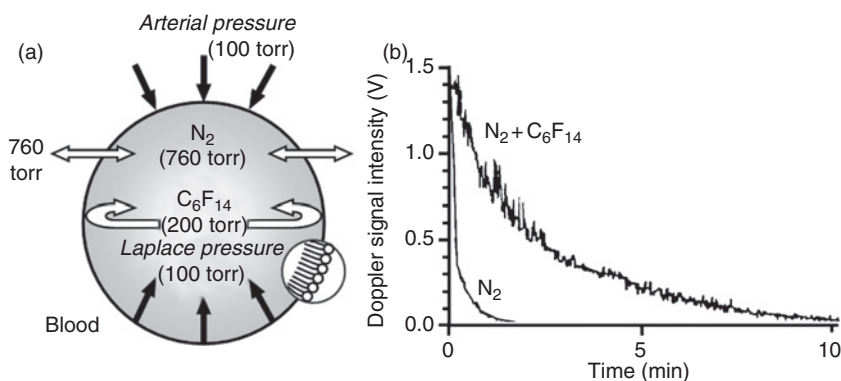


Fig. 10. Micron-size gas bubble with a phospholipid or polymeric shell membrane. (a) Stability enhancement design: Small amounts of a volatile perfluorocarbon, here *F*-hexane, C_6F_{14} , provide substantial osmotic stabilization against Laplace pressure, arterial blood pressure, and oxygen consumption; (b) decay of ultrasound (US) signal (Doppler signal intensity over time) observed in rabbits for nitrogen bubbles stabilized with *F*-hexane (dose: 1 mg/kg body weight) as compared to nitrogen alone. From Ref. [41], with permission.

Image quality and contrast improvement have been obtained by sound wave and signal manipulations. A unique feature of US contrast agents, not found with other imaging modalities, is that the microbubbles interact with the sound waves. They oscillate in the US beam, rapidly contracting and expanding, and resonate at a frequency that depends primarily on bubble size; they then become transmitters themselves. Contrary to blood and other tissues, the response of microbubbles to US is nonlinear, generating harmonic and sub-harmonic sound waves. Separation of harmonic signals from the mostly fundamental frequency backscatter signal from tissues is rather easy (Fig. 11). Use of pulse inversion techniques allows further minimization of the signal from normal tissues, providing “bubble-specific” imaging [42]. These techniques dramatically increased bubble-to-tissue contrast, even allowing the detection of single microbubbles [43].

Because gas bubbles a few microns in diameter do not normally leave the vasculature, they constitute true blood pool contrast agents, that is, agents that, when submitted to US, “light up” the blood, hence the blood vessels and the chambers of the heart. The dose of gas needed for effective contrast enhancement is very small, typically on the order of a fraction of a milliliter, dispersed within some 10^8 bubbles a few microns in diameter. The total amount of PFC administered to a patient is on the order of milligrams. This dose is minuscule when compared with the grams of contrast agents currently used in X-ray or MRI. The PFC is subsequently exhaled by the patient unchanged within minutes.

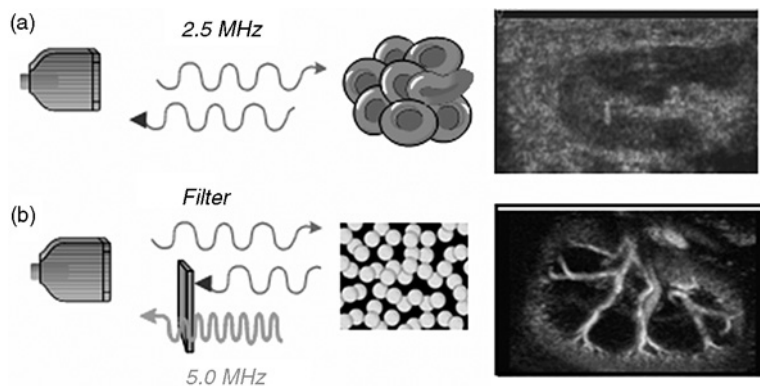


Fig. 11. Fundamental and harmonic imaging: In the fundamental imaging mode (a), a narrow-band pulse of ultrasound (US) centered at a given frequency (e.g., 2.5 MHz) is emitted; the sound reflected by the organs is used to create the image. (b) Microbubbles, because they are extremely compressible in comparison to organ tissue, not only reflect sound more efficiently than tissues but also emit harmonics. In the harmonic mode, the signal from the tissues is filtered out, leaving only the harmonics, resulting in specific imaging of the bubbles [37].

3.1.3. *Products and status*

Several PFC-based US contrast agents have become commercially available. They consist of *Optison*[®] (developed by Molecular Biosystems, Inc., San Diego, CA and commercialized by GE Healthcare, Chalfont St Giles, UK), which contains *F*-propane and has a heat-denatured human albumin shell; *Definity*[®] (developed by ImaRx Therapeutics, Tucson, AZ and Dupont Pharmaceuticals, Newark, DE and commercialized by Bristol Myers Squibb, New York, NY) also contains *F*-propane, but uses a phospholipid monolayer coating; *Sonovue*[®] (Bracco, Princeton, NJ) uses sulfur hexafluoride as the poorly water-soluble gas and has a lipid coating; and *Imagent*[®] (developed by Alliance Pharmaceutical Corp., San Diego, CA and licensed to IMCOR, Phoenix, AZ) consists of phospholipids-coated nitrogen bubbles, osmotically stabilized by a small amount of *F*-hexane. Further products and formulations under investigation include *F*-butane-exposed sonicated dextrose albumin; Acusphere's AI-700, which has a biodegradable synthetic polymer shell; BR14, a lipid-coated *F*-butane microbubble in development by Bracco; Sonazoid[®] (now part of GE Healthcare), a lipid-stabilized *F*-butane microbubble, the development of which appears to have been halted; and MP1950 (Mallinckrodt), a sonicated dispersion of *F*-butane in a micellar dispersion of phospholipids and poly(ethylene glycol) derivatives.

The fact that the microbubbles are restricted to the vascular space makes them ideal for contrast echocardiography and vascular imaging. Echocardiography is used extensively to assess ischemic heart disease. Contrast-enhanced echocardiography improves visualization of the cavities of the heart, the lumen of arteries and veins, and small vessels within solid organs and perfused tissues. Effective endocardial border delineation allows assessment of global heart function and the detection of coronary insufficiency (Fig. 12).

Vascular imaging allows determination of supply vessel occlusions, the presence of clots and wall abnormalities, such as atherosclerotic plaques and possible plaque ulceration, and, if they exist, to assess their effect on blood flow.

3.1.4. *Prospects*

Direct visualization and quantification of blood flow and tissue perfusion are now within reach. It can be achieved by intermittent imaging, in which controlled *in vivo* destruction of the microbubbles (bleaching) by a high-energy US pulse is followed by imaging with a nondestructive pulse, allowing monitoring of tissue replenishment and measurement of perfusion rates. Organ perfusion abnormalities then become detectable. In particular, accurate assessment of myocardial perfusion, hence of microvascular integrity, is key to diagnosing coronary artery disease and myocardial infarction, differentiating stunning from necrosis, quantitatively determining the area at risk of necrosis and infarct area during coronary occlusion, evaluating stenoses and the success of thrombolytic treatment, and providing guidance for patient management.

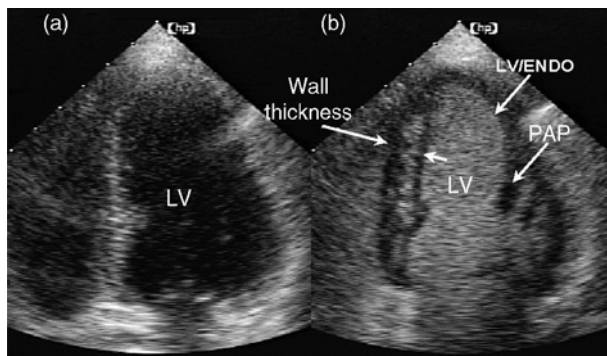


Fig. 12. Left ventricular cavity opacification: (a) View of the left ventricle (LV) of a patient without contrast agent; (b) the same view after a bolus injection of a microbubble contrast agent; the LV, endocardial border (LV/ENDO), and papillary muscle (PAP) are now precisely visualized, allowing myocardial (heart muscle) thickening to be evaluated. When watching the heart in motion, normal functioning heart muscle thickens as it contracts; abnormal functioning heart muscle moves less and does not thicken. From Ref. [106], with permission.

Further applications under investigation concern the detection and assessment of lesions and abnormalities, including tumors, in solid organs, in particular the liver, but also the kidney, spleen, prostate, and ovaries.

Meanwhile, bubble engineering is also progressing. The recent finding of a stabilization synergy between the internal PFC gas (*F*-hexane) and a fluorinated shell component [an *F*-glycerophosphatidylcholine (GPC)] led to significantly prolonged bubble persistence in an acoustic field (Fig. 13) [44]. New pulsing schemes and signal processing methods are also continuously being developed. Manipulation of bubble response to US through particle shell engineering is another facet of this effort.

3.2. Targeted particles for molecular imaging using US and magnetic resonance

Molecular imaging refers to methods that allow detection of specific molecular markers associated with a given pathology. Molecular imaging extends the basis of diagnosis from anatomic abnormalities to detection of biochemical changes. For this purpose, PFC-stabilized microbubbles, as well as PFC-emulsion droplets, are being designed that seek the molecular signature of diseased tissues (Fig. 14). These bubbles and emulsions are made detectable by US or MRI [45,46]. Because microbubbles and emulsion droplets normally do not escape the circulation, targeting is essentially restricted to pathologies that express their specific antigens within the vascular space, typically endothelial cells, leukocytes, and thrombus. Targeting of activated endothelial cells may be particularly

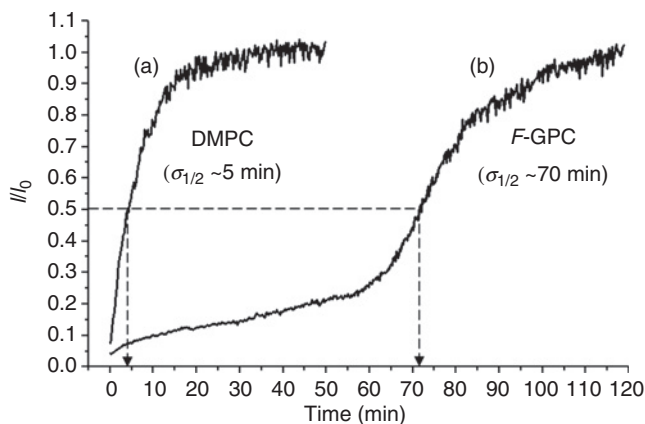


Fig. 13. Synergistic stabilization of microbubbles: Normalized variation of transmitted ultrasound (US) intensity (I/I_0) as a function of time at 25 °C for microbubbles containing *F*-hexane and stabilized (a) by DMPC and (b) by an *F*-alkylated analog of DMPC (*F*-GPC). The half-lives of the microbubbles with DMPC and with *F*-GPC shells are 5 min and 70 min, respectively. From Ref. [44].

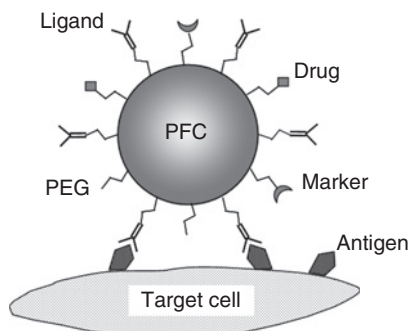


Fig. 14. Targeting of microparticles (e.g., bubbles and emulsion droplets) destined for molecular imaging and drug delivery: Schematic simultaneous binding to a microparticle of a targeting device (antigen-specific ligands), of stealth-providing elements (e.g., PEG strands), and of drugs and markers (e.g., a Gd^{3+} chelate for MRI contrast enhancement).

useful for signaling thrombi, areas of inflammation, atherosclerotic plaques, and angiogenesis in solid tumors.

Numerous strategies are being used to target particles to regions of disease [37]. Passive targeting of microbubbles relies primarily on size and shell characteristics. It allowed, for example, visualization of liver and spleen injury, including tumor metastases, as certain microbubbles are slowed down in the circulation of these organs or taken up by phagocytic cells, thereby highlighting normal organ tissue, but not tumors.

Assessment of inflammation is another important goal. Both albumin- and lipid-coated PFC microbubbles are retained in inflamed tissue, for example, after myocardial ischemia-reperfusion injury. This is because of α_2 -integrin- and complement-mediated attachment to and phagocytosis by activated leukocytes that adhere to vascular endothelium.

Active targeting supposes attachment to the particles' surface of receptor ligands, including monoclonal antibodies, polysaccharides, and small peptides that recognize disease antigens (Fig. 14). Binding to the microbubble can involve covalent or noncovalent (hydrophobic, streptavidin/biotin pairing) interactions.

Active targeting to inflammation sites can be achieved using PFC microbubbles having antibodies to endothelium cell adhesion molecules expressed on the surface of endothelial cells activated during the inflammatory response. Such molecules include intercellular adhesion molecule-1 (ICAM-1), P-selectin, and certain integrins. The adhesion efficiency of microbubbles to target can be improved by simultaneous binding of the contrast agent to two distinct receptors [47].

Detection of thrombus is another clinically important goal. Contrast enhancement of vascular thrombosis has been achieved with a microbubble having a small peptide covalently attached to its surface that selectively binds to the GPIIb/IIIa fibrinogen receptor expressed on the surface of activated platelets that attach to thrombi.

Microbubbles targeted to α_v -integrins (which are overexpressed in regions of angiogenesis) allowed assessment of regions of angiogenesis in mice. Such agents may improve tumor imaging, as tumors promote angiogenesis for their growth, or help monitor promotion of angiogenesis in chronically ischemic tissue.

The pathologies targeted by PFC emulsion droplets are the same as for microbubbles and include inflammation, atherosclerosis, tumor-related angiogenesis, and thrombi. Detection and differentiation from normal tissue also involve binding ligands specific for the epitopes of interest to the droplets (Fig. 14). The basis for the use of PFC emulsions as contrast agents for US imaging is the observation of substantial scattering when the PFC droplets attach in adequate density to a surface, as compared to the rather poor enhancement of ultrasonic scattering by an emulsion in suspension. A thin, contiguous layer of ligand-bound emulsion droplets has essentially the properties of the neat PFC and creates an acoustically reflective interface between the targeted surface and the surrounding medium.

Contrast MRI requires incorporation of paramagnetic material onto the PFC-based targeted particles [48,49]. Incorporation of a gadolinium(III) complex into the lipid monolayer that coats targeted emulsion droplets provides contrast agents useful for both US and MRI modalities. Paramagnetic fibrin-specific PFC emulsion droplets allowed sensitive detection and localization of thrombi by MRI and may allow early identification of fibrin deposits in vulnerable atherosclerotic plaques. The emulsion droplets had both an antifibrin

monoclonal antibody and gadolinium diethylamine-triamine pentaacetic acid-phosphatidylethanolamine attached. A similar Gd-PFC emulsion, targeted to $\alpha_v\beta_3$ integrin (a molecular marker characteristic of angiogenic endothelium), allowed localization of angiogenic regions in rabbits. Such agents show promise for detection of early-stage atherosclerosis and tumors, and monitoring antiangiogenic therapy. ^{19}F MRI was used to confirm and quantify PFC droplet binding.

3.3. Further potential uses of perfluorocarbons in diagnosis

Neat *F*-octyl bromide provides an effective bowel marker during MRI of the gastrointestinal tract. It facilitates detection of pathology by improving stomach and bowel wall delineation. In this case, it is the absence of protons, hence of signal, that creates the desired contrast. PFC emulsions also provide an O_2 sensor that allows mapping of organ and tumor O_2 partial pressure using ^{19}F MRI techniques. Quantitative O_2 mapping involves monitoring the reduction of the ^{19}F spin-lattice relaxation parameter T_1 by the paramagnetic O_2 molecule. Externally applied PFC pads are commercially available that improve magnetic homogeneity, hence image quality, when fat saturation techniques are used during ^1H MRI. The radiopacity of *F*-octyl bromide allowed, for example, X-ray radiography monitoring of PFC distribution in the lungs during liquid ventilation (Fig. 2b).

4. PERFLUOROCARBONS AS DRUGS AND DRUG DELIVERY SYSTEMS

PFCs are being investigated both for drug properties of their own and also for their possible implication in drug delivery [5].

4.1. Lung ventilation

Total and partial liquid ventilations (PLV) with PFCs (usually *F*-octyl bromide) have shown improved gas exchange, lung structure (e.g., reopening of collapsed alveoli), and respiratory mechanics in various animal models of acute lung injury and in the clinic [5,17,50,51]. PLV with PFCs were also repeatedly reported to have an antiinflammatory effect, that is, reduce oxidative damage to lipids and proteins, protect lung epithelial cells, and reduce the release of inflammatory mediators during experimental acute lung injury [52–54]. However, clinical evaluation of PLV, although it showed significant reduction of mortality as compared to historical data, failed to demonstrate an advantage over the most recent, improved mechanical gas ventilation procedures [50]. Specific indications, including smoke inhalation injury, meconium aspiration, poisoning, and neonatal CPB, are still being explored.

Subsequent research explored the effect of vaporized, rather than liquid, PFCs (usually *F*-hexane) [55–57]. Improved gas exchange and lung compliance, as well as antiinflammatory effects, were generally reported. But, although alveolar damage was lower than with gas ventilation with oxygen, no significant improvements of gas exchange and lung mechanics were eventually established [58]. Research now focuses on the capacity for PFCs to attenuate the inflammatory response caused by endotoxin injury, acid aspiration, or viral infection. Pulmonary infusion of cold PFCs is being investigated as a means of rapidly cooling the body and thus protecting the brain after cardiac arrest, myocardial infarction or stroke, or during neurosurgery and cardiac surgery.

4.2. Lung-surfactant replacement

PFCs have recently been shown to prevent formation of a liquid condensed (semicrystalline) phase upon compression of a phospholipid film (Fig. 15). PFCs can also help dissolve semicrystalline domains after they have already formed. This fluidization effect facilitates the respreading of dimyristoylphosphatidylcholine (DMPC), the main component of the lung surfactant, on the surface of lung alveoli upon inspiration [59]. Experimentation on premature rabbits demonstrated a significant increase in tidal lung volume, allowing survival of the treated animals, while controls were all dead within minutes. PFCs may thus prove

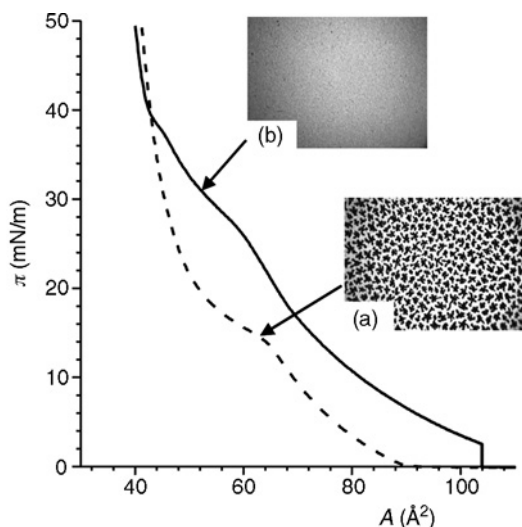


Fig. 15. Compression isotherms (π vs. A) of dipalmitoylphosphatidylcholine (DPPC) measured at 25 °C in an atmosphere of N_2 (dashed line) and of N_2 saturated with *F*-octyl bromide (solid line). Insets: Fluorescence images of (a) the DPPC monolayer compressed at $\pi = 15$ mN/m under N_2 , clearly showing crystalline domains, and (b) the DPPC monolayer in contact with *F*-octyl bromide, showing prevention of crystallization, even at high pressures ($\pi = 30$ mN/m) [107].

useful in lung-surfactant replacement compositions for neonates and possibly for the treatment of the acute respiratory distress syndrome in adults.

4.3. Miscellaneous therapeutic innovations

Appropriate microbubble/sound combinations can provide novel therapeutic tools. Blood clots can, for example, be broken up by a proper targeted bubble/focused sound wave association [60]. Such combinations may also enable non-invasive brain surgery, [61] as well as targeted drug delivery via transient acoustically induced opening of the blood–brain barrier [62].

PFCs have been extensively investigated for cell culture [63]. A PFC emulsion was recently found to prevent the adhesion of certain β -cell lines to cell culture plastic and promoted the formation of pseudo-islets capable of insulin secretion [64].

4.4. Drug and gene delivery

Providing an appropriate drug delivery system has become an essential component of pharmaceutical development and is gaining importance in disease management. Each drug requires its specific delivery system that optimizes efficacy and minimizes side effects (e.g., anticancer agents) through controlled release and, optimally, targeting. Many PFC- and *F*-surfactant-based delivery systems and microreservoirs, including micelles, dendrimers, vesicles, microbubbles, emulsions, and further molecular or self-assembled systems, have been engineered that could help ensure the controlled delivery of fragile biopolymers (e.g., peptides, proteins, and plasmids), as well as protect normal tissue [5,19]. The stability of fluorinated vesicle membranes (Fig. 16) is generally superior to that of vesicles made from standard lipids and their permeability to drugs can be substantially lower. Incorporation of an *F*-alkyl chain into a molecule can modify its diffusion across membranes and across the blood–brain barrier.

The lung, with its large contact area, appears to provide a privileged route for delivery of *F*-colloids. Reverse water-in-PFC emulsions loaded with various drugs, including antibacterial, bronchodilating, mucolytic, tuberculostatic, cholinergic, and antineoplastic agents, can, for example, be administered via metered-dose inhalers [65].

Various types of PFC-based gels and gel-emulsions have been reported [5,66,67]. They may find applications in topical drug delivery, wound healing, and implantable drug depots and as low-friction, gas-permeant, repellent protective-barrier creams against toxic or aggressive media, and in cosmetics.

Incorporation of *F*-chain end-groups into biodegradable polymers can help modulate their biodegradation (e.g., the hydrolysis rate of polyesters) and drug release [68]. Surface treatment of polymer for example, poly(lactic-co-glycolic acid)

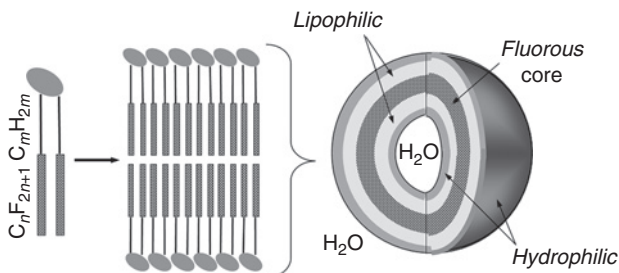


Fig. 16. Schematic representation of a fluorinated vesicle obtained from perfluoroalkylated phospholipids showing separated nanometer-thick domains within their bilayer membrane. The central hydrophobic and lipophobic fluorous core of the membrane is flanked by two lipophilic shells, then by the hydrophilic outermost and innermost layers of polar heads [4].

microcapsules by PFC plasma fluorination can reduce deleterious water penetration [69]. Plasma surface fluorination of polymers such as polyethylene or polypropylene results in lesser wettability and inactivation of enzymes.

Targeted PFC-based colloids, and in particular the micro- and nano-sized emulsions and bubbles described earlier, are being investigated as site-directed drug and gene delivery vehicles. Microbubbles can, for example, be loaded with a thrombolytic agent and directed to a blood clot [60]. The position of microbubbles targeted to diseased tissues can be monitored by US imaging, and release of their drug load can eventually be triggered by a suitable US pulse. Microbubbles were able to effectively enclose and protect adenoviral vectors from inactivation, allowing targeted systemic delivery [70, 71]. US-mediated microbubble destruction improved the efficacy and reduced the nonspecific expression of the gene therapy vector. The simultaneous presence of a Gd^{3+} chelate also allows MRI monitoring of treatment. Like for other colloids, fluorinated colloids may, as needed, be rendered stimuli-dependent (pH, pressure, and temperature).

Further details on PFC-based drug delivery systems can be found in Ref. [5].

5. SURGICAL AIDS

Various gaseous (*F*-propane, SF_6) and liquid (*F*-octane, *F*-decalin, *F*-perhydropheanthren, mixed fluorocarbon-hydrocarbon diblocks, and fluorosilicones) *F*-compounds are being used as intraocular tamponades for use in vitreoretinal surgery [Chapter 9 by Rico-Lattes *et al.*, this volume]. Polymers with *F*-alkyl moieties are used in corneal inlays and implants and in intraocular lenses.

Soft contact lenses incorporating fluorinated polymers (*F*-polyether dimethacrylates, fluorosiloxanes) and showing increased permeability to oxygen and

reduced lipophilicity, thus allowing continuous wear, are being investigated. A fluorosilicon-containing hydrogel lens is commercial [72].

Polymers used in vascular grafts [Chapter 8 by Baquey *et al.*, this volume] need to be stable in biological media and compatible with high pressure and blood-flow conditions. It is essential that the grafts be nonthrombogenic (i.e., do not promote clot formation). They should ideally have viscoelasticity behavior comparable to that of native vessels and should promote neoarterial regeneration. Polymer characteristics should not change over time as the graft needs to remain compliant for a very long time. Surface properties are of utmost importance.

Microporous ePTFE holds a prominent place among fluorinated polymers for reconstructive surgery, especially as vessel substitutes. Polytetrafluoroethylene (PTFE) was made microporous (standard pore size around 30 μm) by extrusion and sintering. Molded microporous ePTFE surfaces display wetting characteristics similar to those of the cardiovascular endothelial lining. Such ePTFE is highly crystalline and nonbiodegradable and displays an electronegative luminal surface that is antithrombogenic. It has also improved cell adhesion characteristics compared to plain PTFE. Its main disadvantage is its relatively high rigidity. ePTFE is widely used, especially as aortic and lower limb bypass grafts, with excellent results [73].

Patency is, however, less satisfactory for small-diameter grafts (<6 mm). Efforts made to modify ePTFE to fill the need for small-diameter vascular grafts include carbon coating to further increase electronegativity, increasing pore sizes to encourage endothelialization, impregnation with or binding of heparin, and coating the grafts with autologous endothelial cells. Inert fluoropolymers can also be surface-modified using plasma or photochemical treatment to introduce chemical functions that allow peptide or poly(ethylene glycol) attachment. For example, a poly(vinylamine) polymer with pendant peptides specifically associated with cell adhesion (integrin-binding peptides), and fitted with *F*-alkyl branches for adsorption onto ePTFE, has been synthesized that facilitates the adhesion and growth of endothelial cells on ePTFE [74]. In another approach, *F*-alkylated oligomers coupled with cell-binding peptides were blended with polyurethane. The bioactive *F*-alkylated species migrated to the polymer surface, providing control of cell adherence [75]. *F*-moieties can thus be used to modify polymer surfaces in view of reducing thrombogenicity, protecting a polymer from enzymatic degradation, controlling/promoting specific cell attachment, or delivering bioactive elements. More compliant fluorinated polymers, having higher elasticity than ePTFE (e.g., poly(vinylidene difluoride) or poly(tetrafluoroethylene-co-hexafluoropropylene)), are being investigated.

ePTFE is also being used in vascular access devices, as for hemodialysis, and in conduits for nerve regeneration. A PFC coating can lower friction of guidewires for catheters, and provide low friction antithrombogenic coating for other cardiovascular devices.

6. RESEARCH TOOLS FOR THE LIFE SCIENCES

Life on our planet is essentially based on carbon and hydrogen. Fluorine, although the most abundant of the halogens, ranking 13th only in order of frequency of the elements in Earth's crust (carbon ranks 14th), is seldom found in natural compounds. Only a handful of (usually toxic) mono- or difluorinated compounds are known. Enzymatic processes exist that form and break the C–F bonds present in these compounds [76]. On the other hand, no natural *perfluorocompounds* or moieties have, as yet, been found. Consequently, the enzymatic machinery that would allow for their generation and recycling has not developed.

The question of how far exogenous PFC (rather than “natural” hydrocarbon) chemistry could provide access to, control of, or interference with living constructs and processes has inevitably been tackled by chemists. The literature on investigations of PFCs in relation to life sciences and biomedical issues is increasing rapidly. Highly fluorinated compounds and moieties can actually allow unique functional modifications of natural compounds, offer surrogate means of molecular recognition and selection, as well as provide unique microenvironments unknown to Nature. PFC-based implements are being used for assaying, separating, and crystallizing biomolecules [9].

6.1. Abiotic tags for controlled recognition, selection, and pairing of biopolymers

Improved selectivity, stability, and performance of drugs, and in particular of therapeutic proteins, are important goals for the pharmaceutical industry. Introduction of *F*-alkyl or aryl groups into peptides and proteins is expected to substantially modify the *in vivo* behavior of these molecules, their interactions with receptors, and their pharmacological characteristics. Remarkably, the examples given below indicate that fluorinated proteins can also retain the structure and activity of their native model. For those engaged in artificial protein and nucleic acid engineering, the introduction of highly fluorinated fragments provides a novel, complementary means for controlling, sorting, and assembling amino acids or nucleosides. It provides new means for templated biosynthesis of peptides from fluorinated amino acids, stabilizing protein folding, achieving selective protein–protein recognition and assembly, DNA recognition and binding, and the modulation of biological processes.

The stability of peptides is generally increased when natural amino acids are substituted by fluorinated analogs (e.g., tri- or hexafluoroleucine, hexafluorovaline). Such stabilization augments with the number of hexafluoroleucine residues introduced [77]. Native-like structure was preserved, but the peptides had a more structured backbone and less fluid hydrophobic core. Substitution of four leucine residues by trifluoroleucines in the leucine zipper peptide GCN4-p1d led to a substantial gain in thermal stability and resistance to chemical denaturation of the

dimeric coiled-coil structure [78]. The DNA-binding behavior of the similarly fluorinated construct GCN4-bZip remained identical in terms of affinity and specificity to that of the wild-type peptide. These examples indicate that some protein domains can tolerate extensive fluorination without loss of function. The coenzyme nicotinamide adenine dinucleotide, when fitted with an *F*-polyether side chain, actually displayed augmented coenzyme activity in horse liver alcohol dehydrogenase-catalyzed oxidation/reduction reactions, the fluorinated coenzyme being dissolved in a fluorous solvent or in liquid CO₂ [79].

Incorporation of fluorinated amino acids creates fluorinated patches within peptides that constitute a new type of highly selective peptide–peptide hydrophobic interaction motif. Disproportionation, under equilibrium conditions, of a heterodimer composed of a highly fluorinated peptide and its nonfluorinated analog led almost exclusively to the homodimers [80]. Phase separation (self-sorting) of such fluorous patches appropriately placed onto hydrophobic folds direct helix–helix self-assembly (pairing or oligomerization) within micelles [81] (Fig. 17). Interactions among fluorous patches, coupled with hydrogen bonds, can be superior and more efficient at directing oligomerization of transmembrane helices within phospholipid bilayer membranes than those based on natural aliphatic interfaces [82]. The self-assembly of the fluorine-patched elements into complex functional biopolymers is here dictated by adaptation to the environment. Systematic studies of the influence of amino acid side chain fluorination on protein folding and stability have been initiated [83].

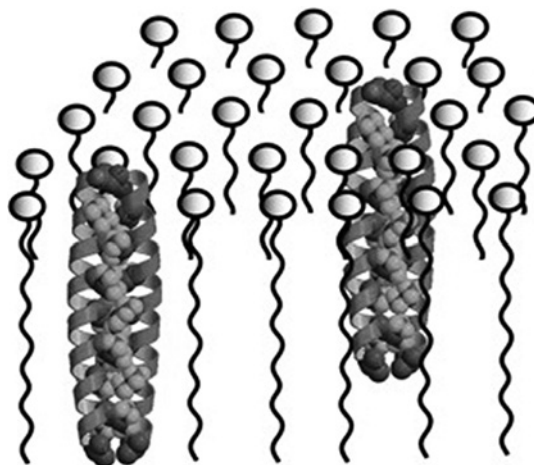


Fig. 17. Fluorous patches direct the pairing of protein segments in lipid micelles. The hydrophobic peptides partition into lipid micelles, forming α -helices. Then, the superhydrophobic hexafluoroleucine residues seek each other, causing self-association into dimers and higher order aggregates. Fluorine is light, while the backbone of the α -helices is dark. From Ref. [81], with permission.

Remarkably, incorporation of fluorinated amino acids into proteins can also be accomplished *in vivo*. This supposes that the fluorinated amino acid analogs are recognized by the appropriate amino acyl-tRNA synthetase enzyme with efficiency similar to that of the natural amino acid. The proliferase response elicited by a fluorinated analog (a trifluoroisoleucine derivative) of murine interleukin-2 produced in an appropriate *Escherichia coli* strain was nearly as high as that of the authentic cytokine, indicating folding into an authentic, native structure [84].

Where nucleic acids are concerned, the enhanced hydrophobicity of abiotic polyfluorinated aromatic bases (e.g., tetrafluorobenzene or tetrafluoroindole deoxyribose derivatives) was exploited as an alternative to “natural” hydrogen bonding to achieve selective and stable nucleic acid base pairing in duplex DNA [85]. The DNA replication was examined using polyfluorinated-nucleotide analogs as substrates. A DNA polymerase active site was able to process the polyfluorinated base pairs more effectively than the analogous hydrocarbon pairs, demonstrating hydrophobic selectivity of polyfluorinated bases for other polyfluorinated bases [86].

Incorporation of nonnatural polyfluorinated bases, capable of enhanced (or “hyper”) hydrophobic interactions, thus expands the genetic alphabet beyond the natural one used in replication. It illustrates the emerging role of *F*-compounds in developing chemistry, including constitutional dynamic biochemistry, that lies well “beyond” nature.

6.2. “Abiotic” environments—“super-nonpolar” fluororous compartments for segregation and confinement

Living organisms are composed of specialized functional subunits that allow exchange processes, including selective transport, and hence, communication. Their structure, therefore, relies heavily on self-assembly of amphiphilic molecules (e.g., phospholipids) into multiple compartments possessing a panoply of specific characters. At the molecular level, functional proteins also exhibit diverse regions offering distinct environments. Substantial efforts are being devoted to producing micron-sized and fluid cell-like compartments that mimic some vital cell functions. *F*-alkylated compounds, because of their exceptional aptitude at developing both hydrophobic and lipophobic effects, are highly effective in generating stable, organized, and compartmented molecular systems with controlled complexity. “Multicompartment micelles” [87] have, for example, been prepared by micellar terpolymerization of acrylamide with both hydrocarbon and fluorocarbon polymerizable surfactants [88]. Other multicompartmented systems have been obtained by self-assembly in water of linear [89] or star-shaped (Fig. 18a) [90] triblock copolymers bearing a highly fluorinated arm, a polystyrene arm, and a polymorpholinium or poly(ethylene oxide) arm.

Exquisite space control at the molecular level is exemplified by the engineering of a spherical shell through spontaneous assemblage of 12 palladium(II) ions with 24 bent *F*-alkylated pyridine-based ligands (Fig. 18b) [91]. The disordered *F*-alkyl chains are tethered to the concave side of the rigid shell, hence providing a fluid inner, nano-droplet-like, fluorinated (fluorous) environment whose size is determined by the length of the *F*-chains. Selective incorporation (cryptation) of PFC molecules was demonstrated. Fluorinated dendrimers also offer precisely shaped nano-size fluorous domains or corona [92,93]. Highly organized helical pyramidal columns were formed by self-assembly of semifluorinated dendrons attached to electron-donor groups [94]. These columns subsequently self-organize into large supramolecular pyramidal liquid crystals.

The exceptionally strong hydrophobic and lipophobic effects constitute a powerful driving force for segregation and self-organization of fluorinated amphiphiles. These effects promote phase separation and ordering among fluorinated components and, within such components, of the fluorinated moieties. Highly fluorinated materials thus offer unique components and tools for the engineering of stable self-assembled supramolecular and colloidal systems [4,6]. These systems can be two- or three-dimensional and usually display several nanocompartmented phases. Such micro- and nanometer-size environments can serve multiple purposes. They can provide microreactors and matrices for polymerization [95]. A fluorosurfactant-stabilized water-in-PFC microemulsion was used to

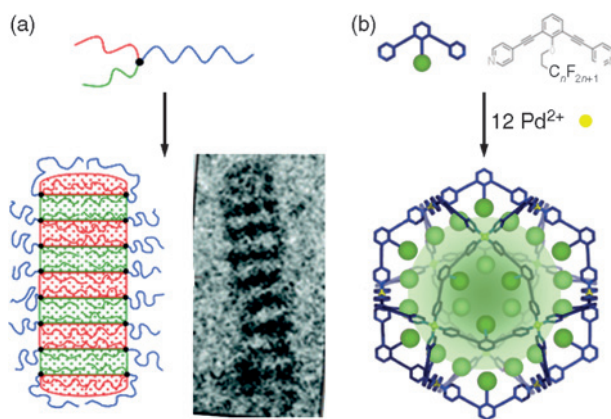


Fig. 18. (a) Schematic representation and cryoTEM image of a multicompartment micelle obtained from self-assembly in water of a star terpolymer having a perfluoropolyether arm (green), a polystyrene arm (red), and a poly(oxyethylene) arm (blue). From Ref. [90], with permission. (b) Self-assembled rigid cage with a fluid perfluorocarbon interior. The cage is made of 12 palladium(II) ions (yellow dots) and 24 linkers with a perfluoroalkyl chain (green dots); the perfluoroalkyl chains-lined cavity within the cage is depicted in light green. From Ref. [91], with permission. (See Colour Plate Section at the end of this book.)

study the influence of confinement on water dynamics [96]. They should allow isolation and investigation of isolated single proteins. It is noteworthy that high enzymatic activity (e.g., lipase-catalyzed alcoholysis) can be preserved and even enhanced in a fluoruous medium [97].

Further examples of controllable spherical or tubular micro- and nano-sized fluorinated environments are found in self-assembled vesicles, tubules, ribbons, as well as in a variety of microbubbles and microdroplets, as in aerosols, emulsions, microemulsions, reverse emulsions, gel-emulsions, and multiple emulsions with highly fluorinated phase or membrane components [6,19]. Two-dimensional constructs with fluorinated microcompartments include monolayer films, bilayer membranes, and interfaces, as found in Langmuir or Langmuir-Blodgett films or within surface micelles [98] and three-dimensional colloids. Figure 16 illustrates the formation of layered hydrophilic, lipophilic, and fluorophilic shells within the bilayer membrane of fluorinated vesicles [19]. These vesicles were obtained either from lipids having *F*-alkylated chains or from combinations of standard phospholipids with fluorocarbon-hydrocarbon diblocks. Segregation of hydrogenated and fluorinated domains within Langmuir monolayers has led to both laterally and vertically phase-separated zones [99].

6.3. Tools for nanogram-scale bioassays and protein crystallization

Achieving selective extraction without denaturation of biopolymers is essential in biochemistry. *F*-surfactants with an *F*-alkyl fragment inserted between a retinoid receptor ligand and a lipidic tail have been designed for the purpose of promoting two-dimensional crystallization of membrane proteins at an air/water interface [100]. The *F*-alkyl segments stabilize the monolayer against solubilization by the detergent used for protein solubilization. It also forces a lipophilic ligand to stay exposed on the aqueous side of the monolayer, while its natural tendency would be to bury itself in the lipidic region of the monolayer.

Other important basic operations in biochemistry include the performance of immunologic and enzymatic assays, and protein crystallization and structure determination. The challenge here is to achieve these operations in great numbers on the smallest possible amount of material, rapidly and cost-efficiently. PFCs play an essential role in the development of dedicated miniaturized “lab-on-a-chip” systems. The approach involves manipulation of discrete droplets of reagents confined and precisely positioned in microchannels [101]. Microfluidic technologies allow handling, transferring, mixing, and separating numerous reactants on the nanoliter scale. PFCs provide the continuous, immiscible, inert carrier fluid that separates and carries the various reactants [102]. They also offer their unique surface properties, allowing flow and friction control and facilitating droplet size and stability control. Microfluidic cartridges preloaded with nanoliter

plugs of reagents separated by gas bubbles [103] within a PFC carrier fluid [102] have been fabricated. The preloaded capillaries are then coupled with microfluidic chips that allow merging of reactant droplets (Fig. 19). Such systems may provide a convenient alternative to well plates for screening [102]. PTFE capillaries can be used to facilitate fluid handling and to allow high-pressure reactions. These tools facilitate the screening and optimization of chemical reactions and of protein crystallization conditions on a large number of very small samples. Crystals grown in plugs inside a microcapillary can be analyzed *in situ* by X-ray diffraction [104].

7. CONCLUSIONS AND PERSPECTIVES

Research and development of highly fluorinated materials for medicine and the life sciences is being actively pursued. PFCs' outstanding chemical and biological inertness and high gas solubilities are the basis for an abiotic means for intravascular oxygen delivery. A stable, injectable PFC emulsion has reached Phase III clinical trials. At this time, however, no effective system, capable of oxygenating tissues and preventing ischemia, is commercially available. Ongoing clinical research focuses on blood sparing and on the important issue of protecting the organs, especially the gut, at risk of ischemia during surgery. PFC-based oxygen carriers could also help cope with blood shortages.

The low water solubility and high vapor pressure of PFCs allowed stabilization of injectable microbubbles that serve as contrast agents for diagnostic US imaging. Several such agents are now commercial and contrast imaging of the cardiac chambers has become part of medical practice. Assessment of microbubble use as flow markers for perfusion and vascular imaging is well advanced. By enabling acquisition of higher quality images, contrast echosonography

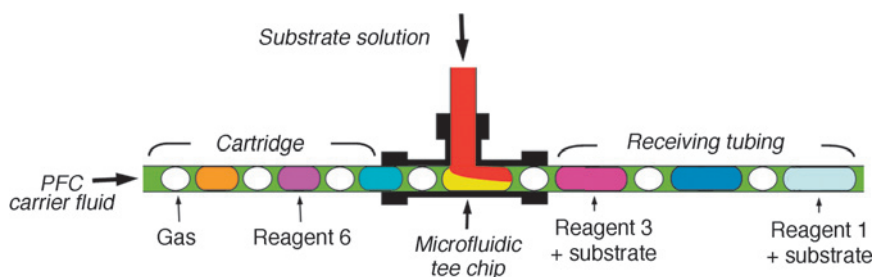


Fig. 19. Schematic view of perfluorocarbon-implemented microfluidics for chemists. Capillary cartridges preloaded with plugs of reagents separated by gas bubbles within a perfluorocarbon carrier fluid are fitted onto a microfluidic chip where the substrate stream merges with the reagent plugs. From Ref. [102], with permission. (See Colour Plate Section at the end of this book.)

provides potential for earlier detection and more accurate characterization of disease, improved confidence in diagnosis, and hence, reduced recourse to more expensive downstream examinations or biopsy. Microbubbles with exceptionally long life (by one order of magnitude) have been obtained using amphiphilic *F*-alkylated bubble wall components.

Targeted PFC-stabilized microbubbles and PFC-in-water emulsions that seek molecular markers of diseases open the door to considerable possibilities to both US and MRI. Substantial efforts will focus on devising affinity ligands (molecular probes) and binding strategies, including multiple epitope binding, suitable for commercial development. These microbubbles and droplets may also provide new vehicles for site-directed drug and gene delivery. PFC-based contrast agents may provide tools for drug development, pharmacokinetic and pharmacodynamic studies, dose regimen and therapeutic efficacy determinations, and the unraveling of the molecular mechanisms of a disease.

Further PFC-based products under investigation include lung-surfactant replacement preparations, and cell and organ preservation media. The anti-inflammatory effects observed upon administration of PFCs in the lungs is also intriguing.

More compliant highly fluorinated polymers for reconstructive surgery (e.g., vascular grafts) and other surgical devices will undoubtedly be developed. Various ophthalmologic aids are also being commonly used.

The intense hydrophobic and lipophobic effects developed by PFC moieties stabilize membranes and generate micro- and nanocompartmented fluoruous environments that can provide confinement, microreactors, and templates. PFCs are also used as inert, apolar carrier fluids for lab-on-a-chip experiments and assays using microfluidic technologies. Faster, more convenient, smaller scale, and cheaper assays are being developed. The outstanding hydrophobic effects of fluorinated tags or patches (e.g., highly fluorinated amino acids) generate powerful noncovalent, binding interactions that can promote molecular recognition, selective sorting, and templated binding (e.g., selective peptide and nucleic acid pairing). Highly fluorinated amino acids or base-substitute shape mimics offer abiotic building blocks for the *de novo* design of novel, abiotic, functional biopolymers, and the extension of biochemistry "beyond natural."

Establishing and understanding the impact of *F*-chains on the formation, structure, dynamics, and properties of molecules and supramolecular self-assemblies comprising fluorinated components is another permanent goal. Such knowledge will help predict and control the formation and properties of *F*-compounds and assemblies.

The unique properties of highly fluorinated materials are thus expected to continue inspire chemists, offer new research tools for the life sciences, and contribute to the emergence of new diagnostic and therapeutic innovations. Pharmaceutical development involves increasing complexity and heavy regulatory, financial, and other constraints, and time. Managing such complexity

and bringing together the required diversity of complementary skills and resources should help turn the unique potential of highly fluorinated materials into useful products.

REFERENCES

- [1] K. Müller, *ChemBioChem* (Special Issue on Fluorine in the Life Science) 5 (2004) 559–722.
- [2] J.P. Bégue, D. Bonnet-Delpon, *Chimie Bioorganique et Médicinale du Fluor*, EDP Sciences, CNRS Editions, Paris, 2005.
- [3] J.G. Riess, in: R.E. Banks (Ed.), *Fluorine at the Millennium*, Elsevier, Amsterdam, 2000, pp. 385–431.
- [4] J.G. Riess, Fluorous micro- and nanophases with a biomedical perspective, *Tetrahedron* 58 (2002) 4113–4131.
- [5] J.G. Riess, in: J.A. Gladysz, D.P. Curran, I. Horváth (Eds.), *Handbook of Fluorous Chemistry*, Wiley-VCH, Weinheim, 2004, pp. 521–573.
- [6] M.P. Krafft, in: J.A. Gladysz, D.P. Curran, I.T. Horvath (Eds.), *Handbook of Fluorous Chemistry*, Wiley-VCH, Weinheim, 2004, pp. 478–490.
- [7] J.G. Riess, Understanding the fundamentals of perfluorocarbons and perfluorocarbon emulsions relevant to *in vivo* oxygen delivery, *Artif. Cells Blood Substit. Immob. Biotech.* 33 (2005) 47–63.
- [8] J.G. Riess, M.P. Krafft, in: R.M. Winslow (Ed.), *Blood Substitutes*, Elsevier, Amsterdam, 2006, pp. 259–275.
- [9] M.P. Krafft, J.G. Riess, Perfluorocarbons, life sciences and biomedical uses, *J. Polym. Sci. Part A: Polym. Chem.* 45 (2007) 1185–1198.
- [10] M.P. Krafft, *Curr. Opin. Colloid Interf. Sci.* (Special issue on Fluorinated Colloids and Interfaces) 8 (2003) 213–314.
- [11] J.M. Lehn, Towards self-organization and complex matter, *Science* 295 (2002) 2400–2403.
- [12] P. Metrangola, H. Neukirch, T. Pilati, G. Resnati, Halogen bonding based recognition processes: A world parallel to hydrogen bonding, *Acc. Chem. Res.* 38 (2005) 386–395.
- [13] J.A. Gladysz, D.P. Curran, *Fluorous Chemistry* (A Special Issue of *Tetrahedron*) 58 (2002) 3823–4131.
- [14] J.A. Gladysz, D.P. Curran, I. Horváth, *Handbook of Fluorous Chemistry*, Wiley-VCH, Weinheim, 2004.
- [15] J.G. Riess, M.P. Krafft, Fluorinated materials for *in vivo* oxygen transport (blood substitutes), diagnosis and drug delivery, *Biomaterials* 19 (1998) 1529–1539.
- [16] R.F. Mattrey, M.A. Trambert, J.J. Brown, S.W. Young, J.N. Bruneton, G.E. Wesbey, Z.N. Balsara, Perflubron as an oral contrast agent for MR imaging: Results of a phase III clinical trial, *Radiology* 191 (1994) 841–848.
- [17] C.L. Leach, J.S. Greenspan, D. Rubenstein, T.H. Shaffer, M.R. Wolfson, J.C. Jackson, R. DeLemos, B.P. Fuhrman, Partial liquid ventilation with perflubron in premature infants with severe respiratory distress syndrome, *New Engl. J. Med.* 335 (1996) 761–766.
- [18] C. Lau, J.L. Butenhoff, J.M. Rogers, The developmental toxicity of perfluoroalkyl acids and their derivatives, *Toxicol. Appl. Pharmacol.* 198 (2004) 231–241.
- [19] M.P. Krafft, J.G. Riess, Highly fluorinated amphiphiles and colloidal systems, and their applications in the biomedical field—A contribution, *Biochimie* 80 (1998) 489–514.
- [20] J.G. Riess, Injectable oxygen carriers (blood substitutes)—Raison d'être, chemistry and some physiology, *Chem. Rev.* 101 (2001) 2797–2920.
- [21] M.P. Krafft, A. Chittofrati, J.G. Riess, Emulsions and microemulsions with a fluorocarbon phase, *Curr. Opin. Colloid Interface Sci.* 8 (2003) 251–258.

- [22] J.G. Riess, Perfluorocarbon-based oxygen delivery, *Artif. Cells Blood Substit. Immobil. Biotech.* 34 (2006) 567–580.
- [23] M.P. Krafft, J.G. Riess, J.G. Weers, in: S. Benita (Ed.), *Submicronic Emulsions in Drug Targeting and Delivery*, Harwood Academic Publication, Amsterdam, 1998, pp. 235–333.
- [24] G.R. Ivanitsky, Biophysics at the turn of the millennium: Perfluorocarbon media and gas-transporting blood substitutes, *Biophysics* 46 (2001) 1–31.
- [25] D.M. Eckman, V.N. Lomivorotov, Microvascular gas embolization clearance following perfluorocarbon administration, *J. Appl. Physiol.* 94 (2003) 860–868.
- [26] P.E. Keipert, in: R.M. Winslow (Ed.), *Blood Substitutes*, Elsevier, Amsterdam, 2006, pp. 312–323.
- [27] D.R. Spahn, K.F. Waschke, T. Standl, J. Motsch, L. Van Huynegem, M. Welte, H. Gombotz, P. Coriat, L. Verkh, S. Faithfull, P. Keipert, Use of perflubron emulsion to decrease allogeneic blood transfusion in high-blood-loss non-cardiac surgery: Results of a European Phase 3 study, *Anesthesiology* 97 (2002) 1338–1349.
- [28] N.S. Faithfull, The concept of hemoglobin equivalency of perfluorochemical emulsions, *Adv. Exp. Med. Biol.* 530 (2003) 271–285.
- [29] R.J. Frumento, L. Mongero, Y. Naka, E. Bennett-Guerrero, Preserved gastric tonometric variables in cardiac surgical patients administered intravenous perflubron emulsion, *Anesth. Analg.* 94 (2002) 809–814.
- [30] K. Yoshitani, F. De Lange, Q. Ma, H.P. Grocott, G.B. Mackensen, Reduction in air bubble size using perfluorocarbons during cardiopulmonary bypass in the rat, *Anesth. Analg.* 103 (2006) 1089–1093.
- [31] S. Marie Bertilla, J.L. Thomas, P. Marie, M.P. Krafft, Co-surfactant effect of a semi-fluorinated alkane at a fluorocarbon/water interface. Impact on the stabilization of fluorocarbon-in-water emulsions, *Langmuir* 20 (2004) 3920–3924.
- [32] S. Audonnet-Blaise, M.P. Krafft, Y. Smani, P.M. Mertes, P.Y. Marie, P. Labrude, D. Longrois, P. Menu, Resuscitation of severe but brief haemorrhagic shock with PFC in rabbits restores skeletal muscle oxygen delivery and does not alter skeletal muscle metabolism, *Resuscitation* 70 (2006) 124–132.
- [33] C.E. Lundgren, G.W. Bergoe, I. Tyssebotn, The theory and application of intravascular microbubbles as an ultra-effective means of transporting oxygen and other gases, *Undersea Hyperb. Med.* 31 (2004) 105–106.
- [34] S.L. Mulvagh, A.N. DeMaria, S.B. Feinstein, P.N. Burns, S. Kaul, J.G. Miller, M. Monaghan, T.R. Porter, L.J. Shaw, F.S. Villanueva, Contrast echography: Current and future applications, *J. Am. Soc. Echocardiogr.* 13 (2000) 331–342.
- [35] H. Becher, P.N. Burns, *Handbook of Contrast Echocardiography—Left Ventricular Function and Myocardial Perfusion*, Springer Verlag, Berlin, 2000.
- [36] B.B. Goldberg, J.S. Raichlen, F. Forsberg, *Ultrasound Contrast Agents—Basic Principles and Clinical Applications*, 2nd edition, Martin Dunitz, London, 2001.
- [37] E.S. Schutt, D.H. Klein, R.M. Mattrey, J.G. Riess, Injectable microbubbles as contrast agents for diagnostic ultrasound imaging: The key role of perfluorochemicals, *Angew. Chem. Int. Ed.* 42 (2003) 3218–3235.
- [38] D. Cosgrove, Ultrasound contrast agents: An overview, *Eur. J. Radiol.* 60 (2006) 324–330.
- [39] P.N. Burns, S.R. Wilson, Microbubble contrast for radiological imaging: 1. Principles, *Ultrasound Q.* 22 (2006) 5–13.
- [40] A. Kabalnov, D. Klein, T. Pelura, E. Schutt, J. Weers, Dissolution of multicomponent microbubbles in the blood stream: 1. Theory, *Ultrasound Med. Biol.* 24 (1998) 739–749.
- [41] A. Kabalnov, J. Bradley, S. Flaim, D. Klein, T. Pelura, B. Peters, S. Otto, J. Reynolds, E. Schutt, J. Weers, Dissolution of multicomponent microbubbles in the blood stream: 2. Experiment, *Ultrasound Med. Biol.* 24 (1998) 751–760.
- [42] N. de Jong, A. Bouakaz, F.J. Ten Cate, Contrast harmonic imaging, *Ultrasonics* 40 (2002) 567–573.

- [43] A.L. Klibanov, P.T. Rasche, M.S. Hughes, J.K. Wojdyla, K.P. Galen, J.H. Wible, G.H. Brandenburger, Detection of individual microbubbles of an ultrasound contrast agent: Fundamental and pulse inversion imaging, *Acad. Radiol.* 9(Suppl. 2) (2002) S279–S281.
- [44] F. Gerber, M.P. Krafft, G. Waton, T.F. Vandamme, Microbubbles with exceptionally long life—Synergy between shell and internal phase components, *New J. Chem.* 30 (2006) 524–527.
- [45] A.L. Klibanov, Microbubble contrast agents: Targeted ultrasound imaging and ultrasound-assisted drug-delivery applications, *Invest. Radiol.* 41 (2005) 354–362.
- [46] C.Z. Behm, J.R. Lindner, Cellular and molecular imaging with targeted contrast ultrasound, *Ultrasound Q.* 22 (2006) 67–72.
- [47] G.E.R. Weller, F.S. Villanueva, E.M. Tom, W.R. Wagner, Targeted ultrasound contrast agents: *In vitro* assessment of endothelial dysfunction and multi-targeting to ICAM-1 and sialyl Lewisx, *Biotechnol. Bioeng.* 92 (2005) 780–788.
- [48] A.M. Morawski, G.A. Lanza, S.A. Wickline, Targeted contrast agents for magnetic resonance imaging and ultrasound, *Curr. Opin. Biotechnol.* 16 (2005) 89–92.
- [49] S.D. Caruthers, P.M. Winter, S.A. Wickline, G.M. Lanza, Targeted magnetic resonance imaging contrast agents, *Methods Mol. Med.* 124 (2006) 387–400.
- [50] R.B. Hirschl, M. Croce, D. Gore, H. Wiedemann, K. Davis, R.H. Bartlett, Prospective, randomized, controlled pilot study of partial liquid ventilation in adult acute respiratory distress syndrome, *Am. J. Respir. Crit. Care Med.* 165 (2002) 781–787.
- [51] J.P. Meinhardt, U. Friess, H.J. Bender, R.B. Hirschl, M. Quintel, Relationship among cardiac index, inspiration/expiratory ratio, and perfluorocarbon dose during partial liquid ventilation in an oleic acid model of acute lung injury in sheep, *J. Pediatr. Surg.* 40 (2005) 1395–1403.
- [52] A.T. Rotta, B. Gunnarsson, L.J. Hernan, B.P. Fuhrman, D.M. Steinhorn, Partial liquid ventilation with perflubron attenuates *in vivo* oxidative damage to proteins and lipids, *Crit. Care Med.* 28 (2000) 202–208.
- [53] U. Merz, B. Klosterhalfen, M. Häusler, M. Kellinghaus, T. Peschgens, H. Hörnchen, Partial liquid ventilation reduces release of leukotriene B₄ and interleukin-6 in bronchoalveolar lavage in surfactant-depleted newborn pigs, *Pediatr. Res.* 51 (2002) 183–189.
- [54] H.A. Haeberle, F. Nesti, H.J. Dieterich, Z. Gatalica, R.P. Garofalo, Perflubron reduces lung inflammation in respiratory syncytial virus infection by inhibiting chemokine expression and nuclear factor-kappaB activation, *Am. J. Respir. Crit. Care Med.* 165 (2002) 1433–1438.
- [55] M.A. Kandler, K. von der Hardt, E. Schoof, J. Dotsch, W. Rascher, Persistent improvement of gas exchange and lung mechanics by aerosolized perfluorocarbon, *Am. J. Resp. Crit. Care Med.* 164 (2001) 31–35.
- [56] J.U. Bleyl, M. Ragaller, U. Tschöh, M. Regner, M. Hübler, M. Kanzow, O. Vincent, M. Albrecht, Changes in pulmonary function and oxygenation during application of perfluorocarbon vapor in healthy and oleic acid-injured animals, *Crit. Care Med.* 30 (2002) 1340–1347.
- [57] K. von der Hardt, E. Schoof, M.A. Kandler, J. Dötsch, W. Rascher, Aerosolized perfluorocarbon suppresses early pulmonary inflammatory response in a surfactant-depleted piglet model, *Pediatr. Res.* 51 (2002) 177–182.
- [58] M. Gama de Abreu, A.D. Quelhas, P. Spieth, G. Bräuer, L. Knels, M. Kasper, A.V. Pino, J.U. Bleyl, M. Hübler, F. Bozza, J. Salluh, E. Kuhlisch, A. Giannella-Neto, T. Koch, Comparative effects of vaporized perfluorohexane and partial liquid ventilation in oleic acid-induced lung injury, *Anesthesiology* 104 (2006) 278–289.
- [59] F. Gerber, M.P. Krafft, T.F. Vandamme, M. Goldmann, P. Fontaine, Preventing crystallization of phospholipids in monolayers: A new approach to lung surfactant therapy, *Angew. Chem. Int. Ed.* 44 (2005) 2749–2752.
- [60] E.C. Unger, T. Porter, W. Culp, R. Labell, T. Matsunaga, R. Zutshi, Therapeutic applications of lipid-coated microbubbles, *Adv. Drug Deliv. Rev.* 56 (2004) 1291–1314.

- [61] N.J. McDannold, N.I. Vykhodtseva, K. Hynynen, Microbubble contrast agent with focused ultrasound to create brain lesion at low power levels: MR imaging and histologic study in rabbits, *Radiology* 241 (2006) 95–106.
- [62] S. Meairs, A. Alonso, Ultrasound, microbubbles and the blood-brain barrier, *Prog. Biophys. Mol. Biol.* 93 (2006) 354–362.
- [63] K.C. Lowe, Perfluorochemical respiratory gas carriers: Benefits to cell culture systems, *J. Fluorine Chem.* 118 (2002) 19–26.
- [64] M. Sanchez Dominguez, M.P. Krafft, E. Maillard, S. Siegrist, A. Belcourt, Prevention of adhesion and promotion of pseudoislets formation from a b-cell line by fluorocarbon emulsions, *ChemBioChem* 7 (2006) 1160–1163.
- [65] N. Butz, C. Porté, H. Courrier, M.P. Krafft, T.F. Vandamme, Reverse water-in-fluorocarbon emulsions for use in pressurized metered-dose inhalers containing hydrofluoroalkane propellants, *Int. J. Pharm.* 238 (2002) 257–269.
- [66] M.P. Krafft, S. Magdassi, E. Touitou (Eds.), *Novel Cosmetic Delivery Systems*, Dekker, New York, 1998, pp. 195–219.
- [67] V.G. Babak, M.J. Stébé, A review on highly concentrated emulsions: Physicochemical principles of formulation, *J. Disp. Sci. Technol.* 23 (2002) 1–15.
- [68] C.S. Ha, J.A. Gardella, Surface chemistry of biodegradable polymers for drug delivery systems, *Chem. Rev.* 105 (2005) 4205–4232.
- [69] K. Tanaka, M. Kogoma, Y. Ogawa, Fluorinated polymer coatings on PLGA microcapsules for drug delivery system using atmospheric pressure glow plasma, *Thin Solid Films* 506–507 (2006) 159–162.
- [70] C.M. Howard, F. Forsberg, C. Minimo, J.B. Liu, D.A. Merton, P.P. Claudio, Ultrasound guided site specific gene delivery system using adenoviral vectors and commercial ultrasound contrast agents, *J. Cell. Physiol.* 209 (2006) 413–421.
- [71] K. Ferrara, R. Pollard, M. Borden, Ultrasound microbubble contrast agents: fundamentals and application to gene and drug delivery, *Ann. Rev. Biomed. Engineer.* 9 (2007) 415–447.
- [72] P.C. Nicolson, J. Vogt, Soft contact lens polymers: An evolution, *Biomaterials* 22 (2001) 3273–3283.
- [73] R.Y. Kannan, H.J. Salacinski, P.E. Butler, G. Hamilton, A.M. Seifalian, Current status of prosthetic bypass grafts: A review, *J. Biomed. Mater. Res. B: Appl. Biomater.* 74B (2005) 570–581.
- [74] C.C. Larsen, F. Kligman, K. Kottke-Marchant, R.E. Marchant, The effect of RGD fluorosurfactant polymer modification of ePTFE on endothelial cell adhesion, growth, and function, *Biomaterials* 27 (2006) 4846–4855.
- [75] M.J. Ernsting, G.C. Bonin, M. Yang, R.S. Labow, J.P. Santerre, Generation of cell adhesive substitutes using peptide fluoroalkyl surface modifiers, *Biomaterials* 26 (2005) 6536–6546.
- [76] C. Dong, F.L. Huang, H. Deng, C. Schaffrath, J.B. Spencer, D. O'Hagan, J.H. Naismith, Crystal structure and mechanism of a bacterial fluorinating enzyme, *Nature* 427 (2004) 561–565.
- [77] H.Y. Lee, K.H. Lee, H.M. Al-Hashimi, E.N.G. Marsh, Modulating protein structure with fluorine amino acids: Increased stability and native-like structure conferred on a 4-helix bundle protein by hexafluoroisoleucine, *J. Am. Chem. Soc.* 128 (2006) 337–343.
- [78] Y. Tang, G. Ghirlanda, N. Vaidehi, J. Kua, D.T. Mainz, W.A. Goddard III, W.F. DeGrado, D.A. Tirrell, Stabilization of coiled-coil peptide domains by introduction of trifluoroisoleucine, *Biochemistry* 40 (2001) 2790–2796.
- [79] J.L. Panza, A.J. Russell, E.J. Beckman, Synthesis of fluorinated NAD as a soluble coenzyme for enzymatic chemistry in fluorine solvents and carbon dioxide, *Tetrahedron* 58 (2002) 4091–4104.
- [80] B. Bilgiçer, X. Xing, K. Kumar, Programmed self-sorting of coiled coils with leucine and hexafluoroisoleucine cores, *J. Am. Chem. Soc.* 123 (2001) 11815–11816.

- [81] B. Bilgiçer, K. Kumar, *De novo* design of defined helical bundles in membrane environments, *Proc. Natl. Acad. Sci. USA* 101 (2004) 15324–15329.
- [82] N. Naarmann, B. Bilgiçer, H. Meng, K. Kumar, C. Steinem, Fluorinated interfaces drive self-association of transmembrane helices in lipid bilayers, *Angew. Chem. Int. Ed.* 45 (2006) 2588–2591.
- [83] C. Jäckel, M. Salwiczek, B. Koksche, Fluorine in a native protein environment—How the spatial demand and polarity of fluoroalkyl groups affect protein folding, *Angew. Chem. Int. Ed.* 45 (2006) 4198–4203.
- [84] P. Wang, Y. Tang, D.A. Tirrell, Incorporation of trifluoroisoleucine into proteins *in vivo*, *J. Am. Chem. Soc.* 125 (2003) 6900–6906.
- [85] J.S. Lai, E.T. Kool, Selective pairing of polyfluorinated DNA bases, *J. Am. Chem. Soc.* 126 (2004) 3040–3041.
- [86] J.S. Lai, E.T. Kool, Fluorous base-pairing effects in a DNA polymerase active site, *Chem. Europ. J.* 11 (2005) 2966–2971.
- [87] H. Ringsdorf, P. Lehmann, R. Weberskirch, Multicompartmentation—a concept for the molecular architecture of life, 217th ACS National Meeting, Anaheim (CA), 1999.
- [88] K. Stähler, J. Selb, F. Candau, Multicompartment polymeric micelles based on hydrocarbon and fluorocarbon polymerizable surfactants, *Langmuir* 15 (1999) 7565–7576.
- [89] S. Kubowicz, J.F. Baussard, J.F. Lutz, A.F. Thünemann, H. von Berlepsch, A. Laschewsky, Multicompartment micelles formed by self-assembly of linear ABC triblock copolymers in aqueous medium, *Angew. Chem. Int. Ed.* 44 (2005) 5262–5265.
- [90] Z. Li, E. Kesselman, Y. Talmon, M.A. Hillmeyer, T.P. Lodge, Multicompartment micelles from ABC miktoarm stars in water, *Science* 306 (2004) 98–101.
- [91] S. Sato, J. Iida, K. Suzuki, M. Kawano, T. Ozeki, M. Fujita, Fluorous nanodroplets structurally confined in an organopalladium sphere, *Science* 313 (2006) 1273–1276.
- [92] A. Garcia-Bernabé, M. Krämer, B. Oláh, R. Haag, Syntheses and phase-transfer properties of dendritic nanocarriers that contain perfluorinated shell structures, *Chem. Eur. J.* 10 (2004) 2822–2830.
- [93] A.M. Caminade, C.O. Turrin, P. Sutra, J.P. Majoral, Fluorinated dendrimers, *Curr. Opin. Colloid Interf. Sci.* 8 (2003) 282–295.
- [94] V. Percec, M. Glodde, M. Peterca, A. Rapp, I. Schnell, H.W. Spiess, T.K. Bera, Y. Miura, V.S.K. Balagurusamy, E. Aqad, P.A. Heiney, Self-assembly of semifluorinated dendrons attached to electron-donor groups mediates their π -stacking via a helical pyramidal column, *Chem. Eur. J.* 12 (2006) 6298–6314.
- [95] M.P. Krafft, L. Schieldknecht, P. Marie, F. Giulieri, M. Schmutz, N. Poulain, E. Nakkache, Fluorinated vesicles allow intrabilayer polymerization of a hydrophobic monomer, yielding polymerized microcapsules, *Langmuir* 17 (2001) 2872–2877.
- [96] J.B. Brubach, A. Mermet, A. Filabozzi, A. Gerschel, D. Lairez, M.P. Krafft, P. Roy, Dependence of water dynamics upon confinement size, *J. Phys. Chem. B* 105 (2001) 430–435.
- [97] T. Maruyama, T. Kotani, H. Yamamura, N. Kamiya, M. Goto, Poly(ethylene glycol)-lipase complexes catalytically active in fluorous solvents, *Org. Biomol. Chem.* 2 (2004) 524–527.
- [98] P. Fontaine, M. Goldmann, P. Muller, M.C. Faure, O. Konovalov, M.P. Krafft, Direct evidence for highly organized networks of circular surface micelles of surfactant at the air/water interface, *J. Am. Chem. Soc.* 127 (2005) 512–513.
- [99] M. Maaloum, P. Muller, M.P. Krafft, Lateral and vertical nanophase separation in Langmuir-Blodgett films of phospholipids and semifluorinated alkanes, *Langmuir* 20 (2004) 2261–2264.
- [100] L. Lebeau, F. Lach, C. Vénien-Bryan, A. Renault, J. Dietrich, T. Jahn, M. G. Palmgren, W. Kühlbrandt, C. Mioskowski, Two-dimensional crystallization of a membrane protein on a detergent-resistant lipid monolayer, *J. Mol. Biol.* 308 (2001) 639–647.
- [101] G.M. Whitesides, The origins and the future of microfluidics, *Nature* 442 (2006) 368–373.

- [102] D.L. Chen, R.F. Ismagilov, Microfluidic cartridges preloaded with nanoliter plugs of reagents: An alternative to 96-well plates for screening, *Curr. Opin. Chem. Biol.* 10 (2006) 226–231.
- [103] V. Linder, S.K. Sia, G.M. Whitesides, Reagent-loaded cartridges for valveless and automated fluid delivery in microfluidic devices, *Anal. Chem.* 77 (2005) 64–71.
- [104] B. Zheng, C.J. Gerdt, R.F. Ismagilov, Using nanoliter plugs in microfluidics to facilitate and understand protein crystallization, *Curr. Opin. Struct. Biol.* 15 (2005) 548–555.
- [105] S.F. Flaim, R.M. Winslow, K.D. Vandegriff, M. Intaglietta (Eds.), *Advances in Blood Substitutes*, Birkhäuser, Boston, 1997, pp. 91–132.
- [106] N.C. Nanda, D.W. Kitzman, L.J. Crouse, H.C. Dittrich, Imagent improves endocardial border delineation, inter-reader agreement, and the accuracy of segmental wall motion assessment, *Echocardiography* 20 (2003) 151–161.
- [107] F. Gerber, M.P. Krafft, T.F. Vandamme, M. Goldman, P. Fontaine, Fluidization of a dipalmitoyl phosphatidylcholine monolayer by fluorocarbon gases: Potential use in lung surfactant therapy, *Biophys. J.* 90 (2006) 3184–3192.

Note from the Editors

Partially adapted from “*Composants et systèmes auto-assemblés hautement fluorés pour le diagnostic et la thérapie*,” M.P. Krafft et J. Riess, *Actualité Chimique*, N° 301–302, November 2006. *Actualité Chimique* and *Société Française de Chimie* are acknowledged for authorization.

CHAPTER 12

Exposure of Humans to Fluorine and Its Assessment

Maja Ponikvar*

Jožef Stefan Institute, Jamova 39, SI-1000 Ljubljana, Slovenia

Contents

1. Introduction	488
2. Fluorine in the environment	490
2.1. Fluoride in the lithosphere	491
2.2. Fluoride in air	491
2.3. Fluoride in natural waters	492
3. Essentiality of fluoride	494
4. Adverse effects of fluoride on humans	495
4.1. Chronic toxicity	495
4.1.1. Dental or enamel fluorosis	496
4.1.2. Skeletal fluorosis	497
4.2. Acute toxicity	498
5. Bioavailability of fluoride	499
6. Absorption, metabolism and excretion of fluoride	500
6.1. Plasma fluoride	501
6.2. Tissue fluoride	501
6.3. Fluoride in placenta and foetus	502
6.4. Elimination of fluoride	502
6.4.1. Excretion via the kidneys and urine	503
6.4.2. Excretion via faeces, saliva and sweat	503
6.4.3. Excretion via breast milk	503
7. Biomarkers of fluoride exposure and their status	503
7.1. Plasma, saliva and urine as contemporary markers	504
7.2. Nails and hair as recent markers	504
7.3. Calcified tissues as historical markers	505
8. Fluoride in diet, fluoride supplements, dental products and fluoridated salt and milk	505
8.1. Drinking water and beverages	505
8.1.1. Concentration of fluoride in drinking water	505
8.1.2. Concentration of fluoride in beverages	507
8.2. Milk and baby formulas	508
8.3. Food	509

*Corresponding author. Tel.: +386-1-477-32-03; Fax: +386-1-477-31-55;
E-mail: maja.ponikvar@ijs.si

8.4. Dietary supplements	514
8.5. Dental products	514
9. Fluoride intake	515
9.1. Fluoride intake in adults	516
9.2. Fluoride intake in children	516
9.2.1. Fluoride intake from diet	521
9.2.2. Fluoride intake from fluoride-containing toothpastes	521
9.2.3. Fluoride intake from fluoride-containing supplements	529
9.2.4. Estimated total intake of fluoride in children	530
10. Analytical methods for fluorine	532
10.1. Sample pre-treatment procedures	533
10.2. Analytical methods for determining fluorine	533
10.3. Determining fluorine in specific types of materials	534
10.3.1. Fluorine in environmental media	534
10.3.2. Fluorine in biological tissues, fluids and related materials	535
10.3.3. Fluorine in fluoride supplements and dental products	535
11. Indicators for estimating requirements for fluoride	535
12. AI of fluoride	536
13. Conclusions – enough or too much fluoride?	537
Appendix: List of acronyms	539
References	539
Note from the Editors	549

Abstract

Fluorine is ubiquitous in the nature and is consequently an inevitable part of the biosphere and human life. The adequate intake (AI) of fluoride ion from all sources is set at 0.05 mg/day/kg body weight; this intake is recommended for all ages above 6 months, because it confers a high level of protection against dental caries and is not associated with any known unwanted health effects. Unfortunately already at this and even lower intakes, there is a risk of dental fluorosis which, on the one hand, is considered as cosmetic and, on the other, as having an adverse effect. This reveals that the border between safe and potentially harmful dosage is narrow and that despite numerous studies knowledge on the fluorine toxicity is still relatively poor.

This paper is written with the aim of providing sufficient background to help understand the mechanism of action of fluoride ion on humans. Current information on the main sources of human exposure to fluoride and current recommendations for AI of fluoride, as well as methods for assessing exposure are reviewed.

1. INTRODUCTION

Elemental fluorine, which is a member of the halogen family, is a pale yellow-green, irritating gas with a sharp odour and atomic mass of 18.998. Fluorine is chemically most reactive of all the elements and does not therefore occur naturally in the free state. In combination it comprises 0.065% of the earth's crust, being the 13th element in abundance [1], and is an inevitable part of the biosphere and human life. The term 'fluorine' is, in this report, used to denote the element in any of its forms and 'fluoride' to denote free inorganic fluoride to which a fluoride ion-selective electrode (ISE) responds.

For over seven decades, it has been recognized that fluoride may have both beneficial and harmful effects on dental health. Small amounts of fluoride have been proven to be beneficial in preventing dental caries because of the greater resistance of enamel-containing fluoride to ingested acids or to acids generated by oral bacteria from ingested sugars; in addition, fluoride also inhibits sugar metabolism in oral bacteria [2]. On the other hand, excessive intake of fluoride during enamel maturation, before tooth eruption, from birth to 7–8 years of age, when enamel formation is complete, can lead to the development of dental fluorosis of deciduous, but predominantly of permanent, teeth. Excessive fluoride intake by children older than 7–8 years does not cause dental fluorosis. Fluoride also has the unique ability to stimulate new bone formation. The actual mechanism of fluoride action is still a subject of debate; however, it is more recently believed that the majority of the benefit from fluoride can be attributed to its topical, rather than systemic, effects [3–5].

A conflict arises from two claims: the first, that fluoride stimulates new bone growth and hence is useful therapeutically in controlling osteoporosis, and the other, that it is the cause of the increasing prevalence of hip fractures in the elderly [6]. Fluoride is currently not recommended for the treatment of osteoporosis, although slow release fluoride therapy is reportedly beneficial. The long-term benefit of the latter is unknown [7].

Fluorine is available to humans, plants and animals mainly in the form of fluoride ion (F^-). Body fluoride status depends on numerous factors, including the total amount of fluoride ingested daily, its bioavailability and metabolism. The adequate intake (AI) of fluoride from all sources is set by the Standing Committee on the Scientific Evaluation of the Dietary Reference Intakes at 0.05 mg/day/kg body weight; this intake is recommended for all ages above 6 months, because it confers a high level of protection against dental caries and is not associated with any known unwanted health effects [8].

Drinking water, beverages and fluoride-containing dentifrices are regarded as the main dietary contributors to human fluoride intake. Food has more recently been recognized as a potentially important source of fluoride. A major source of fluoride in some areas arises from its release into the environment by coal combustion, in process waters and waste from various industrial processes.

Because of the low natural levels of fluoride in some water supplies and correspondingly high levels of dental caries, many authorities worldwide have permitted, or instigated, fluoridation of water supplies, although this has met some opposition, partly because of the potential health or dental effects including fluorosis. In order to prevent dental caries, fluoride is deliberately added to salt or milk in some countries.

Much research has been devoted to fluoride and its health effects, but, although the benefits and risks of exposure to fluoride are well known, it is still not possible to make a firm distinction between a safe daily dose and a potentially harmful one.

Thresholds of 0.05–0.07 and 0.03–0.04 mg/day/kg body weight of fluoride have both been suggested for the appearance of dental fluorosis [9–11]. It is not surprising that few subjects in medicine have proved more controversial than fluoridation of public water supplies, although supported by the World Health Organization (WHO) among other organizations [6]. The controversy is illustrated by the fact that, while the U.S. Centers for Disease Control and Prevention (CDC) claimed that water fluoridation is 1 of the 10 great public health achievements in the United States during the 20th century [12] – nearly two-thirds of the population receives fluoridated drinking water [13] – water fluoridation is banned in most of Europe [14]. Dental fluorosis has also been controversial at times – on the one hand, it is considered as cosmetic and, on the other, as having an adverse effect.

It appears that, in our current state of knowledge, fluoride illustrates surprisingly well the classical medical concept that the effect of a substance depends on the dosage regimen. As Paracelsus (1493–1541) said, ‘All substances are poisons; there is none which is not a poison. The right dose differentiates a poison and a remedy’.

This paper is written with the aim of providing sufficient background to help understand the mechanism of action of fluoride ion on humans. The main focus is on the effects of fluoride on dental health, in-depth discussion of skeletal fluorosis and use of fluoride for treating osteoporosis being outside the scope of this paper. Current information on the main sources of human exposure to fluoride and current recommendations for adequate intake (AI) of fluoride, as well as methods for assessing exposure, will be reviewed.

2. FLUORINE IN THE ENVIRONMENT

Fluorides are released into the environment naturally through the weathering and dissolution of minerals, in emissions from volcanoes and in marine aerosols [15,16]. The anthropogenic sources of fluoride and fluoride-containing emissions include release into the environment through coal combustion and in process waters and waste from various industrial processes, including steel manufacture, primary aluminium, copper and nickel production, phosphate ore processing, phosphate fertilizer production and use, glass, brick and ceramic manufacturing, and glue and adhesive production [17]. See also the first two volumes of this series devoted to fluorine and the environment [18]. The use of fluoride-containing pesticides and the controlled fluoridation of drinking water supplies also contribute to the release of fluoride from anthropogenic sources.

With regard to anthropogenic sources of fluoride, problems have occurred in the mining of phosphates and fluor spar when fluoride rich dust has been blown over long distances by the wind and deposited on plants, thereby entering the food chain. The use of fluoride-containing pesticides can have the same effect, requiring their use to be avoided, or at least limited to the greatest possible

extent. Important sources of undesirable fluoride in soil are the use of fertilizers, the discharge of industrial waste into streams and deposition of airborne fluorides.

2.1. Fluoride in the lithosphere

Fluorine, combined chemically in the form of fluorides, constitutes 0.065% of the earth's crust, being the 13th element in abundance and occurring more widely than chlorine and 5–10 times more abundantly than zinc or copper [1]. In rock and soil, fluoride occurs in a wide variety of minerals, including fluorspar (CaF_2), cryolite (Na_3AlF_6), apatite ($\text{Ca}_5(\text{PO}_4)_3(\text{OH}, \text{F}, \text{Cl})$) and in groups of minerals such as mica, hornblende and a number of pegmatites such as topaz and tourmaline. Despite its obvious abundance, however, most of it is, under normal conditions, firmly bound to minerals and other compounds and therefore not available to plants and animals in its usual biological form of fluoride ion.

Fluoride is a natural component of most types of soil, in which it is mainly bound in complexes and not readily leached. The major source of free fluoride ion in soil is the weathering and dissolution of fluoride rich rock that depends on the natural solubility of the fluoride compound in question, pH, and the presence of other minerals and compounds and of water. The major parameters that control fluoride fixation in soil through adsorption, anion exchange, precipitation, formation of mixed solids and complexes are aluminium, calcium, iron, pH, organic matter and clay [19,20].

Larsen and Widdowson [21] estimated the average fluoride concentration in soil to be about 300 mg/kg. The amount in organic soils is usually lower than in mineral soils.

2.2. Fluoride in air

Airborne fluoride exists in gaseous and particulate forms emitted from both natural and anthropogenic sources. The gaseous fluorides include hydrogen fluoride (HF), carbon tetrafluoride (CF_4), hexafluoroethane (C_2F_6) and silicon tetrafluoride (SiF_4), while particulate fluorides include cryolite (Na_3AlF_6), chiolite ($\text{Na}_5\text{Al}_3\text{F}_{14}$), calcium fluoride (CaF_2), aluminium fluoride (AlF_3) and sodium fluoride (NaF) [17]. The distribution and deposition of airborne fluoride are dependent upon emission strength, meteorological conditions, topography, particle size and chemical reactivity [22,23].

The annual global release of hydrogen fluoride from natural sources, through degassing and explosive eruptions, ranges from 0.06 to 6 Tg, of which 0.05–5 Tg is released into the troposphere and 0.005–0.5 Tg is erupted explosively into the stratosphere [15]. Thus, volcanoes must be regarded, next to the photolysis of anthropogenic halocarbons in the stratosphere, as a significant source of tropospheric and stratospheric HF. Another important natural source

of fluoride is sea salt released from the oceans in the form of marine aerosols, containing ~ 0.02 Tg annually [24].

Anthropogenic sources of fluoride include fossil fuel combustion and industrial waste. Hydrogen fluoride is water soluble and emissions are readily controlled by acid gas scrubbers. HF emission from coal combustion, that is considered to be the main anthropogenic source of HF, was estimated to be 0.18 Tg annually; emission of HF from the combustion of petroleum and natural gas is almost certainly negligible [24]. Apparently only limited data are available concerning total annual emissions of HF from industrial operations; however, there is evidence that emissions of fluorides have been declining [24,25].

Fluorine-containing gases do not disperse so rapidly in the atmosphere as other gases. Smoke is often carried over great distances and can cause considerable damage when it finally descends. Dässler and Grumbach [26], for instance, were able to detect fluorine-containing gases emitted under very humid conditions at a distance of 1–2 km from the source, and reported that fluorine levels at a distance of 7–8 km from the source could be higher than in nearby zones. Molecular fluorine and hydrogen fluoride are largely responsible for the plant damage caused by stack gases [18]. The effects of fluoro-organics on plants and organisms are presented in details in Vol. 1 of this series by Davison and Weinstein [27]. Hydrogen fluoride is reportedly 1000 times as harmful as sulphur dioxide and there can be no doubt that the harmful effect of the latter on plants is greatly exacerbated by traces of fluorine [28].

Fluoride concentrations in ambient air were studied by Thompson *et al.* [29] from 1966 to 1968. A total of 2164 samples were taken in non-urban and 9175 in urban areas. 98.5% of those from non-urban areas contained less than $0.05 \mu\text{g}/\text{m}^3$, 1.3% contained $0.05\text{--}0.09 \mu\text{g}/\text{m}^3$ and only 0.1% contained $0.1\text{--}0.99 \mu\text{g}/\text{m}^3$ of fluoride. Levels in urban areas were slightly higher, 87.8% of samples containing less than $0.05 \mu\text{g}/\text{m}^3$, 4.2% containing $0.05\text{--}0.09 \mu\text{g}/\text{m}^3$, 7.7% containing $0.10\text{--}0.99 \mu\text{g}/\text{m}^3$ and 0.2% more than $1.00 \mu\text{g}/\text{m}^3$ of fluoride. The maximum concentrations observed were 0.16 from non-urban and $1.89 \mu\text{g}/\text{m}^3$ from urban locations.

2.3. Fluoride in natural waters

Natural waters contain fluorides in varying concentrations, which depend mainly on factors such as availability and solubility of minerals containing fluoride, porosity of the rock and soils through which the water passes, residence time, temperature, pH and the presence of other elements. Concentrations of fluoride in water also vary according to the natural sources of emission and to anthropogenic discharges that lead to increased levels of fluoride in the environment. Fluoride levels of groundwater are higher than in surface water because they are more influenced by the rocks through which they pass [25]. Waters with high concentrations of fluoride are usually found at the foot of high mountains and in

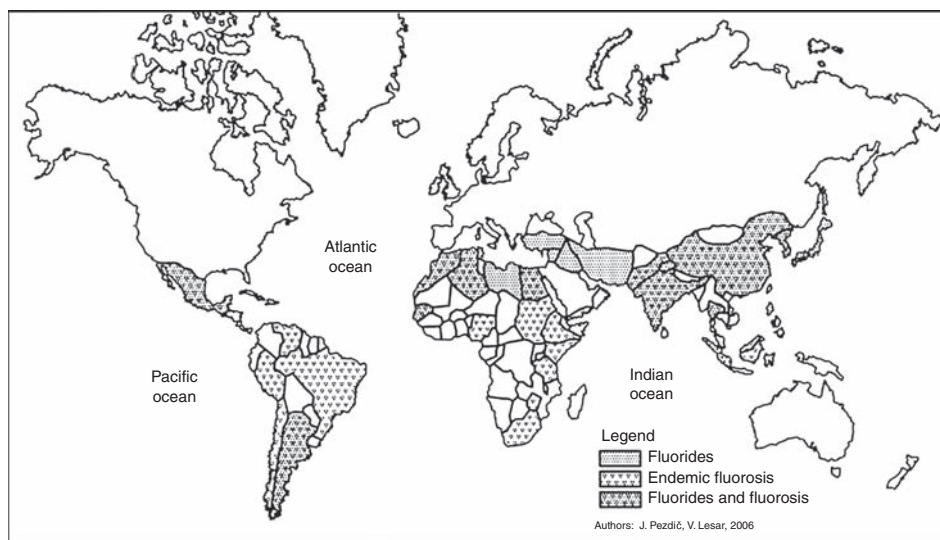


Fig. 1. Areas of the world with endemic fluorosis and areas with high concentrations of fluoride in water.

areas with geological deposits of marine origin. Typical examples are the geographical belt from the Syrian Arab Republic through Jordan, Egypt, the Libyan Arab Jamahiriya, Algeria, Morocco and the Rift Valley. Another belt is that stretching from Turkey through Iraq, the Islamic Republic of Iran and Afghanistan, to India, northern Thailand and China. Similar areas can be found in the America and in China and Japan [6]. Areas of the world with endemic fluorosis and areas with high concentrations of fluoride in water are presented in Fig. 1 prepared by Pezdič and Lesar based on the data from WHO [6] and UNICEF (The United Nations Children's Fund) [30].

Most of the water normally available to humans is involved in the hydrological cycle, which means that it originates in the sea. Fluoride is usually transported through the water cycle bound by an excess of aluminium [31].

Concentrations of fluoride in seawater, $\sim 0.8\text{--}1.5$ mg/L, are higher than in fresh water [6,25]. The concentration of fluoride in non-polluted surface water in areas with low natural fluoride generally ranges between 0.01 and 0.3 mg/L [16,17]. The amount of fluoride in water in areas with high naturally occurring fluoride is usually above 1 mg/L, reaching up to 50 mg/L in springs and geysers. The highest value ever found in water was recorded in Lake Nakuru in the Rift Valley in Kenya, namely 2800 mg/L [17].

The general nature of the geology is not always an indicator of the concentrations of fluoride in groundwater. There are significant variations in the distribution of rocks with readily leaching fluoride. It has been observed that, even within one village community, different wells often show widely divergent concentrations of fluoride, apparently as a result of differences in the local hydrogeological conditions [6].

The concentration of fluoride in rainwater is negligible. Samples of rainwater taken in eight catchments in the heavily industrialized area of Northern Europe revealed median concentrations over 30 days of less than 0.05 mg/L of fluoride [32].

Defluoridation processes of polluted waters are in progress; see for instance recent articles by Pontié *et al.* and by Onyango and Matsuda [18].

3. ESSENTIALITY OF FLUORIDE

Many elements occur in living organisms in such small amounts that early researchers were unable to detect their presence or measure their precise amounts. Interest in trace elements in human and animal physiology began over a century ago with the development and advances in technology that allowed detection and measurement of traces of a number of metal-containing compounds that were not previously suspected to be of biological significance. During the 1930s, a wide range of nutritional disorders of humans and farm stocks were found to be caused by either deficiency or excessive intake of trace elements from the natural environment. In 1931, three research teams independently recognized that fluoride in water consumed during infancy and early childhood resulted in mottling of tooth enamel [33–35].

The criteria for identifying nutritionally essential trace elements have evolved extensively over the past 50 years and may be expected to expand as the result of future research. The definition of elements as essential is thus difficult and, depending on the definition of essentiality, not unanimous. Iyengar *et al.* [36], in 1978, considered an element to be essential if (1) the organism can neither grow nor complete its life cycle if the element is not available in sufficient quantity, (2) the element cannot be wholly substituted by another element and (3) the element has a direct influence on the organism and is involved in its metabolism. Based on this definition, fluorine is not an essential element. Later, in 1987, Underwood and Mertz [37] established essentiality as being when a reduction of the element below the range of tolerable levels, better termed 'range of safe and adequate intake', results in a consistent and reproducible impairment of a physiological function. On this basis, fluorine was included in the list of essential elements because of its proven benefits for dental health and its suggested role in maintaining the integrity of bones.

The old paradigm that dominated nutrition research of the past was dissection. The complex health effects of whole diets were amenable to scientific study only by separating foods into their components, which could be measured and their effects investigated individually. The gradual emergence of 'new' paradigms and their influence on nutrition research increased to the point where they began to modify the old paradigm. 'New', emerging paradigms were addressed by Mertz [38] in 1993: (1) the concern with individual nutrients (dissection) is being complemented by a concern for balanced interactions within the whole diet

(synthesis); (2) the division of the elements into essential and toxic categories is slowly being replaced by the concept of the total dose–response curve and (3) the dominating role of the concept of deficiency in determining nutritional requirements is gradually being complemented by a concern for the total health effects of elements. In accordance with these paradigms, the Expert Consultation of the WHO, Food and Agricultural Organization and International Atomic Energy Agency [39] accepted in 1996 a revised definition of essentiality that says: ‘An element is considered essential to an organism when reduction of its exposure below a certain limit results consistently in reduction in a physiologically important function, or when the element is an integral part of an organic structure performing a vital function in that organism’. This definition is not absolute; it depends on what is considered to constitute a ‘physiologically important function’, ‘consistent’ functional impairment, etc. Caries is not a result of fluoride deficiency; however, since the Expert Consultation considered resistance to dental caries to be a physiologically important function, the element fluorine was regarded as essential. Fluorine was, at the same time, classified into the group of potentially toxic elements, some of which may nevertheless have some essential function at low levels [39].

It has to be recognized that, although fluorine should be probably regarded as an essential element, there is no evidence so far from human studies that overt clinical signs of fluoride deficiency exist. No specifically diagnostic clinical or biochemical parameters have been related to fluoride deficiency [8,39]. It must also be noted that an experimental diet completely free of fluoride, capable of provoking fluoride deficiency, is difficult to obtain. It is also difficult to prove that it is free of fluoride, because of methodological and analytical problems in determining fluorine at low levels.

4. ADVERSE EFFECTS OF FLUORIDE ON HUMANS

Already in 1937 Roholm [40], originator of modern fluoride research, distinguished between chronic and acute toxicity of inorganic fluorides. Chronic toxicity is the result of continuous or repeated exposure of an organism to a toxic substance. Acute toxicity involves harmful effects in an organism through a single or short-term exposure to a toxic substance.

4.1. Chronic toxicity

Fluoride is a cumulative toxin, which accumulates in mineralized tissues, notably in the lattice of bone and tooth crystals [8,39]. The biological effects in humans due to chronic fluoride ingestion depend not only on the total dosage and duration of exposure, but also on associated factors such as nutritional status, functional status of the renal tissue and interaction with other trace elements [41]. The effect of

fluorine is cumulative, so that less serious consequences occur early in the natural course of disease. Whatever may be the type of fluorine exposure, the clinical picture in chronic poisoning occurs in a phased manner [41].

The primary adverse effects associated with chronic, excess fluoride intake are skeletal, and dental or enamel, fluorosis. Other effects, including hypersensitivity reactions, renal insufficiency, immunological effects, possible association with repetitive strain injury, birth defects and cancer have been observed and discussed [17,41–45].

4.1.1. Dental or enamel fluorosis

Dental or enamel fluorosis is an irreversible dose–response effect caused by fluoride ingestion during the pre-eruptive development of teeth. The pre-eruptive maturation of crowns of the anterior permanent teeth, which are of most concern aesthetically, is complete and, together with the risk of fluorosis, is over by the age of 7–8 years [46,47]. After the enamel has completed its pre-eruptive maturation, it is no longer susceptible. Therefore, fluoride intake up to the age of 7–8 years is of most interest. Although it is usually the permanent teeth that are affected, occasionally the deciduous teeth may be also involved.

The symptoms of fluorosis are easy to recognize. The clinical features of mild dental fluorosis vary from thin white striations across the enamel surface to white flecks or small pits on the enamel of the teeth. With increasing severity, the white areas merge and loss of enamel surface can occur. Discrete and confluent pitting of the surface of the teeth is seen in severe cases. The loss of enamel involves only the surface and not the full thickness of the enamel. Fluorosed enamel has a high protein content, resulting in increased porosity; as a consequence, brownish discolouration of the enamel may occur due to uptake of colour from diet into the porous enamel. Mild dental fluorosis has no effect on tooth function and may render the enamel more resistant to caries [8]. This type of fluorosis is not readily apparent to the affected individual or casual observer and often requires a trained specialist to detect it. In contrast, the moderate and severe forms of dental fluorosis are generally characterized by aesthetically (cosmetically) objectionable changes in tooth colour and surface irregularities. Teeth demonstrating fluorosis [48] are showed in Fig. 2.

Several methods have been developed for quantifying dental fluorosis. The most commonly used method is Dean's index [49], which classifies fluorosis on a scale of 0 to 4 as follows: class 0, no fluorosis; class 1, very mild fluorosis (opaque white areas irregularly covering $\leq 25\%$ of the tooth surface); class 2, mild fluorosis (white areas covering 25–50% of the tooth surface); class 3, moderate fluorosis (all surfaces affected, with some brown spots and marked wear on surfaces subject to attrition) and class 4, severe fluorosis (widespread brown stains and pitting). The average score of the two most severely affected teeth is used to derive the classification. Other commonly used methods to rate dental fluorosis include the Thylstrup-Fejerskov Index (TFI) [50] and the tooth surface

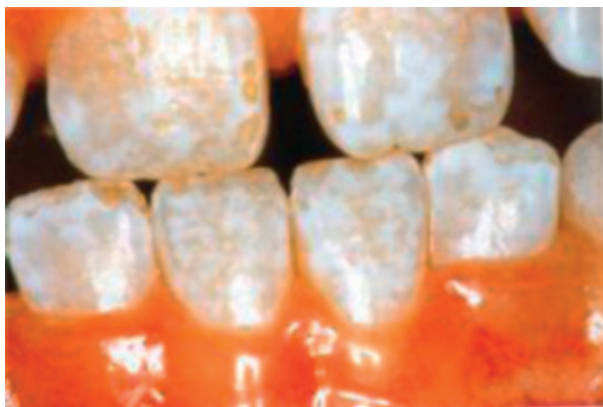


Fig. 2. Teeth demonstrating fluorosis. A high level of dietary fluoride has resulted in much of the enamel becoming opaque in patches, giving a 'mottled' appearance. (Reprinted with permission from [48]. Copyright 2002 Mosby International Limited.) (See Colour Plate Section at the end of this book.)

index of fluorosis (TSIF) [51]. Unlike the Dean's index, the TFI and TSIF use all tooth surfaces to develop the final index score.

Due to ubiquitous exposure to fluoride sources other than drinking water, it is not possible to draw firm conclusions regarding the independent effects of fluoride in drinking water on dental caries and its prevention. It has been estimated that moderate dental fluorosis occurs in 1–2% of the population exposed to fluoride at 1 mg/L in drinking water and in about 10% of the population at 2 mg/L; moderate/severe fluorosis occurs in variable percentages ranging up to 33% of the population exposed to fluoride at 2.4–4.1 mg/L [52].

It is interesting to note that, in the middle of the 20th century, the paradigm was that, to exert its maximum cariostatic effect, fluoride had to become incorporated into dental enamel during development. Hence, a certain prevalence and severity of fluorosis in a population was inevitable if the prevalence and severity of caries among children was to be minimized. Dental fluorosis was thus regarded as an unfortunate side effect of fluoride's caries-protective benefits, and attempts to play down the possible toxic effect of fluoride on developing dental enamel often led the dental profession to present dental fluorosis as merely a cosmetic problem [53].

4.1.2. Skeletal fluorosis

Skeletal fluorosis can be defined as excessive deposition of fluoride in bone. This is a pathological condition that is by far the most important aspect of chronic exposure to elevated levels of fluoride, either by inhalation or by ingestion. The skeletal deformities may be associated with or accentuated by nutritional deficiencies or even malnutrition and hard manual work or, possibly, other conditions found in areas of long-term social and nutritional deprivation [6]. See, for instance Fig. 1 of [54]. The situation is specific also for populations consuming large volumes of water, such as athletes or people with certain medical conditions or

in some tropical areas where, due to higher temperatures, water consumption is increased.

Skeletal fluorosis exhibits several stages. Two pre-clinical asymptomatic changes are characterized by slight, radiographically detectable increases in bone mass. An early symptomatic stage is characterized by sporadic pain and stiffness of joints, arthritic symptoms, slight calcification of ligaments and increased osteosclerosis of cancellous bones, sometimes accompanied by osteoporosis of long bones. Crippling skeletal fluorosis is characterized by marked limitation of joint movements, considerable calcification of ligaments, crippling deformities of the spine and major joints, muscle wasting and neurological defects associated with compression of the spinal cord [52].

Endemic crippling skeletal fluorosis is confined in temperate climates to individuals exposed continuously over many years to very high levels of fluoride; these cases are associated with industrial situations, with unusually high levels of fluoride in drinking water (e.g., 10 mg/L) or the use of high fluoride coal for cooking and drying foodstuffs indoors [6,17,55].

Most data on the occurrence of skeletal fluorosis in occupationally exposed workers have come from older studies. Roholm [40] estimated that, for cryolite workers, the effective daily fluoride intake lies very probably between 0.20 and 0.35 mg/kg (equivalent to 14–25 mg for a 70-kg man). This intake for 10–20 years causes mild to severe signs of osteosclerosis. Hodge and Smith [56] reviewed older studies involving aluminium smelter workers, in which the number of workers examined was usually small and quantitative data on exposure to airborne fluoride were not always provided. They concluded that the incidence of detectable osteosclerosis was often high when the levels of fluoride in the air exceeded 2.5 mg/m³ and/or levels of fluoride in the urine of these workers were greater than 9 mg/L. At airborne concentrations below 2.5 mg/m³ and levels in the urine below 5 mg/L, years of exposure in potrooms produced no osteosclerosis.

Most epidemiological research has indicated that an intake of at least 10 mg/day for 10 or more years is needed to produce clinical signs of the milder forms of osteosclerosis [8]. Water fluoride concentrations of 4–8 mg/L in temperate climates have not been found to be associated with any signs or symptoms of skeletal fluorosis [6]. This data should be regarded with scepticism in view of reports from a number of developing countries that endemic skeletal fluorosis occurs in individuals whose drinking water contains more than 6 mg/L of fluoride [6].

4.2. Acute toxicity

The toxicity of fluoride depends on the type of compound ingested. Generally, the more soluble salts of inorganic fluorides, such as sodium fluoride, are more toxic than those that are either weakly soluble or insoluble [42]. Readily soluble fluoride compounds release free fluoride ions on dissolution, while fluoride compounds that are insoluble or poorly soluble do not [57,58]. Fluoride from the former

group, that includes sodium fluoride (NaF), hydrogen fluoride (HF), fluorosilicic acid (H_2SiF_6) and sodium monofluorophosphate ($\text{Na}_2\text{PO}_3\text{F}$), is easily and almost completely absorbed, while fluoride from substances in the latter group, that include calcium fluoride (CaF_2), magnesium fluoride (MgF_2) and aluminium fluoride (AlF_3), is poorly absorbed [42].

The acute toxic dose of fluoride in humans has been believed to be 2–5 or 8 mg/kg body weight; however, acute fluoride poisoning has occurred at doses from 0.1 to 0.8 mg/kg body weight [59]. Symptoms of acute oral fluoride intoxication may include severe nausea, vomiting, hypersalivation, abdominal pain, cramps and diarrhoea; in severe or fatal cases, these symptoms are followed by convulsion, cardiac arrhythmia and coma [59]. A reasonable, estimated ‘certainly lethal dose’ of sodium fluoride for the average 70 kg adult has been estimated to range between 5 and 10 g, corresponding to 32–65 mg fluoride/kg body weight [60].

The dose range estimated for adults has little utility in cases involving young children. A probable toxic dose of 5 mg/kg body weight of fluoride can be reached in a 10-kg, 1-year-old child after ingestion of approximately fifty 1 mg fluoride tablets, 50 g of toothpaste containing 1000 μg fluoride/g (the old unit ppm is still widely used in the literature; 1 ppm being $\sim 1 \mu\text{g/g}$ or $1 \mu\text{L/L}$), or 50 ml of 0.2% sodium fluoride rinse or 0.4% stannous fluoride rinse gel. Ingestion of approximately twice these amounts can cause toxicity in a 5-year-old child [60].

The basis of the treatment of fluoride poisoning is intravenous or intramuscular calcium therapy [61,62].

5. BIOAVAILABILITY OF FLUORIDE

Bioavailability may be defined as the ‘extent to which, and sometimes rate at which, the active moiety (drug or metabolite) enters the systemic circulation, thereby gaining access to the site of action’ [7]. A common way of studying the bioavailability of drugs is to compare plasma concentration curves and urinary excretion data after a single oral dose, with similar data obtained after intravenous administration. By definition, when a medication is administered intravenously, its bioavailability is 100%. Fluoride compounds that occur naturally or are added to drinking water and yield fluoride ions on dissolution generally exhibit high bioavailability. Bioavailability is lower in the presence of high dietary concentrations of calcium and certain other divalent or trivalent cations with which fluoride can form insoluble or poorly soluble compounds. Nutritional and clinical aspects of fluoride bioavailability have been reviewed by Cerklewski [63].

Most studies assessing bioavailability of fluoride in humans have concentrated on comparing fluoride concentration in the plasma after intake of a substance or food, the values obtained then being compared to plasma values obtained after intravenous or oral administration of sodium fluoride [64–68]. Studies on the bioavailability of fluoride, based on both plasma and urine values of fluoride, were

also reported [69,70]. The methodological approach of these studies is based on the assumptions that sodium fluoride is fully absorbed (100%) on an empty stomach, no endogenous loss of fluoride occurs and urinary excretion is the major route of fluoride elimination.

The bioavailability, from a fasting stomach, of fluoride from sodium fluoride tablets, as used in many caries-prevention programmes, was almost 100% [64]. In studies on adults, this bioavailability was decreased to 50–79% by co-administration of milk or calcium rich products [70]. Yet in another study it was shown that this effect of milk was abolished when fluoride was taken as a part of the breakfast [66]. The authors suggested that formation of calcium salts and entrapment of fluoride in coagulation products of milk are important factors causing the reduction of fluoride bioavailability, and that prolonged stay of chyme after concomitant ingestion of food allows fluoride to become liberated from the bound forms and coagulation products by digestion [66]. The poor fluoride bioavailability, in the range of 4–24%, observed from food such as bone meal, fish bone meal, canned sardines and chicken bone meal, was ascribed to the high content of calcium in these foods so only part of the total fluorine present in the food could be liberated during the digestion process [65]. Low bioavailability of fluoride (2–32%) was reported in humans from diets commonly consumed in India [68]. The data presented show a wide range of bioavailability (2–79%) of fluoride from different foods in adults and that factors such as pH, the amount of ingested food, and the presence and type of minerals in ingested food are also important.

The bioavailability of fluoride from diet and fluoride supplements in infants was about 90% [71].

Results suggest that the mode of administration of a given product is highly important for fluoride bioavailability; bioavailability is thus best determined under conditions that simulate the normal mode of intake of the products or food to be tested.

6. ABSORPTION, METABOLISM AND EXCRETION OF FLUORIDE

The metabolism of fluoride and the effects of normal and abnormal intake of fluoride on body processes have been investigated extensively. The concentration of fluoride ion is generally considered to be more significant than that of total fluorine in assessing the effects of excessive fluorine intake on normal metabolism. However, if fluoride binds to the enzyme, substrate, or the co-factor of a given enzymatic reaction, the bound fluoride will affect the overall process. Although the importance of ionic fluoride is generally recognized, it is total fluorine rather than ionic fluoride concentrations that have been reported in most publications.

In humans, the predominant route of absorption of fluoride is via the gastrointestinal tract. Airborne fluoride may also be inhaled. Dermal absorption is negligible except in cases of hydrofluoric acid burns [42].

When ionic fluoride enters the acidic environment of the stomach lumen, it is largely converted to weak acid hydrogen fluoride (HF) with a pK_a of 3.45 [17]. The higher acidity of the stomach speeds up the process of absorption by passive diffusion from both the stomach and the small intestine, suggesting that fluoride is absorbed from the stomach as undissociated hydrogen fluoride rather than as fluoride ion [63,72]. Most of the fluoride that is not absorbed from the stomach will be rapidly absorbed from the small intestine. There is no convincing evidence that active transport processes are involved [17].

6.1. Plasma fluoride

Fluoride taken in the form of sodium fluoride as a tablet or solution is absorbed rapidly. Only a few minutes after intake, there is a rise in plasma fluoride. The fluctuation in plasma fluoride concentration is dependent on the fluoride dose ingested, the dose frequency and the plasma half-life of fluoride. The half time for absorption is ~ 30 min, so peak plasma concentration usually occurs within 30–60 min [64–69]. Absorbed fluoride is rapidly distributed by the circulation to the intracellular and extracellular fluids and is retained only in calcified tissues. The sensitivity of the serum fluoride concentrations to previous intake, glomerular filtration and the intensity of bone resorption suggests that the human organism exerts no direct homeostatic control and that fluoride concentrations reflect the recent intake [73]. Plasma fluoride levels increase with age, with increasing fluoride content of bone and as a consequence of renal insufficiency [2].

Fluoride is present in human and animal serum in two forms, inorganic fluoride and organic fluorine [74–76]. The former consists of ionic and non-ionic fluoride and the latter of fluorine covalently bound within an organic molecule originating from natural or industrial sources [77,78]. Table 1 shows average concentrations of inorganic fluoride and organic fluorine in human plasma in dependence on the concentration of fluoride in drinking water [76].

The data show that the average concentration of fluoride, but not of organic fluorine, in plasma is directly related to the fluoride concentration in the water ingested. There is apparently no relationship between concentrations of inorganic fluoride and organic fluorine in plasma.

6.2. Tissue fluoride

Fluoride is rapidly distributed in plasma and deposited in bone and other calcified tissues that contain $\sim 99\%$ of the body's fluoride; the remainder is distributed between blood and soft tissues [52]. About 50% of daily fluoride intake is associated with the calcified tissues within 24 h and remaining 50% will be excreted in urine. This 50:50 distribution is strongly shifted to greater retention in the very young and probably towards greater excretion in the later years of life [8].

Table 1. Effect of concentration of inorganic fluoride in drinking water on average concentrations of inorganic fluoride and organic fluorine in plasma [76]

$C(F^-)_{\text{water}}$ [mg/L]	$C(F_{\text{inorg.}}^-)_{\text{plasma}}$ [$\mu\text{g/ml}$] ^a	$C(F_{\text{org.}})_{\text{plasma}}$ [$\mu\text{g/ml}$] ^b
<0.10	0.007	0.023
0.90	0.019	0.025
1.0	0.017	0.030
2.1	0.036	0.045
5.6	0.082	0.021

^a Concentration of inorganic fluoride in plasma.

^b Concentration of organic fluorine in plasma.

Fluoride is incorporated into bone by replacing the hydroxyl ion in hydroxyapatite to form fluorohydroxyapatite. Fluoride in calcified tissues is strongly but not irreversibly bound. It appears that fluoride in bone exists in two pools, one rapidly and the other slowly exchangeable [8]. The former is located in the hydration shell of the bone crystallites, where fluoride can be exchanged isoionically or heteroionically with ions in the surrounding extracellular fluids, while mobilization from the slowly exchangeable pool results from the resorption associated with the process of bone remodelling [8]. Typical levels in adult bone vary between 500 and 4000 mg/kg bone ash [52].

6.3. Fluoride in placenta and foetus

Fluoride readily crosses the placenta and is found in foetal and placental tissue. There appears to be a direct relationship between fluoride levels in maternal blood and cord blood [79–82]. At relatively low maternal blood levels, the cord blood levels were at least 60% of that of maternal blood [80,82]. Although cord fluoride levels were typically lower than maternal levels, one study found no statistical difference between maternal and newborn (1-day-old) serum fluoride levels, suggesting that cord serum fluoride levels do not reflect foetal fluoride status [83]. There is also evidence, however, that the placenta can accumulate fluoride, possibly playing a regulative role that helps protect the foetus from excessive amounts of fluoride, when maternal fluoride intake is high [79,84].

6.4. Elimination of fluoride

Absorbed fluoride that is not deposited in calcified tissue is excreted. The primary pathway for fluoride excretion is via the kidneys and urine; to a lesser extent, fluoride is also excreted in the faeces, sweat and saliva.

6.4.1. Excretion via the kidneys and urine

The major route of fluoride excretion is via the kidney and urine; 40–60% of the daily intake is excreted in the urine with an elimination half-life of about 5 h [17,85]. Fluoride excretion is influenced by a number of factors, including glomerular filtration rate, urinary flow and urinary pH. The excretion of fluoride in urine is reduced in individuals with impaired renal function. Urine fluoride excretion is 0.79 mg/day in humans with normal renal function, 0.53 mg/day in those with questionable and 0.27 mg/day in those with impaired renal function [86].

6.4.2. Excretion via faeces, saliva and sweat

10–25% of the daily intake of fluoride is not absorbed and is excreted in the faeces [6]. It has been estimated that 1% or less of an ingested dose is excreted in saliva [87]; because saliva is swallowed, this amount does not enter mass balance calculations. In contrast to the situation for most electrolytes, the fluoride concentration in saliva appears to be independent of salivary flow rate [87]. Sweat provides only a minor route of fluoride excretion, even under extreme environmental conditions [6].

6.4.3. Excretion via breast milk

The fluoride content of human breast milk usually follows the natural daily fluoride intake during the first 6 months of life. This is especially important when comparing the daily fluoride intake by formula-fed and breastfed infants. In humans, fluoride is poorly transferred from plasma to breast milk [88,89]. A wide range (2–50 µg/L) of fluoride in breast milk has been reported [88–90], although considerably higher levels, exceeding 200 µg/L, have also been reported [91]. The wide range of concentrations reported in human milk can apparently be ascribed to analytical problems at low levels of fluoride.

A single dose of 1.5 mg sodium fluoride did not result in a significant rise in fluoride concentrations in breast milk within 3 h [88]. Although no correlation has been found between concentrations of fluoride in tap water and concentrations of fluoride in breast milk, significantly higher, although still relatively low, concentrations of total fluorine and ionic fluoride were found in breast milk of women living in an area with high concentrations of naturally occurring fluoride in tap water than in those living in areas with low concentrations of fluoride in tap water [90].

7. BIOMARKERS OF FLUORIDE EXPOSURE AND THEIR STATUS

Monitoring human exposure to fluoride can be accomplished with varying degrees of accuracy through the analysis of several biological fluids and tissues. The concentrations of fluoride in plasma, serum and urine have been considered

as useful biomarkers for monitoring deficiency or excessive intake of biologically available fluoride. Concentrations of fluoride in nails or hair and in bones and teeth have also been used as biomarkers of exposure. There are, however, ethical and technical limitations of the use of these fluids and tissues for large-scale monitoring of the body burden of fluoride in humans.

7.1. Plasma, saliva and urine as contemporary markers

The levels of fluoride in body fluids (plasma, saliva, urine) give some indication of recent fluoride intake. Fluoride ion does not produce any metabolites, and so is itself the measured indicator. This indicator, however, does not well reflect the fluoride body burden or the accumulation of fluoride in the body, because the relation between fluoride concentrations in bone and in extracellular fluids is incompletely defined. The concentration of fluoride in plasma, urine, saliva and dental plaque is dependent on the intake via water, diet, fluoride supplements and fluoride-containing dentifrices [92–97].

Fluoride concentrations in ductal and glandular saliva closely follow the plasma concentration but at a lower level. A close relationship was found between the concentrations of fluoride in saliva and plasma, the ratio being 0.55:0.80 [87,93,98].

A commonly used indicator for fluoride exposure is its concentration in urine [85,99]. The urinary excretion rate of fluoride correlates better with its concentration in plasma than in urine [85].

7.2. Nails and hair as recent markers

The concentration of fluoride in nails and hair appears to be proportional to intake over longer periods of time, taking into account their growth rate [100–103]. Exposure to fluoride may occur in the local environment at the place of residence or via occupational exposure. Daily intake from food, water, dentifrices or fluoride supplements also contributes. The major advantage of nails and hair over fluids and tissues as biomarkers for fluoride exposure is that they can easily be obtained in a non-invasive manner. In contrast to plasma, saliva and urine, whose fluoride concentrations provide a snapshot at a certain point of time and are subject to change due to recent fluoride intake and certain physiological variables, the concentration of fluoride in nails and hair is cumulative and reflects the average level of intake over a time period, but depends on how often the nails are clipped or hair cut.

The amount of fluoride in fingernails or toenails as reported in summary table of literature reports prepared by Whitford [103] is about 0.5–5 µg/g, nevertheless also considerably higher values were also reported. The average amount of fluoride found in samples of hair of the low exposure population varied from

1.3 to 2.6 $\mu\text{g/g}$, while the average values were between 400 and 2830 $\mu\text{g/g}$ among aluminium workers and exhibited strong dependence on the type of work exposure to fluoride [102].

7.3. Calcified tissues as historical markers

More than 99% of body burden fluoride is found in calcified tissues. It is generally agreed that the level of chronic exposure extending over period of years is best assessed by determining fluoride concentrations in bone, but this tissue is for obvious reasons collected only rarely. Plasma fluoride concentrations in persons who have had no fluoride intake during the previous several hours can serve as a biomarker for the chronic level of fluoride intake and the total amount of fluoride in the body [104]. Saliva could similarly reflect bone fluoride concentrations, because the ratio of the concentration of fluoride in plasma to that in saliva is relatively constant.

In contrast to skeletal bone and dentine, which accumulate fluoride throughout life and whose levels are proportional to the absorbed dose of fluoride, fluoride in enamel is not an appropriate biomarker, because most of its fluorine was taken up during tooth formation [2]. The post-eruptive fluoride uptake of enamel is expressed only in the outer layer and depends on the concentration of fluoride in the oral cavity [6].

8. FLUORIDE IN DIET, FLUORIDE SUPPLEMENTS, DENTAL PRODUCTS AND FLUORIDATED SALT AND MILK

Drinking water, beverages and dental products containing fluoride are regarded as the main contributors to oral fluoride intake in humans. Food has, more recently, been recognized as a possible important source of fluoride intake. In some countries, fluoride is added to salt and milk.

8.1. Drinking water and beverages

8.1.1. Concentration of fluoride in drinking water

The natural concentration of fluoride in drinking water varies from trace amounts to toxic concentrations. Because of the low natural levels of fluoride in some water supplies and the high levels of dental caries, many authorities worldwide have permitted, or instigated, fluoridation of water supplies. The first artificial fluoridation trials started in 1945 in two towns in America – Newburgh and Grand Rapids [43]. Commonly used compounds for water fluoridation are sodium or potassium fluoride or hexafluorosilicic acid (H_2SiF_6) and its sodium salt (Na_2SiF_6).

According to WHO [6] recommendations, the absolute upper concentration for fluoride in drinking water is 1 mg/L. Yet even this concentration can be too high for many parts of the world due, not only to the greater consumption of water in hot climates, but also to the increasing levels of fluoride in, and increased consumption of, processed drinks and foods, the variety of dental practices and different lifestyles. WHO [6] therefore suggested that the level of 1.0 mg/L should be seen as an absolute upper limit, even in cold climates, while 0.5 mg/L may be appropriate lower limit. The history of water fluoridation and its value in the early years of the 21st century have recently been reviewed by Mullen [105].

Tap water (see Fig. 3), however, is increasingly replaced by the use of bottled water for drinking. Whereas drinking water for human consumption according to E.U. Council Directive 98/83/EC, following the advice of the Scientific Committee on Food (SCF) [106], may not contain more than 1.5 mg/L of fluoride, bottled natural mineral waters may contain higher concentrations of fluoride. According to Directive 2003/40/EEC, the concentration of fluoride in natural mineral waters must be not more than 5 mg/L by 1 January 2008 [2]. Mineral waters exceeding



Fig. 3. A tap water (photo by M. Ponikvar).

concentrations of fluoride 1.5 mg/L shall, in the meantime, bear on the label the words 'contains more than 1.5 mg/L of fluoride: not suitable for regular consumption by infants and children under 7 years of age' and shall indicate the actual concentration of fluoride [2]. According to the U.S. Food and Drug Administration (FDA), imported bottled water to which no fluoride has been added shall not contain fluoride in excess of 1.4 mg/L [107]. The concentration of fluoride in bottled water packaged in the United States depends on the annual average of maximum daily air temperatures at the location where the bottled water is sold at retail. The maximum allowable concentration of fluoride in bottled water with no fluoride added ranges from 1.4 to 2.4 mg/L and in bottled water with fluoride added from 0.8 to 1.7 mg/L [107].

8.1.2. Concentration of fluoride in beverages

Increasing numbers of people are consuming beverages instead of water, so their fluoride content has to be considered when estimating total intake of fluoride.

The tea plant (*Camellia sinensis* L.; family Theaceae) is known to take up fluoride from the soil and accumulate it in the leaves, from where it is readily released during infusion [108,109]. The fluoride content depends on the age of leaves, type of soil, soil pH and on total and extractable fluorine in the top soil [110]. Total fluorine in tea leaves ranges from 100 to 880 mg/kg [110,111]. Black (fermented) and green (unfermented) tea is made from young leaves and contains a lower amount of fluoride than brick tea made from fallen and old leaves. A large percentage of the total fluorine, 25–90%, is released during infusion [110,112], consequently the infusions may contain ~0.70–7.34 mg/L of fluoride [110,111], depending also on the amount of dry tea used, the granulation of the tea, the concentration of fluoride in the added water, the presence of milk, duration of infusion, etc. The results of determining fluoride in some of the locally available bottled teas revealed that in Germany, bottled teas contained 0.03–1.79 mg/L [113]; in the United States, 1.0–4.1 mg/L [114] and in Taiwan, they average an extraordinary 25.7 mg/L of fluoride [115].

It is interesting to note that tea bricks (see Fig. 4) – blocks of whole or finely ground tea leaves that have been packed in moulds and pressed into block form – were used centuries ago as a form of currency due to the high value of tea in many parts of Asia.

Concentrations of fluoride in fruit and vegetable juices are generally low [17]. Concentrations exceeding 1 mg/L of fluoride were determined in 18 out of 43 ready-to-drink juices in the United States, most probably due to contamination with fluoride-containing pesticides [116]. Higher concentrations of fluoride in the range from 0.02 to 2.8 mg/L in 532 juices [117] and 1.2–5.4 mg/L in 20 juices [118] were also reported. Concentrations of fluoride in 332 soft drinks ranged from 0.02 to 1.28 mg/L and exceeded 0.60 mg/L of fluoride for 71% of the



Fig. 4. A tea brick (photo by M. Ponikvar).

products [119]. The range of fluoride concentration in beers brewed and available in England was 0.067–0.451 mg/L and from 0.23 to 1.12 mg/L in other parts of Europe [120]. The higher concentrations of fluoride found in some juices, soft drinks and beers can generally be ascribed to the naturally occurring or artificially added fluoride in water used for preparation.

Wines generally contain less than 1 mg/L of fluoride [121]. Concentrations exceeding 1 mg/L were determined in some Californian wines, most probably the result of using cryolite as a pesticide [122].

8.2. Milk and baby formulas

The concentration of fluoride in human milk generally ranges from 2 to 50 $\mu\text{g/L}$ [88–91]. The concentration in milk of cows fed with a normal diet was 0.103 mg/L and 0.283 mg/L in those fed on contaminated pastures [123].

The concentrations of fluoride in ready-to-feed formulas in the United States and Canada range from 0.1 to 0.3 mg/L while the fluoride concentrations of powdered or liquid-concentrate infant formulas depend mainly on the concentration of fluoride in the water used to reconstitute the product [8]. A study on the concentration of fluoride in infant formula reconstituted with water in Australia revealed concentrations from 0.031 to 0.532 mg/L of fluoride for formulas reconstituted with water not containing fluoride, 0.131 to 0.632 mg/L of fluoride for formulas reconstituted with water containing 0.1 mg/L of fluoride and 1.031 to 1.532 mg/L if formulas were reconstituted with water containing 1.1 mg/L of fluoride [124]. Concentrations of fluoride in 10 samples of powdered milk formulas in Brazil ranged from 0.01 to 0.75 mg/L for those prepared with deionized water, from 0.02 to 1.37 mg/L for those prepared with bottled mineral water containing

0.02–0.69 mg/L of fluoride and from 0.91 to 1.65 mg/L for formulas prepared with fluoridated drinking water containing 0.9 mg/L of fluoride [125].

8.3. Food

Virtually all foods contain at least trace amounts of fluoride. Factors that can influence the level of fluorides in food include the locality in which the food is grown, the amount of fertilizer and pesticides applied, the type of processing the food receives and whether fluoridated water is used in their preparation. Some species of plants and marine organisms, however, appear to accumulate fluoride in large quantities.

Numerous studies have reported the results of determinations of ashed (total) and unashed (inorganic or free) fluoride in different food items. The U.S. Food and Drug Administration (FDA), for example, has collected market basket food collections of representative diets for the average young male 16–19 years of age, for the purpose of estimating the dietary intake of certain metals and of monitoring pesticide residues in the food chain. Food items in this program were divided into the composite food groups described in Table 2 [126].

The total free fluoride contents determined in the different food groups during the market basket programme by San Filippo and Battistone [126],

Table 2. Food groups

Food group	Examples of items
I	Dairy products: milk, ice cream, cheese, butter
II	Meat, fish and poultry: bacon, sausage, pork, chops, eggs, chicken, luncheon meats, roast beef, ground beef, fish (canned and fresh)
III	Grain and cereal products: bread, rolls, cereals, cookies, cakes
IV	Potatoes (boiled, fried and baked, including skins)
V	Leafy vegetables: lettuce, celery, cabbage, spinach, broccoli
VI	Legume vegetables: peas, green beans, lima beans, beans w/pork
VII	Root vegetables: onions, carrot, beet, turnip, rutabaga
VIII	Garden fruits: pepper, tomato, cucumber, eggplant, squash
IX	Fruits: orange, peach, apple, apricot, pear, strawberry, grape, plum
X	Oils, fats and shortening: cooking oil, salad dressing, mayonnaise, shortening, peanut butter
XI	Sugar and adjunct: sugar, jam, jelly, syrup, candy, salt, vinegar, baking soda
XII	Beverages: tea, coffee, soft drinks, drinking water

Singer *et al.* [127] and Singer and Ophaug [128] are presented in Table 3. In addition, the results reported by Taves [129], who also determined the ranges and averages of the amounts of fluoride in individual foods that were then classified into food groups, are listed, for the reason that the ranges of fluoride in specific types of foods give an indication of the variation of the fluoride content within individual groups.

The results presented in Table 3 show that the amount of ashed fluoride, which represents total fluorine, is generally higher than the amount of unashed inorganic or free fluoride, the former being within the range of less than 0.02–2.68 mg/kg and the latter from 0.02 to 2.74 mg/kg, both on a fresh weight basis. The highest average amounts of ashed fluoride were determined in the meat, poultry and fish food group, in the grain and cereal products food group and in beverages. The large amounts of fluoride observed in beverages could be ascribed to the use of fluoridated water for their preparation as well as to tea included in the daily diet. The difference between unashed and ashed samples reflects the amount of non-ionic fluorine in the food that is converted to the ionic form during ashing. The ratio of ashed to inorganic fluoride found by Singer *et al.* [127] was in some cases lower than expected, probably because of analytical difficulties. Taves [129] found generally good agreement between ashed and unashed fluoride while Singer and Ophaug [128] established that the amount of total fluoride is generally higher than that of inorganic fluoride. Of all composites analyzed, the highest ratio was found in dairy products.

The total fluoride content of some food items reported by Lopez and Navia [130] agreed in most cases with those reported by Taves [129] and the ratios of total to free fluoride were in agreement with those obtained by Singer and Ophaug [128].

A comprehensive survey of Finnish foods revealed that fish containing 5.4 mg/kg was the commodity group containing the greatest amount of fluoride on a dry weight basis, with dairy products next at 0.90 mg/kg [131].

Dabeka and McKenzie [132] determined the amount of unashed (inorganic or free) fluoride in 147 food samples. Individual samples with the greatest amount of fluoride were cooked veal (1.23 mg/kg), canned fish (4.57 mg/kg), shellfish (3.36 mg/kg), cooked wheat cereal (1.02 mg/kg) and tea (4.97 mg/kg). Food groups with the highest mean fluoride amounts were fish (2.12 mg/kg), soups (6.06 mg/kg) and beverages (1.15 mg/kg). It is important to add that whether these amounts were calculated on a dry or fresh weight basis was not explicitly stated.

Wide variations in the amount of fluoride are evident in different studies and between and within food groups. Probable explanations for these differences may include (1) differences in origin and growth of foodstuffs, (2) differences in manufacturing procedures, (3) type of water used for preparation and (4) different sample pre-treatment procedures and differences in the analytical procedures.

Table 3. The ranges and averages of amounts of total fluorine (ashed; F_t) and inorganic fluoride (unashed; F_f^-) in different food groups on a fresh weight basis

Group	Examples of items	Reference ^a	$w(F_t)$ [mg/kg]		$w(F_f^-)$ [mg/kg]		Ratio ^c
			Range	Average	Range	Average	
I	Diary products	[126]	/	0.17 ^b	/	/	/
		[127]	/	0.10	/	0.10	1.00
		[129]	0.02–0.95	0.29	0.02–0.82	0.25	1.16
		[128]	/	0.15	/	0.06	2.50
II	Meat, fish, poultry	[126]	/	0.75 ^b	/	/	/
		[127]	/	0.32	/	0.31	1.03
		[129]	0.02–0.48	0.21	0.04–0.51	0.22	0.95
		[128]	/	0.46	/	0.30	1.53
III	Grain and cereal products	[126]	/	0.45 ^b	/	/	/
		[127]	/	0.29	/	0.25	1.16
		[129]	0.08–2.01	0.46	0.08–2.01	0.42	1.10
		[128]	/	0.44	/	0.30	1.47
IV	Potatoes	[126]	/	0.23 ^b	/	/	/
		[127]	/	0.14	/	0.10	1.40
		[129]	0.21–0.82	0.48	0.21–0.84	0.49	0.98
		[128]	/	0.23	/	0.12	1.92
V	Leafy vegetables	[126]	/	0.40 ^b	/	/	/
		[127]	/	0.10	/	0.18	0.56
		[129]	0.11–0.70	0.27	0.08–0.70	0.27	1.00
		[128]	/	0.15	/	0.11	1.36

Table 3. Continued

Group	Examples of items	Reference ^a	w(F _t) [mg/kg]		w(F _f ⁻) [mg/kg]		Ratio ^c
			Range	Average	Range	Average	
VI	Legume vegetables	[126]	/	0.23 ^b	/	/	/
		[127]	/	0.31	/	0.26	1.19
		[129]	0.51–0.57	0.54	0.49–0.57	0.53	1.02
		[128]	/	0.34	/	0.31	1.10
VII	Root vegetables	[126]	/	0.11 ^b	/	/	/
		[127]	/	0.09	/	0.03	3.00
		[129]	0.27–0.46	0.37	0.27–0.48	0.38	0.97
		[128]	/	0.10	/	0.08	1.25
VIII	Garden fruits	[126]	/	0.19 ^b	/	/	/
		[129]	/	0.04	/	0.02	2.00
IX	Fruits	[126]	/	0.11 ^b	/	/	/
		[127]	/	0.06	/	0.06	1.00
		[129]	0.02–0.08	0.04	0.02–0.08	0.06	0.67
		[128]	/	0.11	/	0.11	1.00
X	Oils and fats	[126]	/	0.27 ^b	/	/	/
		[127]	/	0.15	/	0.08	1.88
		[129]	0.02–0.40	0.26	0.02–0.44	0.25	1.04
XI	Sugar and adjunct	[126]	/	0.41 ^b	/	/	/
		[127]	/	0.35	/	0.40	0.88
		[129]	0.02–0.93	0.34	0.02–0.78	0.28	1.21
		[128]	/	0.21	/	0.28	0.75

Table 3. Continued

Group	Examples of items	Reference ^a	w(F _t) [mg/kg]		w(F _f ⁻) [mg/kg]		Ratio ^c
			Range	Average	Range	Average	
XII	Beverages including water	[126]	/	1.12 ^b	/	/	/
		[127]	/	0.83	/	0.63	1.32
		[129]	<0.02–2.68	0.77	0.02–2.74	0.76	1.01
		[128]	/	0.72	/	0.72	1.00
Misc. vegetable and vegetable products		[127]	/	0.17	/	0.13	1.31
		[128]	/	0.29	/	0.19	1.53
Non-classifiable		[129]	0.29–0.86	0.60	0.29–0.87	0.59	1.02

^a References in this table are listed according to the years of publishing for the reason that fluoride analytical methods were modified and developed and therefore reliability of results should be subsequently improved.

^b Average amounts of fluoride in four diets from market basket collections.

^c Ratio between ashed and inorganic fluoride.

8.4. Dietary supplements

Unlike controlled fluoridated drinking water and toothpastes, there is little quantitative information on the cariostatic action of fluoridated salt, although it is considered to act in a manner like that of fluoridated drinking water [17].

Fluoridation of domestic salt for human consumption was initiated in Switzerland in 1955 [133]. Fluoridated salt usually contains 200–250 mg/kg of fluoride, mostly in the form of potassium salt, so 1 g of fluoridated salt provides 0.20–0.25 mg of fluoride [2]. The average daily adult salt intake is estimated to vary from 5 to 10 g [6] so, if all consumed salt were fluoridated, the total daily intake of fluoride would range from 1 to 2.5 mg. Salt fluoridation can reach the entire population, however, addition of fluoride is limited mainly to domestic salt, leaving salt used by bakeries, large kitchens, enterprises and institutions, as well as by the food industry, unfluoridated. Schemes of fluoridation of domestic salt are most developed in France, Germany and Switzerland [134]. Detailed information on the history and experiences of salt fluoridation in Switzerland, France, Germany, Central and Eastern Europe and America were recently reported [133,135–138].

Formerly, the administration of fluoridated milk to children was considered to be a suitable means of increasing their intake of fluoride; however, little quantitative information is available on the efficacy of this delivery system in the prevention of dental caries [17]. Encouraging results have been reported with milk fluoridation; however, Twetman [139] recently commented that there is still a dearth of studies providing high-quality evidence of its effects.

Dietary fluoride supplements, available in the form of tablets, drops, lozenges and rinse supplements, are recommended for caries prevention by medical societies in some countries, especially if the fluoride concentration from drinking water is low. These supplements contain different quantities of fluoride, usually 0.25, 0.50 and 1.00 mg of fluoride per unit, in the form of NaF [60]. Fluoride supplements are rarely prescribed for adults.

8.5. Dental products

Exposure to fluoride occurs through fluoride-containing toothpastes, gels and rinses. Fluoridated toothpastes usually contain from 1000 to 1500 µg/g of fluoride [60]. Because of poor control of the swallowing reflex, toothpastes for children usually contain lower amounts of fluoride, from 250 to 500 µg/g [140]. Yet convincing evidence for the efficacy of fluoridated toothpaste is lacking. In a British study, it was observed that there was significantly less caries in a group receiving 1450 µg/g of fluoride toothpaste than in groups receiving 440 µg/g or fluoride-free toothpaste [141]. Topical mouth rinses marketed for daily home use can contain between 230 and 1000 mg/L [6,60]. Topical gels for application by the

subject contain up to 5000 $\mu\text{g/g}$ and products for professional application up to 12,300 $\mu\text{g/g}$ of fluoride [6,60].

Toothbrush (Fig. 5) is commonly used for teeth brushing. According to the 2003 Lemelson-Massachusetts Institute of Technology (MIT) Invention Index, the toothbrush was selected as the number one invention Americans could not live without [142].

9. FLUORIDE INTAKE

Accurate estimates of fluoride intake are important in order to resolve potential problems of too low or too high exposure. Drinking water, beverages and fluoride-containing dentifrices are regarded as the main contributors to human fluoride intake. The contribution of inhaled airborne fluoride, or fluoride from soil, to total fluoride intake is, under normal conditions, small [17,143,144] and is beyond the scope of this paper.



Fig. 5. Toothbrushes (photo by M. Ponikvar).

9.1. Fluoride intake in adults

The major source of fluoride intake in adults is diet. Estimates for dietary fluoride intake for adults, by age groups and water fluoridation status, are presented in Table 4 [126,127,129,131,132,145–151].

Wide variations in the total intake of fluoride within and between studies are seen from Table 4. This can be ascribed to (1) considerable differences in the amounts of fluoride in similar food items, (2) large variation in the quantities consumed, (3) differences between the age groups and genders studied, (4) differences in the analytical techniques used and (5) the questionable accuracy of data resulting from the early analytical methods used for determining fluoride in diet. It is also important to note that, typically, estimates of quantities of foods consumed, such as standard food tables and market basket surveys, were used, rather than actual quantities of food consumed. In addition, the data required to enable proper comparison of different studies, such as energy value of the total diets, weight of dry and/or fresh matter, and amounts of fluoride in the diet, are usually not given.

The results listed in Table 4 lead to the conclusion that the intake of fluoride was higher in areas with fluoridated than non-fluoridated water. The average daily total fluoride intake in non-fluoridated areas ranged from 0.56 to 1.50 mg (average 1.1 mg) [equivalent to 0.008–0.021 (average 0.016) mg/kg body weight for a 70-kg man]. The daily intake of fluoride in fluoridated areas was almost two-fold higher, being 0.9–3.8 (average 2.1) mg, equivalent to 0.013–0.054 (average 0.030) mg/kg body weight for a 70-kg man. The data from non-fluoridated areas that give the energy value and/or weight of dry or fresh samples were considered further [146–151]. On this basis, the average daily intake of fluoride in non-fluoridated areas, assuming a 2500-kcal diet, was estimated to be 1.08 mg (range 0.58–1.56 mg). This is equivalent to 0.015 mg/kg body weight for a 70-kg man (range 0.008–0.022 mg/kg body weight).

Nevertheless, there are exceptions showing higher fluoride intakes than those listed in Table 4. These include an area in China where the fluoride content of the water is low, but the intake from food and tea is sufficiently high for the incidence of dental fluorosis to exceed 80% [152]. Another, representative example is England, where tea consumption is traditionally high; a study found the daily average intake of fluoride from tea to be 1.26 mg in children and 2.55 mg in adults [153], making a significant contribution to the total daily fluoride intake from diet.

9.2. Fluoride intake in children

Small amounts of fluoride have been proven to be effective in preventing dental caries, but excessive, chronic intake by young children can result in the development of dental fluorosis; the critical period of exposure for all permanent teeth

Table 4. Estimated intake of fluoride from diet for adults by age groups and water fluoridation status expressed as ranges or averages

Reference	Age group [years]	Intake (F_t) [mg/day]	$C(F^-)_{\text{drinking water}}$ [mg/L]	Energy value [kcal/day]	$w(F)_{\text{total diet}}$ [mg/kg]	m (diet) [g]	Diet surveys
San Filippo and Battistone [126] ^{a,b}	Males (16–19)	2.10–2.34 (average 2.20)	1.0	/	/	/	United States (1971)
Osis <i>et al.</i> [145] ^{b,c}	Adults	1.51	/	/	/	/	United States (1974)
Kramer <i>et al.</i> [146] ^{c,d}	Adults	0.78–1.03 (average 0.91) 1.73–3.44 (average 2.63)	0.08–0.44 0.53–1.27	2400–2600	/	/	United States (1974)
Singer <i>et al.</i> [127] ^{a,b}	Males (16–19)	0.912 1.720 0.988 1.215	0.4 0.8 0.9 1.0	/	/	/	United States (1980)

Table 4. Continued

Reference	Age group [years]	Intake (F_i) [mg/day]	$C(F^-)_{\text{drinking water}}$ [mg/L]	Energy value [kcal/day]	$w(F)_{\text{total diet}}$ [mg/kg]	m (diet) [g]	Diet surveys
Varo and Koivistoinen [131] ^{b,c}	Adults	0.56	Presumed to be on a low level	/	/	/	Finland (1980)
Taves [129] ^{a,c}	Adults	1.783	Fluoridated area	/	/	/	United States (1983)
Singer <i>et al.</i> [147] ^{a,b}	Males (15–19)	0.77–1.33 (average 0.89)	<0.1–0.4	2800	/	/	United States (1985)
		1.07–2.08 (average 1.55)	0.5–0.9				
		1.70–2.45 (average 1.97)	1.0–1.3				
Dabeka <i>et al.</i> [148] ^{a,d}	Adults	0.132–1.294 (average 0.563)	0.2	/	/	2569 (wet matter)	Canada (1987)
		0.868–6.700 (average 2.802)	1.0				

Table 4. Continued

Reference	Age group [years]	Intake (F_t) [mg/day]	$C(F^-)_{\text{drinking water}}$ [mg/L]	Energy value [kcal/day]	$w(F)_{\text{total diet}}$ [mg/kg]	m (diet) [g]	Diet surveys
Couzy <i>et al.</i> [149] ^{b,c}	Women	1.25	/	2000 ^d	/	/	France (1988)
	Pregnant or lactating woman	1.39		2500 ^d			
	Males	1.45		2700 ^d			
Haldimann and Zimmerli [150] ^{a,d}	Adults	0.9	0.08–0.09		1.9 (dry matter)	460 (dry matter)	Switzerland (1993)
Dabeka and McKenzie [132] ^{b,c}	12–19, male	1.025	1.0	/	/	/	Canada (1995)
	12–19, female	0.905					
	20–39, male	2.544					
	20–39, female	2.172					
	40–65, male	3.032					

Table 4. Continued

Reference	Age group [years]	Intake (F_t) [mg/day]	$C(F^-)_{\text{drinking water}}$ [mg/L]	Energy value [kcal/day]	$w(F)_{\text{total diet}}$ [mg/kg]	m (diet) [g]	Diet surveys
Ponikvar <i>et al.</i> [151] ^{a,d}	40–65, female	2.615	<0.1	3700	1.84 (dry matter)	820 (dry matter)	Slovenia (2007)
	65+, male	2.588					
	65+, female	2.405					
	Males (18–29)	0.73–2.50 (average 1.50)					
					0.38 (fresh matter)	3957 (wet matter)	

^a Drinking water included.^b Estimates of quantities of foods consumed.^c Drinking water excluded.^d Hospital diets or duplicate diet technique.

being between 11 months and 7–8 years of age [46,47]. The main sources of fluoride intake in children are diet, including drinking water, fluoride-containing dentifrices and fluoride-containing supplements. Intake from fluoridated dental products can be substantial, particularly in young children who have poor control of the swallowing reflex [10,154].

9.2.1. Fluoride intake from diet

Estimates of total dietary fluoride intake for children, by age groups and water fluoridation status, are presented in Table 5 [132,143,155–162]. The data for breastfed infants, who may receive lower amounts of fluoride than those listed in this table, are not included.

Variations in the total daily intake of fluoride within and between studies are evident from Table 5. The intake of fluoride from diet in non-fluoridated areas does not exceed the recommended 0.05 mg/day/kg body weight [8]. The one set that stands out from the rest is that of Wiatrowski *et al.* [156] who reported fluoride intake as high as 0.07–0.16 mg/day/kg body weight. These data have been criticized by Singer and Ophaug [157] on the grounds that the caloric intakes used to estimate the daily fluoride ingestion are too high, thus resulting in overestimates. If that criticism is accepted as valid, then the data listed in Table 5 are remarkably uniform and present no obvious evidence of an increase in fluoride intake over time. So, leaving this study aside, the range of average daily fluoride intake in non-fluoridated areas is estimated between 0.008 and 0.040, with an average of 0.025 mg/kg body weight. The average daily intake of fluoride in fluoridated areas generally exceeds the recommended intake of 0.05 mg/kg body weight [8]; the estimated range, based on average intake, was 0.016–0.127 with an average of 0.058 mg/kg body weight. Nevertheless, it is interesting to note that the intake estimates were generally lower in the studies where duplicate diet technique, which is the most accurate technique of estimating actual daily intake, was used. A possible reason could be overestimates of fluoride intake using, for example, standard food tables or market basket collections instead of the duplicate diet technique.

Intake of fluoride of breastfed infants, that are not included in this table, are usually negligible, because fluoride is poorly transferred from plasma to breast milk [88,89].

9.2.2. Fluoride intake from fluoride-containing toothpastes

Fluoride ingestion from toothpastes is common and often relatively substantial. Reviews by Whitford *et al.* [154], Levy [163] and Levy *et al.* [164] show wide ranges in the amounts of toothpaste used and ingested. These reviews lead to the estimate that younger children (7 and under) ingest, on average, 25–38% of toothpaste per brushing, the amount of toothpaste used per brushing being on average 0.7 g. This amount is considerably higher than the commonly

Table 5. Estimated intake of fluoride from diet for children expressed as ranges or averages by age groups and water fluoridation status in mg/day and mg/day/kg body weight; fluoride intake by breastfed infants is not listed

Reference and comment on the concentration of fluoride in drinking water	Age group	Body weight [kg]	Intake [mg/day]		Intake [mg/day/kg body weight]		Diet surveys
			Non-fluoridated area	Fluoridated area	Non-fluoridated area	Fluoridated area	
McClure [155] ^{a,b} : Fluoridated water contained 1 mg/L of fluoride.	1–3 years	8–16	/	0.417–0.825	/	0.026–0.103	United States (1943)
	4–6 years	13–24		0.556–1.105		0.023–0.085	
	7–9 years	16–35		0.695–1.380		0.020–0.068	
	10–12 years	25–54		0.866–1.725		0.016–0.069	
Wiatrowski <i>et al.</i> [156] ^{b,c} : Nursery drinking water free of fluoride.	1–4 weeks	/	0.32	/	0.07	/	United States (1975)
	4–6 weeks		0.47		0.09		
	6–8 weeks		0.57		0.10		
	2–3 months		0.71		0.12		
	3–4 months		1.02		0.15		
	4–6 months		1.23		0.16		

Table 5. Continued

Reference and comment on the concentration of fluoride in drinking water	Age group	Body weight [kg]	Intake [mg/day]		Intake [mg/day/kg body weight]		Diet surveys
			Non- fluoridated area	Fluoridated area	Non- fluoridated area	Fluoridated area	
Singer and Ophaug [157] ^{a,b} : Non- fluoridated water contained less than 0.16 mg/L and fluoridated 0.85–1.2 mg/ L of fluoride.	2 months	5.0	0.050	0.633	0.010	0.127	United States (1979)
	4 months	6.8	0.102	0.681	0.015	0.100	
	6 months	8.1	0.153	0.763	0.019	0.094	

Table 5. Continued

Reference and comment on the concentration of fluoride in drinking water	Age group	Body weight [kg]	Intake [mg/day]		Intake [mg/day/kg body weight]		Diet surveys
			Non- fluoridated area	Fluoridated area	Non- fluoridated area	Fluoridated area	
Dabeka <i>et al.</i> [158] ^{b,c} : Non- fluoridated water contained 0 mg/L and fluoridated 1 mg/L of fluoride.	<1 month	/	0.15	0.35	0.036	0.087	Canada (1982)
	1–3 months		0.24	0.55	0.040	0.089	
	3–6 months		0.25	0.42	0.035	0.059	
	6–9 months		0.27	0.48	0.033	0.057	
	9–12 months		0.28	0.56	0.027	0.054	
Brunetti and Newbrun [159] ^{a,d} : Optimally fluoridated community.	3–4 years	/	/	0.33	/	/	United States (1983)
Ophaug <i>et al.</i> [160] ^{a,b} : The	6 months	/	0.263	0.400	0.033	0.049	United States (1985)
	2 years		0.251	0.583	0.020	0.047	

Table 5. Continued

Reference and comment on the concentration of fluoride in drinking water	Age group	Body weight [kg]	Intake [mg/day]		Intake [mg/day/kg body weight]		Diet surveys
			Non-fluoridated area	Fluoridated area	Non-fluoridated area	Fluoridated area	
range for non-fluoridated water was taken as between 0.05 and 0.50 mg/L and for fluoridated between 0.54 and 1.04 mg/L of fluoride.							
Schamschula <i>et al.</i> [143] ^{a,b} : Low fluoride water contained	3.9 years 14 years	/	0.22 0.30	0.72 (1.11) 1.00 (1.49)	/	/	Hungary (1988)

Table 5. Continued

Reference and comment on the concentration of fluoride in drinking water	Age group	Body weight [kg]	Intake [mg/day]		Intake [mg/day/kg body weight]		Diet surveys
			Non- fluoridated area	Fluoridated area	Non- fluoridated area	Fluoridated area	
0.06– 0.11 mg/L; intermediate 0.5–1.1 mg/L and high 1.6– 3.1 mg/L of fluoride; intake for high fluoride content water is given in parentheses.							
Dabeka and McKenzie [132] ^{b,c} :	1–4 years 5–11 years	/	/	0.353 0.530	/	/	Canada (1995)

Table 5. Continued

Reference and comment on the concentration of fluoride in drinking water	Age group	Body weight [kg]	Intake [mg/day]		Intake [mg/day/kg body weight]		Diet surveys
			Non-fluoridated area	Fluoridated area	Non-fluoridated area	Fluoridated area	
Drinking water contained 1 mg/L of fluoride.							
Guha-Chowdhury <i>et al.</i> [161] ^{a, d} : Fluoridated water contained 1 mg/L of fluoride.	3–4 years	/	0.05–0.31 (average 0.15)	0.09–0.74 (average 0.36)	0.004–0.02 (average 0.008)	0.004–0.04 (average 0.019)	New Zealand (1996)
Pessan <i>et al.</i> [162] ^{a, d} : Fluoridated water	4–5 years	21.0	/	0.190–1.896 (average 0.455)	/	0.003–0.045 (average 0.021)	Brazil (2003)

Table 5. Continued

Reference and comment on the concentration of fluoride in drinking water	Age group	Body weight [kg]	Intake [mg/day]		Intake [mg/day/kg body weight]		Diet surveys
			Non- fluoridated area	Fluoridated area	Non- fluoridated area	Fluoridated area	
contained 0.6–0.8 mg/L of fluoride.	6–7 years	23.8		0.174–		0.003–	
	4–7 years	22.4		3.270 (average 0.346)		0.034 (average 0.016)	
				0.174–		0.003–0.045	
				3.270 (average 0.398)		(average 0.018)	

^a Drinking water included.^b Estimates of quantities of foods consumed.^c Drinking water excluded.^d Duplicate diet technique.

recommended 'pea size' amount of 0.25 g [2]. Estimates of intake for optimum and average intake of fluoride from toothpaste containing 1000 µg/g of fluoride are presented in Table 6. The estimates were made using a 1000-µg/g formulation, because of lack of convincing evidence for the efficacy of toothpaste containing lower amounts of fluoride (see Section 8.5).

The intake of fluoride from toothpaste listed in Table 6 ranges from 0.003 to 0.012 mg/kg body weight. These data are per brushing estimates and many children brush more than once daily, thus increasing possible intake. Although these quantities may seem to be low at the first sight, they can add considerably to the total daily intake of fluoride.

9.2.3. Fluoride intake from fluoride-containing supplements

Fluoride supplements are recommended by medical societies in some countries for caries prevention, especially if the concentration of fluoride in drinking water is low. It is likely that past use of dietary fluoride supplements has been a prime factor in the increased prevalence of dental fluorosis, a relationship which may stem from the days when fluoride supplement schedules were higher than they are today [11]. Table 7 shows a fluoride supplement dosage schedule that was approved for U.S. and Canadian children by the American Dental Association and Canadian Paediatric Society [8] and a fluoride supplement dosage schedule approved by German Nutrition Society, Austrian Nutrition Society, Swiss Society for Nutrition Research and Swiss Nutrition Association [165].

The various recommended regimens as presented in Table 7 differ considerably with regard to the starting time (birth or 6 months of age), amount in relation to age, and restriction in the presence of salt fluoridation or in dependence on the fluoride concentration in drinking water.

Table 6. Estimated intake for optimum and average intake of fluoride from toothpaste containing 1000 µg/g of fluoride

Age	<i>m</i> [kg] ^a	Intake (F ⁻) [mg/kg body weight] (25% ingestion; use of 0.25 g of toothpaste) ^b	Intake (F ⁻) [mg/kg body weight] (38% ingestion; use of 0.7 g of toothpaste) ^c
7–12 months	9	/	/
1–3 years	13	0.005	0.020
4–8 years	22	0.003	0.012

^a Reference weights taken from Ref. [8].

^b 25% ingestion of 0.25 g of toothpaste represents 0.063 g of toothpaste.

^c 38% ingestion of 0.7 g of toothpaste represents 0.266 g of toothpaste.

Table 7. The fluoride supplement dosage schedule that was approved by the American Dental Association and the Canadian Paediatric Society and the fluoride supplement dosage schedule approved by the German Nutrition Society, Austrian Nutrition Society, Swiss Society for Nutrition Research and Swiss Nutrition Association

Fluoride supplement dosage schedule approved by the American Dental Association and the Canadian Paediatric Society

Age	$m(\text{F}^-)$ [mg] ^a		
	$\text{C}(\text{F}^-)_{\text{drinking water}}$ [mg/L]		
	<0.3	0.3–0.6	<0.6
0–6 months	0	0	/
6 months–3 years	0.25	0	/
3–6 years	0.50	0.25	/
6–16 years	1.00	0.50	/

Fluoride supplement dosage schedule approved by the German Nutrition Society, Austrian Nutrition Society, Swiss Society for Nutrition Research and Swiss Nutrition Association

Age	$m(\text{F}^-)$ [mg] ^a		
	$\text{C}(\text{F}^-)_{\text{drinking water}}$ [mg/L]		
	<0.3	0.3–0.7	>0.7
0–under 4 months	0.50 ^b	0	/
4–under 12 months	0.50 ^b	0	/
1–under 4 years	0.50 ^b	0	/
4–under 7 years	0.5	0.25	/
7–under 10 years	1.0	0.5	/

^a Fluoride supplement values are given in mg/day; 2.2 mg of sodium fluoride contains 1.0 mg of fluoride.

^b The intake in infants and young children from fluoridated salt containing 250 mg/kg of fluoride is, in infants and young children, so low in Germany that additional fluoride tablets appear to be justified.

9.2.4. Estimated total intake of fluoride in children

The total fluoride intake by age groups in children from diet, fluoride supplements and fluoridated toothpastes presented in Table 8 were estimated using the data from Tables 5–7. The lower and higher limits of fluoride intake listed in these were used to provide these estimates.

Table 8. Estimated fluoride intake for infants and children from diet, fluoride supplements and toothpastes based on the intake presented in Tables 5–7

Age	<i>m</i> [kg] ^a	Intake (F ⁻) [mg/day/kg body weight]						
		Diet		Fluoride supplements		Toothpaste	Total	
		Non-fluoridated water ^b	Fluoridated water ^c	Non-fluoridated water ^b	Fluoridated water ^c		Non-fluoridated area ^b	Fluoridated area ^c
2–6 months	7	0.008–0.040 (average 0.025)	0.016–0.127 (average 0.058)	0–0.071 (average 0.036)	0	0	0.008–0.111 (average 0.061)	0.016–0.127 (average 0.058)
7–12 months	9	0.008–0.040 (average 0.025)	0.016–0.127 (average 0.058)	0.028–0.056 (average 0.042)	0	0	0.036–0.096 (average 0.067)	0.016–0.127 (average 0.058)
1–3 years	13	0.008–0.040 (average 0.025)	0.016–0.127 (average 0.058)	0.019–0.038 (average 0.029)	0	0.005–0.020 (average 0.013)	0.032–0.098 (average 0.067)	0.021–0.147 (average 0.071)
4–8 years	22	0.008–0.040 (average 0.025)	0.016–0.127 (average 0.058)	0.023–0.045 (average 0.034)	0	0.003–0.012 (average 0.008)	0.034–0.097 (average 0.067)	0.019–0.139 (average 0.066)

^a Reference weights taken from Ref. [8].^b The concentration of fluoride in non-fluoridated water is lower, being below 0.3 mg/L.^c The concentration of fluoride in fluoridated water is greater than 0.7 mg/L.

The results presented in Table 8 show that the lower limits of ranges of estimated intake of fluoride do not exceed the recommended intake of 0.05 mg/day/kg body weight in either fluoridated or non-fluoridated areas. Yet the higher values of estimated intake generally exceed the recommended intake. Children in non-fluoridated areas receive daily on average 0.066 and in fluoridated areas on average 0.063 mg/kg body weight of fluoride. These intakes exceed the recommended intake. The major sources of fluoride in non-fluoridated areas are fluoride supplements and, in non-fluoridated areas, diet. These approximations are in good agreement with the total fluoride intake estimated in 3- to 6-year-old children in Germany in keeping with a water fluoride concentration of 0.25 mg/L, which was estimated to be within the range of 0.028–0.086 mg/day/kg body weight and with an average of 0.053 mg/kg body weight [166]. The assumptions used in Table 8 are perhaps not applicable to all countries, but the results illustrate well the range of potential exposure to fluoride via oral ingestion in infants and young children under a variety of conditions.

As noted earlier, the data in Tables 4–7 did not consider fluoride intake in breastfeeding infants, who may receive lower amounts of fluoride than shown in these tables. This is nevertheless even favourable, because it is now believed that the majority of benefit from fluoride is from its topical, rather than systematic, effects, so breastfeeding is considered to be protective against dental fluorosis [3–5].

10. ANALYTICAL METHODS FOR FLUORINE

Reliable analytical techniques are a prerequisite for accurate and precise determination of human exposure to fluoride. The goal is to monitor the intake of fluoride and maintain it at adequate levels so that optimal protection against dental caries is achieved, without excessive intake resulting in the appearance of dental or, in the worst case, skeletal fluorosis.

Term 'fluorine' is used to denote the element in any of its forms (and hence total fluorine, F_t) and 'fluoride' to denote free inorganic fluoride (F_f^-) to which fluoride ISEs respond under the conditions of determination, while total fluorine can generally be determined only after total decomposition of the sample (F_t^-). The difference between F_t and F_f^- leads to the amount of bound fluoride (F_b^-) [57]. The extensive classification of different forms of fluorine in biological materials is based on the work of Taves [74] and Venkateswarlu *et al.* [75], and shows that fluorine in biological samples is present in the form of ionic or non-ionic inorganic fluoride and organic fluorine. The latter comprises covalent fluorine that is bound to carbon in all organic fluorine compounds and results from exposure to certain fluorine-containing compounds from natural and/or industrial sources [78]. Total fluorine includes both inorganic fluoride and organic fluorine.

Methods for determining any form of fluorine in any type of material generally rely on the determination of fluorine in the form of free inorganic fluoride ion (F^-).

Four basic requirements for accurate and precise determination of the amount of fluoride or total fluorine in any type of the sample are: (1) the sample has to be appropriately pre-treated so that the required form of fluorine can be determined; (2) interfering reactions have to be effectively suppressed; (3) the final concentration of fluorine must be above the detection limit of the method and (4) if possible, method should be validated using certified reference material (CRM), or the results of analyses compared to the results obtained by an independent method.

The aim of this section is to present a concise overview of separation, concentration and decomposition methods for sample pre-treatment and an overview of the analytical methods available for determining free inorganic fluoride and total fluorine in the environment (natural and drinking water, air and soil), biological and related materials, and fluoride supplements and dental products.

10.1. Sample pre-treatment procedures

In the classical Willard–Winter [167] distillation procedure introduced in 1933, decomposition of compounds and separation of resulting fluoride from interfering substances take place concurrently. This technique and its modifications [168–170] have provided a wealth of information through the middle decades of the 20th century but, mostly because of its cumbersome procedure, have been replaced by simpler methods.

Fluoride can also be separated from interfering substances by using diffusion and microdiffusion techniques that require 6–48 h for quantitative separation of fluoride from the interfering ions [171–174]. Faster procedures, requiring only a few minutes, are the adsorption of fluoride on magnesium oxide or calcium phosphate(V) [75,175], or a reverse extraction procedure [176]. Free inorganic and acid-labile fluoride are determined together by diffusion and reverse extraction, while only free inorganic fluoride is determined by the adsorption technique [177]. Free inorganic fluoride can be also determined directly in filtrates of aqueous solution or suspension of the sample [57,178]. Organic fluorine can be determined after conversion to inorganic fluoride by a rapid procedure using sodium biphenyl, which cleaves covalent C–F bonds [179].

Total decomposition of the sample, the purpose of which is to release fluorine from inorganic or organic matrixes and convert it to fluoride ions, is usually a prerequisite for determining the amount of total fluorine. Commonly used procedures involve oxygen bomb combustion in a closed bomb [176,180], open ashing [181,182], alkali hydroxide or alkali carbonate fusion [151,183–187], pyrohydrolysis [187–191], acid extraction [192,193] and microwave acid digestion [194–196].

10.2. Analytical methods for determining fluorine

Numerous analytical methods have been described for determining fluorine in a variety of samples.

In early methods, the sample was first decomposed, fluoride separated from interfering substances and determined using volumetric [167,168,170], spectrophotometric [169,170] and fluorometric [197,198] methods. These methods have mostly been replaced by the introduction of the fluoride ion-selective electrode (ISE) in 1966 by Frant and Ross [199], a breakthrough method in analytical chemistry of fluorine. Briefly, fluoride ISE is designed to determine fluoride ion activity in aqueous solutions. The observed potential is affected by (1) the total ionic strength of the solution, (2) the pH (H^+ binds fluoride, and OH^- interferes with the measurement) and (3) the presence of any fluoride-complexing cations. The ionic strength and pH of the solution are adjusted and interfering ions complexed by adding a background solution, the so-called TISAB (total ionic strength adjustment buffer). As a consequence, the amount of free inorganic fluoride determined is dependent on the composition of the TISAB employed for the analysis [57]. Fluoride ISE is a widely used technique for determining amounts of free or total fluoride because it is highly selective and covers a wide concentration range. Fluoride ion-selective microelectrodes for determining fluoride in microlitre to nanolitre volumes of samples have also been proposed [200–203].

Other frequently used methods for determining fluoride include ion and gas chromatography [150,204,205] and aluminium monofluoride (AlF) molecular absorption spectrometry [206,207]. Less frequently employed methods include enzymatic [208], catalytic [209], polarographic [210] and voltammetric methods [211], helium microwave-induced [212] or inductively coupled plasma atomic emission spectrometry [213], electrothermal atomic absorption spectrometry [214], inductively coupled plasma-mass spectrometry [215], radioactivation [216], proton-induced gamma emission [217], near-infrared spectroscopy [218] and neutron activation analysis [219].

10.3. Determining fluorine in specific types of materials

10.3.1. Fluorine in environmental media

The concentration of fluoride in water can usually be determined directly without pre-treatment. Among the numerous published analytical techniques, potentiometry with fluoride ISE, ion chromatography, and spectrophotometry are commonly used. If the amount of fluoride present in water is very low, pre-concentration may be required.

Methods for determining gaseous fluorides are generally based on the absorption of gaseous fluorides into a train of absorbing solutions, or collection on a filter with a treated pad and subsequent determination of fluoride.

Determination of total fluoride in soil, sediments, oxides and other raw materials requires complete decomposition of the sample. Accumulation of fluoride in soil can be studied by employing appropriate extraction procedures.

10.3.2. Fluorine in biological tissues, fluids and related materials

Approaches to determining different forms of fluorine in biological and related materials have been reviewed extensively by Venkateswarlu [177,220,221].

Total decomposition is a general pre-requisite for determining the amount of total fluorine in biological materials other than urine. The difference between total fluorine and inorganic fluoride in biological and related materials usually represents organic fluorine. Among the various published decomposition procedures, the most important are open ashing, fusion, oxygen combustion and digestion, followed by a separation or concentration step. A variety of analytical methods have been reported for final quantification of fluoride in such samples.

10.3.3. Fluorine in fluoride supplements and dental products

Total fluorine in fluoride supplements and dental products could be determined with minimal samples pre-treatment as for example by direct acid extraction or heating in TISAB buffer solution and subsequent determination of fluoride using fluoride ISE for the reason that entire fluorine, in these products, should be, by definition, available as free inorganic fluoride.

11. INDICATORS FOR ESTIMATING REQUIREMENTS FOR FLUORIDE

The effectiveness of fluoride against dental caries is a strong indicator for applying an AI of this ion. Epidemiological studies have shown an inverse relationship between dental caries and concentration of fluoride in drinking water. Using the 1942 data from the pioneering research of Dean [222], Hodge [223], in 1950, plotted the average community index of dental fluorosis and the average caries incidence against the concentration of fluoride in community water supplies. Reduction of the average occurrence of dental caries per child was nearly maximal in communities having concentrations of fluoride in water close to 1.0 mg/L. In this way, 1 mg/L became the 'optimal' concentration for fluoride in drinking water and was associated with a high degree of protection against dental caries and low prevalence of the milder forms of dental fluorosis.

Reports published 40–50 years ago suggested that the long-term ingestion of fluoride in amounts slightly above the optimum for caries prevention improved the quality of the human skeleton, and that the risk of osteoporosis might thereby be reduced [17]. Since the 1960s, fluoride at high dose levels (~20–30 mg/day of fluoride) has been used to treat age-dependent osteoporosis [17]. While it appears that such treatment increases trabecular bone density, it apparently has no similar beneficial effect on cortical bone [17]. Although such treatment may protect against vertebral fractures, data on other fractures, including femoral bone, are highly controversial [17]. Assessment of the efficacy of fluoride

therapies for osteoporosis is beyond the scope of this paper. Nevertheless, it is important to note that fluoride is currently not recommended for its treatment. While slow release fluoride is reportedly beneficial, its long-term benefit is unknown [7]. Other data that suggest beneficial effects of fluoride other than prevention of dental caries, or increase bone mineral content, are insufficiently firm to provide the basis for estimating an AI [8].

Several studies have shown that the fluoride balance can be negative [8]. This occurs when the chronic intake is reduced to the extent that concentrations of fluoride in plasma fall and mobilization of fluoride from calcified tissues proceeds. However, there is no evidence so far from human studies that clinical signs of fluoride deficiency exist; no specific clinical or biochemical diagnostic parameters have been related to fluoride deficiency [8,39]. In the present state of knowledge, therefore, negative fluoride balance cannot be used for establishing an AI of fluoride.

12. AI OF FLUORIDE

The estimated average requirement (EAR) is defined as the nutritional intake value that is estimated to meet the requirement defined by a specified indicator of adequacy in 50% of the individuals in a particular life stage and gender group. The recommended dietary allowances (RDA), on the other hand, is the average daily dietary intake level that is sufficient to meet the nutrient requirements of nearly all (97–98%) individuals in a particular life stage and gender group [8]. The RDA applies to individuals, not to groups. The EAR serves as the basis for setting the RDA [8]. If adequate scientific documentation for calculating an EAR is not available, as is the case of fluoride, the AI is set instead of an RDA [8]. The AI is based on observed or experimentally determined estimates of average nutrient intake by a group (or groups) of healthy people.

Burt [11] reviewed the history of development of the 'optimum' intake of fluoride in children and wrote: 'Guidelines on the "optimum" intake of fluoride in children have an interesting history'. In the same 1943 report in which he estimated that the 'average daily diet' contained 1.0–1.5 mg of fluoride, McClure [155] suggested that this same diet provided some 0.05 mg fluoride/day/kg body weight for children aged 1–12 years. This information later came to be interpreted as a recommendation, as when Farkas and Farkas [224] quoted a number of personal opinions which recommended that fluoride intake be measured as a function of body weight. They did not refer to McClure, and not all of their sources who suggested 0.06 mg fluoride/day/kg body weight would be universally accepted as fluoride experts. A few years later, Ophaug *et al.* [225] stated that 0.05–0.07 mg fluoride/day/kg body weight '... is generally regarded as optimum'. Ophaug *et al.* [225] cited as their sources Farkas and Farkas [224], already discussed, and Forrester and Schultz [226], where the reference could not be

found. Despite its dubious genesis, however, empirical evidence suggests that 0.05–0.07 mg fluoride/day/kg body weight remains a useful upper limit for fluoride intake in children.” This has also been applied to adults.

The Standing Committee on the Scientific Evaluation of Dietary Reference Intakes [8] in 1997 defined the AI for fluoride, stating ‘Based on the extensively documented relationship between caries experience and both concentration of fluoride in water and fluoride intake, the AI for fluoride from all sources is set at 0.05 mg/day/kg body weight. This intake range is recommended for ages above 6 months because it confers a high level of protection against dental caries and is associated with no known unwanted health effects’.

An overview of AIs for fluoride, based on an intake of fluoride of 0.05 mg/day/kg body weight for all ages above 6 months is presented by age groups and gender in Table 9.

13. CONCLUSIONS – ENOUGH OR TOO MUCH FLUORIDE?

The beneficial effects of small amounts of fluoride have been established in the prevention of dental caries and thus constitute a strong indicator for an appropriate intake of fluoride, especially in children. On the other hand, excessive intake

Table 9. Overview of adequate intakes (AIs) for fluoride by age groups based on an AI for fluoride of 0.05 mg/day/kg body weight from all sources [8]

Gender	Age	Reference weight [kg]	AI (F ⁻) [mg/day]
Male, female	7–12 months	9	0.45
Male, female	1–3 years	13	0.65
Male, female	4–8 years	22	1.10
Male, female	9–13 years	40	2.00
Male	14–18 years	64	3.20
Female	14–18 years	57	2.85
Male	19 years and over	76	3.80
Female	19 years and over	61	3.05
Pregnancy and lactation	14–18 years	/	2.85
Pregnancy and lactation	19–50 years	/	3.05

of fluoride during enamel maturation before tooth eruption, from birth to 7–8 years of age when enamel formation is complete, can lead to the development of dental fluorosis.

It is the total ingested and bioavailable fluoride that is important when considering the prevention of dental caries together with the occurrence of dental fluorosis. The AI of fluoride from all sources is set at 0.05 mg/day/kg body weight for all ages above 6 months because it confers a high level of protection against dental caries and is associated with no known unwanted health effects [8]. Despite this, thresholds of 0.05–0.07 and of 0.03–0.04 mg/day/kg body weight of fluoride have been suggested for the appearance of dental fluorosis [9–11].

The wide variations in fluoride intake reported in the literature make its accurate estimation difficult. Our estimates show that the total intake of fluoride in infants and children from diet, fluoride supplements and use of fluoridated toothpaste is 0.008–0.111 (average 0.066) mg/day/kg body weight in non-fluoridated areas and 0.016–0.147 (average 0.063) mg/day/kg body weight in fluoridated areas. High intake of fluoride in non-fluoridated areas is ascribed to the use of fluoride supplements and in fluoridated areas to fluoride added into water. Both intakes exceed the lower threshold and are close to the upper threshold of 0.07 mg/day/kg body weight for the appearance of dental fluorosis.

Total dietary fluoride intake, the most important source of fluoride in adults, is estimated to be 0.008–0.021 (average 0.016) mg/day/kg body weight for a 70-kg man in non-fluoridated areas and thus lower than AI. The total dietary intake of fluoride in fluoridated areas was about twofold higher [0.013–0.054 (average 0.03) mg/day/kg body weight for a 70-kg man].

These estimates are based on numerous studies. Nevertheless, the results are difficult to compare because (1) sample pre-treatment methods were used that do not necessarily ensure complete release of fluoride from the sample matrix, (2) adequate information as to how the studies were conducted is not always provided and (3) although advances in analytical techniques for trace amounts have led to re-examination of the many of the published data, the majority of the data on fluoride still comes from older studies.

In order to make reliable comparisons it is therefore suggested that, in future studies, decomposition methods that are known to release *all* the fluoride should be used. Use of certified reference materials (CRM) as part of the quality assurance system should be mandatory. In addition, sufficient information to enable proper comparison of data from different studies must be provided.

Based on the available literature and the current recommendations on fluoride intake, it is hard to say whether the current AI is appropriate, that is, too low or too high. The margin between the beneficial and deleterious effects of fluoride appears to be narrow. More accurate information on background amounts of fluoride intake, especially in children, from food, water, beverages, fluoride supplements and dentifrices is a pre-requisite for making correct decisions on the use of fluoride products. One is currently left with the question 'Enough or too

much fluoride?’ Whether the complex nature of the system precludes there ever being a definite answer, remains to be seen.

APPENDIX: LIST OF ACRONYMS

AI	adequate intake
CDC	Centers for Disease Control and Prevention
CRM	certified reference material
DRI	dietary reference intakes
EAR	estimated average requirement
F^-	fluoride ion
F_b^-	bound fluoride
F_f^-	free inorganic fluoride
F_t	total fluorine
FDA	Food and Drug Administration
FAO	Food and Agricultural Organization
IAEA	International Atomic Energy Agency
ISE	ion-selective electrode
MIT	Massachusetts Institute of Technology
RDA	recommended dietary allowances
SCF	Scientific Committee on Food
TFI	Thylstrup-Fejerskov Index
TISAB	total ionic strength adjustment buffer
TSIF	tooth surface index of fluorosis
UNICEF	The United Nations Children’s Fund
WHO	World Health Organization

REFERENCES

- [1] T.A. O'Donnell, The chemistry of fluorine, in: J.C. Bailar Jr., H.J. Emeléus, R. Nyholm, A.F. Trotman-Dickenson (Eds.), 1st edition, *Comprehensive Inorganic Chemistry*, 1st edition, Vol. 5, Pergamon Press, Oxford, 1973, pp. 1009–1106.
- [2] Opinion of the Scientific Panel on Dietetic Products, Nutrition and allergies on a request from the commission related to the tolerable upper intake level of fluoride, EFSA J. 192 (2005) 1–65 (Available at: http://www.efsa.eu.int/science/nda/nda_opinions/catindex_en.html).
- [3] A. Groeneveld, A.A.M.J. Van Eck, O. Backer Dirks, Fluoride in caries prevention: is the effect pre- or post-eruptive? *J. Dent. Res.* 69 (1990) 751–755.
- [4] D. Brothwell, H. Limeback, Breastfeeding is protective against dental fluorosis in a nonfluoridated rural area of Ontario, Canada, *J. Hum. Lact.* 19 (2003) 386–390.
- [5] E. Hellwig, Á.M. Lennon, Systemic versus topical fluoride, *Caries Res.* 38 (2004) 258–262.
- [6] World Health Organization (WHO) Expert Committee on Oral Health Status and Fluoride Use, *Fluorides and Oral Health: Report of a WHO Expert Committee on Oral Health Status and Fluoride Use*, WHO Technical Report Series 846, World Health Organization, Geneva, 1994.

- [7] M.H. Beers, R. Berkow, *The Merck Manual of Diagnosis and Therapy*, 17th edition, Merck & Co., Inc., New Jersey, 1999 (Available at: <http://www.merck.com/mrksd/mmanual/home.jsp>).
- [8] Standing Committee on the Scientific Evaluation of the Dietary Reference Intakes, *Dietary Reference Intakes (DRI) for Calcium, Phosphorus, Magnesium, Vitamin D, and Fluoride*, National Academy Press, Washington, DC, 1997.
- [9] O. Fejerskov, K.W. Stephen, A. Richards, R. Speirs, Combined effect of systemic and topical fluoride treatments on human deciduous teeth—case studies, *Caries Res.* 21 (1987) 452–459.
- [10] V. Baelum, O. Fejerskov, F. Manji, M.J. Larsen, Daily dose of fluoride and dental fluorosis, *Tandlaegebladet* 91 (1987) 452–456.
- [11] B.A. Burt, The changing patterns of systemic fluoride intake, *J. Dent. Res.* 71 (1992) 1228–1237.
- [12] Centers for Disease Control and Prevention (CDC), Ten great public health achievements – United States, 1900–1999, *MMWR Weekly* 48 (1999) 241–243. (Available at: <http://www.cdc.gov/mmwr/PDF/wk/mm4812.pdf>).
- [13] Centers for Disease Control and Prevention (CDC), Populations receiving optimally fluoridated public drinking water – 2000, United States, 2000, *MMWR Weekly* 51 (2002) 144–147. (Available at: <http://www.cdc.gov/mmwr/PDF/wk/mm5107.pdf>).
- [14] D.W. Cross, R.J. Carton, Fluoridation: A violation of medical ethics and human rights, *Int. J. Occup. Environ. Health* 9 (2003) 24–29.
- [15] R.B. Symonds, W.I. Rose, M.H. Reed, Contribution of Cl- and F-bearing gases to the atmosphere by volcanoes, *Nature* 334 (1988) 415–418.
- [16] Agency for Toxic Substances and Disease Registry (ATSDR), U.S. Department of Health and Human Services, *Toxicological Profile for Fluorides, Hydrogen Fluoride, and Fluorine*, Atlanta, 1993. Available at: <http://www.fluoridealert.org/atsdr-fluoride.pdf>.
- [17] World Health Organization (WHO), *Environmental Health Criteria 227, Fluorides*, World Health Organization, Geneva, 2002.
- [18] A. Tressaud, *Fluorine and the environment: Atmospheric chemistry, emissions and lithosphere*, Vol. 1, and *Fluorine and the environment: Agrochemicals, archaeology, green chemistry and water*, Vol. 2, in: *Advances in Fluorine Science*, Elsevier, Amsterdam, 2006.
- [19] A.K.M. Arnesen, G. Abrahamsen, G. Sandvik, T. Krogstad, Aluminium-smelters and fluoride pollution of soil and soil solution in Norway, *Sci. Total Environ.* 163 (1995) 39–53.
- [20] S. Tripathy, M.K. Panigrahi, N. Kundu, Geochemistry of soil around a fluoride contaminated area in Nayagarh District, Orissa, India: Factor analytical appraisal, *Environ. Geochem. Health* 27 (2005) 205–216.
- [21] S. Larsen, A.E. Widdowson, Soil fluorine, *J. Soil Sci.* 22 (1971) 210–221.
- [22] W.L. Davis, Ambient air fluorides in Salt Lake County, Rocky Mt. Med. J. 69 (1972) 53–56.
- [23] P.S. Low, H. Bloom, Atmospheric deposition of fluoride in the lower Tamar Valley, Tasmania, *Atmos. Environ.* 22 (1988) 2049–2056.
- [24] R.D. Cadle, A comparison of volcanic with other fluxes of atmospheric trace gas constituents, *Rev. Geophys.* 18 (1980) 746–752.
- [25] Agency for Toxic Substances and Disease Registry (ATSDR), U.S. Department of Health and Human Services, *Toxicological Profile for Fluorides, Hydrogen Fluoride, and Fluorine*, Atlanta, 2003. (Available at: <http://www.atsdr.cdc.gov/toxprofiles/tp11.pdf>).
- [26] H.G. Dässler, H. Grumbach, Abgassschäden an Obst in der Umgebung eines Fluorowerkes, *Arch. Pflanzensch.* 3 (1967) 59–69.
- [27] A.W. Davison, L.H. Weinstein, Some problems relating to fluorides in the environment: Effects on plants and animals, in: A. Tressaud (Ed.), *Advances in Fluorine Science*, Vol. 1, Elsevier, Amsterdam, 2006, pp. 251–298.
- [28] W. Bergmann, *Nutritional disorders of plants*, Gustav Fischer Verlag, Jena, 1992.

- [29] R.J. Thompson, T.B. McMullen, G.B. Morgan, Fluoride concentrations in the ambient air, *J. Air Pollut. Control Assoc.* 21 (1971) 484–487.
- [30] UNICEF (The United Nations Children's Fund), Fluoride in water: An overview, UNICEF (Available at: <http://www.unicef.org/wes/fluoride.pdf>).
- [31] J. Ares, Fluoride-aluminium water chemistry in forest ecosystems of central Europe, *Chemosphere* 21 (1990) 597–612.
- [32] C. Reimann, P. De Caritat, J.H. Halleraker, T. Volden, M. Äyräs, H. Niskavaara, V.A. Chekushin, V.A. Pavlov, Rainwater composition in eight arctic catchments in northern Europe (Finland, Norway and Russia), *Atmos. Environ.* 31 (1997) 159–170.
- [33] H.V. Churchill, Occurrence of fluorides in some water of the United States, *Ind. Eng. Chem.* 23 (1931) 996–998.
- [34] M.C. Smith, E.M. Lantz, H.V. Smith, The cause of mottled enamel, *Science* 74 (1931) 244.
- [35] H. Velu, Dystrophie dentaire des mammifères des zones phosphatées (darmous) et fluorose chronique, *C.R. Séances Soc. Biol. Ses. Fil.* 108 (1931) 750–752.
- [36] G.V. Iyengar, W.E. Kollmer, H.J.M. Bowen, *The Elemental Composition of Human Tissues and Body Fluids*, Verlag Chemie, Weinheim, 1978.
- [37] E.J. Underwood, W. Mertz, Introduction, in: W. Mertz (Ed.), *Trace Elements in Human and Animal Nutrition*, 5th edition, Vol. 1, Academic Press, San Diego, 1987, pp. 1–19.
- [38] W. Mertz, Essential trace metals: New definitions based on new paradigms, *Nutr. Rev.* 51 (1993) 287–295.
- [39] The Expert Consultation of World Health Organization/Food and Agriculture Organization of the United Nations/International Atomic Energy Agency (WHO/FAO/IAEA), *Trace Elements in Human Nutrition and Health*, World Health Organization, Geneva, 1996.
- [40] K. Roholm, *Fluorine Intoxication*, NYT Nordisk Forlag, Copenhagen, 1937.
- [41] K.A.V.R. Krishnamachari, Fluorine, in: W. Mertz (Ed.), *Trace Elements in Human and Animal Nutrition*, 5th edition, Vol. 1, Academic Press, San Diego, 1987, pp. 365–415.
- [42] World Health Organization (WHO), *Environmental Health Criteria 36, Fluorine and Fluorides*, World Health Organization, Geneva, 1984.
- [43] G.E. Smith, A surfeit of fluoride, *Sci. Prog. Oxf.* 69 (1985) 429–442.
- [44] E. Marshall, The fluoride debate: One more time, *Science* 247 (1990) 276–277.
- [45] P.T.C. Harrison, Fluoride in water: A UK perspective, *J. Fluorine Chem.* 126 (2005) 1448–1456.
- [46] O. Fejerskov, A. Thylstrup, M.J. Larsen, Clinical and structural features and possible pathogenic mechanisms of dental fluorosis, *Scand. J. Dent. Res.* 85 (1977) 510–534.
- [47] T. Ishii, G. Suckling, The severity of dental fluorosis in children exposed to water with a high fluoride content for various periods of time, *J. Dent. Res.* 70 (1991) 952–956.
- [48] B.K.B. Berkovitz, G.R. Holland, B.J. Moxham, *Oral Anatomy, Histology and Embryology*, 3rd edition, Mosby, Edinburgh, 2002.
- [49] H.T. Dean, Classification of mottled enamel diagnosis, *J. Am. Dent. Assoc.* 21 (1934) 1421–1426.
- [50] A. Thylstrup, O. Fejerskov, Clinical appearance of dental fluorosis in permanent teeth in relation to histologic changes, *Community Dent. Oral* 6 (1978) 315–328.
- [51] H.S. Horowitz, W.S. Driscoll, R.J. Meyers, S.B. Heifetz, A. Kingman, A new method for assessing the prevalence of dental fluorosis—the tooth surface index of fluorosis, *J. Am. Dent. Assoc.* 109 (1984) 37–41.
- [52] L.S. Kaminsky, M.C. Mahoney, J. Leach, J. Melius, M.J. Miller, Fluoride: Benefits and risks of exposure, *Crit. Rev. Oral Biol. Med.* 1 (1990) 261–281.
- [53] T. Aoba, O. Fejerskov, Dental fluorosis: Chemistry and biology, *Crit. Rev. Oral Biol. Med.* 13 (2002) 155–170.
- [54] M. Pontié, C. Diawara, A. Lhassani, H. Dach, M. Rumeau, H. Buisson, J.C. Schrotter, Water defluoridation processes: A review. Application: Nanofiltration (NF) for future large-scale pilot plants, in: A. Tressaud (Ed.), *Advances in Fluorine Science*, Vol. 2, Elsevier, Amsterdam, 2006, pp. 49–80.

- [55] Editorial, Preskeletal phase of fluorosis, *Fluoride* 12 (1979) 169–171.
- [56] H.C. Hodge, F.A. Smith, Occupational fluoride exposure, *J. Occup. Med.* 19 (1977) 12–39.
- [57] J.F. Liebman, M. Ponikvar, Ion selective electrode determination of free versus total fluoride ion in simple and fluoroligand coordinated hexafluoropnictate (PnF_6^- , Pn = P, As, Sb, Bi) salts, *Struct. Chem.* 16 (2005) 521–528.
- [58] M. Ponikvar, J.F. Liebman, Paradoxes and paradigms: When do alkali metal (Na) and alkaline earth (Mg, Ca) halides (F, Cl) completely dissociate? A combined analytical and thermo-chemical approach, *Struct. Chem.* 16 (2005) 587–591.
- [59] K. Akinawa, Re-examination of acute toxicity of fluoride, *Fluoride* 30 (1997) 89–101.
- [60] G.M. Whitford, Fluoride in dental products: Safety considerations, *J. Dent. Res.* 66 (1987) 1056–1060.
- [61] D. Peters, R. Miethchen, Symptoms and treatment of hydrogen fluoride injuries, *J. Fluorine Chem.* 79 (1996) 161–165.
- [62] K. Heard, R.E. Hill, C.B. Cairns, R.C. Dart, Calcium neutralizes fluoride bioavailability in a lethal model of fluoride poisoning, *J. Toxicol. Clin. Toxicol.* 39 (2001) 349–353.
- [63] F.J. Cerklewski, Fluoride bioavailability—Nutritional and clinical aspects, *Nutr. Res.* 17 (1997) 907–929.
- [64] J. Ekstrand, M. Ehrnebo, L.O. Boréus, Fluoride bioavailability after intravenous and oral administration: Importance of renal clearance and urine flow, *Clin. Pharmacol. Ther.* 23 (1978) 329–337.
- [65] K. Trautner, G. Siebert, An experimental study of bio-availability of fluoride from dietary sources in man, *Arch. Oral Biol.* 31 (1986) 223–228.
- [66] K. Trautner, J. Einwag, Influence of milk and food on fluoride bioavailability from NaF and Na_2FPO_3 in man, *J. Dent. Res.* 68 (1989) 72–77.
- [67] E.R. Shulman, M. Vallejo, Effect of gastric contents on the bioavailability of fluoride in humans, *Pediatr. Dent.* 12 (1990) 237–240.
- [68] A. Goyal, K. Gauba, A. Tewari, Bioavailability of fluoride in humans from commonly consumed diets in India, *J. Indian Soc. Pedod. Prev. Dent.* 16 (1998) 1–6.
- [69] C.J. Spak, J. Ekstrand, D. Zylberstein, Bioavailability of fluoride added to baby formula and milk, *Caries Res.* 16 (1982) 249–256.
- [70] J. Ekstrand, M. Ehrnebo, Influence of milk products on fluoride bioavailability in man, *Eur. J. Clin. Pharmacol.* 16 (1979) 211–215.
- [71] J. Ekstrand, E.E. Ziegler, S.E. Nelson, S.J. Fomon, Absorption and retention of dietary and supplemental fluoride by infants, *Adv. Dent. Res.* 82 (1994) 175–180.
- [72] G.M. Whitford, D.H. Pashley, Fluoride absorption: The influence of gastric acidity, *Calcif. Tissue Int.* 36 (1984) 302–307.
- [73] C. Waterhouse, D. Taves, A. Munzer, Serum inorganic fluoride: changes related to previous fluoride intake, renal function and bone resorption, *Clin. Sci.* 58 (1980) 145–152.
- [74] D.R. Taves, Evidence that there are two forms of fluoride in human serum, *Nature* 217 (1968) 1050–1051.
- [75] P. Venkateswarlu, L. Singer, W.D. Armstrong, Determination of ionic (plus ionizable) fluoride in biological fluids. Procedure based on adsorption of fluoride ion on calcium phosphate, *Anal. Biochem.* 42 (1971) 350–359.
- [76] W.S. Guy, D.R. Taves, W.S. Brey Jr., Biochemistry involving carbon-fluorine bond, in: R. Fuller (Ed.), *Plasma Prevalence and Characterization*, ACS Symposium Series 28, 1976, Washington, pp. DC117–134.
- [77] D.R. Taves, B.W. Fry, R.B. Freeman, A.J. Gillies, Toxicity following methoxyflurane anesthesia. II. Fluoride concentrations in nephrotoxicity, *J. Am. Med. Assoc.* 214 (1970) 91–95.
- [78] J. Belisle, Organic fluorine in human serum: Natural versus industrial sources, *Science* 212 (1981) 1509–1510.
- [79] Y.W. Shen, D.R. Taves, Fluoride concentrations in the human placenta and maternal and cord blood, *Am. J. Obstet. Gynecol.* 119 (1974) 205–207.

- [80] S. Gupta, A.K. Seth, A. Gupta, A.G. Gavane, Transplacental passage of fluorides, *J. Pediatr.* 123 (1993) 139–141.
- [81] A. Malhotra, A. Tewari, H.S. Chawla, K. Gauba, K. Dhall, Placental transfer of fluoride in pregnant women consuming optimum fluoride in drinking water, *J. Indian Soc. Pedod. Prev. Dent.* 11 (1993) 1–3.
- [82] E. Brambilla, G. Belluomo, A. Malerba, M. Buscaglia, L. Strohmer, Oral administration of fluoride in pregnant women, and the relation between concentration in maternal plasma and in amniotic fluid, *Arch. Oral Biol.* 39 (1994) 991–994.
- [83] S. Shimonovitz, D. Patz, P. Ever-Hadani, L. Singer, D. Zacut, G. Kidroni, M. Ron, Umbilical cord fluoride serum levels may not reflect fetal fluoride status, *J. Perinat. Med.* 23 (1995) 279–282.
- [84] D.E. Gardner, F.A. Smith, H.C. Hodge, D.E. Overton, R. Feltman, The fluoride content of placental tissue as related to the fluoride content of drinking water, *Science* 115 (1952) 208–209.
- [85] J. Ekstrand, M. Ehrnebo, The relationship between plasma fluoride, urinary excretion rate and urine fluoride concentration in man, *J. Occup. Med.* 25 (1983) 745–748.
- [86] L. Singer, R. Ophaug, Ionic and nonionic fluoride in plasma (or serum), *Crc. Cr. Rev. Cl. Lab. Sc.* 18 (1982) 111–140.
- [87] A. Oliveby, F. Lagerlof, J. Ekstrand, C. Dawes, Studies on fluoride concentrations in human submandibular/sublingual saliva and their relation to flow rate and plasma fluoride levels, *J. Dent. Res.* 68 (1989) 146–149.
- [88] J. Ekstrand, L.O. Boréus, P. De Chateau, No evidence of transfer of fluoride from plasma to breast milk, *Br. Med. J.* 283 (1981) 761–762.
- [89] C.J. Spak, L.I. Hardell, P. De Chateau, Fluoride in human milk, *Acta Paediatr. Scand.* 72 (1983) 699–701.
- [90] S. Esala, E. Vuori, A. Helle, Effect of maternal fluorine intake on breast milk fluorine content, *Br. J. Nutr.* 48 (1982) 201–204.
- [91] Report of Joint World Health Organization/International Atomic Energy Agency (WHO/IAEA), Collaborative Study, Minor and Trace Elements in Breast Milk, World Health Organization, Geneva, 1989.
- [92] J. Ekstrand, G. Alván, L.O. Boréus, A. Norlin, Pharmacokinetics of fluoride in man after single and multiple oral doses, *Eur. J. Clin. Pharmacol.* 12 (1977) 311–317.
- [93] J. Ekstrand, Fluoride concentrations in saliva after single oral doses and their relation to plasma fluoride, *Scand. J. Dent. Res.* 85 (1977) 16–17.
- [94] K. Sjögren, D. Birkhed, L.G. Persson, J.G. Norén, Salivary fluoride clearance after a single intake of fluoride tablets and chewing gums in children, adults, and dry mouth patients, *Scand. J. Dent. Res.* 101 (1993) 274–278.
- [95] J. Ekstrand, Fluoride in plaque fluid and saliva after NaF or MFP rinses, *Eur. J. Oral Sci.* 105 (1997) 478–484.
- [96] S. Twetman, T. Nederfors, L.G. Petersson, Fluoride concentration in whole saliva and separate gland secretions in schoolchildren after intake of fluoridated milk, *Caries Res.* 32 (1998) 412–416.
- [97] W. Stephan Eakle, J.D.B. Featherstone, J.A. Weintraub, S.G. Shain, S.A. Gansky, Salivary fluoride levels following application of fluoride varnish or fluoride rinse, *Community Dent. Oral* 32 (2004) 462–469.
- [98] G.M. Whitford, J.E. Thomas, S.M. Adair, Fluoride in whole saliva, parotid ductal saliva and plasma in children, *Arch. Oral Biol.* 44 (1999) 785–788.
- [99] Z. Tóth, Z. Gintner, J. Bánóczy, The effect of ingested fluoride administered in salt, milk, and tablets on salivary and urinary fluoride concentrations, *Fluoride* 38 (2005) 199–204.
- [100] R.G. Schamschula, E. Sugár, P.S.H. Un, K. Tóth, D.E. Barmes, B.L. Adkins, Physiological indicators of fluoride exposure and utilization: An epidemiological study, *Commun. Dent. Oral* 13 (1985) 104–107.
- [101] W. Czarnowski, K. Stolarska, B. Brzezinska, J. Krechniak, Fluoride in urine, hair and nails of phosphate fertilizer workers, *Fluoride* 29 (1996) 163–165.

- [102] Z. Kokot, D. Drzewiecki, Fluoride levels in hair of exposed and unexposed populations in Poland, *Fluoride* 33 (2000) 196–204.
- [103] G.M. Whitford, Monitoring fluoride exposure with fingernail clippings, *Schweiz. Monatsschr. Zahnmed.* 15 (2005) 685–689.
- [104] Y. Ericsson, K. Gydell, T. Hammarskiöld, Blood plasma fluoride: An indicator of skeletal fluoride content, *Int. Res. Comm. System* 1 (1973) 33.
- [105] J. Mullen, History of water fluoridation, *Br. Dent. J.* 199 (2005) 1–4.
- [106] Scientific Committee on Food (SCF), Reports of the Scientific Committee for Food, 43rd series, European Commission, Luxembourg, 1998. (Available at: http://europa.eu.int/comm/food/fs/sc/scf/reports/scf_reports_43.pdf).
- [107] Food and Drug Administration (FDA), Requirements for Specific Standardized Beverages, Bottled Water, U.S., Title 21, Volume 2, Parts 100 to 169, 2000, Printing Office via GPO Access, CITE: 21CFR165.110. (Available at: <http://frwebgate.access.gpo.gov/cgi-bin/get-cfr.cgi?TITLE=21&PART=165&SECTION=110&YEAR=2000&TYPE=TEXT>).
- [108] Z.M. Xie, Z.H. Ye, M.H. Wong, Distribution characteristics of fluoride and aluminum in soil profiles of an abandoned tea plantation and their uptake by six woody species, *Environ. Int.* 26 (2001) 341–346.
- [109] P. Gulati, V. Singh, M.K. Gupta, V. Vaidya, S. Dass, S. Prakash, Studies on the leaching of fluoride in tea infusions, *Sci. Total Environ.* 138 (1993) 213–222.
- [110] K.F. Fung, Z.Q. Zhang, J.W.C. Wong, M.H. Wong, Fluoride contents in tea and soil from tea plantations and the release of fluoride into tea liquor during infusion, *Environ. Pollut.* 104 (1999) 197–205.
- [111] J. Cao, S.F. Luo, J.W. Liu, Y. Li, Safety evaluation on fluoride content in black tea, *Food Chem.* 88 (2004) 233–236.
- [112] J. Cao, Y. Zhao, J.W. Liu, Safety evaluation and fluorine concentration of Pu'er brick tea and Bianxiao brick tea, *Food Chem. Toxicol.* 36 (1998) 1061–1063.
- [113] A. Behrendt, V. Oberste, W.E. Wetzl, Fluoride concentration and pH of iced tea products, *Caries Res.* 36 (2002) 405–410.
- [114] M.P. Whyte, Fluoride levels in bottled teas, *Am. J. Med.* 119 (2006) 189–190.
- [115] S.C.C. Lung, P.K. Hsiao, K.M. Chiang, Fluoride concentrations in three types of commercially packed tea drinks in Taiwan, *J. Expo. Anal. Environ. Epidemiol.* 13 (2003) 66–73.
- [116] J.G. Stannard, Y.S. Shim, M. Kritsineli, P. Labropoulou, A. Tsamtouris, Fluoride levels and fluoride contamination of fruit juices, *J. Clin. Pediatr. Dent.* 16 (1991) 38–40.
- [117] M.C. Kiritsy, S.M. Levy, J.J. Warren, N. Guha-Chowdhury, J.R. Heilman, T. Marshall, Assessing fluoride concentrations of juices and juice-flavored drinks, *J. Am. Dent. Assoc.* 127 (1996) 895–902.
- [118] L.W. Njenga, D.N. Kariuki, S.M. Ndegwa, Water-labile fluoride in fresh raw vegetable juices from markets in Nairobi, Kenya, *Fluoride* 38 (2005) 205–208.
- [119] J.R. Heilman, M.C. Kiritsy, S.M. Levy, J.S. Wefel, Assessing fluoride levels of carbonated soft drinks, *J. Am. Dent. Assoc.* 130 (1999) 1593–1599.
- [120] S. Warnakulasuriya, C. Harris, S. Gelbier, J. Keating, T. Peters, Fluoride content of alcoholic beverages, *Clin. Chim. Acta* 320 (2002) 1–4.
- [121] M.I. Rodríguez Gómez, A. Hardisson de La Torre, A. Burgos Ojeda, R. Álvarez Marante, L. Díaz-Flores, Fluoride levels in wines of the Canary Islands (Spain), *Eur. Food Res. Technol.* 216 (2003) 145–149.
- [122] A.W. Burgstahler, M.A. Robinson, Fluoride in California wines and raisins, *Fluoride* 30 (1997) 142–146.
- [123] O. Backer Dirks, J.M.P.A. Jongeling-Eijndhoven, T.D. Flissebaalje, I. Gedalia, Total and free ionic fluoride in human and cows milk as determined by gas-liquid-chromatography and fluoride electrode, *Caries Res.* 8 (1974) 181–186.
- [124] M. Silva, E.C. Reynolds, Fluoride content of infant formulae in Australia, *Aust. Dent. J.* 41 (1996) 37–42.

- [125] M.A.R. Buzalaf, J.M. Granjeiro, C.A. Damante, F. de Ornelas, Fluoride content of infant formulas prepared with deionized, bottled mineral and fluoridated drinking water, *J. Dent. Child.* 68 (2001) 37–41.
- [126] P.A. San Filippo, G.C. Battistone, The fluoride content of a representative diet of the young adult man, *Clin. Chim. Acta* 31 (1971) 453–457.
- [127] L. Singer, R.H. Ophaug, B.F. Harland, Fluoride intake of young male adults in the United States, *Am. J. Clin. Nutr.* 33 (1980) 328–332.
- [128] L. Singer, R.H. Ophaug, Determination of fluoride in foods, *J. Agric. Food Chem.* 34 (1986) 510–513.
- [129] D.R. Taves, Dietary intake of fluoride ashed (total fluoride) v. unashed (inorganic fluoride) analysis of individual foods, *Br. J. Nutr.* 49 (1983) 295–301.
- [130] H. Lopez, J.M. Navia, A method to assay fluoride in food, beverages, and diets, *Caries Res.* 22 (1988) 210–216.
- [131] P. Varo, P. Koivistoinen, Mineral element composition of Finnish foods, *Acta Agric. Scand. (Suppl. 22)* (1980) 165–171.
- [132] R.W. Dabeka, A.D. McKenzie, Survey of lead, cadmium, fluoride, nickel, and cobalt in food composites and estimation of dietary intakes of these elements by Canadians in 1986–1988, *J. AOAC Int.* 78 (1995) 897–909.
- [133] T.M. Marthaler, Overview of salt fluoridation in Switzerland since 1955, a short history, *Schweiz. Monatsschr. Zahnmed.* 115 (2005) 651–655.
- [134] T.M. Marthaler, Increasing the public health effectiveness of fluoridated salt, *Schweiz. Monatsschr. Zahnmed.* 115 (2005) 785–792.
- [135] P. Tramini, Salt fluoridation in France since 1986, *Schweiz. Monatsschr. Zahnmed.* 115 (2005) 656–658.
- [136] A.G. Schulte, Salt fluoridation in Germany since 1991, *Schweiz. Monatsschr. Zahnmed.* 115 (2005) 659–662.
- [137] T.M. Marthaler, G.W. Pollak, Salt fluoridation in Central and Eastern Europe, *Schweiz. Monatsschr. Zahnmed.* 115 (2005) 670–674.
- [138] G.M. Gillespie, R. Baez, Development of salt fluoridation in the Americas, *Schweiz. Monatsschr. Zahnmed.* 115 (2005) 663–669.
- [139] S. Twetman, Fluoridated milk may be beneficial to schoolchildren by helping prevent caries, *Evid. Based Dent.* 6 (2005) 88.
- [140] E. Newbrun, Current regulations and recommendations concerning water fluoridation, fluoride supplements, and topical fluoride agents, *J. Dent. Res.* 71 (1992) 1255–1265.
- [141] G.M. Davies, H.V. Worthington, R.P. Ellwood, E.M. Bentley, A.S. Blinkhorn, G.O. Taylor, R.M. Davies, A randomised controlled trial of the effectiveness of providing free fluoride toothpaste from the age of 12 months on reducing caries in 54-year old children, *Community Dent. Health* 19 (2002) 131–136.
- [142] Massachusetts Institute of Technology News Office, Toothbrush beats out car and computer as the invention Americans can't live without, according to Lemelson-MIT Survey (Available at: <http://web.mit.edu/newsoffice/2003/lemelson.html>).
- [143] R.G. Schamschula, J.L. Duppenhaler, E. Sugár, P.S.H. Un, K. Tóth, D.E. Barmes, Fluoride intake and utilization by Hungarian children: Associations and interrelationships, *Acta Physiol. Hung.* 72 (1988) 253–261.
- [144] S. Erdal, S.N. Buchanan, A quantitative look at fluorosis, fluoride exposure, and intake in children using a health risk assessment approach, *Environ. Health Perspect.* 113 (2005) 111–117.
- [145] D. Osis, E. Wiatrowski, J. Samachson, H. Spencer, Fluoride analysis of the human diet and of biological samples, *Clin. Chim. Acta* (1974) 211–216.
- [146] L. Kramer, D. Osis, E. Wiatrowski, H. Spencer, Dietary fluoride in different areas in the United States, *Am. J. Clin. Nutr.* 27 (1974) 590–594.
- [147] L. Singer, R.H. Ophaug, B.F. Harland, Dietary fluoride intake of 15–19-year-old male adults residing in the United States, *J. Dent. Res.* 64 (1985) 1302–1305.

- [148] R.W. Dabeka, A.D. McKenzie, G.M.A. Lacroix, Dietary intakes of lead, cadmium, arsenic and fluoride by Canadian adults: 24 hour duplicate diet study, *Food Addit. Contam.* 4 (1987) 89–102.
- [149] F. Couzy, E. Aubree, C. Magliola, J.P. Mareschi, Average mineral and trace element content in daily adjusted menus (DAM) of French adults, *J. Trace Elem. Electrolytes Health Dis.* 2 (1988) 79–83.
- [150] M. Haldimann, B. Zimmerli, Evaluation of ashing procedures for the gas chromatographic determination of fluoride in biological materials, *Anal. Chim. Acta* 282 (1993) 589–601.
- [151] M. Ponikvar, V. Stibilj, B. Žemva, Daily dietary intake of fluoride by Slovenian Military based on analysis of total fluorine in total diet samples using fluoride ion selective electrode, *Food Chem.* 103(2007) 369–374.
- [152] Y.Z. Han, J.Q. Zhang, X.Y. Liu, L.Z. Zhang, X.H. Yu, J.A. Dai, High fluoride content of food and endemic fluorosis, *Fluoride* 28 (1995) 201–202.
- [153] H.A. Cook, Fluoride and tea, *Lancet* 2 (1969) 329.
- [154] G.M. Whitford, D.W. Allmann, A.R. Shahed, Topical fluorides: Effects on physiologic and biochemical processes, *J. Dent. Res.* 66 (1987) 1072–1078.
- [155] F.J. McClure, Ingestion of fluoride and dental caries, quantitative relations based on food and water requirements of children one to twelve years old, *Am. J. Dis. Child.* 66 (1943) 362–369.
- [156] E. Wiatrowski, L. Kramer, D. Osis, H. Spencer, Dietary fluoride intake of infants, *Pediatrics* 55 (1975) 517–522.
- [157] L. Singer, R. Ophaug, Total fluoride intake of infants, *Pediatrics* 63 (1979) 460–466.
- [158] R.W. Dabeka, A.D. McKenzie, H.B.S. Conacher, B.S. Kirkpatrick, Determination of fluoride in Canadian infant foods and calculation of fluoride intake by infants, *Can. J. Public Health* 73 (1982) 188–191.
- [159] A. Brunetti, E. Newbrun, Fluoride balance of children 3 and 4 years old, *Caries Res.* 17 (1983) 171.
- [160] R.H. Ophaug, L. Singer, B.F. Harland, Dietary fluoride intake of 6-month and 2-year-old children in four dietary regions of the United States, *Am. J. Clin. Nutr.* 42 (1985) 701–707.
- [161] N. Guha-Chowdhury, B.K. Drummond, A.C. Smillie, Total fluoride intake in children aged 3 to 4 years—A longitudinal study, *J. Dent. Res.* 75 (1996) 1451–1457.
- [162] J.P. Pessan, S.M.B. Silva, M.A.R. Buzalaf, Evaluation of the total fluoride intake of 4–7-year-old children from diet and dentifrice, *J. Appl. Oral Sci.* 11 (2003) 150–156.
- [163] S.M. Levy, Review of fluoride exposures and ingestion, *Community Dent. Oral* 22 (1994) 173–180.
- [164] S.M. Levy, M.C. Kiritsy, J.J. Warren, Sources of fluoride intake in children, *J. Public Health Dent.* 55 (1995) 39–52.
- [165] German Nutrition Society, Austrian Nutrition Society, Swiss Society for Nutrition Research, Swiss Nutrition Association, Reference Values for Nutrition Intake, 1st edition, Umschau Braus, Frankfurt, 2002.
- [166] M. Haftenberger, G. Viergutz, V. Neumeister, G. Hetzer, Total fluoride intake and urinary excretion in German children aged 3–6 years, *Caries Res.* 35 (2001) 451–457.
- [167] H.H. Willard, O.B. Winter, Volumetric method for determination of fluorine, *Ind. Eng. Chem., Anal. Ed.* 5 (1933) 7–10.
- [168] G. Pietzka, P. Ehrlich, Fluor-Bestimmung mit Destillation als H_2SiF_6 unter Kreislauf-führung des Wassers, *Angew. Chem.* 65 (1953) 131–134.
- [169] M.A. Wade, S.S. Yamamura, Microdetermination of fluoride using an improved distillation procedure, *Anal. Chem.* 37 (1965) 1276–1287.
- [170] L.H. Andersson, B. Gelin, The separation of fluorine by Willard-Winter distillation and its determination by titration with thorium nitrate or by spectrophotometric measurement, *FOA Rep.* 1 (1967) 1–5.

- [171] L. Singer, W.D. Armstrong, Determination of fluoride. Procedure based upon diffusion of hydrogen fluoride, *Anal. Chem.* 26 (1954) 904–906.
- [172] D.R. Taves, Separation of fluoride by rapid diffusion using hexamethyldisiloxane, *Talanta* 15 (1968) 969–974.
- [173] P. Venkateswarlu, Separation of fluoride from fluoroelastomers by diffusion in test tubes, *Anal. Chem.* 64 (1992) 346–349.
- [174] R. Ikenishi, M. Kanai, M. Ishida, A. Harihara, S. Matsui, I. Yahara, T. Kitagawa, Determination of fluoride ion in animal bone by microdiffusion analysis, *Anal. Chem.* 62 (1990) 2636–2639.
- [175] P. Venkateswarlu, P. Sita, A new approach to the microdetermination of fluoride, adsorption-diffusion technique, *Anal. Chem.* 43 (1971) 758–760.
- [176] P. Venkateswarlu, Determination of total fluorine in serum and other biological materials by oxygen bomb and reverse extraction techniques, *Anal. Biochem.* 68 (1975) 512–521.
- [177] P. Venkateswarlu, Evaluation of analytical methods for fluoride in biological and related materials, *J. Dent. Res.* 69 (1990) 514–521.
- [178] M. Ponikvar, B. Sedej, B. Pihlar, B. Žemva, Determination of fluoride in $M(SbF_6)_x$ compounds, *Anal. Chim. Acta* 418 (2000) 113–118.
- [179] P. Venkateswarlu, Sodium biphenyl method for determination of covalently bound fluorine in organic compounds and biological methods, *Anal. Chem.* 54 (1982) 1132–1137.
- [180] D.A. Levaggi, W. Oyung, M. Feldstein, Microdetermination of fluoride in vegetation by oxygen bomb combustion and fluoride ion electrode analysis, *J. Air Pollut. Control Assoc.* 21 (1971) 277–279.
- [181] L. Singer, R.H. Ophaug, Determination of fluoride in blood plasma, *Anal. Chem.* 49 (1977) 38–40.
- [182] S. Esala, E. Vuori, L. Niinistö, Determination of nanogram amounts of fluorine in breast milk by ashing-diffusion method and the fluoride electrode, *Mikrochim. Acta* 1 (1983) 155–165.
- [183] H.J. Galloway, R.E. Shoaf, C.H. Skaggs, A rapid method for the determination of fluoride in vegetation, *Am. Ind. Hyg. Assoc. J.* 36 (1975) 721–724.
- [184] B. Eyde, Determination of fluoride in plant material with a ion-selective electrode, *Fresenius Z. Anal. Chem.* 311 (1982) 19–22.
- [185] M. Sager, Rapid determination of fluorine in solid samples, *Monatsh. Chem.* 118 (1987) 25–29.
- [186] M. Kjellefold Malde, K. Bjorvatn, K. Julshamn, Determination of fluoride in food by the use of alkali fusion and fluoride ion-selective electrode, *Food Chem.* 73 (2001) 373–379.
- [187] R. Bock, *Handbook of Decomposition Methods in Analytical Chemistry*, Blackie Group, London, 1979.
- [188] J.C. Warf, W.D. Cline, R.D. Tevebaugh, Pyrohydrolysis in the determination of fluoride and other halides, *Anal. Chem.* 26 (1954) 342–346.
- [189] I. Inkielewicz, W. Czarnowski, J. Krechniak, Determination of fluoride in soft tissues, *Fluoride* 36 (2003) 16–20.
- [190] V.L. Dressler, D. Pozebon, E.L.M. Flores, J.N.G. Paniz, E.M.M. Flores, Potentiometric determination of fluoride in geological and biological samples following pyrohydrolytic decomposition, *Anal. Chim. Acta* 466 (2002) 117–123.
- [191] M. Ponikvar, J.F. Liebman, Paradoxes and paradigms: Observations on pyrohydrolytic decomposition of fluorine-containing materials and accompanying thermochemistry, *Struct. Chem.* 17 (2006) 75–78.
- [192] L. Torma, Collaborative study of ion selective electrode method for the direct determination of fluoride in feeds, *J. AOAC* 58 (1975) 477–481.
- [193] A.E. Villa, Rapid method for determining fluoride in vegetation using an ion-selective electrode, *Analyst* 104 (1979) 545–551.

- [194] P. Aysola, P. Anderson, C.H. Langford, Wet ashing in biological samples in a microwave oven under pressure using poly(tetrafluoroethylene) vessels, *Anal. Chem.* 59 (1987) 1582–1583.
- [195] H. Matusiewicz, R.E. Sturgeon, S.S. Berman, Trace element analysis of biological material following pressure digestion with nitric acid–hydrogen peroxide and microwave heating, *J. Anal. At. Spectrom.* 4 (1989) 323–327.
- [196] S.R. Grobler, A.J. Louw, A new microwave acid digestion bomb method for the determination of total fluorine, *Caries Res.* 32 (1998) 378–384.
- [197] D.R. Taves, Determination of submicromolar concentrations of fluoride in biological samples, *Talanta* 15 (1968) 1015–1023.
- [198] H.B. Li, F. Chen, A highly sensitive fluorimetric method for the determination of fluoride in biological material with Al^{3+} -calcein complex, *Fresenius J. Anal. Chem.* 368 (2000) 501–504.
- [199] M.S. Frant, J.W. Ross, Jr., Electrode for sensing fluoride ion activity in solution, *Science* 154 (1966) 1553–1554.
- [200] R.A. Durst, J.K. Taylor, Modification of the fluoride activity electrode for microchemical analysis, *Anal. Chem.* 39 (1967) 1483–1485.
- [201] J. Ekstrand, A micromethod for the determination of fluoride in blood plasma and saliva, *Calcif. Tissue Res.* 23 (1977) 225–228.
- [202] K. Chiba, K. Tsunoda, Y. Umezawa, H. Haraguchi, S. Fujiwara, K. Fuwa, Plate-shaped silver/silver halide reference electrode for determination of fluoride ion in microliter solution with fluoride ion selective electrode, *Anal. Chem.* 52 (1980) 596–598.
- [203] G.L. Vogel, C.M. Carey, L.C. Chow, J. Ekstrand, Fluoride analysis in nanoliter- and microliter-size fluid samples, *J. Dent. Res.* 69 (1990) 522–528.
- [204] Y. Michigami, Y. Kuroda, K. Ueda, Y. Yamamoto, Determination of urinary fluoride by ion chromatography, *Anal. Chim. Acta* 274 (1993) 299–302.
- [205] M.C. Quintana, M.H. Blanco, L. Hernández, Highly sensitive methods for determination of fluoride in biological samples, *J. Liq. Chromatogr. Rel. Technol.* 26 (2003) 763–772.
- [206] K. Tsunoda, K. Fujiwara, K. Fuwa, Subnanogram fluorine determination by aluminum monofluoride molecular absorption spectrometry, *Anal. Chem.* 49 (1977) 2035–2039.
- [207] K. Chiba, K. Tsunoda, H. Haraguchi, K. Fuwa, Determination of fluorine in urine and blood serum by aluminum monofluoride molecular absorption spectrometry and with a fluoride ion selective electrode, *Anal. Chem.* 52 (1980) 1582–1585.
- [208] J. Marcos, A. Townshend, Fluoride determination by its inhibitory effect on immobilized liver esterase, *Anal. Chim. Acta* 310 (1995) 173–180.
- [209] D. Klockow, J. Auffarth, C. Kopp, A catalytic kinetic method for the determination of traces of fluoride in biological material, *Anal. Chim. Acta* 89 (1977) 37–46.
- [210] L. Guanghan, W. Qiongleng, W. Xiaogang, Z. Tong, Y. Xin, Polarographic determination of trace fluoride in foods, *Food Chem.* 66 (1999) 519–523.
- [211] J. Wang, B.S. Grabarić, Application of adsorptive stripping voltammetry for indirect measurement of nonelectroactive ions using competitive complex formation reactions, *Mikrochim. Acta* 100 (1990) 31–40.
- [212] J.M. Gehlhausen, J.W. Carnahan, Determination of aqueous fluoride with a helium microwave-induced plasma and flow injection analysis, *Anal. Chem.* 61 (1989) 674–677.
- [213] J.L. Manzoori, A. Miyazaki, Indirect inductively coupled plasma atomic emission determination of fluoride in water samples by flow injection solvent extraction, *Anal. Chem.* 62 (1990) 2457–2460.
- [214] G. Cobo, M. Gomez, C. Camara, M.A. Palacios, Determination of fluoride in complex liquid matrices by electrothermal atomic absorption spectrometry with in-furnace oxygen-assisted ashing, *Mikrochim. Acta* 110 (1993) 103–110.
- [215] M. Montes Bayón, A. Rodríguez García, J.I. García Alonso, A. Sanz-Medel, Indirect determination of trace amounts of fluoride in natural waters by ion chromatography:

- A comparison of on-line post-column fluorimetry and ICP-MS detectors, *Analyst* 124 (1999) 27–31.
- [216] K. Kobayashi, T. Shigematsu, Trace determination of iron, cobalt, nickel and copper in zirconium fluoride by substoichiometric radioactivation analysis, *J. Radioanal. Nucl. Chem. Articles* 113 (1987) 333–341.
- [217] D.I. Paik, D.S. Ma, D.Y. Park, H.S. Moon, Y.I. Chang, J.B. Kim, Determination of fluorine by PIGE analysis on bovine tooth enamel treated with bamboo salt SMFP toothpaste and fluoride mouth rinsing solution, *J. Radioanal. Nucl. Chem.* 217 (1997) 221–223.
- [218] U. Grummisch, C. Kurowski, D. Timm, H. Grunewald, U. Meyhack, Rapid analysis of organic fluoride compounds for production control by diffuse reflectance near infrared spectroscopy, *J. Near Infrared Spectrosc.* 6 (1998) A239–A241.
- [219] T.P. Cheng, H.D. Anderson, D.S. Mills, V.L. Spate, C.K. Baskett, J.S. Morris, Determination of the fluoride distribution in rabbit bone using instrumental neutron activation analysis, *J. Radioanal. Nucl. Chem.* 217 (1997) 171–174.
- [220] P. Venkateswarlu, Determination of fluorine in biological materials: A review, *Adv. Dent. Res.* 8 (1994) 80–86.
- [221] P. Venkateswarlu, G. Vogel, Fluoride analytical methods, in: O. Fejerskov, J. Ekstrand, B.A. Burt (Eds.), *Fluoride in Dentistry*, Mungsgaard, Copenhagen, 1996, pp. 27–39.
- [222] H.T. Dean, The investigation of physiological effects by the epidemiological method, in: F.R. Moulton (Ed.), *Fluorine and Dental Health*, American Association for the Advancement of Science, Washington, DC, 1942, pp. 23–31.
- [223] H.C. Hodge, The concentration of fluorides in drinking water to give the point of minimum caries with maximum safety, *J. Am. Dent. Assoc.* 40 (1950) 436–439.
- [224] C.S. Farkas, E.J. Farkas, Potential effect of food processing on the fluoride content of infant foods, *Sci. Total Environ.* 2 (1974) 399–405.
- [225] R.H. Ophaug, L. Singer, B.F. Harland, Estimated fluoride intake of average two-year-old children in four dietary regions of the United States, *J. Dent. Res.* 59 (1980) 777–781.
- [226] D.J. Forrester, E.M. Schultz, Proceedings of the International Workshop on Fluorides and Dental Caries Reduction, University of Maryland, Baltimore, MD, 1974.

Note from the Editors

Several chapters dealing with the interaction of fluorine and fluorides with plants, animals and men can be also found in the series “*Advances in Fluorine Science*” Elsevier, Amsterdam (2006),: Effects of fluorine emissions on plants and organisms by A.W. Davison and L.H. Weinstein (Vol. 1); Physiological effects of highly fluorinated waters by M. Pontié *et al.* (Vol. 2.). See also in the present book: interaction between fluorinated biomaterials and the human body by C. Rey *et al.* and fluoride in dentistry by J. W. Nicholson and B. Czarnecka.

This page intentionally left blank

SECTION 3

Pharmaceuticals

This page intentionally left blank

CHAPTER 13

Biological Impacts of Fluorination: Pharmaceuticals Based on Natural Products

Jean-Pierre Bégué and Danièle Bonnet-Delpon*

*Molécules Fluorées, BIOCIS, UMR-8076, Faculté de Pharmacie, Rue J.B. Clément,
Châtenay-Malabry 92296, France*

Contents

1. Introduction	554
2. Biological impact of fluorination	554
2.1. Affinity for the macromolecule target	555
2.1.1. Steric effects	556
2.1.2. Conformational changes	557
2.1.3. Dipolar interactions and electric field	557
2.1.4. Hydrogen bond	558
2.1.5. pK_a of amines	561
2.1.6. Fluorous interactions	562
2.2. Absorption	563
2.2.1. Lipophilicity	563
2.2.2. pK_a and solubility	564
2.3. Metabolism	566
2.3.1. Oxidative metabolism	567
2.3.2. Hydrolytic metabolism	570
2.4. Modification of the chemical reactivity: Conception of enzyme inhibitors	572
2.4.1. Analogue of substrates as inhibitor	572
2.4.2. Inhibition by stabilisation or destabilisation of intermediates of biological processes	574
2.4.3. Irreversible inhibition with based-mechanism inhibitors (suicide-substrates)	575
3. Fluorinated pharmaceuticals based on natural products	577
3.1. Nucleosides and carbohydrates	577
3.1.1. Inhibitors of the thymidylate synthase	578
3.1.2. Inhibitors of RDPR and DNA polymerase	580
3.2. Alkaloids	585
3.2.1. <i>Vinca</i> alkaloids	585
3.2.2. Camptothecin	587
3.3. Lignans	588
3.3.1. Podophyllotoxin	588

*Corresponding author.;

Email: danièle.bonnet-delpon@cep.u-psud.fr

3.4. Anthracyclines	589
3.5. Macrolides	590
3.5.1. Erythromycin	590
3.5.2. Epothilones	591
3.6. Steroids	593
3.6.1. Corticosteroids	593
3.6.2. Fluorosteroids acting on steroid hormone receptors	600
3.6.3. Other fluorinated steroid drugs	601
3.6.4. Vitamin D ₃ metabolites	603
3.7. Prostanoids	606
3.8. Terpenes	608
3.8.1. Artemisinin	608
3.9. Amino acids	610
4. Conclusion	611
References	611

Abstract

This present chapter is devoted to the recent advances, for the last decade, in fluorinated analogues of natural products developed as pharmaceuticals and now marketed or in development (registered or in clinical development). These mainly concern fluorine-substituted nucleosides, alkaloids, macrolides, steroids, amino acids and prostaglandins.

1. INTRODUCTION

Among the numerous marketed pharmaceuticals in the world, more than 150 drugs are fluorinated compounds [1–3]. This is a relatively huge number compared to other halogen-containing pharmaceuticals, and it is all the more striking since organo-chlorine and organo-bromine compounds are far more abundant as natural compounds [4]. The specific properties of the fluorine atom, such as its strong electronegativity, small size, and low polarisability of the C–F bond, can have considerable impact on the behaviour of a small molecule in a biological environment. These aspects are presented in the first part of this chapter, with the aim to illustrate how the presence of fluorine atoms is able to alter properties of a bioactive compound at various biological steps, and possibly to facilitate its emergence as a pharmaceutical [2]. The review is then focused on fluorinated analogues of several families of natural compounds, which have been developed as pharmaceuticals, and is aimed to highlight the latest developments on emerging compounds.

2. BIOLOGICAL IMPACT OF FLUORINATION

The introduction of fluorine atoms into a molecule has an impact on the physical and chemical properties of this molecule, with deep consequences on the biological properties. The absorption, distribution, recognition and interaction or

reaction processes with the biological target, as well as the metabolism and the elimination of this molecule, are affected. This possibility to modify or to modulate the pharmacological profile of a molecule by inserting fluorine atoms clearly explains why bioorganic and medicinal chemistry of fluorine has become so important, and why many drugs and pesticides are fluorinated compounds.

A lightly fluorinated analogue of a natural substance, or of a biologically active molecule, is generally recognised by the same biological macromolecule target (enzyme, receptor, nucleic acids). However, the specific physico-chemical properties of fluorine, especially its strong electronegativity and its own reactivity different from those of other halogens, modify interactions between the molecule and the constituents of the biological medium.

First, a drug must reach its biological target. This latter is localised in a cell located inside a tissue or an organ. The exogenous molecule has to be absorbed, to step over multiple barriers depending on the administration protocol and to be confronted to detoxication enzymes, without being cleared before reaching its target. The presence of fluorine atoms may influence each of these steps: absorption, transport and metabolism. The second phase is the interaction with the target. As it will be shown, the presence of fluorine atoms may have a great influence on the molecular recognition and affinity.

Fluorinated groups (F, CF₂, etc.) are isosteric or isopolar of various functional groups; they can mimic them in the interaction processes with biological macromolecules. They can also interact afterwards with the target, because of the specific reactivity of the fluorinated molecule. This explains the important role played by the incorporation of fluorine atoms in the design of receptor ligands and enzyme inhibitors: substrate analogues, transition state analogues and based-mechanism inhibitors.

It is worth noting that despite the efforts for rationalising and the progresses achieved during the last years, the understanding of the effects of fluorine introduction is still limited. While some of these effects are relatively straightforward to interpret, predicting effect of the overall behaviour of a fluoro compound is often uncertain [2,5–8]. Nevertheless, it will be attempted to clarify and rationalise these fluorination effects with their consequences on the affinity, absorption and metabolism properties. It will also be explained how the electronic properties of a fluorinated substituent (through changes in polarity, in the reactivity of neighbouring functional groups and in the stability of reaction intermediates) allows the design of enzyme inhibitors. These different aspects will be illustrated by means of recent reported examples.

2.1. Affinity for the macromolecule target

The affinity of a substrate with its biological target is first connected to its complementarity with this macromolecule. The molecular recognition and the affinity

depend on the whole favourable interactions that exist in the supramolecular assembly formed between the substrate and the macromolecule. If the presence of fluorine atoms enhances the strength or the number of these favourable interactions, the affinity of the fluorinated substrate will be higher than that of the parent compound. The main parameters involved are the steric and conformational effects, dipolar interactions and hydrogen bonds.

2.1.1. Steric effects

The van der Waals radius of fluorine atom (1.47 Å) is between that of hydrogen (1.20 Å) and that of oxygen (1.52 Å). Many experimental data show that when a hydrogen atom is substituted by a fluorine atom, only weak steric disturbances are induced, despite the difference of size. Conversely, the steric volume of a CF₂ or a CF₃ is much larger than that of a methylene or a methyl group, respectively [9]. More generally, fluoroalkyl groups are much bulkier than alkyl groups. It is considered that the size of a CF₃ group is close to that of an isopropyl group [10]. The steric hindrance induced by the presence of fluoroalkyl groups may destabilise the supramolecular structure formed between the macromolecule and the fluoro analogue of the substrate, or even prevent its formation.

The comparison of the olfactory properties of fluoro analogues of citronellol is a significant example (Fig. 1) [11,12]. While monofluorinated compound exhibit only minor changes in olfactory properties, this is quite different for trifluorocitronellol. In the absence of other factors envisioned, the important differences observed between citronellol and trifluorocitronellol are very likely due to a different recognition by the olfactory receptors, connected to the bigger size of the CF₃ with respect to CH₃ [10].

The rather considerable size of the CF₃ group allows it to efficiently mimic the side chain of several amino acids involved in ligands of receptors or enzyme inhibitors (valine, leucine, phenylalanine, phenylglycine, etc.). Moreover, the hydrophobic character of the CF₃ or R_f group (*vide infra*) favours the complementarity with the lipophilic pockets of the proteins, which are dedicated to receive the side chains of lipophilic amino acids [13]. Interestingly, the ability of a trifluoromethyl group to mimic a large lipophilic group (isobutyl, benzyl, etc.) can be in some cases

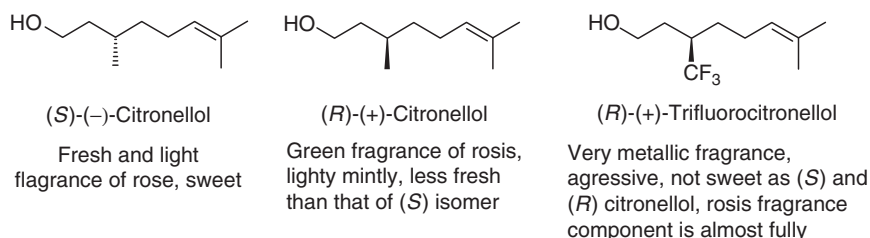


Fig. 1. Comparison of the olfactory properties of citronellols and of trifluorocitronellol [12].

accompanied by a change of the agonist/antagonist character of the ligand, when the binding activity remains unchanged [14].

2.1.2. Conformational changes

Because of the size difference of hydrogen and fluorine atoms, the substitution of a hydrogen by one or several fluorine atoms may modify the conformation of a molecule. Thus, dihedral angles in the lipid chain of fluorinated analogues of tristearine are notably modified by the presence of fluorine atoms, with repercussions on the physical properties [15]. The deep influence of the geometry and of the conformational stability on the affinity of a substrate for its target is well known. However, few studies have been dedicated to the influence of conformational changes, induced by the presence of fluorine atoms, on biological properties.

The gauche effect—which has the same electronic origin as the anomeric effect—is able to stabilise a conformation which should, *a priori*, be disfavoured by steric factors. Thus, the gauche effect disfavours the *trans* anti-periplanar conformation of two electronegative substituents bound by two vicinal carbon atoms (Fig. 2) [16, 17]. *Ab initio* calculations and crystallographic data show that α -fluoroamides and α -fluoroesters prefer adopting *trans* periplanar conformation, with the C–F bond in *anti* with respect to the carbonyl (Fig. 2) [18]. In a similar way, the structure of *N*-fluoroethyl acetamide under crystalline state shows that the conformation stabilised by a gauche effect is the most stable (Fig. 2) [18]. This gauche effect has been used to favour the active conformation of the ribofuranose cycle of sangivamycin analogues, a nucleoside that inhibits the protein kinase C [19]. This effect could also be used to modify the conformation of peptide chains.

2.1.3. Dipolar interactions and electric field

The complementarity of the electric fields of the substrate and of its binding site is an important factor for the affinity, especially because biological macromolecules contain many polar units in their binding site. At an electrostatic level, the energy involved in the interaction between dipoles is even more stabilising when the product of the electric charges is high. The strong electronegativity of the fluorine atom, and thus the strong dipole of the C–F bond, favours dipole–dipole interactions in the binding site. For this reason, a fluorine atom can replace another

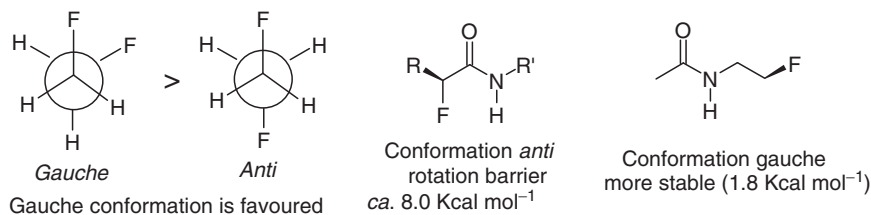


Fig. 2. Gauche effect of fluorinated compounds.

halogen, but also somehow an oxygen atom (or a hydroxyl group). In the same line, an aromatic ring bearing a fluorine atom may mimic a nitrogen-containing heterocycle (pyridine: 2.2 D; fluorobenzene: 1.7 debyes). However, electrons of the lone pairs are strongly retained around the fluorine atom; they are poorly polarisable and thus not so able to induce electric fields. This is also true for the electrons of the C–F bond. As a consequence of this low polarisability, the presence of fluorine atoms lowers the ability of a molecule to respond to electric fields [5,13,20].

2.1.4. Hydrogen bond

Hydrogen bonds play a major role in the interactions of a substrate with its biological target. The latter is generally a protein which bears many possible sites for hydrogen bonds.

Of course, unlike a hydroxyl group, fluorine cannot be a hydrogen bond donor, (Fig. 3). Furthermore, it is a poor acceptor of hydrogen bonds despite its strong electronegativity and its lone pairs of electrons. This is mainly due to the low polarisability of its electron pairs, which thus contribute only weakly to the electron transfer $n \rightarrow \sigma^*$ [5,13,20,21].

Theoretical calculations have shown that the strength of an $F \cdots H$ bond could be estimated between 2.0 and 3.2 kcal/mol, while that of an $O \cdots H$ bond is included between 5 and 10 kcal/mol. The examination of the crystalline structures of protein–ligand complexes taken from databases (Cambridge Crystallographic Data Centre) shows only few examples where fluorine is really involved in narrow contacts with hydrogen atoms, susceptible to reveal the presence of hydrogen bonds [5,13,20–23]. Moreover, these narrow contacts can often rather be interpreted as the result of a geometry imposed by other types of hydrogen bonds, and do not necessarily stem from a dynamic interaction connected to the fluorine atom [24–26].

Nevertheless, some crystalline structures can be found, where the stability seems to stem from $C-F \cdots H-C$ hydrogen bonds and not from $C-O \cdots H$ bonds. For instance, in deoxo-4-fluorophenyl-ribofuranose crystals, the distance between the fluorine atom and the *ortho* hydrogen atom of a second molecule is 2.3 Å, that is, shorter than the sum of the van der Waals radii of the two atoms considered. These $F \cdots H$ interactions should be one of the stabilising forces of oligoribonucleotide duplex formed from these fluorinated nucleotides (Fig. 4) [27]. However, it is worth to note that this example concerns aromatic fluorine and hydrogen atoms, where hydrogen bonds through electron delocalisation are strengthened [16,28].

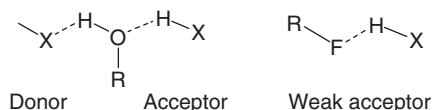


Fig. 3. Comparison of the potential hydrogen bonds between hydroxyl and fluorine.

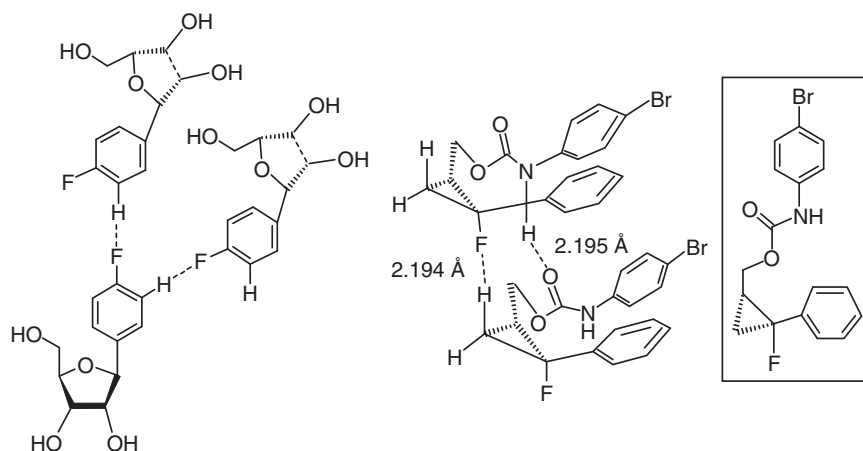


Fig. 4. Hydrogen bonds C–F \cdots H–C [27–29].

A short C–H \cdots F–C distance has also been observed in the crystalline structure of a cyclopropane derivative (2.194 Å) (Fig. 4) [29].

Other non-covalent interactions such as C=O \cdots F–C type, between a fluorine atom and the carbonyl of an amino acid, may take place for the stabilisation of enzyme–inhibitor supramolecular structures [28,30]. It is why the 4-fluorophenyl group is an important motif for binding pocket, as shown by the enhancement of one order of magnitude of the K_i , by introducing one fluorine atom on thrombin inhibitor (Fig. 5) [30].

Moreover, fluorine substitution reduces polarisability, increases the hydrophobic surface area and provides an enhanced driving force for desolvation (estimated driving force 0.2–0.5 kcal/mol) [13].

Pentafluorination diminishes π electron density of phenyl, making it more suitable for participation in stacking or charge transfer with the phenyl groups of other aromatic amino acids of the active site. As an example, the inhibitory power of the carbonic anhydric hydrolase by the pentafluorophenyl analogue of methazolamide is tenfold increased (Fig. 5) [31].

Fluorination has an important indirect impact on hydrogen bonds, via neighbouring functions (hydroxyl, amine, carbonyl, hydrogen). The electron-withdrawing effect of fluorine atom and of fluoroalkyl groups (CF₂, CF₃, etc.) deeply modifies the pK_a of neighbouring functions, and hence their character of hydrogen bond donors or acceptors (Table 1).

The values of the α_2^H parameter, which represents the ability of a substituent to be donor of hydrogen bonds, show that the presence of fluorine atoms notably enhances the hydrogen bond donor ability of a hydroxyl group. Conversely, the values of the β_2^H , which represents the ability to accept hydrogen bonds, are lowered by the presence of fluorine atoms.

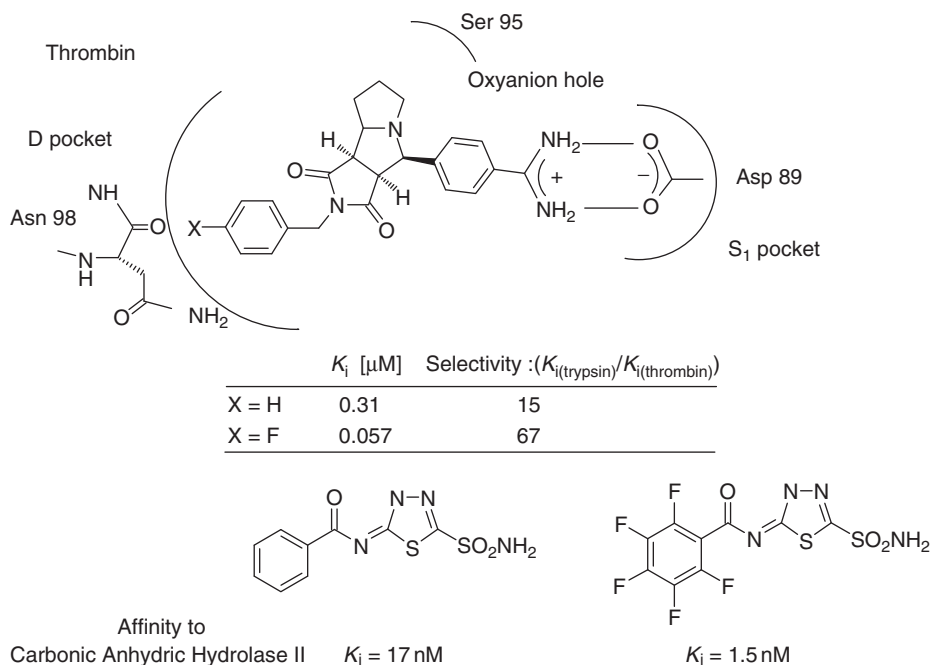


Fig. 5. C–F \cdots O=C interactions of fluorophenyl groups [28,30–31].

Table 1. pK_a , α_2^H and β_2^H values of fluorinated compounds in CCl_4

Compound	pK_a	α_2^H	β_2^H
$\text{CH}_3\text{CH}_2\text{--NH}_2$	10.7	0	0.70
$\text{CF}_3\text{CH}_2\text{--NH}_2$	5.9	—	0.36
MeCONEt_2	—	—	0.71
$\text{CF}_3\text{--CONEt}_2$	—	—	0.47
$\text{CH}_3\text{CH}_2\text{--OH}$	15.9	0.33	0.44
$\text{FCH}_2\text{CH}_2\text{--OH}$	—	0.40	0.36
$\text{CF}_3\text{CH}_2\text{OH}$	12.4	0.57	0.18
$\text{CF}_3\text{--CHOH--CF}_3$	9.3	0.77	0.03
$\text{C}_6\text{H}_5\text{--OH}$	10.0	0.60	0.22
$\text{C}_6\text{F}_5\text{--OH}$	5.5	0.76	0.02
$\text{CH}_3\text{--CO--CH}_3$	—	—	0.48
$\text{CF}_3\text{--CO--CF}_3$	—	—	0.20

The acidic character of fluorinated alcohols, and consequently the excellent ability to donate hydrogen bonds, justifies their interest as central peptidomimetic units in inhibitors of serine and aspartyl proteases [2, p. 59]. An enhancement of

the α_2^H of the OH-11 β of 9-fluorocorticoids has also been invoked to explain their pharmacological properties.

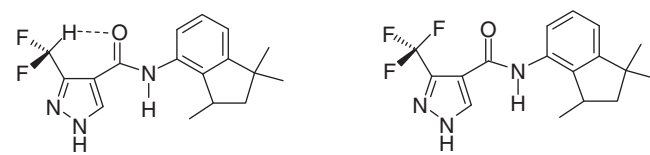
The acidity of the hydrogen of the difluoromethyl group (CF₂H) allows stabilising interactions with electron-withdrawing groups such as a carbonyl. For instance, it has been suggested that the better fungicidal activity of a difluoromethyl amidopyrazole, with respect to the trifluoromethyl parent compound, is due to the stabilisation of the conformation which makes possible an hydrogen bond C=O \cdots H-CF₂ (Fig. 6). This hypothesis is based on semi-empirical calculations of energy, showing a 5 kcal/mol stabilisation of this conformation, with a C-H \cdots O=C bond distance of 2.16 Å. The existence of this hydrogen bond has also been confirmed by nuclear magnetic resonance (NMR) studies [32].

Hydrogen bond involving an acidic hydrogen atom borne by a fluorine-substituted or halogen-substituted carbon seems to contribute to the activity and the selectivity of volatile fluorinated anaesthetics (Table 2). These molecules, although non-functional, can bind stereoselectively with protein targets of the central nervous system [33,34].

2.1.5. pK_a of amines

The lowering of the pK_a induced by the presence of fluorine atoms makes the protonation of an amine function more difficult. This decreased basicity may alter the affinity of a ligand for a receptor, depending whether the ligand acts as neutral or protonated form. As an example, Fig. 7 shows the impact of fluorination on the potency of the 5-HT₂ antagonist mifentidine (an analogue of cimetidine), which acts as neutral form [35]. Conversely, when the ligand interacts as protonated forms, the affinity is decreased.

In a similar way, this lowering may facilitate an enzymatic reaction when the non-protonated species is a better substrate for an enzyme than the protonated one. The rate of the methylation of the β,β -difluoroethylamine by the *N*-methyltransferase of rabbit lung is increased by a factor 4 [36].



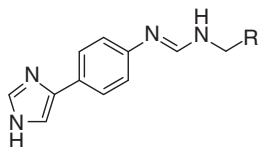
Compound	Dose (ppm)	% of fungicide activity towards control ^a
CF ₂ H	100	92
	20	73
CF ₃	100	62
	20	57

^aFungicide activity towards *Alternaria solani* (tomato parasite)

Fig. 6. Hydrogen bonds induced by CF₂H compounds [32].

Table 2. pK_a and α_2^H values of gaseous general anaesthetics

	pK_a	α_2^H
$CF_3CHClBr$	23.8	0.22
$CHCl_3$	24.1	0.20
$CH_3OCF_2CHCl_2$	26.1	0.17
CHF_2OCF_2CHFCI	26.7	0.19



R	pK_a		Protonated (mol% at pH 7.4)		H_2 affinity (picoM) (guinea pig atrium)
	Imidazole	Amidine	Monocation	Neutral	
CH_3 (Mifentidine)	5.57	8.65	93.2	5.3	177
CH_2F	5.55	8.12	82.6	16	61
CF_2H	4.54	6.60	13.5	86.3	21
CF_3	4.45	6.14	5.1	94.8	7.6

Fig. 7. Activity as H_2 antagonist of fluoro analogue of mifentidine [35].

2.1.6. Fluorous interactions

Fluorous effects in the active site of DNA polymerase have been observed when highly fluorinated nucleotides are present in the DNA template or are supplied as nucleoside triphosphates. When supplied opposite the non-natural bases in the template strand, the hydrophobic fluorinated nucleoside triphosphates have been incorporated more efficiently than the natural deoxynucleoside triphosphates [37]. These results suggest the importance of hydrophobicity, stacking and steric interaction in the polymerase-mediated replication of DNA base pairs that lack hydrogen bonds. These findings and other researches suggest that the enhanced hydrophobicity of highly fluorinated bases could be useful in various applications, for instance in the design of chips for DNA or RNA in genomic technologies.

This fluorous effect can also be effective for the stabilisation of proteins. For example, the selective pairing of peptides which contain perfluorinated chains has been demonstrated, and perfluorinated amino acid side chains have been shown to stabilise the hydrophobic-driven folding of proteins [38,39].

2.2. Absorption

The biological membranes are constituted of lipid bilayers, which form major obstacles for the advance of a drug to its target. In the case of oral administration, the drug must go from the intestine to blood (intestinal barrier), then from blood to an organ, where barriers exist (e.g. the brain–blood barrier). Finally, the molecule must generally go into the cell of the diseased organ or of the pathogenic microorganism by passing through several cell barriers. These steps of transportation and absorption are dependent on various factors, such as lipophilicity, pK_a , solubility and the molecular weight of the drug. The presence of fluorine atoms may have an influence on these parameters [40]. However, this effect is rarely clarified.

2.2.1. Lipophilicity

The lipophilicity of a substance is often evaluated by using its $\log P_{\text{octanol}}$ value, which is the logarithm of its octanol/water partition coefficients. This value is quite representative of the ability of a molecule to pass through a lipidic membrane. However, a high $\log P$ means a strong lipophilicity as well as a strong hydrophobicity. It is worth to note that in the case of highly fluorinated molecules, conversely to hydrocarbon compounds, there is no correlation between lipophilicity and hydrophobicity because fluorinated molecules are both hydrophobic and non-lipophilic. The unique feature of the carbon–fluorine bond stems from the association of the hydrophobic character with a high dipolar hydrophobicity (polar hydrophobicity). The latter property results from a high electronegativity, the small size of fluorine atom and the very low polarisability of the C–F bond [13].

In aromatic series, when hydrogen atoms are replaced by fluorine atoms or by fluoroalkyl groups, an enhancement of the $\log P$ occurs (Table 3) [13]. The CF_3 , CF_3O and CF_3S groups are the most hydrophobic substituents known. They are widely used in crop science [41].

In contrast, there are less experimental data available for aliphatic structures, much more present in natural compounds. Fluorination lowers lipophilicity and enhances the hydrophobicity. However, other factors, like strong hydrogen bonds

Table 3. $\log P$ of fluorinated and non-fluorinated compounds

Compound	$\log P$
C_6H_6	2.1
$\text{C}_6\text{H}_5\text{--F}$	2.3
$\text{C}_6\text{H}_5\text{--CH}_3$	2.1
$\text{C}_6\text{H}_5\text{--CF}_3$	3.0

or the enhancement of the dipolar moment, may lower the hydrophobicity and render the molecule more soluble or make its penetration easier.

For experimental facilities, calculated values of $\log P$ (Clog P) are often used. These latter are calculated by means of commercially available softwares. Nevertheless, relatively important gaps are often observed between calculated and measured values. They depend on parameters and increments used in the software, and a great prudence is required when considering Clog P values, even inside homogeneous series. For instance, the examination of the Clog P values in a series of leucotriene antagonists shows that the substitution by fluorine atoms seems to lower the $\log P$, and hence the lipophilicity [42]. Actually, the measurement of the $\log P$ indicates that calculated values are systematically overestimated (from 0.6 to 1.2 log units) in the case of non-fluorinated compounds, while the correlation fits for fluorinated molecules (Table 4). In this example, fluorinated compounds are slightly more lipophilic than non-fluorinated analogues [42]. However, some other examples illustrate an opposite situation; a bad correlation for fluorinated compounds and a good one for non-fluorinated series. These data highlight that comparison of Clog P has to be used with great caution.

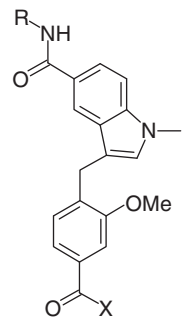
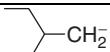
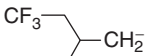
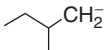
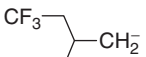
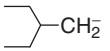
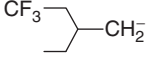
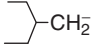
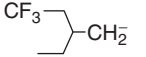
2.2.2. pK_a and solubility

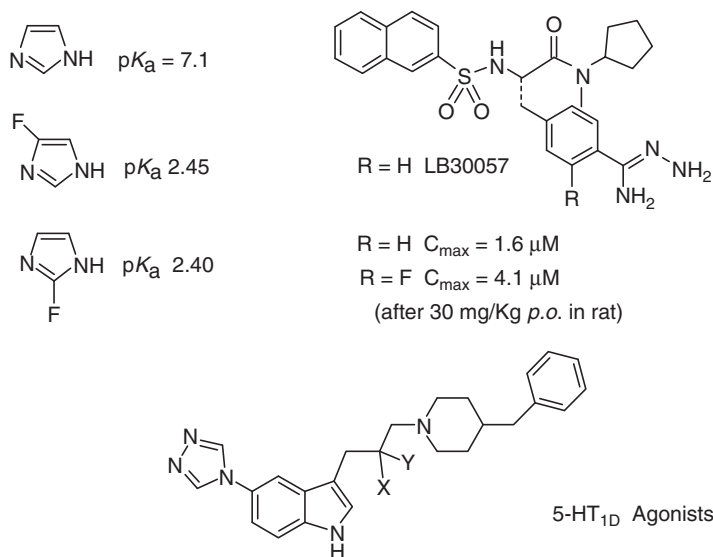
The effect of fluorine atoms on the pK_a of neighbouring ionisable functions is important for the absorption properties of a molecule. It is known that the absorption process of an ionisable drug depends on the respective proportions and lipophilicity of charged and neutral species. The introduction of fluorine atoms may allow to modulate the ionisation of the molecule at physiological pH (pH 7.4). Thus, the lowering of the pK_a of amines and nitrogen-containing heterocycles, by means of fluorinated substituents, can be a very important factor to facilitate the absorption, especially for the oral administration of drugs [43]. β -Trifluoromethyl amines are not protonated at physiological pH, and *ortho* fluorination lowers the pK_a of phenols, anilines and benzoic acids by one unit. The effect on heterocyclic bases, such as an imidazole, is even more important (Fig. 8) [44]. This diminution of the basicity is one of the explanations given to explain the better cellular absorption of anti-bacterial 6-fluoroquinolones with respect to their non-fluorinated analogues [45].

An interesting example concerns the enhancement of absorption of orally active thrombin inhibitors: taking into account that oral absorption can be increased by lowering the basicity of the functions of the P_1 substituent, a fluorine atom has been introduced in *ortho* position of the amidrazone function. This has led to an enhancement of the peak of blood maximal concentration after oral administration of the compound in a rat (Fig. 8) [46].

The lowering of the pK_a provoked by the presence of fluorine atoms renders the protonation of an amine function more difficult. The diminution of the basicity

Table 4. Measured and calculated log *P* values (Clog *P*) of leucotriene antagonists [42]

	R	X	log <i>P</i> (calculated)	log <i>P</i> (measured)	Difference
		<i>o</i> -SO ₂ Tol	6.97	5.85	1.12
		<i>o</i> -SO ₂ Tol	6.38	6.18	0.20
		OH	5.58	4.86	0.72
		OH	4.99	5.12	-0.13
		<i>o</i> -SO ₂ Tol	7.50	6.29	1.21
		<i>o</i> -SO ₂ Tol	6.91	6.45	0.46
		OH	6.11	5.42	0.69
		OH	5.52	5.53	-0.01



X	Y	log <i>P</i>	log <i>D</i> (pH 7)	<i>pK_a</i>	IC ₅₀	EC ₅₀	
H	H	4.97	2.34	9.7	0.3 nM	0.6 nM	<i>very low bioavailability</i>
F	H	4.63	3.25	8.7	0.9 nM	0.9 nM	<i>moderate bioavailability</i>
F	F	4.89	4.80	6.7	78 nM		<i>affinity decreased due to the low <i>pK_a</i></i>

Fig. 8. Influence of fluorine atoms on the pK_a and the absorption [43,45–47].

may lower the affinity for a receptor, like in the case of serotonin 5-HT_{1D} receptor agonists (Fig. 8) [47]. This change in pK_a has strong repercussions on the solubility of the amine in water depending on the pH of the medium, as highlighted by log *D* values at pH 7, while effect on log *P* is negligible (Fig. 8) [41,47].

It is sometimes observed that compounds bearing few fluorinated atoms are more soluble in water than their non-fluorinated analogues [12]. An example reported in Fig. 9 illustrates this effect [48]. Moreover, in this case, it matches with Clog *P* values. However, generalising this effect would be abusive and uncertain.

2.3. Metabolism

The introduction of fluorine atoms in a molecule can be used to modify the processes and the rates of metabolism of the drug, in order to extend the plasma half-life or to avoid the formation of toxic metabolites. Because of the properties of fluorine atom, in particular its electronic effects, it may interact differently on the bio-transformation steps, according to the type of processes involved

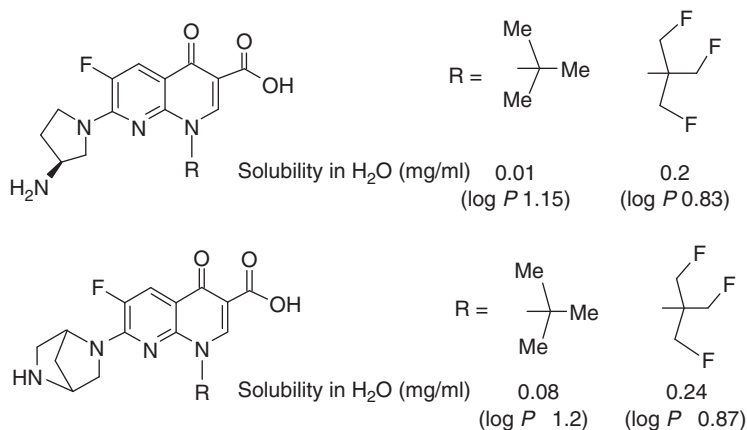


Fig. 9. Solubility of anti-bacterial fluoroquinolones (fluoronaphthyridins) [48].

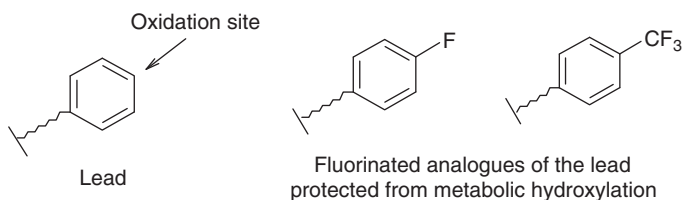


Fig. 10. Biological oxidation of an aryl ring.

(oxidative, reductive, hydrolytic, etc.), which allow the clearance of the exogenous molecule, that is, the elimination of the active principle from the organism.

2.3.1. Oxidative metabolism

The slowing down of the oxidative metabolism process is one of the most frequent reasons for introducing one or several fluorine atoms in a lead compound, in view to transform it into a drug candidate. This approach has largely stood the test of time in many therapeutic classes, and it is usually used 'to block' oxidation sites of aromatic rings. Indeed, the hydroxylation of an aromatic ring is often the first step in the detoxication of an exogenous compound in liver (Fig. 10). While other electron-withdrawing substituents may play the same role, fluorine (or CF₃ group) has the advantage to bring other beneficial effects without engendering too strong disturbances (*vide supra*).

The stability towards oxidative processes is generally attributed to the strength of the C–F bond, which is more important than that of the C–H bond. However, biological oxidations do not only involve the homolysis of a C–X or C–H bond, and then, they cannot be directly associated with the bond strength. It seems more judicious to invoke the difficult formation of the O–F bond to explain the

protection towards the hydroxylation of the *ipso* carbon [5]. Fluoroalkyl groups such as CF_2 , CF_3 , C_2F_5 , exhibit an almost complete inertia towards oxidation. Consequently, they can advantageously replace an alkyl group to avoid the oxidative metabolism. Generally, the metabolism of the molecule does not occur in the neighbouring of fluorine atoms, but goes through alternative mechanisms on other positions (Fig. 11) [49,50,51].

Kinetic parameters of metabolism of fluorinated analogues of propanolol by a cytochrome enzyme (recombinant CYP1A2) have been determined. They clearly indicate that the *N*-dealkylation was almost tenfold lower for the *N*- CH_2CF_3

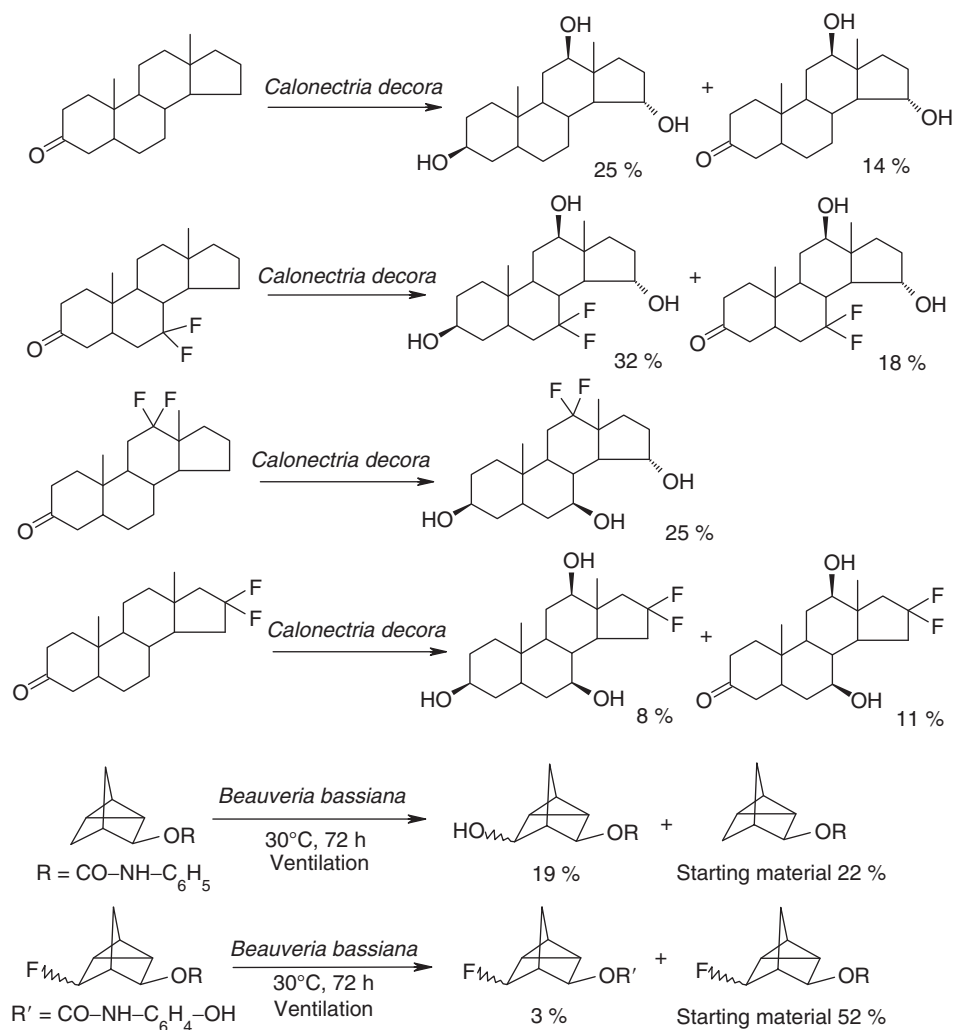


Fig. 11. Influence of the presence of fluorine atoms on microbiological hydroxylation [50,51].

compound with respect to propanolol itself. Hydroxylation of the naphthalene ring is not observed in the case of propanolol, but it becomes the major process with the fluoro analogue (Fig. 12) [52]. The same trends have also been observed with other 'low' pK_a amines on CYP2D6 cytochrome metabolism [52].

Fluoroalkyl groups also protect contiguous carbon atoms, and sometimes hydrogen atoms borne by a β carbon. Most of the oxidations of sp^3 carbons involve cytochrome P450 enzymes with generation of radical-cation intermediates. The electron-withdrawing effect of the fluoroalkyl group interferes with the electronic deficiency connected to the formation of the $C\cdots H\cdots O-Fe^{IV}$ complex [5]. Moreover, the difficult accessibility to the active site also participates to the protective effect of the fluoroalkyl groups [44].

The substitution in the position 2 by a fluorine atom protects the position 3 of Fluparoxan (an α_2 antagonist) from the metabolic hydroxylation. More, it restores a good affinity with the receptor, which was lost when fluorination was performed in the position 1 (Fig. 13) [44].

The presence of the CF_3 group in the compound reported in Fig. 14 protects the side chain from metabolic oxidation during the first hepatic by pass. In other respect, plasma concentration of this compound is strongly increased. Moreover,

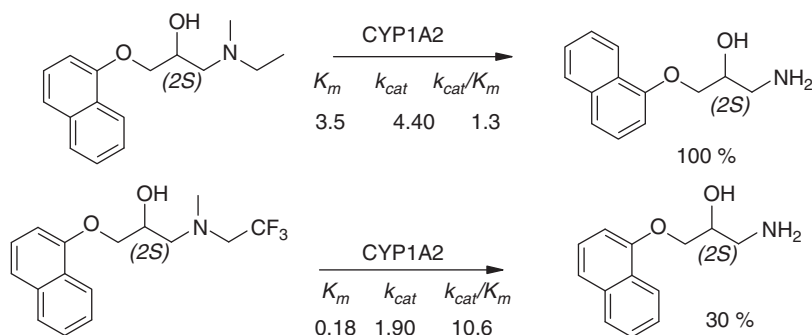


Fig. 12. Metabolism of fluorinated analogues of propanolol by recombinant CYP1A2 [52].

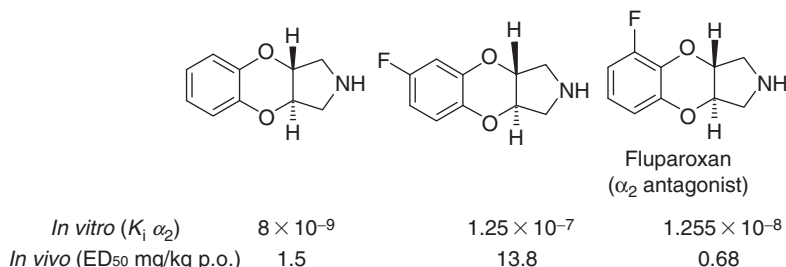


Fig. 13. *In vitro* and *in vivo* activity of the α_2 antagonist Fluparoxan [44].

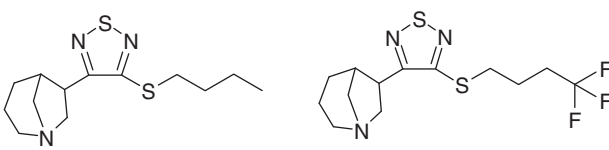
		
	(5S,6S) <i>exo</i>	(5S,6S) <i>exo</i> (LY316108)
Analgesic activity	Affinity for M receptor and analgesic activity <i>in vivo</i> (mice)	
K_i (nM)	0.45	0.40
ED ₅₀ (mg/kg)	0.19	0.10
Plasma concentration (ng/kg) (after 1 h, 30 mg/kg orally)	21	805

Fig. 14. Enhancement of plasma concentration by slowing down the oxidative metabolism of a muscarinic analgesic [53].

the pharmacological activity on the gastrointestinal tract is more selective with the CF₃-compound [53].

The oxidative metabolism leads to the formation of reactive species (epoxides, quinone-imines, etc.), which can be a source of toxicity. Consequently, slowing down or limiting these oxidations is an important second target in medicinal chemistry. Thus, the metabolism of halothane (the first modern general anaesthetic) provides hepatotoxic metabolites inducing an important rate of hepatitis: the oxidation of the non-fluorinated carbon generates trifluoroacetyl chloride. The latter can react with proteins and lead to immunotoxic adducts [54]. The replacement of bromine or chlorine atoms by additional fluorine atoms has led to new families of compounds, preferentially excreted by pulmonary way. These molecules undergo only a very weak metabolism rate (1–3%) [54,55].

Metabolism of the anti-malarial amodiaquine provides quinone-imine, which is an electrophilic metabolite responsible for hepatotoxicity and agranulocytosis. These side effects have severely restricted the clinical use of amodiaquine. The replacement of the phenolic hydroxyl by a fluorine prevents from oxidation process. Then, the *N*-dealkylation becomes the major process. This has led to further refinements, with the preparation of the *N*-*t*-butyl analogue, a compound which resists towards metabolic side-chain cleavage and has an excellent *in vitro* and *in vivo* profile (Fig. 15) [56].

2.3.2. Hydrolytic metabolism

The presence of fluorine atoms does not only protect a molecule from oxidative metabolism but can also protect from proteolysis, by disfavoring the formation of cationic intermediates involved in proteolysis processes. This is particularly important for oral administration of drugs sensitive to acidic media, because of

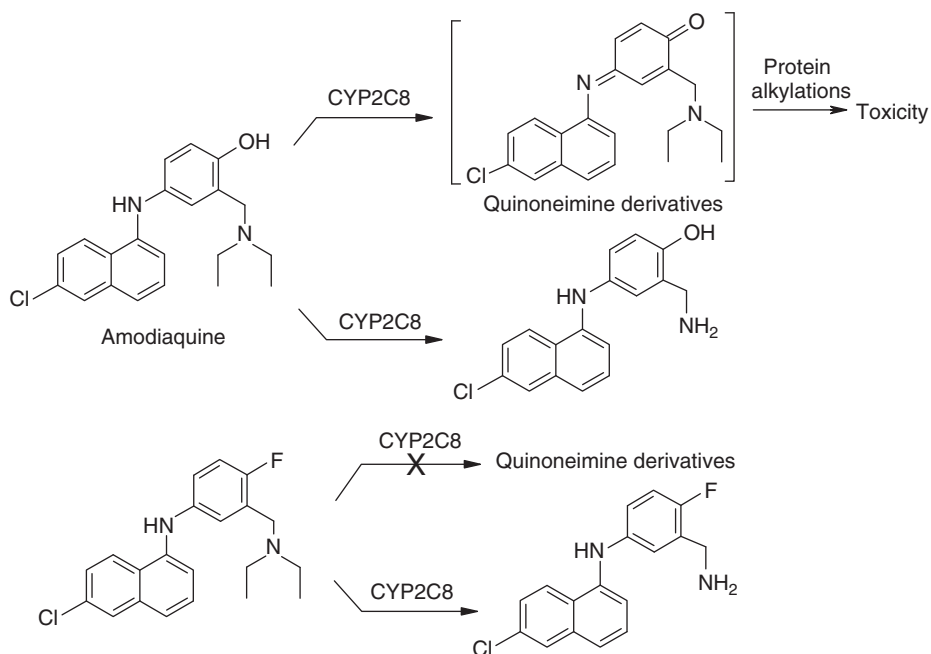


Fig. 15. Amodiaquine and fluoroamodiaquine metabolism [56].

the very acidic pH in the stomach. This approach has been often exploited for structures related to natural compounds.

As an example ddI (2,3-dideoxyinosine), an inhibitor of the HIV reverse transcriptase (RT-HIV), has an only 30-s half-life at pH 1 (at 37°C). Some formulations allow circumventing the problem of the consequent inefficient oral administration. A chemical alternative consists in the introduction of a fluorine atom in 2 β to disfavour the generation of the oxonium ion involved in the proteolysis (Fig. 16) [57,58]. Indeed, the fluorinated analogue is stable in acidic medium while keeping the *in vitro* anti-viral activity. However, it seems that other problems prevented the clinical development [5,57].

Two other examples will be developed latter (see Sections 3.7 and 3.8).

To summarise, it can be considered that the presence of fluorine atoms in a molecule globally enhances its capacity to resist to metabolism, and prevents the generation of toxic electrophilic metabolites. The reduced toxicity of a fluorinated drug with respect to its non-fluorinated analogue is a frequent consequence of the fluorine introduction, as illustrated by the representative case of the volatile general anaesthetics. This effect goes against the frequent feeling that associates fluorine and toxicity, due to the example of monofluoroacetic acid, which is a violent poison. In point of fact, fluorine atoms present in a drug are generally excreted at the ultimate phase as alkaline fluorides or trifluoroacetate salts.

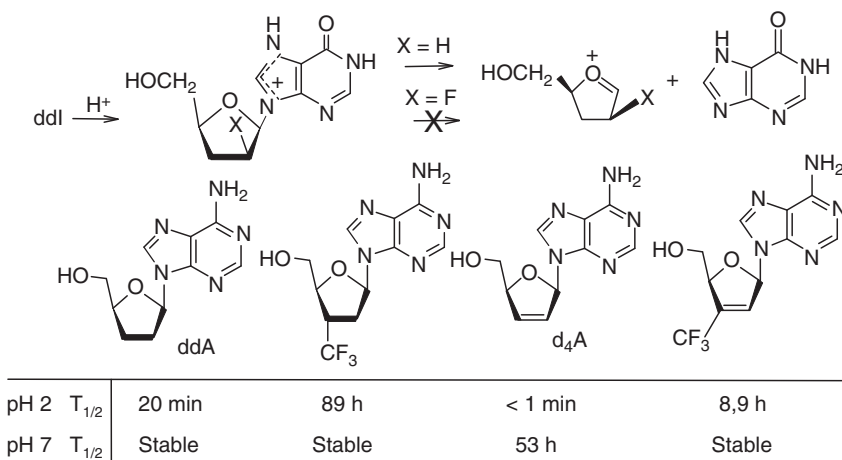


Fig. 16. Effect of fluorination on the stability of *ddl* and *ddA* derivatives towards acidic medium [5,57].

2.4. Modification of the chemical reactivity: Conception of enzyme inhibitors

Modifications of the chemical reactivity, generated by the presence of fluorine atoms in a molecule, are connected to three main factors: the strength of the C–F bond, the electron-withdrawing character of the fluorinated substituents and the possible loss of a fluoride ion or of HF via processes of β -elimination. On these bases and taking into account the ability of fluoro-substituents to sterically or electronically mimic other chemical functions, various strategies have been elaborated for designing enzyme inhibitors. The guiding principles for a design based on fluorine properties will be introduced herein.

2.4.1. Analogue of substrates as inhibitor

A fluorine atom can sterically mimic a hydrogen atom and stereoelectronically a hydroxyl group. This provides quite similar favourable interactions for the affinity in the active site of the enzyme: dipole–dipole interaction, strengthening of the hydrogen bonds (*vide supra*). Some other fluorinated groups are used or proposed to mimic other chemical functions, as illustrated in Fig. 17.

Thus, the monofluoroalkene moiety is a non-hydrolysable isostere of the peptidic bond, and hence can be used as a peptidomimetic unit in the design of protease inhibitors [59,60]. This type of rigid isosteres of the peptidic bond can facilitate the *cis/trans* conformational control of the fragment replaced. Because of the double bond, the bond length and angles of the peptidic bond are suitably mimicked, and the fluorine atom complements the analogy for electronic properties. This approach has been developed in the case of polyamide fragments, in

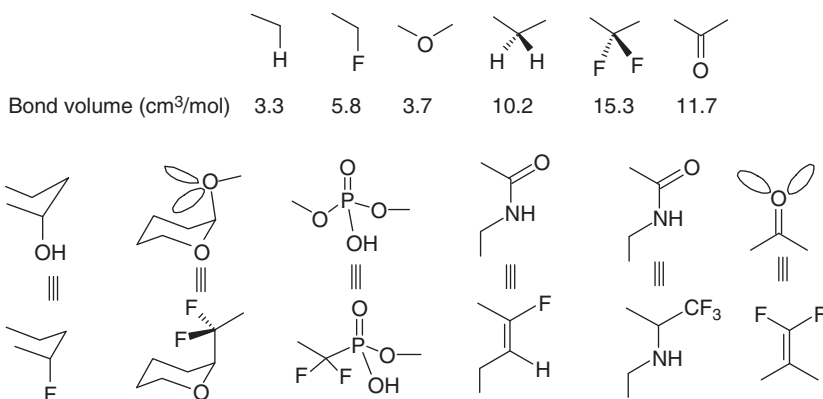


Fig. 17. Fluorinated mimics and bond volume of some functional groups.

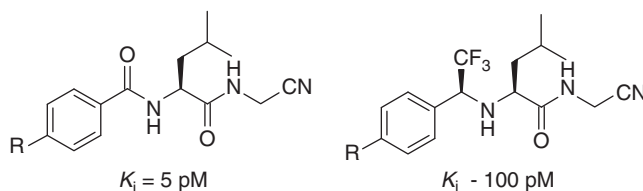


Fig. 18. Inhibitors of human cathepsin K [62a].

view to mimic the *trans*-like conformation of the peptidic bond. Monofluoroalkene moiety can also replace a peptide bond in peptide-nucleic acids (PNA). These latter are DNA mimics, able to complementarily bind oligonucleotides with a high affinity and a sequence specificity [61].

Trifluoroethylamines can also be considered as metabolically stable amide isosteres. A CF₃ group can replace the C=O of an amide and generates a metabolically stable, non-basic amine that maintains the excellent hydrogen bonding. This concept has been developed in the design of protease inhibitors (cathepsin K) (Fig. 18) [62].

Fluorophosphonates, fluoro-C-glycosides and difluorodisaccharides can be used as non-hydrolysable and stable mimics of phosphates, sulfates, disaccharides, where the anomeric oxygen atom is replaced by a CHF or a CF₂ group.

The difluorophosphonates have been the subject of a great number of studies due to their potential applications for the inhibition of numerous phosphatases and kinases [63,64]. Thanks to fluorine atoms, the electronegativity lost by the replacement of the oxygen atom by a CH₂ is recovered (Fig. 19).

Considering the acidity, the monofluorophosphonate is the closest compound to the parent phosphate (Fig. 19). The better results in inhibition obtained with monofluorophosphonates with regard to difluorophosphonates can thus be explained (Fig. 19). Conversely, concerning bond angles, a difluorophosphonate

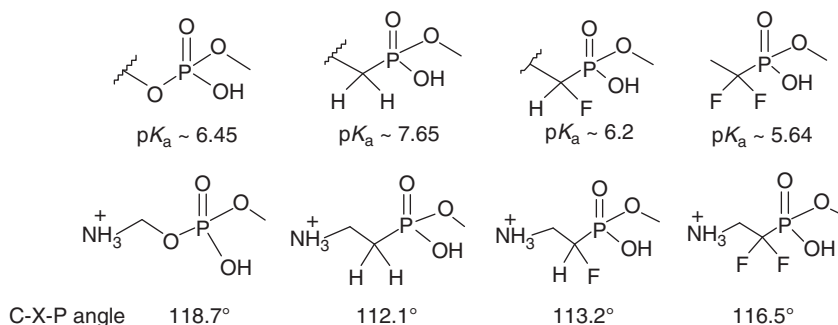


Fig. 19. Acidity of phosphates/phosphonates, and C-X-P angles [15].

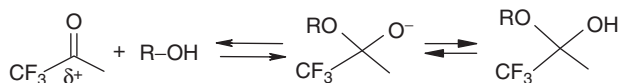


Fig. 20. Stability of tetrahedral hemiketal forms of trifluoromethylketones.

is a better mimic of phosphate than a monofluorophosphonate. However, the replacement of the oxygen by the CF₂ group has a steric impact. Indeed, fluorine atoms are localised in the space usually occupied by the lone pairs of the oxygen.

The replacement of the anomeric oxygen by a CF₂ has been considered to obtain hydrolytically stable difluoro-C-glycosides, difluoro-C-disaccharides and difluoro-C-glycopeptides. These compounds have been synthesized [65–68], but their use as inhibitors does not seem to have been biologically validated.

2.4.2. Inhibition by stabilisation or destabilisation of intermediates of biological processes

2.4.2.1. Stabilisation of the tetrahedral forms of fluoroalkyl ketones

The presence of a fluoroalkyl group in α position of a carbonyl strongly enhances its electrophilicity, and hence its reactivity, towards nucleophiles. The anionic tetrahedral intermediates are stabilised by the electron-withdrawing group Rf (Fig. 20) [69,70]. This phenomenon is illustrated by the ability of fluoroketones to afford stable hydrates in aqueous medium.

These hemiketalic adducts are very good mimics of the tetrahedral transition state involved in the enzymatic hydrolysis of an ester bond or a peptidic bond [71,72]. The nucleophilic entity of the enzyme active site (e.g. the hydroxyl of hydrolytic serine enzymes) can easily add onto the activated carbonyl of a fluoroketone leading to a very stable tetrahedral intermediate. The enzyme is not regenerated and is thus inhibited (Fig. 21) [73].

Di- and trifluoromethylketones inhibit a great number of esterases and proteases with often very high inhibition constants. Although the fluorinated ketone

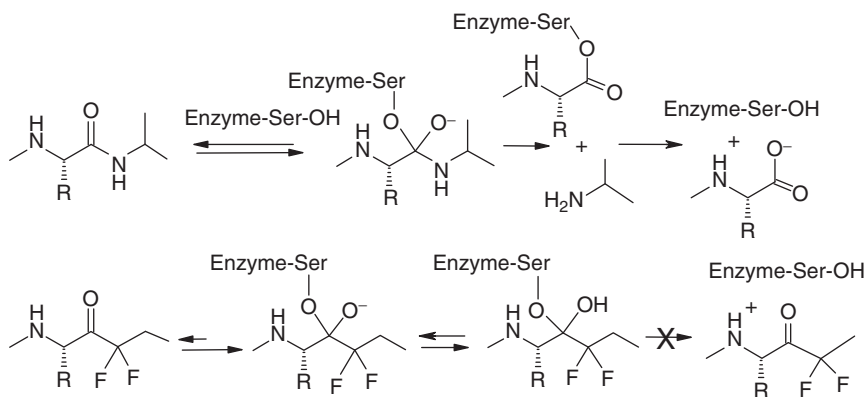


Fig. 21. Inhibition of a serine protease by an amido difluoromethylketone.

is covalently bound to the nucleophilic residue of the enzyme, the inhibition is reversible, since the inhibitor can be displaced by another nucleophile. The covalent nature of interactions as well as the tetrahedral structure of adducts have been demonstrated by kinetic studies, by NMR experiments, and by the X-ray diffraction of the enzyme–substrate complexes [72–74].

2.4.2.2. Destabilisation of cationic intermediates

The electronegative character of a fluorinated substituent can be used to disfavour the development of a positive charge in a biological process, when the latter involves a positively charged transition state. This approach has been used to perform mechanistic studies on the enzymatic farnesyl transfer involved in the synthesis of isoprenoids. The presence of fluorine atoms significantly decreases the transfer rates of the isopentenyl pyrophosphate, catalysed by the diphosphate farnesyl transferase (FPPase) or by the farnesyltransferase protein (FTPase) [75].

Some irreversible inhibitors of the glycosyl transferases have been designed on the basis of the destabilisation, by a fluorinated substituent, of the alkoxy-carbenium ion intermediate. Presence of fluorine atoms renders the formation of the incipient alkoxy-carbenium ion too difficult from an energetic point of view. As a consequence, the elimination of the leaving group from the intermediate resulting from the addition of the enzyme on the fluorinated pseudo-substrate becomes impossible [76].

2.4.3. Irreversible inhibition with based-mechanism inhibitors (suicide-substrates)

The elimination reaction ($E1_{CB}$) of a leaving group in β of an anionic centre is a well-known reaction in organic chemistry, and is commonly called β -elimination. The easy formation of α,β -ethylenic ketones starting from β -chloroketones is a good illustration. Most often, the presence of a negative charge is not necessary, a simple development of negative charge being sufficient to initiate the reaction.

Although the fluoride anion is not a good leaving group (because of the great strength of the C–F bond), ketones, imines and β -fluoroesters easily afford this β -elimination reaction (Fig. 22) [77]. The β -elimination process remains efficient for CF_2 and CF_3 compounds, while the C–F bond is stronger. Indeed, fluorine atoms render more acidic the α proton, which makes easier the formation of the anion.

These transformations are efficient under biological conditions only if another activating group is present (carbonyl, aryl, etc.) [77]. Such an activating group is important to render the elimination product (resulting from the loss of a fluoride ion) a better Michael acceptor. Moreover, if one or several fluorine atoms are present on the double bond, the latter is also more reactive (Fig. 22). Thus, the elimination, promoted by the enzyme, of a fluoride ion from a β -fluoro amino acid leads to a very reactive Michael acceptor. The latter can undergo an irreversible addition of a nucleophile residue of the active site of the enzyme, which is thus inhibited (Fig. 23) [78,79].

Due to the great strength of the C–F bond, with respect to that of other halogens, fluorine is a worse leaving group than chlorine or bromine. This fact gives a great advantage to fluorinated compounds and justifies their choice to set up this type of inhibition: fluorides are bad alkylating reagents and are stable in aqueous or nucleophilic medium. Thus, a fluorinated derivative is stable under physiological conditions and does not interact with the numerous nucleophiles

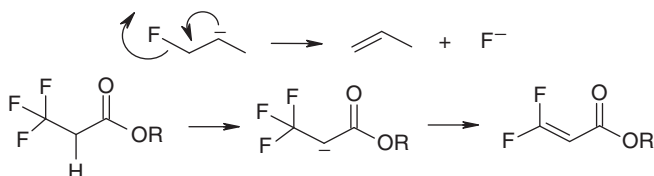


Fig. 22. Fluorine in β -elimination reactions.

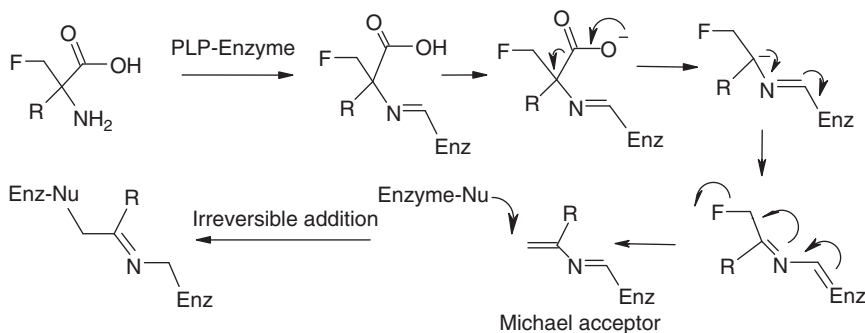


Fig. 23. Principle of the inhibition of an enzyme based on the elimination of a fluoride ion, and formation of a Michael acceptor.

of the medium. Consequently, a fluorocompound does not alkylate nucleophilic sites of the enzyme in a non-specific manner, conversely to chlorinated analogues which are generally non-specific affinity labeller.

3. FLUORINATED PHARMACEUTICALS BASED ON NATURAL PRODUCTS

The development, during the last 15 years, of new synthetic methodologies in fluorine organic chemistry joint to the increasing understanding of fluorine impact on the biological properties of a molecule has facilitated the design and the synthesis of more and more structurally diverse and sophisticated drug candidates. As part of these advances, many fluorinated analogues of natural compounds have been synthesized and investigated. We will not consider here these numerous and often promising synthetic efforts, since we focus this chapter on fluorinated analogues of natural products which have found therapeutic applications. Such fluorinated drugs or drug candidates are present in many therapeutic classes. Some of them are very important drugs known for more than 50 years, such as fluorocorticoids and fluorouracil derivatives, which are still intensively clinically used. Others are much more recent, or are currently in clinical development.

When possible, we have attempted to indicate why fluorination has been performed, according to the general statements described in the first part of this chapter. In some cases, we have included challenging aspects of syntheses. Concerning the marketed or advanced developed drugs, more references can be found in *Chemical Abstracts*, under INN names (International Non-proprietary Names).

3.1. Nucleosides and carbohydrates

The only fluorinated sugar clinically used is the ^{18}F -labelled 2-fluoroglucose, which is a probe in positron emission tomography (PET) medical imagery. Fluorinated analogues of nucleosides are drugs which interact with DNA and RNA. They are essentially developed for the treatment of cancer and viral infection. Fluorine atoms can be present either on the base moiety or on the sugar. Interest in fluorination of nucleosides is widespread. The fluorine atom can mimic a hydrogen or a hydroxyl function, and thus is able to convert a substrate into an inhibitor of a critical enzyme (e.g. 5-fluorouracil). It can protect the nucleoside bond from hydrolytic cleavage (2'-fluoro-nucleoside) and thus improve the stability of the drug (e.g. *clofarabine*). It can also be directly involved in the enzymatic reaction (mechanism-based inhibitor) (e.g. *trifluridine*). Thymidylate synthase (TS), ribonucleotide diphosphate reductase (RDPR), DNA polymerases and viral reverse transcriptases are the main enzymes targeted by fluoronucleosides and fluoronucleobases.

3.1.1. Inhibitors of the thymidylate synthase

The TS mediates the conversion of 2-deoxyuridine monophosphate (dUMP) into deoxythymidine monophosphate (dTMP). This enzymatic methylation reaction is a key step in the synthesis of DNA and involves a ternary complex between the substrate, the enzyme and the co-factor [methylene tetrahydrofolic acid (CH_2FAH_4)] (Fig. 24) [8,80,81]. This transformation represents the sole *de novo* source of dTMP, a building block for DNA synthesis and repair [82].

Anti-cancer properties of 5-fluorouracil (5-FU) were discovered in the 1950s [83]. It was found latter that 5-FU and its derivatives are potent inhibitors of thymidylate synthase [8,84]. The catalytic cycle involves the dissociation of the ternary complex and the elimination of FAH_4 . It is initiated by pulling out the proton H-5, thus generating an exocyclic methylene compound [80]. The active form of the fluoro substrate is generated after its *in vivo* glycosylation and its phosphorylation. It is recognised by the TS and undergoes addition of methylene tetrahydrofolic acid. As the release of an F^+ ion is energetically forbidden [8,85], the fluorine atom which replaces the proton H-5 cannot be pulled out by the base. This leads to the inhibition of the enzyme (Fig. 25).

Although the anti-tumour activity of 5-FU is mainly because of the inhibition of the thymidylate synthase, it is actually multifactor. The incorporation of 5-FU, under F-desoxyuridine form, into various types of RNA generates cytotoxicity. This occurs through the inhibition of the methylation and of the maturation of the ribosomal RNA [86]. The 5-FU is also precursor, by metabolism, of a monofluoroalanine, which is itself toxic.

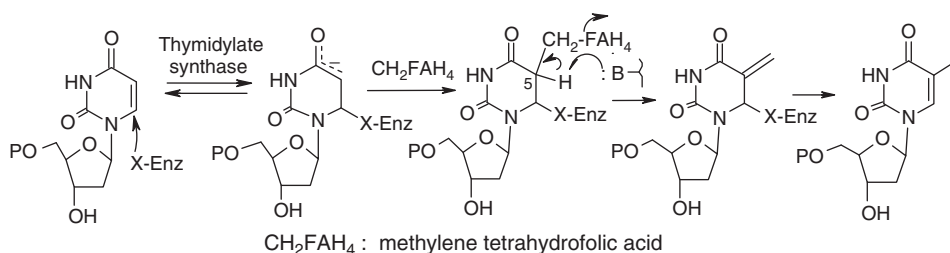


Fig. 24. Mechanism of methylation of deoxyuridine by the thymidylate synthase.

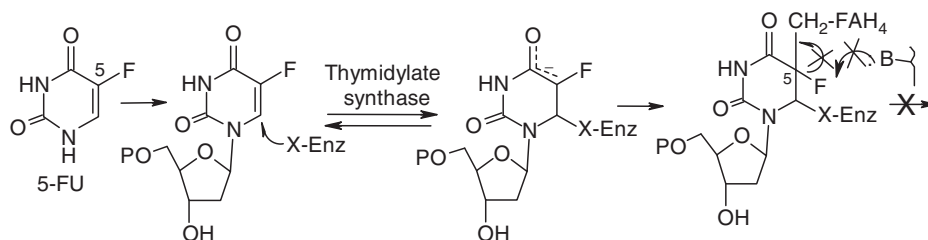


Fig. 25. Inhibition of the thymidylate synthase by the 5-FU [8,80].

5-FU has been extensively used in the treatment of skin cancers and a variety of solid tumours, such as breast, colorectal and gastric cancers, usually via intravenous (i.v.) administration. Although this route is generally the most efficient and the least toxic, it is costly and inconvenient [87]. Furthermore, treatment of cancer with 5-FU has been found to cause neurotoxic and cardiotoxic side effects. Toxicity also derives from the lack of selectivity of the drug towards tumours, and resistance can occur if the cell produces excess of dUMP, for competing with the drug in the active site [88].

It is why many efforts have been done to improve the pharmacological profile of 5-FU with the development of oral 5-FU pro-drugs: *doxifluridine*, *tegafur*, *carmofur* (*ftorafur*), *furtulon*, *capecitabine*, *galocitabine*, *emitefur* (Fig. 26). They are being used clinically either alone or in combination therapy with other anti-cancer agents [89,90].

New formulations are regularly commercialised. Studies on the action mechanism of 5-FU had a large influence on the development of other anti-tumour drugs derived from pyrimidine and purine. The 5-FU is industrially prepared at important tonnage by fluorination of uracil with elemental fluorine.

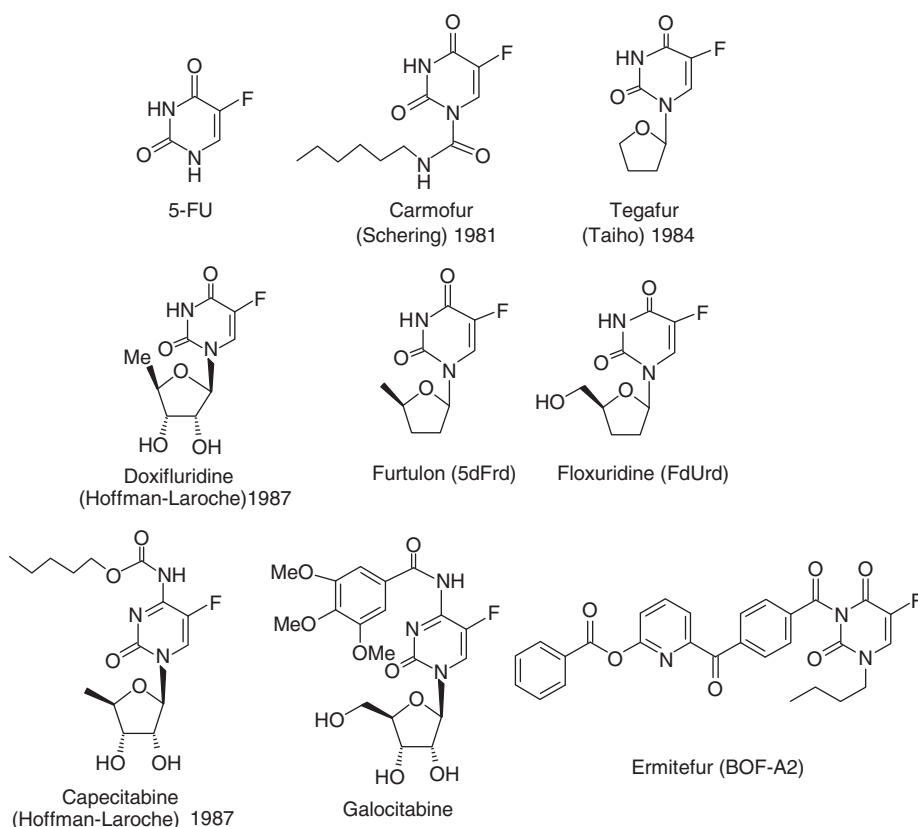


Fig. 26. 5-FU pro-drugs used in cancer therapy.

5-Trifluoromethyl-2'-deoxyuridine, *trifluridine* (Viroptic®), is an anti-viral drug acting on TS via another mechanism. It is a mechanism-based inactivator of thymidylate synthase (Figs. 27 and 28). *Trifluridine* is marketed for the topical treatment of *Herpes simplex virus* infection in eyes.

Trifluridine is synthesized by radical trifluoromethylation of uracil, followed by coupling with the protected deoxyribose (enzymatic or chemical) or by trifluoromethylation of the protected idonucleoside (Fig. 28) [91].

3.1.2. Inhibitors of RDPR and DNA polymerase

Another important target for cancer therapy is the inhibition of the RDPR. This homodimeric enzyme catalyses a crucial step of the DNA biosynthesis, the

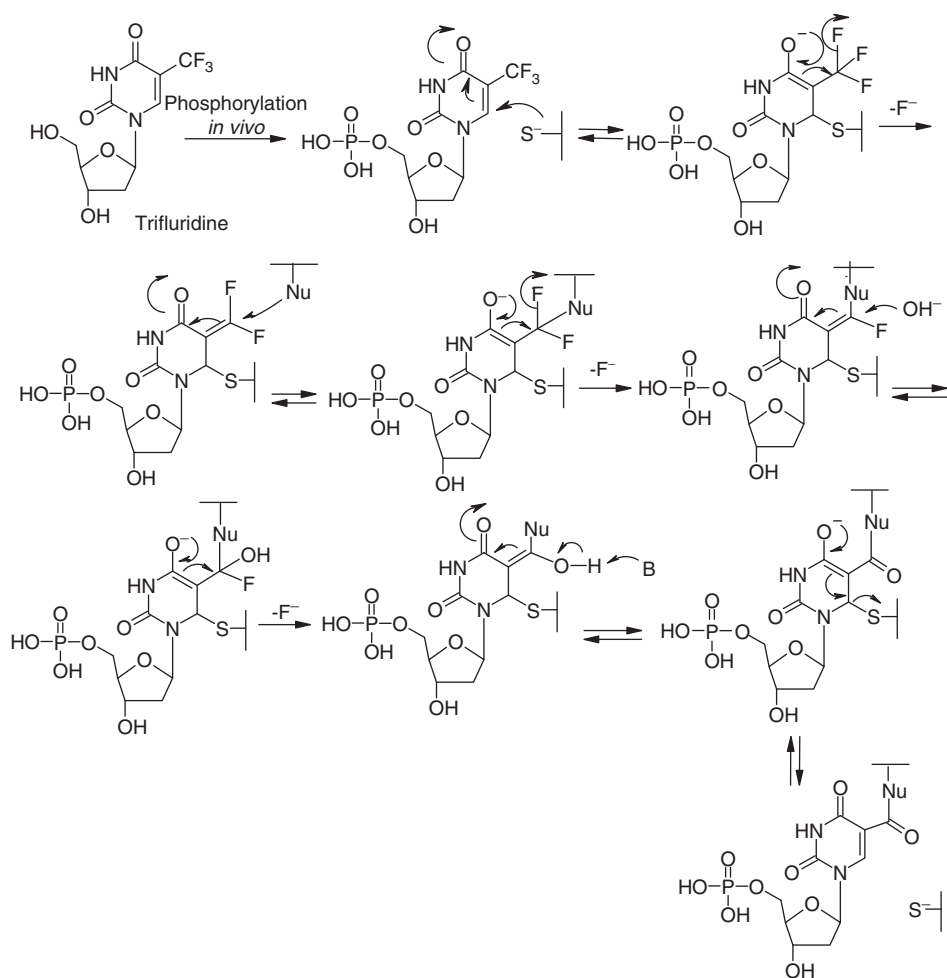


Fig. 27. Inactivation of thymidylate synthase by *trifluridine*.

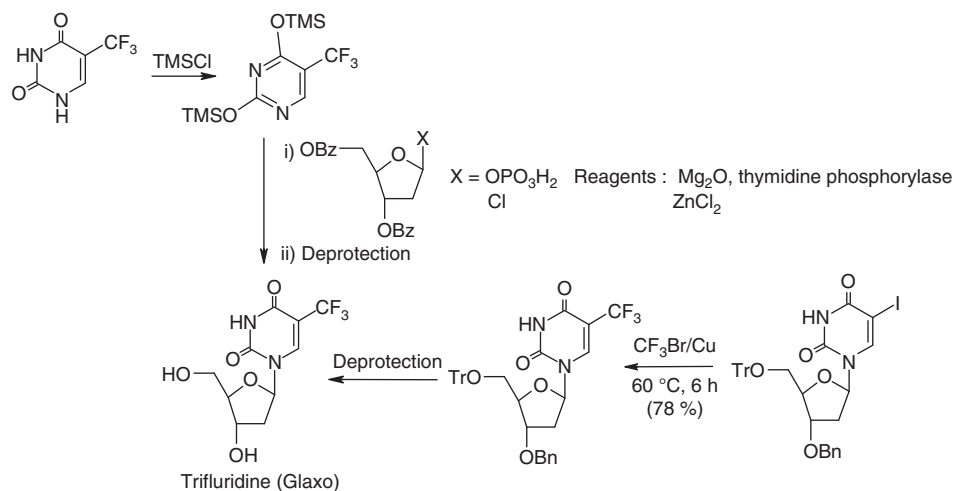


Fig. 28. Syntheses of *trifluridine*.

conversion of nucleotides into deoxynucleotides (Fig. 29). The mechanism of reduction of the nucleotide catalysed by the RDPR is complex. The subunit R1 contains the active site for binding and reduction of the substrate, while the subunit R2 contains the essential tyrosyl radical co-factor. The reduction process involves the abstraction of the hydrogen 3' by a radical generated from the cysteine 439 of R1, generated itself by the tyrosyl radical of the subunit R2. The hydroxyl in 2' is then eliminated as a water molecule and the α -keto radical is successively reduced by cysteines 225 and 462. The further transfer of hydrogen Ha to the new radical provides the deoxynucleotide, and regenerates the sulfur radical (Fig. 29) [92].

In the 1990s, important studies on 2,2-difluoro-2-deoxyribose and corresponding nucleosides have resulted in the discovery of *gemcitabine* (Gemzar®). This 2',2'-difluorodeoxycytidine, an inhibitor of RDPR and of DNA polymerase, was launched in 1996 and is currently used for the treatment of several cancers (non-small cell lung and pancreatic cancer). Its market was more than 2.5 tons in 2001. After metabolic phosphorylation, *gemcitabine* inhibits RDPR, but also interacts with other enzymes involved in the DNA biosynthesis. This explains its great efficiency [93]. More recently novel *O*-alkylglycerophospholipid derivatives of *gemcitabine* have been developed [94].

Gemcitabine (Gemzar®) is prepared from the 2,2-difluoro-2-deoxyribose, itself available by the addition of the Reformatsky reagent of ethyl bromodifluoroacetate on the (*R*)-2,3-*O*-isopropylidene glyceraldehyde. The condensation of the corresponding mesylate with di(trimethylsilyloxy)pyrimidine provides *gemcitabine* [93]. The control of the stereoselectivity of the Reformatsky reaction is difficult (Fig. 30) [95]. Other approaches involving the fluorination of D-pyranoses have been proposed (Fig. 31) [96].

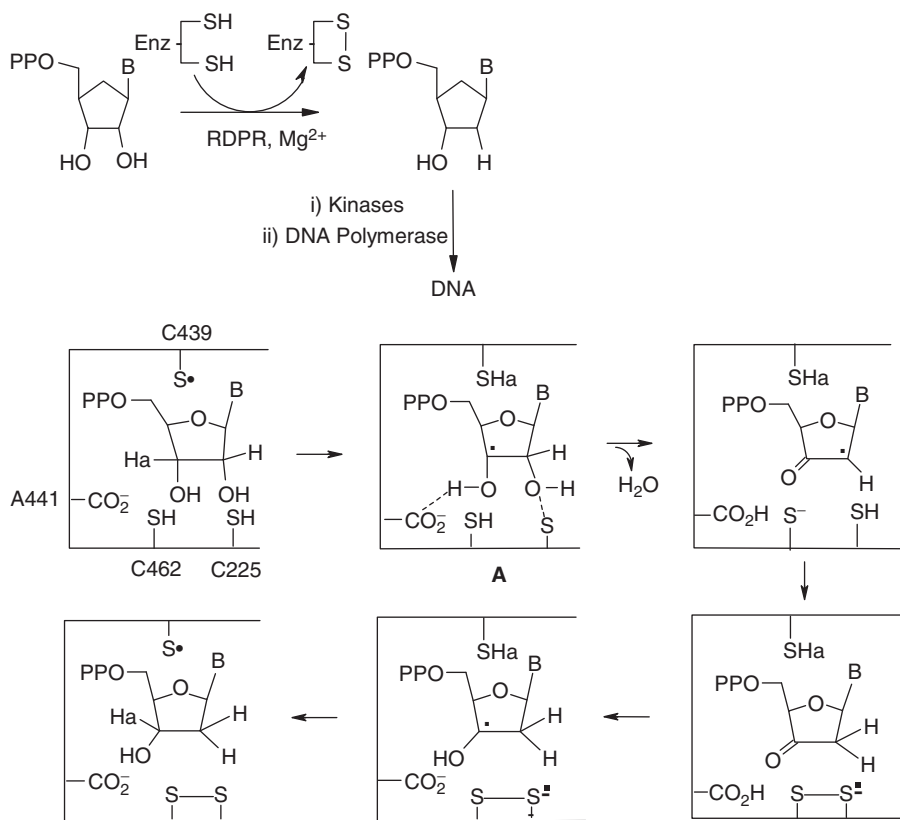


Fig. 29. Mechanism of reduction of nucleotide into deoxynucleotide by RDPR [92].

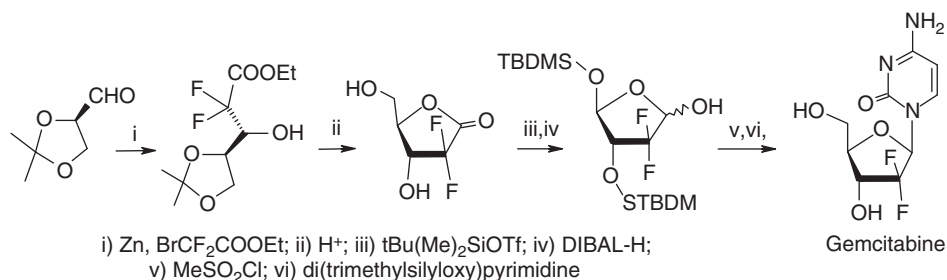


Fig. 30. Preparation of *gemcitabine* (2'-deoxy-2',2'-difluorocytidine) [95].

More recently fluoromethylene deoxycytidines have been rationally designed by McCarthy *et al.* as bio-precursors of mechanism-based inhibitors of RDPR, after phosphorylation *in vivo* by the deoxycytidine kinase. Among these, *tezacitabine* (MDL 101731) [92] has a high anti-proliferative activity and is currently in clinical phase III evaluation for the treatment of solid tumours [92].

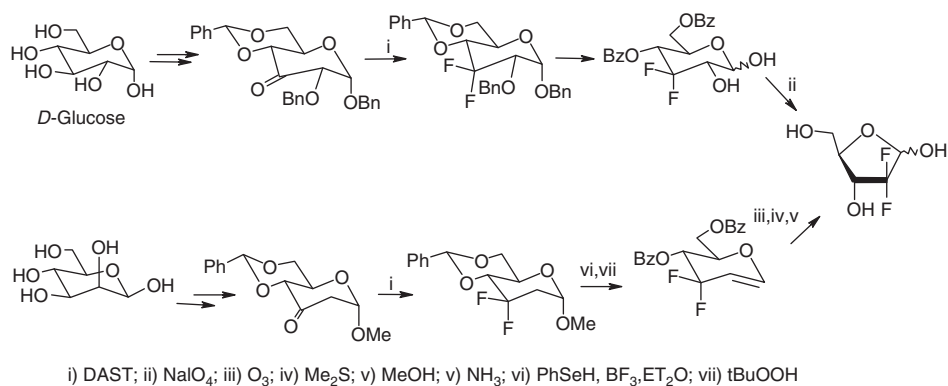


Fig. 31. Synthesis of 2-deoxy-2,2-difluoro-D-ribose from D-pyranoses [96].

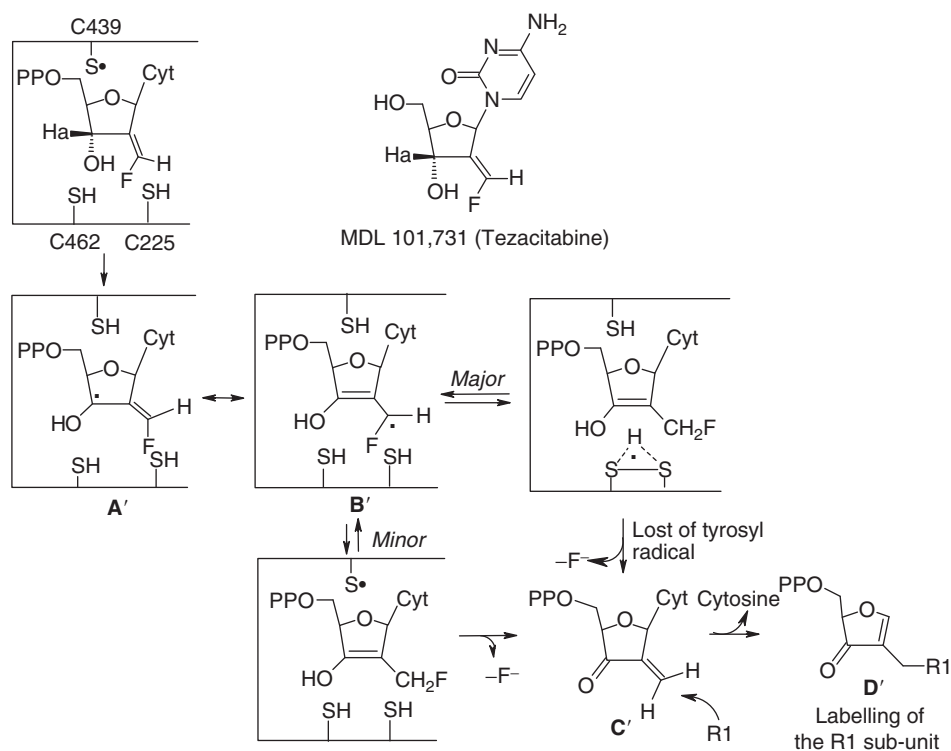


Fig. 32. Proposed mechanism for the inactivation of RDPR by MDL 101731 [92].

In contrast to the radical **A** generated from the cytidine phosphate (Fig. 29), the radical **A'** formed from the 2'-fluoromethylene-2-deoxycytidine cannot eliminate a water molecule (Fig. 32). Instead, it undergoes an isomerisation into a new radical **B'** centred on the fluorine-substituted carbon. The latter finally provides, after

several steps, a high electrophilic entity **D'** able to add the subunit R1 of the enzyme. The resulting covalent adduct of **D'** with the enzyme has been identified (Fig. 32) [92].

Tezacitabine is synthesized from the cytidine protected at 4'-OH, 5'-OH and 4-NH₂. Swern oxidation provides a ketone, which is converted to a *gem*-fluoro-sulfonyl olefin with the anion of sulfonylfluorophosphonate. Reduction of the sulfonyl group is achieved with Bu₃SnH (Fig. 33) [92].

Fludarabine (Fludara®) is a 2-fluorocytarabine (Fig. 34) which inhibits the DNA biosynthesis via the inhibition of DNA polymerase α and of RDPR. It is clinically used for the treatment of leukaemia (chronic lymphomytic leukaemia, CLL).

The structurally similar *clofarabine* is also marketed for the treatment of leukaemia [97]. The fluorine substitution at 2' increases the hydrolytic stability of the drug. Because of its electronegative character, fluorine disfavours the development of positive charge on the anomer carbon, required for the hydrolytic cleavage of nucleosides (see Section 2.3.2.) (Fig. 34) [2, p. 92].

The 5-fluorocytosine (*flucytosine*) is an inhibitor of sterol C-14 demethylase, an enzyme involved in the biosynthesis of ergosterol, an element of fungal wall. It is marketed as an anti-fungal agent, whereas nucleoside derivatives of the

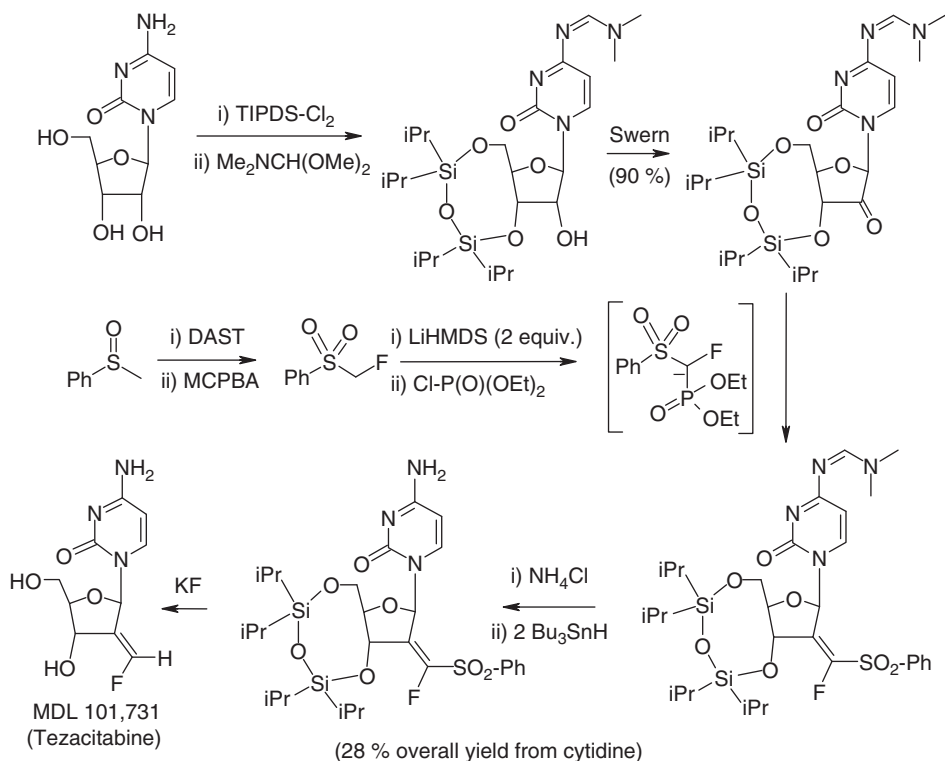


Fig. 33. Synthesis of *tezacitabine* [92].

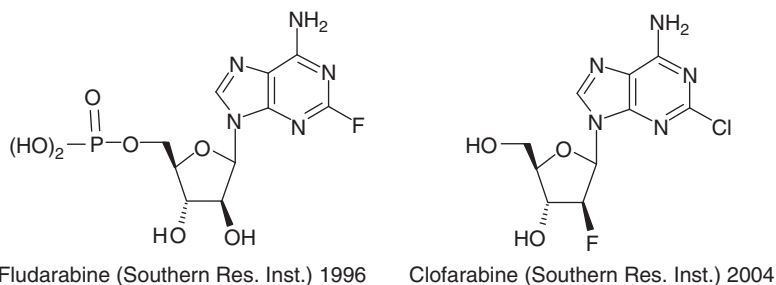


Fig. 34. *Fludarabine and clofarabine.*

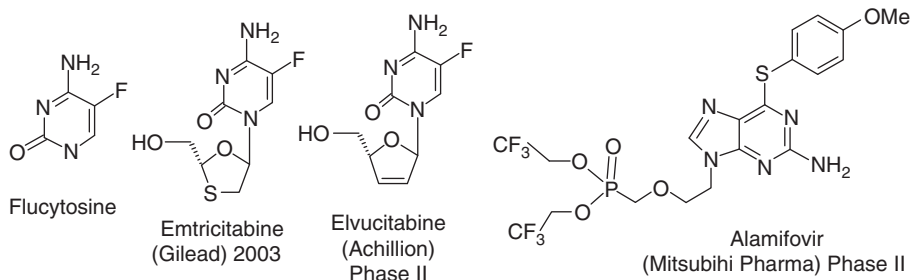


Fig. 35. Anti-viral fluoronucleosides.

5-fluorocytosine (*emtricitabine* and *elvucitabine*) are used for the treatment of viral infection.

Emtricitabine is a nucleoside reverse transcriptase inhibitor, launched for the treatment of HIV infection. It is also currently in phase III for the treatment of hepatitis B virus (HBV) infection (Fig. 35) [98].

Elvucitabine is in phase III development for therapies of HIV and HBV infections. Its anti-viral activity has been shown to result from inhibition of the HIV reverse transcriptase and HBV DNA polymerase (Fig. 35) [99].

Alamifovir is a purine nucleotide in early clinical development for a potential therapy of HBV infection. It is a dinitrfluoroethoxy phosphonate.

3.2. Alkaloids

3.2.1. *Vinca alkaloids*

Vinca dimer indole alkaloids (e.g. *vinblastine*) act as spindle poisons. They bind tubulin, inhibiting polymerisation into microtubules, the major elements of the cytoskeleton [100]. *Vinblastine* itself and its analogue *vinorelbine* (Navelbine®) [101] are marketed for cancer therapies (Fig. 36). *Vinflunine* (Javlor®) is a member of second-generation *Vinca* dimer alkaloids. This 4'-difluoro analogue is more active than *vinorelbine* in several cancers (Fig. 36). It is now in phase III clinical

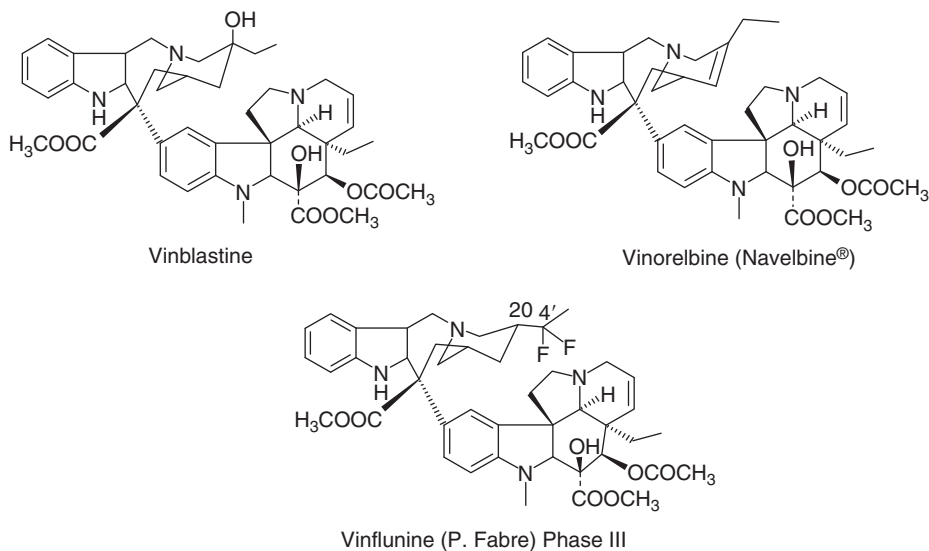


Fig. 36. Anti-mitotic drugs derived from *Vinca* dimer alkaloids.

trials as a chemotherapeutic agent targeted at a variety of cancers (non-small cell lung and bladder cancer) [102]. However, the role of fluorine substitution on the activity is still unknown. Neither an effect on affinity for tubulin nor an effect on metabolism is responsible for the increased anti-tumour efficiency and decreased toxicity [100,102].

Because of the obvious difficulty of synthesis of such highly complex structures, the preparation of fluoro analogues of *Vinca* dimer indole alkaloids had not been envisaged until the remarkable work of Jacquesy's group on super acid media [103,104]. It has been demonstrated that when dissolved in super acid media, complex molecules such as steroids or alkaloids, undergo polyprotonation of reasonably distant functions. This prevents degradation, generally observed under usual strong acidic conditions. Moreover, the lack of basic or nucleophilic entities in the medium avoids further processes responsible for degradation [103]. This approach allowed the fluorination of *vinorelbine* providing the highly potent *vinflunine*.

Fluorination of *vinorelbine* was thus performed in super acid medium (HF-SbF₅). A super electrophilic agent, such as a chloromethyl or a Br⁺ cation is generated *in situ* from a chloromethane (CHCl₃, CCl₄) or from N-Bromo Succinimide (NBS). It is able to abstract a hydrogen from the protonated alkaloid, leading to a cation that can be trapped by an halide anion present in the medium [105,106]. Difluorination remarkably occurs selectively at C-4' of the clavamine fragment (Fig. 37) [105].

The first step of the reaction is a polyprotonation that includes protonation of the double bond. The resulting carbocation at C-20 isomerises into one centered at C-4' more distant from the protonated nitrogen. This C-4' cation is then

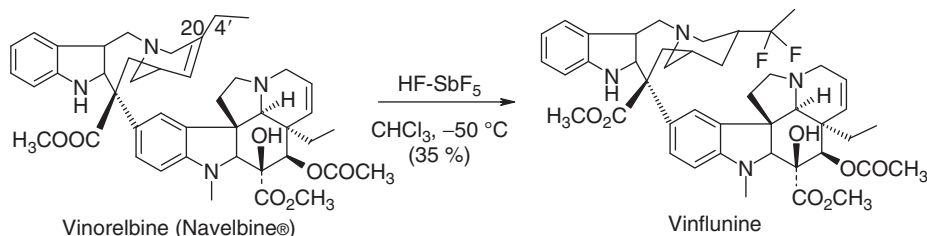


Fig. 37. Preparation of *vinflunine* [106].

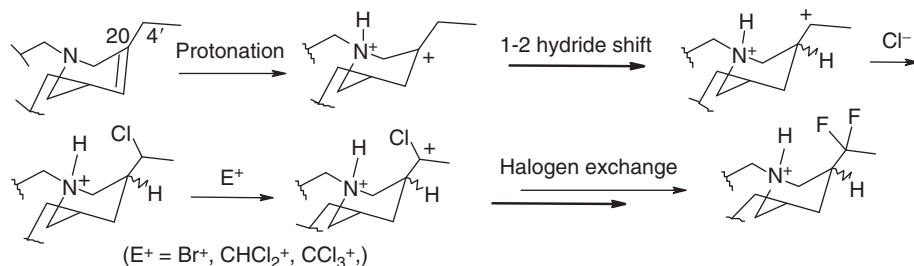


Fig. 38. Mechanism of fluorination of *vinorelbine* [105,106].

trapped by a chloride anion. The 4'-hydrogen geminal to the chlorine atom is abstracted by an oxidative chloromethyl cation, generated in the medium from the added CHCl₃. This provides a new cation at C-4' which again traps a chloride anion, leading to a 4',4'-dichloro compound. Further halogen exchanges, induced by HF, provide the 4',4'-difluoro compound. Although the yield is moderate, it is a remarkable reaction with respect to the complexity of both reaction and substrate (Fig. 38) [105]. Despite the use of very corrosive reagents, the reaction is now performed on an industrial scale [106b].

3.2.2. *Camptothecin*

Camptothecin, an alkaloid isolated from the Chinese tree *Camptotheca acuminata*, is a potent cytotoxic agent, acting by the inhibition of DNA topoisomerase I [107]. Numerous derivatives of camptothecin have been synthesized in order to improve its pharmacological profile for effective anti-tumour drugs. Amongst them, some fluorinated derivatives have been studied and this research has led to two drug candidates. *Exatecan*, fluorinated on the A aromatic ring, is under phase III development, despite the lack of confirmation of initial hopes during the phase II trials [108]. *Diflomotecan*, an E-homocamptothecin difluorinated on the A aromatic ring, is currently in phase II (Fig. 39) [109].

Fluorine has also been introduced on the E-ring. For instance, both epimers of 20-fluoro camptothecin, where the fluorine atom replaces the 20-hydroxyl, have been prepared by total synthesis via stereoselective fluorination with

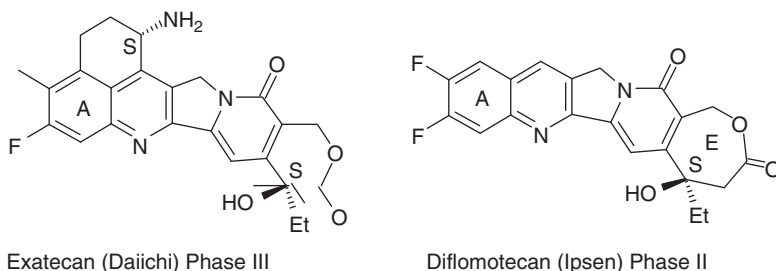


Fig. 39. Fluorinated analogues of camptothecin.

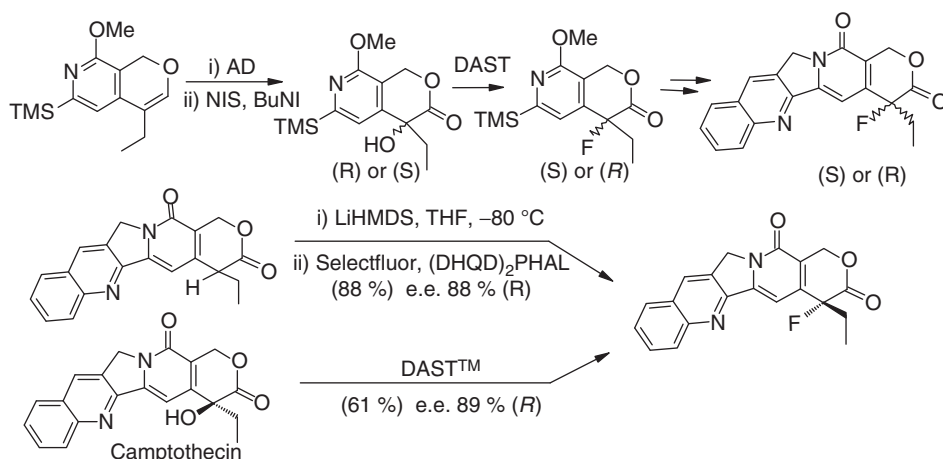


Fig. 40. Preparation of 20-fluorocamptothecins [110,111].

diethylaminosulphur trifluoride (DAST) of the (*R*) and (*S*) α -hydroxylactone precursors (Fig. 40) [110]. An asymmetric fluorination of the 20-deoxycamptothecin lithium enolate, using SelectfluorTM in the presence of $(\text{DHQD})_2\text{PHAL}$, or alternatively, fluorination of camptothecin with DAST, provided the (*R*)-enantiomer (Fig. 40) [111]. Unfortunately, these 20-F-camptothecins are less active or are inactive in topoisomerase I/DNA assays. They are also less hydrolytically stable [110,111].

3.3. Lignans

3.3.1. Podophyllotoxin

Podophyllotoxin is an aryltetralin lignan which has been isolated from several plants of the *Podophyllum* species. It is a potent cytotoxic agent against various cancer cell lines, stopping the cell cycle in metaphase through the inhibition of microtubules assembly by binding the colchicine site of the tubulin [112]. Because of numerous side effects, podophyllotoxin cannot be used as a drug.

Extensive structure modulations were performed to obtain more potent and less toxic anti-cancer agents, such as *etoposide* used in the therapy of numerous cancers (Fig. 41) [113]. In contrast to podophyllotoxin, *etoposide* derivatives act as DNA topoisomerase II inhibitors. *Tafluposide* (F 11782) is an *etoposide* where both hydroxyl functions of the glycoside moiety are acylated with the pentafluorophenoxyacetic acid (Fig. 41). It has been demonstrated that *tafluposide* does not act as a pro-drug of *etoposide*, but through a specific mechanism of interaction with both topoisomerases I and II α [114].

3.4. Anthracyclines

Anthracyclines are anti-tumour quinone-containing antibiotics produced by different strains of *Streptomyces*. Some of them, such as adriamycine (doxorubicine), daunorubicine, are broad-spectrum anti-tumour compounds. They act by binding to DNA, and interfere with DNA replication and gene transcription. Their limitations for clinical use are cardiac toxicity and drug resistance phenomena [115,116]. Consequently, intense structure–activity relationship studies have been carried out in attempts to improve the pharmacological profile. In particular, a number of fluorinated anthracyclines have been prepared with introduction of fluorine atoms onto A or D cycles [117,118] or onto the aglycone side chain linked at C-14 [117]. Fluorination of the aminoglucoside fragment has also been performed in view to increase its hydrolytic stability (Fig. 42). Although some compounds reached a pre-clinical step of development, only the *valrubicine* (trifluoroacetyladiamycine valerate) (Valstar[®]), which is an ester of adriamycine

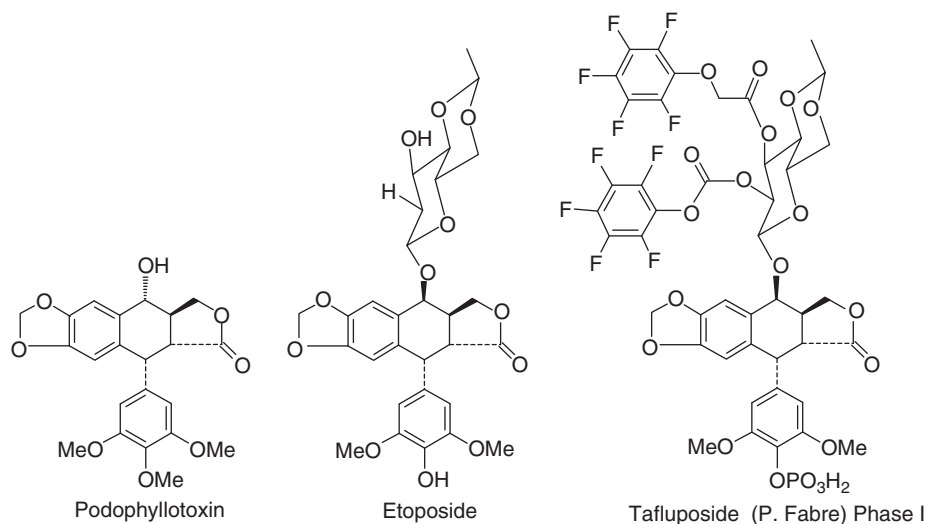


Fig. 41. Podophyllotoxin and its anti-tumour derivatives.

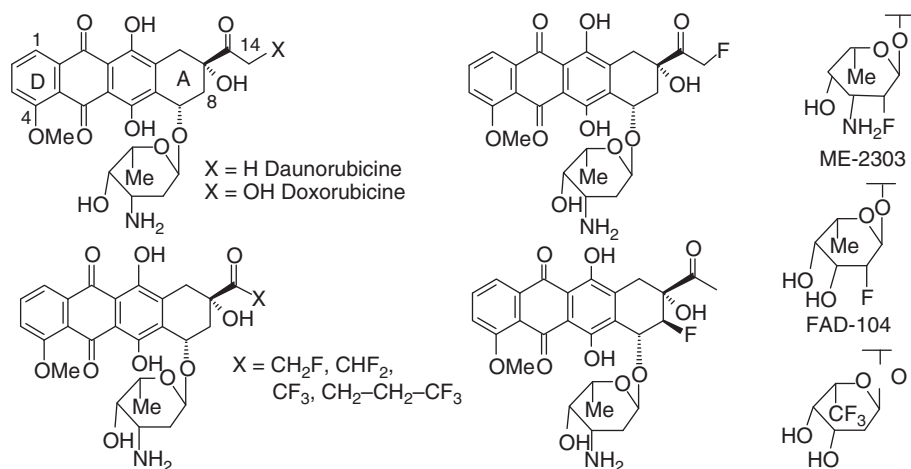


Fig. 42. Examples of fluoroanthracyclines [117,118].

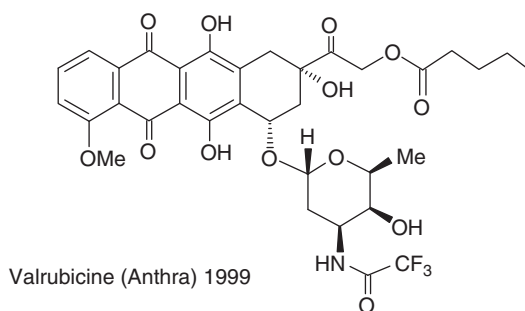


Fig. 43. Valrubicine.

trifluoroacetylated on the aminoglycoside fragment, was fully developed (Fig. 43). It is marketed for the treatment of resistant bladder cancer.

3.5. Macrolides

3.5.1. Erythromycin

Erythromycins are macrolide antibiotics produced by bacterial fermentation. Fluorination of erythromycin has been studied as a strategy to insure better stability in acidic medium and/or to achieve better bioavailability. An erythromycin, fluorinated at C-8, *flurithromycin*, was launched several years ago. Its preparation involves an electrophilic fluorination, with CF_3OF [119] or with an N-F reagent *N*-fluorobenzenesulfonimide (NFSI) [120], of the 8,9-anhydroerythromycin-6,9-hemiacetal or of the erythronolide A (Fig. 44).

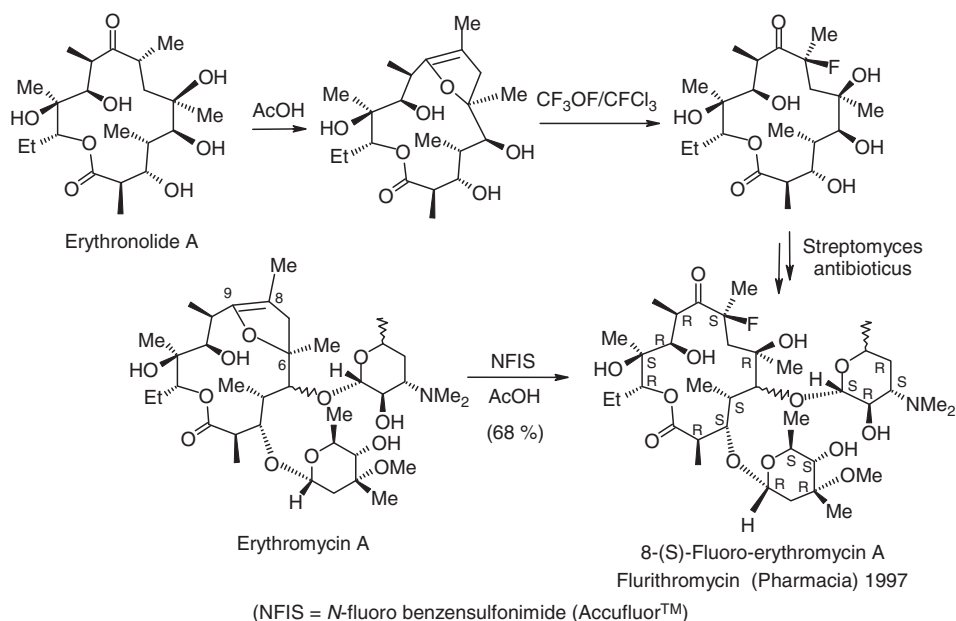


Fig. 44. Synthesis of flurithromycin.

Several 2-fluoroerythromycin derivatives have also been prepared by means of electrophilic fluorination with Selectfluor™ of the enolate of the β -ketoester fragment (Fig. 45) [121]. Fluorination is stereoselective and leads to the α -fluorine compound [122]. Two derivatives of 2-fluoroerythromycin are in clinical development (*HMR-3562* and *HMR-3787*). These compounds are promising agents for the treatment of respiratory pathogens resistant to erythromycin A (Fig. 45) [123].

Recently, a novel fluorinated erythromycin (16-fluoroerythromycin A) has been produced by *Saccharopolyspora erythraea*, using an ω -fluorobutyrate as precursor for the biosynthesis (Fig. 46) [124].

3.5.2. Epothilones

Epothilones are naturally occurring cytotoxic macrolides, which were initially isolated from a mycobacterium. Their anti-tumour activity is similar to that of the clinically established taxoids (taxol, taxotere) by interrupting the dynamic mechanism of microtubule assembly/disassembly. In contrast to taxoids, epothilones are remarkably efficient against multi-drug resistant cells [125]. The precursor of EpoB, the dEpoB, in which the 12,13-oxido linkage is lacking, also exhibits tubulin stabilisation properties, with a better therapeutic index than EpoB. dEpoB is currently in phase II clinical trials. Bioassays were performed on

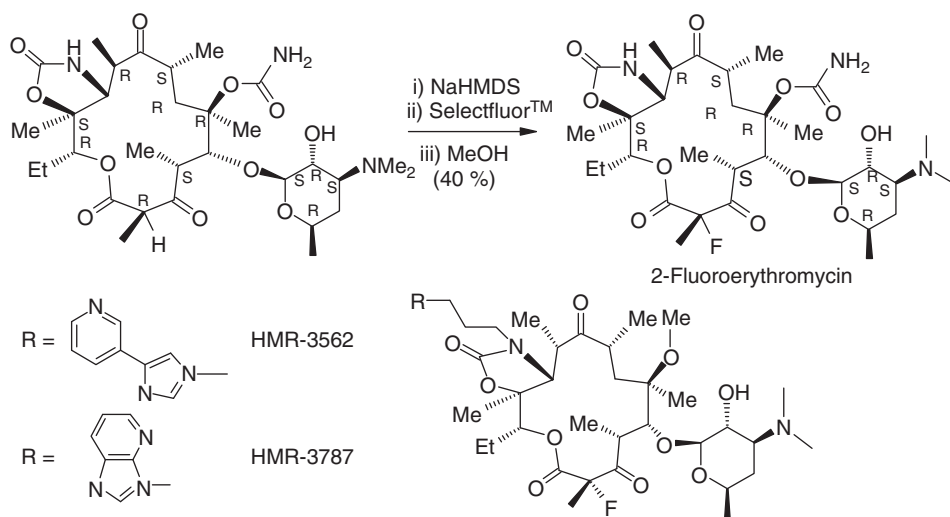


Fig. 45. Synthesis of 2-fluoroerythromycin.

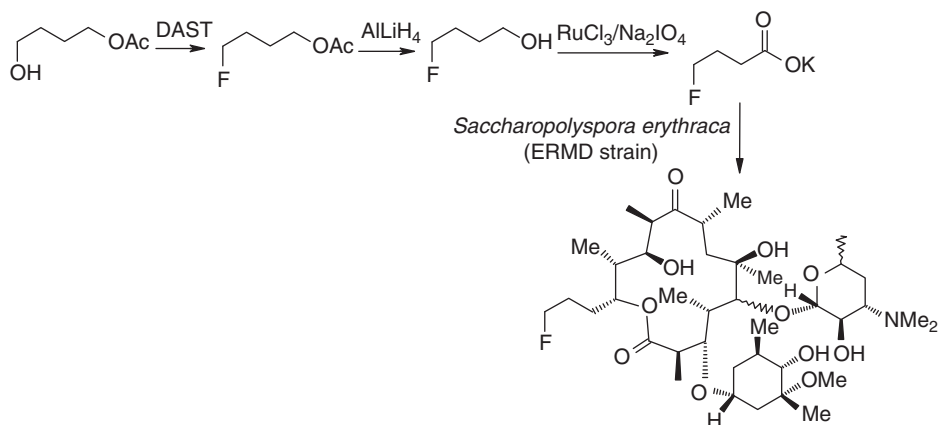
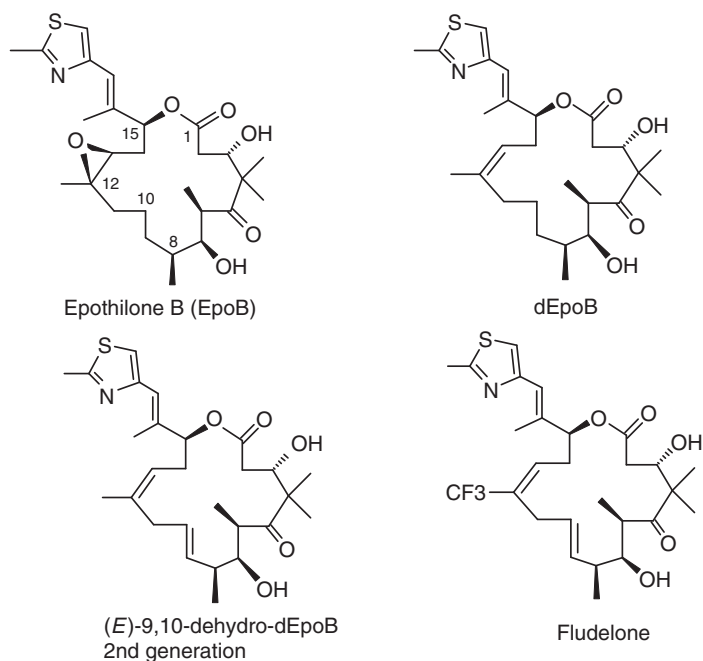


Fig. 46. Biosynthesis of 16-fluoroerythromycin A by *Saccharopolyspora erythraea* (ERMDI strain) [124].

(*E*)-9,10-dehydro-dEpoB, the synthetic intermediate resulting from a ring closure metathesis reaction. These assays revealed that the presence of an (*E*)-9,10 unsaturation in the macrolide framework resulted in a marked increasing in potency and in metabolic stability, despite a rapid hydrolysis by esterases *in vivo* [126]. Its trifluoro analogue (12- CF_3), *fludelone*, exhibited an attenuated cytotoxicity in CCRF-CEM leukaemia cells compared with that of (*E*)-9,10-dehydro-dEpoB). Nevertheless, *in vivo* experiments performed on human tumour xenografts in immunodeficient nude mice showed that *fludelone* is much more active and possesses a twice longer plasma half-life (Fig. 47) [127].



	Fludelone	(E)-9,10-dehydro-dEpoB
IC ₅₀ (nM) (Leukaemia cells CCRF-CEM)	3.2	0.9
Plasma half life (min) (mice)	212 ± 88	84 ± 6
Half life S9 (h) (human liver)	10.5 ± 2.3	4.9 ± 0.7

Fig. 47. Fluoroepothilones [126,127].

The convergent synthesis is based on the closure of the macrolide ring through a ring closure metathesis reaction that can be performed on a multigram scale (Fig. 48) [128]. Clinical trials are ongoing [129].

3.6. Steroids

The medicinal chemistry of fluorosteroids is of course dominated by the fluorocorticoids. Research in fluorocorticoids is now essentially devoted to the search for new formulation of registered drugs. Elsewhere, there is currently a renewal of interest for fluorosteroids in medicinal chemistry mainly in view to develop drugs for hormonal disorders.

3.6.1. Corticosteroids

Glucocorticoids are important metabolic hormones with a central role and many implications. They interact with nuclear receptors. These latter act on

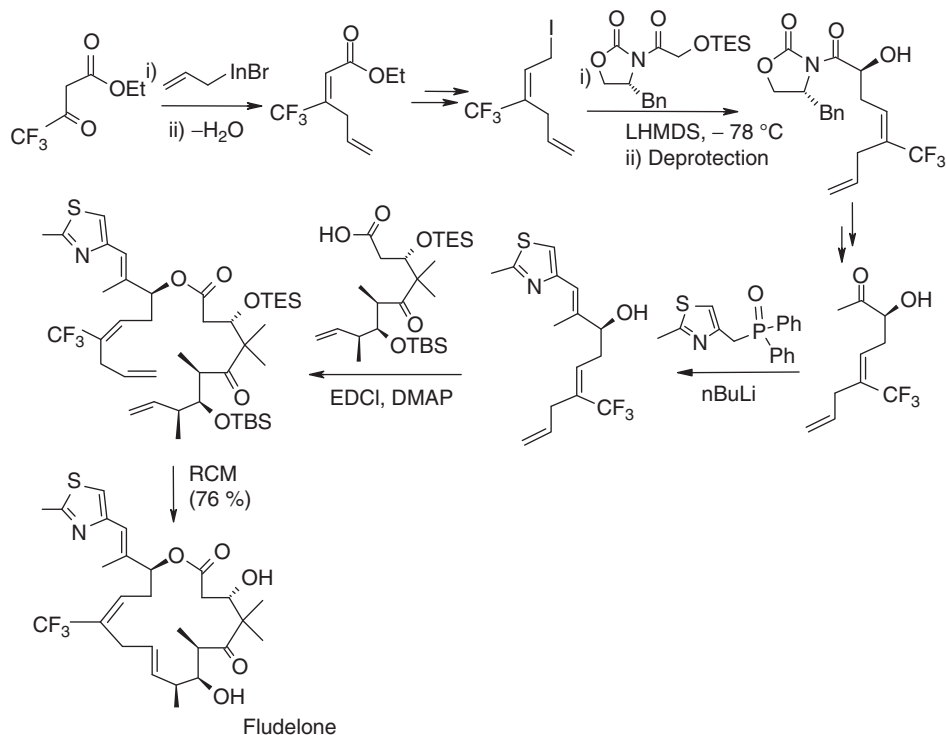


Fig. 48. Synthesis of *fludelone* [128].

transcription factors of the genes coding proteins that are involved in the control of inflammation.

The inhibition of transcription of genes coding for phospholipase A_2 (PLA_2) and the activation of genes coding for lipocortine (endogen inhibitor of PLA_2) reduce the releasing of arachidonic acid (AA) from membrane phospholipids. This explains, at least partially, why glucocorticoids have anti-inflammatory properties.

Glucocorticoids also repress the synthesis of $NF-\kappa B$ (nuclear factor κB), which is an activator of gene transcription coding for pro-inflammatory molecules (Tumor Necrosis Factor (TNF), interleukines 1 and 2, cyclooxygenase 2, etc.). Glucocorticoids also partially neutralise a heterodimeric protein AP-1, formed of proteins Fos and Jun, which activate the transcription of several genes involved in the synthesis of pro-inflammatory proteins: NO synthase (NOS), cyclooxygenase 2 (COX-2) and PLA_2 .

It is in this important family of natural compounds that the first example of the influence of a fluorine atom on biological properties of a molecule has been displayed [130]. This discovery opened the route to very important applications in medicinal field: it has been the starting point of the use of fluorination to modify the biological behaviour of a molecule in view of therapeutic applications.

As soon as corticosteroids, such as cortisone, were used in the treatment of rheumatoid arthritis (glucocorticoid activity), important undesirable side effects appeared (sodium retention). In view of lowering the sodium retention, while increasing the anti-inflammatory activity, Fried performed various chemical modifications. Thus, he could observe that introducing a fluorine atom at the 9α position of the hydrocortisone acetate highly enhanced (11 times) the glucocorticoid activity, while the undesired sodium retention was lowered [130].

Fluorination of corticosteroids at C-9 or/and C-6 increases glucocorticoid activity while the mineralocorticoid activity, responsible of sodium retention (the main adverse effect of corticoids), is decreased. Fluorocorticosteroids were the first fluoro compounds to be used for therapeutic. They are still major drugs against many inflammatory disorders in rheumatology (rheumatoid polyarthritis), Otorhino-laryngology (ORL) (asthma, rhinitis), neurology (brain oedema), dermatology and allergy (anaphylactic shock, Quincke oedema, etc.).

Fluorine substitution can take places at 9α , 6α or at both of these positions (Fig. 49). A very large number of compounds have been designed from corticoid core with these common structural elements, that is, 1,4-diene, 17-hydroxymethylacetyl, 11β -hydroxyl and the main following structural modulation:

A substitution (Me or OH) introduced at C-16 (*difluprednate* excepted) which usually contributes to decrease the mineralocorticoid activity. The substituent can be α (*dexamethasone*, *paramethasone*, *flumetasone*) (16α -Me) or β (*betamethasone*, *diflorasone*) (16β -Me) (Fig. 49). When a hydroxyl is present in

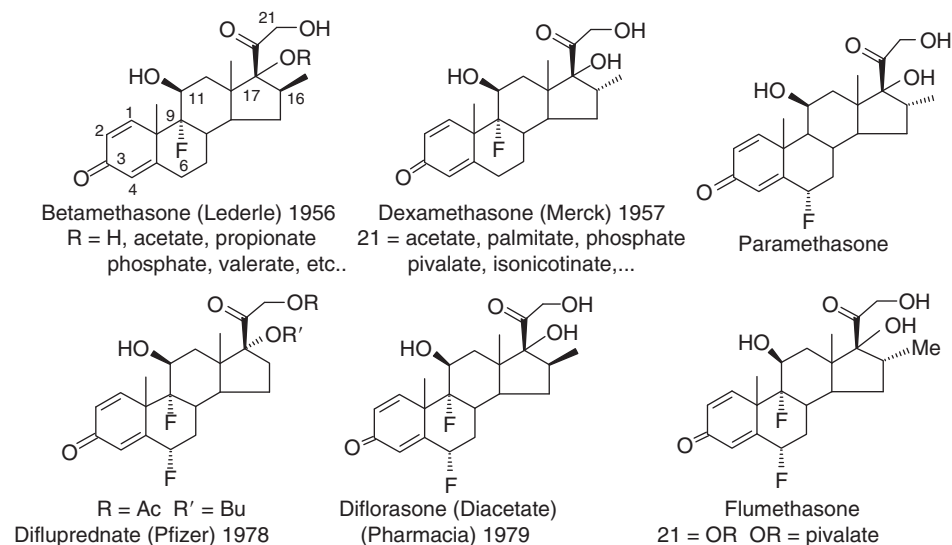


Fig. 49. Examples of 6-, 9- and 6,9-fluorocorticosteroids.

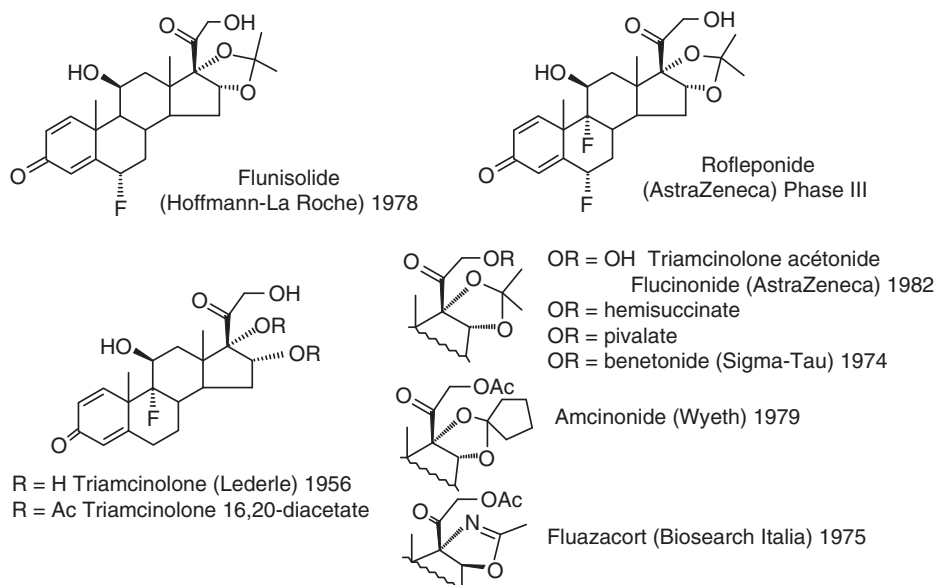


Fig. 50. 16-Hydroxy fluorocorticoids.

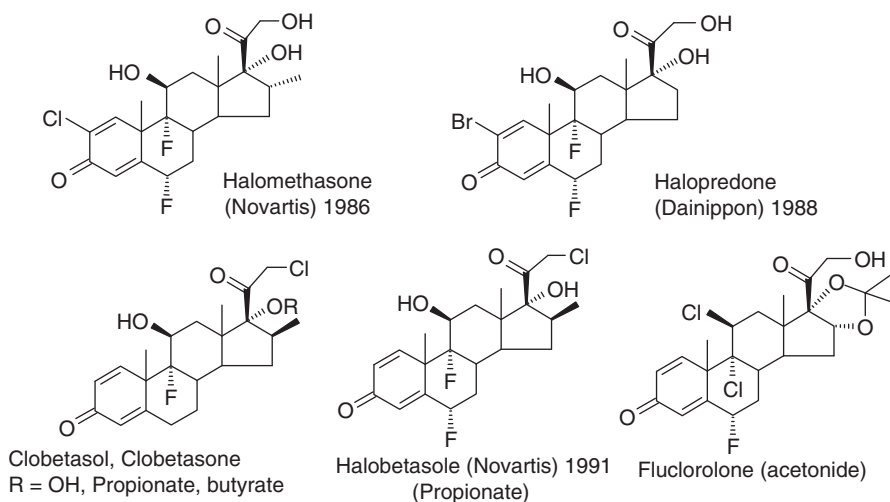


Fig. 51. Halogenofluorocorticosteroids.

C-16 α (*triamcinolone*), it is frequently engaged as an acetonide with the 17-hydroxyl (*flunisolide*, *rofleponide*, etc.) (Fig. 50).

A substitution with another halogen at C-2 (*halomethasone*, *halopredone*) or at C-21 (21-OH \rightarrow 21-Cl) (*clobetasol*, *halobetasol*). *Fluclorolone* is an atypical fluorocorticosteroid, in which the 11 β -OH and the 9 α -F are replaced by chlorine atoms (Fig. 51).

The deletion of 17-hydroxyl (*desoximethasone*, *fluocortolone*, *difluocortolone*, *fluocortine*) (Fig. 52).

There are also several compounds with more atypical substitution, for instance:

fluocortine in which the 20-CH₂OH is replaced by a butyl ester group (Fig. 52),
fluticasone in which the 17-CO-CH₂OH is replaced by an α -fluoromethylthioester (Fig. 53),
fluorometholone which is 6 α -Me-substituted
fluprednidene substituted in C-16 with an *exo*-methylene (Fig. 53).

Fludrocortisone and *fludroxycortide* are mineralocorticoids. They are more potent than cortisol. The reduction of the Δ -1 unsaturation contributes to the decreasing of glucocorticoid and anti-inflammatory activities (Fig. 54).

To all these structural modulations, the esterification of 17- and 21-hydroxyl has been added with the aim to prepare oral, topical, spray and delayed-delivery formulations. A huge number of medicines have been marketed from more than 20 basic molecules (Figs. 48–55). Despite the fact that fluorocorticosteroids

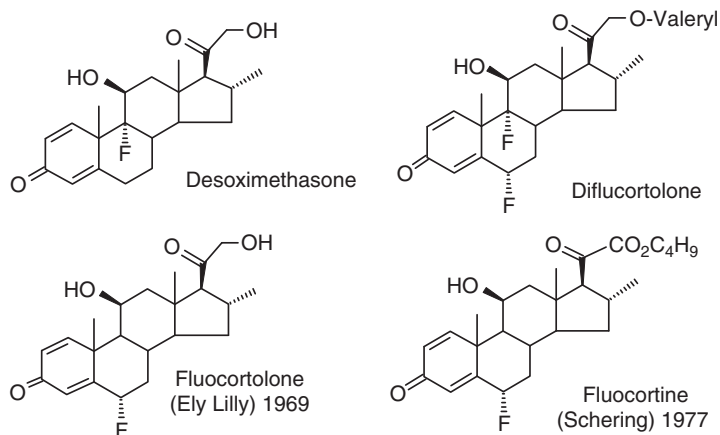


Fig. 52. Fluorocorticosteroids without 17-OH.

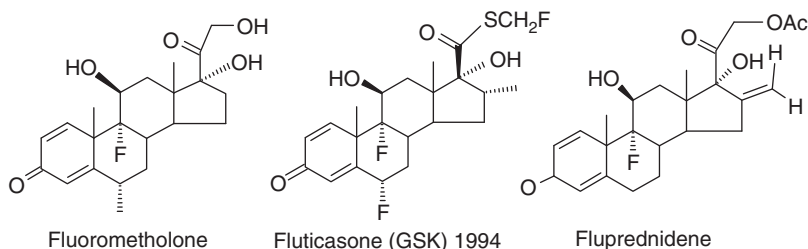


Fig. 53. Examples of fluorocorticosteroids with atypical substitutions.

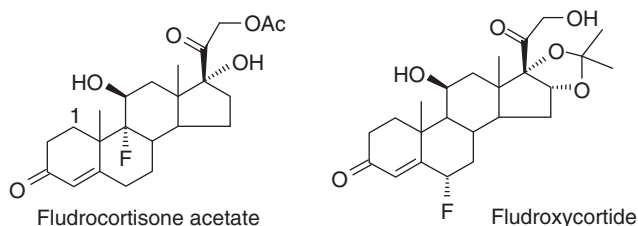


Fig. 54. Fluoro mineralocorticoids.

could be considered as 'old' drugs, they are still major drugs in therapies of inflammation, allergy, asthma, as well in dermatology and ophthalmology, as shown by the new galenic formulations which are regularly launched.

The reason of effects of fluorine atoms at C-6 and C-9 positions on the pharmacological profile (in particular on the enhancement of the glucocorticoid activity and its dissociation from the mineralocorticoid activity) is not always very clear. Three hypothesis coexist:

1. The enhancement of the acidity of the 11β hydroxyl can increase the affinity of the molecule for the receptor which is responsible for the glucocorticoid activity;
2. The slight conformational modification of the cycle A (revealed by X-ray diffraction), which probably comes from an interaction between the fluorine at C-9 and the axial OH at C-1, could contribute to the change in affinity [131]. However X-ray structure of the fluorocortisol co-crystallised with the glucocorticoid receptor does not clearly explain the impact of fluorine on the increased affinity for the receptor (cortisol, $K_i=0.67\mu\text{M}$ vs 9α -fluorocortisol $K_i=0.027\mu\text{M}$) [132,133].
3. The fluorine at C-9 can reduce the oxidative metabolism of the hydroxyl-11. The oxidation the OH-11 into ketone is fast for the cortisol and is accompanied with the loss of the biological activity [134,135].

The original synthesis of 9-fluorocorticoid by Fried involves the opening the 9, 11-epoxy hydrocortisone acetate by HF. This oxirane is prepared in two steps from hydrocortisone acetate. This synthesis still remains the only method to prepare 9-fluorocorticoids (Fig. 55) [130]. To date, there is no alternative known method for this purpose [136].

The introduction of fluorine on the position 6 can be performed according to various pathways: fluorohalogenation [137], via the oxirane 5α - 6α [138], or electrophilic fluorination (FCIO_3 , $\text{CF}_3\text{COONa}/\text{F}_2$ and now F-TEDA-BF_4) (Fig. 56) [139–141]. The stereochemistry of the electrophilic fluorination product is depending on the reagent used. However, the 6α compound is generally the major one. In acidic medium, 6β -F compounds can isomerise into 6α -F compounds [140a].

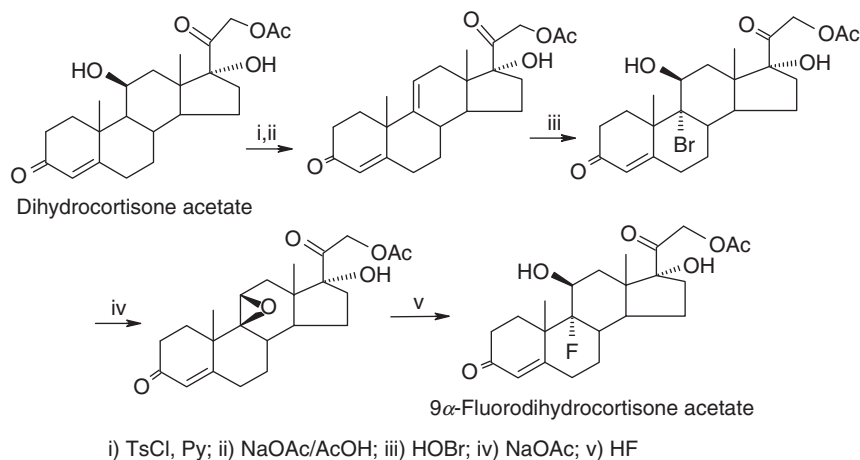


Fig. 55. Synthesis of the 9 α -fluorohydrocortisone [130].

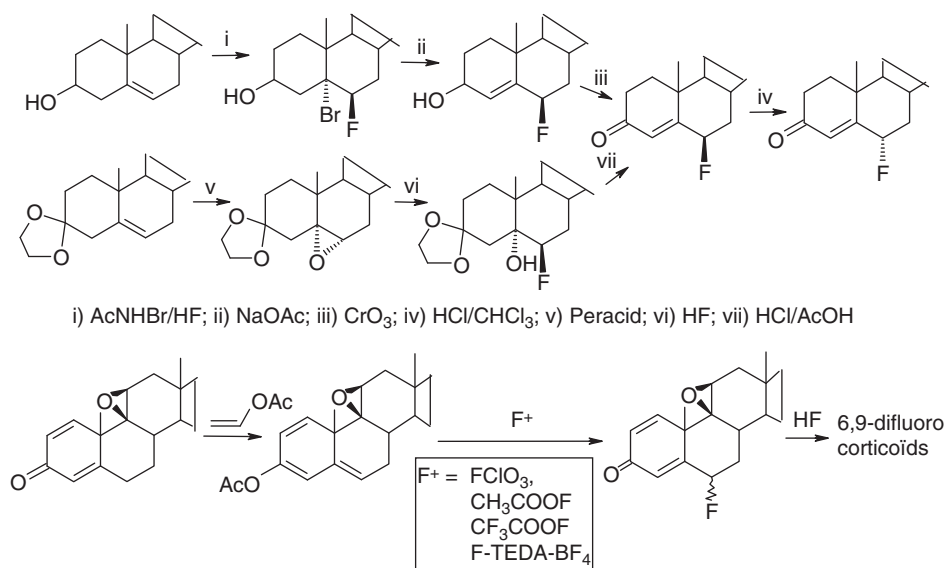


Fig. 56. Synthesis of 6 α -et 6 β -fluorocorticosteroids.

Methods to introduce fluorine on the 6 position are based on electrophilic fluorinations. They are generally adapted to a further introduction of a fluorine on position 9.

Fluorocorticoids are produced at the ton scale (e.g. *fluticasone* 1.1 ton in 2001). The industrial production of fluorocorticosteroids has been a triple chemical challenge: availability of the starting material, use of hazardous and toxic

fluorination reagents and involvement of numbers of chemical or biotechnological step involved in the synthesis, as highlighted by the synthesis of *dexamethazone* (Fig. 57).

The access to corticosteroids from animal or vegetal steroids has been in the focus of important studies. Steroids that are accessible in high tonnage (e.g. diosgenin, hecogenin, stigmasterol, β -sitosterol and biliary acids) have been the industrial precursors of hydrocortison [142–144]. The current industrial processes utilise biliary acids which afford acetoxydehydropregnenolone as precursor (Fig. 58) [142c]. They can also involve the crude mixture of β -sitosterol, extracted from soya oil, and whose fermentation leads to 9 α -hydroxy-androstenolone [144]. The dehydration can be selectively performed to yield the Δ -9–11 compound. The pregnan side chain is then further built.

3.6.2. Fluorosteroids acting on steroid hormone receptors

Fulvestrant is a competitive oestrogen receptor antagonist which binds to the receptor in a competitive manner with an affinity similar to that of estradiol. *Fulvestrant* downregulates the oestrogen receptor in human breast cancer cells. It is marketed for treatments of hormone-dependent breast cancer (Fig. 59) [145].

Although it is a relatively old drug, *Flumedroxone* (Demigran®), marketed as a progestative agent, is worthy of attention here. This derivative of 17-hydroxy

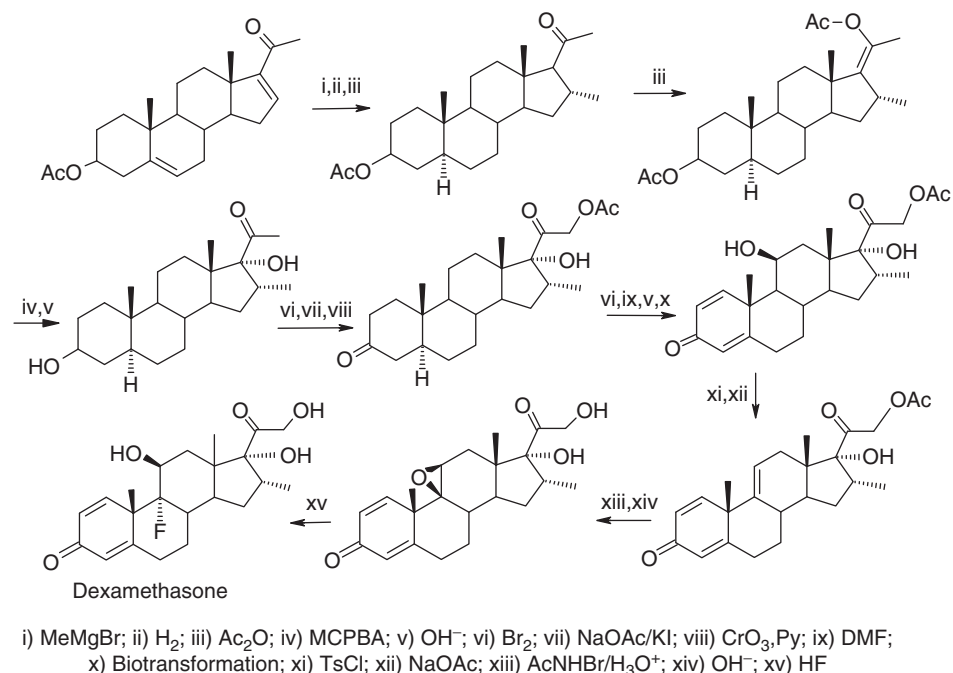


Fig. 57. Synthesis of *dexamethasone* [142].

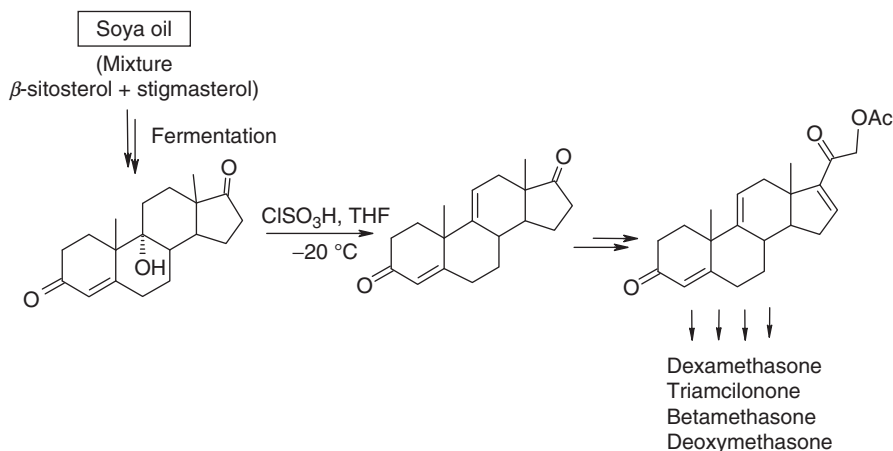


Fig. 58. Upjohn process for the production of precursor of 9 α -fluorocorticosteroids [144].

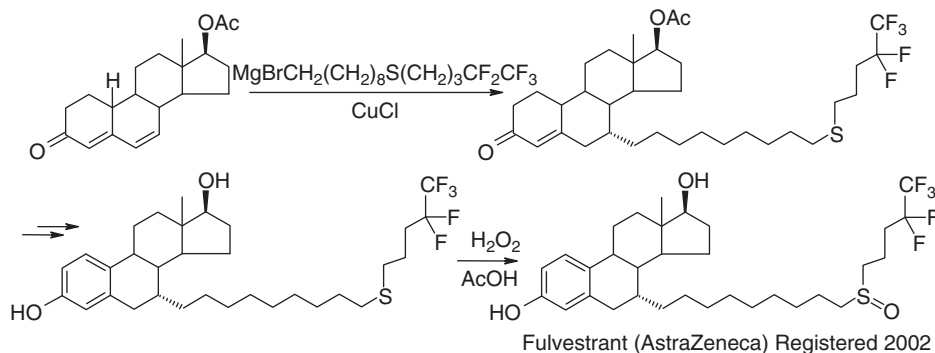


Fig. 59. Synthesis of *fulvestrant* [145].

pregnanolone is substituted at C-6 by a trifluoromethyl group, which is introduced by radical trifluoromethylation, or by electrophilic trifluoromethylation of an enol with the Umemoto reagent (Fig. 60) [146]. Electrophilic fluoroalkylation at C-7 has also been achieved [147].

Antiprogesterone, substituted at C-17 by a hydroxyl (17- β) and a C_2F_5 group (17- α), is an antagonist of the progesterone receptor. It is currently in early clinical development. C_2F_5 is introduced with pentafluoroethyl lithium, prepared *in situ* from pentafluoroethyl iodide and butyllithium (Fig. 61) [148].

3.6.3. Other fluorinated steroid drugs

Dutasteride (Avodart[®]) is a 4-azasteroid, a close analogue of *finasteride*, in which the *t*-butyl of the amide group has been replaced by a bis(trifluoromethyl)

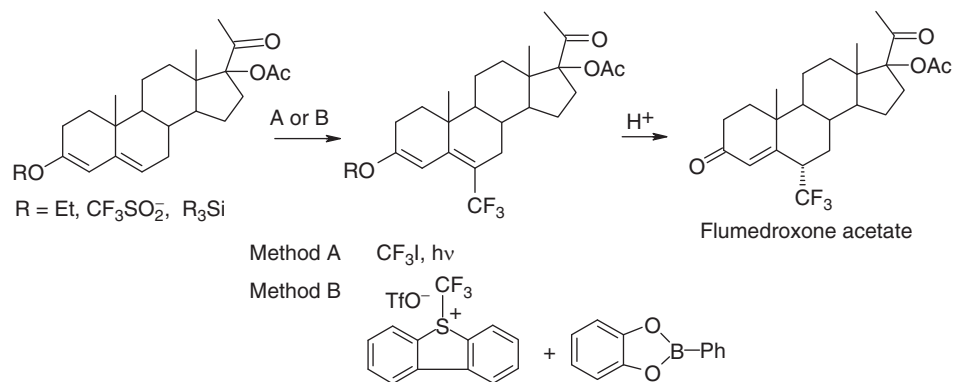


Fig. 60. Synthesis of *flumedroxone* [146c].

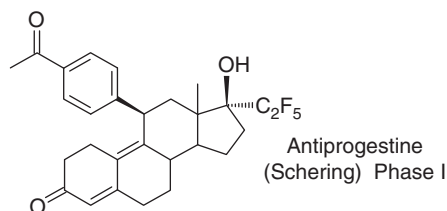


Fig. 61. *Antiprogesterone*.

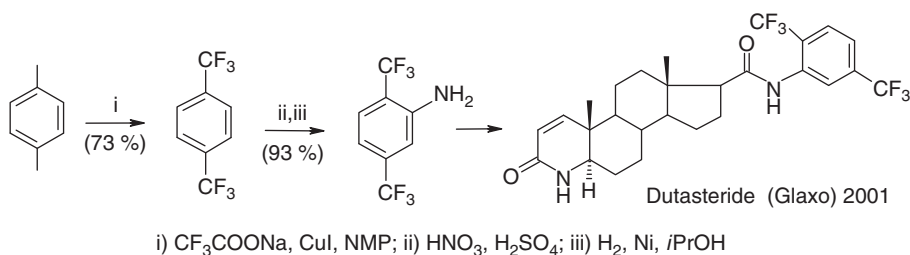


Fig. 62. Synthesis of *dutasteride* [149].

phenyl group. It inhibits both type 1 and type 2 5 α -reductases, enzymes which convert testosterone into dihydrotestosterone in the prostate. *Dutasteride* was recently introduced for the treatment of benign prostatic hyperplasia (BPH). The starting synthon 2,4-bis(trifluoromethyl)-aniline was prepared by trifluoromethylation of the corresponding di-iodobenzene, followed by nitration and reduction (Fig. 62) [149].

Fluasterone is a stable adrenocortical steroid, a 16 α -fluoro analogue of *prasteron* [dehydroepiandrosterone (DHEA)]. It is currently developed (phase II) for the treatment of metabolic syndrome (i.e. insulin resistance). Electrophilic

fluorination with N-F type reagents is well adapted for the synthesis of such an α -fluoroketone (95%, $\alpha:\beta = 95:5$) (Fig. 63) [141].

CCD-3693 is the trifluoro analogue of *ganalozone* (3β -methyl allopregnanolone). It is also a specific ligand for the γ -aminobutyric acid (GABA_A) receptor. However, unlike *ganalozone* which is an anti-convulsive drug, CCD-3693 is currently in early clinical development as a sleep inducer [150]. It is prepared by addition of the Ruppert reagent (CF_3TMS) onto the corresponding ketone (Fig. 63).

3.6.4. Vitamin D_3 metabolites

Vitamin D_3 is transported to liver where it undergoes a hydroxylation at C-25 into $1\alpha,25$ -dihydroxyvitamin D_3 (calcitriol) (Fig. 64). In the kidney, it undergoes further hydroxylations at different sites, depending on the serum Ca^{2+} concentration. The most biologically active metabolite of vitamin D_3 is calcitriol, which plays important roles in the regulation of calcium and phosphorus metabolism. It is used for treating bone diseases, but is also involved in the cell proliferation and the inducement of cell differentiation [151].

Fluorination of calcitriol has been performed on the A-ring and on the side chain. Introduction of fluorine atoms on the A-ring of vitamin D_3 metabolites has been realised on the positions 2 and 4 [152]. Surprisingly, while introduction of fluorine at C-2 strongly decreases the affinity for the calcitriol receptor

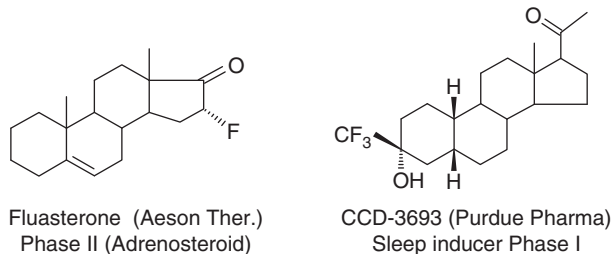


Fig. 63. Fluasterone and CCD-3693.

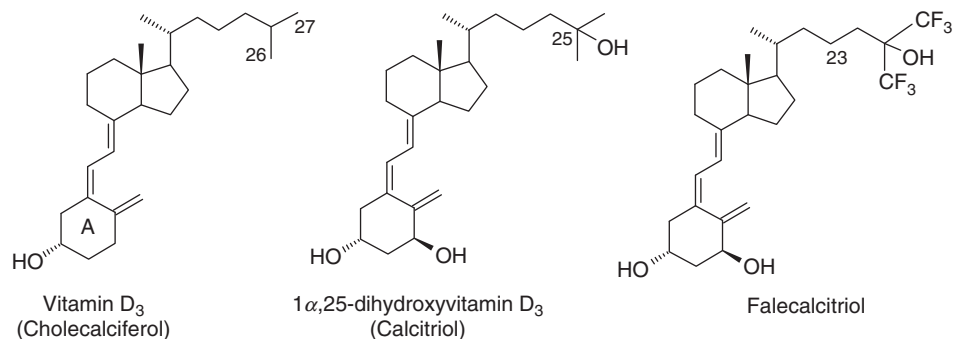


Fig. 64. Vitamin D_3 , calcitriol and falcitriol.

(10% of calcitriol affinity), this modification increases the calcemic activity (higher than that of calcitriol) [152c]. The 1-hydroxyl has also been replaced by a fluorine atom (Fig. 65). Fluorination could also be stereoselectively performed through an electrophilic fluorodesilylation (Fig. 66) [153]. This 1-fluoro analogue *BXL-628* (now *Ro-26-9228*) inhibits the growth factors involved in BPH, without direct androgenic effects. It is currently in phase II of clinical development [154].

Fluorination of the vitamin D₃ side chain was anticipated to have an impact on its metabolism pathway. The 26,27-hexafluorocalcitriol, *falecalcitriol*, was found to be several times more potent than calcitriol in the regulation of Ca²⁺ metabolism and of the immune system [155]. The reason for this higher biological activity was attributed to several mechanisms: a higher activity of its 23(S)-hydroxylated metabolite [hexafluoro-1,23(S),25(OH)₃D₃], a lower affinity for the vitamin D-binding protein (VDR) [156] and a higher affinity of *falecalcitriol*-receptor complex to DNA. *Falecalcitriol* (Hornel®) is prescribed as a hypercalcemicant to treat some bone diseases (hypocalcemia, rickets and osteomalacia) and hyperparathyroidism (Fig. 67). The synthesis of *falecalcitriol* is reported in Fig. 67 [156].

From this success, further efforts have been focused on dissociating the calcemic activity from the anti-proliferative activity, with the aim to limit the former

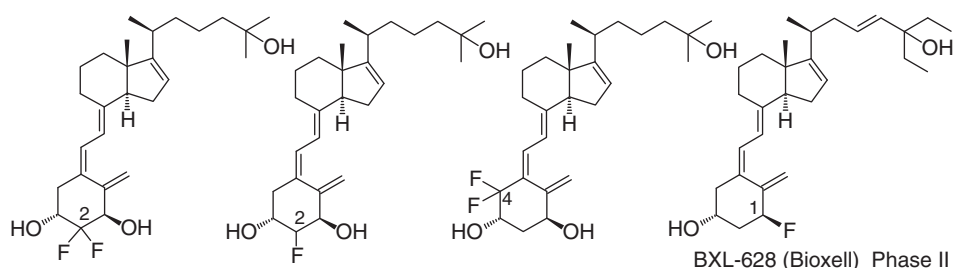


Fig. 65. Fluorination of A-ring of vitamin D₃ metabolites.

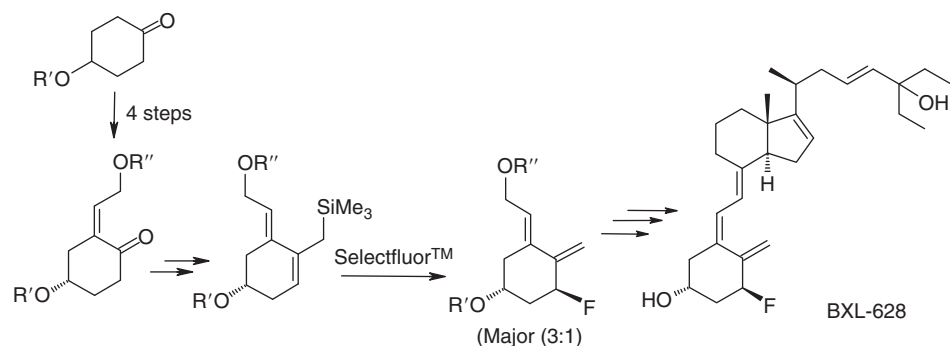


Fig. 66. Enantioselective synthesis of BXL-628 [153].

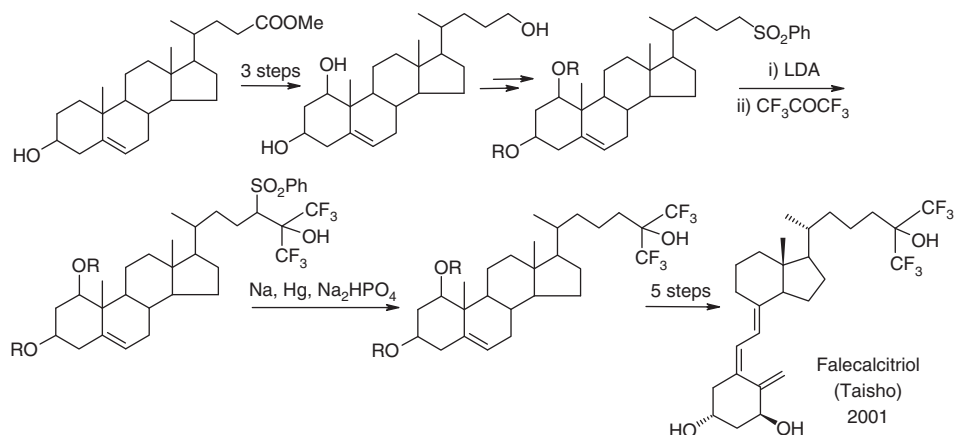


Fig. 67. Synthesis of falecalcitriol [156].

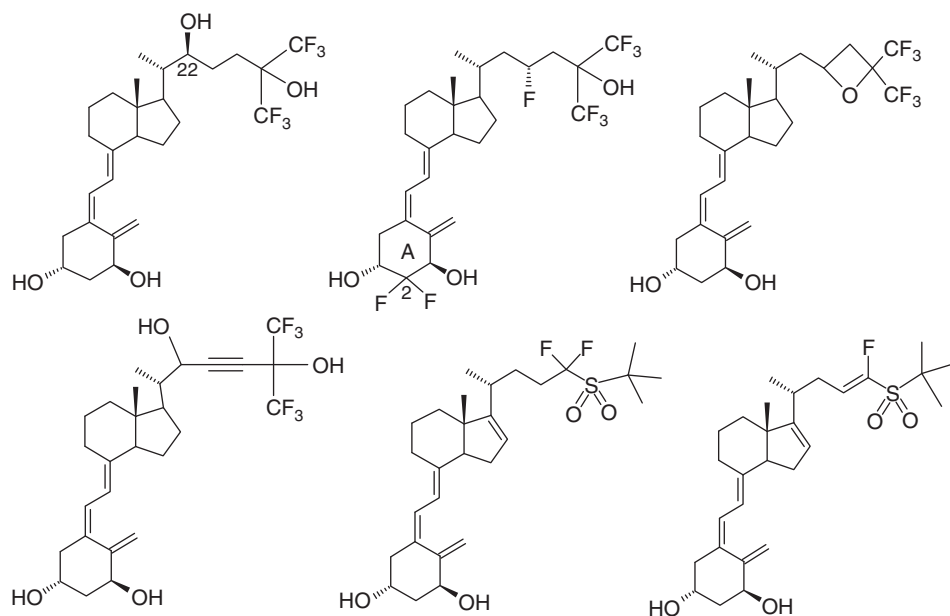


Fig. 68. Fluoro analogues of dihydroxycalciferol.

(hypercalcemia) and to increase the anti-cancer activity. Accordingly, many fluorinated analogues have been synthesized. In particular, starting with falecalcitriol, fluorine atoms have been introduced on positions 22, 23 and 24 of the side chain and on positions 1 and 2 of the A-ring [152,154]. Numerous other structural modifications have also been achieved on the fluorinated side chain (introduction of unsaturation, sulfone, oxetan, etc.), as exemplified in Fig. 68 [156–159].

Some of the resulting compounds, in particular the 22(*S*)-hydroxy-falecalcitriol, exhibit an excellent selectivity, with a very high activity on human carcinoma lines (HT-29) and no calcemic effect, as assessed *in vivo* on rats [156].

Fluorinated analogues of the vitamin D₃ metabolites have also been used as probes in ¹⁹F NMR, to perform studies on the conformation of the complex between vitamin D and its receptor [160].

3.7. Prostanoids

Because of the importance of the arachidonic cascade on a broad range of biological activities, intensive studies have been devoted to the synthesis of prostanoids and other arachidonic acid metabolites. One objective was to acquire a better knowledge of their very puzzling roles in signal transduction, and to elucidate the diverse functions of receptors. Another important objective was to find more stable analogues, able to be developed as potentially valuable drugs. Fluorination of prostanoids was particularly well adapted to these aims, and numerous fluorinated derivatives have been synthesized [2, pp. 125,161,162]. Amongst them, some drug candidates have emerged and are undergoing clinical development or are marketed drugs.

Fluoro analogues of prostacyclins (PGI₁, PGI₂ and PGF_{2α}) have been synthesized in order to enhance the stability of these products, which undergo a very fast metabolism. The instability of PGI₂ under physiological conditions (*t*_{1/2}=5–10 min at pH 7.4 and at 37°C) is connected with both the rapid oxidation of the lateral chain and the presence of the enol ether function. It is so unstable that its functions as a vasodilator and inhibitor of platelet adhesion cannot be clinically exploited. Fluorine atoms have been introduced on the position β to the enolic double bond of *iloprost*, a more stable derivative of PGI₂ (Fig. 69). The proteolysis is dramatically slowed since protonation of the enol ether to give an oxonium ion is disfavoured by the presence of fluorine atoms [163]. Thus, the drug

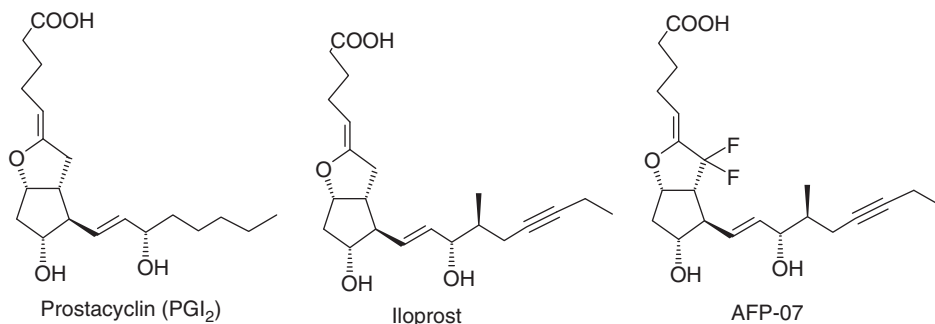


Fig. 69. Fluoro analogues of PGI₂.

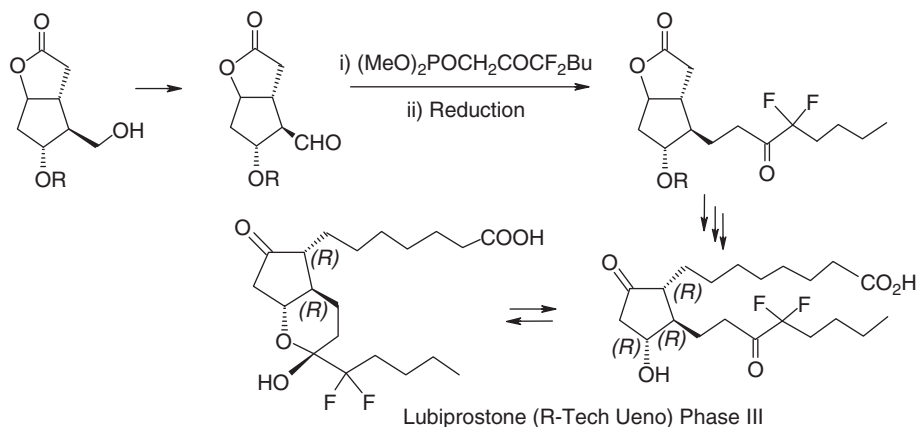


Fig. 71. Synthesis of *lubiprostone*

AFP-168, a deoxy-15,15-difluoro $\text{PGF}_{2\alpha}$ analogue of *travoprost*, where the 15-hydroxyl of the side chain is replaced by a difluoromethylene, is currently under clinical development with the same indication (Fig. 72) [168].

3.8. Terpenes

3.8.1. Artemisinin

Artemisinin is a natural endoperoxide-containing sesquiterpene, isolated from a plant used in traditional Chinese medicine. Acetalic artemisinin derivatives (artemether, artesunate) are very active against chemo-resistant forms of *Plasmodium falciparum*, and are clinically used for the treatment. However, they suffer from an unfavourable pharmacological profile. They are quickly metabolised by fast oxidative metabolism, hydrolytic cleavage and glucuronidation.

Extensive research has been carried out in efforts to increase the duration of action of artemisinin derivatives [169]. A recent approach to design more metabolically stable artemisinins has been developed by introducing a trifluoromethyl group at C-10 [170,171]. Because of its electron-withdrawing character, this substituent was expected to protect efficiently artemisinins from oxidative and hydrolytic cleavages and from glucuronidation when a hydroxyl is present at C-10. The hypothesis has been clearly validated by a comparison of the *in vitro* and *in vivo* anti-malarial activities of fluorinated and non-fluorinated 10-deoxoartemisinins (Fig. 73). The 10-deoxoartemisinin is active *in vitro* against *P. falciparum* strains ($\text{IC}_{50}=20$ nM), but it is completely inactive *in vivo*. The introduction of a trifluoromethyl group on C-10 maintains the *in vitro* activity ($\text{IC}_{50}=6$ nM) and remarkably protect mice *in vivo* [171,172].

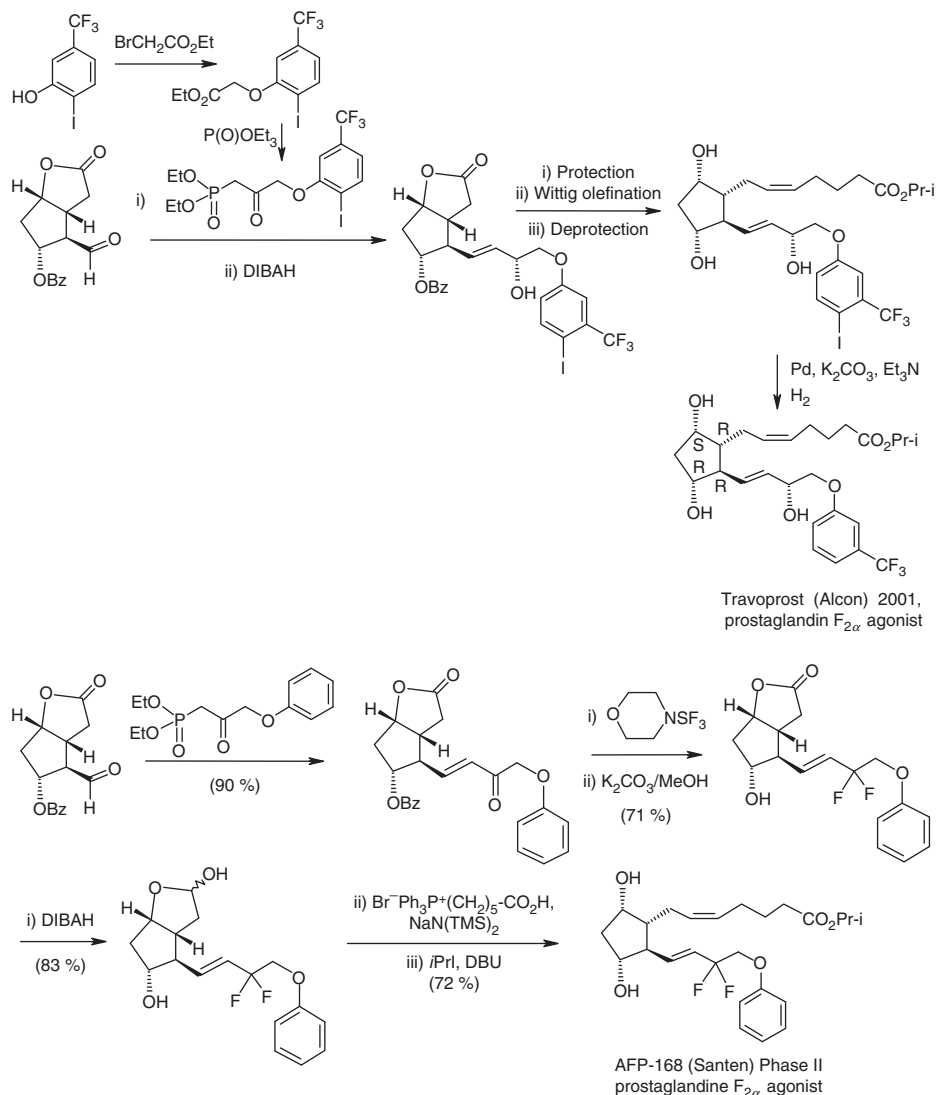


Fig. 72. Syntheses of prostanoids (*Travoprost* and *AFP-168*) used in glaucoma treatment.

Based on these results, 10- CF_3 -analogues of dihydroartemisinin (DHA), artemether, arteether and artesunate have been prepared. They also exhibit very interesting *in vivo* anti-malarial properties, a better stability under stomach acidic conditions. A prolonged plasma half-life was demonstrated for some of them [171,173]. This approach has led to the pre-clinical development of the orally active 10-trifluoromethyl DHA and a 10-trifluoromethyl deoxoartemisinin (Fig. 73) [170–172].

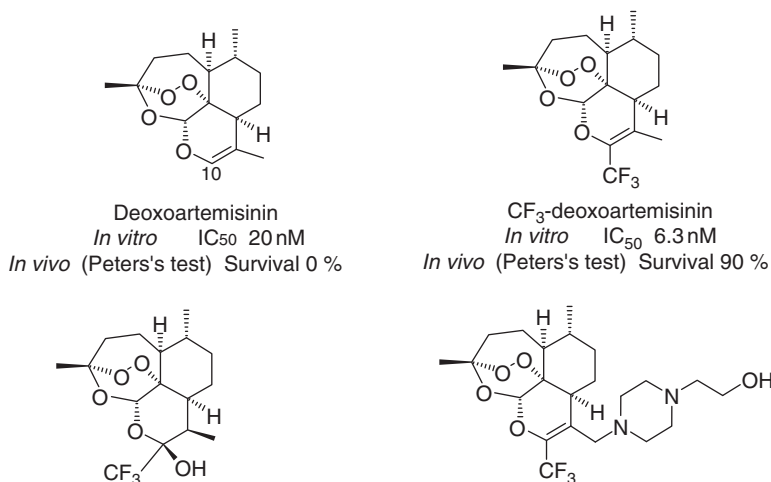


Fig. 73. *In vitro* and *in vivo* anti-malarial activities of fluoro artemisinin derivatives.

3.9. Amino acids

Organic chemists have brought to biologists and chemists specialized in proteins an incredible range of fluorinated amino acids [2, pp. 147–182; 39;174;175]. These fluorinated amino acids have found a great number of uses in enzymology as peptidomimetic units and mechanism-based inhibitors and in protein structural studies [2, pp. 265–270; 8]. However, despite demonstrated biological activities, few of them have resulted in drug candidates for development. Difluoromethylornithine is a notable exception.

The difluoromethylornithine, *eflornithine* (DFMO), is a mechanism-based inhibitor of ornithine decarboxylase. The latter is a pyridoxal-depending key-enzyme of the polyamine biosynthesis from ornithine. Fluorine atoms are essential for the inhibition process [176]. The inhibition mechanism is likely to be similar to that of amino acid decarboxylases by α -fluoromethyl amino acids with an irreversible loss of fluoride anion [2, pp. 265–270; 8]. *Eflornithine* was first clinically developed for cancer treatment, but development was stopped. Activity of *eflornithine* on trypanosome was then discovered [177]. Now, despite its very low bioavailability, *eflornithine* is the best therapy for sleeping sickness (trypanosomiasis) induced by the *Trypanosoma brucei gambiense* parasite, in particular at the cerebral stage. *Eflornithine* is registered with the orphan drug status and is distributed by WHO.

Production of *eflornithine* was temporarily stopped because of environmental concerns associated with the use of HCFC CHF₂Cl, the key reagent in the synthesis (Fig. 74) [178]. However, it seems that now production of *eflornithine* has started again, not only to supply WHO, but also strongly motivated by

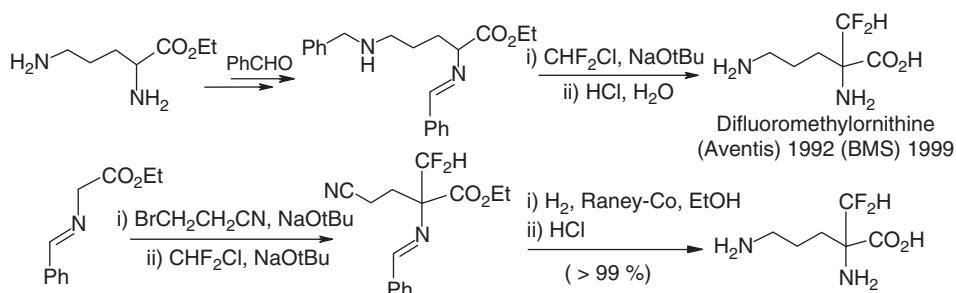


Fig. 74. Synthesis of difluoromethylornithine [178,179].

another application: a topical formulation for the treatment of female hirsutism was recently launched (*Vaniqa*). The synthesis was recently improved and shortened by introducing a selective catalytic reduction of the cyano group. This avoids the side reaction involving cyclisation into lactam. However, the key reagent is still CHF_2Cl [179].

4. CONCLUSION

Nature possesses an inexhaustible repository of chemical diversity that still provides one of the most efficient sources of inspiration for medicinal and drug discovery chemists. This is perfectly demonstrated by recent developments in cancer chemotherapy. Thanks to the important progress realised during the last years in synthetic methodologies that provide more ready access to fluorinated molecules; fluorinated analogues of natural compounds are becoming more and more relevant in drug discovery. This trend is strongly reinforced by the increasing understanding of the influence of fluorine introduction on the modulation and the improvement of pharmacological properties of a molecule. As highlighted in this review, this has resulted in the discovery and the development of important pharmaceuticals based on fluorinated analogues of natural products. It is foreseeable that future progress in fluorine medicinal chemistry of natural products will continue to be important.

REFERENCES

- [1] C. Isanbor, D. O'Hagan, Fluorine in medicinal chemistry: A review of anti-cancer agents, *J. Fluor. Chem.* 127 (2006) 303–319.
- [2] J.P. Bégué, D. Bonnet-Delpon, *Chimie Bioorganique et Médicinale du Fluor*, EDP Science/CNRS Eds, Paris, 2005.
- [3(a)] K. Kirk, Fluorine in medicinal chemistry: Recent therapeutic applications of fluorinated small molecules, *J. Fluor. Chem.* 127 (2006) 1013–1029.

- [3(b)] J.P. Bégué, D. Bonnet-Delpon, Recent advances (1995–2005) in fluorinated pharmaceuticals based on natural products, *J. Fluorine Chem.* 127 (2006) 992–1012.
- [4] H. Deng, D. O'Hagan, C. Schaffrath, Fluorometabolite biosynthesis and the fluorinase from *Streptomyces cattleya*, *Nat. Prod. Rep.* 21 (2004) 773–784.
- [5] P.N. Edwards, Uses of fluorine in chemotherapy, in: R.E. Banks, B.E. Smart, J.C. Tatlow (Eds.), *Organofluorine Chemistry*, Plenum Press, New York, 1994, pp. 501–546.
- [6] R. Filler, Y. Kobayashi, L. Yagupolskii (Eds.), *Organofluorine Compounds in Medicinal and Biomedical Applications*, Elsevier, Amsterdam, 1993.
- [7] I. Ojima, R. McCarthy, J. Welch, (Eds.), *Biomedical Frontiers of Fluorine Chemistry*, ACS Symp. Ser. 639, ACS, Washington, DC, 1996.
- [8] K. Kirk, Biochemistry of Halogenated Organic Compounds, *Biochemistry of the elements*, 9B Plenum Press, New York, 1991, pp. 127–150.
- [9] P. Wang, A. Fichera, K. Kumar, D.A. Tirell, Alternative translations of a single RNA message: An identity switch of (2S,3R)-4,4,4-trifluorovaline between valine and isoleucine codons, *Angew. Chem. Int. Ed.* 43 (2004) 3664–3666.
- [10(a)] G. Bott, L.D. Field, S. Sternhell, Steric effects. A study of a rationally designed system, *J. Am. Chem. Soc.* 102 (1980) 5618–5626.
- [10(b)] T. Nagai, G. Nishioka, M. Koyama, A. Ando, T. Miki, I. Kumadaki, The steric effect of the trifluoromethyl group, *Chem. Pharm. Bull.* 39 (1991) 233–235.
- [11] M. Schlosser, D. Michel, About the “physiological size” of fluorine substituents: Comparison of sensorially active compounds with fluorine and methyl substituted analogues, *Tetrahedron* 52 (1996) 99–108.
- [12] S.P. Götzö, D. Seebach, J.J. Sanglier, EPC Syntheses of trifluorocitronellol and of hexafluoropyrenophorin—A comparison of their physiological properties with the nonfluorinated analogs, *Eur. J. Org. Chem.* (1999) 2533–2544.
- [13] J.C. Biffinger, H.W. Kim, S.G. DiMagno, The polar hydrophobicity of fluorinated compounds, *ChemBioChem.* 5 (2004) 622–627.
- [14] R. Betageri, Y. Zhang, R.M. Zindell, D. Kuzmich, T.M. Kirrane, J. Bentzien, M. Cardozo, A.J. Capolino, T.N. Fadra, R.M. Nelson, Z. Paw, D.T. Shih, C.K. Shih, L. Zuvela-Jelaska, G. Nabozny, D.S. Thomson, Trifluoromethyl group as a pharmacophore: Effect of replacing a CF₃ group on binding and agonist activity of a glucocorticoid receptor ligand, *Bioorg. Med. Chem. Lett.* 15 (2005) 4761–4769.
- [15] D. O'Hagan, H.S. Rzepa, Some influences of fluorine in bioorganic chemistry, *Chem. Commun.* (1997) 645–652.
- [16] K.B. Wiberg, Bent bonds in organic compounds, *Acc. Chem. Res.* 29 (1996) 229–234.
- [17(a)] M. Tavasli, D. O'Hagan, C. Pearson, M.C. Petty, The fluorine *gauche* effect. Langmuir isotherms report the relative conformational stability of (±)-*erythro*- and (±)-*threo*-9,10-difluorostearic acids, *J. Chem. Soc. Chem. Commun.* (2002) 1226–1227.
- [17(b)] D.C. Lankin, G.L. Grunenwald, F.A. Romero, I.Y. Oren, J.P. Snyder, The NH—FC dipole orientation effect for pendant exocyclic CH₂F, *Org. Lett.* 4 (2002) 3557–3560.
- [18(a)] C.R.S. Briggs, D. O'Hagan, J.A.K. Howard, D.S. Yufit, The C–F bond as a tool in the conformational control of amides, *J. Fluor. Chem.* 119 (2003) 9–13.
- [18(b)] C.R.S. Briggs, D. O'Hagan, H.S. Rzepa, A.M.Z. Slawin, Solid state and theoretical evaluation of β -fluoroethyl esters indicate a fluorine-ester *gauche* effect, *J. Fluor. Chem.* 125 (2004) 19–25.
- [18(c)] C.R.S. Briggs, M.J. Allen, D. O'Hagan, D.J. Tozeur, A.M.Z. Slawin, A.E. Goeta, J.A. K. Howard, The observation of a large *gauche* preference when 2-fluoroethylamine and 2-fluoroethanol become protonated, *Org. Biomol. Chem.* 2 (2004) 732–740.
- [19] T. Iimori, Y. Murai, Y. Wakizaka, Y. Ohtsuka, S. Ohuchi, Y. Kodama, T. Oishi, 2'- and 3'-substituted sangivamycins: Conformational restriction by the *Gauche* effect, *Chem. Pharm. Bull.* 41 (1993) 775–777.

- [20] J.A.K. Howard, V.J. Hoy, D. O'Hagan, G.T. Smith, How good is fluorine as a hydrogen bond acceptor? *Tetrahedron* 52 (1996) 12613–12622.
- [21] J.D. Dunitz, R. Taylor, Organic fluorine hardly accepts hydrogen bonds, *Chem. Eur. J.* 3 (1997) 89–98.
- [22] P. Murray-Rust, W.C. Stallings, C.T. Monti, R.K. Preston, J.P. Gluster, Intermolecular interactions of the carbon-fluorine bond: The crystallographic environment of fluorinated carboxylic acids and related structures, *J. Am. Chem. Soc.* 105 (1983) 3206–3214.
- [23] E. Carosati, S. Sciabola, G. Cruciani, Hydrogen bonding interactions of covalently bonded fluorine atoms: From crystallographic data to a new angular function in the GRID force field, *J. Med. Chem.* 47 (2004) 5114–5125.
- [24] L.H. Takashashi, R. Radhakrishnan, R.E. Rosenfield, E.F. Meyer, D.A. Trainor, Crystal structure of the covalent complex formed by a peptidyl α,α -difluoro- β -keto amide with porcine pancreatic elastase at 1.78 Å resolution, *J. Am. Chem. Soc.* 111 (1989) 3368–3374.
- [25] I. Li de la Sierra, E. Papamichael, C. Sakarellos, J.L. Dimicoli, T. Prangé, Interaction of the peptide $\text{CF}_3\text{-Leu-Ala-NH-C}_6\text{H}_4\text{-CF}_3$ (TFLA) with porcine pancreatic elastase; X-ray studies at 1.8 Å, *J. Mol. Recogn.* 3 (1990) 36–44.
- [26] M.R. Groves, Z.J. Yao, P.P. Roller, T.R. Burke Jr, D. Barford, Structural basis for inhibition of the protein tyrosine phosphatase 1B by phosphotyrosine peptide mimetics, *Biochemistry* 37 (1998) 17773–17783.
- [27] J. Parsch, J.W. Engels, $\text{C-F}\cdots\text{H-C}$ Hydrogen bonds in ribonucleic acids, *J. Am. Chem. Soc.* 124 (2002) 5664–5672.
- [28] J.A. Olsen, D.W. Banner, P. Seiler, U.O. Sander, A. d'Arcy, M. Stihle, K. Muller, F. Diederich, A fluorine scan of thrombin inhibitors to map the fluorophilicity fluorophobicity of an enzyme active site: Evidence for $\text{C-F}\cdots\text{C=O}$ interactions, *Angew. Chem. Int. Ed.* 42 (2003) 2507–2511.
- [29] G. Haufe, T.C. Rosen, O.G.J. Meyer, R. Fröhlich, K. Rissanen, Synthesis, reactions and structural features of monofluorinated cyclopropanecarboxylates, *J. Fluor. Chem.* 114 (2002) 189–198.
- [30] F. Hof, D.M. Scofield, W.B. Schweizer, F. Diederich, A weak attractive interaction between organic fluorine and an amide group, *Angew. Chem. Int. Ed.* 43 (2004) 5056–5059.
- [31] X. de Leval, M. Ilies, A. Casini, J.M. Dogné, A. Scozzafava, E. Masini, F. Mincione, M. Starnotti, C.T. Supuran, Carbonic anhydrase inhibitors: Synthesis and topical intraocular pressure lowering effects of fluorine-containing inhibitors devoid of enhanced reactivity, *J. Med. Chem.* 47 (2004) 2796–2804.
- [32] J.A. Erickson, J.I. McLoughlin, Hydrogen bond donor properties of the difluoromethyl group, *J. Org. Chem.* 60 (1995) 1626–1631.
- [33] A.S. Evers, B.A. Berkowitz, D.A. d'Avignon, Correlation between the anaesthetic effect of halothane and saturable binding in brain, *Nature* 328 (1987) 157–160.
- [34] N.P. Franks, W.R. Lieb, Stereospecific effects of inhalational general anesthetic optical isomers on nerve ion channels, *Science* 254 (1991) 427–429.
- [35] A. Donetti, E. Cereda, A. Ezhaya, R. Micheletti, N-(Fluoroethyl)(imidazolylphenyl) formamidines. The issue of the active species of mifentidine, *J. Med. Chem.* 32 (1989) 957–961.
- [36(a)] R.W. Fuller, B.W. Roush, Influence of pK_a on the methylation of arylalkylamines by rabbit lung *N*-methyl transferase, *Res. Comm. Chem. Pathol. Pharmacol.* 10 (1975) 735–738.
- [36(b)] G.L. Grunewald, M.R. Seim, J. Lu, M. Makboul, K.R. Criscione, Application of the goldilocks effect to the design of potent and selective inhibitors of phenylethanolamine *N*-methyltransferase: Balancing pK_a and steric effects in the optimization of 3-methyl-1,2,3,4-tetrahydroisoquinoline inhibitors by b-fluorination, *J. Med. Chem.* 49 (2006) 2939–2952.

- [37] J.S. Lai, E.T. Kool, Fluorous base-pairing effects in a DNA polymerase active site, *Chem. Eur. J.* 11 (2005) 2966–2971.
- [38] Y. Tang, G. Ghirlanda, N. Vaidehi, J. Kua, D.T. Mainz, W.A. Goddard III, W.F. DeGrado, D.A. Tirrell, Stabilization of coiled-coil peptide domains by introduction of trifluoroleucine, *Biochemistry* 40 (2001) 2790–2796.
- [39] C. Jäckel, B. Koksche, Fluorine in peptide design and protein engineering, *Eur. J. Org. Chem.* 2005 (2005) 4483–4503.
- [40] G. Gerebtzoff, X. Li-Blatter, H. Fischer, A. Frentzel, A. Seelig, Halogenation of drugs enhances membrane binding and permeation, *ChemBiochem* 5 (2004) 676–684.
- [41] P. Jeschke, The unique role of fluorine in the design of active ingredients for modern crop protection, *ChemBiochem* 5 (2004) 570–589.
- [42] R.T. Jacobs, P.R. Bernstein, L.A. Cronk, E.P. Vacek, L.F. Newcomb, D. Aharony, C.K. Buckner, E.J. Kusner, Synthesis, structure-activity relationships, and pharmacological evaluation of a series of fluorinated 3-benzyl-5-indolecarboxamides: Identification of 4-[[5-[(2R)-2-methyl-4,4,4-trifluorobutyl]carbamoyl]-1-methylindol-3-yl]methyl]-3-methoxy-N-[(2-methylphenyl)sulfonyl]benzamide, a potent, orally active antagonist of leukotrienes D4 and E4, *J. Med. Chem.* 37 (1994) 1282–1297.
- [43] H.J. Bölm, D. Banner, S. Bendels, M. Kansy, B. Kuhn, K. Müller, U. Obst-Sander, M. Stahl, Fluorine in medicinal chemistry, *ChemBiochem* 5 (2004) 637–643.
- [44] A.B. McElroy, Application of fluorine in medicinal chemistry, in: R.E. Banks, K.C. Lowe (Eds.), *Fluorine in Medicine in the 21st Century*, Manchester University, UMIST, Manchester, 1994, Paper no. 4.
- [45] D.T.W. Chu, P.B. Fernandes, Structure-activity relationships of the fluoroquinolones, *Antimicrob. Agents Chemother.* 33 (1989) 131–135.
- [46] K. Lee, W.-H. Jung, S.Y. Hwang, S.-H. Lee, Fluorobenzamidrazone thrombin inhibitors: Influence of fluorine on enhancing oral absorption, *Bioorg. Med. Chem. Lett.* 9 (1999) 2483–2483.
- [47] M.B. van Niel, I. Collins, M.S. Beer, H.B. Broughton, S.K.F. Cheng, S.C. Goodacre, A. Heald, K.L. Locker, A.M. MacLeod, D. Morrison, C.R. Moyes, D. O'Connor, A. Pike, M. Rowley, M.G.N. Russell, B. Sohal, J.A. Stanton, S. Thomas, H. Verrier, A.P. Watt, J.L. Castro, Fluorination of 3-(3-(piperidin-1-yl)propyl)indoles and 3-(3-(piperazin-1-yl)propyl)indoles gives selective human 5-HT_{1D} receptor ligands with improved pharmacokinetic profiles, *J. Med. Chem.* 42 (1999) 2087–2104.
- [48] P. Remuzon, D. Bouzard, P. Di Cesare, M. Essiz, J.P. Jacquet, J.R. Kiechel, B. Ledoussal, R.E. Kessler, J. Fung-Tomc, Fluoronaphthyridines and -quinolones as antibacterial agents. 3. Synthesis and structure-activity relationships of new 1-(1,1-dimethyl-2-fluoroethyl), 1-[1-methyl-1-(fluoromethyl)-2-fluoroethyl], and 1-[1,1-(difluoromethyl)-2-fluoroethyl] substituted derivatives, *J. Med. Chem.* 34 (1991) 29–37.
- [49] J. Legros, B. Crousse, D. Bonnet-Delpon, J.P. Bégué, M. Maruta, Trifluoromethylcyclohexane as a new solvent? Limits of use, *Tetrahedron* 58 (2002) 4067–4070.
- [50] T.G.C. Bird, P.M. Fredericks, E.R.H. Jones, G.D. Meakins, Microbiological hydroxylation. Part 23. Hydroxylations of fluoro-5 α -androstanones by the fungi *Calonectria decora*, *Rhizopus nigricans*, and *Aspergillus ochraceus*, *J. Chem. Soc. Perkin Trans. 1* (1980) 750–755.
- [51] G. Haufe, D. Wölker, Blocking fluorine substitution in biotransformation of nortricyclanil *N*-phenylcarbamates with *Beauveria bassiana*, *Eur. J. Org. Chem.* (2003) 2159–2166.
- [52] S.L. Boulet, B.M. Mathes, K.J. Hudziak, J.R. Boot, A.H. Clugery, J.D. Findlay, A.A. Lavis, S. Mahadevan, L. Wallace, S.A. Filla, *Abstracts of Papers*, 228th National Meeting of the ACS, Philadelphia, PA, August 22–26, 2004, 58.
- [53] C.H. Mitch, T.J. Brown, F.P. Bymaster, D.O. Calligaro, D. Dieckman, L. Merrit, S.C. Peters, S.J. Quimby, H.E. Shannon, L.A. Shipley, J.S. Ward, K. Hansen, P.H. Olesen, P. Sauerberg, M.J. Sheardown, M.D.B. Swedberg, P. Suzdak, B. Greenwood, Muscarinic analgesics with potent and selective effects on the gastrointestinal tract: Potential application for the treatment of irritable bowel syndrome, *J. Med. Chem.* 40 (1997) 538–546.

- [54] B.K. Park, N.R. Kitteringham, Effects of fluorine substitution on drug metabolism: Pharmaceutical and toxicological implications, *Drug Metab. Rev.* 26 (1994) 605–643.
- [55] B.A. Hitt, R.I. Mazze, M.J. Cousins, H.N. Edmunds, G.A. Barr, J.R. Trudell, Metabolism of isoflurane in Fischer 344 rats and man, *Anesthesiology* 40 (1974) 62–67.
- [56] P.M. O'Neill, S.A. Ward, N. Berry, J.P. Jeyadevan, G. Biagini, E. Asadollaly, B.K. Park, P.G. Bray, A medicinal chemistry perspective on 4-aminoquinoline antimalarial drugs, *Curr. Top. Med. Chem.* 6 (2006) 479–507.
- [57] H. Ford, M. Siddiqui, J.S. Driscoll, V.E. Marquez, J.A. Kelley, H. Mitsuya, T. Shirasaka, Lipophilic, acid-stable, adenosine deaminase-activated anti-HIV prodrugs for central nervous system delivery. 2. 6-Halo- and 6-alkoxy prodrugs of 2'-beta-fluoro-2',3'-dideoxyinosine, *J. Med. Chem.* 38 (1995) 1189–1195.
- [58] F. Jeannot, C. Mathé, G. Gosselin, Synthesis and antiviral evaluation of 3'-C-trifluoromethylnucleoside derivatives bearing adenine as base, *Nucleosides Nucleotides Nucl. Acids* 20 (2001) 755–758.
- [59] T. Allmendinger, E. Felder, E. Hungerbuehler, in: J.T. Welch (Ed.), *Selective Fluorination in Organic and Bioorganic Chemistry*, ACS Symp. Ser. 456, ACS, Washington, DC, 1991, pp. 186–195.
- [60] J.T. Welch, J. Lin, L.G. Boros, B. DeCorte, K. Bergmann, R. Gimi, In: I. Ojima, J. McCarthy, J.T. Welch (Eds.), *Biomedical Frontiers of Fluorine Chemistry*, ACS Symp. Ser. 639, ACS, Washington, DC, 1996, pp. 129–142.
- [61] M. Hollenstein, C.J. Leumann, Fluorinated olefinic peptide nucleic acid: Synthesis and pairing properties with complementary DNA, *J. Org. Chem.* 70 (2005) 3205–3217.
- [62(a)] W.C. Black, C.I. Bayly, D.E. Davis, S. Desmarais, J.P. Falguyret, S. Léger, C.S. Li, F. Massé, D.J. McKay, J.T. Palmer, M.D. Percival, J. Robichaud, N. Tsou, R. Zamboni, Trifluoroethylamines as amide isosteres in inhibitors of cathepsin K, *Bioorg. Med. Chem. Lett.* 15 (2005) 4741–4744.
- [62(b)] C.S. Li, D. Deschenes, S. Desmarais, J.P. Falguyret, J.Y. Gauthier, D.B. Kimmel, S. Léger, F. Massé, M.E. McGrath, D.J. McKay, M.D. Percival, D. Riendeau, S.B. Rodan, M. Thérien, V.L. Truong, G. Wesolowski, R. Zambonia, W.C. Black, Identification of a potent and selective non-basic cathepsin K inhibitor, *Bioorg. Med. Chem. Lett.* 16 (2006) 1985–1989.
- [63] G.M. Blackburn, D.L. Jakemian, A.J. Ivory, M.P. Williamson, Synthesis of phosphonate analogues of 1,3-bis-phosphoglyceric acid and their binding to yeast phosphoglycerate kinase, *Bioorg. Med. Chem. Lett.* 4 (1994) 2573–2578.
- [64] G.M. Blackburn, Phosphonates as analogs of biological phosphates, *Chem. Ind. (London)* (1981) 134–138.
- [65] S. Marcotte, F. D'Hooge, S. Ramadas, C. Feasson, X. Pannecoucke, J.C. Quirion, Synthesis of new α - and β -gem-difluoromethylene C-glycosides in the galactose and glucose series, *Tetrahedron Lett.* 42 (2001) 5879–5882.
- [66] H. Berber, T. Brigaud, O. Lefebvre, R. Plantier-Royon, C. Portella, Reactions of difluoroenoxyasilanes with glycosyl donors: Synthesis of difluoro-C-glycosides and difluoro-C-disaccharides, *Chem. Eur. J.* 7 (2001) 903–909.
- [67] T.F. Herpin, W.B. Motherwell, M.J. Tozer, The synthesis of difluoromethylene-linked C-glycosides and C-disaccharides, *Tetrahedron Asymmetr.* 5 (1994) 2269–2282.
- [68] T.F. Herpin, W.B. Motherwell, J.M. Weibel, Two free radical routes for the preparation of novel difluoromethylene-linked serine-O-glycopeptide analogues, *Chem. Commun.* (1997) 923–924.
- [69] J.P. Guthrie, Carbonyl addition reactions: Factors affecting the hydrate-hemiacetal and hemiacetal-acetal equilibrium constants, *Can. J. Chem.* 53 (1975) 898–906.
- [70] H.P. Braendlin, E.T. McBee, in: M. Stacey, J.C. Tatlow, A.G. Sharp (Eds.), *Advances in Fluorine Chemistry*, Vol. 3, Butterworths, London, 1993, p. 1.
- [71] T.C. Liang, R.H. Abeles, Complex of alpha-chymotrypsin and N-acetyl-L-leucyl-L-phenylalanyl trifluoromethyl ketone: Structural studies with NMR spectroscopy, *Biochemistry* 26 (1987) 7603–7608.

- [72] M.H. Gelb, J.P. Svaren, R.H. Abeles, Fluoro ketone inhibitors of hydrolytic enzymes, *Biochemistry* 24 (1985) 1813–1817.
- [73] K. Brady, A. Wei, D. Ringe, R.H. Abeles, Structure of chymotrypsin-trifluoromethyl ketone inhibitor complexes: Comparison of slowly and rapidly equilibrating inhibitors, *Biochemistry* 29 (1990) 7600–7607.
- [74] L.H. Takahashi, R. Radhakrishnan, R.E. Rosenfield Jr., E.F. Meyer Jr., D.A. Trainor, M. Stein, X-ray diffraction analysis of the inhibition of porcine pancreatic elastase by a peptidyl trifluoromethylketone, *J. Mol. Biol.* 201 (1988) 423–428.
- [75] C.D. Poulter, In: I. Ojima, R. Mc Carthy, J. Welch (Eds.), *Biomedical Frontiers of Fluorine Chemistry*, ACS Books, ACS, Washington, DC, 1996, pp. 158–168.
- [76] M. Namchuk, C. Braun, S.G. Withers, In: I. Ojima, J.R. McCarthy, J.T. Welch (Eds.), *Biomedical Frontiers of Fluorine Chemistry*, ACS Symp. Ser. 639, ACS, Washington, DC, 1996, pp. 279–293.
- [77] M. Hudlicky, *Chemistry of Organic Fluorine Compounds*, 2nd edition, Ellis Horwood, Chitester p. 548.
- [78] J. Kollonitsch, A.A. Patchett, S. Marburg, A.L. Maycock, L.M. Perkin, G.A. Doldouras, D.E. Duggan, S.D. Aster, Selective inhibitors of biosynthesis of aminergic neurotransmitters, *Nature* 274 (1978) 906–908.
- [79(a)] E. Wang, C. Walsh, Suicide substrates for the alanine racemase of *Escherichia coli* B, *Biochemistry* 17 (1978) 1313–1321.
- [79(b)] E. Wang, C. Walsh, Characteristics of β , β -difluoroalanine and β , β , β -trifluoroalanine as suicide substrates for *E. coli* B alanine racemase, *Biochemistry* 20 (1981) 7539–7546.
- [80] J.E. Barrett, D.A. Maltby, D.V. Santi, P.G. Schultz, Trapping of the C5 methylene intermediate in thymidylate synthase, *J. Am. Chem. Soc.* 120 (1998) 449–450.
- [81] G.J. Peters, C.L. van der Wilt, B. van Triest, G. Cadacci-Pisanelli, P.G. Johnston, C.J. van Groeningen, H.M. Pinedo, Thymidylate synthase and drug resistance, *Eur. J. Cancer Part A* 31A(7/8) (1995) 1299–1305.
- [82] G.J. Peters, H.H.J. Backus, S. Freemantle, B. van Triest, G. Cadacci-Pisanelli, C.L. van der Wilt, K. Smid, J. Lunec, A.H. Calvert, S. Marsh, H.L. McLeod, E. Bloemena, S. Meijer, G. Jansen, C.J. van Groeningen, H.M. Pinedo, Induction of thymidylate synthase as a 5-fluorouracil resistance mechanism, *Biochem. Biophys. Acta (Molecular Basis of Disease)* 1587 (2002) 194–205.
- [83] C. Heidelberger, N.K. Chaudhuri, P. Danenberg, D. Mooren, L. Griesbach, R. Duschinsky, J. Schnitzer, E. Plevin, J. Scheiner, Fluorinated pyrimidines: A new class of tumour-inhibitory compounds, *Nature* 179 (1957) 663–666.
- [84] M. Malet-Martino, P. Jolimaitre, R. Martino, The prodrugs of 5-fluorouracil, *Curr. Med. Chem. Anticancer agents* 2 (2002) 267–310.
- [85] K.L. Kirk, R. Filler, In: I. Ojima, J.R. McCarthy, J.T. Welch (Eds.), *Biomedical Frontiers of Fluorine Chemistry*, ACS Symp. Ser. 639, Am. Chem. Soc., Washington, DC, 1996, p. 2.
- [86] K.T. Douglas, *Anticancer drugs* 1, *Chem. Ind. (London)* (1984) 693–698.
- [87] C. Levy-Piedbois, I. Durand-Zaleski, H. Juhel, C. Schmitt, A. Bellanger, P. Piedbois, Cost-effectiveness of second-line treatment with irinotecan or infusional 5-fluorouracil in metastatic colorectal cancer, *Ann. Oncol.* 11 (2000) 157–161.
- [88] R.M. Mader, M.S. Mueller, G.G. Steger, Resistance to 5-fluorouracil, *Gen. Pharmac.* 31 (1998) 661–666.
- [89(a)] C.J.A. Punt, New drugs in the treatment of colorectal carcinoma, *Cancer* 83 (1998) 679–689.
- [89(b)] N.J. Meropol, Oral fluoropyrimidines in the treatment of colorectal cancer, *Eur. J. Cancer* 34 (1998) 1509–1513.
- [89(c)] R.D. Petty, J. Cassidy, Novel fluoropyrimidines: Improving the efficacy and tolerability of cytotoxic therapy, *Curr. Cancer Drug. Targets* 4 (2004) 191–204.
- [90(a)] J. Feliu, J.M. Vicent, C. Garcia-Giron, M. Constella, E. Fonseca, J. Anton-Aparicho, M. Lomas, L.A. Aparicio, F.J. Dorta, M. Gonzalez-Baron, Phase II study of UFT and oxaliplatin in first-line treatment of advanced colorectal cancer, *Br. J. Cancer* 91 (2004) 1758–1762.

- [90(b)] T. Shirasaka, K. Nakano, T. Takechi, H. Siatake, J. Uchda, A. Fujioka, H. Saito, H. Okabe, K. Oyama, S. Takeda, N. Unemi, M. Fukushima, against human colon carcinoma orthotopically implanted into nude rats, *Cancer Res.* 56 (1996) 2602–2606.
- [90(c)] G. Xu, L.H.L. McLeod, Strategies for enzyme/prodrug cancer therapy, *Clin. Cancer Res.* 7 (2001) 3314–3324.
- [91(a)] H. Kawakami, T. Ebata, K. Koseki, H. Matsushita, Y. Naoi, K. Itoh, N. Mizutani, The synthesis of 2'-deoxy-5-trifluoromethyluridine utilizing a coupling reaction, heterocycles 31 (1990) 569–574.
- [91(b)] H. Ishibashi, *Jpn Kokai Tokkyo Koho JP*, Chem. Abstr 143, 2005267194 2005239552.
- [92] R. McCarthy, P.S. Sunkara, D.P. Matthews, A.J. Bitonti, E.J. Jarvi, J.S. Sabol, R.J. Resvick, E.W. Huber, W.A. van der Donk, G. Yu, J.A. Stubbe, In: I. Ojima, J. McCarthy, J.T. Welch (Eds.), *Biomedical Frontiers of Fluorine Chemistry*, ACS Symp. Ser. 639, ACS, Washington, DC, 1996, pp. 246–264.
- [93] L.W. Hertel, J.S. Kroin, C.S. Grossman, G.B. Grindey, A.F. Dorr, A.M.V. Stornio, W. Plunkett, V. Ganghi, P. Huang, In: I. Ojima, J. McCarthy, J.T. Welch (Eds.), *Biomedical Frontiers of Fluorine Chemistry*, ACS Symp. Ser. 639, ACS, Washington, DC, 1996, pp. 265–278.
- [94] H. Brachwitz, J. Bergmann, Y. Thomas, T. Wollny, P. Langen, Synthesis and anti-proliferative potency of 9- β -D-arabinofuranosyl-2-fluoroadenine phospholipid adducts, *Biorg. Chem. Med.* 7 (1999) 1195–1200.
- [95] Y. Matsumura, H. Fujii, T. Nakayama, Y. Morizawa, A. Yasuda, Titanium-promoted highly stereoselective synthesis of α,α -difluoro- β,γ -dihydroxyester. Simple route to 2-deoxy-2,2-difluororibose, *J. Fluor. Chem.* 57 (1992) 203–207.
- [96] R. Fernandez, M.I. Matheu, R. Echarri, S. Castillon, Synthesis of 2-deoxy-3,5-di-O-benzoyl-2,2-difluoro-D-ribose from D-glucose and D-mannose. A formal synthesis of gemcitabine, *Tetrahedron* 54 (1998) 3523–3532.
- [97] K. Chilman-Blair, N.E. Mealy, J. Castaner, Clofarabine. Treatment of acute leukemia, *Drugs Fut.* 29 (2004) 112–120.
- [98] N.E. Mealy, M. Bayés, Annual update 2003: Gastrointestinal drugs, *Drugs Fut.* 28 (2003) 829–840.
- [99(a)] N.E. Mealy, M. Bayés, Annual update 2003: Drugs for pain and anesthesia, *Drugs Fut.* 28 (2003) 493.
- [99(b)] N.E. Mealy, Annual update 2003/2004: Treatment of genitourinary disorders, *Drugs Fut.* 29 (2004) 797.
- [100] J.C. Jacquesy, J. Fahy, In: P.F. Torrence(Ed.), *Biomedical Chemistry: Applying Chemical Principles to the Understanding and Treatment of Disease*, Wiley Ed., New York, 2000, pp. 227–246.
- [101(a)] P. Mangeney, R.Z. Andriamialisoa, J.Y. Lallemand, N. Langlois, Y. Langlois, P. Potier, 5'-Nor anhydrovinblastine: Prototype of a new class of vinblastine derivatives, *Tetrahedron* 35 (1979) 2175–2179.
- [101(b)] B.T. Hill, H.H. Fiebig, W.R. Waud, M.F. Poupon, F. Colpaert, A. Kruczynski, Superior *in vivo* experimental antitumour activity of vinflunine, relative to vinorelbine, in a panel of human tumour xenografts, *Eur. J. Cancer* 35 (1999) 512–520.
- [102] J.A. McIntyre, J. Castaner, Vinflunine. Antimitotic, Vinca alkaloid, *Drugs Fut.* 29 (2004) 574–580.
- [103] J.C. Jacquesy, In: G.K.S. Prakash, P.V.R. Schleyer (Eds.), *Stable Carbocation Chemistry*, Wiley Intersciences, New York, 1997, pp. 549–574 Chapter 17.
- [104] S. Debarge, S. Thibaudeau, B. Violeau, A. Martin-Mingot, M.P. Jouannetaud, J.C. Jacquesy, A. Cousson, Rearrangement or *gem*-difluorination of quinine and 9-epiquinine and their acetates in superacid, *Tetrahedron* 61 (2005) 2065–2073.
- [105] J. Fahy, A. Duflos, J.P. Ribet, J.C. Jacquesy, C. Berrier, M.P. Jouannetaud, F. Zunino, Vinca alkaloids in superacidic media: A method for creating a new family of antitumor derivatives, *J. Am. Chem. Soc.* 119 (1997) 8576–8577.

- [106(a)] C. Berrier, J.C. Jacquesy, M.P. Jouannetaud, C. Lafitte, Y. Vidal, F. Zunino, J. Fahy, A. Duflos, Functionalization of a nonactivated C–H bond: Fluorination of vindoline at C-20 in superacids, *Tetrahedron* 54 (1998) 13761–13770.
- [106(b)] J.C. Jacquesy, C. Berrier, M.P. Jouannetaud, F. Zunino, J. Fahy, A. Duflos, J.P. Ribet, Fluorination in superacids: A novel access to biologically active compounds, *J. Fluorine Chem.* 114 (2002) 139–141.
- [107] M.E. Wall, Camptothecin and taxol: Discovery to clinic, *Med. Res. Rev.* 18 (1998) 299–314.
- [108] K. Chilman-Blair, N.E. Mealy, J. Castaner, M. Bayés, Exatecan mesilate. Anticancer agent, DNA topoisomerase I, *Drugs Fut.* 29 (2004) 9–22.
- [109(a)] O. Lavergne, D. Demarquay, C. Bailly, C. Lanco, A. Rolland, M. Huchet, H. Coulomb, N. Muller, N. Baroggi, J. Camara, C. Le Breton, E. Manginot, J.B. Cazaux, D.C.H. Bigg, Topoisomerase I-mediated antiproliferative activity of enantiomerically pure fluorinated homocamptothecins, *J. Med. Chem.* 43 (2000) 2285–2289.
- [109(b)] N.E. Mealy, M. Bayés, Annual Update 2004–2005 Treatment Respiratory/Thoracic Cancer, *Drugs Fut.* 30 (2005) 109–112.
- [110] R.S. Tangirala, R. Dixon, D. Yang, A. Ambrus, S. Antony, K. Agama, Y. Pommier, D.P. Curran, Total and semisynthesis and *in vitro* studies of both enantiomers of 20-fluorocamptothecin, *Bioorg. Med. Chem. Lett.* 15 (2005) 4736–4740.
- [111] N. Shibata, T. Ishimaru, M. Nakamura, T. Toru, 20-Deoxy-20-fluorocamptothecin: Design and synthesis of Camptothecin isostere, *Synlett* (2004) 2509–2512.
- [112] Y.J. You, Y. Kim, N.H. Nam, S.C. Bang, B.Z. Ahn, Alkyl and carboxylalkyl esters of 4'-demethyl-4-deoxypodophyllotoxin: Synthesis, cytotoxic, and antitumor activity, *Eur. J. Med. Chem.* 39 (2004) 189–193.
- [113] L. Schacter, Etoposide phosphate: What, why, where and how, *Semin. Oncol.* 23 (6 Suppl. 13) (1996) 1–7.
- [114(a)] T. Imbert, Y. Guminski, B. Monse, B. Hill, J.P. Robin, (Pierre Fabre Medicament, Fr.), PCT Int. Appl. (1996) WO 9612727 (*Chem. Abstr.* 125, 115059).
- [114(b)] J.M. Sargent, A.W. Elgie, C.J. Williamson, B.T. Hill, Ex vivo effects of the dual topoisomerase inhibitor tafluposide (F 11782) on cells isolated from fresh tumor samples taken from patients with cancer, *Anticancer Drugs* 14 (2003) 467–473.
- [114(c)] A. Kruczynski, J.M. Barret, B. Van Hille, N. Chansard, J. Astruc, Y. Menon, C. Duchier, L. Creancier, B. Hill, Decreased nucleotide excision repair activity and alterations of topoisomerase II α are associated with the *in vivo* resistance of a P388 Leukemia subline to F11782, a novel catalytic inhibitor of topoisomerases I and II, *Clin. Cancer Res.* 10 (2004) 3156–3168.
- [115] L.W. Hertel, R.J. Ternansky, In: R. Filler (Ed.), *Organofluorine Compounds in Medicinal Chemistry and Biological Applications*, Elsevier, Amsterdam, 1993, pp. 38–52.
- [116] A. Guidi, F. Canfarini, A. Giolitti, F. Pasqui, V. Pestillini, F. Arcamone, In Anthracycline Antibiotics, ACS Symp. Ser. 574 ACS, Washington DC, 1995, pp. 47–58.
- [117(a)] G. Giannini, Fluorinated anthracyclines: Synthesis and biological activity, *Med. Chem. Rev. On line* 1 (2004) 47–71.
- [117(b)] T. Matsumoto, M. Ohsaki, F. Matsuda, S. Terashima, Efficient synthesis and antitumor activity of novel 14-fluoroanthracyclines, *Tetrahedron Lett.* 28 (1987) 4419–4422.
- [117(c)] F. Matsuda, T. Matsumoto, M. Ohsaki, S. Terashima, Synthesis of 14,14-difluoro-4-demethoxydaunorubicin, *Bull. Chem. Soc. Jpn.* 64 (1991) 2983–2989.
- [118] Y. Takagi, K. Nakai, T. Tsuchiya, T. Takeuchi, A 5'-(Trifluoromethyl)anthracycline glycoside: Synthesis of antitumor-active 7-O-(2,6-dideoxy-6,6,6-trifluoro- α -L-lyxohexopyranosyl)adriamycinone, *J. Med. Chem.* 39 (1996) 1582–1588.
- [119] L. Toscano, L. Cappelletti, M. Leonardo (Pierrel S.p.A.), *Eur. Pat. Appl.* (1982) EP 82–200019 19820108 (*Chem. Abstr.* 97, 196812).
- [120] A.J. Poss, G.A. Shia (Allied Signal), PCT Int. Appl. (1996) WO 9608502 WO 95-US11098 19950905 (*Chem. Abstr.* 125, 87097).

- [121] X. Xu, T. Henninger, D. Abbanat, K. Bush, B. Foleno, J. Hilliard, M. Macielag, Synthesis and antibacterial activity of C2-fluoro, C6-carbamate ketolides, and their C9-oximes, *Bioorg. Med. Chem. Lett.* 15 (2005) 883–887.
- [122] C.H. Liang, S. Yao, Y.H. Chiu, P.Y. Leung, N. Robert, J. Seddon, P. Sears, C.K. Hwang, Y. Ichikawa, A. Romero, Synthesis and biological activity of new 5-O-sugar modified ketolide and 2-fluoro-ketolide antibiotics, *Bioorg. Med. Chem. Lett.* 15 (2005) 1307–1310.
- [123] A. Denis, A. Bonnefoy, Novel fluoroketolides: Synthesis and antibacterial activity, *Drugs Fut.* 26 (2001) 975–984.
- [124] R.J.M. Goss, H. Hong, A novel fluorinated erythromycin antibiotic, *Chem. Comm.* (2005) 3983–3985.
- [125] K.C. Nicolaou, F. Roschangar, D. Vourloumis, Chemical biology of Epothilones, *Angew. Chem. Int. Ed.* 37 (1998) 2014–2045.
- [126] T.C. Chou, H. Dong, A. Rivkin, F. Yoshimura, A.E. Gabarda, Y.S. Cho, W.P. Tong, S.J. Danishefsky, Design and total synthesis of a superior family of Epothilone analogues, which eliminate xenograft tumors to a nonrelapsable state, *Angew. Chem. Int. Ed.* 42 (2003) 4762–4767.
- [127] A. Rivkin, T.C. Chou, S.J. Danishefsky, On the remarkable antitumor properties of Fludelone: How we got there, *Angew. Chem. Int. Ed.* 44 (2005) 2838–2850.
- [128] A. Rivkin, F. Yoshimura, A.E. Gabarda, Y.S. Cho, T.C. Chou, H. Dong, S.J. Danishefsky, Discovery of (*E*)-9,10-dehydroepothilones through chemical synthesis: On the emergence of 26-trifluoro-(*E*)-9,10-dehydro-12,13-desoxyepothilone B as a promising anticancer drug candidate, *J. Am. Chem. Soc.* 126 (2004) 10913–10922.
- [129] Y.S. Cho, K.D. Wu, M.A.S. Moore, T.C. Chou, S.J. Danishefsky, Second-generation epothilones: Discovery of fludelone and its extraordinary antitumor properties, *Drugs Fut.* 30 (2005) 737–746.
- [130] J. Fried, E.F. Sabo, 9 α -Fluoro derivatives of cortisone and hydrocortisone, *J. Am. Chem. Soc.* 76 (1954) 1455–1456.
- [131] C.M. Weeks, W.L. Duax, M.E. Wolff, Comparison of the molecular structures of six corticosteroids, *J. Am. Chem. Soc.* 95 (1973) 2865–2868.
- [132] M.E. Wolff, J.D. Baxter, P.A. Kollman, D.L. Lee, I.D. Kuntz, E. Bloom, D.T. Matulich, J. Morris, Nature of steroid-glucocorticoid receptor interactions: Thermodynamic analysis of the binding reaction, *Biochemistry* 16 (1978) 3201–3208.
- [133] B. Kauppi, C. Jakob, M. Färnegårdh, J. Yang, H. Ahola, M. Alarcon, K. Calles, O. Engström, J. Harlan, S. Muchmore, A.K. Ramqvist, S. Thorell, L. Öhman, J. Greer, J.Å. Gustafsson, J. Carlstedt-Duke, M. Carlquist, The three-dimensional structures of antagonistic and agonistic forms of the glucocorticoid receptor ligand-binding domain: RU-486 induces a transformation that leads to active antagonist, *J. Biol. Chem.* 278 (2003) 22748–22754.
- [134] I.E. Bush, V.B. Mahesh, Metabolism of 11-oxygenated steroids. 3. Some 1-dehydro and 9 α -fluoro steroids, *J. Biochem.* 93 (1964) 236–255.
- [135] S.M. Abel, D.J. Back, J.L. Maggs, B.K. Park, Cortisol metabolism by human liver *in vitro*. IV. Metabolism of 9 α -fluorocortisol by human liver microsomes and cytosol, *J. Steroid Biochem. Mol. Biol.* 46 (1993) 833–839.
- [136] J. Fried, E.F. Sabo, Halogenated corticoids. I. 9 α -halogen derivatives of cortisone and hydrocortisone, *J. Am. Chem. Soc.* 79 (1957) 1130–1141.
- [137] A. Bowers, Steroids. CXXIX. A new general route to fluorinated steroids, *J. Am. Chem. Soc.* 81 (1959) 4107–4108.
- [138] J. Fried, J.A. Edwards, *Organic Reactions in Steroid Chemistry*, 1 Von Nostrand, Reinhold Publ., New York, 1972, Vol. 1, p. 432.
- [139] S. Nakanishi, R.L. Morgan, E.V. Jensen, 4-Fluorinated steroids from the reaction of perchloryl fluoride with steroid enamines, *Chem. Ind. (London)* (1960) 1136–1137.
- [140(a)] D.H.R. Barton, J. Lester, S.V. Ley, Electrophilic fluorination of activated olefins: The synthesis of 6-fluorocorticosteroids, *New. J. Chem.* 1 (1977) 315–326.

- [140(b)] Daikin Kogyo Co Ltd EP 0118660 (1984).
- [141] G.S. Lal, Site-selective fluorination of organic compounds using 1-alkyl-4-fluoro-1,4-diazabicyclo[2.2.2]octane salts (selectfluor reagents), *J. Org. Chem.* 58 (1993) 2791–2796.
- [142(a)] G.E. Arth, D.B.R. Johnston, J. Fried, W.W. Spooncer, D.R. Hoff, L.H. Sarett, 16-Methylated steroids. I. 16 α -methylated analogs of cortisone: A new group of anti-inflammatory steroids, *J. Am. Chem. Soc.* 80 (1958) 3160–3161.
- [142(b)] G.E. Arth, J. Fried, D.B.R. Johnston, D.R. Hoff, L.H. Sarett, R.H. Silber, H.C. Stoerk, C.A. Winter, 16-Methylated steroids. I. 16 α -methylated analogs of cortisone, A new group of anti-inflammatory steroids, 9 α -halo derivatives, *J. Am. Chem. Soc.* 80 (1958) 3161–3163.
- [142(c)] Roussel-UCLAF GB 916709 (1963) (Chem. Abstr. 58, 81781).
- [143] J.A. Godard, In: R.E. Banks, K.C. Lowe (Eds.), *Fluorine in Medicine in the 21st Century*, Conference Papers, Manchester University, UMIST, Manchester, 1994.
- [144] K.P. Shephard, (Upjohn), US Patent, 4102907 (1978).
- [145] R. Stevenson, F.W. Kerr, R. Anthony, E.J. Brazier, P.J. Hogan, D.D.P. David (Astra-Zeneca), PCT Int. Appl. 2002032922 (2002) (Chem. Abstr. 136, 340869).
- [146] (a) W.O. Gottfredsen, S. Vangedal, 6 α -Trifluoromethyl-17 α -acetoxyprogesterone and some unsaturated analogs, *Acta Chem. Scand.* 15 (1961) 1786–1788.
- [146(b)] H.Y. Lan-Hargest, J.D. Elliot, D.S. Eggleston, B.W. Metcalf, The photochemical rearrangement of a steroidal dienol triflate, *Tetrahedron Lett.* 28 (1987) 6557–6560.
- [146(c)] G.H. Rasmusson, R.D. Brown, G.E. Arth, Photocatalyzed reaction of trifluoromethyl iodide with steroidal dienones, *J. Org. Chem.* 40 (1975) 672–675.
- [147] J.C. Blazejewski, M.P. Wilmshurst, M.D. Popkin, C. Wakselman, G. Laurent, D. Nonclercq, A. Cleeren, Y. Ma, H.S. Seo, G. Leclercq, Synthesis, characterization and biological evaluation of 7 α -Perfluoroalkylestradiol derivatives, *Bioorg. Med. Chem.* 11 (2003) 335–345.
- [148] U. Fuhrmann, H. Hess-Stumpp, A. Cleve, G. Neef, W. Schwede, J. Hoffmann, K.H. Fritzemeier, K. Chwalisz, Synthesis and biological activity of a novel, highly potent progesterone receptor antagonist, *J. Med. Chem.* 43 (2000) 5010–5016.
- [149] R.K. Bakshi, G.H. Rasmusson, G.F. Patel, R.T. Mosley, B. Chang, K. Ellsworth, G.S. Harris, R.L. Tolman, 4-Aza-3-oxo-5 α -androst-1-ene-17 β -N-arylcarboxamides as dual inhibitors of human type 1 and type 2 steroid 5 α -reductases. Dramatic effect of N-aryl substituents on type 1 and type 2 5 α -reductase inhibitory potency, *J. Med. Chem.* 38 (1995) 3189–3192.
- [150(a)] K.W. Gee, N.C. Lan (Cocensys, Inc., USA), PCT Int. Appl. (1994) WO 9427608 (Chem. Abstr. 122, 291311);
- [150(b)] R.B. Upasani, D.B. Fick, D.J. Hogenkamp, N.C. Lan (Cocensys, Inc., USA), PCT Int. Appl. (1996) WO 9640043 (Chem. Abstr. 126, 131695).
- [151(a)] H.F. DeLuca, H.K. Schnoes, Vitamin D: recent advances, *Ann. Rev. Biochem.* 52 (1983) 411–439.
- [151(b)] L.L. Issa, G.M. Leong, R.L. Sutherland, J.A. Eisman, Vitamin D analogue-specific recruitment of vitamin D receptor coactivators, *J. Bone Miner. Res.* 17 (2002) 879–890.
- [151(c)] R.A. Ettinger, H.F. DeLuca, The vitamin D endocrine system and its therapeutical potential, *Adv. Drug Res.* 28 (1996) 269–312.
- [152(a)] D. Scheddin, H. Moyer, B. Schönecker, S. Gliesling, M. Reichenbacher, Synthesis and biological activities of 2 β -chloro-, 2 β -fluoro-, and 2 β -methoxy-1 α ,25-dihydroxyvitamin D₃, *Steroids* 63 (1998) 633–643.
- [152(b)] M. Shimizu, Y. Terasaki, S. Yamada, 4,4-Difluoro-1 α ,25-dihydroxyvitamin D₃: Analog to probe A-ring conformation in vitamin D-receptor complex, *Tetrahedron Lett.* 40 (1999) 1697–1700.
- [152(c)] G.H. Posner, B.T. Wooddard, K.R. Crawford, S. Peleg, A.J. Brown, P. Dolan, T.W. Kensler, 2,2-Disubstituted analogues of the natural hormone 1 α ,25-dihydroxyvitamin D₃: Chemistry and biology, *Bioorg. Med. Chem.* 10 (2002) 2353–2365.

- [153] G. Giuffredi, C. Bobbio, V. Gouverneur, Enantioselective synthesis of a key "A-Ring" intermediate for the preparation of 1α -Fluoro vitamin D₃ analogues, *J. Org. Chem.* 71 (2006) 5361–5364.
- [154] NME Digest, *Drug News Perspect.* 16 (2003) 122.
- [155(a)] Y. Kobayashi, T. Taguchi, S. Mitsuhashi, T. Eguchi, E. Ohshima, N. Ikekawa, Synthesis in organofluorine chemistry XXXIX. Studies on steroids LXXIX. Synthesis of 1α -hydroxy-26,26,26,27,27,27-hexafluorovitamin D₃, *Chem. Pharm. Bull.* 30 (1982) 4297–4303.
- [155(b)] K. Iseki, T. Nagai, Y. Kobayashi, Synthesis of 24-homo-26,26,26,27,27,27-hexafluoro- 1α ,22,25-trihydroxyvitamin D₃, *Chem. Pharm. Bull.* 40 (1992) 1346–1348.
- [156] K. Iseki, Y. Kobayashi, in: I. Ojima, J. McCarthy, J. Welch (Eds.), *Biomedical Frontiers of Fluorine Chemistry*, ACS Symp. Ser. 639, ACS, Washington, DC, 1996, pp. 214–227.
- [157] K. Ando, F. Kondo, F. Koike, H. Takayama, Synthesis of 24,24-difluoro- 1α -dihydro-vitamin D₃ from vitamin D₂, *Chem. Pharm. Bull.* 40 (1992) 1662–1664.
- [158] G.H. Posner, Q. Wang, G. Han, J.K. Lee, K. Crawford, S. Zand, H. Brem, S. Peleg, P. Dolan, T.W. Kensler, Conceptually new sulfone analogues of the hormone 1α ,25-dihydroxyvitamin D₃: Synthesis and preliminary biological evaluation, *J. Med. Chem.* 42 (1999) 3425–3435.
- [159] M. Ikeda, H. Matsumura, N. Sawada, K. Hashimoto, T. Tanaka, T. Noguchi, M. Hayashi, Synthesis and biological evaluations of C-23-modified 26,26,26,27,27,27-F₆-vitamin D₃ analogues, *Bioorg. Med. Chem.* 8 (2000) 1809–1817.
- [160] A. Ohno, M. Shimizu, S. Yamada, Fluorinated vitamin D analogs to probe the conformation of vitamin D in its receptor complex: ¹⁹F-NMR studies and biological activity, *Chem. Pharm. Bull.* 50 (2002) 475–483.
- [161] Y. Matsumura, T. Nakano, T. Asai, Y. Morizawa, In: I. Ojima, J. McCarthy, J. Welch (Eds.), *Biomedical Frontiers of Fluorine Chemistry*, ACS Symp. Ser. 639, ACS, Washington DC, 1996, pp. 83–94.
- [162] M. Prakesch, D. Grée, S. Chandrasekhar, R. Grée, Synthesis of fluoro analogues of unsaturated fatty acids and corresponding acyclic metabolites, *Eur. J. Org. Chem.* (2005) 1221–1232.
- [163] J.P. Bégué, D. Bonnet-Delpon, F. Benayoud, T.T. Tidwell, R.A. Cox, A. Allen, Comparison of the formation energy of fluorinated alkoxy-carbenium ions, *Gazz. Chim. Ital.* 125 (1995) 399–402.
- [164] C.S. Chang, M. Negishi, T. Nakano, Y. Morizawa, Y. Matsumura, A. Ichikawa, 7,7-Difluoroprostacyclin derivative, AFP-07, a highly selective and potent agonist for the prostacyclin receptor, *Prostaglandins* 53 (1997) 83–90.
- [165] P.W. Collins, R.L. Shone, A.F. Gasieski, W.E. Perkins, R.G. Bianchi, Stabilization of a prostaglandin tertiary allylic alcohol system by fluorine: Synthesis, acid stability studies and pharmacology of a 16-fluoromethyl analog of SC-46275, *Bioorg. Med. Chem. Lett.* 2 (1992) 1761–1766.
- [166] L.A. Sorbera, J. Castaner, N.E. Mealy, Lubiprostone. Treatment of constipation, treatment of irritable bowel syndrome, treatment of postoperative ileus, CIC-2 channel activator, *Drugs Fut.* 29 (2004) 336–342.
- [167] A.I. Graul, A.M. Collins, Annual Update: Ophthalmic Drugs, *Drugs Fut.* 28 (2003) 306.
- [168] Y. Matsumura, N. Mori, T. Nakano, H. Sasakura, T. Matsugi, H. Hara, Y. Morizawa, Synthesis of the highly potent prostanoid FP receptor agonist, AFP-168: A novel 15-deoxy-15,15-difluoroprostaglandin F_{2 α} derivative, *Tetrahedron Lett.* 45 (2004) 1527–1529.
- [169] J.P. Bégué, D. Bonnet-Delpon, The future of antimalarials: Artemisinins and synthetic endoperoxides, *Drugs Fut.* 30 (2005) 509–518.
- [170] N. Truong Thi Thanh, C. Ménage, J.P. Bégué, D. Bonnet-Delpon, J.C. Gantier, B. Pradines, J.C. Doury, T. Truong Dinh, Synthesis and antimalarial activities of fluoroalkyl derivatives of dihydroartemisinin, *J. Med. Chem.* 41 (1998) 4101–4108.

- [171] J.P. Bégué, D. Bonnet-Delpon, Fluoroartemisinins: Metabolically more stable anti-malarial artemisinin derivatives, *ChemMed Chem.* 2 (2007) 608–624.
- [172] F. Grellepois, F. Chorki, M. Ourévitch, S. Charneau, P. Grellier, K.A. McIntosh, W.N. Charman, B. Pradines, B. Crousse, D. Bonnet-Delpon, J.P. Bégué, Orally active antimalarials: Hydrolytically stable derivatives of 10-trifluoromethyl anhydrodi-hydroartemisinin, *J. Med. Chem.* 47 (2004) 1423–1433.
- [173] G. Magueur, B. Crousse, S. Charneau, P. Grellier, J.P. Bégué, D. Bonnet-Delpon, Fluoroartemisinin: Trifluoromethyl analogues of artemether and artesunate, *J. Med. Chem.* 47 (2004) 2694–2699.
- [174] V.P. Kukhar, V.A. Soloshonok *Fluorine-Containing Amino acids, and Properties*, Wiley & Sons, New York, 1995.
- [175] C. Jäckel, W. Seufert, S. Thust, B. Koksche, Evaluation of the molecular interactions of fluorinated amino acids with native polypeptides, *ChemBioChem.* 5 (2004) 717–720.
- [176] W. Metcalf, P. Bey, C. Danzin, M.J. Jung, P. Casara, J.P. Vever, Catalytic irreversible inhibition of mammalian ornithine decarboxylase (E.C.4.1.1.17) by substrate and product analogs, *J. Am. Chem. Soc.* 100 (1978) 2551–2553.
- [177] C. di Bari, G. Pastore, G. Roscigno, P.J. Schechter, A. Sjoerdsma, Late-stage African trypanosomiasis and eflornithine, *Ann. Intern. Med.* 105 (1986) 803–804.
- [178] P. Bey, J.P. Vever, V. Van Dorsselaer, M. Kolb, Direct synthesis of alpha-halogenomethyl-alpha-amino acids from the parent alpha-amino acids, *J. Org. Chem.* 44 (1979) 2732–2742.
- [179] J. Zhu, B.A. Price, J. Walker, S.X. Zhao, Catalytic hydrogenation of ethyl 2-amino-2-difluoromethyl-4-cyanobutanoate and its Schiff base reaction modes, *Tetrahedron Lett.* 46 (2005) 2795–2797.

CHAPTER 14

Synthesis and Pharmacological Properties of Fluorinated Prostanoids

Yasushi Matsumura*

Advanced Organic Synthesis Laboratory, Asahi Glass Co., Ltd, 1150 Hazawa-cho, Kanagawa-ku, Yokohama 221-8755, Japan

Contents

1. Introduction	624
1.1. Biosynthesis and metabolism of prostanoids	624
1.2. Physiological properties of prostanoids and their receptors	626
1.3. Historical background of fluorinated prostanoids research	628
2. PGE Derivatives	630
2.1. 13,14-dihydro-15-keto-PGE derivative	630
2.2. EP1 receptor antagonist	632
2.3. EP2 receptor agonist	635
2.4. EP4 receptor agonist	636
3. PGF derivatives	637
3.1. FP receptor agonist	637
3.2. FP receptor antagonist	641
4. PGD derivatives	642
4.1. DP receptor agonist and antagonist	642
4.2. CRTH2 receptor agonist	644
4.3. CRTH2 receptor antagonist	644
5. PGI derivatives	646
5.1. IP receptor agonist	646
6. Concluding remarks	649
Acknowledgments	652
References	652

Abstract

Prostaglandins (PGs) and thromboxanes (TXs) are locally produced hormones exhibiting a broad variety of biological functions. Application of natural prostanoids as drugs is faced with the problem of both chemical and metabolic instability of these compounds. Consequently, much efforts have been made to find compounds having optimal biological profile. In the seventies and eighties of last century, the high potential of chemical modification with fluorine in drug design of prostanoids has been shown. Substitution of a specific

*Corresponding author. Tel.: +81-45-374-7744; Fax: +81-45-374-8859;
Email: yasushi-matsumura@agc.co.jp

position in prostanoids by a fluorinated moiety affects not only the molecular conformation but also the drug-receptor complex through a possible contribution of fluorine to the nature and strength of the interaction. Enhancement of lipophilicity of prostanoids by fluorination may be an efficient strategy to increase the specific affinity to a hydrophobic pocket of the receptor. In accord with the progress in molecular biology of prostanoid receptors, new fluorinated prostanoids have been developed recently. In this chapter, the synthesis and pharmacological properties of novel fluorinated PGE, PGF, PGD, and PGI derivatives in development are reviewed.

1. INTRODUCTION

1.1. Biosynthesis and metabolism of prostanoids

Prostanoids, which consist of prostaglandins (PGs) and thromboxanes (TXs), are biologically synthesized in the body from arachidonic acid by cyclooxygenase, PG hydroperoxydase, and a family of prostaglandin synthases (Fig. 1). They exert a variety of actions as hormones produced locally in various tissues and cells to maintain homeostasis.

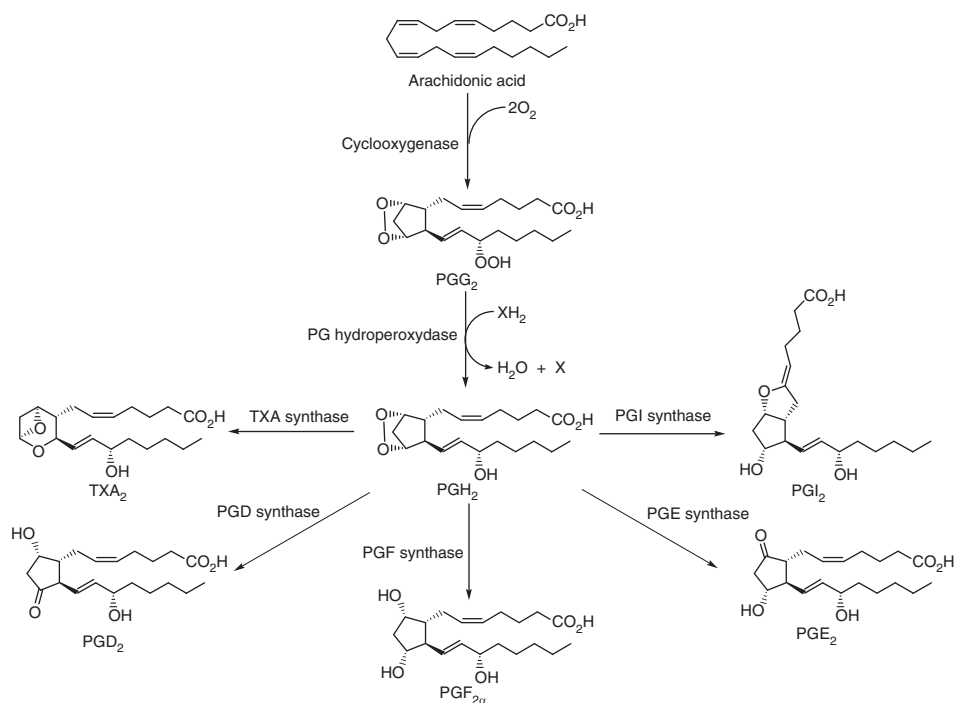


Fig. 1. Biosynthesis of prostanoids.

Research directed toward understanding the physiological and pharmacological roles of prostanoids has stimulated drug development of natural or synthetic analogs in the broad range of therapeutic areas [1]. One of the main problems with the natural prostanoids as drugs has been perceived to be both chemical and metabolic instability. For example, PGI_2 is rapidly hydrolyzed at neutral pH in a few minutes, and TXA_2 is even more labile. PGE_2 is deteriorated by the following metabolism and also by nonenzymatic dehydration of 11-hydroxy group. The initial step in the metabolism of PGE_2 is the oxidation of the 15-hydroxy group to the corresponding 15-oxo- PGE_2 by an NAD^+/NADP -linked enzyme, 15-hydroxy-PG dehydrogenase. The resulting 15-oxo-metabolite is much less biologically active as compared to the parent PG, and the initial metabolic transformation, therefore, generally represent a biological inactivation. Then, reduction of the $\Delta^{13,14}$ double bond by the 15-keto-PG $\Delta^{13,14}$ -reductase produces 13,14-dihydro-15-oxo- PGE_2 as a major metabolite in plasma. Two more enzymatic processes occur to convert the PG into a more polar form suitable for excretion, by shortening the carboxyl side chain (α -chain) through β -oxidation and the linear end of the alkyl chain (ω -chain) through ω -oxidation [2]. The enzymes catalyzing these reactions are present largely in the liver and kidney (Fig. 2).

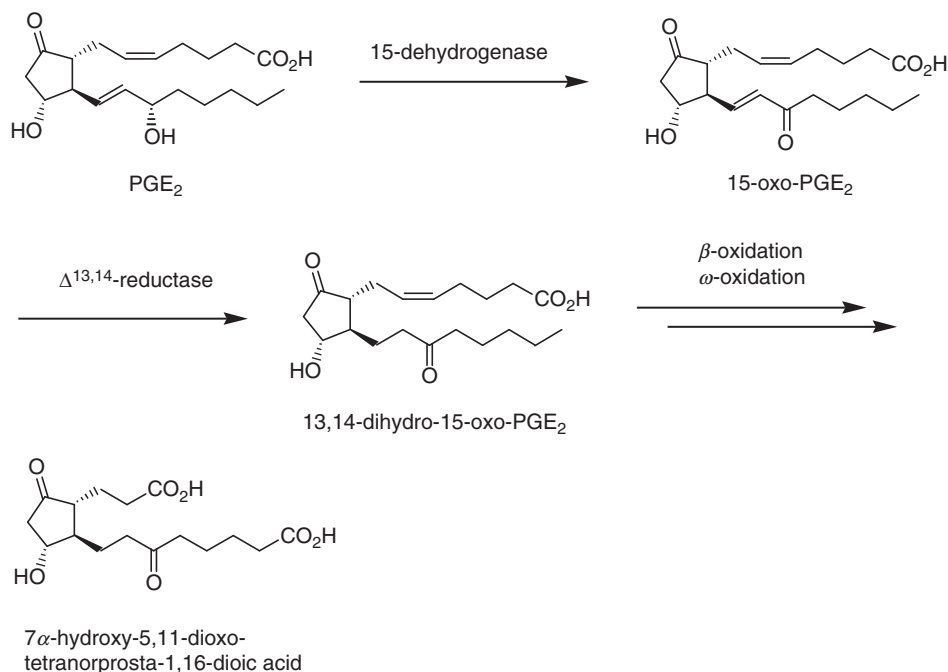


Fig. 2. Major metabolic pathway of PGE_2 in man.

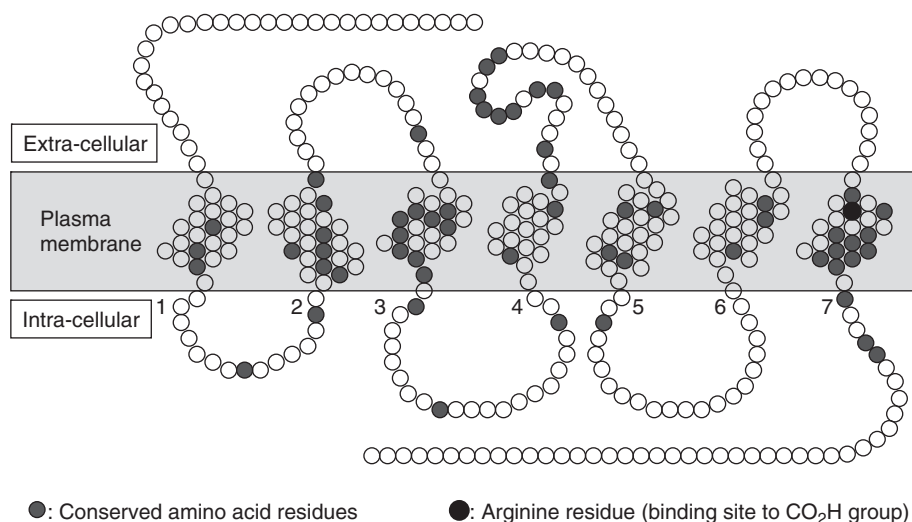
1.2. Physiological properties of prostanoids and their receptors

The prostanoids have been thought to exert their multiple physiological actions via specific protein receptors on the surface of target cells. In early 1980s, the prostanoid receptors were pharmacologically identified from the functional data and classified into DP, EP, FP, IP, and TP receptors, which were specific for PGD₂, PGE₂, PGF_{2α}, PGI₂ (prostacyclin), and TXA₂, respectively [3]. However, none of the receptors had been isolated until TP receptor was purified from human platelets by Ushikubi *et al.* in 1989 [4], and its cDNA was cloned by Hirata *et al.* in 1991 [5]. Since then, the eight prostanoid receptors including four subtypes of EP receptors were identified in various species by homology screening based on the sequence of the TP receptor [6]. The ligand binding properties, second messengers in signal transduction pathways, and tissue distribution of the receptors are summarized in Table 1.

The prostanoid receptors are G-protein coupled rhodopsin-type receptors with seven transmembrane domains [6] (Fig. 3). The overall homology among the receptors is not high, though these receptors conserve the important amino acid sequences in several regions, especially in the seventh transmembrane domain.

Table 1. Properties of prostanoid receptors

Receptor	Rank order of binding affinity	Second messenger	Tissue distribution
DP	PGD ₂ > STA ₂ ≫ PGE ₂ , PGF _{2α}	cAMP ↑	Ileum
CRTH2	PGD ₂ ≫ PGF _{2α} > PGE ₂ > Iloprost	cAMP ↓, Ca ²⁺ ↑	Small intestine, stomach, heart
EP ₁	PGE ₂ > Iloprost > PGE ₁ ≫ PGF _{2α} > PGD ₂	Ca ²⁺ ↑	Kidney
EP ₂	PGE ₂ = PGE ₁ ≫ PGD ₂ , PGF _{2α}	cAMP ↑	Thymus, ileum
EP ₃	PGE ₂ = PGE ₁ ≫ Iloprost > PGD ₂ > PGF _{2α}	cAMP ↓, Ca ²⁺ ↑	Kidney, uterus, stomach
EP ₄	PGE ₂ = PGE ₁ ≫ Iloprost, PGD ₂ , PGF _{2α}	cAMP ↑	Thymus, ileum
FP	PGF _{2α} > PGD ₂ > STA ₂ > PGE ₂ > Iloprost	Ca ²⁺ ↑	Ovary
IP	Iloprost > PGE ₁ ≫ PGD ₂ , PGE ₂ , STA ₂	cAMP ↑, Ca ²⁺ ↑	Thymus, spleen, heart
TP	STA ₂ > PGD ₂ , PGE ₂ , PGF _{2α}	Ca ²⁺ ↑	Thymus, spleen, lung



G protein-coupled rhodopsin-type receptor with 7 putative transmembrane domains

Fig. 3. Prostanoid receptor. Reproduced with permission from Ref. [6d]. Copyright 2001 Tokyo Kagaku Dojin.

It is proposed that the conserved arginine residue in the domain serves as the binding site for the terminal carboxyl group of prostanoid molecules.

In 2001, Nagata *et al.* identified a second PGD₂ receptor, chemoattractant receptor-homologous molecule expressed on T helper (Th) 2 cells (CRTH2), a G-protein-coupled receptor with different functions relative to DP receptor [7]. The CRTH2 receptor shares little sequence homology with DP receptor, but greatest sequence similarity with members of the leukocyte chemoattractant receptor subfamily, which includes the *N*-formyl-methionyl-leucyl-phenylalanine receptor and anaphylatoxin C3a and C5a receptors [8]. The CRTH2 receptor mRNA is expressed not only in hemopoietic cells but also in various tissues such as brain, heart, thymus, spleen, stomach, and small intestine [9].

The physiological and pathophysiological roles of prostanoids have been elucidated from extensive studies using deficient mice in each prostanoid receptor reported by Narumiya and other researchers [10] (Table 2). These knockout mouse studies have become powerful tools for clarifying various physiological functions had been suggested by examining the effects of exogenously added prostanoids, and also for finding important roles of prostanoids that had not been previously known (Table 2). The approach may contribute to the development of novel drugs in testing selective receptor agonists and antagonists which regulate the prostanoid functions. Regarding CRTH2 receptor, it is believed that CRTH2 receptor plays key roles in allergic inflammation through the stimulatory effects

Table 2. Physiological roles of prostanoids revealed by studies using mice deficient in prostanoid receptors

Prostanoids	Receptors	Physiological roles
PGD ₂	DP	A mediator of allergic asthma [12], sleep induction [13]
PGE ₂	CRTH2	(Involvement in allergic inflammation) ^a
	EP1	Attenuation of impulsive behavior [14], augmentation of carcinogenesis [15], development of renal injury [16]
	EP2	Ovulation and fertilization [17], salt-sensitive hypertension [17b,18]
	EP3	A mediator of febrile response to pyrogens [19], duodenal bicarbonate secretion [20], suppression of allergic inflammation [21], urinary concentration [22]
PGF _{2α}	EP4	Patent ductus arteriosus [23], bone resorption [24], suppression of colitis and mucosal damage [25]
	FP	An inducer of labor [26], intraocular pressure lowering effects [27]
PGI ₂	IP	Antithrombotic function [28], a mediator of inflammation [28], enhancement of pain perception [28], augmented cardiac hypertrophy [29], modulation of pulmonary vascular remodeling [30], prevention of atherosclerosis [31]
TXA ₂	TP	Hemostasis [32], development of atherosclerosis [31]

^a Physiological studies using knockout mice have not been reported.

by PGD₂ on Th2 cells, eosinophils, and basophils [11]. Characterization of mice deficient in the CRTH2 receptor will begin to clarify the exact roles that it plays in inflammation and immune modulation.

1.3. Historical background of fluorinated prostanoids research

Since the first successful development of fluorocorticoids in 1950s [33], it has been well known that introduction of fluorine atoms to biologically active substances may lead to improvements in pharmacological properties and an increase in therapeutic efficacy [34]. It has been explained that these advantageous pharmacological effects of fluorinated molecules are mainly derived from

the following physicochemical characters of fluorine: (1) relatively small size, (2) high carbon–fluorine bond energy, (3) high electronegativity, and (4) enhancement in lipophilicity.

A large number of fluorinated prostanoids have been reported since 1970s [35] along with the rapid progress on synthetic studies of the PG framework [36]. In spite of many difficulties in the early years in designing selective drugs without enough information on the structures and the functions of prostanoid receptors, important findings and improvements in biological and physical properties have been made (Fig. 4). For example, fluprostenol having the *m*-trifluoromethylphenoxy group in the ω -chain emerged in 1974 as a first successfully marketed analog applied to a potent luteolytic agent in veterinary medicine [37]. The compound is regarded as one of the most selective FP receptor agonists and widely used for a pharmacological tool. The strong inductive effect and enhancement in lipophilicity caused by the CF_3 group should contribute to improvements of the biological profile. The 16,16-difluoro-PGE₂ was reported in 1975 as a metabolically stabilized analog by 15-dehydrogenase inhibition of the degradation pathways *in vitro* [38]. The inhibition of enzymatic oxidation is accounted for by the destabilization of carbonyl group substituted by electron-withdrawing fluorine atoms causing a shift in equilibrium between the allyl alcohol and the enone favoring the reduced form. Fried *et al.* reported 10,10-difluoro-13,14-dehydro-PGI₂ in 1980 [39] and 10,10-difluoro-TXA₂ in 1989 [40] as important examples which showed the inductive effects of fluorine caused an increase in the stability of PGI₂ and TXA₂ against hydrolysis, respectively.

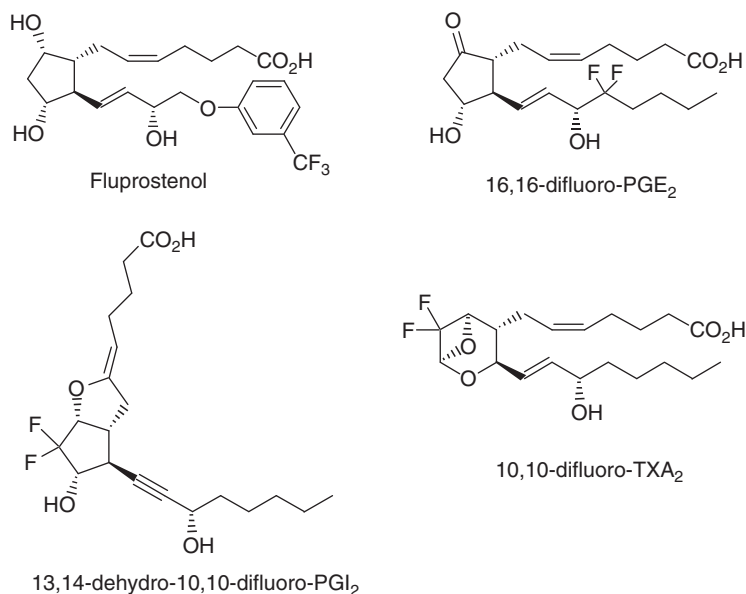


Fig. 4. Fluorinated prostanoids reported before 1990.

The above instances demonstrated the high potential of chemical modification with fluorine in drug design of prostanoids. Generally, prostanoids are flexible molecules that change their conformation in response to changes in environments by the intramolecular hydrogen bonding between the terminal carboxylic acid and the hydroxy group at C-9, C-11, or C-15 [41]. In the drug-receptor complex, the prostanoids can make a preferred conformation by the forces involved in ionic interactions and dipole–dipole interactions including hydrogen bonding between these functional groups and the corresponding amino acid residues of receptors [42]. If a specific position of the prostanoids is substituted by fluorine, it should affect not only the molecular conformation but also the drug–receptor complex through a possible participation of the fluorine to the interactions. Prostanoids themselves are regarded as lipophilic molecules, but the enhancement in lipophilicity introducing a fluorinated building block as a rigid template may be an effective methodology to increase the specific affinity to a hydrophobic pocket of the receptors.

Recently, new fluorinated prostanoids that utilized unique properties of fluorine have been developed in accord with rapid advances in molecular biology on prostanoid receptors. This chapter reviews the synthesis and pharmacological properties of novel fluorinated prostanoids in development.

2. PGE DERIVATIVES

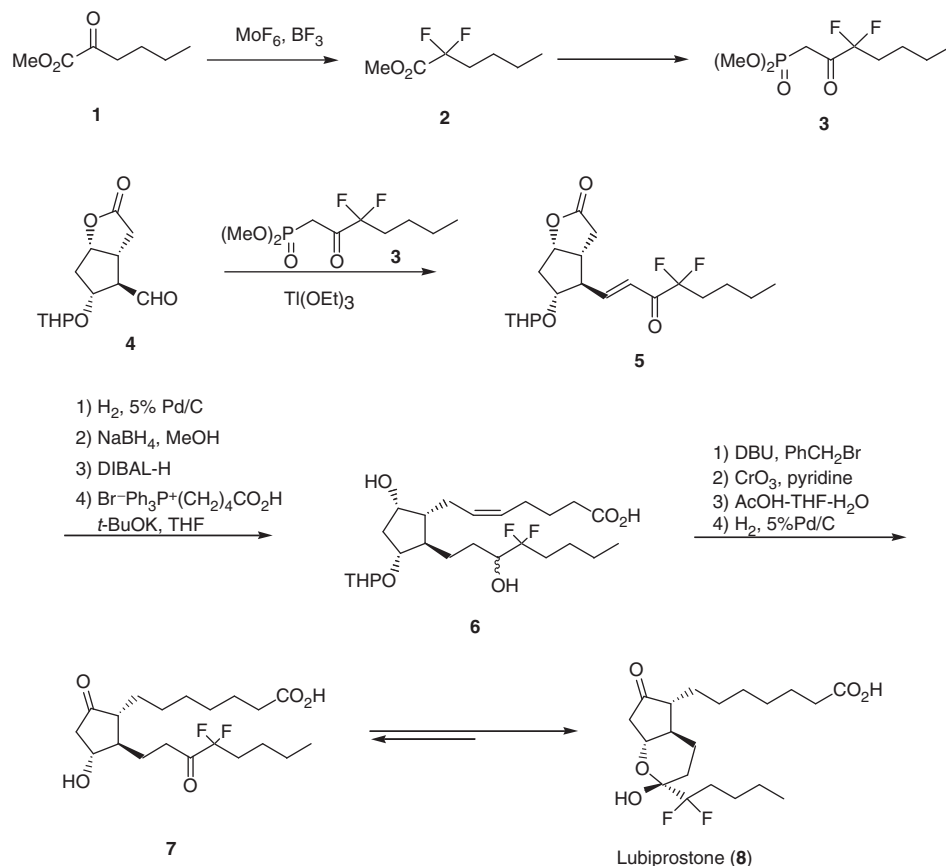
The PGE receptors are classified into four subtypes: EP1, EP2, EP3, and EP4 receptors, all of which respond to the naturally occurring agonist PGE₂, but differ in their actions and in their responses to various analogs. In comparison to PGE₂, natural PGE₁ has a weaker affinity with EP1 receptor, but similarly strong affinities with EP2, EP3, and EP4 receptors. In addition, PGE₁ also binds strongly to the IP receptor [43]. It is thought that PGE₂ or PGE₁ works as a local hormone by showing that the multiple physiological actions in any tissues depend on the interactions to these receptors. The PGE derivatives have been used as drugs for ischemic peripheral vascular disease, Raynaud's phenomenon, management of gastroduodenal ulceration, and cervical ripening and labor induction [1]. If more specific drugs to each receptor are developed to regulate the complex pharmacological actions of the PGE derivatives, new treatment in a wider therapeutic area can be achieved.

2.1. 13,14-dihydro-15-keto-PGE derivative

Ueno *et al.* have studied the physiological functions of 13,14-dihydro-15-keto-PG derivatives for many years, and they have found unique biological activities of these metabolites previously regarded as inactive compounds. Recently, they

have reported that the synthesis of lubiprostone introduced fluorine atoms to C-16 of the PG [44] (Scheme 1).

The compound was synthesized in a similar manner with 16,16-difluoro-PGE₂ reported by Magerlein [38]. The α -keto ester **1** was fluorinated with MoF₆-BF₃ to afford methyl 2,2-difluorohexanoate **2**, which was then transformed to phosphonate **3**. The ω -chain of PG skeleton was introduced to the Corey aldehyde **4** by Horner-Emmons type reaction. After hydrogenation and reduction of ketone **5**, diisobutylaluminum hydride (DIBAL-H) reduction was followed by the Wittig reaction of the resulting lactol to give the difluoro-PGF derivative **6**. The esterification of carboxylic acid **6** with benzyl bromide in the presence of 1,8-diazabicyclo [5.4.0]undec-7-ene (DBU) and oxidation of both hydroxy groups gave the corresponding diketone. After deprotection of the tetrahydropyranyl (THP) group, cleavage of the benzyl ester accompanying hydrogenation of the double bond afforded 15-keto-PGE analog **7**. It was cyclized between hydroxy group at



Scheme 1. Synthesis of lubiprostone.

C-11 and carbonyl group at C-15 to give lubiprostone **8** because of the electron-withdrawing effect of the fluorine atoms. The compound is mainly formed as bicyclic hemiacetal **8** as stable crystals or crystalline powder.

Lubiprostone has used as a novel PG compound for an oral treatment of constipation with a unique action directed to the target tissue, although it has low systemic availability following oral administration. It activates a locally acting chloride channel, which is a normal constituent of the apical membrane of the human intestine, and enhances a chloride-rich intestinal fluid secretion without altering sodium and potassium concentration in the serum. In fasted rats administered doses of 1, 10, or 100 $\mu\text{g/kg}$ of the compound, dose-dependent increases in the concentration of chloride ions in the bowel were detected, indicating that the compound opens chloride channels and promotes chloride ion transport *in vivo* [45].

The standard pharmacokinetic parameters of the compound such as a half-life or bioavailability cannot be reliably calculated, because the concentrations in plasma are below 10 pg/mL. As analogously expected from the results on the shift in keto-alcohol equilibrium of 16,16-difluoro-PGE₂, it is rapidly metabolized by C-15 reduction mediated by the ubiquitously expressed carbonyl reductase. The metabolism followed by β -oxidation and ω -oxidation forms a mixture of α and β epimers at the 15-hydroxy moiety as a sole measurable metabolite [46]. In 2006, the US Food and Drug Administration approved the drug application for an oral treatment of chronic idiopathic constipation in adults, estimating that 4–5 million Americans are affected. Lubiprostone has also completed a phase II trial in constipation-predominant irritable bowel syndrome, and has been further evaluated for other bowel dysfunctions.

2.2. EP1 receptor antagonist

Prostanoids produced in the spinal cord may play an important role in the development of hyperalgesia, an increased sensitivity to a painful stimulus, and allodynia, a pain response to a usually not painful stimulus [47]. EP1 receptor gains considerable attention as one of selective targets for an analgesic drug of similar effects as nonsteroidal anti-inflammatory drugs that achieve analgesic activity through the inhibition of cyclooxygenases, but fewer potential side effects [48].

The dibenzoxazepine derivatives, SC-51089 and SC-51234A (Fig. 5), were reported as EP1 receptor blocking compounds [49]. The antinociceptive effects were examined in rats using the formalin test. The specific nociceptive behaviors evoked by formalin injection into the paw were attenuated by spinal administration of these EP1 antagonists [50].

Ohuchida *et al.* have studied to synthesize a series of sulfonamide and carboxamide derivatives having an affinity with EP1 receptor. They have discovered that ONO-8713 having 2-sulfonylamino-5-trifluoromethylphenol as a core

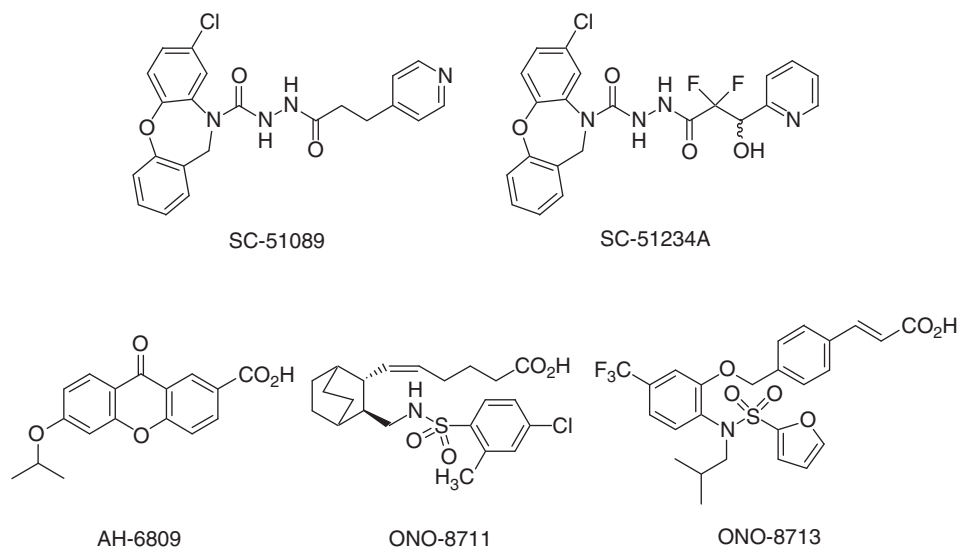


Fig. 5. EP1 receptor antagonists.

template with a cinnamic acid moiety in the α -chain showed a highly potent and selective EP1 receptor antagonist activity [51]. In contrast to AH-6809 [52] conventionally used as an EP1 receptor antagonist or ONO-8711 [15,53], another EP1 receptor antagonist similar in structure to typical TP antagonists, ONO-8713 presented at least 3000-fold selectivity between EP1 receptor and other prostanoid receptors (Table 3).

Since ONO-8713 shows a good bioavailability (>50%) in oral administration, it has been used for various studies as a pharmacological tool to analyze functions of EP1 receptor. The EP1 receptor antagonist reduced hyperalgesia and allodynia and revealed a protective effect in excitotoxic neuronal damage caused by *N*-methyl-D-aspartic acid [54]. The studies on the progression of nephropathy in streptozotocin-induced diabetic rats indicated that the compound prevented glomerular hypertrophy, proteinuria, and mesangial expansion [55]. In stroke-prone spontaneously hypertensive rats, the treatment with the antagonist inhibited the development of renal injury, including renal fibrosis, proteinuria, and decreased creatinine clearance [16]. These observations suggested a novel therapeutic potential of the EP1 receptor antagonist for the treatment of renal damage caused by both hypertension and diabetes. Furthermore, the compound has been examined for the role of EP1 receptor in cancer development because a role of cyclooxygenases had been demonstrated in the many types of cancer [56]. Administration of the compound resulted in suppression of chemically induced colon cancer development [57] and UVB light induced skin cancer development [58].

Table 3. Binding affinities of the EP1 receptor antagonists to the mouse prostanoid receptors

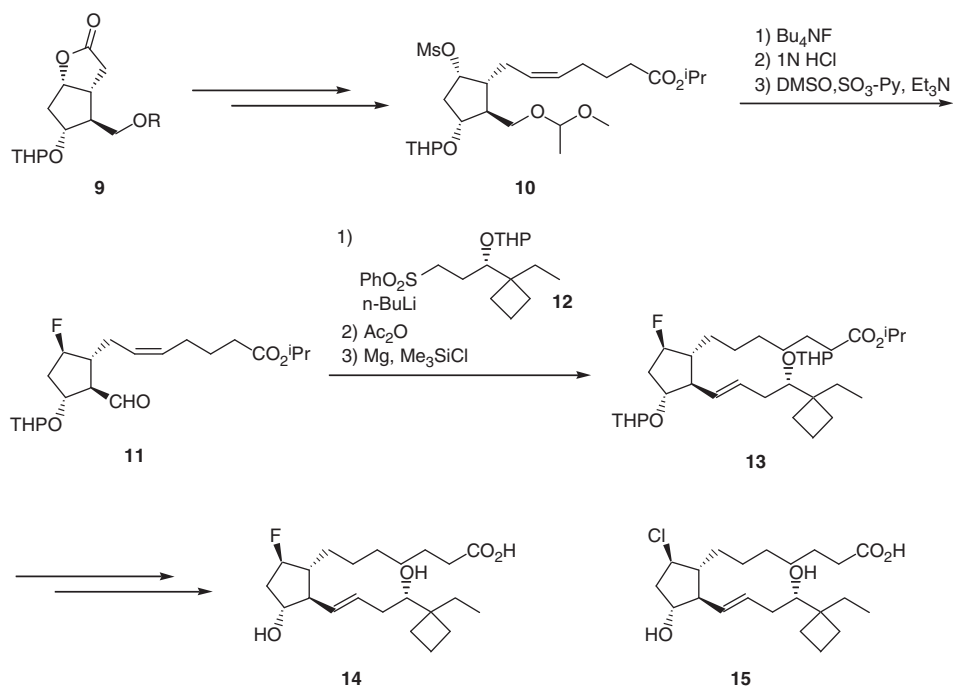
Compounds	(K _i value: nM)							
	DP	EP1	EP2	EP3	EP4	FP	IP ^a	TP ^a
ONO-8713	>10,000	0.3	3000	1000	>10,000	1400	10,000	10,000
ONO-8711	1800	1.7	5300	67	>10,000	>10,000	>10,000	76
AH-6809	>10,000	>10,000	240	82	>10,000	>10,000	>10,000	>10,000

^a Human prostanoid receptors.

2.3. EP2 receptor agonist

Ohuchida *et al.* also reported synthesis of the fluorinated analog in the cyclopentane ring of PG structure (Scheme 2) [59]. The mesylate **10** prepared by commonly used Corey method was fluorinated with Bu_4NF to give the fluoride, which was transformed to the corresponding aldehyde **11**. The reaction of the aldehyde **11** with lithiated (3*S*)-3-tetrahydropyranyloxy-4,4-propanohexylphenyl-sulfone **12** and quenching with acetic anhydride afforded the corresponding acetoxy sulfone, which was converted to the PG derivative **13** in the treatment with $\text{Mg}/\text{Me}_3\text{SiCl}$. The desired product **14** has a similar ω -chain as butaprost, often used physiologically as an EP2 receptor agonist. In comparison to butaprost, the linear carbon length is one carbon shorter, but the hydroxy group is similarly positioned at C-16 next to the cyclobutane ring.

In the binding assay of the derivatives, it is shown that both fluoride **14** and chloride **15** [60] strongly bind to EP2 receptor. In contrast to chlorinated derivative **15**, which also has some affinities to EP1 and EP4 receptors, the fluoride **14** showed any significant affinities to EP1, EP3, or EP4 receptors at $10\ \mu\text{M}$ [59]. From these results, it seems that β -fluoride or β -chloride can be substituted for the carbonyl group at C-9 of PGE structure, and the substitution by a fluorine atom is more suitable for binding selectively to the EP2 receptor. The fluorinated



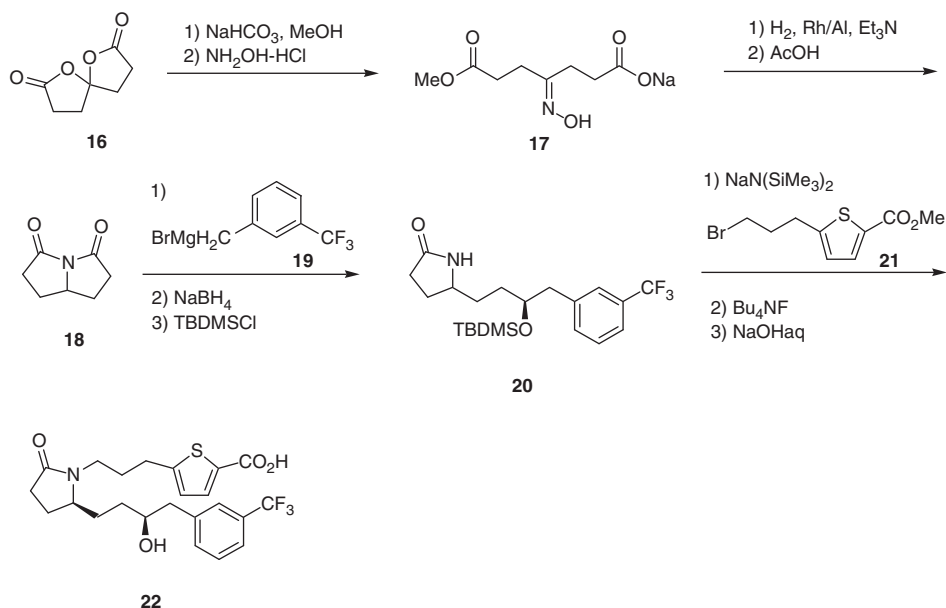
Scheme 2. Synthesis of 9 β -fluoro-PGE₁ analog.

compound was described as useful for treatment of immunological disease, asthma, dysfunction of bone formation, premature labor, abortion, and liver dysfunction.

2.4. EP4 receptor agonist

EP4 receptor agonists have drawn much attention to the effects of promoting osteogenesis [61] or suppressing colitis and mucosal damage [62], because the potential of an EP4 receptor agonist for treatment in bone diseases or inflammatory bowel disease has been examined in clinical trial [61].

Cameron *et al.* reported the synthesis of a new EP4 receptor agonist, a heterocyclic PG derivative bearing *m*-CF₃-phenyl group in the ω -chain [63] (Scheme 3). The tetrahydropyrrolizine-3,5-dione **18** was prepared from the 4-ketopimeric acid dilactone **16** by cyclization via oxime **17**. The treatment with the Grignard reagent **19**, reduction with NaBH₄, and protection with *t*-butyldimethylsilyl (TBDMS) chloride gave pyrrolidinone **20**. *N*-alkylation with (3-bromopropyl)thiophene-1-carboxylic acid methyl ester **21** and removal of the protective group afforded heterocyclic PGE derivative **22**. The compound **22** was reported as a selective EP4 receptor agonist, which can be useful for the treatment of hypertension, liver failure, loss of patency of the ductus arteriosus, glaucoma, or ocular hypertension in a patient according to the literature [63].



Scheme 3. Synthesis of EP4 receptor agonist.

3. PGF DERIVATIVES

3.1. FP receptor agonist

The natural PGF_{2 α} derivatives have been used as a drug for cervical ripening prior to induction of labor. Cloprostenol and fluprostenol were marketed for luteolytic agents in many kinds of domestic animal species [37] (Fig. 6). Since the discovery that PGF_{2 α} reduces intraocular pressure (IOP) in an animal model in 1980s [64], extensive efforts have been dedicated to develop FP receptor agonists as new promising antiglaucoma agents [65]. Glaucoma is one of the most common but serious eye disease that gradually steals sight often without symptoms. Main risk factor of the disease is thought to be high IOP, which causes damage to the optic nerve.

Isopropyl unoprostone [66], a PGF_{2 α} metabolite derivative, was developed by Ueno *et al.* and first marketed in Japan for the treatment of glaucoma in 1994. Stjerschantz *et al.* later developed latanoprost [67] regarded as a representative FP receptor agonist. These PG drugs have been widely used for the treatment of ocular hypertension in many countries, because they have good IOP-reducing effects without causing serious systemic side effects. However, application of the drugs causes local adverse effects, such as hyperemia and iris/skin pigmentation [68]. Furthermore, the existing PG-related ocular hypotensive drugs, even latanoprost, do not produce satisfactory IOP control in all patients.

Travoprost is an isopropyl ester of fluprostenol, which shows an IOP-reducing effect as potent as latanoprost [69]. The synthetic route of travoprost **31** is shown in Scheme 4 [70]. The cleavage of the three-membered ring of tricyclic ketone **26** by the attack of the cuprate prepared from vinyl iodide **25** gave the compound **27**.

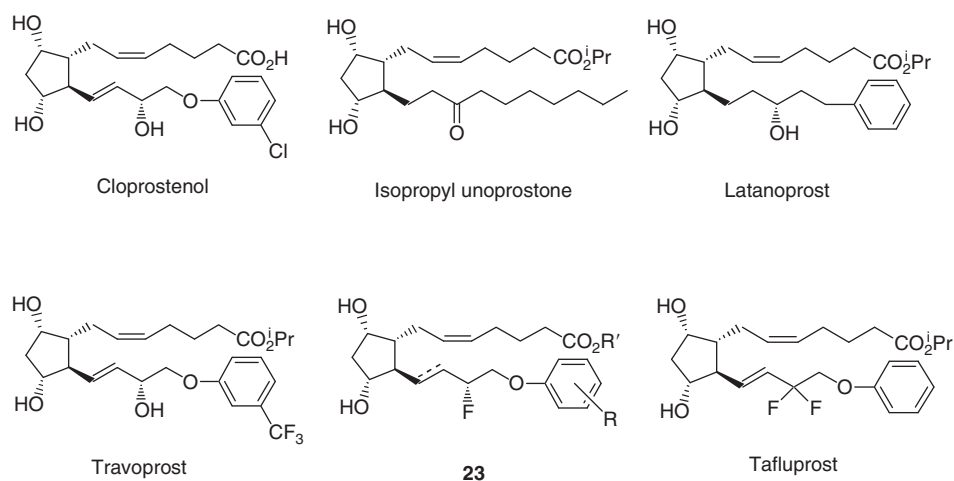
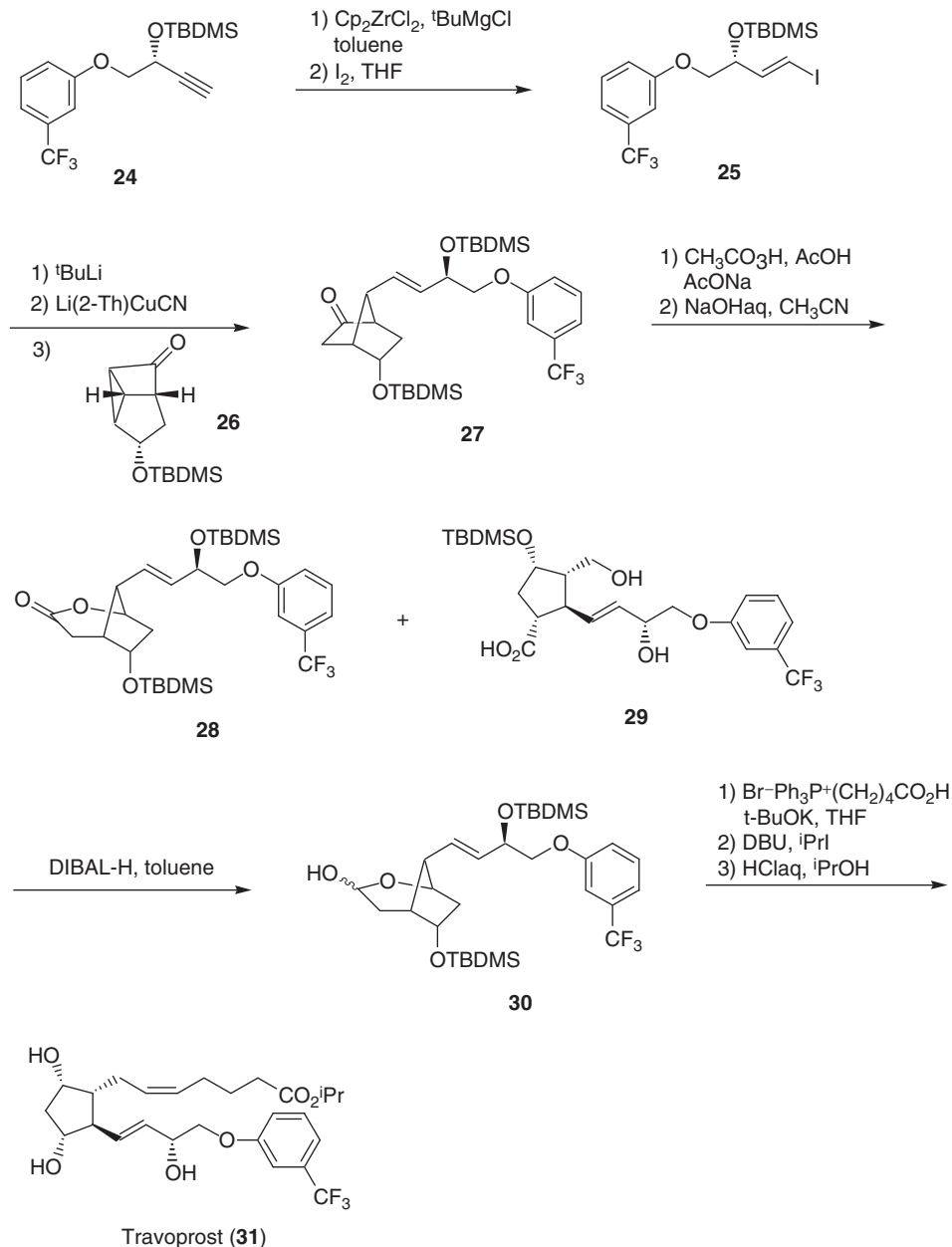


Fig. 6. Prostaglandin F_{2 α} derivatives.

Baeyer-Villiger oxidation afforded the desired lactone **28** accompanied with hydroxycarboxylic acid **29** as a byproduct. After removal of the acid **29**, the lactone was reduced with DIBAL-H and employed in the Wittig reaction to form the PG structure **31** (Scheme 4).



Scheme 4. Synthesis of travoprost.

In the search for a new FP receptor agonist having more potent IOP-reducing activity and weaker side effects, our research group has recently discovered a 15-deoxy-15,15-difluoro-PGF_{2α} derivative, tafluprost (AFP-168), which shows highly potent and selective affinity to the FP receptor [71].

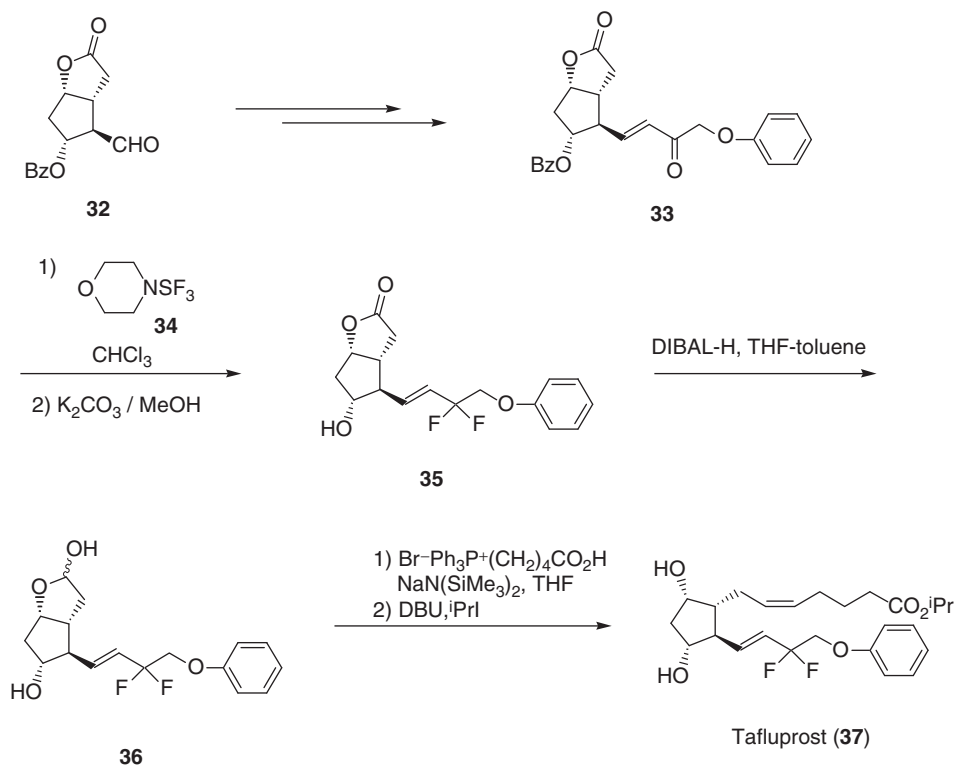
In the functional FP receptor affinity assay *in vitro*, we found 15-deoxy-15-fluoro-16-phenoxy-tetranorPGF_{2α} derivatives **23** strongly caused constriction of the cat isolated iris sphincter [72] (Table 4). It suggested that exchanging the 15-hydroxy group for fluorine preserved agonistic activities on the FP receptor [73]. Interestingly, 15, 15-difluorinated analogs demonstrated much more potent agonistic activities than the monofluorinated derivatives. Among all, tafluprost, isopropyl ester of AFP-172, displayed the best pharmacological profile.

A synthetic route of tafluprost is shown in Scheme 5 [71]. The synthesis was started from the Corey aldehyde **32**, which was converted to enone **33** by Horner-Emmons reaction. Since the general method to prepare allyl difluorides from enones had not been reported, we studied the fluorination reaction. It was found that the reaction of the enone **33** with morpholinosulfur trifluoride **34** and successive deprotection gave the desired geminal difluoride **35**. DIBAL-H reduction of the lactone **35** and the Wittig reactions yielded the 15-deoxy-15,15-difluoro-PGF_{2α} derivative as a mixture of 5*Z* and 5*E* isomers. The Wittig reaction used sodium bis(trimethylsilyl)amide as a base and gave the best result for the stereoselectivity (5*Z*/5*E* = 99/1). The esterification of the crude acid treated with

Table 4. Functional assay of PG derivatives on FP receptor^a

Compounds	A	X	R ₁	R ₂	R ₃	R ₄	EC ₅₀ (nM)
Latanoprost acid form	Single bond	CH ₂	H	OH	H	H	13.6
AFP-159	Single bond	O	H	F	H	H	6.6
AFP-120	Double bond	O	H	F	Cl	Cl	37.9
AFP-164	Single bond	O	F	F	H	Cl	9.4
AFP-157	Double bond	O	F	F	H	Cl	1.9
AFP-162	Single bond	O	F	F	H	H	2.4
AFP-172	Double bond	O	F	F	H	H	0.6

^a Constriction effects of PG derivatives on cat iris sphincters.



Scheme 5. Synthesis of tafluprost.

Table 5. Affinity of $\text{PGF}_{2\alpha}$ derivatives for the human prostanoid FP receptor

Compounds (acid form)	K_i (nM)	Ratio (tafluprost = 1)
Tafluprost	0.40	1
Latanoprost	4.7	12
Unoprostone	680	1700

isopropyl iodide and 1,8-diazabicyclo[5.4.0]undec-7-ene afforded the desired 15-deoxy-15,15-difluoro- $\text{PGF}_{2\alpha}$ derivative **37** (tafluprost).

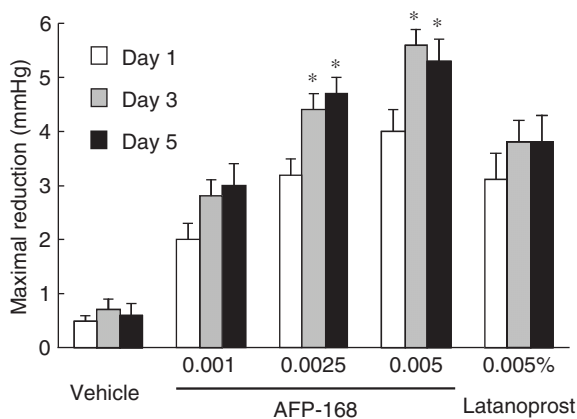
The affinity for the FP receptor of the corresponding carboxylic acid of tafluprost was 0.4 nM, which was 12 times and 1700 times higher than those of latanoprost and isopropyl unoprostone, respectively (Table 5) [74]. It should be noted that substitution of difluoro-moiety for the hydroxy group at C-15 of $\text{PGF}_{2\alpha}$ increases binding to the FP receptor to such a large extent, because the hydroxy group was thought to be essential to show their pharmacological activity [75]. Since the acid form of tafluprost did not show significant affinities for other prostanoid receptors, the drug was proven to be a highly selective compound.

In cultured melanoma cells, a carboxylic acid of latanoprost has been reported to increase melanogenesis [76]. However, a carboxylic acid of tafluprost did not have the stimulatory effects on melanin content in cultured B16-F10 melanoma cells [72]. It suggests the application of tafluprost may cause less pigmentation than do latanoprost.

Tafluprost has a potent IOP-reducing effect in animal models [74,77]. For example, the maximal IOP reduction achieved with tafluprost at 0.0025% was greater than with latanoprost at 0.005% in both laser-induced glaucomatous and ocular normotensive monkeys. The effects of tafluprost and latanoprost on IOP reduction in conscious ocular normotensive monkeys are indicated in Fig. 7. Furthermore, tafluprost significantly increases retinal blood flow and blood velocity in animal models [78]. The improvement of ocular blood flow is thought to be meaningful in glaucoma therapy, especially for normal tension glaucoma patients, because recently it has been assumed that optic nerve damage is concerned not only in mechanical compression caused by IOP but also in impairment of ocular blood flow. Tafluprost has been developed in clinical trials and currently it is being prepared for new drug application in glaucoma.

3.2. FP receptor antagonist

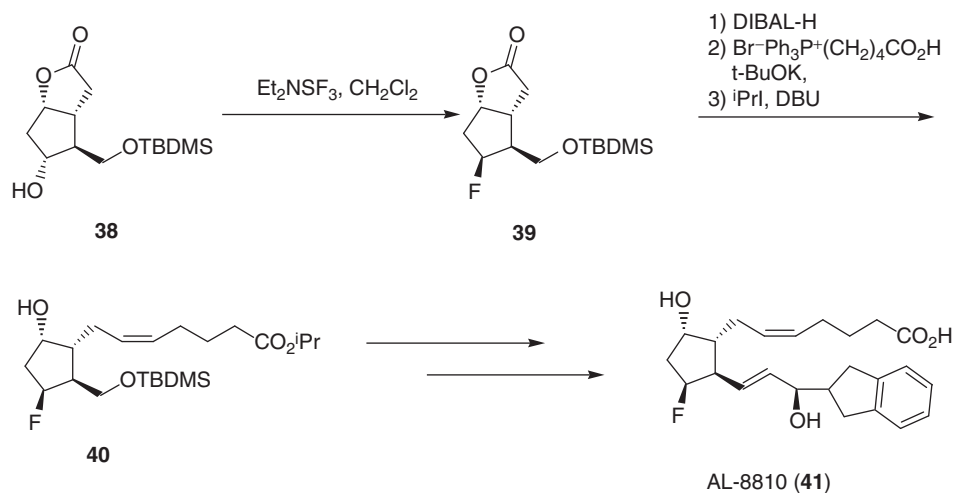
Sharif *et al.* reported 11-deoxy-16-fluoro-PGF_{2 α} , AL-3138 [79], and 11 β -fluoro-15 β -hydroxy-PGF_{2 α} analog, AL-8810 [80], as FP receptor antagonists. The synthesis of AL-8810 was shown in Scheme 6 [81]. The fluorination of



Drugs were instilled once daily at 10:30 AM of Day 1 to Day 5. Data represent the mean \pm SE of 10 animals.

* $p < 0.05$ vs. Day 1 (dunnett multiple-range test)

Fig. 7. Effects of tafluprost (AFP-168) and latanoprost on maximal reduction of intraocular pressure in conscious ocular normotensive monkeys. Reproduced with permission from Ref. [74]. Copyright 2004 Elsevier.



Scheme 6. Synthesis of AL-8810.

hydroxylactone **38** with diethylaminosulfur trifluoride provided the β -fluoride **39**. The α -chain was connected to the compound **39** in the series of DIBAL-H reduction and Wittig reaction. The resulting compound **40** was further transformed to the desired 11 β -fluoro-15 β -15-indanyl-PGF_{2 α} derivative **41** according to conventional synthetic methods. Both AL-3138 and AL-8810 exhibited FP receptor antagonist potencies against fluprostenol accompanied with weak agonist potencies as partial FP receptor agonists. Neither compound significantly inhibits functional responses of EP2, EP4, DP, and TP receptors. These compounds are often used in pharmacological experiments to characterize functions mediated through the FP receptor.

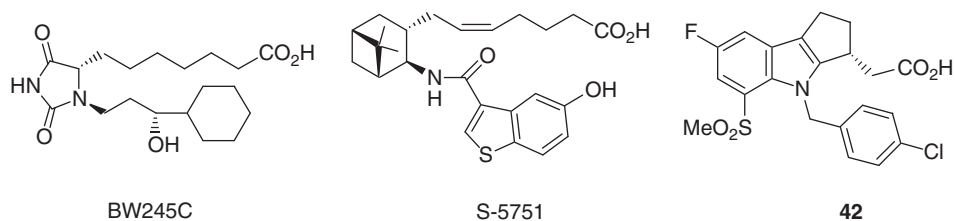
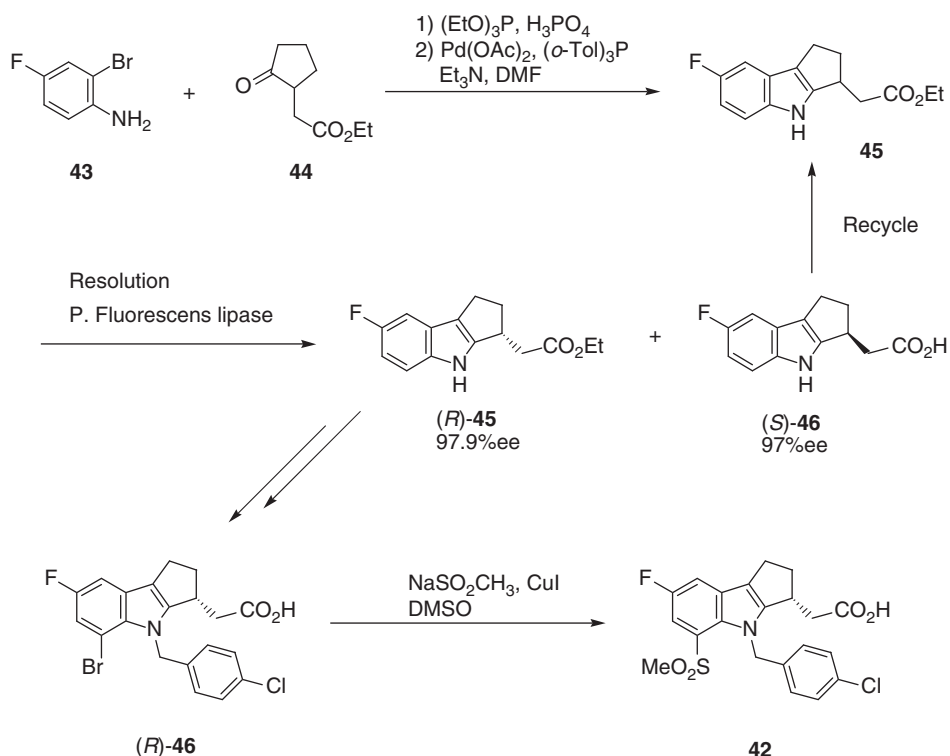
4. PGD DERIVATIVES

4.1. DP receptor agonist and antagonist

PGD₂ has been implicated in various physiological actions such as sleep induction, cell survival, and allergic response through the activation of the DP receptor. The discovery of BW245C [82], a selective and stable synthetic agonist of DP receptor, has allowed the identification of DP-specific effects mediated by PGD₂ such as vasodilation, relaxation of smooth muscle, and platelet aggregation (Fig. 8).

The DP receptor antagonists such as S-5751 [83] and compound **42** have been developed as promising leads in the alleviation of various allergic disorders.

Campos *et al.* reported asymmetric synthesis of the DP receptor antagonist **42** starting from (*R*)-2-cyclopentene-1-acetic acid obtained via asymmetric allylic

**Fig. 8.** DP receptor agonist and antagonists.**Scheme 7.** Synthesis of DP receptor antagonist.

alkylation of cyclopentyl acetate [84]. Shafree *et al.* reported alternative synthesis by means of lipase-catalyzed enzymatic resolution of an indole ester **45**, a key intermediate for the DP receptor antagonist **42** (Scheme 7) [85]. Condensation of 2-bromo-4-fluoroaniline **43** with ketoester **44** followed by intramolecular Heck reaction provided the indole ester **45**. They found asymmetric hydrolysis of the racemic indole ethyl ester **45** using *Pseudomonas fluorescens* lipase was an efficient way to produce optically pure indole ethyl ester **(R)-45**. The enzyme converted the undesired **(S)** enantiomer to its corresponding acid **(S)-46**, while

leaving the desired (*R*) enantiomer untouched, yielding (*R*)-ester with 95%ee at 48% conversion.

A study of substrate solubility and phase-partitioning behavior in a wide range of solvent concentrations by Truppo *et al.* led to a fourfold decrease in enzyme charge with an increase in product enantiomeric excess. The process was successfully run at 400-L scale yielding the desired product with 99.73%ee at 50% conversion with the optimized conditions [86]. The DP receptor antagonist **42** is being evaluated in clinical trials for the treatment of allergic rhinitis.

4.2. CRTH2 receptor agonist

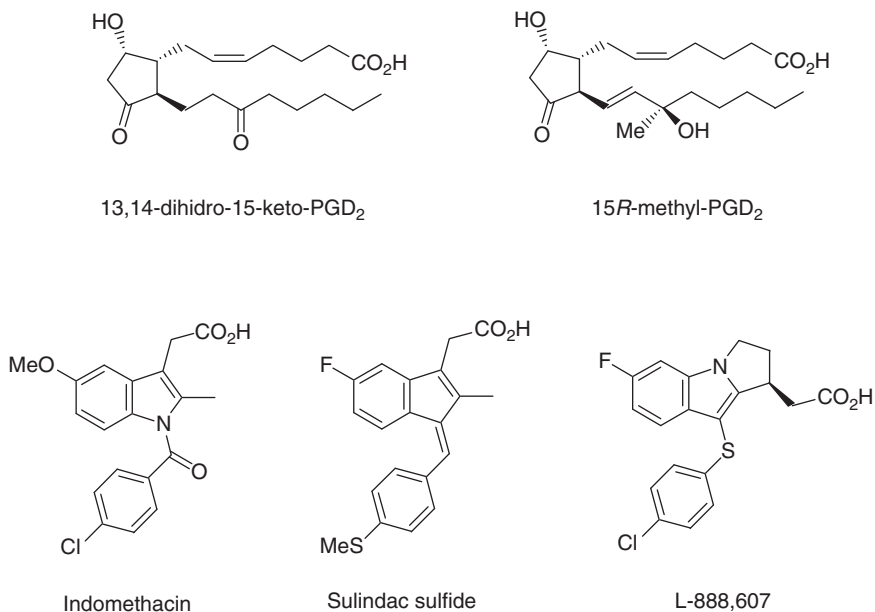
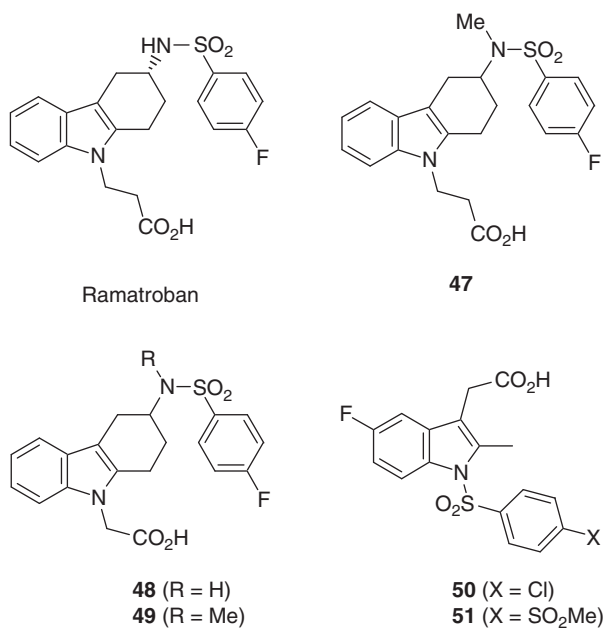
The second receptor for PGD₂, CRTH2, is selectively expressed on Th2 cells, eosinophils, and basophils, all of which are implicated in asthma and allergic reactions. The effects on the activation of Th2 lymphocytes and eosinophils were elicited by selective CRTH2 receptor agonists 13,14-dihydro-15-keto-PGD₂ and 15*R*-methyl-PGD₂ (Fig. 9), and blocked by an antiCRTH2 antibody [7a,87]. However, the roles played by the receptor *in vivo* have not been fully investigated. Since these agonists are unstable *in vivo*, a stable CRTH2 receptor agonist is necessary for studies to examine the functions of the receptor.

One of representative nonsteroidal anti-inflammatory drugs, indomethacin, was shown to bind to the human CRTH2 receptor and to act in an agonistic fashion *in vitro* [88]. Another NSAID, sulindac sulfide, was also shown to bind with moderate affinity to the human CRTH2 receptor [9] and murine CRTH2 receptor [89]. These two compounds belong to indolylacetic acid analogs having very similar spatial arrangement of acetic acid and aromatic groups.

Gervais *et al.* reported L-888,607 as the first synthetic potent and selective CRTH2 receptor agonist which does not inhibit cyclooxygenases at a concentration up to 10 μM [90]. The compound also possesses a fluoroindole core and a carboxylic acid side chain. In the structure–activity relationship study, they suggested the *S*-configuration at the chiral center bearing the acetic acid group allows the compound to give a better conformation to fit the CRTH2 receptor than the DP receptor. Replacement of the fluorine atom by larger atoms or groups led to a less potent compound. The stable CRTH2 receptor agonist, L-888,607, became a useful tool to identify the role of CRTH2 receptor *in vivo* in distinguishing from the function of DP receptor.

4.3. CRTH2 receptor antagonist

The synthesis of selective CRTH2 receptor antagonists has been more extensively studied to develop them as potential clinical candidates for the treatment of allergy, asthma, or other inflammatory disorders (Fig. 10). Ramatroban, a TP receptor antagonist, clinically used in asthma and allergic rhinitis, was recently

**Fig. 9.** CRTH2 receptor agonists.**Fig. 10.** CRTH2 receptor antagonists.

shown to antagonize the CRTH2 receptor as well [91]. Ramatroban completely inhibited the PGD₂-stimulated human eosinophil migration mediated through activation of CRTH2. It suggested that the clinical efficacy of ramatroban may be in part mediated through its action on the CRTH2 receptor.

Ulven *et al.* reported that minor structural modifications of ramatroban led to potent CRTH2 receptor antagonists with complete lack of activity on the TP receptor [92]. The binding affinities and antagonistic potencies of ramatroban and the analogs on CRTH2, TP, and DP receptors were examined. The *N*-methylated analog **47** showed equipotency with ramatroban on the CRTH2 receptor, but 2000 times weaker affinity on the TP receptor. Shortening the acidic side chain of ramatroban by one carbon atom increased affinity and antagonistic potency on the CRTH2 receptor over the TP receptor, by 1000 and 400 times, respectively.

Armer *et al.* indicated fluoroindolylacetic acid derivatives were potent and selective CRTH2 receptor antagonists having good oral bioavailability [93]. They studied indolylacetic acid derivatives **50** and **51** based on the structural similarity with the endogeneous CRTH2 receptor agonists, indomethacin and sulindac sulfide. The most significant improvements in CRTH2 receptor binding were achieved with modification of the indole core with *N*-sulfonyl moieties. The selectivity for CRTH2 receptor over the DP receptor of the compound **51** was high with >160-fold selectivity. The compound **51** showed activity in cellular assays such as eosinophil shape change or Th2 cell chemotaxis. The CRTH2 receptor antagonist **51** has good oral pharmacokinetic properties in rats.

5. PGI DERIVATIVES

5.1. IP receptor agonist

Prostacyclin (PGI₂) was discovered and named by Vane in 1976 when the structure was elucidated [94], just after the isolation and identification of TXA₂ [95]. It is produced by the vessel wall and has potent actions being a vasodilator and an inhibitor of platelet aggregation. It has opposite actions to TXA₂ made by platelets as a strong vasoconstrictor. The balance between PGI₂ and TXA₂ formation largely contributes to maintain homeostasis in the cardiovascular system.

The natural PGI₂ is a very unstable compound, easily hydrolyzed to give inactive 6-oxo-PGF_{1 α} under physiological conditions (Fig. 11). The half-life of the compound in physiological pH was 1.6 min at 37 °C [96]. Therefore, therapeutic applications of natural PGI₂ have been very limited. A large number of derivatives have been synthesized to stabilize the chemical structures. Among them, iloprost [97], beraprost [98], and uniprost [99] have been clinically used.

The fluorine-containing PGI₂ derivatives have also been studied to modify the physical and physiological properties by utilizing unique characters of fluorine atoms [35]. Most of the modifications were aimed at preventing hydrolysis by

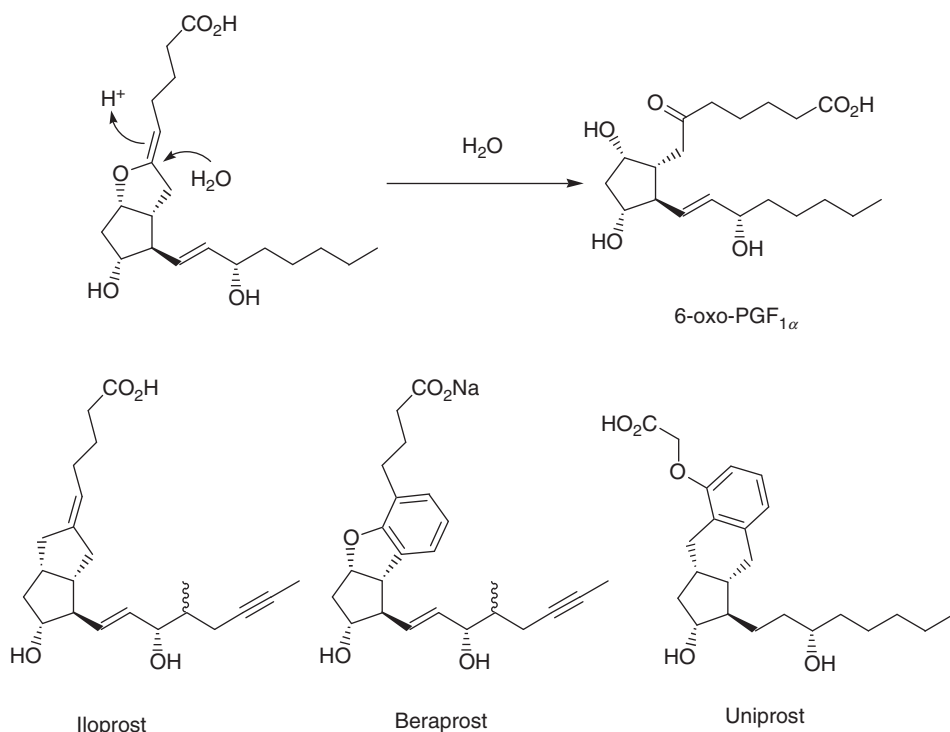
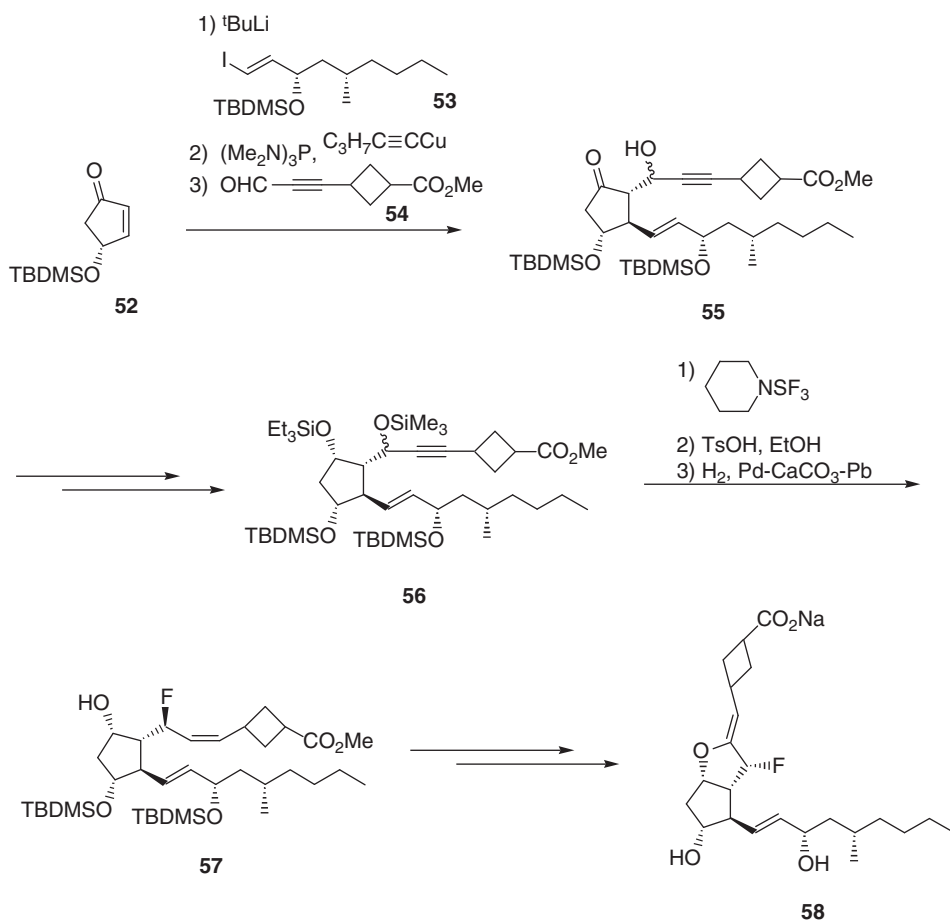


Fig. 11. Degradation mechanism of natural PGI₂ and the stabilized PGI₂ analogs.

decreasing the electron density of the enol ether of the PGI₂. Fried *et al.* reported that the half-life of the synthesized 10,10-difluoro-13,14-dehydro-PGI₂ was 24 h at pH 7.4 [39]. Bannai *et al.* and Djuric *et al.* reported 7β-fluoro-PGI₂ [100] and 5-fluoro-PGI₂ [101], respectively.

We designed 7α-fluoro-PGI₂ derivatives having cycloalkylene α-side chains not only to protect the enol ether from hydrolysis but also to prevent it from being metabolized by β-oxidation. The synthesis of the representative derivative, 7-fluoro-2,4-methylene-17,20-dimethyl-PGI₂, is shown in Scheme 8 [102]. The PG structure of **55** was synthesized by three-component coupling approach [103] from enone **52**, iodide **53**, and aldehyde **54**. The stereospecific fluorination of trimethylsilyl ether **56** with piperidinosulfur trifluoride, deprotection, and partial hydrogenation gave the fluoride **57**. The cyclization of the alcohol **57** afforded the targeted fluorinated PGI₂ derivative **58**. The 7α-fluoro-PGI₂ **58** was alternatively synthesized by utilization of methylenecyclopentanone [104].

The pharmacological results on the antiplatelet activity of the analogs are summarized in Table 6. Among the cycloalkylene derivatives, the cyclobutylene compound indicated most potent inhibition of ADP-induced platelet aggregation *in vitro*. The antianigral effects of the *cis* and *trans* cyclobutylene compounds **58** given intravenously and orally were 10–100-fold more potent than iloprost on vasopressin-induced ST depression of rat electrocardiogram [105]. Although



Scheme 8. Synthesis of 7 α -fluoro-17,20-dimethyl-2,4-methylene-PGI₂.

the compound showed strong biological effects, the half-life of the compound in aqueous media turned out to be just 2–3 h unexpectedly.

The author next tried to stabilize the PGI₂ structure by introducing second fluorine atom to the 7-position. However, it had been unknown to make such a difluorovinyl ether unit in the literature. We studied difluorination and Wittig reaction as key steps in the synthetic route of the target difluoro-PGI₂ from the Corey lactone. After searching the difluorination reaction, it was found that fluorination with *N*-fluorobenzenesulfonimide in the presence of potassium bis(trimethylsilyl) amide and manganese dibromide effectively provided the desired difluoride (Table 7) [106].

The synthesis of AFP-07 is shown in Scheme 9 [107]. The enone **59** prepared from the Corey lactone was reduced with aluminum reagent and protected with *t*-butyldimethylsilyl chloride. Fluorination of the lactone **60** under the standard conditions gave the difluorolactone **61**. The carbonyl group of the difluorolactone

Table 6. Inhibitory effects of α -chain modified 7-fluoro-PGI₂ derivatives on ADP-induced platelet aggregation

Compounds (R=)							
Relative potency to PGE ₁ (PGE ₁ =1)	0.34	13.3	3.4	1.27	7.0	0.6	0.05

61 becomes more reactive to the nucleophilic attack because of the strong electron-withdrawing effect of the fluorine atoms. The Wittig reaction proceeded well to afford the vinyl ether **62** with high 5Z/5E selectivity, which converted to the desired difluoro-PGI₂ (AFP-07).

In the binding study to the prostanoid receptors, AFP-07 showed strong affinity with IP receptor, but weak affinities with the EP1~EP4 receptors [108]. The compound was found to be one of the most potent IP receptor agonists reported in literature with high receptor selectivity. The stability in aqueous solution and the activities of antiplatelet aggregation of the PGI₂ derivatives are shown in Table 8. From these results, it was proved that the fluorinated PGI₂, AFP-07, was stabilized by at least 10,000 times compared with the natural one [106]. Moreover, the potent antiplatelet activities shown *in vitro* and *in vivo* demonstrate high therapeutic potential of AFP-07 in the application for ischemic peripheral vascular disease [109] and pulmonary hypertension [110].

6. CONCLUDING REMARKS

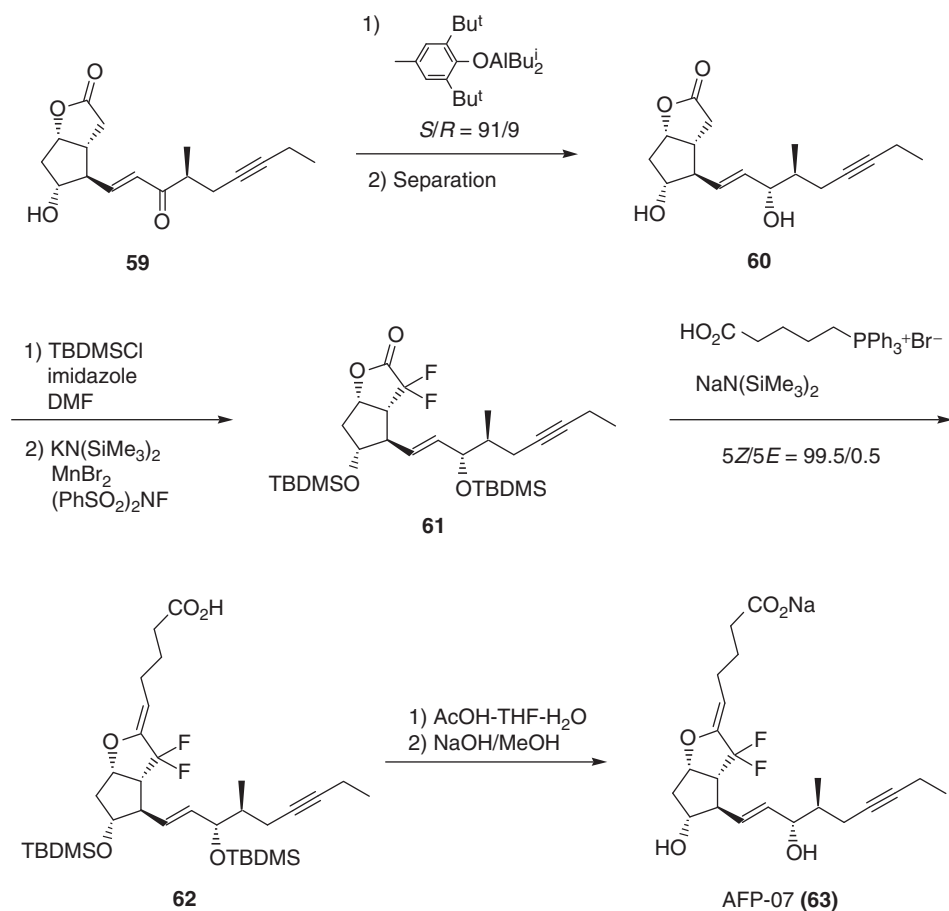
Since molecular cloning of the prostanoid receptors, the research in this field has been evolved quite fast. Information obtained from the studies on the receptor

Table 7. Electrophilic difluorination of carbonyl compounds

$ \text{R}^1-\text{C}(=\text{O})-\text{CH}_2-\text{R}^2 \xrightarrow[\text{KN}(\text{SiMe}_3)_2, \text{THF}]{\text{MnBr}_2, (\text{PhSO}_2)_2\text{NF}} \text{R}^1-\text{C}(=\text{O})-\text{CF}_2-\text{R}^2 + \text{R}^1-\text{C}(=\text{O})-\text{CHF}-\text{R}^2 $			
Substrates	Difluorinated products	Yield (%)	Selectivity (di:mono)
		93	>99:1
		80	>98:2
	complex mixture	-	-
		57	>98:2

structures and properties is utilized for computer-aided molecular modeling and structure-based drug design. The use of expressed receptors aids in screening of compounds for the specific receptor agonists or antagonists. The studies using mice lacking specific prostanoid receptors have uncovered several important physiological roles of prostanoids. The involvement of prostanoid receptors in broad areas of pathological phenomena has drawn much attention and explored their potential use as a therapeutic target in intractable diseases. In addition, identification and characterization of prostanoid transporters [111] are expected to be informative to design a new formulation for drug targeting or drug delivery system.

In this chapter, the recent development of the fluorinated prostanoids, which take advantage of the unique properties caused by fluorine atoms, was introduced. It is remarkable that a subtle change in structures of a series of compounds markedly

**Scheme 9.** Synthesis of AFP-07.**Table 8.** Chemical stability and biological activity of fluoro-PGI₂ derivatives

Compounds	Half-life in saline ^{a)}	Inhibitory effects on human platelet aggregation <i>in vitro</i> (PGE ₁ = 1) ^{c)}
PGI ₂	10 min	10
7 α -Fluoro-17,20-dimethyl-2,4-methylene-PGI ₂ (58)	2–3 h ^{b)}	3–13
AFP-07 (63)	>90 days	237

^{a)} 25 °C, pH 7, concentration 10 $\mu\text{g}/\text{ml}$.^{b)} 37 °C, pH 7, concentration 2 $\mu\text{g}/\text{ml}$.^{c)} Relative potency, ADP = 2 μM .

affects the affinities to the receptors or physical properties of the molecule. These fluorinated prostanoids may also be useful as a new probe in spectroscopic analysis on drug–receptor interactions by nuclear magnetic resonance [112] or molecular imaging *in vivo* using positron emission tomography [113].

In the synthesis of fluorinated prostanoids, there are still limited methods to introduce fluorine atoms selectively to the target molecule. It is hoped that the development of new fluorination reactions will contribute to the progress on the prostanoid research, and possibly discovery of novel drugs addressing unmet medical needs in future.

ACKNOWLEDGMENTS

The author thanks the coworkers whose names are shown in published papers for their essential contributions.

REFERENCES

- [1] J.R. Vane, J. O'Grady, *Therapeutic Applications of Prostaglandins*, Edward Arnold, London, 1993.
- [2(a)] M.H.F. Sullivan, C.K. Roseblade, N.B. Rendell, G.W. Taylor, M.G. Elder, Metabolism of prostaglandins E_2 and F_2 alpha by human fetal membranes, *Biochem. Biophys. Acta* 1123 (1992) 342.
- [2(b)] S.E. Barrows, J. Cockcroft, C.T. Dollery, N.E. Hickling, J.M. Ritter, Identification of 13,14-dihydro-15-oxo-prostaglandin F_2 alpha in the circulation during infusions of bradykinin and prostaglandin E_2 in man, *Br. J. Pharmacol.* 91 (1987) 245.
- [3] R.A. Coleman, I. Kennedy, P.P.A. Humphery, K. Bunce, P. Lumley, in: J.C. Emmett (Ed.), *Comprehensive Medicinal Chemistry*, Vol. 3, Pergamon, Oxford, p. 643.
- [4] F. Ushikubi, M. Nakajima, M. Hirata, M. Okuma, M. Fujiwara, S. Narumiya, Purification of the thromboxane A_2 /prostaglandin H_2 receptor from human blood platelets, *J. Biol. Chem.* 264 (1989) 16496.
- [5] M. Hirata, Y. Hayashi, F. Ushikubi, Y. Yokota, R. Kageyama, S. Nakanishi, S. Narumiya, Cloning and expression of cDNA for a human thromboxane A_2 receptor, *Nature* 349 (1991) 617.
- [6(a)] R.A. Coleman, W.L. Smith, S. Narumiya, International Union of Pharmacology classification of prostanoid receptors: Properties, distribution, and structure of the receptors and their subtypes, *Pharmacol. Rev.* 46 (1994) 205.
- [6(b)] S. Narumiya, Y. Sugimoto, F. Ushikubi, Prostanoid receptors: Structures, properties, and functions, *Physiol. Rev.* 79 (1999) 1193.
- [6(c)] A.N. Hata, R.M. Breyer, Pharmacology and signaling of prostaglandin receptors: Multiple roles in inflammation and immune modulation, *Pharmacol. Ther.* 103 (2004) 147.
- [6(d)] A. Ichikawa, in: S. Murota, S. Yamamoto (Eds.), *New Development of Prostaglandin Research*, Vol. 38, Tokyo Kagaku Dojin, Tokyo, p. 8.
- [7(a)] H. Hirai, K. Tanaka, O. Yoshie, K. Ogawa, K. Kenmotsu, Y. Takamori, M. Ichimasa, K. Sugamura, M. Nakamura, S. Takano, K. Nagata, Prostaglandin D_2 selectively induces chemotaxis in T helper type 2 cells, eosinophils, and basophils via seven-transmembrane receptor CRTH2, *J. Exp. Med.* 193 (2001) 255.
- [7(b)] K. Nagata, K. Tanaka, K. Ogawa, K. Kemmotsu, T. Imai, O. Yosie, H. Abe, K. Tada, M. Nakamura, K. Sugamura, S. Takano, Selective expression of a novel surface molecule by human Th2 cells *in vivo*, *J. Immunol.* 162 (1999) 1278.

- [8] H. Abe, T. Takeshita, K. Nagata, T. Arita, Y. Endo, T. Fujita, H. Takayama, M. Kubo, K. Sugamura, Molecular cloning, chromosome mapping and characterization of the mouse CRTH2 gene, a putative member of the leukocyte chemoattractant receptor family, *Gene* 227 (1999) 71.
- [9] N. Sawyer, E. Cauchon, A. Chateaufneuf, R.P.G. Cruz, D.W. Nicholson, K.M. Metters, G.P. O'Neill, F.G. Gervais, Molecular pharmacology of the human prostaglandin D₂ receptor, CRTH2, *Br. J. Pharmacol.* 137 (2002) 1163.
- [10(a)] F. Ushikubi, Y. Sugimoto, A. Ichikawa, S. Narumiya, Roles of prostanoids revealed from studies using mice lacking specific prostanoid receptors, *Jpn. J. Pharmacol.* 83 (2000) 279.
- [10(b)] S. Narumiya, G.A. FitzGerald, Genetic and pharmacological analysis of prostanoid receptor function, *J. Clin. Invest.* 108 (2001) 25.
- [11] K. Nagata, H. Hirai, The second PGD₂ receptor CRTH2: Structure, properties, and functions in leukocytes, *Prostaglandins Leukot. Essent. Fatty Acids* 69 (2003) 169.
- [12] T. Matsuoka, M. Hirata, H. Tanaka, Y. Takahashi, T. Murata, K. Kabashima, Y. Sugimoto, T. Kobayashi, F. Ushikubi, Y. Aze, N. Eguchi, Y. Urade, N. Yoshida, K. Kimura, A. Mizoguchi, Y. Honda, H. Nagai, S. Narumiya, Prostaglandin D₂ as a mediator of allergic asthma, *Science* 287 (2000) 2013.
- [13] A. Mizoguchi, N. Eguchi, K. Kimura, Y. Kiyohara, W.M. Qu, Z.L. Huang, T. Mochizuki, M. Lazarus, T. Kobayashi, T. Kaneko, S. Narumiya, Y. Urade, O. Hayaishi, Dominant localization of prostaglandin D receptors on arachnoid trabecular cells in mouse basal forebrain and their involvement in the regulation of non-rapid eye movement sleep, *Proc. Natl. Acad. Sci. USA* 98 (2001) 11674.
- [14] Y. Matsuoka, T. Furuyashiki, K. Yamada, T. Nagai, H. Bito, Y. Tanaka, S. Kitaoka, F. Ushikubi, T. Nabeshima, S. Narumiya, Prostaglandin E receptor EP1 controls impulsive behavior under stress, *Proc. Natl. Acad. Sci. USA* 102 (2005) 16066.
- [15] K. Watanabe, T. Kawamori, S. Nakatsugi, T. Ohta, S. Ohuchida, H. Yamamoto, T. Maruyama, K. Kondo, F. Ushikubi, S. Narumiya, T. Sugimura, K. Wakabayashi, Role of the prostaglandin E receptor subtype EP1 in colon carcinogenesis, *Cancer Res.* 59 (1999) 5093.
- [16] T. Suganami, K. Mori, I. Tanaka, M. Mukoyama, A. Sugawara, H. Makino, S. Muro, K. Yahata, S. Ohuchida, T. Maruyama, S. Narumiya, K. Nakao, Role of prostaglandin E receptor EP1 subtype in the development of renal injury in genetically hypertensive rats, *Hypertension* 42 (2003) 1183.
- [17(a)] H. Hizaki, E. Segi, Y. Sugimoto, M. Hirose, T. Saji, F. Ushikubi, T. Matsuoka, Y. Noda, T. Tanaka, N. Yoshida, S. Narumiya, A. Ichikawa, Abortive expansion of the cumulus and impaired fertility in mice lacking the prostaglandin E receptor subtype EP2, *Proc. Natl. Acad. Sci. USA* 96 (1999) 10501.
- [17(b)] C.R. Kennedy, Y. Zhang, S. Brandon, Y. Guan, K. Coffee, C.D. Funk, M.A. Magnuson, J.A. Oate, M.D. Breyer, R.M. Breyer, Salt-sensitive hypertension and reduced fertility in mice lacking the prostaglandin EP2 receptor, *Nat. Med.* 5 (1999) 217.
- [18] S.L. Tilly, L.P. Audoly, E.H. Hicks, H.S. Kim, P.J. Flannery, T.M. Coffman, B.H. Koller, Reproductive failure and reduced blood pressure in mice lacking the EP2 prostaglandin E₂ receptor, *J. Clin. Invest.* 103 (1999) 1539.
- [19] F. Ushikubi, E. Segi, Y. Sugimoto, T. Murata, T. Matsuoka, T. Kobayashi, H. Hizaki, K. Tuboi, M. Katsuyama, A. Ichikawa, T. Tanaka, N. Yoshida, S. Narumiya, Impaired febrile response in mice lacking the prostaglandin E receptor subtype EP3, *Nature* 395 (1998) 281.
- [20] K. Takeuchi, H. Urawa, S. Kato, O. Furukawa, H. Araki, Y. Sugimoto, A. Ichikawa, F. Ushikubi, S. Narumiya, Impaired duodenal bicarbonate secretion and mucosal integrity in mice lacking prostaglandin E-receptor subtype EP3, *Gastroenterology* 117 (1999) 1128.
- [21] T. Kunikata, H. Yamane, E. Segi, T. Matsuoka, Y. Sugimoto, S. Tanaka, H. Tanaka, H. Nagai, A. Ichikawa, S. Narumiya, Suppression of allergic inflammation by the prostaglandin E receptor subtype EP3, *Nat. Immunol.* 6 (2005) 524.

- [22] E.F. Fleming, K. Athirakul, M.I. Oliverio, M. Key, J. Goulet, B.H. Koller, T.M. Coffman, Urinary concentrating function in mice lacking EP3 receptors for prostaglandin E₂, *Am. J. Physiol.* 275 (1998) F955.
- [23(a)] M. Nguyen, T. Camenisch, J.N. Snouwaert, E. Hicks, T.M. Coffman, P.A. Anderson, N.N. Malouf, B.H. Koller, The prostaglandin receptor EP4 triggers remodelling of the cardiovascular system at birth, *Nature* 390 (1997) 78.
- [23(b)] E. Segi, Y. Sugimoto, A. Yamasaki, Y. Aze, H. Oida, T. Nishimura, T. Murata, T. Matsuoka, F. Ushikubi, M. Fukumoto, T. Tanaka, N. Yoshida, S. Narumiya, A. Ichikawa, Patent ductus arteriosus and neonatal death in prostaglandin receptor EP4-deficient mice, *Biochem. Biophys. Res. Commun.* 246 (1998) 7.
- [24] C. Miyaura, M. Inada, T. Suzawa, Y. Sugimoto, F. Ushikubi, A. Ichikawa, S. Narumiya, T. Suda, Impaired bone resorption to prostaglandin E₂ in prostaglandin E receptor EP4-knockout mice, *J. Biol. Chem.* 275 (2000) 19819.
- [25] K. Kabashima, T. Saji, T. Murata, M. Nagamachi, T. Matsuoka, E. Segi, K. Tsuboi, Y. Sugimoto, T. Kobayashi, Y. Miyachi, A. Ichikawa, S. Narumiya, The prostaglandin receptor EP4 suppresses colitis, mucosal damage and CD4 cell activation in the gut, *J. Clin. Invest.* 109 (2002) 883.
- [26] Y., Sugimoto, A. Yamasaki, E. Segi, K. Tsuboi, Y. Aze, T. Nishimura, H. Oida, N. Yoshida, T. Tanaka, M. Katsuyama, K. Hasumoto, T. Murata, M. Hirata, F. Ushikubi, M. Negishi, A. Ichikawa, S. Narumiya, Failure of parturition in mice lacking the prostaglandin F receptor, *Science* 277 (1997) 681.
- [27] T. Ota, M. Aihara, S. Narumiya, M. Araie, The effects of prostaglandin analogues on IOP in prostanoid FP-receptor-deficient mice, *Invest. Ophthalmol. Vis. Sci.* 46 (2005) 4159.
- [28] T. Murata, F. Ushikubi, T. Matsuoka, M. Hirata, A. Yamasaki, Y. Sugimoto, A. Ichikawa, Y. Aze, T. Tanaka, N. Yoshida, A. Ueno, S. Oh-ishi, S. Narumiya, Altered pain perception and inflammatory response in mice lacking prostacyclin receptor, *Nature* 388 (1997) 678.
- [29] A. Hara, K. Yuhki, T. Fujino, T. Yamada, K. Takayama, S. Kuriyama, O. Takahata, H. Karibe, Y. Okada, C.-Y. Xiao, H. Ma, S. Narumiya, F. Ushikubi, Augmented cardiac hypertrophy in response to pressure overload in mice lacking the prostaglandin I₂ receptor, *Circulation* 112 (2005) 84.
- [30] Y. Hoshikawa, N.F. Voelkel, T. Gesell, M.D. Moore, K.G. Morris, L. Alger, S. Narumiya, M.W. Geraci, Prostacyclin receptor-dependent modulation of pulmonary vascular remodeling, *Am. J. Respir. Crit. Care Med.* 164 (2001) 314.
- [31] T. Kobayashi, Y. Tahara, M. Matsumoto, M. Iguchi, H. Sano, T. Murayama, H. Arai, H. Oida, T. Yurugi-Kobayashi, J.K. Yamashita, H. Katagiri, M. Majima, M. Yokode, T. Kita, S. Narumiya, Roles of thromboxane A(2) and prostacyclin in the development of atherosclerosis in apoE-deficient mice, *J. Clin. Invest.* 114 (2004) 784.
- [32] D.W. Thomas, R.B. Mannon, P.J. Mannon, A. Latour, J.A. Oliver, M. Hoffman, O. Smithies, B.H. Koller, T.M. Coffman, Coagulation defects and altered hemodynamic responses in mice lacking receptors for thromboxane A₂, *J. Clin. Invest.* 102 (1998) 1994.
- [33] J. Fried, E.F. Sabo, 9 α -Fluoro derivatives of cortisone and hydrocortisone, *J. Am. Chem. Soc.* 76 (1954) 1455.
- [34(a)] R. Filler, Y. Kobayashi, *Biomedical Aspects of Fluorine Chemistry*, Kodansya and Elsevier Biomedical, Tokyo and Amsterdam, 1982.
- [34(b)] J.T. Welch, S. Eswar Krishnan, *Fluorine in Bioorganic Chemistry*, John Wiley & Sons, New York, 1991.
- [34(c)] R. Filler, Y. Kobayashi, L.M. Yagupolskii, *Organofluorine Compounds in Medicinal Chemistry and Biomedical Applications*, Elsevier, Amsterdam, 1993.
- [34(d)] V.P. Kukhar, V.A. Soloshonok, *Fluorine-containing Amino Acids: Synthesis and Properties*, Wiley, Chichester, 1995.
- [34(e)] I. Ojima, J.R. McCarthy, J.T. Welch, *Biomedical Frontiers of Fluorine Chemistry*, American Chemical Society, Washington, DC, 1996.
- [34(f)] T. Hiyama, *Organofluorine Compounds, Chemistry and Applications*, Springer, Berlin, 2000.

- [35(a)] W.E. Barnette, The synthesis and biology of fluorinated prostacyclins, *CRC Crit. Rev. Biochem.* 15 (1984) 201.
- [35(b)] A. Yasuda, Ref. [34] (c) p. 275.
- [35(c)] Y. Matsumura, Recent developments in fluorinated prostanoids, *J. Synth. Org. Chem. Jpn.* 63 (2005) 40.
- [36(a)] S.M. Roberts, F. Scheimann, *New Synthetic Routes to Prostaglandins and Thromboxanes*, Academic Press, London, 1982.
- [36(b)] P.W. Collins, S.W. Djuric, Synthesis of therapeutically useful prostaglandin and prostacyclin analogs, *Chem. Rev.* 93 (1993) 1533.
- [37] M. Dukes, W. Russel, A.L. Walpole, Potent luteolytic agents related to prostaglandin $F_{2\alpha}$, *Nature* 250 (1974) 330.
- [38] B.J. Magerlein, W.L. Miller, 16-Fluoroprostaglandins, *Prostaglandins* 9 (1975) 527.
- [39] J. Fried, M. Mitra, M. Nagarajan, M.M. Mehrotra, 10,10-Difluoro-13-dehydroprostacyclin: A chemically and metabolically stabilized potent prostacyclin, *J. Med. Chem.* 23 (1980) 234.
- [40(a)] T.A. Morinelli, A.K. Okwu, D.E. Mais, P.V. Halushka, V. John, C.-K. Chen, J. Fried, Difluorothromboxane A_2 and stereoisomers: Stable derivatives of thromboxane A_2 with differential effects on platelets and blood vessels, *Proc. Natl. Acad. Sci. USA* 86 (1989) 5600.
- [40(b)] J. Fried, V. John, M.J. Szewedo, C.K. Chen, C. O'Yang, T.A. Morinelli, A.K. Okwu, P. V. Halushka, Synthesis of 10,10-difluorothromboxane A_2 , a potent and chemically stable thromboxane agonist, *J. Am. Chem. Soc.* 111 (1989) 4510.
- [41] M. Takasuka, M. Kishi, M. Yamakawa, FTIR spectral study of intramolecular hydrogen bonding in thromboxane A_2 receptor agonist (U-46619), prostaglandin (PG) E_2 , PGD $_2$, PGF $_2$. α , prostacyclin receptor agonist (carbacyclin) and their related compounds in dilute carbon tetrachloride solution: Structure-activity relationships, *J. Med. Chem.* 37 (1994) 47.
- [42] A report of PGF derivatives on ligand docking experiments to a human FP receptor model: Y. Wang, J.A. Wos, M.J. Dirr, D.L. Soper, M.A. deLong, G.E. Mieling, B. De, J.S. Amberg, E.G. Suchanek, C.J. Taylor, Design and synthesis of 13,14-Dihydro prostaglandin F_{1a} analogues as potent and selective ligands for the human FP receptor, *J. Med. Chem.* 43 (2000) 945.
- [43] M. Kiriya, F. Ushikubi, T. Kobayashi, M. Hirata, Y. Sugimoto, S. Narumiya, Ligand binding specificities of the eight types and subtypes of the mouse prostanoid receptors expressed in Chinese hamster ovary cells, *Br. J. Pharmacol.* 122 (1997) 217.
- [44(a)] R. Ueno, EP 0503887 (2005).
- [44(b)] R. Ueno, US 6414016 (2002).
- [44(c)] L.A. Sorbera, J. Castaner, N.E. Mealy, Lubiprostone, *Drug Fut.* 29 (2004) 336.
- [45] R. Ueno, J. Cuppoletti, WO 0330912 (2003).
- [46] Scampo Pharmaceuticals; <http://www.sucampo.com>.
- [47] H. Kawahara, A. Sakamoto, S. Takeda, H. Onodera, J. Imaki, R. Ogawa, A prostaglandin E_2 receptor subtype EP1 receptor antagonist (ONO-8711) reduces hyperalgesia, allodynia, and c-fos gene expression in rats with chronic nerve constriction, *Anesth. Analg.* 93 (2001) 1012.
- [48] P.F. Durrenberger, P. Facer, M.A. Casula, Y. Yiangou, R.A. Gray, I. P. Chessell, N.C. Day, S.D. Collins, S. Bingham, A.W. Wilson, D. Elliot, R. Birch, P. Anand, Prostanoid receptor EP1 and Cox-2 in injured human nerves and a rat model of nerve injury: A time-course study, *BMC Neurol.* 6 (2006) 1.
- [49] E.A. Hallinan, T.J. Hagen, R.K. Husa, S. Tsybalov, S.N. Rao, J.P. vanHoeck, M.F. Rafferty, A. Stapelfeld, M.A. Savage, M. Reichman, N-substituted dibenzoxazepines as analgesic PGE $_2$ antagonists, *J. Med. Chem.* 36 (1993) 3293.
- [50] A.B. Malmberg, M.F. Rafferty, T.L. Yaksh, Antinociceptive effect of spinally delivered prostaglandin E receptor antagonists in the formalin test on the rat, *Neurosci. Lett.* 173 (1994) 193.
- [51(a)] S. Ohuchida, Y. Nagao, WO 9827053 (1998).

- [51(b)] S. Narumiya, Prostanoid receptors and new drug development, *Folia Pharmacol. Jpn.* 117 (2001) 243.
- [52] R.A. Coleman, I. Kennedy, R.L.G. Sheldrick, AH6809, a prostanoid EP 1 receptor blocking drug, *Br. J. Pharmacol.* 85 (1985) 273.
- [53] S. Ohuchida, Y. Nagao, T. Maruyama, EP 878465 (1998).
- [54] A.S. Ahmad, S. Saleem, M. Ahmad, S. Dore, Prostaglandin EP1 receptor contributes to excitotoxicity and focal ischemic brain damage, *Toxicol. Sci.* 89 (2006) 265.
- [55] H. Makino, I. Tanaka, M. Mukoyama, A. Sugawara, K. Mori, S. Muro, T. Suganami, K. Yahata, R. Ishibashi, S. Ohuchida, T. Maruyama, S. Narumiya, K. Nakao, Prevention of diabetic nephropathy in rats by prostaglandin E receptor EP1-selective antagonist, *J. Am. Soc. Nephrol.* 13 (2002) 1757.
- [56(a)] M. Oshima, J.E. Dinchuk, S.L. Kargman, H. Oshima, B. Hancock, E. Kwong, J.M. Trzaskos, J.F. Evans, M.M. Taketo, Suppression of intestinal polyposis in *Apc delta716* knockout mice by inhibition of cyclooxygenase 2 (COX-2), *Cell* 87 (1996) 803.
- [56(b)] S.M. Fischer, H.-H. Lo, G.B. Gordon, K. Seibert, G. Kelloff, R.A. Lubet, C.J. Conti, Chemopreventive activity of celecoxib, a specific cyclooxygenase-2 inhibitor, and indomethacin against ultraviolet light-induced skin carcinogenesis, *Mol. Carcinog.* 25 (1999) 231.
- [57] K. Watanabe, T. Kamimori, S. Nakatsugi, T. Ohta, S. Ohuchida, H. Yamamoto, T. Maruyama, K. Kondo, S. Narumiya, T. Sugimura, K. Wakabayashi, Inhibitory effect of a prostaglandin E receptor subtype EP1 selective antagonist, ONO-8713, on development of azoxymethane-induced aberrant crypt foci in mice, *Cancer Lett.* 156 (2000) 57.
- [58] K.L. Tober, T.A. Wilgus, D.K. Kusewitt, J.M. Thomas-Ahner, T. Maruyama, T.M. Oberyszyn, Importance of the EP1 receptor in cutaneous UVB-induced inflammation and tumor development, *J. Invest. Dermatol.* 126 (2006) 205.
- [59] S. Ohuchida, K. Tani, JP 2000-95755 (2000).
- [60] K. Tani, A. Naganawa, A. Ishida, H. Egashira, K. Sagawa, H. Harada, M. Ogawa, T. Maruyama, S. Ohuchida, H. Nakai, K. Kondo, M. Toda, Design and synthesis of a highly selective EP2-receptor agonist, *Bioorg. Med. Chem. Lett.* 11 (2001) 2025.
- [61(a)] K. Yoshida, H. Oida, T. Kobayashi, T. Maruyama, M. Tanaka, T. Katayama, K. Yamaguchi, E. Segi, T. Tsuboyama, M. Matsushita, K. Ito, Y. Ito, *et al.* Stimulation of bone formation and prevention of bone loss by prostaglandin E EP4 receptor activation, *Proc. Natl. Acad. Sci. USA* 99 (2002) 4580.
- [61(b)] T. Maruyama, S. Kuwabe, Y. Kawanaka, T. Shiraishi, Y. Shinagawa, K. Sakata, A. Seki, Y. Kishida, H. Yoshida, T. Maruyama, S. Ohuchida, H. Nakai, S. Hashimoto, M. Kawamura, K. Kondo, M. Toda, Design and synthesis of a selective EP4-receptor agonist. Part 4: practical synthesis and biological evaluation of a novel highly selective EP4-receptor agonist, *Bioorg. Med. Chem.* 10 (2002) 2103.
- [62] M. Nitta, I. Hirata, K. Toshina, M. Murano, K. Maemura, N. Hashimoto, S. Sasaki, H. Yamauchi, K. Katsu, Expression of the EP4 prostaglandin E₂ receptor subtype with rat dextran sodium sulphate colitis: Colitis suppression by a selective agonist, ONO-AE1-329, *Scand. J. Immunol.* 56 (2002) 66.
- [63] K.O. Cameron, B.A. Lefker, D.R.J. Knight, WO 0377910 (2003).
- [64] L.Z. Bito, Comparison of the ocular hypotensive efficacy of eicosanoids and related compounds, *Exp. Eye Res.* 38 (1984) 181.
- [65(a)] J. Stjernschantz, B. Resul, Phenyl substituted prostaglandin analogs for glaucoma treatment, *Drugs Fut.* 17 (1992) 691.
- [65(b)] N. Ishida, N. Odani-Kawabata, A. Shimazaki, H. Hara, Prostanoids in the therapy of glaucoma, *Cardiovasc. Drug Rev.* 24 (2006) 1.
- [66] M. Sakurai, M. Araie, T. Oshika, M. Mori, K. Masuda, R. Ueno, M. Takase, Effects of topical application of UF-021, a novel prostaglandin derivative, on aqueous humor dynamics in normal human eyes, *Jpn. J. Ophthalmol.* 35 (1991) 156.

- [67] B. Resul, J. Stjernschantz, K. No, C. Liljebris, G. Selen, M. Astin, M. Karlsson, L.Z. Bito, Phenyl-substituted prostaglandins: Potent and selective antiglaucoma agents, *J. Med. Chem.* 36 (1993) 243.
- [68] M. Wand, R. Ritch, E.K.J. Isbey, T.J. Zimmerman, Latanoprost and periocular skin color changes, *Arch. Ophthalmol.* 119 (2001) 614.
- [69] P.A. Netland, T. Landry, E.K. Sullivan, R. Andrew, L. Silver, A. Weiner, S. Mallick, J. Dickerson, M.V. Bergamini, S.M. Robertson, A.A. Davis, Travoprost compared with latanoprost and timolol in patients with open-angle glaucoma or ocular hypertension, *Am. J. Ophthalmol.* 132 (2001) 472.
- [70] L.T. Boulton, D. Brick, M.E. Fox, M. Jackson, I.C. Lennon, R. McCague, N. Parkin, D. Rhodes, G. Ruecroft, Synthesis of the potent antiglaucoma agent, travoprost, *Org. Proc. Res. Dev.* 6 (2002) 138.
- [71] Y. Matsumura, N. Mori, T. Nakano, H. Sasakura, T. Matsugi, H. Hara, Y. Morizawa, Synthesis of the highly potent prostanoid FP receptor agonist, AFP-168: A novel 15-deoxy-15,15-difluoroprostaglandin $F_{2\alpha}$ derivative, *Tetrahedron Lett.* 45 (2004) 1527.
- [72] T. Nakajima, T. Matsugi, W. Goto, M. Kageyama, N. Mori, Y. Matsumura, H. Hara, New fluoroprostaglandin $F(2\alpha)$ derivatives with prostanoid FP-receptor agonistic activity as potent ocular-hypotensive agents, *Biol. Pharm. Bull.* 26 (2003) 1691.
- [73(a)] Synthesis of 15-deoxy-15-fluoro-PGF $_{2\alpha}$: V.V. Bezuglov, L.D. Bergelson, Synthesis of fluoroprostacyclins, *Dokl. Akad. Nauk SSSR* 250 (1980) 468.
- [73(b)] Independently reported ocular hypotensive effects of 15-deoxy-15-fluoro-PGF $_{2\alpha}$ derivatives: P. Klimko, M. Hellberg, M. McLaughlin, N. Sharif, B. Severns, G. Williams, K. Haggard, J. Liao, 15-Fluoro prostaglandin FP agonists: A new class of topical ocular hypotensives, *Bioorg. Med. Chem.* 12 (2004) 3451.
- [74] Y. Takagi, T. Nakajima, A. Shimazaki, M. Kageyama, T. Matsugi, Y. Matsumura, B.T. Gabelt, P.L. Kaufman, H. Hara, Pharmacological characteristics of AFP-168 (tafluprost), a new prostanoid FP receptor agonist, as an ocular hypotensive drug, *Exp. Eye Res.* 78 (2004) 767.
- [75] B. Resul, J. Stjernschantz, Structure-activity relationships of prostaglandin analogues as ocular hypotensive agents, *Curr. Opin. Ther. Pat.* 3 (1993) 781.
- [76] K. Bergh, P. Wentzel, J. Stjernschantz, Production of prostaglandin E_2 by iridial melanocytes exposed to latanoprost acid, a prostaglandin $F_{2\alpha}$ analogue, *J. Ocular Pharmacol. Ther.* 18 (2002) 391.
- [77] T. Ota, H. Murata, E. Sugimoto, M. Aihara, M. Araie, Prostaglandin analogues and mouse intraocular pressure: Effects of tafluprost, latanoprost, travoprost, and unoprostone, considering 24-hour variation, *Invest. Ophthalmol. Vis. Sci.* 46 (2005) 2006.
- [78] N. Izumi, T. Nagaoka, E. Sato, F. Mori, A. Takahashi, A. Yoshida, DE-085 increases retinal blood flow, *Invest. Ophthalmol. Vis. Sci. Abst.* 45 (2004) 2340.
- [79] N.A. Sharif, J.Y. Crider, T.L. Davis, AL-3138 antagonizes FP prostanoid receptor-mediated inositol phosphates generation: Comparison with some purported FP antagonists, *J. Pharm. Pharmacol.* 52 (2000) 1529.
- [80] B.W. Griffin, P. Klimko, J.Y. Crider, N.A. Sharif, AL-8810: A novel prostaglandin F_2 α analog with selective antagonist effects at the prostaglandin F_2 α (FP) receptor, *J. Pharmacol. Exp. Ther.* 290 (1999) 1278.
- [81] N.A. Sharif, B.W. Griffin, US 6441033 (2002).
- [82] B.J. Whittle, S. Moncada, K. Mullane, J.R. Vane, Platelet and cardiovascular activity of the hydantoin BW245C, a potent prostaglandin analogue, *Prostaglandins* 25 (1983) 205.
- [83(a)] T. Tsuji, T. Honma, Y. Hiramatsu, S. Mitsumori, M. Inagaki, A. Arimura, K. Yasui, F. Asanuma, J. Kishino, M. Ohtani, Bicyclo[2.2.1]heptane and 6,6-dimethylbicyclo[3.1.1]heptane derivatives: Orally active, potent, and selective prostaglandin D_2 receptor antagonists, *J. Med. Chem.* 40 (1997) 3504.
- [83(b)] A. Arimura, K. Yasui, J. Kishino, F. Asanuma, H. Hasegawa, S. Kakudo, M. Ohtani, H. Arita, Prevention of allergic inflammation by a novel prostaglandin receptor antagonist, S-5751, *J. Pharmacol. Exp. Ther.* 298 (2001) 411.

- [84] K.R. Campos, M. Journet, S. Lee, E.J.J. Grabowski, R.D. Tillyer, Asymmetric synthesis of a prostaglandin D₂ receptor antagonist, *J. Org. Chem.* 70 (2005) 268.
- [85] A. Shafree, V. Upadhyay, E. Corley, M. Biba, D. Zhao, J.-F. Marcoux, K. Campos, M. Journet, A. King, R. Larsen, E. Grabowski, R. Volante, R. Tillyer, An efficient enzyme-catalyzed kinetic resolution: Large-scale preparation of an enantiomerically pure indole-ethyl ester derivative, a key component for the synthesis of a prostaglandin D₂ receptor antagonist, an anti-allergic rhinitis drug candidate, *Tetrahedron Asymmetry* 16 (2005) 3094.
- [86] M.D. Truppo, M. Journet, A. Shafree, J.C. Moore, Optimization and scale-up of a lipase-catalyzed enzymatic resolution of an indole ester intermediate for a prostaglandin D₂ (DP) receptor antagonist targeting allergic rhinitis, *Org. Proc. Res. Dev.* 10 (2006) 592.
- [87] G. Monneret, C. Cossette, S. Gravel, J. Rokach, W.S. Powell, 15R-methyl-prostaglandin D₂ is a potent and selective CRTH2/DP2 receptor agonist in human eosinophils, *J. Pharmacol. Exp. Ther.* 304 (2003) 349.
- [88] H. Hirai, K. Tanaka, S. Takano, M. Ichimasa, M. Nakamura, K. Nagata, Agonistic effect of indomethacin on a prostaglandin D₂ receptor, CRTH2, *J. Immunol.* 168 (2002) 981.
- [89] A.N. Hata, T.P. Lybrand, L.J. Marnett, R.M. Breyer, Structural determinants of arylacetic acid nonsteroidal anti-inflammatory drugs necessary for binding and activation of the prostaglandin D₂ receptor CRTH2, *Mol. Pharmacol.* 67 (2005) 640.
- [90] F.G. Gervais, J.P. Morello, C. Beaulieu, N. Sawyer, D. Denis, G. Greig, D. Malebranche, G.P. O'Neill, Identification of a potent and selective synthetic agonist at the CRTH2 receptor, *Mol. Pharmacol.* 67 (2005) 1834.
- [91] H. Sugimoto, M. Shichijo, T. Iino, Y. Manabe, A. Watanabe, M. Shimazaki, F. Gantner, K.B. Bacon, An orally bioavailable small molecule antagonist of CRTH2, ramatroban (BAY u3405), inhibits prostaglandin D₂-induced eosinophil migration *in vitro*, *J. Pharmacol. Exp. Ther.* 305 (2003) 347.
- [92] T. Ulven, E. Kostenis, Minor structural modifications convert the dual TP/CRTH2 antagonist ramatroban into a highly selective and potent CRTH2 antagonist, *J. Med. Chem.* 48 (2005) 897.
- [93] R.E. Armer, M.R. Ashton, E.A. Boyd, C.J. Brennan, F.A. Brookfield, L. Gazi, S.L. Gyles, P.A. Hay, M.G. Hunter, D. Middlemiss, M. Whittaker, L. Xue, *et al.* Indole-3-acetic acid antagonists of the prostaglandin D₂ receptor CRTH2, *J. Med. Chem.* 48 (2005) 6174.
- [94] S. Moncada, R.J. Gryglewski, S. Bunting, J.R. Vane, An enzyme isolated from arteries transforms prostaglandin endoperoxides to an unstable substance that inhibits platelet aggregation, *Nature* 263 (1976) 663.
- [95] M. Hamberg, J. Svensson, T. Wakabayashi, B. Samuelsson, Thromboxanes: A new group of biologically active compounds derived from prostaglandin endoperoxides, *Proc. Natl. Acad. Sci. USA* 72 (1975) 2994.
- [96] M.J. Cho, M.A. Allen, Chemical stability of prostacyclin (PGI₂) in aqueous solutions, *Prostaglandins* 15 (1978) 943.
- [97] W. Skuballa, H. Vorbruggen, A new route to 6a-carbacyclin. Synthesis of a stable, biologically active prostacyclin analogue, *Angew. Chem. Int. Ed. Engl.* 20 (1981) 1046.
- [98] T. Murata, S. Sakaya, T. Hoshino, T. Umetsu, T. Hirano, S. Nishio, General pharmacology of beraprost sodium. 1st Communication: Effect on the central nervous system, *Arzneim. Forsch.* 39(II) (1989) 860.
- [99(a)] D.B. Badesch, V.V. McLaughlin, M. Delcroix, C. Vizza, H. Olschewski, O. Sitbon, R.J. Barst, Prostanoid therapy for pulmonary arterial hypertension, *J. Am. Coll. Cardiol.* 43 (2004) 56S.
- [99(b)] R.M. Moriarty, N. Rani, L.A. Enache, M.S. Rao, H. Batra, L. Guo, R.A. Penmasta, J.P. Staszewski, S.M. Tuladhar, O. Prakash, D. Crich, A. Hirtopeanu, R. Gilardi, The intramolecular asymmetric Pauson-Khand cyclization as a novel and general stereoselective route to benzindene prostacyclins: Synthesis of UT-15 (Treprostinil), *J. Org. Chem.* 69 (2004) 1890.

- [100] K. Bannai, T. Toru, T. Oba, T. Tanaka, N. Okamura, K. Watanabe, A. Hazato, S. Kurozumi, Synthesis of chemically stable prostacyclin analogs, *Tetrahedron* 39 (1983) 3807.
- [101] S.W. Djuric, R.B. Garland, L.N. Nysted, R. Pappo, G. Plume, L. Swenton, Synthesis of 5-fluoroprostacyclin, *J. Org. Chem.* 52 (1987) 978.
- [102(a)] T. Asai, Y. Morizawa, T. Shimada, T. Nakayama, M. Urushihara, Y. Matsumura, A. Yasuda, Synthesis of new stable fluoroprostacyclin analogs with potent anti-anginal activity, *Tetrahedron Lett.* 36 (1995) 273.
- [102(b)] Y. Matsumura, T. Shimada, T. Nakayama, M. Urushihara, T. Asai, Y. Morizawa, A. Yasuda, Synthesis of 7-fluoro-2,4-methylene-17,20-dimethylprostacyclins. Novel stable prostacyclin analogs as potent anti-anginal agents, *Tetrahedron* 51 (1995) 8771.
- [102(c)] Y. Matsumura, T. Nakano, T. Asai, Y. Morizawa, Ref. [34] (e), p. 83.
- [103] R. Noyori, M. Suzuki, New synthetic methods. (49). Prostaglandin syntheses by three-component coupling, *Angew. Chem. Int. Ed. Engl.* 23 (1984) 847.
- [104(a)] Y. Matsumura, S.-Z. Wang, T. Asai, T. Shimada, Y. Morizawa, A. Yasuda, Facile and efficient synthesis of fluoroprostacyclin analogs, *Synlett* (1995) 260.
- [104(b)] Y. Matsumura, T. Shimada, S.-Z. Wang, T. Asai, Y. Morizawa, A. Yasuda, Study of efficient synthetic routes for 7-fluoroprostaglandin F_{2x} and 7-fluoro-17,20-dimethyl-2,4-methyleneprostacyclin, *Bull. Chem. Soc. Jpn.* 69 (1996) 3523.
- [105] Y. Matsumura, T. Asai, T. Shimada, T. Nakayama, M. Urushihara, Y. Morizawa, A. Yasuda, T. Yamamoto, B. Fujitani, K. Hosoki, Novel fluoroprostacyclin analogs with modified cycloalkylenyl chains. Highly potent and orally active anti-anginal agents, *Chem. Pharm. Bull.* 43 (1995) 353.
- [106] T. Nakano, M. Makino, Y. Morizawa, Y. Matsumura, Synthesis of novel difluoroprostacyclin derivatives: Unprecedented stabilizing effect of fluorine substituents, *Angew. Chem. Int. Ed. Engl.* 35 (1996) 1019.
- [107] Y. Matsumura, T. Nakano, N. Mori, Y. Morizawa, Synthesis and biological properties of novel fluoroprostaglandin derivatives: Highly selective and potent agonists for prostaglandin receptors, *Chimia* 58 (2004) 148.
- [108] C.S. Chan, M. Negishi, T. Nakano, Y. Morizawa, Y. Matsumura, A. Ichikawa, 7,7-Difluoroprostacyclin derivative, AFP-07, a highly selective and potent agonist for the prostacyclin receptor, *Prostaglandins* 53 (1997) 83.
- [109] A.K. Sim, M.E. Cleland, A.B. Pottage, Y. Matsumura, T. Nakano, The antithrombotic activity of AFP-07, a potent novel prostacyclin analogue, *10th Int. Conf. Prostaglandins Rel. Comp.*, Vienna (1996).
- [110] L. Alger, M. Geraci, R.M. Tuderand, N.F. Voelkel, AFP-07 prevents chronic hypoxic pulmonary hypertension in rats, *Abst. of the 91th Int. Conf. Am. Heart Assoc. Am. Thor. Soc.*, C46-K7, Chicago (1998).
- [111(a)] N. Kanai, R. Lu, J.A. Satriano, Y. Bao, A.W. Wolkoff, V.L. Schuster, Identification and characterization of a prostaglandin transporter, *Science* 268 (1995) 866.
- [111(b)] S. Itoh, R. Lu, Y. Bao, J.D. Morrow, L.J. Roberts, V.L. Schuster, Structural determinants of substrates for the prostaglandin transporter PGT, *Mol. Pharmacol.* 50 (1996) 736.
- [111(c)] V.L. Schuster, Molecular mechanism of prostaglandin transport, *Ann. Rev. Physiol.* 60 (1998) 221.
- [112] K.-H. Ruan, J. Wu, S.-P. So, L.A. Jenkins, Evidence of the residues involved in ligand recognition in the second extracellular loop of the prostacyclin receptor characterized by high resolution 2D NMR techniques, *Arch. Biochem. Biophys.* 418 (2003) 25.
- [113] M. Suzuki, H. Doi, K. Kato, M. Bjorkman, B. Langstrom, Y. Watanabe, R. Noyori, Rapid methylation for the synthesis of a ¹¹C-labeled tolylisocarbacyclin imaging the IP₂ receptor in a living human brain, *Tetrahedron* 56 (2000) 8263.

This page intentionally left blank

CHAPTER 15

Synthesis and Biochemical Evaluation of Fluorinated Monoamine Oxidase Inhibitors

Kenneth L. Kirk,^{*,1} Shinichi Yoshida,² and Günter Haufe³

¹*Laboratory of Bioorganic Chemistry, National Institute of Diabetes and Digestive and Kidney Diseases, National Institutes of Health, DHHS, 8 Center Drive, MSC 0810, Bethesda, MD 20814, USA*

²*Tottori Institute of Industrial Technology, 7-1-1, Wakabadai-minami, Tottori 689-1112, Japan*

³*Organisch-Chemisches Institut, Westfälische Wilhelms-Universität Münster, D-48149 Münster, Germany*

Contents

1. Introduction	662
1.1. Amine oxidases	662
1.1.1. Monoamine oxidases (EC 1.4.3.4)	662
1.1.2. Polyamine oxidase (EC 1.4.3.4)	664
1.1.3. Semicarbazide-sensitive amine oxidases (EC 1.4.3.6)	664
1.2. Drugs targeting amine oxidases	664
1.2.1. MAO inhibitors	664
1.2.2. SSAO inhibitors	665
1.3. Fluorine in drug design	665
2. Ring-fluorinated MAO inhibitors	666
2.1. Fluorine-substituted benzylamines and 2-phenylethylamines	666
2.2. 4-Fluorotranlylcypromine	669
2.3. Aryl- <i>N</i> -aminoethylamide derivatives, for example, Ro-41-1049 and Ro-16-6491	670
3. Aromatic side chain-fluorinated MAO and SSAO inhibitors	671
3.1. β,β -Difluorinated phenethylamines	672
3.2. Fluoroallylamines as irreversible MAO inhibitors	672
3.3. Haloallylamines as SSAO inhibitors	673
3.4. Allyl hydrazines as SSAO inhibitors	674
3.5. Fluorinated aryl-oxazolidinone derivatives, for example, befloxtone	674
3.6. Fluorinated 5 <i>H</i> -indeno[1,2- <i>c</i>]pyridazin-5-one MAO B-selective inhibitors	675
4. Fluorinated MAO inhibitors as PET-scanning agents	676
4.1. Fluorinated amine oxidase inhibitors as PET-imaging agents in the CNS	676
4.2. ¹¹ C-Labeled MAO inhibitors	677
4.3. ¹⁸ F-Labeled MAO inhibitors	677

^{*}Corresponding author. Tel.: +1-301-496-2619; Fax: +1-301-402-4182;
E-mail: kennethk@bdg8.niddk.nih.gov

5. Fluorinated cyclopropylamines as inhibitors of SSAO and MAO	679
5.1. Cyclopropylamines as inhibitors of SSAO and MAO	679
5.1.1. Overview of the development of cyclopropylamines as MAO inhibitors	679
5.1.2. Isozyme selectivity of cyclopropylamine MAO inhibitors	680
5.1.3. Mechanisms of inhibition	681
5.2. Effects of fluorine substitution on inhibition of SSAO by cyclopropyl amines	683
5.3. Effects of fluorine substitution on MAO inhibition	684
6. Final comments	687
Acknowledgment	688
References	688

Abstract

The selective introduction of fluorine provides many advantages in the design of analogues of biologically important molecules. This strategy has been applied successfully in the design of pharmacological probes and medicinal agents over the broad spectrum of available biological targets. As targets for therapeutic intervention, amine oxidases have critically important functions in both prokaryotic and eukaryotic life forms. Because of the potent biological activities of amines, both endogenous and exogenous, efficient mechanisms for their deactivation have evolved and amine oxidase-catalyzed oxidation plays a large role in this deactivation. It is not surprising that these enzymes became the focus of intense research as therapeutic potential of modulating their activities became apparent. The special properties of fluorine have been exploited successfully in many aspects of research on these amine oxidases. These include development of selective inhibitors, tools for studies of reaction mechanisms, agents for positron emission tomography (PET) imaging, and development of medicinal agents. In this chapter, we focus on the use of fluorine substitution in research on two types of enzymes, the flavin-dependent monoamine oxidases (MAO) A and B and the copper-containing amine oxidases (CAO), also known as semicarbazide-sensitive amine oxidases (SSAO).

1. INTRODUCTION

1.1. Amine oxidases

Amine oxidases catalyze the oxidative deamination of both xenobiotic and biogenic amines, and thus have many critical biological functions. Two distinct classes differ in the nature of their prosthetic groups [1]. The flavin-(FAD: flavin adenine dinucleotide)-dependent amine oxidases include monoamine oxidases (MAO A and B) and polyamine oxidases. Amine oxidases not containing FAD, the so-called semicarbazide-sensitive amine oxidases (SSAO), include both plasma amine oxidases and tissue amine oxidases. These contain quinonoid structures as redox cofactors that are derived from posttranslationally modified tyrosine or tryptophan side chains, topaoquinone frequently playing this role [2].

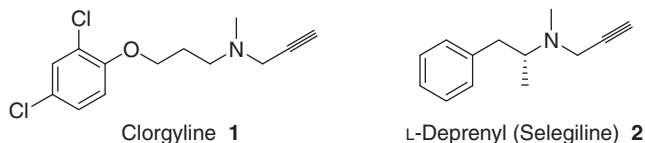
1.1.1. Monoamine oxidases (EC 1.4.3.4)

Maintaining a proper balance of neurotransmitter synthesis and storage, release to the postsynaptic cleft, reuptake into neuronal vesicles, and metabolism is an

absolute requirement for normal neuronal function. With catecholamine- and serotonin-containing neurons, reuptake is the principal mechanism for rapid curtailment of neurotransmitter action and maintaining transmitter homeostasis. However, oxidative deamination by MAO (amine:oxygen oxidoreductase, deaminating, flavin-containing), is also a decisive mechanism for deactivation of catecholaminergic and serotonergic neurotransmitters, and is one of the important functions of these enzymes. In addition, intestinal MAO metabolizes dietary pressor amines, vascular MAO protects organs from circulating pressor amines, and liver MAO controls blood levels of these amines. MAO will oxidize a wide variety of primary aliphatic and aromatic amines, as well as some secondary and tertiary amines, an important requirement being the presence of an α -hydrogen atom [3].

In the late 1960s, two groups reported results that indicated the possibility of more than one form of MAO. In 1967, Maître suggested that tissue (brain vs liver)-dependent potencies of inhibitors could be explained by the presence of different forms of MAO [4]. In 1968, Johnston published an analysis of unusual kinetics observed with the new MAO inhibitors that were being developed. He concluded that the most reasonable hypothesis to explain such results as double sigmoid curves was the existence of at least two forms of the enzyme [5]. By the mid-1980s, differences of substrate and inhibitor specificity of two MAOs, now called MAO A and B, were well understood [6].

MAO A and B differ in primary structure and in substrate specificity [5,7]. The two isozymes, located on the mitochondrial outer membranes, have 70% homology in peptide sequence and share common mechanistic details. It is now recognized that these are different proteins encoded by different genes, but probably derived from a common ancestral gene. Crystal structures for both MAO A and B complexes with inhibitors have recently been reported [8]. Serotonin is selectively oxidized by MAO A, whereas benzylamine and 2-phenylethylamine are selective substrates for MAO B. Dopamine, norepinephrine, epinephrine, tryptamine, and tyramine are oxidized by both MAO A and B in most species [9]. In addition, MAO A is more sensitive to inhibition by clorgyline (**1**), whereas MAO B is inhibited by low concentrations of L-deprenyl ((*R*)-(-)-deprenyl) (**2**) [5,6c]. Development of inhibitors that are selective for each isozyme has been an extremely active area of medicinal chemistry [8].



A single electron transfer (SET) mechanism involving initial transfer of an electron from the FAD cofactor has been proposed for MAO-catalyzed oxidations [10]. An alternative polar nucleophilic mechanism has also received support [11].

1.1.2. Polyamine oxidase (EC 1.4.3.4)

Polyamine oxidase (amine:oxygen oxidoreductase, deaminating, flavin-containing), is also a FAD-dependent enzyme and has many similarities to MAO. It is responsible for the oxidation of the secondary amino group in such substrates as *N*-acetyl spermine and spermidine in the biosynthesis of spermidine and putrescine [1,12]. This enzyme will not be covered in this chapter.

1.1.3. Semicarbazide-sensitive amine oxidases (EC 1.4.3.6)

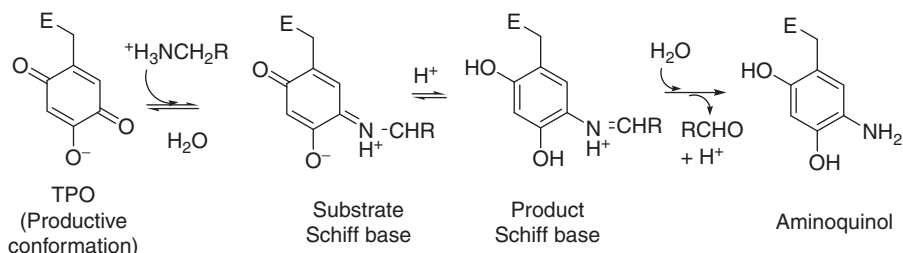
Semicarbazide-sensitive amine oxidases (SSAOs, amine:oxygen oxidoreductase, deaminating, copper-containing) are copper-dependent amine oxidases (CAO) which occur widely in bacteria, yeast, plants, and mammals and have a strict preference for oxidation of primary amines. Most of these enzymes contain a topaquinone cofactor that is derived posttranslationally from an active site tyrosine residue. SSAOs are receiving increasing attention as more and more important roles for these amine oxidases are being identified in eukaryotes [13]. SSAOs are found in various mammalian tissues, especially in vascular smooth muscle cells, but also in cartilage, adipose tissue, and plasma. Of particular relevance are the reports of increased levels of activities, as well substrates, in congestive heart failure, Alzheimer's disease, and in patients with advanced diabetes. The proposal has been made that SSAO-mediated oxidative stress may contribute to cardiovascular deterioration in these patients [14]. The influence of selective inhibitors on the activity of membrane-bound SSAOs in mammalian tissues is the subject of a recent review [15].

The mechanism proposed for SSAO-catalyzed oxidations is shown in Scheme 1 [16]. A molecular oxygen-dependent oxidation converts the reduced cofactor back to the quinone with the formation of hydrogen peroxide and ammonia.

1.2. Drugs targeting amine oxidases

1.2.1. MAO inhibitors

Some 50 years ago, Zellers demonstrated that MAOs were the targets of antidepressant drugs, a reflection of the important physiologic role these enzymes have



Scheme 1. Proposed mechanism for SSAO-catalyzed oxidation of amines [16].

in regulating the levels of amine neurotransmitters. Both reversible and irreversible inhibitors of MAO A and B have been used clinically in the treatment of many neurological disorders including depression, Parkinson's disease, and Alzheimer's disease. However, the therapeutic potential of MAO inhibitors for the treatment of disorders related to amine imbalance has been complicated by undesirable side effects. An important example of these results from the fact that MAO is needed to metabolize pressor amines, such as tyramine, that are present in the diet. If MAO inhibition results in the failure to clear such amines by metabolism, hypertension can result. The presence of tyramine in cheese led to the term "cheese effect" for this unwanted consequence of MAO inhibition. Organ distribution—for example, intestinal enzyme is primarily MAO A—and structure activity relationships (SARs) for MAO A and B suggested that an MAO B-selective inhibitor would have decreased likelihood to elicit the cheese effect. Antidepressant effects are due to selective MAO A inhibition in the central nervous system (CNS) and reversible MAO A inhibitors such as moclobemide are particularly effective for the treatment of depression. (The reversible nature of the inhibition allows tyramine and other pressor amines to be metabolized because increased concentrations of substrate will displace the inhibitor.) MAO B inhibitors, free of the cheese effect, have no antidepressant activity but have other therapeutic applications. For example, MAO B inhibitors, such as L-deprenyl, are used to increase CNS dopamine levels as an adjunct to L-DOPA therapy in Parkinson's disease [17]. MAO B inhibitors are also currently in clinical trials for the treatment of Alzheimer's disease, based on the detection of an increased level of MAO B in plaque-associated astrocytes of brains from Alzheimer's patients [18]. Recent reviews provide an excellent current perspective on the therapeutic potential of MAO inhibitors [9,19].

1.2.2. SSAO inhibitors

Literature reports also suggest inhibitors of SSAO to be potential therapeutic agents. Plasma SSAO levels are increased in patients with congestive heart failure, as well as in diabetes mellitus and the elevation is greater with increasing severity of the disease. The possibility that SSAO not only increases after vascular endothelial damage but also may even play a role in the development of the damage has implications with respect to diagnosis, prognosis, and even preventive therapy. However, it has been noted that a lack of inhibitors with high potency and selectivity has hampered progress in defining the roles of SSAO more precisely [20].

1.3. Fluorine in drug design

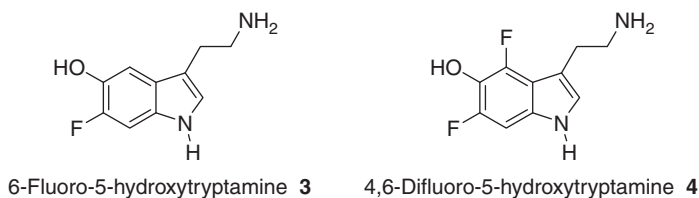
The special advantages of selective substitution of fluorine in drug design and development are well recognized and have been reviewed extensively [21]. Small size and high electronegativity impart special properties to fluorinated

molecules that have been exploited extensively to modulate such properties as biological half-lives and receptor binding, and in the design of reversible and irreversible enzyme inhibitors. Altered lipophilicity in fluorine-substituted molecules affects biological properties, particularly with respect to transport and interactions with membranes and recognition sites. Fluorine is frequently introduced to enhance metabolic stability through inhibition of oxidative metabolism [22]. Enhanced binding of fluorinated molecules has been ascribed to specific interactions of the C–F bond with binding site amino acid residues [23] as well as to polar hydrophobic effects [24]. Whereas fluorine has often been introduced based on rational mechanistic principles, this element also is frequently introduced as a part of SAR studies in the empirical component of drug development [25]. Effects of fluorine substitution can be analyzed after the fact, and such analyses often provide additional information to guide further exploitation of fluorine in drug design. In this chapter, we review the use of fluorinated molecules in the design of inhibitors of amine oxidases.

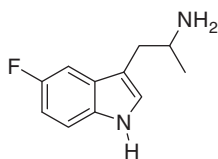
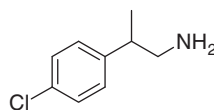
2. RING-FLUORINATED MAO INHIBITORS

2.1. Fluorine-substituted benzylamines and 2-phenylethylamines

In Section 1.3, the general effects of fluorine substitution on drug activity and selectivity have been treated. As seen frequently with other enzymatic reactions, introduction of fluorine can have dramatic effects on the properties of substrates and inhibitors of MAOs [26]. For example, preliminary studies indicated that fluorination of 5-hydroxytryptamine in the 6- or the 4,6-positions (**3,4**) causes this predominantly MAO A substrate to be metabolized significantly by platelet MAO B [27]. Although no direct evidence was obtained, this may be caused by increased lipophilicity introduced by fluorine substitution.



Over the years, many reversible competitive inhibitors selective for MAO A have been developed, including many α -methylamines. In contrast, very few effective MAO B-selective reversible inhibitors have been reported to date. Accumulated experience has indicated that α -alkylamines are inhibited sterically from binding to MAO B—and thus are MAO A selective. No complementary steric inhibition selective for MAO A is available [6b]. However, it was demonstrated that, while 5-fluoro- α -methyltryptamine (**5**) is a selective MAO A substrate, β -substitution, as in *p*-chloro- β -methylphenylamine (**6**), favors MAO B selectivity [28].

5-Fluoro- α -methyltryptamine 5*p*-Chloro- β -methylphenylamine 6

In an early study, *p*-fluorobenzylamine was reported to be a better substrate for MAO than is benzylamine. This was ascribed to higher acidity of the benzyl group of the former that would facilitate proton removal, considered to be an initial step in the oxidation process [29].

Edmondson has carried out extensive SAR on the oxidation of benzylamine analogues with both MAO A [11] and B [30]. Binding efficiency to MAO B of *para*-substituted benzylamines increased with increasing lipophilicity. The rate of oxidation (k_{cat}) was more influenced by steric factors, *p*-CF₃ having the slowest rate in the series studied and benzylamine having the highest rate, with *p*-F intermediate in value. Thus, steric factors appear to be more important than electronic factors in determining the rate of MAO B oxidation of *para*-substituted benzylamines. In these studies, no evidence was found for radical intermediates. This and other results from this study were discussed in terms of the validity of the SET mechanism proposed by Silverman [10].

In 1995, Silverman and Hawe published structure–activity studies of fluorine-substituted benzylamines and substituted 2-phenylethylamines. Introduction of one or several fluorine atoms makes these compounds good substrates for MAO B (see Table 1), but none of them was an inactivator of the enzyme [31].

It was found that the turnover number decreases as the electron withdrawing character of the benzene ring increases [32]. This is consistent with mechanistic assumptions involving electron transfer from the amine to the flavin [32]. In addition, the trend of decreasing catalytic efficiency ($k_{\text{cat}}/K_{\text{m}}$) with increased lipophilicity ($\log P$) is consistent with the “stickiness” due to binding of hydrophobic substituents to a hydrophobic active site of an enzyme. In contrast, for substituted 2-phenylethylamines there was no correlation observed between the catalytic efficiency and electronic, hydrophobic, or steric factors of different substituents in aliphatic positions, among them 2-fluoro-2-phenylethylamine, 2,2-difluoro-2-phenylethylamine, and racemic, or enantiomerically pure 2-methyl-2-trifluoromethyl-2-phenylethylamine. This indicates that many parameters determine the binding and turnover of these more flexible molecules compared to the fluorinated benzylamines. At higher concentrations, the latter racemic compound was shown to be a competitive inhibitor with K_i of 3.3 μM . This may indicate that the increased hydrophobicity assists in stabilizing the enzyme adduct [32].

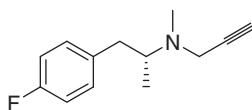
Miller and Edmondson [11] studied the reaction rates and binding efficiencies of MAO A with 17 different *para*-substituted benzylamines. In the anaerobic half

Table 1. Kinetic constants of fluorine-substituted benzylamine derivatives for oxidation by monoamine oxidases (MAO) B (pH 9.0, 25 °C) [31]. Adapted by permission of Harwood Academic Publishers GmbH. Copyright 1995.

Entry	Compound	k_{cat} (min^{-1})	K_{m} (μM)	$k_{\text{cat}}/K_{\text{m}}$ ($\mu\text{M}^{-1} \text{min}^{-1}$)
1	Benzylamine	1024	253	4.05
2	2-Fluorobenzylamine	31	19	1.63
3	3-Fluorobenzylamine	168	51	3.30
4	4-Fluorobenzylamine	448	147	3.01
5	2,4-Difluorobenzylamine	25	15	1.67
6	2,6-Difluorobenzylamine	14	20	0.70
7	2,4,5-Trifluorobenzylamine	14	7	2.00
8	Pentafluorobenzylamine	7	22	0.32

reaction, a strong correlation was found between the rate of flavin reduction and electron withdrawing properties of the substituents, suggesting proton removal as the mode of oxidation by MAO A. Binding of the substrates to MAO A was favored by large groups in the *para*-position, suggesting a large hydrophobic-binding pocket. Differences in binding of substrates to MAO A and B were proposed to explain greater dependence on electronic factors with MAO A. The authors suggest that their results favor a polar mechanism over the alternative SET mechanism.

In Section 1.1.1, L-deprenyl (**2**) was discussed as a potent selective MAO B inhibitor. Its *p*-fluoro analogue, fludeprenyl (**7**), was shown to retain the irreversible and selective inhibitory effects of its parent compound, with similar potency *in vitro* in rat tissue and *in vivo* in mice [33]. Both compounds have also been reported to have similar protective actions against transient global cerebral ischemia in gerbils. With L-deprenyl (**2**), these effects occurred at doses below those which inhibit MAO B, while the effects of the *p*-fluoro analogue **7** occurred only at doses that also inhibit MAO B activity [33b,34].



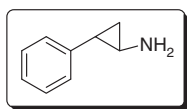
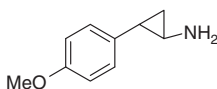
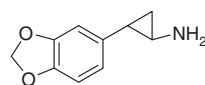
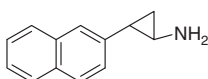
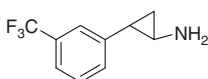
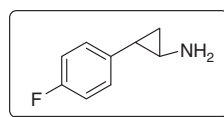
Fludeprenyl **7**

Fludeprenyl (**7**) also has methamphetamine-like discriminative-stimulus properties in squirrel monkeys that appear at twofold higher doses than the L-deprenyl-induced response [35]. These behavioral activities were ascribed to formation of the metabolites, *p*-fluoroamphetamine and *p*-fluorometamphetamine.

2.2. 4-Fluorotransylcypromine

Transylcypromine (*trans*-2-phenylcyclopropylamine, TCP, **8a**) has close structural similarity to amphetamine (2-amino-1-phenylpropane) and is known as a nonhydrazine, nonselective, and irreversible inhibitor of both MAO A and B. It is also a potent reversible inhibitor of CAOs [36,37]. Transylcypromine has an important clinical use for treatment of certain depressive illnesses, particularly of nonendogenous and atypical depressions and depressions associated with anxiety, agitation, phobias, and anergia [38–40]. In combination with lithium, it is also applied for treatment of refractory depression [41]. Recent reports also discussed MAO inhibitors as useful agents against neurodegenerative disorders such as Parkinson's or Alzheimer's diseases [42]. Despite impressive clinical successes, clinical use of transylcypromine and other MAO inhibitors is limited by various problems, including the “cheese effect” discussed in Section 1.

A short biological half-life is one disadvantage of TCP [43], as shown by studies in experimental animals [44–46] as well as in humans [47–51]. It is known that *p*-hydroxylation is an important initial step in metabolism of many biologically relevant aromatic compounds, including transylcypromine [52,53]. In that regard, several *p*-substituted analogues of TCP, such as 4-methoxy- (**9**) and 3,4-methylenedioxytransylcypromine (**10**) and 2-naphthylcyclopropylamine (**11**) as well as 3-trifluoromethyltransylcypromine (**12**), have been shown to be equipotent or even more potent than TCP in inhibiting MAO *in vitro* [54].

Transylcypromine, TCP **8a**4-Methoxytransylcypromine **9**3,4-Methylenedioxytransylcypromine **10**2-Naphthylcyclopropylamine **11**3-Trifluoromethyltransylcypromine **12**4-Fluorotransylcypromine, FTCP **13**

Since fluorine is known to greatly retard, if not block aromatic hydroxylation, a particularly relevant derivative of TCP is *trans*-2-(4-fluorophenyl)cyclopropylamine (FTCP, **13**). FTCP was shown to be 10 times more potent as an inhibitor of MAO A and B *in vitro* in rat brain homogenates. After intraperitoneal (ip) administration, FTCP attained higher brain and liver levels and provided greater availability than did TCP after injection of an equimolar amount. Moreover, there was no difference in the *ex vivo* MAO A and B inhibitory profiles in brain and liver over a period of 24 h following treatment with TCP or FTCP. FTCP also increased the concentrations of catecholamines, serotonin, and trace amines in brain at most time intervals following ip injection [55]. Later studies with the male

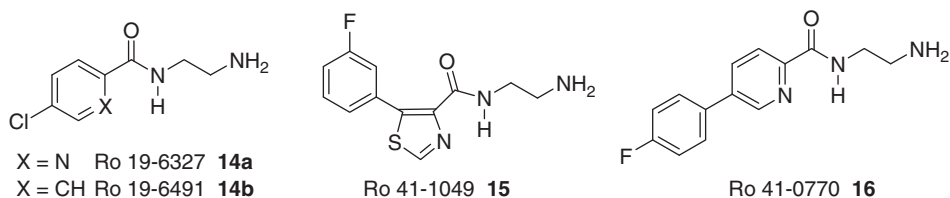
Sprague-Dawley rats have shown that chronic administration of low doses of the nonselective TCP, of FTCP, and of the MAO A-selective clorgyline leads to sustained increases in brain amine concentrations in the frontal cortex, nucleus accumbens, caudate nucleus, hippocampus, and hypothalamus with minimal regional differences [56].

Other studies have shown that the fluorinated drug attains longer-lasting and more consistent concentrations in brain than does TCP. This might result in lowering the clinical dose and hence might also reduce the incidence of side effects apparently contributed to the action of TCP on uptake and release of neurotransmitter amines [57–63]. However, comparisons of effects of TCP and FTCP on uptake and release of these amines *in vivo* and *ex vivo* in brain and heart will be necessary to clarify this situation.


2.3. Aryl-*N*-aminoethylamide derivatives, for example, Ro-41-1049 and Ro-16-6491

Reversible MAO inhibitors are generally more suitable than substrates for studying the relationship between the chemical structure of molecules and their recognition by the active site of the enzymes because the affinity for the inhibitors is often higher than it is for the substrates. The following examples illustrate the extent to which selectivity is sometimes dramatically dependent on very limited modifications of the chemical structure.

Basically, the catalytic site of MAOs is thought to consist of two distinct parts, namely a polar-binding site for the amino group and a hydrophobic entrance cavity [64]. Several 2-aminoethylcarboxamides are potent MAO inhibitors. The monocyclic compounds Ro 19-6327 (**14a**) and Ro 19-6491 (**14b**) have been shown to be highly selective for MAO B and the fluorinated dicyclic Ro 41-1049 (**15**) is a potent MAO A inhibitor, while Ro 41-0770 (**16**) was found to be quite nonselective [65].




By tritiation experiments, Cesura *et al.* have shown that both molecules bind exclusively to the active site of the enzyme and behave as mechanism-based reversible MAO inhibitors [66,67]. The selectivity for MAO A of Ro 41-1049 (**15**) appears to be higher than that of clorgyline, which loses its selectivity and also inhibits MAO B at micromolar concentrations [6b]. The common *N*-2-aminoethylcarboxamide group present in the Ro derivatives seems to interact



R_5 R_4

X



R_4 R_7

		IC ₅₀ (nM)		Selectivity ratio	
		5-HT	PEA	5-HT/PEA	
X = CH, R ₄ = CF ₃ , R ₅ = Br	17a	470	0.44	1068	
X = CH, R ₄ = H, R ₅ = Br	17b	9500	0.32	29,688	
X = CH, R ₄ = H, R ₅ = Cl	17c	20,500	0.37	55,405	
X = N, R ₄ = H, R ₅ = H	17d	195	13.5	14	
X = N, R ₄ = CF ₃ , R ₅ = H	17e	510	9.8	52	
<hr/>					
Clorgylin (1)		0.56	440	0.0013	
L-Deprenyl (2)		1800	4.7	383	

		IC ₅₀ (nM)		Selectivity ratio	
		5-HT	PEA	5-HT/PEA	
R ₄ = H, R ₇ = COOCH ₃	18a	9.0	4200	0.002	
R ₄ = H, R ₇ = C ₆ H ₅	18b	12.0	2200	0.005	
R ₄ = CH ₃ , R ₇ = Cl	18c	3.3	13	0.25	
R ₄ = CH ₃ , R ₅ = CH ₃	18d	3.9	7.2	0.54	
R ₄ = H, R ₇ = Cl	18e	11.5	20.0	0.58	
R ₄ = F, R ₇ = CH ₃	18f	28.5	5.3	5.4	
R ₄ = CN, R ₇ = H	18g	120	6.8	18.0	

Fig. 1. Influence of substituents in the aromatic ring on the selectivity of 3-(2-aminoethoxy)-1,2-benzisoxazole derivatives as monoamine oxidases (MAO) A or B inhibitors. Ratio of selectivity was calculated from IC_{50} values of MAO A and B determined by an *in vitro* assay of mouse brain mitochondria using 5-hydroxy tryptamine (5-HT) and 2-phenylethylamine (PEA) as specific substrates, respectively (see Ref. [9]). Smaller values indicate that inhibitors are MAO A selective [71].

with a domain on MAO, which is likely to be very similar in the two isoforms of the enzyme, and most probably are not essential for substrate and inhibitor selectivity [64]. Since MAO A and B differ in primary structure with about 70% homology [6,68,69], the difference in selectivity of Ro 19-6327 (**14a**) and Ro 19-6491 (**14b**) on the one hand and Ro 41-1049 (**15**) on the other hand may be the result of these constitutive differences between the isoforms of MAO in the hydrophobic-binding domain and/or its environment [64]. X-ray structural analysis of the adduct of MAO B and Ro-19-6491 showed that the inhibitor is bound to the enzyme as a flavin N(5) adduct [70].

Furthermore, 3-(2-aminoethoxy)-1,2-benzisoxazole derivatives were reported to change selectivity for MAO A and B, depending on the substituents attached to the aromatic ring [71]. For example, **18a** and **18b** selectively inhibited MAO A, while **17b** and **17c** were selective to MAO B. Substituents at the 7-position increased MAO A selectivity and halogen at the 5-position increased MAO B selectivity (Fig. 1). Although the correlation of chemical structure of these derivatives and selectivity was not discussed in this report, selectivity change might reflect the differences of active site cavity of MAO A and B. A recent report suggested that human MAO A has a single substrate cavity of 550 Å³, which is shorter in length and wider than the longer and narrower cavity in human MAO B which has a size of 700 Å³ [8b]. The role of the fluorine substituent in all mentioned inhibitors was not investigated in detail.

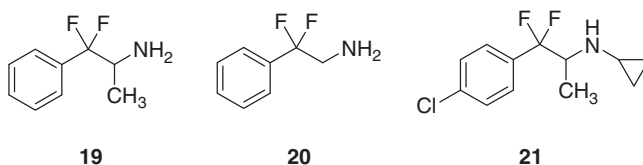
3. AROMATIC SIDE CHAIN-FLUORINATED MAO AND SSAO INHIBITORS

Examples of material included in this section will be earlier work dealing with β -fluorinated arylethyl amines that have lowered amine pK_{as} and a series of

fluoro-allyl amines that have been developed as irreversible MAO inhibitors. Our own research, involving aryl-side chain-fluorinated amines that incorporate the cyclopropyl moiety, will be discussed in Section 5.

3.1. β,β -Difluorinated phenethylamines

In the 1970s, Fuller examined the effects of β,β -difluoro substitution on the biological properties of a series of arylethylamines. Among the compounds prepared were β,β -difluoroamphetamine (**19**), β,β -difluoro phenethylamine (**20**), and *N*-cyclopropyl-4-chloro- β,β -difluorophenylethylamine (**21**). A drop in amine pK_a of about 2.5 pH units resulted from the fluorine substitution. Included in biological studies were effects on activities toward MAO. *In vitro* β,β -difluoroamphetamine was a less active inhibitor of MAO than amphetamine and β,β -difluorophenylethylamine was a poorer substrate for deamination than phenylethylamine. *N*-Cyclopropyl-4-chlorophenylethylamine is an irreversible inhibitor of MAO. There was little difference *in vivo* in MAO inhibition in various tissues of the rat [72].



3.2. Fluoroallylamines as irreversible MAO inhibitors

In the 1980s, problems associated with the irreversible MAO A inhibition related to the cheese effect prompted chemists at Merrell Dow to initiate a program to develop MAO B-selective inhibitors. Allylamines had been shown earlier to be “pseudoirreversible” inhibitors (activity restored by the substrate benzylamine) of MAO [73]. (*E*)-2-(3,4-dimethoxyphenyl)-3-fluoroallylamine (Fig. 2, **22d**) was prepared and found to be an irreversible inhibitor of MAO with good MAO B selectivity [74]. It was also devoid of indirect sympathomimetic and uptake-blocking properties, actions that also can lead to unwanted side effect. A series of 3-haloallylamines possessing the same properties were prepared (Fig. 2) [75,76]. The proposed mechanism of action involved addition of either an active site nucleophile of the enzyme or the flavin cofactor to the double bond. Halogen, preferably *cis* to the aromatic ring, was necessary for efficient inactivation. Ring methoxyl groups favored MAO B selectivity, whereas hydroxyl groups were detrimental to this selectivity. Further work led to the development of extremely selective MAO B inhibitors such as Merrell Dow Laboratories (MDL) 72887 (**24**) and MDL 72974A (**25**) [77].

A strategy was developed to target such inhibitors to the CNS. (*E*)- β -Fluoromethylene-*m*-tyrosine (**26**), the amino acid bioprecursor to **22f**, was synthesized. The amino acid crosses the blood–brain barrier and is decarboxylated by

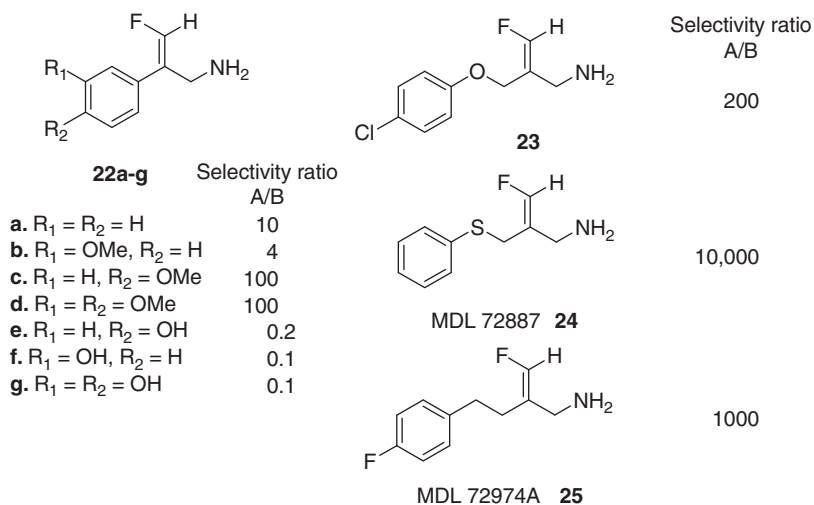
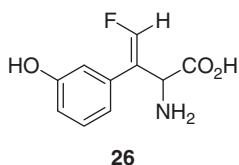


Fig. 2. Isozyme selectivity of fluoroallyl amine monoamine oxidases (MAO) inhibitors. The selectivity ratio was defined as the ratio of the concentrations of inhibitors required to decrease the activity of both forms of the enzyme at the same rate [77]. A high ratio thus indicates a B-selective inhibitor.

aromatic amino acid decarboxylase (AADC) intraneuronally to produce **22f** that now functions in the neuron as a potent MAO inhibitor (slight MAO A selectivity). (2*S*)-3-(3,4-dihydroxyphenyl)-2-hydrazinyl-2-methyl-propanoic acid (carbidopa) was used to inhibit peripheral AADC activity so MAO inhibition is limited to the CNS, thus providing another strategy to avoid the cheese effect [76]. Use of [¹⁸F]-labeled β -fluoromethylenetyramine precursors as positron emission tomography (PET)-scanning agents will be discussed in Section 4.



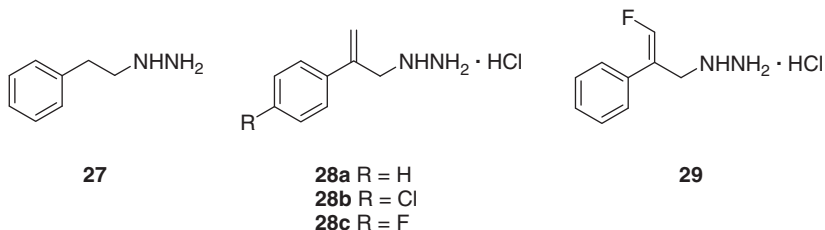
3.3. Haloallylamines as SSAO inhibitors

2-Haloallyl amines also have been studied as inhibitors of SSAO. The 2-aryl-3-haloallylamines proved to be potent irreversible inhibitors of rat aorta SSAO. Hydrophobic substituents on the aryl ring enhanced activity, while phenolic groups decreased activity [78]. The MAO B selective (*E*)-2-(3',4'-dimethoxyphenyl)-3-fluoroallylamine (**22d**) inhibited rat SSAO in vascular and brown adipose tissues and was selective relative to inhibition of MAO A [79]. MDL 72974A (**25**) is a potent irreversible inhibitor of both MAO B and SSAO with a 190-fold lower affinity for MAO A [80].

Examination of the Merrell Dow series of haloallyl amines as inactivators of bovine plasma amine oxidase recently has been reported. The (*E*)- and (*Z*)-3-fluoroallyl amines were more potent than the 3-bromo analogues. In addition, the *Z*-isomers were more potent than the *E*-isomers, in contrast to the result reported for inactivation of MAO [81].

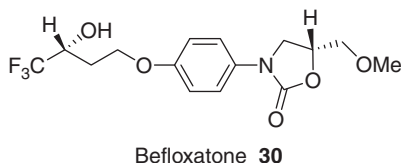
3.4. Allyl hydrazines as SSAO inhibitors

Carbonyl reagents, such as semicarbazide and phenelzine (**27**), are inactivators of SSAO. In a strategy that includes two inactivating structural motifs (allylamine and hydrazine), a series of allyl hydrazines including the series **28a–c** as well as the fluoroallyl analogue **29** were prepared. Compounds **28a–c** were potent irreversible inhibitors of SSAO, and compounds **28a,c** had particularly good selectivity with respect to MAO inhibition. The presence of the vinyl fluoride in **29** had little effect on potency but did result in a loss in selectivity [82].



3.5. Fluorinated aryl-oxazolidinone derivatives, for example, befloxatone

The structural diversity of MAO A and B-selective inhibitors clearly indicates that a relationship between the structural features of a given molecule and its selective recognition by either MAO A or B cannot be established *a priori* [83]. However, there are many examples showing that the affinity of any active molecule can markedly be improved by chemical modulation of the lead structure [64]. As an example the mode of interaction of befloxatone (**30**) was investigated [84].

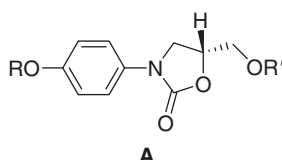


Early classical MAO inhibitors used clinically, such as tranylcypromine and phenelzine, generate reactive species, which are trapped by MAO by formation of strong covalent bonds with the enzyme [32,64,85]. For this reason, effects could be of

long-lasting duration. Befloxatone (**30**) belongs to the chemical family of aryl-oxazolidinones, the structures of which differ significantly from classical MAO inhibitors by the absence of an amino function. It does not form a stable complex with the enzyme and thus has shorter duration of action, an advantage that reduces side effects [86]. Detailed structural and electronic analysis [87] and binding studies revealed that this compound is a potent, selective, and reversible MAO A inhibitor *in vitro* and *ex vivo*, which does not interact with a large number of receptors, monoamine transporters, or other amine oxidases [88]. Befloxatone (**30**) selectively and competitively inhibited MAO A in human and rat brain, heart, liver, and duodenum homogenates with K_i values ranging from 1.9 to 3.6 nM for MAO A and from 270 to 900 nM for MAO B [89]. It was selected as a drug candidate for the treatment of depression and the clinical pharmacology has been investigated [90].

From detailed X-ray analysis and *ab initio* molecular orbital calculations, it has been suggested that the planar electron-rich aryl-oxazolidinone moiety interacts reversibly via the π -system with the flavin cofactor of the enzyme, which is also planar and known to be an electron acceptor [91]. Additionally, the side chains of the inhibitor, including the trifluoromethyl group, are engaged in interactions with the peptide core of the enzyme [87].

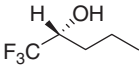
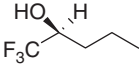
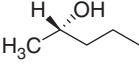
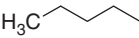
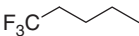
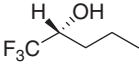
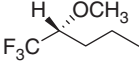
Binding constants of several fluorinated and nonfluorinated analogues and corresponding diastereomers of the general structure **A** have also been determined in order to study the influence of the fluorine moiety and the stereochemical requirements on the inhibition of MAO A and B (Table 2) [92].



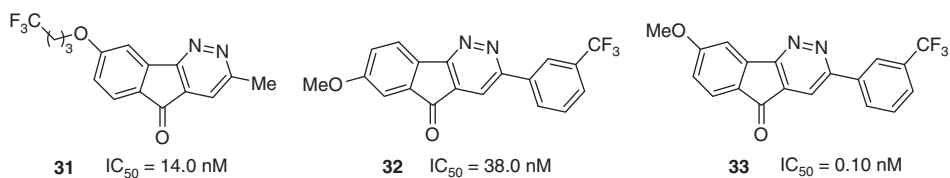
3.6. Fluorinated 5*H*-indeno[1,2-*c*]pyridazin-5-one MAO B-selective inhibitors

Wouters *et al.* analyzed stereoelectronic properties of MAO B inhibitors to develop a pharmacophore model for reversible MAO B inhibitors. Apparent requirements for specific H-bonds and hydrophobic interactions were used to design the pyridazinone **31** that proved to have a low nanomolar K_i and 7000-fold selectivity for MAO B [93]. In a related series, among reversible MAO-B selective 5*H*-indeno[1,2-*c*]pyridazin-5-ones reported by Kneubühler *et al.*, a methoxy-substituted analogue, assigned structure **32**, was the most potent [94]. Based on X-ray analysis, Frédéricick *et al.* reassigned the structure as **33** and found it to be significantly more potent ($IC_{50} = 0.10$ nM) than authentic **32** ($IC_{50} = 38.0$ nM) isolated as a minor substituent in the synthetic sequence [95]. None of the compounds studied inhibited MAO A at

Table 2. Affinity of different befloxtone analogues A expressed in terms of K_i for monoamine oxidases (MAO) A and B [92]. Adapted, by permission of Elsevier Science Ltd. Copyright 1999.

R	R'	K_i MAO A (nM)	K_i MAO B (nM)
	CH ₃	2.5	222
	CH ₃	28	16
	CH ₃	6.1	1460
	CH ₃	9.3	31
	CH ₃	2.4	4
CH ₃	CH ₃	130	769
	H	13	9.2
	CH ₃	53	2

1000 nm. The potency of inhibition was found to be highly dependent on the regio-chemistry of the alkoxy substituent.



4. FLUORINATED MAO INHIBITORS AS PET-SCANNING AGENTS

4.1. Fluorinated amine oxidase inhibitors as PET-imaging agents in the CNS

The development of PET as a research tool and diagnostic procedure has had particularly valuable CNS applications. Metabolic studies using [^{18}F]-2-fluoro-2-dexoy glucose ([^{18}F]-FDG), quantitation of regional dopaminergic function with

6- ^{18}F fluoro-3,4-dihydroxyphenylalanine (^{18}F -6-fluoro-DOPA), and the use of ^{18}F -cyclofoxy to study opiate receptors are examples of the effective targeting of ^{18}F -labeled agents to the CNS (see also Chapters 1-4, this volume). In these studies, the strategy takes advantage of known biochemical factors that concentrate the positron-emitting compound to the target of interest. For example, phosphorylation traps ^{18}F -FDG in the brain, ^{18}F -6-fluoro-DOPA is decarboxylated enzymatically and the product ^{18}F -6-fluorodopamine is taken up and stored in dopaminergic neurons, and ^{18}F -(-)-cyclofoxy binds with high affinity to the opiate receptor [96].

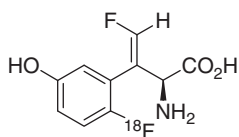
4.2. ^{11}C -Labeled MAO inhibitors

Another strategy to effectively trap a positron-emitting species, thus localizing it, is to design an irreversible inhibitor that is labeled with the emitting isotope. Localization of MAO by this procedure was done initially by Fowler *et al.* who mapped human brain MAO A and B with the ^{11}C -labeled MAO A-selective irreversible inhibitor clorgyline (**1**) and the ^{11}C -labeled MAO B-selective irreversible inhibitor L-deprenyl (**2**) [97]. Several studies were carried out with ^{11}C -L-deprenyl and ^{11}C -clorgyline [98] including studies that have revealed lower MAO activity in the brain and peripheral organs of smokers relative to nonsmokers [99]. In addition, cerebral MAO A has been mapped using the reversible, selective inhibitor ^{11}C -befloxatone [100] as a PET-scanning agent. The acute inhibition of cardiac MAO A activity after tobacco smoke inhalation also was measured using the same technique [101].

4.3. ^{18}F -Labeled MAO inhibitors

The longer half-life of ^{18}F (109.6 min) compared to ^{11}C (20.4 min) is one of the advantages of this isotope in the design and synthesis of PET agents (see Chapter 1, this volume). Therefore, there has been much interest in the development of irreversible MAO inhibitors labeled with ^{18}F as biological probes to map MAO activity.

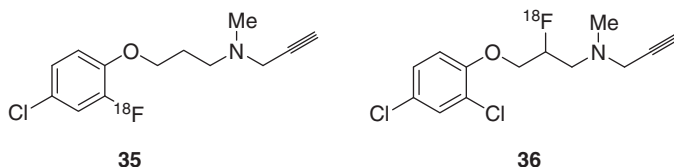
This ability to target the fluoroallylamine irreversible inhibitors of MAO to the CNS was exploited further for PET imaging using ring- ^{18}F -fluorinated analogues of β -fluoromethylene-*m*-tyrosine. Stereoisomers (D and L), geometric isomers (*E* and *Z*), and regioisomers (2-, 4-, and 6-aryl ring positions) were prepared. Brain localization was favored by 6- ^{18}F -fluorination of the L-enantiomer having the (*E*)-double bond configuration (6- ^{18}F -fluoro-(*E*)- β -fluoromethylene-*meta*-L-tyrosine (**34**)) [102].



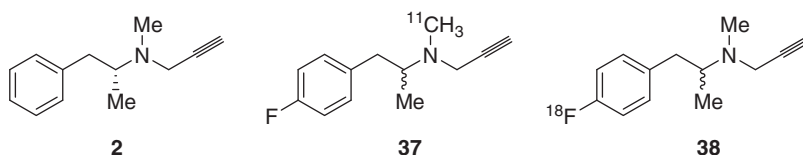
34

Inhibitors known to be selective for MAO A or B have been labeled with [^{18}F]-fluorine for PET studies. For example, [^{18}F]-fluoroclogyline (**35**) labeled on the aromatic ring with low specific activity [^{18}F]-fluorine was shown to have favorable properties for mapping MAO A activity in the brain [103].

Carrier-free [^{18}F]-fluorine with high specific activity is produced as ionic fluoride, as opposed to low activity [^{18}F]-enriched fluorine gas suitable for electrophilic fluorinations or for producing electrophilic fluorinating agents. However, labeling electron-rich aromatic rings with fluoride by nucleophilic substitution has presented synthetic problems. To obviate this difficulty, Mukherjee and Yang prepared a radiofluorinated analogue **36** of clogyline with the label on the side chain using nucleophilic displacement of a precursor mesylate [104]. Binding of **36** showed a greater than 1000-fold selectivity for MAO A versus MAO B. Intravenously administered **36** accumulated in rodent brain in areas that are known to have significant concentrations of MAO A.

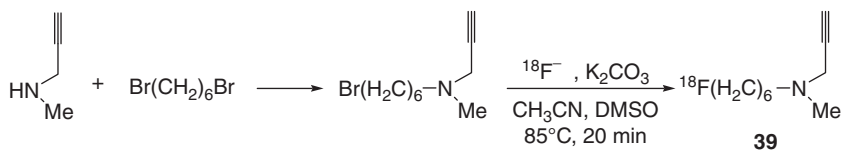


As previously discussed, L-deprenyl (**2**) is a selective suicide inhibitor of MAO B. As part of a program to develop [^{18}F]-labeled L-deprenyl for PET studies, Fowler and coworkers prepared [^{11}C]-labeled D- and L-4-fluorodeprenyl (**37**) to study the effects of fluorine substitution on kinetics of uptake and localization [105]. Subsequently, no-carrier-added D,L-4-[^{18}F]-fluorodeprenyl (**38**) was made by a nucleophilic aromatic substitution reaction [106].



In order to have a more convenient synthesis of a MAO B-selective [^{18}F]-labeled inhibitor, Mukherjee and coworkers employed a similar strategy to the one they used to make [^{18}F]-labeled clogyline. The synthesis of [^{18}F]-labeled N-(6-fluorohexyl)-N-methylpropargylamine (**39**) is shown in Scheme 2. Binding of **39** had over 200-fold selectivity for MAO B over MAO A. *In vitro* autoradiography of rat brain slices showed that **39** accumulated in regions known to have high concentrations of MAO B activity [107].

Fowler and coworkers have recently reviewed the development of [^{11}C]- and [^{18}F]-labeled PET-scanning agents targeted to MAO activity [108].



Scheme 2. Synthesis of [^{18}F]-labeled *N*-(6-fluorohexyl)-*N*-methylpropargylamine (**39**).

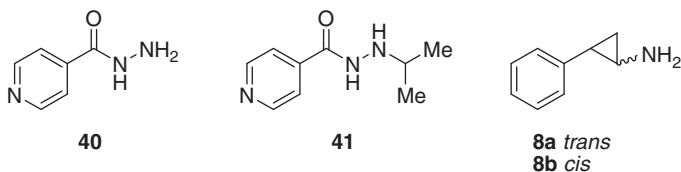
5. FLUORINATED CYCLOPROPYLAMINES AS INHIBITORS OF SSAO AND MAO

5.1. Cyclopropylamines as inhibitors of SSAO and MAO

5.1.1. Overview of the development of cyclopropylamines as MAO inhibitors

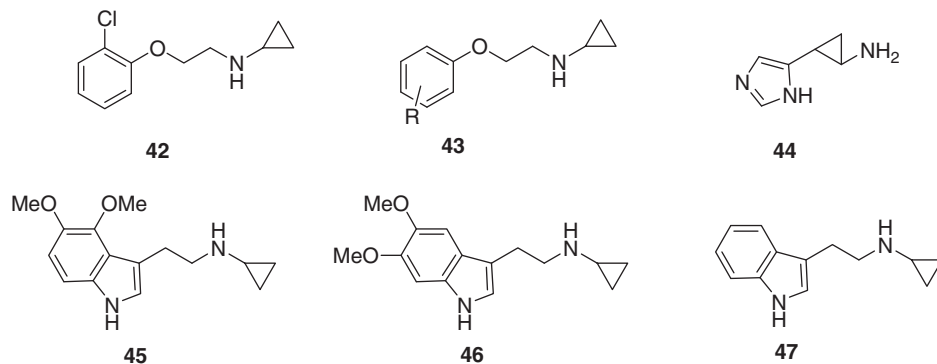
The first inhibitors of flavin-dependent MAO that were developed for clinical use were hydrazines and hydrazides. The chance discovery that the antitubercular drug, 4-pyridine carboxylic acid hydrazide (isoniazid, **40**), was also a potent MAO inhibitor led to the development of the related drug, iproniazid (**41**), used for the treatment of depressive illness. Although this compound demonstrated remarkable antidepressant action, its clinical value was seriously compromised by side effects [19].

Cyclopropylamines have been the subject of extensive research over a long period for a variety of reasons. Included in the results of this research was the discovery that certain cyclopropylamines were inhibitors of flavin-containing MAO. Lacking a hydrazide moiety, these compounds were expected to be devoid of liver toxicity. *Trans*-2-phenylcyclopropylamine (tranylcypromine) (**8a**), discussed in Section 2.2, appears to be the first cyclopropylamine to be used in clinical trials [109]. Norepinephrine concentrations in the rat brain could be increased by oral administration of lower doses of **8a** in comparison to iproniazid [110].



In the late 1960s, different types of cyclopropylamines, the *N*-substituted cyclopropylamines, were reported [111]. One of the most interesting compounds in the new class was *N*-[2-*o*-chlorophenoxy]-ethyl]-cyclopropylamine (Lilly 51641) (**42**). This compound noncompetitively inhibited the MAO-catalyzed oxidation of serotonin, tyramine, phenylethylamine, and tryptamine *in vitro* and increased the serotonin concentration in the whole rat brain *in vitro*. In structure–activity studies on a series of *m*- and *p*-aromatic substituted *N*-(phenoxyethyl)cyclopropylamines (**43**), the degree of inhibition correlated well with σ and π values [112].

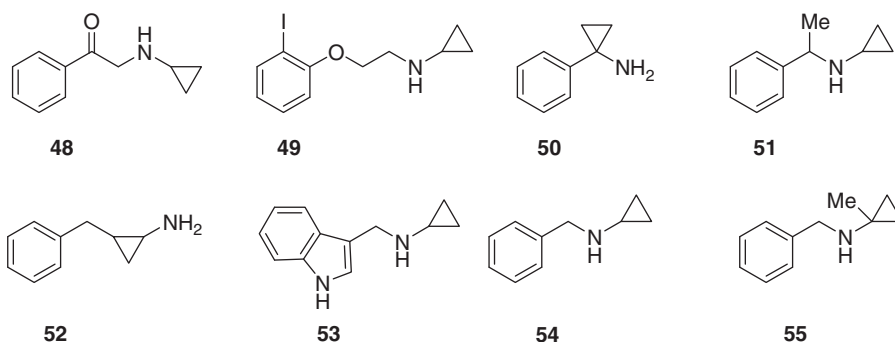
Another *N*-substituted cyclopropylamine, 2-(4-imidazolyl)cyclopropylamine (**44**), is also a potent inhibitor of rat brain MAO *in vitro* [113], and *N*-cyclopropyl derivatives of tryptamine (**45–47**) were reported to be inhibitors for mitochondrial and bovine plasma MAOs [114].



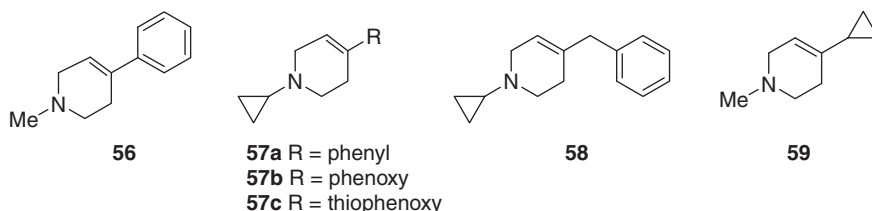
5.1.2. Isozyme selectivity of cyclopropylamine MAO inhibitors

With the recognition in the late 1960s that there are two forms of MAO (Section 1.1.1), potential therapeutic implications related to isozyme selectivity needed to be considered in MAO inhibitor development. (The early literature also reveals some lack of distinction between copper-containing and flavin-containing MAOs.) An important case in point involves the clinical side effects associated with the “cheese effect” (Section 1.2.1) that made clear that there would be important clinical advantages to having available isozyme-selective inhibitors [115]. Follow-up studies with the well-known cyclopropylamine inhibitor *trans*-2-phenylcyclopropylamine (**8a**) demonstrated that this clinically useful compound is an irreversible inhibitor of MAO, but that it had no selectivity toward either MAO A or B [116].

Fuller reported that *N*-phenacyl-cyclopropylamine hydrochloride (**48**) displayed a slight preference for MAO B inhibition, and that analogues with various substituents on the phenyl ring were inhibitors of MAO A [117]. Subsequent research revealed that *N*-[2-(*o*-chlorophenoxy)-ethyl]-cyclopropylamine (Lilly 51641) (**42**) had selectivity toward MAO A [118]. The iodo analogue of compound **42**, *N*-[2-(*o*-iodophenoxy)-ethyl]-cyclopropylamine (LY121768) (**49**), also proved to be a MAO A-selective irreversible inhibitor [119]. Silverman and coworkers reported that 1-phenylcyclopropylamine (**50**) and *N*-cyclopropyl- α -methylbenzylamine (**51**) are 50 times more potent irreversible inhibitors for MAO B than MAO A, while 1-benzylcyclopropylamine (**52**) showed some selectivity for MAO A [120]. *N*-Cyclopropyl-indolylmethylamine (**53**), *N*-cyclopropylbenzylamine (**54**), and *N*-(1-methylcyclopropyl)benzylamine (**55**) were also shown to be good inhibitors, but the selectivities were not reported [121].



1-Methyl-4-phenyl-1,2,3,6-tetrahydropyridine (**56**, MPTP) is a well-known Parkinsonian-inducing neurotoxin. From the 1990s to the present time, Castagnoli and coworkers have focused on cyclopropyl analogues (**57–59**) of MPTP in a strategy for development of MAO B inactivators [122]. As expected, 1-cyclopropyl-4-phenyl-1,2,3,6-tetrahydropyridine (**57a**) was an efficient time- and concentration-dependent inhibitor of MAO B. 4-Benzyl-1-cyclopropyl-1,2,3,6-tetrahydropyridine (**58**) is also a time- and concentration-dependent inhibitor of MAO B, but this compound proved to be an excellent MAO B substrate. 4-Thiophenoxy and 4-phenoxy analogues (**57c**, **57b**) are substrates but not inactivators of MAO B. Although not possessing a cyclopropylamine moiety, the 4-cyclopropyl analogue (**59**) also proved to be an excellent MAO B substrate.



5.1.3. Mechanisms of inhibition

In the early 1960s, Burger and coworkers prepared a series of analogues of *trans*-2-phenylcyclopropylamine (**8a**) and studied the relationship between chemical structures and efficiency of MAO inhibition [123]. From this they determined that the structural requirements for inhibition in this class of compounds are (1) a cyclopropane ring, (2) an amino group attached directly to the cyclopropane ring, and (3) a 2-substituent containing an aromatic moiety. These findings were very interesting and useful but it should be noted that at this time (early 1960s), the presence of two forms of MAO was still not recognized. Riley and Brier reported in 1972 that (1*S*,2*R*)-enantiomer is more potent than the (1*R*,2*S*)-enantiomer, demonstrating the importance of absolute configuration on inhibitory potency [124].

Silverman and coworkers have carried out extensive research on the mechanism of inactivation of MAO by cyclopropylamine analogues. They first reported in the early 1980s that *N*-cyclopropyl-*N*-arylalkylamines are mechanism-based inactivators of MAO [121,125]. The mechanism proposed was enzyme-catalyzed one electron oxidation of *N*-cyclopropylamines to give reactive ring-opened products which further react with either flavin and/or a cysteine residue, depending on the structure of the inactivator. According to their reports [120,125, 126], 1-phenylcyclopropylamine (**50**) attached reversibly to a cysteine residue and irreversibly to the flavin when it activated MAO B, whereas **50** modified only the flavin during inactivation of MAO A. In the case of *trans*-2-phenylcyclopropylamine (**8a**) and *N*-cyclopropyl- α -methylbenzylamine (**51**), both MAO A and B are inactivated by attachment to a cysteine residue (Fig. 3).

On the other hand, a recent crystallographic study revealed that the *trans*-2-phenylcyclopropylamine (**8a**) forms a cyclopropyl ring-opened adduct with MAO B at the flavin C(4a), and no evidence was obtained for inhibitor binding at Cys-365 [70,127]. From this observation, Edmondson and coworkers suggested [70] that the inhibition mechanism might be accommodated by a mechanism similar to that proposed by Sayre *et al.* for the quinone-mediated oxidative cleavage of cyclopropylamines [128].

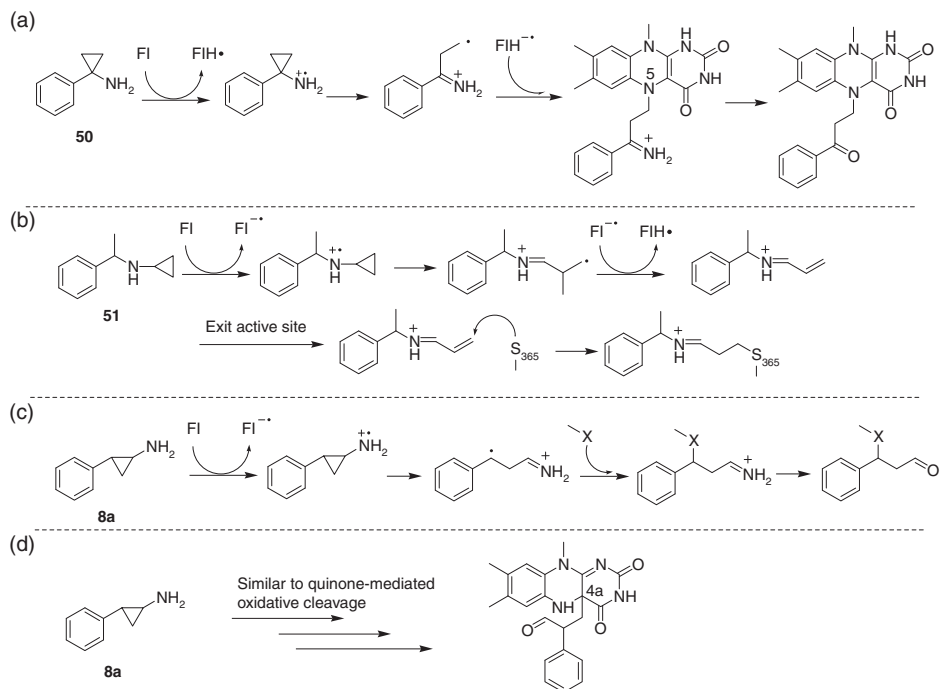


Fig. 3. Proposed inhibition mechanisms by cyclopropylamines. (a) From Ref. [126e]; (b) from Ref. [125a]; (c) from Ref. [126a]; (d) from Ref. [70].

Inhibition mechanisms by *N*-cyclopropyl MPTP analogues are also discussed in terms of two catalytic pathways, one of which is based on an initial SET step from the nitrogen lone pair, as proposed by Silverman, and the second is based on an initial α -carbon hydrogen atom transfer (HAT) step, as proposed by Edmondson, leading to a radical and dihydropyridinium product formation. The observation that MAO B catalyzes the efficient oxidation of certain 1-cyclopropyl-4-substituted-1,2,3,6-tetrahydropyridines to the corresponding dihydropyridinium metabolites suggests that the catalytic pathway for these cyclic tertiary allylamines may not proceed via the putative SET-generated aminyl radical cations [122]. Further studies will be necessary to clarify all the facets of the mechanism of inhibition of MAO by cyclopropylamines.

In contrast to the substantial work with MAO, relatively little research has been reported on the mechanism of inhibition of copper-containing amine oxidases and SSAO by cyclopropylamines. Bovine plasma amine oxidase, equine plasma amine oxidase, *Escherichia coli* amine oxidase, and *Arthrobacter globiformis* amine oxidase were inhibited by *trans*-2-phenylcyclopropylamine (**8a**) and the mode of inhibition was shown by spectral and crystal structure analyses to be competitive and reversible [36,37,129].

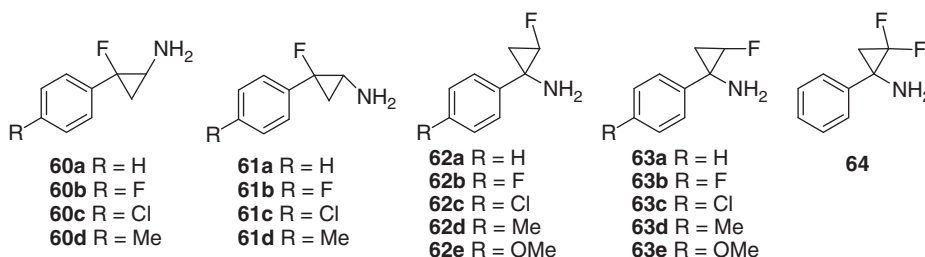
5.2. Effects of fluorine substitution on inhibition of SSAO by cyclopropyl amines

As discussed above, many cyclopropylamines are good inhibitors of MAOs. In addition, as discussed in Section 3.2, fluorine substitution had substantial effects on the inhibition of MAOs by such analogues as allylamines. We undertook a broadly based study of the effects of fluorine substituted on the cyclopropyl ring of cyclopropyl amines on potency and selectivity of amine oxidase inhibition. In addition to effects on amine pK_a and lipophilicity, we expected additional consequences resulting from altered geometry and ring strain due to the presence of fluorine.

Trans-2-phenylcyclopropylamine (**8a**) and its *cis*-isomer (**8b**) are competitive inhibitors of microbial copper-containing SSAO [37,130]. Introduction of fluorine at position 2 of **8a** and **8b** had dramatic effects on the inhibition of microbial tyramine oxidase from *Arthrobacter* sp. by these compounds [130]. Compound **60a** with a *cis* arrangement of the fluorine substituent and the amino group was 10 times more potent an inhibitor than compound **8a**. In contrast, the corresponding diastereomer **61a** with a *trans* arrangement of the two substituents was five times less active than **8a** (Table 3).

A series of *p*-substituted 2-fluoro-2-arylcylopropylamines (**60b–d**, **61b–d**) were shown to be competitive inhibitors of this enzyme [131]. The nature of the *p*-substituents in the more potent *trans*-isomer (*cis*-relationship between fluorine and the amino group) of 2-fluoro-2-arylcylopropylamine influenced the inhibitory potency in a consistent fashion. Thus, electron-withdrawing groups (F, Cl) slightly

decreased the activity, while the methyl group (+I substituent) increased the activity by a factor of ca. 9 compared to *trans*-2-fluoro-phenylcyclopropylamine (**60a**) and by a factor of 90 compared to tranlycypromine. This copper-containing enzyme contains 2,4,5-trihydroxyphenylalanine quinone (TPQ) as an organic cofactor in its active site. In the catalytic mechanism, it is well established that the substrate forms a Schiff's base adduct with TPQ [16,132]. Crystallographic studies showed that the reversible inhibitor, *trans*-2-phenylcyclopropylamine (**8a**), also forms a Schiff's base adduct with the O-5-position of the TPQ as the site of substrate binding [36,37,129]. It should be noted that no cyclopropane ring opening was observed in this case. The increase of the inhibitory potency, resulting from introduction of electron-donating groups to the aromatic ring suggests that the basicity/nucleophilicity of the amino group may be important for activity. As expected, pK_a values of fluorinated phenylcyclopropylamines showed that the aromatic methyl group enhanced the basicity of the amino group ($pK_a = 7.41$ for Me > 7.35 for H > 7.31 for F > 7.19 for Cl) (Table 3). However, fluorination of the cyclopropane ring caused a decrease in basicity of the amino group ($pK_a = 8.47$ for **8a** to 7.35 for **60a**), showing, as would be expected, that pK_a values were more influenced by fluorination of the cyclopropane ring than by ring substitution of aromatic ring. Because ring substitution with a methyl group and cyclopropane fluorination have opposing effects on amine basicity, it is difficult to ascribe the fluorine-induced increased inhibitory activity to effects on amine basicity alone. Log *D* values also showed no clear correlation with the inhibitory potency (Table 3). Further work will be required to explain the effects of fluorine substitution on activity.



Activity also was strongly dependent on the absolute configuration. The (1*S*,2*S*)-enantiomer of **60a** was an excellent inhibitor of tyramine oxidase, whereas the (1*R*,2*R*)-enantiomer was essentially devoid of activity.

Inhibition of copper-containing tyramine oxidase by fluorinated 1-phenylcyclopropylamines (**62a–e**, **63a–e**, **64**) also was investigated. These compounds displayed relatively poor activity as inhibitors [130, 133] (Table 3).

5.3. Effects of fluorine substitution on MAO inhibition

With respect to the effects of fluorine substitution on the behavior of cyclopropylamines as MAO inhibitors, the results of the work of Fuller and Molloy with

Table 3. IC₅₀ values and inhibition type of 2-aryl-2-fluoro and 1-aryl-2-fluorocyclopropylamines for tyramine oxidase^{d,e} [130, 131, 133]

Compound	Isomer type ^a	NH ₂ /F relationship	R	IC ₅₀ (μM)	Inhibition type	pK _a ^b	log <i>D</i> ^c
8a	<i>trans</i>	—	H	35 ± 6	Competitive	8.47	Nd
60a	<i>trans</i>	<i>cis</i>	H	3.6 ± 1.5	Competitive	7.35	1.53
(1 <i>R</i> ,2 <i>R</i>)- 60a	<i>trans</i>	<i>cis</i>	H	Ni	Nd	—	—
(1 <i>S</i> ,2 <i>S</i>)- 60a	<i>trans</i>	<i>cis</i>	H	2.3 ± 0.1	Competitive	—	—
60b	<i>trans</i>	<i>cis</i>	F	8.1 ± 1.6	Competitive	7.31	1.60
60c	<i>trans</i>	<i>cis</i>	Cl	3.7 ± 0.3	Competitive	7.19	2.23
60d	<i>trans</i>	<i>cis</i>	Me	0.39 ± 0.17	Competitive	7.41	1.83
8b	<i>cis</i>	—	H	33 ± 1	Irreversible	8.50	1.41
61a	<i>cis</i>	<i>trans</i>	H	190 ± 90	Partial irreversible	6.98	1.78
61b	<i>cis</i>	<i>trans</i>	F	75 ± 12	Partial irreversible	6.88	2.14
61c	<i>cis</i>	<i>trans</i>	Cl	89 ± 25	Partial irreversible	6.81	2.66
61d	<i>cis</i>	<i>trans</i>	Me	51 ± 5	Nd	7.04	Nd
62a	<i>trans</i>	<i>trans</i>	H	Ni	Nd	—	—
62b	<i>trans</i>	<i>trans</i>	F	Ni	Nd	—	—
62c	<i>trans</i>	<i>trans</i>	Cl	Ni	Nd	—	—
62d	<i>trans</i>	<i>trans</i>	Me	Ni	Nd	—	—
62e	<i>trans</i>	<i>trans</i>	OMe	Ni	Nd	—	—
63a	<i>cis</i>	<i>cis</i>	H	Ni	Nd	—	—
63b	<i>cis</i>	<i>cis</i>	F	110 ± 0	Irreversible	—	—
63c	<i>cis</i>	<i>cis</i>	Cl	Ni	Nd	—	—
63d	<i>cis</i>	<i>cis</i>	Me	220 ± 10	Irreversible	—	—
63e	<i>cis</i>	<i>cis</i>	OMe	Ni	Nd	—	—
64	—	—	—	Ni	Nd	—	—
Semicarbazide	—	—	—	6.7 ± 0.2	Nd	—	—

^a Relative configuration of aromatic ring and amine.

^b Ionization constants (pK_a) were measured pH-metrically in 0.1 M KNO₃ at 21 °C.

^c log *D* values were measured from the partition coefficients for 1-octanol/0.05 N NaOH + 5% vol dimethylsulfoxide at pH 7.4.

^d Ni = no inhibition was observed.

^e Nd = could not be determined.

N-cyclopropyl-4-chloro- β,β -difluorophenethylamine (**21**) were discussed in Section 3.1 [72]. Likewise, certain of the properties of *p*-fluorophenylcyclopropylamine (**13**) were reviewed in Section 2.2

We have examined the above-described series of *trans*- and *cis*-2-fluoro-2-phenylcyclopropylamine analogues (**60a–d**, **61a–d**) as inhibitors of recombinant human liver MAO A and B [134]. The presence of fluorine attached to a cyclopropane ring, especially for *trans*-isomer **8a**, was found to result in an increase in inhibitory activity toward both MAO A and B (Table 4). In addition, *p*-substitution of electron-withdrawing groups, such as Cl and F, in the aromatic ring of the *trans*-isomers (**60b–d**) increased the inhibition of both enzymes. On the other hand, the introduction of fluorine at 2-position of *cis*-isomer **8b** resulted in loss of inhibitory activity for both MAO A and B, and no further *p*-aromatic substitution for *cis*-isomer greatly affected on the inhibitory activity with either enzymes. In addition, both MAO A and B were selectively inhibited by the (1*S*,2*S*)-enantiomer of **60a**, while no inhibition was observed with the (1*R*,2*R*)-enantiomer [134]. As already described in the former section, several questions on the mechanistic pathway for MAO inhibition by cyclopropylamines still remain. However,

Table 4. IC₅₀ values and inhibition type of 2-fluoro-2-phenylcyclopropylamines for recombinant human liver monoamine oxidases (MAO) A and B^{c,d} [134a]. Adapted by permission of Elsevier Ltd. Copyright 2004.

Compound	Isomer type ^a	R	MAO A		MAO B	
			IC ₅₀ (μM)	Inhibition type	IC ₅₀ (μM)	Inhibition type
8a	<i>trans</i>	H	20 ± 0	Irreversible	19 ± 0	Irreversible
60a	<i>trans</i>	H	12 ± 1	Irreversible	6.4 ± 0.1	Irreversible
60b	<i>trans</i>	F	3.6 ± 0.2	Irreversible	4.9 ± 0.1	Irreversible
60c	<i>trans</i>	Cl	1.6 ± 0	Irreversible	3.7 ± 0.1	Irreversible
60d	<i>trans</i>	Me	13 ± 0	Irreversible	13 ± 0	Irreversible
8b	<i>cis</i>	H	11 ± 1	Irreversible	19 ± 1	Irreversible
61a	<i>cis</i>	H	65 ± 42	Irreversible	19 ± 1	Irreversible
61b	<i>cis</i>	F	270 ± 70	Irreversible	10 ± 0	Irreversible
61c	<i>cis</i>	Cl	89 ± 9	Irreversible	4.8 ± 0.1	Irreversible
61d	<i>cis</i>	Me	230 ± 120	Irreversible	30 ± 1	Irreversible
Deprenyl ^b	–	–	Ni	Nd	0.6 ± 0.1	Nd
Clorgyline	–	–	0.13 ± 0.01	Nd	25 ± 1.2	Nd

^a Relative configuration of aromatic ring and amine.

^b (*R*)-(-)-form.

^c Ni = no inhibition was observed.

^d Nd = could not be determined.

the rapid opening of the cyclopropane ring seems to be a key step for the inhibition. This step is also consistent with the irreversible inhibition found for *trans*-2-phenylcyclopropylamine (**8a**). Fluorine substitution is known to increase the ring strain in cyclopropyl rings [135]. Therefore, it can be expected that introduction of fluorine at the 2-position of **8a** would result in a more rapid opening of cyclopropane ring of the fluoro analogue **60a**.

Interestingly, fluorination at the 2-position of 1-phenylcyclopropylamine (**50**), which is known as a selective inhibitor of MAO B relative to MAO A, reversed the selectivity and resulted in a potent inhibitor selective for MAO A [133,134] (Table 5). *p*-Substituted analogues of 1-phenylcyclopropylamine (**62b–e**, **63b–e**) are also MAO A-selective inhibitors and showed the same level of inhibitory potency as **62a** and **63a**.

6. FINAL COMMENTS

Several strategies are used in medicinal chemistry to exploit selective fluorination in the design of biologically active molecules, and this is true in the development

Table 5. IC₅₀ values and inhibition type of 2-fluoro-1-phenylcyclopropylamines for recombinant human liver MAO A and B^{b,c} [133]. Adapted by permission of Elsevier Ltd. Copyright 2005.

Compound	R	Isomer type ^a	MAO A		MAO B	
			IC ₅₀ (μM)	Inhibition type	IC ₅₀ (μM)	Inhibition type
50	—	—	730 ± 150	Nd	190 ± 20	Irreversible
62a	H	<i>trans</i>	1.1 ± 0.1	Irreversible	290 ± 50	Irreversible
62b	F	<i>trans</i>	1.2 ± 0.0	Irreversible	38 ± 0	Irreversible
62c	Cl	<i>trans</i>	0.7 ± 0.1	Irreversible	39 ± 1	Irreversible
62d	Me	<i>trans</i>	0.2 ± 0.0	Irreversible	110 ± 0	Irreversible
62e	OMe	<i>trans</i>	0.7 ± 0.0	Irreversible	81 ± 5	Irreversible
63a	H	<i>cis</i>	0.9 ± 0.1	Irreversible	72 ± 1	Irreversible
63b	F	<i>cis</i>	0.6 ± 0.0	Irreversible	13 ± 1	Irreversible
63c	Cl	<i>cis</i>	0.5 ± 0.0	Irreversible	24 ± 1	Irreversible
63d	Me	<i>cis</i>	0.2 ± 0.0	Irreversible	40 ± 2	Irreversible
63e	OMe	<i>cis</i>	0.6 ± 0.1	Irreversible	23 ± 0	Irreversible
64	—	—	110 ± 10	Irreversible	Ni	Nd

^a Relative configuration of aromatic ring and amine.

^b Ni = no inhibition was observed.

^c Nd = could not be determined.

of inhibitors of amine oxidases as well. The effects of aromatic ring fluorination on benzyl- and phenylethylamines were studied with respect to potency and selectivity of inhibition of MAO A and B. Included in early biological studies of β,β -difluorophenylethylamines of Fuller *et al.* were an examination of effects of altered amine pK_a and lipophilic character on activities as MAO inhibitors. In the Merrell Dow research to develop MAO B-selective inhibitors, the presence of a fluorovinyl moiety played a key role in the enhancement of selectivities and potencies of a series of fluorovinyl amines. PET-scanning agents designed to map the regional concentrations of MAOs have taken advantage of irreversible binding of [^{18}F]-labeled inhibitors selective for each isozyme. Our own work with cyclopropane ring-fluorinated arylcyclopropyl amines has revealed dramatic effects on potencies and selectivities. In our own work, we have found that fluorination of arylcyclopropyl amines can have a strong effect on activities as inhibitors of both MAO and SSAO. In the future, more work with fluorinated MAO and SSAO inhibitors undoubtedly will reveal new and interesting effects of fluorine on potency and selectivity.

ACKNOWLEDGMENT

This research was supported in part by the intramural research program of NIDDK, NIH (KLK), the Tottori Prefectural Government (SY), and the Deutsche Forschungsgemeinschaft (GH).

REFERENCES

- [1] M.S. Benedetti, Biotransformation of xenobiotics by amine oxidases, *Fundam. Clin. Pharmacol.* 15 (2001) 75–84.
- [2] M. Mure, S.A. Mills, J.P. Klinman, Catalytic mechanism of the topa quinone containing copper amine oxidases, *Biochemistry* 41 (2002) 9269–9278.
- [3] K.E. Tipton, S. Boyce, J. O'Sullivan, G.P. Davey, J. Healy, Monoamine oxidases: Certainties and uncertainties, *Curr. Med. Chem.* 11 (2004) 1965–1982.
- [4] L. Maître, Monoamine oxidase inhibiting properties of SU-11,739 in the rat. Comparison with pargyline, tranlylcypromine, and iproniazid, *J. Pharmacol. Exp. Ther.* 157 (1967) 81–88.
- [5] J.P. Johnston, Some observations upon a new inhibitor of monoamine oxidase in brain tissue, *Biochem. Pharmacol.* 17 (1968) 1285–1297.
- [6(a)] R.M. McCauley, E. Racker, Separation of two monoamine oxidases from bovine brain, *Mol. Cell. Biochem.* 1 (1973) 73–81.
- [6(b)] C.J. Fowler, S.B. Ross, Selective inhibitors of monoamine oxidase A and B: Biochemical, pharmacological, and clinical properties, *Med. Res. Rev.* 4 (1984) 323–358.
- [6(c)] J. Knoll, K. Magyar, Some puzzling pharmacological effects of monoamine oxidase inhibitors, *Adv. Biochem. Psychopharmacol.* 5 (1972) 393–408.
- [7] A.W.J. Bach, N.C. Lan, D.L. Johnson, C.W. Abell, M.E. Bembenek, S.W. Kwan, P. H. Seeburg, J.C. Shih, cDNA cloning of human-liver monoamine oxidase-A and oxidase-B—molecular-basis of differences in enzymatic properties, *Proc. Natl. Acad. Sci. USA* 85 (1988) 4934–4938.

- [8(a)] C. Binda, F. Hubálek, M. Li, Y. Herzig, J. Sterling, D.E. Edmondson, A. Mattevi, Crystal structures of monoamine oxidase B in complex with four inhibitors of the N-propargylaminoindan class, *J. Med. Chem.* 47 (2004) 1767–1774.
- [8(b)] L. De Colibus, M. Li, C. Binda, A. Lustig, D.E. Edmondson, A. Mattevi, Three-dimensional structure of human monoamine oxidase A (MAO A): Relation to the structures of rat MAO A and human MAO B, *Proc. Natl. Acad. Sci. USA* 102 (2005) 12684–12689.
- [9] M.B.H. Youdim, D. Edmondson, K.F. Tipton, The therapeutic potential of monoamine oxidase inhibitors, *Nat. Rev. Neurosci.* 7 (2006) 295–309.
- [10] R. Silverman, Radical ideas about monoamine oxidase, *Acc. Chem. Res.* 28 (1995) 335–342.
- [11] R. Miller, D.E. Edmondson, Structure-activity relationships in the oxidation of para-substituted benzylamine analogues by recombinant human liver monoamine oxidase A, *Biochemistry* 38 (1999) 13670–13683.
- [12] N. Seiler, Catabolism of polyamines, *Amino Acids* 26 (2004) 217–233.
- [13] J. O'Sullivan, M. Unzeta, J. Healy, M.I. O'Sullivan, G. Davey, K. F. Tipton, Semicarbazide-sensitive amine oxidases: Enzymes with quite a lot to do, *Neurotoxicology* 25 (2004) 313–315.
- [14(a)] F. Boomsma, D.J. van Veldhuisen, P.J. de Kam, A.J. Man in 't Veld, A. Mossterd, J.I. Lie, M.A.D.H. Schalekamp, Plasma semicarbazide-sensitive amine oxidase is elevated in patients with congestive heart failure, *Cardiovas. Res.* 33 (1997) 387–391.
- [14(b)] F. Boomsma, U.M. Bhaggoe, A.M.B. van der Houwen, A.H. van den Meiracker, Plasma semicarbazide-sensitive amine oxidase in human (patho)physiology, *Biochem. Biophys. Acta* 1647 (2003) 48–54.
- [14(c)] H. Vidrio, Semicarbazide-sensitive amine oxidase: Role in the vasculature and vasodilation after in situ inhibition, *Auton. Autacoid Pharmacol.* 23 (2004) 275–283.
- [15] H. Kinemuchi, H. Sugimoto, T. Obata, N. Satoh, S. Ueda, Selective inhibitors of membrane-bound semicarbazide-sensitive amine oxidase activity in mammalian tissues, *Neurotoxicology* 25 (2004) 325–335.
- [16(a)] J.P. Klinman, Mechanisms whereby mononuclear copper proteins functionalize organic substrates, *Chem. Rev.* 96 (1996) 2541–2561.
- [16(b)] J.P. Klinman, The multi-functional topaquinone copper amine oxidases, *Biochem. Biophys. Acta* 1647 (2003) 131–137.
- [17] A.M. Cesura, A. Pletscher, The new generation of monoamine oxidase inhibitors, *Prog. Drug Res.* 38 (1992) 171–297.
- [18] J. Saura, J.M. Luque, A.M. Cesura, M. Da Prada, V. Chan-Palay, G. Huber, J. Löffler, J. Richards, Increased monoamine oxidase B activity in plaque-associated astrocytes of Alzheimer brains revealed by quantitative enzyme radioautography, *Neuroscience* 62 (1994) 15–30.
- [19] B.M.H. Youdim, Y.S. Bakhle, Monoamine oxidase isoforms and inhibitors in Parkinson's disease and depressive illness, *Br. J. Pharmacol.* 147 (2006) 5287–5296.
- [20] P. Mátyus, B. Dajka-Halász, Á. Földi, N. Haider, D. Barlocco, K. Magyar, Semicarbazide-sensitive amine oxidases: Current status and perspectives, *Curr. Med. Chem.* 11 (2004) 1285–1298.
- [21] K.L. Kirk, Selective fluorination in drug design and development, an overview of biochemical rationales, *Curr. Top. Med. Chem.* 6 (2006) 1447–1456.
- [22] P.N. Edwards, Uses of fluorine in chemotherapy, in: R.E. Banks, B.E. Smart, J.C. Tatlow (Eds.), *Organo Fluorine Chemistry, Principles and Commercial Applications*, Plenum Press, New York, 1994 pp. 501–541.
- [23] J. Olsen, D.W. Banner, P. Seiler, B. Wagner, T. Tschoop, U. Obst-Sander, M. Kansy, K. Müller, F.A. Diedrich, Fluorine interactions at the thrombin active site: Protein backbone fragments H-C_α-C=O comprise a favorable C-F environment and interactions of C-F with electrophiles, *ChemBioChem* 5 (2004) 666–675.

- [24] J.C. Biffinger, H.W. Kim, S.G. DiMagno, The polar hydrophobicity of fluorinated compounds, *ChemBioChem* 5 (2004) 622–627.
- [25] K.L. Kirk, Fluorine in medicinal chemistry: Recent therapeutic applications of fluorinated small molecules, *J. Fluorine Chem.* 127 (2006) 1013–1029.
- [26] K.L. Kirk, Biochemistry of halogenated organic compounds, in: *Biochemistry of the Elements* Plenum Press, New York, 1991 pp. 340–352.
- [27] K.L. Kirk, D. Cantacuzene, C.R. Creveling, Synthesis and biological properties of ring-fluorinated biogenic amines, in: R. Filler, Y. Kobayashi (Eds.), *Biomedical Aspects of Fluorine Chemistry*, Kondasha Ltd., Tokyo, 1982 pp. 75–91.
- [28] H. Kinemuchi, Y. Arai, Y. Toyoshima, T. Tanona, K. Kisara, Studies on 5-fluoro- α -methyltryptamine and *p*-chloro- β -methylphenethylamine—Determination of the MAO-A or MAO-B selective inhibition in vitro, *Jpn. J. Pharmacol.* 46 (1988) 197–199.
- [29] C.H. Williams, Monoamine-oxidase. 1. Specificity of some substrates and inhibitors, *Biochem. Pharmacol.* 23 (1974) 615–628.
- [30] M.C. Walker, D.E. Edmondson, Structure-activity relationships in the oxidation of benzylamine analogues by bovine liver mitochondrial monoamine oxidase B, *Biochemistry* 33 (1994) 7088–7098.
- [31] R.B. Silverman, W.P. Hawe, SAR studies of fluorine-substituted benzylamines and substituted 2-phenylethylamines as substrates and inactivators of monoamine-oxidase-B, *J. Enzyme Inhib.* 9 (1995) 203–215.
- [32] R.B. Silverman, Electron transfer chemistry of monoamine oxidase, in: P.S. Mariano, (Ed.), *Advances in Electron Transfer Chemistry*, Vol. 2, JAI Press, Greenwich, CT 1992 pp. 177–213.
- [33(a)] I.A. Terleckyj, R.E. Heikkila, *In vivo* and *in vitro* pharmacologic profile of two new irreversible MAO B inhibitors: MDL 72,974A and fluorodeprenyl, *Ann. NY Acad. Sci.* 648 (1992) 365–367.
- [33(b)] F. Erdo, A. Baranyi, J. Takacs, P. Aranyi, Different neurorescue profiles of selegiline and *p*-fluoro-selegiline in gerbils, *NeuroReport* 11 (2000) 2597–2600.
- [34] W.G. Tatton, J.S. Wadia, W.Y. Ju, R.M. Chalmers-Redman, N.A. Tatton, (–)-Deprenyl reduces neuronal apoptosis and facilitates neuronal outgrowth by altering protein synthesis without inhibiting monoamine oxidase, *J. Neural. Transm. Suppl.* 48 (1996) 45–59.
- [35] S. Yasar, J. Gaal, Z. Justinova, J. Bergman, Discriminative stimulus and reinforcing effects of *p*-fluoro-*l*-deprenyl in monkeys, *Psychopharmacology* 182 (2005) 95–103.
- [36] C.G. Saysell, W.S. Tambyrajah, J.M. Murray, C.M. Wilmot, S.E.V. Philips, M.J. McPherson, P.F. Knowles, Probing the catalytic mechanism of *Escherichia coli* amine oxidase using mutational variants and a reversible inhibitor as a substrate analogue, *Biochem. J.* 365 (2002) 809–816.
- [37] E.M. Shepard, H. Heather, G.A. Juda, D.M. Dooley, Inhibition of six copper-containing amine oxidases by the antidepressant drug tranylcypromine, *Biochim. Biophys. Acta* 1647 (2003) 252–259.
- [38] J.M. Himmelhoch, C.Z. Fuchs, J.B. Symons, A double blind study of tranylcypromine treatment of major anergic depression, *J. Nerv. Ment. Dis.* 170 (1982) 628–634.
- [39] F. Quitkin, A. Rifkin, D.F. Klein, Monoamine oxidase inhibitors. A review of antidepressant effectiveness, *Arch. Gen. Psychiatry* 36 (1979) 749–760.
- [40] K. White, J. Razani, B. Cadow, R. Gelfand, R. Palmer, G. Simpson, R.B. Sloane, Tranylcypromine vs. nortriptyline vs. placebo in depressed out patients: A controlled trial, *Psychopharmacology* 82 (1984) 258–262.
- [41] L.H. Price, D.S. Charney, G.R. Heninger, Efficacy of lithium-tranylcypromine treatment in refractory depression, *Am. J. Psychiatry* 142 (1985) 619–623.
- [42] P. Foley, M. Gerlach, M.B.H. Youdim, P. Riederer, MAO inhibitors: Multiple roles in the therapy of neurodegenerative disorders? *Parkinsonism Relat. Disord.* 6 (2000) 25–47.
- [43(a)] G.B. Baker, L.J. Urchuk, K.F. McKenna, S.H. Kennedy, Metabolism of monoamine oxidase inhibitors, *Cell. Mol. Neurobiol.* 19 (1999) 411–426.

- [43(b)] G.B. Baker, R.T. Coutts, A.J. Greenshaw, Neurochemical and metabolic aspects of antidepressants: an overview, *J. Psychiatry Neurosci.* 25 (2000) 481–496.
- [44] J.A. Fuentes, M.A. Oleshansky, N.H. Neff, Comparison of the antidepressant activity of (-)- and (+)-tranylcypromine in an animal model, *Biochem. Pharmacol.* 25 (1976) 801–804.
- [45] D.G. Calverley, G.B. Baker, R.T. Coutts, W.G. Dewhurst, A method for the measurement of tranylcypromine in rat brain regions using gas chromatography with electron capture detection, *Biochem. Pharmacol.* 30 (1981) 861–867.
- [46] D.R. Hampson, G.B. Baker, R.T. Coutts, A comparison of the neurochemical properties of the stereoisomers of tranylcypromine in the central nervous system, *Cell. Mol. Biol.* 32 (1986) 593–599.
- [47] R.C. Baselt, C.B. Steward, E. Shaskan, Determination of serum and urine concentrations of tranylcypromine by electron-capture gas-liquid chromatography, *J. Anal. Toxicol.* 1 (1977) 215–217.
- [48] V.A. Lang, H.E. Geissler, E. Mutschler, Bestimmung und Vergleich der Plasma- und Urin-Konzentrationen nach Gabe von (+)- und (-)-Tranylcypromin, *Arzneimittelforschung* 29 (1979) 154–157.
- [49] H. Weber, H. Spahn, W. Mahrke, E. Mutschler, Pharmacokinetics of tranylcypromine enantiomers in healthy volunteers, *J. Pharm. Pharmacol.* 36 (1984) 50W.
- [50] D.J. Edwards, A.G. Mallinger, S. Knopf, J. Himmelhoch, Determination of tranylcypromine in plasma using gas chromatography-chemical-ionization mass spectrometry, *J. Chromatogr. Biomed. Appl.* 344 (1985) 356–361.
- [51] A.G. Mallinger, D.J. Edwards, J.M. Himmelhoch, S. Knopf, J. Ehler, Pharmacokinetics of tranylcypromine in patients who are depressed—relationship to cardiovascular effects, *Clin. Pharmacol. Ther.* 40 (1986) 444–450.
- [52] G.B. Baker, D.R. Hampson, R.T. Coutts, R.G. Micetich, T.W. Hall, T.S. Rao, Detection and quantitation of a ring-hydroxylated metabolite of the antidepressant drug tranylcypromine, *J. Neural Transm.* 65 (1986) 233–244.
- [53] A.J. Nazarali, G.B. Baker, R.T. Coutts, A.J. Greenshaw, Para-hydroxytranylcypromine: Presence in rat brain and heart following administration of tranylcypromine and *N*-cyanoethyl analogue, *Eur. J. Drug Metab. Pharmacokinet.* 12 (1987) 207–214.
- [54] T.S. Rao, R.T. Coutts, G.B. Baker, T.W. Hall, R.G. Micetich, Analogs of tranylcypromine: Comparison of effects on monoamine oxidase *in vitro*, *Proc. West Pharmacol. Soc.* 29 (1986) 279–281.
- [55] R.T. Coutts, T.S. Rao, G.B. Baker, R.G. Micetich, T.W.E. Hall, Neurochemical and neuropharmacological properties of 4-fluorotranylcypromine, *Cell. Mol. Neurobiol.* 7 (1987) 271–290.
- [56] A.J. Greenshaw, T.S. Rao, A.J. Nazarali, G.B. Baker, R.T. Coutts, Chronic effects of tranylcypromine and 4-fluorotranylcypromine on regional brain monoamine metabolism in rats: A comparison with clorgyline, *Biol. Psychiatry* 25 (1989) 1014–1020.
- [57] E.D. Hendley, S.H. Snyder, The relationship between the action of monoamine oxidase inhibitors on the noradrenaline uptake system and their antidepressant efficacy, *Nature* 220 (1968) 1330–1331.
- [58] J.J. Schildkraut, Tranylcypromine: Effects on norephedrine metabolism in rat brain, *Am. J. Psychiatry* 126 (1970) 925–931.
- [59] A.S. Horn, S.H. Snyder, Steric requirements for catecholamine uptake by rat brain synaptosomes, studies with rigid analogues of amphetamine, *J. Pharmacol. Exp. Ther.* 180 (1972) 523–530.
- [60] G.B. Baker, H.R. McKim, D.G. Calverley, W.G. Dewhurst, Effects of the monoamine oxidase inhibitors tranylcypromine, phenelzine and pheniprazine on the uptake of catecholamines in slices from rat brain regions, *Proc. Eur. Soc. Neurochem.* 1 (1978) 536.
- [61] G.B. Baker, L.E. Hio, W.G. Dewhurst, Effects of monoamine oxidase inhibitors on release of dopamine and 5-hydroxytryptamine from rat striatum *in vivo*, *Cell. Mol. Biol.* 26 (1980) 182–186.

- [62] J. Tuomisto, D.F. Smith, Effects of tranlylcypromine enantiomers on monoamine uptake and release and imipramine binding, *J. Neural Transm.* 65 (1986) 135–145.
- [63] R.L. Sherry, R.T. Coutts, G.B. Baker, Fluorotranlylcypromine, a novel monoamine oxidase inhibitor. Neurochemical effects in rat brain after short- and long-term administration, *Drug Dev. Res.* 48 (1999) 61–69.
- [64] P. Dostert, Can our knowledge of monoamine oxidase (MAO) help in the design of better MAO inhibitors? *J. Neural Transm. Suppl.* 41 (1994) 269–279.
- [65] M. Da Prada, R. Kettler, H.H. Keller, A.M. Cesura, J.G. Richerds, J. Saura Marti, D. Muggli-Maniglio, P.-C. Wyss, E. Kyburz, R. Imhof, From moclobemide to Ro 19-6327 and Ro 41-1049: The development of a new class of reversible, selective MAO A and MAO B inhibitors, *J. Neural Transm. Suppl.* 29 (1990) 279–292.
- [66] A.M. Cesura, M.D. Galva, R. Imhof, E. Kyburz, G.B. Picotti, M. Da Prada, [3H]Ro 19-6327: A reversible ligand and affinity labelling probe for monoamine oxidase-B, *Eur. J. Pharmacol.* 162 (1989) 457–465.
- [67] A.M. Cesura, M. Bös, M.D. Galva, R. Imhof, M. Da Prada, Characterization of the binding of [3H]Ro 41-1049 to the active site of human monoamine oxidase-A, *Mol. Pharmacol.* 37 (1990) 358–366.
- [68] A. Ito, T. Kuwahara, S. Inadome, Y. Sagara, Molecular cloning of a cDNA for rat liver monoamine oxidase B, *Biochem. Biophys. Commun.* 157 (1988) 970–976.
- [69] J.F. Powell, P.P. Hau, W. Weyler, S. Chen, J. Salach, K. Adrikopoulos, J. Mallet, X.O. Breakefield, The primary structure of bovine monoamine oxidase type A: Comparison with peptide sequences of bovine monoamine oxidase type B and other flavoenzymes, *Biochem. J.* 259 (1989) 407–413.
- [70] C. Binda, M. Li, F. Hubálek, N. Restelli, D.E. Edmondson, A. Mattevi, Insights into the mode of inhibition of human mitochondrial monoamine oxidase B from high-resolution crystal structures, *Proc. Natl. Acad. Sci. USA* 100 (2003) 9750–9755.
- [71] K. Yoshimi, M. Kozuka, J. Sakai, T. Iizawa, Y. Shimizu, I. Kaneko, K. Kojima, N. Iwata, Novel monoamine oxidase inhibitors, 3-(2-aminoethoxy)-1,2-benzisoxazole derivatives, and their differential reversibility, *Jpn. J. Pharmacol.* 88 (2002) 174–182.
- [72] R.W. Fuller, B.B. Molloy, The effect of aliphatic fluorine on amine drugs, in: R. Filler (Ed.), *Biochemistry Involving Carbon-Fluorine Bonds*, ACS, Washington, D.C., 1976 pp. 77–98.
- [73] R.R. Rando, A. Eigner, The pseudoirreversible inhibition of monoamine oxidase by allylamine, *Mol. Pharmacol.* 13 (1977) 1005–1013.
- [74] P. Bey, J. Fozard, J.M. Lacoste, I.A. McDonald, M. Zreika, M.G. Palfreyman, (*E*)-2-(3,4-Dimethoxyphenyl)-3-fluoroallylamine: A selective, enzyme-activated inhibitor of type B monoamine oxidase, *J. Med. Chem.* 27 (1984) 9–10.
- [75] I.A. McDonald, J.M. Lacoste, P. Bey, M.G. Palfreyman, M. Zreika, Enzyme-activated irreversible inhibitors of monoamine oxidase: Phenylallylamine structure-activity relationships, *J. Med. Chem.* 28 (1985) 186–193.
- [76] M.G. Palfreyman, I.A. McDonald, J.R. Fozard, Y. Mely, A.J. Sleight, M. Zreika, J. Wagner, P. Bey, P.J. Lewis, Inhibition of monoamine oxidase selectively in brain monoamine nerves using the bioprecursor (MDL 72394), a substrate for aromatic L-amino acid decarboxylase, *J. Neurochem.* 45 (1985) 1850–1860.
- [77] M.G. Palfreyman, P. Bey, A. Sjoerdsma, Enzyme-activated/mechanism-based inhibitors, *Essays Biochem.* 23 (1987) 28–81.
- [78] G.A. Lyles, C.M.S. Marshall, I.A. McDonald, P. Bey, M.G. Palfreyman, Inhibition of rat aorta semicarbazide-sensitive amine oxidase by 2-phenyl-3-haloallylamines and related compounds, *Biochem. Pharmacol.* 36 (1987) 2847–2853.
- [79] J. Elliot, B.A. Callingham, M.A. Barrand, *In-vivo* effects of (*E*)-2-(3',4'-dimethoxyphenyl)-3-fluoroallylamine (MDL 72145) on amine oxidase activities in the rat. Selective inhibition of semicarbazide-sensitive amine oxidase in vascular and brown adipose tissue, *J. Pharm. Pharmacol.* 41 (1989) 37–41.
- [80] M.G. Palfreyman, I.A. McDonald, P. Bey, C. Danzin, M. Zreika, G. Cremer, Haloallylamine inhibitors of MAO and SSAO and their therapeutic potential, *J. Neural. Transm.* 41 (1994) 407–414.

- [81] J. Kim, Y. Zhang, C. Ran, L.M. Sayre, Inactivation of bovine plasma amine oxidase by haloallylamines, *Bioorg. Med. Chem. Lett.* 14 (2006) 1444–1453.
- [82] E.Y. Wang, H. Gao, L. Salter-Cid, J. Zhang, E.M. Podar, A. Miller, J. Zhao, A. O'Rourke, M.D. Linnik, Design, synthesis, and biological evaluation of semicarbazide-sensitive amine oxidase (SSAO) inhibitors with anti-inflammatory activity, *J. Med. Chem.* 49 (2006) 2166–2173.
- [83] P. Dostert, M. Strolin Benedetti, K.F. Tipton, Interactions of monoamine oxidase with substrates and inhibitors, *Med. Res. Rev.* 9 (1989) 45–89.
- [84(a)] O. Curet, G. Damoiseau, N. Aubin, Biochemical profile of befloxtatone, a new reversible MAO-A inhibitor, *Clin. Neuropharmacol.* 15 (suppl 1) (1992) 428B.
- [84(b)] V. Rovei, D. Caille, O. Curet, D. Ego, F.-X. Jarreau, Biochemical pharmacology of befloxtatone (MD370503), a new potent reversible MAO A inhibitor, *Neural. Transm. Suppl.* 41 (1994) 339–347.
- [84(c)] O. Curet, G. Damoiseau, J.-P. Rovei, F.-X. Jarreau, Effects of befloxtatone, a new potent reversible MAO A inhibitor, on cortex and striatum monoamines in freely moving rats, *J. Neural. Transm. Suppl.* 41 (1994) 349–355.
- [85] A.S. Kalgutkar, N. Castagnoli, B. Testa, Selective inhibitors of monoamine oxidase (MAO A and MAO B) as probes of its catalytic site and mechanism, *Med. Res. Rev.* 15 (1995) 325–388.
- [86] N. Brunello, S.Z. Langer, J. Perez, G. Racagni, Current understanding of the mechanism of action of classic and newer antidepressant drugs, *Depression* 2 (1995) 119–126.
- [87] J. Wouters, F. Moureau, G. Vercauteren, G. Evrard, F. Durant, J.J. Koenig, F. Ducrey, F.X. Jarreau, Experimental and theoretical study of reversible monoamine oxidase inhibitors: Structural approach of the active site of the enzyme, *J. Neural. Transm. Suppl.* 41 (1994) 313–319.
- [88] O. Curet, G. Damoiseau-Ovens, C. Sauvage, N. Sontag, P. Avenet, H. Depoortere, D. Caille, O. Bergis, B. Scatton, Preclinical profile of befloxtatone, a new reversible MAO A inhibitor, *J. Affect. Disord.* 51 (1998) 287–303.
- [89] O. Curet, G. Damoiseau, N. Aubin, N. Sontag, V. Rovei, F.-X. Jarreau, Befloxtatone, a new reversible and selective monoamine oxidase-A inhibitor. I. Biochemical profile, *J. Pharmacol. Exp. Ther.* 277 (1996) 253–264.
- [90] P. Rosenzweig, A. Patat, O. Curet, G. Durrieu, C. Dubruc, I. Zieleniuk, Clinical pharmacology of befloxtatone: A mini review, *J. Affect. Disord.* 51 (1998) 305–312.
- [91] F. Moureau, J. Wouters, D.P. Vercauteren, S. Collin, G. Evrard, F. Durant, F. Ducrey, I.J. Koenig, F.X. Jarreau, A reversible monoamine oxidase inhibitor, toloxtatone: structural and electronic properties, *Eur. J. Med. Chem.* 27 (1992) 939–948.
- [92] J. Wouters, F. Moureau, G. Evrard, J.-J. Koenig, S. Jegham, P. George, F. Durant, A reversible monoamine oxidase A inhibitors, befloxtatone: Structural approach of its mechanism of action, *Bioorg. Med. Chem.* 7 (1999) 1683–1693.
- [93] F. Ooms, R. Frédérick, F. Durant, J.P. Petzer, N. Castagnoli, C.J. Vand der Schyf, J. Wouters, Rational approaches towards reversible inhibition of type B monoamine oxidase. Design and evaluation of a novel 5H-indeno[1,2-c]pyridazin-5-one derivative, *Bioorg. Med. Chem. Lett.* 13 (2003) 69–73.
- [94] S. Kneubühler, U. Thull, C. Altomare, V. Carta, P. Gaillard, P.A. Carrupt, A. Carotti, B. Testa, Inhibition of monoamine oxidase-B by 5H-indeno[1,2-c]pyridazines: Biological activities, quantitative structure-activity relationships (QSARs) and 3D-QSARs, *J. Med. Chem.* 38 (1995) 3874–3883.
- [95] R. Frédérick, W. Dumont, F. Ooms, L. Aschenbach, Jr., C.J. Van der Schyf, N. Castagnoli, J. Wouters, A. Krief, Synthesis, structural reassignment, and biological activity of type B MAO inhibitors based on the 5H-indeno[1,2-c]pyridazin-5-one core, *J. Med. Chem.* 49 (2006) 3743–3747.
- [96(a)] J.S. Fowler, The synthesis and application of F-18 compounds in positron emission tomography, in: R. Filler, Y. Kobayashi, L.M. Yagupolskii (Eds.), *Organofluorine Compounds in Medicinal Chemistry and Biomedical Application*, Elsevier, Amsterdam, 1993 pp. 309–338.

- [96(b)] S. Sun, A. Adejare, Fluorinated molecules as drugs and imaging agents in the CNS, *Curr. Top. Med. Chem.* 6 (2006) 1457–1464.
- [97] J.S. Fowler, R.R. MacGregor, A.P. Wolf, C.D. Arnett, S.L. Dewey, D. Schlyer, D. Christman, J. Logan, M. Smith, H. Sachs, S.M. Aquilonius, P. Bjurling, C. Halldin, P. Hartvig, K.L. Leenders, H. Lundqvist, L. Orelund, C.-G. Stålnacke, B. Långström, Mapping human brain monoamine oxidase A and B with ^{11}C -labeled suicide inactivators and PET, *Science* 235 (1987) 481–485.
- [98] J.S. Fowler, J. Logan, G.-J. Wang, N.D. Volkow, F. Telang, Y.-S. Ding, C. Shea, V. Garza, Y. Xu, Z. Li, D. Alexoff, P. Vaska, R. Ferrieri, D. Schlyer, W. Zhu, S.J. Gatley, Comparison of the binding of the irreversible monoamine oxidase tracers, [^{11}C]clorgyline and [^{11}C]l-deprenyl in brain and peripheral organs in humans, *Nucl. Med. Biol.* 31 (2004) 313–319.
- [99] J.S. Fowler, J. Logan, G.-J. Wang, N.D. Volkow, F. Telang, W. Zhu, D. Franceschi, C. Shea, V. Garza, Y. Xu, Y.-S. Ding, D. Alexoff, D. Warner, N. Netusil, P. Carter, M. Jayne, P. King, P. Vaska, Comparison of monoamine oxidase A in peripheral organs in nonsmokers and smokers, *J. Nucl. Med.* 46 (2005) 1414–1420, and references therein.
- [100(a)] M. Bottlaender, F. Dollé, I. Geunther, D. Roumenov, C. Fuseau, Y. Bramoulle, O. Curet, J. Jegham, J.-L. Pinquier, P. George, H. Valette, Mapping the cerebral monoamine oxidase type A: Positron emission tomography characterization of the reversible selective inhibitor [^{11}C]befloxatone, *J. Pharmacol. Exp. Ther.* 305 (2003) 467–473.
- [100(b)] F. Dollé, Y. Bramoulle, F. Hinnen, S. Demphel, P. George, M. Bottlaender, Efficient synthesis of [^{11}C]befloxatone, a selective radioligand for the *in vivo* imaging of MAO-A density using PET, *J. Labelled Compd. Radiopharm.* 46 (2003) 783–792.
- [101] H. Valette, M. Bottlaender, F. Dollé, C. Coulon, M. Ottaviani, A. Syrota, Acute inhibition of cardiac monoamine oxidase A after tobacco smoke inhalation: Validation study of [^{11}C]befloxatone in rats followed by a positron emission tomography application in baboons, *J. Pharmacol. Exp. Ther.* 314 (2005) 431–436.
- [102] S.-C. Huang, J. Quintana, N. Satyamurthy, G. Lacan, D.-C. Yu, M.E. Phelps, J.R. Barrio, [^{18}F]Fluoro- β -fluoromethylene-*m*-tyrosine derivatives show stereo, geometrical, and regio specificities as *in vivo* central dopaminergic probes in monkeys, *Nucl. Med. Biol.* 26 (1999) 365–370.
- [103] M. Hirata, Y. Magata, Y. Ohmono, H. Saji, C. Tanaka, A. Yokoyama, Radiofluorinated clorgyline derivative for mapping MAO-A activity in brain with PET, *J. Labelled Compd. Radiopharm.* 35 (1994) 234–235.
- [104] J. Mukherjee, Z.-Y. Yang, Development of *N*-[3-(2',3'-Dichlorophenoxy)-2- ^{18}F -fluoropropyl]-*N*-methylpropargylamine (^{18}F -fluoroclogyline) as a potential PET radiotracer for monoamine oxidase-A, *Nucl. Med. Biol.* 26 (1999) 619–625.
- [105] A. Plenevaux, S.L. Dewey, J.S. Fowler, M. Guillaume, A.P. Wolf, Synthesis of (R)-(-) and (S)-(+)-4-fluorodeprenyl and (R)-(-) and (S)-(+)-[N - ^{11}C -methyl]-4-fluorodeprenyl and positron emission tomography studies in baboon brain, *J. Med. Chem.* 33 (1990) 2015–2019.
- [106] A. Plenevaux, J.S. Fowler, S.L. Dewey, A.P. Wolf, M. Guillaume, The synthesis of no-carrier-added dl-4-[^{18}F]fluorodeprenyl via nucleophilic aromatic substitution reaction, *Int. J. Radiat. Appl. Instrument. Part A, Appl. Radiat. Isot.* 42 (1991) 121–127.
- [107] J. Mukherjee, Z.-Y. Yang, R. Lew, *N*-(6- ^{18}F -Fluorohexyl)-*N*-methylpropargylamine: A Fluorine-18-labeled monoamine oxidase B inhibitor for potential use in PET studies, *Nucl. Med. Biol.* 26 (1999) 111–116.
- [108] J.S. Fowler, J. Logan, N.D. Volkow, G.-J. Wang, R.R. MacGregor, Y.-S. Ding, Monoamine oxidase: Radiotracer development and human studies, *Methods* 27 (2002) 263–277.

- [109(a)] R.E. Tedeschi, D.H. Tedeschi, P.L. Ames, L. Cook, P.A. Mattis, E.J. Fellows, Some pharmacological observations on tranlylcypromine (SKF trans-385), A potent inhibitor of monoamine oxidase, *Proc. Soc. Exp. Biol. Med.* 102 (1959) 380–381.
- [109(b)] M.C. Petersen, J.W. McBrayer, Treatment of affective depression with *trans* d, l-phenylcyclopropylamine hydrochloride; A preliminary report, *Am. J. Psychiatry* 116 (1959) 67–68.
- [110(a)] H. Green, R.W. Erickson, Effect of *trans*-2-phenylcyclopropylamine upon norepinephrine concentration and monoamine oxidase activity of rat brain, *J. Pharmacol. Exp. Ther.* 129 (1960) 237–242.
- [110(b)] H. Green, J.H. Sawyer, Intracellular distribution of norepinephrine in rat brain. I. Effect of reserpine and the monoamine oxidase inhibitors, *trans*-2-phenylcyclopropylamine and 1-isonicotinyl-2-isopropyl hydrazine, *J. Pharmacol. Exp. Ther.* 129 (1960) 243–249.
- [111(a)] R.W. Fuller, Kinetic studies and effects *in vivo* of a new monoamine oxidase inhibitor, *N*-[2-*o*-(chlorophenoxy)-ethyl]-cyclopropylamine, *Biochem. Pharmacol.* 17 (1968) 2097–2106.
- [111(b)] J. Mills, R. Kattau, I.H. Slater, R.W. Fuller, *N*-Substituted cyclopropylamines as monoamine oxidase inhibitors. Structure-activity relationship. Dopa potentiation in mice and *in vitro* inhibition of kynuramine oxidation, *J. Med. Chem.* 11 (1968) 95–97.
- [112] R.W. Fuller, M.M. Marsh, J. Mills, Inhibition of monoamine oxidase by *N*-(phenoxyethyl)cyclopropylamines. Correlation of inhibition with Hammett constants and partition coefficients, *J. Med. Chem.* 11 (1968) 397–398.
- [113] A. Burger, M. Bernabé, P.W. Collins, 2-(4-Imidazolyl)cyclopropylamine, *J. Med. Chem.* 13 (1970) 33–35.
- [114(a)] F. Chimenti, M.C. Casanova, P. Turini, S. Sabatini, Monoamine oxidase inhibitors. I. Synthesis of *N*-cyclopropyltryptamines, *Farmaco [Sci]* 35 (1980) 785–790.
- [114(b)] F. Chimenti, M.C. Casanova, V. Zagarese, P. Turini, S. Sabatini, Substances inhibiting monoamine oxidase. II. Inhibition of bovine plasma amine oxidase by *N*-cyclopropyltryptamines, *Farmaco [Sci]* 38 (1983) 425–428.
- [115(a)] D.G. Folks, Monoamine oxidase inhibitors: Reappraisal of dietary considerations, *J. Clin. Psychopharmacol.* 3 (1983) 249–251.
- [115(b)] M.B. Youdium, J.P. Finberg, Monoamine oxidase B inhibition and the “gcheese effect”, *J. Neural Transm. Suppl.* 25 (1987) 27–33.
- [116] N.H. Neff, H.Y. Yang, Another look at the monoamine oxidases and the monoamine oxidase inhibitor drugs, *Life Sci.* 14 (1974) 2061–2074.
- [117] R.W. Fuller, S.K. Hemrick, J. Mills, Inhibition of monoamine oxidase by *N*-phenacylcyclopropylamine, *Biochem. Pharmacol.* 27 (1978) 2255–2261.
- [118] R.W. Fuller, S.K. Hemrick-Luecke, Elevation of epinephrine concentration in rat brain by LY51641, a selective inhibitor of type A monoamine oxidase, *Res. Commun. Chem. Pathol. Pharmacol.* 32 (1981) 207–221.
- [119] R.W. Fuller, S.K. Hemrick-Luecke, B.B. Molloy, *N*-[(2-*o*-Indophenoxy)ethyl]cyclopropylamine hydrochloride (LY121768), a potent and selective irreversible inhibitor of type A monoamine oxidase, *Biochem. Pharmacol.* 32 (1983) 1243–1249.
- [120(a)] R.B. Silverman, C.K. Hiebert, Inactivation of monoamine oxidase A by the monoamine oxidase B inactivators 1-phenylcyclopropylamine, 1-benzylcyclopropylamine, and *N*-cyclopropyl- α -methylbenzylamine, *Biochemistry* 27 (1988) 8448–8453.
- [120(b)] R.B. Silverman, Effect of alpha-methylation on inactivation of monoamine oxidase by *N*-cyclopropylbenzylamine, *Biochemistry* 23 (1984) 5206–5213.
- [121(a)] R.B. Silverman, S.J. Hoffman, Mechanism of inactivation of mitochondrial monoamine oxidase by *N*-cyclopropyl-*N*-arylalkyl amines, *J. Am. Chem. Soc.* 102 (1980) 884–886.
- [121(b)] R.B. Silverman, S.J. Hoffman, *N*-(1-Methy)cyclopropylbenzylamine: A novel inactivator of mitochondrial monoamine oxidase, *Biochem. Biophys. Res. Commun.* 101 (1981) 1396–1401.

- [121(c)] R.B. Silverman, R.B. Yamasaki, Mechanism-based inactivation of mitochondrial monoamine oxidase by *N*-(1-methylcyclopropyl)benzylamine, *Biochemistry* 23 (1984) 1322–1332.
- [122(a)] L. Hall, S. Murray, K. Castagnoli, N. Castagnoli, Jr., Studies on 1,2,3,6-tetrahydropyridine derivatives as potential monoamine oxidase inactivators, *Chem. Res. Toxicol.* 5 (1992) 625–633.
- [122(b)] S. Kuttub, A. Kalgutkar, N. Castagnoli Jr., Mechanistic studies on the monoamine oxidase B catalyzed oxidation of 1,4-disubstituted tetrahydropyridines, *Chem. Res. Toxicol.* 7 (1994) 740–744.
- [122(c)] J.M. Rimoldi, Y.X. Wang, S.K. Nimkar, S.H. Kuttub, A.H. Anderson, H. Burch, N. Castagnoli, Jr., Probing the mechanism of bioactivation of MPTP type analogs by monoamine oxidase B: Structure-activity studies on substituted 4-phenoxy-, 4-phenyl-, and 4-thiophenoxy-1-cyclopropyl-1,2,3,6-tetrahydropyridines, *Chem. Res. Toxicol.* 8 (1995) 703–710.
- [122(d)] J.M. Rimoldi, S.G. Puppali, E. Isin, P. Bissel, A. Khalil, N. Castagnoli, Jr., A novel and selective monoamine oxidase B substrate, *Bioorg. Med. Chem.* 13 (2005) 5808–5813.
- [122(e)] C. Franot, S. Mabic, N. Castagnoli, Jr., Chemical model studies on the monoamine oxidase-B catalysed oxidation of 4-substituted 1-cyclopropyl-1,2,3,6-tetrahydropyridines, *Bioorg. Med. Chem.* 6 (1986) 283–291.
- [123(a)] A. Burger, C.S. Davis, H. Green, D.H. Tedeschi, C.L. Zirkle, 1-Methyl-2-phenylcyclopropylamine, *J. Med. Pharm. Chem.* 4 (1961) 571–574.
- [123(b)] C. Kaiser, B. Lester, C.L. Zirkle, 2-Substituted cyclopropylamines. I. Derivatives and analogues of 2-phenylcyclopropylamine, *J. Med. Pharm. Chem.* 5 (1962) 1243–1265.
- [123(c)] C.L. Zirkle, C. Kaiser, D.H. Tedeschi, R.E. Tedeschi, A. Burger, 2-Substituted cyclopropylamines. II. Effect of structure upon monoamine oxidase-inhibitory activity as measured *in vivo* by potentiation of tryptamine convulsions, *J. Med. Pharm. Chem.* 5 (1962) 1265–1284.
- [124] T.N. Riley, C.G. Brier, Absolute configuration of (+)- and (–)-*trans*-2-phenylcyclopropylamine hydrochloride, *J. Med. Chem.* 15 (1972) 1187–1188.
- [125(a)] A.P. Vintém, N.T. Price, R.B. Silverman, R.R. Ramsay, Mutation of surface cysteine 374 to alanine in monoamine oxidase A alters substrate turnover and inactivation by cyclopropylamines, *Bioorg. Med. Chem.* 13 (2005) 3487–3495.
- [125(b)] M.L. Vanquez, R.B. Silverman, Revised mechanism for inactivation of mitochondrial monoamine oxidase by *N*-cyclopropylbenzylamine, *Biochemistry* 24 (1985) 6538–6543.
- [126(a)] R.B. Silverman, Mechanism of inactivation of monoamine oxidase by *trans*-2-phenylcyclopropylamine and the structure of the enzyme-inactivator adduct, *J. Biol. Chem.* 258 (1983) 14766–14769.
- [126(b)] R.B. Silverman, P.A. Zieske, Mechanism of inactivation of monoamine oxidase by 1-phenylcyclopropylamine, *Biochemistry* 24 (1985) 2128–2138.
- [126(c)] R.B. Silverman, P.A. Zieske, 1-Benzylcyclopropylamine and 1-(phenylcyclopropyl)-methylamine: An inactivator and a substrate of monoamine oxidase, *J. Med. Chem.* 28 (1985) 1953–1957.
- [126(d)] R.B. Silverman, J.M. Cesarone, X. Lu, Stereoselective ring opening of 1-phenylcyclopropylamine catalysed by monoamine oxidase-B, *J. Am. Chem. Soc.* 115 (1993) 4955–4961.
- [126(e)] D.J. Mitchell, D. Nikolic, R.B. van Breemen, R.B. Silverman, Inactivation of monoamine oxidase B by 1-phenylcyclopropylamine: Mass spectral evidence for the flavin adduct, *Bioorg. Med. Chem. Lett.* 11 (2001) 1757–1760.
- [127] D.E. Edmondson, A. Mattevi, C. Binda, M. Li, F. Hubálek, Structure and mechanism of monoamine oxidase, *Curr. Med. Chem.* 11 (2004) 1983–1993.
- [128] L.M. Sayre, M.P. Singh, P.B. Kokil, F. Wang, Non-electron-transfer quinone-mediated oxidative cleavage of cyclopropylamines. Implications regarding their utility as probes of enzyme mechanism, *J. Org. Chem.* 56 (1991) 1353–1355.

- [129] C.M. Wilmot, C.G. Saysell, A. Blessington, D.A. Conn, C.R. Kurtis, M.J. McPherson, P.F. Knowles, S.E. Phillips, Medical implications from the crystal structure of a copper-containing amine oxidase complexed with the antidepressant drug tranylcypromine, *FEBS Lett.* 576 (2004) 301–305.
- [130] S. Yoshida, O.G.J. Meyer, T.C. Rosen, G. Haufe, S. Ye, M.J. Sloan, K.L. Kirk, Fluorinated phenylcyclopropylamines. 1. Synthesis and effect of fluorine substitution at the cyclopropane ring on inhibition of microbial tyramine oxidase, *J. Med. Chem.* 47 (2004) 1796–1806.
- [131] T.C. Rosen, S. Yoshida, R. Fröhlich, K.L. Kirk, G. Haufe, Fluorinated phenylcyclopropylamines. 2. Effects of aromatic ring substitution and of absolute configuration on inhibition of microbial tyramine oxidase, *J. Med. Chem.* 47 (2004) 5860–5871.
- [132] S. Hirota, T. Iwamoto, S. Kishishita, T. Okajima, O. Yamauchi, K. Tanizawa, Spectroscopic observation of intermediates formed during the oxidative half-reaction of copper/topa quinone-containing phenylethylamine oxidase, *Biochemistry* 40 (2001) 15789–15796.
- [133] S. Ye, S. Yoshida, R. Fröhlich, G. Haufe, K.L. Kirk, Fluorinated phenylcyclopropylamines. Part 4. Effects of aryl substituents and stereochemistry on the inhibition of monoamine oxidases by 1-aryl-2-fluoro-cyclopropylamines, *Bioorg. Med. Chem.* 13 (2005) 2489–2499.
- [134(a)] S. Yoshida, T.C. Rosen, O.G.J. Meyer, M.J. Sloan, S. Ye, G. Haufe, K.L. Kirk, Fluorinated phenylcyclopropylamines. Part 3: Inhibition of monoamine oxidase A and B, *Bioorg. Med. Chem.* 12 (2004) 2645–2652.
- [134(b)] T.C. Rosen, S. Yoshida, K.L. Kirk, G. Haufe, Fluorinated phenylcyclopropylamines as inhibitors of monoamine oxidases, *ChemBioChem* 5 (2004) 1033–1043.
- [135] W.R. Dolbier, Jr., M.A. Battiste, Structure, synthesis and chemical reactions of fluorinated cyclopropanes and cyclopropenes, *Chem. Rev.* 103 (2003) 1071–1098.

This page intentionally left blank

CHAPTER 16

Fluoroolefin Dipeptide Isosteres: Structure, Syntheses, and Applications

John T. Welch*

Department of Chemistry, University at Albany, Albany, NY 12222, USA

Contents

1. Introduction	700
1.1. Peptide isosteres	700
1.1.1. Peptidomimetics	701
1.1.2. Amide bond isosteres	701
1.1.3. Nomenclature and terminology	702
2. Fluoroolefin dipeptide isosteres	702
2.1. Alkenes as amide bond substitutes	702
2.2. Fluoroolefins as one of the best amide bond replacements	703
2.3. Synthesis of fluoroolefin peptide isosteres	704
2.3.1. Carbine insertion. Synthesis of Gly- ψ [(Z)-CF=CH]Gly (4) and Phe- ψ [(Z)-CF=CH]Gly (5)	704
2.3.2. Claisen condensation–dehydration. Synthesis of tripeptide analogs Cbz-Gly- ψ [(Z)-CF=CH]LeuXaa (10)	705
2.3.3. Alkylation reactions. Synthesis of asparagine analogs (17) and (18)	705
2.3.4. Imine addition reactions in the synthesis of Val- ψ [(Z)CF=CH]Gly (23)	707
2.3.5. Fluorotris(trimethylsilyl)methane addition reactions. Synthesis of fluoroolefin depsipeptide precursor (27)	707
2.3.6. Nozaki-Hiyama-Kishi-type reactions to construct a fluoroolefin depsipeptide precursor (28)	708
2.3.7. Negishi-type reactions to construct a fluoroolefin depsipeptide precursor (29)	708
2.3.8. Horner-Emmons. Replacement of a nonpeptidomimetic amide (32) with the fluoroolefin isostere (33)	709
2.3.9. Horner-Emmons. Fluorophosphono dithioacetate (34) in the preparation of fluoroolefin peptide isostere precursors	710
2.3.10. Horner-Emmons. Synthesis of Phe- ψ [(E)-CF=CH]Gly (37)	710
2.3.11. Horner-Emmons. The use of 2-fluoro-2-diethylphosphonoacetic acid (41) or acylfluorodiethylphosphonoacetate to prepare fluoroolefin dipeptide isostere precursors (42)	711
2.3.12. Horner-Emmons. The synthesis of DPP IV inhibitors (44)	712

*Corresponding author. Tel.: +1-518-442-4455;
Email: jwelch@uamail.albany.edu

2.3.13. Horner-Emmons. The use of (diphenylphosphinoyl)fluoroacetonitrile (48) to introduce the amino group	712
2.3.14. Peterson fluoroolefination. Synthesis of the Ala ψ [(Z)-CFC]-pro isostere (50) DPP IV inhibitors using the Peterson fluoroolefination reaction	713
2.3.15. Peterson fluoroolefination. Synthesis of 2-(2-amino-1-fluoro-propylidene)-cyclopentanecarbonitrile (55) as DPP IV inhibitors	714
2.3.16. Stereoselective construction of (Z)-fluoroalkene depsipeptide (60) through a Cu(I)-mediated allylic substitution reaction	714
2.3.17. Synthesis of Boc-Phe ψ [(Z)-CF=CH]Gly-OEt (64) utilizing organocopper-mediated reduction of γ,γ -difluoro- α,β -enoates	715
2.3.18. Synthesis of functionalized (Z)-fluoroalkene-type dipeptide isosteres (36) via SmI ₂ -mediated reduction of γ,γ -difluoro- α,β -enoates	716
2.3.19. Reductive formation of fluoroolefins and subsequent conversion to diketopiperazine mimics (71). Nonpeptidic amide bond replacement	717
3. Related methods for the synthesis of α -fluoro- α,β -unsaturated ketones	717
3.1. Conversion from trifluoromethyl ketones via Mg(0)-promoted successive double defluorination	717
3.2. Synthesis of α -fluoro- α,β -unsaturated ketones via palladium-catalyzed cross-coupling reaction of 1-fluorovinyl halides (79) with organostannanes (80)	719
3.3. Synthesis of α -fluoro- α,β -unsaturated ketone via allylic hydroxylation of vinyl fluoride	719
3.4. Synthesis of α -fluoroenone from 1,1,1,2-tetrafluoroethane	719
3.5. Miscellaneous reactions	720
4. Metathesis reactions	721
5. Biological applications and utility of fluoroolefin peptide isosteres	722
5.1. Background	722
5.1.1. Role of <i>cis-trans</i> geometry in biological systems	722
5.1.2. Fluorine in biological mimics	722
5.2. Peptidyl prolyl isomerases (PPlases)	723
5.2.1. Cyclophilin (CyP) inhibitors	724
5.2.2. Pin1	725
5.3. Dipeptidyl peptidase IV	725
5.3.1. DPP IV inhibition	727
5.3.2. Quiescent proline peptidase (QPP)	728
5.4. Thermolysin	728
5.5. β -turn mimics	728
References	730

Abstract

The preparation of the fluoroolefin amide isosteres is reviewed. The incorporation of the amide isosteres in peptidomimetics and the influence of that isosteric substitution on biological activity on inhibition of peptidyl prolyl isomerases cyclophilin (CyP) and Pin1, dipeptidyl peptidase IV/CD26 (DPP IV) and thermolysin is described. In addition, select fluoroolefination procedures which may have utility in the construction of fluoroolefin amide isosteres are illustrated.

1. INTRODUCTION

1.1. Peptide isosteres

1.1.1. Peptidomimetics

The potential utility of peptides as therapeutic agents with clinical applications is limited as a consequence of intrinsic peptide properties such as metabolic instability or poor transmembrane mobility. Hence, the design and synthesis of metabolically stable peptide analogs that can either mimic or block the bioactivity of natural peptides or enzymes is an important area of medicinal chemistry research. Numerous structural modifications to peptides have been examined in pursuit of molecules with more desirable properties [1–3]. These modified structures, peptidomimetics, are nonpeptide molecules that imitate the desired properties of the natural substances.

1.1.2. Amide bond isosteres

The isosteric replacement of a peptide bond is a potentially important and general approach to the design of peptidomimetics [4]. The peptide bond is rigid, polar, and prefers to be planar. The hydrogen of the amino group and oxygen of the amide carbonyl are nearly antiperiplanar. The backbone conformations of peptides are defined by the torsion angles of the $C_\alpha-N$ bond (ϕ) and $C_\alpha-C$ bond (ψ) (Fig. 1). Though ϕ and ψ angles describe potentially freely rotating single bonds, rotation of those bonds is often restricted by steric interactions of substituents at the C_α and N atoms. A basic underlying principle in design of peptide isosteres is that any modification of the peptide backbone may alter the physical and chemical properties of the molecule and reduce the peptidic character [5] and that in turn has an impact on biological interactions. Such interactions include changes in the metabolic stability, receptor selectivity, and pharmacological and pharmacokinetic properties such as oral bioavailability. Therefore, important considerations in selection of an amide bond replacement are the potential of the surrogate to mimic both the steric and electronic properties of the amide bond [3].

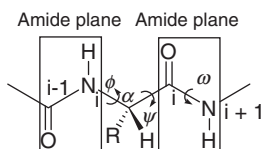


Fig. 1. Definitions for amide bond isosteres.

1.1.3. Nomenclature and terminology

Spatola introduced the term “pseudopeptide” to refer to any peptide analog involving a peptide backbone modification [6]. According to Spatola’s terminology, an amide bond surrogate can be designated by the symbol “ ψ []” with the functionality that replaces the peptide bond, including geometrical (*E* or *Z*) or stereochemical (*R* or *S*) descriptors, specified within the brackets. For example, (*E*) alkene isostere of the dipeptide [7] prolylglycine Pro-Gly (**1**), is represented as Pro ψ [(*E*)-CH=CH]Gly (**2**) (Fig. 2). This nomenclature is general and accommodates any amide bond replacement.

2. FLUOROOLEFIN DIPEPTIDE ISOSTERES

2.1. Alkenes as amide bond substitutes

A superior amide bond replacement should achieve the closest topographical similarity to the amide unit, particularly the *trans* geometry of the amide bond [8] (see Fig. 3). In this regard, the carbon–carbon double bond ψ [(*E*)CH=CH] isosteres (**3a**) (Fig. 3) replicates the amide bond in terms of bond length, bond angle, and rigidity. The C_{*x*}–C_{*x*}+1 (Fig. 1) distance in the isostere is nearly equal to those found in dipeptides (ca., 3.8 Å) with subtle variations in their spatial orientations [9,10]. Peptide analogs bearing the *E*-alkene isostere retain much of biological activity of parent peptide and do not significantly alter the overall conformation of a peptide molecule. The utility of *E*-alkene dipeptide isosteres (EADIs) as potential mimics of amide bond in bioactive peptides has been investigated by many research groups [11–15]. But of particular interest is the

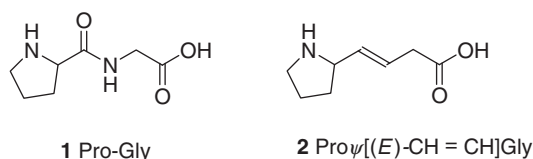


Fig. 2. Comparison of prolyl amide and the corresponding olefin isostere.

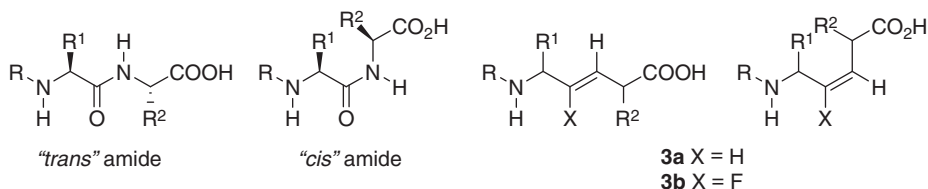


Fig. 3. *Cis* and *trans* amides and the corresponding olefin isosteres.

incorporation of the alkene isostere in fixing prolyl amide bond geometry since the amino acyl-proline *cis-trans* interconversion is one of the limiting steps in protein folding [16]. Both $\psi[(E)\text{-CH=CH}]$ [7,17,18] and $\psi[(Z)\text{-CH=CH}]$ [19,20] acyl prolyl amide isosteres have been described. These prolyl amide isosteres have found utility in the study of peptidyl prolyl isomerase action [21–23], cell cycle regulatory enzymes, Pin1, Chk1, and histone deacetylases [24], and κ -selective opioid analgesics [25]. Alkene peptide isosteres have also found utility in RGD peptidomimetics [26,27] and bombesin antagonists [28]. Additionally, introduction of the alkene isostere is effective in promoting enzymatic cyclization reactions [29].

Various EADIs have been synthesized using different synthetic routes [30–34]. One of the widely used methods of preparation of *E*-alkene peptide bond isosteres involving ring opening of vinyl aziridines by cuprates has recently been reviewed [35,36].

Alkene dipeptide isosteres do however have limitations, for example, the polarity of $\psi[\text{CH=CH}]$ is very low. The high electronegativity of the carbonyl oxygen is obviously not reproduced well by —CH=CH— and therefore the electronic consequences of this replacement do not mimic the carbonyl group well. Certain intrinsic properties of amide bonds such as dipole interactions and hydrogen bonding which is lacking in alkene isosteres can be compensated using fluorinated derivatives like fluoroalkene and vinyl fluorides.

2.2. Fluoroolefins as one of the best amide bond replacements

In 1984, the fluoroolefin $\psi[\text{CF=CH}]$ isostere (**3b**) (Fig. 3) was first proposed as a superior isoelectronic and isosteric replacement for peptide amide bond on the basis of its planar geometry and polarization [37] (see Fig. 4). Not only does this amide isostere have similar bond lengths and bond angles to an amide bond, but also $\psi[\text{CF=CH}]$ is able to fix the conformation at the peptide linkages depending on whether the (*E*) or (*Z*) double-bond isomer is employed. The steric demand of fluorine in biological interactions has been discussed at length [38,39]. However, the importance of the influence of fluorination on electrostatic interactions has also been recognized [40] and studied computationally [5,41]. The high electronegativity of fluorine introduces a dipole moment in the olefin unit in a direction analogous to the dipole moment created by the carbonyl oxygen of the amide bond efficiently mimicking the electronic features of the amide bond (Fig. 8).

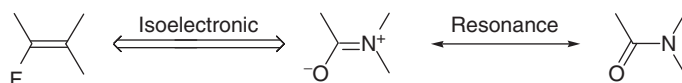


Fig. 4. Fluoroolefins as isoelectronic amide isosteres.

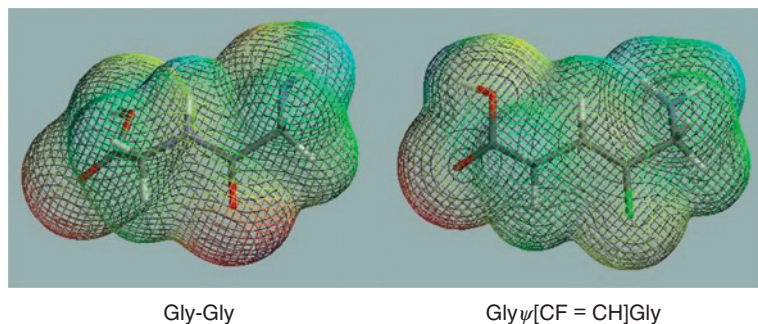


Fig. 5. Electrostatic potential surfaces computed with B3LYP/6-31G** using Titan 1.05. (See Colour Plate Section at the end of this book.)

Theoretical studies [42,43], including estimation of the dipole moment, have strongly supported the original hypothesis behind introduction of the fluoroolefin amide surrogates.

Electrostatic potential surfaces of Gly-Gly and the fluoroolefin isostere created with B3LYP/6-31G** by using Titan 1.0.5 (Fig. 5) illustrates that reduced polarization of the fluoroolefin relative to the amide bond. The original postulates described above were confirmed in independent findings from two groups [14,44] (Fig. 5).

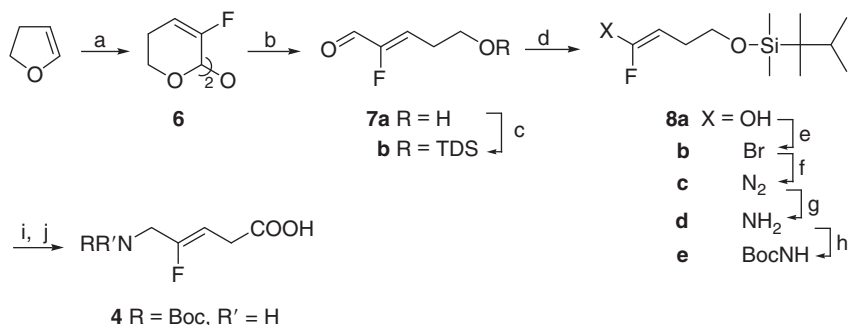
2.3. Synthesis of fluoroolefin peptide isosteres

The synthesis and utility of fluoroolefin peptide isosteres has previously been reviewed [45]. The fluoroolefin isostere preparations summarized below are organized by the synthetic method employed to introduce the fluoroolefin rather than by the dipeptide isostere formed.

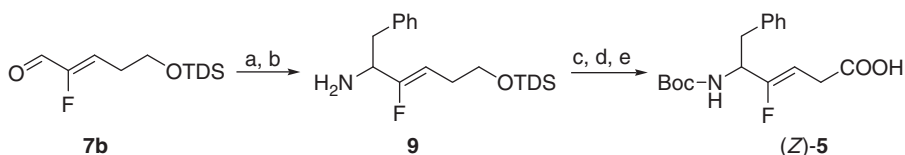
2.3.1. Carbine insertion. Synthesis of Gly-ψ[(Z)-CF=CH]Gly (**4**) and Phe-ψ[(Z)-CF=CH]Gly (**5**)

The preparations of Gly-ψ[CF=CH]Gly (**4**) and Phe-ψ[CF=CH]Gly (**5**) were described by Allmendinger and his coworkers [46,47]. The Gly-Gly fluoroolefin dipeptide isostere (**4**) was synthesized from cyclic acetal (**6**), obtained by the procedure of Dehmlow [48] involving a carbene insertion and reexpansion reaction. Further elaboration as detailed in Scheme 1 ultimately afforded the *N*-protected amino acids (**4**).

The Phe-Gly isostere (Z)-**5** was prepared starting with the aldehyde (**7b**) (Scheme 2). The *N*-Boc protected dipeptide isostere (Z)-**5** was obtained as a racemate.



Scheme 1. Reagents and conditions: (a) CHCl_2F , CH_2Cl_2 , 50% NaOH, $\text{PhCH}_2\text{NEt}_3\text{Cl}$, 41%; (b) aq. HCl, dioxane, reflux, 34%; (c) TDS-Cl, imidazole, DMF, rt, 65%; (d) diisobutylaluminum hydride (DIBAH), toluene, -70°C , 80%; (e) CBr_4 , Ph_3P , CH_2Cl_2 , 0°C , 50%; (f) NaN_3 , DMF, rt, 64%; (g) LiAlH_4 , ether, rt, 80%; (h) $(\text{Boc})_2\text{O}$, CH_2Cl_2 , 85%; (i) R, R' = Phth : 1% HCl in EtOH, R = Boc , R' = H : Bu_4NF ; (j) Jones oxidation, 68%.



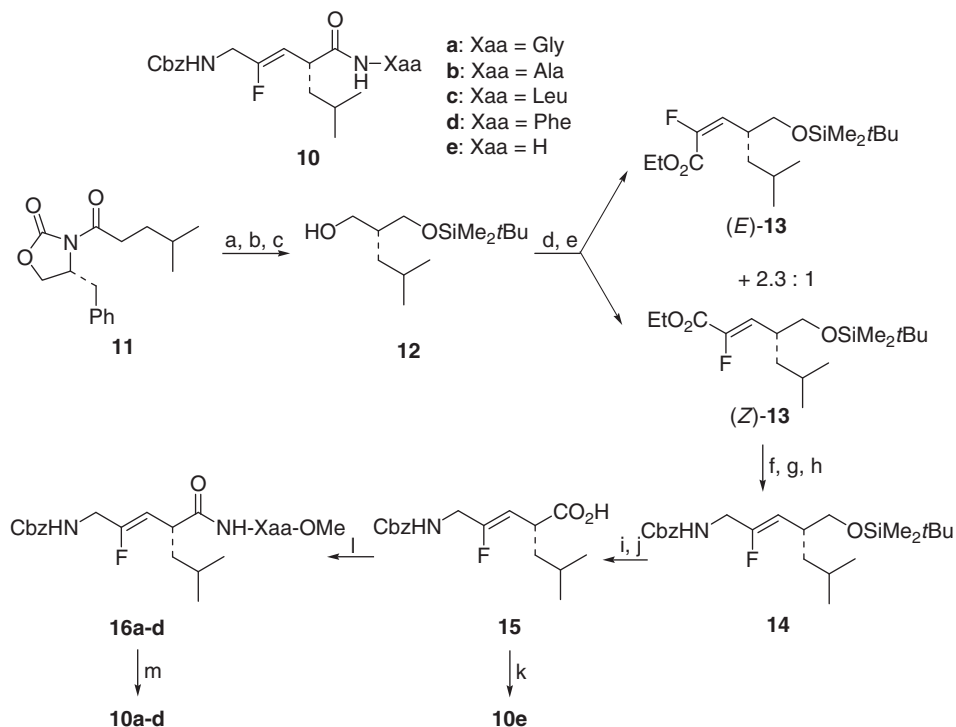
Scheme 2. Reagents and conditions: (a) $\text{LiN}(\text{SiMe}_3)_2$, THF, hexane, -25°C ; (b) PhCH_2MgCl , ether, -70°C , 48%; (c) $(\text{Boc})_2\text{O}$, CH_2Cl_2 , rt, 100%; (d) Bu_4NF , THF, rt, 96%; (e) Jones oxidation, 68%.

2.3.2. Claisen condensation–dehydration. Synthesis of tripeptide analogs *Cbz*-Gly-ψ[(*Z*)-CF=CH]LeuXaa (**10**)

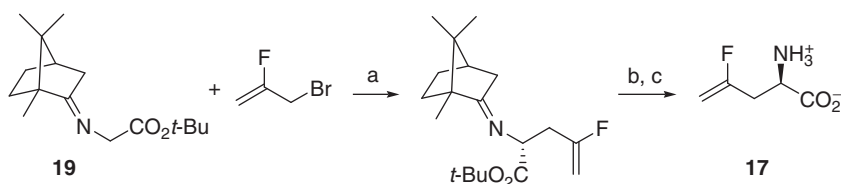
Bartlett *et al.* [14] described the synthesis of a series of fluoroolefin tripeptide isosteres *Cbz*-Gly-ψ[(*Z*)-CF=CH]LeuXaa (Xaa = Gly, Ala, Leu, Phe, and NH_2) (**10**) (Scheme 3) as the ground-state analog inhibitors of thermolysin. Treatment of acid (**15**) with ammonia gave **10e**. The inhibitors **10a–d** are formed by conventional amide acid coupling reactions of suitably protected amino acids followed by saponification with lithium hydroxide.

2.3.3. Alkylation reactions. Synthesis of asparagine analogs (**17**) and (**18**)

Diastereoselective alkylation of (*R*)-(+)-camphor-based glycyimine (**19**) with 3-bromo-2-fluoropropene gave (*R*)-(+)-2-amino-4-fluoropent-4-enoic acid with 38% overall yield and 90% ee after hydrolytic deprotection, or in the case of the alanylimine, (*R*)-(+)-2-amino-4-fluoro-2-methyl-pent-4-enoic acid (19% overall yield, 59% ee) [49]. Deprotection under drastic conditions was accompanied by hydrolysis of the fluorovinyl moiety to give (*R*)-(–)-2-amino-4-oxo-pentanoic acid hydrochloride with 28% overall yield and >95% ee (Scheme 4).

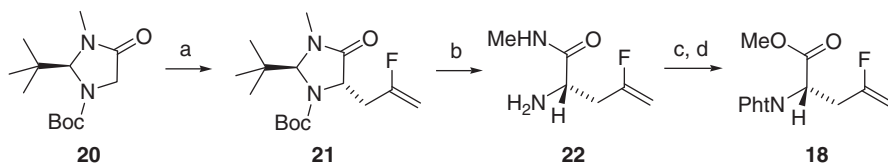


Scheme 3. Reagents and conditions: (a) TiCl_4 , trioxane, $i\text{Pr}_2\text{NEt}$, 85%; (b) imidazole, SSiCl , DMF 99%; (c) LiBH_4 , ether, 76%; (d) PCC, CH_2Cl_2 ; (e) NaH, $(\text{CO}_2\text{Et})_2$, $\text{FCH}_2\text{CO}_2\text{Et}$, 53%; (f) NH_3 , MeOH, 89%; (g) LiAlH_4 , ether; (h) CbzCl , Et_3N , 67%; (i) TBAF, 99%; (j) Jones, 91%; (k) NH_3 , EDC, HOBT, 70%; (l) Xaa-OMe, EDC, HOBT, $i\text{Pr}_2\text{NEt}$, 87–90%; (m) LiOH , quant.

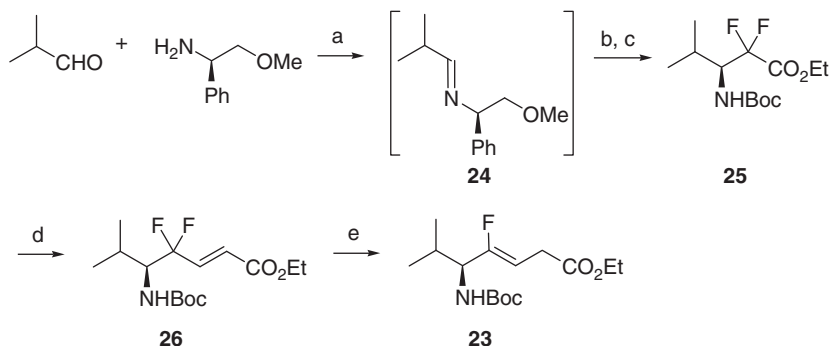


Scheme 4. Reagents and conditions: (a) LDA, DMPU, THF -108°C ; (b) trifluoroacetic acid; (c) propylene oxide.

Asymmetric alkylation of (*S*)-*Boc*-2-*tert*-butyl-3-methylimidazolidin-4-one (**20**) with 2-fluoroallyl tosylate, followed by first mild acidic deprotection of the products **21**, and then basic hydrolysis of the *N'*-methylamides (**22**) gave (*S*)-2-amino-4-fluoropent-4-enoic acid [50]. Basic hydrolysis of **22** was accompanied by partial racemization, a problem which was subsequently overcome by a nitrosative deamidation procedure to form **18** (Scheme 5).



Scheme 5. Reagents and conditions: (a) LDA, DMPU, THF, $\text{CH}_2=\text{CFCH}_2\text{X}$ -50°C ; (b) 1N HCl/MeOH/ H_2O reflux; (c) phtA, $\text{C}_2\text{Cl}_2\text{O}_2$, CHCl_3 ; (d) NaNO_2 , Ac_2O $0-4^\circ\text{C}$ then dioxane reflux.



Scheme 6. Reagents and conditions: (a) mole sieves 3 \AA ; (b) $\text{BrCF}_2\text{CO}_2\text{Et}$, Et_2Zn , $\text{RhCl}(\text{PPh}_3)_3$; (c) $\text{Pd}(\text{OH})_2$, H_2 , then Boc_2O ; (d) DiBALiH then $(\text{EtO})_2\text{P}(\text{O})\text{CH}_2\text{CO}_2\text{Et}$, LiCl , $i\text{-Pr}_2\text{NEt}$; (e) SmI_2 , $t\text{-BuOH}$.

2.3.4. Imine addition reactions in the synthesis of Val- ψ [(Z)CF=CH]Gly (**23**)

A Rh-catalyzed Reformatsky reaction of chiral imine (**24**) led to the stereoselective preparation of the α,α -difluoro- β -amino acid (**25**). **25** was converted to difluoroalkene (**26**), and subsequently L-Val- ψ [(Z)CF=CH]Gly derivative (**23**) in greater than 82% for both steps. The samarium diiodide-mediated reductive transformation of the γ,γ -difluoro- α,β -enoates proceeded via successive two-electron transfers to form a dienolate species which upon kinetically controlled trapping with *tert*-BuOH formed **23** (Scheme 6).

2.3.5. Fluorotris(trimethylsilyl)methane addition reactions. Synthesis of fluoroolefin depsipeptide precursor (**27**)

Depsipeptide analogs (Fig. 6) have been prepared by a variety of methods some of which will be summarized below.

Fluorotris(trimethylsilyl)methane reacted with 2 M equiv. of an aromatic aldehyde in the presence of potassium fluoride/18-crown-6 to give 1,3-disubstituted 2-fluoro-2-propen-1-ols (**27**) in 65–78% yields [51] (Scheme 7).

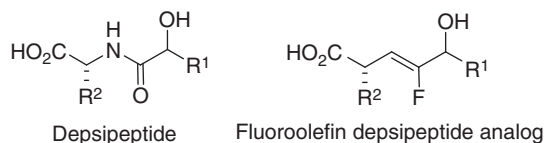
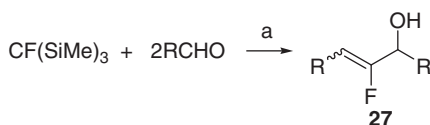
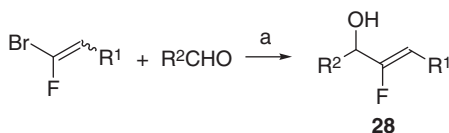


Fig. 6. Comparison of depsipeptide and fluoroolefin depsipeptide isostere.



Scheme 7. Reagents and conditions: (a) KF, 18-crown-6.



Scheme 8. Reagents and conditions: (a) NiCl_2 (30 mol%), CrCl_2 (3 equiv.), DMF.

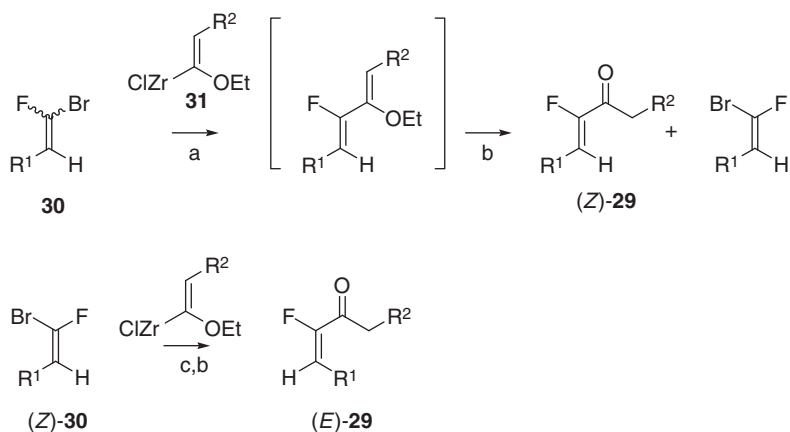
2.3.6. Nozaki-Hiyama-Kishi-type reactions to construct a fluoroolefin depsipeptide precursor (**28**)

Two research groups have reported nickel–chromium promoted addition of bromofluoro alkenes to aldehydes where the product is the desired depsipeptide analog. CrCl_2 - and NiCl_2 -mediated coupling reactions of *E/Z* mixture (with *Z* in slight excess) of 1-bromo-1-fluoroalkenes with aldehydes proceeded in a high stereoselectivity to give the differentially substituted corresponding (*Z*)-2-fluoroallylic alcohol (**28**) [52] (Scheme 8).

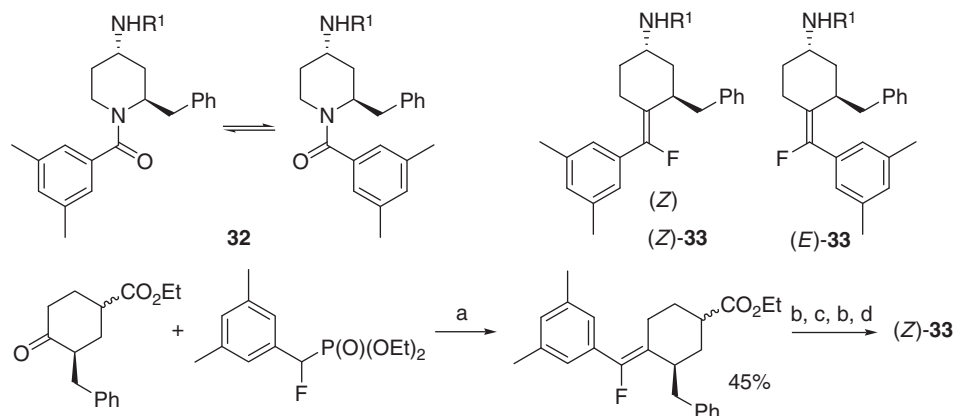
The principal difference between the two groups lay in the relative ratio of chromous ion to nickel employed [53].

2.3.7. Negishi-type reactions to construct a fluoroolefin depsipeptide precursor (**29**)

A kinetically controlled Negishi palladium-catalyzed coupling reaction was used in a highly stereospecific synthesis of (*E*)- or (*Z*)- α -fluoro- α,β -unsaturated ketone (**29**), an intermediate to the above described depsipeptides [54]. Reaction of *E/Z* gem-bromofluoroolefin (**30**) and alkoxyvinylzinc species (**31**) yielded (*Z*)-**29** in 70–99% yields. When the unreacted (*Z*) bromo, fluoroolefin was allowed to react in tetrahydrofuran (THF) under reflux, (*E*)-**29** was formed in up to 98% yield (Scheme 9).



Scheme 9. Reagents and conditions: (a) 0.85 equiv. $\text{Pd}(\text{OAc})_2$, 2.5% PPh_3 , 5% THF, 10 °C; (b) 1N HCl; (c) 2 equiv. $\text{Pd}(\text{OAc})_2$, 5% PPh_3 , 10% THF, reflux.



Scheme 10. Reagents and conditions: (a) KHMDS , THF; (b) LiOH , THF/ H_2O ; (c) ClCO_2Bu , Et_3N , NaN_3 20–65 °C; (d) quinolone-4-carboxylic acid, propane phosphonic acid anhydride, Et_3N .

2.3.8. Horner-Emmons. Replacement of a nonpeptidomimetic amide (32) with the fluoroolefin isostere (33)

As a prelude to the use of olefination reactions to introduce the fluoroolefin amide isostere, the synthesis of fluoroolefin analogs of CGP 49823 is described where a nonpeptidic amide bond was replaced with a fluoroolefin [55]. Comparison of the binding affinities of these analogs for the NK1 receptor enabled determination of the active conformation of the amide containing compound CGP 49823. It was otherwise not easy to establish that the *syn* orientation of the aromatic ring of the benzamide towards the 2-benzyl substituent was the active conformation (Scheme 10).

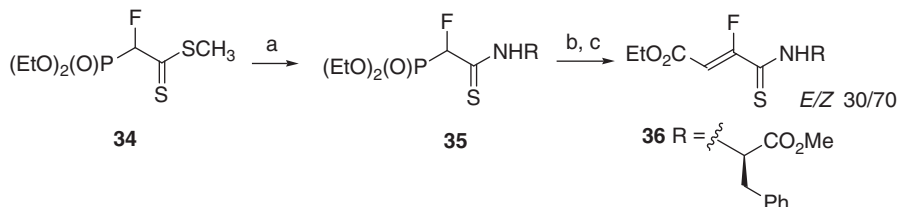
2.3.9. Horner-Emmons. Fluorophosphono dithioacetate (**34**) in the preparation of fluoroolefin peptide isostere precursors

Methyl fluoro(diethoxyphosphono)dithioacetate (**34**) has been prepared from difluorinated precursors [56]. Fluorophosphonothioacetamides (**35**) derived from this dithioester, have been successfully transformed into highly functionalized fluoroalkenes (**36**). Judicious selection of the aldehyde coupling partner can lead expeditiously to the preparation of fluoroolefin dipeptide isosteres following elaboration of the carboethoxy group and desulfurization (Scheme 11).

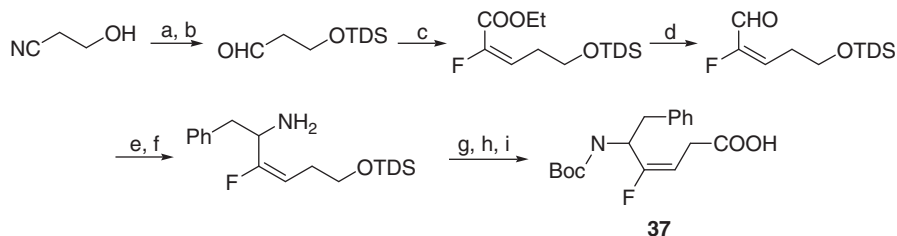
2.3.10. Horner-Emmons. Synthesis of *Phe* ψ [(*E*)-CF=CH]Gly (**37**)

Phe ψ [(*E*)-CF=CH]Gly was synthesized utilizing an olefination as the key step (Scheme 3) [46,47] (Scheme 12).

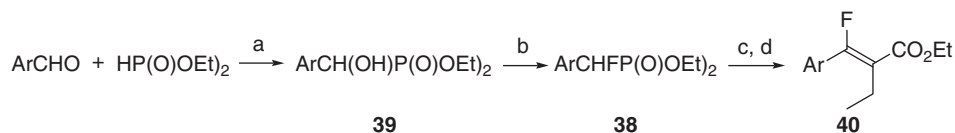
In related studies, it has been shown that α -fluorobenzylphosphonates $\text{ArCHFPO}(\text{OEt})_2$ (**38**) will undergo Wadsworth-Emmons-type olefination reactions with aldehydes and ketones [57]. **39** was prepared from benzaldehydes and $\text{HP}(\text{O})(\text{OEt})_2$, which was fluorinated using diethylaminosulfur trifluoride; for example, diethyl [(3,5-dimethylphenyl)(fluoro)methyl]phosphonate (**38**) was formed in 91%. An 82% yield of Me 2-[(fluoro)(4-fluorophenyl)methylene]butanoate (1:1 *E:Z*) (**40**) was obtained from **38** and methyl 2-oxobutanoate (Scheme 13).



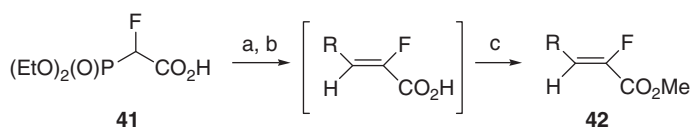
Scheme 11. Reagents and conditions: (a) RNH_2 and Et_3N ; (b) BuLi , THF, -78°C ; (c) EtO_2CCHO .



Scheme 12. Reagents and conditions: (a) TDS-Cl, DBU, CH_2Cl_2 , 80%; (b) diisobutylaluminum hydride (DiBAIH), toluene, -70 to -20°C , 65%; (c) $(\text{EtO})_2\text{PO-CHF-COOEt}$, LDA, THF, -70°C , 76%; (d) DiBAIH , toluene, -70°C , 72%; (e) $\text{LiN}(\text{SiMe}_3)_2$, -25°C ; (f) PhCH_2MgCl , 14%; (g) $(\text{Boc})_2\text{O}$, CH_2Cl_2 , rt, 86%; (h) Bu_4NF , THF, rt, 77%; (i) Pt/C , O_2 , 28%.



Scheme 13. Reagents and conditions: (a) Et_3N ; (b) Et_2NSF_3 , CH_2Cl_2 , 0°C ; (c) LDA, THF, -70°C ; (d) methyl 2-oxobutanoate, -70 to 20°C .



Scheme 14. Reagents and conditions: (a) BuLi; (b) RCHO; (c) TMSCHN₂.

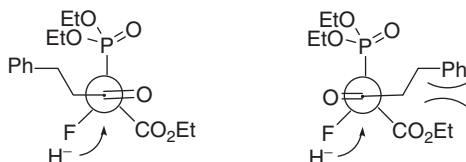
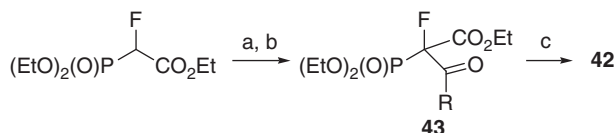


Fig. 7. *Re* and *Si* face attack of hydride ion.



Scheme 15. Reagents and conditions: (a) BuLi, THF, 0 °C; (b) RCOCl; (c) NaBH₄, EtOH, -78 °C

2.3.11. *Horner-Emmons. The use of 2-fluoro-2-diethylphosphonoacetic acid (41) or acylfluorodiethylphosphonoacetate to prepare fluoroolefin dipeptide isostere precursors (42)*

The stereoselective Horner–Wadsworth–Emmons reaction of aldehydes with 2-fluoro-2-diethylphosphonoacetic acid utilizing isopropyl magnesium bromide afforded (*Z*)- α -fluoro- α,β -unsaturated carboxylates (**42**) as the major products in 81–98% yield [58] (Scheme 14).

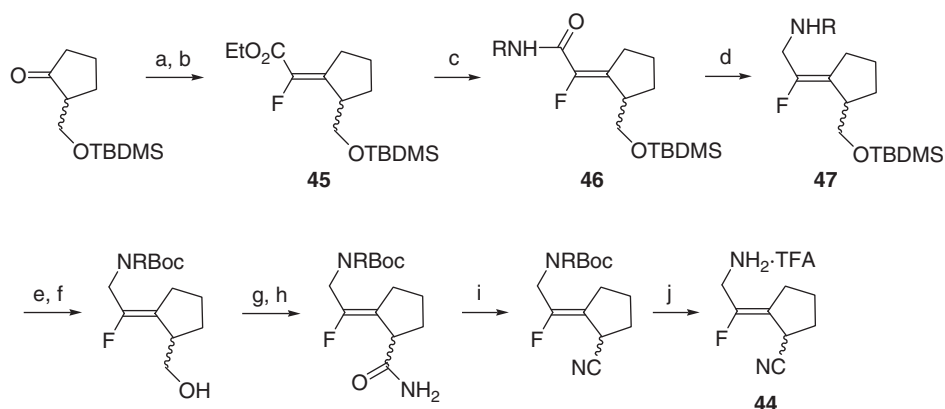
In related experiments, it was reported that reduction with sodium borohydride of acyl intermediate **43** forms the α,β -unsaturated product **42** in excellent stereoselectivity and in 58–84% yield [59]. The diastereoselectivity of the reduction was predicted by the Felkin–Anh model (Fig. 7) (Scheme 15).

2.3.12. Horner-Emmons. The synthesis of DPP IV inhibitors (**44**)

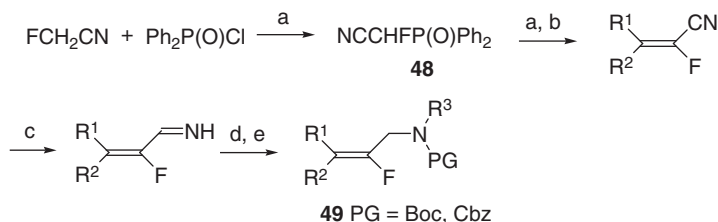
(*E*)- and (*Z*)-fluoroolefin analogs (**44**) ($R = 2$ -phenylethyl, 1-adamantyl, 4-fluorobenzyl) of potent DPP IV inhibitors were synthesized utilizing the Wadsworth–Horner–Emmons reaction. The use of sodium hydride as the base in the Wadsworth–Horner–Emmons transformation was central to achieving useful yields of **45** in this reaction (74%). Following amide (**46**) formation and reduction, the desired α -fluoro- α,β -unsaturated amine functionality **47** was revealed [60,61] (Scheme 16).

2.3.13. Horner-Emmons. The use of (diphenylphosphinoyl) fluoroacetonitrile (**48**) to introduce the amino group

α -Fluoroacrylonitriles were synthesized in moderate to good yields by Horner–Wittig reaction of aldehydes and ketones with (diphenylphosphinoyl)fluoroacetonitrile, prepared *in situ* from fluoroacetonitrile and diphenylphosphinyl chloride [62]. Diisobutylaluminum hydride (DiIBALH)-reduction and transimination resulted in the direct conversion to 2-fluoroallylamines (**49**) (Scheme 17).



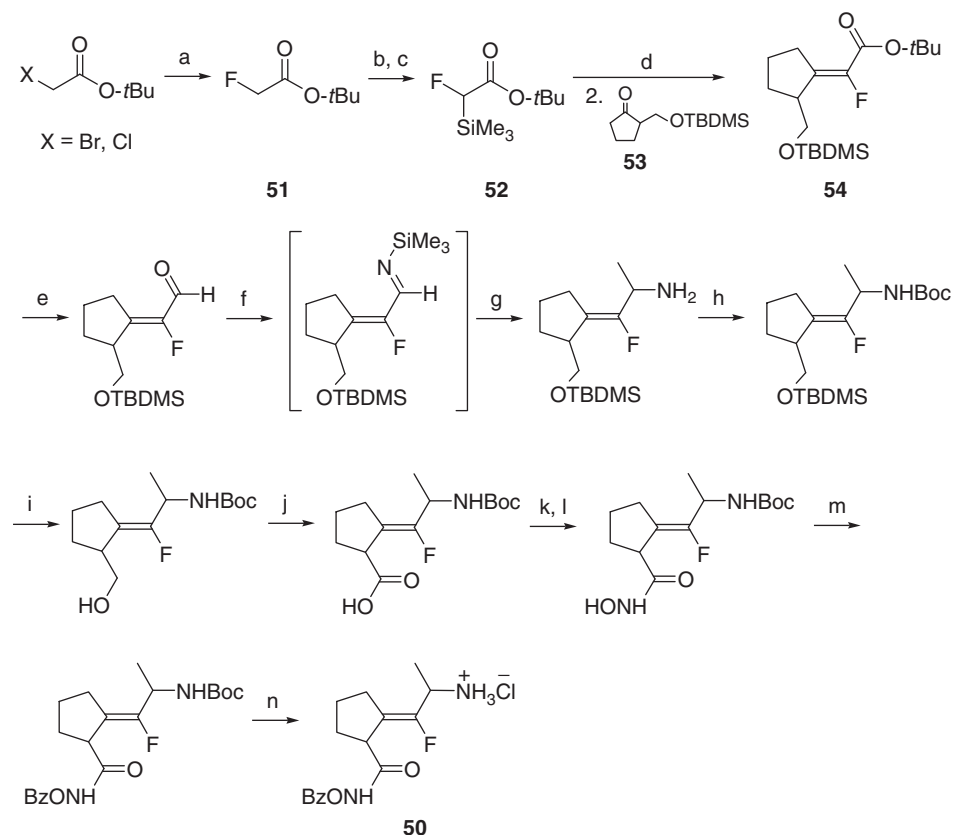
Scheme 16. Reagents and conditions: (a) NaH, ethyl(diethoxyphosphoryl)fluoroacetate; (b) KOH, MeOH; (c) TBTU, diisopropylethylamine (DIPEA), RNH_2 ; (d) $POCl_3$, DIPEA, $LiAlH_4$; (e) $(Boc)_2O$, DIPEA; (f) $AcOH/H_2O/THF$; (g) Jones; (h) i -BuOC(O)Cl, DIPEA then NH_4OH ; (i) $POCl_3$, imidazole, pyridine; (j) TFA, CH_2Cl_2 , 30 min.



Scheme 17. Reagents and conditions: (a) LiHMDS (or LDA), $-78^\circ C$; (b) aldehyde or ketone; (c) DiIBALH, MeOH; (d) R^3NH_2 , $NaBH_4$; (e) Boc_2O or CbzCl.

2.3.14. Peterson fluoroolefination. Synthesis of the Alaψ[(Z)-CFC]-pro isostere (**50**) DPP IV inhibitors using the Peterson fluoroolefination reaction

Alaψ[(Z)-CF=C]-Pro containing *N*, *O*-diacylhydroxamic acid type protease inhibitors have been prepared as shown in Scheme 18 [63,64]. The synthesis is based upon the use of *tert*-butyl- α -fluoro-trimethylsilylacetate in a variation of the Peterson olefination procedure to construct the necessary functionalized fluoroolefin. Treatment of **51** with 4 equiv. of lithium diisopropylamide (LDA) and 6 equiv. of chlorotrimethylsilane at -78°C formed **52** in 71% yield. The key step is the Peterson olefination reaction of the TBDMS-protected 2-(hydroxymethyl)cyclopentanone (**53**) with *tert*-butyl- α -fluoro- α -trimethylsilylacetate (**52**). The fluoroolefin product was obtained as a mixture of (*Z*):(*E*) isomers (**54**). Separation of the double-bond isomers by column chromatography provided (*Z*) isomer (**54**) in 43% yield. Further



Scheme 18. Reagents and conditions: (a) KF, AcNH₂ 90 °C; (b) LDA, TMSCl; (c) aqueous tartaric acid; (d) LDA; (e) DiBAIH, ether, -70°C ; (f) LHMDs, -30°C ; (g) MeLi, -78°C ; (h) Boc-ON, TEA, dioxane; (i) AcOH/H₂O/THF; (j) Cr₃O, H₂SO₄; (k) Im₂CO; (l) NH₂OH·HCl; (m) BzCl; (n) 1 M HCl/AcOH.

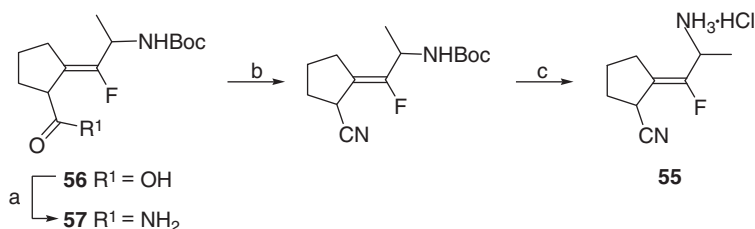
transformations provide the target compound **50**. **50** showed superior inhibitory properties for DPP IV, yet was stable in aqueous solution at neutral pH for a period of 25 h (see Section 5.3.1).

2.3.15. Peterson fluoroolefination. Synthesis of 2-(2-amino-1-fluoro-propylidene)-cyclopentanecarbonitrile (**55**) as DPP IV inhibitors

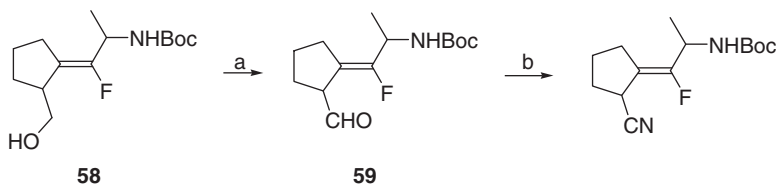
2-(2-Amino-1-fluoro-propylidene)-cyclopentanecarbonitriles (**55**), ψ [CF=C] isostere of 2-cyanopyrrolidides, were prepared from **56**, an intermediate in the synthesis of **50** (Scheme 19) [65]. A better route was conversion of the primary alcohol (**58**), another intermediate in the synthesis of **50**, to the aldehyde (**59**) through Swern oxidation followed by treatment with hydroxylamine-O-sulfonic acid (Scheme 10). Both pairs of diastereomer *u*-**55** and *l*-**55** exhibited inhibitory activity against DPP IV. *u*-**55** and *l*-**55** also were very stable in buffer (pH 7.6) as assessed by UV-vis spectroscopy over the range of 190–1,100 nm at 30 and 50 °C (Scheme 20).

2.3.16. Stereoselective construction of (*Z*)-fluoroalkene depsipeptide (**60**) through a Cu(I)-mediated allylic substitution reaction

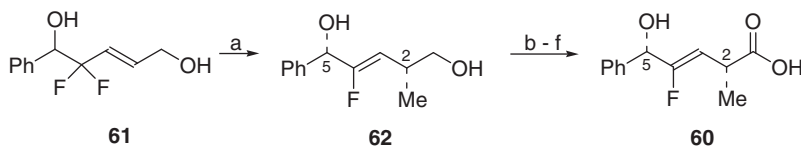
Strategies centered on reductive introduction of the fluoroolefin via a geminal difluoro allylic array have been reviewed [66]. In an introductory example to this synthetic approach, Okada *et al.* [67] developed a completely stereoselective synthesis of (*Z*)-2,5-*syn* 2-alkyl-4-fluoro-5-hydroxy-3-alkenoic acids through the Cu(I)-mediated allylic substitution reaction of trialkylaluminum with the (*E*)-4,4-difluoro-5-hydroxyallylic alcohol derivative (**61**) (Scheme 21). Reaction



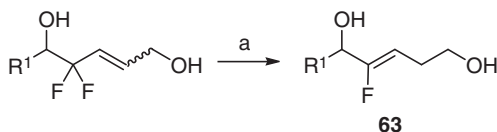
Scheme 19. Reagents and conditions: (a) *N*-hydroxysuccinimide, NH_4OH , DCC; (b) POCl_3 , pyr; (c) 10% $\text{HCl-H}_2\text{O}$.



Scheme 20. Reagents and conditions: (a) Swern; (b) $\text{NH}_2\text{OSO}_2\text{H}$, $\text{CH}_2\text{Cl}_2\text{-H}_2\text{O}$.



Scheme 21. Reagents and conditions: (a) Me_3Al , $\text{CuI} \cdot 2 \text{ LiCl}$; (b) TBDMSCl , imidazole, DMF; (c) Ac_2O , Et_3N , THF; (d) TBAF , THF; (e) CrO_3 , H_2SO_4 , acetone; (f) KOH , H_2O - MeOH , then 10% HCl .



Scheme 22. Reagents and conditions: (a) LiAlH_4 , Me_3Al .

of (*E*)-difluoroallylic alcohol (**61**) with a combination of trialkylaluminum (Me_3Al , 5–10 equiv.) and $\text{CuI} \cdot 2 \text{ LiCl}$ (2.5 equiv.) in THF at 0°C for 15–20 h, provided the desired 4-fluoro-5-hydroxyhomoallylic alcohol (**62**) in excellent 98% yield with complete *Z*-selectivity and 2,5-syn diastereoselectivity. After protection of the secondary hydroxyl group as the acetate, oxidation of the primary hydroxyl group of **62** to carboxylic acid by Jones' oxidation gave the desired acid (**60**) in 53% overall yield (Scheme 21).

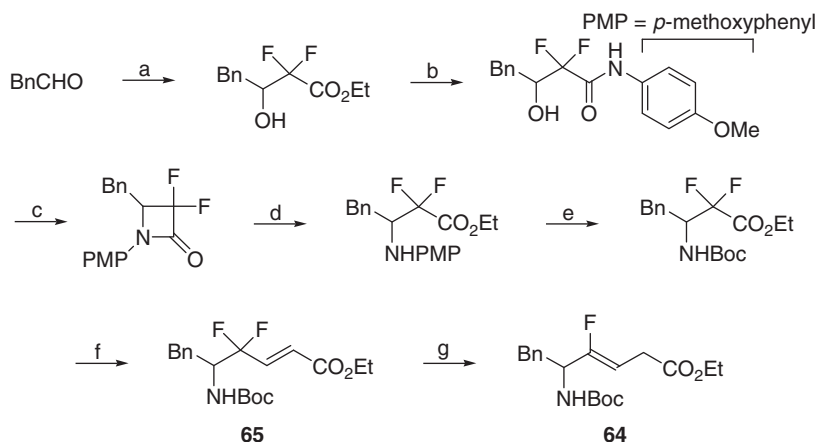
Taguchi [68] has also reported a reductive transformation which allows preparation of the unsubstituted **63** shown below. The free hydroxyl group is essential for the reaction to proceed (Scheme 22).

2.3.17. Synthesis of *Boc-Phe*/[*(Z)*-CF=CH]Gly-OEt (**64**) utilizing organocopper-mediated reduction of γ,γ -difluoro- α,β -enoates

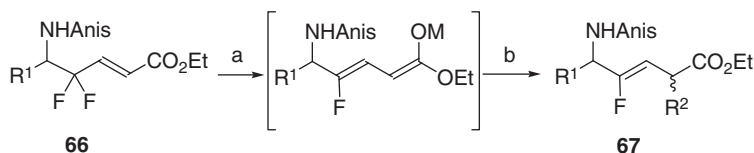
Otaka *et al.* reported the synthesis of (*Z*)-fluoroalkene dipeptide isosteres utilizing an organocopper-mediated reduction (Scheme 23) [69,70]. Reduction of **65** with $\text{Me}_2\text{Cu}(\text{CN})\text{Li}_2 \cdot 2 \text{ LiBr} \cdot 2 \text{ LiCl}$ (4 equiv.) in THF- Et_2O at -78°C for 15 min, proceeded unequivocally to yield the desired (*Z*)-fluoroalkene dipeptide isostere, *Boc-Phe*/[*(Z)*-CF=CH]Gly-OEt (**64**) in 85% isolated yield.

It has also been found to be possible to effect the reductive fluoroolefination with the amine group protected as an anisidine derivative [71] (**66**) and thereby obviate the aforementioned amine deprotection–reprotection scheme (Scheme 24).

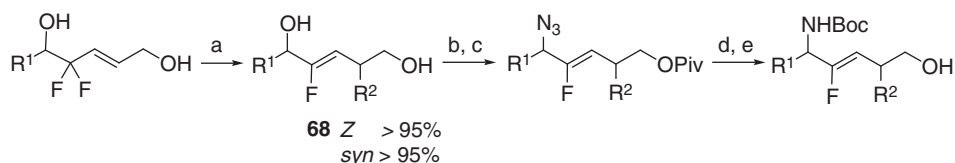
Alternatively, the amino group was introduced subsequent to the reductive formation of the fluoroalkene [72]. The regio- and stereoselective conversion of the C5-hydroxyl group of the fluoroolefin to an amino group could be achieved through one-pot mesylation and azidation reaction (Scheme 25).



Scheme 23. Reagents and conditions: (a) $\text{BrZnCF}_2\text{CO}_2\text{Et}$, THF; (b) NaOH, THF- H_2O , then bis(2-oxo-3-oxazolidinyl)-phosphinic chloride, *p*-anisidine, diisopropylethylamine, CH_2Cl_2 ; (c) Ph_3P , diethylazodicarboxylate (DEAD), THF; (d) NaOH, THF- H_2O , then H_2SO_4 , MeOH; (e) CAN, MeCN- H_2O , then $(\text{Boc})_2\text{O}$, THF; (f) diisobutylaluminium hydride (DiBAIH), CH_2Cl_2 -toluene, then $(\text{EtO})_2\text{P}(\text{O})\text{CH}_2\text{CO}_2\text{Et}$, LiCl, diisopropylethylamine, CH_3CN ; (g) $\text{Me}_2\text{Cu}(\text{CN})\text{Li}_2 \cdot 2\text{LiBr} \cdot 2\text{LiCl}$, THF- Et_2O .



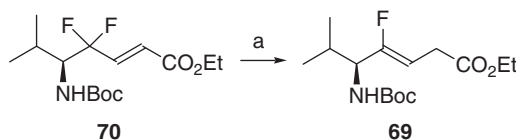
Scheme 24. Reagents and conditions: (a) Me_2CuLi ; (b) R^2X .



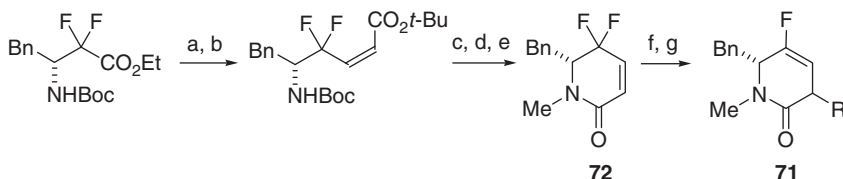
Scheme 25. Reagents and conditions: (a) R^2_3Al , $\text{CuI} \cdot 2\text{LiCl}$, THF, 0°C ; (b) PivCl , py; (c) 4-dimethylaminopyridine (DMAP) (3 equiv.), NaN_3 (20 equiv.), methanesulfonyl chloride (MsCl) (3 equiv.), RT then DMSO 3 h; (d) LiAlH_4 ; (e) $(\text{Boc})_2\text{O}$, Et_3N , CH_2Cl_2 .

2.3.18. Synthesis of functionalized (*Z*)-fluoroalkene-type dipeptide isosteres (**36**) via Sml_2 -mediated reduction of γ,γ -difluoro- α,β -enoates

Recently, the synthesis of functionalized (*Z*)-fluoroalkene-type dipeptide isosteres (**36**) via Sml_2 -mediated reduction of γ,γ -difluoro- α,β -enoates (**37**) (Scheme 7) was reported [73] (Scheme 26).



Scheme 26. Reagents and conditions: (a) Sml_2 , *t*-BuOH THF.



Scheme 27. Reagents and conditions: (a) DIBALH , $\text{CH}_2\text{Cl}_2/\text{toluene}$; (b) $(o\text{-MePhO})_2\text{POCH}_2\text{CO}_2t\text{-Bu}$, NaI , DBU ; (c) 4 M HCl ; (d) 1-ethyl-3-[3-(dimethylamino)propyl]carbodiimide (EDC), HOAt , $(i\text{-Pr})_2\text{Net}$, DMF ; (e) MeI , NaH ; (f) Me_3CuLi_2 , $\text{LiI} \cdot 3 \text{ LiBr}$; (g) electrophile.

2.3.19. Reductive formation of fluoroolefins and subsequent conversion to diketopiperazine mimics (**71**). Nonpeptidic amide bond replacement

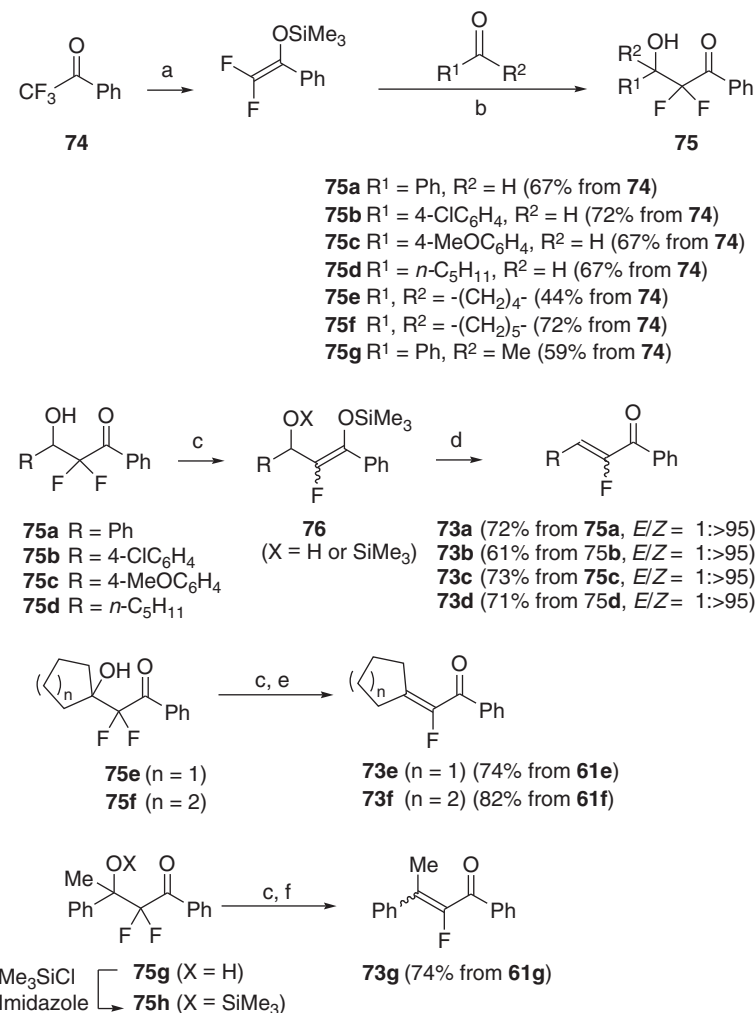
Reduction of difluorolactam (**72**) with higher-order cuprate reagent ($\text{Me}_3\text{CuLi}_2 \cdot \text{LiI} \cdot 3 \text{ LiBr}$), followed by trapping the resulting metal dienolate with an electrophile gave the α -alkylated- β,γ -unsaturated- δ -lactams in good yields [74]. Because of side chain steric repulsion, alkylation with relatively sterically demanding electrophiles such as benzyl bromide gave mostly 3,6-*trans* isomers on kinetic trapping of the metal enolates. On the other hand, methyl iodide-mediated alkylations predominantly provided the 3,6-*cis* isomers despite the presence of a bulky benzyl side chain (Scheme 27).

3. RELATED METHODS FOR THE SYNTHESIS OF α -FLUORO- α,β -UNSATURATED KETONES

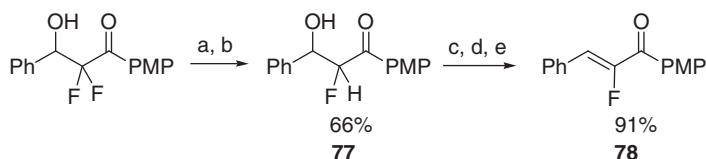
α -Fluoro- α,β -unsaturated carbonyl compounds are promising precursors for fluoroalkene oligopeptide isosteres, and have been prepared by a variety of approaches. Here, some more recent general synthetic methods are briefly outlined.

3.1. Conversion from trifluoromethyl ketones via $\text{Mg}(0)$ -promoted successive double defluorination

Reductive $\text{Mg}(0)$ -promoted double defluorination reactions for the synthesis of α -fluoro- α,β -unsaturated ketones (**73**) (Scheme 11) from readily accessible trifluoromethylketones has been described [75] (Scheme 28).



Scheme 28. Reagents and conditions: (a) Mg, TMSCl, THF; (b) TiCl_4 , CH_2Cl_2 , -78°C aldehydes or 0°C ketones; (c) Mg, TMSCl, THF, 0°C ; (d) 25% HCl; (e) 10% HCl; (f) conc. HCl.



Scheme 29. Reagents and conditions: (a) Mg, Me_3SiCl , THF; (b) TBAF, MeOH; (c) *m*-chloropbenzoic acid (*m*-CPBA), CH_2Cl_2 -hexafluoroisopropanol; (d) MsCl, Et_3N ; (e) DBU, THF.

Uneyama has also modified the olefination step as in the transformation of **77** to **78** so that more nearly neutral conditions can be utilized [75]. This is especially important in those cases with acid-sensitive protection or stereogenic centers (Scheme 29).

3.2. Synthesis of α -fluoro- α,β -unsaturated ketones via palladium-catalyzed cross-coupling reaction of 1-fluorovinyl halides (**79**) with organostannanes (**80**)

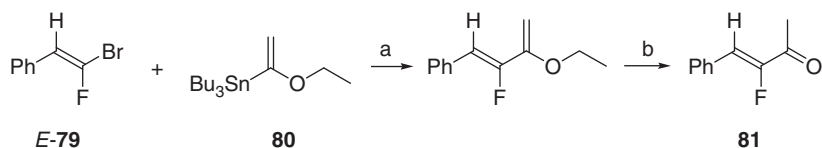
α -Fluoro- α,β -unsaturated ketone may also be prepared via palladium-catalyzed cross-coupling reaction of 1-fluorovinyl halides (**79**) with organostannanes (**80**) to form on aqueous work up olefin (**81**) (Scheme 12) [76] (Scheme 30).

3.3. Synthesis of α -fluoro- α,β -unsaturated ketone via allylic hydroxylation of vinyl fluoride

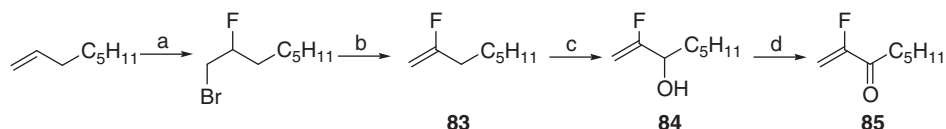
2-Fluoro-oct-1-en-3-one (**82**) has been synthesized by allylic hydroxylation of vinyl fluoride (Scheme 31) [77,78]. Oxidation of vinyl fluoride (**83**) using 0.5 equiv. of SeO_2 and 2 equiv. of *tert*-butyl hydroperoxide with a catalytic amount of acetic acid followed by elimination formed to 2-fluoroalk-1-en-3-ols (**84**) in 32% overall yield for three steps. Subsequent pyridinium dichromate-oxidation of **84** yielded 2-fluoro-oct-1-en-3-one (**83**) in 81% (Scheme 31).

3.4. Synthesis of α -fluoroenone from 1,1,1,2-tetrafluoroethane

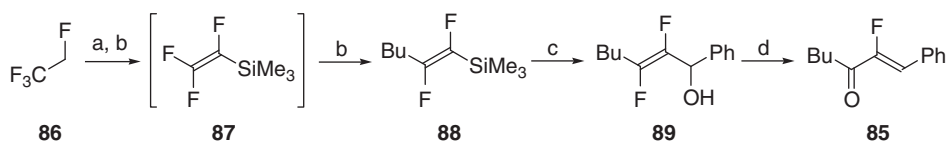
α -Fluoroenone (**85**) has been constructed using 1,1,1,2-tetrafluoroethane (HFC-134a) as a building block (Scheme 32) [79]. Dehydrofluorination/metallation of HFC-134a (**86**) was followed by trapping with chlorotrimethylsilane. Vinylsilane (**87**) underwent further reaction *in situ* with a second equivalent of *n*-butyllithium to afford the vicinal difluoride (**88**) in good yield (82%). Exposure to catalytic TAS-F (20 mol%) in the presence of benzaldehyde, followed by mild



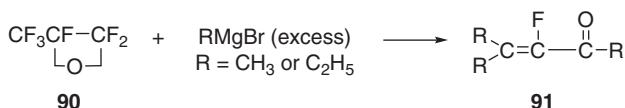
Scheme 30. Reagents and conditions: (a) $\text{Pd}(\text{PPh}_3)_4$, dioxane (95%); (b) aqueous workup (14%).



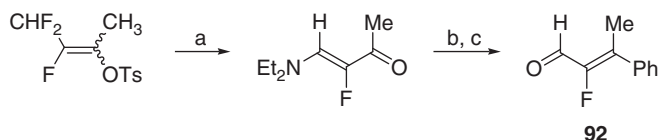
Scheme 31. Reagents and conditions: (a) NBS, $\text{Et}_3\text{N} \cdot 3 \text{HF}$, CH_2Cl_2 ; (b) $\text{KO}^t\text{-Bu}$, pentane (60% over two steps); (c) SeO_2 , *t*-BuOOH, HOAc (cat.), CH_2Cl_2 (54%); (d) PDC, MS 10 Å, CH_2Cl_2 (81%).



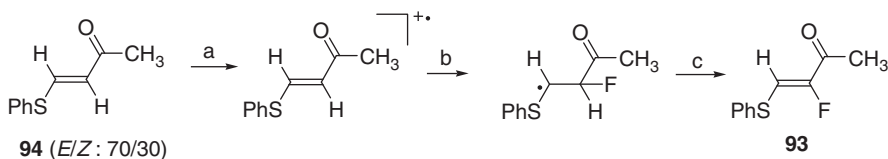
Scheme 32. Reagents and conditions: (a) *n*-BuLi, THF, -78°C ; (b) TMSCl; (c) PhCHO, 20% TAS-F, THF, -30°C to rt; (d) 1 M HCl.



Scheme 33. Grignard addition to a perfluorinated epoxide.



Scheme 34. Reagents and conditions: (a) Et_2NH , Et_3N , 10 mol% tetrabutyl ammonium fluoride (TBAF), DMSO, 70°C ; (b) PhLi, THF, -78°C ; (c) 10% HCl aq., rt.



Scheme 35. Reagents and conditions: (a) $-\text{e}^-$, $\text{Et}_3\text{N} \cdot 3 \text{ HF}$, CH_3CN ; (b) F^- ; (c) Na_2CO_3 , H_2O .

acid work-up led (via the allylic alcohol (**88**)) to the isolation in an acceptable 55% yield of α -fluoroenone (**85**) as a crystalline solid (Scheme 32).

3.5. Miscellaneous reactions

The reaction of hexafluoropropene oxide (HFPO) (**90**) with excess Grignard reagents formed alkylated α,β -unsaturated ketones (**91**) (Scheme 33) [80].

Funabiki prepared α -fluoro- β -phenylacrylaldehyde (**92**), a particularly useful synthetic intermediate, by an addition elimination strategy (Scheme 34) [81].

Electrochemical fluorination of β -phenylsulfenyl- α,β -unsaturated ketones can form α -fluoro- α,β -unsaturated carbonyl compounds (Scheme 35) [82]. α -Fluoro- β -thio- α,β -unsaturated ketone (**93**) was synthesized by the selective nucleophilic

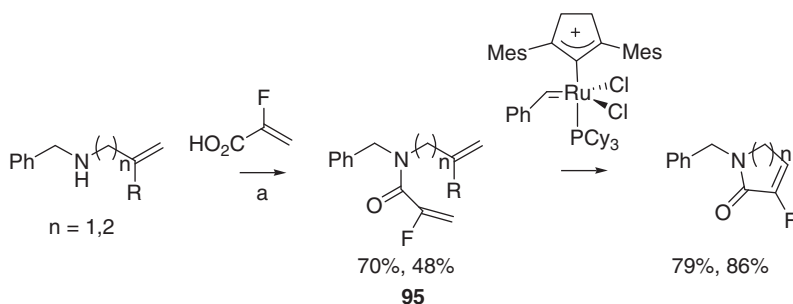
anodic fluorination of the β -phenylthio- α,β -unsaturated ketone (**94**) in $\text{Et}_3\text{N} \cdot 3 \text{ HF} / \text{CH}_3\text{CN}$, followed by treatment with Na_2CO_3 to complete the dehydrofluorination.

4. METATHESIS REACTIONS

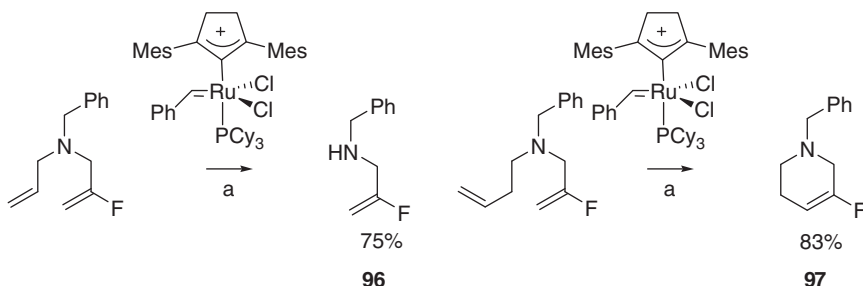
With the ready availability of 2-fluoro-allylic halides and α -fluoroacrylic acid derivatives, incorporation of a pendant fluorovinyl unit is easier than ever. The utility of these products is markedly enhanced by the reactivity of the fluorovinyl unit in olefin metathesis reactions. Some success has been found in cyclization reactions as shown below [83] (Scheme 36).

Interestingly, the reaction is clearly sensitive to substituent; the absence of a carbonyl present in the reactant amide (**95**) above, with slight changes in electronic or conformational effects enough to perturb reaction outcome [84]. In the amine example below, the substituted pyrrolidine (**96**) was not isolated, while a slight increase in chain length facilitated the desired cyclization to **97** (Scheme 37).

With these promising results, application of metathesis reactions for the construction of the substituted fluoroolefins required in peptide isosteres is potentially very useful.



Scheme 36. Reagents and conditions: (a) ethyl 3-(3-dimethyl aminopropyl) carbodiimide (EDC), hydroxybenzotriazole (HOBT).



Scheme 37. Reagents and conditions: (a) TFA, 100°C .

5. BIOLOGICAL APPLICATIONS AND UTILITY OF FLUOROOLEFIN PEPTIDE ISOSTERES

5.1. Background

As described in the beginning of this chapter, the peptide bond is rigid, polar, and prefers a planar structure with hydrogen of the amino group and oxygen of the carbonyl almost *trans*. It is easily understood that this conformational preference and rigidity has profound implications to the tertiary and quaternary structure of proteins and similarly on the binding of smaller peptides to receptors.

5.1.1. Role of *cis*–*trans* geometry in biological systems

An excellent synopsis of the influence of double-bond (and pseudo double bonds, such as the amide bond) geometry on biological activity has been published [8]. The central role of the amide pseudo double bond on the architecture of proteins is illustrated when the *trans* preference of amide bonds is recognized. The enthalpic difference between the two conformers has been shown to lie between 0.5 and 2.5 kcal/mol with a barrier to *cis*–*trans* interconversion of approximately 61–22 kcal/mol [8] (Fig. 8).

And most importantly for a discussion of the replacement of amide bonds by fluoroolefin isosteres, the *cis* and *trans* amide bonds have different hydration shells [43,85]. The role of solvation and desolvation is understood to be crucial not only in amide bond isomerization but also in peptide transport generally.

Tertiary amides, such as those associated with prolyl amide bonds frequently influence turn architectures. The importance of the *cis* Xaa-Pro bond on activity was recognized and proposed to be the source of differentiation in biological activity [86]; therefore, isomerization of the prolyl amide bond is central to regulation of protein folding, immunosuppression, and mitosis. These functions are not surprisingly associated with several disease states and thus substitution of the acyl-proline amide bond with the fluoroolefin isostere has received considerable attention.

5.1.2. Fluorine in biological mimics

The use of fluorine has become well established in the analysis of protein structure and function, for example, in tools such as ^{19}F NMR (nuclear magnetic

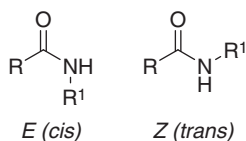


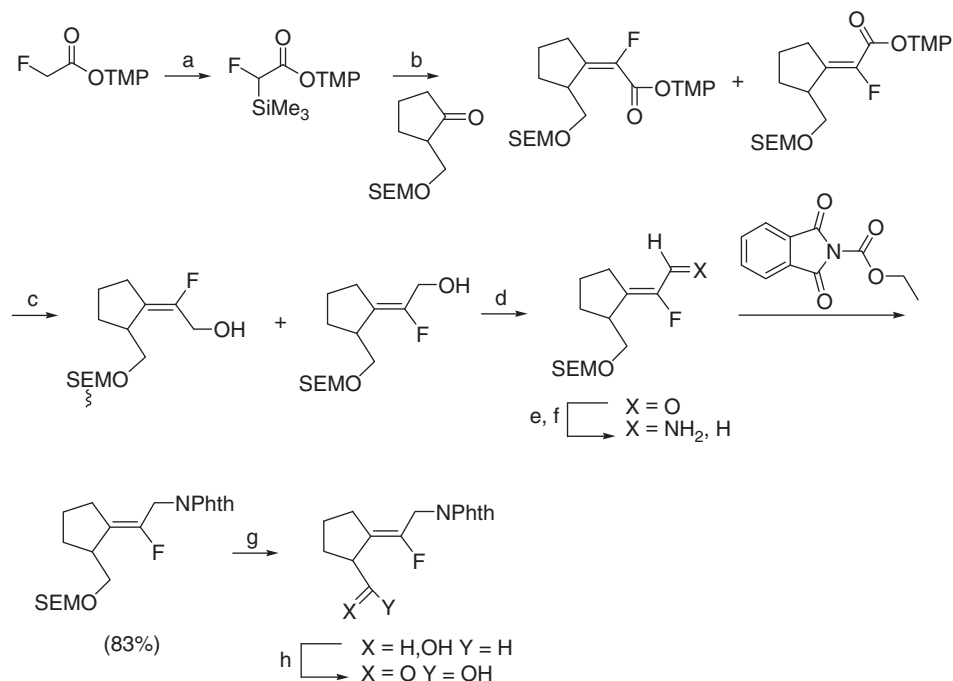
Fig. 8. *Cis* and *trans* amides.

resonance) spectroscopy [39]. The application of the unique electronic properties of this element for the structural and chemical modification of peptides and proteins is well recognized. The influences of fluorination, and selective fluorination in particular, can be complex [38]. The carbon fluorine bond length compares favorably with the carbonyl carbon–oxygen bond, from 1.35 to 1.4 Å and 1.23 to 1.25 Å, respectively. The Taft E_s° parameter for F of 0.46 compares favorably with a value of 0.55 for OH. While the magnitudes of the associated dipoles are quite different, the dipoles are aligned similarly [87]. The influence of fluorination on other important parameters including but not limited to lipophilicity, basicity, or acidity have been summarized [88]. When substitution is affected to mimic existing electronic effects, such as dipoles, the electrostatic surface of fluorinated mimic compares favorably with the parent compound. An important influence of fluorination that was elegantly described recently is the increase in efficiency of binding of fluorinated substrates induced by the hydrophobic nature of fluorine. In this argument, as fluorinated materials are only poorly solvated in an aqueous environment the energetic requirement for desolvation prior to binding is dramatically diminished with the result that the overall efficiency of binding increases [89]. Selective fluorination can also be employed to simply block metabolism, a consequence of the carbon–fluorine bond strength; in such cases, the electronic surfaces can be quite different. The combination of the through-bond electronic interactions, which influence nucleophilicity of neighboring groups, electrostatic interactions, and hydrophobicity can lead to complex effects in a polar aqueous environment thereby confounding our predictions of the influence of fluorination on reactivity. Examples of these phenomena are the often seemingly unpredictable participation of fluorine in hydrogen bonds and the apparent steric demand of fluorine in biological receptors [38].

5.2. Peptidyl prolyl isomerases (PPIases)

In contrast to secondary amide bonds which exist almost exclusively in the *trans* conformation as a consequence of interactions with sequentially adjacent residues, 10–30% of acyl-proline bonds can be found in the *cis* conformation [21]. With *cis*–*trans* isomerization of amide bonds playing a crucial role in protein structure and function, the amino acyl-proline *cis*–*trans* interconversion is one of the limiting steps of protein folding. To facilitate protein folding to form fully functional constructs, acyl-proline bond isomerization is accelerated by a family of proteins called immunophilins or peptidyl-prolyl isomerases (PPIases). The PPIases, include cyclophilin (CyP), Pin1, and FK506 binding protein (FK506BP), are associated with several biological processes [90–92]. CyP and FK506BP are involved in immunosuppression, calcium ion-dependent signaling, and chaperone function. Folding processes facilitated by CyP are also known to be essential for HIV-1 core packaging and therefore viral replication processes [93]. Pin1,

Fig. 9. *Cis* and *trans* isomers of prolyl amide olefin isosteres.



Scheme 38. Reagents and conditions: (a) 4 equiv. LDA, 8 equiv. TMSCl then saturated tartaric acid (92%); (b) LDA (65%, 4:1 *E/Z*); (c) diisobutylaluminum hydride (DiBAIH) (97%); (d) CrO₃, pyridine (78%); (e) LHMDs; (f) DiBAIH; (g) BF₃·Et₂O (89%); (h) CrO₃, H₂SO₄ (59%); (i) HOBT, DCC, *N*-methylmorpholine (77%); (j) CH₃NHNH₂; (k) Boc-(L)-Ala, HOBT, DCC, *N*-methylmorpholine; (l) TFA (overall yield last four steps 22%).

5.2.2. Pin1

Pin1, a human homolog of *Escherichia coli* parvulin, interacts with cell cycle regulatory proteins and is required for mitosis [21]. In addition, Pin1 has been implicated as a potential therapeutic target in cancer pathogenesis and Alzheimer's disease [96]. Pin1 is distinguished from CyP in that it specifically interacts with phosphorylated serine/threonine-proline peptide bonds. To date Ser/[(*E*)CH=C]-Pro and Ser/[(*Z*)CH=C]-Pro analogs have been prepared [22,24] and it has been found that the (*Z*) isostere is significantly more potent inhibitor. However, the corresponding fluoroolefin isosteres have yet to be prepared and represent a significant opportunity for an additional application of this isosteric replacement.

5.3. Dipeptidyl peptidase IV

DPP IV/CD26 (DPP IV), a cell-surface protease, selectively removes an *N*-terminal dipeptide from peptides with proline or alanine in the second position. DPP IV

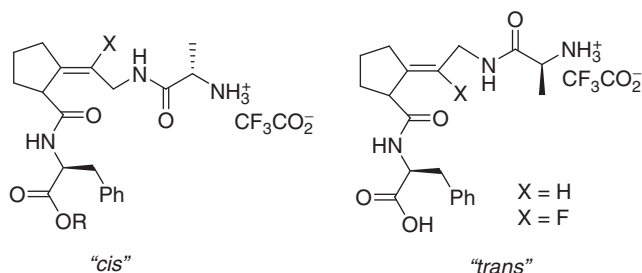


Table 1. Percent inhibition of cyclophilin (CyP)^a by Gly-ψ[(*E/Z*)C=CH]-Pro and Gly-ψ[(*E/Z*)C=CF]-Pro isosteres

Peptide orientation ^b	X	Inhibitor concentration			
		0.5 mM	0.25 mM	0.1 mM	0.05 mM
"Cis 1"	H	50 ± 4 (2) ^c	17 ± 2 (4)	15 ± 6 (4)	1 ± 1 (5)
	F	30 ± 2 (2)	0 (2)		
"Cis 2"	H	39 (2)	34 ± 3 (3)	27 ± 7 (4)	
	F	30 ± 13 (2)	7 ± 2 (2)		
"Trans 1"	H	14 ± 8 (2)	15 ± 4 (2)		
	F	34 ± 6 (3)	24 ± 4 (2)		
"Trans 2"	H	23 ± 27 (3)	28 ± 6 (3)	3 ± 3 (5)	2 ± 3 (6)
	F	43 (1)	26 (1)		

^a Substrate Suc-Ala-Ala-Pro-Phe-*p*-NA (0.07 mM) and cyclophilin (0.5 μM).

^b 1 and 2 refer to separated diastereomers of (*E*)- and (*Z*)-Ala-Glyψ[CF=C]-Pro-Phe. While absolute configuration was not determined, the relative configuration for each separated diastereomer was established by NMR methods [44].

^c Percent enzyme inhibition.

is expressed on a specific set of T lymphocytes, where it is upregulated after activation. It is also expressed in a variety of tissues, primarily on endothelial and epithelial cells. The role of DPP IV/CD26 within the immune system results from combination of exopeptidase activity and interaction with other substances. DPP IV/CD26 thereby functions as a costimulatory molecule influencing T cell activity and modulating chemotaxis [97]. DPP IV is also a validated target for the treatment of Type 2 diabetes, with several inhibitors currently in Phase III clinical trials [98]. Glucagon-like peptide-1 (GLP-1 (7–36) amide) is released in the small intestine in response to the ingestion of nutrients and enhances the glucose-dependent secretion of insulin from pancreatic B-cells. In type 2 diabetic patients, the continuous infusion of GLP-1 (7–36) amide decreases plasma glucose and Hb A1c concentrations and improves B-cell function. However, this desirable effect is rapidly terminated by the *N*-terminal cleavage of GLP-1 at

Ala2 by DPP IV. With the short *in vivo* half-life of GLP-1 (<3 min) limiting the utility of exogenous GLP-1-based therapy, inhibition of endogenous GLP-1 degradation by reduction of DPP IV activity has been shown to be an effective strategy to enhance the *in vivo* incretin activity of GLP-1 [99]. The promising therapeutic potential of DPP IV inhibitors in the treatment of type 2 diabetes and in the treatment of immunological disorders has been reviewed [100–102]. DPP IV is also implicated in HIV-1 entry, malignant transformation, and tumor invasion [97]. While inhibitor development preceded structural information the crystal structure of DPP IV is now available [103].

5.3.1. DPP IV inhibition

The activity of DPP IV inhibitors has been reported by two groups [61,63,65]. The findings from our work are summarized in Table 2 [64,65].

From this work, it is apparent that the inactivation of DPP IV by *u* and *l* nitrile does not follow pseudo-first-order reaction kinetics. The inactivation process is dependent principally on inhibitor concentration, and only slightly changes with incubation time. Secondly, the inhibitory potency of inhibitor *u* and *l* nitrile is nearly equivalent (for *u* K_i = 6.03 μ M and for *l* K_i = 7.69 μ M), that is, the inhibitors interact with DPP IV relatively little difference in potency. K_i of both *u* and *l* are four to five times lower than Ala-Pro-NHO-Bz(4-NO₂). Both *u* and *l* nitrile exhibit superior inhibitory activity to the previously prepared Ala-Pro-NHO-Bz(4-NO₂) compound. Surprisingly both the *u* and *l* nitrile have superior activity to mechanism based Ala ψ [CF=C]-Pro-NHO-Bz inhibitor.

Table 2. Percent inhibition of dipeptidyl peptidase IV (DPP IV) by Ala ψ [(*E*) C=CF]-Pro derived inhibitors

Inhibitors	[<i>l</i>] μ M ^a	% Inhibition	
		Incubation time = 2 min	Incubation time = 30 min
<i>u</i> Ala ψ [CF = C]-Pro CN ^b	1	16%	22%
	10	50%	49%
<i>u</i> Ala ψ [CF = C]-Pro-NHOBz	10	42%	39%
<i>l</i> Ala ψ [CF = C]-Pro CN	1	14%	12%
	10	47%	52%
<i>u</i> Ala ψ [CF = C]-Pro-NHOBz	10	4%	1%
Ala-Pro-NHOBz (4-NO ₂)	1,100	29%	60%

^a Inhibitor concentration.

^b The *u* diastereomeric pair was not separated for these analyses; therefore, the activity might reasonably be higher.

Augustyns' findings allow the direct comparison of the *E* and *Z* forms of the peptide isostere with the parent peptide [61]. These authors reported that fluoroolefin peptide isostere containing compounds were much more potent inhibitors of DPP II but possessed little activity against DPP IV (Table 3).

5.3.2. Quiescent proline peptidase (QPP)

Interestingly, the selectivity of the hydroxamic acid inhibitor of DPP IV was crucial in experiments to establish the role and existence of quiescent cell proline dipeptidase, QPP, a serine protease whose inhibition leads to the death of quiescent peripheral blood monocytes [104]. All other DPP IV inhibitors did not exhibit sufficient selectivity to discriminate between DPP IV and QPP.

5.4. Thermolysin

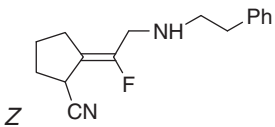
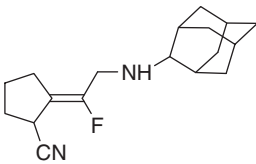
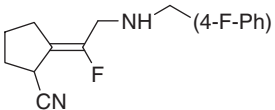
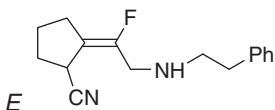
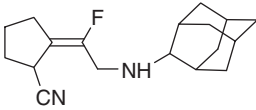
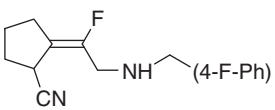
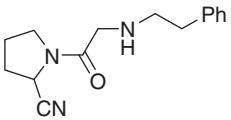
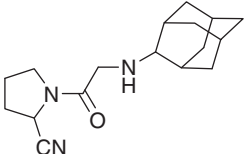
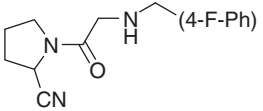
Tripeptide analogs of the form Cbz-Gly ν [(*Z*)-CF=CH] LeuXaa (1, Xaa = Gly, Ala, Leu, Phe, and NH₂) were synthesized to assess the ability of the fluoroalkene moiety to mimic a peptide linkage [14]. These compounds are modest inhibitors of the zinc endopeptidase thermolysin ($0.19 \text{ mM} < K_i < 1.8 \text{ mM}$); the K_i values correlate strongly with the K_m values, but not K_m/k_{cat} , for hydrolysis of the corresponding peptides. The K_i versus K_m correlation indicates that the P₂' residue of these inhibitors sits in the thermolysin active site in the same manner as the substrate in the Michaelis complex. However, the lack of correlation between K_i and K_m/k_{cat} indicates that these inhibitors bind as ground-state analogs with no relationship between the affinities of the inhibitors and the transition-state form of nonisostere containing inhibitors. This report represented the first direct assessment of the fluoroalkene unit as a peptide surrogate.

5.5. β -turn mimics

One future potential application is the use of fluoroolefin isostere constructs to modulate the folding of larger peptide assemblages [105]. The β -strand is well known as a central peptide folding motif associated with specific receptors. The control of β -strand conformations may lead to potent enzyme inhibitors or conversely increase affinity of β -strand receptors for substrates. Strand mimetics suggest the possibility, by virtue of rigidity, of surface protein analogs in scaffolds for separating protein domains as might be required in cell surface interactions between multiple receptors. The role of alkenes in such processes is still in progress.

One strategy to control folding is to direct folds by introduction of β -hairpins, turns which are often associated with Pro incorporation in a polypeptide sequence. Constrained turn mimics have previously been employed in investigations of the active conformation of peptides. Clearly, from the above discussion of CyP and

Table 3. Inhibition of DPP IV by Gly ψ [C=CF]-Pro derived inhibitors^a [61]

Inhibitors	IC ₅₀ (μ M)
	>500
	12
	>1,000
	>1,000
	15
	>500
	2.13 \pm 0.11
	0.35 \pm 0.03
	3.7 \pm 0.2

^a If the IC₅₀ was greater than the highest measured solubility, the value was reported as >X.

DPP IV inhibitors, access to potent *cis*-proline mimics, (*E*)-fluoroolefin isosteres, is convenient. The utility of (*Z*)-alkene amide isosteres in such applications has been established [106].

REFERENCES

- [1] J. Gante, Peptide mimetics—tailor-made enzyme inhibitors, *Angew. Chem. Int. Ed.* 33 (1994) 1699–1720.
- [2] J.M. Ahn, N.A. Boyle, M.T. MacDonald, K.D. Janda, Peptidomimetics and peptide backbone modifications, *Mini Rev. Med. Chem.* 2 (2002) 463–473.
- [3] B. Penke, G. Toth, G. Varadi, Analogue and conformational studies on peptides, hormones and other biologically active peptides, *Amino Acids Pept. Proteins* 34 (2003) 55–148.
- [4] M.L. West, D. Fairlie, Targeting HIV-1 protease: A test of drug-design methodologies, *Trends Pharmacol. Sci.* 16 (1995) 67–74.
- [5] P. Gillespie, J. Cicariello, G.L. Olson, Conformational analysis of dipeptide mimetics, *Biopolymers* 43 (1997) 191–217.
- [6] A.F. Spatola, Peptide backbone modifications: A structure-activity analysis of peptides containing amide bond surrogates, conformational constraints, and related backbone replacements, in: B. Weinstein (Ed.), *Chemistry and Biochemistry of Amino Acids, Peptides and Proteins*, Marcel Dekker, New York, 1983, pp. 267–357.
- [7] M.M. Vasbinder, S.J. Miller, Synthesis of the Pro-Gly dipeptide alkene isostere using olefin cross-metathesis, *J. Org. Chem.* 67 (2002) 6240–6242.
- [8] C. Dugave, L. Demange, *Cis-trans* isomerization of organic molecules and biomolecules: Implications and applications, *Chem. Rev. (Washington, DC, United States)* 103 (2003) 2475–2532.
- [9] M.M. Hann, P.G. Sammes, P.D. Kennewell, J.B. Taylor, On double bond isosteres of the peptide bond; an enkephalin analog, *J. Chem. Soc. Chem. Commun.* (1980) 234–235.
- [10] M.M. Hann, P.G. Sammes, P.D. Kennewell, J.B. Taylor, On the double bond isostere of the peptide bond: Preparation of an enkephalin analog, *J. Chem. Soc. Perkin Trans. 1* (1982) 307–314.
- [11] K. Fujimoto, R. Doi, R. Hosotani, M. Wada, J.-U. Lee, T. Koshiba, T. Ibuka, H. Habashita, K. Nakai, N. Fujii, M. Imamura, Effects of structural modulation on biological activity of bombesin analogues with (*E*)-alkene bond, *Life Sci.* 60 (1997) 29–34.
- [12] K. Miyasaka, S. Kanai, M. Masuda, T. Ibuka, K. Nakai, N. Fujii, A. Funakoshi, Involvement of cholinergic processes in cholecystokinin (CCK) release [corrected] by luminal oleic acid, *J. Auton. Nerv. Syst.* 63 (1997) 179–182.
- [13] T.E. Christos, A. Arvanitis, G.A. Cain, A.L. Johnson, R.S. Potorf, S.W. Tam, W.K. Schmidt, Stable isosteres of neurotensin C-terminal pentapeptides derived by modification of the amide function, *Bioorg. Med. Chem. Lett.* 3 (1993) 1035–1040.
- [14] P.A. Bartlett, A. Otake, Fluoroalkenes as peptide isosteres: Ground state analog inhibitors of thermolysin, *J. Org. Chem.* 60 (1995) 3107–3111.
- [15] J.S. Wai, D.L. Bamberger, T.E. Fisher, S.L. Graham, R.L. Smith, J.B. Gibbs, S.D. Mosser, A.I. Oliff, D.L. Pompliano, E. Rands, N.E. Kohl, Synthesis and biological activity of Ras farnesyl protein transferase inhibitors. Tetrapeptide analogs with amino methyl and carbon linkages, *Bioorg. Med. Chem.* 2 (1994) 939–947.
- [16] C. Dugave, Study of the *cis-trans* isomerization of the amino-acyl prolyl peptide bond. Application to the design of novel inhibitors of immunophilins, *Curr. Org. Chem.* 6 (2002) 1397–1431.
- [17] N.G. Bandur, K. Harms, U. Koert, First stereoselective synthesis of a Pro-Pro *E*-alkene dipeptide isostere, *Synlett* (2005) 773–776.

- [18] A. Otaka, F. Katagiri, T. Kinoshita, Y. Odagaki, S. Oishi, H. Tamamura, N. Hamanaka, N. Fujii, Regio- and stereoselective synthesis of (*E*)-Alkene *trans*-Xaa-Pro dipeptide mimetics utilizing organocopper-mediated Anti-S_N2' reactions, *J. Org. Chem.* 67 (2002) 6152–6161.
- [19] Y. Sasaki, A. Niida, T. Tsuji, A. Shigenaga, N. Fujii, A. Otaka, Stereoselective synthesis of (*Z*)-alkene-containing proline dipeptide mimetics, *J. Org. Chem.* 71 (2006) 4969–4979.
- [20] S.A. Hart, M. Sabat, F.A. Etzkorn, Enantio- and regioselective synthesis of a (*Z*)-alkene *cis*-proline mimic, *J. Org. Chem.* 63 (1998) 7580–7581.
- [21] X.J. Wang, F.A. Etzkorn, Peptidyl-prolyl isomerase inhibitors, *Biopolymers* 84 (2006) 125–146.
- [22] X.J. Wang, S.A. Hart, B. Xu, M.D. Mason, J.R. Goodell, F.A. Etzkorn, Serine-*cis*-proline and Serine-*trans*-proline isosteres: Stereoselective synthesis of (*Z*)- and (*E*)-alkene mimics by still-wittig and ireland-claisen rearrangements, *J. Org. Chem.* 68 (2003) 2343–2349.
- [23] S.A. Hart, (*Z*)- and (*E*)-alkene *cis*- and *trans*-proline isosteres as mimics of cyclophilin and pin1 substrates, Ph.D. Dissertation, University of Virginia, 2001.
- [24] F.A. Etzkorn, Protein mimics inhibit enzymes that regulate the cell cycle, 2004 Abstracts of papers 228th ACS National meeting, Aug. 22–26.
- [25] C.Y. Cheng, B.I. Liou, S.T. Jih, Stereoselective synthesis of *trans*-(*E*)-*N*-{2-[4-(3,4-dichlorophenyl)but-2-en-2-yl]cyclohexyl}pyrrolidine as an alkene mimetic of the arylacetamide analgesics, *J. Chinese Chem. Soc. (Taipei, Taiwan)* 40 (1993) 67–71.
- [26] S. Oishi, T. Kamano, A. Niida, Y. Odagaki, N. Hamanaka, M. Yamamoto, K. Ajito, H. Tamamura, A. Otaka, N. Fujii, Diastereoselective synthesis of new γ [(*E*)-CH=CMe]- and Ψ [(*Z*)-CH=CMe]-type alkene dipeptide isosteres by organocopper reagents and application to conformationally restricted cyclic RGD peptidomimetics, *J. Org. Chem.* 67 (2002) 6162–6173.
- [27] S. Oishi, K. Miyamoto, A. Niida, M. Yamamoto, K. Ajito, H. Tamamura, A. Otaka, Y. Kuroda, A. Asai, N. Fujii, Application of tri- and tetrasubstituted alkene dipeptide mimetics to conformational studies of cyclic RGD peptides, *Tetrahedron* 62 (2006) 1416–1424.
- [28] N. Fujii, K. Nakai, H. Habashita, A. Otaka, T. Ibuka, M. Wada, R. Doi, R. Hosotani, M. Imamura, Highly stereoselective synthesis of (*E*)-alkene dipeptide isosteres via organocopper mediated 1,3-chirality transfer reaction and its application to the synthesis of a potent bombesin antagonist with no agonistic activity in Peptides 1994, Proceedings of the 23rd European Peptide Symposium, Braga, Port., 1995 Sept. 4–10, 1994, 1995.
- [29] D. Garbe, S.A. Sieber, N.G. Bandur, U. Koert, M.A. Marahiel, Enzymatic cyclization of peptidomimetics with incorporated (*E*)-alkene dipeptide isosteres, *ChemBioChem* 5 (2004) 1000–1003.
- [30] M.T. Cox, D.W. Heaton, J. Horbury, Preparation of protected *trans*-olefinic dipeptide isosteres, *J. Chem. Soc. Chem. Commun.* (1980) 799–800.
- [31] R.L. Johnson, Inhibition of renin by substrate analogue inhibitors containing the olefinic amino acid 5(*S*)-amino-7-methyl-3(*E*)-octenoic acid, *J. Med. Chem.* 27 (1984) 1351–1354.
- [32] R. Beresis, J.S. Panek, A concise enantioselective synthesis of *trans*-olefin dipeptide isosteres, *Bioorg. Med. Chem. Lett.* 3 (1993) 1609–1614.
- [33] A. Spaltenstein, P.A. Carpino, F. Miyake, P.B. Hopkins, A stereocontrolled synthesis of *trans*-alkene isosteres of dipeptides, *Tetrahedron Lett.* 27 (1986) 2095–2098.
- [34] C. Charrier, L. Ettouati, J. Paris, New application of the Julia olefination for the synthesis of Tyr-Gly *E*-alkene and carba isostere pseudopeptides, *Tetrahedron Lett.* 40 (1999) 5705–5707.
- [35] T.C. Henninger, P. Wipf, (*E*)-Alkene peptide bond isosteres by cuprate opening of vinyl aziridines, *Methods Mol. Med.* 23 (1999) 125–136.

- [36] P. Wipf, T.C. Henninger, Solid-phase synthesis of peptide mimetics with (*E*)-alkene amide bond replacements derived from alkenylaziridines, *J. Org. Chem.* 62 (1997) 1586–1587.
- [37] S.L. Ellison, Ph.D. Dissertation, University of Liverpool, 1984.
- [38] M. Schlosser, in: V.A. Soloshonok (Ed.), *The Chemical and Physiological Size of Fluorine in Enantiocontrolled Synthesis of Fluoro-Organic Compounds*, John Wiley & Sons Ltd., Chichester, 1999, pp. 613–659.
- [39] C. Jaeckel, B. Koksche, Fluorine in peptide design and protein engineering, *Eur. J. Org. Chem.* (2005) 4483–4503.
- [40] J.T. Welch, I.H. Jeong, W.J. Chung, K. Zhao, J. Lin, Fluorination and electrostatic interactions in enzyme binding, in: *Fluorinated Bio-active Compounds; Proceedings of a conference held in Brussels, 13–15 Sept 1999*, 1999.
- [41] J. Xiao, B. Weisblum, P. Wipf, Electrostatic versus steric effects in peptidomimicry: Synthesis and secondary structure analysis of gramicidin S analogues with (*E*)-alkene peptide isosteres, *J. Am. Chem. Soc.* 127 (2005) 5742–5743.
- [42] R.J. Abraham, S.L.R. Ellison, P. Schonholzer, W.A. Thomas, A theoretical and crystallographic study of the geometries and conformations of fluoro-olefins as peptide analogs, *Tetrahedron* 42 (1986) 2101–2110.
- [43] P. Cieplak, P.A. Kollman, Peptide mimetics as enzyme inhibitors: Use of free energy perturbation calculations to evaluate isosteric replacement for amide bonds in a potent HIV protease inhibitor, *J. Comput. Aided Mol. Des.* 7 (1993) 291–304.
- [44] L.G. Boros, B.D. Corte, R.H. Gimi, J.T. Welch, Y. Wu, R.E. Handschumacher, Fluoroolefin peptide isosteres—tools for controlling peptide conformations, *Tetrahedron Lett.* 35 (1994) 6033–6036.
- [45] J.T. Welch, T. Allmendinger, Fluoroolefin isosteres, *Methods Mol. Med.* 23 (1999) 357–384.
- [46] T. Allmendinger, P. Furet, E. Hungerbuehler, Fluoroolefin dipeptide isosteres. I. The synthesis of Gly[CF=CH]Gly and racemic Phe[CF=CH]Gly, *Tetrahedron Lett.* 31 (1990) 7297–7300.
- [47] T. Allmendinger, E. Felder, E. Hungerbuehler, Fluoroolefin dipeptide isosteres. II. Enantioselective synthesis of both antipodes of the Phe-Gly dipeptide mimic, *Tetrahedron Lett.* 31 (1990) 7301–7304.
- [48] E.V. Dehmlow, K. Franke, Uses of phase transfer catalysis. 11. Phase transfer catalytic reactions of heterocycles with dihalocarbenes, *Liebigs Ann. der Chemie* (1979) 1456–1464.
- [49] K.W. Laue, C. Muck-Lichtenfeld, G. Haufe, Enantioselective syntheses of 2-amino-4-fluoropent-4-enoic acids. Isosteres of asparagine, *Tetrahedron* 55 (1999) 10413–10424.
- [50] D.M. Shendage, R. Froehlich, K. Bergander, G. Haufe, Asymmetric synthesis of γ -fluorinated α -amino acid derivatives, *Eur. J. Org. Chem.* (2005) 719–727.
- [51] M. Shimizu, T. Hata, T. Hiyama, Novel C1 building blocks for fluoro olefin synthesis: FC(SiMe₃)₃ and FC(SiMe₃)₂SnBu₃, *Bull. Chem. Soc. Japan* 73 (2000) 1685–1690.
- [52] A. Saito, M. Nakagawa, T. Taguchi, Chromium-mediated fluoroalkenylation reactions of 1,1-dibromo-1-fluoroalkane and 1-bromo-1-fluoroalkene derivatives, *J. Fluor. Chem.* 126 (2005) 1166–1173.
- [53] G. Dutheil, X. Lei, X. Pannecoucke, J.C. Quirion, A novel diastereoselective synthesis of (*Z*)-fluoroalkenes via a Nozaki-Hiyama-Kishi-Type reaction, *J. Org. Chem.* 70 (2005) 1911–1914.
- [54] G. Dutheil, C. Paturel, X. Lei, S. Couve-Bonnaire, X. Pannecoucke, First stereospecific synthesis of (*E*)- or (*Z*)- α -fluoroenones via a kinetically controlled Negishi coupling reaction, *J. Org. Chem.* 71 (2006) 4316–4319.
- [55] S.J. Veenstra, K. Hauser, P. Felber, Studies on the active conformation of the NK1 antagonist CGP 49823. Part 2. Fluoro-olefin analogs of tertiary amide rotamers, *Bioorg. Med. Chem. Lett.* 7 (1997) 351–354.

- [56] E. Pfund, S. Masson, M. Vazeux, T. Lequeux, Syntheses of α -fluoro- α,β -unsaturated thioamides and thiazolines from a fluorophosphonodithioacetate, *J. Org. Chem.* 69 (2004) 4670–4676.
- [57] T. Allmendinger, R. Fujimoto, F. Gasparini, W. Schilling, Y. Satoh, α -Fluoro-benzylphosphonates as reagents for the preparation of 1-fluoro-1-aryl alkenes and α -fluoro-stilbenes, *Chimia* 58 (2004) 133–137.
- [58] S. Sano, R. Teranishi, Y. Nagao, Toward (Z)-selective Horner-Wadsworth-Emmons reaction of aldehydes with 2-fluoro-2-diethylphosphonoacetic acid, *Tetrahedron Lett.* 43 (2002) 9183–9186.
- [59] S. Sano, K. Saito, Y. Nagao, Tandem reduction-olefination for the stereoselective synthesis of (Z)- α -fluoro- α,β -unsaturated esters, *Tetrahedron Lett.* 44 (2003) 3987–3990.
- [60] P. Van der Veken, I. Kertesz, K. Senten, A. Haemers, K. Augustyns, Synthesis of (E)- and (Z)-fluoro-olefin analogs of potent dipeptidyl peptidase IV inhibitors, *Tetrahedron Lett.* 44 (2003) 6231–6234.
- [61] P. Van der Veken, K. Senten, I. Kertesz, I. De Meester, A.M. Lambeir, M.B. Maes, S. Scharpe, A. Haemers, K. Augustyns, Fluoro-olefins as peptidomimetic inhibitors of dipeptidyl peptidases, *J. Med. Chem.* 48 (2005) 1768–1780.
- [62] J.H. van Steenis, A.M.C.H. van den Nieuwendijk, A. van der Gen, α -fluoroacrylonitriles: Horner-Wittig synthesis and conversion into 2-fluoroallyl amines and C-(1-fluorovinyl)nitrones, *J. Fluor. Chem.* 125 (2004) 107–117.
- [63] J. Lin, P.J. Toscano, J.T. Welch, Inhibition of dipeptidyl peptidase IV by fluoroolefin-containing N-peptidyl-O-hydroxylamine peptidomimetics, *Proc. Natl. Acad. Sci. USA* 95 (1998) 14020–14024.
- [64] J.T. Welch, J. Lin, Fluoroolefin containing dipeptide isosteres as inhibitors of dipeptidyl peptidase IV(CD26), *Tetrahedron* 52 (1996) 291–304.
- [65] K. Zhao, D.S. Lim, T. Funaki, J.T. Welch, Inhibition of dipeptidyl peptidase IV (DPP IV) by 2-(2-amino-1-fluoro-propylidene)-cyclopentanecarbonitrile, a fluoroolefin containing peptidomimetic, *Bioorg. Med. Chem.* 11 (2003) 207–215.
- [66] A. Otaka, E. Mitsuyama, J. Watanabe, H. Watanabe, N. Fujii, Synthesis of fluorine-containing bioisosteres corresponding to phosphoamino acids and dipeptide units, *Biopolymers* 76 (2004) 140–149.
- [67] M. Okada, Y. Nakamura, A. Saito, A. Sato, H. Horikawa, T. Taguchi, Stereoselective construction of functionalized (Z)-fluoroalkenes directed to decapeptide isosteres, *Tetrahedron Lett.* 43 (2002) 5845–5847.
- [68] Y. Nakamura, M. Okada, H. Horikawa, T. Taguchi, Preparation of δ -fluorinated homoallylic alcohol derivatives via regioselective hydride reduction of allylic alcohol derivatives, *J. Fluor. Chem.* 117 (2002) 143–148.
- [69] A. Otaka, H. Watanabe, A. Yukimasa, S. Oishi, H. Tamamura, N. Fujii, New access to α -substituted (Z)-fluoroalkene dipeptide isosteres utilizing organocopper reagents under 'reduction-oxidative alkylation (R-OA)' conditions, *Tetrahedron Lett.* 42 (2001) 5443–5446.
- [70] A. Otaka, H. Watanabe, E. Mitsuyama, A. Yukimasa, H. Tamamura, N. Fujii, Synthesis of (Z)-fluoroalkene dipeptide isosteres utilizing organocopper-mediated reduction of γ,γ -difluoro- α,β -enoates, *Tetrahedron Lett.* 42 (2001) 285–287.
- [71] M. Okada, Y. Nakamura, A. Saito, A. Sato, H. Honkawa, T. Taguchi, Synthesis of α -alkylated (Z)- γ -fluoro- β,γ -enoates through organocopper mediated reaction of γ,γ -difluoro- α,β -enoates: A different reactivity of $R_3Al-Cu(I)$ and Me_2CuLi , *Chem. Lett.* (2002) 28–29.
- [72] Y. Nakamura, M. Okada, A. Sato, H. Horikawa, M. Koura, A. Saito, T. Taguchi, Stereoselective synthesis of (Z)-fluoroalkenes directed to peptide isosteres: Copper mediated reaction of trialkylaluminum with 4,4-difluoro-5-hydroxyallylic alcohol derivatives, *Tetrahedron* 61 (2005) 5741–5753.
- [73] A. Otaka, J. Watanabe, A. Yukimasa, Y. Sasaki, H. Watanabe, T. Kinoshita, S. Oishi, H. Tamamura, N. Fujii, Sml_2 -mediated reduction of γ,γ -difluoro- α,β -enoates with

- application to the synthesis of functionalized (Z)-fluoroalkene-type dipeptide isosteres, *J. Org. Chem.* 69 (2004) 1634–1645.
- [74] A. Niida, M. Mizumoto, T. Narumi, E. Inokuchi, S. Oishi, H. Ohno, A. Otaka, K. Kitaura, N. Fujii, Synthesis of (Z)-alkene and (E)-fluoroalkene-containing diketopiperazine mimetics utilizing organocopper-mediated reduction-alkylation and diastereoselectivity examination using DFT calculations, *J. Org. Chem.* 71 (2006) 4118–4129.
- [75] H. Hata, T. Kobayashi, H. Amii, K. Uneyama, J.T. Welch, A new sequential defluorination route to α -fluoro- α,β -unsaturated ketones from trifluoromethyl ketones, *Tetrahedron Lett.* 43 (2002) 6099–6102.
- [76] C. Chen, K. Wilcoxon, C.Q. Huang, N. Strack, J.R. McCarthy, New methods for the synthesis of fluoro olefins via the palladium catalyzed cross-coupling reaction of 1-fluorovinyl halides with organoboranes and organostannanes, *J. Fluor. Chem.* 101 (2000) 285–290.
- [77] T. Ernet, G. Haufe, Allylic hydroxylation of vinyl fluorides, *Synthesis* (1997) 953–956.
- [78] M. Essers, C. Mück-Lichtenfeld, G. Haufe, Diastereoselective diels-alder reactions of α -Fluorinated α,β -unsaturated carbonyl compounds: Chemical consequences of fluorine substitution, *J. Org. Chem.* 67 (2002) 4715–4721.
- [79] J.M. Bainbridge, S. Corr, M. Kanai, J.M. Percy, HFC-134a as a fluorinated building block: Short synthesis of α -fluoro enones, *Tetrahedron Lett.* 41 (2000) 971–974.
- [80] R.O. Watts, C.G. Allison, K.P. Barthold, P. Tarrant, Reaction of hexafluoropropene oxide with Grignard reagents, *J. Fluor. Chem.* 3 (1973) 7–15.
- [81] K. Funabiki, T. Kurita, M. Matsui, K. Shibata, An efficient and general entry to (Z)- α -fluoro- β -substituted acrylaldehydes based on the coupling reaction of α -fluoro- β -amino acrylaldehydes with organolithium reagents, *Chem. Lett.* (1997) 739–740.
- [82] D.F. Andr  s, U. Dietrich, E.G. Laurent, B.S. Marquet, Anodic fluorination of vinyl sulfides - synthesis of α -fluoro- β -thio- α,β -unsaturated carbonyl compounds, *Tetrahedron* 53 (1997) 647–658.
- [83] M. Marhold, A. Buer, H. Hiemstra, J.H. van Maarseveen, G. Haufe, Synthesis of vinyl fluorides by ring-closing metathesis, *Tetrahedron Lett.* 45 (2004) 57–60.
- [84] S.S. Salim, R.K. Bellingham, V. Satcharoen, R.C.D. Brown, Synthesis of heterocyclic and carbocyclic fluoro-olefins by ring-closing metathesis, *Org. Lett.* 5 (2003) 3403–3406.
- [85] E.S. Eberhardt, R.T. Raines, Amide-amide and amide-water hydrogen bonds: Implications for protein folding and stability, *J. Am. Chem. Soc.* 116 (1994) 2149–2150.
- [86] G. Fischer, Enzymes that catalyse the restructuring of proteins, *Curr. Opin. Struct. Biol.* 10 (2000) 40–45.
- [87] J.T. Welch, Bond strengths and reactivity in organo-fluorine compounds, in: B. Baasner (Ed.), *Houben Weyl Methoden der Organische Chemie, E10b Part 2 Fluorine*, Georg Thieme Verlag, Stuttgart, (1999), pp. 293–305.
- [88] B.E. Smart, Fluorine substituent effects (on bioactivity), *J. Fluor. Chem.* 109 (2001) 3–11.
- [89] J.C. Biffler, H.W. Kim, S.G. DiMagno, The polar hydrophobicity of fluorinated compounds., *ChemBioChem* 5 (2004) 622–627.
- [90] F.A. Etzkorn, L.A. Stolz, Z.Y. Chang, C.T. Walsh, Role of the cyclosporin-A-cyclophilin complex, FK506-FK506-binding protein complex and calcineurin in the inhibition of T-cell signal transduction, *Curr. Opin. Struct. Biol.* 3 (1993) 929–933.
- [91] S.F. Gothel, M.A. Marahiel, Peptidyl-prolyl cis-trans isomerases, a superfamily of ubiquitous folding catalysts, *Cell. Mol. Life Sci.* 55 (1999) 423–436.
- [92] J.D. Joseph, E.S. Yeh, K.I. Swenson, A.R. Means, The peptidyl-prolyl isomerase Pin1, *Prog. Cell Cycle Res.* 5 (2003) 477–487.
- [93] Q. Li, M. Moutiez, J.B. Charbonnier, K. Vaudry, A. Menez, E. Quemeneur, C. Dugave, Design of a gag pentapeptide analogue that binds human cyclophilin a more efficiently than the entire capsid protein: New insights for the development of novel anti-HIV-1 drugs, *J. Med. Chem.* 43 (2000) 1770–1779.

- [94] L. Demange, M. Moutiez, K. Vaudry, C. Dugave, Interaction of human cyclophilin hCyp-18 with short peptides suggests the existence of two functionally independent subsites, *FEBS Lett.* 505 (2001) 191–195.
- [95] H.C. Wang, K. Kim, R. Bakhtiar, J.P. Germanas, Structure-activity studies of ground- and transition-state analogue inhibitors of cyclophilin, *J. Med. Chem.* 44 (2001) 2593–2600.
- [96] Y. Zhang, Inhibitors targeting the enzymatic activity and biological function of Pin1, *Mini Rev. Org. Chem.* 1 (2004) 359–366.
- [97] A.M. Lambeir, C. Durinx, S. Scharpe, I. De Meester, Dipeptidyl-peptidase IV from bench to bedside: An update on structural properties, functions, and clinical aspects of the enzyme DPP IV, *Crit. Rev. Clin. Lab. Sci.* 40 (2003) 209–294.
- [98] K. Augustyns, P. Van der Veken, A. Haemers, Inhibitors of proline-specific dipeptidyl peptidases: DPP IV inhibitors as a novel approach for the treatment of Type 2 diabetes, *Expert Opin. Ther. Patents* 15 (2005) 1387–1407.
- [99] P.E. Wiedeman, J.M. Trevillyan, Dipeptidyl peptidase IV inhibitors for the treatment of impaired glucose tolerance and type 2 diabetes, *Curr. Opin. Investig. Drugs (Thomson Curr. Drugs)* 4 (2003) 412–420.
- [100] A.E. Weber, Dipeptidyl Peptidase IV Inhibitors for the Treatment of Diabetes, *J. Med. Chem.* 47 (2004) 4135–4141.
- [101] K. Augustyns, P. Van der Veken, K. Senten, A. Haemers, The therapeutic potential of inhibitors of dipeptidyl peptidase IV (DPP IV) and related proline-specific dipeptidyl aminopeptidases, *Curr. Med. Chem.* 12 (2005) 971–998.
- [102] K. Augustyns, P. Van der Veken, K. Senten, A. Haemers, Dipeptidyl peptidase IV inhibitors as new therapeutic agents for the treatment of type 2 diabetes, *Expert Opin. Ther. Patents* 13 (2003) 499–510.
- [103] M. Engel, T. Hoffmann, L. Wagner, M. Wermann, U. Heiser, R. Kiefersauer, R. Huber, W. Bode, H.U. Demuth, H. Brandstetter, The crystal structure of dipeptidyl peptidase IV (CD26) reveals its functional regulation and enzymatic mechanism, *Proc. Natl. Acad. Sci. USA* 100 (2003) 5063–5068.
- [104] M. Chiravuri, T. Schmitz, K. Yardley, R. Underwood, Y. Dayal, B.T. Huber, A novel apoptotic pathway in quiescent lymphocytes identified by inhibition of a post-proline cleaving aminodipeptidase: A candidate target protease, quiescent cell proline dipeptidase, *J. Immunol.* 163 (1999) 3092–3099.
- [105] W.A. Loughlin, J.D.A. Tyndall, M.P. Glenn, D.P. Fairlie, Beta-Strand Mimetics, *Chem. Rev. (Washington, DC, United States)* 104 (2004) 6085–6117.
- [106] F.A. Etzkorn, J.M. Travins, S.A. Hart, Rare protein turns: γ -turn, helix-turn-helix, and cis-proline mimics, *Adv. Amino Acid Mimet. Peptidomimet.* 2 (1999) 125–163.

This page intentionally left blank

CHAPTER 17

Molecular Interactions of Fluorinated Amino Acids in a Native Polypeptide Environment

Mario Salwiczek, Christian Jäckel, and Beate Kokschr*

*Department of Chemistry and Biochemistry, Free University of Berlin,
Takustr. 3, 14195 Berlin, Germany*

Contents

1. Introduction	738
2. Unique and versatile: The properties of fluoroalkyl groups	739
2.1. Spatial demand and steric effects	739
2.2. The electrostatic properties of the C–F bond	740
3. Effects of fluorine in protein environments: Metabolism and structural integrity	742
3.1. Proteolytic stability of C ^α -fluoroalkyl amino acids	742
3.1.1. α -Chymotrypsin: A natural protein environment	742
3.1.2. Fluorine's ambiguity: Can polar properties of fluororalkyl groups compete with conformational restrictions?	743
3.1.3. Summary	746
3.2. The "orthogonal" properties of fluoroalkyl amino acid side chains	747
3.2.1. The α -helical coiled coil: A versatile, amphiphilic model system	747
3.2.2. Fluorinated alkyl side chains in a hydrophobic environment	751
3.2.3. Fluorinated alkyl side chains in a hydrophilic environment	752
3.2.4. Summary	754
4. Conclusions and future perspectives	755
References	756

Abstract

Protein folding and activity are based on a multitude of molecular interactions. Single amino acid side chains modulate the nature and strength of such interactions. The metabolic and structural stability of peptides and proteins that contain fluorinated substituents have been studied extensively in recent years. However, the application of fluorinated building blocks to the *de novo* design of peptides and proteins requires a detailed knowledge of molecular interactions directed by the fluorine atom. Our research focuses on the effect of fluorine substitutions on the structure and biological activity of peptides. We have designed and systematically investigated a model peptide system based on the α -helical coiled-coil motif to evaluate the properties of different fluorinated amino acids within a

*Corresponding author;
Email: kokschr@fu-berlin.de

hydrophobic and hydrophilic protein environment. We found that even interactions of single fluorinated amino acids can highly affect polypeptide folding.

1. INTRODUCTION

Intermolecular interactions represent the main regulatory machinery of a wide variety of biological processes such as signal transduction, cell–cell communication, catalysis, as well as metabolism and hormone regulation. Peptides and proteins play a powerful role in these functions because of their structural and functional versatility [1]. They can take part in various interactions of a hydrophobic as well as dipolar and ionic nature depending on the side chain functionalities of the amino acids within the sequence. Because of steric effects, the three-dimensional structure of a protein may also contribute to molecular recognition. Physiological and psychological disorders often originate from peptide and protein malfunctions. Protein mutation can result in the deactivation or hyperstimulation of a specific signal transduction pathway and may greatly affect enzyme activity. Undesirable interactions that occur in the course of viral and bacterial infections may also induce diseases. Therefore, research on new biologically active peptides as possible drugs for the treatment of infections and metabolic, hormonal, and brain diseases has been an important subject of biological chemistry for the last decades. Peptides that are exclusively composed of the 20 canonical amino acids often exhibit a comparably low metabolic stability as well as low membrane permeability, which both result in an unsatisfactory pharmacological activity. The rational design of peptides that are partly composed of non-canonical amino acids with nonnatural side chain functional groups as well as chemical modifications of the peptide bond is a promising way to improve metabolic stability, membrane permeability, and, thus, pharmacological activity [2–4].

In addition to solid phase peptide synthesis [5,6], newly developed strategies for the synthesis of peptides and proteins, including segment condensation [7], native chemical ligation [8–10], expressed protein ligation [11,12], as well as *in vivo* expression using aminoacylated suppressor-tRNA [13–16], have significantly improved the methods for incorporating a wide variety of nonnatural building blocks into synthetic peptides and proteins. Fluorinated amino acids have been shown to be interesting tools for modulating the structure and bioactivity of peptide-based drugs [17]. Although the metabolic stability and the interaction of fluoromodified peptides with different enzymes have already been studied, the interpretation of these results with respect to molecular interactions of the fluorine atom is yet to be fully accomplished [18]. This may be attributed to the fact that some important properties of fluorinated hydrocarbon analogs, such as hydrophobicity, spatial demand, and the ability to participate in dipolar interactions, especially hydrogen bonds, have not yet been systematically studied within a protein environment.

This chapter aims to summarize our efforts to investigate the effects of fluorinated amino acid substitutes on the interactions with natural protein environments. In addition to a rather specific example concerning the interactions of small peptides with a proteolytic enzyme, we present a simple polypeptide model that aids for a systematic investigation of the interaction pattern of amino acids that differ in side chain length as well as fluorine content within both a hydrophobic *and* hydrophilic protein environment. Amino acid side chain fluorination highly affects polypeptide folding due to steric effects, polarization, and fluororous interactions.

2. UNIQUE AND VERSATILE: THE PROPERTIES OF FUOROALKYL GROUPS

The interactions of peptides and proteins in biological environments can sometimes be so complex that it is often difficult to unambiguously interpret the data observed. Therefore, many investigations on the molecular interactions of fluorine comprise more or less small organic molecules that contain a limited number of functional groups. The results of these studies lead to a better understanding of the properties of “organic fluorine” in biological environments. The next two subchapters shortly summarize the general properties of fluoroalkyl groups as a prerequisite to understand their interactions with proteins.

2.1. Spatial demand and steric effects

In comparison to the van der Waals radii of oxygen (1.52 Å) and hydrogen (1.20 Å), the fluorine atom with its radius of 1.47 Å is expected to exhibit approximately the same spatial demand as oxygen and should be more sterically demanding than hydrogen [19]. However, various studies have shown that the substitution of one hydrogen atom by fluorine does not seem to disturb the overall structural features of a molecule and, therefore, has often been considered to be isosteric [20]. The substitution of a hydrogen atom or a hydroxy group by fluorine has been used to improve the metabolic stability of drug candidates against oxidizing enzymes such as cytochrome P450 without significantly disturbing the binding affinity of the drug to its target protein [21]. This concept has led to the synthesis of numerous nonpeptidic fluorinated drugs, some of which are already in clinical use [22]. While the isosterism of fluorine and hydrogen has been widely accepted, the spatial demand of higher fluorinated alkyl groups is still being controversially debated [17]. The above-described influences of monofluorine substitutions have led to the assumption that a trifluoromethyl group is approximately as large as a methyl substituent. However, a comparison of the van der Waals volumes (CH_3 : 21.6 Å³; CF_3 : 39.8 Å³) [23] clearly proves a trifluoromethyl group to have approximately twice the spatial demand as a methyl substituent.

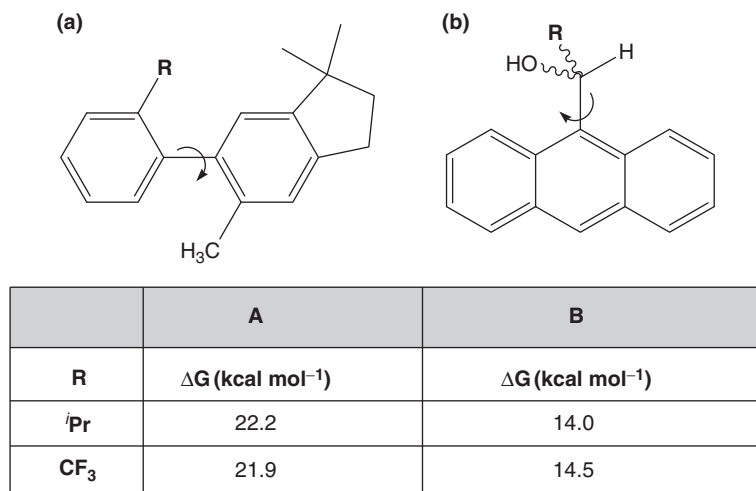


Fig. 1. Rotational barriers of (a) substituted 6-aryl-1,1,5-trimethylindanes and (b) (9-anthryl)carbinol derivatives depending on the substituent R.

Furthermore, the estimation of the rotational barriers of ortho-substituted 6-aryl-1,1,5-trimethylindanes (Fig. 1a) [24] by NMR as well as conformational NMR-studies of (9-anthryl)carbinol derivatives (Fig. 1b) [25] have shown the CF₃ substituent to have steric effects that are comparable to those of an isopropyl group (Fig. 1).

Therefore, comparing CF₃ with isopropyl has become quite common. It should be taken into account, however, that these two groups are not comparable with respect to their three-dimensional shape [23]. Moreover, the isopropyl group is much more flexible and even though it occupies a much larger van der Waals volume (56.2 Å³) [23] than CF₃, their steric effects seem to be comparable. Thus, the terms *steric size* and *steric effect* should not be mixed [26]. The steric size of a molecule or substituent can be evaluated relatively easily by estimating its van der Waals volume, whereas the interpretation of the steric effects of a substituent strongly depends on the method applied for their investigation. Investigations on the enantiodirecting properties of a CF₃ substituent in chemical reactions, for example, have led to comparing its spatial demand to *tert*-butyl, and the question arises as to whether it could be even bulkier than a phenyl substituent [27].

2.2. The electrostatic properties of the C–F bond

Combining the highest electronegativity (4,0) with a rather small polarizability volume which amounts to not more than 0.5 Å³ makes fluorine a unique element. Its incorporation into hydrocarbon frameworks results in different electrostatic effects, which are sometimes rarely predictable. However, the influence of fluorine substituents on the acidity of nearby functional groups such as OH, NH,

and CH has been thoroughly studied [28]. The introduction of fluorine into the side chain of amino acids has been shown to have a higher impact on the basicity of the amino function than on the acidity of the carboxy function. Both the pK_a and pK_b value can significantly shift depending on the degree of fluorination and the substitution position. Therefore, the inductive effect of the fluorine atom alters the electrostatic properties of the peptide bond and directs molecular interactions of fluorinated peptides with proteins.

The ability of carbon-bound fluorine to accept hydrogen bonds is one of the most controversially discussed issues [29]. Numerous studies have been published describing the direct measurement of hydrogen bond strengths and distances involving the fluorine atom as an acceptor function applying NMR and crystal structure analysis [30–33]. In addition, quantum mechanical approaches have been used to prove this rather rarely observable interaction to be theoretically possible [34–39]. These investigations comprise interactions of the type $C-F\cdots H-X$ where X is either O, N, an aromatic C, or a CH_xF_y moiety. Surveys of crystallographic databases have shown that fluorine does accept hydrogen bonds but only in the absence of any better acceptors [40]. However, interactions of proteins have not been the subject of such investigations. In a semitheoretical study by Dunitz et al., a screen for $C-F\cdots H-X$ ($X = O, N$) distances within small molecule crystal structures revealed that contacts closer than 2.3 Å are rarely observed. Nevertheless, some $C-F\cdots H-X$ hydrogen bonds in protein–ligand complexes have been postulated and confirmed by quantum mechanical calculations [41,42]. At least 16 examples have been discussed where a fluorine atom might accept a hydrogen bond from a protein XH group. These interactions are generally denoted as “possible” and are referred to as very weak.

Despite the highly dipolar nature of the C–F bond, fluorinated hydrocarbons generally tend to be more hydrophobic than their nonfluorinated analogs. This may be because fluorine lowers the molecules’ overall polarizability and is itself a very weak hydrogen bond acceptor. Furthermore, fluoroalkyl groups occupy much larger van der Waals volumes than their fluorine free analogs. This property is often described as “polar hydrophobicity of fluorinated compounds” [43]. However, it must be taken into account that the increase in hydrophobicity does not generally imply an increase in lipophilicity. Aromatic fluorination, perfluoroalkylation, as well as the attachment of fluorine atoms to π -bonded carbon atoms with minor exceptions increases lipophilicity, whereas the mono- and trifluorination of saturated alkyl groups generally decreases it [26]. Nevertheless, the aromatic trifluoromethylation of various pharmacological lead compounds has been shown to enhance membrane binding and permeation [44]. Therefore, fluorination of drug candidates including peptides is expected to be a useful concept to facilitate membrane permeation, especially, the diffusion across the blood–brain barrier.

3. EFFECTS OF FLUORINE IN PROTEIN ENVIRONMENTS: METABOLISM AND STRUCTURAL INTEGRITY

3.1. Proteolytic stability of C $^{\alpha}$ -fluoroalkyl amino acids

3.1.1. α -Chymotrypsin: A natural protein environment

The investigation of the proteolytic stability of fluorosubstituted peptides using an enzyme with well-known structure and catalytic mechanism allows a rough analysis of the interactions of fluorosubstituents with the active site. α -Chymotrypsin is a pancreatic serine protease whose catalytic mechanism as well as three-dimensional structure and substrate specificity have been especially well investigated [45,46]. The catalytic triad consists of Ser195, His57, and Asp102. Substrate binding is mediated by aromatic residues (Phe, Trp, and Tyr) which fit into the hydrophobic binding pocket near the active site. The first step of the cleavage reaction is the nucleophilic attack of the Ser195 side chain oxygen on the carbonyl function of the peptide bond. A tetrahedral, intermediate oxyanion is thus formed which resembles the transition state of this reaction. In the course of this process the peptide backbone undergoes a conformational transition. The new conformation perfectly fits into the oxyanion hole which is formed by the enzyme. In addition, the intermediate is stabilized by at least three additional hydrogen bonds. The cleavage reaction is accompanied by a proton transfer from Ser195 oxygen to the imidazole nitrogen of His57 supported by Asp102. A model of substrate binding and stabilization of the intermediate is depicted in Fig. 2 [47,48].

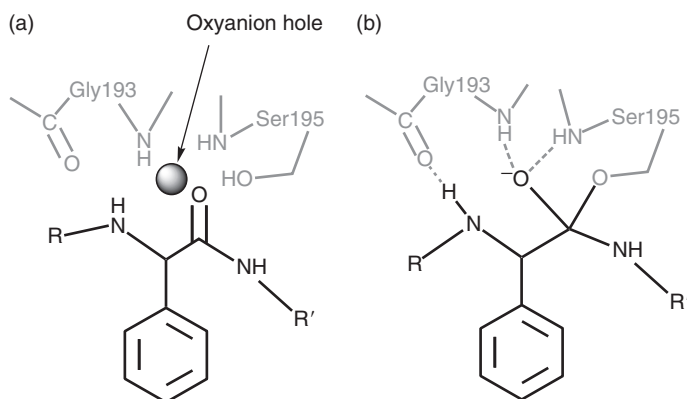
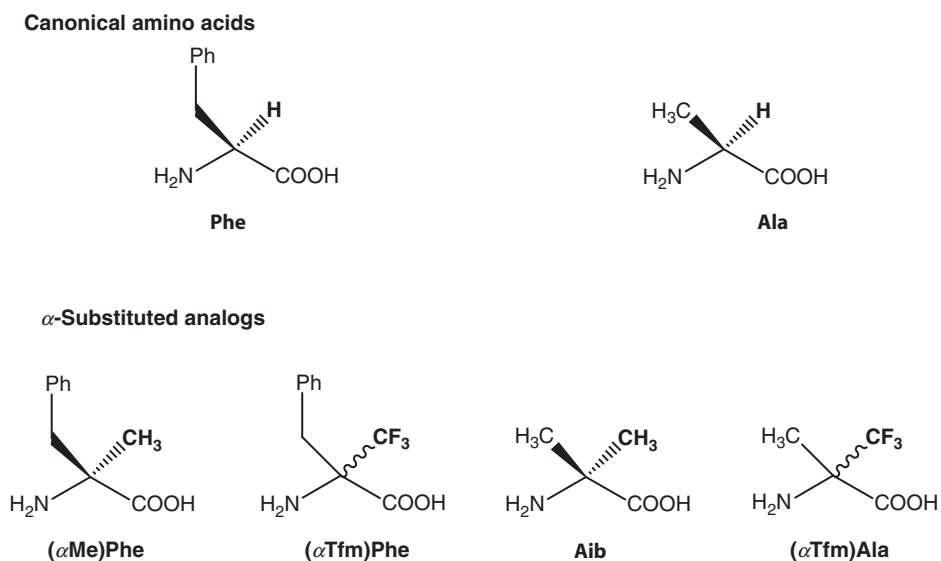


Fig. 2. Model image of a typical substrate bound to α -Chymotrypsin. (a) Binding of the substrate. (b) Three additional hydrogen bonds stabilize the intermediate oxyanion.

3.1.2. Fluorine's ambiguity: Can polar properties of fluororalkyl groups compete with conformational restrictions?

Various diastereomeric di-, tri-, and tetrapeptides that carry the sterically demanding trifluoromethyl group instead of the natural α -proton at different positions within these short peptide sequences have been designed, and their stability towards enzymatic hydrolysis has been investigated. The structures of the α -trifluoromethyl (α Tfm)-substituted amino acids are shown in Scheme 1. From these studies we gained valuable information on how α -trifluoromethyl-substituted peptides may interact with proteins. The α Tfm amino acids used in this study combine the conformational restrictions [49–52] of $C^{\alpha,\alpha}$ -dialkylation with the unique stereoelectronic properties of the fluorine atom and have shown interesting effects on peptide–enzyme interactions [53,54].

Based on the known substrate specificity of α -chymotrypsin, phenylalanine has been chosen as the amino acid at the P_1 position (P-nomenclature according to Schechter and Berger) [55]. The α -proton at P_1 has been substituted either by methyl or trifluoromethyl. Substitutions beyond P_1 contain trifluoromethyl alanine or aminoisobutyric acid. Therefore, each fluorosubstitution can be compared to its natural as well as fluorine-free α -substituted analog, thereby enabling differentiation of the steric and electronic effects. Scheme 2 summarizes the amino acids that have been used in this study.



Scheme 1. Structures of the native amino acids and their nonnatural α -substituted analogs. α -Trifluoromethyl phenylalanine as well as α -trifluoromethyl alanine have been used as racemic mixtures.

In Fig. 3 the sequences of 12 modified as well as two natural peptides which serve as control sequences are given [54]. The diastereomers of all Tfm-substituted peptides were separately studied regarding their protease stability. The results of this hydrolysis study are summarized in Fig. 4.

Cleavage site					
	P ₃	P ₂	P ₁	P ₁ '	P ₂ '
	Z	Ala	Phe	Leu	NH ₂
Z	(α Tfm)Ala	Ala	Phe	Leu	NH ₂
Z	Aib	Ala	Phe	Leu	NH ₂
	Z	(α Tfm)Ala	Phe	Leu	NH ₂
	Z	Aib	Phe	Leu	NH ₂
		Z	(α Tfm)Phe	Leu	NH ₂
		Z	(α Me)Phe	Leu	NH ₂
		Z	Phe	(α Tfm)Ala	Ala
		Z	Phe	Aib	Ala
		Z	Phe	Leu	(α Tfm)Ala
		Z	Phe	Leu	Aib
		Z	Phe	Ala	Ala

Fig. 3. Sequence representation of Aib- and Tfm-substituted peptides. The cleavage site is highlighted in grey. Diastereomeric Tfm-substituted peptides have been separated prior to hydrolysis.

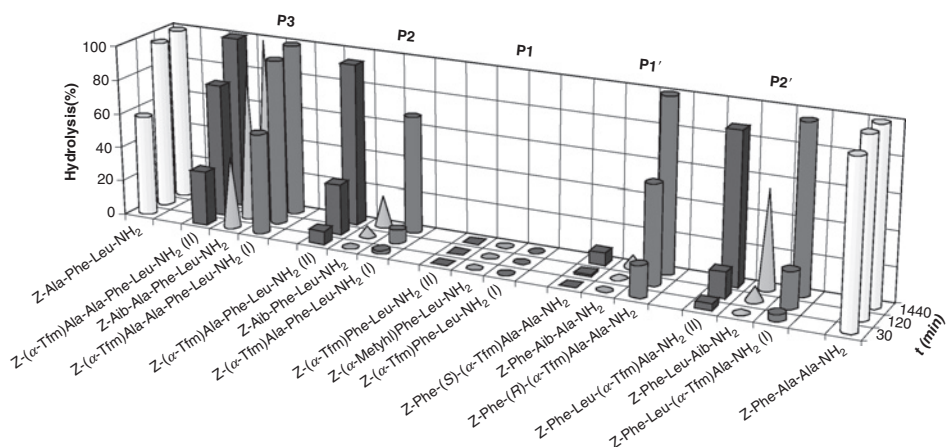


Fig. 4. Summary of the quantitative hydrolysis study.

As shown in Fig. 4, a substitution of the α -proton of Phe at the P_1 position by Tfm completely inhibits proteolysis while the native peptide Z-Ala-Phe-Leu-NH₂ has been completely degraded within a short time. The comparison of this result to the one obtained for the α -methyl analog reveals that this stabilization is probably not an effect of fluorination but of steric restrictions. $C^{\alpha,\alpha}$ -Dialkylated amino acids are known to impart conformational constraints on the peptide backbone, inducing a kink or β -turns. Such a conformation would obviously disfavor a proper binding of the substrate in the active site [53,56]. $C^{\alpha,\alpha}$ -Dialkylated amino acids missing the α -proton are known to extraordinarily slow down the enzymatic degradation of peptides containing such substitutions in proximity to the cleavage site [57]. Besides the induction of helical structures on the peptide backbone, the α,α -dialkylation stabilizes the peptide bond against proteolytic cleavage [58].

The increased steric demand of the trifluoromethyl group presumably aggravates this effect, but as the methyl analog of TfmAla itself is fully stable, this effect cannot be exclusively considered as steric effects of fluorine substitution. All substitutions beyond P_1 show that the stabilizing effect of α -dialkylation decreases along with its distance to the cleavage site. However, even peptides substituted in P_3 are more stable than the natural control sequences. Besides this general trend, which has been shown for both α -methylation and α -trifluoromethylation, two other interesting effects have been observed. With the exception of P_1 substitutions, the fluorinated peptides are generally less stable than their Aib-containing counterparts, and the proteolytic stability highly depends on the absolute stereochemistry of the α Tfm amino acid. As the Aib-containing peptides prove the increase in proteolytic stability to be an effect of C^{α} -dialkylation, the destabilizing effect of fluorination cannot be exclusively explained by the steric effects of Tfm. Fluorination considerably enhances the spatial demand of a methyl group. If steric hindrance were the only explanation for this, the Aib effect could also be expected to increase. The experiment, however, has revealed the opposite. Both observations imply that Tfm-substituted peptides exhibit interactions with enzyme residues within the active site that are impossible for their nonfluorinated counterparts. Considering the electrostatic properties of fluoroalkyl groups, these effects are very likely to be a consequence of fluorine's high electronegativity and, thus, an electrostatic rather than a steric effect. Hydrogen bonds between the trifluoromethyl substituent and the enzyme may account for a better binding of the substrate, thereby accelerating degradation.

The strongest influence of configuration has been observed for P_1' -substituted diastereomers of Z-Phe-(α Tfm)Ala-Ala-NH₂. The crystal structures of both diastereomers have been solved, which enables a better interpretation of this rather interesting effect. While the (S,S,S)-diastereomer has been shown to be almost as stable as the Aib-substituted peptide, the (S,R,S)-diastereomer was hydrolyzed very quickly within the same time range. Molecular modeling studies readily support the formation of hydrogen bonds as a possible explanation for this effect [18,54]. With the known crystal structure of the α -chymotrypsin/phenyl boronic

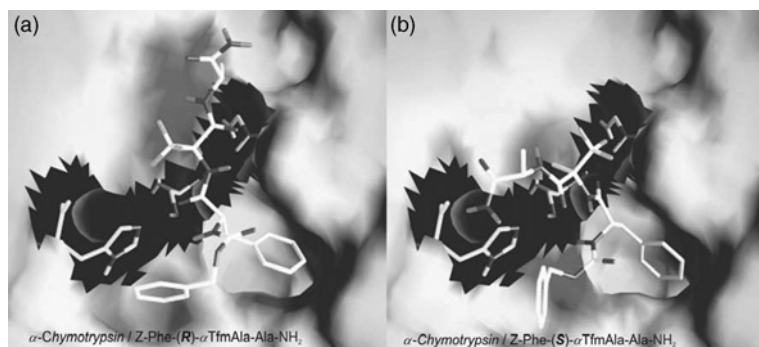


Fig. 5. Conformations of the two diastereomeric Z-Phe-(α Tfm)Ala-Ala-NH₂ peptides within the active site of α -chymotrypsin B. Kocsch, M. Thorman, unpublished results.

acid complex taken from the Brookhaven Protein Data Bank [59], the identical backbone of Z-Phe-Aib-Ala-NH₂, Z-Phe-Ala-Ala-NH₂, and the two epimeric peptides of Z-Phe-(α Tfm)Ala-Ala-NH₂ was fitted into the active site of the protease in such a way that the aromatic Phe residue occupies the hydrophobic-binding pocket and the cleavage site is located next to Ser195. These starting arrangements were energy minimized using the program CHARMm 22 force field (Quanta). These results, together with support from a docking study where the best binding conformations of both diastereomers were computationally selected, provide a detailed picture of the enzyme-bound conformation of both diastereomers (Fig. 5).

In Fig. 5a, the Tfm group of the (S,R,S)-diastereomer forms an equilateral triangle with the side chains of Ser195 and His57. A possible hydrogen bond between fluorine and the OH group decreases the O–H bond strength and thereby supports His57 in attracting the proton. Consequently, the oxygen nucleophilicity is increased. In contrast, the Tfm group of the (S,S,S)-diastereomer is shown to exhibit an attractive interaction with the backbone NH group of Gly193, thereby stabilizing a rather unfavorable conformation, which causes the cleavage site to point away from Ser195 (Fig. 5b).

3.1.3. Summary

With the support of quantum mechanics this proteolysis study has readily shown that fluorinated amino acid side chains are able to direct enzyme substrate interactions, which can have an influence on proteolytic stability. Depending on the absolute stereochemistry and on the position within the sequence, α Tfm amino acids can considerably stabilize peptides against proteolysis. The unique electrostatic properties of carbon-bound fluorine, however, may also induce a contrary effect. The conformational restrictions of C $^{\alpha}$ -dialkylation seem to be partly diminishable by the electrostatic consequences of fluorination. With this knowledge,

the application of Tfm groups in *de novo* designed peptides and peptide mimetics may be used to enhance substrate binding to receptors.

3.2. The “orthogonal” properties of fluoroalkyl amino acid side chains

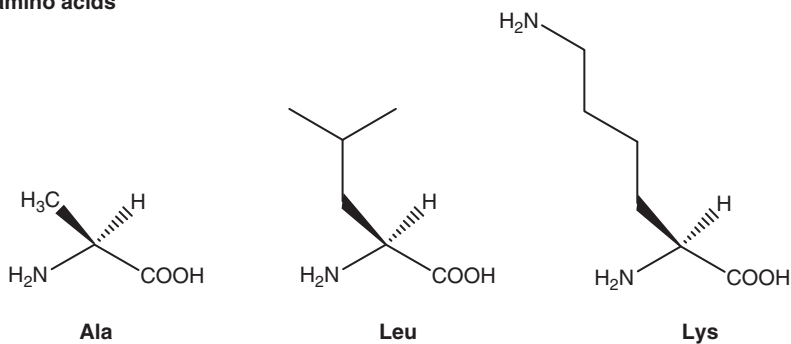
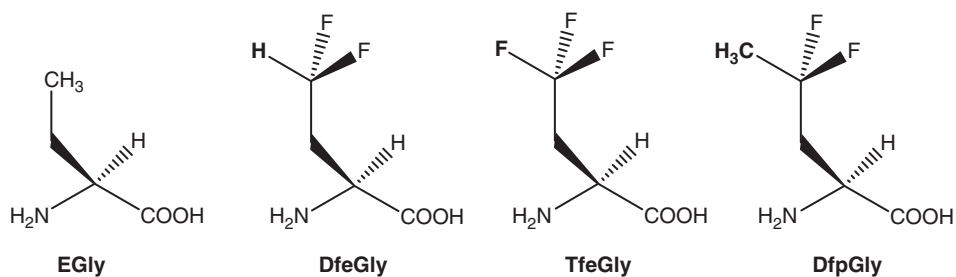
3.2.1. The α -helical coiled coil: A versatile, amphiphilic model system

In the previous chapter we described a systematic study of the interactions of small model peptides with a rather specific enzyme. In our attempt to systematize the effects of fluorinated amino acids on peptide and protein interactions we have established a model system that lays the foundation for a more general approach. How do the steric effects and the degree of fluorination as well as the polarity of fluoroalkyl amino acid side chains affect the folding of proteins and the strength of peptide–protein interactions? In order to answer this central question we choose a very common folding motive, the α -helical coiled coil.

Coiled coils are naturally occurring peptide oligomers of enormous biological importance. Their stability strongly depends on complementary hydrophobic and hydrophilic interaction surfaces. They typically consist of two to five monomers that form α -helices on oligomerization and wrap around each other to a left-handed superhelical structure [60]. This tertiary structure directly arises from the well-defined repetitive amino acid sequence of the monomers, the heptad repeat (abcdefg)_n. Positions **a** and **d** are typically occupied by hydrophobic residues, whereas positions **e** and **g** contain charged amino acids. Oligomerization is driven by the formation of a hydrophobic core between residues **a** and **d** by a zipper-like “knobs-into-holes” packing. Positions **e** and **g** contribute to oligomerization specificity by the formation of interhelical salt bridges. The remaining positions mainly contain hydrophilic amino acids to provide solubility and show only marginal effects on the structural stability. Every single side chain of the amino acids in position **a**, **d**, **e**, and **g** has well-defined interaction partners. This feature of the coiled coil folding motif provides the basis for our model system as it allows an unambiguous interpretation of the data with respect to side chain interactions in the context of a protein environment. Figure 6 provides an overview about the features of the amphiphilic coiled coil interaction surfaces.

The screening system is based on an antiparallel 41 amino acid residue α -helical coiled-coil homodimer [61] which is able to detect single fluorine substitutions within both recognition domains [62]. The peptide is presented as a helical wheel diagram and as an extended sequence in Fig. 7. Using this rationally designed model system, amino acids differing in side chain length and fluorine content have been studied in the context of a hydrophobic and hydrophilic polypeptide environment [63].

The structures of all amino acids, which have been included into the study, are shown in Scheme 2. Starting from (S)-aminobutyric acid (EGly), the spatial

Native amino acids**Noncanonical amino acids**

Scheme 2. Structures of the native amino acid residues compared to their fluorinated analogs. Aminobutyric acid and its fluorinated analogs are referred to as substituted glycines (EGly).

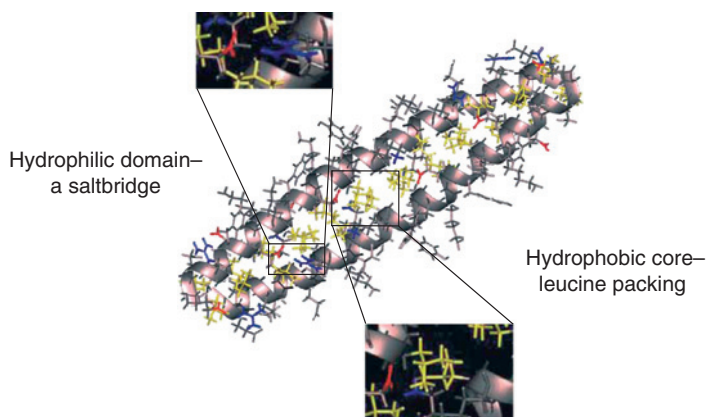


Fig. 6. Model of a typical coiled coil dimer with focus on hydrophobic core packing and interhelical salt bridges. (See Colour Plate Section at the end of this book.)

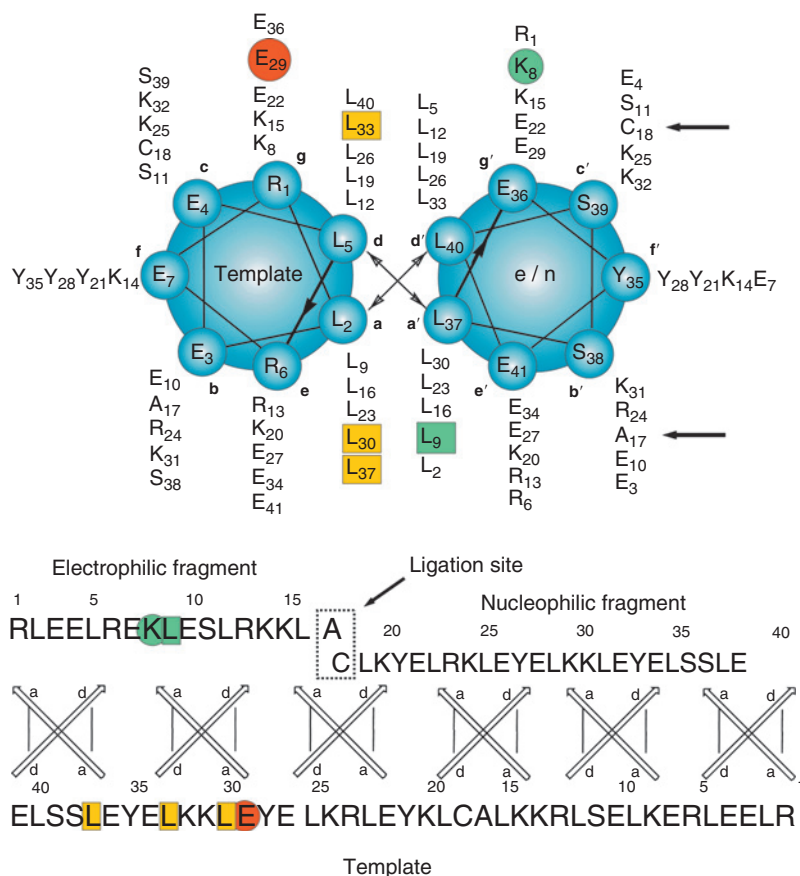


Fig. 7. Helical wheel and sequence representation of the parental homodimeric coiled coil. The substitution positions within the hydrophobic domain are highlighted with open squares and those in the charged domain with open circles. Their interaction partners are highlighted with shaded squares and circles, respectively. The arrows mark the ligation site of nucleophilic and electrophilic fragments. (See Colour Plate Section at the end of this book.)

demand of the side chain has been gradually increased by stepwise fluorination. According to literature arguments the amino acid (S)-trifluoroethyl glycine bearing a trifluoromethyl group instead of an isopropyl group is expected to have steric *effects* that are comparable to those of native leucine. An additional methyl substitution instead of a fluorine substituent exceeds the spatial demand of a CF₃ group and may, therefore, be expected to be comparable to leucine in steric *size*.

Two independent screens have been developed to investigate the effects of fluorinated building blocks on the interactions of the dimeric peptide assembly. The impact of fluorine side chain substitutions on the stability of coiled coil folding has been studied using temperature-dependant CD spectroscopy. The second screen is based on the ability of α -helical peptides to self-replicate. Thus, peptide

sequences that follow the 3–4 heptad repeat motif are able to act as catalysts for the native chemical ligation of two sequence homologs under physiological conditions either as ligases or replicases [64,65]. Our investigations are based on the replicase activity. The initial step of the replication cycle is one spontaneous peptide bond formation between the N-terminal cysteine of the nucleophilic fragment and the C-terminal benzyl thioester of the electrophilic fragment. In the first cycle, the full-length monomer acts as a template for the coiled coil-like assembly of both fragments and the template. This noncovalent association induces a close proximity of the reactive functional groups and thereby promotes fragment condensation via chemical ligation [66]. The mechanism of native chemical ligation and the replicase reaction cycle are shown in Fig. 8. In the last step of the cycle, the dissociation of the coiled coil dimer releases a new monomer, which acts as a catalyst for following replicase cycles. The strength of complementary interactions between the amino acids highly affects association and dissociation and, therefore, determines the overall rate of peptide bond formation. As a result, recording the time dependence of the replication rate provides valuable information about the impact of a certain nonnatural substitution on amino acid interactions within the coiled coil polypeptide environment.

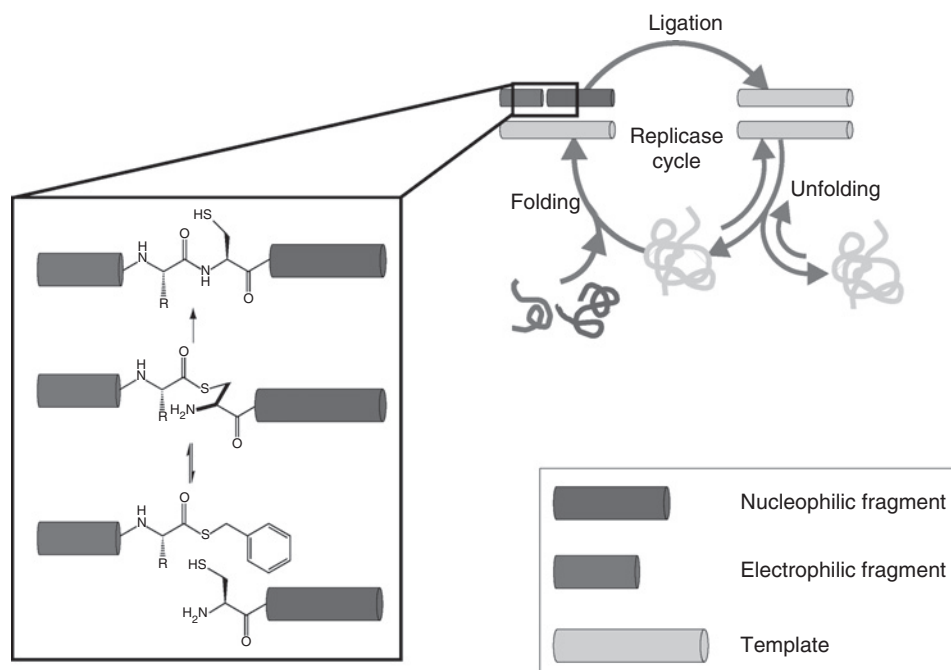


Fig. 8. The replicase reaction cycle with a focus on the native chemical ligation.

3.2.2. Fluorinated alkyl side chains in a hydrophobic environment

The substitution of Leu9 by alanine, ethyl glycine, and its fluorinated derivatives within the hydrophobic core generally decreases the overall thermal stability of the dimer as shown by melting points, which are lowered by 14.9–22.3 K (Fig. 9a).

The decrease in spatial demand of the side chain from isobutyl (Leu) to methyl (Ala) disturbs hydrophobic core packing, which causes severe destabilization of the dimeric assembly. Compared to Leu9Ala, a subsequent increase in spatial demand by side chain elongation to ethyl (EGly) increases the melting point again. The thermal stability of the coiled coil assembly further increases on step-wise fluorination of the EGly residue. The increase in stability correlates with the fluorine content, which indicates an increase in steric demand upon fluorination. Surprisingly, an even further increase in spatial demand by the replacement of one fluorine atom in TfeGly by methyl (Leu9DfpGly) leads to a dramatic loss of structural stability. This peptide, although bearing a side chain that is expected to be most comparable to the leucine side chain, was shown to be even less stable than the peptide with alanine in the same substitution position. This loss of structural integrity is obviously a consequence of fluorine's inductive effect. The stability of the dimer decreases along with the increasing number of hydrogen atoms (TfeGly > DfeGly > DfpGly), which are strongly polarized by the adjacent fluorine atoms. The electrostatic consequences of fluorination can, thus, have a much stronger effect on hydrophobic protein interactions than the increase in molecular volume does. The effects of fluorinated alkyl side chains in hydrophobic protein environments are summarized in Fig. 10.

Substituting a leucine residue within the hydrophobic core as discussed above has been shown to generally retard the replication. EGly side chain fluorination, although it has a stabilizing effect on coiled coil folding, does not accelerate product formation (Fig. 9b). The first step of the cycle is highly dependent on the

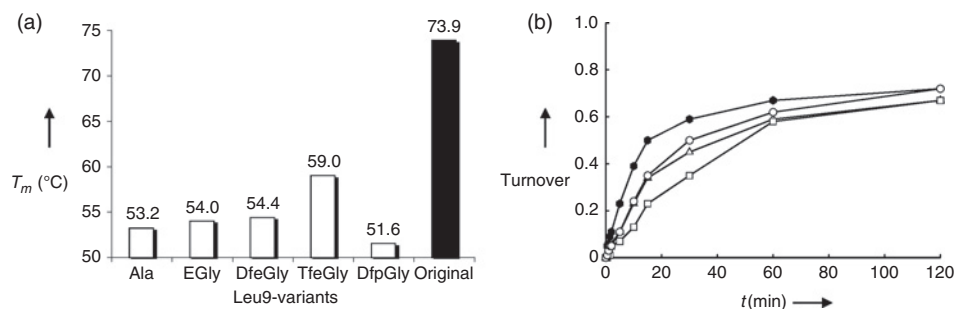


Fig. 9. (a) Melting points and (b) replicase turnover of the Leu9-modified peptides. Parental peptide (filled hexagons); other peptides with the following substitutions: EGly (○), DfeGly (△), TfeGly (□).

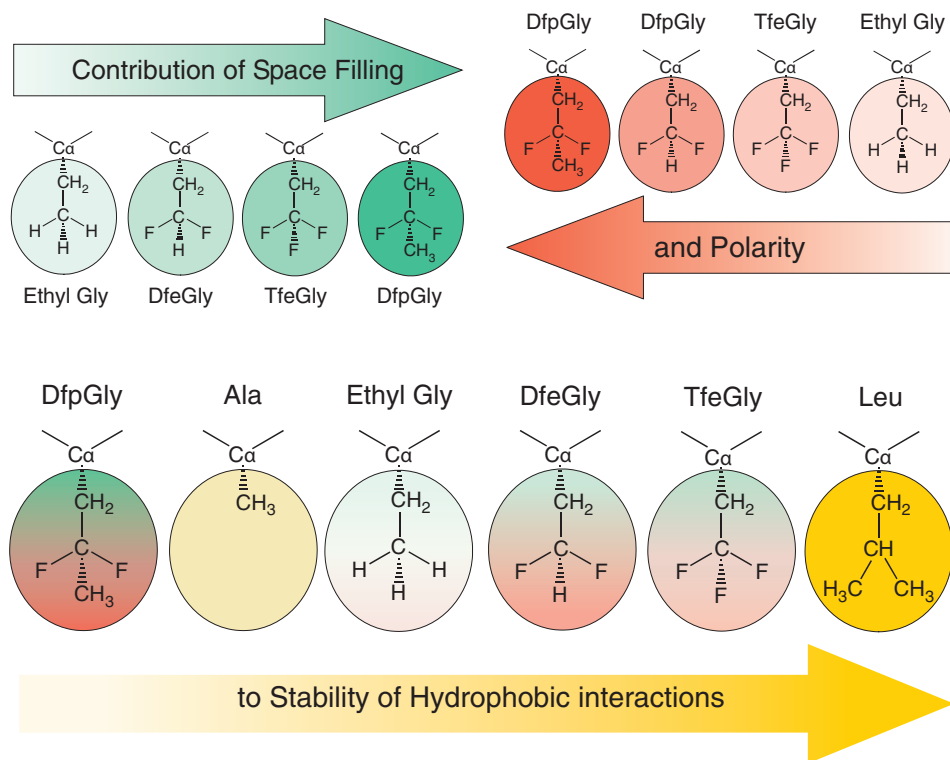


Fig. 10. The contrary effects of spatial demand and polarization on side chain fluorination on hydrophobic interactions. (See Colour Plate Section at the end of this book.)

stability of the complementary hydrophobic interactions between **a** and **d** positions. The association of the electrophilic and nucleophilic fragment should, thus, accelerate on the introduction of a stabilizing amino acid residue. Instead, replicase turnover is decreased. This effect has been shown to correlate with the number of fluorine atoms in the amino acid side chain. Fluorinated side chains, therefore, seem to induce polypeptide interactions that cannot be observed for the fluorine-free counterparts. A possible explanation would be that fluorine–fluorine interactions in the unfolded state of the fluorinated fragments prevent the fragments from properly associating with the template. The higher the degree of fluorination, the more F–F interactions in the unfolded state compete with coiled coil folding and, as a result, shift the equilibrium. Consequently, the association of the two small fragments with the template is retarded and the overall rate of product formation decreases.

3.2.3. Fluorinated alkyl side chains in a hydrophilic environment

Substitutions of Lys8 within the charged domain generally tend to have a lower impact on the thermal stability compared to the same substitutions within the

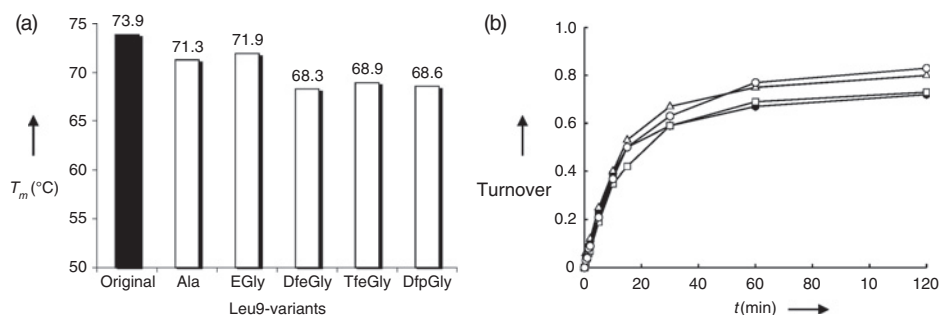


Fig. 11. (a) Melting points and (b) replicase turnover of the Lys8-modified peptides. Parental peptide (filled hexagons); other peptides with the following substitutions: EGly (○), DfeGly (△), TfeGly (□).

hydrophobic core. The loss of one salt bridge between positions g29 and g'8 causes the melting points to be only slightly lowered (Fig. 11a). In addition, the hydrophobic nature of the fluorinated amino acid side chains drives them to be separated from the aqueous solvent. The resulting desolvation of residues within the charged domain causes a general destabilization of the folding motive. Interestingly, the nonfluorinated peptides Lys8Ala and Lys8EGly are slightly more stable than their fluorinated analogs. This indicates an increase in hydrophobicity upon alkyl side chain fluorination. Furthermore, it can be concluded that fluorine–fluorine interactions may shift the folding equilibrium to the unfolded state, thereby generally aiding thermal unfolding.

As shown by several studies, the formation of fluorous cores is a strong driving force. The groups of Kumar [67], Tirrell [68–70], and Marsh [71,72] have shown that highly fluorinated analogs of leucine, isoleucine, and valine can stabilize helical peptide oligomers driven by the preferred interaction of the fluoro alkyl groups with one another. Interactions via fluorine contacts are highly specific as shown by the segregation of fluorinated peptides from similar aliphatic protein interfaces [73]. They are favored even in membrane environments, which emphasizes the *lipophobic* character of fluorinated aliphatic alkyl groups [74–76].

It is interesting that the peptides carrying a substitution within the charged interface show an increase in replicase turnover (Fig. 11b). This may be attributed to an acceleration of the dissociation within the last step of the cycle due to the loss of a single salt bridge. However, the stepwise introduction of fluorine atoms causes the product formation to decelerate. This effect nicely correlates with the fluorine content as previously shown for the Leu9-substituted peptides. Therefore, the interactions of fluorine atoms within the smaller electrophilic fragments show a higher impact on the association with the template than on the dissociation of the full-length coiled coil dimer. This observation is in accordance with those obtained for the stability of Lys8-substituted peptides. Substitutions within the charged domain have been shown to affect the stability as well as

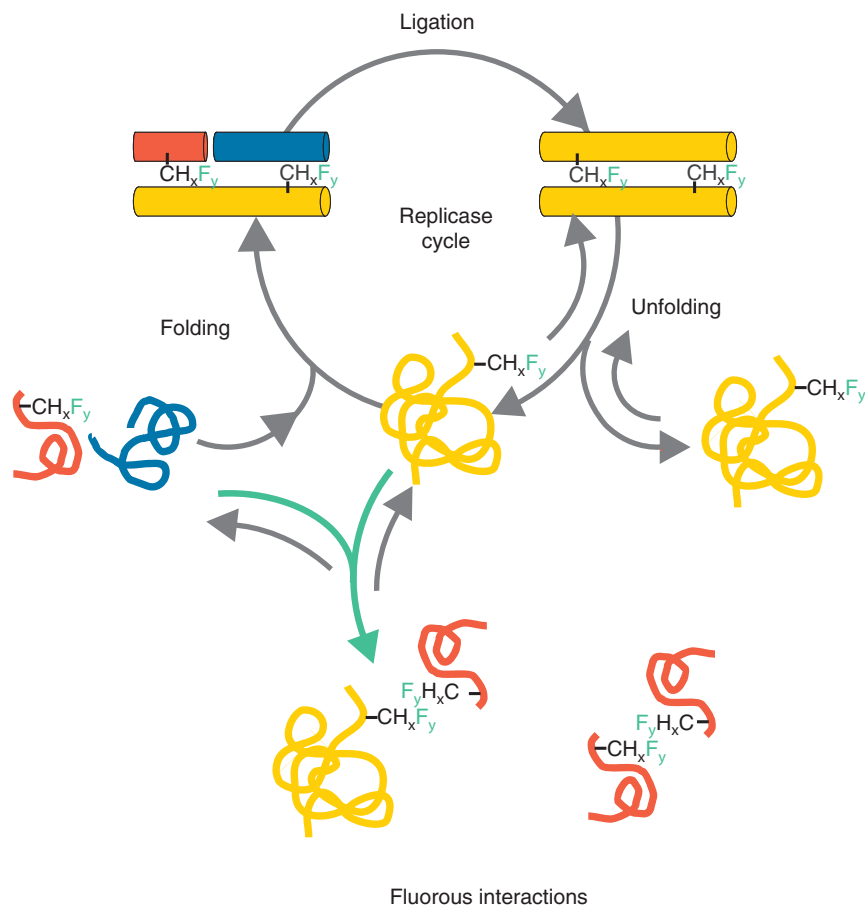


Fig. 12. The template-assisted autocatalyzed peptide replication cycle and the influence of fluorine–fluorine interactions (yellow, template; red, electrophilic fragment; blue, nucleophilic fragment). (See Colour Plate Section at the end of this book.)

the replication to a much lower extent. The replication cycle and the role of the “fluorous effect” on product formation and, therefore, on protein folding are summarized in Fig. 12.

3.2.4. Summary

The α -helical coiled coil-based screening system already provided a wide variety of information about the interactions of fluorinated amino acids within hydrophobic and hydrophilic protein environments. Investigations on the thermal stability as well as the replicase activity have both emphasized the “orthogonal” properties of fluorinated aliphatic amino acid side chains. The term “orthogonal” in this context has been chosen by us to demonstrate that they are in fact hydrophobic

but due to their strong dipoles less lipophilic. Thus, fluorinated amino acids combine properties that are normally considered as orthogonal. Fluorination does increase the spatial demand of a methyl group as shown by the stabilization of hydrophobic core interactions upon EGly side chain fluorination. However, the amino acid TfeGly, which is expected to have the same steric effects as native leucine, causes the stability of the folding motive to decrease. Therefore, the electrostatic consequences of aliphatic fluorination seem to have a stronger impact on hydrophobic interactions than the increase in hydrophobicity. Furthermore, it has to be taken into account that fluorinated amino acids favor fluorine–fluorine interactions that may strongly influence peptide and protein folding.

4. CONCLUSIONS AND FUTURE PERSPECTIVES

We have systematically studied the complex interactions of fluoroalkyl amino acid side chains with native protein environments. In comparison to their alkyl analogs, fluoroalkyl amino acids are characterized by enhanced spatial demand and higher hydrophobicity. At the same time, the increase in polarity on fluorination causes their lipophilicity to decrease. The combination of these “orthogonal” properties causes fluorine’s role in peptide and protein design to be ambiguous. In the context of large proteins, the effects of fluorine substitutions are difficult to predict. As a result, rational peptide and protein design comprising fluorinated amino acids still remains a challenge. However, model studies using appropriate polypeptides that mimic a native protein environment as presented in Section 3.2 have already led to a more comprehensive understanding of peptide interactions directed by fluorinated amino acids:

- Under certain conditions, such as conformational restrictions or absence of any better acceptors, carbon-bound fluorine presumably accepts hydrogen bonds from protein functional groups (Section 2.2.1).
- Fluoroalkyl side chains are hydrophobic but due to the polarization of adjacent hydrogen atoms are also polar and thus disturb hydrophobic-polypeptide interactions (Section 3.3).
- Being highly hydrophobic but less lipophilic than their hydrocarbon analogs, fluoroalkyl amino acid side chains tend to interact with one another by fluorine–fluorine contacts. Therefore, even one single fluorinated amino acid can direct polypeptide folding due to strong character of fluorine–fluorine interactions (Section 3.3 and 3.4).

Our research will further focus on the development of new and related methodologies for the investigation of interactions of carbon-bound fluorine in the context of peptide and protein environments. The rationalization of the properties of side chain-bound fluorine aims at the *de novo* design of peptides and peptide mimetics with new biological and pharmacological properties.

REFERENCES

- [1] N. Sewald, H.D. Jakubke, *Biologically active peptides*, Peptides: Chemistry and Biology Wiley-VCH, Weinheim, 2002, pp. 61–134.
- [2] A. Giannis, T. Kolter, Peptidomimetics for receptor ligands—Discovery, development, and medical perspectives, *Angew. Chem. Int. Ed.* 32(9) (1993) 1244–1267.
- [3] J.C.M. van Hest, D.A. Tirrell, Protein-based materials, toward a new level of structural control, *Chem. Commun.* 19 (2001) 1897–1904.
- [4] A.J. Link, M.L. Mock, D.A. Tirrell, Non-canonical amino acids in protein engineering, *Curr. Opin. Biotechnol.* 14(6) (2003) 603–609.
- [5] G. Jung, A.G. Beck-Sickinger, Multiple peptide synthesis methods and their applications. New synthetic methods (87), *Angew. Chem. Int. Ed.* 31(4) (1992) 367–486.
- [6] K.H. Altmann, M. Mutter, Die chemische Synthese von Peptiden und Proteinen, *Chem. unserer Zeit* 27(6) (1993) 274–286.
- [7] D.Y. Jackson, J. Burnier, C. Quan, M. Stanley, J. Tom, J.A. Wells, A designed peptide ligase for total synthesis of ribonuclease A with unnatural catalytic residues, *Science* 266(5381) (1994) 243–247.
- [8] J.P. Tam, Y.A. Lu, C.F. Liu, J. Shao, Peptide synthesis using unprotected peptides through orthogonal coupling methods, *Proc. Natl. Acad. Sci. USA* 92(26) (1995) 12485–12489.
- [9] J.P. Tam, Q. Yu, Z. Miao, Orthogonal ligation strategies for peptide and protein, *Biopolymers (Peptide Science)* 51(5) (2000) 311–332.
- [10] J.P. Tam, J. Xu, K.D. Eom, Methods and strategies of peptide ligation, *Biopolymers* 60 (3) (2001) 194–205.
- [11] T.W. Muir, D. Sondhi, P.A. Cole, Expressed protein ligation: A general method for protein engineering, *Proc. Natl. Acad. Sci. USA* 95(12) (1998) 6705–6710.
- [12] R. David, M.P.O. Richter, A.G. Beck-Sickinger, Expressed protein ligation, *Eur. J. Biochem.* 271(4) (2004) 663–667.
- [13] V.W. Cornish, D. Mendel, P.G. Schultz, Probing protein structure and function with an expanded genetic code, *Angew. Chem. Int. Ed.* 34(6) (1995) 621–633.
- [14] J.W. Chin, T.A. Cropp, J.C. Anderson, M. Mukherji, Z. Zhang, P.G. Schultz, An expanded eukaryotic genetic code, *Science* 301(5635) (2003) 964–967.
- [15] J.C. Anderson, N. Wu, S.W. Santoro, V. Lakshman, D.S. King, P.G. Schultz, An expanded genetic code with a functional quadruplet codon, *Proc. Natl. Acad. Sci. USA* 101(20) (2004) 7566–7571.
- [16] A. Stormgaard, A.A. Jensen, K. Stormgaard, Site-specific incorporation of unnatural amino acids into proteins, *ChemBioChem* 5(7) (2004) 909–916.
- [17] C. Jäckel, B. Koksche, Fluorine in peptide design and protein engineering, *Eur. J. Org. Chem.* 21 (2005) 4471–4477.
- [18] R. Smits, B. Koksche, How C^α-fluoroalkyl amino acids and peptides interact with enzymes: Studies concerning the influence on proteolytic stability, enzymatic resolution and peptide coupling, *Curr. Top. Med. Chem.* 6(14) (2006) 1483–1498.
- [19] A. Bondi, Van der Waals volumes and radii, *J. Phys. Chem.* 68(3) (1964) 441–451.
- [20] D. O'Hagan, H.S. Rzepa, Some influences of fluorine in bioorganic chemistry, *Chem. Commun.* 7 (1997) 645–651.
- [21] H.J. Böhm, D. Banner, S. Bendels, M. Kansy, B. Kuhn, K. Müller, U. Obst-Sander, M. Stahl, Fluorine in medicinal chemistry, *ChemBioChem* 5(5) (2004) 637–643.
- [22] F.M.D. Ismail, Important fluorinated drugs in experimental and clinical use, *J. Fluorine Chem.* 118(1–2) (2002) 27–33.
- [23] F. Leroux, Atropisomerism, biphenyls, and fluorine: A comparison of rotational barriers and twist angles, *ChemBioChem* 5(5) (2004) 644–649.
- [24] G. Bott, L.D. Field, S. Sternhell, Steric effects: A study of a rationally designed system, *J. Am. Chem. Soc.* 102(17) (1980) 5618–5626.

- [25] I. Riggi, A. Virgili, M. de Moragas, C. Jaime, Restricted rotation and NOE transfer: A conformational study of some substituted (9-anthryl)carbinol derivatives, *J. Org. Chem.* 60(1) (1995) 27–31.
- [26] B.E. Smart, Fluorine substituent effects (on bioactivity), *J. Fluorine Chem.* 109(1) (2001) 3–11.
- [27] P.V. Ramachandran, A.V. Teodorovic', H.C. Brown, Chiral synthesis via organoboranes. 38. Selective reductions. 48. Asymmetric reduction of trifluoromethyl ketones by B-chlorodiisopinocampheylborane in high enantiomeric purity, *Tetrahedron* 49(9) (1993) 1725–1738.
- [28] M. Schlosser, Parametrization of substituents: Effects of Fluorine and other heteroatoms on OH, NH, and CH acidities, *Angew. Chem. Int. Ed.* 37(11) (1998) 1497–1513.
- [29] G.R. Desiraju, Hydrogen bridges in crystal engineering: Interactions without borders, *Acc. Chem. Res.* 35(7) (2002) 565–573.
- [30] H. Takemura, M. Kotoku, M. Yasutake, T. Shinmyozu, 9-Fluoro-18-hydroxy-[3.3]metacyclophane: Synthesis and estimation of a C-F...H-O hydrogen bond, *Eur. J. Org. Chem.* 9 (2004) 2019–2024.
- [31] V.R. Thalladi, H.C. Weiss, D. Bläser, R. Boese, A. Nangia, G.R. Desiraju, C-H...F interactions in the crystal structures of some fluorobenzenes, *J. Am. Chem. Soc.* 120 (34) (1998) 8702–8710.
- [32] T.J. Barbarich, C.D. Rithner, S.M. Miller, O.P. Anderson, S.H. Strauss, Significant inter- and intramolecular O-H...F-C hydrogen bonding, *J. Am. Chem. Soc.* 121(17) (1999) 4280–4281.
- [33] R. Fröhlich, T.C. Rosen, O.G.J. Meyer, K. Rissanen, G. Haufe, New indications for the potential involvement of C-F-bonds in hydrogen bonding, *J. Mol. Struct.* 787(1–3) (2006) 50–62.
- [34] T.A. Evans, K.R. Seddon, Hydrogen bonding in DNA—A return to the *status quo*, *Chem. Commun.* 21 (1997) 2023–2024.
- [35] X. Wang, K.N. Houk, Difluorotoluene, a thymine isostere, does not hydrogen bond after all, *Chem. Commun.* 23 (1998) 2631–2632.
- [36] K.S. Schmidt, R.K.O. Sigel, D.V. Filippov, G.A. van der Marel, B. Lippert, J. Reedijk, Hydrogen bonding between adenine and 2,4-difluorotoluene is definitely not present, as shown by concentration-dependent NMR studies, *New J. Chem.* 24(4) (2000) 195–197.
- [37] E. Carosati, S. Sciabola, G. Cruciani, Hydrogen bonding interactions of covalently bonded fluorine atoms: From crystallographic data to a new angular function in the GRID force field, *J. Med. Chem.* 47(21) (2004) 5114–5125.
- [38] I. Hyla-Kryspin, G. Haufe, S. Grimme, Weak hydrogen bridges: A systematic theoretical study on the nature and strength of C-H...F-C interactions, *Chem. Eur. J.* 10(14) (2004) 3411–3422.
- [39] H. Mollendal, Structural and conformational properties of 1,1,1-trifluoro-2-propanol investigated by microwave spectroscopy and quantum chemical calculations, *J. Phys. Chem. A* 109(42) (2005) 9488–9493.
- [40] L. Shimon, J.P. Glukser, The geometry of intermolecular interactions in some crystalline fluorine-containing organic compounds, *Struct. Chem.* 5(6) (1994) 383–397.
- [41] J.D. Dunitz, R. Taylor, Organic fluorine hardly ever accepts hydrogen bonds, *Chem. Eur. J.* 3(1) (1997) 89–98.
- [42] J.D. Dunitz, Organic fluorine: Odd man out, *ChemBioChem* 5(5) (2004) 614–621.
- [43] J.C. Biffinger, H.W. Kim, S.G. DiMaggio, The polar hydrophobicity of fluorinated compounds, *ChemBioChem* 5(5) (2004) 622–627.
- [44] G. Gerebtzoff, X. Li-Blatter, H. Fischer, A. Frentzel, A. Seelig, Halogenation of drugs enhances membrane binding and permeation, *ChemBioChem* 5(5) (2004) 676–684.
- [45] A.R. Fersht, *Enzyme Structure and Mechanism*, 2nd edition, Freeman, New York, 1985.

- [46] V. Schellenberger, U. Schellenberger, Y.V. Mitin, H.D. Jakubke, Characterization of the S'-subsite specificity of bovine pancreatic α -chymotrypsin via acyl transfer to added nucleophiles, *Eur. J. Biochem.* 187(1) (1990) 163–167.
- [47] H. Dutler, S. Bizzozero, Mechanism of the serine protease reaction. Stereoelectronic, structural, and kinetic considerations as guidelines to deduce reaction paths, *Acc. Chem. Res.* 22(9) (1989) 322–327.
- [48] D. Voet, J.G. Voet, C.W. Pratt, *Fundamentals of Biochemistry—Life at the Molecular Level* 2nd edition, Wiley, USA, 2006, pp. 346–350.
- [49] J. Rizo, L.M. Gierasch, Constrained peptides: Models of bioactive peptides and protein substructures, *Ann. Rev. Biochem.* 61 (1992) 387–418.
- [50] G. Valle, M. Crisma, C. Toniolo, S. Polinelli, W.H.J. Boesten, H.E. Schoemaker, E. M. Meijer, J. Kamphuis, Peptides from chiral C $^{\alpha}$, α -disubstituted glycines. Crystallographic characterization of conformation of C $^{\alpha}$ -methyl, C $^{\alpha}$ -isopropylglycine [(α Me)Val] in simple derivatives and model peptides, *Int. J. Pept. Protein Res.* 37(6) (1991) 521–527.
- [51] V.A. Bindra, A. Kuki, Conformational preferences of oligopeptides rich in α -aminoisobutyric acid. III. Design, synthesis and hydrogen bonding in 310-helices, *Int. J. Pept. Protein Res.* 44(6) (1994) 539–548.
- [52] K.H. Altmann, E. Altmann, M. Mutter, Conformational studies on peptides containing enantiomeric α -methyl- α -amino acids. Part I. Differential conformational properties of (*R*)- and (*S*)-2-methylaspartic acid, *Helv. Chim. Acta* 75(4) (1992) 1198–1210.
- [53] B. Kokschi, N. Seewald, K. Burger, H.D. Jakubke, Peptide modification by incorporation of α -trifluoromethyl substituted amino acids, *Amino Acids* 11(3–4) (1996) 425–434.
- [54] B. Kokschi, N. Seewald, H.J. Hofmann, K. Burger, H.D. Jakubke, Proteolytically stable peptides by incorporation of α -Tfm amino acids, *J. Pept. Sci.* 3(3) (1997) 157–167.
- [55] I. Schechter, A. Berger, On the size of the active site in proteases. I. Papain, *Biochem. Biophys. Res. Commun.* 27(2) (1967) 157–162.
- [56] T. Michel, B. Kokschi, S.N. Osipov, A.N. Golubev, J. Sieler, K. Burger, Peptide synthesis with α -(difluoromethyl)-substituted α -amino acids, *Coll. Czech. Chem. Commun.* 67(10) (2002) 1533–1559.
- [57] C. Toniolo, F. Fromaggio, M. Crisma, G.M. Bonora, S. Pegoraro, S. Polinelli, W.H. J. Boesten, H.E. Schoemaker, Q.B. Broxterman, J. Kamphuis, Synthesis, characterization, and solution conformational analysis of C $^{\alpha}$ -methyl-, C $^{\alpha}$ -benzylglycine [(α Me)Phe] model peptides, *Pept. Res.* 5(1) (1992) 56–61.
- [58] V. Mat'ha, A. Jegerov, M. Kiess, H. Brückner, Morphological alterations accompanying the effect of peptaibiotics, α -aminoisobutyric acid-rich secondary metabolites of filamentous fungi, on *Culex pipiens* larvae, *Tissue Cell* 24(4) (1992) 559–564.
- [59] A. Tulinsky, R.A. Belvins, Structure of a tetrahedral transition state complex of α -chymotrypsin dimer at 1.8-Å resolution, *J. Biol. Chem.* 262(16) (1987) 7737–7743.
- [60] A. Rose, I. Meier, Scaffolds, levers, rods and springs: Diverse cellular functions of long coiled-coil proteins, *Cell. Mol. Life Sci.* 61(16) (2004) 1996–2009.
- [61] J.M. Mason, K.M. Arndt, Coiled coil domains: Stability, specificity, and biological implications, *ChemBioChem* 5(2) (2004) 170–176.
- [62] K. Pagel, B. Seiwert, K. Seeger, S. Berger, A. Mark, B. Kokschi, Advanced approaches for the characterization of a *de novo* designed antiparallel coiled-coil peptide, *Org. Biomol. Chem.* 3(7) (2005) 1189–1194.
- [63] C. Jäckel, W. Seufert, S. Thust, B. Kokschi, Evaluation of the molecular interactions of fluorinated amino acids with native polypeptides, *ChemBioChem* 5(5) (2004) 717–720.
- [64] C. Jäckel, M. Salwiczek, B. Kokschi, Fluorine in a native polypeptide environment—How the spatial demand and polarity of fluoroalkyl groups affect protein folding, *Angew. Chem. Int. Ed.* 45(25) (2006) 4198–4203.
- [65] K. Severin, D.H. Lee, J.A. Martinez, M.R. Ghadiri, Peptide Self-Replication Via Template-Directed Ligation, *Chem. Eur. J.* 3(7) (1997) 1017–1024.
- [66] A. Saghatelian, Y. Yokobayashi, K. Soltani, M.R. Ghadiri, A chiroselective peptide replicator, *Nature* 409 (2001) 797–801.

- [67] P.E. Dawson, T.W. Muir, I. Clark-Lewis, S.B.H. Kent, Synthesis of proteins by native chemical ligation, *Science* 266(5186) (1994) 776–779.
- [68] N.C. Yoder, K. Kumar, Fluorinated amino acids in protein design and engineering, *Chem. Soc. Rev.* 31(6) (2002) 335–341.
- [69] Y. Tang, G. Ghirlanda, W.A. Petka, T. Nakajima, W.F. DeGrado, D.A. Tirrell, Fluorinated coiled coil proteins prepared *in vivo* display enhanced thermal and chemical stability, *Angew. Chem. Int. Ed.* 40(8) (2001) 1494–1496.
- [70] Y. Tang, G. Ghirlanda, N. Vaidehi, J. Kua, D.T. Mainz, W.A. Goddard III, W. F. DeGrado, D.A. Tirrell, Stabilization of coiled coil peptide domains by introduction of trifluoroleucine, *Biochemistry* 40(9) (2001) 2790–2796.
- [71] Y. Tang, D.A. Tirrell, Biosynthesis of a highly stable coiled coil protein containing hexafluoroleucine in an engineered bacterial host, *J. Am. Chem. Soc.* 123(44) (2001) 11089–11090.
- [72] K.H. Lee, H.Y. Lee, M.M. Slutsky, J.T. Anderson, E.N.G. Marsh, Fluorous effect in proteins: *De novo* design and characterization of a four- α -helix bundle protein containing hexafluoroleucine, *Biochemistry* 43(51) (2004) 16277–16248.
- [73] H.Y. Lee, K.H. Lee, H.M. Al-Hashimi, E.N.G. Marsh, Modulating protein structure with fluorous amino acids: Increased stability and native-like structure conferred on a 4-helix bundle protein by hexafluoroleucine, *J. Am. Chem. Soc.* 128(1) (2006) 337–343.
- [74] B. Bilgiçer, K. Kumar, Synthesis and thermodynamic characterization of self-sorting coiled coils, *Tetrahedron* 58(20) (2002) 4105–4112.
- [75] B. Bilgiçer, K. Kumar, De novo design of defined helical bundles in membrane environments, *Proc. Natl. Acad. Sci. USA* 101(43) (2004) 15324–15329.
- [76] N. Naarmann, B. Bilgiçer, H. Meng, K. Kumar, C. Steinem, Fluorinated interfaces drive self-association of transmembrane α -helices in lipid bilayers, *Angew. Chem. Int. Ed.* 45 (16) (2006) 2588–2591.
- [77] A. Niemz, D.A. Tirrell, Self-association and membrane-binding behavior of melittins containing trifluoroleucine, *J. Am. Chem. Soc.* 123(30) (2001) 7407–7413.

This page intentionally left blank

CHAPTER 18

Biological Fluorination in *Streptomyces cattleya*: The Fluorinase

Hai Deng,¹ Fang-Lu Huang,² James H. Naismith,¹ David O'Hagan,^{1,*}
Jonathan B. Spencer,² and Xiaofeng Zhu¹

¹*School of Chemistry and Centre for Biomolecular Sciences, University of St Andrews,
North Haugh, St Andrews, KY16 9ST, UK*

²*The University Chemical Laboratory, Lensfield Road, Cambridge, CB2 1EW, UK*

Contents

1. Introduction	761
2. Characterisation of the fluorinase	764
3. Mechanism of the fluorinase	765
4. Reversibility of the fluorinase	768
5. The fluorinase is a chlorinase	768
6. Substrate specificity	770
7. Genetic basis of fluorination in <i>S. cattleya</i>	771
8. The biosynthetic pathway to fluoroacetate and 4-fluorothreonine	772
9. The fluorinase as a tool for synthesis and formation of C– ¹⁸ F bonds for positron emission tomography	774
References	776

Abstract

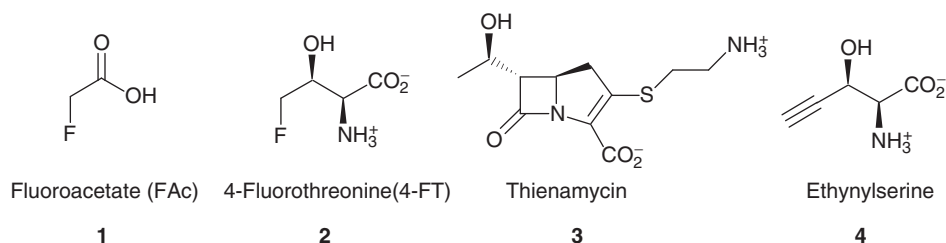
Recent developments on research into a bacterial C–F bond forming enzyme are reviewed. The fluorinase enzyme was isolated from *Streptomyces cattleya* in 2002 and shown to catalyse the conversion of fluoride ion and S-adenosyl-L-methionine (SAM) to 5'-fluoro-5'-deoxyadenosine (5'-FDA) and L-methionine. Subsequently, the enzyme has been the subject of cloning, crystallisation, mechanism and substrate specificity studies. This review summarises the current status of this research.

1. INTRODUCTION

In 1986, a research group from Merck discovered that the soil bacterium *Streptomyces cattleya* was able to elaborate two fluorinated metabolites. *S. cattleya* is

*Corresponding author.;
Email: do1@st-andrews.ac.uk

the producing organism for the β -lactam antibiotic, thienamycin **3**, and during the efforts by Merck to improve the production titre of this antibiotic, they discovered a novel antibiotic activity when a particular soya protein was used in the fermentation nutrient. It subsequently transpired that the soya protein had significant levels of fluoride ion and that the novel antibiotic activity was due to 4-fluorothreonine (4-FT) **2** production [1].



If exogenously added fluoride was used to supplement cell growth, then both fluoroacetate (FAC) **1** and 4-FT **2** accumulated in the fermentation media of *S. cattleya*. In fact at millimolar concentrations, all of the added fluoride could be converted to these organo-fluorine metabolites in a batch fermentation. FAC **1** is a well-known toxin, and had already been identified as a natural product in many highly toxic plant species, particularly in plants from Africa and Australia [2]. 4-FT **2** was purified from *S. cattleya* based on its antibiotic activity and it was subsequently shown to have the L-threonine absolute stereochemistry [3]. Its mode of action as an antibiotic has not been determined, but it is interesting that it is a direct analogue of the amino acid L-threonine and presumably its role lies in its ability to mimic this amino acid in some metabolic transformation. Interestingly, the same organism also produces ethynylserine **4** [4], another threonine analogue with antibiotic activity.

The identification of the fluorinated metabolites **1** and **2** from *S. cattleya* immediately raised the question as to how inorganic fluoride was converted to organic fluorine and clearly the organism has an enzyme capable of forming a C–F bond. We began a biosynthetic investigation on this organism with a particular focus on identifying the fluorination activity [5]. Early experiments focused on cell-free transformations and the first significant step towards identifying the fluorination enzyme involved a cell-free extract incubation of ATP **7** and fluoride ion. Cell-free extracts were generated by sonication of washed cell suspensions in a buffer, followed by removal of the cell wall debris by centrifugation. The resultant protein solution contains all of the enzymes liberated from the cells, and this solution can then be assayed for individual enzyme activities, and forms the starting point for enzyme purification. The reaction of ATP **7** and fluoride ion in the cell-free extract was followed by ¹⁹F NMR and the progress of enzymatic fluorination monitored over time. A typical ¹⁹F NMR profile is shown in Fig. 1. It was observed that

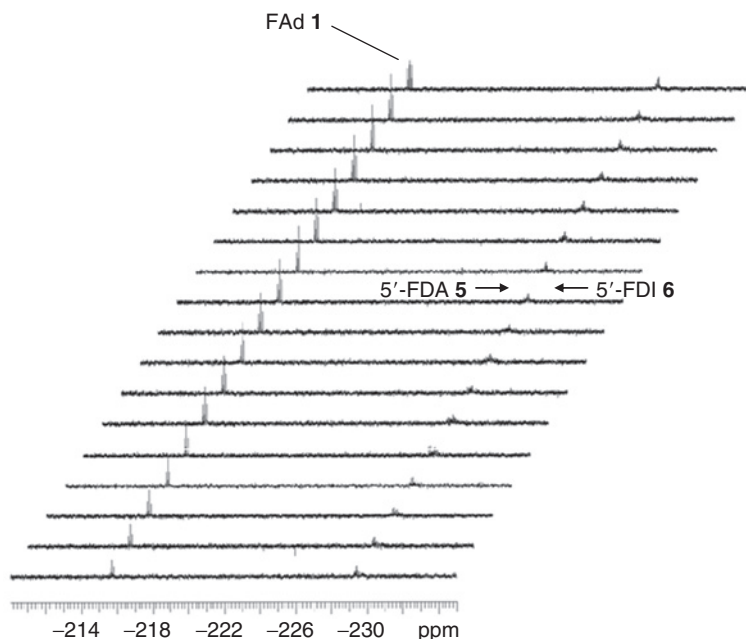
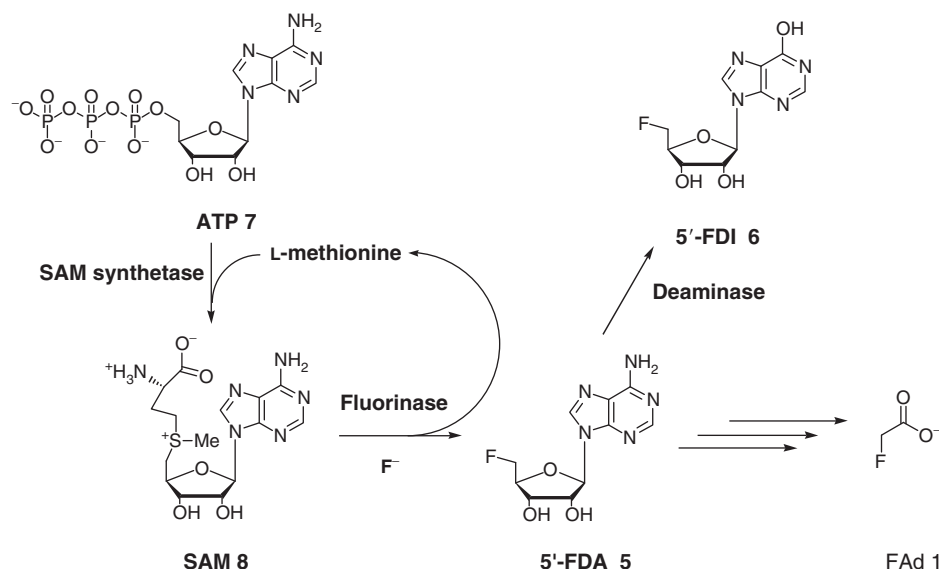


Fig. 1. ^{19}F NMR time course of the *Streptomyces cattleya* cell-free extract incubation of ATP **7** and fluoride ion in buffer, monitored every hour for 17 h. Three fluorine containing products are apparent. These are 5'-FDA **5**, 5'-FDI **6** and FAc **1** [6].

ATP **7** was converted to two, at that time unknown organo-fluorine compounds, 5'-fluoro-5'-deoxyadenosine (5'-FDA) **5** and 5'-fluoro-5'-deoxyinosine (5'-FDI) **6** as well as FAc **1** [6].

It was interesting that the cell-free extract had the capacity to support the biosynthesis all the way to FAc **1**, an end product of one of the fluorometabolite pathways. This observation indicates that all of the enzymes and cofactors required to support FAc biosynthesis were present and active in the cell-free extract, even though the integrity of the cells had been destroyed. This experiment showed that organic fluoride production was achievable *in vitro* from the *S. cattleya* protein extract. Subsequent purification of the fluorinase (5'-fluoro-5'-deoxyadenosine synthase), using standard purification protocols revealed that the true substrate for the enzyme was SAM **8** and not ATP **7** [8]. It transpired that ATP **7** and L-methionine (L-Met) were converted to SAM **8** in the crude cell-free extract and that the resultant SAM **8** was then processed by the fluorinase with the release of L-Met. Thus, a catalytic cycle where L-Met was regenerated to drive these two reactions had been inadvertently established (Scheme 1). The fluorinase catalyses the conversion of SAM **8** and fluoride ion to make 5'-FDA **5** as shown in Scheme 1 [8].



Scheme 1. The reactions of the *Streptomyces cattleya* cell-free extract incubation of ATP 7 and fluoride ion, illustrating the formation of 5'-FDA 5, 5'-FDI 6 and FAd 1. L-methionine is recycled between SAM synthetase and the fluorinase [7].

2. CHARACTERISATION OF THE FLUORINASE

The fluorinase enzyme was purified by standard protein purification methods with an HPLC assay monitoring the conversion of SAM 8 to 5'-FDA 5, to identify the active protein fractions [9]. It is a relatively robust protein with no particular problems associated with its stability during purification or on storage. Overall, it is a slow enzyme with a low k_{obs} . The origin of this relative inefficiency lies in a high K_m for fluoride ion, which is in the millimolar range, and a low k_{cat} . Also, it is an enzyme with quite complex kinetics and in particular it shows product (5'-FDA 5) inhibition and as 5 accumulates, the rate of the reaction slows further. This turnover problem is solved in the whole organism by coupling the fluorinase activity to the second enzyme on the metabolic pathway, a purine nucleotide phosphorylase (*vide infra*) which rapidly depletes 5'-FDA 5.

Amino acid sequence analysis of the purified protein, obtained by Edman degradation, provided sections of partial amino acid sequence and this sequence information allowed the construction of DNA primers for amplification of the fluorinase gene (*flA*) from *S. cattleya* genomic DNA, using the polymerase chain reaction (PCR). The fluorinase gene was located and cloned in this manner in collaboration with Dr. Joe Spencer's laboratory at Cambridge University. This then enabled the fluorinase gene to be identified and amplified. The gene was placed into the pET28a(+) plasmid for over-expression in *E. coli* BL21(DE3) cells.

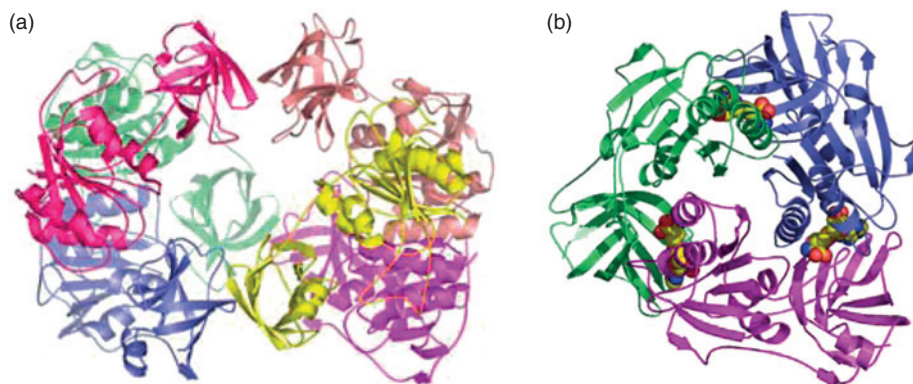


Fig. 2. A representation of the X-ray-derived structure of the fluorinase. Inset (a) shows the full structure as a hexamer (dimer of trimers) and inset (b) shows the protein trimer with three *S*-adenosyl-L-methionine (SAM) **8** substrate molecules bound at the subunit interfaces [10]. (See Colour Plate Section at the end of this book.)

With over-expressed protein available in milligram quantities, the enzyme was crystallised and its structure was solved by X-ray diffraction analysis [10].

The X-ray structural study revealed an enzyme that was a dimer of trimers as illustrated in Fig. 2. The monomeric unit represented a new protein fold with no previously solved analogues in the gene or protein sequence databases. SAM **8** binds at three sites in the trimer, a binding site located at the three subunit interfaces. A closer inspection of SAM **8** bound to the enzyme reveals that the ribose sugar ring has the four ring carbons essentially in a plane, an unusually strained conformation for the ribose moiety of nucleotides on a protein. This is shown in Fig. 3. The planarity appears to be held by a hydrogen bonding array between the 2' and 3' hydroxyl groups of the ribose and the carboxylate residue of Asp-16 as shown in Fig. 3. It is also anchored by a hydrogen bond to the backbone NH of Tyr-77.

3. MECHANISM OF THE FLUORINASE

The fluorinase enzyme mediates a substitution reaction whereby fluoride ion displaces L-methionine with formation of a C–F bond and cleavage of a C–S bond. In order to explore the mechanism in detail, the process has been explored both experimentally and theoretically. The stereochemical course of the reaction was of immediate interest, particularly to delineate between direct inversion or double inversion during the substitution process. A direct substitution will proceed with inversion of configuration at the C5' carbon, whereas a double inversion process will proceed with an overall retention of configuration at the C-5' carbon. To explore this, it was important to prepare SAM **8** carrying a stereospecifically

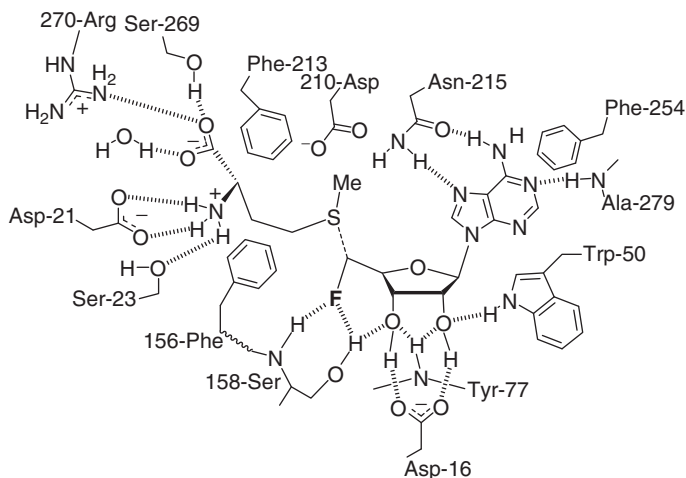
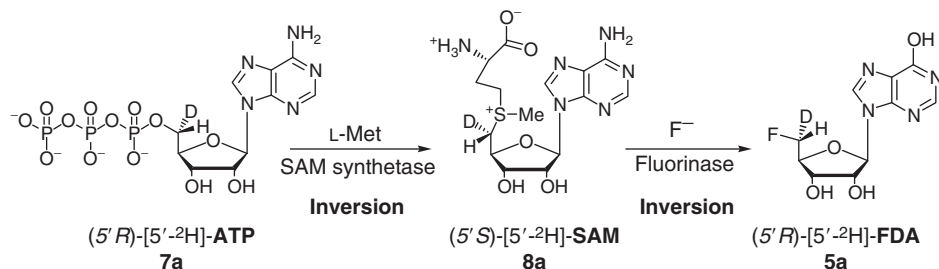


Fig. 3. S-adenosyl-L-methionine (SAM) **8** bound to the fluorinase showing hydrogen bonding contacts [10].

positioned deuterium isotope C-5'. In the event, a sample of SAM **8** was synthesised with deuterium at the 5'-*pro-S* site of SAM **8**. This substrate was prepared enzymatically using SAM synthetase, from a sample of (5'*R*)-[5'-²H]-ATP **7a**, which was itself prepared by a previously established synthetic method [11]. Incubation of (5'*S*)-[5'-²H]-SAM **8a** with the fluorinase generated a sample of (5'*R*)-[5'-²H]-FDA **5a** with a 'chiral fluoromethyl' group. A challenge was to establish the absolute stereochemistry at the resultant C-5' centre of 5'-FDA **5**. This aspect of the experiment was achieved by using chiral liquid crystalline ²H NMR in collaboration with Jacques Courtieu and Abdelkrim Meddour at the CNRS, Orsay. When the ²H NMR of (5')- **5a** or (5'*S*)- [5'-²H]-FDA **5b** is recorded in a chloroform solution of poly- γ -benzyl-L-glutamate, the medium forms a lyotropic liquid crystalline phase, and the quadrupolar deuterium nucleus of (*R*)-**5a** or (*S*)-[5'-²H]-FDA **5b** interacts differently with the chiral medium generating signals with distinct chemical shifts and distinct deuterium quadrupolar couplings. Using a synthetic reference sample of (5'*S*)-[5'-²H]-FDA **5b**, it was established that the material from the enzymatic reaction had the 5'*R* configuration at C-5' of 5'-FDA **5a**, and thus that an inversion of configuration had occurred during the fluorinase reaction. This is summarised in Scheme 2. The experiment supported a straightforward S_N2 reaction mechanism for fluorinase-mediated C–F bond formation [12].

This mechanistic conclusion is further supported by a recent QM/MM theory study [13] where the conformation of the reactants and products in the reactive complexes and of the transition state has been examined. Both the crystallographic [10] and theory studies [13] suggest that fluoride ion is stripped of all of its hydrated water and that this heat of hydration loss is compensated for by at least three hydrogen bonds to the surface of the protein. Fluoride ion makes



Scheme 2. The stereochemical course of the fluorinase reaction was established by stereospecific labelling at C-5' of ATP **7** and SAM **8** with deuterium. The fluorinase reaction proceeds with an inversion of configuration [12].

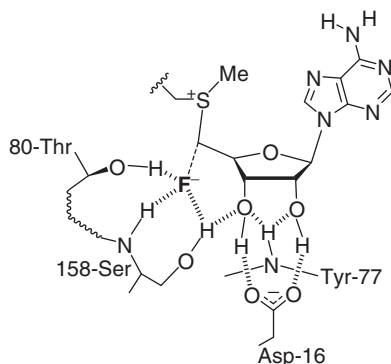


Fig. 4. Working hypothesis for fluoride ion hydrogen bonding prior to nucleophilic attack at the active site of the fluorinase as deduced by X-ray crystallography [10] and QM/MM calculations [13].

hydrogen bonding contacts to both the NH and OH hydrogens of Ser-158 in the reactive complex and possibly also to the OH side chain of Thr-80 in the transition state. This last contact is not observed in the ground state X-ray-derived structures but was a conclusion drawn for the theory study as shown in Fig. 4. It remains to be experimentally verified.

The enzyme appears to catalyse the reaction by predisposition of these hydrogen bonding interactions and the calculated activation energy is 53 kJ mol^{-1} . This is a significant lowering of the activation barrier compared to the barrier found in the solution reaction (92 kJ mol^{-1}) and represents an enzymatic rate acceleration of one million fold. In another theory study [14] which modelled this reaction in a simulated water matrix, the electrostatic interaction between F^- and the positively charged sulphur (R_3S^+) of SAM **8** was deduced to confer significant stability to the reaction complex. These theory studies also support a

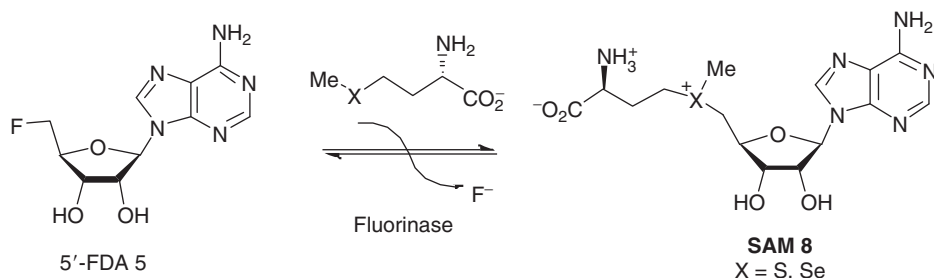
mechanism where the fluorination reaction occurs by an S_N2 reaction process consistent with the stereochemical study with deuterium labelling at C5' as described above.

4. REVERSIBILITY OF THE FLUORINASE

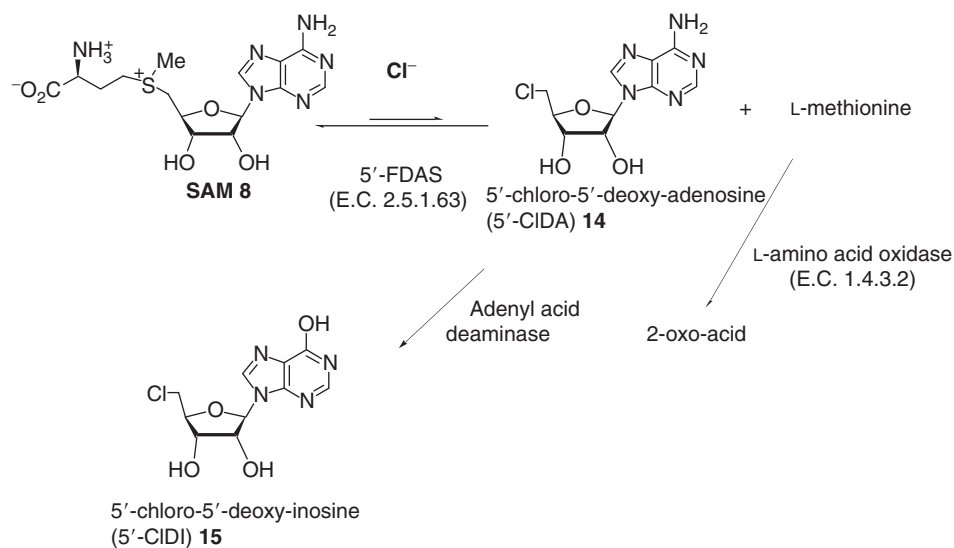
Despite the high bond dissociation energy of the C–F bond, the fluorinase is also able to operate in the reverse direction. Incubation of 5'-FDA **5** with L-[^{13}C -methyl]-methionine resulted in the formation of [^{13}C -methyl]-SAM **8c** as illustrated in Scheme 3. A similar experiment with L-selenomethionine (L-Se-Met) and 5'-FDA **5** resulted in a more efficient reaction (sixfold) to generate L-Se-SAM, which was readily identifiable via a mass spectral fragmentation product (MeSeAdo) by its signature isotope fingerprint again by LC-MS. Comparison of the V_{max} calculated at saturating kinetics, for assays run in each direction, indicated that the equilibrium lies in favour of 5'-FDA **5**.

5. THE FLUORINASE IS A CHLORINASE

Efforts to replace fluoride by chloride ion as a substrate for the fluorinase do not result in the efficient production of 5'-chloro-5'-deoxyadenosine (5'-CIDA) **14**. This is due to the equilibrium of the chloride reaction lying significantly in favour of substrate ($\text{Cl}^- + \text{SAM}$) over products (5'-CIDA **14** and L-Met), rather than an inherent inability of the fluorinase to activate chloride toward nucleophilic attack. This was revealed in two separate coupled enzyme assays which were designed to shift the equilibrium of the reaction towards the organo-chlorine product 5'-CIDA **14** as shown in Scheme 4. The first of these involved an assay in which the fluorinase was coupled to an L-amino acid oxidase. Removal of L-methionine, the co-product of halide substitution by enzymatic oxidation, inhibits the reverse reaction. In the eventm this assay generated 5'-CIDA **14** and allowed the detection of this product from SAM **8** and chloride.



Scheme 3. The fluorinase operates in reverse with both L-Met and L-Se-Met.



Scheme 4. Coupled enzyme assays shifting the fluorinase reaction in favour of 5'-chloro-5'-deoxyadenosine (5'-CIDA) **14** synthesis [15].

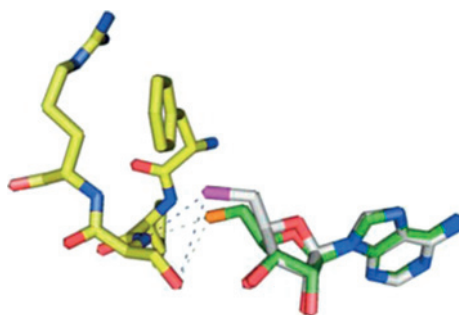


Fig. 5. The X-ray-derived structure of the 5'-chloro-5'-deoxyadenosine (5'-CIDA)-fluorinase co-complex overlaid with the 5'-FDA structure. It can be seen that the chlorine atom is displaced relative to the location of the fluorine due to its larger size [15]. (See Colour Plate Section at the end of this book.)

A related experiment involved a coupled fluorinase/adenyl acid deaminase (*Aspergillus* sp.) assay. In this reaction, the resultant 5'-CIDA **14** is converted to 5'-chloro-5'-deoxyinosine (5'-CIDI) **15**. These experiments indicate that the fluorinase can process chloride ion in a similar manner to fluoride.

The product, 5'-CIDA **14** was co-crystallised with the fluorinase but without added L-Met. This resulted in a structure with 5'-CIDA **14** bound to the active site of the enzyme as shown in Fig. 5 [15].

The use of either chloride ion in the forward direction and 5'-CIDA **14** in the reverse extends the repertoire of the fluorinase and also reveals a novel nucleophilic enzymatic chlorination reaction.

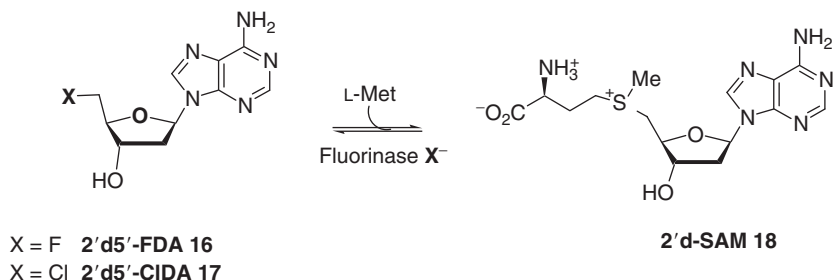
6. SUBSTRATE SPECIFICITY

Substrate specificity studies have revealed that the fluorinase can catalyse the conversion of 2'-deoxyadenosine substrates **16** and **17** to 2'-d-SAM **18** (Scheme 5).

Both the 2'-d-F and 2'-d-Cl analogues **16** and **17** were synthesised and assessed as substrates in these experiments and although both were less efficient than 5'-FDA **5**, the chloro analogue showed about 50% activity and the fluoro analogue about 10% activity relative to the natural substrate. Removal of the hydrogen bonding interaction between the 2'-hydroxyl group and Asp-16 surprisingly does not appear to kill this reaction [16].

To gain further insight into how these substrates bind at the active site, a co-crystallisation study of 2'-d-FDA **16** with the fluorinase was carried out for X-ray structure analysis and the resultant structure is shown in Fig. 6. The analogue 2'-d-FDA **16** bound at the active site is overlaid with 5'-FDA **5**. It is clear that the orientation and conformation of the ribose ring is altered. The 2-deoxy-ribose ring is puckered in a more classical conformation, whereas 5'-FDA **5** has a planar and more highly strained conformation. The aspartate carboxylate has moved a little towards the 2'-OH group and the 3'-OH moved in the other direction to accommodate a more central bifurcated hydrogen bond.

With the fluorinase gene cloned, gene walking experiments have been carried out to explore the genes immediately surrounding the fluorinase (*flA*) gene [17]. This sequencing study revealed a 10-kb DNA fragment which contains about 12 genes. These genes were all tentatively assigned a function based on sequence homologies to known genes (Fig. 7).



Scheme 5. 2'-Deoxyanalogues are substrates for the fluorinase.

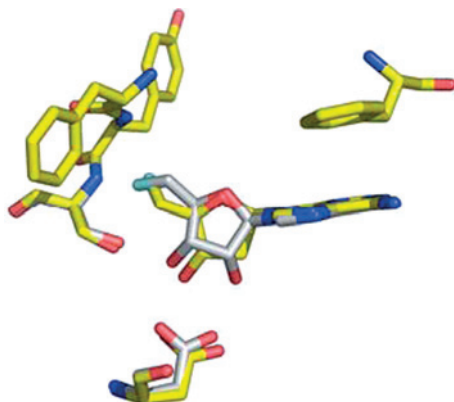


Fig. 6. Structure of the 2'-d-FDA **16**-fluorinase co-complex, overlaid with the structure of 5'-FDA **5** bound to the enzyme [16]. (See Colour Plate Section at the end of this book.)

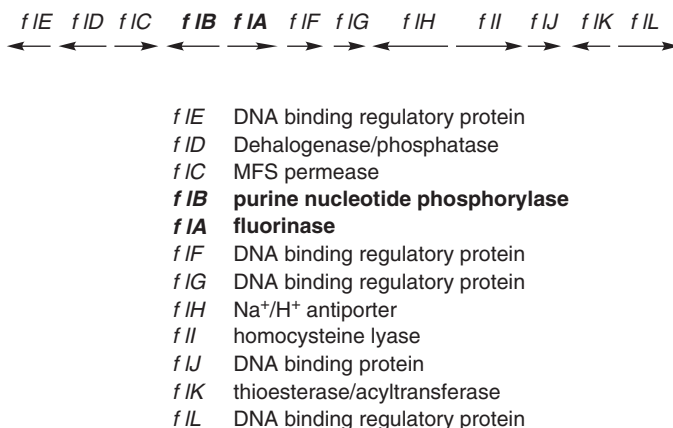
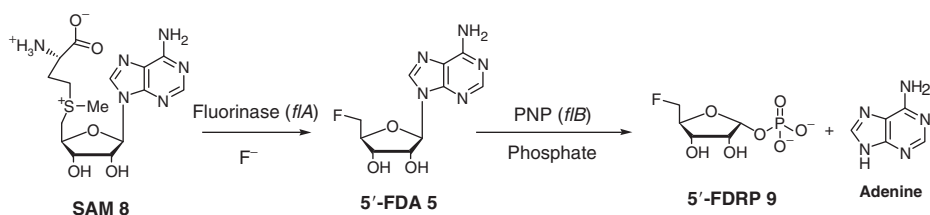


Fig. 7. Relative arrangement and annotation of a 10-kb gene cluster around the fluorinase gene (*flA*) of *Streptomyces cattleya*. The *flB* gene codes the second step on the biosynthesis pathway to the fluorometabolites, operating directly after the fluorinase [17].

7. GENETIC BASIS OF FLUORINATION IN *S. CATTLEYA*

Immediately adjacent to the fluorinase gene (*flA*) is a purine nucleotide phosphorylase (PNP) gene (*flB*), and this gene codes for the next enzyme on the biosynthetic pathway to the fluorometabolites, FAc **1** and 4-FT **2**. This enzyme was already purified from *S. cattleya* and was shown to mediate the phosphorolytic cleavage of 5'-FDA **5** to generate 5-fluoro-5-deoxy ribose-1-phosphate (FDRP) **9**. When the product of the *flB* gene was cloned and over-expressed, it was found to mediate an identical reaction confirming its role and relationship to the fluorinase



Scheme 6. The reactions of the *flA* and *flB* gene products, the fluorinase and a PNP constitute the first two steps in fluorometabolite biosynthesis.

gene. Thus, the genes for the first two enzymes on the pathway lie immediately adjacent to each other on the *S. cattleya* genome as illustrated in Scheme 6.

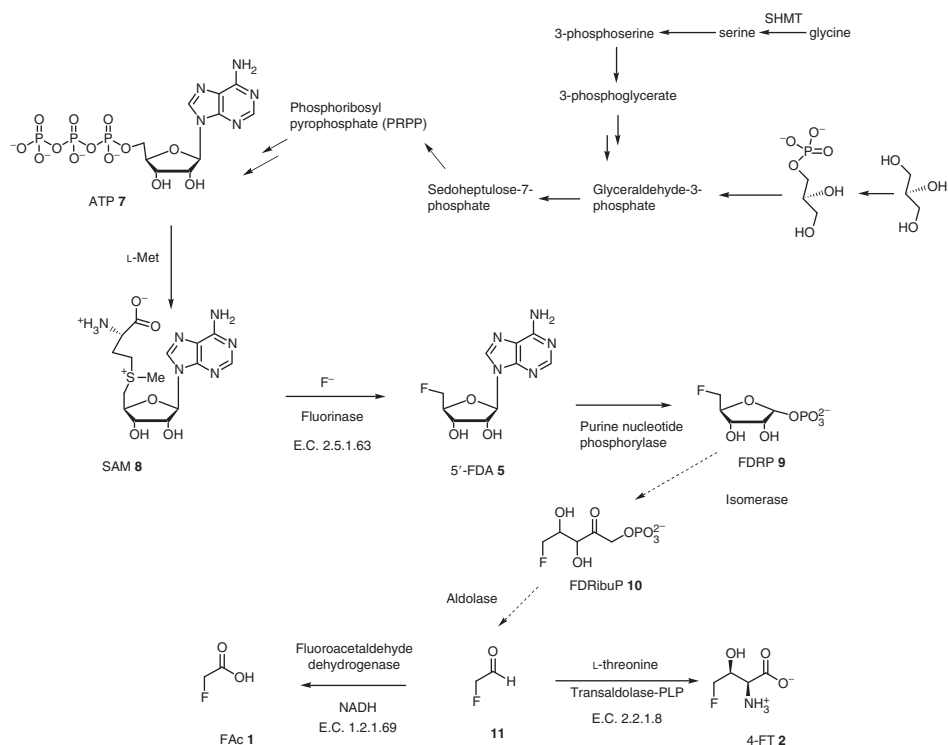
Further analysis of the gene cluster did not reveal any more biosynthetic genes; however, many of the genes appear to be involved in the management of fluoride ion uptake and fluorometabolite toxicity. Intriguingly, *flK* has homology to a thioesterase and appears to be the fluoroacetate resistance gene. FAc **1** is toxic because it is converted to fluoroacetyl-CoA in the cells and then to fluorocitrate by the action of citrate synthase. Some plants have developed a resistance mechanism to this toxin by possessing a thioesterase which rapidly hydrolyses fluoroacetyl-CoA to FAc, keeping it in the metabolically benign form. The product of the *flK* gene does this. The enzyme has been over-expressed and shown to rapidly hydrolyse fluoroacetyl-CoA but it does not hydrolyse acetyl-CoA. Other genes in the cluster may code for management proteins possibly for importing, for example, fluoride/FAc (*flC*, *flH*) in and out of the cell. A gene coding for *S*-adenosylhomocysteine lyase (*flI*) is present in the cluster. *S*-Adenosylhomocysteine (SAH), which is the demethylated form of SAM **8**, is a potent inhibitor of the fluorinase [9], and the role of this enzyme appears to be to reduce intracellular SAH levels to maximise the efficiency of the fluorinase.

8. THE BIOSYNTHETIC PATHWAY TO FLUOROACETATE AND 4-FLUOROTHREONINE

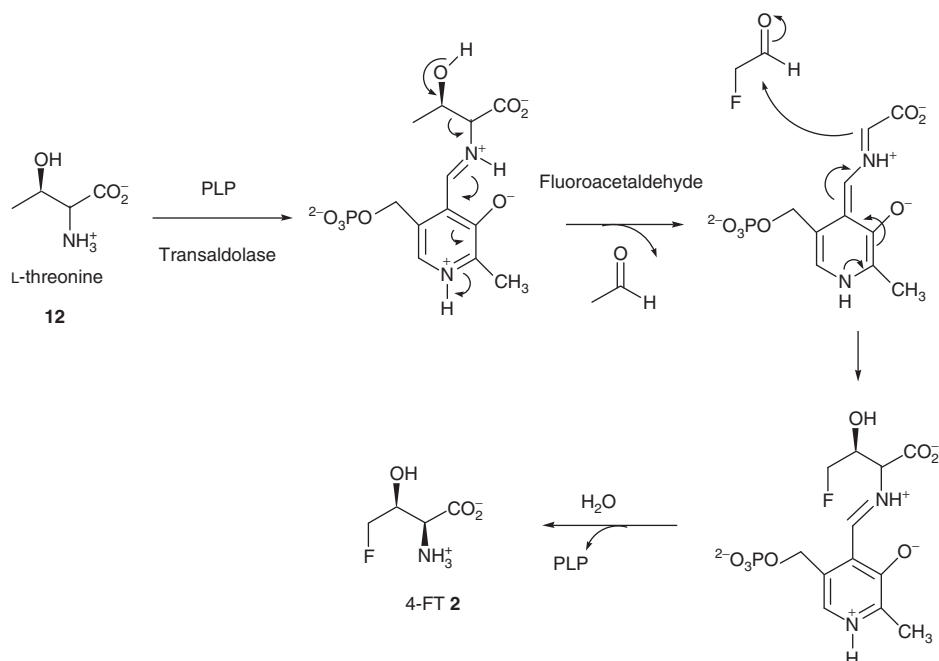
Our early experiments reported that isotopically (^{13}C , ^2H) labelled glycine, serine and glycerol were efficiently incorporated into the fluorometabolites, FAc **1** and 4-FT **2**, and these observations can now be rationalised with a knowledge that the biosynthesis proceeds via SAM **8** and 5'-FDA **5**. Glycine is related to serine via the enzyme serine hydroxymethyl transferase (SHMT), and serine can undergo phosphorylation and can feed into the glycolytic pathway. Glycerol also feeds directly into the glycolytic pathway. Conversion of *sn*-glycerol-3-phosphate to glyceraldehyde-3-phosphate and then via sedoheptulose-7-phosphate and

into the ribose ring of ATP **7** and SAM **8** accounts for the observed incorporation of glycerol into the ribose moiety of ATP **7** and then SAM **8**. The fluorinase then operates to convert SAM **8** to 5'-FDA **5**. The next transformation involves the action of a purine nucleotide phosphorylase (PNP) as discussed above, which converts 5'-FDA **5** to FDRP **9**.

The product of the PNP enzyme, FDRP **9** has been purified and characterised. The evidence suggests that FDRP **9** is then isomerised to 5-fluoro-5-deoxyribose-1-phosphate **10**, acted upon by an isomerase (Scheme 7). Such ribulose phosphates are well-known products of aldolases and a reverse aldol reaction will clearly generate fluoroacetaldehyde **11**. Fluoroacetaldehyde **11** is then converted after oxidation to FAc **1**. We have also shown that there is a pyridoxal phosphate (PLP)-dependent enzyme which converts fluoroacetaldehyde **11** and L-threonine **12** to 4-FT **2** and acetaldehyde in a transaldol reaction as shown in Scheme 8. Thus, all of the biosynthetic steps from fluoride ion to FAc **1** and 4-FT **2** can be rationalised as illustrated in Scheme 7.



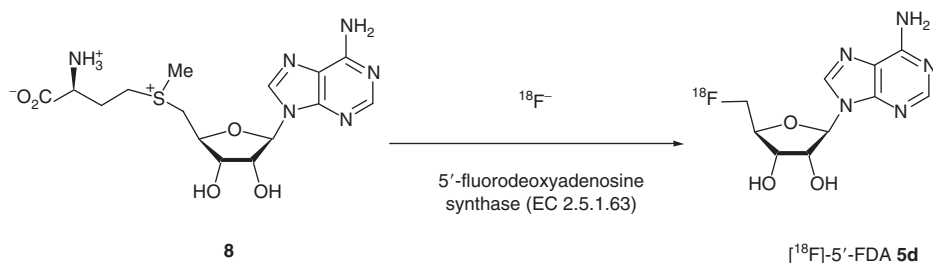
Scheme 7. The biosynthesis of FAc **1** and 4-FT **2** in *Streptomyces cattleya*.



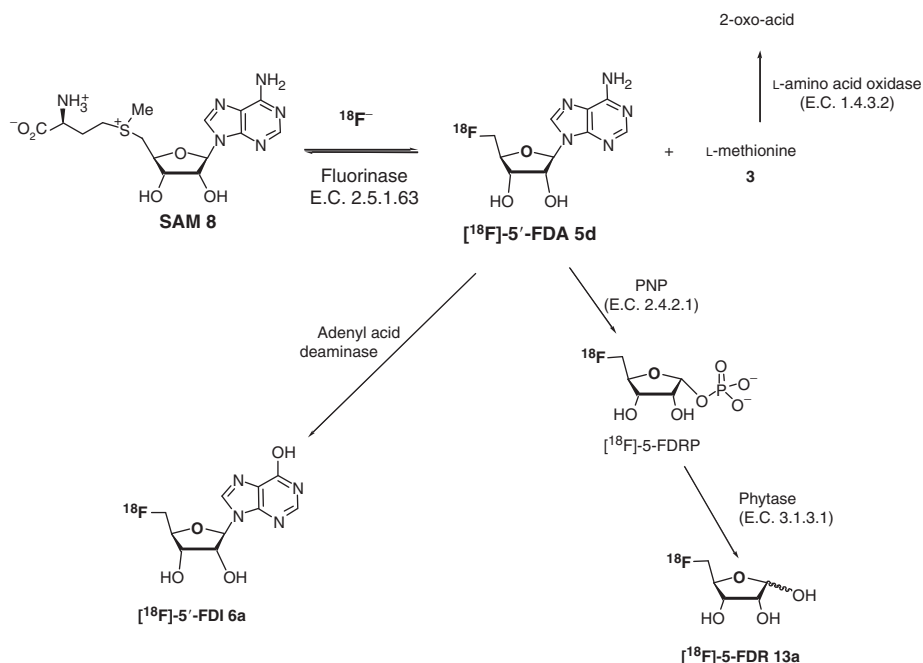
Scheme 8. The conversion of L-threonine **12** and fluoroacetaldehyde **11** to 4-FT **2** and acetaldehyde catalysed by the PLP enzyme threonine transaldolase from *Streptomyces cattleya* [18].

9. THE FLUORINASE AS A TOOL FOR SYNTHESIS AND FORMATION OF C–¹⁸F BONDS FOR POSITRON EMISSION TOMOGRAPHY

Positron emission tomography (PET) is an important non-invasive diagnostic method in the clinic for imaging tumours. It is used for monitoring the distribution of drugs within the body and for identifying cell and receptor degeneration in the brain. Synthesis methods are required to incorporate appropriate positron emitting isotopes into suitable organic molecules, which can be used as ‘ligands’ to bind to appropriate biological targets. The two most widely used positron emitting isotopes in PET are ¹¹C ($t_{1/2}$ —11 min) and ¹⁸F ($t_{1/2}$ —110 min). Enzymes have not been used in PET ligand syntheses due to the virtual absence of appropriate enzymes to utilise the common sources of these isotopes. However, access to the fluorinase has opened up some prospects for biocatalysis in this area with [¹⁸F]-fluoride. Fluoride ion is the preferred starting point because [¹⁸F]-fluoride is generated directly by the cyclotron in very high specific radioactivity (typically GBqs). Due to the relatively short half lives of the isotopes, syntheses methods for PET should ideally be rapid and incorporate isotope of high specific radioactivity.



Scheme 9. Enzymatic synthesis of [^{18}F]-5'-FDA **5d** from [^{18}F]-fluoride.



Scheme 10. The synthesis routes to ^{18}F -labelled nucleosides and ribose in coupled enzyme systems [20].

Despite their absence, enzymatic methods offer an attractive prospect in PET synthesis also because in general, enzymes mediate stereo- and regio-selective reactions. In this regard, the fluorinase has been investigated as a catalyst for the synthesis of [^{18}F]-FDA **5c** [19,20] (Scheme 9).

With over-expressed fluorinase and under optimised reaction conditions, a synthesis of [^{18}F]-FDA **5d** from [^{18}F]-fluoride was achieved in a radiochemical yield (RCY) of 95%. Also in coupled enzyme systems, where the fluorinase is co-incubated with other enzymes, the syntheses of [^{18}F]-5'-fluoro-5'-deoxy-inosine

([¹⁸F]-5'-FDI **6a**) and [¹⁸F]-5-fluoro-5-deoxy-D-ribose ([¹⁸F]-5-FDR **13a**) has been achieved also in good radiochemical yields as shown in Scheme 10.

In summary, the recent developments on fluorinase enzyme research have explored the structure, mechanism and substrate specificity in some detail. Progress has been made at the genetic level which is beginning to inform our understanding of the organisation of the fluorometabolite pathway within *S. cattleya* although much more remains to be uncovered here. In terms of applications of this enzyme, its utility as a synthesis tool for the incorporation of the fluorine-18 isotope from [¹⁸F]-fluoride ion has proven practical, and there may be a role for the fluorinase in the synthesis of some PET ligands.

REFERENCES

- [1] M. Sanada, T. Miyano, S. Iwadare, J.M. Williamson, B.H. Arison, J.L. Smith, A.W. Douglas, J.M. Liesch, E. Inamine, Biosynthesis of fluorothreonine and fluoracetic acid by the thienamycin producer, *Streptomyces cattleya*, J. Antibiot. 39 (1986) 259–265.
- [2] D.B. Harper, D. O'Hagan, The fluorinated natural products, Nat. Prod. Rep. 11 (1994) 123–134.
- [3] M.R. Amin, D.B. Harper, J.M. Moloney, C.D. Murphy, J.A.K. Howard, D. O'Hagan, A short highly stereoselective synthesis of the fluorinated natural product (2S,3S)-4-fluorothreonine, Chem. Comm. (1997) 1471–1472.
- [4] C. Schaffrath, C.D. Murphy, J.T.G. Hamilton, D. O'Hagan, Biosynthesis of fluoroacetate and 4-fluorothreonine in *Streptomyces cattleya*. Incorporation of oxygen-18 from [2-²H,2-¹⁸O]-glycerol and the role of serine metabolites in fluoroacetaldehyde biosynthesis, J. Chem. Soc. Perkin Trans. 1 (2001) 3100–3105.
- [5] S.J. Moss, C.D. Murphy, J.T.G. Hamilton, W.C. McRoberts, D. O'Hagan, C. Schaffrath, D.B. Harper, Fluoroacetaldehyde: A precursor of both fluoroacetate and 4-fluorothreonine in *Streptomyces cattleya*, Chem. Commun. (2000) 2281–2282.
- [6] C. Schaffrath, S.L. Cobb, D. O'Hagan, Cell-free biosynthesis of fluoroacetate and 4-fluorothreonine in *Streptomyces cattleya*, Angew. Chem. Int. Ed. 41 (2002) 3913–3915.
- [7] H. Deng, D. O'Hagan, C. Schaffrath, Fluorometabolite biosynthesis and the fluorinase from *Streptomyces cattleya*, Nat. Prod. Rep. 21 (2004) 773–784.
- [8] D. O'Hagan, C. Schaffrath, S.L. Cobb, J.T.G. Hamilton, C.D. Murphy, Biosynthesis of an organofluorine molecule, Nature 416 (2002) 279.
- [9] C. Schaffrath, H. Deng, D. O'Hagan, Isolation and characterisation of 5,-fluorodeoxyadenosine synthetase, a fluorination enzyme from *Streptomyces cattleya*, FEBS Lett. 547 (2003) 111–114.
- [10] C. Dong, F.L. Huang, H. Deng, C. Schaffrath, J.B. Spencer, D. O'Hagan, J.H. Naismith, Crystal structure and mechanism of a bacterial fluorinating enzyme, Nature 427 (2004) 561–565.
- [11] E. Trevisiol, E. Defrancq, J. Lhomme, A. Laayoun, P. Cros, Synthesis of nucleoside triphosphates that contain an aminooxy for post-amplification labelling, Eur. J. Org. Chem. (2000) 211–217.
- [12] C.D. Cadicamo, J. Courtieu, H. Deng, A. Meddour, D. O'Hagan, Enzymatic fluorination in *Streptomyces cattleya* takes place with an inversion of configuration consistent with an S_N2 reaction mechanism, ChemBioChem 5 (2004) 685–690.
- [13] H.M. Senn, D. O'Hagan, W. Thiel, Insight into enzymatic C–F bond formation from QM and QM/MM calculations, J. Am. Chem. Soc. 127 (2005) 13643–13655.

- [14] M.A. Vincent, I.H. Hillier, The solvated fluoride anion can be a good nucleophile, *Chem Commun.* (2005) 5902–5903.
- [15] H. Deng, S.L. Cobb, A. McEwan, R.P. McGlinchey, J.H. Naismith, D. O'Hagan, D.A. Robinson, J.B. Spencer, The fluorinase from *Streptomyces cattleya* is also a chlorinase, *Angew Chem. Int. Ed.* 45 (2006) 759–762.
- [16] S.L. Cobb, H. Deng, A.R. McEwan, J.H. Naismith, D. O'Hagan, D.A. Robinson, Substrate specificity in enzymatic fluorination. The fluorinase from *Streptomyces cattleya* accepts 2'-deoxyadenosine substrates, *Org. Biomol. Chem.* 4 (2006) 1458–1460.
- [17] F. Huang, S.F. Haydock, D. Spiteller, T. Mironenko, T.-L. Li, D. O'Hagan, P.F. Leadlay, J.B. Spencer, The gene cluster for fluorometabolite biosynthesis in *Streptomyces cattleya*: A thioesterase confers resistance to fluoroacetyl-coenzyme A, *Chem & Biol.* 13 (2006) 475–484.
- [18] C. Schaffrath, C.D. Murphy, D. O'Hagan, *Angew Chem. Int. Ed.* 40 (2001) 4479–4481.
- [19] L. Martarello, C. Schaffrath, H. Deng, A.D. Gee, A. Lockhart, D. O'Hagan, The first enzymatic method for C-¹⁸F bond formation: The synthesis of 5'-[¹⁸F]-fluoro-5'-deoxyadenosine for imaging with PET, *J. Labelled Compd. Radiopharm.* 46 (2003) 1181–1189.
- [20] H. Deng, S.L. Cobb, A.D. Gee, A. Lockhart, L. Martarello, R.P. McGlinchey, D. O'Hagan, M. Onega, Fluorinase mediated C-¹⁸F bond formation, an enzymatic tool for PET labelling, *Chem. Commun.* (2006) 652–654.

SUBJECT INDEX

- AADC. *See* Aromatic amino acid decarboxylase
- α -Adrenoceptors, 112
density of cardiac, 113
subtypes of, 113
- Acetyl [^{18}F] hypofluorite ($\text{CH}_3\text{CO}_2[^{18}\text{F}]\text{F}$), 14, 15
- Acid-functional monomer, 362
- Acute normovolemic hemodilution, 452
- Acyclovir, 25
- Adenosine triphosphate (ATP), 240
- β -Adrenoceptors (β -ARs)
density in heart, 100
 ^{18}F -labeled radioligands for PET
imaging of, 100
[^{18}F]fluoroacetone as radiolabeling building block, 106
[^{18}F]fluorocarazolol 5, 102, 108, 109
[^{18}F]fluoroisopropyl-penbutolol 1, 101, 106
[^{18}F]fluorometoprolol 6, 103, 109–110
(*R,R*)(*S,S*)-[^{18}F]fluoroethylfenoterol 9, 111–112
(*S*)-[^{18}F]fluoroethylcarazolol 8, 111
subtypes of, 100
- Adriamycin (doxorubicine), 589
- Agrochemical agents, 215
- AlF. *See* Aluminium monofluoride
- Aliphatic nucleophilic substitution, 28
- Alkenes, as amide bond substitutes, 702–703
- Alkenes fluorination, 18
- Allyl hydrazines as SSAO inhibitors, 674
- Aluminium monofluoride, 534
- Alumino-fluoride complexes, 364
- Alzheimer's disease (AD)
pathophysiological mechanisms of, 67
PET and SPECT imaging in, 69
- Ameloblast cells, 319
- Amine oxidases, 662
- Amino acid side chain fluorination
effects of, 739
hydrophobicity in, 753
- o*-Aminophenol-*N,N,O*-triacetic acid (APTRA), 241
- Amodiaquine, metabolism of, 570, 571
- Amyloid cascade hypothesis, 68
- Amyloid deposits, 77–78
- Aneurysm rupture, 380
- Angiogenesis, 220
- ANH. *See* Acute normovolemic hemodilution
- Anhydrous electrophilic fluorine, 12
- Anhydrous [^{18}F]fluorine, 14
- Anoxic relaxation, 221
- Anthracyclines
aminoglucoside fragment fluorination, 589–590
mechanism of action of, 589
- Anthropogenic sources of fluoride, 490–492
- Antiprogesterone, 601
- Antithrombin, 392
- Apatite, 284–310
- Apatite-wollastonite glass-ceramic (AW-GC), 302
- Aprotic polar solvents, 36
- Arenium ion mechanism, 23
- Aromatic amino acid decarboxylase, 673
- Aromatic fluorination and lipophilicity, 741
- Aromatic nucleophilic substitutions, 27–28
- Arsenic penta[^{18}F]fluoride, 13
- Artemisinin
fluoro derivatives of, 610
pharmacological profile of, 608
- Arthrobacter globiformis*, 683
- Aryl- α -tri[^{18}F]fluoromethylketones, 22
- Asparagine analogs, synthesis, 705–707
- Atherosclerosis
and MMP overexpression, 92
risk factors and progression of, 91
- Atherosclerotic plaques
imaging based on assessment of degree of inflammation, 91
imaging with ^{18}F -labeled MMPis, 92–93
- Atomic force microscopy (AFM), use in chemical force mode, 300
- Atraumatic restorative treatment (ART)
technique, 357
- Balz-Schiemann and Wallach reactions, 35, 40–41
- Behavioral and psychological symptoms of dementia (BPSD), 72
- Benzodiazepine receptors, 76–77
- Benzylamines, fluorine substituted, 666–668
- Bioactive chemical structures, 6
- Bioceramics
applications of fluoridated, 281
biological properties of, 319
fluoride-containing coatings
high-energy processing, 312–314
solution-mediated processing, 314–316
processing techniques for, 311
- Biocompatible emulsions, 224

This page intentionally left blank

- Bioglasses
 - bioactivity of, 302
 - clinical use of, 302
- Bioinert alumina substrate, 303
- Biological apatites, fluoride ions in, 316–319
- Biological membranes
 - absorption in
 - lipophilicity, 563–564
 - pK_a and solubility, 564–566
- Biological system, β -turn mimics role in, 728–730
- Biological target
 - hydrogen bonds, 558
 - substrate affinity for, 555
- Biomaterials cardiovascular surgery, 380–402
- Biomedical cyclotrons, 7, 8
- Biomimetic nanocrystalline apatite crystals, 301
- Bioreductive drugs, 173
- Blood coagulation cascade triggering, 392–393
- Blood interaction with vessel wall
 - electric potential role, 381–382
 - plasma protein–material interaction, 382–384
 - shear stress role, 384–385
 - surface tension/surface free energy role, 381
- Blood–material interactions, 382–384
- Blood oxygen level dependent (BOLD), 221
- Blood substitute emulsion, 224
- BMD. *See* Bone mineral density
- Bone cells, effect of fluoride-containing
 - substrates on, 321
- Bone-implant bonding, 312
- Bone-implant interface, 322
- Bone mineral density, 283, 319, 346
- Bone scanning, 14
- Brain tumor imaging, [^{18}F]DOPA for, 181
- Breast cancer
 - [^{18}F]-FDG-PET/CT imaging of, 159
 - [^{18}F]-FDG-PET imaging
 - for primary and initial staging of, 157–158
 - for recurrence detection, 158–159
- Bromine [^{18}F]fluoride ($\text{Br}[^{18}\text{F}]\text{F}$), 13
- Bromo [^{18}F]fluoride, 18, 21
- Bromo perfluoro-*n*-octan (PFOB), 411
- B-type carbonate-apatites, 287
- BXL-628, vitamin D3 metabolite, 604

- Calcitriol
 - calcemic activity, 604
 - fluorination of, 603
- Calcium phosphate cements (CPC), 305
- Camellia sinensis*, 507
- Camptothecin
 - derivatives of, 587
 - fluorinated analogues of, 588
 - fluorination with DAST, 588
- Cancer chemotherapeutics
 - fluoropyrimidines, 216
 - other anticancer drugs, 217–218
- Cancer Imaging Program (CIP), 199
- CAO. *See* Copper-dependent amine oxidases
- Carbanions, 22
- (9-anthryl)Carbinol derivatives, rotational barriers
 - of, 739–740
- Carbon–carbon double bond, electrophilic
 - fluorination, 19
- Carbon–fluorine covalent bond, 14
- Carbon nuclear magnetic resonance
 - (^{13}C -NMR), 36
- Cardiac 'uptake-1' mechanism, ^{18}F -labeled
 - compounds for imaging
 - catecholamines, 118
 - 4- and 6-[^{18}F]fluorometaraminol, 121–123
 - 6-[^{18}F]fluorodopamine and 6-[^{18}F]
 - fluoronorepinephrine, 119–121
 - guanethidine analogs
 - 4-[^{18}F]fluoro-3-iodobenzonitrile, 124–125
 - [^{18}F]MFBG, 123
- Cardiopulmonary bypass, 458
- Cathepsin K, inhibitors of, 573
- Caveats, development and exploitation of
 - reporter molecules, 242
- Cellular hypoxia, 244
- Central nervous system disorders, 77
- Ceramic microstructure, 307
- Certified reference material, 533
- C–F bond
 - dipolar nature of, 741
 - effect on acidity of functional groups, 740–741
 - fluorine, 8
- Charged particles, cyclotron acceleration of, 10
- Chemical interactions
 - enzyme reporters, 245
 - FDG metabolism, 243–244
 - hypoxia, 244–245
- Chemical shift imaging (CSI), 215
- Chlorinase. *See* Fluorinase
- 5'-Chloro-5'-deoxyadenosine(5'-CIDA)
 - enzyme assays shifting, 769
 - x-ray-derived structure of, 769
- Chlorotrifluoromethane (freon-11), 26
- Choline
 - for imaging of malignancies, 177
 - importance of, 176
 - normal biodistribution of, 177
 - phosphorylcholine formation with, 176–177
- Cholinergic system, 74–76
- α -Chymotrypsin
 - catalytic triad and cleavage reaction of, 742
 - peptide conformations within active sites of, 747
- Citronellol, olfactory properties of, 556
- ^{11}C -labeled MAO inhibitors as PET-scanning
 - agent, 677
- Cleavage sites, Tfm-substituted peptides
 - α -dialkylation stabilizing effect on, 745–746
 - enzymatic degradation, 744
- Clinical dentistry, 338
- Coiled coils. *See also* α -Helical coiled coil
 - folding assembly, 748
 - EGly side chain fluorination effects on, 751
 - and F–F interactions, 752
 - fluorine–fluorine interactions effects on, 753

- impact of fluorine side chain substitutions on
 - stability of, 749–750
 - thermal stability of, 748
 - Colon cancer, 252
 - Colorectal cancer
 - causes of, 144
 - conventional imaging modalities, limitations of, 145–146
 - cost-effective analysis of management of
 - recurrent, 152–153
 - [¹⁸F]-FDG-PET imaging for
 - clinical management of recurrent or metastatic, 147–148
 - hepatic metastases detection, 148
 - preoperative staging of, 146
 - recurrence of, 146
 - survival rates, 144–145
 - therapy monitoring with [¹⁸F]-FDG-PET imaging, 148
 - lesion location, 149–150
 - for restaging of recurrent, 150–151
 - Compomers. *See* Polyacid-modified composite resins
 - Copper-dependent amine oxidases, 664
 - Corticosteroids, fluorination of, 595
 - CPB. *See* Cardiopulmonary bypass
 - Crippling skeletal fluorosis, 498
 - CRM. *See* Certified reference material
 - CRTH2 receptor agonist and antagonist,
 - synthesis, 644–646
 - CRTH2 receptor (prostanoid receptor), 627, 628
 - Cryptand Kryptofix-222®, 12
 - Crystal growth method, 307
 - Cs⁺-Kryptofix-222® complex, 16
 - Curie level, 9
 - Cyclophilin inhibitors, 723–725
 - Cyclopropylamines MAO inhibitors
 - development of, 679–680
 - inhibition mechanisms, 681–683
 - isozyme selectivity, 680–681
 - CyP. *See* Cyclophilin inhibitors
 - Cytotoxicity test, 431–432
 - Czochralski method, 307
-
- Dean's index, in dental fluorosis rating, 496–497
 - Definity®, PFC-based product, 465
 - Densiron 68®, 408, 429–430
 - Dental amalgams, 357
 - Dental or enamel fluorosis, 334, 496–497
 - Dental restorative materials, 335
 - Dentifrices, 351–353
 - Dexamethasone, synthesis of, 600
 - Dexfenfluramine, 218
 - DFMO. *See* Difluoromethylornithine
 - C^{α,α}-Dialkylated amino acids, 745
 - α-Dialkylation
 - conformational restrictions of, 747
 - peptide bond stabilization, 745
 - Diastereomers, crystal structures of, 745–746
 - DiBAIH. *See* Diisobutylaluminum hydride
 - α,ω-Dichloro-F-octane, 454
 - Diethylaminosulphur tri[¹⁸F]fluoride ([¹⁸F]DAST), 13
 - Diflomotecan, 587
 - 1,1-Difluoroethylene polymerisation, 396
 - Difluoromethyl amidopyrazole, fungicidal activity of, 561
 - Difluoromethylornithine (DFMO), 232
 - ornithine decarboxylase inhibitor, 610
 - synthesis of, 611
 - Difluorophosphonates, 573
 - Dihydroxycalciferol, fluoro analogues of, 605
 - Diisobutylaluminum hydride, 712
 - Dimethyl sulfoxide (DMSO), 36
 - Dimyristoylphosphatidylcholine, 470
 - Dipeptidyl peptidase IV, 725–728
 - Diphosphoglycerate (DPG), 215
 - Dipole–dipole interactions, 291
 - Disk diffusion test, 432
 - Dissociation energy, C–F bond, 768
 - DMPC. *See* Dimyristoylphosphatidylcholine
 - DNA polymerases, 217
 - fluorous effects in active site of, 562
 - inhibitors of
 - elvucitabine, 585
 - fludarabine, 584
 - gemcitabine, 581–582
 - Dopaminergic system, 73–74
 - DPP IV. *See* Dipeptidyl peptidase IV
 - DP receptor antagonists, synthesis of, 642–644
 - DP receptor (prostanoid receptor), 627, 628
 - Drinking water, fluoridation of, 335, 349
 - Drug delivery system and PFCs, 471–472
 - Dual-particle cyclotrons, 10
 - Dutasteride, 4-azasteroid, 601–602
 - Dynamic oxygen mapping, 229
-
- EADIs. *See* E-alkene dipeptide isosteres
 - E-Alkene dipeptide isosteres, 702
 - EAR. *See* Estimated average requirement
 - Echo planar imaging, 229
 - Efficiency (ED50), biological information, 7
 - Egg yolk phospholipids, 455
 - Electron-donating reactant, 14
 - Electron spin resonance (ESR), 221
 - Electron-withdrawing group (EWG), 35
 - Electrophilic fluorination reagents
 - application of
 - acetyl [¹⁸F]hypofluorite, 15–16
 - bromo [¹⁸F]fluoride, 18
 - N-[¹⁸F]fluoro-N-alkylsulphonamides, 17–18
 - N-[¹⁸F]fluoropyridinium triflate, 17
 - 1-[¹⁸F]fluoro-2-pyridone, 17
 - molecular [¹⁸F]fluorine, 15
 - perchloryl [¹⁸F]fluoride, 16
 - trifluoromethyl [¹⁸F]hypofluorite, 15
 - xenon di[¹⁸F]fluoride, 16
 - Electrophilic [¹⁸F]radiofluorinations, 11, 14
 - Electrophilic radiofluorinating agents, 49
 - Elvucitabine, 585
 - Emtricitabine, 585

- Emulsification, 410
- Enamel crystals characteristics, 318
- Enamel mineralisation, 342
- Endotamponade medias
 - drop shapes of, 440
 - tissue penetration of, 439
- [¹⁸F] ET-1 ([¹⁸F] Endothelin-1), 93
 - binding potency for ET_A receptor, 94
 - ¹⁸F-labeled nonpeptidyl ligand for receptors of, 95
 - isoforms of, 94
- Enol structures, fluorination, 21–22
- Enzymatic carbon-[¹⁸F]fluorine bond formation, 43–44
- Epothilones, anti-tumour activity of, 591
- EP2 receptor agonist, 9 β -fluoro-PGE₁ analog, 635
- EP4 receptor agonists, synthesis of, 636
- EP1 receptor antagonist(s)
 - dibenzoxazepine derivatives, 632
 - ONO-8713 and ONO-8711, 633–634
 - SC-51089 and SC-51234A, 633
- Erythromycins
 - fluorination of, 590
 - 2-fluoroerythromycin derivatives, 591
- Escherichia coli*, 476, 683
- Esophageal cancer
 - [¹⁸F]-FDG-PET/CT imaging, 162–163
 - [¹⁸F]-FDG-PET imaging
 - diagnostic accuracy of, 161
 - locoregional lymph node metastases, 160
 - for primary and initial staging, 159–160
 - recurrence detection, 161–162
 - therapeutic approaches for, 159
- Estimated average requirement, 536
- ET_A and ET_B receptors, 94
- N-Ethylaminophenol (NEAP), 234
- S-Ethyl trifluoroacetate (SETFA), 205
- Etoposide derivatives, 589
- European Medical Device Directive (MDD), 427
- Expanded polytetrafluoroethylene, 389, 391–396, 450, 473
- EYP. *See* Egg yolk phospholipids

- FAD. *See* Flavin adenine dinucleotide
- Falecalcitriol
 - selectivity of, 606
 - synthesis of, 604, 605
- Fatty acids
 - during fasting, 86
 - as myocardium energy source, 89
 - oxidation
 - diseases associated with dysregulation of, 89
 - 14F6THA and FTP, 90–91
 - methyl-branched-chain ω -¹⁸F-fluorofatty acids, 89
- FCLs. *See* Fluorocarbon liquids
- FCLs for ophthalmic use, test scheme
 - test procedures, 433–435
 - toxicological tests, 431–432
- F-compounds usage, environmental issues in, 451

- Femoral bone density, 346
- Fermentable carbohydrates, 340
- [¹⁸F]ET-1
 - radiosynthesis of, 95
 - in vivo* ET receptor imaging, 94
- [¹⁸F]FDG/[¹⁸F]FDM ratio, 19
- [¹⁸F]-FDG-PET/CT imaging
 - comparison with [¹⁸F]-FDG-PET, 148
 - image acquisition in, 170
 - lung cancer
 - initial staging, 154–155
 - recurrence detection, 155
 - methodical considerations and limitations of, 169–170
 - sensitivity, specificity, and accuracy of, 150
 - for staging and restaging of colorectal cancer patients, 148–151
 - therapy monitoring with, 149
 - therapy response, 169–170
- [¹⁸F]-FDG-PET imaging
 - breast cancer
 - histopathologic response in locally advanced, 168
 - for primary and initial staging of, 157–158
 - for recurrence detection, 158–159
 - gastrointestinal stromal tumors (GIST), 167–168
 - image acquisition in, 170
 - of locally advanced head and neck squamous cell carcinoma (HNSCC), 168
 - lung cancer
 - initial staging of, 153–154
 - recurrence detection of, 154
 - malignant lymphomas, 167
 - metabolic response, 169
 - methodical considerations and limitations of, 169–170
 - ovarian cancer, 168–169
 - for staging and restaging of tumor patients, 144
 - colorectal cancer, 146–148
- [¹⁸F]-FLT. *See* [¹⁸F]-fluorothymidine
- [¹⁸F]-Fluoride-PET for imaging of bone metastases, 178–179
- [¹⁸F]-Fluorine based radiotracers, 143
 - 3'-deoxy-3'-[¹⁸F]-fluorothymidine
 - noninvasive proliferation assessment and tumor imaging, 171
 - as PET tracer, 173
 - for therapeutic monitoring, 172–173
 - and thymidine kinase 1 (TK1) activity, 172
 - uptake in lymphomas, 172
 - [¹⁸F]FET-PET, cerebral gliomas imaging, 180
 - [¹⁸F]-Fluoride-PET for imaging of bone metastases, 178–179
 - [¹⁸F]-Fluorocholine-PET for prostate cancer imaging, 176–178
 - [¹⁸F]-Galacto-RGD-PET
 - breast cancer staging with, 176
 - integrin expression imaging, 175–176
 - fluorinated dihydroxyphenylalanine [¹⁸F] DOPA, 181
- 8-[¹⁸F]Fluoroacyclovir, 25

- [¹⁸F]Fluorobenzene, 23
- [¹⁸F]-Fluorocholine-PET for prostate cancer imaging, 176–178
- 5-[¹⁸F]Fluorocytosine, 25
- 2-[¹⁸F]Fluoro-2-deoxy-D-glucose ([¹⁸F]FDG), 4–5, 13
- 2-[¹⁸F]Fluoro-2-deoxy-D-mannose ([¹⁸F]FDM), 19
- 2-Deoxy-2-[¹⁸F]fluoro-D-glucose, metabolic radiotracer
 - accumulation mechanism in myocytes, 88
 - radiosynthesis of
 - hydrolytic deprotection, 89
 - nucleophilic substitution, 88
 - uses of, 87
- 8-[¹⁸F]Fluoroganciclovir, 25
- α -[¹⁸F]Fluoroketone, 14
- 6-[¹⁸F]Fluoro-L-DOPA, 13
- 2-[¹⁸F]Fluoro-L-phenylalanine, 25
- 3-[¹⁸F]Fluoro-L-tyrosine, 25
- 2-[¹⁸F]Fluoromalonate, 16
- [¹⁸F]-Fluoromisonidazole, PET agent, 174
- 1-[¹⁸F]Fluoronaphthalene, 23
- 8-[¹⁸F]Fluoropenciclovir, 25
- 6 α -[¹⁸F]Fluoroprogesterone, 21
- 1-[¹⁸F]Fluoro-2-pyridone, 14, 17, 23
- 14-[¹⁸F]Fluoro-6-thiaheptadecanoic acid, 90
- 16-[¹⁸F]Fluoro-4-thiahexadecanoic acid
 - as metabolically trapped FAO probe, 90
 - radiosynthesis of, 91
- [¹⁸F]-Fluorothymidine
 - for noninvasive proliferation assessment and tumor imaging, 171
 - as PET tracer, 173
 - for therapeutic monitoring, 172–173
 - and thymidine kinase 1 (TK1) activity, 172
 - uptake in lymphomas, 172
- 4-[¹⁸F]Fluoro-tri-*N*-methylanilinium cation ([¹⁸F]FTMA), MBF tracer, 97
- 5-[¹⁸F]Fluorouracil, 20
- 5-[¹⁸F]Fluorouridine, 21
- Fibrin deposition, 384–385
- ¹⁹F Isotropic chemical shift distribution, 291
- FK506 binding protein, 723
- ¹⁸F-Labeled MAO inhibitors as PET-scanning agent, 677–679
- ¹⁸F-Labelled 2-fluoroglucose, 577
- Flame spray pyrolysis process, 307
- Flavin adenine dinucleotide, 662
- Fluasterone, adrenocortical steroid, 602–603
- Flucytosine, 584
- Fludarabine, 584
- Fludrocortisone, 597
- Fludroxycortide, 597
- Flumedroxone (Demigran®), progestative agent, 600–601
- Fluocortine, 597
- Fluorapatite, 284–310
- Fluorapatite
 - structure, 285–288
 - FTIR, 289
- NMR, 291–298
- Fluorcanasite, 303
- Fluor-containing glasses, 302–305
- Fluorescence imaging, 200
- Fluorhydroxyapatites, 286, 298, 306
- Fluoridated apatites
 - difficulties related to characterisation of, 296
 - dissolution properties of, 296–297
 - fluoridation effects of, 300–301
 - fluoridation reactions of, 297–298
 - mechanical properties of, 301–302
 - physico-chemical characterisation technique
 - FTIR spectroscopy, 289–290
 - solid-state NMR, 290–296
 - X-ray diffraction, 288
 - preparation and synthesis routes of
 - high-temperature methods, 306–307
 - low-temperature methods, 308–311
 - substitution of, 286–288
 - surface characteristics
 - adsorption properties, 300
 - surface charge, 300
 - surface energy, 299–300
 - thermal stability, 298
 - thermodynamic characteristics of, 299
- Fluoridated bioceramics, 281
- Fluoridated cements, 305
- Fluoridated toothpastes, 351
- Fluoridation
 - effects, 300
 - reaction, 297
- Fluoride
 - absorption, metabolism in humans, 500–502
 - acute toxicity in human, 498–499
 - adequate intake determination of, 536–538
 - in air, 491–492
 - beneficial and harmful effects, 489–490
 - bioavailability in humans, 499–500
 - biomarkers of, 503–505
 - chronic toxicity in human, 495–498
 - in dental products, 514–515
 - in dietary supplements, 514
 - in drinking water and beverages, 505–508
 - efficacy assessment, 535–536
 - excretion in humans, 502–503
 - in foods, 509–514
 - importance of, 494–495
 - intake in adults, 516
 - intake in children from, 516–521
 - diet, 521–528
 - fluoride-containing toothpastes, 521, 529
 - fluoride supplements, 529–530
 - in lithosphere, 491
 - in milk and baby formulas, 508–509
 - in natural waters, 492–494
 - in tea brick, 507–508
 - in the environment, 490–493
 - topical applications, 354
 - toxicology, 495–499
- Fluoride-containing composite resins, 364–365
- Fluoride gels, 355

- Fluoride ion hydrogen bonding, working hypothesis, 767
- Fluoride ions
- adverse effects of
 - fluorosis, 344–345
 - potential systemic effects, 345–347
 - antimicrobial effect of, 339–340
 - biological fluids related to, 321
 - delivering methods
 - dentifrices, 351–353
 - drinking water, 347–350
 - fluoride mouthrinses, 353–354
 - fluoride-releasing restorative materials, 355
 - salt and milk, 350–351
 - topical fluoride applications, 354–355
 - in dentistry, 335
 - effects on bacteria, 320–321
 - effects on mineralising cells, 319
 - effects on osteoclasts cells, 319–320
- Fluoride therapy, 337
- Fluorinase
- active site of, 767
 - characterisation of, 764
 - 2'-deoxyanalogues, substrates, 770
 - mechanism of, 765
 - reversibility of, 768
 - SAM 8 bound to, 766
 - stereochemical course of, 767
 - substrate specificity study of, 770
 - x-ray-derived structure of, 765
- Fluorinase gene (flA), 764, 771
- reactions of, 772
- Fluorinated amino acids, 738. *See also* C^α-Fluoroalkyl amino acids
- Fluorinated compounds
- Gauche effect of, 557
 - pK_a, α^H2 and β^H2 values of, 559–560
- Fluorinated dihydroxyphenylalanine, brain tumor imaging, 181
- Fluorinated drugs/pharmaceuticals
- alkaloids
 - camptothecin, 587–588
 - vinca dimer indole alkaloids, 585–587
 - amino acids
 - difluoromethylornithine (eflornithine), 610–611
 - amino acids, difluoromethylornithine (eflornithine), 610–611
 - anthracyclines, 589–590
 - based on nucleosides and carbohydrate
 - inhibitors of RDPR and DNA polymerase, 580–585
 - inhibitors of thymidylate synthase, 578–580
 - lignans, podophyllotoxin, 588–589
 - macrolides
 - epothilones, 591–593
 - erythromycin, 590–591
 - prostanoids
 - lubiprostone and travoprost, 607–608
 - prostacyclins (PGI₁, PGI₂ and PGF_{2 α}), 606–607
 - reduced toxicity of, 571
 - steroids
 - antiprogesterone, 601
 - corticosteroids, 593–600
 - dutasteride, 601
 - fluasterone, 602–603
 - fulvestrant and flumedroxone, 600
 - terpenes
 - artemisinin, 608
 - dihydroartemisinin (DHA), 609
 - vitamin D3 metabolites
 - calcitriol, 603
 - falecalcitriol, 604, 605
- Fluorinated gases, 253
- Fluorinated hydrocarbons, hydrophobic nature of, 741
- Fluorinated MAO inhibitors as PET-imaging agents, 676–679
- Fluorinated patch formation, 474–475
- Fluorinated polymers, 394–402
- Fluorinated surfactants, problems of, 452
- Fluorination
- affinity for macromolecule target, 555
 - conformational changes, 557
 - dipolar interactions and electric field, 557–558
 - fluorous interactions, 562
 - hydrogen bonds, 558–561
 - pK_a of amines, 561–562
 - steric effects, 556
 - of aromatic rings
 - fluorodehydrogenation, 24–25
 - fluorodemetalation, 25–27
 - biological impact of
 - lipophilicity, 563–564
 - pK_a and solubility, 564–566
 - of carbanions, 22–23
 - chemical reactivity modification
 - inhibition by destabilisation of cationic intermediates, 575
 - inhibition by stabilisation of fluoroalkyl ketones, 574–575
 - irreversible inhibition, 575–577
 - substrates as inhibitor, 572–574
 - of double-bond structures
 - alkenes, 18–21
 - enol structures, 21–22
 - metabolism
 - of drug, 567
 - hydrolytic, 570–572
 - oxidative, 567–570
 - mifentidine, 561
 - physical and chemical properties, 554
 - polyfluoroalkene with [¹⁸F]F₂, 20
- Fluorine
- chemical characteristics, 488
 - determination, analytical methods in, 532–535
 - in drug design and development, 665–666
 - electronegativity of, 557

- electronic effects, 566
- extractable content and cell growth inhibition rate, 427
- hydrolytic metabolism of, 570
- inductive effect of, 741
- influence on microbiological hydroxylation, 568
- in inhibitors, 575
- neon gas mixtures, 14
- non-covalent interaction with carbonyl of amino acid, 559
- physico-chemical properties of, 555
- polymers, use in vascular prostheses, 388
- substitution, 559
- substitution ratio, 293
- use in eye surgery, 408–412
- Fluorine-18
 - design of radiotracers and radiopharmaceuticals labeled with, 7
 - labeled anhydrous reagents, 12
 - labeled precursors for, 12–14
 - labeled radiopharmaceuticals, 12
 - macromolecule labeling with, 45
 - physical and nuclear characteristics of, 4
 - production of, 10–11
 - reagents for labeling of oligonucleotides, 48–49
 - as short-lived positron emitters for PET, 5
- α -Fluoro- α,β -unsaturated ketones, synthesis, 717–721
- 11 β -[^{18}F]Fluoro-5 α -dihydrotestosterone, 21
- Fluoroalkenyltropene derivatives, 31
- C $^{\alpha}$ -Fluoroalkyl amino acids
 - enzymatic hydrolysis analysis of, 743
 - polypeptide interactions, 752
 - proteolytic stability of, 742
 - side chains, orthogonal properties of
 - α -helical coiled coil, 747–750
 - in hydrophilic environment, 752–754
 - in hydrophobic environment, 751–752
- Fluoroalkyl groups
 - electronegative character of, 575
 - electrophilicity due to, 574
 - electrostatic properties of C–F bond, 740–741
 - polar properties effect on conformational restrictions of
 - α -trifluoromethyl phenylalanine, 743–744
 - C $^{\alpha,\alpha}$ -dialkylated amino acids, 745
 - response to oxidation, 568
 - spatial demand and steric effects, 739–740
 - steric hindrance induced by, 556
- Fluoroamodiaquine, metabolism of, 571
- Fluorocarbon liquids, 422
- Fluorocorticoids, 599–600
- Fluorocorticosteroids, 595
 - with atypical substitutions, 597
 - types of, 595
- 2-fluorocytarabine. See Fludarabine
- Fluorodehydrogenation, 23
- Fluorodemetalation reactions, 23
- 5'-Fluoro-5'-deoxyadenosine (5'-FDA), 761
- enzymatic synthesis of, 775
- formation of, 764
- organo-fluorine compound, 763
- structure of, 771
- 3-Fluoro-3-deoxy-D-glucose isomer (3-FDG), 244
- Fluoroepothilones, 593
- 2-Fluoroerythromycin
 - derivatives of, 591
 - synthesis of, 592
- Fluorometholone, 597
- Fluoro mineralocorticoids, 598
- Fluoroolefin dipeptide isosteres, 702
 - biological applications of, 722–730
 - metathesis reactions in, 721
 - in peptide amide bond replacement, 703
 - synthesis of
 - alkylation reactions, 705–707
 - carbine insertion, 704–705
 - claisen condensation–dehydration, 705
 - fluorotris(trimethylsilyl)methane addition reaction, 707–708
 - Horner–Wadsworth–Emmons reaction, 709–712
 - imine addition reactions, 707
 - Negishi-type reactions, 708–709
 - Nozaki–Hiyama–Kishi-type reactions, 708
 - Peterson fluoroolefination, 713–714
 - stereoselective synthesis of (Z)-fluoroalkene depsipeptide, 714–715
- Fluorapatite (FA)
 - adsorption properties of, 300
 - atomic positions in stoichiometric, 285
 - crystal structure of stoichiometric, 284–286
 - hydrolysis of, 283
 - precipitation of, 310
 - precipitation of crystals of, 342
 - single crystals of, 307
 - surface energy of, 299
- Fluoro-prostanoids, 607
- 6-Fluoropyridoxol (6-FPOL), 231
- Fluoroquinolone
 - antibiotics, 219
 - solubility of, 567
- Fluorosilicates, 347–350
- Fluorosis, 344–345
- 5-Fluorouracil (5-FU)
 - anti-cancer properties of, 578
 - pro-drugs for cancer therapy, 579–580
 - side effects in cancer treatment, 579
- 5'-deoxy-5-[^{18}F]Fluorouridine, 21
- Fluorous effects, 562
- Fluorous interactions, 754
- Fluosol emulsion development, 455–456
- Fluprednidene, 597
- Flurithromycin, 590–591
- ^{19}F NMR
 - hypoxia indicators, 246
 - oximetry, 226
 - spectrum of fluorapatite and fluorhydroxyapatite, 291–293
 - spin lattice relaxation, 221

- F-octyl bromide, 454, 469
 F-octylethane, 454
¹⁸F-radiopharmaceuticals, 69
 FREDOM-tissue oxygen dynamics, 230
 Free acid resonances, 232
 Frontotemporal dementia, 70
 [¹⁸F]SB209670
 ¹⁸F-labeled nonpeptidyl ligand for ET receptors, 95
 radiosynthesis of, 96
¹⁹F SPE-MAS NMR spectrum, 292
 FTCP. *See* Trans-2-(4-fluorophenyl) cyclopropylamine
 14F6THA. *See* 14-[(¹⁸F)]Fluoro-6-thiaheptadecanoic acid
 FTP. *See* 16-[(¹⁸F)]Fluoro-4-thiahexadecanoic acid
 Fulvestrant
 competitive oestrogen receptor antagonist, 600
 synthesis of, 601

 Gamma rays, 9
 Ganciclovir, 25
 Gastrointestinal stromal tumors, glivec treatment, 167–168
 Gastrointestinal tract, 163
 histopathologic response, locally advanced adenocarcinoma of esophagogastric junction, 165
 metabolic imaging with [¹⁸F]-FDG, 165
 therapy-induced changes, 164–165
 Gauche effect of fluorinated compounds, 557
 Gemcitabine (Gemzar®), 581
 Gene reporter molecules, 220
 Gene therapy, 247
 GI. *See* Gastrointestinal tract
 GIST. *See* Gastrointestinal stromal tumors
 Glass ionomer cements (GIC), 305
 Glass-ionomers, 356–361
 GLP-1. *See* Glucagon-like peptide-1
 Glucagon-like peptide-1, 726
 Glucocorticoids
 anti-inflammatory properties, 594
 electrophilic fluorination of, 598
 metabolic hormones, 593
 Glucose metabolic reductions, 70
 Glucose transport proteins, 88
 Glycerophosphatidylcholine, 466
bis-Glycidyl ether dimethacrylate (bisGMA), 362
 Gly-Gly fluoroolefin dipeptide isostere, synthesis of, 704
 Good Laboratory Practice (GLP), 10
 Good Manufacturing Practice (GMP), 10
 GPC. *See* Glycerophosphatidylcholine
 GPCRs. *See* G-protein-coupled receptors
 G-protein-coupled receptors, 94
 G-protein coupled rhodopsin-type receptors.
 See also Prostanoid(s)
 amino acid sequences in, 626
 transmembrane domains of, 627
 Green fluorescent protein (GFP), 200

 Haloallylamines as SSAO inhibitors, 673–674
 Halogenofluorocorticosteroids, 596
 Halothan, metabolism of, 570
 HAT. *See* Hydrogen atom transfer
 'Heavier than water' internal tamponade, 410
 Heavy oil extraction system, 416
 Heavy silicone oils, 408
 α-Helical coiled coil
 chemical ligation and replicase activity, 750
 florination, 749
 hydrophobic core packing, 748
 impact of fluorine side chain substitutions on folding stability, 749–750
 noncovalent association, 750
 Hemoglobin (Hb), oxygen transport and delivery mechanism, 452–453
 Henderson–Hasselbalch equation, 231
 Heteroaromatic nucleophilic substitutions, 42
 Heterocorrelation chemical shift (HetCor) NMR measurements, 292
 Heterodimeric transmembrane glycoproteins.
 See Integrins
 Hexafluorobenzene (HFB), 221
 26,27-Hexafluorocalcitriol. *See* Falecalcitriol
 Hexafluoropropene oxide, 720
 HFPO. *See* Hexafluoropropene oxide
 High-molecular-weight macromolecules, 6
 High performance liquid chromatography (HPLC), 200
 application of, 10
 Hildebrandt coefficients, 452
 Histamine receptors, 76–77
¹H NMR, 293–295
 Hodgkin's disease, 32
 1H-perfluorooctane in PFO, 441
 Human eye anatomy, 422–423
 2-Hydroxyethyl methacrylate (HEMA), 357, 361
 Hydrofluoric acid (HF), 13
 Hydrogen atom transfer, 683
 Hydrogen bonds
 acidic hydrogen atom and halogen-substituted carbon, 561
 between hydroxyl and fluorine, 558
 Hydrogen [¹⁸F]fluoride (H[¹⁸F]F), 12
 Hydrophobic protein interactions, 751–752
 Hydroxyapatite (HA)
 effect of fluoride on physico-chemical properties of, 280
 electrical conductivity of, 300
 fluoridation of, 280
 fluoride interaction with, 340
 formation of, 298
 gaseous fluoridation of, 306
 plasma spray technique used for, 313
 precipitation of, 343
 5-Hydroxy-6-[(¹⁸F)]fluoro-L-tryptophan, 25
 Hydroxyl ion exchange, 341
 Hypoxia, 173

- Hypoxia-selective cytotoxins. *See* Bioreductive drugs
- Hypoxia-specific PET tracers, molecular imaging with, 174
- Hypoxic tumors, 220
- IAD. *See* Intraoperative blood donation
- ICAM-1. *See* Intercellular adhesion molecule-1
- ICER. *See* Incremental cost-effectiveness ratio
- Imagent[®], PFC-based product, 465
- Implant–tissue interface, 282
- Incremental cost-effectiveness ratio, 152
- Injectable micron-size gas bubbles, development and challenges, 462
- Integrins, 175
- Intensity modulated radiation therapy (IMRT), 221
- Intercellular adhesion molecule-1, 468
- Intermolecular interactions, 738
- Internal tamponade potency, 409
- Intraocular pressure, 637
- Intraoperative blood donation, 458
- Intratumoral (IT) injection, 228
- Iodinated azomycin galactoside (IAZG), 245
- Ion beam sputter deposition techniques, 313
- Ionomer glasses, for dental applications, 322
- Ion-selective electrode, 360, 488
- IOP. *See* Intraocular pressure
- IP receptor agonist, synthesis of, 646–649
- ISE. *See* Ion-selective electrode
- Kaplan–Meier analysis, [¹⁸F]-FDG-PET scans, 167
- Krebs–Henseleit buffer, 226
- Kryptofix-222[®], 13
- Lab on-a-chip systems, PFCs role in, 478
- Latent tracks, 398–399
- L-DOPA compound, 26
- Lineic Energy Transfer (LET), 399
- Liquid–liquid extraction, 9
- Liquid perfluorocarbons, 408, 410–411
- Locally advanced rectal cancer, prognostic value of, 166
- LPFC. *See* Liquid perfluorocarbons
- LPFC, properties of, 410–411
- Lubiprostone
- fluoro-prostanoid, 607
 - for oral treatment of constipation, 632
 - synthesis of, 608, 631
- Lung cancer
- [¹⁸F]-FDG-PET/CT imaging for
 - initial staging of, 154–155
 - recurrence detection of, 155 - [¹⁸F]-FDG-PET imaging for
 - initial staging of, 153–154
 - prediction of prognosis for patients with, 166–167
 - recurrence detection of, 154
- Lung-surfactant replacement and PFCs usages, 470–471
- Lung ventilation, PFCs usage in, 469–470
- Lymphomas, malignant
- [¹⁸F]-FDG-PET imaging
 - for progression free survival and overall survival prediction, 167
 - for staging and restaging of, 156
 - staging and restaging of malignant, by [¹⁸F]-FDG-PET/CT imaging, 156–157
- Lys8-substituted peptides, stability of, 753–754
- Magic angle spinning (MAS), 291
- Magnetic resonance imaging, 197, 451
- Malaria (anti-malarial drugs), 570–611
- MAO. *See* Monoamine oxidases
- MAO inhibitors
- aromatic side chain-fluorinated, 671–676
 - β,β -fluorinated phenethylamines as, 672
 - befloxatone as, 674–675
 - cyclopropylamines as, 679–683
 - fluorinated 5H-indeno[1,2-c]pyridazin-5-one as, 675–676
 - fluorine substitution effects on, 684–687
 - fluoroalkylamines as, 672–673
 - in neurological disorders treatment, 665
 - ring fluorinated
 - aryl-*n*-aminoethylamide derivatives, 670–671
 - benzylamines and 2-phenylethylamines, 666–668
 - 4-Fluorotranlylcypromine, 669–670
- MAOs inhibitors and substrates, fluorine effects of, 666
- Matrix metalloproteinases, pathological expression and activation of, 92
- MBF. *See* Myocardial blood flow
- MDL. *See* Tezacitabine
- Medial temporal hypometabolism, 71
- Medical radioisotopes, 10
- Metabolic trapping, 88
- Metafluoro isomers, 234
- Metal functionalisation, 26
- Metal ions, roles in cellular physiological processes, 235
- Methyl-branched-chain ω -¹⁸F-fluorofatty acids, 89
- Methyl [¹⁸F]fluoride (CH₃[¹⁸F]F), 11
- Methyl lithium, 22
- Microfluidics technologies, PFCs role in, 478–479
- Micron-size bubbles osmotic stabilization, perfluorochemical in, 463–464
- Microwave technology, 9
- Mild cognitive impairment (MCI), 71
- Milk fluoridation, 351
- Mineralizing cells, 319
- Mitogen-activated protein kinase system (MAPK), 319
- MMP inhibitors (MMPi), radiolabeled
- lead structures for, 92
 - radiosynthesis of, 93
- MMPs. *See* Matrix metalloproteinases
- Molecular imaging method, 466
- Molecular *in vivo* imaging, 4

- Molecular recognition, 555
 Monoamine oxidases, 662–663
 Mono[¹⁸F]fluoride (Cl[¹⁸F]F), 13
 MRI. *See* Magnetic resonance imaging
 Multicompartmented micelle formation, 476–477
 Multi-quantum (MQ) coherences, 291
 Muscarinic acetylcholine receptors
 density in heart, 114
 ¹⁸F-labeled diastereomers for imaging of
 4-[¹⁸F]fluorodexetimide (4-[¹⁸F]FDEX),
 115–117
 [¹⁸F]FP-TZT, M₂-subtype, 115, 116
 (*R,R*)-[¹⁸F]FQNPc, 117–118
 (*R,R*)-quinuclidinyl- 4-[¹⁸F]fluoromethyl-
 benzilate, 115
 (*R,S*)-quinuclidinyl- 4-[¹⁸F]fluoromethyl-
 benzilate, 114
 subtypes of, 113
 Muscarinic acetylcholinergic receptors
 (mAChRs), 74–75
 Myocardial blood flow
 tracers, 96
 7'-[¹⁸F] fluoro-6',7'-dihydrorotenone ([¹⁸F]
 FDHR), 98
 ¹⁸F-labeled amines and quaternary
 ammonium salts, 97
 [¹⁵O]H₂O and [¹³N]NH₃, 96
 SPECT, 98
 Myocardial oxygenation, 224–225
 Myocardial physiology, 224
 Myocardium
 energy metabolism in, 86–87
 energy source for, 89
 innervation of
 α-adrenoceptors, 112–113
 β-adrenoceptors, 100–112
 muscarinic receptor, 113–114
 radioligands for imaging, 99–100
 sympathetic and parasympathetic, 98–100
 molecular imaging of
 with [¹⁸F]FDG and ¹⁸F-labeled fatty acids,
 86
 neurotransmission process of, 99
 perfusion analysis of, 96–98
 Myocardium infarctus, 380
 Myocytes
 [¹⁸F]FDG accumulation mechanism in, 88
 uptake of glucose in, 88

 Natural compounds (pharmaceuticals), 553–611
 Natural hydroxyapatite, 341
 N-dealkylation
 of fluorinated analogues of propranolol, 568
 N-t-butyl analogue, 570
 Neoadjuvant chemotherapy/radiochemotherapy,
 metabolic effects of, 165
 Neodymium-doped yttrium aluminium garnet (Nd:
 YAG) laser deposition, 313
 NET. *See* Nonrepinephrine transporter
 NET₂S[¹⁸F]F₃, 13
 Neurodegenerative disorder, 68

 Neuroendocrine tumors (NETs), 181
 N-[¹⁸F]Fluoro-N-alkylsulphonamides, 14, 17, 23
 N-[¹⁸F]Fluoropyridinium triflate, 14, 17, 23
 Nitrosyl [¹⁸F]fluoride (ON[¹⁸F]F), 14
 NMR. *See* Nuclear magnetic resonance
 NMR oximetry, 221
 Non-covalent interactions, 559
 Nonrepinephrine transporter, neurotransmitter
 uptake process, 118
 Nonsteroidal anti-inflammatory agents, 219
 Nuclear magnetic resonance, 197–253, 290
 Nucleophilic aliphatic substitution, 29–30
 Nucleophilic aromatic substitution, homoaromatic
 series, 35–36
 Nucleophilic radiofluorinations, 11, 12, 27–28
 Nucleoside reverse transcriptase inhibitor, 585

 OCP hydrolyzate, 342
 Octacalcium phosphate (OCP), 310, 342
 Ocular endotamponade
 improvement in, 428–431
 local effects, evaluation of
 drop shapes/contact angles, 440–441
 high density effects, 435
 impurities effect, 441
 oxygen content, 435–436
 physicochemical behaviors effects, 437
 structure based effects, 437–440
 perfluorocarbons as, 426
 requirements for, 427–428
 Ocular tamponade, principle of, 409
 Optison[®], PFC-based product, 465
 Oral 5-fluorouracil (5-FU) pro-drugs, 579
 Organic aminofluorides, 352
 Organic porogenic agents, 311
 Ornithine decarboxylase, inhibitor of, 610
 Osteoblast cells, 321
 effect of fluoride ion on, 319–320
 proliferation of, 319
 Osteoblast-like cell adhesion, 303
 Osteoclast cells, 321–322
 Osteoporosis treatment and fluoride therapy,
 489–490, 535–536
 Ovarian cancer, [¹⁸F]-FDG-PET imaging of,
 168–169
 Oxane Hd[®], 408
 biocompatibility of, 415
 characteristics of, 412
 clinical study, 415–417
 intra-ocular bubble of, 430
 Oxidative metabolism
 reactive species formation, 570
 slowing down of, 567
 Oxyfluor emulsion development, 456
 Oxygen extraction fraction, 221
 Oxygent[™] emulsion development, 455–458
 applications of, 459

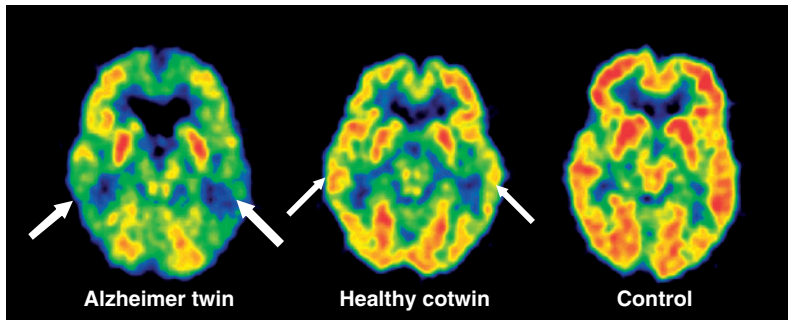
cis-9,10-Palmitoleic acid, 19
 Pancreatic serine protease. *See* α-Chymotrypsin

- Para-methoxy-methamphetamine (PMMA)
 cement, 303
- Partial liquid ventilations, 469
- Partially fluorinated compounds, 428–430
- Passive reporter molecules, 252
- Pauling's scale, electronegative atom, 8
- Penciclovir, 25
- Pentafluorination, 559
- Peptide isosteres, 701–702
- Peptidomimetics design, 701–702
- Peptidyl prolyl isomerases, 723
- Perchloryl [^{18}F]fluoride ($[\text{}^{18}\text{F}]\text{FCIO}_3$), 14, 16
- Perflubron, 454
- Perfluorocarbon gases use, 409
- Perfluorocarbon liquids, 424
 biocompatibility of, 425–426
 contact angle, 440
 ophthalmic use of, 426
 quality of, 427
- Perfluorocarbons (PFCs), 198
 biocompatibility and environmental issues of, 451–452
 biomedical uses of, 448–451
 as drugs and drug delivery systems, 469–472
 as life sciences and biomedical tools, 474–479
 oxygen delivery to tissues and organs, 452–453
 product and applications of, 465–466
 product developments, 455–458
 solubility, 450
 as surgical aids, 472–473
 uses in diagnosis, 466–469
- Perfluorochemicals, 448, 450
- Perfluorocyclohexan (PFE), 411
- Perfluorodecaline (PFD), 411
- Perfluorohexyl-ethane, 437
- Perfluorohexyl-ethene oligomers, 442
- Perfluoro-*n*-octan (PFO), 411
- Perfluorophenanthren (PFPN), 411
- Perfluorotributylamine (PFBA), 411
- Perfluorotributylamine (PFTB), 221
- Perftoran development, 456
- PET. *See* Polyethylene terephthalate
- PET, *See* Positron emission tomography
- PET, trade names, 389
- PET/CT scanner, functionality of, 144
- PET imaging, 33
- PET radionuclide, 49
- PET radiopharmaceutical, 5, 67
- PFC-based oxygen carriers
 applications of, 458–460
 challenges in developing, 454–455
- PFC emulsions, 224
- PFCLs. *See* Perfluorocarbon liquids
- PFC $p\text{O}_2$ reporters, 221–224
- PFCs. *See* Perfluorochemicals
- PFOB. *See* F-octyl bromide; Perflubron
- PG (*See* Prostaglandins)
- PGD derivatives
 CRTH2 receptor agonist and antagonist, 644–646
 DP receptor agonist and antagonist, 642–644
- PGD2 receptor (prostanoid receptor), 627, 628
- PGE derivatives
 13,14-dihydro-15-keto-PGE derivative, 630–632
 EP2 receptor agonist, 635–636
 EP4 receptor agonist, 637
 EP1 receptor antagonist, 632–634
- PGE receptors
 subtypes of, 630
- PGF_{2 α} derivatives, role as drugs, 637
- PGF derivatives
 FP receptor agonist, 637–641
 FP receptor antagonists, 641–642
- PGI₂ degradation mechanism, 647
- PGI derivatives, IP receptor agonist, 646–649
- pH, indicator of tissue health and acidosis, 231
- Pharmacokinetics, 7
- Phe-Gly isostere, synthesis, 704–705
- 2-phenylethyl-amines, fluorine substituted, 666–668
- Phosphates/phosphonates, acidity of, 574
- Pin1, therapeutic role, 725
- pK_a (acid dissociation constant)
 of amines, 561–562
 of fluorinated compounds, 559–560
 of gaseous general anaesthetics, 562
- Placenta and foetus, fluoride concentration in, 502
- Plasma fibronectin, 303
- Plasma fluoride levels in human, 501
- Plasma spray process, 313
- Platelet deposition, 384–385
- PLV. *See* Partial liquid ventilations
- ^{31}P NMR, 295–296
- Podophyllotoxin
 cytotoxic agent, 588
 etoposide derivatives (anti-tumour derivative), 589
- Polarographic electrodes, 231
- Polyacid-modified composite resins, 362–364
- Poly(ADP-ribo) polymerase1 (PARP-1), 217
- Polyamine oxidases, 664
- Polyethylene terephthalate, 380
- Polymerase chain reaction (PCR), 764
- Polypeptide interactions, fluorinated side chains, 752
- Polytetrafluoroethylene, 380, 473
- Polyvinylidene difluoride, 394
 chemical modification of, 396
 conversion diagram of, 397
 scanning electron microscopy
 microphotographies of, 399–400
 and swift heavy ions (SHI), 396, 398–399
 tubular conduit by, 398
- Positron emission tomography (PET) technique, 67, 200, 673, 774
 impact of fluorine-18 on, 5
 for molecular in vivo imaging, 4
 positron emission, 142
 short-lived positron-emitting radionuclides
 for, 5
 use in nuclear medicine, 4

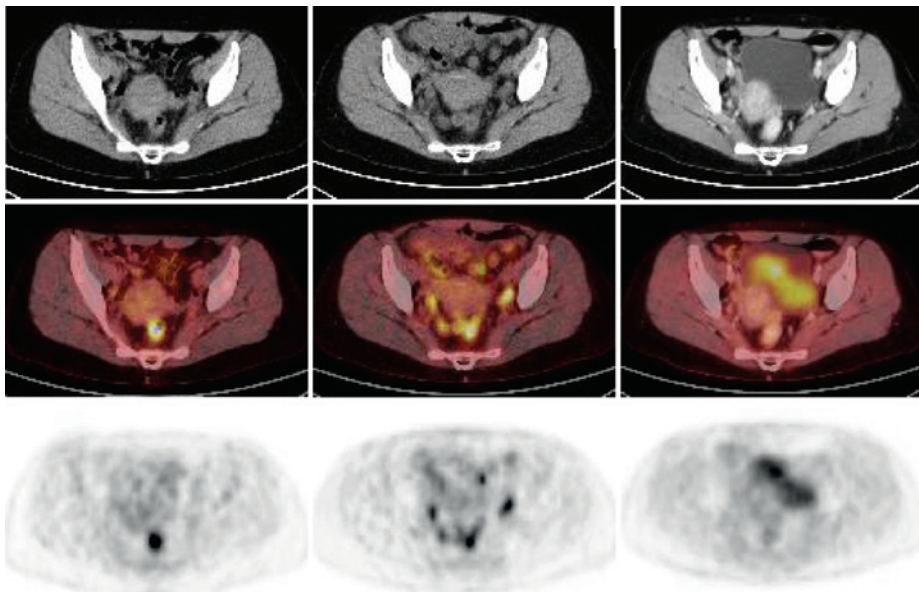
- Positron emitter
 challenges in radiochemistry with, 8–10
 design of radiotracers and
 radiopharmaceuticals labeled with, 7
 development of methods and techniques for
 synthesis of, 8
- Positron-emitting radiohalogens, 6
- Positron-emitting radionuclides, for PET
 imaging, 6
- Posterior cingulate cortex, 71
- PPlases. *See* Peptidyl prolyl isomerases
- Progesterone receptor antagonist. *See*
 Antiprogesterone
- Proliferative diabetic vitreoretinopathy (PDR),
 423
- Proliferative vitreoretinopathy, 416, 423
- Prostacyclins (PGI₁, PGI₂ and PGF_{2α}), fluoro
 analogues of, 606
- Prostaglandins (PG), drugs, role of, 637
- Prostanoid(s)
 biosynthesis of, 624
 fluorinated, 628
 in drug design, 630
 fluprostenol and 6,16-difluoro-PGE₂,
 629
 lubiprostone and travoprost, 607–608
- PGE2
 metabolism of, 625
 and prostanoid receptor, 628
 receptors, 630–631
 physiological properties of, 626, 628
 prostacyclins (PGI₁, PGI₂ and PGF_{2α}),
 606–607
 receptors
 homology, 626, 627
 PGD2 and CRTH2, 627–628
- Prostate cancers, 30
- Protein structure and function, role of fluorine,
 722–723
- Pseudo first-order reaction kinetics, 9
- Pseudomonas fluorescens*, 643
- ³¹P SPE-MAS NMR spectra, 295
- PTFE. *See* Polytetrafluoroethylene
- ePTFE. *See* Expanded polytetrafluoroethylene
- PTFE, properties of, 388–389
- ePTFE prostheses
 chemical modification of, 395
 development and use of, 391–392
 formation of, 389
 improvement strategies, 392–393
 tapered arterial prostheses, 394
- Pulsed laser deposition, 313
- Purine nucleotide phosphorylase (PNP) gene
 (fIB), 771
 reactions of, 772
- PVDF. *See* Polyvinylidene difluoride
- P(VDF-HFP) copolymers, 394
 chemical modification of, 401–402
- PVR. *See* Proliferative vitreoretinopathy
- Pyrolysis method, 307
- Quiescent proline peptidase (QPP), 728
- Racemic *erythro*-9,10-*d*[[18F]fluoropalmitic
 acid, 19
- Radiation-induced cytotoxic products, 173
- Radiofluorinations, 4
 methods of, 11–12
- Radiohalogens, positron-emitting, 5
- Radioisotope, half-lives of, 8
- Radiolabeled amino acid tracers, 180
- Radiopharmaceuticals, 174
- Radiotracer, 6
- Ramatroban, therapeutic role of,
 644, 646
- RDA. *See* Recommended dietary allowances
- RDPR. *See* Ribonucleotide diphosphate
 reductase
- Reactive [¹⁸F] fluoride anion, preparation of,
 28–29
- Recommended dietary allowances, 536
- Remineralisation and demineralisation
 processes, 339
- Replicase
 activity and chemical ligation, 750
 template-assisted autocatalyzed peptide
 replicase cycle, 754
 turnover of Leu9-modified peptides,
 751–752
 turnover of Lys8-modified peptides, 753
- Reporter molecules
 physical interactions
 myocardial oxygenation, 224–226
 PFC *p*O₂ reporters, 221–224
 tumor oxygenation, 226–231
 in vivo oximetry, 220–221
- RES. *See* Reticuloendothelial system
- Resin-modified glass-ionomers, 361–362
- Respiratory gating, 170
- Reticuloendothelial system, 455
- Retinal detachment, 423
- Retinal oxygenation, 228
- Retinal reapplication force, 409
- RGD (arginin-glycin-aspartic acid) triade, 393
- Rhegmatogenous retinal detachment (RD),
 definition of, 407
- Ribonucleotide diphosphate reductase, 580
 inhibitors of
 2',2'-difluorodeoxycytidine, 581
 fludarabine, 584
 fluoromethylene deoxycytidines, 582
 mechanism for inactivation of, 583
 nucleotide reduction catalysis, 581, 582
- Rietveld refinement method, 287
- RMN3
 biocompatibility of, 413–415
 RMN3-silicone oil mixture, experimental study,
 414–415
 structure of, 413
 synthesis of, 412–413
- Rotational echo double resonance (REDOR), 292

- S-adenosylhomocysteine (SAH), 772
S-adenosyl-L-methionine (SAM), 44, 761, 765
Saliva proteins, adsorption of, 318
SAM synthetase, 764, 766, 767
SARs. *See* Structure activity relationships
Scanning Electron Microscopy (SEM), 399
Scientific Committee on Food (SCF), 506
Secondary ion mass spectroscopy (SIMS), 360
Semicarbazide-sensitive amine oxidases, 662, 664
Semifluorinated alkanes, 411
Sep-Pak[®] cartridges, 9
Serine hydroxymethyl transferase (SHMT), 772
Serine protease inhibition, 575
Serotonergic system, 72–73
SET. *See* Single electron transfer
SHI. *See* Swift heavy ions
Signal-to-noise ratio (SNR), 221
Silica-phosphate glass-ceramic, 302
Silicone oil, properties of, 410
Silicone oil tamponade, 408
Silicon tetra[¹⁸F]fluoride (Si[¹⁸F]F₄), 13
Single electron transfer, 663
Single photon emission computed tomography (SPECT), 67, 200
Skeletal fluorosis, 497–498
Sodium iodine symporter, 248
Soft contact lenses and PFCs usages, 472–473
Sol-gel method, 310
Solid-phase extraction (SPE), 36
Sonazoid[®], PFC-based product, 465
Sonovue[®], PFC-based product, 465
Spatial demand
 effect on side chain fluorination, 752
 of fluorinated alkyl groups, 739, 749
 of fluoroalkyl amino acids, 755
 of methyl group, 746, 755
 side chain elongation effect on, 751
Specific surface area (SSA), 307
Specific transformation protocol, 389
SPECT radiopharmaceuticals, 68
Spin echo formation, 291
Spin lattice relaxation, 221, 228
SSAO-catalyzed oxidation of amines, mechanism, 664
SSAO inhibitors
 allyl hydrazines as, 674
 cyclopropylamines as, 679–683
 fluorine substitution effects on, 683–684
 haloallyl amines as, 673–674
 therapeutic role, 665
SSAOs. *See* Semicarbazide-sensitive amine oxidases
Steric effects
 of fluorine substitution in amino acids, 745
 of isopropyl group and trifluoromethyl group, 740
 of α Tfm amino acid, 746
Sterol C-14 demethylase inhibitor, 584
Streptococcus mutans, 336, 340
Streptomyces cattleya
 FAC 1 and 4-TF 2, biosynthesis of, 773
 fluorinated metabolites, 761
 fluorination, genetic basis of, 770–771
 fluorometabolite pathway, 763, 771, 772, 776
 ¹⁹F NMR time course of, 763
 reactions of, 764
 relative arrangement and annotation of fIA, 771
Structure activity relationships, 665
Subendothelium, platelet attachment to, 384
Sulphur hexafluoride (SF₆), 409
Sulphur tetra[¹⁸F]fluoride (S[¹⁸F]F₄), 13
Surface protonated phosphates, 294
Surgical vascular suture, 388
Swift heavy ions, 396, 398–399
Synthetic prostaglandin (SC-46275), anti-secretory activity of, 607
Tafluprost and FP receptor, 639–641
Tamponades, in vitreoretinal surgery, 408
Tanker effect, 437
TCP. *See* Tricalcium phosphate
Teflon FEP, 388
Tetramethylsilan (TMS), 294
Tezacitabine
 RDPR inhibitor, 582–583
 synthesized from, 584
TFI. *See* Thylstrup-Fejerskov Index in dental fluorosis rating
 α Tfm-substituted amino acids
 enzymatic degradation of, 744
 phenylalanine and alanine, 743
 proteolysis inhibition, 744
 stereochemistry and steric effects of, 746
Thermolysin, role in biological system, 728
Thrombin time, 399–400
Thrombomodulin (TM), 393
Thrombosis, 381–382
Thylstrup-Fejerskov Index in dental fluorosis rating, 496–497
Thymidylate synthase (TS)
 inhibitors of, 5-fluorouracil (5-FU), 578
 methylation of deoxyuridine by, 578
TISAB. *See* Total ionic strength adjustment buffer
TISAB decomplexation, 360
Tissue fluoride levels in human, 501–502
Tissue oxygenation, 220
Tooth enamel crystals, 296
Tooth mottling, 334. *See also* Dental fluorosis
Tooth surface index of fluorosis, 496–497
Total global ischemia (TGI), 225, 226
Total ionic solubility acid buffer (TISAB), 360
Total ionic strength adjustment buffer, 534
Toxicology (LD50), biological information, 7
TPQ. *See* 2,4,5-trihydroxyphenylalanine quinine
Trans-2-(4-fluorophenyl)cyclopropylamine, 669
Tranylcypromine, clinical role, 669
Travoprost synthesis, 607, 637–638

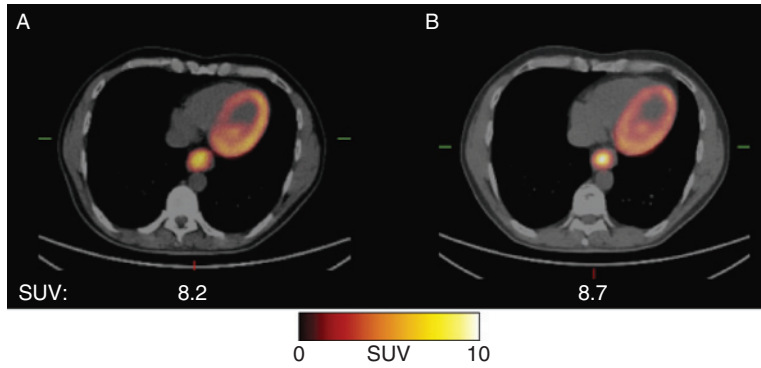
- Triazene decomposition reaction, aromatic labeling in, 13. *See also* Wallach reaction
 Tricalcium phosphate(TCP), 282, 669
 Tricarboxylic acid (TCA) cycle, 214
 Triethylene glycol dimethacrylate (TEGDMA), 362
 Trifluorocitronellol, olfactory properties of, 556
 Trifluoroethylamines, 573
 Trifluoromethyl [^{18}F]hypofluorite ($\text{CF}_3\text{O}[^{18}\text{F}]\text{F}$), 14, 15
 Trifluridine, 5-FU pro-drug, 580
 2,4,5-Trihydroxyphenylalanine quinine, 684
 6-aryl-1,1,5-Trimethylindanes, rotational barriers of, 739–740
 Trimethylsilyl enol ethers, 22
 Tripeptide isosteres, synthesis, 705
 TSIF. *See* Tooth surface index of fluorosis
 TT. *See* Thrombin time
 Tumor hypoxia
 bioreductive drugs for, 173
 doses of radiation therapy in, 173
 PET and PET/CT imaging for, 174–175
 tumor oxygenation evaluation methods, 174
 Tumor hypoxiation, 228
 Tumor oxygenation, 226–231
 Tumor response, 163
 Tumour imaging agents, 25
- Ultrasound (US) imaging
 application of, 462
 PFCs properties in, 463
- U.S. Centers for Disease Control and Prevention (CDC) water fluoridation standard, 490
- U.S. Food and Drug Administration and fluosol development, 455–456
- Valrubicine, 590
 van der Waals radius, fluorine, 8
 Varnishes, 355
 Vascular prostheses, 388–389, 394, 396
 Vasoactive drugs, 217
 Vesicular monoamine transporter, isoforms of, 118
- Vinca dimer indole alkaloids
 anti-mitotic drugs derived from, 586
 vinblastine, 585
 vinflunine, 585–586, 585–587
- Vitrectomy, 423–424
 Vitreoretinal diseases, 423
 Vitreoretinal (VR) surgery, 424
 Vitro-retinal proliferation (VRP), 408
 VMAT. *See* Vesicular monoamine transporter
- Wallach reaction, 13
 Water fluoridation, 347
 Weft and warp, 389–390
 White spot lesion, 338
 Willard–Winter distillation procedure in fluoride determination, 533
 World Health Organization (WHO) water fluoridation standard, 490, 493, 506
- Xenon $d[^{18}\text{F}]$ fluoride ($\text{Xe}[^{18}\text{F}]\text{F}_2$), 13–14, 16
 X-ray photoelectron spectroscopy (XPS)
 quantitative analysis, 395



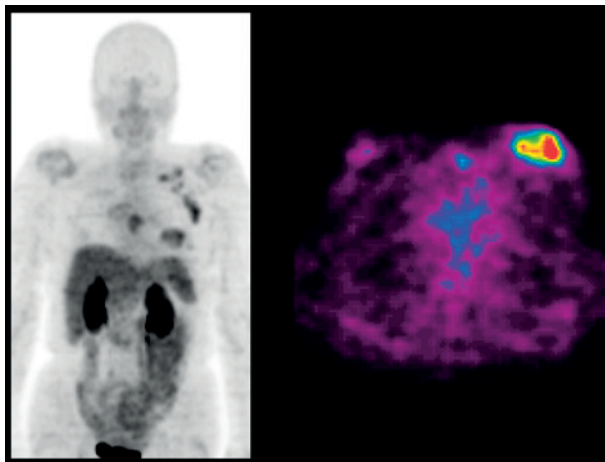
Chapter 2, Fig. 1. An [^{18}F]FDG-PET scan depicting glucose metabolism in a monozygotic twin pair and in a control subject. Note the clear reduction in [^{18}F]FDG uptake especially in temporoparietal areas (thick arrows) in the cotwin having AD (on the left), and similar, but less pronounced reduction in same brain areas (thin arrows) in the cognitively healthy cotwin (in the middle) as compared with the uptake in a control subject (on the right).



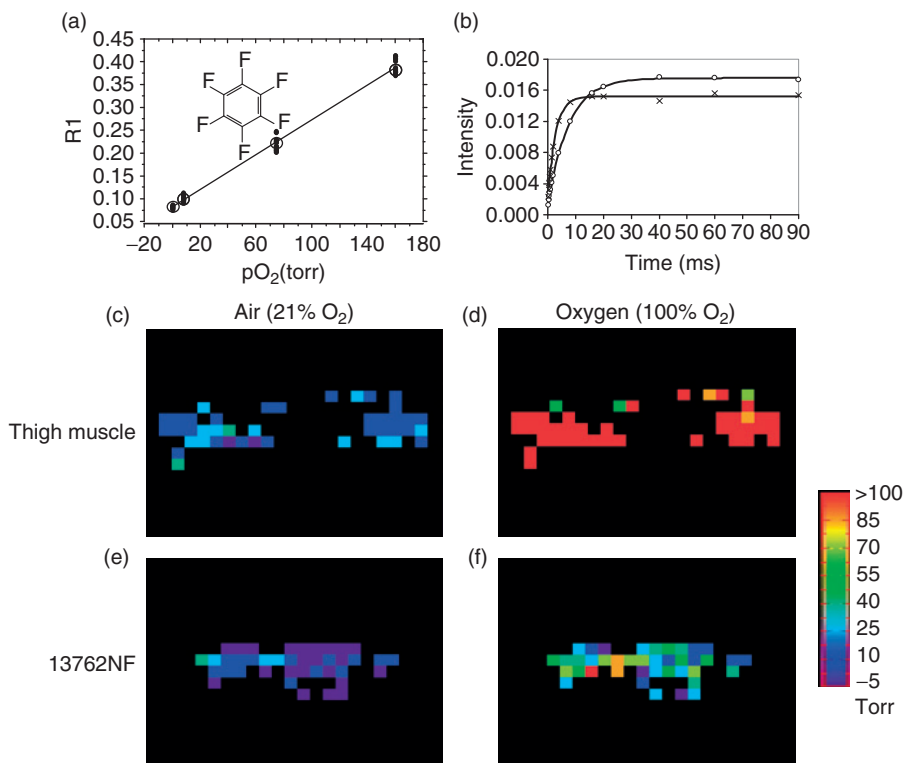
Chapter 4, Fig. 1. Example of FDG-PET/CT studies in a patient with rectal cancer and metabolic response. FDG uptake decreases 14 days after initiation and after completion of radiochemotherapy. First row shows the CT-scan, second row displays the fusion of FDG-PET and CT-scans and the third row represents the corresponding FDG-PET scan.



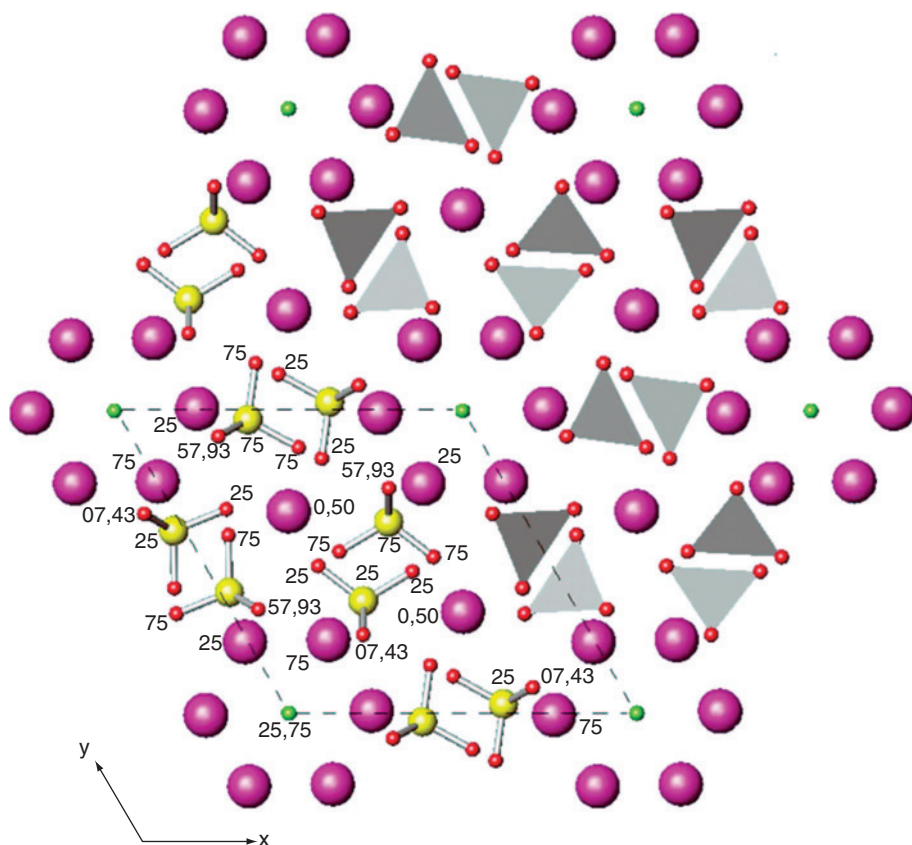
Chapter 4, Fig. 2. Example of FDG-PET/CT studies (fused images) in a patient with adenocarcinomas of the esophagus and metabolic non-response. High focal initial FDG uptake in the tumor (A) which is almost unchanged 14 days (B) after initiation of chemotherapy.



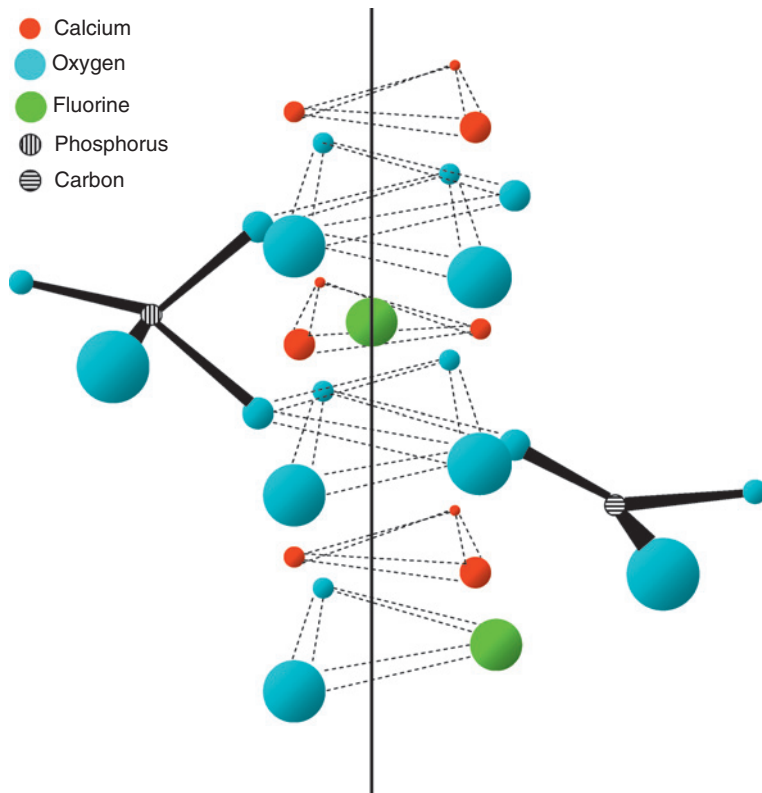
Chapter 4, Fig. 4. Patient with breast cancer: Staging with [^{18}F]-RGD-PET.



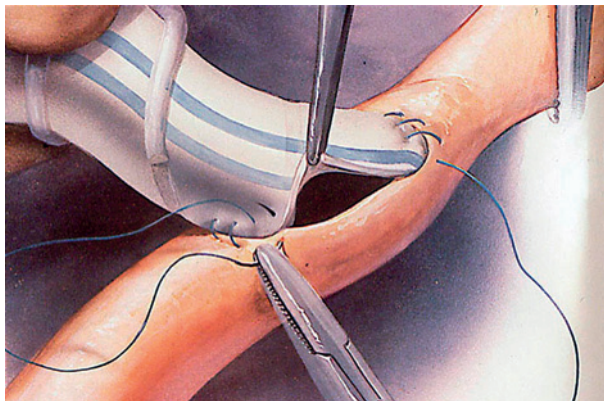
Chapter 5, Fig. 7. *FREDOM-tissue oxygen dynamics.* (a) A linear relationship is found between the spin lattice relaxation rate R_1 of hexafluorobenzene (HFB) and pO_2 (reprinted from *Methods in Enzymology*, 386, Zhao D, Jiang L, Mason RP, Measuring Changes in Tumor Oxygenation., 378–418, Copyright (2004), with permission from Elsevier) [10]. (b) ^{19}F NMR relaxation curves from a single voxel in rat leg muscle after direct administration of 50 μ l HFB. Curves are shown during air breathing (circles; $T_1 = 7.37$ s, $pO_2 = 28$ Torr) and following switch to oxygen for about 20 min (crosses; $T_1 = 2.65$ s, $pO_2 = 156$ Torr), respectively. (c) pO_2 map of rat thigh muscle during air breathing. Data obtained in 6.5 min, showing heterogeneity of baseline oxygenation. Mean $pO_2 = 20 \pm 1$ Torr. (d) Following 20 min oxygen breathing, all the voxels in (c) showed increased pO_2 reaching a new mean $pO_2 = 158 \pm 6$ Torr. (e) pO_2 map of 13762NF rat breast tumor, while rat breathed air (mean $pO_2 = 13 \pm 2$ Torr). Oxygenation is clearly lower than for muscle, above. (f) During oxygen breathing, tumor pO_2 increased, though showing considerable heterogeneity of response with mean $pO_2 = 52 \pm 4$ Torr.



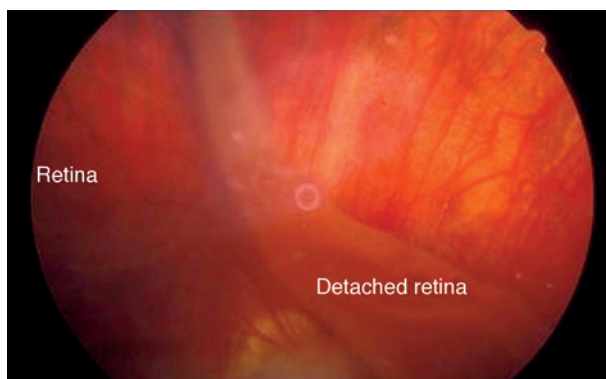
Chapter 6, Fig. 2. Structure of fluorapatite. Projection on the (001) crystallographic plane, perpendicular to the c axis of the hexagonal structure. (Reproduced by permission of IUCr from Ref. [2]). Purple: Calcium; green: Fluorine; red: Oxygen; yellow: Phosphorus.



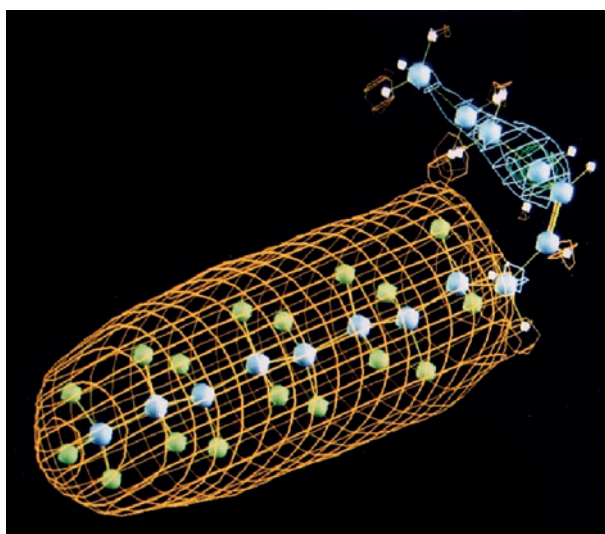
Chapter 6, Fig. 3. Split view of atoms along the c axis of the hexagonal structure showing the two possible fluoride ion locations. In stoichiometric fluorapatite, fluoride ions locate in the equilateral triangle formed by Ca(II) ions. In type B carbonate apatite, the replacement of PO_4^{3-} ions by CO_3^{2-} ions creates an oxygen atom vacancy which may be occupied by a second kind of fluoride ion (adapted from Ref. [4]).



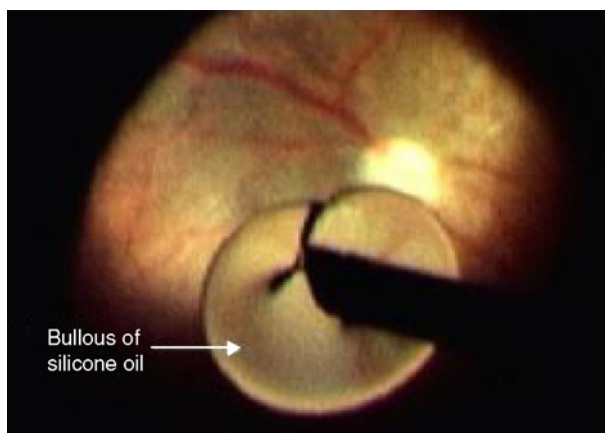
Chapter 8, Fig. 2. A type of surgical vascular suture.



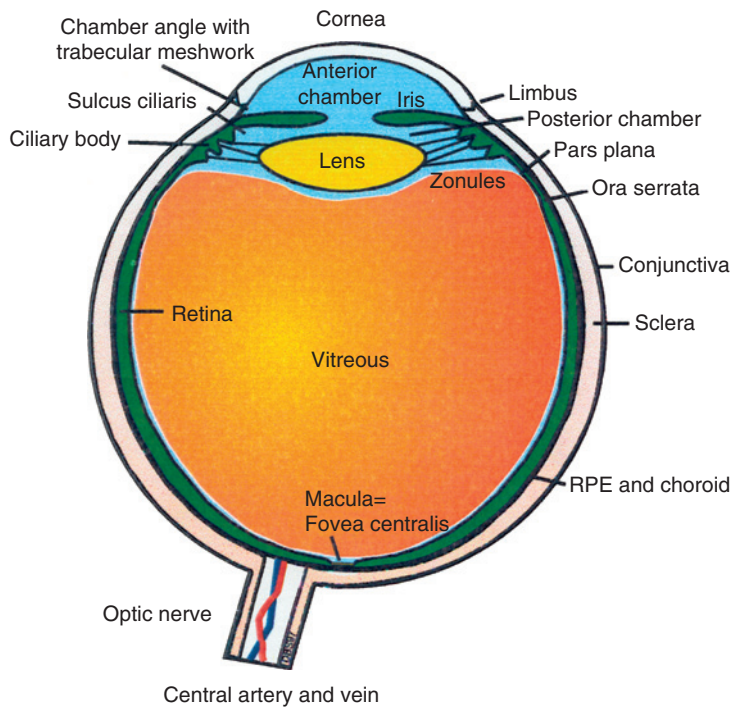
Chapter 9, Fig. 1. Photograph of fundus with a retinal detachment.



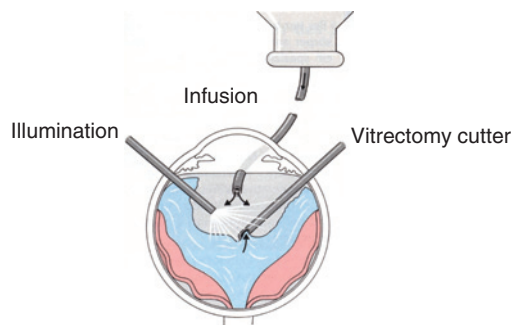
Chapter 9, Fig. 3. Structure of RMN3.



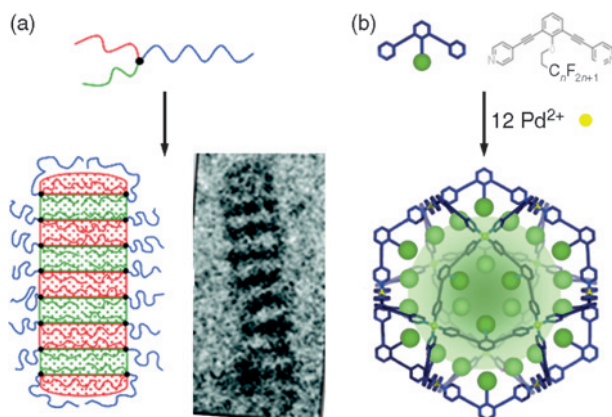
Chapter 9, Fig. 5. Preoperative picture showing the 'heavy oil' extraction system.



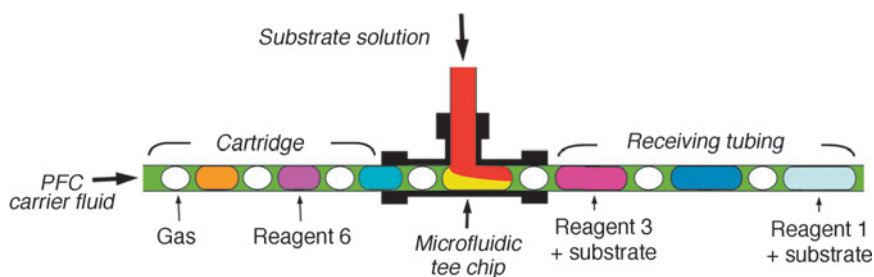
Chapter 10, Fig. 1. Cross section of the human eye.



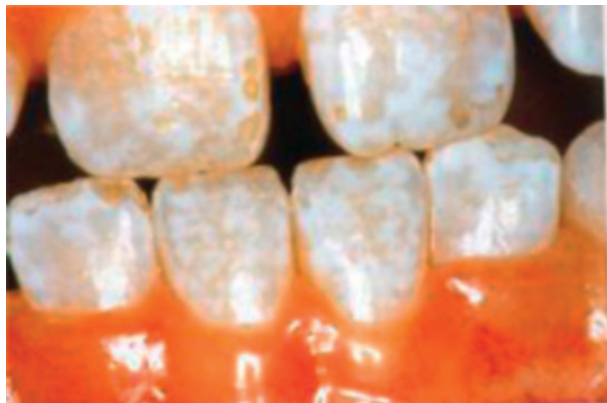
Chapter 10, Fig. 2. Vitrectomy.



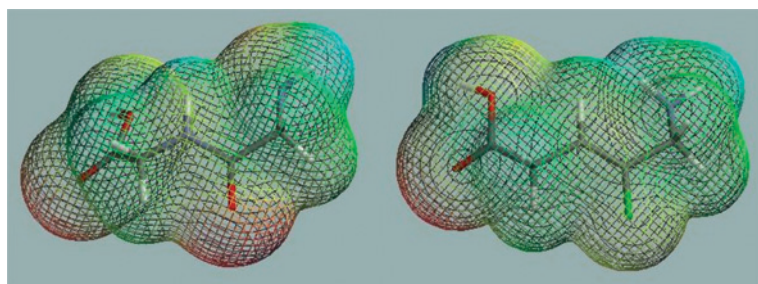
Chapter 11, Fig. 18. (a) Schematic representation and cryoTEM image of a multicompartment micelle obtained from self-assembly in water of a star terpolymer having a perfluoropolyether arm (green), a polystyrene arm (red), and a poly(oxyethylene) arm (blue). From Ref. [90], with permission. (b) Self-assembled rigid cage with a fluid perfluorocarbon interior. The cage is made of 12 palladium(II) ions (yellow dots) and 24 linkers with a perfluoroalkyl chain (green dots); the perfluoroalkyl chains-lined cavity within the cage is depicted in light green. From Ref. [91], with permission.



Chapter 11, Fig. 19. Schematic view of perfluorocarbon-implemented microfluidics for chemists. Capillary cartridges preloaded with plugs of reagents separated by gas bubbles within a perfluorocarbon carrier fluid are fitted onto a microfluidic chip where the substrate stream merges with the reagent plugs. From Ref. [102], with permission.



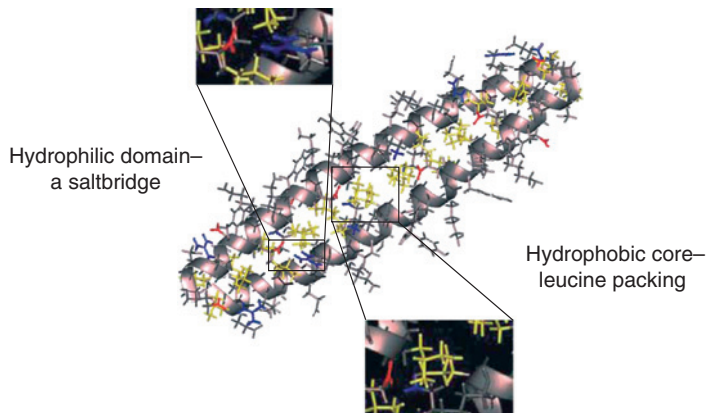
Chapter 12, Fig. 2. Teeth demonstrating fluorosis. A high level of dietary fluoride has resulted in much of the enamel becoming opaque in patches, giving a 'mottled' appearance. (Reprinted with permission from [48]. Copyright 2002 Mosby International Limited.)



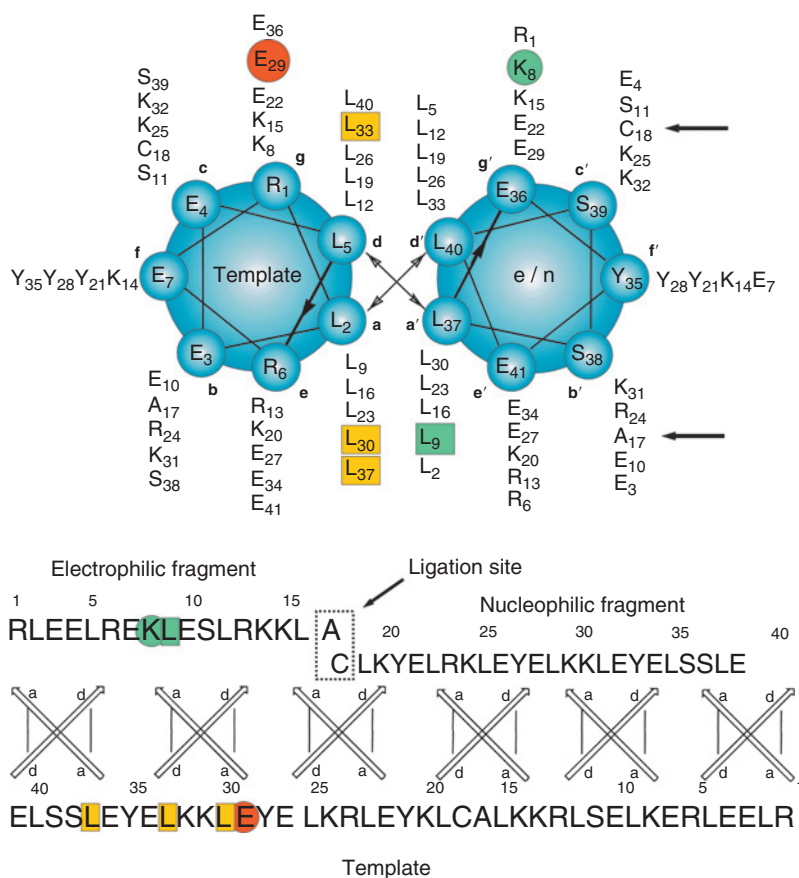
Gly-Gly

Gly ψ [CF = CH]Gly

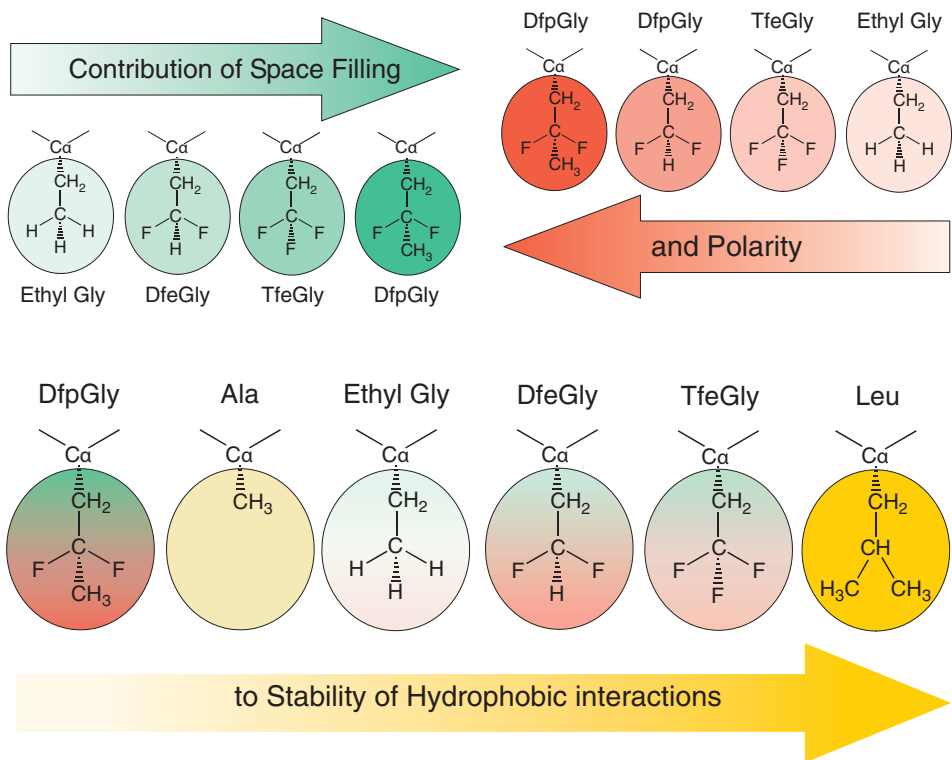
Chapter 16, Fig. 5. Electrostatic potential surfaces computed with B3LYP/6-31G** using Titan 1.05.



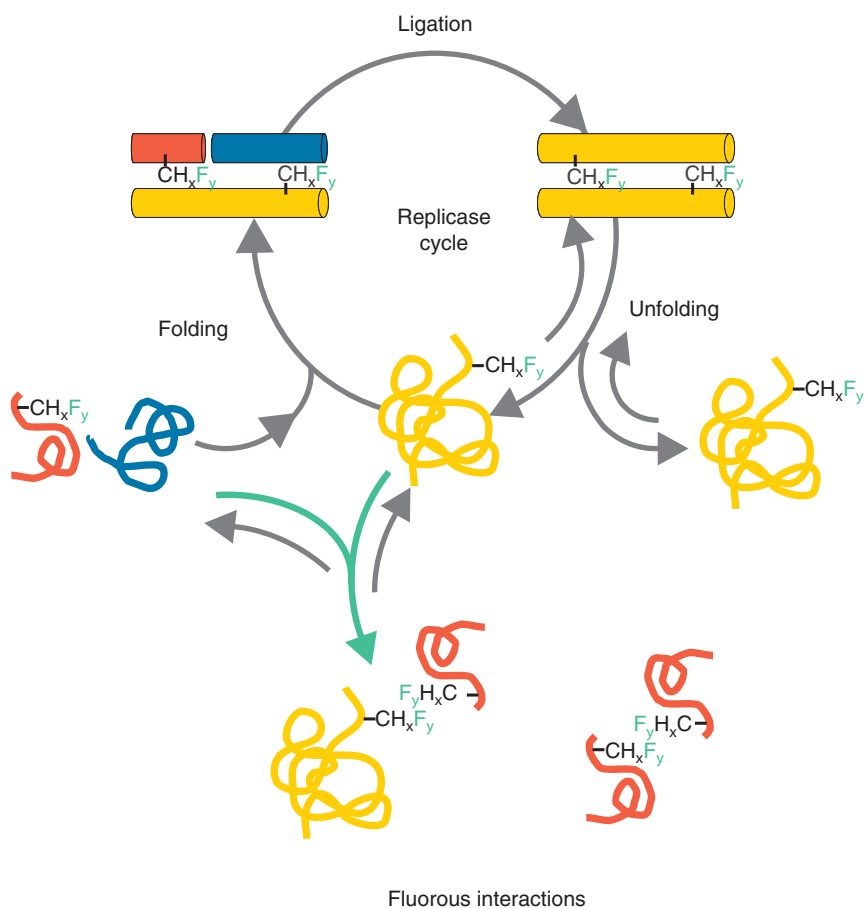
Chapter 17, Fig. 6. Model of a typical coiled coil dimer with focus on hydrophobic core packing and interhelical salt bridges.



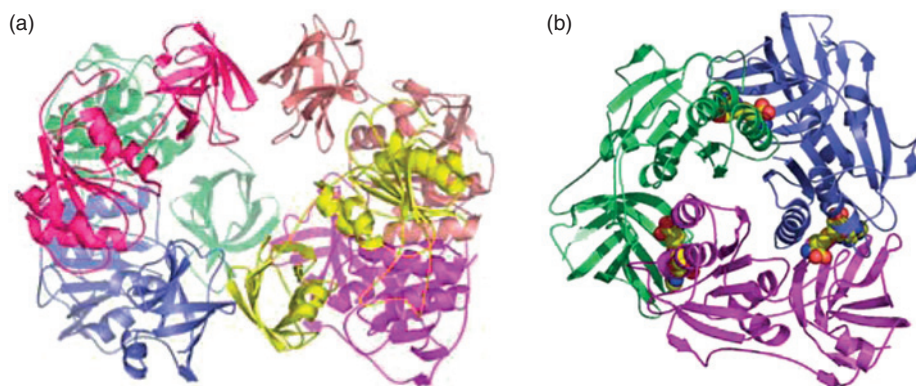
Chapter 17, Fig. 7. Helical wheel and sequence representation of the parental homodimeric coiled coil. The substitution positions within the hydrophobic domain are highlighted with open squares and those in the charged domain with open circles. Their interaction partners are highlighted with shaded squares and circles, respectively. The arrows mark the ligation site of nucleophilic and electrophilic fragments.



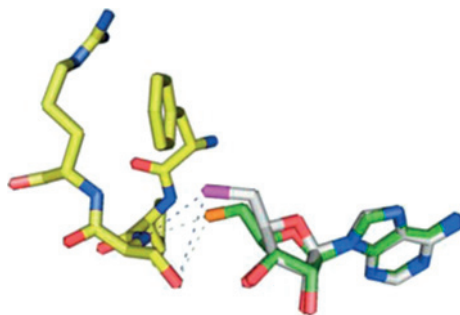
Chapter 17, Fig. 10. The contrary effects of spatial demand and polarization on side chain fluorination on hydrophobic interactions.



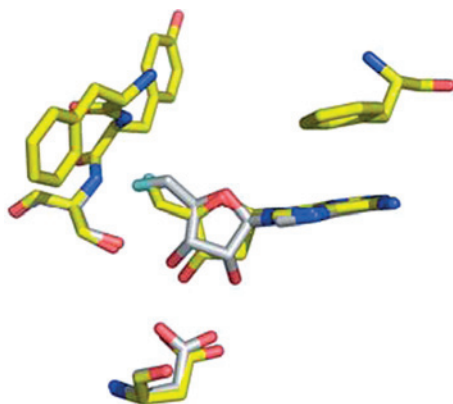
Chapter 17, Fig. 12. The template-assisted autocatalyzed peptide replication cycle and the influence of fluorine–fluorine interactions (yellow, template; red, electrophilic fragment; blue, nucleophilic fragment).



Chapter 18, Fig. 2. A representation of the X-ray-derived structure of the fluorinase. Inset (a) shows the full structure as a hexamer (dimer of trimers) and inset (b) shows the protein trimer with three *S*-adenosyl-L-methionine (SAM) **8** substrate molecules bound at the subunit interfaces [10].



Chapter 18, Fig. 5. The X-ray-derived structure of the 5'-chloro-5'-deoxyadenosine (5'-CIDA)-fluorinase co-complex overlaid with the 5'-FDA structure. It can be seen that the chlorine atom is displaced relative to the location of the fluorine due to its larger size [15].



Chapter 18, Fig. 6. Structure of the 2'-d-FDA **16**-fluorinase co-complex, overlaid with the structure of 5'-FDA **5** bound to the enzyme [16].